



HAL
open science

Analytical methods and field theory for disordered systems

Thimothée Thiery

► **To cite this version:**

Thimothée Thiery. Analytical methods and field theory for disordered systems. Physics [physics]. Université Paris sciences et lettres, 2016. English. NNT : 2016PSLEE017 . tel-01361896v2

HAL Id: tel-01361896

<https://theses.hal.science/tel-01361896v2>

Submitted on 16 Feb 2017

HAL is a multi-disciplinary open access archive for the deposit and dissemination of scientific research documents, whether they are published or not. The documents may come from teaching and research institutions in France or abroad, or from public or private research centers.

L'archive ouverte pluridisciplinaire **HAL**, est destinée au dépôt et à la diffusion de documents scientifiques de niveau recherche, publiés ou non, émanant des établissements d'enseignement et de recherche français ou étrangers, des laboratoires publics ou privés.

THÈSE DE DOCTORAT

de l'Université de recherche Paris Sciences et Lettres
PSL Research University

Préparée à l'École Normale Supérieure

Analytical methods and field theory for disordered systems

Ecole doctorale n°564

Physique en Île-de-France

Spécialité Physique Théorique

Soutenue par Thimothée THIERY
le 5 septembre 2016

Dirigée par **Pierre LE DOUSSAL**

COMPOSITION DU JURY :

M. MÜLLER Markus
PSI-Villigen, Rapporteur

M. POVOLOTSKY Alexander
BLTP-Dubna, Rapporteur

M. BIROLI Giulio
CEA-Saclay, Membre du jury

M. COMETS Francis
LPMA-Paris VII, Membre du jury

M. LE DOUSSAL Pierre
LPT-ENS, Directeur de thèse

M. ROSSO Alberto
LPTMS-Paris XI, Membre du jury

M. WIESE Kay
LPT-ENS, Co-Directeur de thèse



Contents

| | |
|---|-------------|
| Remerciements | ix |
| Introduction, goal and outline of the manuscript | xi |
| Index of notations and abbreviations | xvii |
| I Disordered elastic systems | 1 |
| I.1 The Hamiltonians | 1 |
| I.1.1 The state space | 1 |
| I.1.2 The elastic Hamiltonian | 2 |
| I.1.3 The disorder Hamiltonian | 3 |
| I.1.4 The confining Hamiltonian | 5 |
| I.2 Static phase diagram and the strong disorder regime | 6 |
| I.2.1 The pure system and the thermal fixed point | 6 |
| I.2.2 Relevance and irrelevance of short-range disorder at the thermal fixed point | 9 |
| I.2.3 Static phase diagram | 10 |
| I.2.4 Early attempts at characterizing the strong disorder regime: Flory arguments and the Larkin model | 13 |
| I.3 Various problems considered in this thesis | 15 |
| I.3.1 Shocks in the statics at zero temperature for elastic interfaces . | 15 |
| I.3.2 Avalanche dynamics at the depinning transition for elastic in- terfaces | 16 |
| I.3.3 Static problem at finite temperature for directed polymers with SR elasticity and the KPZ universality class | 19 |
| I.4 Experimental realizations | 23 |
| I.4.1 Disordered elastic systems pinned in a quenched random envi- ronment | 23 |
| I.4.2 Out-of-equilibrium interface growth | 26 |
| II Avalanches and shocks of disordered elastic interfaces | 29 |
| II.1 Introduction | 29 |
| II.2 Avalanches for a particle | 30 |
| II.2.1 Shocks between ground states for toy models of a particle with- out disorder | 30 |
| II.2.2 Avalanches in the dynamics of a particle on the real line | 32 |

| | | |
|------------|--|------------|
| II.2.3 | Shock process versus avalanche process for a particle | 38 |
| II.3 | Avalanches for an interface | 40 |
| II.3.1 | Shocks for an interface | 40 |
| II.3.2 | Avalanches for an interface | 45 |
| II.4 | FRG approach to shocks | 49 |
| II.4.1 | The functional renormalization group for the statics of disordered elastic interfaces | 49 |
| II.4.2 | Applying the functional renormalization group to shocks | 58 |
| II.5 | FRG approach to avalanches | 63 |
| II.5.1 | The functional renormalization approach to the depinning transition | 63 |
| II.5.2 | Applying the functional renormalization group to avalanches | 68 |
| II.6 | Summary of the thesis | 77 |
| II.6.1 | Introduction | 78 |
| II.6.2 | Presentation of the main results of [1] | 81 |
| II.6.3 | Presentation of the main results of [2] | 83 |
| II.6.4 | Presentation of the main results of [3] | 87 |
| II.7 | Conclusion | 92 |
| III | Exactly solvable models of directed polymer | 95 |
| III.1 | The KPZ universality class in $1 + 1d$ | 96 |
| III.1.1 | A few models in the KPZ universality class | 96 |
| III.1.2 | The KPZ fixed point - strong universality | 107 |
| III.1.3 | Universality of the KPZ equation: notion of weak universality and universal scaling limits of DP on the square lattice | 109 |
| III.2 | Exact solvability properties | 112 |
| III.2.1 | Symmetries of the continuum KPZ equation | 112 |
| III.2.2 | An analytical exact solvability property: the stationary measure | 113 |
| III.2.3 | An algebraic exact solvability property: Bethe ansatz integrability of the continuum DP | 118 |
| III.2.4 | A few words on other exact solvability properties | 126 |
| III.3 | Summary of the thesis | 127 |
| III.3.1 | Introduction | 127 |
| III.3.2 | Presentation of the main results of [4] | 129 |
| III.3.3 | Presentation of the main results of [5] | 135 |
| III.3.4 | Presentation of the main results of [6] | 143 |
| III.3.5 | Presentation of the main results of [7] | 147 |
| III.4 | Conclusion | 153 |
| | Conclusion | 155 |
| A | Paper: Spatial shape of avalanches in the BFM | 157 |
| A.1 | Introduction | 157 |
| A.2 | The Brownian force model | 158 |
| A.2.1 | Model | 158 |
| A.2.2 | Velocity Theory | 159 |

| | | |
|----------|---|------------|
| A.2.3 | Avalanche-size observables | 159 |
| A.2.4 | The ABBM model | 159 |
| A.3 | Derivation of the avalanche-size distribution in the BFM | 160 |
| A.4 | Avalanche densities and quasi-static limit | 161 |
| A.4.1 | Center of mass: ABBM | 161 |
| A.4.2 | BFM | 162 |
| A.5 | Fully-connected model | 163 |
| A.6 | Spatial shape in small systems $N = 2, 3$ | 164 |
| A.7 | Continuum limit | 166 |
| A.7.1 | Avalanche size PDF and density in the continuum limit | 166 |
| A.7.2 | Rewriting the probability measure on avalanche sizes | 166 |
| A.7.3 | The saddle point for large aspect ratio S/ℓ^4 | 167 |
| A.7.4 | Simulations: Protocol and first results | 168 |
| A.8 | Fluctuations around the saddle point | 170 |
| A.8.1 | Field theoretic analysis | 170 |
| A.8.2 | Generating a random configuration, and importance sampling | 173 |
| A.8.3 | The leading correction to the shape at large sizes | 174 |
| A.8.4 | Fluctuations of the shape for large avalanches | 174 |
| A.8.5 | Asymmetry of an avalanche | 174 |
| A.8.6 | Comparison of the perturbative corrections to the numerics | 175 |
| A.8.7 | The optimal shape beyond extreme value statistics | 176 |
| A.9 | Application to stationary driving | 176 |
| A.10 | Conclusion | 177 |
| A.11 | App A | 177 |
| A.12 | App B | 178 |
| A.13 | App C | 178 |
| A.14 | App D | 180 |
| A.15 | App E | 181 |
| A.16 | App F | 182 |
| A.17 | App G | 182 |
| A.18 | App H | 183 |
| A.19 | App I | 183 |
| B | Paper: Universality in the spatial shape of avalanches | 185 |
| B.1 | Letter | 185 |
| B.2 | Supplemental Material | 190 |
| C | Paper: Universal correlations between shocks | 205 |
| C.1 | Introduction | 205 |
| C.2 | Main results | 206 |
| C.3 | Model, shock observables and method | 208 |
| C.3.1 | Model | 208 |
| C.3.2 | The ground state and the scaling limit | 209 |
| C.3.3 | Properties of $\tilde{\Delta}^*(u)$ and static universality classes | 209 |
| C.3.4 | Shocks observables: Densities | 210 |
| C.3.5 | Shocks observables: Probabilities | 210 |

| | | |
|----------|--|------------|
| C.3.6 | Relation between avalanche-size moments and renormalized force cumulants: First moment | 211 |
| C.3.7 | Generating functions | 212 |
| C.3.8 | Relation between avalanche-size moments and renormalized force cumulants: Kolmogorov cumulants and chain rule | 212 |
| C.3.9 | Strategy of the calculation and validity of the results | 213 |
| C.3.10 | Connected versus non-connected averages and the ϵ -expansion | 214 |
| C.4 | Correlations between total shock sizes | 214 |
| C.4.1 | Reminder of the diagrammatic rules and extraction of shock mo- ments | 214 |
| C.4.2 | Lowest moments | 214 |
| C.4.3 | Generating function for all moments | 215 |
| C.4.4 | Results for the densities | 216 |
| C.4.5 | Analysis of the results | 217 |
| C.5 | Local structure of correlations | 218 |
| C.5.1 | Reminder: one-shock case | 219 |
| C.5.2 | Two-shock case: Notation and diagrammatic result | 219 |
| C.5.3 | First moments: arbitrary sources and kernels | 220 |
| C.5.4 | First moment: correlations between the local shock sizes for short-ranged elasticity. | 221 |
| C.5.5 | First moment: correlations between the local shock sizes for long- ranged elasticity. | 222 |
| C.6 | Measurement of correlations in simulations of $d = 0$ toy models. | 222 |
| C.6.1 | Models and goals | 222 |
| C.6.2 | Numerical Results: RB model | 223 |
| C.6.3 | Numerical Results: RF model | 223 |
| C.7 | Conclusion | 223 |
| C.8 | App A | 226 |
| C.9 | App B | 227 |
| C.10 | App C | 228 |
| C.10.1 | Algebraic derivation of Eq. (C.5.17) | 228 |
| C.10.2 | More explicit solution for avalanches measured on parallel hy- perplanes | 231 |
| C.11 | App D | 232 |
| D | Paper: Log-Gamma directed polymer and BA | 233 |
| D.1 | Introduction | 233 |
| D.2 | Model | 234 |
| D.2.1 | Model | 234 |
| D.2.2 | Rescaled Potential | 235 |
| D.3 | Evolution equation and Brunet Bethe ansatz | 236 |
| D.3.1 | Evolution equation | 236 |
| D.3.2 | Bethe-Brunet Ansatz | 236 |
| D.4 | Time evolution of the moments, symmetric transfer matrix | 237 |
| D.4.1 | Symmetric transfer matrix and scalar product | 237 |
| D.4.2 | Time-evolution of the moments | 237 |

| | | |
|----------|---|------------|
| D.5 | The continuum/Lieb-Liniger limit | 238 |
| D.6 | Norm of the eigenstates | 239 |
| D.7 | Large L limit | 239 |
| D.7.1 | Strings | 240 |
| D.7.2 | Eigenvalue of a string: energy | 240 |
| D.7.3 | Momentum of a string | 241 |
| D.7.4 | Phase space | 241 |
| D.7.5 | Norm of the string states | 241 |
| D.8 | Formula for the integer moments $\overline{Z^n}$ | 241 |
| D.9 | Generating function | 242 |
| D.9.1 | Generating function for the moments | 242 |
| D.9.2 | Generating function: Laplace transform | 243 |
| D.9.3 | Probability distribution | 243 |
| D.10 | Limit of very long polymers and universality | 244 |
| D.11 | Comparison with other results | 246 |
| D.12 | Conclusion | 248 |
| D.13 | App A | 249 |
| D.14 | App B | 249 |
| D.14.1 | finite L | 249 |
| D.14.2 | in the limit $L \rightarrow +\infty$ | 250 |
| D.15 | App C | 250 |
| D.16 | App D | 251 |
| D.17 | App E | 252 |
| D.18 | App F | 252 |
| D.19 | App G | 253 |
| D.20 | App H | 254 |
| D.21 | App I | 254 |
| D.22 | App J | 255 |
| D.23 | App K | 255 |
| E | Paper: On integrable DP models on the square lattice | 257 |
| E.1 | Introduction and main results | 257 |
| E.1.1 | overview | 257 |
| E.1.2 | Main results and outline of the paper | 258 |
| E.2 | DPs on \mathbb{Z}^2 : Replica method and integrability | 260 |
| E.2.1 | Definition of the model | 260 |
| E.2.2 | The replica method and the coordinate Bethe Ansatz. | 260 |
| E.2.3 | The constraint of integrability on integer moments. | 261 |
| E.3 | Integrable polymer models | 264 |
| E.3.1 | The $ q < 1$ case. | 264 |
| E.3.2 | The $q \rightarrow 1$ limit | 264 |
| E.4 | Study of the Inverse-Beta Polymer | 266 |
| E.4.1 | Moments Formula and Coordinate Bethe Ansatz | 266 |
| E.4.2 | Fredholm determinant formulas and KPZ universality | 269 |
| E.4.3 | The large length limit and the KPZ universality. | 271 |
| E.4.4 | A low temperature limit. | 273 |

| | | |
|----------|---|------------|
| E.5 | Conclusion | 275 |
| E.6 | App A | 276 |
| E.7 | App B | 277 |
| E.8 | App C | 280 |
| E.9 | App D | 281 |
| F | Paper: Beta polymer | 283 |
| F.1 | Introduction and main results | 283 |
| | F.1.1 Overview | 283 |
| | F.1.2 Main results and outline of the paper | 284 |
| F.2 | Model and earlier work | 285 |
| | F.2.1 The Beta polymer | 285 |
| | F.2.2 Relation to a random walk in a random environment | 286 |
| | F.2.3 Relation to the problem and notations of Barraquand-Corwin | 287 |
| F.3 | Bethe Ansatz solution of the Beta polymer | 287 |
| | F.3.1 Bethe ansatz on a line with periodic boundary conditions | 287 |
| | F.3.2 Resolution of the Bethe equations in the large L limit: repulsion and free particles | 288 |
| | F.3.3 Bethe ansatz toolbox | 289 |
| | F.3.4 A large contour-type moment formula | 290 |
| F.4 | Asymptotic analysis in the diffusive regime | 291 |
| | F.4.1 The issue of the first site | 291 |
| | F.4.2 Cauchy type Fredholm determinant formulas | 292 |
| | F.4.3 Asymptotic analysis of the first-moment: definition of the opti- mal direction and of the asymptotic regimes | 292 |
| | F.4.4 Asymptotic analysis in the diffusive vicinity of the optimal di- rection on the Cauchy-type Fredholm determinant | 294 |
| | F.4.5 Multi-point correlations in a diffusive vicinity of the optimal di- rection | 295 |
| F.5 | Asymptotic analysis in the large deviations regime: KPZ universality | 296 |
| | F.5.1 Recall of the results of Barraquand-Corwin | 296 |
| | F.5.2 An inherent difficulty and a puzzle | 297 |
| | F.5.3 A formal formula for the moments of the Beta polymer in terms of strings | 297 |
| | F.5.4 A formal Fredholm determinant and KPZ universality | 298 |
| | F.5.5 Crossover between Gamma and Tracy-Widom fluctuations | 299 |
| F.6 | Nested-Contour integral formulas | 300 |
| | F.6.1 Alternative moments formulas | 300 |
| | F.6.2 Mellin-Barnes type Fredholm determinant | 302 |
| F.7 | Numerical results | 302 |
| | F.7.1 In the diffusive regime. | 302 |
| | F.7.2 In the large deviations regime. | 304 |
| F.8 | Conclusion | 304 |
| F.9 | App A | 306 |
| F.10 | App B | 307 |
| F.11 | App C | 307 |

| | | |
|----------|--|------------|
| F.11.1 | Two equivalent formulas for the Strict-Weak polymer | 307 |
| F.11.2 | A formal formula for the moments of the Beta polymer. | 308 |
| F.12 | App D | 309 |
| G | Paper: Stationary measures of DPs on \mathbb{Z}^2 | 311 |
| G.1 | Introduction | 311 |
| G.2 | Recall: stationary measure of the Log-Gamma polymer | 312 |
| G.3 | Overview: definitions, main results and outline | 314 |
| G.3.1 | Definitions of the models of directed polymers | 314 |
| G.3.2 | Stationarity and reversibility properties | 318 |
| G.3.3 | Quenched free-energy in point to point models without boundaries | 319 |
| G.3.4 | Convergence of point to point models to their stationary state | 320 |
| G.3.5 | Outline and some additional results not presented here | 320 |
| G.4 | Stationary measure of the Inverse-Beta polymer | 320 |
| G.4.1 | Stationary property of the model with boundaries | 321 |
| G.4.2 | Stationarity property of the model with stationary initial condition | 321 |
| G.4.3 | Reversibility of the stationary measure: detailed balance property | 322 |
| G.4.4 | Relation to other models | 325 |
| G.5 | Stationary measure of the Bernoulli-Geometric polymer | 326 |
| G.5.1 | Stationarity properties of the Bernoulli-Geometric polymer | 326 |
| G.5.2 | Relation to other models | 327 |
| G.6 | Convergence to the stationary measure | 329 |
| G.6.1 | Free-energy in models with boundaries | 329 |
| G.6.2 | Free-energy in models without boundaries | 330 |
| G.6.3 | Convergence to the stationary measures | 333 |
| G.6.4 | A remark on optimal paths and energy fluctuations in models with boundaries | 334 |
| G.7 | Numerical results for the zero-temperature model | 336 |
| G.8 | Conclusion | 336 |
| G.9 | App A | 338 |
| G.10 | App B | 339 |
| | Bibliographie | 341 |

Remerciements

Ces trois années de thèse écoulées furent riches en rencontres et je voudrais ici remercier les personnes impliquées de près¹ dans mon expérience de thésard qui touche à sa fin.

Je voudrais tout d'abord remercier Markus Müller et Alexander Povolotsky pour avoir accepté d'être les rapporteurs de ma thèse et pour leurs nombreuses remarques qui ont permis d'améliorer ce manuscrit. Merci aussi à Giulio Biroli, Francis Comets et Alberto Rosso pour avoir accepté de compléter le jury de la soutenance.

Un grand merci à Pierre Le Doussal et Kay Wiese pour avoir accepté de diriger mon stage de M2 puis ma thèse. J'ai énormément appris à leurs cotés, beaucoup de belle physique, les techniques parfois arides permettant d'extraire la dite physique des équations, à être persévérant devant des problèmes complexes et à avoir le flair pour les attaquer du bon angle. J'étais bien loin d'être un chercheur au début de cette thèse et j'espère en être plus proche aujourd'hui grâce à eux. Le temps passant au cours de cette thèse j'ai été amené à travailler essentiellement avec Pierre que j'aimerais remercier plus particulièrement, pour l'attention soutenue qu'il a portée à mon travail; pour tout le temps passé à des discussions dans son bureau, qui m'ont souvent été immensément bénéfiques grâce à sa capacité à jauger mon niveau et à s'y adapter pour mieux l'élever; pour sa velléité à m'envoyer dans des endroits ensoleillés; pour la justesse qu'il a montrée dans sa manière de me guider à travers une belle aventure scientifique à la recherche de Tracy Widom et autres merveilles... J'espère que nous continuerons à l'avenir nos recherches communes.

Je tiens aussi à remercier Viviane Sebillé et Sandrine Patacchini pour tout le travail fourni au cours de ces trois ans, ainsi que Marc-Thierry Jaekel pour m'avoir aidé à de maintes reprises à apprivoiser les équipements informatiques du LPT. Merci aussi à mes nombreux collègues de bureau Antoine Bourget, Matthieu Delorme, Alexander Dobrinevski, Bruno Le Floch, Thomas Gueudré, Thibaud Maimbourg, Antoine Tilloy, Romain Vasseur et Éric Vernier, pour la convivialité constante au cours de ces années de pérégrinations dans un laboratoire au décor parfois post-apocalyptique. Je voudrais remercier plus particulièrement mes illustres prédécesseurs Alexander et Thomas pour m'avoir guidé avec beaucoup de gentillesse au début de ma thèse et pendant le stage de M2 dans les méandres des avalanches, FRG, polymère dirigé et ansatz de Bethe. Leur impact positif sur mon travail et ma compréhension de ces sujets à ces stades précoces de ma thèse a été énorme. Outre les apports scientifiques je les remercie également évidemment pour leur amitié qui m'a été précieuse durant ces années. Je remercie

¹Désolé pour ceux que j'oublie!

également mes collègues thésards et post-docs de l'ens par delà mon bureau Jacopo De Nardis et Andrea De Luca, ainsi que Jean Barbier, Ralph Bourdoukan, Alice Coucke, Christophe Gardella et Alaa Saade, pour tous les moments partagés autour de gros dwichs, fat flans, d'eau municipale et de ramens.

Je voudrais également remercier toutes les personnes avec qui j'ai partagé des moments sympas pendant ces nombreuses vacances écoles d'été et conférences, je pense notamment à Nicolas Posé et Mathias Van Regemortel pour ces durs moments de dolce vita à Trieste; Grégory Schehr et l'équipe des Houches: Nicola Allegra, Charlie Duclut, Tony Prat et Malo Tarpin; ainsi qu'Élizabeth Agoristas et Vivien Lecomte, notamment pour le marathon gastronomique qui nous a permis de mieux accepter le rythme harassant de la vie en Californie.

Je remercie également mes professeurs de sciences du lycée qui ont su éveiller en moi un intérêt pour les sciences pourtant au début très profondément enfoui, en particulier Mme Capron qui a été le principal artisan de cet éveil, mais aussi Mr Morand et les autres, ainsi que Mme Biolet et Mme Guest dont les cours en prépa m'ont permis d'en arriver là.

Finalement je tiens à profiter de ce premier espace formel de remerciements qui m'est offert pour redire mon affection aux personnes qui me sont chères. Merci ainsi à tous mes amis parisiens et tourangeaux pour toutes ces années. Merci à ma famille. Merci Suzanne.

Introduction, goal and outline of the manuscript

The theoretical analysis of disordered systems is an outstanding challenge of modern statistical physics and probability theory that finds applications in (disorder is present in any experimental setup and *might* play a crucial role) and outside of physics (e.g. error-correcting codes and optimization problems). In such systems the interplay between thermal (and/or quantum) fluctuations, the disordered environment and interactions often creates a rich ‘glassy’ phenomenology. In this thesis we focus on d -dimensional elastic interfaces in a $(d + 1)$ -dimensional disordered media, described by a single valued function $u : x \in \mathbb{R}^d \rightarrow u(x) \in \mathbb{R}$ (the height of the interface). The latter are remarkable examples of disordered systems. On one hand they can be used to describe a variety of physical situations such as domain walls in disordered magnets, fractures fronts in brittle materials, contact lines of viscous fluids on rough substrates... On the other hand they are sufficiently simple to allow analytical approaches and tremendous theoretical progress. For such systems, while the elasticity tends to flatten the interface, thermal fluctuations and the disordered environment tend to roughen it. The energy landscape of the interface is fractioned into a multitude of metastable states which in some cases dramatically influence the static and dynamic properties of the interface.

Shocks and Avalanches

In the case of the statics, one can show that in ‘small’ dimensions ($d \leq 4$ for interfaces with short-range elasticity), the temperature is irrelevant at large scale and the large scale properties of the interface are those of its ground state: the system is *pinned* by disorder (there are subtleties linked with the fact that the temperature is dangerously irrelevant). At least in some cases, this pinning phenomena is collective and one expects some *universality* and *scale invariance* to emerge: large scale properties of the interface are, up to some non universal constants, independent of the underlying disorder distribution (although there are several *universality classes* that one would like to classify). In particular the interface is *rough* and its static *roughness exponent*, ζ_s loosely defined by $u(x) - u(0) \sim x^{\zeta_s}$ is universal. As we will review this problem has been already well studied and a good understanding of these universal properties has been reached. A more recent question is to understand the properties of several successive metastable states of the interface. Confining the interface around some position w and studying the evolution of the ground state of the interface as w is varied,

the ground state changes abruptly at a discrete sequence of positions w_i . These changes in the ground state $u(x) \rightarrow u(x) + S(x)$ define a sequence of *shocks* $S(x)$. As both $u(x)$ and $u(x) + S(x)$ are legitimate ground states of the interface displaying scaling and universality, one expects the shocks $S(x)$ to display scaling and universality inherited from the universal physics of disordered elastic interfaces.

A closely related phenomenon occurs in the zero temperature dynamics of the interface of sufficiently low dimensions when it is slowly driven with a mean velocity $\partial_t u(t, x) \sim v \rightarrow 0^+$ (at the ‘*depinning transition*’). The system reaches an out-of-equilibrium steady-state displaying scaling and universality with a depinning roughness exponent $u(t, x) - u(t, 0) \sim x^{\zeta_d}$ that differs from the static one. In the steady-state, most of the time the interface is actually pinned by disorder in a metastable state, $\partial_t u(t, x) \sim 0$, and very rarely manages to cross an energy barrier. When it does the interface moves with a macroscopic velocity of order $O(1)$ during a finite time window $\Delta t = O(1)$ until it is pinned again in a new metastable state. The next jump occurs after a period of quiescence $T \sim 1/v \gg \Delta t$. The motion of the interface in between these metastable states is called an *avalanche*. The latter are very close cousins of the shocks between static ground states mentioned above, but are richer as they are a complex time-dependent phenomena for which more questions can be asked. Again these avalanches inherit the scale invariance and the universality of disordered elastic interfaces at the depinning transition.

More generally avalanches occur in a wide range of complex systems, from snow avalanches to avalanches in the neural activity of the brain. While avalanches in some systems will fall in the universality class of the disordered elastic interface model, other may not. Important counter examples are e.g. avalanches at the yielding transition of amorphous materials (for which plastic deformations play an important role) or earthquakes (for which the presence of aftershocks, whose origin is still controversial, is certainly not captured by the simplest elastic interface model). In any case, characterizing and understanding the universality in avalanche processes, and in particular for the elastic interface model for which powerful analytical methods exist, is an important challenge. It indeed allows to understand and compare efficiently seemingly unrelated phenomena such as the fracture process of a brittle material or the jerky motion of a contact line between a viscous fluid and a rough substrate, and to assess the importance of various mechanisms in the dynamics. Important questions in the context of shocks and avalanches are the characterization of the distribution of the avalanche total size S (the area swept by the interface), the duration T ... As the avalanche processes mentioned above (at least for the elastic interface case) are scale-invariant processes, the latter are distributed with probability distribution functions (PDF) displaying (in a certain regime) a power-law behavior $P(S) \sim S^{-\tau_S}$, $P(T) \sim T^{-\tau_T}$. The critical exponents thereby defined are believed to be universal and related to the critical exponents of the depinning transition (for avalanches) or of the statics (for shocks). Scaling and universality is however not restricted to critical exponents and there exist *universal scaling functions*, allowing a refined characterization of universality classes. A perfect example of such universal scaling functions is the temporal shape of avalanches, which received much attention lately and was computed at and beyond mean-field. Going back to experiments, while on one hand the study of the temporal shape indeed showed

universality between different avalanche processes, on the other hand it permitted to highlight the (non-universal) influence of Eddy currents for avalanches in Barkhausen noise experiments.

Out-of-equilibrium growth and the KPZ universality class

Another, seemingly unrelated phenomenon, is the out-of-equilibrium growth of an elastic interface $h(t, x) \in \mathbb{R}$ driven by thermal fluctuations in the absence of quenched noise, typically thought of as separating a stable and an unstable phase of a thermodynamic system. The interface is rough $h(t, x) - h(t, 0) \sim x^\alpha$ and exhibits non-trivial fluctuations and spatio-temporal patterns. For one dimensional interface $x \in \mathbb{R}$ and local growth mechanisms with other reasonable assumptions, it is believed that a single universality class, the Kardar-Parisi-Zhang (KPZ) universality class, controls the large scale properties of growing interfaces. Remarkably, there is a very close connection with the statics of disordered elastic interfaces: the fluctuations of the free-energy $F(L, u)$ of a directed polymer ($d = 1$ elastic interface case) of length L at the temperature T in a short-range random potential with end-points fixed as $u(0) = 0$, $u(L) = u$, defines a growing interface $h(t, x) := F(L = t, u = x)$ in the KPZ universality class. The KPZ universality class also encompasses models of interacting particles in one-dimension and has emerged over the years as a paradigmatic example of universality in out-of-equilibrium statistical physics. In this case the critical exponents are known exactly: the roughness exponent is $\alpha = 1/2$ and the height of the interface fluctuates widely on a scale of order $t^{1/3}$ (where here t refers to the duration since the beginning of the growth).

As for avalanches, universality goes however well beyond the sole critical exponents and the full distribution of the (rescaled) fluctuations of the interface are universal and, interestingly, depend only on global properties of the initial condition of the growing interface. As an example, for an interface growing from a flat initial condition, the fluctuations of the interface at a given point are distributed with the Tracy-Widom distribution for the largest eigenvalue of a random matrix in the Gaussian orthogonal ensemble, thus unveiling a remarkable connection between random matrix theory and the KPZ universality class. Observed in modern experiments, the emergence of such universal distributions related to extreme value statistics of random matrix theory is understood at the theoretical level through the analysis of *exactly solvable models* in the KPZ universality class, in particular models of directed polymers. While this property still lacks a ‘simple’ explanation, the wide range of application of KPZ universality, of KPZ scaling and of the Tracy-Widom distribution, has the flavor of an extension of the central limit theorem to strongly correlated random variables. This has motivated in the past years a vast research effort aiming at the understanding of the KPZ fixed point, which thus still relies on the use of exactly solvable models.

Analytical methods and the results obtained during the thesis

While in a general setting I have tried throughout the thesis to improve the understanding and characterization of universal properties for models of disordered elastic interfaces in their strong disorder regime, my work can be divided following the subjects

mentioned above.

On avalanches

On one hand I have been interested in shocks and avalanche statistics for disordered elastic interfaces. To this aim I have used the functional renormalization group (FRG), a method already well developed. As any renormalization procedure, the latter directly aims at characterizing the large scale properties of the system through the identification of the appropriate fixed point. As I will review, the fixed points are perturbative in $\epsilon = 4 - d$ (for interfaces with short-range elasticity) and I have obtained results for avalanche statistics using this expansion at one-loop order, i.e. at first order beyond mean-field, i.e. at order $O(\epsilon)$.

I have first focused on the spatial shape of avalanches. While on one hand the temporal shape of avalanches received a lot of attention, the spatial shape did not, surely because of the involved technical difficulties and the absence of an analytically tractable (and experimentally relevant) precise definition, in particular a centering procedure. I first obtained results at the mean-field level for the shape of peaked avalanches for model with short-range elasticity in $d = 1$: there the shape becomes deterministic and given by a well defined spatial profile [1]. Secondly, I focused on the mean shape of avalanches of fixed size centered on their seed for which I obtained results beyond mean-field, valid at order $O(\epsilon)$ [2]. This ‘seed-centering’ procedure introduced in this work appears as the most natural way, at least from the analytical point of view, to center spatial observables in the avalanche motion, and it could be used for other observables. In [2] I perform simulations that show that the seed-centering can be successfully implemented in numerics, and in the future it would be interesting to confront these results with experiments for which the spatial shape is an accessible quantity, as is the case in some fractures experiments.

In another project I investigated the correlations between successive avalanches and shocks. In general the question of correlations in avalanche processes has received a lot of attention, in particular in the context of earthquakes where these are linked to the notion of aftershocks, but in the elastic interface model they were always neglected and their sole existence was not put forward in the previous literature. While there are no correlations at the mean-field level where the avalanche process is a Lévy jump process [1], beyond mean-field I showed that there are always correlations. Furthermore these correlations are universal, of order $O(\epsilon)$, and controlled by the structure of the FRG fixed point [3]. While these correlations do not correspond to the correlations observed in e.g. earthquake statistics, similar correlations probably exist in any system and understanding them is likely to be necessary to obtain a quantitative understanding of the correlations. In other systems well described by the elastic interface model, this work shows that in most cases (for interfaces of dimension below the upper critical dimension), there exist important correlations in the sequence of avalanches. Comparing these results with experiments would be very interesting.

On directed polymers

On the other hand I have been interested in understanding the emergence of KPZ universality, or lack of thereof, in models of directed polymer on the square lattice. To this aim I have studied and discovered models with exact solvability properties, extending the already known exact solvability properties of the continuum directed

polymer, the Bethe ansatz solvability and the exactly known stationary measure. In particular I have obtained: (i) Tracy-Widom GUE fluctuations for the point to point free-energy of the Log-Gamma polymer [4]; (ii) Tracy-Widom GUE fluctuations for the point to point free-energy of the Inverse-Beta polymer (a model I discovered during the thesis) and a classification of finite temperature Bethe ansatz exactly solvable models of directed polymer on the square lattice [5]; (iii) Tracy-Widom fluctuations for the large deviation function of a random walk on \mathbb{Z} in a time-dependent Beta distributed random environment, equivalent to the point to point free energy of the Beta polymer, and Gamma fluctuations in the diffusive regime of the random walk (suggesting a local breaking of KPZ universality due to an additional conservation law for the Beta polymer) [6]; (iv) the stationary measures and mean quenched free-energy/optimal energy in the Inverse-Beta polymer and in the Bernoulli-Geometric polymer, an exactly solvable model of directed polymer on the square lattice at zero temperature dual to the Inverse-Beta polymer which I also discovered during the thesis [7].

This ‘world’ of exactly solvable models of directed polymer on the square lattice, in part unveiled by this thesis, now offers a set of models with different properties allowing to ask precise question about the KPZ fixed point and directed polymers in general. The Bethe ansatz approach to finite temperature models of directed polymer on the square lattice, developed in this thesis and at the same time by others, provides a new versatile tool which hopefully will permit to obtain a variety of interesting results for these models.

Goal and outline of the manuscript

The goal of this manuscript is to provide a self-contained and pedagogical review of the subjects mentioned above, with an emphasis on theoretical techniques and aspects important to the understanding of the research papers [1, 2, 3, 4, 5, 6, 7] written during the thesis and regrouped in Appendices A-G, whose main results will also be presented in the core of the manuscript.

In Chapter I I provide a broad introduction to disordered elastic systems, which will serve as a background for the understanding of the two main subjects studied during the thesis and presented thoroughly in the next chapters. In particular I re-obtain the static phase diagram of these systems, discuss the notion of strong disorder and the associated phenomenology, review early theoretical approaches and their caveats to motivate the use of the more sophisticated methods already mentioned, give a brief introduction to the more specialized subjects studied during the thesis and discuss some experimental evidences.

In Chapter II I focus on the avalanche processes of disordered elastic interfaces in the statics and in the dynamics (at the depinning transition) at zero temperature. I first introduce the notion of shocks and avalanches in $d = 0$ toy models, and then generalize it to interfaces. I review the functional renormalization group approach to the statics and dynamics (at the depinning transition) of disordered elastic interfaces at zero temperature, with an emphasis on its applications to the computation of shocks and avalanches observables. I discuss the recent progresses made on the understanding of avalanche processes to motivate the main subjects studied during the thesis, the

spatial structure of avalanches and the correlations in avalanche processes. The results obtained in the research papers [1, 2, 3], regrouped in Appendix A-C, are presented in the end of the chapter.

In Chapter III I focus on the problem of the statics of a directed polymer at finite temperature in a random potential in dimension $1 + 1$. I recall the connection of this problem with the out-of-equilibrium growth of an interface in the KPZ universality class. I give an introduction to the KPZ universality class and review some recent remarkable progresses that were made (through the study of peculiar exactly solvable models) in the understanding of the KPZ universality class in $1 + 1$ d. In particular I will present some known exact solvability properties of the continuum directed polymer -symmetries, stationary measure, Bethe ansatz solvability- that I tried in this thesis to generalize in discrete settings. I will then present the results obtained in the research papers [4, 5, 6, 7], regrouped in Appendix D-G.

Index of notations and abbreviations

- use of subscripts: in this thesis the value at x of an arbitrary function $f : x \in U \rightarrow f(x) \in V$ will often be denoted using a subscript: $f_x \equiv f(x)$. To avoid confusions, we will NEVER use subscripts to denote derivatives.

For $x \in \mathbb{R}^d$, $\int_x \equiv \int_{x \in \mathbb{R}^d} d^d x$

For $q \in \mathbb{R}^d$, $\int_q \equiv \int_{q \in \mathbb{R}^d} \frac{d^d q}{(2\pi)^d}$

$\hat{\delta}^{(d)}(q) = (2\pi)^d \delta^{(d)}(q)$ where $\delta^{(d)}(q)$ is the usual Dirac delta distribution in d dimension.

The Fourier transform of a function f_x is denoted $f_q = \int_x e^{-iq \cdot x} f_x$. Thus $f_x = \int_q e^{iq \cdot x} f_q$.

$\overline{(\)}$ is the average over disorder.

\sim denotes the equality in law between random variables

$\theta(x)$ is the Heaviside theta function

$\Gamma(x)$ is Euler's Gamma function

$$A_d^\gamma = \frac{(2\sqrt{\pi})^d}{2} \frac{\Gamma(\gamma)}{\Gamma(\gamma+1-d/2)}$$

$$C_n^m = \frac{n!}{m!(n-m)!}$$

$$(a)_n = \prod_{k=0}^{n-1} (a+k)$$

-
- ABBM: Allesandro-Beatrice-Bertotti-Montorsi
 - BA: Bethe ansatz
 - BFM: Brownian-Force-Model
 - BW: Boltzmann Weight
 - CDF: Cumulative Probability Distribution
 - DES: Disordered Elastic System
 - DP: Directed-Polymer
 - DR: Dimensional Reduction
 - FP: Fixed Point
 - FPP: First Passage Percolation
 - FRG: Functional Renormalization Group
 - GOE/GUE/GSE: Gaussian Orthogonal/Unitary/Symplectic Ensemble of Random Matrix Theory.
 - gRSK: geometric/tropical RSK
 - GWN: Gaussian white noise

IR: Infra-Red
KPZ: Kardar-Parisi-Zhang
KPZUC: KPZ universality class in $1 + 1d$
LL: Lieb-Liniger
LPP: Last Passage Percolation
LR: Long-Range
LT: Laplace Transform
MSHE: Multiplicative Stochastic-Heat-Equation
NF: Narayan-Fisher
PDF: Probability Distribution Function
RB: Random Bond
RF: Random Field
RG: Renormalization Group
RMT : Random Matrix Theory
RSK: Robinson-Schensted-Knuth
RV: Random Variable
RW: Random Walk
RWRE: Random Walk in a Random Environment
SHE: Stochastic-Heat-Equation
SR: short-range
TD-RWRE: Random Walk in a Time-Dependent Random Environment
TFP: Thermal Fixed Point
TW: Tracy-Widom
UV: Ultra-Violet
ZRP: Zero-Range-Process

Chapter I

Disordered elastic systems

The focus of this thesis is on disordered elastic systems (DES) and the goal of this section is to discuss some general properties of the latter that will underline all the manuscript. We will start by very general theoretical considerations on DES that are introduced in Sec. I.1, discuss the relevance of the disorder and draw the well-known static phase diagram in Sec. I.2. In Sec. I.3 we briefly introduce the more specialized topics that are the focus of Chapter II and III. Finally in Sec. I.4 we discuss some experimental systems for which a theoretical approach using DES has been proposed. An alternative way to read this chapter is to start by the experimental observations of Sec. I.4. Here we have decided to first present the theoretical objects we will study in order to already try to be precise on the specific model with which one can attempt to understand a given experimental situation. The content of I.1 and I.2 is now standard and similar presentations can be found in [8, 9, 10]

I.1 The Hamiltonians

Although in this thesis we will also consider discrete systems, let us here focus on continuous systems introduce a general Hamiltonian for a DES of *internal dimension* $d \in \mathbb{N}^*$ and *external dimension* $N \in \mathbb{N}^*$. Let us first discuss the state space,

I.1.1 The state space

A state of the system is a real function

$$u : x \in \mathbb{R}^d \rightarrow u(x) \equiv u_x \in \mathbb{R}^N . \quad (\text{I.1.1})$$

Where here we have introduced the subscript notation to indicate the dependence on the position in the internal space. The latter will be heavily used in the following. The space \mathbb{R}^d will be referred to as the *internal space*, whereas \mathbb{R}^N will be referred to as the *external space*. A state of the system can be embedded in the *total space* of dimension $d + N$ as the set of points $(x, u_x) \in \mathbb{R}^{d+N}$. The case of *elastic interfaces* refers to the $N = 1$ case. Indeed in this case the DES can be thought of as separating two phases of a thermodynamic system living in the total space. The case of *directed polymers* on the other hand refers to the $d = 1$ case. Note that we already made a restricting hypothesis

that will hold for all theoretical analysis present in this manuscript since more general DES not described by a single-valued function (I.1.1) could be considered. For the case of interfaces this is the hypothesis that there are no *overhangs*, while for the directed polymer case, this is precisely the hypothesis from which the word directed comes. More generally a point of the DES can thus be labeled by its internal coordinate x and can only move in the external space.

In all the manuscript, whenever such a continuum description is used, we will assume the existence of two length-scales in the internal space: (i) a small-size cutoff a below which the elastic and continuum description of the system breaks down; (ii) a large scale cutoff L which represents the lateral extension of the system (the system is thus finite). Boundary conditions will be discussed later. Let us already say here that all the results obtained in this thesis actually concern the case of elastic *interfaces*, that is the special case $N = 1$. The Hamiltonian of the system will be generally the sum of three contributions

$$\mathcal{H}_{V,w}[u] := \mathcal{H}^{\text{el}}[u] + \mathcal{H}_V^{\text{dis}}[u] + \mathcal{H}_w^{\text{conf}}[u]. \quad (\text{I.1.2})$$

As we detail below, $\mathcal{H}^{\text{el}}[u]$ is the *elastic Hamiltonian* of the system, $\mathcal{H}_V^{\text{dis}}[u]$ is the *disorder Hamiltonian* (that depends on the realization of a random potential V) and $\mathcal{H}_w^{\text{conf}}[u]$ is a *confining Hamiltonian* that confines the system around an average position w . Here $\mathcal{H}^{\text{el}}[u]$ and $\mathcal{H}_V^{\text{dis}}[u]$ are the main players but the presence of a confining Hamiltonian will be important to define various quantities and to study avalanches. In this section we will keep N arbitrary, mainly to emphasize the influence of the external dimension on the importance of the disorder on large scale properties. Let us now be more precise and define/give examples for each term that appears in (I.1.2).

I.1.2 The elastic Hamiltonian

Our typical choice for the elastic Hamiltonian will be the case of *short-range elasticity* that is modeled by the Hamiltonian

$$\mathcal{H}_{\text{SR}}^{\text{el}}[u] := \frac{c}{2} \int_x (\nabla_x u_x)^2, \quad (\text{I.1.3})$$

where $c \geq 0$ is a constant. By rescaling the x axis we will assume $c = 1$. We will also sometimes consider other types of elasticity. In the most general case the elastic Hamiltonian will be defined by,

$$\mathcal{H}_g^{\text{el}}[u] := \frac{1}{2} \int_{x,y} g_{x,y}^{-1} u_x \cdot u_y, \quad (\text{I.1.4})$$

where we introduced the *elasticity kernel* $g_{x,y}^{-1}$. We will suppose that the elasticity kernel is rotationally and translationally invariant (in internal space) $g_{x,y}^{-1} = g_{|x-y|}^{-1}$ and to be such that $\mathcal{H}^{\text{el}}[u]$ defined above is a convex functional that attains its minimum for *flat* systems: $\mathcal{H}^{\text{el}}[cst] = 0$. We also suppose translational and rotational invariance in external space: $\mathcal{H}^{\text{el}}[u + cst] = \mathcal{H}^{\text{el}}[u]$. Note that the ground state of the elastic

Hamiltonian is thus degenerate. Introducing the Fourier-transform of the elasticity kernel, $g_q^{-1} = \int_x e^{-iqx} g_{x,y}^{-1}$, the elastic Hamiltonian can be rewritten as

$$\mathcal{H}_g^{\text{el}}[u] = \frac{1}{2} \int_q g_q^{-1} u_{-q} \cdot u_q . \quad (\text{I.1.5})$$

And the case of short-range (SR) elasticity thus corresponds to the choice $g_q^{-1} = \sigma q^2$. In this introduction we will consider elastic kernels of the form $g_q^{-1} = |q|^\gamma$ and the important examples will be $\gamma = 2$ (SR elasticity) and $\gamma = 1$. The latter is known to be relevant in describing some systems with long-range (LR) elasticity as will be recalled in Sec. I.4.

I.1.3 The disorder Hamiltonian

The disorder Hamiltonians will be taken as the integral of a disorder potential $V : (x, u) \in \mathbb{R}^d \times \mathbb{R}^N \rightarrow V(x, u) \in \mathbb{R}$:

$$\mathcal{H}_V^{\text{dis}}[u] := \int_x V(x, u_x) . \quad (\text{I.1.6})$$

Here $\{V(x, u)\}$ is a collection of random variables (RVs) that is drawn from a known probability distribution function (PDF). In Chapter III we will define precisely the PDF of $\{V(x, u)\}$, as we will restrict our analysis to some specific distributions allowing exact treatments. We will however have in mind that some large scale properties should be *universal*, where here by universal we mean independent of the distribution of V apart from some precise properties. In Chapter II on the other hand we will almost never specify the PDF of $\{V(x, u)\}$ as we will directly use methods that will make clear the universal character of our conclusions. Here let us only define the global properties of the PDF of $\{V(x, u)\}$ for which our results will hold.

We will restrict our analysis to the case where the distribution of $V(x, u)$ at one point has no fat tails: all the positive moments $\overline{V(x, u)^n}$ (where from now on the overline $\overline{(\)}$ denotes the average over the random environment, i.e. over the distribution of $\{V(x, u)\}$) are finite for $n \geq 0$: $\overline{V(x, u)^n} < +\infty$ (e.g. a Gaussian distributed disorder). We will suppose that $V(x, u)$ is homogeneously distributed. The symmetry in law $V(x + \Delta x, u + \Delta u) \sim V(x, u)$ (where here and throughout this manuscript \sim means ‘distributed in law as’) will sometimes be referred to as the *statistical translational invariance of the disorder*. Concerning the *correlations* in the set of RVs $\{V(x, u)\}$, the two most important cases that we will consider, motivated by physical applications, are (i) disorder of the *random bond* type for which the correlations of the potential $V(x, u)$ are *short range* (SR); (ii) disorder of the *random field* type for which it is the *force* $F(x, u) := -\nabla_u V(x, u)$ acting on the system which has SR correlations. More precisely we will suppose

$$\begin{aligned} \overline{V(x, u)V(x', u')^c} &= \delta^{(d)}(x - x') R_0(u - u') , \\ \overline{F(x, u)F(x', u')^c} &= \delta^{(d)}(x - x') \Delta_0(u - u') , \end{aligned} \quad (\text{I.1.7})$$

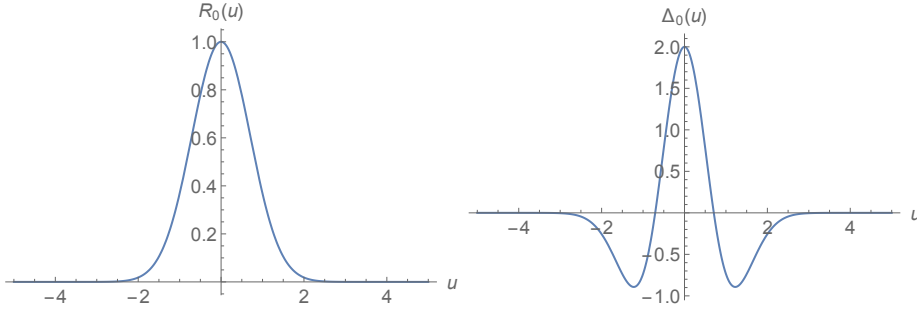


Figure I.1: Typical shape of the second cumulant of the disorder potential and of the disorder force for disorder of the random bond type with $N = 1$ and correlation length $u_c \sim 2$.

where $\Delta_0(u) = -\nabla_u^2 R_0(u)$. Both are radial functions (i.e. even functions for $N = 1$). In the random bond (RB) case $R_0(u)$ is decaying faster than any-power law at large u , i.e. typically as $R_0(u) \sim e^{-|u|/u_c}$ where u_c is the *correlation length of the disorder*. The typical shape we have in mind for this case is shown in Fig. I.1, $R_0(u)$ is positive while $\Delta_0(u)$ is positive at small $|u|$ and negative at large $|u|$. If $R_0(u)$ is flat at 0 and at infinity, we have $\int_u |u|^{d-1} \Delta_0(u) = 0$. The case of 0 correlation length $u_c = 0$ corresponds to $R_0(u) = \delta^{(N)}(u)$. In the random field (RF) case, $\Delta_0(u)$ has the same properties as $R_0(u)$ in the RB case with a correlation length u_c . In this case $R_0(u) \sim_{|u| \rightarrow \infty} -\sigma|u|$, see Fig. I.2. Finally we will also sometimes briefly consider periodic disorder: in this case $V_0(x, u + \Delta u) = V_0(x, u)$ where Δu is the period (this case is relevant e.g. in the context of charge density waves [11]).

Remark: The distinction between the internal and external space in the form of the correlations (I.1.7) might seem strange. The reason for this is that in our renormalization procedure, in Chapter II, we will try to describe the *effective disorder felt at large scale* by the interface. In doing so we will see that, e.g. starting from a RB disorder with 0 correlation length $R_0(u) = \delta^{(N)}(u)$ the effective disorder at large scale will acquire a finite correlation length in the u space. Conversely, starting with a non-

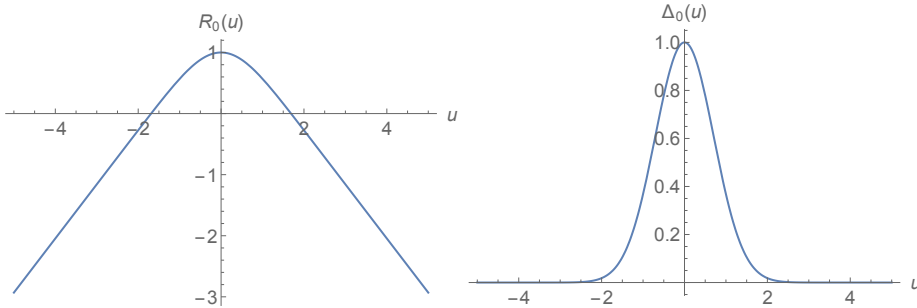


Figure I.2: Typical shape of the second cumulant of the disorder potential and of the disorder force for disorder of the random field type with $N = 1$ and correlation length $u_c \sim 2$.

zero correlation length in the internal space, the effective disorder at large scale will have a (decreasing to) 0 correlation length in the internal space. For this reason we will already start our renormalization procedure with disorder having the same type of correlations than the effective disorder at large scale. Long-range correlations in internal space can break this picture and we will not study them, see e.g. [12].

I.1.4 The confining Hamiltonian

Most of the questions one can ask about a disordered elastic system with Hamiltonian defined as in (I.1.2) would be ill-defined without a confining term $\mathcal{H}_w^{\text{conf}}[u]$ that confines the system around an average position $w \in \mathbb{R}^N$. For example, due to the translational invariance in external space of $\mathcal{H}^{\text{el}}[u]$, the ground state of the Hamiltonian $\mathcal{H}^{\text{el}}[u] + \mathcal{H}_V^{\text{dis}}[u]$ for a ‘typical realization of a typical’ disorder in an infinite space would be at infinity. There are various ways of regularizing the problem and in this thesis we will consider two possibilities.

In Chapter II we will confine the system around an average position $w \in \mathbb{R}^N$ using a parabolic well as, for the case of a system with SR elasticity,

$$\mathcal{H}_w^{\text{conf}}[u] := \frac{m^2}{2} \int_x (u_x - w)^2, \quad (\text{I.1.8})$$

and the parameter $m > 0$, which is the stiffness of the well, will be called the mass. In this case we have

$$\mathcal{H}_{\text{SR}}^{\text{el}}[u] + \mathcal{H}_w^{\text{conf}}[u] = \frac{1}{2} \int_q (q^2 + m^2)(u_{-q} - w_{-q}) \cdot (u_q - w_q). \quad (\text{I.1.9})$$

Here we have noted $w_q = w \hat{\delta}^{(d)}(q)$. More generally for other types of elasticity we will consider confinement such that

$$\mathcal{H}_g^{\text{el}}[u] + \mathcal{H}_w^{\text{conf}}[u] = \frac{1}{2} \int_q \tilde{g}_q^{-1} (u_{-q} - w_{-q}) \cdot (u_q - w_q) \quad (\text{I.1.10})$$

with

$$\tilde{g}_q^{-1} = (\mu^2 + q^2)^{\frac{\gamma}{2}} \quad (\text{I.1.11})$$

and in these cases we will denote the mass as

$$m = \sqrt{\tilde{g}_{q=0}^{-1}} = \mu^{\frac{\gamma}{2}}. \quad (\text{I.1.12})$$

Conversely we will note $\tilde{g}_{x,y}^{-1} = \int_q e^{iq \cdot (x-y)} \tilde{g}_q^{-1}$. In the remainder of the manuscript we will actually drop the tilde and except otherwise stated, the ‘elastic kernel’ g_q^{-1} will thus also contain the confining term as in (I.1.10). Note that the confining Hamiltonian introduces a length-scale $\ell_\mu := 1/\mu$ above which different parts of the interface are essentially elastically independent. Being interested in the regime where elasticity and disorder compete on equal footing, we will be interested in length-scales $|x - x'| \ll \ell_\mu$. We will thus consider the small μ limit. Taking also into account the scales a and L

discussed earlier we will be interested in the regime $a \ll |x - x'| \ll \ell_\mu \ll L$. As such, boundary conditions will not play a role in this case and we will not discuss them. As we will recall below in Chapter II, adding such a confining term permits a convenient renormalization group approach to disordered elastic interfaces (the case $N = 1$). There ℓ_μ plays the role of an infra-red cutoff that smoothly cuts off fluctuations of the system at large length and $-\log \mu$ will play the role of time for the renormalization group flow. More precisely we will be interested in understanding the properties of the system as w is varied. In particular, under some conditions that will be discussed, we will see that as w is varied, the ground state of the interface changes discontinuously as a function of w . These abrupt changes define the notion of *shocks* or *static-avalanches*. Understanding universal properties of avalanche processes is one of the main goals of this thesis. In Chapter II the confining term (I.1.8) will thus play a major role as moving w will allow us to probe a certain sequence of metastable states of the interface.

In Chapter III on the other hand we will consider the case of a *directed polymer in a two dimensional random medium*, that is the case $d = N = 1$. There we will mostly consider the so-called point-to-point problem and suppose that both ends of the polymer at $x = 0$ and $x = L$ are fixed as $u_0 = 0$ and $u_L = w$. This can be implemented by a confining Hamiltonian $\mathcal{H}_w^{\text{conf}}[u] = -E \left(\delta^{(N)}(u_0) + \delta^{(N)}(u_L - w) \right)$ with $E \rightarrow \infty$. There the focus will be on lattice models and on determining statistical properties of the DP at a finite temperature using exact methods. We will obtain finite L results but we will mostly be interested in understanding some bulk properties for $L \rightarrow \infty$ which are believed to be universal. One of the reasons why we will use in this chapter a different confining Hamiltonian compared to Chapter II is that (I.1.8) does not permit an exact solution.

1.2 Static phase diagram and the strong disorder regime

In this section we consider the statistical mechanics of a disordered elastic system described by an Hamiltonian of the form (I.1.2) at a finite temperature T and confined around $w = 0$ as in (I.1.10). The goal of this section is to discuss qualitatively the relevance at large scale of the disorder and of the temperature and to draw the well known equilibrium phase diagram of DES. We will start by discussing the case of the pure system $V = 0$ and describe the *thermal fixed point*.

1.2.1 The pure system and the thermal fixed point

We thus consider an elastic system $u : x \in \mathbb{R}^d \rightarrow \mathbb{R}^N$ described by the Hamiltonian, written in Fourier space,

$$\mathcal{H}_{\text{pure}}[u] = \frac{1}{2} \int_q (q^2 + \mu^2)^{\frac{\gamma}{2}} u_{-q} \cdot u_q . \quad (\text{I.2.1})$$

At a given temperature T , the thermal average of an observable O of the u field is defined by the path-integral

$$\langle O[u] \rangle := \frac{1}{Z[T]} \int \mathcal{D}[u] O[u] e^{-\frac{1}{T} \mathcal{H}_{\text{pure}}[u]} \quad , \quad Z[T] = \int \mathcal{D}[u] e^{-\frac{1}{T} \mathcal{H}_{\text{pure}}[u]} . \quad (\text{I.2.2})$$

The Hamiltonian (I.2.1) is quadratic and the theory is Gaussian: arbitrary integer moments of u_x can be computed exactly using Wick's theorem. In particular the two-point function is obtained as

$$\begin{aligned}\langle u_q \cdot u_{q'} \rangle &= \hat{\delta}(q + q') \frac{T}{(q^2 + \mu^2)^{\frac{\gamma}{2}}} \\ \langle u_x \cdot u_{x'} \rangle &= T \int_q \frac{e^{iq \cdot (x-x')}}{(q^2 + \mu^2)^{\frac{\gamma}{2}}}\end{aligned}\tag{I.2.3}$$

Hence we have

$$\begin{aligned}\langle (u_x - u_{x'})^2 \rangle &= 2T \int_q \frac{1 - e^{iq \cdot (x-x')}}{(q^2 + \mu^2)^{\frac{\gamma}{2}}} \\ &= 2T |x - x'|^{2\zeta_{\text{Th}}} F_d \left(\frac{|x - x'|}{\ell_\mu} \right)\end{aligned}\tag{I.2.4}$$

where we have introduced the *thermal roughness exponent*

$$\zeta_{\text{Th}} := \frac{\gamma - d}{2}, \tag{I.2.5}$$

as well as the scaling function $F_d(y) = \int_q \frac{1 - \cos(q_1)}{(q^2 + y^2)^{\frac{\gamma}{2}}}$ where q_1 is the first coordinate of the d -dimensional vector q and we recall $\ell_\mu = 1/\mu$. At large distance $F_d(y)$ decays algebraically as $\frac{1}{|y|^{2\zeta_{\text{Th}}}}$: the different points along the interface become elastically independent and $\langle (u_x - u_{x'})^2 \rangle$ tends to a constant. In the regime we are interested in $|x - x'| \ll \ell_\mu$, F_d in (I.2.4) is constant and can be forgotten and the mean square displacement $\langle (u_x - u_{x'})^2 \rangle$ displays a power-law behavior determined by the roughness exponent ζ_{Th} . Hence for $d \leq \gamma$, $\zeta_{\text{Th}} \geq 0$ and the interface is rough (it displays a logarithmic scaling for $d = \gamma$), while it is flat for $d > \gamma$ ($\zeta_{\text{Th}} < 0$). Hence, as expected, the effect of the temperature on the large scale fluctuations of a system of fixed internal dimension d gets stronger as the range of elasticity is decreased.

The thermal fixed point

Let us now discuss the notion of Thermal fixed point (TFP), first at the level of the Hamiltonian (I.2.1), and we consider the limit $\mu \rightarrow 0$ (which is the regime we are interested in). In this limit, the following scale transformation, equivalently written in Fourier or real space,

$$\begin{aligned}x &= b\tilde{x} \quad , \quad \tilde{u}_{\tilde{x}} = b^{-\zeta_{\text{Th}}} u_{x=b\tilde{x}} \\ q &= b^{-1}\tilde{q} \quad , \quad \tilde{u}_{\tilde{q}} = b^{-d-\zeta_{\text{Th}}} u_{q=b^{-1}\tilde{q}}\end{aligned}\tag{I.2.6}$$

leaves the Hamiltonian $\mathcal{H}_{\text{pure}}[u]$ invariant: it is a fixed point of the above scaling transformation. Note that physical observables are sensitive to the combination $\frac{1}{T}\mathcal{H}_{\text{pure}}[u]$ (and not $\mathcal{H}_{\text{pure}}[u]$ alone). In this theory, conserving the thermal averages of observables under the thermal rescaling (I.2.6) does not impose a rescaling of the temperature: this is the thermal fixed point of the theory. The question of its stability can be simply considered by adding other terms in the Hamiltonian (I.2.1) and checking whether or

not they decay to 0 under the rescaling (I.2.6) as $b \rightarrow \infty$ increases. Indeed finite \tilde{x} corresponds to large x if $b \gg 1$ and the theory in the variables $(\tilde{x}, \tilde{u}_{\tilde{x}})$ can be thought of as a coarse-grained effective theory describing the physics of the system at a larger scale. As an example, consider adding higher order derivative terms of the form, schematically, $\int_x (\nabla_x)^n u^p$ with $n \geq p$ and p even (so that the elastic Hamiltonian is still invariant under translation and parity in the external space: $\mathcal{H}^{\text{el}}[u] = \mathcal{H}^{\text{el}}[u + cst] = \mathcal{H}^{\text{el}}[-u]$) in the Hamiltonian (I.2.1) for the case of short-range elasticity. Applying the scaling transformation we obtain

$$\int_x (\nabla_x)^n u^p \longrightarrow b^{d-n+p\frac{2-d}{2}} \int_{\tilde{x}} (\nabla_{\tilde{x}})^n (\tilde{u}_{\tilde{x}})^p . \quad (\text{I.2.7})$$

Such a term always decays to zero under the coarse-graining procedure: the large scale physics will be described by the simple thermal fixed point we have considered. A similar analysis will allow us to discuss the relevance of the disorder at the TFP below but let us warn the reader here that this ‘renormalization procedure’ will *not* be the one adopted in Chapter II to truly discuss the renormalization of the theory with disorder. The point of view we will adopt there will be to study the *effective action* of the field theory (which will be a replicated field theory in the case of the static problem). We will keep ℓ_μ finite as a convenient infra-red cutoff, and compute the effective action in the limit $\mu \rightarrow 0$ and show that it takes a universal scaling form. Let us now briefly translate here the properties of the thermal fixed point in this language. The effective action of the theory at finite μ is defined as

$$e^{W_{\mu,T}[J]} := \int \mathcal{D}[u] e^{-\frac{1}{T} \mathcal{H}_{\text{pure}}[u] + \int_x J_x \cdot u_x} \quad (\text{I.2.8})$$

$$\Gamma_{\mu,T}[u] := -W_{\mu,T}[J] + \int_x J_x \cdot u_x \quad , \text{ where } J \text{ is such that } u_x = \frac{\delta W_{\mu,T}[J]}{\delta J_x} ,$$

where we have emphasized the dependence on μ and on the temperature of the effective action $\Gamma_{\mu,T}[u]$ and on the *generating function for connected diagrams* $W_{\mu,T}[J]$. For a Gaussian theory described by the quadratic Hamiltonian (I.2.1), it is trivial to compute these functionals and one obtains, up to an unimportant constant term, $\Gamma_{\mu,T}[u] = \frac{1}{T} \mathcal{H}_{\text{pure}}[u]$: $\Gamma_{\mu,T}[u]$ can be computed for arbitrary μ . In this language the scale invariance can be written by introducing the rescaled effective action

$$\tilde{\Gamma}_\mu[\{\tilde{u}_{\tilde{x}}\}] = \Gamma_\mu[\{u_x = \mu^{-\zeta_{\text{Th}}} \tilde{u}_{\tilde{x}=\mu x}\}] . \quad (\text{I.2.9})$$

As $\mu \rightarrow 0$, for $\tilde{x} \leq 1$ fixed of order $O(1)$, the field $\tilde{u}_{\tilde{x}}$ describes the large scale fluctuations in the scaling regime of the field u_x in the original theory. At fixed T , $\tilde{u}_{\tilde{x}}$, the scale invariance of the thermal fixed point reads in this language

$$-\mu \partial_\mu \tilde{\Gamma}_\mu[\{\tilde{u}_{\tilde{x}}\}] = 0. \quad (\text{I.2.10})$$

And this holds $\forall \mu$. In the theory with disorder the analysis will be much harder but we will in the end obtain an equation similar to (I.2.10). We will only be able to obtain information on the effective action $\Gamma_\mu[u]$ in the limit $\mu \rightarrow \infty$ and in the limit $\mu \rightarrow 0$. In the latter limit, that is the one we will truly be interested in, the key point will notably be to identify the rescalings of the field u and of the temperature T such that a rescaled effective action $\Gamma_\mu[u]$ converges to a fixed point of a non-trivial FRG equation.

I.2.2 Relevance and irrelevance of short-range disorder at the thermal fixed point

Let us now consider the effect of adding a small Gaussian short-range disorder to the pure Hamiltonian (I.2.1):

$$\begin{aligned}\mathcal{H}_V^{\text{dis}}[u] &:= \int_x V(x, u_x) \\ \mathcal{H}[u] &= \mathcal{H}_{\text{pure}}[u] + \mathcal{H}_V^{\text{dis}}[u].\end{aligned}\quad (\text{I.2.11})$$

And we suppose for simplicity that $V(x, u)$ is Gaussian, with mean 0 and a two-point correlation function

$$\overline{V(x, u)V(x', u')} = g\delta^{(d)}(x - x')\delta^{(N)}(u - u'), \quad (\text{I.2.12})$$

with $g \geq 0$ a parameter (a RB type disorder with 0 correlation length). Under a general rescaling $x = b\tilde{x}$ and $\tilde{u}_{\tilde{x}} = b^{-\zeta}u_{x=b\tilde{x}}$, the disorder energy is rescaled as

$$\mathcal{H}_V^{\text{dis}}[u] = \int_x V(x, u_x) \quad \longrightarrow \quad b^d \int_{\tilde{x}} V(b\tilde{x}, b^\zeta \tilde{u}_{\tilde{x}}) \sim b^{\frac{d-N\zeta}{2}} \int_{\tilde{x}} \tilde{V}(\tilde{x}, \tilde{u}_{\tilde{x}}). \quad (\text{I.2.13})$$

Here and throughout the rest of the manuscript \sim means ‘distributed in law as’ and $\tilde{V}(\tilde{x}, \tilde{u})$ is a (new) centered Gaussian disorder with correlations $\overline{\tilde{V}(\tilde{x}, \tilde{u})\tilde{V}(\tilde{x}', \tilde{u}')} = g\delta^{(d)}(\tilde{x} - \tilde{x}')\delta^{(N)}(\tilde{u} - \tilde{u}')$. Note that the rescaling (I.2.13) effectively assumes that the configuration of the field u_x on which the rescaling is performed is independent of the disorder in order to use $\overline{V(x, u_x)V(x', u_{x'})} = g\delta^{(d)}(x - x')\delta^{(N)}(u_x - u_{x'})$. This will be true here in the sense of the leading approximation for an expansion in V since at leading order fluctuations of u_x are controlled by the thermal fixed point and here u_x can be thought of as a typical configuration of the DES at the TFP. Using $\zeta = \zeta_{\text{Th}}$, one obtains that the disorder energy scales as $b^{\frac{d-N(\gamma-d)/2}{2}}$. Hence small disorder is perturbatively irrelevant at the thermal fixed point if

$$N > \frac{2d}{\gamma - d}. \quad (\text{I.2.14})$$

The result (I.2.14) however only holds for $d < \gamma$ as we now explain. Indeed in larger dimension $d > \gamma$, the thermal roughness exponent ζ_{Th} is smaller than 0. The system at the thermal fixed point is not rough but flat. The exponent ζ_{Th} describes the algebraic speed at which the fluctuations $\langle (u_x - u_{x'})^2 \rangle$ converge to their asymptotic value. Using the rescaling $\tilde{u}_{\tilde{x}} = b^{-\zeta}u_x$ with $b \gg 1$ and $\zeta \leq 0$ means that distances of order 1 in the coordinates \tilde{u} correspond to infinitesimal distances in the coordinates u : for a realistic model this is dangerous since at small distances one expects the continuum description to break down. One also necessarily starts at some point to see the effect of the non-zero correlation length of the disorder V which was assumed to be zero for simplicity here. For these reasons, for a realistic model of a disordered elastic system in a flat phase, comparing the effect of the elastic energy and of the disorder energy at large scale should rather be made by rescaling the lengths as $x = b\tilde{x}$ and $u = \tilde{u}$. In such a rescaling the elastic energy is rescaled as $\mathcal{H}^{\text{el}}[u] \rightarrow b^{d-\gamma}\mathcal{H}^{\text{el}}[\tilde{u}]$ while the disorder energy is rescaled as $\mathcal{H}^{\text{el}}[u] \rightarrow b^{\frac{d}{2}}\mathcal{H}^{\text{el}}[\tilde{u}]$. Hence starting from a flat interface, i.e. e.g.

in $d \geq \gamma$ for a model at the thermal fixed point or in arbitrary d at zero temperature, weak disorder is relevant at large scale if

$$d \leq d_{\text{uc}} := 2\gamma. \quad (\text{I.2.15})$$

Where we have introduced the *upper-critical dimension of the problem*. Let us now summarize our findings.

I.2.3 Static phase diagram

1. At finite temperature for $\gamma \leq d \leq 2\gamma$ and for $d \leq \gamma$ and $N > \frac{2d}{\gamma-d}$ and at zero temperature for $d \leq 2\gamma$, for arbitrary weak disorder, the elastic system is always rough at large scale with a roughness exponent larger than the thermal roughness exponent (the system pays more elastic energy than in the thermal phase to be able to visit regions of space with low values of the disorder potential). From the renormalization point of view, we will see that the effective action of the theory flows to a new fixed point at which scaling holds and in the scaling regime $|x - x'| \ll \ell_\mu$,

$$\overline{\langle (u_x - u_{x'})^2 \rangle} \sim |x - x'|^{2\zeta_s} \quad (\text{I.2.16})$$

where we defined the statics roughness exponent $\zeta_s \geq 0$. At the upper-critical dimension of the problem $d_{\text{uc}} = 2\gamma$, since the disorder is only marginally relevant at large scale, the roughness exponent ζ_s is expected to be 0 and (I.2.16) to be replaced by a logarithmic scaling. Here the fact that the large scale cutoff scale ℓ_μ is equal to the one of the pure theory $\ell_\mu = 1/\mu$ is a consequence of the so-called *Statistical-Tilt-Symmetry* (STS) of the problem as will be discussed later. At this fixed point, taken as a parameter of the effective action, the temperature of the systems is irrelevant and flows to 0 when μ goes to 0 as μ^θ . Asking that the combination $\frac{1}{T} \int_q (q^2 + \mu^2)^{\frac{\gamma}{2}} u_{-q} \cdot u_q$ that will enter into the effective action (again as a consequence of STS) of the problem converges to a well defined limit imposes

$$\theta = d - \gamma + 2\zeta_s = 2(\zeta_s - \zeta_{\text{Th}}) \geq 0. \quad (\text{I.2.17})$$

This regime will be called the *strong disorder regime* in the remainder of the manuscript. In this regime thus the temperature at large scale is irrelevant and the system optimizes its energy by balancing elasticity and disorder. We will also say that in this phase the system is *pinned* by disorder.

2. On the other hand, for $d \leq \gamma$ and $N > \frac{2d}{\gamma-d}$ (i) there exists a strong disorder fixed point at $T = 0$ (ii) the thermal fixed-point is stable to weak-disorder. There are thus at least two phases. Starting from the strong disorder, zero temperature fixed point, it is believed that at least for small N , the strong disorder fixed point is stable to a perturbation by a small temperature. The question of whether or not there exists a finite critical value $N_{\text{uc}} < \infty$ such that for $N > N_{\text{uc}}$ an arbitrary small temperature makes the system depart from the strong disorder fixed point and converge to the thermal fixed point is a difficult question which

remains unanswered. This is true even in what might be the simplest case of SR elasticity ($\gamma = 2$) in $d = 1$, the so-called directed polymer problem, see Sec. I.3. In this case, the problem is equivalent to the KPZ equation in dimension N (see Sec. I.3), and in this language N_{uc} is the unknown upper-critical dimension of the KPZ equation, which could be equal to $+\infty$. In this phase, for a sufficiently large temperature / weak disorder, the large scale physics is described by the thermal fixed point, the system is rough but it is not pinned: its fluctuations are thermal.

3. Finally, for $d > 2\gamma$ the system is always flat and the elasticity wins at large scale: the system is in its *ordered phase*.

From the above discussion we thus obtain the well-known phase diagram for the statics of disordered elastic systems as a function of the internal and external dimension d and N for RB disorder and elasticity of the type (I.1.4) with $g_q^{-1} = |q|^\gamma$ as presented in (I.3). This diagram can be more or less modified if one changes some assumptions that were made. For example

(i) Disorder with long-range correlations: if the disorder has long-range correlations in either the external or internal space its influence is expected to increase and the large scale properties of the system can be different. Let us see qualitatively what changes for the case of random field disorder which will also be considered in this thesis (see Sec. I.1) with 0 correlation length. In this case under rescaling the disorder energy behaves as, schematically,

$$\int_x V(x, u_x) = \int_x \int_{u'} F(x, u'_x) \longrightarrow b^{\frac{d-N\zeta}{2} + \zeta} \int_{\tilde{x}} \int_{\tilde{u}'} \tilde{F}(\tilde{x}, \tilde{u}'_{\tilde{x}}) = b^{\frac{d-(N-2)\zeta}{2}} \int_{\tilde{x}} \tilde{V}(\tilde{x}, \tilde{u}_{\tilde{x}}) \quad (\text{I.2.18})$$

Following the same path as before, one sees that such correlations do not modify the upper-critical dimension of the problem which is still 2γ , but increases the minimal value of N above which the thermal phase is stable to weak disorder as $N_{\text{min}} = 2 + \frac{2d}{\gamma-d} = \frac{2\gamma}{\gamma-d}$. For a study of long-range correlations in internal space we refer to [12] and references therein.

(ii) Disorder with fat-tails: although it is not clearly visible in our derivation, disorder with fat-tails (i.e. for which there exists a finite n_{max} such that $\overline{V^n(x, u)} = +\infty$ for $n \geq n_{\text{max}}$) can strongly modify the static phase diagram and corresponds to new universality classes. Naive intuition coming from the study of sums of independent random variables would suggest that $n_{\text{max}} > 2$ would not change the phase diagram. In general not much is known about the behavior of disordered elastic systems in presence of fat-tail disorder. For the case of the directed polymer (DP) in a two-dimensional random media $N = d = 1$ with SR elasticity $\gamma = 2$, it is known from a Flory argument confirmed by numerical studies that $n_{\text{max}} \leq 5$ actually suffices to change the behavior of the DP [13, 14]. The physical origin of this modification is that the strategy of optimization of energy of the DP changes in the presence of fat-tails disorder. While for a Gaussian disorder the DP optimizes its energy homogeneously along its internal direction, the optimization of energy becomes dominated by extreme

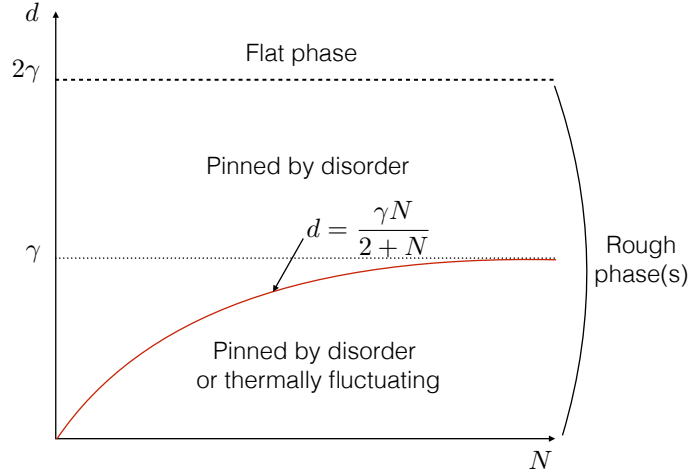


Figure I.3: Static phase diagram for a DES with elasticity kernel $g_q^{-1} = |q|^\gamma$ in a RB disorder potential at temperature T . For $d \geq 2\gamma$ the system is always asymptotically flat. For $d \leq 2\gamma$ and $N < \frac{2d}{\gamma-d}$, i.e. $d > \frac{\gamma N}{2+N}$ the system is always pinned by disorder and is in a strong disorder / 0 temperature phase. For $d < \frac{\gamma N}{2+N}$ the system can a priori be either pinned by disorder (at the strong disorder FP), or thermally fluctuating (at the thermal FP), but is in any case always rough. The existence of a critical value N_{uc} above which the system is always in the thermal phase remains debated.

value statistics in the presence of fat tails with $n_{\max} \leq 5$. The presence of a few sites in the energy landscape with very low values of the disorder potential then dominates the energy of the DP. We will not consider further in this thesis this complex question and restrict our analysis to $n_{\max} = +\infty$.

The goal of this thesis is to understand properties of disordered elastic systems in the strong disorder regime of the phase diagram of Fig. I.3. In this regime one expects (and would like to prove) that the system is rough with a non-zero roughness exponent ζ_s as in (I.2.16). Furthermore one expects the roughness exponent ζ_s to be independent of the details of the distribution of $V(x, u)$: since the pinning of the DES is clearly a collective phenomenon (at least if the PDF of $V(x, u)$ has no fat tails) and ζ_s is a large scale property, one expects some universality to exist. As we will see in Chapter II using the Functional Renormalization Group, for disorder as discussed in Sec. I.1.3 and in the case of interfaces $N = 1$, there is indeed universality in the large scale properties of disordered elastic interfaces. The different universality classes are indexed by the choice of the range of elasticity (the experimentally most important being LR $\gamma = 1$ and SR $\gamma = 2$) and of the correlations of the disorder (RB, RF or random periodic).

I.2.4 Early attempts at characterizing the strong disorder regime: Flory arguments and the Larkin model

Let us now review two early theoretical approaches aiming at describing the strong disorder regime of Fig. I.3. As usual we consider disordered elastic systems with an elastic kernel $g_q^{-1} \sim |q|^\gamma$.

a Flory scaling argument

The Flory argument is a RG-type argument that consists in equating the scaling dimension of the elastic energy term and of the disorder term using simple rescaling of the different terms in the Hamiltonian as was performed in the last section to check the relevance of small disorder close to the thermal fixed point. In this sense it is similar to a dimensional analysis. We thus rescale $x = b\tilde{x}$ with $\tilde{u}_{\tilde{x}} = b^{-\zeta_s} u_{x=b\tilde{x}}$. The elastic Hamiltonian is rescaled as before as $\mathcal{H}^{\text{el}}[u] \rightarrow b^{d-\gamma+2\zeta_s} \mathcal{H}^{\text{el}}[\tilde{u}]$. For RB type disorder (see Sec. I.1.3) the rescaling of the disorder part of the Hamiltonian is as in (I.2.13) and we obtain

$$d - \gamma + 2\zeta_s = \frac{d - N\zeta_s}{2} \implies \zeta_s = \frac{2\gamma - d}{4 + N}. \quad (\text{I.2.19})$$

In the RF type (see Sec. I.1.3) on the other hand we obtain, using (I.2.18)

$$d - \gamma + 2\zeta_s = \frac{d - (N - 2)\zeta_s}{2} \implies \zeta_s = \frac{2\gamma - d}{2 + N}. \quad (\text{I.2.20})$$

The flow in the Flory argument is the following. Here we are assuming that we are at a RG fixed point and that the effective disorder felt at large scale transforms as in (I.2.13) or (I.2.18). However, during such a coarse-graining procedure, there can be a non-trivial renormalization of the disorder coming from the optimization of the energy of the interface on small scales. This scaling argument should thus be taken with caution.

In particular we will see that (I.2.19) disagrees with the *exact result* for directed polymers in $1 + 1d$ with short-range elasticity for which $\zeta_s = 2/3$. Remarkably for the RF case at least for $N = 1$, it is believed that (I.2.20) is exact. This is due to the fact that, although the disorder is also corrected by the renormalization in this case and the hypothesis leading to (I.2.20) are not correct, it is possible to show using the Functional Renormalization Group that the tail of $R_0(u) \sim -\sigma|u|$ is not corrected, and it is this uncorrected large distance behavior of $R_0(u)$ which dominates the optimization of the interface energy. For the RF case this remarkable result calls for a precise explanation showing that there are no corrections coming from the optimization on small scales, and for the important RB case the failure of the argument motivates the development of a true renormalization scheme.

b The Larkin model

Larkin model

The Larkin model, introduced by Larkin in [15], is a perturbative attempt at understanding the properties of the strong disorder fixed point by directly looking at the

$T = 0$ problem, i.e. by considering the ground state of the interface. It consists in linearizing the random potential $V(x, u)$ (taken e.g. of the RB type) around a given position and retaining only the first order term. If the system is confined around a position $w = 0$ the potential is linearized as $V(x, u) = V(x, 0) + \partial_u V(x, 0)u = V(x, 0) - F(x)u$, where we introduced the force $F(x) := -\partial_u V(x, 0)$. Note that by definition $F(x)$ does not depend on u . The latter is chosen centered, Gaussian with short-range correlations in the internal space and second moment $\overline{F(x)F(x')} = \delta^{(d)}(x - x')\Delta$ where $\Delta \geq 0$. Taking as usual an elastic Hamiltonian $\mathcal{H}^{\text{el}}[u] = \frac{1}{2} \int_q (q^2 + \mu^2)^{\frac{\gamma}{2}} u_{-q} u_q$, the ground state of the system satisfies

$$(q^2 + \mu^2)^{\frac{\gamma}{2}} u_q - F(q) = 0. \quad (\text{I.2.21})$$

Hence, the position field is Gaussian, with correlations in Fourier space

$$\overline{u_{q'} u_q} = \hat{\delta}^{(d)}(q + q') \frac{\Delta}{(q^2 + \mu^2)^\gamma}. \quad (\text{I.2.22})$$

And in real space, for $d \leq d_{\text{uc}} = 2\gamma$ and for lengths $|x - x'| \ll 1/\mu$, it is rough

$$\overline{(u_x - u_{x'})^2} \sim C_d \Delta |x - x'|^{2\zeta_L} \quad (\text{I.2.23})$$

with $C_d = 2^{1-2\gamma} \pi^{-d/2} \frac{\Gamma(d/2-\gamma)}{\Gamma(\gamma)}$ and the roughness exponent known as the Larkin exponent

$$\zeta_L := \frac{2\gamma - d}{2}. \quad (\text{I.2.24})$$

Dimensional reduction

Again the Larkin exponent (I.2.24) is not correct. One example is that it does not reproduce the exact result already cited above $\zeta_s = 2/3$ for the RB case with $N = d = 1$ and $\gamma = 2$. A natural question however is to understand whether or not one could extend and improve the previous calculation by taking into account higher order terms in the series expansion of the potential: $V(x, u) = \sum_{n=0}^{\infty} \frac{u^n}{n!} \partial_u^n V(x, u)|_{u=0}$. Solving the minimization problem (I.2.21) in an expansion in u by adding higher order terms leads to a remarkable result: *to all orders in perturbation theory, it predicts (I.2.22) and the Larkin roughness exponent (I.2.24)*. In the context of interfaces, this simplification of naive perturbation theory was first discussed in [16]. In the more general context of disordered systems it is known as the phenomenon of *dimensional reduction* which asserts that disorder averaged observables of a theory at $T = 0$ are equivalent to thermal averages in the pure theory at finite temperature in dimension $d_{\text{dr}} = d - \gamma$ (see [17] for a theoretical analysis of this property using supersymmetry and e.g. [18] for a diagrammatic approach). The thermal roughness exponent (I.2.5) $\zeta_{\text{Th}} = \frac{\gamma-d}{2}$ is indeed equal to (I.2.24) using $d \rightarrow \gamma - d$. Of course, if dimensional reduction was true everything would be rather simple. The problem here is that the Larkin analysis misses important non-perturbative effects and can only work at small scale as we now discuss. First, since the Larkin model is based on a perturbation theory with the disorder expanded around the flat interface configuration $u = 0$, it is hard to believe that it is correct at large length scales for $d \leq 2\gamma$ since it predicts a rough interface. More precisely, note that it effectively assumes that the force $F(x)$ does not depend on

u while a generic RB disorder has a finite correlation length $u_c < \infty$. For this reason, while on small scales $|x - x'| \leq L_c$ such that Δu is small $|\Delta u| \leq u_c$ the Larkin model can accurately describe the fluctuations of the system, it should certainly fail above. The length L_c is known as the *Larkin length* and it can be estimated as, using (I.2.23),

$$\sqrt{C_d \Delta} L_c^{\zeta_L} \sim r \quad \text{i.e.} \quad L_c \sim \left(\frac{u_c}{\sqrt{\Delta C_d}} \right)^{\frac{2}{2\gamma-d}}. \quad (\text{I.2.25})$$

In particular note that for $u_c = 0$, $L_c = 0$ and the Larkin model is nowhere consistent. What happens to the system above the Larkin length is that the elastic energy cost paid by the system to wander in the energy landscape on distances $\Delta u \gg u_c$ becomes manageable and the system starts to fully exploit the fact that there are a lot of minima. We will see in Chapter II that the Larkin length is linked to the notion of *shocks* and *avalanches*. Describing the optimization of energy on large scales is a complex problem that will be tackled using renormalization method in Chapter II and exact methods in Chapter III.

I.3 Various problems considered in this thesis

In this section we consider a disordered elastic system described by the Hamiltonian (I.1.2) and briefly introduce some questions that will be tackled during the thesis.

I.3.1 Shocks in the statics at zero temperature for elastic interfaces

In Chapter II we will be interested in the statics at zero temperature for elastic interfaces, i.e. the $d \geq 1$ and $N = 1$ problem. We will thus be interested in the (V -dependent) ground state $u_x^V(w)$ of the total Hamiltonian:

$$\begin{aligned} u_x^V(w) &:= \operatorname{argmin}_{u_x: \mathbb{R}^d \rightarrow \mathbb{R}} \mathcal{H}_{V,w}[u] \\ &= \operatorname{argmin}_{u_x: \mathbb{R}^d \rightarrow \mathbb{R}} \left(\mathcal{H}^{\text{el}}[u] + \mathcal{H}_V^{\text{dis}}[u] + \mathcal{H}_w^{\text{conf}}[u] \right). \end{aligned} \quad (\text{I.3.1})$$

More explicitly we will be interested in the case of an elastic kernel $g_q^{-1} = \sqrt{q^2 + \mu^2}$ for an interface confined around a parabolic well at position w .

$$u_x^V(w) = \operatorname{argmin}_{u_x: \mathbb{R}^d \rightarrow \mathbb{R}} \left(\frac{1}{2} \int_q g_q^{-1} (u_{-q} - w_{-q}) \cdot (u_q - w_q) + \int_x V(x, u_x) \right). \quad (\text{I.3.2})$$

Following the previous section, the interesting case on which we will focus will be the low-dimension case $d \leq 2\gamma$ (condition for the interface to be pinned by the disorder at large scale) and in the range of scales $a \ll |x - x'| \ll \ell_\mu \ll L$. In this range of scales one indeed expects scaling and universality to hold and we will be interested in understanding the process $u_x^V(w)$ as a function of w . Since for any w the interface is pinned by disorder one expects that the evolution of $u_x^V(w)$ with w contains jumps in between different metastable states of the disorder Hamiltonian. This will be made precise in Chapter II, and we will see that these jumps, also called *shocks* will inherit the universality present in the physics of disordered elastic systems (yet to be precisely discussed).

Irrelevance of the temperature? A natural question is to ask why we are only considering the zero temperature static problem in the questions outlined above. Indeed, we have ‘shown’ in the previous section that the thermal fixed point of the interface is unstable and the large scale physics of the system is described by a strong disorder fixed point at zero temperature whenever $\frac{2d}{\gamma-d} > 1$, that is for $d \geq \gamma/3$. Since short-range elasticity is described by $\gamma = 2$ and we will only be interested in the cases with a longer range of elasticity, especially $\gamma = 1$, for true interfaces of dimension $d \geq 1$, the thermal fixed point will always be unstable and the system is always expected to be in the pinned phase. Although it is true that for these problems the temperature does not play a role for large scale properties such as the roughness exponent, it does affect some small scales properties and in particular we will see that it smoothes the jump process described above. Therefore, though some of our results might also be relevant for the non-zero temperature case as we will discuss, we will focus on the zero-temperature problem.

1.3.2 Avalanche dynamics at the depinning transition for elastic interfaces

a Introduction to the depinning transition

Another question we will be interested in is the dynamics of the interface at the depinning transition that we now introduce. The depinning transition is a dynamical phase transition that occurs in the over-damped dynamics (with viscosity coefficient η) of elastic interfaces with elastic kernel $g_{x,y}^{-1} = \int_q e^{iq(x-y)} |q|^\gamma$, driven by a non-zero force f in a random force field $F(x, u_x)$ with second moment as in (I.1.7), and we typically have in mind the case of a Gaussian force where $\Delta_0(u - u')$ is a short-range function with correlation length u_c . The equation of motion of the interface is

$$\eta \partial_t u_{tx} = \int_y g_{x,y}^{-1} u_y + F(x, u_x) + f. \quad (\text{I.3.3})$$

Note that this dynamics (which corresponds to type A in the classification of [19]) is a somehow arbitrary choice on which we will focus. The presence of inertial or viscoelastic effects are not taken into account here and thus not all disordered elastic interfaces moving in nature can surely not be described by this dynamics. For some of them however, at least in some regime, this type of dynamics have been proposed as a relevant description (see Sec. I.4). For the case of SR elasticity $\gamma = 2$ this equation is often referred to as the Quenched-Edwards-Wilkinson equation. Here the initial condition will be basically unimportant: we will be looking at the *out-of-equilibrium steady state* reached by the interface at $t \rightarrow \infty$. Indeed it can be proved that in our setting, starting from an initial condition such that all velocity along the interface are either positive or 0 (i) they remain so for all time; (ii) up to a time translation the interface position field reaches a single well-defined steady state. The two last statements are often referred to as the Middleton theorem in the literature and were proved by Middleton in [20]. The first question in the depinning transition is to understand the *velocity-force characteristic* of the interface, that is

$$v(f) := \lim_{t \rightarrow \infty} \frac{u_{tx}}{t}. \quad (\text{I.3.4})$$

And here we are interested in the limit of an infinitely large interface $L \rightarrow \infty$. The basic physics of the depinning transition that we recall below is known since the work of Larkin in the framework of superconductors [15], and was later developed in the interface context, see e.g. [21] and references therein. The main observation is that for $f \leq f_c$, the interface does not move, $v(f) = 0$ and for f larger but close to f_c , the velocity force characteristic exhibits a power-law behavior with an exponent $\beta \geq 0$:

$$v(f) \sim (f - f_c)^\beta \quad \text{for } f \geq f_c. \quad (\text{I.3.5})$$

To estimate f_c , first note that when $f = 0$, the interface is at rest. For $d \leq 2\gamma$, the interface is rough while for $d \geq 2\gamma$ is asymptotically flat. For a flat interface of internal length L , the typical disorder force acting on the interface scales as $F \sim \sqrt{\Delta(0)}L^{d/2}$, while the total driving force acting on the interface is fL^d . The latter always wins for $L \rightarrow \infty$ and the interface starts to move: $f_c = 0$ for $d \geq 2\gamma$, the disorder is irrelevant at large scale and $\beta = 1$. For $d \leq 2\gamma$, the interface is rough when $f = 0$. On scales smaller than the Larkin length (I.2.25) $L \leq L_c$, the displacements of the interface are small, and one can estimate again the typical force acting on this portion of the interface as $F \sim \sqrt{\Delta(0)}L^{d/2}$. Such a small portion of the interface can stay pinned for sufficiently small F . Seeing the interface as a collection of $N = (L/L_c)^d$ domains of length L_c pinned by fluctuations of the disorder, an estimate of the critical force (due to Larkin) is thus:

$$f_c \sim \sqrt{\Delta(0)}L_c^{-d/2}, \quad (\text{I.3.6})$$

and an estimate of L_c was given in (I.2.25).

b The depinning transition as a continuous out of equilibrium phase transition

Following this simple analysis, the zero temperature dynamics of disordered elastic interfaces of dimension $d \leq 2\gamma$ as described by (I.3.3) appears to exhibit a *dynamical phase transition* where the order parameter is the velocity of the interface and f is the control parameter (see Fig. I.4). The description of this phase transition can be made in analogy with ordinary continuous phase transitions in equilibrium statistical mechanics, with the additional ‘complication’ that there is also a time direction in the problem (see [11] for the discussion of this point of view in the case of sliding charge density waves). The usual space scale invariance at the point of a continuous equilibrium phase transition becomes a space-time scale invariance in the steady state at the point of the dynamical phase transition which is basically summarized by saying that time scale as $t \sim x^z$ where z is the *dynamics exponent* of the transition. In the steady-state, approaching the transition from above $f \rightarrow f_c^+$, there exists a growing correlation length $\xi \sim (f - f_c)^{-\nu}$ ($\nu \geq 0$ is another exponent) such that, for $|x - x'| \leq \xi$ and $|t - t'| \leq \xi^z$, the fluctuations of the position field satisfy the scaling form

$$\overline{(u_{tx} - u_{t'x'})^2} \sim |x - x'|^{2\zeta_d} \mathcal{G}\left(\frac{|t - t'|}{|x - x'|^z}\right) \quad (\text{I.3.7})$$

where ζ_d is the *roughness exponent* and $\mathcal{G}(y)$ is a scaling function that satisfies

$$\mathcal{G}(y) \xrightarrow{y \rightarrow 0} cst \quad , \quad \mathcal{G}(y) \sim_{y \rightarrow \infty} (y^{2\zeta_d/z}). \quad (\text{I.3.8})$$

The different critical exponents β , ν , ζ_d and z introduced above are, as will be shown later, not independent. More precisely the depinning transition can be described by only two independent critical exponents, which will be taken as ζ_d and z in the following. ζ_d is analogous to the roughness exponent in the static problem ζ_s but is a priori different. As the depinning transition appears as a collective phenomenon, it is expected that these exponents have some universality. As we will recall in Chapter II, there are actually fewer universality classes at the depinning transition of the interface than in the corresponding static problem since it is now known that there is *a single universality class for short-range random forces*, corresponding to a random field universality class (although different from the corresponding universality class in the statics). In particular at depinning, the large scale properties in a random potential of the RF and RB type are similar. As the dimension becomes close to the upper-critical dimension $d_{uc} = 2\gamma$, the disorder becomes irrelevant at large scale and the roughness exponent ζ_d must converge to 0, while the value of the dynamic exponent converges to, as can simply be read off from (I.3.3), $z = \gamma$. As we know from the study of the static problem, for $d \leq 2\gamma$ and without driving force, the system is pinned. As we will see, the non-trivial dynamics that occurs at the depinning transition is due to the fact that the interface will be most of the time pinned by disorder in a metastable state (as we will argue these are different from the static ground states). From time to time the interface will manage to cross the energy barrier and then moves with a velocity of order 1 until it is pinned again by a new metastable state. Thus the interface dynamics at the depinning transition appears as an avalanche process. At large force the system is never pinned and flows with $v(f) \sim f/\eta$: disorder is washed out and only leads to small fluctuations around the deterministic behavior. The interesting regime to understand is thus clearly the avalanche process close to the depinning transition. The universal properties of this avalanche process will be, together with shocks between ground states presented before, at the core of Chapter II.

c Creep and the temperature

The influence of the temperature on the depinning transition is much more subtle than on the large scale properties of the static ground state (although it can also be quite subtle). In the static problem, as we will see in Chapter II, non-zero temperature smoothes the shocks at small scales when the energy differences between successive minima become of the same order as the thermal energy. In particular in the static problem, the role of *energy barriers* between successive minima will be inexistent. On the contrary, the slow, non-trivial dynamics that is observed at the depinning transition of the interface is all about the interface being able to cross energy barriers (the fast motion observed after such a barrier has been crossed being an avalanche). Since a non-zero temperature allows the interface to cross an arbitrary large energy barrier, it has important effects on the dynamics, and the temperature is not irrelevant at large scale. In particular, *at non-zero T , for arbitrary force $f \geq 0$, the interface moves with a non-zero velocity $v(f)$* . This phenomenon is known as *creep*. It was first described theoretically [22, 23, 24, 25]. Rather non-trivial assumptions and scaling arguments

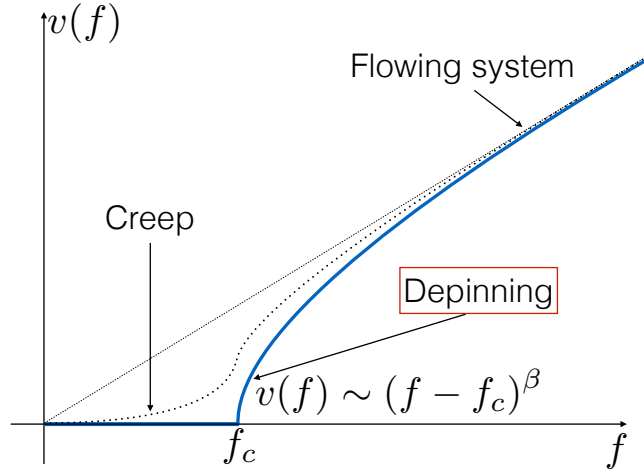


Figure I.4: Velocity-force characteristic of an infinite interface of dimension $d \leq 2\gamma$ for the over-damped dynamics (I.3.3). Blue line: depinning velocity-force characteristic for the interface at $T = 0$. Dotted black line: creep velocity-force characteristic for the interface at low temperature.

led to the creep law, valid for $f \ll f_c$,

$$v(f) \sim e^{-\frac{U_c}{T} \left(\frac{f_c}{f}\right)^\mu}, \quad \mu = \frac{D - 2 + 2\zeta_s}{2 - \zeta_s}, \quad (\text{I.3.9})$$

where U_c is a system-dependent energy scale. Note in particular that (I.3.9) involves the static roughness exponent, while the creep is a non-equilibrium phenomenon. On the theoretical side the relation (I.3.9) was confirmed up to one loop accuracy using FRG [26, 27]. For the case of SR elasticity in $d = 1$ in a random bond potential (for which the static exponent $\zeta_s = 2/3$ is exactly known and thus $\mu = 1/4$), it was also confirmed numerically in [28], and even experimentally using measurements on the dynamics of magnetic domain walls [29]. Understanding more thoroughly the creep regime of an elastic interface is still a very active area of research [30, 31] that we will not discuss in this thesis. Let us only note the recent numerical study [32] that suggests that avalanches of the interface during the slow creep motion of the interface exhibit in different regimes scalings corresponding with either the scaling of static shocks, or the one of dynamic avalanches at the depinning transition studied in this thesis. From now on we will always restrict ourselves, for the dynamics, to the zero temperature case.

I.3.3 Static problem at finite temperature for directed polymers with SR elasticity and the KPZ universality class

a From the DP with SR elasticity to the KPZ equation

Another focus of this thesis is the Kardar-Parisi-Zhang (KPZ) equation which is associated with the statics of a short-range elastic directed polymer ($d = 1$ case) in

dimension N at finite temperature T as we now recall. The partition sum for directed polymer (DP) with starting point $u_0 = 0$ and endpoint $u_L = u \in \mathbb{R}^N$ can be written as a path integral

$$Z_L(u) = \int_{u(0)=0}^{u(L)=u} \mathcal{D}[u] e^{-\frac{1}{2T} \int_0^L dx (\nabla_x u_x)^2 - \frac{1}{T} \int_0^L dx V(x, u_x)}, \quad (\text{I.3.10})$$

and for now we suppose that the random potential is Gaussian with correlations

$$\overline{V(x, u)V(x', u')}^c = \delta(x - x') R_0(|u - u'|) \quad (\text{I.3.11})$$

with $R_0(u)$ a SR function (RB disorder). We will see in Chapter III that (up to a subtlety on which we will comment later) that $Z_L(u)$ satisfies a stochastic partial differential equation (SPDE) known as the multiplicative stochastic heat equation (MSHE). In this equation L plays the role of the time in the heat equation and we will thus make the change of variables

$$L \rightarrow t, \quad u \rightarrow x. \quad (\text{I.3.12})$$

In these variable $Z_L(u) \rightarrow Z_t(x)$ satisfies

$$\frac{\partial}{\partial t} Z_t(x) = \left(\frac{T}{2} (\nabla_x)^2 - \frac{1}{T} V(t, x) \right) Z_t(x). \quad (\text{I.3.13})$$

And the initial condition is $Z_{t=0}(x) = \delta^{(N)}(x)$. Introducing the free-energy of the directed polymer through the change of variables $F_t(x) = -T \log Z_t(x)$, we obtain, for $V(t, x)$ a smooth disorder,

$$\partial_t F_t(x) = -\frac{1}{2} (\nabla_x F)^2 + \frac{T}{2} (\nabla_x)^2 F_t(x) + V(t, x). \quad (\text{I.3.14})$$

Finally, making the change of variables $h(t, x) = -F_t(x)$, we obtain

$$\partial_t h(t, x) = \frac{1}{2} (\nabla_x h(t, x))^2 + \frac{T}{2} (\nabla_x)^2 h(t, x) - V(t, x). \quad (\text{I.3.15})$$

For the case of $V(t, x)$ taken as a Gaussian white noise, this SPDE is known in the literature as the N -dimensional Kardar-Parisi-Zhang (KPZ) equation. Beware that x now corresponds, in the elastic system language, to the N dimensional coordinates in the external space, while t corresponds to the one-dimensional coordinate that spans the internal space. The change of variables $Z_t(x) = e^{Th(t, x)}$ that maps the MSHE to the KPZ equation is known in the literature as the Cole-Hopf transform.

b The KPZ equation as a model of out-of-equilibrium growth of interfaces

Note that the KPZ equation (I.3.15) appears rather similar to the quenched Edwards-Wilkinson equation (i.e. (I.3.3) with SR elasticity $g_{x,y}^{-1} = -\delta^{(d)}(x - y) \nabla_y^2$) for the overdamped dynamics of a d dimensional interface at zero temperature except for the few *important* differences that (i) it contains a non linear term $(\nabla_x h_{tx})^2$ (ii) the disorder is not quenched but rather depends on time and can be interpreted as a thermal disorder.

Let us now interpret h_{xt} as a N -dimensional interface and (I.3.15) has a SPDE for the dynamics of h_{xt} . Note that the non-linear term breaks the symmetry $h \rightarrow -h$ and makes the interface grow in the upward direction. In particular, even without driving term and at zero disorder $V = 0$, an interface described by the dynamics (I.3.15) starting from a non-flat initial condition would grow indefinitely: $\lim_{t \rightarrow \infty} h_{xt} = +\infty$. This should be compared with the Edwards-Wilkinson equation (I.3.3) with neither disorder nor driving. In this case the pure dynamics is rather simple: starting from an initial configuration $u_{x,t=0}$ the interface flattens through the effect of the elastic force. The interface dynamics described by (I.3.3) and (I.3.15) are thus radically different. While (I.3.3) can be thought of as the dynamics of an interface that separates two equivalent phases, (I.3.15) describes an *out-of-equilibrium* situation where one phase (the one below the interface) is favored compared to the other one. This is precisely for the purpose of describing such physical situations that (I.3.15) was first introduced in the seminal paper [33]. While in (I.3.3) all the complexity comes from the fact that the disorder is static, in (I.3.15) the complexity comes from the presence of the non-linear term that makes the problem an out-of-equilibrium problem. Indeed, without the non-linear term, solving (I.3.15) is trivial since the equation is linear in h_{tx} .

c Introduction to KPZ universality in 1 + 1d

At least in 1 + 1d (i.e. $N = 1$) the equation (I.3.15) is believed to represent an important universality class of out-of-equilibrium *local* growth processes sharing the following properties [34]

1. The interface is elastic, of the short-range type such as $(\nabla_x)^2 h$ in (I.3.15).
2. The growth rate at x is non-linear in the local slope $(\nabla_x h)$ and thus favors one phase, as $(\nabla_x h)^2$ in (I.3.15).
3. The interface is subjected to thermal fluctuations, i.e. $V(t, x)$ in (I.3.15) has short-range correlations.
4. There is no quenched disorder in the system.

The importance of the KPZ universality class goes however well beyond growth processes (for recent review see [34, 35, 36]). One example is also that as we showed, it is equivalent to the static problem of a DP at a finite temperature T (hence although the KPZ equation does describe an out-of-equilibrium situation, it is fair to say that it is a rather peculiar one). In the special case $N = 1$ which will be the focus of Chapter III, much is known about the problem and the associated universality. Let us recall here a few important features of this universality class (that will be proved in specific models in Chapter III). Noting $v_\infty(\varphi) = \lim_{t \rightarrow \infty} \frac{1}{t} h(t, x = \varphi t)$ ¹ (the non universal, deterministic asymptotic growth speed of the interface) for $h(t, x)$ an interface growing from an initial profile $h(t = 0, x) = h_0(x)$ with a growth process in the 1 + 1d KPZ universality class, we have

¹The ballistic scaling in this definition can be expected from the non-disordered case, e.g. starting from an initial condition $Z_{t=0}(x) = \delta(x)$ we obtain $Z_t(x) \sim \frac{1}{\sqrt{t}} e^{-\frac{x^2}{2Tt}}$ and taking the log one obtains $h(t, x) \sim t \frac{x^2}{2T^2 t^2}$.

Scale invariance and universality of critical exponents

The centered profile

$$\underline{h}(t, x) := h(t, x) - tv_\infty(x/t), \quad (\text{I.3.16})$$

has large time fluctuations such that for $t \gg 1$ and $\forall b, t, x$, we have the equality in law

$$\underline{h}(t, x) \sim b^{-\alpha} \underline{h}(b^z t, bx), \quad (\text{I.3.17})$$

with the *universal exponents*

$$\alpha = 1/2 \quad , \quad z = 3/2. \quad (\text{I.3.18})$$

The critical exponent α is the roughness exponent of the interface. Note that it is equal to the roughness exponent of a Brownian motion. The critical exponent z is the dynamic exponent. Note that going back to the DP language amounts to taking $x \rightarrow u$ and $t \rightarrow x$: in this language the roughness exponent of the DP $u \sim x^{\zeta_s}$ is thus $\zeta_s = 1/z = 2/3$ as already announced. Using (I.3.17), one obtains, for $t \gg 1$ and $\forall x$

$$\overline{(\underline{h}(t, x) - \underline{h}(0, 0))^2} = |x|^{2\alpha} \mathcal{G}_1\left(\frac{t}{|x|^z}\right) = t^{2\beta} \mathcal{G}_2\left(\frac{t}{|x|^z}\right). \quad (\text{I.3.19})$$

Where the choice of the writing is a matter of taste and $\mathcal{G}_1(y)$ are two scaling functions related by $\mathcal{G}_1(y) = y^{2\beta} \mathcal{G}_2(y)$,

$$\beta = \alpha/z = 1/3 \quad (\text{I.3.20})$$

is the *growth exponent*, often measured in numerics, $\mathcal{G}_1(y) \sim_{y \rightarrow 0^+} cst$ and $\mathcal{G}_1(y) \sim_{y \rightarrow \infty} y^{2\alpha/z}$. Note finally that, even if one takes $V(t, x)$ in (I.3.15) as a GWN, there is no simple way to see that the exponents (I.3.18) are the true critical exponents of the KPZ universality class and that the equality in law (I.3.17) holds: the KPZ equation is not invariant by rescaling (I.3.18) and is certainly *not* the FP of its own universality class. This will be further discussed in Chapter III.

Universality beyond critical exponents: universality of fluctuations

The following convergence in law holds

$$\lim_{t \rightarrow \infty} \frac{\underline{h}(t, 0)}{t^{\frac{1}{3}}} = \lambda X, \quad (\text{I.3.21})$$

where λ is a non-universal constant and X is a RV whose distribution is *universal and depends only on some global properties of the boundary conditions*. The classification of ‘sub-universality’ classes corresponding to boundary conditions is probably still not complete (but almost, see [34]) but a few robust examples are: (i) starting from ‘droplet’ initial condition, i.e. $h_0(x) = -w|x|$ with $w \rightarrow \infty$, leads to X distributed with the Tracy-Widom GUE distribution, corresponding to the (rescaled) probability distribution function of the largest eigenvalue of a random matrix in the GUE ensemble [37]; (ii) starting from flat initial condition, i.e. $h_0(x) = 0$, leads to X distributed with the Tracy-Widom GOE distribution, the distribution of the largest eigenvalue

of a random matrix in the GOE ensemble [38]; (iii) starting from a stationary initial condition (see Chapter III) leads to X distributed with the Baik-Rains distribution [39]. Note that in the DP language (I.3.21) means that the fluctuations of the DP free-energy scale with the length as $L^{1/3}$ and are distributed according to the same distributions.

Other remarkable known universal properties of the KPZ universality class in $1 + 1d$ will be reviewed in Chapter III. Let us close this section by mentioning that the theoretical knowledge of this remarkable universality is due to the existence of various models in the $1 + 1d$ KPZ universality class that possess *exact solvability properties*. This notably includes the usual continuum KPZ equation itself as we will recall but our focus in this thesis will be on *discrete exactly solvable models of directed polymers on the square lattice*.

I.4 Experimental realizations

In this chapter we introduce a few of the physical systems for which a description by a disordered elastic interface has been proposed. They all have in common the fact that, at a mesoscopic scale in some regimes, they can be described by an interface with different elastic behaviors which look rough and exhibit complex fluctuations. They can however be regrouped in two different classes. In Sec. I.4.1 we will give examples of interfaces pinned by quenched disorder, at or close to equilibrium (more precisely such that if no force acts on the system the interface is at rest). They will be described by various types of elasticities and disorder. In Sec. I.4.2 on the other hand we will give examples of growing interfaces that are fundamentally out of equilibrium: they grow indefinitely. We will present interfaces whose large scale dynamics is believed to be captured by the standard KPZ universality class in $d = 1 + 1$.

I.4.1 Disordered elastic systems pinned in a quenched random environment

a Domain walls in magnetic systems and Barkhausen noise

Considering a piece of ferromagnetic material of dimension $D \geq 2$ below its Curie temperature, it is known that a variety of static and dynamic properties of the material can be understood at a coarse grained level by describing only the *domain walls* (DW) between several domains of constant magnetization. If impurities are present in the material (without destroying the ferromagnetic order) and that the deformations of the DW are small (e.g. at sufficiently low temperature) it is possible to describe the domain wall by a simple elastic interface in a disordered medium without overhangs [40, 22, 41, 29] as in (I.1.1) with $d = D - 1$ and $N = 1$. Preparing the sample at low-temperature such that there are a few domain walls, the pinning of the domain walls by the disorder will make inhomogeneities in the magnetization persist. If the disorder is made of random magnetic impurities it will naturally be of the random bond type, but random field type disorder can also be studied in antiferromagnetic systems with random impurities under a constant field (see [9] and references therein). The elasticity

of the domain wall is naturally short-range ($\gamma = 2$) as the energy cost of creating a domain wall is local and proportional to the area of the domain, but under certain conditions it is known that long-range elastic interactions can be relevant (see below). From this point a variety of situations can be investigated, in particular the static properties of the domain wall and its dynamics under an external magnetic field.

In some experimental situations it is possible to directly visualize the domain walls and to investigate properties such as the roughness of the interface or its response to an external force. In particular in [29] the authors investigated the so-called creep-regime of a domain wall in an effectively two-dimensional ferromagnetic material ($D = 2$) and investigated the so-called creep regime, that is the velocity-force characteristics of the domain-wall at very small applied force (=magnetic field). The authors obtained a remarkable confirmation of the so-called creep law discussed above (I.3.9), and also measured the roughness exponent of the domain-wall as $\zeta \simeq 0.69 \pm 0.07$, corresponding well to the theoretical exact value of the static roughness exponent of a directed polymer ($d = N = 1$) in a RB disorder with SR elasticity $\zeta_s = 2/3$.

The influence of the physics of domain walls has however also direct consequences on macroscopic properties of the sample. An important example is linked to the notion of *Barkhausen noise*. Applying a slowly increasing magnetic field to a magnetic sample, the magnetization increases following the hysteresis curve. The increase in magnetization is however non-smooth and proceeds by jumps. These can directly be measured (see [42, 43]), and the first experimental report of the existence of this noisy signal is due to H. Barkhausen in [44]. Research on this process has led to distinguish two classes of magnets: (i) hard magnets, characterized by a ‘wide’ hysteresis curve; (ii) soft magnets, characterized by ‘small’ hysteresis curve. In the first class, the microscopic origin of the Barkhausen noise is attributed to the coherent reversal of domains of magnetizations. In the second class, the Barkhausen noise is attributed to the motion of domain walls which alternate periods where they are pinned for a long time by impurities, and period of fast motion where they jump from pinning configurations to pinning configurations. Plotting the magnetization as a function of time $M(t)$, the latter exhibits a so-called *avalanche dynamics* characterized by jumps $M(t + \Delta t) - M(t) = S$ interrupted by ‘long’ ($\gg \Delta t$) periods of quiescence. Following the domain wall interpretation for the origin of these jumps, the size S of the jumps of the magnetization are directly proportional to the volume (for samples in $D = 3$) swept by the DW during its motion. It was found (see [45, 46] and references therein) that the distribution of jumps S and time T are power law distributed in between two (widely separated) cutoffs:

$$P(S) \sim S^{-\tau_S} \quad , \quad P(T) \sim T^{-\alpha} . \quad (\text{I.4.1})$$

As we will see in Sec. II.3.2, these power-laws were argued to be related to the critical exponents of the interface at the depinning transition, and thus such measurements give access to properties of the interface (and vice versa). In Barkhausen experiments two universality classes for soft magnets in $D = 3$ were found [45, 46]: (i) polycrystalline materials for which the exponents depend on the driving rate and for which the exponent at slow driving are $\tau_S \simeq 3/2$. In this class it was argued that due to the

presence of dipolar interactions, the elasticity of the domain-walls are effectively long-range with $\gamma = 1$ [47]. Taking a look at the phase diagram in Sec. I.2.3, although here we are not in a static situation, we see that these systems have $d = 2 = 2\gamma = d_{uc}$: they sit right at the upper-critical-dimension of the problem. We will see in the following that the above exponents are indeed the mean-field exponents of avalanche motion. (ii) amorphous materials, for which the empiric exponents are $\tau_S \simeq 1.27$ and $\alpha \simeq 1.25$, independently of the driving rate, and for which the elasticity of the domain wall is short-range.

b Fractures fronts in brittle materials

Another physical process for which the model of an elastic interface has been used is for the fracture of brittle materials (see [48] for a review). Indeed it has been argued that for these systems the propagation of the crack front can be understood as the zero temperature over-damped dynamics of a line with long-range elasticity ($d = \gamma = 1$) [49, 50, 51, 52] in a disordered medium. The fracture proceeds again by avalanches, whose statistics can be experimentally measured by acoustic techniques, or in some experimental setup by direct visualization of the crack front [53, 54, 55, 56]. The experimentally obtained value of the roughness exponent was there reported as $\zeta \sim 0.35$ on large scales, while at small scales a value of $\zeta \sim 0.63$ was reported. In these systems, due to the long-range nature of the elasticity, an avalanche at one point of the interface generally triggers several avalanches at different points and when speaking about the distribution of the size of avalanches, one has to distinguish whether the size of single avalanches or of the cluster of avalanches is measured. In [57] the distribution of the size of single avalanches was reported to have a power-law exponent of $\tau_S^{\text{ind}} \sim 1.56 \pm 0.04$.

c Some other related situations

Contact lines of fluids on rough substrates

It has been argued that the slow motion of the contact line of a fluid on a rough substrate could be well approximated by the motion of an elastic line with long-range elasticity at the depinning transition [58, 59, 60]. While some aspect of this dynamics agree (e.g. avalanches) well with the elastic interface theory, [61], the value of the experimentally measured roughness exponent $\zeta \sim 0.5$ is still not understood, although it has been argued that it could be the sign of non-linear elastic terms [62].

Earthquakes

It has been argued that some features of earthquakes and geological faults could be captured by the model of an elastic interface in a disordered medium [63, 64, 65, 66]. It is however a rather controversial issue and it is now clear that some important features of earthquakes, such as aftershocks and the Omori law [67] are not contained in *the simplest* elastic interface model. We will come back to this specific issue in Sec. II.6.1.

Vortex lattices in superconductors

Although it not a disordered elastic interface, let us mention here that features of the deformation of the vortex lattice in high- T_c superconductors ($d = 3$, $N = 2$) are similar

to those of disordered elastic interfaces. In particular it is known that the pinning of the lattice by the disorder plays an important role in high- T_c superconductivity and that a similar depinning transition is observed. See [68] for a review.

Imbibition

Let us finally mention here the problem of the invasion of a viscous fluid in a porous medium known as ‘imbibition’ where in some regime the dynamics resembles the dynamics of an elastic interface and scale invariant avalanches are also observed [69]. Some aspects of the problem are however not captured by elastic interfaces (in particular in the experimentally much studied context of so-called forced flow imbibition, the conservation of the volume of the fluid imposes the mean velocity of the fluid at all time and thus generates a complex non-local dynamics along the front). We refer the reader to [70] for a review of this related subject.

1.4.2 Out-of-equilibrium interface growth

We now give a few examples of situations where the out-of-equilibrium growth of a 1-dimensional interface was shown to display scale-invariant behavior in agreement with the $1 + 1$ -d KPZ universality class. It should be stressed here that it is easier to find in the literature experimentally observed growth processes in $d = 1 + 1$ for which the scaling behavior notably differs from the one of the KPZ universality class, see e.g. [71, 72]. This obviously does not mean that the KPZ universality class does not exist in nature, but it is true that some of its conditions are not always easy to realize experimentally (e.g. absence of quenched noise). Below we mention three convincing experiments.

a Growth of bacterial colonies and cancerous cells

Bacterial colonies growing on a Petri dish provide an experimental realization of a growing interface in $1 + 1d$. In [73] experiments on the growth of two types (B and D) of bacteria were performed. From microscopic observation it was observed that the microscopic growth mechanisms of the two types were quite different. While the type B bacteria formed long chain advancing simultaneously (thus inducing a non-local growth), for the type D bacteria the growth mechanisms were argued to be local. The found roughness exponent of the interface were found to be $\alpha_B \simeq 0.78 \pm 0.02$ and $\alpha_D \simeq 0.50 \pm 0.01$. The growth of type D bacteria was therefore argued to provide an experimental example of a growing interface in the $1 + 1d$ KPZ universality class.

More recently in another biological context, the growth of cell colonies for cancerous and non cancerous cells on Petri dishes was investigated in [74] with the aim of distinguishing both types of cells from their growth mechanisms. Although some distinguishing features were reported, both types of colonies were found to exhibit a KPZ type growth scaling with exponents measured as $\alpha \simeq 0.50 \pm 0.05$, $\beta \simeq 0.32 \pm 0.04$ and $z \simeq 1.5 \pm 0.2$.

b Burning paper fronts

Slowly burning sheets of paper also provide an example of interface growth in $1 + 1d$. In [75] this growth process was investigated for two different types of papers. The

exponents were found in good agreement with the KPZ expected values: $\alpha \simeq 0.48 \pm 0.01$ and $\beta = 0.32 \pm 0.01$.

c Liquid crystal growths

The most convincing experimental evidence of KPZ universality in growth process in $1 + 1d$ comes from recent experiments on turbulent liquid crystal [76, 77, 78, 79, 80]. This experiment is very close in spirit to the original motivation for introducing the KPZ equation [33]: the interface is a true interface between two phases (called DSM1 and DSM2) of the same system. While the microscopic properties of each phase are rather complicated, at high electric field the DSM1 phase is unstable and the growth of a nucleus of the DSM2 phase in an initially prepared liquid crystal in the DSM1 phase exhibit fluctuation statistics in amazing agreement with the KPZ theory in $1+1d$. These highly reproducible experiments indeed allowed the authors to obtain the scaling exponents $\alpha \simeq 0.5 \pm 0.05$ and $\beta \simeq 0.336 \pm 0.001$, but also to exhibit strong evidence that the full rescaled fluctuations of the interface height at large time converges to the GUE and GOE distributions, depending on the shape of the original nucleus of stable phase. Traces of the Baik-Rains distribution in the stationary state were also obtained.

Chapter II

Avalanches and shocks of disordered elastic interfaces

II.1 Introduction

Avalanche-type dynamics occur in a large variety of complex systems: snow avalanches, earthquakes, fracture processes in disordered materials, fluctuations in the stocks market, Barkhausen noise in magnets, avalanches in the neural activity of the brain... In a general sense, a system is said to display avalanches if its response to a slow, smooth, external loading is discontinuous and proceeds via jumps. The most interesting situation to the statistical physicist is the case where these jumps span a wide range of space and time scales. If this occurs, then one might hope that the precise underlying dynamics of each system is mostly (except e.g. symmetries, etc) unimportant at large scales, i.e. that avalanche processes display some *universality*. In fact such systems do exist in nature, and the experimental and theoretical analysis of systems and models displaying avalanches has created a large research activity over the past decades [81]. Some key conceptual frameworks on the theoretical side have been the analysis of avalanches in (i) cellular automaton models exhibiting *Self-Organized-Criticality* [82], as e.g. the Manna sandpile model [83] and the Abelian sandpile model [84], see [85] for a review; (ii) the random field Ising model [86, 87, 88] and the mean-field spin glass SK model [89, 90]; (iii) models related to the concept of marginal stability [91]; (iv) disordered elastic systems.

In this part of the manuscript we will review some known results on avalanches (and the closely related notion of shocks) in disordered elastic interfaces. Understanding avalanche processes in this type of systems is an important issue. Indeed on one hand it is known that the model of an elastic interface in a disordered medium is relevant to describe a variety of physical situations (see Sec. I.4), and therefore on the theoretical side it is a perfect candidate to understand universality in some avalanche processes. On the other hand disordered elastic systems permit the use of a variety of existing analytical techniques. Theoretical progresses on this type of system are thus already possible and understanding them is a good starting point for other problems. For example it was recently argued that the Manna sandpile model is in the same universality class as the depinning of an interface in a short-range disordered medium [92],

or that the yielding transition in amorphous solids share some interesting properties with the depinning transition [93] (although it is in a different universality class, in particular there is an additional independent critical exponent).

The outline of this section is as follows: In Sec. II.2 we introduce the notion of shocks and avalanches in toy models of a particle on the real line ($d = 0$ elastic interfaces). These notions are generalized to the case of interfaces in Sec. II.3. There we review the phenomenology associated with avalanches, in particular we discuss their scaling. In Sec. II.4 and Sec. II.5 we review the functional renormalization group approach to the statics and to the depinning transition of disordered elastic interfaces, with an emphasis on its application to the study of shocks and avalanches. Finally in Sec. II.6, we will review some important results on avalanches in disordered elastic interfaces, and summarize the results obtained during the thesis on this subject. These are presented more thoroughly in the original research papers [1, 2, 3] reproduced in Appendix A B C.

II.2 Introduction: the avalanche process(es) of a particle on the real line

In this section we begin our study of avalanche processes of elastic interfaces by studying toy models in $d = 0$, i.e. a particle on the real line in a disordered medium. This analysis will prove relevant when discussing the avalanche processes of true elastic interfaces as a basis on which we will build some intuition on shocks and avalanches processes. In Sec. II.2.1 we introduce the notion of shocks and in Sec. II.2.2 we introduce the notion of avalanches. We will conclude by comparing these two notions in Sec. II.2.3

II.2.1 Shocks between ground states for toy models of a particle without disorder

In this section we introduce the notion of shocks using toy models of a particle in a deterministic potential V exhibiting several local minimas as would a true disorder potential. We study this simple case in order to maximize the clarity of the exposition. Exact results can also be obtained for models of shocks for a particle in a random potential: this includes the case of $V(u)$ taken with the correlations of a Brownian motion (the Sinai model [94], a toy-model for the random field universality class of elastic interfaces) or with short-range correlations (that corresponds to the Kida problem in the context of Burgers's turbulence [95] and to a toy-model for the random bond universality class for elastic interfaces). We refer the reader to [96] and references therein for exact results on these models, and we now begin our study of shocks.

a Shocks for a particle in a cosine potential

We consider the toy model of a particle on the real line $u \in \mathbb{R}$ subject to a cosine potential $V(u) = \cos(u)$ and to a confining potential $\frac{1}{2}m^2(w-u)^2$. The total Hamiltonian

of the particle is

$$\mathcal{H}_w[u] := \cos(u) + \frac{1}{2}m^2(w - u)^2 . \quad (\text{II.2.1})$$

The ‘disorder potential’ $V(u)$ has an infinite number of exactly degenerate minima at $u_k = \pi + 2\pi k$, $k \in \mathbb{Z}$. For $m \neq 0$, the confining potential $\frac{1}{2}m^2(w - u)^2$ breaks this degeneracy, except at some special points w_k (the points where $V(w)$ is maximum, that is when $w_k = 2\pi k$, $k \in \mathbb{Z}$) and the ground state

$$u(m; w) := \operatorname{argmin}_{u \in \mathbb{R}} \mathcal{H}_w[u] , \quad (\text{II.2.2})$$

is well defined except in this discrete set of points. Graphically the position of the ground state of the system can be obtained using the so-called ‘Maxwell construction’: for a given w with a non-degenerate ground state $u(m, w)$ with energy $E(m, w)$, by definition, $V(u) > E(m, w) - \frac{1}{2}m^2(u - w) \forall u \neq u(m, w)$, with the equality at $u = u(m, w)$. Hence, $\forall C < E(m, w)$, the parabola $C - \frac{1}{2}m^2(u - w)$ does not intersect $V(u)$. Increasing C from $-\infty$, the position of the ground state $u(m, w)$ is given by the abscissa of the first point of intersection of the parabola $C - \frac{1}{2}m^2(u - w)$ with $V(u)$ (see Fig. II.1). For large m , the ground state $u(m; w)$ closely follows w and $u(m; w)$ is smooth as a function of w . For m small enough, at the point $w = w_k$, the ground state of the system is degenerate between one point $u^+(m; w)$ that is close to u_k , and $u^-(m, w)$, that is close to u_{k-1} . The critical value where this degeneracy first occurs satisfies the equation $\frac{1}{2}m_c^2 = \frac{1}{2} \frac{d^2V(u)}{du^2} \Big|_{u=0} = \frac{1}{2}$, that is $m_c = 1$. As $m \rightarrow 0$, it is trivial to see that $u^+(m; w)$ converges to u_k and $u^-(m; w)$ converges to u_{k-1} . We obtain

$$\begin{aligned} \lim_{m \rightarrow 0} u(m; w) &= \sum_{k \in \mathbb{Z}} \theta(w - w_k) \theta(w_{k+1} - w) u_k \\ &= u_{-1} + \sum_{k=0}^{+\infty} \theta(w - w_k) S_k \quad \text{for } w > 0 . \end{aligned} \quad (\text{II.2.3})$$

Here θ denotes the Heaviside theta function, and in the second line we have introduced the size of the k^{th} shock $S_k = u_k - u_{k-1}$. In this simple model these are of course all equal to $S_k = S = 2\pi$ and $u_{-1} = -\pi$. The above formulae are ambiguous at the shock points $w = w_k$ since precisely at these points the ground state is degenerate, and thus $u(m; w)$ is ill defined. This is resolved by using e.g. the convention that $u(m, w)$ is left continuous. At small, but non-zero m , $m \ll m_c$, the shock process gets slightly modified, as $u(m; w)$ is not exactly constant between w_k and w_{k+1} . Small m corrections are given by, for $w_k < w < w_{k+1}$,

$$u(m; w) = u_k + m^2 \delta u_k(w) + O(m^4) \quad , \quad \delta u_k(w) := w - u_k . \quad (\text{II.2.4})$$

Let us now discuss the influence of the temperature in a toy model of a particle in a double-well potential.

b Smoothing of the shocks by the temperature

We now consider a particle on the real line $u \in \mathbb{R}$ at equilibrium at a finite temperature $T > 0$ in a double well potential $V(u) = -\frac{u^2}{2} + \frac{u^4}{4}$ and subject to a confining potential

$\frac{1}{2}m^2(w - u)^2$. The Hamiltonian is

$$\mathcal{H}_w[u] = -\frac{u^2}{2} + \frac{u^4}{4} + \frac{1}{2}m^2(w - u)^2. \quad (\text{II.2.5})$$

And we consider the average position of the particle:

$$u(m, T; w) := \frac{\int_{-\infty}^{\infty} ue^{-\frac{1}{T}\mathcal{H}_w[u]}}{\int_{-\infty}^{\infty} e^{-\frac{1}{T}\mathcal{H}_w[u]}}. \quad (\text{II.2.6})$$

First note that in the limit $m \rightarrow 0$, we obtain $\lim_{m \rightarrow 0} u(m, T; w) = 0$. On the other hand, taking first the zero temperature limit we obtain, for m sufficiently small $m \leq m_c = 1$,

$$\lim_{T \rightarrow 0} u(m, T; w) = \theta(w)u^+(m) + \theta(-w)u^-(m) \quad (\text{II.2.7})$$

with for $m \ll m_c$,

$$u^+(m, w) = 1 + \frac{m^2}{3}(w - 1)^3 + O(m^4) \quad , \quad u^-(m, w) = -1 + \frac{m^2}{3}(w + 1)^3 + O(m^4). \quad (\text{II.2.8})$$

Let us now consider the limit T small but non zero, with $m \leq m_c$ fixed. The integrals in (II.2.6) are dominated by two saddle-points at $u^-(m, w)$ and $u^+(m, w)$. One easily obtains, noting $\Delta E(m, w) := \mathcal{H}[u^+(m, w)] - \mathcal{H}[u^-(m, w)]$ the difference of energy between the right minimum and the left minimum,

$$u(m, T; w) = \frac{\text{sign}(u^+(m, w))e^{-\frac{1}{T}\Delta E(m, w)} + \text{sign}(u^-(m, w))}{\frac{1}{|u^+(m, w)|}e^{-\frac{1}{T}\Delta E(m, w)} + \frac{1}{|u^-(m, w)|}} + O(1/\sqrt{T}) \quad (\text{II.2.9})$$

Taking now the small m limit on this expression we obtain

$$u(m, T; w) \simeq \tanh\left(\frac{m^2w + O(m^4)}{T}\right) + O(1/\sqrt{T}). \quad (\text{II.2.10})$$

In particular, one retrieves for large $|w|$ or for small temperature the shock limit (II.2.7). For non-zero T , the shock is smoothened on a scale

$$w_T \sim \frac{T}{m^2}. \quad (\text{II.2.11})$$

Read differently, the shock is smoothened on small scales when the energy difference between the two minima $\sim m^2w$ is smaller than the thermal energy $\sim T$. Note that the height of the barrier of potential between the two minima does not play a role in this problem.

II.2.2 Avalanches in the dynamics of a particle on the real line

In this section we now discuss the notion of avalanches in the zero temperature overdamped dynamics of a particle. We first consider the case of a particle in an abstract force landscape $F(u)$, and then recall some features of the very instructive exact solution of the Alessandro-Beatrice-Bertotti-Montorsi (ABBM) model where the force $F(u)$ is a Brownian motion. We refer the reader to [97] for the study of other cases.

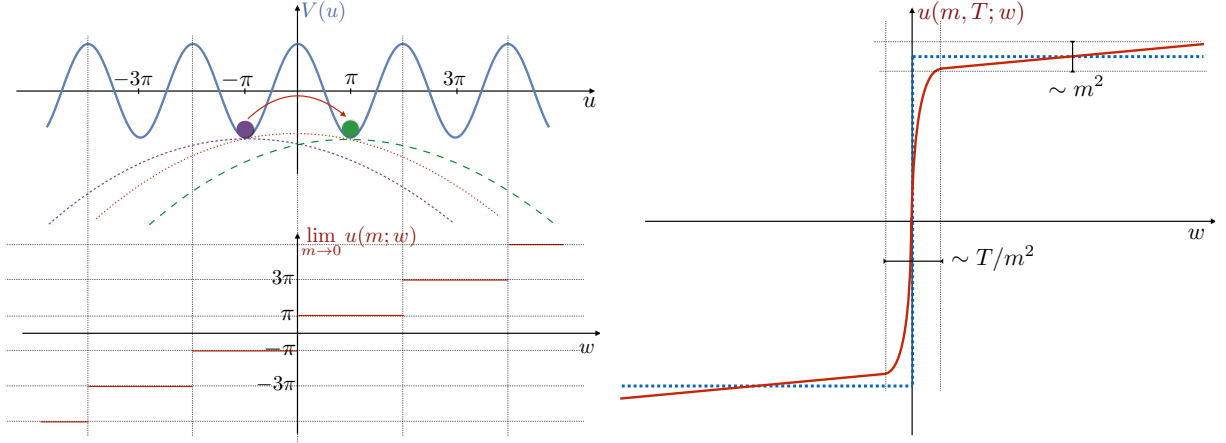


Figure II.1: Left: Shock process for a particle at zero temperature in a cosine potential. Left-up: The Maxwell construction allows to graphically find the position of the minimum of $V(u) + \frac{1}{2}m^2(u - w)^2$ for $m \neq 0$: the parabola $-\frac{1}{2}m^2(u - w)^2$ is raised until it intersects $V(u)$. The point of intersection corresponds to the position of the minimum. For $-2\pi < w < 0$ (resp. $0 < w < 2\pi$), the minimum is at $-\pi$ (purple dot) (resp. $+\pi$, green dot) (up to $O(m^2)$ corrections). At $w = 0$ (red dotted parabola) the minimum is degenerate. Left-bottom, the jump process obtained from the above picture in the limit $m \rightarrow 0$. Right: smoothening of a perfect shock for a particle in a double-well potential by non-zero T and m in the limit $T \ll m^2$ and $m \ll m_c$.

a The avalanche process of a particle in a smooth force landscape $F(u)$.

Let us thus consider the over-damped dynamics of a particle in a force landscape $F(u)$. Here we typically have in mind the case $F(u) = a(u)\sin(b(u)u)$ with $a(u)$ and $b(u) > 1$ some smooth bounded functions: the force landscape has a lot of minims and does not wander too far away from zero (see Fig. II.2). The temperature is 0 and similarly to the static problem, we consider the over-damped dynamics of a particle driven by a parabolic well at a constant velocity $v > 0$:

$$\eta \partial_t u_t = m^2(vt - u_t) + F(u_t) . \quad (\text{II.2.12})$$

Let us suppose that at $t = 0$ the particle is at rest and sits in a stable minima of its energy landscape: $u_{t=0} = u_0$ with

$$m^2 u_0 = F(u_0) \quad , \quad m^2 - F'(u_0) > 0 . \quad (\text{II.2.13})$$

Now, note that since $F(u)$ is continuous, it is clear from (II.2.12) that u_t is \mathcal{C}^1 and

$$\forall t \geq 0 \quad , \quad \partial_t u_t \geq 0 . \quad (\text{II.2.14})$$

This allows to make the change of variable $u(v, m; w) = u_{t=w/v}$. Plugging it into (II.2.12) one obtains

$$\eta v \partial_w u(v, m; w) = m^2(w - u(v, m; w)) + F(u(v, m; w)) . \quad (\text{II.2.15})$$

Hence taking the limit $v \rightarrow 0$, the *quasi-static process*

$$u(m; w) := \lim_{v \rightarrow 0} u(v, m; w) = \lim_{v \rightarrow 0} u_{t=w/v}, \quad (\text{II.2.16})$$

satisfies

$$0 = m^2(w - u(m; w)) + F(u(m; w)). \quad (\text{II.2.17})$$

Of course, $\forall v > 0$, the function $u(v, m; w)$ is \mathcal{C}^1 as a function of w . However, the limit $v \rightarrow 0$ can be singular, and indeed as in the case of shocks in the statics, if m is sufficiently small $m < m_c$ (the latter being now given by $m_c^2 = \max_u F'(u)$), the quasi-static process $u(m; w)$ can exhibit discontinuities as a function of w . The classic construction of $u(m; w)$ is given in red in Fig. II.2: starting from $u(m; 0) = u_0$, it is obtained by following whenever possible the root of (II.2.17) (hence $u(m; w)$ is left continuous, $\forall w > 0$, $u(m; w^-) = \lim_{\delta w \rightarrow 0^+} u(m; w - \delta w) = u(m; w)$), or when not possible at some w_k with $k \in \mathbb{N}$, $u(m; w_k^+) = \lim_{\delta w \rightarrow 0} u(m; w_k + \delta w)$ is given by the smallest root of (II.2.17) that is larger than $u(m; w_k^-)$. At these points of discontinuity the quasi-static process makes a jump $S_k = u(m; w_k^+) - u(m; w_k^-)$ that we call an avalanche. Following similar arguments as before for the case of shocks in the statics, it is clear that in the limit $m \rightarrow 0$, this process becomes a pure jump process

$$u^{\text{jump}}(w) := \lim_{m \rightarrow 0} m^{-\zeta} u(m; m^{-\zeta} w) = u_0 + \sum_{k=0}^{\infty} \theta(w - w_k) S_k. \quad (\text{II.2.18})$$

Here we have introduced the *roughness exponent* $\zeta \geq 0$. The latter accounts for the fact that in general, e.g. for the case of a random process $F(u)$, the jumps become rarer and bigger as $m \rightarrow 0$. In the case of shocks in the periodic potential, we had $\zeta = 0$ precisely because the potential was periodic and in the limit $m \rightarrow 0$ only one shock occurred per period of the potential, with its size being equal to the period. Scaling u and w by ζ in (II.2.18) allows us to obtain a non-trivial jump process in the limit. The value of ζ depends on the precise properties of $F(u)$ and is therefore non-universal. Why this exponent is called ζ , i.e. how it is related to the roughness exponent for interfaces, will become clearer in the next section. In the following we will set $\zeta = 0$ for simplicity but the discussion can be repeated with $\zeta \geq 0$.

Let us now come back to the time process u_t and draw some conclusions on the dynamics of the particle. Between jumps, $w_k < w < w_{k+1}$, $\partial_w u^{\text{jump}}(w) = 0$. Inverting the derivative and the limits with $t = w/v$ we obtain,

$$0 = \partial_w u^{\text{jump}}(w) = \lim_{m \rightarrow 0} \lim_{v \rightarrow 0} \frac{1}{v} \partial_t u_t = 0. \quad (\text{II.2.19})$$

Hence between jumps, in the successive limit $v \rightarrow 0$ and (= then) $m \rightarrow 0$ the velocity of the particle is *not* of order v . Rather it is $o(v)$. Let us now ‘zoom in’ around the k^{th} jump and look at a window around t_k , i.e. $t_k < t < w_k/v + \Delta t$ with by definition $\Delta t = o(1/v)$ since this smooth process happens during a time scale that is not captured by the jump process (II.2.18). Since this process happens on such a short-time scale, we

can forget during the jump that the well keeps moving and approximate $vt \sim w_k + o(1)$ and the dynamics during the jump is given by

$$\eta \partial_t u_t = m^2(w_k - u_t) + F(u_t) + o(1) \quad (\text{II.2.20})$$

At $t = 0$ the right hand-side is approximately equal to $m^2(w_k - u(m; w_k)) + F(u(m; w_k)) = 0$, but here this equilibrium point is unstable since a jump occurs. After a short transient time of order $\tau_m = \eta/m^2$, the right hand-side is soon of order 1 and in the limit of small m , it is dominated by the force $F(u)$. Hence during the jump the velocity of the particle is of order 1 and the jump occurs on a time scale of order 1. This discussion highlights a characteristic feature of the temporal dynamics of the avalanche process we are interested in. Although it is clear that, since $F(u)$ is bounded, the mean velocity (here mean refers to the average over space) of the particle is equal to v (i.e. $\lim_{t \rightarrow \infty} \frac{u_t - u_0}{t} = v$), the dynamics is *intermittent*. Most of the time the particle is actually pinned by disorder and its velocity is $o(v)$ (if one again uses a notion of probability by taking a random time t this occurs with a probability of order 1), and from time to time the particles is in an avalanche and its velocity is of order 1 (this occurring with probability $O(v)$). This is quite different for a smooth motion (obtained e.g. either by taking $F \rightarrow 0$ or $v \rightarrow \infty$) for which one expects to observe the velocity of the particle to be of order v with probability 1. These considerations will become clearer in the ABBM model.

b The ABBM model.

Let us now study our first true random process and consider the ABBM model. A possible definition of the latter is the stochastic process

$$\eta \partial_t u_t = m^2(vt - u_t) + F(u_t) , \quad (\text{II.2.21})$$

with the initial condition $u_{t=0} = 0$ and the force $F(u)$ is a one-sided (i.e. $F(0) = 0$) Brownian-motion (BM) with correlations

$$\overline{(F(u') - F(u))^2} = 2\sigma |u - u'| . \quad (\text{II.2.22})$$

This is one definition of the so-called Alessandro-Beatrice-Bertotti-Montorsi (ABBM) model. It was first introduced as a phenomenological model to describe Barkhausen noise [98, 99]. In this context u_t denotes the measured magnetization of the disordered magnetic sample under the applied magnetic field $\sim vt$. It was later argued, first on phenomenological grounds [100], then from first principles using FRG [101] that it correctly describes the avalanche of the center of mass of realistic interfaces at the depinning transition at the mean-field level. The model presents the peculiarity of being in some sense exactly solvable and a lot of exact quantities can be computed (see [42, 43] for a review). We will not recall them all here, but only focus on analyzing the exact results for the stationary velocity distribution and for the avalanche size distribution to highlight in a more concrete model some of the considerations of the previous section.

To simplify the discussion first note that, using the scale invariance of the BM, (II.2.17) can almost be entirely rescaled so that all parameters are equal to 1. Indeed,

introducing $S_m := \sigma/m^4$ and $\tau_m := \eta/m^2$, rescaling $u_t = S_m \tilde{u}_{\tilde{t}}$, $t = \tau_m \tilde{t}$, noting $\tilde{v} = v/v_m$ with $v_m = S_m/\tau_m$, one obtains in these dimensionless units

$$\partial_t u_t = vt - u_t + F(u_t) \quad (\text{II.2.23})$$

where here we have dropped the tildes and now $F(u)$ is a one-sided Brownian-Motion (BM) with correlations $\overline{(F(u') - F(u))^2} = 2|u - u'|$.

Stationary velocity distribution

The stationary distribution of the velocity of the particle was already obtained in the original paper of ABBM [98]. At long time $t \gg \tau_m$, the probability distribution function (PDF) of the velocity of the particle $\dot{u}_t := \partial_t u_t$ is stationary and equal to

$$P(v; \dot{u}) = \frac{1}{\Gamma(v)} (\dot{u})^{-1+v} e^{-\dot{u}} \theta(\dot{u}), \quad (\text{II.2.24})$$

where $\Gamma(v)$ is the Euler's Gamma function. As expected the mean-velocity of the particle is equal to v : $\int_0^\infty \dot{u} P(v; \dot{u}) = v$. The behavior of the PDF (II.2.24) is however completely different depending on whether $v > v_m = 1$ or $v < 1$. For $v > 1$, $P(v; \dot{u} = 0) = 0$: in the stationary state the particle is never pinned by the potential. In this phase the PDF $P(v, \dot{u})$ is maximum for $\dot{u} = v - 1$ and both the most probable velocity and the mean velocity are of order $O(v)$: the motion of the particle is more or less smooth and the particle mostly follows the imposed driving. On the other hand when $v < 1$, $P(v; \dot{u} = 0) = +\infty$ and there is an accumulation of the probability at 0: the particle is almost always at rest. In the limit $v \rightarrow 0$, in the sense of distribution, $\lim_{v \rightarrow 0} P(v; \dot{u}) = \delta(\dot{u})$. At $\dot{u} = O(1)$ fixed on the other hand

$$P(v; \dot{u}) = v \hat{\rho}(\dot{u}) + O(v^2) \quad , \quad \hat{\rho}(\dot{u}) := \frac{1}{\dot{u}} e^{-\dot{u}}. \quad (\text{II.2.25})$$

While $\hat{\rho}(\dot{u})$ is not normalizable, i.e. $\hat{\rho}_0 = \int \hat{\rho}(\dot{u}) = +\infty$, it controls all the moments of $P(v; \dot{u})$. To see this, it is useful to consider the Laplace transform of $P(v; \dot{u})$, defined as, for $\lambda < 1$,

$$\begin{aligned} \int_0^\infty d\dot{u} e^{\lambda \dot{u}} P(v; \dot{u}) &= e^{-v \log(1-\lambda)} = e^v \int_0^\infty d\dot{u} (e^{\lambda \dot{u}} - 1) \hat{\rho}(\dot{u}) \\ &= 1 + v \int_0^\infty d\dot{u} (e^{\lambda \dot{u}} - 1) \hat{\rho}(\dot{u}) \\ &\quad + \frac{v^2}{2} \int_0^\infty \int_0^\infty d\dot{u}_1 d\dot{u}_2 (e^{\lambda \dot{u}_1} - 1) (e^{\lambda \dot{u}_2} - 1) \hat{\rho}(\dot{u}_1) \hat{\rho}(\dot{u}_2) + \dots \end{aligned} \quad (\text{II.2.26})$$

Now, if $\hat{\rho}_0$ defined above was finite, we could define a normalized probability distribution $P_{\text{ava}}(\dot{u}) := \frac{\hat{\rho}(\dot{u})}{\hat{\rho}_0}$ and the above equality could be rewritten

$$\int_0^\infty d\dot{u} e^{\lambda \dot{u}} P(v; \dot{u}) = \sum_{m=0}^\infty \frac{(\hat{\rho}_0 v)^m}{m!} e^{-\hat{\rho}_0 v} \int d\dot{u}_1 \dots d\dot{u}_m e^{\lambda(\dot{u}_1 + \dots + \dot{u}_m)} P_{\text{ava}}(\dot{u}_1) \dots P_{\text{ava}}(\dot{u}_m). \quad (\text{II.2.27})$$

Proving explicitly that (II.2.26) can be resummed into (II.2.27) if $\hat{\rho}_0$ is finite is not complicated. A similar equality is shown in Appendix D of [1] (see Appendix A). The

formula (II.2.27) can equivalently be rewritten

$$P(v; \dot{u}) = \sum_{m=0}^{\infty} \frac{(\hat{\rho}_0 v)^m}{m!} e^{-\hat{\rho}_0 v} \underbrace{(P_{\text{ava}} \star \cdots \star P_{\text{ava}})}_{m \text{ times self-convolution of } P_{\text{ava}}}(\dot{u}) \quad (\text{II.2.28})$$

The interpretation of this formula is as follows. At each time, the velocity \dot{u} of the particle is the sum of m velocities that are independently drawn from $P_{\text{ava}}(\dot{u})$. $P_{\text{ava}}(\dot{u})$ is thought of as the PDF of the velocity during an avalanche, and m is the number of active avalanches at an arbitrary time t . The latter is drawn from a Poisson distribution with intensity $\hat{\rho}_0 v$. Thus in the ABBM model, avalanches are independent from one another. This is characteristic of a Lévy jump process. One of the question tackled in this thesis is to understand if this independence property is also true for models of interfaces in a short-range random force landscape (we will see that it is not!). Taking the limit $v \rightarrow 0$ of (II.2.28) we obtain

$$P(v; \dot{u}) = (1 - \hat{\rho}_0 v) \delta(\dot{u}) + \hat{\rho}_0 v P_{\text{ava}}(\dot{u}) + O(v^2). \quad (\text{II.2.29})$$

This is the picture of avalanche motion that was described in the last section. At small v the particle does not move at all with a probability close to 1, and sometimes move (with a probability of order v) at a velocity of order 1. For the ABBM model, we note that $\hat{\rho}_0$ is infinite and the previous interpretation is a bit tedious. This is due to the scale invariance of the BM even at small scales: the particle is never truly pinned in a typical realization of the BM and it always makes microscopic jumps, formula (II.2.29) does not truly hold. For a realistic model with a smooth disorder at small scale (II.2.29) will truly hold. Even in the ABBM model however, this interpretation holds at the level of the moments as seen using (II.2.27). In particular

$$\begin{aligned} \int_0^{\infty} d\dot{u} (\dot{u})^n P(v; \dot{u}) &= \frac{\Gamma(v+n)}{\Gamma(v)} = v \times (v+1) \times \dots \times (v+n-1) \\ &= v(n-1)! + O(v^2) \\ &= v \int d\dot{u} \rho(\dot{u}) \dot{u} + O(v^2). \end{aligned} \quad (\text{II.2.30})$$

While for $v \gg 1$, the n^{th} integer moment is of order v^n , characteristic of a smooth motion at the typical velocity v , for $v \ll 1$ all integer moments are of order v : an avalanche occurs with probability of order v but if it does, the velocity inside the avalanche is of order 1.

Avalanche sizes

The most convenient way to define the PDF of avalanche sizes in the ABBM model is to consider a driving during a finite duration T_d (i.e. $w(t) = v\theta(T_d - t)\theta(t)$). Defining the avalanches size as the total motion of the particle $S = u(t = +\infty) - u(t = 0) = \int_0^{\infty} \dot{u}_t$, the PDF of avalanche sizes $P(S)$ was computed in [102]. The result is

$$P(S) = \frac{vT_d}{2\sqrt{\pi}S^{3/2}} e^{-\frac{(S-vT_d)^2}{4S}}. \quad (\text{II.2.31})$$

Hence, for $vT_d \ll 1$ (small driving) the PDF of avalanche size exhibits a power-law behavior $S^{-3/2}$ (this exponent was first identified in [103]) in between two cutoff scales,

a small scale cutoff $\sim \frac{(vT_d)^2}{S_m}$ and a large scale cutoff $\sim S_m$ (here $S_m = \sigma/m^4 = 1$) in dimensionless units. Since the limit $m \rightarrow 0$ can obviously be taken on the expression (II.2.31), this shows that the proper rescaling of u that we discussed earlier in the general case here corresponds to $u \rightarrow m^{-\zeta}u$ with $\zeta = 4$ for the ABBM model. The limit $vT_d \rightarrow 0$ at S fixed defines the *avalanche size density in the ABBM model*:

$$P(S) = vT_d\rho(S) + O((vT_d)^2) \quad , \quad \rho(S) := \frac{1}{2\sqrt{\pi}S^{3/2}}e^{-S/4} . \quad (\text{II.2.32})$$

As for the case of the stationary velocity distribution, the density $\rho(S)$ is not normalizable due to a divergence at small S . One could apply a similar treatment as we did before for the stationary velocity distribution and show that $P(S)$ can be rewritten in a certain sense as an infinite series of self-convolutions of $\rho(S)$ with itself, a property that defines a Lévy jump process (see also Appendix D of [1] in Appendix A). It is also possible to precisely relate $\rho(S)$ to the avalanches observed in the quasi-static dynamics (this will be shown in Sec. II.5.2), and show that the motion of the particle in the ABBM model between two points where the velocity is zero are distributed according to (II.2.32). Again the accumulation of avalanches of small sizes is due to the scale invariance of the BM. Note finally that the exponent $3/2$ can simply be understood as follows. Assume that at a time $t = 0$ an avalanche has started and the velocity of the particle is v_0 and its initial position is u_0 . Taking the limit $v \rightarrow 0$ in (II.2.21) and differentiating with respect to u we obtain

$$\frac{d\dot{u}_t}{du} = -1 + \xi(u) . \quad (\text{II.2.33})$$

Where now the velocity $\dot{u}_t = \partial_t u_t$ is seen as a function of the position of the particle u and $\xi(u)$ is a GWN. Hence the velocity of the particle performs a Brownian motion in ‘time’ u with a unit negative drift -1 . Hence the next point $u = u_0 + S$ where \dot{u}_t is 0 corresponds to the next passage time to the origin of a Brownian motion with a unit negative drift, which is indeed power-law distributed with an exponent $3/2$ (see e.g. [104]), and the unit drift provides an exponential cutoff as in (II.2.32). The exponent $\tau = 3/2$ plays an important role in avalanche statistics (recall that it is observed in some Barkhausen noise experiments [45]) and it is interesting to understand its value as a consequence of this well-known property of the BM.

II.2.3 Shock process versus avalanche process for a particle

Let us conclude this section by comparing the shock and avalanche processes defined before for a particle in a smooth, bounded potential $V(u)$ that has a lot of minimas. The shock process was defined by the minimization of the total energy of the particle

$$u^{\text{shock}}(m; w) := \operatorname{argmin}_{u \in \mathbb{R}} \left(V(u) + \frac{1}{2}m^2(u - w)^2 \right) . \quad (\text{II.2.34})$$

And the latter becomes a true jump process in the limit $m \rightarrow 0$ as discussed before. In all this section we will keep m small but finite. Assuming that $V(u)$ is differentiable, the shock process verifies $\forall w \in \mathbb{R}$,

$$0 = m^2(w - u^{\text{shock}}(m; w)) + F(u^{\text{shock}}(m; w)) \quad (\text{II.2.35})$$

and it is by definition the root of this equation with the smallest energy. On the other hand in the dynamical case, the quasi-static process was defined again as a root of the same equation (see (II.2.17))

$$0 = m^2(w - u^{\text{q.s.}}(m; w)) + F(u^{\text{q.s.}}(m; w)) \quad (\text{II.2.36})$$

with a specific rule that we recall. Starting from an arbitrary root of (II.2.36) $u^{\text{q.s.}}(m; w)$ is always increasing (since the driving was positive $v = 0^+$), is continuous whenever possible (i.e. it follows a given root when the root exist), and whenever the root it follows ceases to exist, it jumps to the smallest of bigger roots. Let us now note, $\forall w \in \mathbb{R}$, the set of $n(w)$ roots of the equation $0 = m^2(w - u) + F(u)$ as $(u_1(w), \dots, u_{n(w)}(w))$ with $u_i(w) < u_{i+1}(w)$. Of course $n(w)$ a priori varies as a function of w . Let us suppose that at a given $w = w_0$, $u^{\text{q.s.}}(m; w_0)$ is the i_0^{th} root of the equation (II.2.36): $u^{\text{ava}}(m; w) = u_{i_0}(w)$. Note that as w increases, from the rules specified before, $\forall w \geq w_0$, $u^{\text{q.s.}}(m; w)$ is the $i^{\text{th}}(w)$ root of (II.2.36): $u^{\text{q.s.}}(m; w) = u_{i(w)}(w)$ and it is clear that $i(w)$ cannot increase if $F(u)$ is continuous. On the contrary it decreases as we now explain. Since $F(u)$ is bounded, the first root of the equation $u_1(w)$ ceases to exist at some finite $w = w_1 \geq w_0$. In the sequence of roots of the equation $(u_1(w), \dots, u_{n(w)}(w))$, at $w = w_1$, $u_1(w)$ is then replaced by $u_2(w)$ (the second smallest root becomes the smallest root as the smallest root ceases to exist). Hence when this occurs, either $i(w)$ decreases by one unit at w_1 (since the sequence of roots is shifted to the left at w_1), or just before w_1 , $u^{\text{q.s.}}(m; w)$ is already the smallest root and continues being the smallest root at w_1^+ . This shows that after a finite driving ΔW (which however diverges as $m \rightarrow 0$), the quasi-static process *follows the smallest root of the equation* (II.2.36). Hence if one starts the dynamics at $w_0 = -\infty$, the quasi-static process driven to the right $v = 0^+$, noted $u_+^{\text{q.s.}}(m; w)$ always follows the smallest root of (II.2.36). Similarly, the quasi-static process starting at $+\infty$ and driven to the left with $v = 0^-$ always follows the largest root of (II.2.36). Hence there are two canonical quasi-static processes and the shock process. They all follow a sequence of roots of the same equation and

$$u_+^{\text{q.s.}}(m; w) = u_{i_1(w)}(w) \quad , \quad u_-^{\text{q.s.}}(m; w) = u_{i_{n(w)}(w)}(w) \quad , \quad u^{\text{shock}}(m; w) = u_{i_{\text{shock}}(w)}(w) \quad . \quad (\text{II.2.37})$$

where $\forall w$, $u_{i_{\text{shock}}(w)}(w)$ is the root with the smallest energy. In general there is no symmetry between these different jump processes that would allow to get one from a simple translation/reflection of another. While $u^{\text{shock}}(m; w)$ always follows the ground state of the system, in general $u_+^{\text{q.s.}}(m; w)$ visits a sequence of *metastable states*. This sequence of states is sometimes referred to in the literature, especially in the case of interfaces, as the Middleton states [20]. An interesting consequence/characterization of this is related to the irreversibility of the quasi-static process.

Dissipation of energy and hysteresis in the avalanche process

Let us first remark that, at the point of a shock in the static ground state of the particle, the total energy of the particle is conserved: $\mathcal{H}_{w_k}[u^{\text{shock}}(m; w_k^+)] = \mathcal{H}_{w_k}[u^{\text{shock}}(m; w_k^-)]$. This is true since shocks between ground states precisely occur at the position where the latter is degenerate. On the other hand in the dynamics, one should not forget that between the beginning and the end of an avalanche

$u_+^{\text{q.s.}}(m; w_k) = u_0$ and $u_+^{\text{q.s.}}(m; w_k^+) = u_0 + S$, $S > 0$, the dynamics of the particle actually (II.2.23) plays a role. During the shock $vt = w_k$ and the dynamics is

$$\eta \partial_t u_t = m^2(w_k - u_t) + F(u_t) . \quad (\text{II.2.38})$$

Multiplying by $\partial_t u_t$ and integrating between the beginning t_0 and the end t_f of the shock one obtains

$$\eta \int_{t_0}^{t_f} (\partial_t u_t)^2 = \mathcal{H}_{w_k}[u_0] - \mathcal{H}_{w_k}[u_0 + S] > 0 . \quad (\text{II.2.39})$$

Note that the left-hand side has no reasons to vanish in the limit $m \rightarrow 0$. This shows that there is a dissipation of energy in the avalanche process (graphically it can be represented as an area as in Fig. II.2). In a protocol where one drags slowly the particle from $-\infty$ to $+\infty$ and back, the particle first follows the forward quasi-static process $u_+^{\text{q.s.}}(m; w)$, and then the backward quasi-static process $u_-^{\text{q.s.}}(m; w)$. These are different, see Fig. II.2, and the system exhibits *hysteresis* (we refer to [43] for a study of avalanches on the hysteresis loop of the ABBM model).

II.3 Shocks and Avalanches of elastic interfaces

In this section we discuss the generalization of the notion of shocks and avalanches introduced in the previous section for models of particle to d -dimensional interfaces. We begin with the case of shocks in Sec. II.3.1, and study the case of avalanches in Sec. II.3.2.

II.3.1 Shocks for an interface

a Introduction

Let us begin with the notion of shocks for an interface. We consider a d -dimensional elastic interface $u : x \in \mathbb{R}^d \rightarrow u_x \in \mathbb{R}$ with elasticity of range γ pinned by an harmonic well at the position $w \in \mathbb{R}$ and subject to a ‘nice’ random potential $V(x, u_x)$ with short-range correlations (by nice we mean as discussed in Sec. I.1.3). The Hamiltonian is thus

$$\mathcal{H}_{V,w}[u] := \frac{1}{2} \int_{x,y} g_{x,y}^{-1}(u_x - w)(u_y - w) + \int_x V(x, u_x) , \quad (\text{II.3.1})$$

where we recall $g_{x,y}^{-1} = \int_q e^{iq(x-y)} \sqrt{q^2 + \mu^2}$ with $\mu > 0$. Here and throughout the rest of the manuscript μ is thought of as small (i.e. $\ell_\mu = 1/\mu$ is very large compared to all eventual microscopic scales of the models, as e.g. the Larkin length (I.2.25)), although ℓ_μ is kept small compared to L (in order not to feel the boundary conditions). As seen in Sec. I.2, for $d < 2\gamma$, the ground state of the interface at fixed w ,

$$u_x(w) := \operatorname{argmin}_{u_x: \mathbb{R}^d \rightarrow \mathbb{R}} \mathcal{H}_{V,w}[u] , \quad (\text{II.3.2})$$

is rough with a non zero roughness exponent $\zeta_s > 0$:

$$\overline{(u_x(w) - u_{x'}(w))^2} \sim |x - x'|^{2\zeta_s} \quad , \quad \text{for } |x - x'| \leq \ell_\mu = 1/\mu . \quad (\text{II.3.3})$$

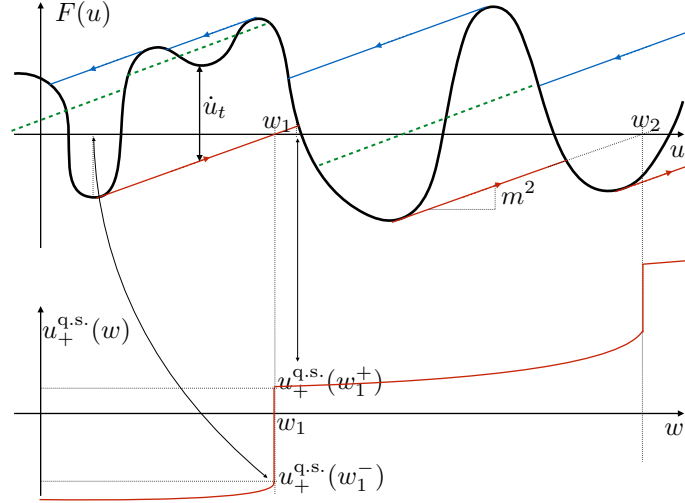


Figure II.2: Top: The different jump processes (here smoothed by a non zero m) of a particle in a force landscape $F(u)$ (black line). The forward quasi-static process $u_+^{\text{q.s.}}(m; w)$ follows the smallest root of the equation $m^2(u-w) = F(u)$ (red construction above). When the root ceases to exist, $u_+^{\text{q.s.}}(m; w)$ jumps to the smallest one on the right (such as the shock at w_1 above). During the jumps of the forward quasi-static process, the particle moves with a velocity equal to $m^2(w_k - u_t) + F(u_t)$, that is the difference of height between the red line and $F(u)$. During such a jump, the particle thus dissipates an energy equal to the area between the red line and $F(u)$. In the backward quasi-static process (blue construction above), the particle follows a different sequence of metastable states. In the static shock-process (green-dashed construction above), the particle jumps between ground states at the same-energy. Hence, during a jump in the static shock process, the algebraic area enclosed in between the green-dashed line and $F(u)$ is 0. Dragging slowly the particle from $-\infty$ to $+\infty$ and back, the dissipated energy ('the area of the hysteresis loop') is equal to the sum of the areas enclosed in between the blue and black line and red and black line. Bottom: Forward quasi-static process deduced from the top picture. Here two avalanches at w_1 and w_2 are visible.

Here again the fact that the large scale cutoff scale ℓ_μ is equal to the one of the pure theory $\ell_\mu = 1/\mu$ is a consequence of the Statistical-Tilt-Symmetry (STS) of the problem, of which we postpone the discussion to Sec. II.4.1. What happens to the ground state as a function of w ? Although it cannot be proved in all generality, as in the $d = 0$ problem of a particle discussed in the last section, one expects the ground state of the interface to exhibit jumps at an ensemble of discrete locations $\{w_i, i \in \mathbb{Z}\}$ (whose density increases with the system size as L^d) as w is changed (at these precise points the ground state (II.3.2) is ill-defined since it is actually degenerate). This was confirmed numerically in e.g. [105, 106]. Hence we write, $\forall i \in \mathbb{Z}$,

$$u_x(w_i^+) = u_x(w_i^-) + S_x^{(i)}. \quad (\text{II.3.4})$$

Here $S_x^{(i)}$ is the *local size at x* of the i^{th} avalanche. Using a stability argument it is trivial to show that $u_x(w)$ is strictly increasing as a function of w and hence $S_x^{(i)} \geq 0$. The *sequence of shocks* $(w_i, S_x^{(i)})$ is random and characterizing its statistical properties is one of the main problems studied in this thesis. In the study of shocks for particles on the real line of the previous section, we saw that shocks only occurred for a small enough confinement. Using FRG we will see in Sec. II.4 that a similar property holds for interfaces, and that shocks only occur for $\mu \leq \mu_c$ where μ_c is linked to the Larkin length (see Sec. I.2.3) as $\mu_c := 1/L_c$. Similarly, for non-zero μ , as for the $d = 0$ case, one expects the motion of the interface to also contain some smooth part. We will discuss later the appropriate scaling limit that one should take in order for $u_x(w)$ to be a pure jump process. Before we continue let us write here

A word of caution

Let us stress that most of what we will say about shocks and avalanches for disordered elastic interfaces relies on a large number of unproven assumptions. The notion of shocks and avalanches can be seen as a phenomenological picture and it is rather hard to see it emerge from the theory ‘from first principles’ (except e.g. in $d = 0$ as in the previous section). It is mostly built from studies of toy models and numerical simulations. However as we will see, it is a very useful phenomenological picture as it allows to efficiently interpret -and is consistent with- the output of the calculations of the Functional Renormalization Group. In this sense, the existence of shocks can be seen as a hypothesis, or an ansatz, that will be plugged into the theory, and the consistency of the ansatz will always have to be verified.

b Shock observables and scaling

A few important shock observables are (i) the *lateral extension of the shocks* $\ell^{(i)}$; (ii) its total size $S^{(i)}$ and (iii) its local size at x , $S_x^{(i)}$.

(i) The lateral extension $\ell^{(i)}$ denotes the diameter of the domain $x \in \mathbb{R}^d$ where $S_x^{(i)}$ is non-zero. Note that in general it is actually not obvious that the latter is not infinite (this was recently shown in a specific model, the Brownian Force Model with SR elasticity in $d = 1$, defined below, in [107]), but here we will assume that it is so, and this eventually implies that there is some small cutoff scale δu such that by $S_x^{(i)} = 0$ we mean $S_x^{(i)} \leq \delta u$.

(ii) The total size of the shock is defined as $S^{(i)} := \int_x S_x^{(i)}$. Let us now introduce the *density of avalanche sizes* $\rho(S)$, defined as

$$\rho(S) := \overline{\sum_i \delta(S - S^{(i)}) \delta(w - w_i)}. \quad (\text{II.3.5})$$

The latter does not depend on w for a statistically translationally invariant disorder. $\rho_0 = \int_0^\infty dS \rho(S)$ is the mean number of shocks per unit of w , and

$$P(S) := \frac{1}{\rho_0} \rho(S) \quad (\text{II.3.6})$$

is the normalized probability distribution function (PDF) of avalanche sizes. In the following we will denote $\langle \rangle_\rho$ and $\langle \rangle_P$ the average with respect to ρ and P .

Let us now discuss some properties of the avalanche observable previously defined.

Scaling of avalanches

Since two points x and x' with $x - x' \geq \ell_\mu$ are essentially statistically independent, one expects not to observe avalanches with an extension much larger than ℓ_μ : ℓ_μ is a large scale cutoff for the avalanches lateral extension probability distribution function (PDF) $P(\ell)$. On the other hand in the regime of lengths smaller than ℓ_μ , one expects scale invariance to hold. That is, reintroducing an eventual short scale cutoff ℓ_0 , *no* length scale should have any influence for $\ell_0 \ll |x - x'| \ll \ell_\mu$. This leads us to the scaling hypothesis that in the scaling regime $P(x\ell)/P(\ell)$ does not depend on ℓ , i.e. it is a function of x , $f(x) \leq 0$. It is easily seen that $f(x_1 x_2) = f(x_1) f(x_2)$ and is f is continuous, it well known that $f(x)$ must be a power-law. Hence we expect, in the scaling regime that

$$\ell_0 \ll \ell \ll \ell_\mu \implies P(\ell) \sim \frac{1}{\ell^{\tau_\ell}}. \quad (\text{II.3.7})$$

i.e. $P(\ell)$ is a power-law in the scaling regime characterized by an exponent τ_ℓ . Since both ground states $u_x(w_i^+)$ and $u_x(w_i^-)$ are statistically equivalent and scale as in (II.3.3), one also expects the local shape S_x to scale as $|x - x_0|^{\zeta_s}$ where x_0 denotes a point on the border of the avalanche and the scaling is expected to hold for $\ell_0 \ll |x - x_0| \ll \ell$. Hence the local size well inside the avalanche $S_x \sim \ell^{\zeta_s}$ must be power-law distributed as, in the scaling regime $\ell_0^{\zeta_s} \ll S_x \ll \ell_\mu^{\zeta_s}$,

$$P(S_x) \sim \frac{1}{S_x^{\tau_S^{\text{loc}}}} \quad , \quad \tau_S^{\text{loc}} := 1 + \frac{\tau_\ell - 1}{\zeta_s}. \quad (\text{II.3.8})$$

Similarly, one expects the total size to scale as $S \sim \ell^{d+\zeta_s}$ and to be distributed as, in the scaling regime

$$S_0 \sim \ell_0^{-d-\zeta} \ll S \ll S_\mu \sim \mu^{-d-\zeta} \quad (\text{II.3.9})$$

one expects

$$P(S) \sim \frac{1}{S^{\tau_S}} \quad , \quad \tau_S := 1 + \frac{\tau_\ell - 1}{d + \zeta_s}. \quad (\text{II.3.10})$$

Hence, as $\mu \rightarrow 0$ avalanches become larger and larger. It is thus expected that the appropriate scaling to obtain a non-trivial pure-jump process is to take

$$\begin{aligned} \tilde{u}_{\tilde{x}}(\tilde{w}) &:= \lim_{\mu \rightarrow 0} \mu^{\zeta_s} u_{x=\mu^{-1}\tilde{x}}(w = \mu^{-\zeta_s}\tilde{w}) \\ &= cst + \sum_{i \in \mathbb{Z}} \theta(\tilde{w} - \tilde{w}_i) \tilde{S}_x^{(i)}. \end{aligned} \quad (\text{II.3.11})$$

This a posteriori justifies the notation ζ used in (II.2.18). In these units the large scale cutoff on the total size of avalanches $\tilde{S} = \int_x \tilde{S}_x$ is now of order 1, while the low scale cutoff is now of order $\mu^{d+\zeta}$. In the following we will temporarily ignore the rescaling (II.3.11) and do as if $u_x(w)$ itself was performing a jump process:

$$u_x(w) = cst + \sum_{i \in \mathbb{Z}} \theta(w - w_i) S_x^{(i)}. \quad (\text{II.3.12})$$

Knowing that in doing so we are ignoring some smooth parts (typically of order $O(\mu^\gamma)$, see (II.3.1)) that disappear in the scaling limit (II.3.11). Using the fact that $\overline{u_x(w)} = w$ and using the definition (II.3.5), we obtain the first moment of the avalanche total size density:

$$\langle S \rangle_\rho = L^d. \quad (\text{II.3.13})$$

As was shown in (II.3.7), (II.3.8) and (II.3.10), the different power-law exponents of avalanche observable distributions are not independent. Rather they are linked to one another by scaling relations involving the roughness exponent ζ_s . As for the roughness exponent ζ_s , an important question is to understand whether are not the power-law exponents defined above are universal or not, and how many universality classes they are. A conjecture by Narayan and Fisher (NF), originally proposed in [108] in the context of avalanches at depinning, actually states that the exponents can all be obtained from the sole knowledge of ζ_s . If the latter is true, it means that there is a single critical exponent governing both the static ground state of an elastic interface in a disorder media (that can be measured using a snapshot of the interface), and the power law exponents (that describe the complex shock process of switches between the ground states of the interface). This also implies that there are exactly as many universality classes of shocks as there are universality classes for the statics of disordered elastic interfaces. Let us derive here the NF conjecture following e.g. [109] (see also [110, 43] for a closely related approach).

c The NF conjecture

The NF conjecture permits to obtain the power-law exponent of the avalanche total size distribution τ_S self consistently when $1 < \tau_S < 2$. It is based on several hypotheses. The first is that the avalanche size density obeys the following scaling form, already motivated by the previous discussion,

$$\rho(S) = L^\alpha \mu^\rho \frac{1}{S^{\tau_S}} f_{\text{cut}} \left(\frac{S}{S_\mu} \right) g_{\text{cut}} \left(\frac{S}{S_0} \right). \quad (\text{II.3.14})$$

Where (i) $f_{\text{cut}}(x)$ is a large scale cutoff function such that $f_{\text{cut}}(x) \approx 1$ for $x \leq 1$ and $f_{\text{cut}}(x)$ quickly decays to 0 for $x \geq 1$; (ii) $g_{\text{cut}}(x)$ is a small scale cutoff function such that $g_{\text{cut}}(x) \approx 1$ for $x \geq 1$ and $g_{\text{cut}}(x)$ quickly decays to 0 for $x \leq 1$. The presence of the large scale cutoff function was already justified before. The presence of a small scale cutoff function is necessary for $\tau_S > 1$ since in this case, the mean number of avalanches per unit w diverges as $S_0 \rightarrow 0$: it is dominated by the small scale cutoff as

$$\rho_0 = \int_0^\infty dS \rho(S) \sim L^\alpha \mu^\rho S_0^{1-\tau_S}. \quad (\text{II.3.15})$$

The low scale cutoff S_0 is a priori purely of microscopic origin (or set to an arbitrary value in a simulation) and does not scale with either μ or L . For $\tau < 2$, the first moment of the avalanche size density is dominated by the large scale cutoff and

$$\langle S \rangle_\rho = L^d \sim L^\alpha \mu^\rho S_\mu^{2-\tau_S} \sim L^\alpha \mu^{\rho-(2-\tau_S)(d+\zeta_s)}. \quad (\text{II.3.16})$$

Hence we obtain from this relation

$$\alpha = d \quad , \quad \tau_S = 2 - \frac{\rho}{d + \zeta_s}. \quad (\text{II.3.17})$$

The true difficulty is therefore to obtain ρ . The NF conjecture is that *the density of avalanches per unit of applied force stays constant as $\mu \rightarrow 0$* . ρ_0 in (II.3.15) must therefore be proportional to the applied force which scales as μ^γ , and the NF conjecture thus states

$$\tau_S = 2 - \frac{\gamma}{d + \zeta_s}. \quad (\text{II.3.18})$$

Although its derivation assumed here $\tau_S > 1$ (if $\tau_S < 1$, ρ_0 is convergent at small S_0 but dominated by the large scale cutoff as $\rho_0 \sim \mu^\rho S_\mu^{1-\tau_S}$), i.e. $\gamma/(d + \zeta_s) < 1$, its validity might actually be more general as suggested e.g. in [32]. The NF conjecture was confirmed up to one-loop accuracy by FRG calculations in [109, 111, 101]. Note that for models of interfaces at their upper-critical dimension $d = d_{\text{uc}} = 2\gamma$, since the fluctuations of the interface are there expected to show a logarithmic scaling (hence $\zeta_s = 0$ at $d = d_{\text{uc}}$) we obtain $\tau_S = 3/2$. That is, we obtain the same exponent as the avalanche size exponent in the ABBM model (see Sec. II.2.2). We will see later that this is not a coincidence.

II.3.2 Avalanches for an interface

In this section we now discuss the notion of avalanches for a d -dimensional interface at the depinning transition.

a Alternative approach to the depinning transition and avalanches

To discuss the notion of avalanches at the depinning transition we will actually not discuss the dynamics described by the equation of motion (I.3.3) (elastic interface

driven by a force f), but rather, in analogy with the static problem and as in the $d = 0$ models of Sec. II.2.2, study the interface dynamics when driven by a harmonic well:

$$\begin{aligned} \eta \partial_t u_{tx} &= \int_y g_{x,y}^{-1}(u_{ty} - w(t)) + F(x, u_{tx}) \\ w(t) &= vt . \end{aligned} \quad (\text{II.3.19})$$

Here $v > 0$, the hypotheses on the random force are as in Sec. I.1.3 and as usual $g_{x,y}^{-1} = \int_q (q + \mu^2)^{\frac{z}{2}} e^{iq(x-y)}$ with $\mu \geq 0$. Here again, taking an initial condition such that the velocities of the interface are positive at $t = 0$, they remain so for all time and at late times the interface position field converges to a well-defined steady state (Middleton theorem [20]). Here the driving $w(t) = vt$ imposes the mean velocity of the interface, in the steady-state,

$$\overline{\partial_t u_{tx}} = v . \quad (\text{II.3.20})$$

Since we are actually interested in describing the dynamics at the depinning transition, we will be interested in the limit $v \rightarrow 0^+$. In this limit, the interface fluctuations are expected to display a scale invariant behavior identical to (I.3.7) (only the exponents are the same, the scaling function can be different). As for our study of the static problem, this scale invariant behavior is expected to occur in the range of scales $|x - x'| \leq \ell_\mu$, $|t - t'| \leq \ell_\mu^z$ with $\ell_\mu^{-1} = 1/\mu$. As in the static problem, the fact that the large scale cutoff ℓ_μ is equal to the one of the pure theory $\ell_\mu = 1/\mu$ is a consequence of the Statistical-Tilt-Symmetry (STS) of the problem, of which we postpone the discussion to Sec. II.5.1. To study the depinning transition, we will consider the quasi-static process, as we did for the $d = 0$ model of a particle (see Sec. II.2.2),

$$u_x(w) := \lim_{v \rightarrow 0^+} u_{t=w/v, x} . \quad (\text{II.3.21})$$

The latter satisfies, $\forall w \in \mathbb{R}$,

$$0 = \int_y g_{x,y}^{-1}(u_y(w) - w) + F(x, u_x(w)) . \quad (\text{II.3.22})$$

Note that the static ground state of the interface studied in Sec. II.3.1 is also a solution of this equation, and is by definition the one of minimum energy. As for the $d = 0$ models, in the steady-state, the correct solution of (II.3.22) is the leftmost one (see Sec. II.2.3) and a priori differs from the ground state. This sequence of Middleton states can have roughness different from the one of the ground state and a result of FRG is that they are indeed different. As in the statics we expect that for $\mu \leq \mu_c$ (associated with the Larkin length as $\mu_c := 1/L_c$, see (I.2.25)), the quasi-static process $u_x(w)$ is non-analytic and displays avalanches at discrete locations w_k , $k \in \mathbb{Z}$. In the appropriate scaling limit $u \sim \mu^{-\zeta_d}$, $x \sim \mu^{-1}$ and $w \sim \mu^{-\zeta_d}$, it is expected to become a pure jump process:

$$u_x(w) = cst + \sum_{k \in \mathbb{Z}} \theta(w - w_k) S_x^{(k)} . \quad (\text{II.3.23})$$

During an avalanche, the interface dynamics plays an important role and is described by (II.3.19) with $vt \rightarrow w_k^+$. This is a clear difference with the statics, which is in particular

responsible for the fact that energy is dissipated during the quasi-static process (see Sec. II.2.3 for the complete discussion in $d = 0$). Note that since the sequence of metastable states visited by the interface in this forward quasi-static process is a priori different from the sequence of ground states in the static problem (in particular these states have different roughness exponent), the sequence of avalanches is also different. As for the static problem, we however expect similar scaling and universality to occur in avalanches in the interface dynamics, with different exponents however. Interesting observables associated with the k^{th} avalanches are (i) as in the static case: w_k the location of the avalanche, $\ell^{(k)}$ the lateral extension of the avalanche, $S_x^{(k)}$ the local size of the avalanche at x , $S^{(k)} = \int_x S_x^{(k)}$ the total size of the avalanche; (ii) observables that only exist in the dynamics: $T^{(k)}$ the duration of the avalanches, $x_0^{(k)}$ the first point that becomes unstable at the beginning of the avalanche (the ‘seed’ of the avalanche, note that this is another important difference with avalanches in the statics where this notion does not make sense), $v^{(k)}(t, x) = \partial_t u_{t=w_k/v+tx}$ the velocity field inside the avalanche, $\bar{v}^{(k)}$ the mean velocity inside the avalanche, $E^{(k)} = \eta \int_{tx} (\partial_t u_{tx})^2$ the energy dissipated during the avalanche. For these observables, scaling now notably imposes similar relations as in the static case and some new relations, associated with new observables and that involve the dynamic exponent z :

$$S_x \sim \ell^{\zeta_d} \quad , \quad S \sim \ell^{d+\zeta_d} \quad , \quad T \sim \ell^z \quad , \quad v \sim \ell^{\zeta_d - z} . \quad (\text{II.3.24})$$

These observables are expected to be distributed with PDF with power-law behavior as in the static case. From (II.3.24) it is clear that the different power-law exponents are not independent. It is in this context that the Narayan-Fisher conjecture was first introduced [108]. It can be ‘shown’ using the exact same arguments as in Sec. II.3.1 and reads

$$\tau_S = 2 - \frac{\gamma}{d + \zeta_d} . \quad (\text{II.3.25})$$

b A side remark/a word of caution: avalanche power-law exponents depend on the driving

We have up to now discussed avalanches for an elastic interface driven by a parabolic well: the driving is soft ($\mu \rightarrow 0$) and homogeneous on the system. This type of driving is known to be relevant in various experimental situations and in particular to reproduce the driving by a force right at the depinning transition, but other driving can be considered and can be relevant in other situations. Another driving that has already been considered is the case of avalanches for an interface such that the position of part of the interface is imposed to be w (see e.g. [112, 113]). Here we consider the situation where an interface of internal length L , dimension d , elastic Hamiltonian (I.1.4) with $g_q^{-1} = |q|^\gamma$, in a random potential $V(x, u)$, is free to move in \mathbb{R} , except on a subspace $\mathbb{E}_{d_{\text{dr}}} \in \mathbb{R}^d$ of dimension d_{dr} where its position is imposed to be $w(t) = vt$. The extreme case $d_{\text{dr}} = 0$ corresponds to an interface driven at a single point. Noting $x = (x_1, \dots, x_d) \in \mathbb{R}^d$ the d -dimensional coordinates of x and taking for concreteness $\mathbb{E}_{d_{\text{dr}}} = \{x = (x_1, \dots, x_{d_{\text{dr}}}, 0, \dots, 0) \in \mathbb{R}^d, (x_1, \dots, x_{d_{\text{dr}}}) \in \mathbb{R}^{d_{\text{dr}}}\}$ we thus study the

problem

$$\begin{aligned}\eta\partial_t u_{tx} &= \int_y g_{x,y}^{-1} u_y + F(x, u_x) \\ u_{tx} &= w(t) \quad \text{for } x \in \mathbb{E}_{d_{\text{dr}}}\end{aligned}\tag{II.3.26}$$

for a very slow driving $w(t) = vt$ and $v \simeq 0^+$, and we study the forward quasi-static process $u_x(w) = \lim_{v \rightarrow 0^+} u_{t=w/v, x}$. Obviously for $x \in \mathbb{E}_{d_{\text{dr}}}$, $u_x(w) = w$ is a smooth function of w , but for $x \notin \mathbb{E}_{d_{\text{dr}}}$ one still expects to observe scale invariance and some non-analytic behavior with avalanches at discrete positions w_i : $u_x(w_i^+) = u_x(w_i^-) + S_x^{(i)}$. Since the roughness exponent ζ_d is a bulk property of the system, it is expected that the total size of these shocks still satisfies the relation $S \sim \ell^{d+\zeta_d}$ with the same roughness exponent as before, where ℓ is the linear extension of the shocks in the space perpendicular to the driven space $\mathbb{E}_{d_{\text{dr}}}^\perp$. Here the only large scale cutoff for the avalanche linear extension is L and the large scale cutoff for the avalanche total sizes is $S_L \sim L^{d+\zeta_d}$. Defining again the avalanche size distribution as $\rho(S) := \sum_i \delta(S - S^{(i)})\delta(w - w_i)$, we thus expect that it displays a power-law behavior in between two cutoff scales S_0 and S_L , as

$$\rho(S) = L^\alpha \frac{1}{S^{\tau_S}} f_{\text{cut}}\left(\frac{S}{S_L}\right) g_{\text{cut}}\left(\frac{S}{S_0}\right),\tag{II.3.27}$$

where f_{cut} and g_{cut} are two scaling functions such that $f_{\text{cut}}(x) \approx 1$ for $x \leq 1$, $f_{\text{cut}}(x)$ quickly decays to 0 for $x \geq 1$, $g_{\text{cut}}(x) \approx 1$ for $x \geq 1$ and $g_{\text{cut}}(x)$ quickly decays to zero for $x \leq 1$. Let us now apply a reasoning similar to the one used in the derivation of the NF conjecture (II.3.18). If $1 < \tau_S < 2$ the mean-density of avalanches per unit w is dominated by the small scale cutoff as

$$\rho_0 = \int_0^\infty \rho(S) dS \sim L^\alpha S_0^{1-\tau_S}.\tag{II.3.28}$$

The first moment of the avalanche size distribution must still be $\langle S \rangle_\rho = L^d$ and is dominated by the large scale cutoff as

$$\langle S \rangle_\rho = L^d \sim L^\alpha S_L^{2-\tau_S} \sim L^{\alpha+(2-\tau_S)(d+\zeta_s)}.\tag{II.3.29}$$

In this setting, it is natural to think that the mean number per unit of w of avalanches scales as $L^{d_{\text{dr}}}$, implying $\alpha = d_{\text{dr}}$. Indeed, here avalanches can only be triggered by the depinning of one of the points in the vicinity of one of the driven points $\mathbb{E}_{d_{\text{dr}}}^\perp$ and the number of avalanches is thus expected to be proportional to the number of driven points. Using (II.3.29) we thus obtain a generalization of the Narayan-Fisher conjecture:

$$\tau_S = 2 - \frac{d - d_{\text{dr}}}{d + \zeta_d}.\tag{II.3.30}$$

This relation is in agreement with the result [112, 113] for the case $d = 1$ and $d_{\text{dr}} = 0$. We are unaware whether or not this general conjecture already appeared in the literature.

II.4 The functional renormalization group treatment of shocks in disordered elastic systems: a short review

In this section we now review the use of the functional renormalization group to calculate shock observables. We will begin by recalling the important results of FRG for the statics of d -dimensional interfaces in Sec. II.4.1, and in Sec. II.4.2 we will show how to apply FRG to the study of shocks.

II.4.1 The functional renormalization group for the statics of disordered elastic interfaces

a Introduction

We thus consider the static problem of determining the statistical properties of the ground state of a disordered elastic interface of internal dimension d in a quenched random potential $V(x, u)$

$$\begin{aligned} u_x(w) &:= \operatorname{argmin}_{u: \mathbb{R}^d \rightarrow \mathbb{R}} \mathcal{H}_{V,w}[u] \\ &= \operatorname{argmin}_{u: \mathbb{R}^d \rightarrow \mathbb{R}} \left(\frac{1}{2} \int_{x,y} g_{x,y}^{-1}(u_x - w)(u_y - w) + \int_x V(x, u_x) \right). \end{aligned} \quad (\text{II.4.1})$$

where as usual $g_{x,y}^{-1} = \int_q e^{iq(x-y)}(q^2 + \mu^2)^{\frac{\gamma}{2}}$. The disorder potential is chosen centered, e.g. Gaussian, with second cumulant¹

$$\overline{V(x, u)V(x', u')} = \delta^{(d)}(x - x')R_0(u - u'), \quad (\text{II.4.2})$$

where R_0 is the *bare disorder cumulant* that will be chosen either as associated with disorder of the random bond type, the random field type, or eventually periodic disorder $R_0(u + \Delta u) = R_0(u)$ that can be relevant to some applications (see Sec. I.1.3 for definitions). In low dimensions $d \leq 2\gamma$, we know from Sec. I.2.3 that the disorder is relevant at large scale, that the ground state is rough and exhibits scaling in the range of scales $|x - x'| \ll \ell_\mu := 1/\mu$, and we will be interested in the $\mu \rightarrow 0^+$ limit. The application of renormalization group ideas to disordered elastic systems has a long and rich history that we will not thoroughly review here. The phenomenon of dimensional reduction recalled in Sec. I.2.3 warns us that naive perturbation theory in the disorder badly fails and one has to find a way to do better. The way out proposed by the FRG is as follows. Let us first introduce here the replicated action of the theory.

A convenient way to perform disorder averages is to consider the replicated action of the theory (see [96] for some background on replicas) for the statics at temperature T . Replicating the field $u_x \rightarrow u_x^a$, $a = 1, \dots, n$, the action is

$$S[w; \{u_x^a\}] := \frac{1}{2T} \sum_{a=1}^n \int_{x,y} g_{x,y}^{-1}(u_x^a - w)(u_y^a - w) - \frac{1}{2T^2} \sum_{a,b=1}^n \int_x R_0(u_x^a - u_x^b) + \dots \quad (\text{II.4.3})$$

¹The fact that we simply assume here that the correlations of the potential in the internal space x are described by a δ distribution, while the correlations in the external space u are given by a function $R_0(u)$ even for short-range disorder notably comes from the fact that this structure is stable under renormalization. That is, starting from a bare disorder with more complex short-range correlations in internal space, at large scale it will look just as if we started from (II.4.2). Conversely, starting from a bare disorder with ‘trivial’ short-range correlations $R_0(u - u') = \sigma\delta(u - u')$, the renormalized disorder at large scale will still be short-range in u space, but with a finite correlation length.

here the dots indicate the eventual presence of higher cumulants of the random potential that will be generated by the renormalization procedure anyway. Physical, disorder averaged observables of the ground state (II.4.1) of the Hamiltonian are obtained by taking the limit of a path integral formula

$$\overline{O[\{u_x(w)\}]} = \lim_{n, T \rightarrow 0} \int \prod_{a=1}^n O[\{u_x^a\}] \mathcal{D}[u^a] e^{-S[w; \{u_x^a\}]} . \quad (\text{II.4.4})$$

Fisher's breakthrough and the development of FRG

Performing the naive perturbation theory of an observable (II.4.4) using an analytic $R_0(u)$ again gives the dimensional reduction result with the Larkin roughness exponent $\zeta_L = \frac{2\gamma-d}{2}$. What is even more surprising with this result is the following: expanding the even and analytic function $R_0(u)$ in (II.4.3) as $R_0(u) = \sum_{n=0}^{+\infty} \frac{1}{2n!} C_{2n} u^{2n}$ and performing the rescaling valid at the Larkin fixed point

$$x = \mu^{-1} \tilde{x} \quad , \quad u_x^a = \mu^{-\zeta_L} \tilde{u}_{\tilde{x}=\mu x}^a \quad , \quad T = \mu^{-d+\gamma-2\zeta_L} , \quad (\text{II.4.5})$$

the disordered part of the action (II.4.3) is rescaled as

$$\frac{1}{2\tilde{T}^2} \int_{\tilde{x}} \sum_{a,b=1}^n \sum_{n=0}^{\infty} \mu^{\alpha_n} \frac{1}{2n!} C_{2n} (\tilde{u}_{\tilde{x}}^a - \tilde{u}_{\tilde{x}}^b)^{2n}$$

$$\alpha_n = -d - 2n\zeta_L - 2(-d + \gamma - 2\zeta_L) = (2\gamma - d)(1 - n) . \quad (\text{II.4.6})$$

Here for $d < 2\gamma$, C_0 thus flows to 0 and is unimportant at large scale at the Larkin FP, $C_1 = R''(0)$ is left invariant as expected, but all the higher cumulants C_{2n} with $n > 1$ do flow and are relevant at the Larkin FP. This should lead the system to flow away from the Larkin FP. However, as observed in [16], the contribution of all higher cumulants simplify in the calculation of observables (the dimensional reduction (DR) property). This was attributed to an underlying supersymmetric property of the FT [17], or equivalently in a diagrammatic language, to the ‘mounting property’ of diagrams associated with the field theory (II.4.3) [18]. The Larkin result is however as we know incorrect (see the discussion in Sec. I.2.3). Escaping the Larkin FP using a RG procedure calls for (i) a functional RG to take into account the fact that all cumulants of the potential become simultaneously relevant for $d < 2\gamma$; (ii) a RG scheme that somehow escapes DR. The solution first noted by Fisher in [114] is as follows. Using a one-loop Wilson’s shell RG on the replicated action (II.4.3) with $\mu = 0$ but with a UV cutoff $\Lambda > 0$ that is sent to $\Lambda_l = \Lambda e^{-l}$ to renormalize the complete function $R_0(u)$ the bare cumulant $R_0(u)$ is renormalized into a function $R_l(u)$ (it corresponds to the cumulant of a renormalized disorder seen at large scale by the manifold, see below). Following the RG flow, remarkably, the function $R_l(u)$ becomes *non-analytic at a finite scale* $l = l_c < \infty$: the function $\Delta_l(u) = -R_l''(u)$ exhibits a cusp around 0: $\Delta_l(u) - \Delta_l(0) \sim \Delta_l'(0^+) |u| + O(u^2)$. The non-analyticity forbids the expansion (II.4.6) and escapes DR. Several fixed point (FP) functions $R(u)$ were found corresponding² to the three classes listed above, i.e. random bond, random field and random periodic. The found fixed point functions are of order $O(\epsilon)$ with $\epsilon = d_{\text{uc}} - d = 2\gamma - d$, hence

²Other FP functions exist and correspond to disorder with long range correlations $R_0(u) \sim_{u \rightarrow \infty} u^\alpha$.

allowing to compute perturbatively any observable in an expansion in the non-analytic renormalized disorder second cumulant $R'_l(u)$. It was later argued in [115] that the non-analyticity in $R_l(u)$ is related to the presence of shocks in the ground state (this will be clear below). Many developments followed this work and here we name a few: (i) refinement of the result to two-loops using perturbative RG [116, 117]; (ii) development of exact RG approaches [18, 118]; (iii) clarification of the role of the temperature [119, 96]. References for the application of FRG to the depinning transition and to avalanches will be discussed in Sec. II.5.1. In the following we will use the most modern approach to FRG as presented e.g. in [96] and only state the results. We refer the reader to [120, 121] for what are probably the most pedagogical introductions to FRG.

b Definition of the different functionals and the statistical-tilt-symmetry

Our preferred approach to FRG, as presented [96] to which we refer the reader for more details, is to study the flow of the effective action of the replicated theory as the strength of the confining well is varied from $\mu \rightarrow \infty$ to $\mu \rightarrow 0$. In the limit $\mu \rightarrow \infty$ the fluctuations are frozen and the effective action is basically the bare action of the theory, while in the limit $\mu \rightarrow 0$ that we want to study, the effective action takes a universal scaling form. This type of approach is common in non-perturbative RG (see [122] for a review) but here our final results will be perturbative. Although this presentation can be quite cumbersome the first time it is probably the clearest way to understand the validity and the interpretation of the main results of the FRG.

The renormalized disorder functional

Let us first define, for each realization of the disorder V , the *renormalized disorder at the scale μ for a well centered at w_x* , $\hat{V}_\mu[\{w_x\}]$ as

$$e^{-\frac{1}{T}\hat{V}_\mu[\{w_x\}]} = \int \mathcal{D}[u] e^{-\frac{1}{T} \left(\frac{1}{2} \int_{x,y} g_{x,y}^{-1}(u_x - w_x)(u_y - w_y) + \int_x V(x, u_x) \right)} \quad (\text{II.4.7})$$

Hence here we are considering the usual theory with a well position that is now inhomogeneous in space. The renormalized disorder $\hat{V}_\mu[\{w_x\}]$ is a functional of the well position w_x . It converges in the limit $T \rightarrow 0$ to the energy of the ground state of the Hamiltonian in the well w . In the limit $\mu \rightarrow \infty$, $u_x = w_x$ and $V_\mu[\{w_x\}] = \int_x V(x, w_x)$. More generally the renormalized disorder combines the effects of the elasticity, the thermal fluctuations and the disorder and we think of it as a renormalized disorder seen by the interface on a scale $\ell_\mu = 1/\mu$.

The W functional

On the other hand, let us consider, in the theory with $w_x = 0$, the *generating functional for connected correlations in the replicated field theory*:

$$e^{W_\mu[\{j_x^a\}]} := \int \prod_{a=1}^n \mathcal{D}[u^a] e^{-S[0, \{u_x^a\}] + \sum_a \int_x j_x^a u_x^a} \quad (\text{II.4.8})$$

This functional is a standard object considered in field theory and is the sum of all connected diagrams. Writing $\langle \rangle_{S[0, \cdot]}$ the average with respect to the replicated action

with $w = 0$ (II.4.3), the connected correlations $G_{x_1, \dots, x_n}^{a_1, \dots, a_n} := \langle u_{x_1}^{a_1} \cdots u_{x_n}^{a_n} \rangle_{S[0, \cdot]}$ appear in the polynomial expansion of W_μ as

$$W_\mu[\{j_x^a\}] = W_\mu[0] + \frac{1}{2} \sum_{ab} \int_{x,y} G_{x,y}^{a,b} j_x^a j_y^b + \frac{1}{4!} \sum_{abcd} \int_{x,y,z,t} G_{x,y,z,t}^{a,b,c,d} j_x^a j_y^b j_z^c j_t^d + O(j^6). \quad (\text{II.4.9})$$

And connected correlations of the replicated field are obtained by applying functional derivatives to W_μ . W_μ is an even functional of j_x by statistical parity invariance of the disorder. Here we assumed that it is analytic $\forall T > 0$.

The STS symmetry and the form of $G_{x,y}^{a,b}$

The Statistical-Tilt-Symmetry originates from the statistical translational invariance of the disorder. The latter implies, for an arbitrary function ϕ_x (constant in replica space)

$$S[0, \{u_x^a + \phi_x\}] = S[0, \{u_x^a\}] + \frac{1}{T} \int_{x,y} g_{x,y} u_x^a \phi_y + \frac{1}{2T} \sum_{a,b} \int_{x,y} g_{x,y} \phi_x \phi_y. \quad (\text{II.4.10})$$

This implies the identity for $W_\mu[\{j_x^a\}]$, using $j_x = \frac{1}{T} \int_y g_{x,y}^{-1} \phi_y$,

$$W_\mu[\{j_x^a + j_x\}] = W_\mu[\{j_x^a\}] + T \sum_a \int_{x,y} g_{x,y}^{-1} j_x^a j_y + n \frac{T}{2} \int_{x,y} g_{x,y}^{-1} j_x j_y. \quad (\text{II.4.11})$$

Taking a derivative with respect to j_x at $j_x = 0$ we obtain

$$\sum_a \frac{\delta}{\delta j_x^a} W_\mu[\{j_x^a\}] = T \sum_a \int_y g_{x,y} j_y^a \quad (\text{II.4.12})$$

This being valid $\forall n \in \mathbb{N}$ and for any sources j_x^a , this implies an infinite series of identities for the ‘coefficients’ of the series expansion of $W_\mu[\{j_x^a\}]$. In particular, it implies for the quadratic part

$$\sum_b G_{x,y}^{ab} = T g_{x,y}, \quad (\text{II.4.13})$$

This is the same result as the one that would be obtained in the pure theory: *the sum of the connected correlations $\sum_b \langle u_x^a u_y^b \rangle_{S[0, \cdot]} = T g_{x,y}$ is not modified by the disorder.* This indicates that connected correlations decay as $e^{-|x-y|/\ell_\mu}$ with $\ell_\mu := 1/\mu$. The parameter μ is not modified by the renormalization. This fact was already heavily used before. Other relations extracted from (II.4.12) are $\sum_{a_{2n}} G_{x_1, \dots, x_{2n}}^{a_1, \dots, a_{2n}} = 0$

Relating the W_μ functional and the renormalized disorder V_μ .

It is an elementary calculation to show that the W_μ functional is related to the renormalized disorder functional defined in (II.4.7) as

$$e^{W_\mu[\{j_x^a = \frac{1}{T} \int_y g_{x,y}^{-1} w_x^a\}]} e^{-\frac{1}{2T} \sum_a \int_{x,y} g_{x,y}^{-1} w_x w_y} = \overline{\prod_{a=1}^n e^{-\frac{1}{T} \hat{V}_\mu[\{w_x^a\}]}}, \quad (\text{II.4.14})$$

This important relation (its consequences will be shown below) was first shown in [123, 96]. Expanding in cumulants the right hand side of (II.4.9), and in replica sums the

W_μ functional, one sees that *the expansion in cumulants of the renormalized disorder functional exactly gives* $W_\mu[\{j_x^a = \frac{1}{T} \int_y g_{x,y}^{-1} w_x^a\}]$ as, noting $\tilde{W}_\mu[\{w_x^a\}] := W_\mu[\{j_x^a = \frac{1}{T} \int_y g_{x,y}^{-1} w_x^a\}]$

$$\begin{aligned} \tilde{W}_\mu[\{w_x^a\}] &= \tilde{W}_\mu[0] + \frac{1}{2T} \sum_{ab} \int_{x,y} g_{x,y}^{-1} w_x^a w_y^b + \frac{1}{2T^2} \sum_{ab} \hat{R}[\{w_x^{a,b}\}] + \\ &+ \sum_{m \geq 3} \frac{1}{n! T^m} \sum_{a_1, \dots, a_m} \hat{S}^{(m)}[\{w_{x_1}^{a_1}\}, \dots, \{w_{x_m}^{a_m}\}]. \end{aligned} \quad (\text{II.4.15})$$

where we have introduced the notation $w_x^{a,b} = w_x^a - w_x^b$ and

$$\tilde{W}_\mu[0] = -\frac{n}{T} \overline{\hat{V}_\mu[\{w_x^a\}]} \quad (\text{II.4.16})$$

$$\hat{R}[\{w_x^{a,b}\}] := \overline{\hat{V}_\mu[\{w_x^a\}] \hat{V}_\mu[\{w_x^c\}]^c} \quad (\text{II.4.17})$$

$$\hat{S}^{(m)}[\{w_{x_1}^{a_1}\}, \dots, \{w_{x_m}^{a_m}\}] := (-1)^m \overline{\hat{V}_\mu[\{w_{x_1}^1\}] \dots \hat{V}_\mu[\{w_{x_m}^m\}]^c} \quad (\text{II.4.18})$$

Here STS implies that $\tilde{W}_\mu[0]$ does not depend on $\{w_x^a\}$, $\hat{R}[\{w_x^{a,b}\}]$ only depends on the difference $w_x^a - w_x^b$, and similarly the higher order cumulants of the renormalized disorder satisfy $\hat{S}^{(m)}[\{w_{x_1}^{a_1} + w_x\}, \dots, \{w_{x_m}^{a_m} + w_x\}] = \hat{S}^{(m)}[\{w_{x_1}^{a_1}\}, \dots, \{w_{x_m}^{a_m}\}]$. Note that this expansion in cumulants is not trivially related to the expansion in j_x^a performed in (II.4.9) (e.g. $\hat{R}[\{w_x^{a,b}\}]$ itself has an expansion in w).

The effective action

The last functional to introduce before we give the important results of the FRG is *the effective action functional* $\Gamma_\mu[\{u_x^a\}]$. As usual in Field-Theory it is defined as the Legendre transform of the W_μ functional:

$$\begin{aligned} \Gamma_\mu[\{u_x^a\}] &= -W_\mu[\{j_x^a\}] + \sum_a \int_x j_x^a u_x^a = -\tilde{W}_\mu[\{w_x^a\}] + \frac{1}{T} \int_{x,y} g_{x,y}^{-1} u_x^a w_y^a \\ u_x^a &= \frac{\delta W_\mu[\{j_y^b\}]}{\delta u_x^a} = T \int_z g_{x,z} \frac{\partial \tilde{W}_\mu[\{w_y^b\}]}{\delta w_x^a}. \end{aligned} \quad (\text{II.4.19})$$

In terms of diagrams it corresponds to the sum of 1-particle irreducible diagrams generated by the action $S[0; \{u_x^a\}]$. The physical, disordered averaged observables are contained in W_μ which can be obtained from the effective action Γ_μ by inverting the Legendre transform (the latter is actually an involution). This was performed in [96]. In particular, it is shown that $\Gamma_\mu[\{u_x^a\}]$ admits an expansion as

$$\begin{aligned} \Gamma_\mu[\{u_x^a\}] &= \Gamma_\mu[0] + \frac{1}{2T} \sum_{ab} \int_{x,y} g_{x,y}^{-1} u_x^a u_y^b - \frac{1}{2T^2} \sum_{ab} R[\{u_x^{a,b}\}] + \\ &- \sum_{m \geq 3} \frac{1}{n! T^m} \sum_{a_1, \dots, a_m} S^{(m)}[\{u_{x_1}^{a_1}\}, \dots, \{u_{x_m}^{a_m}\}]. \end{aligned} \quad (\text{II.4.20})$$

And inverting the Legendre transform gives ‘nice’ relations between the cumulants of the renormalized disorder and the ‘Gamma cumulants’. In particular we have $\Gamma_\mu[0] = -\tilde{W}_\mu[0]$ and what will turn out to be the most important relation, the equality between functionals

$$R[\{w_x\}] = \hat{R}[\{w_x\}]. \quad (\text{II.4.21})$$

c Exact RG approach: The Morris-Wetterich equation and the scaling hypothesis

Let us first formulate the FRG result using an exact RG formalism and later connect it to perturbative approaches. To formulate the exact RG equation, it is convenient to define a slightly different effective action functional

$$\hat{\Gamma}_\mu[\{u_x^a\}] = \Gamma_\mu[\{u_x^a\}] - \frac{1}{2T} \sum_{ab} \int_{x,y} g_{x,y}^{-1} u_x^a u_y^b. \quad (\text{II.4.22})$$

The latter behaves well even for $\mu \rightarrow \infty$. Indeed, for $\mu \rightarrow \infty$, it is clear that the functional W_μ in (II.4.8) can be evaluated using a saddle-point calculation around $u_x^a = w_x^a$. Inserting the result into the Legendre transform (II.4.13) shows that $\lim_{\mu \rightarrow \infty} \hat{\Gamma}_\mu[\{u_x^a\}]$ is exactly the expansion in cumulants of the bare disorder $V(x, u)$:

$$\lim_{\mu \rightarrow \infty} \hat{\Gamma}_\mu[\{u_x^a\}] = -\frac{1}{2T^2} \sum_{a,b=1}^n \int_x R_0(u_x^a - u_x^b) + \dots, \quad (\text{II.4.23})$$

where again we have added dots to signify the presence of higher order cumulants if the initial disorder is non-Gaussian³. As a function of μ , the effective action functional satisfies the Morris-Wetterich equation [124, 125, 118, 96]

$$-\mu \partial_\mu \hat{\Gamma}_\mu[\{u_x^a\}] = \beta[\hat{\Gamma}_\mu[\{u_x^a\}]], \quad (\text{II.4.24})$$

where the functional β function is

$$\beta[\hat{\Gamma}_\mu[\{u_x^a\}]] = -\frac{1}{2} \sum_a \int_{x,y,z} \mu (\partial_\mu g_{x,y}) g_{y,z}^{-1} (G^{-1})_{z,x}^{a,a}, \quad G_{x,y}^{a,b} = 1 - T \int_z g_{x,z} \frac{\delta^2 \hat{\Gamma}_\mu}{\delta u_z^a \delta u_y^b}. \quad (\text{II.4.25})$$

At our level of rigor (II.4.23) is an (awfully complicated) well posed problem: we have an initial condition at $\mu \rightarrow \infty$ ⁴ for a differential equation that we want to solve. Actually we do not want to follow completely the RG flow from $\mu \rightarrow \infty$ to $\mu = 0^+$, but rather, although it is not obvious, show that close to $\mu = 0$, an appropriately rescaled version of $\hat{\Gamma}_\mu[\{u_x^a\}]$ tends to a fixed point functional. More precisely, reintroducing explicitly T as a parameter and rescaling,

$$x = \mu^{-1} \tilde{x}, \quad u_x = \mu^{-\zeta_s} \tilde{u}_{\tilde{x}}, \quad T \sim \mu^{-\theta} \tilde{T} \quad (\text{II.4.26})$$

the scaling hypothesis can be phrased in an unambiguous way as follows. We require that the effective action in the ‘tilde’ variables, that describe the large scale physics of the original theory,

$$\tilde{\Gamma}_\mu[\tilde{T}; \{\tilde{u}_{\tilde{x}}\}] = \Gamma_\mu[T = \mu^{-\theta} \tilde{T}, \{u_x = \mu^{\zeta_s} \tilde{u}_{\tilde{x}=\mu x}\}] \quad (\text{II.4.27})$$

converges, as $\mu \rightarrow 0$, to a constant, well-defined action:

$$\lim_{\mu \rightarrow 0} \tilde{\Gamma}_\mu[\tilde{T}; \{\tilde{u}_{\tilde{x}}\}] = \tilde{\Gamma}^*[\tilde{T}; \{\tilde{u}_{\tilde{x}}\}]. \quad (\text{II.4.28})$$

³Note here that something bad can happen if the bare disorder has fat tails since then the expansion in cumulants is ill-defined.

⁴If a small scale cutoff a is assumed then the initial condition (II.4.23) holds at $\mu = 1/a$.

Inserting the scaling form (II.4.27) into the RG equation (II.4.24), $\tilde{\Gamma}_\mu[\tilde{T}; \{\tilde{u}_x\}]$ itself satisfies a Morris-Wetterich equation with a rescaled β function:

$$-\mu\partial_\mu\tilde{\Gamma}_\mu[\tilde{T}; \{\tilde{u}_x\}] = \tilde{\beta}[\tilde{\Gamma}_\mu][\{\tilde{u}_x\}]. \quad (\text{II.4.29})$$

And since $-\mu\partial_\mu = -\partial_{\log(\mu)}$ and $\log(\mu) \rightarrow_{\mu \rightarrow 0} -\infty$, (II.4.28) actually implies that the limiting functional is a fixed point of the rescaled Beta function

$$\tilde{\beta}[\tilde{\Gamma}^*] = 0. \quad (\text{II.4.30})$$

The hypothesis (II.4.28) is thus rather strong and allows us not to follow completely the RG flow (since we are thus only interested in the fixed point), while defining the Beta function in (II.4.24) as generating the flow associated with $-\mu\partial_\mu$ (an not e.g. ∂_μ) is not a random choice. Obviously these are all strong hypotheses (that will not be proven). Before we describe the solution of this problem at $T = 0$, let us note that since the effective action contains the term $\frac{1}{2T} \sum_{ab} \int_{x,y} g_{x,y}^{-1} u_x^a u_y^b$ where $g_{x,y}^{-1}$ is the bare propagator that is not corrected by the renormalization (STS), the exponent θ must be given by $d - \gamma + 2\zeta_s$ and there is only one unknown critical exponent here.

d Solving the Morris-Wetterich equation at $T = 0$ in $d = d_{uc} - \epsilon$: the multi-local expansion

The main result of the FRG approach to disordered elastic interface is: there exists a solution of (II.4.30) such that, in the $T \rightarrow 0$ limit, it converges to a fixed point functional $\tilde{\Gamma}^*$ that admits a perturbative expansion in $\epsilon = 2\gamma - d$. In this limit the action is non-analytic around $u_x^a = 0$. This non-analyticity is smoothed at $T \neq 0$ on a small scale called the *thermal boundary layer*, $u_x^a \sim \tilde{T} \sim \mu^\theta T$. Considering carefully the $T \rightarrow 0$ by taking this smoothing into account allows to obtain the β function directly at $T = 0$ [96]. In the end the structure of the solution is as follows. The functional $R[\{u_x\}]$ can be separated into its local $R(u)$ and non-local part $\tilde{R}[u]$ as

$$R[\{u_x\}] = \int_x R(u_x) + \tilde{R}[\{u_x\}] \quad (\text{II.4.31})$$

where the decomposition is unambiguously defined by the fact that $\tilde{R}[\{u_x\}]$ is 0 for a constant field $u_x = u$ for which $R[\{u_x = u\}] = L^d R(u)$. At the fixed point, the function $R(u)$ is $O(\epsilon)$, the non-local part $\tilde{R}[\{u_x\}]$ is $O(\epsilon^2)$ and the higher-order cumulants are $S^{(m)}[\{u_{x_1}^{a_1}\}, \dots, \{u_{x_m}^{a_m}\}]$ are $O(\epsilon^m)$. They can be computed by plugging the decomposition (II.4.20) into (II.4.24) and assuming that they scale with ϵ as written above. Using this decomposition, the differential equation for the local part can be closed, in principle, up to an arbitrary order in ϵ . We now show this differential equation up to order $O(\epsilon^2)$ as obtained in [116]. Let us first introduce the loop integrals

$$\begin{aligned} I_1 &= \mu^{d-2\gamma} \tilde{I}_1 \quad , \quad \tilde{I}_1 = \int_q \frac{1}{(q^2 + 1)^\gamma} \\ I_A &= \mu^{2d-4\gamma} \tilde{I}_A \quad , \quad \tilde{I}_A = \int_{q_1, q_2} \frac{1}{(q_1^2 + 1)^{\frac{\gamma}{2}} (q_2^2 + 1)^{\frac{\gamma}{2}} ((q_1 + q_2)^2 + 1)^\gamma} + O(\epsilon) \end{aligned} \quad (\text{II.4.32})$$

Note that the combination $\epsilon \tilde{I}_1$ stays finite as $\epsilon \rightarrow 0$. We will often use

$$A_d^\gamma := \frac{1}{\epsilon \tilde{I}_1} = \frac{(2\sqrt{\pi})^d}{2} \frac{\Gamma(\gamma)}{\Gamma(\gamma + 1 - d/2)} \quad (\text{II.4.33})$$

$$= 2^{-1+2\gamma} \pi^\gamma \Gamma(\gamma). \quad (\text{II.4.34})$$

Rescaling

$$R(u) = A_d^\gamma \mu^{\epsilon-4\zeta_s} \tilde{R}(\mu_s^\zeta u) \quad (\text{II.4.35})$$

one obtains [116, 96]

$$\begin{aligned} -\mu \partial_\mu \tilde{R}(u) &= \underbrace{(\epsilon - 4\zeta_s) \tilde{R}(u) + \zeta u \tilde{R}'(u)}_{\text{rescaling}} + \underbrace{\left(\frac{1}{2} \tilde{R}''(u)^2 - \tilde{R}''(0) \tilde{R}''(u) \right)}_{\text{1-loop}} \\ &+ \underbrace{\frac{1}{2} X \left((\tilde{R}''(u) - \tilde{R}''(0)) \tilde{R}'''(u)^2 \right) - \frac{\lambda_s}{2} X (\tilde{R}'''(0^+)^2) \tilde{R}''(u)}_{\text{2-loops}} \\ &+ O(\tilde{R}^4) \end{aligned} \quad (\text{II.4.36})$$

where $\lambda_s = 1$ and $X = \frac{2\epsilon(2\tilde{I}_A - \tilde{I}_1^2)}{(\epsilon \tilde{I}_1)^2}$, i.e. $X = 1 + O(\epsilon)$ for $\gamma = 2$ (short-range elasticity) and $X = 4 \ln(2) + O(\epsilon)$ for $\gamma = 1$. We are looking for a solution of the equation $-\mu \partial_\mu \tilde{R}(u) = 0$. Since we are expanding around $d = d_{\text{uc}}$ where the disorder is only marginally relevant, ζ_s is expected to be $O(\epsilon)$ and thus the solution of $-\mu \partial_\mu \tilde{R}(u) = 0$ in (II.4.36) is also, as announced, $O(\epsilon)$. The value of the exponent $\zeta_s = \epsilon \zeta_1 + \epsilon^2 \zeta_2^2 + O(\epsilon^3)$ has to be adjusted so that a solution of (II.4.36) with the desired properties hold. Note that if $\tilde{R}^*(u)$ is a fixed point of (II.4.36), $\tilde{R}(u) = \frac{1}{\kappa^4} \tilde{R}^*(\kappa u)$ is also a fixed point and thus there are several *families* of fixed points. Thus when talking about a FP one has to specify one scale. Universal quantities can nevertheless be constructed as e.g. $\tilde{R}''''(0)$, $\tilde{R}(0)/(\tilde{R}''(0))^2 \dots$ (see [116]). A standard choice is to fix the value at 0 as $\tilde{R}^*(0) = \epsilon$. It was found that

- A single value of ζ_1 , ζ_2 leads to a fixed point function in the random bond universality class with $\tilde{R}^*(u)$ quickly decaying to 0. The latter was obtained using a shooting method in ([116]) as (the $O(\epsilon)$ result is coherent with the previous result from [114]) $\zeta_1 = 0.20829806(3)$ and $\zeta_2 = 0.006858(1)$ for SR elasticity ($\gamma = 2$).
- A single value of ζ_s leads to a FP in the random field universality class, i.e. with $\tilde{R}^*(u) \sim_{|u| \rightarrow \infty} |u|$ and $\tilde{R}''(u)$ decaying quickly to 0. It is given by $\zeta_s = \epsilon/3 + O(\epsilon^2)$ (independently of γ). This result was actually argued to hold to any order [116] in ϵ , in agreement with the simple Flory argument of Sec. I.2.3.
- For periodic disorder $\tilde{R}^*(u) = \tilde{R}^*(u+1)$, the value of ζ is necessarily 0. Interestingly in this case it was found in [116] that $\tilde{R}^*(u) = f(\epsilon)u(1-u)$ with $f(\epsilon) = O(\epsilon)$ a function. This form was also conjectured to hold to all order.

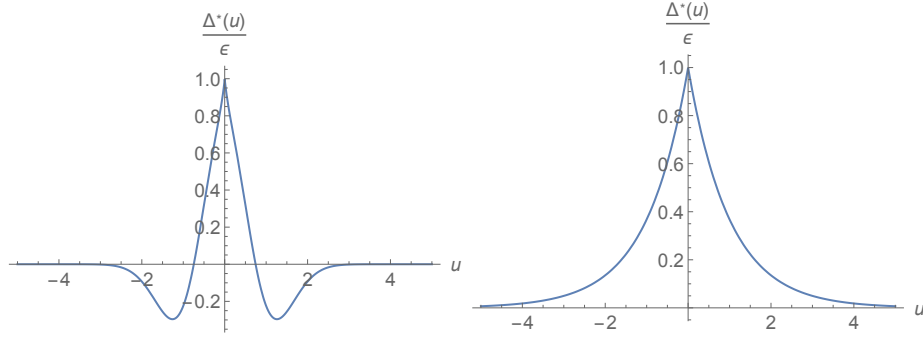


Figure II.3: Cartoon of the shape of FRG fixed point functions $\Delta^*(u) = -R^{**}(u)$ for the RB universality class (left) and the RF universality class (right).

These different fixed points were argued to be stable in [114, 116]. The typical shape of the RF and RB FP functions $\Delta^*(u) = -R^{**}(u)$, here normalized as $\Delta^*(0) = \epsilon$, are plotted in Fig. II.3. Other generic long-range fixed points with $\tilde{R}(u) \sim_{u \rightarrow \infty} u^{2(1-\alpha)}$ with $\zeta_s^\alpha = \frac{\epsilon}{2(1+\alpha)}$ (holding presumably to all order) were also found and argued to be stable as long as they lead to a roughness exponent larger than the RB roughness exponent [116] (otherwise the system flows to the RB FP). Let us conclude this section with a few remarks:

1. The first line of (II.4.36) (i.e. the rescaling and the one-loop part) were already obtained by Fisher in [114] using a Wilson's RG scheme and can be easily obtained using a standard perturbative RG from the beginning.
2. It is instructive to study the flow of $\tilde{R}''(0)$ and $\tilde{R}''''(0)$: to one-loop these close as $-\mu \partial_\mu \tilde{R}''(0) = (\epsilon - 2\zeta_s) \tilde{R}''(0) + \tilde{R}''''(0)^2$ and $-\mu \partial_\mu \tilde{R}''''(0) = \epsilon \tilde{R}''''(0) + 3\tilde{R}''''(0)^2 + 4\tilde{R}''(0)\tilde{R}''''''(0)$. Starting from an initially smooth disorder at some scale μ_0 , $R_{\mu_0}(u)$, at the beginning of the flow the function stays analytic: $\tilde{R}''(0) = \tilde{R}''''(0) = 0$. At the beginning of the flow $\tilde{R}''(0)$ thus does not flow, and if it were so for all time one would find $\zeta_s = \epsilon/2$ i.e. the dimensional reduction result. However, $\tilde{R}''''(0)$ becomes infinite, and thus the function non-analytic around 0, in a finite renormalization time. More precisely, for $\mu > \mu_c = \mu_0 \left(\frac{3\tilde{R}''''(0)}{3\tilde{R}''''(0) + \epsilon} \right)^{\frac{1}{\epsilon}}$, one obtains $\tilde{R}''''(0) = \frac{\tilde{R}''''(0)\epsilon\mu_0^\epsilon}{(3\tilde{R}''''(0) + \epsilon)\mu^\epsilon - 3\tilde{R}''''(0)\mu_0^\epsilon}$ and \tilde{R} becomes non-analytic around 0 for $\mu \leq \mu_c$: the function $\tilde{\Delta}(u) = -\tilde{R}''(u)$ acquires a linear cusp around 0: $\tilde{\Delta}(u) - \tilde{\Delta}(0) \simeq \tilde{\Delta}'(0^+) |u| + O(u^2)$. The occurrence of this cusp will be related to shocks below. Note that once the cusp appears, $\tilde{R}''(0)$ starts to flow and the system escapes dimensional reduction. Note that the cusp appears when the system probes length scales larger than $L'_c := 1/\mu_c = \frac{1}{\mu_0} \left(1 + \frac{\epsilon}{3\tilde{R}''''(0)} \right)^{\frac{1}{\epsilon}}$. Using the simple estimate $\tilde{R}''''(0) \sim \frac{\Delta(0)}{u_c^2}$, one shows that L'_c essentially reproduces the Larkin length L_c computed in (I.2.25). Thus, following the renormalization group flow, the system actually believes that it is flowing to the Larkin fixed point up to a scale corresponding to the Larkin length where the cusp, associated with

metastability in the system (see below), appears. The fact that no ‘supercusp’ appears later in the flow, i.e. all derivative of \tilde{R} at 0 up to the fourth one remain finite, was discussed in [116].

3. The second line of (II.4.36) was first obtained in [116] where the authors used standard (although functional) perturbative RG to directly attempt to renormalize the field theory at $T = 0$. The problem with this approach is that one then encounters so-called ‘anomalous terms’ involving $\tilde{R}'''(0)$ and one has to decide whether it is $\tilde{R}'''(0^+)$ or $\tilde{R}'''(0^-)$. The proper way to do so is to regularize the non-analytic behavior by studying the zero temperature limit of the renormalized theory at finite temperature as outlined above and reviewed in [96]. In [116] the authors nevertheless obtained (II.4.36) with a value of λ a priori not specified by the perturbative method, which was imposed to be one to respect the ‘potentiality’ of the problem, i.e. the existence of FP function of the RB type (see [116]).
4. The FRG equation (II.4.36) is both UV *and* IR universal. It is UV universal in the sense that, by construction, it does not depend on the microscopic details of the models. The more subtle property is to prove that it does not depend on the chosen IR cutoff scheme [116], that was here chosen as a massive scheme.

II.4.2 Applying the functional renormalization group to shocks

In this section we now discuss the application of FRG methods presented in Sec. II.4.1 to the study of the shock statistics of the interface presented in Sec. II.3.1. We begin by linking the non-analyticity of the fixed point effective action of FRG with the occurrence of shocks. We then show how FRG can be used to compute shock observables on the example of the density of total size of shocks.

a The cusp and the shocks

As already remarked we first note that as $T \rightarrow 0$, the renormalized disorder potential for a constant well $\hat{V}_\mu(w) := \hat{V}_\mu[\{w_x = w\}]$ defined in (II.4.7) converges to (assuming no degeneracy of the ground state, which is true with probability 1 except at some discrete positions)

$$\hat{V}_\mu(w) = \frac{1}{2} \int g_{x,y}^{-1}(u_x(w) - w)(u_y(w) - w) + \int_x V(x, u_x(w)), \quad (\text{II.4.37})$$

where as usual $u_x(w)$ denotes the ground state of the interface as defined in (II.4.1). Using the saddle-point structure in (II.4.1), one shows that the *renormalized force at the scale μ* , defined by

$$\hat{F}_\mu(w) := -\partial_w \hat{V}_\mu(w) \quad (\text{II.4.38})$$

admits the expression at zero temperature

$$\hat{F}_\mu(w) = \int_{x,y} g_{x,y}^{-1}(w - u_x(w)) = \int_x f_x(w) \quad \text{with} \quad f_x(w) = m^2(w - u_x(w)). \quad (\text{II.4.39})$$

where the second equality is true for elastic kernel of the form $g_{x,y}^{-1} = \int_q e^{iq(x-y)}(q^2 + \mu^2)^{\frac{\gamma}{2}}$ and we recall that $m = \mu^{\frac{\gamma}{2}}$. Hence, using (II.4.16), (II.4.21) and the definition of the local part (II.4.31), one sees that the *local part of the second cumulant of the renormalized force at the scale μ* , defined by,

$$\Delta(u) := -R''(u) \quad (\text{II.4.40})$$

is linked to an observable of the ground state as

$$\Delta(w - w') = \frac{1}{L^d} \partial_w \partial_{w'} \overline{\hat{V}_\mu(w) \hat{V}_\mu(w')} = \frac{m^4}{L^d} \int_x \int_y \overline{(w - u_x(w))(w - u_y(w))^c}. \quad (\text{II.4.41})$$

Or equivalently, in terms of the position of the *center of mass of the interface* defined by

$$u(w) := \frac{1}{L^d} \int_x u_x(w), \quad (\text{II.4.42})$$

we have

$$\Delta(w - w') = L^d m^4 \overline{(u(w) - w)(u(w') - w')}. \quad (\text{II.4.43})$$

This relation, first shown in [123, 96], has deep consequences. On its left hand side it involves the second cumulant of the renormalized disorder that naturally appears in the effective action of the replicated theory. As a function of $m = \mu^{\frac{\gamma}{2}}$, the rescaled cumulant

$$\tilde{\Delta}(w) := (A_d^\gamma)^{-1} \mu^{2\zeta_s - \epsilon} \Delta(\mu^{-\zeta_s} w) \quad (\text{II.4.44})$$

obeys a RG equation that is the second derivative of (II.4.36). In the limit $\mu \rightarrow 0$ it converges to a fixed point function, depending on the universality class of the initial bare disorder. This fixed point function is non-analytic and exhibits a cusp around 0 (see Fig. II.3) and for small μ we thus have $\tilde{\Delta}(w) - \tilde{\Delta}(0) \simeq \tilde{\Delta}'(0^+) |w| + O(w^2)$. On the right hand side on the other hand it involves a simple observable linked to the ground state of the interface. This relation thus provides a protocol to *measure the FRG function $\Delta(u)$* . The latter was first implemented in numerics with an excellent agreement with the theory [105], and later also in experiments [61] (for the related case of the depinning). On the other hand, since the left hand side of (II.4.43) is non-analytic beyond the Larkin scale $\mu_c \sim L_c^{-1}$ this *shows that the right-hand side is also non-analytic beyond the Larkin scale*. More precisely, using $\overline{u(w)} = w$, (II.4.43) can be rewritten as, introducing $\hat{u}(w) = u(w) - w$,

$$\overline{(\hat{u}(w) - \hat{u}(0))^2} = -2 \frac{\Delta(w)}{L^d m^4}. \quad (\text{II.4.45})$$

For a smooth motion, the left-hand side of (II.4.45) is $O(w^2)$ for small w . Obviously this could just mean that with some probability $\hat{u}(w) \sim \sqrt{w}$ close to $w = 0$. The natural interpretation from the study of $d = 0$ models, numerics (and physical intuition) is, however, that with a small probability proportional to w , the center of mass of the

interface makes a jump of size S/L^d , distributed with a PDF $P(S)$ and (II.4.45) is rewritten

$$\rho_0 w \frac{\langle S^2 \rangle_P}{L^{2d}} + O(w^2) = -\frac{2\Delta'(0^+)w}{L^d m^4} + O(w^2), \quad (\text{II.4.46})$$

where $\langle \rangle_P$ denotes the average with respect to P and ρ_0 already introduced in Sec. II.3.1, is the density of shocks per unit length. Equivalently, using the definitions of the density $\rho(S)$ and PDF $P(S) = \rho(S)/\rho_0$ of avalanche total size introduced in Sec. II.3.1, see (II.3.5) and (II.3.6), as well as the relation shown there $\langle S \rangle_\rho = \rho_0 \langle S \rangle_P = L^d$, (II.4.46) is rewritten

$$S_m := \frac{\langle S^2 \rangle_\rho}{2\langle S \rangle_\rho} = \frac{\langle S^2 \rangle_\rho}{2\langle S \rangle_\rho} = \frac{\sigma}{m^4}, \quad \sigma = -\Delta'(0^+) \geq 0. \quad (\text{II.4.47})$$

Note that the relation (II.4.47) is exact here since $\Delta(w)$ is exactly given by (II.4.43)⁵. It can also be easily obtained by *assuming that the shock decomposition*

$$u_x(w) = cst + \sum_i S_x^{(i)} \theta(w - w_i), \quad (\text{II.4.48})$$

holds at small μ . The basic idea of applying FRG to shocks is to *interpret* the short-scale singularities that appear in the FRG flow of the effective action as consequences of the presence of shocks as written in (II.4.48). Here (II.4.47) actually does not tell much about the shock statistics since $\Delta'(0^+)$ contains one non-universal scale κ as discussed in Sec. II.4.1. Here we have thus linked this non-universal scale to a precise (non-universal) observable in (II.4.47). On the other hand the result of the FRG is that all higher order cumulants of the renormalized disorder potential and the full effective action can be obtained using the structure of the ϵ expansion as functions of $\Delta(u)$. In the end this will imply that all higher order moments of the shock total size density $\langle S^n \rangle_\rho$ (and other shocks observables) can be expressed using the ϵ expansion in terms of only one non-universal scale, that we can choose as S_m . The true input of FRG in the study of shock statistics basically works in three steps:

- (i) Assume the shock decomposition (II.4.48) and relate a given shock observable to a disorder averaged observable of $u_x(w)$ (actually we will need disorder average observables of the ground state for different well position w in the same environment, see below).
- (ii) Compute the disorder averaged observable in the limit $\mu \rightarrow 0$ using the results of the FRG.
- (iii) Draw the consequences for the shock observable.

b Shocks and the ϵ expansion: the case of the one-shock total size distribution

Let us now briefly recall how the above program goes for the one-shock total size density $\rho(S)$. The following is based on [109, 111]. Let us first study the scaling of S_m

⁵Up to a non-universal scale it can also be computed in an ϵ expansion using FRG but that is not what we are doing here.

defined in (II.4.47) with μ and ϵ . Note that since for small m , $\Delta(w)$ takes the scaling form $\Delta(w) = A_d^\gamma \mu^{\epsilon-2\zeta_s} \tilde{\Delta}(\mu^{\zeta_s} w)$ with $\tilde{\Delta}(w) = O(\epsilon)$ a function close to one of the fixed points of the FRG equation, we have, defining $\tilde{\sigma} = \tilde{\Delta}'(0^+)$,

$$S_m = \frac{\langle S^2 \rangle_\rho}{2\langle S \rangle_\rho} = A_d^\gamma \frac{\mu^{\epsilon-\zeta_s}}{m^4} \tilde{\sigma} = A_d^\gamma \mu^{-d-\zeta_s} \tilde{\sigma}, \quad (\text{II.4.49})$$

and we recall $m = \mu^{\gamma/2}$. First, note that S_m diverges as $\mu \rightarrow 0$ and that the scaling (II.4.49) is consistent with the scaling hypothesis

$$\rho(S) = L^\alpha \mu^\rho \frac{1}{S\tau_S} f_{\text{cut}}\left(\frac{S}{S_m}\right) g_{\text{cut}}\left(\frac{S}{S_0}\right). \quad (\text{II.4.50})$$

with $\tau_S \leq 2$ that was made in the derivation of the NF conjecture in Sec. II.3.1 (there S_m was denoted S_μ in (II.3.14)). Indeed, the second moment $\langle S \rangle_\rho$ diverges as $S_m \rightarrow \infty$ and is controlled by the massive cutoff.

On the other hand, note that $S_m = O(\epsilon)$. Therefore it is natural to assume, and the end result will be consistent with this assumption, that all moments of the avalanche size distribution scale as, for $n \geq 2 \in \mathbb{N}$, $\langle S^n \rangle_\rho \sim S_m^{n-1} \sim \epsilon^{n-1} \mu^{-(n-1)(d+\zeta_s)}$. The proper object which is expected to have a well defined (and universal) $\mu \rightarrow 0, \epsilon \rightarrow 0$ limit is thus the density of shocks total size in units of S_m :

$$\tilde{\rho}(\tilde{S}) := S_m \rho(S_m \tilde{S}). \quad (\text{II.4.51})$$

which is $O(1)$. The latter is normalized as $\int_{\tilde{S}>0} \tilde{S} \tilde{\rho}(\tilde{S}) d\tilde{S} = L^d$ and $\int_{\tilde{S}>0} \tilde{S}^2 \tilde{\rho}(\tilde{S}) d\tilde{S} = 2L^d$. Let us introduce (almost) its Laplace transform (dropping from now on the tilde)

$$Z(\lambda) := L^{-d} \int_{S>0} (e^{\lambda S} - 1) \rho(S) dS. \quad (\text{II.4.52})$$

Here the -1 in the definition of $Z(\lambda)$ is to ensure that (II.4.52) is finite even when $\tau_S > 1$ (which will be true, at least close to $\epsilon = 0$) and the small scale cutoff S_0 in (II.4.50) is sent to 0. The L^{-d} ensures that it is finite as $L \rightarrow \infty$. Altogether, $Z(\lambda) = \lambda + 2\lambda^2 + O(\lambda^3)$, and note that the coefficient in front of λ and λ^2 are exact (i.e. they are consequences of our definition). The real input of FRG is to provide the ϵ expansion of the coefficients in front of the higher order terms in λ^n , $n \geq 3$.

(i) The first step is now to relate $Z(\lambda)$ to a disorder averaged observable of the position field, assuming that the shock decomposition (II.4.48) holds. This was done in [109, 111] and the result is

$$Z(\lambda) = \partial_\delta G_\delta(\lambda)|_{\delta=0^+}, \quad G_\delta(\lambda) := L^{-d} \overline{e^{\frac{\lambda L^d}{S_m} (\hat{u}(w+\delta) - \hat{u}(w))}} \quad (\text{II.4.53})$$

Here $\hat{u}(w+\delta) = \frac{1}{L^d} \int (u_x(w) - w)$. Let us give a quick justification that (II.4.53) holds: if there is no shock between w and $w+\delta$, $L^{nd} (\hat{u}(w+\delta) - \hat{u}(w))^n$ is of order $O(\delta^n)$ and such events do not contribute to (II.4.53). The order $O(\delta)$ in $L^{nd} (\hat{u}(w+\delta) - \hat{u}(w))^n$ is thus dominated by the probability $\rho_0 \delta$ that one shock occurred and $(\hat{u}(w+\delta) - \hat{u}(w))^n \sim \rho_0 \delta \langle S^n \rangle_P + O(\delta^2) = \delta \langle S^n \rangle_\rho + O(\delta^2)$. (Here we neglect possible contributions coming from the simultaneous occurrence of more than one shock at w^+ , this hypothesis is

sometimes referred to as the fact that the shocks are dilute, and the probability that two shocks occurred is thus $O(\delta^2)$). This justifies (II.4.53) at each order in an expansion in λ .

(ii) In the second step, we now want to compute the right hand-side of (II.4.53) using FRG. To do this we need to consider the replicated action for several copies of the same disordered elastic system. We therefore consider the theory for $r = 2$ position fields u_x^i coupled to different parabolic wells centered at positions w_i in the same disordered environment ($w_1 = w$ and $w_2 = w + \delta$). The Hamiltonian of the problem is

$$\mathcal{H}[\{u\}, \{w\}] = \sum_{i=1}^r \mathcal{H}_{\text{el}}[u^i, w^i] + \sum_{i=1}^r \int_x V(u_x^i, x). \quad (\text{II.4.54})$$

This leads to a replicated action of the form

$$S[u] = \frac{1}{2T} \sum_{a,i} \int_{xx'} g_{xx'}^{-1}(u_{ax}^i - w_i)(u_{ax'}^i - w_i) - \frac{1}{2T^2} \sum_{a,i;b,j} \int_x R_0(u_{ax}^i - u_{bx}^j) + \dots \quad (\text{II.4.55})$$

where a is a replica index and R_0 is, as in (II.4.2), the bare cumulant of the disorder $V(x, u)$. The results from FRG of the previous section for the $r = 1$ case can be generalized⁶ to this new problem [109, 111]. In particular one shows that the effective action of the theory is given by, in the limit $\mu \rightarrow 0$,

$$\Gamma[u] = \frac{1}{2T} \sum_{a,i} \int_{xx'} g_{xx'}^{-1}(u_{ax}^i - w_i)(u_{ax'}^i - w_i) - \frac{1}{2T^2} \sum_{a,i;b,j} \int_x R(u_{ax}^i - u_{bx}^j) + O(\epsilon^2). \quad (\text{II.4.56})$$

Here $R(u) = O(\epsilon)$ is the same renormalized disorder correlator as already introduced in the previous section, while the neglected terms are higher-order terms in ϵ that can be expressed as loop integrals with higher powers of R . Using the effective action (II.4.56) is often referred to as the improved tree theory. Here one can a priori use either the renormalized disorder correlator $R(u)$ as computed to order $O(\epsilon)$ from the FRG, or the true renormalized disorder correlator $R(u)$, since (II.4.56) is then still true up to $O(\epsilon^2)$. The observable $G_\delta(\lambda)$ is then computed by singling out the first replica as

$$G_\delta(\lambda) = L^{-d} \lim_{T,n \rightarrow 0} \int \mathcal{D}[u] e^{\frac{\lambda}{S_m} \int_x (u_{1x}^2(w_2) - u_{1x}^1(w_1) - w_2 + w_1) - S[u]} \quad (\text{II.4.57})$$

This path integral is evaluated using a saddle-point calculation on the effective action (II.4.56). The saddle-point equations are solved in the limit $T, n \rightarrow 0$ (see [111]).

(iii) In the end one obtains the result, valid for $\lambda < 1/4$,

$$\begin{aligned} Z(\lambda) &= \lambda + Z(\lambda)^2 + O(\epsilon) \\ Z(\lambda) &= \frac{1}{2} \sqrt{1 - 4\lambda} + O(\epsilon). \end{aligned} \quad (\text{II.4.58})$$

Which corresponds to a tree result for $\rho(S)$:

$$\rho(S) = \frac{L^d}{2\sqrt{\pi} S^{3/2}} e^{-S/4} + O(\epsilon). \quad (\text{II.4.59})$$

⁶Actually it is exactly the same theory since (II.4.55) is equivalent to taking all $w_i = 0$ but coupling the action to a source that depends on the replica index as done in Sec. II.4.1, see (II.4.14).

In terms of the avalanche size distribution exponent we have thus

$$\tau_S = \frac{3}{2} + O(\epsilon) = 2 - \frac{\gamma}{d + \zeta_s} + O(\epsilon). \quad (\text{II.4.60})$$

i.e. the result agrees well with the NF conjecture to order $O(1)$ since $\zeta_s = O(\epsilon)$ and $d = 2\gamma - \epsilon$. The results (II.4.58), (II.4.59), (II.4.60) have the status of mean-field theory results for the shock total size density. We will see that these are equivalent to the mean-field theory results obtained in the dynamics and there we will describe more precisely what this mean-field theory corresponds to. Before we turn to the analysis of avalanches at depinning let us make a few comments on (II.4.59)

- Dimensions in (II.4.59) are reintroduced using (II.4.51), in particular note that, as announced, the dimensionful result for $\rho(S)$ contains only one non-universal scale that was here chosen as S_m (defined in (II.4.49)).
- The exponent $\tau_S = 3/2$ appears completely universal, i.e. independent of both the UV (hidden in σ) and IR (the massive cutoff) details of the models.
- The form of the distribution (II.4.59) (i.e. the exponential cutoff) is UV independent but non-universal in the sense that it depends on the chosen IR regularizing scheme, here a massive cutoff with $\ell_\mu = 1/\mu \ll L$. We note that such massive cutoffs have been argued to be relevant in some experimental setups, as e.g. for fluid contact line experiments [61].
- The above calculations have been extended using FRG to one-loop accuracy in [109, 111]. One of the result shown there is that the avalanche size exponent τ_S does agree with the NF conjecture. To this date this is the most precise calculation and we thus have $\tau_S = 2 - \frac{\gamma}{d + \zeta_s} + O(\epsilon^2)$.

II.5 The functional renormalization group treatment of avalanches in disordered elastic systems: a short review

In this section we now review the use of the functional renormalization group to calculate avalanche observables. We will begin by recalling the important results of FRG for the dynamics of d -dimensional interfaces at the depinning transition in Sec. II.5.1, and in Sec. II.5.2 we will show how to apply FRG to the study of avalanches.

II.5.1 The functional renormalization approach to the depinning transition

a Introduction

In this section we now review important FRG results on the depinning transition. We will try to make as many parallels as possible with the FRG theory for the static problem and therefore give less details in this section. As for the static problem at $T = 0$, a naive perturbative approach to the depinning transition gives the trivial dimensional reduction result. The FRG approach escapes this phenomenon through a renormalization procedure which involves a non-analytic action. As for the statics, this

was first found by a one-loop perturbative analysis using Wilson's RG [126, 127, 128, 108]. This analysis surprisingly led to results identical to the one-loop results in the static problem, while the two problems are clearly different (in particular the random bond universality class is unstable at depinning, see below). The FRG analysis was extended to two-loops in [129], and there the differences with the statics appeared. An interesting extension to the creep regime was also made in [26], though some questions remain open. Pedagogical reviews of FRG for the depinning transition can be found in [9, 43]. Let us now introduce the main objects and state the results. We study the problem

$$\begin{aligned}\eta_0 \partial_t u_{tx} &= \int_y g_{x,y}^{-1} (w(t) - u_{ty}) + F(x, u_{tx}) \\ w(t) &= vt .\end{aligned}\tag{II.5.1}$$

As usual $g_{x,y}^{-1} = \int_q \sqrt{q^2 + \mu^2} e^{iq(x-y)}$ and the random force is chosen centered, Gaussian with a second cumulant

$$\overline{F(x, u)F(x', u')} = \delta^{(d)}(x - x') \Delta_0(u - u') .\tag{II.5.2}$$

We are interested to study (II.5.1) in the successive limits: (i) $t \rightarrow \infty$ (more precisely we want to describe correlations in the steady state reached by an interface described by (II.5.1), the latter being uniquely defined up to trivial time-translations [20] and thus the initial condition of (II.5.1) will be unimportant); (ii) $v \rightarrow 0^+$ (depinning regime); (iii) $\mu \rightarrow 0$ (where observables are expected to reach a universal scaling limit and avalanches to occur). Disorder-averaged observables of the position field are computed using the Martin-Siggia-Rose (MSR) formalism (see [130, 131] for historical references and [132, 133] for reviews).

$$\begin{aligned}\overline{O[\{u_{tx}\}]} &:= \int \mathcal{D}u \mathcal{D}\hat{u} O[\{u_{tx}\}] e^{-S[u, \hat{u}]}, \\ S[u, \hat{u}] &:= S_0[u, \hat{u}] + S_{\text{dis}}[u, \hat{u}] + S_{\text{dri}}[u, \hat{u}].\end{aligned}\tag{II.5.3}$$

Where here $\hat{u}_{t,x} \in i\mathbb{R}$ is the MSR response field and we have split the action between the quadratic part S_0 , the disorder part S_{dis} and the driving part S_{dri} as:

$$\begin{aligned}S_0[u, \hat{u}] &:= \int_{tx} \hat{u}_{tx} \left(\eta_0 \partial_t u_{tx} + \int_y g_{x,y}^{-1} u_{ty} \right), \\ S_{\text{dis}}[u, \hat{u}] &:= -\frac{1}{2} \int_{t,t',x} \hat{u}_{tx} \hat{u}_{t'x} \Delta_0(u_{tx} - u_{t'x}) + \dots, \\ S_{\text{dri}}[u, \hat{u}] &= -\int_x \int_y \hat{u}_{tx} g_{x,y}^{-1} w(t) = -m^2 \int_x \hat{u}_{tx} vt .\end{aligned}\tag{II.5.4}$$

Here we have implicitly adopted the Ito convention to interpret (II.5.1) and the dots in $S_{\text{dis}}[u, \hat{u}]$ indicates eventual higher order cumulants of the bare disorder force if the latter is non Gaussian. In the following we will denote by $\langle \rangle_S$ the average with respect to the MSR action (II.5.3). The latter is identical to the disorder average $\overline{(\)}$ in the steady state of (II.5.1) for observables of the position field u_{tx} , but in the following we will also consider averages involving the MSR field \hat{u}_{tx} .

b Definition of the different functionals and the statistical tilt symmetry

As in the statics, we consider the generating function for connected correlations:

$$e^{W_\mu[\{j_{tx}\},\{\hat{j}_{t,x}\}]} := \langle e^{\int_{t,x} j_{t,x} u_{tx} + \int_{t,x} \hat{j}_{t,x} \hat{u}_{tx}} \rangle_S, \quad (\text{II.5.5})$$

and its Legendre transform, the effective action of the theory,

$$\Gamma_\mu[u, \hat{u}] := -W[j, \hat{j}] + \int_{t,x} j_{t,x} u_{tx} + \int_{t,x} \hat{j}_{t,x}, \quad (\text{II.5.6})$$

where on the right hand side the sources j and \hat{j} are given in terms of the fields u and \hat{u} by inverting

$$u_{t,x} = \frac{\delta W}{\delta \hat{j}_{t,x}}, \quad \hat{u}_{tx} = \frac{\delta W}{\delta j_{t,x}}. \quad (\text{II.5.7})$$

Let us begin with

The Statistical Tilt Symmetry in the dynamics and the relation statics/dynamics

Note that the total action $S[u, \hat{u}]$ has the symmetry, for any *time-independent* function ϕ_x , $S[u + \phi_x, \hat{u}] = S[u, \hat{u}] + \int_{txy} \hat{u}_{tx} g_{x,y}^{-1} \phi_y$. Hence, for any observable $O[u, \hat{u}]$, we obtain the STS relation,

$$\langle O[u - \phi, \hat{u}] \rangle_S = \int \mathcal{D}u \mathcal{D}\hat{u} O[\{u_{tx}\}] e^{-S[u+\phi, \hat{u}]} = \langle O[u, \hat{u}] e^{-\int_{txy} \hat{u}_{tx} g_{x,y}^{-1} \phi_y} \rangle_S. \quad (\text{II.5.8})$$

In a differential form the latter is rewritten, applying $\frac{\delta}{\delta \phi_x} |_{\phi_x=0}$ to the last identity,

$$\int_t \langle \frac{\delta}{\delta u_{tx}} O[u, \hat{u}] \rangle_S = \langle O[u, \hat{u}] \int_{t,y} g_{x,y}^{-1} \hat{u}_{ty} \rangle_S, \quad (\text{II.5.9})$$

where we have explicitly used the symmetry $g_{x,y}^{-1} = g_{y,x}^{-1}$. For the observable $O[u, \hat{u}] = u_{t_f, x_f}$, we thus obtain

$$\delta^{(d)}(x - x_f) = \int_{ty} g_{x,y}^{-1} \langle \hat{u}_{t,y} u_{t_f, x_f} \rangle_S. \quad (\text{II.5.10})$$

Introducing the response function

$$\mathbf{R}(x_f - x_i, t_f - t_i) := \langle \hat{u}_{t_i, x_i} u_{t_f, x_f} \rangle_S, \quad (\text{II.5.11})$$

(recall here that from causality and the Ito convention that $\mathbf{R}(*, t) = 0$ for $t \leq 0$) we thus obtain that

$$\int_{t,y} g_{x,y}^{-1} \mathbf{R}(x_f - y, t_f - t) = \delta^{(d)}(x - x_f). \quad (\text{II.5.12})$$

I.e. inverting the elastic kernel and going into Fourier space we obtain

$$\mathbf{R}(q, \omega = 0) = \frac{1}{(q^2 + \mu^2)^{\frac{d}{2}}}, \quad \mathbf{R}(q, \omega) := \int_{q, \omega} e^{-iqx - i\omega t} \mathbf{R}(x, t). \quad (\text{II.5.13})$$

On the other hand, note that in the theory without disorder, the bare response function $R_0(x_f - x_i, t_f - t_i) := \langle \hat{u}_{t_i, x_i} u_{t_f, x_f} \rangle_{S_0}$ is easily obtained as

$$R_0(q, \omega) = \frac{1}{i\eta_0\omega + (q^2 + \mu^2)^{\frac{\gamma}{2}}}. \quad (\text{II.5.14})$$

Hence the zero frequency part of the response function $R(q, \omega)$ is not modified by the disorder. Note that STS does not say anything on the non-zero frequency part. Indeed the latter will be modified and the viscosity coefficient η receives a correction from the disorder. Before we proceed, let us emphasize here an idea that can be seen in much of the calculation performed in the dynamics: there is an analogy between the time in the dynamic theory and the replica index in the statics. This can be seen by comparing the calculations performed above with the one in the discussion of STS in the static theory in Sec. II.4.1. This analogy can be pushed quite far [129]. Note that in the dynamics, when two position fields are far from each other in time, they are effectively independent but see the same disorder, just as would two replicated fields with different replica index in the statics. More generally there will be close links between observables at 0 frequency in the dynamics and observables in the static theory.

c Main Results of FRG in the dynamics

The result of FRG for depinning is that the effective action of the theory $\Gamma_\mu[u, \hat{u}]$ takes, in the limit $v \rightarrow 0^+$ first and $\mu \rightarrow 0$ then, a scaling form as follows. Rescaling

$$\begin{aligned} x &= \mu^{-1}\tilde{x} \quad , \quad t = \mu^{-z}\tilde{t} \quad , \\ u_{t,x} &= \mu^{-\zeta_d}\tilde{u}_{\tilde{t},\tilde{x}} \quad , \quad \hat{u}_{t,x} = \mu^{d+z-\gamma+\zeta_d}\tilde{\hat{u}}_{\tilde{t},\tilde{x}}. \end{aligned} \quad (\text{II.5.15})$$

The rescaled effective action

$$\tilde{\Gamma}_\mu[\{\tilde{u}_{\tilde{t},\tilde{x}}\}, \{\tilde{\hat{u}}_{\tilde{t},\tilde{x}}\}] = \Gamma_\mu[\{u_{t,x} = \mu^{-\zeta_d}\tilde{u}_{\tilde{t}=\mu^z t, \tilde{x}=\mu x}\}, \{\hat{u}_{t,x} = \mu^{d+z-\gamma+\zeta_d}\tilde{\hat{u}}_{\tilde{t}=\mu^z t, \tilde{x}=\mu x}\}] \quad (\text{II.5.16})$$

converges, as $\mu \rightarrow 0$, to a fixed point of a rescaled functional Beta function

$$\lim_{\mu \rightarrow 0} \tilde{\Gamma}_\mu[\{\tilde{u}_{\tilde{t},\tilde{x}}\}, \{\tilde{\hat{u}}_{\tilde{t},\tilde{x}}\}] = \tilde{\Gamma}^*[\{\tilde{u}_{\tilde{t},\tilde{x}}\}, \{\tilde{\hat{u}}_{\tilde{t},\tilde{x}}\}] \quad , \quad \tilde{\beta}[\tilde{\Gamma}^*] = 0. \quad (\text{II.5.17})$$

In this limit the effective action can be computed in an expansion in $\epsilon = 2\gamma - d$. As for the statics the critical exponents ζ and z are adjusted so that a fixed point indeed exists. The latter has the same form as the initial action of the theory, except that

(i) one must replace η by a renormalized value

$$\eta \rightarrow \mu^{\gamma-z}\tilde{\eta}_\mu \quad (\text{II.5.18})$$

where $\tilde{\eta}_\mu$ flows with the RG and converges to a constant $\eta^* := \lim_{\mu \rightarrow 0} \eta_\mu$ (which depends on the flow, i.e. it is non-universal). The Beta function associated with the flow of η was computed up to order $O(\epsilon^2)$ in [129].

(ii) The disorder part of the effective action is changed to

$$\Gamma_{\text{dis}}[u, \hat{u}] := -\frac{1}{2} \int_{t,t',x} \hat{u}_{t,x} \hat{u}_{t',x} \Delta(u_{tx} - u_{t',x}) + O(\epsilon^2), \quad (\text{II.5.19})$$

where, as in the statics, the $O(\epsilon^2)$ contains higher order cumulants (and the non-local part of the second order cumulant) of the renormalized pinning force. The latter admits an expansion in Δ , that can be computed using a standard loop expansion and handling carefully the non-analyticities (see below). Close to the fixed point, $\Delta(u)$ takes a scaling form

$$\Delta(u) = A_d^\gamma \mu^{\epsilon - 2\zeta_d} \tilde{\Delta}(\mu^{\zeta_d} u) \quad (\text{II.5.20})$$

where $\tilde{\Delta}(u) = O(\epsilon)$ is closed to a FP of the following FRG flow equation (computed up to two-loops in [129]):

$$\begin{aligned} -\mu \partial_\mu \tilde{\Delta}(u) &= \underbrace{(\epsilon - 2\zeta_d) \tilde{\Delta}(u) + \zeta_d u \tilde{\Delta}'(u)}_{\text{rescaling}} - \underbrace{\frac{1}{2} [(\tilde{\Delta}(u) - \tilde{\Delta}(0))^2]''}_{\text{1-loop}} \\ &+ \underbrace{\frac{1}{2} X[(\Delta(u) - \Delta(0)) \Delta'(u)^2]'' - \frac{\lambda_d}{2} X(\tilde{\Delta}'(0^+)^2) \tilde{\Delta}''(u)}_{\text{2-loops}} \\ &+ O(\tilde{\Delta}^4) \end{aligned} \quad (\text{II.5.21})$$

where $\lambda_d = -1$. As in the statics, if $\tilde{\Delta}^*(u)$ is a fixed point, $\frac{1}{\kappa^2} \tilde{\Delta}^*(\kappa u)$ is also a fixed point and thus there are several families of fixed points. The fixed point toward which the system flows depends on the full flow (in particular it depends on the starting point, i.e. microscopic parameters). Remarkably, to one-loop order, the flow equation (II.5.21) is identical to the one of the statics. Namely, taking two derivatives of (II.4.36) and defining $\tilde{\Delta}(u) = -\tilde{R}''(u)$, one obtains exactly (II.5.21), up to the change $\lambda_s \rightarrow \lambda_d$ (we remind $\lambda_s = 1$). Hence, up to two loop order, the FRG equation for the depinning and the statics only differs by the coefficient in front of the ‘anomalous terms’ involving the $\tilde{R}'''(0^+) = -\tilde{\Delta}'(0^+)$. This change has drastic consequences:

- The random bond universality class of the statics, the universality class for short-range correlated disorder, is unstable in the dynamics and flows to the random field universality class (see below). This is a signature of irreversibility in the depinning process: since the interface always moves forward in the dynamics, it does not know whether it is dragged in a random force landscape that is the derivative of a potential or not. This difference was confirmed numerically in [134].
- The random field universality class thus appears as the unique universality class for the depinning with non-periodic short-range disorder. Moreover this random field universality class is different from the static one. The roughness exponent was shown to be different with $\zeta_d \simeq \frac{\epsilon}{3}(1 + 0.143313\epsilon) + O(\epsilon^3)$ for SR elasticity ($z \simeq 2 - \frac{2}{9}\epsilon - 0.0432087\epsilon^2 + O(\epsilon^3)$) and $\zeta_d \simeq \frac{\epsilon}{3}(1 + 0.39735\epsilon) + O(\epsilon^3)$ ($z = 1 - \frac{2}{9}\epsilon - 0.1132997\epsilon^2 + O(\epsilon^3)$) for LR elasticity. The fixed point function $\tilde{\Delta}^*(u)$ is also different from the static one, as confirmed numerically in [134].
- The random periodic universality class is also different and the fixed-point function is non-potential. See [129] for more details.

This shows that it is crucial, when performing a perturbative calculation in the statics or in the dynamics in terms of the non-analytic, renormalized disorder, to evaluate carefully the possible non-analytical terms that arise because of the short-distance singularities of the fixed point functions. In the statics as we explained, the correct evaluation of such anomalous terms require to take very carefully the $T \rightarrow 0$ limit. In the dynamics the situation is somehow simpler and the short-distance singularities are regularized by the non-zero velocity: since the renormalized disorder correlator always comes with $\Delta(u_{xt} - u_{xt'})$ and $u_{xt} \geq u_{xt'}$ if $t \geq t'$, there should never be ambiguities regarding the side of the cusp that appears. In particular, the higher cumulants of the renormalized pinning force (the $O(\epsilon^2)$ in (II.5.19)) can be computed using a standard loop expansion (at least up to two-loop [129]) directly at $T = 0$ and $v = 0^+$.

Other exponents at the depinning transition

In our field theory approach to depinning, the correlation length ξ mentioned in the introduction to the depinning transition in Sec. I.3.2 is equal to $\ell_\mu := 1/\mu$ since μ is not corrected by the renormalization (STS). On the other hand, an appropriate definition of the critical force is the mean force exerted by the well on the interface as $v \rightarrow 0^+$ in the steady state:

$$f_c(\mu) := \lim_{v \rightarrow 0^+} \overline{\mu^\gamma v t - u_{tx}}. \quad (\text{II.5.22})$$

Hence, at non-zero velocity, slightly above the depinning transition, we expect that $f - f_c(\mu) = \overline{\mu^\gamma v t - u_{tx}} - \lim_{v \rightarrow 0} \overline{\mu^\gamma v t - u_{tx}}$ to scale as $\mu^{\gamma - \zeta_d}$. Hence the exponent ν defined by $\xi \sim (f - f_c)^{-\nu}$ is thus

$$\nu = \frac{1}{\gamma - \zeta_d}. \quad (\text{II.5.23})$$

On the other hand the exponent β defined by $v = \overline{\partial_t u_{tx}} \sim (f - f_c)^\beta$ must scale as $\mu^{z - \zeta_d} = \mu^{\beta(\gamma - \zeta_d)}$ and hence

$$\beta = \frac{z - \zeta_d}{\gamma - \zeta_d}. \quad (\text{II.5.24})$$

II.5.2 Applying the functional renormalization group to avalanches

a Introduction

Let us now extend our analysis of Sec. II.3.2 of shocks in the statics to the case of avalanches in the dynamics. We first note the relation, shown in [97], that extends the relation (II.4.43) of the statics:

$$\Delta(w - w') = L^d m^4 \overline{(u(w) - w)(u(w') - w')^c}, \quad (\text{II.5.25})$$

where $\Delta(w - w')$ is the renormalized second cumulant of the pinning force at depinning and $u(w)$ is the center of mass of the interface in the forward quasi-static process

$$u(w) := \frac{1}{L^d} \int_x u_x(w) \quad , \quad u_x(w) := \lim_{v \rightarrow 0^+} u_{t=w/v, x}. \quad (\text{II.5.26})$$

Note that it slightly differs from (II.4.43) by the fact that the average in (II.5.25) is a connected average. While in the statics we have $u(w) = w$, in the dynamics $u(w) \neq w$ and the difference $m^2(w - \overline{u(w)})$ is the critical force of the system. Apart from this the interpretation and consequences of the formula (II.5.25) are mostly equivalent to those of (II.4.43) and we refer the reader to the discussion after (II.4.43). In particular as $\mu \rightarrow 0$, beyond the Larkin length, the left-hand-side of (II.5.25) takes a universal, non-analytic scaling form (II.5.20). This non-analyticity is interpreted as the occurrence of avalanches in the forward quasi-static process and we assume that in the scaling limit $u_x(x) \sim \mu^{-\zeta_d}$,

$$u_x(w) = cst + \sum_i S_x^{(i)} \theta(w - w_i). \quad (\text{II.5.27})$$

As in the statics, the density for the total size of the shocks, $S^{(i)} = \int_x S_x^{(i)}$, is defined as

$$\rho(S) := \overline{\sum_i \delta(w - w_i) \delta(S - S^{(i)})}, \quad (\text{II.5.28})$$

and does not depend on w in the steady-state. Without repeating the same discussion as in the statics we obtain the two important exact relations

$$\langle S \rangle_\rho = L^d, \quad S_m := \frac{\langle S^2 \rangle_\rho}{2 \langle S \rangle_\rho} = \frac{\sigma}{m^4} = A_d^\gamma \mu^{-d-\zeta_d} \tilde{\sigma}, \quad (\text{II.5.29})$$

where $\sigma = -\Delta'(0^+)$ and $\tilde{\sigma} = -\tilde{\Delta}'(0^+)$ are $O(\epsilon)$. Let us now see how to relate more generally an observable associated with the avalanche motion of the interface to an observable of the MSR field theory. Before we do so let us note that it is important to have in mind the discussion of avalanches in the $d = 0$ case given in Sec. II.2.2.

b The MSR response field as the generator of avalanche motion

Let us now consider the theory for the interface velocity field $\dot{u}_{tx} = \partial_t \dot{u}_{tx}$. It is obtained by taking a derivative of (II.5.1)

$$\eta_0 \partial_t \dot{u}_{tx} = \int_y g_{x,y}^{-1} (v - \dot{u}_{ty}) + \partial_t F(x, u_{tx}) \quad (\text{II.5.30})$$

We consider, for an arbitrary source λ_{tx} , the generating functional of the velocity field in the steady state of (II.5.30)

$$G[\lambda_{tx}] := \overline{e^{\int_{tx} \lambda_{tx} \dot{u}_{tx}}}. \quad (\text{II.5.31})$$

Let us suppose that λ_{tx} is non-zero only in a time window $t \in [0, T]$. The latter is taken to be large compared to the typical time scale of the avalanche motion (so that every avalanche that occurs in this time window terminates), and small compared to the waiting time in between successive avalanche (that is of order $O(1/v)$). This will be automatically ensured later by taking the limit $v \rightarrow 0$ first and $T \rightarrow \infty$ afterwards. Let us now denote: (i) $p_{t_i}[\dot{u}_{tx}]$ the probability distribution functional of the velocity

field of the interface knowing that an avalanche started somewhere along the interface at time t_i , normalized as $\int \mathcal{D}[\dot{u}] \rho_{t_i}[\dot{u}_{tx}] = 1$; (ii) ρ_0 the mean number of avalanches per unit of driving. From the general picture of avalanche motion built on $d = 0$ toy models in Sec. II.2.2, we know (i.e. that is how we would like to interpret the FRG results) that in the limit $v \rightarrow 0^+$, $G[\lambda_{tx}]$ admits the expansion

$$G[\lambda_{tx}] = (1 - \rho_0 v T) + \rho_0 v \int_{t_i=0}^T \int \mathcal{D}[\dot{u}] e^{\int_{tx} \lambda_{tx} \dot{u}_{tx}} \rho_{t_i}[\dot{u}_{tx}] + O(v^2). \quad (\text{II.5.32})$$

Equivalently we can write, introducing the *density functional of the velocity field inside an avalanche starting at time t_i* : $\rho_{t_i}[\dot{u}_{tx}] = \rho_0 \rho_{t_i}[\dot{u}_{tx}]$,

$$G[\lambda_{tx}] - 1 = v \int_{t_i=0}^T \int \mathcal{D}[\dot{u}] \left(e^{\int_{tx} \lambda_{tx} \dot{u}_{tx}} - 1 \right) \rho_{t_i}[\dot{u}_{tx}] + O(v^2). \quad (\text{II.5.33})$$

On the other hand, $G[\lambda_{tx}]$ can be computed using the MSR field theory associated with the velocity theory. The latter is a simple adaptation of (II.5.3)-(II.5.4) and we obtain

$$G[\lambda_{xt}] = \int D[\tilde{u}] D[\dot{u}] e^{\int_{xt} \lambda_{xt} \dot{u}_{xt} - S[\dot{u}, \tilde{u}] + m^2 v \int_{tx} \tilde{u}_{tx}}, \quad (\text{II.5.34})$$

where $S[\dot{u}, \tilde{u}] := S_0[\dot{u}, \tilde{u}] + S_{\text{dis}}[\dot{u}, \tilde{u}]$ with

$$\begin{aligned} S_0[\dot{u}, \tilde{u}] &:= \int_{tx} \tilde{u}_{tx} \left(\eta_0 \partial_t \dot{u}_{tx} + \int_y g_{x,y}^{-1} \dot{u}_{ty} \right), \\ S_{\text{dis}}[\dot{u}, \tilde{u}] &:= -\frac{1}{2} \int_{t,t',x} \tilde{u}_{tx} \tilde{u}_{t'x} \partial_t \partial_{t'} \Delta_0(u_{tx} - u_{t'x}). \end{aligned} \quad (\text{II.5.35})$$

Taking now the expansion in v of (II.5.34) we obtain

$$G[\lambda_{xt}] - 1 = m^2 v \langle \int_{tx} \tilde{u}_{tx} e^{\int_{xt} \lambda_{xt} \dot{u}_{xt}} \rangle_S + O(v^2). \quad (\text{II.5.36})$$

Hence, comparing (II.5.36) with (II.5.34) we identify

$$Z[\lambda] := \int_{t_i=0}^T \int \mathcal{D}[\dot{u}] \left(e^{\int_{tx} \lambda_{tx} \dot{u}_{tx}} - 1 \right) \rho_{t_i}[\dot{u}_{tx}] = m^2 \int_{tx} \langle \tilde{u}_{tx} e^{\int_{xt} \lambda_{xt} \dot{u}_{xt}} \rangle_S. \quad (\text{II.5.37})$$

Note now that from a diagrammatic point of view, all diagrams that contribute to $\langle \tilde{u}_{tx} e^{\int_{xt} \lambda_{xt} \dot{u}_{xt}} \rangle_S$ correspond to ‘histories of the interface motion’ such that the first non-zero velocity of the interface is at a time larger or equal to t and at a position x . It is thus natural to identify

$$Z_{t_i, x_i}[\lambda] := \int \mathcal{D}[\dot{u}] \left(e^{\int_{tx} \lambda_{tx} \dot{u}_{tx}} - 1 \right) \rho_{t_i, x_i}[\dot{u}_{tx}] = m^2 \langle \tilde{u}_{t_i, x_i} e^{\int_{xt} \lambda_{xt} \dot{u}_{xt}} \rangle_S, \quad (\text{II.5.38})$$

where $\rho_{t_i, x_i}[\dot{u}_{tx}]$ is the density for the velocity field inside *avalanches that are triggered at time t_i at the position x_i* . This formula first appeared in [2] (see Appendix B). Although, as it is usual when dealing with avalanches, one could debate some heuristic steps that were taken in its derivation, it is also coherent with the more controlled

setting of avalanches following a kick in the force in a non-stationary setting in a solvable model, and we refer to [2] (see Appendix B) for a more complete discussion of (II.5.38). Let us now discuss how to use FRG to obtain a simplified action that allows us to compute the ϵ expansion of the right-hand side of (II.5.38) in the limit $\mu \rightarrow 0$, and thus obtain the ϵ expansion of a generic observable associated with the avalanche motion.

c The simplified action for the motion inside avalanches in the velocity theory

One way to use FRG to compute avalanche observables at depinning is to follow the same route as presented for the statics in Sec. II.4.2. This route is presented in detail in [101] and shown to be equivalent, to one-loop accuracy and for observables associated with a single avalanche such as (II.5.38), to a simplified theory. We now present this simplified theory following [101] and [43]. The essential steps will be:

- (i) Express the bare disorder force-force cumulant $\Delta_0(u)$ and viscosity coefficient η_0 of the theory by formally inverting the one-loop expressions for $\Delta(u)$ and η obtained from one-loop perturbative FRG.
- (ii) Express the MSR action for the *velocity theory* in terms of the renormalized disorder $\Delta(u)$ and viscosity η .
- (iii) Take into account the fact that the scale of avalanches, S_m , is $O(\epsilon)$ to obtain a simplified action valid to describe the velocity field inside a single avalanche.

Let us start with the first step. The one-loop expression for $\Delta(u)$ in terms of $\Delta_0(u)$ is [129]

$$\Delta(u) = \Delta_0(u) - I_1(\Delta_0(u) - \Delta_0(0))\Delta'_0(u). \quad (\text{II.5.39})$$

It can formally be inverted⁷ as

$$\Delta_0(u) = \Delta(u) + I_1(\Delta(u) - \Delta(0))\Delta'(u). \quad (\text{II.5.40})$$

In the same way [129]

$$\eta = \eta_0(1 - \Delta''_0(0^+)I_1) \quad , \quad \eta_0 = \eta(1 + \Delta''(0^+)I_1). \quad (\text{II.5.41})$$

Of course these expressions and the inversions that were made are completely formal: while the bare disorder correlator appearing on the left of (II.5.40) can be a smooth function of u , we know that the renormalized disorder on the right of (II.5.40) is non-analytic for $\mu \leq \mu_c$. As usual with perturbative RG, this type of manipulations and one-loop expression (II.5.39) are only appropriate to obtain the RG flow of the parameters close to a perturbative FP (see e.g. [135]). More precisely, taking the derivative $-\mu\partial_\mu$ of (II.5.39) at fixed $\Delta_0(u)$ and then replacing on the right-hand side $\Delta_0(u)$ by the expression (II.5.40) leads to the correct one-loop Beta function (II.5.21). This inversion allows however to obtain self-consistently a bare action that will lead, using a one-loop perturbative calculation of an observable, to the correct result up to

⁷The formal expansions and inversions of series performed here are controlled under the assumption that Δ and Δ_0 are small and of the same order.

order $O(\epsilon)$. Hence to obtain our avalanche observables (II.5.38) we will perform one-loop perturbative calculations with an action similar to (II.5.35) with the replacement $\eta_0 \rightarrow \eta$, $\Delta_0 \rightarrow \Delta$ and reminding ourselves in the end that counter-terms involving the loop-integral I_1 as in (II.5.40), (II.5.41) must be added.

The above considerations are the steps (i) and (ii) in the announced program. Let us now finally perform the last step, namely use that S_m , the upper-cutoff of the avalanche size distribution, is $O(\epsilon)$. We thus need to rescale (II.5.38) in a way that allows us to study the limit $\mu \rightarrow 0$ and $\epsilon \rightarrow 0$. We will do the rescaling in two steps for clarity. We thus consider

$$\tilde{Z}_{t_i, x_i}[\tilde{\lambda}] := Z_{t_i, x_i}[\lambda = \tilde{\lambda}/S_m] = m^2 \langle \tilde{u}_{t_i, x_i} e^{\int_{xt} \frac{\tilde{\lambda} x t}{S_m} \dot{u}_{xt}} \rangle_S \quad (\text{II.5.42})$$

Let us first take care of the scaling with μ : we must adapt the scaling of (II.5.15) to the fields of the velocity theory. We thus take,

$$\begin{aligned} x &= \mu^{-1} \bar{x} \quad , \quad t = \mu^{-z} \bar{t} \quad , \\ \dot{u}_{t, x} &= \mu^{z-\zeta_d} \dot{\bar{u}}_{\bar{t}, \bar{x}} \quad , \quad \tilde{u}_{t, x} = \mu^{d-\gamma+\zeta_d} \tilde{\bar{u}}_{\bar{t}, \bar{x}} \quad , \end{aligned} \quad (\text{II.5.43})$$

using here $\bar{(\)}$ for rescaled quantity, and where the dots mean either ∂_t or $\partial_{\bar{t}}$, depending on the field to which they are applied. The elastic kernel is rescaled as $g_{\mu^{-1}\bar{x}, \mu^{-1}\bar{y}}^{-1} = \mu^{d+\gamma} \bar{g}_{\bar{x}, \bar{y}}^{-1}$ with $\bar{g}_{\bar{x}, \bar{y}}^{-1} = \int_q e^{iq\mu^{-1}(x-y)} (q^2 + 1)^{\frac{\gamma}{2}}$ and we remind ourselves that in the limit $\mu \rightarrow 0$ the rescaled renormalized disorder and friction are close to one of the fixed points of the FRG flow:

$$\eta \sim \mu^{\gamma-z} \tilde{\eta}^* \quad , \quad \Delta(u) \sim A_d^\gamma \mu^{\epsilon-2\zeta_d} \tilde{\Delta}^*(\mu^{\zeta_d} u) \quad . \quad (\text{II.5.44})$$

Using this rescaling, our ‘model’ avalanche observable (II.5.38) is expressed as, using that $S_m = A_d^\gamma \mu^{-d-\zeta_d} \tilde{\sigma}^*$,

$$\tilde{Z}_{t_i, x_i}[\tilde{\lambda}] = \mu^{d+\zeta_d} \int \mathcal{D}\dot{\bar{u}} \mathcal{D}\tilde{\bar{u}} \tilde{\bar{u}}_{\bar{t}_i, \bar{x}_i} e^{(A_d^\gamma)^{-1} \int_{\bar{t}, \bar{x}} \tilde{\lambda}_{t\bar{x}} \frac{\dot{\bar{u}}_{t\bar{x}}}{\tilde{\sigma}^*} - \bar{S}[\tilde{\bar{u}}, \tilde{\bar{u}}]} \quad , \quad (\text{II.5.45})$$

where the action $\bar{S}[\tilde{\bar{u}}, \tilde{\bar{u}}]$ is now as in (II.5.34) with $\eta \rightarrow \tilde{\eta}^*$, $\tilde{\Delta} \rightarrow \tilde{\Delta}^*$ and the dependence on μ has completely disappeared (apart from the prefactor). Finally, we must now ‘zoom’ in on the $O(\epsilon)$ scale of the avalanche motion that is controlled by $\tilde{\sigma}^* = -\tilde{\Delta}^{*\prime}(0^+) = O(\epsilon)$. To this aim we thus rescale

$$\dot{\bar{u}}_{\bar{t}, \bar{x}} = A_d^\gamma \tilde{\sigma}^* \dot{\bar{u}}_{\bar{t}, \bar{x}} \quad , \quad \tilde{\bar{u}}_{\bar{t}, \bar{x}} = (A_d^\gamma \tilde{\sigma}^*)^{-1} \tilde{\bar{u}}_{\bar{t}, \bar{x}} \quad . \quad (\text{II.5.46})$$

This final rescaling allows us to make an expansion of the renormalized disorder correlator around $u = 0$: for \underline{u} of order 1 we have

$$\tilde{\Delta}^*(A_d^\gamma \tilde{\sigma}^* \underline{u}) = \tilde{\Delta}^*(0) - A_d^\gamma (\tilde{\sigma}^*)^2 |\underline{u}| + \frac{1}{2} \tilde{\Delta}^{*\prime\prime}(0) (A_d^\gamma \tilde{\sigma}^*)^2 \underline{u}^2 + O(\epsilon^4) \quad . \quad (\text{II.5.47})$$

This rescaling leaves the quadratic part of the action invariant but changes the disorder part as, following the different changes of variables,

$$\begin{aligned}
S_{\text{dis}}[\dot{u}, \tilde{u}] &= -\frac{1}{2} \int_{t,t',x} \tilde{u}_{tx} \tilde{u}_{t'x} \partial_t \partial_{t'} \Delta(u_{tx} - u_{t'x}) \\
&= -\frac{A_d^\gamma}{2} \int_{\bar{t}, \bar{t}', \bar{x}} \tilde{u}_{\bar{t}\bar{x}} \tilde{u}_{\bar{t}'\bar{x}} \partial_{\bar{t}} \partial_{\bar{t}'} \tilde{\Delta}^*(\bar{u}_{\bar{t}\bar{x}} - \bar{u}_{\bar{t}'\bar{x}}) \\
&= -\frac{1}{2A_d^\gamma (\tilde{\sigma}^*)^2} \int_{\bar{t}, \bar{t}', \bar{x}} \tilde{u}_{\bar{t}\bar{x}} \tilde{u}_{\bar{t}'\bar{x}} \partial_{\bar{t}} \partial_{\bar{t}'} \tilde{\Delta}^*(A_d^\gamma \tilde{\sigma}^*(\underline{u}_{\bar{t}\bar{x}} - \underline{u}_{\bar{t}'\bar{x}})) \quad (\text{II.5.48}) \\
S_{\text{dis}}[\dot{u}, \tilde{u}] &= - \int_{\bar{t}, \bar{x}} (\tilde{u}_{\bar{t}\bar{x}})^2 \dot{u}_{\bar{t}, \bar{x}} + \frac{A_d^\gamma \tilde{\Delta}^{*''}(0)}{2} \int_{\bar{t}, \bar{t}', \bar{x}} \tilde{u}_{\bar{t}\bar{x}} \tilde{u}_{\bar{t}'\bar{x}} \dot{u}_{\bar{t}\bar{x}} \dot{u}_{\bar{t}'\bar{x}} + O(\epsilon^2).
\end{aligned}$$

We refer the reader to [101] for more details on the simplification in the last line that notably uses $\dot{u}_{\bar{t}\bar{x}} \leq \dot{u}_{\bar{t}'\bar{x}}$ for $\bar{t} \leq \bar{t}'$. Hence our model observable (II.5.45) can be calculated when μ is close to 0 using the ϵ expansion as

$$\tilde{Z}_{t_i, x_i}[\tilde{\lambda}] = \frac{1}{S_m} \int \mathcal{D}\underline{\dot{u}} \mathcal{D}\underline{\tilde{u}} \tilde{u}_{t_i x_i} e^{\int_{\bar{t}, \bar{x}} \tilde{\lambda}_{tx} \dot{u}_{tx} - \underline{S}[\underline{\dot{u}}, \underline{\tilde{u}}]}, \quad (\text{II.5.49})$$

where the action $\underline{S}[\underline{\dot{u}}, \underline{\tilde{u}}]$ is similar to (II.5.34) with $\eta \rightarrow \tilde{\eta}^*$, $\mu \rightarrow 1$ and the disorder part is as in (II.5.48). The observable can be computed to order $O(\epsilon)$ using one loop perturbative RG. Possible divergences appearing in the calculation are canceled by counter-terms associated to the renormalization of η and Δ (II.5.40) and (II.5.41)⁸. In the following we conclude our introduction to the analysis of avalanches using FRG by focusing on the mean-field theory that is obtained by retaining only the terms of order $O(1)$ in (II.5.48), i.e. we set $\tilde{\Delta}^{*''}(0) \rightarrow 0$.

d The mean-field theory: the Brownian Force Model

Let us now discuss in more details avalanche observables in the dynamics of elastic interfaces to lowest order in $\epsilon = 2\gamma - d$. As discussed in the previous section we thus only need to consider an interface whose *velocity field* dynamics inside an avalanche is described by the action

$$\begin{aligned}
\overline{O\{\dot{u}_{tx}\}} &:= \int \mathcal{D}\dot{u} \mathcal{D}\tilde{u} O\{\dot{u}_{tx}\} e^{-S[\dot{u}, \tilde{u}]}, \\
S[\dot{u}, \tilde{u}] &:= S_0[\dot{u}, \tilde{u}] + S_{\text{dis}}[\dot{u}, \tilde{u}] + S_{\text{dri}}[\dot{u}, \tilde{u}] \\
S_0[\dot{u}, \tilde{u}] &:= \int_{tx} \tilde{u}_{tx} \left(\eta \partial_t \dot{u}_{tx} + \int_y g_{x,y}^{-1} \dot{u}_{ty} \right), \\
S_{\text{dis}}[\dot{u}, \tilde{u}] &:= -\sigma \int_{tx} \tilde{u}_{tx}^2 \dot{u}_{tx}, \\
S_{\text{dri}}[\dot{u}, \tilde{u}] &:= -m^2 v \int_{tx} \tilde{u}_{tx}. \quad (\text{II.5.50})
\end{aligned}$$

Here we have reintroduced a possible driving velocity $v \geq 0$, the different units and the renormalized parameters η and σ . Let us first comment on the nature of this theory.

⁸A subtlety linked to calculations using the simplified action (II.5.48) is that one has also to take care of a formal renormalization of μ forbidden by STS in the full theory. We refer the reader to [43, 101] for more details on this issue.

The Brownian Force Model

It is a simple exercise [101] to show that the MSR action (II.5.50) is equivalent to the following stochastic equation for the velocity field of the interface:

$$\eta \partial_t \dot{u}_{tx} = \int_y g_{x,y}^{-1} (v - \dot{u}_{tx}) + \sqrt{2\sigma \dot{u}_{tx}} \xi_{tx}, \quad (\text{II.5.51})$$

where ξ_{xt} is a centered and normalized Gaussian white noise (GWN):

$$\overline{\xi_{tx} \xi_{t',x'}} = \delta^{(d)}(x - x') \delta(t - t'). \quad (\text{II.5.52})$$

In turn, the equation (II.5.51) appears as the time derivative of an equation for the position field of the interface as

$$\eta \partial_t u_{tx} = \int_y g_{x,y}^{-1} (vt - u_{tx}) + F(x, u_{xt}), \quad (\text{II.5.53})$$

where for each x , $F(x, u)$ is a Brownian motion (BM) in u independent of the others and with increments

$$\overline{(F(x, u) - F(x, u'))^2} := 2\sigma |u - u'|. \quad (\text{II.5.54})$$

This theory was called the Brownian Force Model (BFM) in [111, 101, 102]. Note that the emergence of a BM should not be surprising: we obtained the BFM as the mean-field theory for the depinning of interfaces in short-range disorder by linearizing the correlator of the renormalized pinning force around the cusp because avalanches are small, that is of order $O(\epsilon)$. For an arbitrary pinning force $\tilde{F}(x, u)$ that is stationary with $\overline{\tilde{F}(x, u) \tilde{F}(x', u')^c} = \delta^{(d)}(x - x') \Delta(u - u')$ and has a cusp, we have

$$\overline{(\tilde{F}(x, u) - \tilde{F}(x, u'))^2} = 2(\Delta(0) - \Delta(u - u')) \simeq -2\Delta'(0^+) |u - u'| + O(|u - u'|^2). \quad (\text{II.5.55})$$

hence we retrieve generally the BFM with $\sigma = -\Delta'(0^+)$ through such considerations. A subtle issue here is, however, that the BM is not a stationary process. While in (II.5.51) we did not define precisely the initial condition since it is implicit that we are looking at the stationary process for the velocity field \dot{u}_{tx} (which exists), the process in (II.5.53) has generally no stationary state. The definition (II.5.53) thus requires some precisions. One way is to make the Brownian motion $F(x, u)$ stationary in u by considering Brownian bridges in a large box [101] $F(x, 0) = F(x, W) = 0$ with $W \gg 1$ and looking at the process in the middle of the box in a width of order 1: $u \rightarrow W/2 + u$ with $u = O(1)$. The correlations between the different BM constructed in this way are then to leading order $\overline{F(x, u) F(x', u')^c} = \delta^{(d)}(x - x') (\Delta(0) - \sigma |u - u'|)$. This is, however, a bit artificial and in this setup $\Delta(0)$ is huge, $\Delta(0) \sim W$. From a more pragmatic point of view one can consider one-sided Brownian motion with the initial condition that the interface is at rest at $t = 0$:

$$F(x, 0) = 0, \quad \dot{u}_{tx} = u_{tx} = 0, \quad (\text{II.5.56})$$

In this setup one can now consider an arbitrary (non-stationary) driving $w(t)$ with the equation of motion

$$\eta \partial_t u_{tx} = \int_y g_{x,y}^{-1} (w(t) - u_{tx}) + F(x, u_{xt}), \quad (\text{II.5.57})$$

and $w(t=0) = 0$. If $w(t)$ is always increasing, $\dot{w}(t) \geq 0$, the interface dynamics in the velocity theory is described by the same MSR action as in (II.5.50) with $S_{\text{dri}}[\dot{u}, \tilde{u}] = m^2 \int_{tx} \tilde{u}_{tx} \dot{w}(t)$.

The BFM as a FRG fixed point in any d and the scaling exponents of the BFM
As was first remarked in [111], and can be checked by differentiating the static FRG equation for $\tilde{R}(u)$ (II.4.36) three times with respect to u or the dynamic FRG equation (II.5.21) once with respect to u to obtain in both cases a FRG equation for $\tilde{\Delta}'(u)$, the model defined by

$$\tilde{\Delta}'(u) = \frac{d}{du} (-\tilde{\sigma}|u|) = -\tilde{\sigma}\text{sign}(u) \quad (\text{II.5.58})$$

is a fixed point of the FRG equation in any d with the exponent $\zeta_s = \zeta_d = \epsilon$ and the dynamic exponent $z = \gamma$. Furthermore this fixed point was argued in [111] to be stable and to be an exact fixed point for an arbitrary number of loops. In [102] it was even shown that it is a fixed point of the (more complicated and not shown in this manuscript) FRG equation for the dynamics at non-zero velocity. Note that inserting the scaling (II.5.43) in (II.5.50) it is easily seen that the critical exponents $z = \gamma$ and $\zeta = \epsilon$ does lead to a μ independent action (this is linked to the exact scale invariance of the BM).

Back to the ABBM model

Let us now look at the dynamics of the center of mass in the BFM model. Defining $u_t = \frac{1}{L^d} \int_x u_{tx}$, we obtain from (II.5.51)

$$\eta \partial_t \dot{u}_t = m^2 (v - \dot{u}_t) + \sqrt{2\sigma_L} \xi_t \quad (\text{II.5.59})$$

where we have used the identity in law $\frac{1}{L^d} \int_x \sqrt{\dot{u}_{t,x}} \xi_{tx} = \sqrt{\sigma_L} \dot{u}_t \xi_t$ with $\sigma_L = \sigma/L^d$ and ξ_t a unit centered GWN $\overline{\xi_t \xi_{t'}}^c = \delta(t - t')$. The equation (II.5.59) is equivalent to the time-derivative of the equation of motion of a particle in the ABBM model already considered in Sec. II.2.2b. Hence *the mean-field theory for the motion of the center of mass of an elastic interface inside an avalanche at the depinning transition is the ABBM model*. In particular, the mean-field value for the power-law exponent τ_S is, as in the shocks case, $3/2$. Note that this value is also consistent with the NF conjecture applied to the BFM in any d since $\tau_S = 2 - \gamma/(d + \zeta) = 3/2$ as $\zeta = \epsilon = 2\gamma - d$. Let us remind here the reader that this mean-field exponent is linked to the first return time to the origin of the one-dimensional BM as shown in Sec. II.2.2. The mean-field nature of the ABBM model was already argued on phenomenological grounds in [100, 42]. Here it has been derived from first principles using FRG but more importantly it is now clear how to go beyond the predictions of the ABBM model. Namely, the BFM, first introduced in [136, 101, 102], provides the proper mean-field theory to describe *spatial correlations* in the avalanche process. Finally, FRG also permits to go beyond mean-field and to compute corrections in an ϵ expansion. Before we close this chapter, let us finally recall here that the BFM has an important exact solvability property and show an application of this property.

e Exact solvability of the BFM and the avalanche size distribution

We now discuss a remarkable solvability property of the BFM. We consider a non-stationary case with an inhomogeneous driving $w_x(t)$ described by the equation of motion

$$\eta \partial_t u_{tx} = \int_y g_{x,y}^{-1}(w_x(t) - u_{tx}) + F(x, u_{xt}), \quad (\text{II.5.60})$$

where as before the BM is one sided $F(x, 0) = 0$ and at $t = 0$ the interface is at rest $u_{tx} = 0$ and $w_x(t = 0) = 0$. We suppose that the driving is always increasing $\dot{w}_x(t) \geq 0$ during a finite amount of time and note the total displacement $w_x = \int_0^\infty \dot{w}_x(t) dt$. Our goal is to compute the generating function for the velocity field for an arbitrary source λ_{xt} :

$$\begin{aligned} G(\lambda_{xt}) &:= \overline{e^{\int_{t \geq 0, x} \lambda_{xt} \dot{u}_{xt}}} \\ &= \int \mathcal{D}[\dot{u}] \mathcal{D}[\tilde{u}] e^{-\int_{tx} \tilde{u}_{tx} \left(\eta \partial_t \dot{u}_{tx} + \int_y g_{x,y}^{-1} \dot{u}_{ty} \right) + \sigma \int_{tx} \tilde{u}_{xt}^2 \dot{u}_{tx} + m^2 \int_{tx} \tilde{u}_{tx} \dot{w}_x(t)} e^{\int_{t \geq 0, x} \lambda_{tx} \dot{u}_{xt}} \end{aligned} \quad (\text{II.5.61})$$

Here we have rewritten the average over disorder using the MSR action. As first remarked in [136], a remarkable simplification of the BFM is that the action for the velocity theory is *linear in \dot{u}_{tx}* . The path integral over \dot{u} thus simply leads to a functional Dirac delta distribution. One then easily obtains

$$G(\lambda_{xt}) = e^{m^2 \int_{tx} \tilde{u}_{tx}^\lambda \dot{w}_x(t)}, \quad (\text{II.5.62})$$

where \tilde{u}_{tx}^λ is the solution of the ‘instanton’ equation:

$$\eta \partial_t \tilde{u}_{tx} - \int_y g_{x,y}^{-1} \tilde{u}_{ty} + \sigma \tilde{u}_{tx}^2 + \lambda_{tx} = 0 \quad (\text{II.5.63})$$

with the condition $\tilde{u}_{tx} = 0$ for $t \geq t_{\max} = \min\{t \in \mathbb{R}, \lambda_{xt'} = 0 \forall t' \geq t\}$. A remarkable feature of (II.5.63) is that it does not depend on the driving: the dependence of the observable on the driving only appears in (II.5.62). Before we show a simple application of this formula let us mention that the solution (II.5.62-II.5.63) can also be obtained without using the MSR formalism, see [102].

Distribution of avalanche total size in the BFM

As an application of (II.5.62-II.5.63) consider the calculation of the PDF $P(S)$ of the total displacement of the interface $S = \int_{t \geq 0, x} \dot{u}_{tx}$ for a homogeneous driving $w_x = w$. The Laplace transform of $P(S)$

$$G(\lambda) := \int_{S=0}^\infty P(S) e^{\lambda S} dS, \quad (\text{II.5.64})$$

is obtained using (II.5.62-II.5.63) with $\lambda_{xt} = \lambda$. The solution of II.5.63 is time and space independent and reads

$$\tilde{u}_{tx}^\lambda = \frac{m^2}{\sigma} Z(\lambda S_m), \quad Z(\lambda) = \frac{1}{2} \left(1 - \sqrt{1 - 4\lambda} \right), \quad S_m := \sigma/m^4. \quad (\text{II.5.65})$$

Note that the function $Z(\lambda)$ already appeared in the mean-field calculation of the shocks total size density in (II.4.58). Here we thus obtain

$$G(\lambda) = e^{\frac{L^d w}{S_m} Z(\lambda S_m)}. \quad (\text{II.5.66})$$

Performing the Inverse-Laplace transform of (II.5.66) as in [101], we obtain the result given in the discussion of the ABBM model (II.2.31) (there it was given in dimensionless units $S_m = 1$ and with $vT_d = L^d w$):

$$P(S) = \frac{L^d w}{2\sqrt{\pi}\sqrt{S_m}S^{3/2}} e^{-\frac{(S-L^d w)^2}{4SS_m}} \quad (\text{II.5.67})$$

In order to see the link between this quantity and avalanches in the quasi-static steady state of the interface, consider now the density of avalanche total size $\rho_{x=0}(S)$ triggered at an arbitrary time t at position $x = 0$ in the quasi-static steady state (for the velocity theory) of the BFM. Its ‘Laplace transform’ is obtained using (II.5.65) with $\lambda_{xt} = \lambda$. We can again use the instanton equation to evaluate the path-integral over \dot{u}_{tx} and we obtain

$$\int_{S>0} (e^{\lambda S} - 1) \rho_{x=0}(S) = m^2 \langle \tilde{u}_{t,x=0} \rangle_S = m^2 \tilde{u}_{t,x=0}^\lambda = \frac{1}{S_m} Z(\lambda S_m). \quad (\text{II.5.68})$$

Inverting (see e.g. [101]), we obtain

$$\rho_{x=0}(S) = \frac{1}{2\sqrt{\pi}\sqrt{S_m}S^{3/2}} e^{-\frac{S}{4S_m}}. \quad (\text{II.5.69})$$

And we note the equality

$$\rho_{x=0}(S) = \frac{1}{L^d} \frac{\partial P(S)}{\partial w} \Big|_{w=0}, \quad (\text{II.5.70})$$

that shows the link between avalanches defined in the quasi-static steady state or in the non-stationary setting. Here the factor $\frac{1}{L^d}$ accounts for the fact that avalanches contributing to $P(S)$ can be triggered with equal probability at any point of the interface. Using the fact that the BFM is a Lévy jump process it is also possible to ‘invert’ (II.5.70) and obtain $P(S)$ in terms of $\rho_{x=0}(S)$. This is a similar calculation as the one given in Sec. II.2.2 for the stationary velocity distribution of the ABBM model and it is detailed in [1] (see Appendix A). Let us conclude this section by remarking that the density of avalanche total size in the BFM (II.5.69) is the same as the one for shocks in the statics (II.4.59) at the level of mean-field theory. This is not surprising since the differences between depinning and statics only appear at two-loop order in FRG.

II.6 Summary of (and more context around) the results obtained during the thesis

In this section we present the main results obtained on shocks and avalanches during this thesis. We begin in Sec. II.6.1 with a quick summary of the previous section and also present the actual research context around the obtained results. The next sections present the main results obtained in [1, 2, 3].

II.6.1 Introduction

Summary of the previous sections

In the last section we have introduced the notion of shocks and avalanches in disordered elastic systems. We have shown how the Functional Renormalization Group can be efficiently used to calculate universal properties of these jump processes: the latter inherit the universality and the scale invariance of the FRG fixed points and gives a natural interpretation to the non-analytic nature of these FPs. For non periodic, short-range disorder we have shown that there are a priori two universality classes for shocks, random bond and random field disorder, and a unique universality class for avalanches that corresponds to random field disorder, which is however different from the Random Filed universality class for shocks. Close to the upper-critical-dimension, which depends on the range of the elasticity of the interface as $d_{\text{uc}} = 2\gamma$, we have identified the relevant mean-field theory to describe the motion inside avalanches at the depinning transition as the BFM model. The center of mass dynamics in the BFM model was shown to be equivalent to the ABBM model. Based on these constructions, we can now ask various questions about the universality in avalanche processes using mean-field approaches, but also beyond mean-field in a controlled $\epsilon = d_{\text{uc}} - d$ expansion of observables using the structure of the FRG FPs. Let us now review some known results and introduce the subjects which will be the focus of Sec. II.6.2, Sec. II.6.3 and Sec. II.6.4.

Critical exponents

The first focus of the community has been on the determination of the exponents characterizing the power-law distribution of quantities such as the extension, duration or total size of the avalanches. Since those are linked to one another by scaling relations involving the critical exponents of the statics (for shocks) or of the depinning transition (for avalanches), an important question was to understand whether or not the exponents can be entirely deduced from the exponents of the statics and depinning transition. The NF conjecture that was presented earlier, first proposed for avalanches at depinning [108] and later generalized to the case of shocks [106, 109], provides a precise affirmative answer to this question. Since it is however based on unproven assumptions, it is still important to obtain an independent derivation of these exponents. At the mean-field level the exponent $\tau_S = 3/2$, first derived in [103], agrees with the NF conjecture. More recently, the NF conjecture was shown to hold up to one-loop both for shocks and avalanches in [109, 111, 101].

Universal distribution

Besides critical exponents, it is interesting to obtain the full PDF of avalanche observables. Although these in general depend on the IR cutoff of the theory (i) cutoffs such as the massive scheme discussed in this thesis have proved relevant in the description of some experimental setups [61]; (ii) the scaling with the cutoff of the different avalanche observables distributions on the IR cutting length is also expected to be universal, e.g. here $S_\mu \sim \mu^{-d-\zeta}$; (iii) this implies the universal scaling behavior of various avalanche observables since the (sufficiently high order) moments of avalanche observables distributions are dominated by their cutoff. For the ABBM model the PDF of avalanche size and duration were obtained in [97, 136, 137, 102]. Still in the ABBM model, the distribution of the maximum velocity inside an avalanche was also

computed in [137, 138] where the authors also obtained the dependence of the exponents on the velocity. The joint distribution of size and duration was obtained in [102]. The distribution of the extension of avalanches was computed in the BFM with SR elasticity in $d = 1$ in [107]. Results beyond-mean field for the avalanche total and local size distribution were obtained at one loop-order in [109, 111] (shocks) and [101] (avalanches). These notably predicted the characteristic ‘bump’ that is observed in numerics [139] in the avalanche size distribution close to the large-scale cutoff.

Universal scaling functions

Recently universality in avalanche processes has been pushed one step further and a lot of attention was devoted to the study of *universal scaling functions*. Indeed, the full velocity field of the interface $\dot{u}(t, x)$ inside an avalanche (where t refers to the time since the beginning of the avalanche and x is the d -dimensional internal coordinate according to some centering procedure) is expected to be universal and scale invariant. For example, using the scaling (II.3.24) and a sum rule, for avalanches of fixed duration T inside the scaling regime $T_0 \ll T \ll T_m$, one expects to have the equality in law

$$\dot{u}(t, x) \sim T^{\zeta_d/z-1} \sqrt{\text{fixed duration}}(t/T, x/T^{1/z}), \quad (\text{II.6.1})$$

where the rescaled spatio-temporal process $\sqrt{\text{fixed duration}}(t, x)$ is a well defined T -independent stochastic process. Alternatively, for avalanches of fixed total size S in the scaling regime, one expects

$$\dot{u}(t, x) \sim S^{1-(z+d)/(\zeta_d+d)} \sqrt{\text{fixed size}}(t/S^{z/(d+\zeta_d)}, x/S^{1/(d+\zeta_d)}), \quad (\text{II.6.2})$$

where the rescaled spatio-temporal process $\sqrt{\text{fixed size}}(t, x)$ is a well defined S -independent stochastic process. Of course it is one thing to write (II.6.1) or (II.6.2) but it is another to prove it and to characterize in some way these rescaled stochastic processes. In recent years a lot of attention has been devoted to the study of the *mean temporal shape of avalanches at fixed duration or size*.

$$\begin{aligned} \mathcal{F}_{\text{temporal shape}}^{\text{fixed duration}}(t) &:= \overline{\int_x \mathbf{u}^{\text{fixed duration}}(t, x)}, \\ \mathcal{F}_{\text{temporal shape}}^{\text{fixed size}}(t) &:= \overline{\int_x \mathbf{u}^{\text{fixed size}}(t, x)}. \end{aligned} \quad (\text{II.6.3})$$

At the mean-field level in the ABBM model, the closely related mean temporal shape at fixed size as a function of the interface position was first computed in [140, 141]. The mean temporal shape at fixed duration was computed in [142], with the remarkably simple result $\mathcal{F}_{\text{temporal shape}}^{\text{fixed duration}}(t) \sim t(1-t)$. Interestingly, these remarkable observables are also well suited to investigate non-universal effects in avalanche processes which are also interesting for practical applications. In particular, it was known experimentally that the mean temporal shape at fixed duration of Barkhausen pulses present an asymmetry and are skewed to the left, a fact which was attributed to the slow relaxation of Eddy currents affecting the domain wall dynamics [143, 42]. Years later these effects were introduced in a modified ABBM model, the temporal shape was again computed analytically and presented the asymmetry observed experimentally [144]. Finally, results beyond mean-field (at one-loop) were recently obtained for the average temporal shape at fixed duration and size in [43, 110]. The very recent comparison

with experiments confirmed the increase of precision brought by one-loop corrections [145].

The spatial shape of avalanches

On the other hand the equally interesting *spatial shape of avalanches* was left aside from theoretical studies until recently. This was a rather disappointing state of affairs since the latter could also be measured in some modern experimental setups on e.g. fracture processes. In [1] (presented in Sec. II.6.2 and Appendix A), as will be detailed in the next section, we made the first progress in this direction and showed that at the mean-field level, i.e. in the BFM, the shape of avalanches in $d = 1$ becomes *deterministic* in the limit of peaked avalanches $S/\ell^{d+\zeta} \gg 1$ and we identified the limiting shape. Fluctuations around this deterministic profile were also studied in an expansion in $\ell^{d+\zeta}/S$. Comparison with numerical simulations showed a good to perfect agreement. In [2] (presented in Sec. II.6.3 and Appendix B) we went further in analyzing the spatial shape of avalanches. We first obtained *the mean velocity field* inside avalanches of fixed total size at the mean-field level. This observable contains both the mean temporal shape at fixed size previously studied and a new result, the mean *spatial shape at fixed total size*. Going beyond mean field we were able to compute the one-loop corrections to the mean spatial shape at fixed total size. Comparison with numerical simulations showed a good agreement.

What about correlations?

Up to now all the observables that were mentioned concern what one may call ‘one-shock/avalanche statistics’. However, an interface in a given disordered medium generally experiences a *sequence of shocks/avalanches* $\{w_i, S_x^{(i)}\}$. The observables mentioned before do not fully characterize the properties of this sequence since there can be correlations between different shocks/avalanches. In the context of earthquakes the study of these correlations has been a major focus of the field. From the phenomenological point of view the main result is the Omori law that characterizes the number of aftershocks after a main shock [67]. Several mechanisms have been advanced to explain these strong correlations, all involving an additional dynamical variable [146, 147]. For elastic interfaces, in an attempt to explain the Omori law from simple mechanisms, correlations between avalanches were until recently only studied as a result of such additional degrees of freedom in the interface dynamics, such as relaxation processes [148, 149] or memory effects [144]. Overall there is a belief that these correlations are not captured by the simple interface model. While this is certainly true, it is still clearly of interest to understand first the correlations in interface models (as the example of the temporal shape of Barkhausen avalanches teach us, it is important to first thoroughly understand what is universal to understand what is not!). These universal correlations were remarkably left aside from all theoretical studies until recently. There was even a belief that avalanches were uncorrelated in elastic interfaces model. While this is certainly true for the ABBM and the BFM model, as we very precisely show in [1] (presented in Sec. II.6.2 and Appendix A), correlations always exist in non mean-field models. Using FRG we showed in [3] (presented in Sec. II.6.4 and Appendix C) that correlations between shocks in disordered elastic interfaces are universal, of order ϵ and are controlled by the renormalized disorder correlator $\Delta(u)$. While as we showed, the one-shock statistics is only sensitive to the behavior of $\Delta(u)$

around the cusp, correlations between static shocks feel the full shape of $\Delta(u)$. We obtained quantitative results on the correlations that notably permits and original and unambiguous distinction between the RB and RF universality class.

Before we begin a more detailed presentation of the results obtained during the thesis (we will only present the main results and encourage readers to look at the original research papers in Appendices A-B-C), let us mention here that the list of problems introduced above is of course very incomplete. Other interesting important open problems of the field will be mentioned in the conclusion.

II.6.2 Presentation of the main results of [1]

An exact formula for the local size of avalanches following an arbitrary driving in the BFM on an arbitrary graph

In [1] we consider the BFM on an arbitrary graph and consider the avalanches following a stepped driving (defined below). That is we consider the equation of motion

$$\eta \partial_t u_{it} = \sum_{j=1}^N c_{ij} u_{jt} - m^2 (u_{it} - w_{it}) + F_i(u_{it}) \quad (\text{II.6.4})$$

where (i) $i = 1, \dots, N \in \mathbb{N}$ label the points of the graph; (ii) u_{it} is the position of the i^{th} point at time t ; (iii) the points are linked to one another by a time-independent elasticity matrix c_{ij} such that $\sum_j c_{ij} = 0$ and $c_{ij} \geq 0$ for $i \neq j$; (iv) the random forces $F_i(u)$ are a collection of independent one-sided BM with $\overline{[F_i(u) - F_i(u')]^2} = 2\sigma|u - u'|$ and $\sigma \geq 0$; (v) the interface is at rest at time 0 and $u_{it=0} = F_i(0) = w_{it=0} = 0$; (vi) for $t \geq 0$ the driving verifies $\dot{w}_{it} \geq 0$ and $w_i := w_{i,t=+\infty} < \infty$.

Under these conditions, we obtain an exact formula for the joint distribution of avalanche local size defined as $S_i := u_{i,t=\infty}$ (which is smaller than ∞ with probability 1) for an arbitrary driving $\vec{w} = (w_1, \dots, w_N)$. We obtain (in dimensionless units $w_i \rightarrow w_i/S_m$ and $S_i \rightarrow S_i/S_m$ with $S_m = \sigma/m^4$)

$$P_{\vec{w}}(\vec{S}) = \left(\frac{1}{2\sqrt{\pi}} \right)^N \left(\prod_{i=1}^N S_i \right)^{-\frac{1}{2}} \exp \left(-\frac{1}{4} \sum_{i=1}^N \frac{(w_i - \sum_{j=1}^N C_{ij} S_j)^2}{S_i} \right) \det (M_{ij})_{N \times N}$$

$$M_{ij} = C_{ij} + \delta_{ij} \frac{w_i - \sum_{k=1}^N C_{ik} S_k}{S_i} \quad , \quad C_{ij} = \delta_{ij} - \frac{1}{m^2} c_{ij} \quad . \quad (\text{II.6.5})$$

The formula is obtained both (i) using an ‘instanton’ method similar as (II.5.61-II.5.63) to obtain formally the Laplace Transform (LT) of (II.6.5), the LT is then formally inverted using heuristic calculations involving Grassmann variables; (ii) an exact proof by deriving the Kolmogorov backward equation satisfied by (II.6.5) in the case where the driving is $\dot{w}_{it} = w_i \delta(t)$.

Exact formula for the densities and the BFM as a Lévy-Jump process

Based on the formula (II.6.5) and on the form of its Laplace Transform, we show that the BFM is an infinitely divisible process. Namely $\forall k \in \mathbb{N}, \forall \vec{w}_1, \dots, \vec{w}_k \in (\mathbb{R}_+)^N$ such that $\vec{w} = \sum_{i=1}^k \vec{w}_i$, we have

$$P_{\vec{w}}(\vec{S}) = (P_{\vec{w}_1} \star P_{\vec{w}_2} \star \dots \star P_{\vec{w}_k})(\vec{S}) \quad . \quad (\text{II.6.6})$$

This rigorously shows that the BFM on an arbitrary graph is a Lévy jump process (see e.g. [104]). The motion of the interface is a succession of jumps independently generated in time and in space by the densities $\rho_i(\vec{S}) = \frac{\partial P_{\vec{w}}(\vec{S})}{\partial w_i} |_{\vec{w}=0}$ which, for each site i , corresponds to the density of avalanches triggered at the i^{th} site (which depends non-trivially on i on an arbitrary graph). Based on (II.6.5) we obtain an exact formula for these densities and are able to take the $k \rightarrow \infty$ limit of (II.6.6) as

$$\int d^N \vec{S} e^{\vec{\lambda} \cdot \vec{S}} P_{\vec{w}}(\vec{S}) = \sum_{n=0}^{\infty} \sum_{(i_1, \dots, i_n)} \frac{w_{i_1} \dots w_{i_n}}{n!} \prod_{l=1}^n \int d^N \vec{s}_{i_l} (e^{\lambda \vec{s}_{i_l}} - 1) \rho_{i_1}(\vec{s}_{i_1}) \dots \rho_{i_n}(\vec{s}_{i_n}) \quad (\text{II.6.7})$$

In (II.6.7) each term $w_{i_1} \dots w_{i_n}$ corresponds to events where the total motion \vec{S} of the interface was generated by n elementary avalanches triggered by the density ρ_i at the site i_1, \dots, i_n and $\vec{S} = \vec{s}_{i_1} + \dots + \vec{s}_{i_n}$ (note that there can be several avalanche triggered from the same seed, i.e. the terms $i_k = i_{k'}$ are contained in the above summation).

The formulae (II.6.5) and (II.6.7) are rather remarkable as they contain in principle all the information on the spatial structure of avalanches in a completely general version of the BFM model. The possibility to obtain such a formula is linked to the non-trivial exact solvability property of the BFM. Although it was previously known that the avalanches in the BFM are independent, this independence property was never described as precisely as in (II.6.7). It is however fair to say that extracting more information (e.g. a marginal probability) from these formulae is quite hard. In [1] we are able to make progress in the fully connected model for arbitrary N . The study of the large N limit from these formulae is rather instructive and we encourage readers to read the 5th section of [1] (see Appendix A). Here we present only one result extracted from (II.6.5) namely the deterministic shape taken by peaked avalanches in the continuum BFM model with SR elasticity in $d = 1$.

The shape of peaked avalanches in the BFM with SR elasticity in $d = 1$

Taking the continuum limit of the above formulae, we obtain a formula for the density of avalanches in the BFM with SR elasticity in $d = 1$ on a line of length L with periodic boundary conditions as (in dimensionless unit, see Appendix A for more details and Sec. II.5.2 for the definition of the BFM in the continuum)

$$\rho[S_x] \sim \frac{(\int_0^L dx S_x) \int_0^L \frac{1}{S_x^2}}{(\prod_x S_x)^{\frac{1}{2}}} \exp \left(- \int_0^L dx \frac{(S_x - \nabla^2 S_x)^2}{4S_x} \right). \quad (\text{II.6.8})$$

This allows us to obtain observable such as the mean shape of avalanches using a path integral on the shape of avalanches S_x with statistical weight $\rho[S_x]$. We show that for avalanches of extension ℓ and total size S , in the limit of peaked avalanches $S/\ell^4 \gg 1$, the *centered, reduced* shape $s(x) = \frac{1}{S\ell} S_{(x-x_0)/\ell}$, defined such that the support of the reduced shape is $x \in [-1/2, 1/2]$ and $\int_{-1/2}^{1/2} s(x) dx = 1$, becomes deterministic $s(x) = s_0(x)$ (given by a saddle-point of the path integral associated with (II.6.8)) and solves

$$\mathcal{A} \phi(x) = \phi^{(4)}(x) + \frac{5\phi'(x)^4}{\phi(x)^3} - \frac{10\phi'(x)^2\phi''(x)}{\phi(x)^2}. \quad (\text{II.6.9})$$

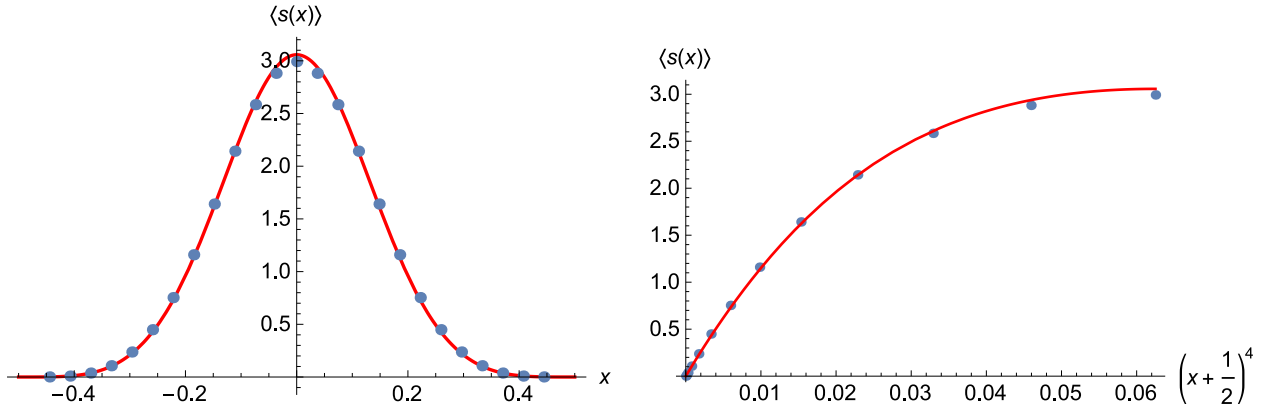


Figure II.4: Left: Mean shape obtained by averaging over the 1000 avalanches with the largest S/ℓ^4 in the simulations of the BFM of [1] (blue dots, compared to the optimal shape $s_0(x)$ solution of (II.6.9) (red line). Right: test of the predicted behavior $s_0(x) \sim (x + 1/2)^4$ close to the boundaries. Figures taken from [1].

where $s_0(x) = \phi_0(x)^2$ with $\phi_0(x)$ the solution of (II.6.9) with the saddle-point parameter \mathcal{A}_0 ensuring $\int_{-1/2}^{1/2} \phi_0(x)^2 = 1$. (II.6.9) was solved numerically with a high precision. The solution is predicted to decay close to the boundary as $s_0(x) \sim_{x \rightarrow 1/2^-} (1/2 - x)^4$. This is confronted with numerical simulations of the BFM (see Appendix A for more details) with a very good agreement, as shown in Fig. II.4. In [1] we also investigate the $\sqrt{\ell^4/S}$ corrections to this deterministic behavior and obtain, based on the optimal shape $s_0(x)$, the tails of the PDF of aspect ratios S/ℓ^4 . These additional results are successfully confronted with numerical simulations (see [1] in Appendix A).

II.6.3 Presentation of the main results of [2]

The seed-centering

In [2] we pursued the analysis of the spatial shape of avalanche processes. One of the main contributions of our work was to remark that the most convenient way to center the shape of avalanches (from the perspective of performing analytical calculations) is to center them around their seed. Indeed, as was shown with (II.5.38), the structure of the MSR action for the depinning of elastic interface allows quite naturally to isolate in any observable $O[\dot{u}_{tx}]$ the contribution of avalanches starting at a given time t_i and position x_i . In some sense this is natural since this is the only centering which respects the causal structure of avalanche processes: the seed centering is a conditioning on the stochastic process of the velocity field inside an avalanche with respect to its initial condition. Another type of centering, e.g. the centering with respect to the maximum or to the center of mass of the avalanche, does not respect this causality since it corresponds to a conditioning on the full history of the stochastic process. It is reasonable to think that it is this absence of an adapted centering procedure that made the mean spatial shape of avalanches ignored from theoretical studies until this paper. Of course, having a centering procedure that is analytical-work friendly is almost useless if the observable cannot be measured in numerical simulations and experiments.

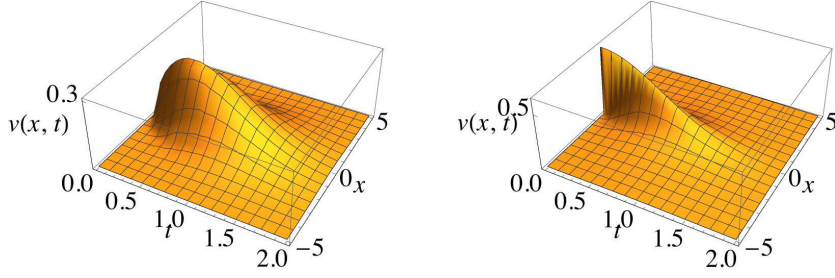


Figure II.5: Plot of the mean-field result for the space-time mean velocity profile inside an avalanche in $d = 1$ for SR (left, see (II.6.11)) and LR elasticity (right, see (II.6.12)). Figures taken from [2].

One of the challenge of [2] was therefore to devise an algorithm allowing a simple study of seed-centered shapes. We refer the reader to the paper [2] presented in Appendix B for a description of this algorithm and only give the results here, everywhere presented in dimensionless units $x = \tilde{x}/m$, $t = \tau_m \tilde{t}$, $S = S_m \tilde{S}$ with $\tau_m = \eta/m^2$ and $S_m = \sigma/m^4$ (as usual m is the mass of the driving spring and η and σ are linked to the renormalized parameters of the models, see Appendix B for details and Sec. II.3.2 and Sec. II.5.2 for the notations and definitions used in this section)

The mean velocity field inside avalanches of fixed size in the BFM in arbitrary d

We first showed that for the BFM in arbitrary d with SR and LR elasticity, the scaling formula for the *mean value of the velocity field inside seed-centered avalanches of fixed size S in the scaling regime*

$$\langle \dot{u}_{tx} \rangle_S = S^{\frac{\zeta-z}{d+\zeta}} F(t/S^{\frac{z}{d+\zeta}}, x/S^{\frac{1}{d+\zeta}}), \quad (\text{II.6.10})$$

holds with a simple scaling function for SR elasticity in arbitrary d , $\forall S$

$$F(t, x) = 2te^{-t^2} \frac{1}{(4\pi t)^{d/2}} e^{-x^2/(4t)}, \quad (\text{II.6.11})$$

and for LR elasticity (obtained in arbitrary d in Fourier space and in $d = 1$ in real space) $\forall S \ll S_m$

$$F(t, x) = 2te^{-t^2} \int_q e^{iqy-|q|t} \stackrel{d=1}{=} \frac{2t^2 e^{-t^2}}{\pi(x^2 + t^2)}. \quad (\text{II.6.12})$$

These are shown in Fig. II.5 but have not been measured in simulations.

The mean spatial shape of avalanches of fixed size in the BFM and at one loop for SR elasticity

Integrating (II.6.11) with respect to time leads to the *mean shape of seed centered avalanches in the BFM for SR elasticity in arbitrary d* . The latter can be checked to satisfy the following scaling form $\forall S$, equivalently written in Fourier or real space

$$\langle S(x) \rangle_S = S^{1-\frac{d}{d+\zeta}} \mathcal{F}_d\left(\frac{x}{S^{\frac{1}{d+\zeta}}}\right), \quad \langle S(q) \rangle_S = S \tilde{\mathcal{F}}_d(qS^{\frac{1}{d+\zeta}}). \quad (\text{II.6.13})$$

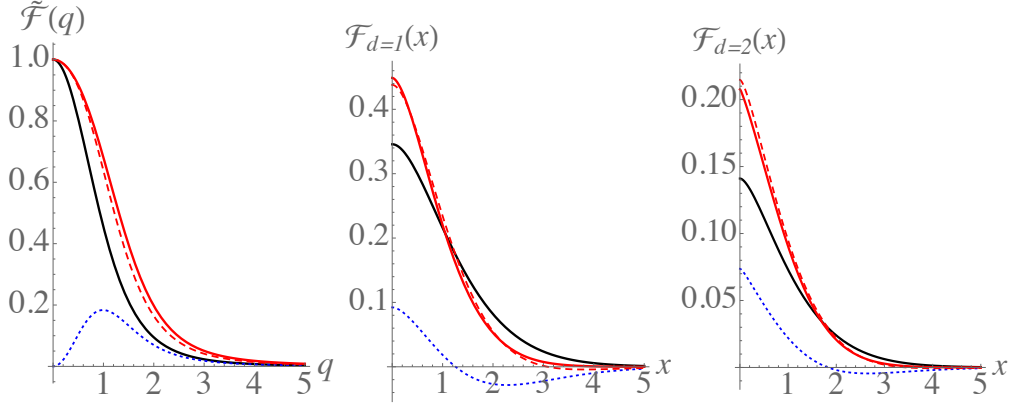


Figure II.6: Analytical results at MF and $O(\epsilon)$ level for the universal scaling function $\tilde{\mathcal{F}}_{d=1}$ in Fourier space (Left) and \mathcal{F}_d in real space for $d = 1$ (Middle) and $d = 2$ (Right) for SR elasticity. Black lines: tree/mean-field results. Dotted blue lines: universal corrections, $\delta\tilde{\mathcal{F}}_1(q)$ (left, $O(\epsilon)$ correction in Fourier space in $d = 1$), $\delta\mathcal{F}_1(x)$ (middle) and $\delta\mathcal{F}_2(x)$ (right). Red-dashed lines: $O(\epsilon)$ estimate obtained by simply adding the corrections to the MF value. Red lines: improved $O(\epsilon)$ estimate, which, through a re-exponentiation procedure, takes properly into account the modification of exponents (II.6.17) and (II.6.18) (see [2] in Appendix B). Note that the cusp at the origin of the avalanche shape at $O(\epsilon)$ is not obvious in this plot since the non-analyticity is rather small, but it can be emphasized using a log-log scale. Figures taken from [2].

$\mathcal{F}_d(x)$ can be expressed using hypergeometric functions (see [2] in Appendix B), and $\tilde{\mathcal{F}}_d(q)$ has the remarkably simple, d -independent form

$$\tilde{\mathcal{F}}_d^{\text{BFM}}(q) = \tilde{\mathcal{F}}^{\text{BFM}}(q) = 1 - \frac{\sqrt{\pi}q^2}{2} e^{\frac{q^4}{4}} \text{erfc}\left(\frac{q^2}{2}\right). \quad (\text{II.6.14})$$

The result for these scaling functions in the BFM in any d in Fourier space and in $d = 1, 2$ in real space are shown in black in Fig. II.6.

For more realistic models of interfaces in a short-range (SR) correlated disorder, the above results are the $O(\epsilon^0)$ results to the mean spatial shape of avalanches. In order to go beyond mean-field, we use the results of FRG and in [2], using the simplified action (II.5.48), we were able to compute the $O(\epsilon)$ corrections to the mean shape. In Fourier space we show that the scaling (II.6.13) is still compatible with one-loop FRG in the scaling regime $S \ll S_m$ and we obtain the $O(\epsilon)$ correction

$$\tilde{\mathcal{F}}_d^{\text{BFM}}(q) = \tilde{\mathcal{F}}^{\text{MF}}(q) + \delta\tilde{\mathcal{F}}_d(q) + O(\epsilon^2), \quad (\text{II.6.15})$$

where $\delta\tilde{\mathcal{F}}_d(q) = \epsilon\tilde{\mathcal{F}}^{(1)}(q)$. Here $\tilde{\mathcal{F}}^{(1)}(q) = \int_{\mathcal{C}} \frac{d\mu}{2i\pi} e^{\mu} \tilde{H}(\mu, q)$ is obtained as an Inverse Laplace Transform (ILT) $\mu \rightarrow 1$ of:

$$\begin{aligned} \tilde{H}(\mu, q) = & \frac{4\sqrt{\pi}}{9} \left[\frac{2 - 3\gamma_E}{8} \frac{1}{q^2 + 2\sqrt{\mu}} - \frac{4\sqrt{\mu}}{(q^2 + 2\sqrt{\mu})^2} \right. \\ & \left. \times \left(\frac{q^2 + 9\sqrt{\mu}}{q\sqrt{q^2 + 8\sqrt{\mu}}} \sinh^{-1}\left(\frac{q}{2\sqrt{2\sqrt{\mu}}}\right) - 1 + \frac{3}{16} \ln(4\mu) \right) \right], \end{aligned} \quad (\text{II.6.16})$$

where γ_E is Euler's Gamma constant (see [2] in Appendix B for the choice of the contour \mathcal{C}). We then define the correction to the mean shape in real space as the d -dimensional Fourier transform $\delta\mathcal{F}_d(x) = \int \frac{d^d q}{(2\pi)^d} e^{-iqx} \delta\tilde{\mathcal{F}}_d(q)$. We were not able to perform the ILT of (II.6.16) in full generality but obtained the behavior of the mean shape in Fourier space at small and large q and in real space at small and large x . In particular we show that:

(i) At large q in Fourier space,

$$\tilde{\mathcal{F}}_d(q) \simeq_{q \gg 1} \tilde{A}_d q^{-\tilde{\eta}_d} \quad , \quad \tilde{\eta}_d = 4 - \frac{4\epsilon}{9} + O(\epsilon^2) \quad , \quad (\text{II.6.17})$$

with a universal prefactor $\tilde{A}_d = 2(1 - (2 + \frac{\gamma_E}{4})\frac{2\epsilon}{9})$. In real space this implies, in the expansion of $\mathcal{F}_d(x)$ at small x , a non-analytic term $\sim |x|^{\eta_d}$ with $\eta_d = \tilde{\eta}_d - d = \frac{5\epsilon}{9} + O(\epsilon^2)$.

Restoring the S dependence from (II.6.13) this leads to $\langle S(q) \rangle_S \sim_{q \rightarrow +\infty} S^{1 - \frac{\tilde{\eta}_d}{d+\zeta}} q^{-\tilde{\eta}_d}$ and the non-analytic part $\langle S(x) \rangle_S^{n,a} \sim_{x \rightarrow 0} S^{1 - \frac{\tilde{\eta}_d}{d+\zeta}} |x|^{\eta_d}$. Note that in the BFM case (retrieved by taking $\epsilon = 0$) the value $\tilde{\eta}_d = 4 = d + \zeta_{BFM}$ implies that the large q behavior of $\langle S(q) \rangle_S$ *does not depend on S* . This may seem natural: in the BFM the small scales do not know about the total size of the avalanche. A generalization of this property to the SR disorder case would suggest the guess $\tilde{\eta}_d^{\text{guess}} = d + \zeta$. Our $O(\epsilon)$ result however explicitly shows that this property fails and $\tilde{\eta}_d > d + \zeta$ (at least close to $\epsilon = 0$). Hence in the SR disorder case the *large avalanches tend to be more smooth than small avalanches*. Note that the predicted value of η_d is smaller than 2 in all physical dimensions: *this non-analytic term should actually dominate the behavior of $\mathcal{F}_d(x)$ around 0* (and thus lead to a cusp singularity).

(ii) At large x in real space, we obtain that the mean shape has a stretched exponential decay as:

$$\mathcal{F}_d(x) \sim e^{-Cx^\delta} \quad , \quad \delta = \frac{4}{3} + \frac{2}{27}\epsilon + O(\epsilon^2) \quad , \quad (\text{II.6.18})$$

with a universal prefactor $C = \frac{3}{4} + (\frac{7\sqrt{3}}{36} - 1)\frac{2}{9}\epsilon$. Remarkably, using $\zeta = \epsilon/3 + O(\epsilon^2)$, this agrees to $O(\epsilon)$ with the general conjecture $\delta = \frac{d+\zeta}{d+\zeta-1}$ that we justify in [2].

Comparison with numerical simulations

In [2], using an original algorithm to retrieve the seed of the avalanches we compare the above theoretical results with simulations of the BFM and of a model with SR disorder in $d = 1$, both with short-range elasticity. For the BFM (as it should since our results are exact) we obtain a perfect agreement, see Fig. II.7. This demonstrates that our observable is measurable in numerical simulations. For the model with SR disorder, our results compare reasonably well with the results of the numerical simulations and bring a substantial improvement compared to the mean-field results, see Fig. II.8. The results look better in Fourier space: when integrated, the small discrepancy $\forall q$ in Fourier space gives a larger discrepancy around the origin in real space. Additional numerical results are shown [2]. In particular it is shown that the cusp of the mean shape for model with SR disorder that is predicted by our one-loop result is indeed compatible with numerical simulations.

Some additional results can be found in [2], in particular we introduce and compute to order $O(\epsilon)$ some *universal ratios*, which are quantities allowing us to efficiently com-

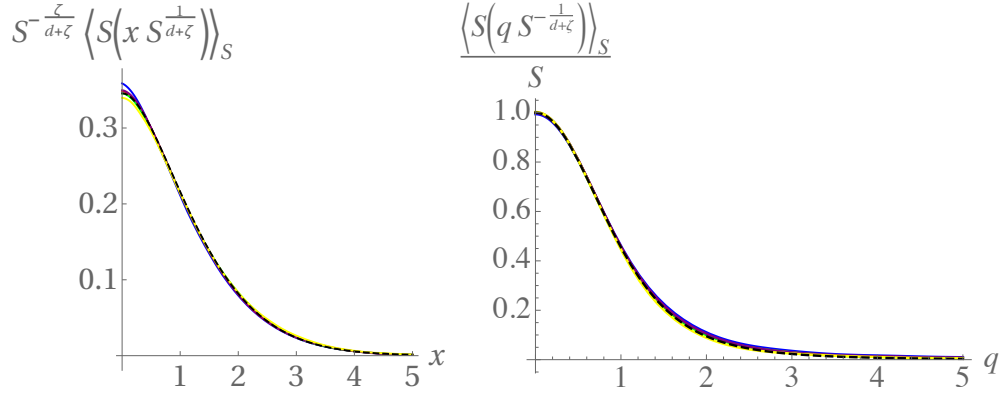


Figure II.7: Lines: rescaled mean shapes of avalanches at fixed size S obtained from the simulations of the BFM model in $d = 1$ in real (left) and Fourier (right) space, for $S = 10$ (blue), $S = 10^2$ (red), $S = 10^3$ (green), $S = 10^4$ (purple) and $S = 10^5$ (yellow). Dashed black lines: exact theoretical results in the BFM. No fitting parameter. Figures taken from [2].

pare different shape functions when one scale is unknown. This could be particularly useful for comparison with experiments.

II.6.4 Presentation of the main results of [3]

The two-shock density

In [3], presented in Appendix C, we investigated the presence of correlations at order $O(\epsilon)$ in the sequence of shocks of the ground state $(w_i, S_x^{(i)})_{i \in \mathbb{Z}}$ for a d -dimensional elastic interface in a disordered medium (we refer the reader to Sec. II.3.1 for definitions). Since depinning/avalanches and statics/shocks at zero temperature for disordered elastic interfaces are, for all we know, equivalent up to order $O(\epsilon^2)$, our results are expected to apply equally well for avalanches at the depinning transition. The phenomenology is, however, as we will see, richer in the case of shocks due to the presence of one more universality class (random bond) for short-range correlated disorder. We investigate these correlations by looking at the two-shock density at a distance $W > 0$, defined as,

$$\rho_W(S_1, S_2) := \overline{\sum_{i \neq j} \delta(w - w_i) \delta(S_1 - S^{(i)}) \delta(w + W - w_j) \delta(S_2 - S^{(j)})} .$$

Here $\int_{w_1}^{w'_1} dw \int_{w_2}^{w'_2} dw' \int_{S_1}^{S'_1} dS \int_{S_2}^{S'_2} dS' \rho_{w'-w}(S, S')$ counts the mean number of pairs of shocks such that the first shock occurred between w_1 and w'_1 , and the second between w_2 and w'_2 , with sizes between S_1 and S'_1 , resp. S_2 and S'_2 . An absence of correlations in the sequence of shocks would imply $\rho_W(S_1, S_2) = \rho(S_1)\rho(S_2)$ where the one-shock density $\rho(S)$ was defined in (II.3.5). To investigate the presence of correlations we thus study the *connected two-shock size density* $\rho_W^c(S_1, S_2)$, defined as

$$\rho_W^c(S_1, S_2) := \rho_W(S_1, S_2) - \rho(S_1)\rho(S_2) . \quad (\text{II.6.19})$$

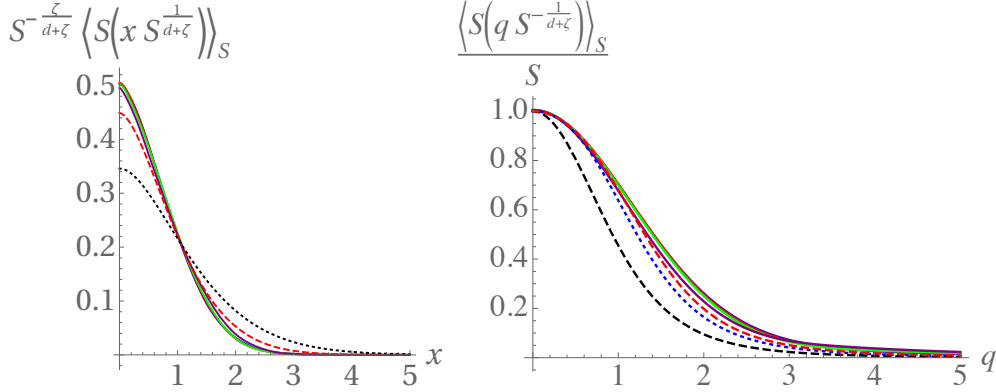


Figure II.8: Lines: rescaled mean shapes of avalanches at fixed size S from the simulation of the model with SR disorder in $d = 1$ in real (left) and Fourier (right) space for $S = 50$ (blue), $S = 10^2$ (red), $S = 10^3$ (green), $S = 10^4$ (purple). Dashed black lines: theoretical MF result. Red dashed line: improved $O(\epsilon)$ result taking into account the modification of exponents (II.6.17) and (II.6.18). Blue dashed line on the right: $O(\epsilon)$ obtained by simply adding one-loop corrections to the MF result. No fitting parameter. Figures taken from [2].

At the mean-field level in the BFM, as we know (see Sec. II.6.2) shocks are independent thus $\rho_W^c(S_1, S_2) = 0$. At order $O(\epsilon)$ however as we show below this is not the case and $\rho_W^c(S_1, S_2) = O(\epsilon)$ is given by a universal scaling function.

An exact formula for the first connected moment

We first obtain an *exact formula* for the first connected moment

$$\frac{\langle S_1 S_2 \rangle_{\rho_W^c}}{[\langle S \rangle_{\rho}]^2} = -\frac{\Delta''(W)}{L^d m^4}. \quad (\text{II.6.20})$$

Here a subscript indicates the density with respect to which the average is taken. For uncorrelated shocks the right-hand side of (II.6.20) would be 0. Here as usual $\Delta(W)$ is the universal scaling function of the FRG, which can be measured as an observable using (II.4.43). The above equation is a generalization to the two-shocks case of the exact formula for $S_m = \langle S^2 \rangle_{\rho} / (2\langle S \rangle_{\rho})$ given in (II.4.47). For m close to 0 as we know (see Sec. II.4.1) $\Delta(W)$ takes a universal scaling form with

$$\Delta(u) = A_d^\gamma \mu^{\epsilon - 2\zeta_d} \kappa^2 \Delta^*(\mu^{\zeta_d} u / \kappa) \quad (\text{II.6.21})$$

where κ is a non-universal microscopic scale. Depending on the range of correlations of the initial disorder, $\Delta^*(u) = O(\epsilon)$ is the fixed point of the FRG equation with $\Delta^*(0) = \epsilon$ of the RB or RF universality class. From II.6.20 the shocks appear positively correlated for $\Delta''(W) \leq 0$ and anti-correlated for $\Delta''(W) \geq 0$. Taking a look at the cartoon of the typical shape of the RB and RF fixed points presented in Fig. II.9, correlations between shocks thus give an unambiguous distinction between these two universality classes: for RF shocks are always anti-correlated, while for RB they are anti-correlated at small distances and positively correlated at large distances. An exact equation

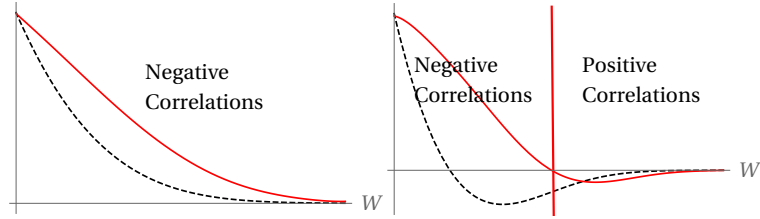


Figure II.9: Cartoons of the typical shape of the renormalized disorder correlator $\Delta(W)$ (black-dashed line) and of its second derivative $\Delta''(W)$ (red line) for the random field (left) and random bond (right) universality classes (not to scale). Our results predict that the shock sizes are always negatively correlated in the random field universality class, whereas the random bond universality class exhibits a richer structure with negatively (resp. positively) correlated shock sizes at small (resp. large) distances. Figures taken from [3].

similar to (II.6.21) can be proved for avalanches at depinning. In this case random bond bare disorder flows at large scale to random field disorder and thus avalanches at the depinning are always anti-correlated.

The two-shock density at $O(\epsilon)$

To go beyond the exact result (II.6.20) we use FRG in [3] to obtain $\rho_W^c(S_1, S_2)$ at first order in $O(\epsilon)$. We obtain

$$\rho_W^c(S_1, S_2) = \frac{1}{(L\mu)^d} \frac{L^{2d}}{S_m^4} \mathcal{F}_d\left(\frac{W}{W_\mu}, \frac{S_1}{S_\mu}, \frac{S_2}{S_\mu}\right). \quad (\text{II.6.22})$$

Where $W_\mu \simeq \kappa\mu^{-\zeta}$, $S_m \simeq A_d^\gamma \kappa \Delta^{*'}(0^+) \mu^{-(d+\zeta)}$ and the function \mathcal{F}_d is universal and apart from its three arguments depends only on the spatial dimension and range of elasticity inside the interface (the form of the large scale cutoff, here exponential, depends also on the chosen IR cutoff scheme of the theory). To first order in $d = d_{uc} - \epsilon$, and in the limit of large L and small μ , it is given by

$$\mathcal{F}_d(w, s_1, s_2) \simeq A_d^\gamma \frac{\tilde{\Delta}^{*''}(w)}{16\pi\sqrt{s_1 s_2}} e^{-(s_1+s_2)/4} + O(\epsilon^2). \quad (\text{II.6.23})$$

In [3] we use (II.6.23) to obtain a variety of results: the normalized PDF for shocks sizes at a distance W , the conditional probability to observe one shock given that another one occurred, and in particular the mean-density of pairs of shocks at a distance W :

$$\rho_2(W) = \int dS_1 dS_2 \rho_W(S_1, S_2) = \rho_0^2 \left[1 - \frac{\Delta''(W)}{L^d m^4} \left(\frac{\langle S \rangle_P}{2S_m} \right)^2 \right] + O(\epsilon^2). \quad (\text{II.6.24})$$

Generalization to the local shapes

The factor $\frac{1}{(L\mu)^d}$ in (II.6.22) highlights the fact that correlations are local and avalanches are correlated only if they occur in regions of space that are elastically connected (that is at a distance $|x - x'| \ll \ell_\mu$). To emphasize this local structure in [3] we investigated the correlations between the local size of the shocks measured on arbitrary subspace

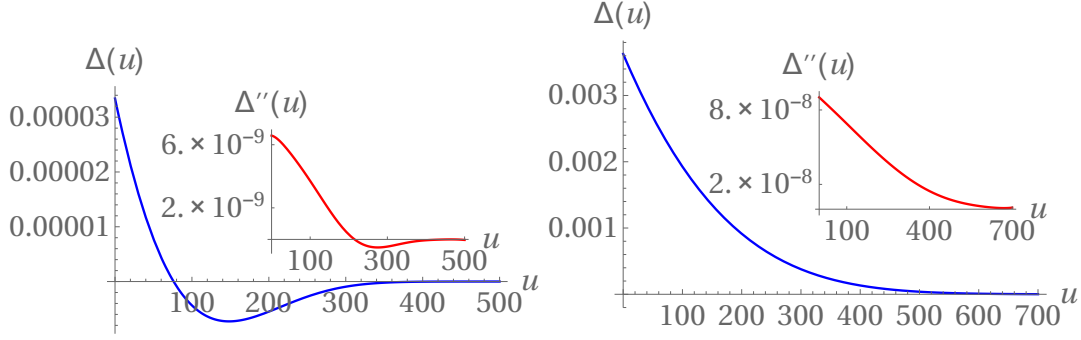


Figure II.10: Left: Renormalized disorder $\Delta(u)$ measured in the $d = 0$ RB toy model. Inset: its second derivative $\Delta''(u)$, computed using a numerical fit of the measured $\Delta(u)$. Right: The same for the RF toy model. Figures taken from [3].

(see [3] in Appendix C for precise definitions). We obtained a result for the generating function of all connected moments. Here we only show the results for the first connected moments for SR and LR elasticity: for SR we obtain

$$\langle\langle S_{1x_1} S_{2x_2} \rangle\rangle_{\rho_W^c} = \mathcal{F}_d^{11}\left(\frac{W}{W_\mu}, m|x_1 - x_2|\right) \quad (\text{II.6.25})$$

$$\begin{aligned} \mathcal{F}_d^{11}(w, x) &= -2^{-\frac{d}{2}-1} \pi^{-\frac{d}{2}} A_d \Delta^{*''}(w) x^{2-\frac{d}{2}} K_{2-\frac{d}{2}}(x) \\ &+ O(\epsilon^2). \end{aligned} \quad (\text{II.6.26})$$

where $K_n(x)$ is a modified Bessel function of the second kind. For LR elasticity we obtain

$$\langle\langle S_{1x_1} S_{2x_2} \rangle\rangle_{\rho_W^c} = \mathcal{F}_{d,\text{LR}}^{11}\left(\frac{W}{W_\mu}, m^2|x_1 - x_2|\right) \quad (\text{II.6.27})$$

$$\mathcal{F}_d^{11}(w, x) = -(2\pi)^{-\frac{d}{2}} A_d \Delta^{*''}(w) x^{1-\frac{d}{2}} K_{1-\frac{d}{2}}(x) + O(\epsilon^2).$$

Comparison with numerical simulations of toy models in $d = 0$

In [3] we confronted our results with numerical simulations of toy models of a particle on \mathbb{Z} with either a random bond type potential, or a random field type potential. In both cases, we measure the renormalized disorder correlator $\Delta(W)$, the first and second connected moment $\langle S_1 S_2 \rangle_{\rho_W^c}$ and $\langle S_1^2 S_2 \rangle_{\rho_W^c}$, and the mean density of pairs of shocks at a distance W , $\rho_2(W)$. As shown in Fig. II.10 to Fig. II.12, we obtain in both cases a perfect agreement for our exact formula (II.6.20). We also obtain a surprisingly good agreement with our $O(\epsilon)$ formula for $\rho_2(W)$ (II.6.24), considering that here $\epsilon = 4$. The results for the second connected moments $\langle S_1^2 S_2 \rangle_{\rho_W^c}$ are poorer and not shown here. These simulations were more a proof of principle than a real test of our theory since what we are really interested in is the case of interfaces for which FRG should work better. However, we clearly see that these correlations exist, are not negligible, and as theoretically found, possess an interesting structure since they allow to distinguish between the RB and RF universality class.

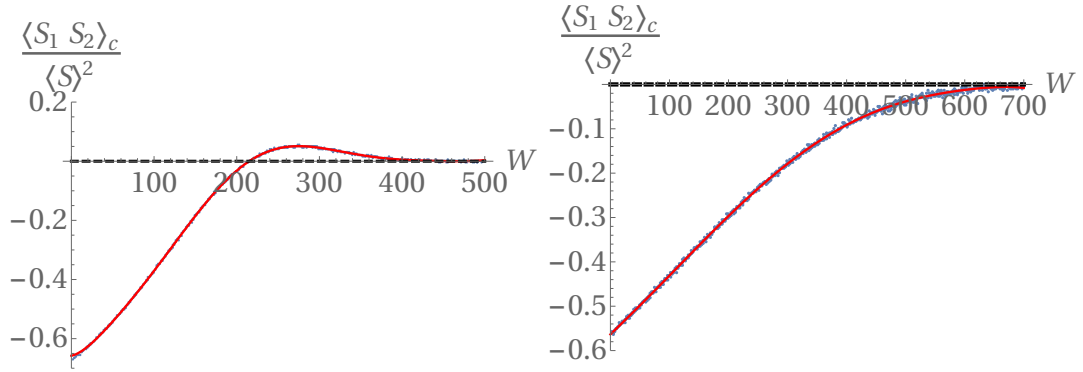


Figure II.11: Left: Comparison between the measurement of the normalized moment $\frac{\langle S_1 S_2 \rangle_{\rho_W^c}}{\langle S \rangle^2}$ (blue dots) and the prediction from the exact result (II.6.20) using the measurement of $\Delta(u)$ (red curve) in the RB toy model. The agreement is perfect as expected. Right: The same for the RF toy model. Figures taken from [3].

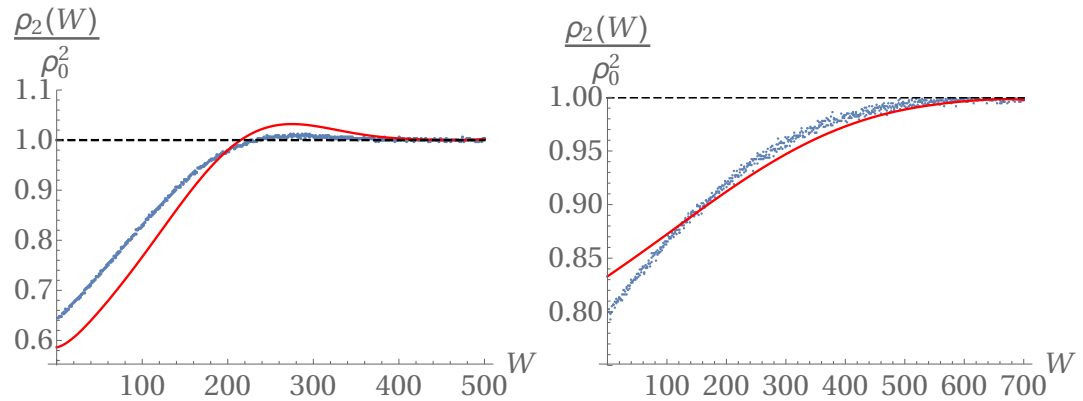


Figure II.12: Left: Comparison between the measurement of $\rho_2(W)$ (blue dots) and the prediction from the $O(\epsilon)$ result (II.6.24) using the measurement of $\Delta(u)$ (red curve) in the RB toy model. We obtain a surprisingly good agreement. Right: the same for the RF toy model. Figures taken from [3].

II.7 Conclusion

The study of shocks and avalanche processes in disordered elastic interfaces is of outstanding interest. On one hand avalanche type processes are observed in nature in a variety of physical situations. From the statistical physics perspective, as complex scale free spatio-temporal processes, they represent a remarkable field of applications of universality ideas outside the standard study of continuous phase transitions in equilibrium statistical mechanics. From a more conceptual perspective, they are fundamental processes at the core of the theory of disordered elastic systems. Indeed, they are a direct consequence, and a characterization, of the presence of many metastable states in the energy landscape of the system, and they dominate both the physics of the statics and of depinning. Understanding avalanche processes has brought new light to the functional renormalization group approach to disordered elastic systems. The ‘curiosity’ at the center of the theory, the non-analyticity of the effective action, is now directly linked to avalanches: measuring the functional renormalization group fixed point function in numerics and experiments is now possible.

In this thesis we have focused on the study of correlations and spatial shapes of avalanches. In both cases we have obtained results beyond mean-field that unveiled a rich structure. Many directions remain to extend these results. Concerning the spatial shape of avalanches, a natural extension would be to obtain one-loop results for the spatial shape with a long-range elastic kernel, which is of immediate experimental interest, or also one-loop results for the mean-velocity field inside avalanches. Concerning the correlations in avalanche processes, it would be interesting to extend our results to the dynamics. Although we have argued that our results obtained in the case of shocks should apply equally well to avalanches at depinning, it surely remains to be shown. More importantly, some features of the avalanche process at depinning are not present in the case of shocks, in particular the notion of seeds. Analyzing the correlation between the seeds of successive avalanches would be a very natural characterization of the non-Lévy nature of the avalanche process beyond mean-field. A complementary direction of research would be to gain a better understanding of correlations induced by mechanisms not captured by the elastic interface model, e.g. memory effects in the dynamics as in [144]. Finally, for both the shape of avalanches and correlations, it would be highly interesting to compare the results with refined simulations (particularly for the correlations where ours were performed in $d = 0$), and with experiments. Comparing the temporal shape of avalanches computed in the ABBM model with the shape of Barkhausen pulses measured in soft magnets has triggered important developments that we reviewed. It would be interesting if similarly we could learn new aspects of the (eventually non-universal) physics e.g. of fracture processes by comparing the spatial shape of avalanches with our results.

Many other interesting open (and difficult) questions not tackled during this thesis remain. For example a better understanding of the functional renormalization group approach to the dynamics of disordered elastic interfaces at finite temperature and/or velocity would be of great interest. For avalanches this would lead to a better characterization of avalanches during the creep dynamics, as recently investigated in [32]. In Barkhausen noise experiments, it is observed that a non-zero velocity modifies the avalanche exponents in materials with an effective LR elasticity, but not for materi-

als with SR elasticity [45]. While the velocity dependence of the exponents is known in the ABBM model, a FRG approach is surely necessary to understand such thinner effects. Similarly as for the effect of the temperature on avalanches, the effect of quantum fluctuations on avalanches (related to the notion of quantum creep) remains to be understood. Another interesting problem, of immediate experimental interest for fracture experiments, is to understand the statistics of clusters in avalanches for disordered elastic interfaces with LR elasticity (a question which was swept under the carpet during most of this chapter since we were effectively considering the total avalanche, which is eventually formed of several smaller avalanches). Finally it would be interesting to understand how to extend our results and methods to models close but not equivalent to disordered elastic interfaces, e.g. by taking into account plastic deformations or an additional conservation law as would be relevant for forced-flow imbibition experiments.

Chapter III

Exact solvability, directed polymers in 1+1d random media and KPZ universality

In this chapter we will focus on the study of the static properties of directed polymers (DPs, the $d = 1$ problem) with short-range elasticity ($\gamma = 2$) in a random bond type potential at a finite temperature T in dimension $N = 1$. Taking a look at the phase diagram of Fig. I.3 drawn in Chapter I, the large scale properties of the system are predicted to always be described by a strong disorder fixed point. Of course one can use the results of Sec. II.4.1 to study this FP by taking $\epsilon = 3$ (assuming the ϵ expansion has a sufficiently large radius of convergence) but that is not what we will do here. In fact in this chapter we will not focus so much on this FP. Rather, guided by the belief that it exists, we will study very specific models with *exact solvability properties*, i.e. for which exact analytical methods are available¹. The large scale analysis of exact results obtained for peculiar models will then lead to indirect information about the FP. The main issues with these methods is that they will not be robust to arbitrary small perturbations of the model. In particular we will study models of DP on the square lattice that are exactly solvable, for a given distribution of random energies, at a unique temperature. Guided by the qualitative analysis of Chapter I we however know that the temperature is irrelevant at large scales and therefore believe that the universal properties do not depend on its choice. Determining from the solution of the model which property is universal will not always be trivial, however, see in particular Sec. III.3.4. From the point of view of universality, while the choice $\gamma = 2$, $d = N = 1$ and RB disorder can seem awfully restrictive compared to the more general analysis performed in Chapter I and Chapter II, we will see that (i) by restricting to this choice we will obtain very sharp results; (ii) this universality class is actually very large; (iii) results that, to this date, have only been obtained using exact methods have been measured in modern experimental settings. For these first two points we already refer the reader to Sec. I.3.3 where the links between the continuum DP problem and

¹To be fair with FRG, let us mention here more precisely that it is also an exact method since it provides an exact perturbative expansion of observables in an ϵ expansion. Its application in $d = 1$ is, however, necessarily inexact since in practice one needs to truncate the expansion to a given order.

the KPZ equation was recalled (thus already bringing in models of out-of-equilibrium growth in $1 + 1d$ in the large universality class mentioned above) together with some important results on the KPZ equation. For the last point we refer to Sec. I.4.2 for good to amazing experimental verifications of properties of KPZ universality in $1 + 1d$.

The outline of this chapter is as follows: in Sec. III.1 we will present a more complete introduction to the KPZ universality class in $1 + 1d$. In Sec. III.2 we will present a few exact solvability properties that played an important role over the years. In Sec. III.3 we will finally present the results obtained during the thesis.

III.1 The KPZ universality class in $1 + 1d$

In this section we review some results about the KPZ universality class in $1 + 1d$. We will start by presenting a few models in the KPZ universality class in Sec. III.1.1, with an emphasis on directed polymers models. We will then review important results obtained in some models and present the notion of *strong universality* and KPZ fixed point in Sec. III.1.2. Finally in Sec. III.1.3 we will discuss the notion of *weak universality* and the universal scaling limits of directed polymers on the square lattice. The material contained in this section is by now standard and inspired by a few excellent reviews on the subject [34, 35, 150, 36, 151].

III.1.1 A few models in the KPZ universality class

In this section we present a few models believed, under some mild assumptions, to be in the KPZ universality class. We mainly focus on models of DPs: in the continuum, on the square lattice, at finite and zero temperature. But we also present some links with interacting particle systems and growing interfaces.

a The continuum DP and the KPZ equation Vs The Edwards-Wilkinson case

The continuum KPZ equation is in the KPZ universality class. Behind this statement lies a rather long history that highlights the fact that many results on the KPZ universality class were obtained using exact solutions of some discrete models that resisted proof directly in the continuum setting until recently (2010). For now we just wish to make here a few more comments on the links between the continuum DP and the KPZ equation. Only in this section we keep the dimension arbitrary.

Derivation of the Stochastic Heat Equation

We recall that the partition sum of the continuum DP at temperature T in a random potential $V(t, x)$ with both endpoints fixed was defined in (I.3.10) as the path integral (here with the change of notations $L \rightarrow t$ and $u \rightarrow x$)

$$Z_t(x) := \int_{u(0)=0}^{u(t)=x} \mathcal{D}[u] e^{-\frac{1}{2T} \int_0^t (\frac{du}{dt})^2 dt' - \frac{1}{T} \int_0^t V(t', u(t')) dt'} . \quad (\text{III.1.1})$$

And here, keeping the notations of Chapter I, $u(t') \in \mathbb{R}^N$ and the random potential is taken Gaussian with RB correlations (I.3.11), $\overline{V(t, x)V(t', x')} = \delta(t - t')R_0(x - x')$.

In order to obtain the differential equation satisfied by $Z_t(x)$ (I.3.13), it is already convenient to adopt a stochastic process language and note that the term in the path measure $\mathcal{D}[u]e^{-\frac{1}{2T}\int_0^t(\frac{du}{dt})^2 dt'}$ is just the measure on N -dimensional Brownian motion $u(t)$. The partition sum $Z_t(x)$ is thus written as²

$$Z_t(x) = \mathbb{E} \left(e^{-\frac{1}{T}\int_0^t dt' V(t', u(t'))} \delta^{(N)}(u(t) - x) \right), \quad (\text{III.1.2})$$

where here the average \mathbb{E} is over the stochastic process $u(t)$ now defined by

$$\begin{aligned} \partial_t u(t) &= \sqrt{T}\xi(t) \\ u(0) &= 0. \end{aligned} \quad (\text{III.1.3})$$

Here $\xi(t) = (\xi_1(t), \dots, \xi_N(t))$ is a vector of unit centered Gaussian white noise (GWN) with δ correlations

$$\langle \xi_i(t)\xi_j(t') \rangle_\xi = \delta_{ij}\delta(t - t'), \quad (\text{III.1.4})$$

and $\langle \rangle_\xi$ is the average over the GWN. Note that in this interpretation, the elasticity of the DP is of pure entropic origin (paths of the BM are more numerous close to the diagonal), and the fact that it is short-range comes partly from the fact that the BM satisfies a local stochastic partial differential equation (SPDE). Using the Feynman-Kac formula it is possible to show that $Z_t(x)$ solves a SPDE. Let us now give a simple derivation of this SPDE. We compute $Z_{t+dt}(x)$ as given by (III.1.2) and separate in the expectation value the contribution of the last time step between t and $t + dt$:

$$\begin{aligned} Z_{t+dt}(x) &= Z_t(x) + \frac{\partial}{\partial t} Z_t(x)dt + o(dt) \\ &= \mathbb{E} \left(e^{-\frac{1}{T}\int_0^t dt' V(t', u(t')) - \frac{dt}{T} V(t, u(t))} \delta^{(N)}(u(t+dt) - x) \right) + o(dt) \\ &= \left(1 - \frac{dt}{T} V(t, x) \right) \mathbb{E} \left(e^{-\frac{1}{T}\int_0^t dt' V(t', u(t'))} \delta^{(N)}(u(t+dt) - x) \right) + o(dt). \end{aligned} \quad (\text{III.1.5})$$

Let us now discretize the last time step between t and $t + dt$ as

$$u(t+dt) = u(t) - \sqrt{Tdt}\xi \quad (\text{III.1.6})$$

with ξ a unit centered normal distribution. Hence we can write

$$\begin{aligned} Z_{t+dt}(x) &= \left(1 - \frac{dt}{T} V(t, x) \right) \mathbb{E} \left(e^{-\frac{1}{T}\int_0^t dt' V(t', u(t'))} \delta^{(N)}(u(t) - (x + \sqrt{Tdt}\xi)) \right) + o(dt) \\ &= \left(1 - \frac{dt}{T} V(t, x) \right) \frac{1}{(2\pi dt)^{\frac{N}{2}}} \int d^N \xi e^{-\frac{\xi^2}{2dt}} Z_t(x + \sqrt{T}\xi) + o(dt) \\ &= \left(1 - \frac{dt}{T} V(t, x) \right) \frac{1}{(2\pi)^{\frac{N}{2}}} \int d^N \xi e^{-\frac{\xi^2}{2}} \left(Z_t(x) + \sum_{i=1}^N \left(\sqrt{Tdt}\xi_i \frac{\partial}{\partial x_i} Z_t(x) + \frac{Tdt}{2} \xi_i^2 \frac{\partial^2}{\partial x_i^2} Z_t(x) \right) \right) + o(dt) \\ &= \left(1 - \frac{dt}{T} V(t, x) \right) \left(Z_t(x) + \frac{Tdt}{2} (\nabla_x)^2 Z_t(x) \right) + o(dt) \end{aligned}$$

²I thank Francis Comets for noticing a mistake in (III.1.2) in a preliminary version of this manuscript.

Hence, comparing the terms of order dt in the first and last line of the above calculation, we obtain,

$$\frac{\partial}{\partial t} Z_t(x) = \left(\frac{T}{2} (\nabla_x)^2 - \frac{1}{T} V(t, x) \right) Z_t(x), \quad (\text{III.1.7})$$

with the initial condition $Z_{t=0}(x) = \delta^{(N)}(x)$.

A subtlety

There is a non-trivial subtlety in the equivalence between (III.1.1), (III.1.2) and (III.1.7) on which we now comment. On one hand, looking at (III.1.7), for a centered potential, it seems that the mean value of $Z_t(x)$ is just the transition probability for a random walk on \mathbb{R}^N (since we are using Ito's convention). On the other hand, looking at (III.1.1) or (III.1.2) it seems that this mean value should contain a term involving $R_0(0)$. The equivalence between (III.1.2) and (III.1.7) is ensured if one takes as a definition of the exponential the so-called time/Wick ordered exponential as:

$$e^{-\frac{1}{T} \int_0^t V(t, u(t))} := \sum_{n=0}^{\infty} (-1/T)^n \int_{0 \leq t_1 < t_2 < \dots < t_n \leq t} V(t_1, u(t_1)) \dots V(t_n, u(t_n)). \quad (\text{III.1.8})$$

The difference with the ordinary exponential is obviously immaterial for non-random smooth potentials $V(t, x)$. For the case of a random potential with δ interaction in the t direction it however makes a big difference: here the ordering $t_i < t_{i+1}$ ensures the equivalence between (III.1.2) and (III.1.7), which was actually implicit in the derivation of (III.1.2)³. Finally, denoting now by $\check{Z}_t(x)$ the object defined by the path integral (III.1.1), the equivalence with $Z_t(x)$ defined by (III.1.2) (with the time-ordered exponential) or (III.1.7) (interpreted in the Ito sense) is

$$\begin{aligned} Z_t(x) &= \check{Z}_t(x) e^{-\frac{1}{2T^2} \int_0^t dt' R_0(0)} \\ \check{Z}_t(x) &= \int_{u(0)=0}^{u(t)=x} \mathcal{D}[u] e^{-\frac{1}{2T} \int_0^t dt' \left(\frac{du}{dt} \right)^2 - \frac{1}{T} \int_0^t dt' V(t', u(t'))}. \end{aligned} \quad (\text{III.1.9})$$

This subtlety will be particularly important to make sense of the path integral formula (III.1.1) in the important case where $V(t, u)$ is taken as a centered Gaussian white noise and $R_0(u - u') \sim \delta^{(N)}(u - u')$. From now on we will adopt this convention.

From the MSHE to the KPZ equation

In Sec. I.3.3 we already saw that taking the logarithm of the MSHE (III.1.7), assuming that $V(t, x)$ is smooth, one obtains that $h(t, x) = T \log(Z_t(x))$ satisfies the KPZ equation (I.3.15). This derivation, however, assumed a smooth random potential $V(t, x)$. In the same spirit as above, let us take into account the fact that the random potential is rough in the time direction and use Ito's lemma (see e.g. [104]) to compute the time

³To see this, consider for example the exponential of the integral of a GWN $Y(t) = e^{\int_0^t \xi(t') dt'}$. Using a similar derivation as above one obtains $\partial_t Y = \xi(t) Y(t)$ and thus Ito's convention imposes $\partial_t \overline{Y(t)} = 0$. This is true only if $Y(t)$ is interpreted as $Y(t) = \sum_n \int_{0 < t_1 < \dots < t_n < t} \xi(t_1) \dots \xi(t_n)$. Using the regular interpretation of the exponential one obtains $\overline{Y(t)} = e^{t/2}$.

derivative of $h(t, x) = T \log(Z_t(x))$. We obtain

$$\begin{aligned} \partial_t h(t, x) &= \frac{T}{Z_t(x)} \left(\left(\frac{T}{2} (\nabla_x)^2 - \frac{1}{T} V(t, x) \right) Z_t(x) \right) - \frac{1}{2Z_t(x)^2} R_0(0) (Z_t(x))^2 \\ &= \frac{1}{2} (\nabla_x h)^2 + \frac{T}{2} \nabla_x^2 h - V(t, x) - \frac{R_0(0)}{2}. \end{aligned} \quad (\text{III.1.10})$$

Hence we see that the Ito's lemma precisely makes the short-distance correlations of the disorder play a role again. Making a change of variables

$$\check{h}(t, x) = h(t, x) + \frac{R_0(0)t}{2}, \quad (\text{III.1.11})$$

$\check{h}(t, x)$ solves

$$\partial_t \check{h}(t, x) = \frac{1}{2} (\nabla_x \check{h})^2 + \frac{1}{2} \nabla_x^2 \check{h} - V(t, x). \quad (\text{III.1.12})$$

And note that $\check{h}(t, x) = T \log \check{Z}_t(x)$ where $\check{Z}_t(x)$ was defined through the path-integral formula (III.1.9). The KPZ equation usually refers to the equation (III.1.12) satisfied by \check{h} . In the following we will drop the different checkmarks, knowing that $h(t, x) = \log Z_t(x)$ is a (sometimes dangerous) shortcut. From now on we will also restrict ourselves to the case $N = 1$, i.e. the directed polymer in a two dimensional random environment, or the one-dimensional KPZ equation, hereafter referred to as the 1 + 1d case. Before we continue we remind the reader that we already commented in Sec. I.3.3 on the interpretation of the KPZ equation as a model of out-of-equilibrium growth.

The continuum DP and KPZ equation

The continuum directed polymer and KPZ equation generally refer to the case where $V(t, x) = -\xi(t, x)$ with ξ a Gaussian white noise (GWN) with correlations

$$\overline{\xi(t, x)\xi(t', x')} = 2\sigma\delta(t - t')\delta(x - x'). \quad (\text{III.1.13})$$

In this case, let us emphasize that the MSHE (III.1.7) and the KPZ equation (III.1.12) have a very different status. Focusing now on the case $N = 1$, while the MSHE, interpreted in the Ito sense, remains well defined, the KPZ equation a priori is not: we will see that $\log(Z_t(x))$ looks locally like a BM and thus taking the square of its derivative is ill advised. The $R_0(0)$ ($= +\infty$ in this case) wandering around in between (III.1.7) and (III.1.12) is a sign of this issue. This calls for a regularization technique and making sense of the 'solution of the KPZ equation' is a hard problem. In fact well before a precise sense was given to solving the KPZ equation [152] people believed that the right way to interpret the KPZ equation is through the Cole-Hopf transform, and thus $\log(Z_t(x))$ with $Z_t(x)$ the solution of the MSHE has long been thought of as the solution of the KPZ equation. Accordingly in this chapter when we mention the solution of the KPZ equation, we actually mean the Cole-Hopf solution.

Ignoring from now on these issues and taking $V(t, x) = -\xi(t, x)$ a GWN with correlations (III.1.13), let us first note that the change of variables,

$$\begin{aligned} t = a\tilde{t} \quad , \quad x = b\tilde{x} \quad , \quad a = \frac{T^{\frac{5}{3}}}{(2\sigma)^{\frac{2}{3}}} \quad , \quad b = (2\sigma/T)^{\frac{2}{3}} \quad , \\ \tilde{Z}_{\tilde{t}}(\tilde{x}) = Z_{t=a\tilde{t}}(x = b\tilde{x}) \quad , \quad \tilde{h}(\tilde{t}, \tilde{x}) = h(t = a\tilde{t}, x = b\tilde{x}) \quad , \end{aligned} \quad (\text{III.1.14})$$

make the equations (III.1.7) and (III.1.12) equivalent to (dropping the tildes)

$$\begin{aligned}\frac{\partial}{\partial t}Z_t(x) &= \frac{1}{2}(\nabla_x)^2Z_t(x) + \xi(t, x)Z_t(x), \\ \partial_t h(t, x) &= \frac{1}{2}(\nabla_x h(t, x))^2 + \frac{1}{2}(\nabla_x)^2h(t, x) + \xi(t, x).\end{aligned}\quad (\text{III.1.15})$$

where now $\xi(t, x)$ is a centered GWN with $\overline{\xi(t, x)\xi(t', x')} = \delta(t - t')\delta(x - x')$. Note that this simple calculation shows that there cannot be any phase transition in the large scale properties of the DP at a finite critical value of the temperature or of the noise strength: the system is always in the same phase. This was expected from the static phase diagram Fig. I.3 and we know that this phase corresponds to a strong disorder, zero temperature phase for the DP.

The Edwards-Wilkinson equation

Only at e.g. vanishing non-linearity can one obtain a different large scale behavior. The resulting equation in this case is known as the Edwards-Wilkinson equation. It reads

$$\partial_t h(t, x) = \frac{1}{2}(\nabla_x)^2h(t, x) + \xi(t, x).\quad (\text{III.1.16})$$

Note that in this case the growth favors neither direction. The critical exponents are easily extracted in this case by a simple scaling argument, leading to $z = 2$, $\alpha = 1/2$ and $\beta = 1/4$ (see Sec. I.3.3 for definitions). The full solution is easily obtained by going to Fourier space $x \rightarrow q$: each Fourier component performs an independent Ornstein-Uhlenbeck process with diffusivity $\sim q^2$ and

$$h(t, q) = h(0, q)e^{-\frac{1}{2}tq^2} + \int_0^t e^{-\frac{1}{2}q^2(t-t')}\xi(t', q).\quad (\text{III.1.17})$$

The problem is thus essentially solved and fluctuations at the Edwards-Wilkinson fixed point are Gaussian. The solution of the KPZ equation at non-zero linearity and the description of the associated FP will be much more difficult. Before we discuss some known properties of this FP, let us now present a few models in the KPZ universality class in 1 + 1d (KPZUC).

b Models of DP on the square lattice at finite temperature

The definition (III.1.2) of the partition sum of the continuum DP makes it transparent how to discretize the DP on any graph: given an underlying ‘free’ measure on directed paths π on the graph, one associates to each path a random energy $E(\pi)$ that is the sum of all energies encountered by the path along the way. In this thesis we will be interested in models of DP on the square lattice which is a natural discretization of the continuum DP problem in $d = 1 + 1$. We thus consider the square lattice \mathbb{Z}^2 , with Euclidean coordinates (x_1, x_2) . Directed paths on \mathbb{Z}^2 are up-right paths: they jump either to the right $(x_1, x_2) \rightarrow (x_1 + 1, x_2)$, or upward $(x_1, x_2) \rightarrow (x_1, x_2 + 1)$ (see Fig. III.1). Given a temperature T and an ensemble of random energies $\{\mathcal{E}_{x_1, x_2}, (x_1, x_2) \in \mathbb{Z}^2\}$ that are

drawn from a given PDF, the *point-to-point partition sum* of the DP with starting point $(0, 0)$ and endpoint $(x_1, x_2) \in \mathbb{N}^2$ is

$$Z_{x_1, x_2} := \sum_{\pi: (0,0) \rightarrow (x_1, x_2)} e^{-\frac{1}{T} \sum_{(x'_1, x'_2) \in \pi} \mathcal{E}_{x'_1, x'_2}}. \quad (\text{III.1.18})$$

Here $\sum_{\pi: (0,0) \rightarrow (x_1, x_2)}$ denotes the sum over all up-right paths on \mathbb{N}^2 from $(0, 0)$ to $(x_1, x_2) \in \mathbb{N}^2$. Introducing the random Boltzmann weights $W_{x_1, x_2} := e^{-\frac{1}{T} \mathcal{E}_{x_1, x_2}}$, (III.1.18) is equivalently rewritten as

$$Z_{x_1, x_2} := \sum_{\pi: (0,0) \rightarrow (x_1, x_2)} \prod_{(x'_1, x'_2) \in \pi} W_{x'_1, x'_2}. \quad (\text{III.1.19})$$

Alternatively we will use, in analogy with the continuum DP case, the coordinate t defined by

$$t = x_1 + x_2. \quad (\text{III.1.20})$$

The latter is thus the length of the DPs. When using t , the space coordinate will be taken either as

$$x = x_1, \quad \text{or} \quad \hat{x} = \frac{x_1 - x_2}{2}, \quad (\text{III.1.21})$$

as schematized in Fig. III.1. The factor $1/2$ in the definition of \hat{x} is to ensure that neighboring lattice sites at the same time coordinate t are distant from 1 in units of \hat{x} . The coordinate t is thus strictly increasing along a DP path, x is weakly increasing, while \hat{x} decreases or increases and is the coordinate that is the closest in spirit to the x coordinate of the continuum DP. Using these coordinates, directed paths π from $(0, 0)$ to (x_1, x_2) identify with functions $x(t) = \hat{x}(t) + \frac{t}{2}$ such that $x(0) = 0$, $x(x_1 + x_2) = x_1$ and $x(t+1) - x(t) \in \{0, 1\}$ (and similarly for $\hat{x}(t)$). Using these coordinates we will note the partition sum equivalently as

$$Z_t(x) = Z_{x_1=x, x_2=t-x_1}, \quad Z_t(\hat{x}) = Z_{x_1=(t+2\hat{x})/2, x_2=(t-2\hat{x})/2}. \quad (\text{III.1.22})$$

We will adopt a similar notation for any function on the lattice.

In each random environment and for $t \geq 0$, the partition sum of the DP can also be defined recursively as

$$\begin{aligned} Z_{t+1}(x) &= W_{t+1}(x) (Z_t(x) + Z_t(x-1)) \quad \text{with} \quad Z_{t=0}(x) = \delta_{x,0} \\ \iff Z_{t+1}(\hat{x}) &= W_{t+1}(\hat{x}) (Z_t(\hat{x} + 1/2) + Z_t(\hat{x} - 1/2)) \quad \text{with} \quad Z_{t=0}(\hat{x}) = \delta_{\hat{x},0} \end{aligned} \quad (\text{III.1.23})$$

Note that (III.1.23) appears as a discrete analogue of the MSHE (III.1.15) (this will be made more precise in Sec. III.1.3). The KPZ universality hypothesis then basically states that, for sufficiently nice disorder (such that all the moments of the random energy are finite, $(\overline{\mathcal{E}_{x_1, x_2}})^n < \infty$, and the disorder has short-range correlations), the large scale properties of $\log Z_t(\hat{x})$ are similar to those of $h(t, x)$ in the KPZ equation (this will be made more precise in Sec. III.1.3). In this thesis we will often look at the

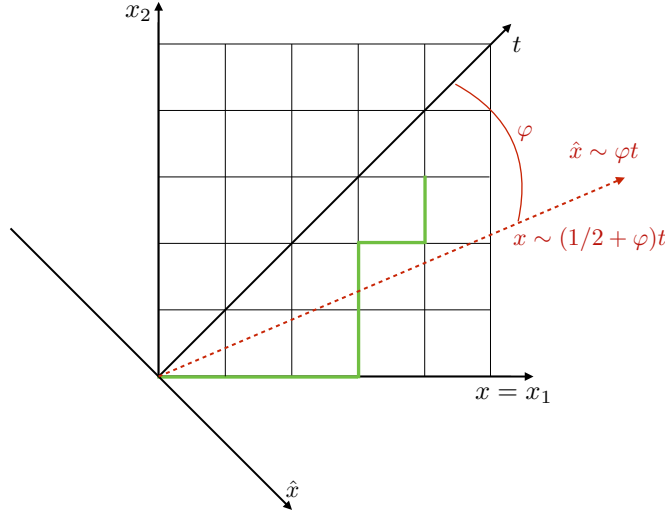


Figure III.1: Different coordinate systems for directed polymers on the square lattice. Green: an admissible directed path, i.e. up-right path, from $(0, 0)$ to $(x_1, x_2) = (4, 3)$ i.e. $(t, x) = (7, 4)$ i.e. $(t, \hat{x}) = (7, 1/2)$. Red, convention used for the asymptotic analysis of polymers of large length $t \gg 1$ in a given direction φ .

large scale properties in an arbitrary direction φ , referring to $t \gg 1$ with the ballistic scaling

$$x \sim (1/2 + \varphi)t \iff \hat{x} \sim \varphi t, \quad (\text{III.1.24})$$

i.e. the ‘angle’ φ is measured with respect to the diagonal of the square lattice see Fig. III.1.

We should stress here that for most models in the KPZUC, there is often one observable whose large scale properties is similar to the height in the KPZ equation, but that does not mean that the properties of any observable of any model in the KPZUC are related to some observable in the KPZ equation. More generally interesting observables in one language may not necessarily be relevant in the other and vice-versa. In particular in the DP framework, the ‘KPZ-height’ like variable is the free-energy of the DP. The latter is certainly interesting, but does not contain all DP properties. Before being a model in the KPZUC, the DP is the statistical mechanics of directed paths in a random environment, and Z_{x_1, x_2} is the normalization factor that allows to define the *quenched measure on paths as*, for all paths from $(0, 0)$ to $(x_1, x_2) \in \mathbb{N}^2$,

$$Q_{x_1, x_2}(\pi) := \frac{e^{-\frac{1}{T} \sum_{(x'_1, x'_2) \in \pi} \mathcal{E}_{x'_1, x'_2}}}{Z_{x_1, x_2}}. \quad (\text{III.1.25})$$

The latter is a deformed version of the underlying free measure on directed paths that favors the energy, it is a probability measure on paths from $(0, 0)$ to (x_1, x_2) and it is itself a random (disorder dependent) object. The *annealed measure* is the average over disorder of the quenched measure:

$$P_{x_1, x_2}(\pi) := \overline{Q_{x_1, x_2}(\pi)}. \quad (\text{III.1.26})$$

With these definitions, for a given observable on paths $O(\pi)$, one is interested in the quenched and annealed averages as

$$\langle O(\pi) \rangle_Q := \sum_{\pi} O(\pi) Q_{x_1, x_2}(\pi) \quad , \quad \overline{\langle O(\pi) \rangle_Q} := \sum_{\pi} O(\pi) P_{x_1, x_2}(\pi) . \quad (\text{III.1.27})$$

In the DP framework, understanding the properties of the quenched and annealed measure are the most challenging questions. Some of these properties are indeed contained in KPZ universality: taking (x_1, x_2) along the diagonal $(x_1, x_2) = (T/2, T/2)$ with $T \rightarrow \infty$, parametrizing paths by functions $\hat{x}(t)$, one expects that (i) with probability 1 at large T the support of the quenched measure Q is on paths scaling like $\hat{x}(t) \sim T^{\zeta} \tilde{\hat{x}}(t/T)$ with ζ the roughness exponent of the DP related to the dynamic exponent of KPZ as $\zeta = 1/z = 2/3$ (see Sec. I.3.3); (ii) a similar (less strong) statement for the annealed measure P . More subtle properties like the shape of the rescaled path $\tilde{\hat{x}}(t)$ or its localization properties are not trivially related to observables in the growing interface language. In the DP framework, localization refers to the fact that, even in the limit of infinite polymer $T \rightarrow \infty$, with probability 1 (i.e. for almost any drawing of the random environment), there exists a point at time $t = T/2$ which is visited by the polymer with a non-zero probability. This should be compared to a standard random walk where the point visited with maximum probability is on the diagonal and the probability is of order $1/\sqrt{T}$ in $d = 1 + 1$. A stronger statement of localization of the full path in the DP case is the fact that there are paths for which the quenched measure $Q_{T/2, T/2}(\pi)$ remains non-zero in the limit $T \rightarrow \infty$. This is consistent with the idea of Chapter I and Chapter II that temperature is (although dangerously [96]) irrelevant at large scales.

Let us finally mention that such models of DPs on the square lattice and in higher dimensions have received a considerable amount of attention from the mathematical community, independently of any exact solvability properties and using purely probabilistic approaches, starting with the work of Imbrie and Spencer [153] and Bolthausen [154]. Rigorous results in particular confirm the static phase diagram of Fig. I.3. We refer the reader to [155] for a review, in particular for the mathematical definition of the strong disorder regime in terms of martingales or localization properties of the path [156].

c Models of DPs on the square lattice at zero temperature

As temperature is irrelevant at the strong disorder FP of the DP, it is natural that models of DPs at zero temperature are also in the KPZ universality class. A model of DP at zero temperature can be obtained as the limit of the model previously considered as

$$\mathbf{E}_{x_1, x_2} := \lim_{T \rightarrow \infty} -T \log Z_{x_1, x_2} = \min_{\pi: (0,0) \rightarrow (x_1, x_2)} \sum_{(x'_1, x'_2) \in \pi} \mathcal{E}_{x'_1, x'_2} . \quad (\text{III.1.28})$$

\mathbf{E}_{x_1, x_2} is thus the energy of the optimal path from $(0, 0)$ to (x_1, x_2) . KPZ universality says here that the large scale properties of \mathbf{E}_{x_1, x_2} should be the same as those of the height in the growing interface language. At a given time the profile $\mathbf{E}_t(x)$ is interpreted

as an interface. For $t \geq 0$, it evolves according to

$$\mathbf{E}_{t+1}(\hat{x}) = \mathcal{E}_t(\hat{x}) + \min(\mathbf{E}_t(\hat{x} - 1/2), \mathbf{E}_t(\hat{x} + 1/2)) , \quad (\text{III.1.29})$$

with the initial condition $\mathbf{E}_{t=0}(0) = 0$ and $\mathbf{E}_{t=0}(\hat{x}) = -\infty$ for $\hat{x} \neq 0$. Let us denote here for future use

$$h^{(1)}(t, \hat{x}) = -\mathbf{E}_t(\hat{x}) , \quad (\text{III.1.30})$$

the ‘growing interface’ defined in this way. Two particular subclasses of zero temperature DP models have been much studied, each having links with interesting other models.

The first is the case where the random energies are bounded from below, say by 0. In this case the DP model is usually referred to as a *directed first passage percolation problem* (FPP). The random energies \mathcal{E}_{x_1, x_2} are interpreted as waiting times $\mathbf{t}_{x_1, x_2} := \mathcal{E}_{x_1, x_2}$ and the optimal energy \mathbf{E}_{x_1, x_2} as a first passage time \mathbb{T}_{x_1, x_2} . This type of model was originally introduced in [157] to describe the invasion of a fluid into a porous medium. These models can provide examples of the fact that KPZ universality should always be applied with caution: if the \mathbf{t}_{x_1, x_2} can be zero with a finite probability p , there can be a region of space where the first passage time converges to 0 in the large time limit with probability 1. This precisely occurs if p is large enough and that a percolation threshold is reached. Of course in this case the fluctuations of T_{x_1, x_2} do not scale with the KPZ exponent $t^{1/3}$. We will see an example of such a model in Sec. III.3.5.

The second subclass is the case where the random energies are bounded from above, say by 0. In this case the DP model is usually referred to as a *directed last passage percolation problem* (LPP). The random energies \mathcal{E}_{x_1, x_2} are interpreted as the opposite of waiting times $\mathbf{t}_{x_1, x_2} := -\mathcal{E}_{x_1, x_2}$ and the optimal energy \mathbf{E}_{x_1, x_2} as the opposite of the last passage time $\mathbb{T}_{x_1, x_2} := -\mathbf{E}_{x_1, x_2} = \max_{\pi: (0,0) \rightarrow (x_1, x_2)} \sum_{(x'_1, x'_2) \in \pi} \mathbf{t}_{x'_1, x'_2}$. See [158] for a review. In this case it is usual to define a growing interface different from the one mentioned previously by looking at the boundary of the set $B(t) := \{(x_1, x_2) \in \mathbb{N}^2, \mathbb{T}_{x_1, x_2} \leq t\}$ see Fig. III.2. This growing interface fall in the more general class of so-called corner growth models as we will show in the next section. Note that the recursion equation for the last passage time reads

$$T_{x_1+1, x_2+1} = \mathbf{t}_{x_1+1, x_2+1} + \max(T_{x_1+1, x_2}, T_{x_1, x_2+1}) . \quad (\text{III.1.31})$$

And the growing interface thus necessarily has the shape shown in Fig. III.2: the boundary is a *down-right* path $(x_1(i), x_2(i))_{i=0, \dots, N}$ on \mathbb{N}^2 : its starting point on the vertical edge is $(x_1(0), x_2(0)) = (x_1^{\max}, 0)$, with $x_1^{\max} = \max_{x_1 \in \mathbb{N} | T_{x_1, 0} \leq t} x_1$. Switching to the t, \hat{x} coordinate, the growing interface is thus defined now as

$$h^{(2)}(t, \hat{x}) := \max\{t' | T_{t'}(\hat{x}) \leq t\} . \quad (\text{III.1.32})$$

The fluctuations of this growing interface are believed to be in the KPZUC for sufficiently nice distributions of weights [158]. We will see in the next section that growth models defined in this way fall in a class of models known as corner growth models, and

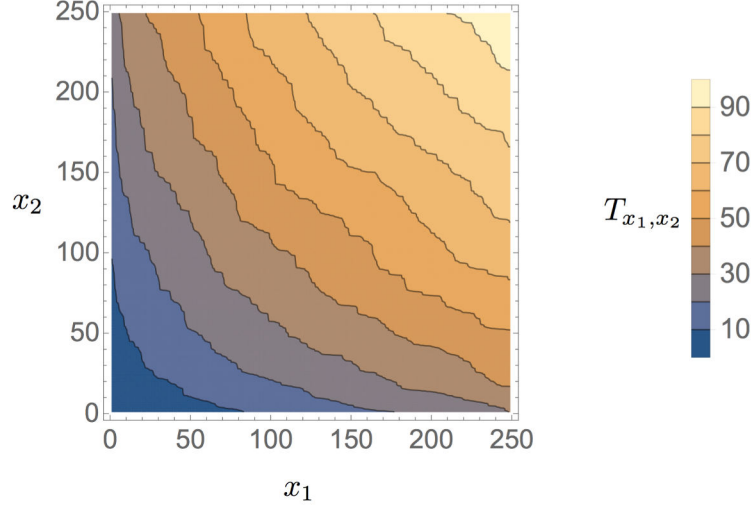


Figure III.2: Starting from a model of last passage percolation, a growing interface is defined as the level lines of T_{x_1, x_2} . The interface evolves according to a corner growth model type dynamics. Figure obtained using a simulation of LPP on a square lattice of 256×256 sites and using exponentially distributed waiting times with rate 10.

it is actually for a model of LPP with geometric or exponentially distributed weights that the emergence of Tracy-Widom type fluctuations in the DP context was first shown in [159]. Note that the two growing interfaces $h^{(1)}$ and $h^{(2)}$ are $\forall \hat{x}$ the inverse of one another: $\forall(t, \hat{x}), h^{(1)}(h^{(2)}(t, \hat{x}), \hat{x}) = t$, and

$$\begin{aligned} \text{Prob}(h^{(1)}(t, \hat{x}) \leq H) &= \text{Prob}(T_t(\hat{x}) \leq H) \\ \text{Prob}(h^{(2)}(t, \hat{x}) \leq H) &= \text{Prob}(T_H(\hat{x}) \geq t). \end{aligned} \quad (\text{III.1.33})$$

Their large scale fluctuations are thus linked. Assuming that, for \hat{x} fixed, $h^{(1)}(t, \hat{x}) \sim c_1 t + \lambda_1 t^{1/3} X$ with X a $O(1)$ RV and $c_1 \geq 0$, then $\lim_{t \rightarrow \infty} \text{Prob}(h^{(1)}(t, \hat{x}) \leq c_1 t + \lambda_1 t^{1/3} z) = F(z)$ with $F(z)$ the CDF of X . We thus must have

$$\begin{aligned} F(z) &= \lim_{t \rightarrow \infty} \text{Prob}(T_t(\hat{x}) \leq c_1 t + \lambda_1 t^{1/3} z) \\ &= 1 - \lim_{t' \rightarrow \infty} \text{Prob}(T_{\frac{t'}{c_1} - \frac{\lambda_1}{c_1^{1/3}} (t')^{1/3} z}(\hat{x}) \geq t') \\ &= 1 - \lim_{t' \rightarrow \infty} \text{Prob}(h^{(2)}(t', \hat{x}) \leq \frac{t'}{c_1} - \frac{\lambda_1}{c_1^{1/3}} (t')^{1/3} z) \end{aligned} \quad (\text{III.1.34})$$

Hence $h^{(2)}(t, \hat{x}) \sim c_2 t - \lambda_2 t^{1/3} X'$ with $c_2 = 1/c_1$, $\lambda_2 = \frac{\lambda_1}{c_1^{1/3}}$ and the CDF of X' is $\text{Prob}(X' \leq z) = 1 - F(z)$.

d Interacting particle systems

The simple exclusion process and the corner growth model

‘Some’ interacting particle systems on \mathbb{Z} are in the KPZ universality class. To make the discussion clearer we consider the simple exclusion process (SEP) with exponential waiting times (see Fig. III.3). Particles are labeled by $i \in \mathbb{N}$ or \mathbb{Z} depending on the setting and their position is denoted $x_i(t)$. Each particle carries two exponential clocks and attempt jumps to the right with rate p and jumps to the left with rate q . Jumps are suppressed if the target site is already occupied. Let us introduce the ‘spin’ variable $\hat{\eta}(t, y)$, which is taken as $+1$ if y is occupied by a particle at time t and -1 if it is empty. Denoting $N(t)$ the number of particles that jumped from 0 to 1 up to time t , a growing interface is defined as (see e.g. [34])

$$\begin{aligned} h(0, t) &= N(t) \\ h(x > 0, t) &:= N(t) - \sum_{y=1}^x \hat{\eta}(t, y) \\ h(x < 0, t) &:= N(t) + \sum_{y=x}^{-1} \hat{\eta}(t, y) . \end{aligned} \quad (\text{III.1.35})$$

Which basically consists in saying that $-\hat{\eta}(t, y)$ is, at each time, the discrete derivative of the height field: $-\hat{\eta}(t, y) = h(t, x) - h(t, x - 1)$. From this point of view the spin variables in the exclusion process are related to a discretization of the noisy Burgers equation and $\eta(t, y)$ is the velocity of the fluids particles (see Sec. III.2.2 for the continuum Burgers equation). Note that the velocity field is conserved locally: $\sum_{y=a}^b \hat{\eta}(t, y)$ only evolves when events at the boundaries a, b occur. From the exclusion rule and the fact that particle jumps are local, the interface evolves only at points where its slope changes: a local valley is transformed into a local hill with rate p and a local hill is transformed into a local valley with rate q . It is clear that the interface grows upward if $p > q$ and downward if $p < q$. For this reason the case $p = q$ (symmetric simple exclusion process) is very special and the associated field does not display fluctuations in the KPZUC, but rather in the Edwards-Wilkinson universality class. All other cases $p \neq q$ (asymmetric simple exclusion process, ASEP) are expected to be in the KPZUC. Let us now draw the connection with last passage percolation previously defined by considering the case of the totally-asymmetric exclusion process (TASEP), i.e. the SEP with $q = 0$ and $p \neq 0$ (see e.g. [160]).

From the TASEP to LPP

To do so we will consider the so-called *step initial condition*: particles are labelled by $i \in \mathbb{N}$ and at $t = 0$ we take

$$x_i(t = 0) = -i . \quad (\text{III.1.36})$$

And let us denote by $T(i, j)$ the time where the particle i makes her $(j + 1)^{\text{th}}$ jump. The height at the origin $N(t)$ defined in (III.1.35) is thus equal to

$$N(t) = i_{\max}(t) + 1 \quad i_{\max}(t) := \max_{i \in \mathbb{N}} \{i, T(i, i) \leq t\} . \quad (\text{III.1.37})$$

On the other hand we have that, for $(i, j) \in \mathbb{N}^2$

$$\begin{aligned} T(0, j + 1) &= T(0, j) + \mathbf{t}_{0, j+1} , \\ T(i + 1, 0) &= T(i, 0) + \mathbf{t}_{i+1, 0} , \\ T(i + 1, j + 1) &= \mathbf{t}_{i+1, j+1} + \max(T(i + 1, j), T(i, j + 1)) . \end{aligned} \quad (\text{III.1.38})$$

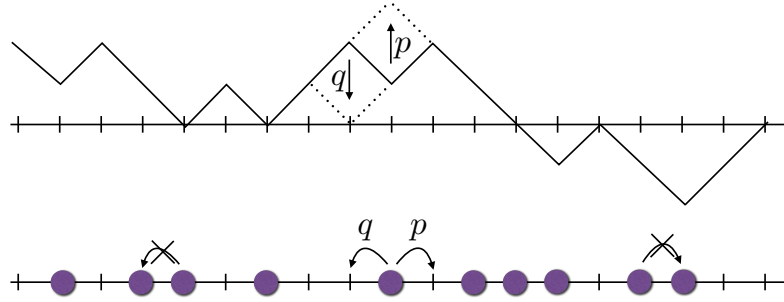


Figure III.3: Illustration of the mapping between the ASEP and the corner growth model, that is also related in the totally asymmetric case $q = 0$ to LPP.

Here the $t_{i,j}$ are independent, exponentially distributed RVs with parameter q . Indeed the first line corresponds to saying that the time it takes for the 0^{th} particle to make her $(j + 2)^{th}$ jump is just the time it takes her to make her $(j + 1)^{th}$ jump + an exponentially distributed RV. The second line corresponds to saying that the time it takes for the $(i + 1)^{th}$ particle to make her first jump is just the time it takes to the i^{th} particle to make her first jump + an exponentially distributed RV. Finally the last line corresponds to saying that, before she makes her $(j + 2)^{th}$ jump, the $(i + 1)^{th}$ particle has to wait that the i^{th} particle makes her $(j + 2)^{th}$ jump (so that the arrival site is empty) and that she first has to do her $(j + 1)^{th}$ jump and finally wait for an exponentially distributed amount of time. Note that all this is true with the updating rules that were given because an exponential clock is memoryless. This will be more generally true for arbitrary waiting time distributions if the clock is started each time it is possible to make a jump. We have thus shown here that the waiting times of the TASEP (III.1.38) corresponds to the last passage time in a directed last passage percolation problem. The height in the corner growth model (III.1.35) is exactly the height $h^{(2)}$ defined in the LPP context. The TASEP with exponentially distributed waiting times with step initial condition thus provides an example where it is possible to switch between the interacting particle language, the language of directed polymer at zero temperature and the growing interface language.

III.1.2 The KPZ fixed point - strong universality

There is various degrees of precision which can be achieved when describing the so-called KPZ fixed point and we refer the reader to [161] for the most complete description. Once the identification of a ‘growing interface’ $h(t, x)$ in a model has been made, the KPZUC hypothesis is that the appropriately rescaled large time fluctuations of the interface are completely universal. More precisely, starting from a given initial condition, one first has to subtract the deterministic (angle-dependent) growth rate of the interface

$$v_\infty(\varphi) := \lim_{t \rightarrow \infty} \frac{h(t, \varphi t)}{t}, \quad (\text{III.1.39})$$

which is generally expected to be well-defined and non random (i.e. the above convergence holds with probability 1). One then defines

$$\underline{h}(t, x) := h(t, x) - tv_\infty(x/t). \quad (\text{III.1.40})$$

And the rescaled process that involves the roughness exponent $\alpha = 1/2$ and dynamic exponent $z = 3/2$.

$$h(\mathbf{t}, \mathbf{x}) := \lim_{b \rightarrow \infty} b^{-\alpha} \underline{h}(t = b^z \mathbf{t}, x = b\mathbf{x}). \quad (\text{III.1.41})$$

Then,

(i) The universality of critical exponents amounts to saying that $h(\mathbf{t}, \mathbf{x})$ is a well defined, non trivial stochastic process.

(ii) The stronger universality property is that, up to three non-universal constants associated with the measure of time, space, and height C_t , C_x and C_h , the random process $h(\mathbf{t}, \mathbf{x})$ is model independent. i.e. $\tilde{h}(\mathbf{t}, \mathbf{x}) := h(\mathbf{t}/C_t, \mathbf{x}/C_x)/C_h$ is fully universal and depends only on the initial condition. Furthermore there are only a few attractive subclasses of initial conditions (in the sense that the large-time statistics for an arbitrary initial condition will fall into one of these subclasses). The classification of these subclasses is not complete and does not rely on rigorous results but the three main classes that are commonly considered are the so called droplet initial condition, the flat initial condition and the stationary initial condition (see below). For each of these classes the limiting process at a fixed time $\tilde{h}(\mathbf{t}, \mathbf{x})$ is known:

1. The droplet case: in the interface language, it corresponds to an initial condition such that the interface stays curved for all time (i.e. the mean profile $v_\infty(\varphi)$ is not flat). For the KPZ equation itself, the appropriate initial condition is often taken as $h(t = 0, x) := -\lim_{w \rightarrow \infty} w|x|$. In the DP case the latter is clearer and corresponds to directed polymers with fixed starting point $Z_{t=0}(x) = \delta(x)$, and $Z_t(x)$ is the *point to point* partition sum. For the corner growth model it corresponds to ASEP with a step initial condition. In this case, for a given time \mathbf{t} and point \mathbf{x} , the one point distribution of $h(\mathbf{t}, \mathbf{x})$ is the GUE Tracy-Widom (TW) distribution (introduced in [37]). Moreover at a fixed time \mathbf{t} , as a function of \mathbf{x} , $\tilde{h}(\mathbf{t}, \mathbf{x})$ is a process known as the Airy2 process $\mathcal{A}_2(\mathbf{x})$ (introduced in [162]). It is a process that is stationary in \mathbf{x} , that satisfies $\overline{\mathcal{A}_2(\mathbf{x})\mathcal{A}_2(0)^c} \rightarrow_{\mathbf{x} \rightarrow \infty} 0$, whose one point distribution is the GUE-TW distribution and which locally looks like a Brownian motion, $\overline{(\mathcal{A}_2(\mathbf{x}) - \mathcal{A}_2(0))^2} \sim_{\mathbf{x} \rightarrow 0} |\mathbf{x}|$.
2. The flat case: in the interface language, it corresponds to a flat initial condition $h(t = 0, x) = cst$. In this case $v_\infty(\varphi) = cst'$. In the DP framework this corresponds to a directed polymer with the starting point free to move on a line $Z_{t=0}(x) = 1$, and $Z_t(x)$ is the *point to line* partition sum. For the corner growth model it corresponds to ASEP with particles only on even sites. In this case, for a given time \mathbf{t} and point \mathbf{x} , the one point distribution of $h(\mathbf{t}, \mathbf{x})$ is the GOE Tracy-Widom (TW) distribution (introduced in [38]). Moreover at a fixed time \mathbf{t} , as a function of \mathbf{x} , $\tilde{h}(\mathbf{t}, \mathbf{x})$ is a process known as the Airy 1 process $\mathcal{A}_1(\mathbf{x})$ (introduced in [163]). It has properties similar to the Airy 2 process: stationarity in \mathbf{x} , $\overline{\mathcal{A}_1(\mathbf{x})\mathcal{A}_1(0)^c} \rightarrow_{\mathbf{x} \rightarrow \infty} 0$, and it locally looks like a Brownian motion.

3. The stationary initial condition is a random initial condition that ensures a stationarity property in the model dynamics. Examples and the nature of this stationarity property will be discussed in Sec. III.2.2. In this case at large time as a function of x , $h(t, x)$ is given by $\tilde{h}(t, x) = X_{BR} + B(x)$ where X_{BR} is a RV distributed according to the Baik-Rains distribution (introduced in [39]) and $B(x)$ is a two-sided Brownian motion. X_{BR} and $B(x)$ have non-trivial correlations.

Many other things are known about these limiting spatial processes, including for example other initial ‘crossover initial conditions’ (half flat, Brownian-flat, half Brownian), see [164]. In contrast to this accurate description of spatial correlations at large time, much less is known about two-time correlations. In an abstract setting these are related to the notion of ‘Airy sheet’ [161], but explicit formulae are rare (see however [165, 166, 167, 168]). Finally we should mention here the related question of growth from a given initial condition in a restricted geometry, for example directed polymers in a half-space, which, when both starting points are taken ‘close to the wall’, exhibit large scale fluctuations of free energy scaling as $t^{1/3}$ and governed by the GSE Tracy-Widom distribution [38], see [169] for DP in the continuum.

The belief in these remarkable properties of the KPZUC comes from exact solutions of peculiar models. At the level of one point distribution for the droplet case the emergence of the TW-GUE distribution was first shown in the LPP model with geometric weights in [159] (a similar result was shown just before in the related context of the longest increasing subsequence of a random permutation in [170]). The corresponding result for the KPZ equation itself is more recent [171, 172, 173, 165] (thus the fact that the KPZ equation is in its own universality class is a recent result). Extension to multi-points were first shown for the PNG model [162, 174], and later for the KPZ equation in [175]. For the flat case, one-point formulae were again first shown in discrete models [176] then for the KPZ equation [177, 178, 179, 180], while multi-point correlations were only studied in a discrete setting [163]. A similar story goes for the stationary case [181, 182, 183, 184, 185]. We should here that the works cited here are not all at the same level of rigor and many other works could be cited. We will review later the appropriate references for the scope of this chapter, namely discrete models of directed polymers, and refer to [34] for other references.

III.1.3 Universality of the KPZ equation: notion of weak universality and universal scaling limits of DP on the square lattice

The limiting spatial process (III.1.41) does not obey the KPZ equation: the KPZ equation is not the KPZ fixed point. Under a general rescaling, if $h(t, x)$ solves the KPZ equation (III.1.15), $\tilde{h}(\tilde{t}, \tilde{x}) := b^{-\alpha}h(t = b\tilde{t}, x = b^z\tilde{x})$ solves (dropping the tildes)

$$\partial_t h(t, x) = \frac{b^{\alpha+z-2}}{2} c_1 (\nabla_x h(t, x))^2 + \frac{b^{z-2}}{2} (\nabla_x)^2 c_2 h(t, x) + b^{(z-2\alpha-1)/2} c_3 \xi(t, x), \quad (\text{III.1.42})$$

where we have reintroduced explicit constants in front of each term on the right hand side. There is no way to fix z and α to get a scale invariant equation. The values $\alpha = 1/2$ and $z = 3/2$ of the KPZUC, a property of the KPZ FP, are not trivially

obtained through scaling.

In all the models in the KPZUC, however, the KPZ equation/the continuum DP plays a peculiar role that is linked with the notion of weak universality [186]. The latter refers to two limits:

(i) The weak asymmetry limit. Symmetric growth models ($c_1 = 0$) are in the Edwards-Wilkinson universality class and are characterized by exponents $\alpha = 1/2$ and $z = 2$. If an asymmetry is present $c_1 \neq 0$, the large scale properties are those of the KPZ FP. Note that rescaling (III.1.42) with $\alpha = 1/2$, $z = 2$ and $c_1 \sim b^{-1/2}$ leaves the KPZ equation itself invariant. More generally it is conjectured that (under the usual assumptions such as locality, etc...) the KPZ equation itself is the universal scaling limit of weakly asymmetric growth models in $1 + 1$ d when rescaling space $x \sim b$, $t \sim b^2$ and the asymmetry as $b^{-1/2}$. For this reason the KPZ equation is sometimes referred to as implementing the universal crossover between the EW FP and the KPZ FP. An important example of this weak-universality property is provided by the work of Bertini and Giacomin [187] that states that, upon scaling space as $x \sim b$, $t \sim b^2$ and the asymmetry $p - q$ as $b^{-1/2}$ in the corner growth model previously defined, the corner growth model height profile converges to the Cole-Hopf solution of the KPZ equation.

(ii) On the other hand the weak noise limit is linked with the DP in a disordered medium. At zero disorder, $c_3 = 0$, DPs are equivalent to random walks, are diffusive $z = 2$ and have no disorder fluctuations $\alpha = 0$. For $c_3 \neq 0$, the large scale properties of DPs are described by the KPZ FP. Noting that the rescaling (III.1.42) with $\alpha = 0$, $z = 2$ and $c_3 \sim b^{-1/2}$ leaves the KPZ equation invariant, it is conjectured that the KPZ/MSHE is the universal scaling limit of weakly disordered DPs. This scaling has also been called the intermediate disorder regime in the literature [188]. Let us illustrate it heuristically on the case of DPs on the square lattice, using the notations of Sec. III.1.1. We start with the discrete version of the MSHE in the variables t, \hat{x} given in (III.1.23) which we recall here

$$Z_{t+1}(\hat{x}) = e^{-\frac{1}{T}\mathcal{E}_{t+1}(\hat{x})} (Z_t(\hat{x} + 1/2) + Z_t(\hat{x} - 1/2)) . \quad (\text{III.1.43})$$

We thus scale

$$t = b^2 D \tilde{t} \quad , \quad \hat{x} = b \tilde{x} \quad , \quad \mathcal{E}_{t+1}(\hat{x}) = 1/\sqrt{b} V(t, \hat{x}) \quad , \quad (\text{III.1.44})$$

with V a centered $O(1)$ RV, take b very large, $b \gg 1$, and consider the limiting partition sum

$$\tilde{Z}_{\tilde{t}}(\tilde{x}) := \lim_{b \rightarrow \infty} A^{b^2 D \tilde{t}} Z_{t=b^2 D \tilde{t}}(\hat{x} = b \tilde{x}) , \quad (\text{III.1.45})$$

with A left undetermined for now. We thus obtain from III.1.43

$$\frac{1}{A} \left(\tilde{Z}_{\tilde{t}}(\tilde{x}) + \frac{1}{b^2 D} \partial_{\tilde{t}} \tilde{Z}_{\tilde{t}}(\tilde{x}) \right) = \left(1 - \frac{1}{\sqrt{b} T} V(t, \hat{x}) \right) \left(2 \tilde{Z}_{\tilde{t}}(\tilde{x}) + \frac{1}{4b^2} (\partial_{\tilde{x}})^2 \tilde{Z}_{\tilde{t}}(\tilde{x}) \right) . \quad (\text{III.1.46})$$

This suggests to take $A = 1/2$ and we obtain

$$\partial_{\tilde{t}} \tilde{Z}_{\tilde{t}}(\tilde{x}) = \frac{D}{8} (\partial_{\tilde{x}})^2 \tilde{Z}_{\tilde{t}}(\tilde{x}) + \frac{D}{T} b^{3/2} V(b^2 D \tilde{t}, b \tilde{x}) \tilde{Z}_{\tilde{t}}(\tilde{x}). \quad (\text{III.1.47})$$

In the limit $b \rightarrow 0$, $D b^{3/2} V(b^2 D \tilde{t}, b \tilde{x})$ converges to a GWN. To see this explicitly, consider for example a random potential which is uncorrelated from site to site with cumulant $\overline{(V(t, x))^n} = c_n$ and the cumulant generating function

$$\begin{aligned} G[\lambda] &:= \overline{e^{\int_{\tilde{x}=0}^1 \int_{\tilde{t}=0}^1 D b^{3/2} V(b^2 D \tilde{t}, b \tilde{x}) \lambda(\tilde{t}, \tilde{x})}} \\ &= e^{\overline{D b^{3/2} \frac{1}{b^3 D} \sum_{\tilde{x}=0}^b \sum_{\tilde{t}=0}^{b^2 D} V(b^2 D \tilde{t}, b \tilde{x}) \lambda(t/(D b^2), x/b)}} \\ &= e^{\frac{c_2}{2 b^3} \sum_{\tilde{x}=0}^b \sum_{\tilde{t}=0}^{b^2 D} \lambda^2(t/(D b^2), x/b) + \frac{c_3}{3! b^{9/2}} \sum_{\tilde{x}=0}^b \sum_{\tilde{t}=0}^{b^2 D} \lambda^3(t/(D b^2), x/b) + \dots} \\ &= e^{\frac{c_2 D}{2} \int_{\tilde{x}=0}^1 \int_{\tilde{t}=0}^1 \lambda^2(\tilde{t}, \tilde{x}) + \frac{c_3}{3! b^{3/2}} \int_{\tilde{t}=0}^1 \lambda^3(\tilde{t}, \tilde{x}) + \dots} \\ &=_{b \rightarrow \infty} e^{\frac{c_2 D}{2} \int_{\tilde{x}=0}^1 \int_{\tilde{t}=0}^1 \lambda^2(\tilde{t}, \tilde{x})}. \end{aligned} \quad (\text{III.1.48})$$

Hence in the limit $b \rightarrow \infty$ the cumulant generating function G is equal to

$$G[\lambda] = e^{\overline{\int_{\tilde{x}=0}^1 \int_{\tilde{t}=0}^1 \sqrt{c_2 D} \xi(\tilde{t}, \tilde{x}) \lambda(\tilde{t}, \tilde{x})}}, \quad (\text{III.1.49})$$

where $\xi(\tilde{t}, \tilde{x})$ is a unit GWN with correlations $\overline{\xi(\tilde{t}, \tilde{x}) \xi(\tilde{t}', \tilde{x}')} = \delta(\tilde{t}' - \tilde{t}) \delta(\tilde{x}' - \tilde{x})$. Hence the rescaled partition sum (III.1.45) with $A = 1/2$ converges, as $b \rightarrow \infty$, to the rescaled solution of the MSHE

$$\partial_{\tilde{t}} \tilde{Z}_{\tilde{t}}(\tilde{x}) = \frac{D}{8} (\partial_{\tilde{x}})^2 \tilde{Z}_{\tilde{t}}(\tilde{x}) + \sqrt{2c} \xi(\tilde{t}, \tilde{x}) \tilde{Z}_{\tilde{t}}(\tilde{x}), \quad (\text{III.1.50})$$

with $c = D \overline{V^2} / (2T^2)$. This establishes that the MSHE is the universal scaling limit of DPs on the square lattice with weak disorder under diffusive scaling. We refer the reader to [188] for a rigorous approach. Note that the weak disorder regime is equivalent to the regime of high temperature $T \sim \sqrt{b}$ at fixed disorder. In this phrasing, the continuum DP is the universal high temperature limit of DPs, see in particular [173, 189] for a discussion of this property and an extension to disorder with non-zero correlation length.

Before we close this chapter let us mention here that there exists another universal scaling limit of DPs on the square lattice that has played an important role in recent developments. Taking \mathbb{T} and N finite, it is obtained by taking $x_1 = b\mathbb{T}$, $x_2 = N$ and $\mathcal{E}_{x_1, x_2} \sim 1/\sqrt{b} \tilde{\mathcal{E}}_{x_1, x_2}$ and taking $b \rightarrow \infty$ with N and the distribution of $\tilde{\mathcal{E}}_{x_1, x_2}$ fixed so that the $\tilde{\mathcal{E}}_{x_1, x_2}$ are independent $O(1)$ centered random variables with at least a well defined second moment. This is the limit of long directed polymers on the square lattice conditioned to stay close to the horizontal axes. The polymer makes an infinite number ($\sim b$) of horizontal jumps, and a finite number (N) of vertical jumps. In this case the possible polymer paths can be indexed by $(s_1, s_2, \dots, s_N) \in [0, \mathbb{T}]^N$ where $x_1 = b s_i$ is the position of the jump from $x_2 = i$ to $x_2 = i + 1$. Between two jumps the random energy of the DP is a sum of all the random energies encountered on the horizontal line at $x_2 = i - 1$. This sum is equivalent in law to a centered Gaussian

random variable that we can write down as the difference of two Brownian motions in s :

$$\sum_{x_1=N s_i}^{x_1=N s_{i+1}} \mathcal{E}_{x_1, i-1} \sim B_i(s_{i+1}) - B_i(s_i) \quad (\text{III.1.51})$$

where $B_i(s)$ is a BM with $B_i(0) = 0$ and $B'_i(s) = \sqrt{\tilde{\mathcal{E}}^2} \xi_i(s)$ where $\xi_i(s)$ are a collection of independent GWN with $\overline{\xi_i(s) \xi_{i'}(s')} = \delta_{i, i'} \delta(s - s')$. Thus in this limit the partition sum is rewritten as

$$\begin{aligned} Z_T^{s.d.}(N) &:= \lim_{b \rightarrow \infty} Z_{x_1=bT, x_2=N} \\ &= \int_{0 \leq s_1, \dots, s_N \leq T} e^{-\frac{1}{T} \sum_{i=0}^N B_i(s_{i+1}) - B_i(s_i)}, \end{aligned} \quad (\text{III.1.52})$$

with by definition $s_0 = 0$ and $s_{N+1} = T$. This is the definition of the O'Connell-Yor semi-discrete directed polymer which was introduced in [190] and for which KPZ universality (more precisely GUE TW fluctuations) in the limit $N \rightarrow \infty$ was shown in [191, 192]. This was later used in [193] to prove a universality result of TW-GUE fluctuations for point to point partition sum of directed polymer in 'thin rectangles' [193].

III.2 A partial selection of analytical miracles in models in the KPZ universality class

In the previous section we discussed the notion of weak and strong KPZ universality and introduced a few models in the KPZUC. In this chapter we now present a few *exact solvability properties* that permitted over the years to build the belief in the remarkable properties of the KPZUC and focus on DPs. We will discuss: (i) in Sec. III.2.1 the symmetries of the KPZ equation; (ii) in Sec. III.2.2 the stationary measure of the the KPZ equation and some models of DPs on \mathbb{Z}^2 ; (iii) in Sec. III.2.3 the Bethe-ansatz solvability of the continuum DP; (iv) in Sec. III.2.4 some other exact solvability properties: the RSK and gRSK correspondences and Macdonald processes (briefly discussed).

III.2.1 Symmetries of the continuum KPZ equation

Hydrodynamic point of view: Galilean symmetry

The KPZ equation (III.1.15) enjoys Galilean invariance: for a given realization of the GWN $\xi(t, x)$, if $h(t, x)$ is a solution of the KPZ equation, then

$$h_v(t, x) = h(t, x - tv) - vx + \frac{v^2 t}{2}, \quad (\text{III.2.1})$$

is a solution of the KPZ equation in the noise $\xi_v(t, x) = \xi(t, x - tv)$. Defining $u(t, x) = \partial_x h(t, x)$, $u(t, x)$ solves the equation

$$\partial_t u(t, x) = u(t, x) \partial_x u(t, x) + \frac{1}{2} \partial_x^2 u(t, x) + \partial_x \xi(t, x). \quad (\text{III.2.2})$$

Which is the Burgers's equation for a randomly forced fluid, much studied in the literature in the context of turbulence: here $u(t, x)$ is interpreted as the velocity field of a one-dimensional fluid (see [194] for a review). In this framework the above symmetry reads $u_v(t, x) = u(t, x - tv) - v$ and really is the Galilean symmetry associated with a change of Galilean referential.

Directed polymer point of view: STS

From the DP point of view this symmetry is easily seen using the path integral formula for the point to point partition sum (I.3.10) of the DP in a potential $V(t, x)$ (here rewritten using dimensionless units, i.e. $T = 1$)

$$\begin{aligned}
 Z_t(x - tv) &:= \int_{u(0)=0}^{u(t)=x-tv} \mathcal{D}[u] e^{-\frac{1}{2} \int_0^t dt' (\partial_{t'} u(t'))^2 - \frac{1}{2} \int_0^t dt' V(t', u(t'))} \\
 &= \int_{u(0)=0}^{u(t)=x} \mathcal{D}[u] e^{-\frac{1}{2} \int_0^t dt' (\partial_{t'} u(t'))^2 + v \int_0^t dt' \partial_{t'} u(t') - \frac{v^2}{2} \int_0^t dt' - \frac{1}{2} \int_0^t dt' V(t', u(t') - tv)} \\
 &= e^{vx - \frac{v^2}{2} t} \int_{u(0)=0}^{u(t)=x} \mathcal{D}[u] e^{-\frac{1}{2} \int_0^t dt' (\partial_{t'} u(t'))^2 - \frac{1}{2} \int_0^t dt' V(t', u(t') - tv)} \quad (\text{III.2.3})
 \end{aligned}$$

and by taking the logarithm, one obtains the symmetry (III.2.1). For a random potential which satisfies the symmetry in law $\forall v, V(t, x) \sim V(t, x - tv)$, we then have a statistical symmetry and in law we have $h_v(t, x) \sim h(t, x)$. In particular this holds for a GWN $V(t, x) = \xi(t, x)$. In Chapter I and II this symmetry was called the statistical tilt symmetry. In the DES context we saw that it implies a non-renormalization of the elastic coefficient. In particular, the effective action of the theory contains the term $-\frac{1}{2T} \sum_{a=1}^n \int_x (\nabla u_x^a)^2$. This implied the symmetry between the roughness exponent of the DP ζ_s and the exponent θ of the fluctuations of the free energy as.

$$\theta = 1 - 2 + 2\zeta_s = -1 + 2\zeta_s . \quad (\text{III.2.4})$$

Interpreted in the KPZ context, the roughness exponent ζ_s of the DP is $1/z$ with z the dynamic exponent, and θ is the growth exponent β , related to the roughness exponent of the interface α as $\beta = \alpha/z$. Hence we have

$$\frac{\alpha}{z} = -1 + \frac{2}{z} \iff \alpha + z = 2 . \quad (\text{III.2.5})$$

The KPZUC is thus characterized by a single critical exponent. Note that this symmetry holds in any dimension N .

III.2.2 An analytical exact solvability property: the stationary measure

a Stationary measure of the 1d Burgers equation: the continuum KPZ case

In any model in the KPZUC, the appropriate height field is never stationary itself but grows with time. The height gradients, however, can be stationary and the stationary measure is known since [195, 33]. For the KPZ equation in particular, one studies the Burgers's equation for $u(t, x) = \partial_x h(t, x)$ already written in (III.2.2). Let us first

study the case where the non-linearity is zero (Edwards-Wilkinson case), the equation for $u(t, x)$ is now

$$\partial_t u(t, x) = \frac{1}{2} \partial_x^2 u(t, x) + \partial_x \xi(t, x). \quad (\text{III.2.6})$$

where $\xi(t, x)$ is a unit centered GWN. Let us now show that a family of stationary processes is obtained by taking $u(t, x)$ as $u(t, x) = \mu + \eta_t(x)$ where μ is the average slope of the KPZ interface (this labels the family) and $\eta_t(x)$ is distributed as a unit centered GWN for each t . Let us start from an initial condition $u(t=0, x) = \mu + \eta(x)$ with $\eta(x)$ a GWN independent of $\xi(t, x)$ and show that $\forall t$, $u(t, x) = \mu + \eta_t(x)$ with $\eta_t(x)$ a unit centered GWN. (III.2.6) is easily solved in Fourier space as

$$u(t, q) = e^{-1/2q^2 t} (\mu + \eta(q)) + \int_0^t e^{-\frac{1}{2}q^2(t-t')} i q \xi(t, q) dt'. \quad (\text{III.2.7})$$

This is sufficient to show that $u(t, x)$ is Gaussian distributed and one easily concludes the calculation by computing the first moment $\overline{u(t, q)} = \mu$ and the first cumulant $\overline{u(t, q)u(t, q')^c} = \hat{\delta}(q + q')$. Of course a priori this concerns only the EW universality class but remarkably the same stationary measure works for the KPZ equation. Checking this property directly in the continuum setting is, however, non-trivial due to the non-linear term and one has to be more precise here about what is meant by the continuum KPZ equation. Writing a functional Fokker-Planck equation for the PDF of $u(t, x)$, $\mathcal{P}_t[u]$, one obtains

$$\frac{\partial}{\partial t} \mathcal{P}_t[f] = - \int_x \frac{\delta}{\delta f(x)} \left((f \partial_x f + \frac{1}{2} \partial_x^2 f) \mathcal{P}_t[f] \right) + \frac{1}{2} \int_{x,y} \frac{\delta^2}{\delta f(x) \delta f(y)} (\partial_x \partial_y \delta(x-y) \mathcal{P}_t[f]) \quad (\text{III.2.8})$$

And since

$$\mathcal{P}_{stat}[f] \sim e^{-\frac{1}{2} \int dx f(x)^2 + \mu f(x)} \quad (\text{III.2.9})$$

is already stationary for the Edwards-Wilkinson case, it is stationary for the KPZ case iff

$$- \int_x \frac{\delta}{\delta f(x)} (f \partial_x f \mathcal{P}_{stat}[f]) = 0. \quad (\text{III.2.10})$$

Acting with the functional derivative on the $f \partial_x f$ is however rather ambiguous and one has to define a discretization procedure. It was argued in [196] that the proper way to discretize the non linear term in the KPZ equation is, taking $h(x, t) \rightarrow h_i(t)$,

$$(\partial_x h(x, t))^2 \rightarrow \frac{1}{3} ((\nabla_i h)^2 + (\nabla_i h)(\nabla_{i-1} h) + (\nabla_{i-1} h)^2). \quad (\text{III.2.11})$$

With $\nabla_i h(t) := h_{i+1}(t) - h_i(t)$. For the corresponding discretized Burgers equation, this implies the discretization, writing $u_i(t) := \nabla_i h(t)$

$$u \partial_x u \rightarrow \frac{1}{3} ((u_{i+1} - u_{i-1})(u_{i+1} + u_{i-1}) + u_i(u_{i+1} - u_{i-1})). \quad (\text{III.2.12})$$

With this discretization, the functional derivative is thus interpreted as

$$\begin{aligned}
 \int_x \frac{\delta}{\delta f(x)} (f \partial_x f) &\sim \sum_i \frac{d}{df_i} \frac{1}{3} ((f_{i+1} - f_{i-1})(f_{i+1} + f_{i-1}) + f_i(f_{i+1} - f_{i-1})) \\
 &\sim \sum_i \frac{1}{3} (f_{i+1} - f_{i-1}) \\
 &\sim \int_x \frac{2}{3} \partial_x f_x .
 \end{aligned} \tag{III.2.13}$$

And hence

$$- \int_x \frac{\delta}{\delta f(x)} (f \partial_x f \mathcal{P}_{stat}[f]) = - \int_x \frac{2}{3} \partial_x f_x \mathcal{P}_{stat}[f] - \int_x (f \partial_x f)(-f + \mu) \mathcal{P}_{stat}[f] . \tag{III.2.14}$$

Note that all three terms in this expression are total derivatives: hence $\mathcal{P}_{stat}[f]$ is indeed a stationary measure of the continuum KPZ equation (provided appropriate boundary conditions are assumed). Note that this property only holds because the discretization (III.2.11) was chosen and it is thus legitimate to ask what the KPZ equation actually means? This reflects the difficulties related to tackling the KPZ equation directly in the continuum. The right way to interpret it is really through the Cole-Hopf transform. Note that at the level of the Burgers velocity field, the discretization (III.2.12) precisely ensures that the velocity field is locally conserved: the right hand side of (III.2.12) can be written as a difference. We already noticed this property of the velocity field (i.e. height gradients) when we discussed the case of the corner growth model in Sec. III.1.1. Since the derivation of the stationary measure is at this stage quite unsatisfactory we will recover the result below in an unambiguous way starting from a model of DP on the square lattice. Let us first draw the consequences of the existence of this stationary measure. In the interface language, let us start from an initial condition

$$h(t = 0, x) = \mu x + B(x) , \tag{III.2.15}$$

where $B(x)$ is a two-sided Brownian motion. Although the interface grows, the slope field is stationary and

$$h(t, x) = h(t, x = 0) + \mu x + B_t(x) , \tag{III.2.16}$$

where for each t , $B_t(x)$ is a two-sided BM. This invariance of the Brownian motion implies that the roughness exponent of the interface is $\alpha = 1/2$, and together with (III.2.5) this entirely determines the critical exponents of the KPZUC. Note that the interface dynamics itself is not stationary and, as mentioned in Sec. III.1.2 (i) the fluctuations of $h(t, x = 0)$ grows at large time as $t^{1/3}$ and are distributed with the Baik-Rains distribution; (ii) $h(t, x = 0)$ and $B_t(x)$ are non-trivially correlated. In the DP language the free-energy of the polymer thus performs a Brownian motion.

It is expected that, starting from any initial condition, the slope field of the interface at large time will be stationary on local scales. Denoting as before $v_\infty(\varphi)$ the large time asymptotic velocity of the interface in the direction φ , it is expected that, in law, we have

$$h(T + t, \varphi T + x) - h(T, \varphi T) \sim_{T \rightarrow \infty} X_t + \mu x + B_t(x) \tag{III.2.17}$$

where $\mu = \partial_\varphi v_\infty(\varphi)$ (to ensure the equality of the mean value on both sides of (III.2.17)), $B_t(x)$ is a two-sided BM, X_t is a RV whose fluctuations grow at large time as $t^{1/3}$ and are distributed according to the Baik-Rains distribution, and $x, t = O(1)$. Of course if one scales x as $T^{2/3}$ one will see non-trivial correlations in the spatial direction and the process in x is not anymore a BM but, as discussed before, the Airy process. Conversely this explains why the Airy process and the interface at large time locally looks like a BM.

b Stationary measure of the Log-Gamma polymer

We now recover the stationary measure of the continuum KPZ equation in the DP framework. To this aim we first consider a model of DP on the square lattice introduced by Seppäläinen in the landmark paper [197], the Log-Gamma polymer. It is defined as in Sec. III.1.1 through the recursion equation (III.1.23)

$$Z_{t+1}(\hat{x}) = W_{t+1}(\hat{x}) (Z_t(\hat{x} + 1/2) + Z_t(\hat{x} - 1/2)) , \quad (\text{III.2.18})$$

where the random Boltzmann weights are all independent and distributed as the inverse of a Gamma RV with parameter $\gamma > 0$:

$$W_t(x) \sim \text{Gamma}(\gamma)^{-1} . \quad (\text{III.2.19})$$

And we recall that a RV X is distributed as a Gamma RV with parameter γ iff its PDF is

$$X \sim \text{Gamma}(\gamma) \iff p(X) = \frac{1}{\Gamma(\gamma)} X^{1+\gamma} e^{-X} . \quad (\text{III.2.20})$$

In [197] it was shown that, now interpreting (III.2.18) $\forall t$ as the definition of a Markov process, if at $t = 0$ the successive ratios of partition sums are chosen to be distributed as quotients of independent Gamma RV with

$$\frac{Z_{t=0}(\hat{x} + 1)}{Z_{t=0}(\hat{x})} \sim \frac{\text{Gamma}(\gamma - \lambda)}{\text{Gamma}(\lambda)} , \quad (\text{III.2.21})$$

where $0 < \lambda < \gamma$, then they remain so for all time. This model provided the first example of a discrete model of DP on the square lattice at finite temperature where the stationary measure is known exactly - a sign of the existence of *exact solvability properties*. The model was later shown to be exactly solvable using the gRSK correspondence (see Sec. III.2.4) in [198] and Bethe ansatz in [4]. As in the continuum KPZ case, the partition sum $Z_t(\hat{x})$ is not stationary but $\log Z_t(\hat{x})$ performs a random walk $\forall t$. The random walk is in general biased, except if $\lambda = \gamma/2$. As already shown in [4] and as we now recall, this model has a weak noise limit in the $\gamma \rightarrow \infty$ limit where the partition sum of the Log-Gamma polymer converges to the solution of the MSHE. Normalizing by definition the temperature T to 1, the random energies of the model are

$$\mathcal{E}_t(\hat{x}) = -\text{Log}(W_t(x)) \sim \log(\text{Gamma}(\gamma)) . \quad (\text{III.2.22})$$

And the first two moments are given in terms of the diGamma function $\psi = \Gamma'/\Gamma$ as

$$\bar{\mathcal{E}} = \psi(\gamma) \sim_{\gamma \gg 1} \log(\gamma) + O(1/\gamma) \quad , \quad \overline{\mathcal{E}^2}^c \sim \psi'(\gamma) \sim_{\gamma \gg 1} \frac{1}{\gamma} + O(1/\gamma^2) . \quad (\text{III.2.23})$$

This shows that, taking $\gamma = b\gamma'$, we can use the weak universality of the MSHE as discussed in Sec. III.1.3⁴. More precisely, adapting (III.1.50) to take into account the mean value of the energies, we now define

$$\tilde{Z}_{\tilde{t}}(\tilde{x}) := \lim_{b \rightarrow \infty} e^{b^2 D \tilde{t} \log(\gamma/2)} Z_{t=b^2 D \tilde{t}}(\hat{x} = b\tilde{x}) , \quad (\text{III.2.24})$$

and $\tilde{Z}_{\tilde{t}}(\tilde{x})$ satisfies the stochastic equation

$$\partial_{\tilde{t}} \tilde{Z}_{\tilde{t}}(\tilde{x}) = \frac{D}{8} (\partial_{\tilde{x}})^2 \tilde{Z}_{\tilde{t}}(\tilde{x}) + \sqrt{2c} \xi(\tilde{t}, \tilde{x}) . \quad (\text{III.2.25})$$

with $c = D/(2\gamma')$. To compare with our previous results on the stationary measure we thus take $D = 4$ and $c = 1/2$, i.e. $\gamma' = 4$. In order for the stationary initial condition (III.2.21) of the discrete model to have a well-defined limit as $b \rightarrow \infty$ we take $\lambda = \gamma/2 - \mu = b\gamma'/2 - \mu$ with $\mu = O(1)$. In this limit $\log \tilde{Z}_{\tilde{t}}(\tilde{x})$ performs a drifting Brownian motion with

$$\begin{aligned} \overline{\log \tilde{Z}_{\tilde{t}}(\tilde{x}) - \log \tilde{Z}_{\tilde{t}}(0)} &\sim b\tilde{x}(\psi(\gamma - \lambda) - \psi(\lambda)) \\ &\sim \mu\tilde{x} \end{aligned} \quad (\text{III.2.26})$$

and

$$\begin{aligned} \overline{(\log \tilde{Z}_{\tilde{t}}(\tilde{x}) - \log \tilde{Z}_{\tilde{t}}(0))^2}^c &\sim b\tilde{x}(\psi'(\gamma - \lambda) + \psi'(\lambda)) \\ &\sim \tilde{x} . \end{aligned} \quad (\text{III.2.27})$$

And thus we obtain in an unambiguous way that the family of stationary measures of the MSHE corresponds to $\log \tilde{Z}_{\tilde{t}}$ performing a drifting BM (one easily checks that higher cumulants $\overline{(\log \tilde{Z}_{\tilde{t}}(\tilde{x}) - \log \tilde{Z}_{\tilde{t}}(0))^n}^c$ with $n \geq 3$ are $O(1/b^{n-2})$).

c Stationary measure of exponential and geometric Last-Passage-Percolation

An elegant way to obtain results on last-passage-percolation with exponential waiting times is to use the zero-temperature limit of the Log-Gamma polymer. Although the Log-Gamma polymer does not contain a parameter corresponding to the temperature (which is one by definition) we saw in the last section that sending $\gamma \rightarrow \infty$ corresponds to a weak-noise limit, similar to a large temperature limit. Conversely, sending $\gamma \rightarrow 0^+$ yields a zero-temperature limit. More precisely, setting $\gamma = \epsilon\gamma'$ with $(\epsilon, \gamma') \in \mathbb{R}_+^2$, one easily shows that rescaled random energies in the Log-Gamma model (III.2.22) converge in law to (minus) exponential random variables:

$$\tilde{\mathcal{E}}_t(\hat{x}) := \frac{\mathcal{E}_t(\hat{x})}{\epsilon} = -\frac{\text{Log}(W_t(\hat{x}))}{\epsilon} \sim_{\epsilon \rightarrow 0^+} -\text{Exp}(\gamma') . \quad (\text{III.2.28})$$

⁴This is a slight adaptation of the weak universality since we are taking a weak noise limit while changing the shape of the distribution at the same time. The ideas are, however, identical.

We recall that the PDF of an exponential random variable is

$$x \sim \text{Exp}(\gamma') \iff p(x) = \frac{1}{\gamma'} e^{-\gamma' x}. \quad (\text{III.2.29})$$

Hence, introducing

$$\mathbf{E}_t(\hat{x}) = \lim_{\epsilon \rightarrow 0^+} -\frac{\log Z_t(\hat{x})}{\epsilon}, \quad (\text{III.2.30})$$

the linear recursion relation of the Log-Gamma polymer becomes, in the limit $\epsilon \rightarrow 0$, equivalent to

$$\mathbf{E}_{t+1}(\hat{x}) = \tilde{\mathcal{E}}_t(\hat{x}) + \min(\mathbf{E}_t(\hat{x} - 1/2), \mathbf{E}_t(\hat{x} + 1/2)). \quad (\text{III.2.31})$$

Switching to the waiting-time language as in Sec. III.1.1, one sees that this recursion equation corresponds to a problem of last passage percolation with exponential waiting times. We can now take the limit of the stationary initial condition of the Log-Gamma polymer (III.2.21). Setting $\lambda = \epsilon\lambda'$ we obtain that, if at $t = 0$ the energy is taken as a two-sided random walk with increments distributed as differences of independent random variables with

$$\mathbf{E}_{t=0}(\hat{x} + 1) - \mathbf{E}_{t=0}(\hat{x}) = \text{Exp}(\lambda') - \text{Exp}(\gamma' - \lambda'), \quad (\text{III.2.32})$$

then they remain so at all time. This exact solvability property of last passage percolation with exponential waiting times was first proved by Burke in [199] in the language of stochastic queuing systems. As for the Log-Gamma case, this exact solvability property is only the tip of the iceberg and last passage percolation with exponential weights enjoy other remarkable properties. These notably include: (i) the possibility to use the RSK (see Sec. III.2.4) correspondence [159]; (ii) Bethe ansatz solvability of the associated particle system, the TASEP with exponential clocks (see [200] and references therein). Let us finally mention here that these different exact solvability properties can be generalized to the geometric case where the random energies are discrete and distributed as $\tilde{\mathcal{E}}_t(\hat{x}) \sim -\text{Geo}(q)$ where $0 < q < 1$ and we use the convention

$$X = \text{Geo}(q) \iff \text{Proba}(X = k) = (1 - q)q^k. \quad (\text{III.2.33})$$

In particular in this case the stationary initial condition is obtained by setting

$$\mathbf{E}_{t=0}(\hat{x} + 1) - \mathbf{E}_{t=0}(\hat{x}) = \text{Geo}(q_b) - \text{Geo}(q/q_b) \quad (\text{III.2.34})$$

with $q < q_b < 1$. This is a generalization of the exponential case since the limit $q = 1 - \gamma'\epsilon$ of the geometric distribution is the exponential distribution.

III.2.3 An algebraic exact solvability property: Bethe ansatz integrability of the continuum DP

In this section we discuss the Bethe ansatz integrability of the continuum DP and recall the main steps that led to the results for the fluctuations of the point-to-point free-energy of the DP obtained in [173] (as well as in [165]).

a From the stochastic-heat-equation to the attractive Lieb-Liniger model

We now discuss the replica Bethe ansatz solution of the continuum DP which was first initiated by Kardar in [201]. In this section, to conform with recent works on the subject, we will study the MSHE with the following normalization,

$$\partial_t Z_t(x) = (\partial_x)^2 Z_t(x) + \sqrt{2\bar{c}} \xi(t, x) Z_t(x), \quad (\text{III.2.35})$$

with as usual $\xi(t, x)$ a unit Gaussian white noise with correlation $\overline{\xi(t, x)\xi(t', x')} = \delta(t - t')\delta(x - x')$. It can be obtained from the universal scaling limit of DP on the square lattice discussed in (III.1.47) with $D = 8$. For concreteness we also consider the initial condition

$$Z_{t=0}(x) = \delta(x = 0), \quad (\text{III.2.36})$$

and $Z_t(x)$ is thus a point to point partition sum. Let us introduce the ‘wave-function’

$$\psi_t(x_1, \dots, x_n) = \overline{Z_t(x_1) \cdots Z_t(x_n)}, \quad (\text{III.2.37})$$

from which the n^{th} integer moment of the partition sum is obtained by taking coinciding points. Introducing n auxiliary independent Brownian motions

$$b'_i(t) = \sqrt{2}\eta_i(t) \quad , \quad b_i(0) = 0, \quad (\text{III.2.38})$$

with $\eta_i(t)$ independent unit centered GWN, $\psi_t(x_1, \dots, x_n)$ is obtained as a conditional expectation value through the Feynman-Kac representation of the solution of the MSHE (see (III.1.2)) as

$$\psi_t(x_1, \dots, x_n) = \mathbb{E} \left(\overline{e^{\sum_{i=1}^n \int_0^t dt' \sqrt{2\bar{c}} \xi(t', b_i(t'))} \prod_{i=1}^n \delta(b_i(t) - x_i)} \right). \quad (\text{III.2.39})$$

Exchanging the two averages we obtain⁵

$$\psi_t(x_1, \dots, x_n) = \mathbb{E} \left(e^{\sum_{1 \leq i < j \leq n} \int_0^t dt' 2\bar{c} \delta(b_i(t) - b_j(t'))} \prod_{i=1}^n \delta(b_i(t) - x_i) \right). \quad (\text{III.2.40})$$

Using again the Feynman-Kac type formula (or an elementary derivation as in Sec. I.3.3) one obtains that ψ_t satisfies the PDE

$$\begin{aligned} \partial_t \psi_t &= -H_n \psi_t \quad , \quad H_n := - \sum_{j=1}^n \frac{\partial^2}{\partial x_j^2} - 2\bar{c} \sum_{1 \leq i < j \leq n} \delta(x_i - x_j), \\ \psi_{t=0}(x_1, \dots, x_n) &= \prod_{i=1}^n \delta(x_i). \end{aligned} \quad (\text{III.2.41})$$

Remarkably, this equation corresponds to the Schrödinger equation written in imaginary time for bosons (the wave function (III.2.39) is manifestly symmetric) in the

⁵Note that here there is no contribution from the term $i = j$ since we are using a time-ordered exponential, see the discussion in Sec. III.1.1.

attractive ($\bar{c} \geq 0$ is the strength of the white noise) Lieb-Liniger (LL) model [202]. Note that comparing (III.2.37) with (III.2.40), we have replaced the average over disorder by an average over interacting Brownian paths. This is an example of stochastic duality relations which relates the observables of two a priori unrelated stochastic processes and the LL model is dual to the MSHE. The particles of the LL model correspond to replica of the partition sum and we will use indifferently both denominations.

b Bethe ansatz solution of the LL model

The strategy adopted to solve (III.2.41) is to first compute all the symmetric eigenfunctions of the Lieb-Liniger Hamiltonian H_n :

$$H_n \psi_\mu = \Lambda_\mu \psi_\mu, \quad (\text{III.2.42})$$

where μ labels the different eigenvectors. As already noticed in [202], the symmetric eigenfunctions of H_n are obtained using the Bethe ansatz (see [203] for a review) as we now recall. Since we are looking for symmetric eigenfunctions of H_n it is sufficient to specify their values in the so-called *Weyl chamber* $x_1 \leq x_2 \leq \dots \leq x_n$ as

$$\psi_\mu(x_1 \leq \dots \leq x_n) = \tilde{\psi}_\mu(x_1, \dots, x_n), \quad (\text{III.2.43})$$

where $\tilde{\psi}_\mu$ is a priori not symmetric and the other sectors are obtained by using the symmetry of ψ_μ . In the interior of the Weyl chamber $x_1 < x_2 < \dots < x_n$, the interaction has no influence and the spectral equation (III.2.42) just amounts to the *free spectral equation*

$$H_n^{\text{free}} \tilde{\psi}_\mu = \Lambda_\mu \tilde{\psi}_\mu, \quad H_n^{\text{free}} = - \sum_i \frac{\partial^2}{\partial x_i^2}. \quad (\text{III.2.44})$$

And since the values of $\tilde{\psi}_\mu(x_1, \dots, x_n)$ outside the Weyl chamber have no influence on ψ_μ , we might as well take (III.2.43) to hold $\forall (x_1, \dots, x_n) \in \mathbb{R}^n$. We thus look for $\tilde{\psi}_\mu$ as a superposition of plane waves:

$$\tilde{\psi}_\mu := \sum_{\sigma \in S_n} A_\sigma \prod_{i=1}^n z_{\sigma(i)}^{x_i}, \quad (\text{III.2.45})$$

where S_n is the group of permutations of $\{1, \dots, n\}$, the $n!$ complex numbers A_σ are called *amplitudes* and the n complex numbers z_i are called *rapidities*. Alternatively we will consider the *quasi-momenta* λ_i defined by

$$z_j = e^{i\lambda_j}. \quad (\text{III.2.46})$$

The eigenvalue of the spectral problem (III.2.42) is completely specified by the free equation (III.2.44) as

$$\Lambda_\mu = \sum_{i=1}^n \lambda_i^2. \quad (\text{III.2.47})$$

Note that each of the $n!$ terms in $\tilde{\psi}_\mu$ independently solve (III.2.44) with the same eigenvalue. Here we are considering for now the most general superposition of plane

waves to try to maintain the maximum liberty with the aim of solving the full spectral problem (III.2.42). For now the spectral problem is already solved in the interior of the Weyl chamber. Let us now consider the condition of solvability at the ‘two particles boundary’ of the Weyl chamber $x_1 < x_2 < \dots < x_i = x_{i+1} < x_{i+2} < \dots < x_n$. From (III.2.42) and the form of the LL Hamiltonian (III.2.41) it is clear that we are looking for solutions ψ_μ that are continuous everywhere but not \mathcal{C}^1 . More precisely the derivatives of ψ_μ must exhibit jumps at coinciding points to compensate the δ interaction. Assuming that these discontinuities only concern the derivatives on coinciding points we must have

$$\begin{aligned} \frac{\partial^2 \psi_\mu}{\partial x_i^2} &= \left(\frac{\partial \psi_\mu}{\partial x_i} \Big|_{x_i=x_{i+1}^+} - \frac{\partial \psi_\mu}{\partial x_i} \Big|_{x_i=x_{i+1}^-} \right) \delta(x_{i+1} - x_i) + \dots \\ \frac{\partial^2 \psi_\mu}{\partial x_{i+1}^2} &= \left(\frac{\partial \psi_\mu}{\partial x_{i+1}} \Big|_{x_{i+1}=x_i^+} - \frac{\partial \psi_\mu}{\partial x_{i+1}} \Big|_{x_{i+1}=x_i^-} \right) \delta(x_{i+1} - x_i) + \dots \end{aligned} \quad (\text{III.2.48})$$

where the dots denote more regular terms. Using the symmetry of the wave-function one easily obtains that these singular parts are actually equals and expressed in terms of $\tilde{\psi}_\mu$ as, considering only the most singular terms

$$\frac{\partial^2 \psi_\mu}{\partial x_i^2} \simeq \frac{\partial^2 \psi_\mu}{\partial x_{i+1}^2} \simeq \left(\frac{\partial}{\partial x_{i+1}} - \frac{\partial}{\partial x_i} \right) \tilde{\psi}_\mu \Big|_{x_{i+1}=x_i} \delta(x_{i+1} - x_i) + \dots \quad (\text{III.2.49})$$

Let us now integrate, for all x_j fixed, distinct and ordered except x_i and x_{i+1} , the spectral equation (III.2.42) from $x_i = x_{i+1} - \epsilon$ to $x_i = x_{i+1} + \epsilon$. We obtain,

$$\int_{x_i=x_{i+1}-\epsilon}^{x_i=x_{i+1}+\epsilon} \left(-\frac{\partial^2}{\partial x_i^2} - \frac{\partial^2}{\partial x_{i+1}^2} \right) \psi_\mu - 2\bar{c}\psi_\mu + O(\epsilon) = O(\epsilon). \quad (\text{III.2.50})$$

implying, using (III.2.48) and (III.2.49)

$$-\left(\frac{\partial}{\partial x_{i+1}} - \frac{\partial}{\partial x_i} \right) \tilde{\psi}_\mu \Big|_{x_{i+1}=x_i} = \bar{c}\tilde{\psi}_\mu. \quad (\text{III.2.51})$$

And this implies for the amplitudes A_σ , that any amplitudes differing from one another by a transposition of $i \leftrightarrow j$, noted τ_{ij} , must satisfy

$$\frac{A_{\sigma \circ \tau_{ij}}}{A_\sigma} = \frac{\lambda_{\sigma(j)} - \lambda_{\sigma(i)} - i\bar{c}}{\lambda_{\sigma(j)} - \lambda_{\sigma(i)} + i\bar{c}}. \quad (\text{III.2.52})$$

There are thus $\frac{1}{2}C_n^2 n!$ equations for $n!$ variables, but they are mutually consistent [202]. The solution is defined up to a constant (i.e. the choice of A_{Id}) and we will choose here, in agreement with e.g. [178],

$$A_\sigma = \prod_{1 \leq \alpha < \beta \leq n} \left(1 + \frac{i\bar{c}}{\lambda_{\sigma(\beta)} - \lambda_{\sigma(\alpha)}} \right). \quad (\text{III.2.53})$$

We have now obtained a complete solution of the spectral problem (III.2.42). Here we have only taken care of the two-body interaction, but the Lieb-Liniger Hamiltonian (III.2.41) has indeed only two-bodies interactions. Note that we have not yet specified the values of the rapidities z_i . We now must do so in such a way that we obtain a complete basis of symmetric functions.

c The string solution

Here we will adopt the same strategy as e.g. in [178] and adopt periodic boundary conditions on a line of length L . More precisely we look for solutions such that $\forall(x_1, \dots, x_n) \in \mathbb{R}^n$ we have

$$\psi_\mu(x_1, \dots, x_{i-1}, x_i + L, \dots, x_n) = \psi_\mu(x_1, \dots, x_n). \quad (\text{III.2.54})$$

This implies the Bethe equations for the quasi-momenta:

$$e^{i\lambda_\alpha L} = \prod_{\beta \neq \alpha} \frac{\lambda_\alpha - \lambda_\beta - i\bar{c}}{\lambda_\alpha - \lambda_\beta + i\bar{c}}. \quad (\text{III.2.55})$$

These boundary conditions are appropriate to study the problem of the continuum DP on a cylinder as in [204, 205]. For our purpose they are only a trick to obtain a well defined complete basis⁶ of eigenfunctions and we will study the limit $L \rightarrow \infty$. The solution in this case was first described in [207] and here we recall the main features. In the large L limit a set of solutions λ_α can be decomposed in n_s packets, also called *strings*, of m_i particles (the string *multiplicities*) with $i = 1, \dots, n_s$ and $n = \sum_{i=1}^{n_s} m_j$. Inside the j^{th} string, the quasi-momenta are labeled by $a = 1, \dots, m_j$ and take the form

$$\lambda^{j,a} := k_j + \frac{i\bar{c}}{2}(m_j + 1 - 2a) + i\delta^{ja}, \quad (\text{III.2.56})$$

where k_j is quantized as for free-particles, $k_j = 2\pi I_j/L$ with $I_j \in \mathbb{Z}$ and δ^{ja} are corrections to this leading behavior that decay exponentially with L . Note that the quasi-momenta inside a string are symmetric with respect to the real axis. To understand this structure let us consider the two-particle case and take the log of the Bethe equations (III.2.55): we obtain

$$\begin{aligned} \lambda_1 &= \frac{2\pi I_1}{L} + \frac{1}{iL} (\log(\lambda_1 - \lambda_2 - i\bar{c}) - \log(\lambda_1 - \lambda_2 + i\bar{c})) \\ \lambda_2 &= \frac{2\pi I_2}{L} - \frac{1}{iL} (\log(\lambda_1 - \lambda_2 - i\bar{c}) - \log(\lambda_1 - \lambda_2 + i\bar{c})), \end{aligned} \quad (\text{III.2.57})$$

with $(I_1, I_2) \in \mathbb{Z}^2$ and note that $\lambda_1 + \lambda_2$ is always real. The naive solution of this equation in an expansion in $1/L$ would thus be $\lambda_j = \frac{2\pi I_j}{L} + O(1/L^2)$, i.e. an asymptotic solution equivalent to free-particles. This however neglects the fact that the singularity of the logarithm at 0 can kill the $1/L$ decay before it. More precisely if $\lambda_1 = \lambda_2 + i\bar{c} + O(e^{-\delta L})$ with $\delta > 0$, then $I_1 = I_2$ and we obtain

$$\lambda_1 = \frac{2\pi I_1}{L} + \frac{1}{iL}(-\delta L) \quad , \quad \lambda_2 = \frac{2\pi I_1}{L} - \frac{1}{iL}(-\delta L). \quad (\text{III.2.58})$$

By consistency we must have $\lambda_1 - \lambda_2 \simeq i\bar{c} = 2i\delta$. Hence this solution is only consistent if $\bar{c} > 0$: strings only exist in the attractive phase of the Lieb-Liniger model. Finally since $\lambda_1 + \lambda_2$ must be real this implies the string form (III.2.56) for $m = 2$. This reasoning

⁶Proving the completeness of the Bethe solutions is in general a very non-trivial problem, see [206] and references therein for the case studied here.

can be generalized to any m and leads to (III.2.56). Note that these considerations do not constitute in any case a proof that the string states form a complete basis in the large L limit, but they indeed do, see [208]. In the large L limit the dynamics of the system is thus relatively simple and the particles form string states that move essentially independently. In particular, the wave function associated with n particles forming a single n -string is

$$\psi_\mu(x_1, \dots, x_n) := n! e^{ik \sum_i x_i - \frac{\bar{c}}{2} \sum_{1 \leq i < j \leq n} |x_i - x_j|}. \quad (\text{III.2.59})$$

String states thus correspond to bound states. The contribution to the eigenvalue Λ_μ of a string of m_j particles is the energy of the string

$$E_j := \sum_{a=1}^{m_j} (\lambda^{j,a})^2 = m_j k_j^2 - \frac{(\bar{c})^2}{12} m_j (m_j^2 - 1). \quad (\text{III.2.60})$$

The ground state of the system is thus obtained by forming a single n -string. Finally, noting that the Bethe wavefunction (III.2.45) with (III.2.53) is symmetric by exchange $z_i \leftrightarrow z_j$ the sum over eigenstates can be computed as

$$\sum_\mu = \sum_{n_s=1}^n \frac{1}{n_s!} \sum_{(m_1, \dots, m_{n_s})_n} \prod_{j=1}^{n_s} \int_{\mathbb{R}} \frac{m_j L dk_j}{2\pi}, \quad (\text{III.2.61})$$

where the $n_s!$ avoids a double counting of the states, the sum $\sum_{(m_1, \dots, m_{n_s})_n}$ is over all n_s -uplets such that $\sum_{j=1}^{n_s} m_j = n$ and the last terms comes from the fact that each string-state should be considered as a free-particle with total moment $K_j := \sum_{a=1}^{m_j} \lambda^{j,a} = m_j k_j$ (see [209]).

d Norm of the states

As the eigenfunctions of a symmetric operator, the Bethe eigenfunctions are orthogonal. They are however not normalized and for many practical applications it is important to know their norm. A remarkable formula due to Gaudin [210] is that the norm of the eigenstates of the system with periodic boundary conditions can be computed, at finite L , as

$$\begin{aligned} \|\psi_\mu\|^2 &= \int_{[0,L]^n} dx_1 \cdots dx_n \psi_\mu^*(x_1, \dots, x_n) \psi_\mu(x_1, \dots, x_n) \\ &= n! \prod_{1 \leq \alpha < \beta \leq n} \frac{(\lambda_\alpha^{LL} - \lambda_\beta^{LL})^2 + (\bar{c}^{LL})^2}{(\lambda_\alpha^{LL} - \lambda_\beta^{LL})^2} \det G^{LL} \end{aligned} \quad (\text{III.2.62})$$

where G^{LL} is the Gaudin matrix whose entries are:

$$G_{\alpha\beta}^{LL} = \delta_{\alpha\beta} \left(L + \sum_{\gamma=1}^n K(\lambda_\alpha^{LL} - \lambda_\gamma^{LL}) \right) - K(\lambda_\alpha^{LL} - \lambda_\beta^{LL}) \quad (\text{III.2.63})$$

$$K(x) = \frac{-2\bar{c}^{LL}}{x^2 + (\bar{c}^{LL})^2} \quad (\text{III.2.64})$$

Note that the entries of the Gaudin matrix in the LL case are the derivatives of the logarithm of the Bethe equations. Performing the asymptotic analysis of this formula at large L for string states is a non-trivial problem (due to the divergences or zeros both in the prefactor and in the Gaudin kernel) which was only accomplished recently in [209]. The result is

$$\|\psi_\mu\|^2 = \frac{n!L^{n_s}}{(\bar{c})^{n-n_s}} \prod_{j=1}^n m_j^2 \prod_{1 \leq i < j \leq n_s} \frac{4(k_i - k_j)^2 + (m_i + m_j)^2 \bar{c}^2}{4(k_i - k_j)^2 + (m_i - m_j)^2 \bar{c}^2} + O(L^{n_s-1}). \quad (\text{III.2.65})$$

Note in particular that this norm scales as L^{n_s} , a scaling that would be obtained for n_s free particles.

e Point-to-point free-energy fluctuations of the continuum DP

Starting from

$$\overline{Z_t(x)^n} = \sum_{\mu} \frac{\langle \psi_\mu, \psi_{t=0} \rangle}{\|\psi_\mu\|^2} \Lambda_\mu^t \psi_\mu(x, \dots, x), \quad (\text{III.2.66})$$

and combining the ingredients presented with the previous section together with the fact that $\psi_\mu(x, \dots, x) = n! e^{i \sum_{j=1}^{n_s} m_j k_j x}$ one obtains the formula that first appeared in [173, 165]:

$$\begin{aligned} \overline{Z_t(x)^n} = & \sum_{n_s=1}^n \frac{n! \bar{c}^n}{n_s! (2\pi \bar{c})^{n_s}} \sum_{(m_1, \dots, m_{n_s})_n} \prod_{j=1}^{n_s} \frac{dk_j}{m_j} \prod_{1 \leq i < j \leq n_s} \frac{4(k_i - k_j)^2 + (m_i - m_j)^2 \bar{c}^2}{4(k_i - k_j)^2 + (m_i + m_j)^2 \bar{c}^2} \\ & \times \prod_{j=1}^{n_s} e^{i \sum_{j=1}^{n_s} m_j k_j x - t \left(m_j k_j^2 - \frac{(\bar{c})^2}{12} m_j (m_j^2 - 1) \right)}. \end{aligned} \quad (\text{III.2.67})$$

This formula is exact, but does not determine the probability distribution of $Z_t(x)$: the moments grow as $e^{tn^3 \frac{(\bar{c})^2}{12}}$ (contribution from the ground state), i.e. too fast to determine the distribution. Hence determining the Laplace transform

$$g_{t,x}(u) := \overline{e^{-u Z_t(x)}} \quad (\text{III.2.68})$$

from (III.2.66) is impossible from a mathematical point of view. Exchanging the average over disorder and the series expansion of the exponential in (III.2.68) leads to a diverging series. This is a caveat of the replica method for the continuum DP and one has to devise a recipe to resum the diverging series. The correct way used for example in [173, 165] is to use the Airy trick $\int_{\mathbb{R}} dy Ai(y) e^{ys} = e^{\frac{s^3}{3}}$ (valid for $Re(s) > 0$) to ‘linearize’ the energies of the string. Let us now give the result for the Laplace transform at $x = 0$ (which is not restrictive since STS holds, see Sec. III.2.1). Introducing the rescaled Laplace transform

$$\tilde{g}(s) = \overline{\exp \left(-e^{\lambda s} \frac{Z_t(0)}{\bar{c} e^{-\frac{\bar{c}^2 t}{12}}} \right)} = \overline{\exp \left(-e^{\lambda(s-ft)} \right)} \quad (\text{III.2.69})$$

where we have introduced the parameter λ and the rescaled free-energy

$$\lambda = \left(\frac{\bar{c}^2 t}{4}\right)^{\frac{1}{3}} \quad , \quad f_t := \frac{-\log Z_t(0) + \log(\bar{c}) + \frac{\bar{c}^2 t}{12}}{\lambda} . \quad (\text{III.2.70})$$

Then $\tilde{g}(s)$ can be rewritten as a Fredholm determinant (see [211] and references therein for background on Fredholm determinants):

$$\tilde{g}(s) = \text{Det}(I + K) \quad (\text{III.2.71})$$

with the kernel

$$K(v, v') = - \int_{\mathbb{R}} \frac{dk}{2\pi} dy Ai(y + k^2 - s + v + v') \frac{e^{\lambda y - ik(v-v')}}{1 + e^{\lambda y}} . \quad (\text{III.2.72})$$

K is an operator $K : L^2(\mathbb{R}^+) \rightarrow L^2(\mathbb{R}^+)$, i.e. the v, v' variables above live on \mathbb{R}_+ . The essential steps to go from (III.2.69) to (III.2.71) are (i) (wrongfully) inverting the average with respect to disorder and the series expansion of the exponential in (III.2.69); (ii) use the exact formula (III.2.66); (iii) exchange in the resulting (diverging) expression the sum over n (originating from step (i)) and the sum over n_s in (III.2.66); (iv) use the Airy trick; (v) notice the determinantal structure using the formula

$$\det \left[\frac{1}{i(k_i - k_j) + (m_i + m_j)/2} \right]_{n_s \times n_s} = \prod_{i=1}^{n_s} \frac{1}{m_i} \prod_{1 \leq i < j \leq n_s} \frac{4(k_i - k_j)^2 + (m_i - m_j)^2}{4(k_i - k_j)^2 + (m_i + m_j)^2} . \quad (\text{III.2.73})$$

The emergence of a determinant thus in the end comes from the remarkable formula for the norm of string states in the large L limit. We refer the reader to [173] for more details on the derivation of (III.2.71)-(III.2.72). Finally, starting from (III.2.71) it is possible to perform the large time (i.e. large λ) limit of the Fredholm determinant. Assuming that the rescaled free-energy f_t defined in (III.2.70) is a $O(1)$ RV (and thus $\frac{\bar{c}^2}{12}$ is the extensive part of the free-energy of the DP while λ is the scale of the fluctuations of the free-energy), one obtains [173] (using $\lim_{\lambda \rightarrow \infty} \exp(-e^{\lambda(s-f)}) = \theta(f - s)$)

$$\lim_{t \rightarrow \infty} \text{Prob} \left(\frac{-\log Z_t(0) + \frac{\bar{c}^2 t}{12}}{\lambda} > s \right) = \text{Prob}(f_\infty > s) = F_2 \left(-\frac{s}{2^{2/3}} \right) , \quad (\text{III.2.74})$$

where $F_2(s)$ is the CDF of the Tracy-Widom GUE distribution which also admits an expression as a Fredholm determinant [37].

f A few results obtained using Bethe ansatz

The replica Bethe ansatz approach to DP has led to a variety of exact results. Known since the work of Kardar [201], it was first applied for technical reasons, to the study of DP properties that can be deduced more or less from the sole knowledge of the ground state energy, i.e. the limit of DPs of large length $t \gg 1$ on a finite cylinder L (the limit $L \rightarrow \infty$ being eventually taken afterwards). This was used to already determine the critical exponents [201, 212] or the large deviation function for the fluctuations of the free-energy of the DP on the cylinder [204, 205]. Obtaining the universal distribution

of fluctuations for the growth of an interface in an infinite space, however, requires to consider the limit $t \rightarrow \infty$ with at least $L \gg t^{2/3}$. The study of this limit from BA requires a summation over all excited states. This was only achieved recently, partly thanks to the work of Calabrese and Caux [209] who managed to compute the norm of string states (III.2.65).

Even with this knowledge it is still far from trivial to obtain exact results. Additionally since the method is not rigorous from a mathematical point of view due to the too rapid growth of moments, it requires a large number of tricks. Once a solid recipe to tackle this issue has been devised (a recipe that sometimes appears retrospectively to be the shadow of a rigorous derivation, as e.g. by considering a q -deformed model, see [208]), the replica Bethe ansatz approach has led a variety of new (presumably exact) results. Here we name a few: (i) TW-GUE distribution of fluctuations for the point-to-point free energy [173, 165]; (ii) TW-GOE distribution of fluctuations for the point-to-line free energy [177, 178, 179]; (iii) multi-point correlations for the point-to-point free-energy and the Airy process [175, 213]; (iv) one point (Baik-Rains) and multi-point distributions of fluctuations for the point-to-Brownian (i.e. the DP with stationary initial condition) free-energy [183, 184]; (v) TW-GSE distribution of fluctuations for the point-to-point free energy of a directed polymer in a half-space [169]; (vi) fluctuations of free-energy in the crossover from droplet to stationary initial condition [184]; (vii) fluctuations of free-energy in the crossover from droplet to flat initial condition [214]; (viii) distribution of the endpoint of the polymer [215]; (ix) extension to two-times [166]. Some of these results have been shown rigorously since then (see [34]), giving credit to the replica method.

III.2.4 A few words on other exact solvability properties

In the next chapter we will review the recent progresses that have been made on applying the replica Bethe ansatz to models of DPs on \mathbb{Z}^2 , which are one of the major focus of this thesis. Additionally we will see that these BA exactly solvable models of DPs have another exact-solvability property that has also been discussed previously, namely their stationary measure can be written down exactly. Before we do so we now mention other exact solvability properties that have played an important role in the study of DPs, particularly for discrete models.

a A combinatorial exact solvability property: RSK and gRSK correspondence

As we mentioned, the first proof of TW-GUE fluctuations for a point-to-point directed polymer was in [159] for a model of DP at zero temperature with (minus) exponential or geometric distribution of random energies, i.e. equivalently a model of LPP with exponential or geometric distribution of waiting times (see Sec. III.1.1). The exact solvability used there appears to be of purely combinatorial origin and proceeds in three steps. It consists, for the geometric case, in: (i) mapping the problem of finding the last passage time $T(x_1, x_2)$ to the problem of finding the length of the longest increasing subsequence in a sequence of pairs of integers (x'_1, x'_2) where the number of times (x_1, x_2) appears in the sequence is given by the value of the random waiting time

t_{x_1, x_2} ; (ii) using the Robinson-Schensted-Kuth (RSK) algorithm to map this problem onto the problem of finding the length of the first row in a pair of ‘semi-standard Young tableaux’; (iii) obtain a representation of the PDF of the latter using Schur polynomials. The formula obtained in the last step shares striking similarities with formulae obtained in random matrix theory. The asymptotic analysis is carried out using the theory of symmetric polynomials, and the role played by the Hermite polynomials for the GUE is played by the Meixner polynomials. We refer to [160] for a pedagogical review of this approach to LPP with geometric waiting times. This approach was later adapted to study a model of first passage percolation with geometric waiting times on horizontal edges of \mathbb{Z}^2 only [216]. The RSK correspondence was later ‘tropicalized’ in [217] to obtain the proof of GUE-TW distribution of free-energy fluctuations for the semi-discrete directed polymer. This new combinatorial mapping has since then been referred to as the geometric RSK (gRSK) correspondence. LPP with geometric and exponential waiting times was a precursor of the first discovered exactly solvable model of DP on the square lattice at finite temperature, the Log-Gamma polymer. Introduced in [197] for the possibility of writing down exactly its stationary measure, it was later shown that the gRSK correspondence could be used to tackle this finite temperature case as well [198], the results were then later used in [218] to obtain the first proof of the emergence of TW-GUE fluctuations in a finite temperature model of DP on \mathbb{Z}^2 . Similarly, the LPP model discussed previously was a precursor of the ‘Strict-Weak’ polymer, the second exactly solvable model of finite temperature DP on \mathbb{Z}^2 . Introduced in [219, 220], three exactly solvable properties were shown simultaneously for this model: exact stationary measure, Bethe ansatz solvability and gRSK correspondence. TW-GUE fluctuations were shown too. The links between RSK and gRSK correspondence was recently clarified in [221] where the authors obtained a general correspondence that interpolates between both.

b Macdonald processes

The theory of Macdonald processes, developed in [192], has provided important results for various models in the KPZUC. Macdonald processes are a two-parameter family of stochastic processes which, in several limits, converge to models now known to belong to the KPZUC in particular the q-TASEP, the semi-discrete DP and the continuum DP. The exact solvability property of Macdonald processes notably relies on results from the theory of symmetric functions (Macdonald functions) and Macdonald processes in general constitute a class of processes different from BA solvable processes (but their intersection is not empty).

III.3 Summary of (and more context around) the results obtained during the thesis

III.3.1 Introduction

In the last sections we have thus discussed some aspects of the KPZUC and presented some exact solvability properties that, in the DP context, contributed to the statement of the KPZ universality hypothesis. Before we continue, let us emphasize here that

there is still no simple explanation for the values of the exponents in the KPZUC, and even less for the emergence of universal distributions related to extreme value statistics of RMT⁷. Despite this, this universality class seems remarkably robust. *The emergence of the KPZ exponents and of the Tracy-Widom GUE distribution in so many different models has the flavor of an analogue of the central limit theorem in the case of strongly correlated RVs.* Understanding simple mechanisms explaining this universality is one of the major objectives of research in this field. This task, however, still appears beyond reach, and most of the research in the KPZUC still relies on the study of exactly solvable models. It is in this spirit that in this thesis we studied directed polymers on the square lattice and tried to understand how KPZUC appears in these models (see Sec. III.3.4).

As we discussed in the last section, the RSK and gRSK correspondences have played a major role in the study of DPs on \mathbb{Z}^2 . While the RSK correspondence provided the first proof of TW-GUE type fluctuations of free-energy for LPP with geometric waiting times [159], the gRSK correspondence led to a similar result, for the first time, in a model of a DP on \mathbb{Z}^2 at finite temperature, the Log-Gamma polymer [197, 198, 218].

On the other hand, for the continuum DP, as reviewed in the last section, the Bethe ansatz approach, although non-rigorous, is a powerful and versatile technique that was recently applied to obtain a variety of *exact* results. This state of affairs provided the motivation to obtain a Bethe ansatz approach to the Log-Gamma polymer. Similarly to the continuum case, the moment problem is mapped into a discrete-time and discrete-space dynamics of replica on \mathbb{Z} . It was found by Éric Brunet that the transfer matrix of the problem (equivalent to the LL Hamiltonian), could be diagonalized using the Bethe ansatz. As we showed in the last section, this BA solvability is, however, only the beginning of the route to the ‘proof’ of GUE-TW-type fluctuations for the DP free-energy. The paper [4] showed how the route used for the continuum DP could be successfully adapted to this discrete case. The results obtained in [4] will be presented in Sec. III.3.2 and the original research paper can be found in Appendix. D.

The dynamics of the replica on \mathbb{Z} for the Log-Gamma polymer is very similar to the dynamics of interacting particle systems referred to as zero-range-processes (ZRP). In the seminal paper [222], Povolotsky obtained a classification of BA solvable models of ZRP on \mathbb{Z} with parallel updates⁸. The purpose of the paper [5] was to understand whether or not this classification could be adapted to obtain a classification of finite temperature BA solvable models of DP on \mathbb{Z}^2 . As we will discuss in Sec. III.3.3, with some specific hypothesis, this classification is very close to being complete. In particular it encompasses all known models of exactly solvable models of DP on \mathbb{Z}^2 : the already discussed Log-Gamma and Strict-Weak polymer, but also (i) the Beta polymer introduced shortly before by Barraquand and Corwin in [224]; (ii) the Inverse-Beta polymer, a new integrable model of DP on the square lattice that remarkably interpolates between the Inverse-Beta and Log-Gamma polymer, and for which we showed TW-GUE fluctuations for the point-to-point free energy. The results obtained in [5] will be presented in Sec. III.3.3 and the original research paper can be found in Appendix. E.

⁷Note that the Baik-Rains distribution has no equivalent in RMT.

⁸A classification later extended in [223] to the case of non-parallel updates.

Among the classification of BA exactly solvable models of DP obtained in [5], the Beta polymer has the remarkable peculiarity that it can also be interpreted as a model of a random walk on \mathbb{Z} in a time-dependent random environment (TD-RWRE). This is the first example of an exactly solvable model of TD-RWRE and it brings to this field the possibility of using exact techniques and the scope of KPZUC. In [224] the authors obtained exact results for the point to half-line partition sum of the DP. In the correspondence with TD-RWRE these correspond to results for the cumulative distribution function (CDF) of the TD-RWRE transition probability. They notably showed a convergence at large time of the fluctuations of the point to half-line free-energy of the DP, in the large deviations regime of the TD-RWRE, to the GUE-TW distribution. This suggests that KPZ universality does apply in the large deviations regime, but the behavior of the TD-RWRE in the diffusive regime was not considered in [224]. In [6], using the techniques developed in [4, 5], we obtained complementary exact results for the point to point partition sum of the DP, equivalent in the correspondence with TD-RWRE to the PDF of the TD-RWRE transition probability. We performed the asymptotic analysis of these formulae both in the large deviations regime and in the diffusive regime. While in the large deviations regime we obtain TW-GUE type fluctuations for the point to point DP free-energy, in the diffusive regime we obtain that the fluctuations of the partition sum are Gamma distributed. This permits a discussion of the crossover between both regimes. The results obtained in [6] will be presented in Sec. III.3.4 and the original research paper can be found in Appendix. F.

Finally in [7], on one hand we pursued the analysis of the Inverse-Beta polymer and obtained its stationary measure exactly. Using the stationary measure we additionally recovered rigorously some results obtained in [5]. On the other hand we used this knowledge to go back to zero temperature models of DPs on the square lattice and we introduced a new exactly solvable model, the Bernoulli-Geometric polymer. The motivation to look for this model came from the fact that (i) the Inverse-Beta polymer appears as a general model encompassing the two gRSK solvable finite temperature models of DP on \mathbb{Z}^2 , the Log-Gamma and the Strict-Weak polymer; (ii) the Log-Gamma and the Strict-Weak polymer are both linked with RSK solvable zero-temperature models of DP on \mathbb{Z}^2 with discrete energies, namely models of first and last passage percolation with geometric waiting times. It was thus natural to conjecture that a zero-temperature model of DP on \mathbb{Z}^2 , linked with the Inverse-Beta polymer and with discrete random energies should exist. The Bernoulli-Geometric model introduced in this paper appears as this missing model and we obtained its stationary measure exactly and deduced from it several results. The results obtained in [7] will be presented in Sec. III.3.5 and the original research paper can be found in Appendix. G.

We now give a more detailed overview of the main results obtained in [4, 5, 6, 7]. We only focus on the main results and encourage the reader to look directly at the original research papers in Appendices D-E-F-G. We begin with [4] on which we will be quite exhaustive since many of the methods developed in [4] are used in [5, 6].

III.3.2 Presentation of the main results of [4]

Introduction, our strategy and an issue

In [4] we attempted to solve the Log-Gamma polymer model, already presented in

Sec. III.2.2, using the coordinate Bethe ansatz. The model is defined through the recursion equation for the partition sum, for $t \geq 0$,

$$Z_t(\hat{x}) = W_{t+1}(\hat{x}) (Z_t(\hat{x} - 1/2) + Z_t(\hat{x} + 1/2)) \quad , \quad Z_0(\hat{x}) = \delta_{\hat{x},0} W_0(0) . \quad (\text{III.3.1})$$

Where the random Boltzmann weights $W_t(\hat{x})$ are independent and distributed according to the inverse of Gamma random variables with parameter $\gamma > 0$ (see (III.2.20)). Note that here we have added a Boltzmann weight on the first site of the DP. The moments of $W_t(\hat{x})$ are well defined for $n \leq \gamma$ and are given by

$$\overline{(W_t(\hat{x}))^n} = \frac{\Gamma(\gamma - n)}{\Gamma(\gamma)} = \frac{(-1)^n}{(1 - \gamma)_n} , \quad (\text{III.3.2})$$

where we introduced the Pochhammer symbol $(a)_n = \prod_{k=0}^{n-1} (a + k)$. For $n > \gamma$, $\overline{(W_t(\hat{x}))^n} = +\infty$. In this paper, our goal is to compute the PDF of $Z_t(\hat{x})$ from the knowledge of its integer moments $\overline{(Z_t(\hat{x}))^n}$ that we will compute using BA. This problem is obviously ill-defined since only a finite number (the first γ) of moments of $Z_t(\hat{x})$ exist. The problem here is thus in some sense even worse than in the continuum DP where the moments were ‘only’ growing too fast.

A way out

Note, however, that using the analytical continuation of the Gamma function, the right-hand side of (III.3.2) is well-defined $\forall n$, although these are not the moments of the Inverse-Gamma distribution (the moments only exist for n in the complex plane with $\text{Re}(n) < \gamma$). The question we ask here is: ‘can we still somehow use these analytically continued moments to obtain (non-rigorously) the Laplace transform of $W_t(\hat{x})$ ’, which is defined by

$$g(u) := \overline{e^{-W_t(\hat{x})}} = \sum_{n=0}^{\infty} \frac{(-u)^n}{n!} \overline{(W_t(\hat{x}))^n} . \quad (\text{III.3.3})$$

If we find a ‘solution’ to this ill-defined problem, then our goal will be to adapt this solution to obtain the Laplace transform of $Z_t(\hat{x})$ from similarly analytically continued moments. First note that in the expression (III.3.3), it is not possible to exchange the series expansion of the exponential and the average over disorder since only a finite number of moments of $W_t(\hat{x})$ exist. We can, however, rewrite this series expansion using a Mellin-Barnes representation:

$$g(u) = \frac{-1}{2i\pi} \int_{s \in \mathcal{C}} \frac{\pi ds}{\sin(\pi s)} u^s \frac{\overline{(W_t(\hat{x}))^s}}{\Gamma(1 + s)} , \quad (\text{III.3.4})$$

where \mathcal{C} is a vertical contour oriented from down to top with $\mathcal{C} = -a + i\mathbb{R}$ and $0 < a < 1$. The identity between (III.3.3) and (III.3.4) follows from the (legitimate) application of the residue theorem when closing the contour on the right and taking the poles of the sine function in the denominator. Using (III.3.2), $g(u)$ can thus be obtained as

$$g(u) = \frac{-1}{2i\pi} \int_{s \in \mathcal{C}} \frac{\pi ds}{\sin(\pi s)} u^s \frac{\Gamma(\gamma - s)}{\Gamma(\gamma)\Gamma(1 + s)} . \quad (\text{III.3.5})$$

This integral converges and the inversion of the integral and of the average over disorder is legitimate. We can now ‘un-do’ the Mellin-Barnes transform. Closing the contour \mathcal{C} on the right and taking into account the poles of the sine function *and* of the Γ function at the numerator, we obtain (using Euler’s reflection formula)

$$\begin{aligned} g(u) &= g_{\text{mom}}(u) + g_{\text{non-analytic}}(u), \quad (\text{III.3.6}) \\ g_{\text{mom}}(u) &:= \sum_{n=0}^{\infty} \frac{(-u)^n}{n!} \frac{\Gamma(\gamma - n)}{\Gamma(\gamma)}, \\ g_{\text{non-analytic}}(u) &:= \sum_{n=0}^{\infty} \frac{(-1)^n}{n!} u^{\gamma+n} \frac{\Gamma(-\gamma - n)}{\Gamma(\gamma)}. \end{aligned}$$

The Laplace Transform thus admits a non-analytic series expansion. Note that the analytic part of the series expansion $g_{\text{mom}}(u)$ can also be obtained by naively (and wrongfully) inverting the series expansion of the exponential and the average over disorder in (III.3.3) and using (III.3.2) $\forall n$. The question now is *how one can guess $g(u)$ from the sole knowledge of $g_{\text{mom}}(u)$?* The answer is: wrongfully (again) apply a Mellin-Barnes transform using the proper analytical continuation of the coefficients of the series expansion of $g_{\text{mom}}(u)$ to $n \in \mathbb{C}$:

$$g_{\text{mom}}(u) = \sum_{n=0}^{\infty} \frac{(-u)^n}{\Gamma(1+n)} \frac{\Gamma(\gamma - n)}{\Gamma(\gamma)} \rightarrow \frac{-1}{2i\pi} \int_{s \in \mathcal{C}} \frac{\pi ds}{\sin(\pi s)} u^s \frac{\Gamma(\gamma - s)}{\Gamma(\gamma)\Gamma(1+s)} = g(u). \quad (\text{III.3.7})$$

Note that there is a single analytical continuation that provides the right answer and it has to be guessed. This ‘trick’ gives us hope to solve the problem for the Log-Gamma polymer as follows: (i) compute the ‘moments’ $\overline{(Z_t(\hat{x}))^n} \forall n$ using BA, as if the moments of $W_t(\hat{x})$ were given by the right hand side of (III.3.2) $\forall n$; (ii) compute the ‘moment generating function’ $g_{t,x}^{\text{mom}}(u) = \sum_{n=0}^{\infty} \overline{Z_t(\hat{x})^n} u^n$; (iii) perform an ‘illegal’ Mellin-Barnes transform on $g_{t,x}^{\text{mom}}(u)$ using an analytical continuation and obtain a function $g_{t,x}(u)$; (iv) check that $g_{t,x}(u)$ is indeed the Laplace transform of $Z_t(\hat{x})$ for low values of t and \hat{x} and hope that it holds $\forall(t, \hat{x})$.

Bethe-Brunet ansatz

Introducing the mean value of the Boltzmann weights $w_0 = \overline{W_t(\hat{x})} = \frac{1}{\gamma-1}$ we consider the ‘wave-function’ (denoting from now on \hat{x} by x as in [4])

$$\psi_t(x_1, \dots, x_n) = \frac{1}{(2)^{nt} (w_0)^{n(t+1)}} \overline{Z_t(x_1) \cdots Z_t(x_n)}. \quad (\text{III.3.8})$$

The normalization of the wave-function ensures an easy comparison with the continuum DP case (see (III.2.24)) that is also discussed independently in the paper. Defining

$$h_n = \frac{\overline{(W_t(x))^n}}{w_0^n}, \quad (\text{III.3.9})$$

the transfer matrix is obtained as

$$\begin{aligned} \psi_{t+1}(x_i) &= (T_n \psi_t)(x_i) = \frac{1}{2^n} a_{x_1, \dots, x_n} \sum_{(\delta_1, \dots, \delta_n) \in \{-\frac{1}{2}, \frac{1}{2}\}^n} \psi_t(x_1 - \delta_1, \dots, x_n - \delta_n) \\ a_{x_1, \dots, x_n} &= \prod_x h_{\sum_{\alpha=1}^n \delta_{x, x_\alpha}}. \end{aligned} \quad (\text{III.3.10})$$

As shown by Éric Brunet, the symmetric eigenfunction of T_n

$$T_n \psi_\mu = \theta_\mu \psi_\mu, \quad (\text{III.3.11})$$

takes a Bethe-Ansatz form: for $x_1 \leq \dots \leq x_n$, $\psi_\mu(x_1, \dots, x_n) = \tilde{\psi}_\mu(x_1, \dots, x_n)$ with

$$\begin{aligned} \tilde{\psi}_\mu(x_1, \dots, x_n) &= \sum_{\sigma \in S_n} A_\sigma \prod_{\alpha=1}^n z_{\sigma(\alpha)}^{x_\alpha}, \quad A_\sigma = \prod_{1 \leq \alpha < \beta \leq n} \left[1 + \frac{\bar{c}}{2(t_{\sigma(\alpha)} - t_{\sigma(\beta)})} \right], \\ z_\alpha &= e^{i\lambda_\alpha}, \quad t_\alpha = i \tan\left(\frac{\lambda_\alpha}{2}\right) = \frac{z_\alpha - 1}{z_\alpha + 1}, \end{aligned} \quad (\text{III.3.12})$$

and

$$\theta_\mu = \prod_{i=1}^n z_\alpha^{\frac{1}{2}} \frac{1 + z_\alpha^{-1}}{2}. \quad (\text{III.3.13})$$

The form (III.3.12) should be compared with (III.2.53). In an appropriate scaling limit (the $\gamma \rightarrow \infty$ weak noise limit, see Sec. III.2.2) (III.3.12) converges to (III.2.53). Imposing periodic boundary conditions on a line of length L (immaterial in the computation of a moment as long as $t \geq L$) one obtains the following Bethe equations

$$e^{i\lambda_\alpha L} = \prod_{1 \leq \beta \leq n, \beta \neq \alpha} \frac{2t_\alpha - 2t_\beta + \bar{c}}{2t_\alpha - 2t_\beta - \bar{c}} = \prod_{1 \leq \beta \leq n, \beta \neq \alpha} \frac{2 \tan(\frac{\lambda_\alpha}{2}) - 2 \tan(\frac{\lambda_\beta}{2}) - i\bar{c}}{2 \tan(\frac{\lambda_\alpha}{2}) - 2 \tan(\frac{\lambda_\beta}{2}) + i\bar{c}} \quad (\text{III.3.14})$$

which should be compared with (III.2.55).

Symmetric transfer matrix, weighted scalar product and norm formula

The above transfer matrix is not symmetric and the eigenfunctions (III.3.12) are not orthogonal with respect to the canonical scalar product on $(\mathbb{Z}/(L\mathbb{Z}))^n$. In [4] we argue that the eigenfunctions (III.3.12) are orthogonal with respect to the following weighted scalar product:

$$\langle \phi, \psi \rangle = \sum_{(x_1, \dots, x_n) \in \{0, \dots, L-1\}^n} \frac{1}{a_{x_1, \dots, x_n}} \phi^*(x_1, \dots, x_n) \psi(x_1, \dots, x_n) \quad (\text{III.3.15})$$

We then conjecture a generalization of the Gaudin formula for the norm of the eigenfunctions (see [4] for some checks)

$$\|\psi_\mu\|^2 := \langle \psi_\mu, \psi_\mu \rangle = n! \prod_{1 \leq \alpha < \beta \leq n} \frac{(2t_\alpha - 2t_\beta)^2 - \bar{c}^2}{(2t_\alpha - 2t_\beta)^2} \det G \quad (\text{III.3.16})$$

with

$$\begin{aligned} G_{\alpha\beta} &= \delta_{\alpha\beta} \left(L + (1 - t_\alpha^2) \sum_{\gamma=1}^n \tilde{K}(t_\alpha - t_\gamma) \right) - (1 - t_\beta^2) \tilde{K}(t_\alpha - t_\beta) \\ \tilde{K}(t) &= \frac{-2\bar{c}}{-4t^2 + \bar{c}^2}. \end{aligned} \quad (\text{III.3.17})$$

This formula should be compared with (III.2.62). It is rather remarkable since the Gaudin formula does not a priori seem to know that we have defined the weighted scalar product (III.3.15).

The large L limit and the string solution

We assume $\bar{c} > 0$ (i.e. $\gamma > 1$, which is true if the first moment of the partition sum is well defined so that it makes sense to use the Bethe ansatz at least for small n). We then argue in [4] that the Bethe equations are solved in the large L limit similarly as in the continuum case (see Sec. III.2.3). Namely, a general eigenstate is given by partitioning n into n_s strings, each string containing m_j particles where the index $j = 1, \dots, n_s$ labels the string and

$$t_\alpha = t_{j,a} = i \frac{k_j}{2} + \frac{\bar{c}}{4}(m_j + 1 - 2a) + \frac{\delta_{j,a}}{2}, \quad (\text{III.3.18})$$

where we introduce an index $a = 1, \dots, m_j$ that labels the rapidity inside a string, and $\delta_{j,a}$ are deviations that fall off exponentially with L . This formula should be compared with (III.2.56). To compute the norm of the string states, we adapt the derivation of the Calabrese-Caux formula [209] to our formula (III.3.16) and obtain

$$\|\psi_\mu\|^2 = n! L^{n_s} \prod_{1 \leq i < j \leq n_s} \frac{4(k_i - k_j)^2 + \bar{c}^2(m_i + m_j)^2}{4(k_i - k_j)^2 + \bar{c}^2(m_i - m_j)^2} \prod_{j=1}^{n_s} \left[\frac{m_j}{\bar{c}^{m_j-1}} \left(\sum_{a=1}^{m_j} \frac{1}{1 - t_{j,a}^2} \right) \prod_{b=1}^{m_j} (1 - t_{j,b}^2) \right], \quad (\text{III.3.19})$$

which should be compared with (III.2.65). Note that as in the LL case the norm is almost a determinant. Here however, the additional factor $\sum_{a=1}^{m_j} \frac{1}{1 - t_{j,a}^2}$ which comes from the careful large L analysis of (III.3.16) spoils the algebraic structure⁹. ‘Luckily’ it will be canceled out in the final calculation by a factor coming from the phase space: we argue that the sum over eigenstates can be computed as

$$\sum_\mu = \sum_{n_s=1}^n \frac{1}{n_s!} \sum_{(m_1, \dots, m_{n_s})_n} \prod_{j=1}^{n_s} \int_{\mathbb{R}} \frac{L dk_j}{2\pi} \sum_{a=1}^{m_j} \frac{1}{1 - t_{j,a}^2}, \quad (\text{III.3.20})$$

which should be compared with (III.2.61). Finally noting that the contribution to the eigenvalue associated with the unit translation in time and on the lattice \mathbb{Z} are $\theta_\mu = \prod_{j=1}^{n_s} \theta_{m_j, k_j}$ with

$$\theta_{m_j, k_j} = \left(\frac{2}{\bar{c}} \right)^{m_j} \left(\frac{\Gamma(-\frac{m_j}{2} + \frac{\gamma}{2} - i \frac{k_j}{\bar{c}}) \Gamma(-\frac{m_j}{2} + \frac{\gamma}{2} + i \frac{k_j}{\bar{c}})}{\Gamma(\frac{m_j}{2} + \frac{\gamma}{2} - i \frac{k_j}{\bar{c}}) \Gamma(\frac{m_j}{2} + \frac{\gamma}{2} + i \frac{k_j}{\bar{c}})} \right)^{\frac{1}{2}}, \quad (\text{III.3.21})$$

and $\prod_\alpha z_\alpha = \prod_{j=1}^{n_s} \prod_{a=1}^{m_j} \frac{1 + t_{j,a}}{1 - t_{j,a}}$ with

$$\prod_{a=1}^{m_j} \frac{1 + t_{j,a}}{1 - t_{j,a}} = \frac{\Gamma(-\frac{m_j}{2} + \frac{\gamma}{2} - i \frac{k_j}{\bar{c}}) \Gamma(\frac{m_j}{2} + \frac{\gamma}{2} + i \frac{k_j}{\bar{c}})}{\Gamma(\frac{m_j}{2} + \frac{\gamma}{2} - i \frac{k_j}{\bar{c}}) \Gamma(-\frac{m_j}{2} + \frac{\gamma}{2} + i \frac{k_j}{\bar{c}})}. \quad (\text{III.3.22})$$

⁹It could obviously be integrated into a determinant, but not in a symmetric form.

An exact formula for the moments of the Log-Gamma polymer

Combining the precedent results, we obtain, for $\gamma < n$:

$$\begin{aligned} \overline{Z_t(x)^n} &= n! \sum_{n_s=1}^n \frac{1}{n_s!} \sum_{(m_1, \dots, m_{n_s})_n} \prod_{j=1}^{n_s} \int_{-\infty}^{+\infty} \frac{dk_j}{2\pi} \prod_{1 \leq i < j \leq n_s} \frac{4(k_i - k_j)^2 + (m_i - m_j)^2}{4(k_i - k_j)^2 + (m_i + m_j)^2} \\ &\quad \prod_{j=1}^{n_s} \frac{1}{m_j} \left(\frac{\Gamma(-\frac{m_j}{2} + \frac{\gamma}{2} - ik_j)}{\Gamma(\frac{m_j}{2} + \frac{\gamma}{2} - ik_j)} \right)^{\frac{t}{2}+1+x} \left(\frac{\Gamma(-\frac{m_j}{2} + \frac{\gamma}{2} + ik_j)}{\Gamma(\frac{m_j}{2} + \frac{\gamma}{2} + ik_j)} \right)^{\frac{t}{2}+1-x}, \end{aligned} \quad (\text{III.3.23})$$

which should be compared with (III.2.67). Note that the right hand side of (III.3.23) makes sense $\forall n$. We can use this fact to perform the rest of the program announced earlier.

Fredholm determinant formulae for the Laplace transform of the partition sum in the Log-Gamma polymer

Let us first perform the step (ii): we compute

$$g_{t,x}^{\text{mom}}(u) = \sum_{n \in \mathbb{N}} \frac{(-u)^n}{n!} \overline{Z_t(x)^n}, \quad (\text{III.3.24})$$

where $\overline{Z_t(x)^n}$ denotes $\forall n$ the right hand side of (III.3.23). Adapting the route followed in the continuum DP case (see Sec. III.2.3) we obtain a Fredholm determinant formula for $g_{t,x}^{\text{mom}}(u)$ as

$$g_{t,x}^{\text{mom}}(u) = \text{Det} \left(I + K_{t,x}^{\text{mom}} \right), \quad (\text{III.3.25})$$

with the kernel:

$$\begin{aligned} K_{t,x}^{\text{mom}}(v_1, v_2) &= \sum_{m=1}^{\infty} \int_{-\infty}^{+\infty} \frac{dk}{\pi} (-u)^m e^{-2ik(v_1-v_2)-m(v_1+v_2)} \\ &\quad \left(\frac{\Gamma(-\frac{m}{2} + \frac{\gamma}{2} - ik)}{\Gamma(\frac{m}{2} + \frac{\gamma}{2} - ik)} \right)^{\frac{t}{2}+1+x} \left(\frac{\Gamma(-\frac{m}{2} + \frac{\gamma}{2} + ik)}{\Gamma(\frac{m}{2} + \frac{\gamma}{2} + ik)} \right)^{\frac{t}{2}+1-x} \end{aligned} \quad (\text{III.3.26})$$

and $K_{t,x}^{\text{mom}} : L^2(\mathbb{R}_+) \rightarrow L^2(\mathbb{R}_+)$. Performing now the step (iii), we conjecture a formula for the Laplace transform of the Log-Gamma polymer by changing the sum over m in the above kernel to an integral on the complex plane as for a Mellin-Barnes transform. We obtain

$$g_{t,x}(u) = \overline{\exp -uZ_t(x)} = \text{Det} \left(I + K_{t,x} \right) \quad (\text{III.3.27})$$

with

$$\begin{aligned} K_{t,x}(v_1, v_2) &= \int_{-\infty}^{+\infty} \frac{dk}{\pi} \frac{-1}{2i} \int_{\mathcal{C}} \frac{ds}{\sin(\pi s)} u^s e^{-2ik(v_1-v_2)-s(v_1+v_2)} \\ &\quad \left(\frac{\Gamma(-\frac{s}{2} + \frac{\gamma}{2} - ik)}{\Gamma(\frac{s}{2} + \frac{\gamma}{2} - ik)} \right)^{\frac{t}{2}+1+x} \left(\frac{\Gamma(-\frac{s}{2} + \frac{\gamma}{2} + ik)}{\Gamma(\frac{s}{2} + \frac{\gamma}{2} + ik)} \right)^{\frac{t}{2}+1-x}, \end{aligned} \quad (\text{III.3.28})$$

where $\mathcal{C} = a + i\mathbb{R}$ with $0 < a < \min(1, \gamma)$ (note that the sum over m in (III.3.26) starts at $m = 1$) and $K_{t,x} : L^2(\mathbb{R}_+) \rightarrow L^2(\mathbb{R}_+)$.

KPZUC in the Log-Gamma polymer

Performing the asymptotic analysis of (III.3.28) we finally obtain

$$\lim_{t \rightarrow \infty} \text{Prob} \left(\frac{\log Z_t(\varphi t) + tc_\varphi}{\lambda_\varphi} < 2^{\frac{2}{3}} z \right) = F_2(z) \quad (\text{III.3.29})$$

where $F_2(z)$ is the standard GUE Tracy-Widom cumulative distribution function, and the (angle-dependent) constants are determined by the system of equations:

$$0 = \left(\frac{1}{2} + \varphi\right)\psi'\left(\frac{\gamma}{2} - k_\varphi\right) - \left(\frac{1}{2} - \varphi\right)\psi'\left(\frac{\gamma}{2} + k_\varphi\right) \quad (\text{III.3.30})$$

$$c_\varphi = \left(\frac{1}{2} + \varphi\right)\psi\left(\frac{\gamma}{2} - k_\varphi\right) + \left(\frac{1}{2} - \varphi\right)\psi\left(\frac{\gamma}{2} + k_\varphi\right) \quad (\text{III.3.31})$$

$$\lambda_\varphi = \left(-\frac{t}{8} \left(\left(\frac{1}{2} + \varphi\right)\psi''\left(\frac{\gamma}{2} - k_\varphi\right) + \left(\frac{1}{2} - \varphi\right)\psi''\left(\frac{\gamma}{2} + k_\varphi\right) \right) \right)^{\frac{1}{3}}. \quad (\text{III.3.32})$$

We recall that $\psi = \Gamma'/\Gamma$ is the diGamma function. Here k_φ , which is implicitly defined by the first equation, encodes the position of the saddle-point at $(s, k) = (0, k_\varphi)$ in the kernel (III.3.28). This formula reproduces the results obtained from the gRSK correspondence in [218] for $\varphi = \varphi^* = 0$, that is $c_{\varphi^*} = \psi(\gamma/2)$ and $\lambda_{\varphi^*} = (\frac{-t}{8}\psi''(\gamma/2))^{1/3}$, and generalize it to arbitrary angles. It is successfully confronted to numerical simulations in [4].

Other results contained in [4] (see Appendix D) are (i) additional formulae for the PDF of $Z_t(x)$ at any t, x as differences of two Fredholm determinant formulae; (ii) additional Fredholm determinant formulae for $g_{t,x}(u)$ closer to those usually encountered in the mathematical literature; (iii) the comparison at each step of our Bethe ansatz approach with the BA approach to the continuum DP using the weak-universality of the continuum DP and thus the convergence of our results to the continuum case; (iv) the study of the limit to the semi-discrete DP; (v) many checks of the above formulae.

III.3.3 Presentation of the main results of [5]

Classification of BA solvable models of a DP on \mathbb{Z}^2 : step 1

The BA solvability of the Log-Gamma polymer is not an accident and comes from the algebraic structure of the model, more precisely as we will see below, it comes from the structure of its moments (III.3.2) that satisfy the simple recursion relation $\overline{(W_t(\hat{x}))^{n+1}} = \overline{(W_t(\hat{x}))^n} / (\gamma - n - 1)$. It is a natural question to understand whether or not the Inverse-Gamma distribution is the only distribution that permits BA solvability. For this purpose in [5] we investigated the conditions of BA solvability of a DP at finite temperature on \mathbb{Z}^{210} . For this purpose we consider a ‘general’ model of DP on \mathbb{Z}^2 where (see Fig. III.4) (i) the Boltzmann weights (BW) live on the edges; (ii) the couple of BWs leading to the vertex (t, x) is noted $(u_{t,x}, v_{t,x})$ where $u_{t,x}$ is the

¹⁰By BA solvability here we mean BA solvability of the moments problem. There could be other types of BA solvability. For example the partition sum of the Log-Gamma polymer can be obtained as the limit of an observable of a BA solvable interacting particle system on \mathbb{Z} , the q-Push TASEP [221]. This BA solvability does not seem trivially related to the one studied in [4].

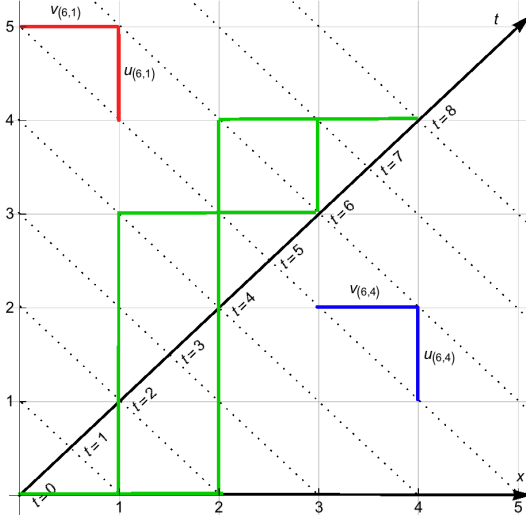


Figure III.4: General scheme for the models of directed polymer in the classification of [5]. Blue (resp. Red) : couple of correlated Boltzmann weight on edges arriving at $(t = 6, x = 1)$ (resp. $(t = 6, x = 4)$). Green: two admissible (i.e. up/right) paths for polymers with starting point $(0, 0)$ and endpoint $(8, 4)$. Figure taken from [5].

BW on the vertical edge and $v_{t,x}$ is the BW on the horizontal edge; (iii) BWs leading to different vertices are not correlated; (iv) the BWs are homogeneously distributed as $(u_{t,x}, v_{t,x}) \sim (u, v)$ with $(u, v) \in \mathbb{R}_+^2$ two (a priori correlated) positive RVs. Note that this class of models contains models with on-site Boltzmann weights since $u_{t,x}$ and $v_{t,x}$ can be correlated. For example the Log-Gamma case is reproduced taking $u_{t,x} = v_{t,x} \sim \text{Gamma}(\gamma)^{-1}$. The extent of the ‘generality’ of this class of models is precisely the one that allows us to perform the classification (see below). Other models outside this class could be considered and are not covered by our results.

In this framework the point-to-point partition sum satisfies the recursion relation

$$\begin{aligned} Z_{t=0}(x) &= \delta_{x,0} \\ Z_{t+1}(x) &= u_{t+1,x} Z_t(x) + v_{t+1,x} Z_t(x-1). \end{aligned} \quad (\text{III.3.33})$$

And this can be translated to a recursive (i.e. transfer matrix) equation for ψ_t :

$$\begin{aligned} \psi_{t=0}(x_1, \dots, x_n) &= \delta_{x_1,0} \dots \delta_{x_n,0} \\ \psi_{t+1}(x_1, \dots, x_n) &= \sum_{\{\delta_1, \dots, \delta_n\} \in \{0,1\}^n} a_{x_1, \dots, x_n}^{\delta_1, \dots, \delta_n} \psi_t(x_1 - \delta_1, \dots, x_n - \delta_n) = (T_n \psi_t)(x_1, \dots, x_n) \\ a_{x_1, \dots, x_n}^{\delta_1, \dots, \delta_n} &= \prod_{y \in \mathbb{Z}} (u)^{\sum_{i=1}^n \delta_{x_i, y} \delta_{\delta_i, 0}} (v)^{\sum_{i=1}^n \delta_{x_i, y} \delta_{\delta_i, 1}}. \end{aligned} \quad (\text{III.3.34})$$

The latter generalizes the recursion equation of the Log-Gamma case (III.3.10) and we are interested in models for which all the symmetric eigenfunctions of the transfer matrix

$$T_n \psi_\mu = \Lambda_\mu \psi_\mu \quad (\text{III.3.35})$$

can be obtained in the BA form

$$\begin{aligned}\psi_\mu(x_1, \dots, x_n) &= \tilde{\psi}_\mu(x_1, \dots, x_n) \text{ if } x_1 \leq \dots \leq x_n, \\ \tilde{\psi}_\mu(x_1, \dots, x_n) &= \sum_{\sigma \in S_n} A_\sigma \prod_{i=1}^n z_{\sigma(i)}^{x_i}.\end{aligned}\quad (\text{III.3.36})$$

The class of models we consider is precisely the one that makes (III.3.34) similar to the recursion equation for the PDF for the position of n particles moving on \mathbb{Z} with a ZRP (with parallel updates) type dynamics. In this interpretation the transfer matrix must be stochastic (i.e. conserve the probability) and the recursion equation (III.3.34) is often called the Master equation. In a recent work [222], Povolotsky managed to classify all the ZRP with parallel updates for which the transfer matrix T_n can be diagonalized by the Bethe ansatz. This construction precisely encodes the fact that ‘the n particle problem must be reminiscent of the 2 particle problem’¹¹ in the form of a deformed Binomial formula for non-commutative variables. For our purpose this classification must be slightly adapted since we are not a priori only interested in stochastic transfer matrix T_n . We will not repeat here the arguments that lead to the classification (see [5] in Appendix E), but only give the result: the spectral problem (III.3.35) is solved by the BA (III.3.36) iff the moments take the form

$$\overline{u^{n_1} v^{n_2}} = (\epsilon_1)^{n_1} (\epsilon_2)^{n_2} \frac{(\frac{\nu}{\mu}; q)_{n_1} (\mu; q)_{n_2}}{(\nu; q)_{n_1+n_2}} \frac{(q; q)_{n_1+n_2}}{(q; q)_{n_1} (q; q)_{n_2}} \frac{1}{C_{n_1+n_2}^{n_1}}, \quad (\text{III.3.37})$$

with $(\epsilon_1, \epsilon_2, q, \mu, \nu) \in \mathbb{R}^5$ and $(a; q)_n = \prod_{k=0}^{n-1} (1 - aq^k)$. In this case the symmetric eigenfunctions of T_n are obtained as (III.3.36) with the condition (which can be solved)

$$\frac{A_{\sigma \circ \tau_{ij}}}{A_\sigma} = - \frac{c + b z_{\sigma(j)} + a z_{\sigma(i)} z_{\sigma(j)} - z_{\sigma(i)}}{c + b z_{\sigma(i)} + a z_{\sigma(i)} z_{\sigma(j)} - z_{\sigma(j)}}. \quad (\text{III.3.38})$$

with

$$\mathbf{a} = \frac{\overline{u^2} - (\overline{u})^2}{(\overline{u})(\overline{v})} \quad \mathbf{b} = \frac{2\overline{uv} - (\overline{u})(\overline{v})}{(\overline{u})(\overline{v})} \quad \mathbf{c} = \frac{\overline{v^2} - (\overline{v})^2}{(\overline{u})(\overline{v})}. \quad (\text{III.3.39})$$

Classification of BA solvable models of DP on \mathbb{Z}^2 : step 2

It remains to understand whether or not (III.3.37) are indeed the moments of positive random variables for some choice of the parameters. In ([5]) we consider, for $(\epsilon_1, \epsilon_2, q, \mu, \nu) \in \mathbb{R}^5$ fixed and $x \in \mathbb{R}$

$$P(x) = \overline{(u + xv)^2}^c. \quad (\text{III.3.40})$$

If (III.3.37) are moments of real variables, then $P(x)$ must be positive $\forall x \in \mathbb{R}$ (and maybe 0 at some x_c if u and v are correlated as $u + x_c v = 0$). $P(x)$ being a degree 2 polynomial, its root can easily be studied and we arrive to the conclusion that the

¹¹A feature that was not present in the continuum DP model where there are only two-bodies interactions.

only possibility for (III.3.37) to be the moments of real variables is to consider the degenerate limit

$$\nu = q^{\alpha+\beta} \quad , \quad \mu = q^\beta \quad , \quad q \rightarrow 1 . \quad (\text{III.3.41})$$

Taking this limit using $(q^a; q)_n \simeq_{q \rightarrow 1} (1-q)^n (a)_n$ (where $(a)_n = \prod_{k=0}^{n-1} (a+k)$) we thus restricted our search for integrable models of DP to those with moments as

$$\overline{u^{n_1} v^{n_2}} = (\epsilon_1)^{n_1} (\epsilon_2)^{n_2} \frac{(\alpha)_{n_1} (\beta)_{n_2}}{(\alpha + \beta)_{n_1+n_2}} . \quad (\text{III.3.42})$$

A combinatorial identity shows that in this case $\forall n, \overline{(u/\epsilon_1 + v/\epsilon_2)^n} = 1$ and the BWs are thus strongly correlated as $u/\epsilon_1 + v/\epsilon_2 = 1$. At this point we cannot obtain more general results and only exhibit models for which the moments are given by (III.3.42). We consider both (i) models for which the moments of the BWs are indeed given by (III.3.42) $\forall (n_1, n_2)$; (ii) models for which only a finite number of moments exist, namely for $n_1 + n_2 \leq n_{\max}$ with some $n_{\max} \in \mathbb{N}^*$. In the second case (inspired by the Log-Gamma case) the BA a priori only allows us to compute the first n_{\max} moments of the partition sum. First, this classification indeed contains the Log-Gamma case as a degenerate limit: taking $(\epsilon_1, \epsilon_2) = (+1, -1)$, $\alpha + \beta = 1 - \gamma$ with $\gamma \geq 0$, $\beta \rightarrow \infty$ and rescaling the Boltzmann weights as (implying a corresponding rescaling of the partition sum) $u = \beta u^{LG}$, $v = \beta v^{LG}$ we obtain

$$((u^{LG})^{n_1}, (v^{LG})^{n_2}) = \lim_{\beta \rightarrow \infty} \frac{1}{\beta^{n_1+n_2}} (-1)^{n_2} \frac{(1-\gamma-\beta)_{n_1} (\beta)_{n_2}}{(1-\gamma)_{n_1+n_2}} = \frac{(-1)^{n_1+n_2}}{(1-\gamma)_{n_1+n_2}} , \quad (\text{III.3.43})$$

which indeed reproduces the moments of the Log-Gamma polymer (III.3.2). In between our work on the Log-Gamma polymer [4] and this work [5], two new exactly solvable models of DP on \mathbb{Z}^2 were obtained: the Strict-Weak (SW) polymer and the Beta polymer. Both were shown to be solvable by BA in [219] and [224]. In the SW case Boltzmann weights are given by $v^{SW} = 1$ and $u^{SW} \sim \text{Gamma}(\alpha)$. It is obtained from our framework by taking the limit $(\epsilon_1, \epsilon_2) = (1, 1)$ and $\beta \rightarrow \infty$ with $\alpha > 0$ fixed and $u^{SW} = \beta u$, $v^{SW} = v$. Indeed in this limit the moments are:

$$((u^{SW})^{n_1}, (v^{SW})^{n_2}) = \lim_{\beta \rightarrow \infty} \beta^{n_1} \frac{(\alpha)_{n_1} (\beta)_{n_2}}{(\alpha + \beta)_{n_1+n_2}} = (\alpha)_{n_1} . \quad (\text{III.3.44})$$

This corresponds to the distribution described above. In the Beta polymer the Boltzmann weights are distributed as $u^B + v^B = 1$ and $u \in [0, 1]$ is a Beta random variable with parameters (α, β) . Its PDF is

$$u \sim \text{Beta}(\alpha, \beta) \iff p(u) = \frac{\Gamma(\alpha + \beta)}{\Gamma(\alpha)\Gamma(\beta)} u^{\alpha-1} (1-u)^{\beta-1} . \quad (\text{III.3.45})$$

and the moments are as above with $(\epsilon_1, \epsilon_2) = (1, 1)$. We will come back to this model in the next section. Finally in [5] we introduce a new exactly solvable model of DPs on \mathbb{Z}^2 , the Inverse-Beta polymer. In this model $(\epsilon_1, \epsilon_2) = (1, -1)$, $v = u - 1$ and u is distributed as the inverse of a Beta random variable: $u \sim \text{Beta}(\gamma, \beta)^{-1} > 1$. The moments are as above with $\alpha = 1 - \beta - \gamma$. In the limit $\beta \rightarrow \infty$, this model converges

to the Log-Gamma polymer, while in the limit $\gamma \rightarrow \infty$ it converges to the Strict-Weak model (this limit is different from the one mentioned above, which corresponds to the degeneration from the Beta to the Strict-Weak polymer). In [5] we attempted a more systematic study of possible models of DPs, but it remains inconclusive. In any case, for now, all exactly solvable models of DPs on \mathbb{Z}^2 are thus BA solvable and can be regrouped using our notations as in Fig. III.5. Note that in Fig. III.5 we also include the symmetrized version (with respect to the diagonal of \mathbb{Z}^2) of the Inverse-Beta and Strict-Weak polymer which are both anisotropic models that favor one edge. The rest of this section is devoted to the Inverse-Beta polymer, which thus generalizes both the Log-Gamma and Strict-Weak polymer.

BA solution of the Inverse-Beta polymer

In the Inverse-Beta polymer, the moments of the Boltzmann weights are well defined for $(s_1, s_2) \in \mathbb{C}^2$ with $\text{Re}(s_1 + s_2) \leq \gamma$ and $\text{Re}(s_2) > -\beta$ and are given by

$$\overline{u^{s_1} v^{s_2}} = \frac{\Gamma(\gamma + \beta) \Gamma(\gamma - s_1 - s_2) \Gamma(\beta + s_2)}{\Gamma(\gamma) \Gamma(\beta) \Gamma(\gamma + \beta - s_1)}. \quad (\text{III.3.46})$$

The replica Bethe ansatz approach to this model suffers from exactly the same problem as the one for the Log-Gamma case: only a finite number of integer moments of the partition sum exist. It is however possible to use the same strategy as for the Log-Gamma case. The two approaches are actually remarkably similar: defining again $\bar{c} = 4/(\gamma - 1)$, we showed in [5] that *the eigenfunctions of the transfer matrix T_n in the Log-Gamma and Inverse-Beta case are equal*. A simple incarnation of this remarkable property is that the quotient of two amplitudes of the Bethe wave-function in (III.3.38), which controls completely the structure of the wave-function and the Bethe equations, does not depend on β . In particular they are equal to those in the Log-Gamma limit $\beta \rightarrow \infty$. We can thus use the same results as in the Log-Gamma case: string solution at large L , Gaudin formula... The only things that differs is the eigenvalue associated with the unit translation in time: the Inverse-Beta polymer is an anisotropic model with $v = u - 1$, and the vertical direction is thus favored in this model. In [5] we showed that this change leads to the following formula for the integer moments of the DP partition sum:

$$\begin{aligned} \overline{Z_t(x)^n} &= n! \frac{\Gamma(\gamma)}{\Gamma(\gamma - n)} \sum_{n_s=1}^n \frac{1}{n_s!} \sum_{(m_1, \dots, m_{n_s})_n} \prod_{j=1}^{n_s} \int_{-\infty}^{+\infty} \frac{dk_j}{2\pi} \prod_{1 \leq i < j \leq n_s} \frac{4(k_i - k_j)^2 + (m_i - m_j)^2}{4(k_i - k_j)^2 + (m_i + m_j)^2} \\ &\prod_{j=1}^{n_s} \frac{1}{m_j} \left(\frac{\Gamma(-\frac{m_j}{2} + \frac{\gamma}{2} - ik_j)}{\Gamma(\frac{m_j}{2} + \frac{\gamma}{2} - ik_j)} \right)^{1+x} \left(\frac{\Gamma(-\frac{m_j}{2} + \frac{\gamma}{2} + ik_j)}{\Gamma(\frac{m_j}{2} + \frac{\gamma}{2} + ik_j)} \right)^{1-x+t} \left(\frac{\Gamma(\beta + ik_j + \frac{\gamma}{2} + \frac{m_j}{2})}{\Gamma(\beta + ik_j + \frac{\gamma}{2} - \frac{m_j}{2})} \right)^t, \end{aligned} \quad (\text{III.3.47})$$

which is valid for $n \leq \gamma$ and very similar to the corresponding formula for the Log-Gamma case (III.3.23). The first factor $\frac{\Gamma(\gamma)}{\Gamma(\gamma - n)}$, which comes out of the structure of the BA, forbids to express $\overline{e^{-uZ_t(x)}}$ as a Fredholm determinant. As in the Log-Gamma case we thus consider a partition sum with a BW added at the origin:

$$\tilde{Z}_t(x) = w_{00} Z_t(x), \quad (\text{III.3.48})$$

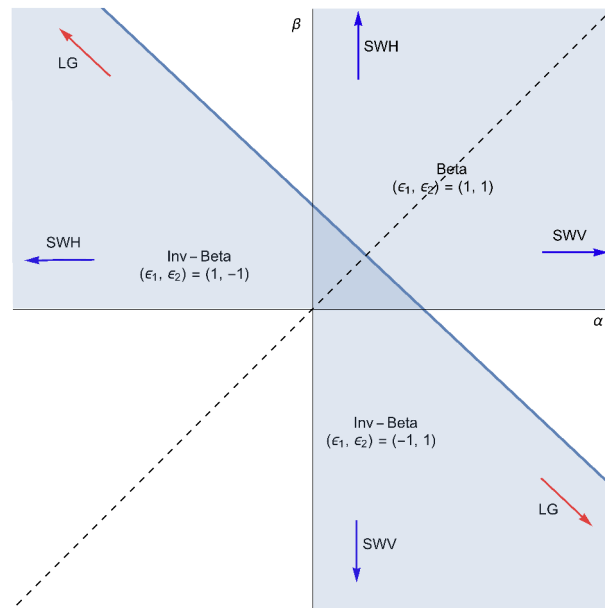


Figure III.5: Classification of exactly solvable finite temperature models of DPs on \mathbb{Z}^2 following the notations of [5]. The dashed line represents the axis of symmetry $\alpha \leftrightarrow \beta$, or equivalently the symmetry between vertical and horizontal edges. The blue line indicates the line $\alpha + \beta = 1$ or equivalently $\gamma = 1 - (\alpha + \beta) = 0$. Limiting polymer models are indicated by red arrows for the log-Gamma (LG) and blue arrows for the Strict-Weak (with weights either on horizontal edges (SWH) or vertical edges (SWV)). We also emphasize the values of (ϵ_1, ϵ_2) which corresponds to the polymer considered. Notice that the region $\alpha > 0, \beta > 0$ and $\gamma < 1$ is a region of coexistence of the Inverse-Beta and the Beta polymer, only distinguished by the value of (ϵ_1, ϵ_2) . Figure taken from [5].

where $w_{00} \sim \text{Gamma}(\gamma)^{-1}$ is independent of $Z_t(x)$. The moments of $\tilde{Z}_t(x)$ are given by (III.3.47), but without the factor $\frac{\Gamma(\gamma)}{\Gamma(\gamma-n)}$. Following the same route as in the Log-Gamma case we express the moment generating function of $\tilde{Z}_t(x)$ as a Fredholm determinant. Using a Mellin-Barnes transform inside the associated kernel, we conjecture a formula for the Laplace transform $g_{tx}(u) = \text{Det}(I + K_{tx})$ with

$$K_{t,x}(v_1, v_2) = \int_{-\infty}^{+\infty} \frac{dk}{\pi} \frac{-1}{2i} \int_C \frac{ds}{\sin(\pi s)} u^s e^{-2ik(v_1-v_2)-s(v_1+v_2)} \quad (\text{III.3.49})$$

$$\left(\frac{\Gamma(-\frac{s}{2} + \frac{\gamma}{2} - ik)}{\Gamma(\frac{s}{2} + \frac{\gamma}{2} - ik)} \right)^{1+x} \left(\frac{\Gamma(-\frac{s}{2} + \frac{\gamma}{2} + ik)}{\Gamma(\frac{s}{2} + \frac{\gamma}{2} + ik)} \right)^{1-x+t} \left(\frac{\Gamma(\beta + ik + \frac{\gamma}{2} + \frac{s}{2})}{\Gamma(\beta + ik + \frac{\gamma}{2} - \frac{s}{2})} \right)^t,$$

where $C = a + i\mathbb{R}$ with $0 < a < \min(1, \gamma)$ and $K_{t,x} : L^2(\mathbb{R}_+) \rightarrow L^2(\mathbb{R}_+)$. Performing the asymptotic analysis of this formula we obtain TW-GUE fluctuations in the Inverse-Beta polymer:

$$\lim_{t \rightarrow \infty} \text{Prob} \left(\frac{\log Z_t((1/2 + \varphi)t) + tc_\varphi}{\lambda_\varphi} < 2^{\frac{2}{3}} z \right) = F_2(z), \quad (\text{III.3.50})$$

where the (φ -dependent) constants are determined by the system of equations:

$$0 = \left(\frac{1}{2} + \varphi\right)\psi'\left(\frac{\gamma}{2} - k_\varphi\right) - \left(\frac{1}{2} - \varphi\right)\psi'\left(\frac{\gamma}{2} + k_\varphi\right) + \psi'\left(\beta + \frac{\gamma}{2} + k_\varphi\right), \quad (\text{III.3.51})$$

$$c_\varphi = \left(\frac{1}{2} + \varphi\right)\psi\left(\frac{\gamma}{2} - k_\varphi\right) + \left(\frac{1}{2} - \varphi\right)\psi\left(\frac{\gamma}{2} + k_\varphi\right) - \psi\left(\beta + \frac{\gamma}{2} + k_\varphi\right),$$

$$\lambda_\varphi = \left(-\frac{t}{8} \left(\left(\frac{1}{2} + \varphi\right)\psi''\left(\frac{\gamma}{2} - k_\varphi\right) + \left(\frac{1}{2} - \varphi\right)\psi''\left(\frac{\gamma}{2} + k_\varphi\right) - \psi''\left(\beta + \frac{\gamma}{2} + k_\varphi\right) \right)\right)^{\frac{1}{3}} \dots$$

These cannot be solved in full generality, except for the optimal angle φ^* , defined by $\partial_\varphi c_\varphi = 0$ for which we find

$$\varphi^* = -\frac{1}{2} \frac{\psi'(\beta + \gamma/2)}{\psi'(\gamma/2)} < 0$$

$$c^* = c_{\varphi^*} = \psi(\gamma/2) - \psi(\beta + \gamma/2)$$

$$\lambda_{\varphi^*} = \left(\frac{t}{8} (\psi''(\beta + \gamma/2) - \psi''(\gamma/2))\right)^{1/3}. \quad (\text{III.3.52})$$

The optimal angle is the angle of maximum probability chosen by the endpoint of the polymer with one end free to move on the line. Note that its value is non-trivial (it is different from the value expected in an averaged environment). This thus generalizes the explicit results obtained in the Log-Gamma case where $\varphi^* = 0$ (note that here $\varphi^* \rightarrow_{\beta \rightarrow \infty} 0$ and $\varphi^* \rightarrow_{\gamma \rightarrow \infty} -1/2$, corresponding to the Log-Gamma and Strict-Weak limits).

Zero-temperature limit of the Inverse-Beta polymer: Bernoulli-Exponential polymer

As we saw in Sec. III.2.4, the $\gamma \rightarrow 0$ limit of the Log-Gamma polymer leads to LPP with exponential waiting times. Similarly, the Inverse-Beta polymer admits a zero temperature limit obtained by setting $\gamma = \epsilon\gamma'$, $\beta = \epsilon\beta'$. In this limit one shows

[5] that the rescaled random energies of the model $(\mathcal{E}^u, \mathcal{E}^v) = (-\epsilon \log(u), -\epsilon \log(v))$ converge in law to

$$(\mathcal{E}^u, \mathcal{E}^v) \sim_{\epsilon \rightarrow 0} (-\zeta E_{\gamma'}, (1 - \zeta)E_{\beta'} - \zeta E_{\gamma'}) = (\mathcal{E}'_u, \mathcal{E}'_v), \quad (\text{III.3.53})$$

where ζ is a Bernoulli random variable of parameter $p = \beta' / (\gamma' + \beta')$, $E_{\gamma'}$ and $E_{\beta'}$ are exponential random variables of parameter $\gamma' > 0$ and $\beta' > 0$, independent of ζ (the PDF of exponential RVs was given in (III.2.29) and the Bernoulli RV is by definition 1 with probability p). The optimal energy in the model satisfies the recursion

$$\mathbf{E}_{t+1}(x) = \min(\mathbf{E}_t(x) + \mathcal{E}_{t+1}^u(x), \mathbf{E}_t(x-1) + \mathcal{E}_{t+1}^v(x)) . \quad (\text{III.3.54})$$

And the initial condition is $\mathbf{E}_t(x=0) = 0$ and $\mathbf{E}_t(x) = -\infty$ for $x \neq 0$. In the limit $\beta' \rightarrow \infty$ the model corresponds to LPP with exponential waiting times, while in the limit $\gamma' \rightarrow \infty$ it converges to the zero temperature limit of the Strict-Weak polymer, which is a model of FPP with exponentially distributed waiting times on horizontal edges only. This model thus remarkably interpolates between a model of first and last passage percolation on \mathbb{Z}^2 . Based on our exact results for the Inverse-Beta polymer, we obtain various exact results for this zero-temperature model. In particular we show that $\text{Prob}(\mathbf{E}_t(x) > r) = \text{Det}(I + K_{tx}^{T=0})$ with

$$K_{t,x}^{T=0}(v_1, v_2) = - \int_{-\infty}^{+\infty} \frac{dk}{\pi} \int_{\tilde{C}} \frac{ds}{2i\pi s} e^{sr - 2ik(v_1 - v_2) - s(v_1 + v_2)} \quad (\text{III.3.55})$$

$$\left(\frac{\frac{s}{2} + \frac{\gamma'}{2} - ik}{-\frac{s}{2} + \frac{\gamma'}{2} - ik} \right)^{1+x} \left(\frac{\frac{s}{2} + \frac{\gamma'}{2} + ik}{-\frac{s}{2} + \frac{\gamma'}{2} + ik} \right)^{1-x+t} \left(\frac{\beta' + ik + \frac{\gamma'}{2} - \frac{s}{2}}{\beta' + ik + \frac{\gamma'}{2} + \frac{s}{2}} \right)^t ,$$

where $\tilde{C} = a + i\mathbb{R}$ with $0 < a < \gamma'$ and $K_{t,x}^{T=0} : L^2(\mathbb{R}_+) \rightarrow L^2(\mathbb{R}_+)$. The asymptotic analysis then leads to Tracy-Widom fluctuations for the optimal energy in this zero temperature model:

$$\lim_{t \rightarrow \infty} \text{Prob} \left(\frac{\mathbf{E}_t(x = (1/2 + \varphi)t) - t\tilde{c}_\varphi}{\tilde{\lambda}_\varphi} > -2^{\frac{2}{3}} \tilde{z} \right) = F_2(\tilde{z}) \quad (\text{III.3.56})$$

with

$$0 = \frac{(\frac{1}{2} + \varphi)}{(\frac{\gamma'}{2} - \tilde{k}_\varphi)^2} - \frac{(\frac{1}{2} - \varphi)}{(\frac{\gamma'}{2} + \tilde{k}_\varphi)^2} + \frac{1}{(\beta' + \frac{\gamma'}{2} + \tilde{k}_\varphi)^2} , \quad (\text{III.3.57})$$

$$\tilde{c}_\varphi = -\frac{(\frac{1}{2} + \varphi)}{\frac{\gamma'}{2} - \tilde{k}_\varphi} - \frac{(\frac{1}{2} - \varphi)}{\frac{\gamma'}{2} + \tilde{k}_\varphi} + \frac{1}{\beta' + \frac{\gamma'}{2} + \tilde{k}_\varphi} , \quad (\text{III.3.58})$$

$$\tilde{\lambda}_\varphi = \left(\frac{t}{8} \left(\frac{(1+2\varphi)}{(\frac{\gamma'}{2} - \tilde{k}_\varphi)^3} + \frac{(1-2\varphi)}{(\frac{\gamma'}{2} + \tilde{k}_\varphi)^3} - \frac{2}{(\beta' + \frac{\gamma'}{2} + \tilde{k}_\varphi)^3} \right) \right)^{\frac{1}{3}} . \quad (\text{III.3.59})$$

In this case the system can be solved exactly since the equation for \tilde{k}_φ is a quartic equation.

Let us conclude this section by mentioning that other results and many details are given in [5] (see Appendix E). In particular we conjecture interesting n -fold integral formulae for the Laplace transform of the partition sum/optimal energy PDF of the Inverse-Beta/Bernoulli-Exponential model that are reminiscent of those obtained using the gRSK/RSK correspondence for the Log-Gamma/LPP model.

III.3.4 Presentation of the main results of [6]

The Beta Polymer and its TD-RWRE interpretation

The Beta polymer is a BA solvable model of DP on \mathbb{Z}^2 introduced in [224] and included in the classification of [5]. In [224] the authors studied the half-line to point partition sum and our initial motivation was to use the results of [5] to study the point to point partition sum. The Beta polymer is, however, a very peculiar model and in doing so we have notably unveiled a novel fluctuation behavior (see below). The Beta polymer has two parameters $(\alpha, \beta) \in \mathbb{R}_+^2$ and its random BWs are correlated as $u + v = 1$ with $u \sim \text{Beta}(\alpha, \beta)$ as in (III.3.45). Thanks to these correlations and as already noticed in [224], given a random environment specified by a drawing of the $(u_{tx}, v_{tx} = 1 - u_{tx})$, the partition sum of the point to point Beta polymer can also be interpreted as a transition probability for a random walk on \mathbb{Z} in a time-dependent random environment (TD-RWRE). Introducing the time coordinate t and the hopping probabilities

$$t = -t \quad , \quad p_{t,x} = u_{t,x} \in [0, 1] \quad , \quad (\text{III.3.60})$$

the TD-RWRE is defined as follows: denoting X_t the position of the particle at time t , the particle performs a RW on \mathbb{Z} with the following transition probabilities

$$\begin{aligned} X_t \rightarrow X_{t+1} = X_t & \text{ with probability } p_{t,X_t} = u_{t=-t,X_t} \quad , \\ X_t \rightarrow X_{t+1} = X_t - 1 & \text{ with probability } 1 - p_{t,X_t} = v_{t=-t,X_t} \quad . \end{aligned} \quad (\text{III.3.61})$$

In the RWRE language, the point to point partition sum of the Beta polymer $Z_t(x)$ is the probability, given that a particle starts at position x at time $t = -t \leq 0$, that it arrives at position 0 at time $t = t = 0$:

$$Z_t(x) = P(X_0 = 0 | X_{t=-t} = x) \quad . \quad (\text{III.3.62})$$

In this interpretation, the recursion equation for the polymer partition sum (III.3.33) is a Backward equation for the probability $P(X_0 = 0 | X_t = x)$:

$$\begin{aligned} P(X_0 = 0 | X_{t-1} = x) &= p_{t-1,x} P(X_0 = 0 | X_t = x) + (1 - p_{t-1,x}) P(X_0 = 0 | X_t = x - 1) \\ P(0, 0 | 0, x) &= \delta_{x,0} \quad . \end{aligned} \quad (\text{III.3.63})$$

Note finally that the starting point of the polymer corresponds to the endpoint of the RW and vice-versa.

Definition of the optimal direction

The optimal direction can be defined by considering the *annealed* PDF, defined as

$$P_{\text{ann}}(X_0 = 0 | X_{-t} = x) := \overline{P(X_0 = 0 | X_{-t} = x)} = \overline{Z_t(x)} \quad , \quad (\text{III.3.64})$$

which is the transition PDF for a RW defined as above with $p_{t,x}$ replaced by its average: $p_{t,x} \rightarrow \overline{p_{t,x}} = \bar{u} = \alpha / (\alpha + \beta)$. By translational invariance of the averaged environment we have $P_{\text{ann}}(X_0 = 0 | X_{-t} = x) = P_{\text{ann}}(X_t = -x | X_0 = 0) = \overline{Z_t(x)} = \frac{\alpha^x \beta^{t-x}}{(\alpha + \beta)^t}$. In

general, the annealed PDF decreases at large time in a given direction as, scaling $x = (1/2 + \varphi t)$,

$$\overline{Z_t(x = (1/2 + \varphi t))} = \sqrt{\frac{2}{\pi t(1 - 4\varphi^2)}} \left(\frac{2}{\sqrt{1 - 4\varphi^2}} \left(\frac{1 - 2\varphi}{2\varphi + 1} \right)^\varphi \frac{r^{(1/2 + \varphi)}}{1 + r} \right)^t \left(1 + O(1/\sqrt{t}) \right). \quad (\text{III.3.65})$$

where we have introduced the asymmetry parameter

$$r = \beta/\alpha \in \mathbb{R}_+. \quad (\text{III.3.66})$$

It is easily seen that $\overline{Z_t(x = (1/2 + \varphi t))}$ decreases exponentially in every direction, except at its maximum $\varphi = \varphi_{opt}(r)$ which defines the *optimal angle*

$$\varphi_{opt}(r) = \frac{r - 1}{2(r + 1)} \in] - 1/2, 1/2[, \quad (\text{III.3.67})$$

The optimal angle thus appears as the most probable space-time direction taken by a RW in an averaged environment. Below we will see that the fluctuations of $Z_t(x)$ will depend on the chosen direction and we will mainly consider the *large deviations regime*, corresponding to the scaling $x = (1/2 + \varphi t)$ with $\varphi \neq \varphi_{opt}(r)$, and the *diffusive regime around the optimal direction*, corresponding to the scaling $x = (1/2 + \varphi_{opt}(r)t) + \kappa\sqrt{t}$ where (III.3.65) takes a Gaussian form.

Bethe ansatz solution of the Beta polymer

In [2] we show that, defining $c = \frac{4}{\alpha + \beta} > 0$ and

$$z_j = e^{i\lambda_j} \quad , \quad \tilde{t}_j = -i \cot\left(\frac{\lambda_j}{2}\right) = \frac{z_j + 1}{z_j - 1} \quad , \quad z_j = -\frac{1 + \tilde{t}_j}{1 - \tilde{t}_j} \quad , \quad (\text{III.3.68})$$

the eigenfunctions and the Bethe equations of the Beta polymer are identical to those of the Log-Gamma and Inverse-Beta polymer (III.3.12)-(III.3.14), up to the change $t_i \rightarrow \tilde{t}_i$ and $\bar{c} \rightarrow c$. However, in [2], we show that this change has important consequences: the string solutions are not stable and $c > 0$ can be interpreted as a repulsive interaction parameter. In the large L limit the replica thus behave as free particles and do not form bound states. The repulsive nature of the model is interpreted as a consequence of the TD-RWRE nature of the model. In this case we therefore obtain a formula for the moments of the partition sum which is simpler (compared to (III.3.23) and (III.3.47)) and does not contain a summation over string states:

$$\overline{Z_t(x)^n} = (-1)^n \frac{\Gamma(\alpha + \beta + n)}{\Gamma(\alpha + \beta)} \quad (\text{III.3.69})$$

$$\prod_{j=1}^n \int_{-\infty}^{+\infty} \frac{dk_j}{2\pi} \prod_{1 \leq i < j \leq n} \frac{(k_i - k_j)^2}{(k_i - k_j)^2 + 1} \prod_{j=1}^n \frac{(ik_j + \frac{\beta - \alpha}{2})^t}{(ik_j + \frac{\alpha + \beta}{2})^{1+x} (ik_j - \frac{\alpha + \beta}{2})^{1-x+t}} .$$

Making the link with the nested contour integral approach to BA used in [224] we also obtain a formula for the multi-point moments: for $0 \leq x_1 \leq \dots \leq x_n$:

$$\overline{Z_t(x_1) \cdots Z_t(x_n)} = (-1)^n \frac{\Gamma(\alpha + \beta + n)}{\Gamma(\alpha + \beta)} \quad (\text{III.3.70})$$

$$\prod_{j=1}^n \int_{\mathbb{R}} \frac{dk_j}{2\pi} \prod_{1 \leq i < j \leq n} \frac{k_i - k_j}{k_i - k_j + i} \prod_{j=1}^n \frac{(ik_j + \frac{\beta - \alpha}{2})^t}{(ik_j + \frac{\alpha + \beta}{2})^{1+x_j} (ik_j - \frac{\alpha + \beta}{2})^{1-x_j+t}} .$$

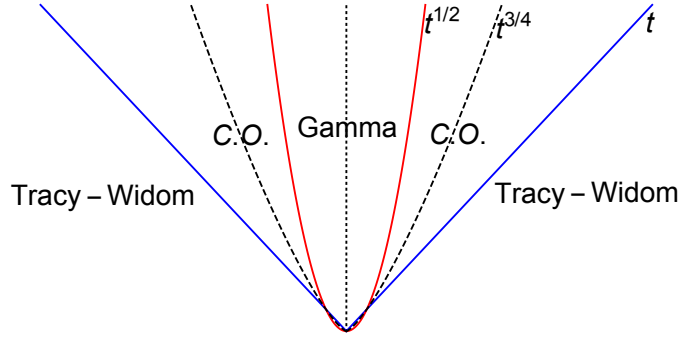


Figure III.6: The different regimes of sample to sample fluctuations of the PDF in the Beta TDRWRE problem around the optimal direction (indicated by a dotted line) for different scaling of the deviation with respect to the optimal direction $\check{x} = x - (1/2 + \varphi_{opt})t$. In the diffusive regime $\check{x} \sim \sqrt{t}$ the fluctuations of the PDF are Gamma distributed. In the large deviations regime $\check{x} \sim t$, fluctuations of the logarithm of the PDF are distributed according to the GUE Tracy-Widom distribution with exponents in agreement with the usual KPZ universality expected in point to point directed polymers problem. These two regimes are connected by a cross-over regime (C.O.) at a scale $\check{x} \sim t^{3/4}$. Figure taken from [6].

Cauchy-type Fredholm determinant formula

A further simplification that is specific to the Beta polymer is that, since the Boltzmann weights are bounded, the moments of the partition sum $\overline{(Z_t(x))^n}$ do not grow too fast in this case and indeed determine unambiguously the distribution of $Z_t(x)$. As in the Inverse-Beta case, the first factor $\frac{\Gamma(\alpha+\beta+n)}{\Gamma(\alpha+\beta)}$ in front of (III.3.69) forbids to express the LT of $Z_t(x)$ as a Fredholm determinant. For this reason we consider the generating function $g_{t,x}(u) = \sum_{n=0}^{\infty} \frac{(-u)^n}{n!} Z_n$ with $Z_n = \frac{\Gamma(\alpha+\beta)}{\Gamma(\alpha+\beta+n)} \overline{(Z_t(x))^n}$. We obtain several equivalent Fredholm determinant formulae for $g_{t,x}(u)$, and notably

$$g_{t,x}(u) = \text{Det} \left(I + u \hat{K}_{t,x} \right) \tag{III.3.71}$$

with the kernel $\hat{K}_{t,x} : L^2(\mathbb{R}) \rightarrow L^2(\mathbb{R})$:

$$\hat{K}_{t,x}(q_1, q_2) = -\frac{2}{\pi} \frac{(1 + iq_1(\alpha - \beta))^{-x+t}}{(1 + iq_1(\alpha + \beta))^{1-x+t}} \frac{(1 + iq_2(\alpha - \beta))^x}{(1 - iq_2(\alpha + \beta))^{1+x}} \frac{1}{2 + i(q_2^{-1} - q_1^{-1})} . \tag{III.3.72}$$

The procedure to go from $g_{t,x}(u)$ to the PDF of $Z_t(x)$ is discussed in [6]. Note that compared to the Fredholm-determinant formula presented up to now (III.2.72)-(III.3.28)-(III.3.49), (III.3.72) has the distinguishing feature that the Laplace Transform variable appears simply linearly in front of the kernel. This type of Fredholm determinant formula is known in the literature as Cauchy-type formulae and first appeared in the KPZ-related literature in the work of Tracy and Widom on the ASEP [225].

Asymptotic analysis in the optimal direction

In [6] we show that

$$\mathcal{Z}_t(\kappa) = \alpha \sqrt{2\pi r t} e^{\frac{(r+1)^2}{2r} \kappa^2} Z_t \left(x = \left(\frac{1}{2} + \varphi_{opt}(r) \right) t + \kappa \sqrt{t} \right), \quad (\text{III.3.73})$$

converges at fixed t , in the large time limit to a process, constant in κ , with marginal distribution a Gamma distribution with parameter $\alpha + \beta$

$$\mathcal{Z}_\infty(\kappa) \sim \text{Gamma}(\alpha + \beta). \quad (\text{III.3.74})$$

From the point of view of DPs on \mathbb{Z}^2 , this result can be thought of as a breaking of KPZUC in the optimal direction, due to the presence of an additional conservation law, namely the conservation of the probability, encoded in the correlations of the random BWs as $u + v = 1$. From the point of view of TD-RWRE this result shows that, in a given environment, $P(X_0 = 0 | X_{t-1} = x = (1/2 + \varphi_{opt}(r))t + \kappa\sqrt{t})$ converges to a Gaussian distribution, which is modulated by a κ (= starting-point) independent Gamma distributed RV. The origin of the Gamma distribution can be traced back to the first factor in (III.3.69), which thus plays a very important role here.

Asymptotic analysis in the large deviations regime

To perform the asymptotic analysis in the large deviations regime we find that our formula (III.3.71)-(III.3.72) is not adapted. This was already remarked on the Cauchy-type Fredholm determinant formula obtained by Tracy and Widom in [225] and performing the asymptotic analysis required to obtain another Fredholm determinant representation [226]. The Beta polymer is thus an example of a model where performing the asymptotic analysis using Cauchy-type formulae is well adapted to the study of the diffusive regime of the TD-RWRE. For the large deviations regime, we thus first obtain a *formal* Fredholm determinant formula for $g_{t,x}(u)$: $g_{t,x}(u) = \text{Det} \left(I + \check{K}_{t,x} \right)$ with

$$\begin{aligned} \check{K}_{t,x}(v_1, v_2) = & \int_L \frac{dk-1}{\pi} \int_C \frac{ds}{2i} \frac{ds}{\sin(\pi s)} u^s e^{-2ik(v_1-v_2)-s(v_1+v_2)} \\ & \left(\frac{\Gamma(-\frac{s}{2} + \alpha + \beta + ik)}{\Gamma(\frac{s}{2} + \alpha + \beta + ik)} \right)^{1+x} \left(\frac{\Gamma(-\frac{s}{2} + ik)}{\Gamma(\frac{s}{2} + ik)} \right)^{1-x+t} \left(\frac{\Gamma(\beta + ik + \frac{s}{2})}{\Gamma(\beta + ik - \frac{s}{2})} \right)^t, \end{aligned} \quad (\text{III.3.75})$$

which now appears rather similar to those for the Log-Gamma and Inverse-Beta polymer (III.3.28)-(III.3.49) (see [6] for the precise sense in which this formula is formal). Performing the asymptotic analysis of (III.3.75) we obtain, for $\varphi_{opt}(r) < \varphi < 1/2$ (the other case being obtained by symmetry)

$$\lim_{t \rightarrow \infty} \text{Prob} \left(\frac{\log Z_t((1/2 + \varphi)t) + tc_\varphi}{\lambda_\varphi} < 2^{\frac{2}{3}} z \right) = F_2(z), \quad (\text{III.3.76})$$

with

$$\varphi = \frac{\psi'(\beta + k_\varphi) - \frac{1}{2}(\psi'(k_\varphi) + \psi'(\alpha + \beta + k_\varphi))}{\psi'(\alpha + \beta + k_\varphi) - \psi'(k_\varphi)}, \quad (\text{III.3.77})$$

$$c_\varphi = -G'_\varphi(k_\varphi) = \left(\varphi + \frac{1}{2} \right) \psi(k_\varphi + \alpha + \beta) - \psi(k_\varphi + \beta) + \left(\frac{1}{2} - \varphi \right) \psi(k_\varphi),$$

$$\frac{8\lambda_\varphi^3}{t} = G''''_\varphi(k_\varphi) = - \left(\varphi + \frac{1}{2} \right) \psi''(k_\varphi + \alpha + \beta) + \psi''(k_\varphi + \beta) - \left(\frac{1}{2} - \varphi \right) \psi''(k_\varphi).$$

From the point of view of DPs, this result shows that KPZUC is restored away from the optimal direction of the TD-RWRE. The value of c_φ was already determined in [224] using a general theorem of [227], the value of λ_φ was, however, still unknown. Our result (III.3.77) actually appears equivalent to the one of [224] in the large deviations regime if one replaces the point to point partition sum in (III.3.76) by the half-line to point partition sum that is studied in [224].

Let us conclude this section by mentioning other results obtained in [6] (see Appendix F) (i) alternative Fredholm determinant formulae for $g_{t,x}(u)$, in particular a formula that gives a rigorous meaning to the formal formula (III.3.75); (ii) relations of our approach with the nested contour integral approach to the Bethe ansatz; (iii) formula for the PDF of $Z_t(x)$ at any time; (iv) a discussion of the crossover between the diffusive region and the large deviations regime, identified with deviations from the optimal direction of order $t^{3/4}$ (see Fig. III.6); (v) an extensive numerical study of the validity of our results using simulations of the Beta polymer.

III.3.5 Presentation of the main results of [7]

In Sec. III.2.2 we recalled that the Log-Gamma polymer was first introduced for the possibility of writing down exactly its stationary measure, an example of an exact solvability property that led to many developments. The initial motivation of [7] was to investigate whether or not the stationary measure of the Inverse-Beta polymer could also be obtained. This is interesting from several points of view, in particular (i) the links between the different types of exact solvability properties mentioned up to now are not yet understood; (ii) the stationary measure encodes the space-time correlations of the DP free-energy at large t on distances $\ll t^{2/3}$, an information which is notoriously hard to obtain from the BA; (iii) the results obtained using BA for the Inverse-Beta polymer required the use of several mathematically non-rigorous tricks and some of them can be obtained rigorously from the stationary measure, thus partially confirming the approach of [5]; (iv) the knowledge of the stationary measure of the Log-Gamma is at the basis of the derivation of a variety of results, e.g. the fluctuation exponents of the DP [197], the large deviation function of the partition sum [228], localization properties of the DP [229]. These results can thus probably be generalized to a richer model using the results of [7]. On the other hand the possibility to write down exactly the stationary measure indicates the presence of exact solvability properties. Considering the fact that LPP is both exactly solvable for exponential and geometric distributions of waiting times, it was natural to conjecture that the zero temperature limit of the Inverse-Beta polymer, the Bernoulli-Exponential polymer, could be generalized to an exactly solvable model with discrete energies. In [7] the Bernoulli-Geometric polymer is introduced and corresponds to this model: we obtain its stationary measure and deduce from it several results.

Stationary measure of the Inverse-Beta polymer

Keeping the notations of [5] and Sec. III.3.3¹², we thus consider the Inverse-Beta

¹²These notations have been changed in [7] so that the v (resp. u) BWs live on the vertical (resp. horizontal) edges of \mathbb{Z}^2 .

consider an initial condition such that at $t = 0$ they are independent and distributed as $\check{U}_{t=0}(x) \sim U$ and $\check{V}_{t=0}(x) \sim V$ with

$$U \sim (\text{Beta}(\gamma - \lambda, \beta + \lambda))^{-1} - 1 \quad , \quad V \sim (\text{Beta}(\lambda, \beta))^{-1} . \quad (\text{III.3.82})$$

Here $0 < \lambda < \gamma$ is a parameter that labels a family of stationary measures. In [7] we show that for all down-right paths π_{dr} on \mathbb{Z}^2 that can be obtained from the down-right path

$$\pi_{dr}^{(0)} = \{(x_1, x_2) = (m, -m) \rightarrow (m, -m - 1) \rightarrow (m + 1, -m - 1), m \in \mathbb{Z}\} \quad (\text{III.3.83})$$

by a sequence of down-left to top-right transformation (which amounts to changing a down-left corner of a down-right path to a top-right corner, see Fig. III.7 for a self-explanatory definition of these notions), the variables $\check{U}_t(x)$ and $\check{V}_t(x)$ living on the down-right path are independent and distributed as in (III.3.82). Furthermore, this stationary measure is reversible in the following sense. Considering the stationary process (III.3.80) during a finite time window T , the time-reversed process

$$\check{U}_{t_R}^R(x_R) = \check{U}_{t=T-t_R}(x = -x_R + 1) \quad , \quad \check{V}_{t_R}^R(x_R) = \check{V}_{t=T-t_R}(x = -x_R) , \quad (\text{III.3.84})$$

satisfies the identity in law

$$\left(\check{U}_t(x), \check{V}_t(x) \right)_{t=0, \dots, T; x \in \mathbb{Z}} \sim \left(\check{U}_{t_R}^R(x_R), \check{V}_{t_R}^R(x_R) \right)_{t_R=0, \dots, T; x_R \in \mathbb{Z}} . \quad (\text{III.3.85})$$

For the original process of the partition sum (III.3.78) this implies that, if one starts from an initial condition such that successive partition sum quotients are random and distributed as

$$\frac{\check{Z}_{t=0}(x+1)}{\check{Z}_{t=0}(x)} \sim \frac{(\text{Beta}(\gamma - \lambda, \beta + \lambda))^{-1} - 1}{(\text{Beta}(\lambda, \beta))^{-1}} , \quad (\text{III.3.86})$$

where the different Beta RVs appearing in this initial condition are all independent, then these quotients remain distributed as so for all time (and are independent at t fixed). Finally, adding for convenience the initial condition $\check{Z}_{t=0}(0) = 1$ we show in [7] that the partition sum in the stationary state in the upper-right quadrant of \mathbb{Z}^2 , $(\check{Z}_t(x))_{x \in \mathbb{N}}$, are equivalent in law to the *point to point* partition sum $\hat{Z}_t(x)$ of a model defined on \mathbb{N}^2 with peculiar boundary conditions: $(\check{Z}_t(x))_{x \in \mathbb{N}} \sim (\hat{Z}_t(x))_{x \in \mathbb{N}}$. We refer the reader to [7] for the precise definition of this model.

The Bernoulli-Geometric polymer

In [7] we define the Bernoulli-Geometric polymer as a geometric discretization of the Bernoulli-Exponential polymer defined in Sec. III.3.3 and introduced in [5]. It is a zero-temperature model of DP on \mathbb{Z}^2 with random energies on-edges and where the optimal energy satisfies the relation

$$\mathbf{E}_{t+1}(x) = \min (\mathbf{E}_t(x) + \mathcal{E}_{t+1}^u(x), \mathbf{E}_t(x-1) + \mathcal{E}_{t+1}^v(x)) , \quad (\text{III.3.87})$$

with the initial condition $E_{t=0}(0) = 0$ and $E_{t=0}(x) = -\infty$ for $x \neq 0$. The random energies are distributed as¹³

$$\begin{aligned}\mathcal{E}^u &\sim -\zeta_{uv}G_q \in \mathbb{Z}_- , \\ \mathcal{E}^v &\sim (1 - \zeta_{uv})(1 + G_{q'}) - \zeta_{uv}G_q \in \mathbb{Z} ,\end{aligned}\quad (\text{III.3.88})$$

where $(q, q') \in]0, 1[^2$ are the two parameters of the model, and G_q generally denotes a Geometric RV $G_q \sim \text{Geo}(q)$ (see (III.2.33)). ζ_{uv} is a Bernoulli RV with parameter

$$p_{uv} = \frac{1 - q'}{1 - qq'} \in]0, 1[. \quad (\text{III.3.89})$$

This value ensures an exact solvability property. This model generalizes the Bernoulli-Exponential polymer which is now retrieved in a limit $q = 1 - \gamma'\epsilon$, $q' = 1 - \beta'\epsilon$ and $\epsilon \rightarrow 0^+$. The case $q' = 0$ corresponds to LPP with geometric waiting times as studied in [159], while the case $q = 0$ is FPP with geometric waiting times on the horizontal edges only as in [216].

Stationary Bernoulli-Geometric polymer

We now discuss the stationary measure of the Bernoulli-Geometric polymer. The stationary optimal energy $\check{E}_t(x)$ satisfies the recursion equation (III.3.87) but with a different initial condition. Similarly as for the Inverse-Beta polymer, to describe the stationary measure, we consider the horizontal and vertical energy differences variables defined as

$$\check{U}_t(x) = \check{E}_t(x) - \check{E}_{t-1}(x-1) \quad , \quad \check{V}_t(x) = \check{E}_t(x) - \check{E}_{t-1}(x) . \quad (\text{III.3.90})$$

These satisfy the recursion relation

$$\begin{aligned}\check{U}_{t+1}(x) &= \phi_{T=0}^{(1)}(\check{U}_t(x), \check{V}_t(x-1), \mathcal{E}_{t+1}^v(x), \mathcal{E}_{t+1}^u(x)) \\ \check{V}_{t+1}(x) &= \phi_{T=0}^{(2)}(\check{U}_t(x), \check{V}_t(x-1), \mathcal{E}_{t+1}^v(x), \mathcal{E}_{t+1}^u(x)) ,\end{aligned}\quad (\text{III.3.91})$$

where $\phi_{T=0}$ is the $T = 0$ *stationarity map* defined as: $\phi_{T=0} : (\mathbf{U}, \mathbf{V}, \mathbf{u}, \mathbf{v}) \rightarrow (\mathbf{U}', \mathbf{V}')$ with

$$\mathbf{U}' = \min(\mathbf{u}, \mathbf{v} + \mathbf{U} - \mathbf{V}) \quad , \quad \mathbf{V}' = \min(\mathbf{u} + \mathbf{V} - \mathbf{U}, \mathbf{v}) . \quad (\text{III.3.92})$$

An elementary (but non-trivial) property of $\phi_{T=0}$ then shows the following. Taking (III.3.91) as the definition, $\forall t$, of a stochastic process for the $\check{U}_t(x)$ and $\check{V}_t(x)$ variables, we consider an initial condition such that at $t = 0$ they are independent and distributed as $\check{U}_{t=0}(x) \sim \mathbf{U}$ and $\check{V}_{t=0}(x) \sim \mathbf{V}$ with

$$\mathbf{U} \sim (1 - \zeta_{\mathbf{U}})(1 + G_{q_b q'}) - \zeta_{\mathbf{U}}G_{q/q_b} \quad , \quad \mathbf{V} \sim -\zeta_{\mathbf{V}}G_{q_b} . \quad (\text{III.3.93})$$

where $q < q_b < 1$ is a parameter that labels a family of stationary measure and $\zeta_{\mathbf{U}}$ and $\zeta_{\mathbf{V}}$ are Bernoulli RVs with parameters

$$p_{\mathbf{U}} = \frac{1 - q_b q'}{1 - qq'} \quad , \quad p_{\mathbf{V}} = \frac{1 - q'}{1 - q_b q'} . \quad (\text{III.3.94})$$

¹³Here we keep the notations adopted for the Bernoulli-Exponential polymer in Sec. III.3.3, which differs from those adopted in [7].

Similarly as before, in [7] we then show that for all down-right paths π_{dr} on \mathbb{Z}^2 that can be obtained from $\pi_{dr}^{(0)}$ by a sequence of down-left to top-right transformation, the variables $\check{U}_t(x)$ and $\check{V}_t(x)$ living on the down-right path are independent and distributed as in (III.3.93). Finally we show that the stationary measure is reversible through the equality in law, similarly as for (III.3.85)

$$\left(\check{U}_t(x), \check{V}_t(x) \right)_{t=0, \dots, T; x \in \mathbb{Z}} \sim \left(\check{U}_{t_R}^R(x_R), \check{V}_{t_R}^R(x_R) \right)_{t_R=0, \dots, T; x_R \in \mathbb{Z}} \quad (\text{III.3.95})$$

where the time-reversed process on a finite time window T is now

$$\check{U}_{t_R}^R(x_R) = \check{U}_{t=T-t_R}(x = -x_R + 1) \quad , \quad \check{V}_{t_R}^R(x_R) = \check{V}_{t=T-t_R}(x = -x_R) . \quad (\text{III.3.96})$$

This implies for the optimal energy $\check{E}_t(x)$ that, taking for initial condition $\check{E}_{t=0}(0) = 0$ and independent energy increments distributed as

$$\check{E}_{t=0}(x+1) - \check{E}_{t=0}(x) \sim (1 - \zeta_U)(1 + G_{q_b q'}) - \zeta_U G_{q/q_b} + \zeta_V G_{q_b} , \quad (\text{III.3.97})$$

then they remain distributed as so for all time. As before, the optimal energy in the model with stationary initial condition in the upper-right quadrant is shown to be identical in law to a point to point optimal energy $\hat{E}_t(x)$ in a model with special boundaries: $(\check{E}_t(x))_{x \in \mathbb{N}} \sim (\hat{E}_t(x))_{x \in \mathbb{N}}$. Note that in the case $q' = 0$ this reproduces the known result for LPP with geometric waiting times (III.2.34).

Optimal energy per unit length in the Bernoulli-Geometric polymer

Defining the mean energy of the horizontal and vertical energy differences in the stationary state of the Bernoulli-Geometric polymer

$$\begin{aligned} f_U^{q, q'}(q_b) &:= \bar{U} = \frac{q_b^2 q' - q}{(q_b - q)(1 - q_b q')} , \\ f_V^{q, q'}(q_b) &:= \bar{V} = -\frac{1 - q'}{1 - q_b q'} \frac{q_b}{1 - q_b} . \end{aligned} \quad (\text{III.3.98})$$

We show that the mean optimal energy per unit length in the direction $\varphi \in]-1/2, 1/2[$ in the stationary Bernoulli-Geometric polymer is linear in φ with

$$\begin{aligned} \check{f}^{p.u.l.}(\varphi, q_b) &:= \lim_{t \rightarrow \infty} \frac{1}{t} \overline{\check{E}_t(x = (1/2 + \varphi)t)} \\ &= (1/2 + \varphi) f_U^{q, q'}(q_b) + (1/2 - \varphi) f_V^{q, q'}(q_b) . \end{aligned} \quad (\text{III.3.99})$$

And using the model with boundaries we obtain a formula for the mean optimal energy per unit length in the direction φ in the point to point Bernoulli-Geometric polymer:

$$\begin{aligned} f^{p.u.l.}(\varphi) &:= \lim_{t \rightarrow \infty} \frac{1}{t} \overline{E_t(x = (1/2 + \varphi)t)} \\ &= \check{f}^{p.u.l.}(\varphi, q_b^*(\varphi)) . \end{aligned} \quad (\text{III.3.100})$$

where $q_b^*(\varphi)$ is the solution of the equation

$$\partial_{q_b} \check{f}^{p.u.l.}(\varphi, q_b) |_{q_b = q_b^*(\varphi)} = 0 . \quad (\text{III.3.101})$$

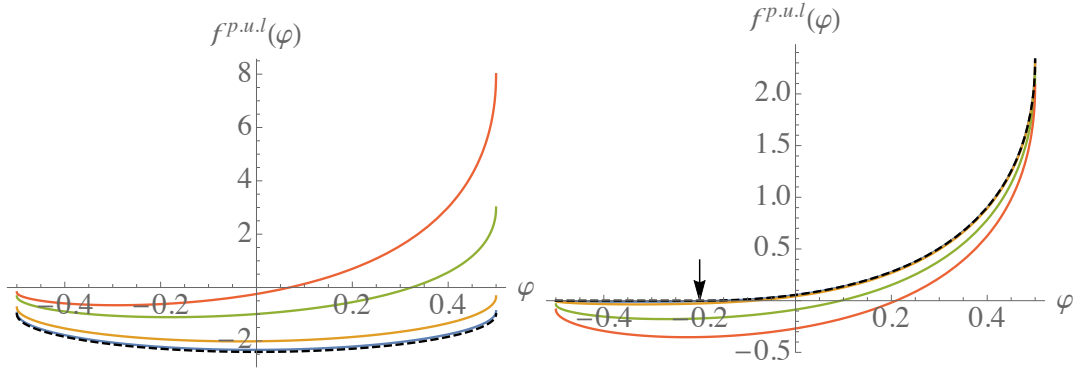


Figure III.8: Left: Optimal energy per-unit-length $f^{p.u.l.}(\varphi)$ (III.3.100) in the Bernoulli-Geometric polymer for $q = 0.5$ and $q' = 0.1, 0.4, 0.8, 0.9$ (plain lines, blue, orange, green and red) and in the last passage percolation limit $q' \rightarrow 0$ (black dashed line). Right: Optimal energy per-unit-length $f^{p.u.l.}(\varphi)$ in the Bernoulli-Geometric polymer for $q' = 0.7$ and $q = 0.001, 0.01, 0.1, 0.2$ (plain lines, blue, orange, green and red) and in the first passage percolation limit $q \rightarrow 0$ (black dashed line). The arrow indicates the percolation threshold of the $q \rightarrow 0$ limit $\varphi_{q'=0.7} = -0.2$. Figures taken from [7].

This is a quartic equation for $q_b^*(\varphi)$ that can be solved exactly, leading to an explicit expression for $f^{p.u.l.}(\varphi)$ which is plotted in Fig. III.8 for various parameters q, q' , and in particular close to the LPP and FPP limits $q' \rightarrow 0$ and $q \rightarrow 0$. Note the non-analytic behavior in the FPP limit where $f^{p.u.l.}(\varphi) = 0$ for $-1/2 \leq \varphi \leq \varphi_{q'} = 1/2 - q'$ and $f^{p.u.l.}(\varphi) > 0$ for $\varphi > 1/2 - q'$. This is interpreted as a percolation threshold where for $\varphi < 1/2 - q'$, the optimal path manages to pass with probability 1 only on edges with 0 energy (a feature that can only be observed in the Bernoulli-Geometric polymer and not in the Bernoulli-Exponential polymer). Fluctuations in this region of space should differ from naive KPZUC expectations. We obtain results similar to (III.3.99)-(III.3.100) for the Inverse-Beta polymer that bring a rigorous confirmation of the value of c_φ obtained from the Bethe Ansatz in [5], see (III.3.51).

Convergence to the stationary measure

Finally we discuss more qualitatively the convergence of the point-to-point partition sum $Z_t(x)$ in the Inverse-Beta polymer / point-to-point optimal energy $E_t(x)$ in the Bernoulli-Geometric polymer and we conjecture that the following limit holds in law (for $x, t = O(1)$)

$$\lim_{T \rightarrow \infty} E_{T+t}(\varphi T + x) - E_T(\varphi T) \sim \check{E}_t(x), \quad (\text{III.3.102})$$

where as before $\check{E}_t(x)$ is the optimal energy in the stationary Bernoulli-Geometric polymer (i.e. with initial condition III.3.97), with the stationary parameter q_b chosen as $q_b = q^*(\varphi)$, the solution of the quartic equation (III.3.101). A similar conjecture is proposed for the Inverse-Beta polymer.

Finally, in [7] (see Appendix G), we successfully check our main results (III.3.100) and (III.3.102) for the Bernoulli-Geometric polymer using simulations of the model. Many details on the above results are given, in particular the definition and the prop-

erties of the Inverse-Beta and Bernoulli-Geometric polymer with boundaries briefly mentioned here, that are actually at the center of [7].

III.4 Conclusion

In this chapter we have reviewed some recent progress in the understanding of the KPZ universality class in $1 + 1d$ based on the existence of models with exact solvability properties. In particular we reported the results obtained in this thesis on exactly solvable models of directed polymers on the square lattice. We have showed how the Bethe ansatz approach developed for the continuum case could be adapted in the discrete setting. The Bethe ansatz approach was also used to classify exactly solvable models of DP at finite temperature containing all known models and a new one, the Inverse-Beta polymer. This ‘world’ of exactly solvable models of directed polymers contain models with very different properties. In the Inverse-Beta and Log-Gamma polymer we could show, using the Bethe ansatz, that the model have fluctuations of free-energy scaling with $t^{1/3}$ and distributed according to the Tracy-Widom GUE distribution with explicit non-universal constants. In the Beta polymer, also interpreted as a model of random walk in a time-dependent one-dimensional random environment, we obtained similar results for the fluctuations in the large deviations regime, and completely different ones in the diffusive regime. This model teaches us a lot about TD-RWRE and DPs: on one hand special short-range correlations of the disorder lead to an additional conservation law and break KPZ universality in the diffusive region, on the other-hand in the other directions KPZ universality is recovered in the TD-RWRE framework. Finally in a complementary work we studied the stationary measure of models of DPs on the square lattice and obtained the one of the Inverse-Beta polymer. With this knowledge, we returned to zero temperature models and introduced the Bernoulli-Geometric polymer. We showed that the latter has an exact solvability property, namely we obtained its stationary measure exactly, and deduced from it several exact results. A tentative cartoon of the relations between the models of directed polymers considered in this manuscript is presented in Fig. III.9.

At this stage many directions of research remain. Understanding the remarkable universality unveiled by models in the KPZUC, and more particularly directed polymers, is still a work in progress for which the models we have studied and the techniques we have developed provide valuable tools. Obvious extensions are the study of DPs on the square lattice with different boundary conditions and extension of our results to multi-point statistics. It would also be interesting to gain a better understanding of the localization properties of DPs on the square lattice and in the continuum using a Bethe ansatz approach. The Beta polymer also brought exact solvability techniques to the TD-RWRE field and much work in this direction also remains, in particular testing the universality of our results for more general models of TD-RWRE. Another question is to gain a better understanding of models of DPs with complex weights, which are related to problems of Anderson localization. In this question we already made progress since at least some part of the classification of [5] also applies to this case, and if an exactly solvable model of DP on \mathbb{Z}^2 with complex weights exists, then under some mild assumptions some signs of its existence should already be visible in

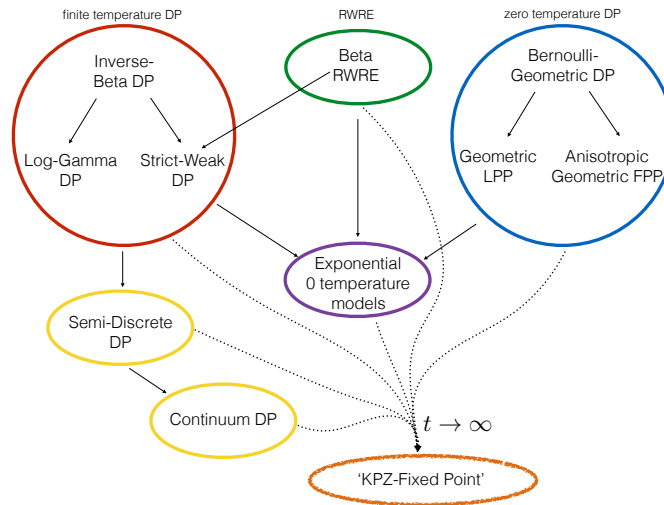


Figure III.9: The different models of DPs encountered during this thesis can be re-grouped in several families. Solid arrows represent various scaling limits of the models, while the dotted arrows represent the conjectured large time convergence of the fluctuations of all these models to the KPZ FP. These dotted arrows have to be taken with caution and sometimes miss important properties: the fluctuations of the free-energy in the Beta RWRE in the diffusive regime, or of the first passage time in the anisotropic Geometric FPP model considered above in the percolating region, do not converge to those of the KPZ FP.

our work (no such signs were found). A more conceptual issue is the understanding of the links between the different exact solvability properties discussed in the manuscript. Finally a long-standing issue is to build techniques allowing to understand the properties of the KPZ FP without relying on the use of exactly solvable models. Indeed, although exactly solvable models allow a remarkable description of the properties of the KPZ FP, it would be highly desirable to get a simple explanation for the emergence of boundary condition dependent extreme value RMT type statistics, or even of the critical exponents. This is particularly important in the aim of understanding the higher-dimensional case where (at least for now) no exactly solvable model exists.

Conclusion

In this thesis we have made progress in the understanding of the properties of elastic interfaces in disordered media in their strong disorder regime. In Chapter II we have been interested in characterizing the universal properties of avalanches and shocks for disordered elastic interfaces with arbitrary elastic kernels in arbitrary dimensions, working directly at zero temperature. In Chapter III we focused on the study of the statics of a directed polymer in a $1 + 1d$ random media at finite temperature and were interested in properties related to the KPZ universality class. We refer the reader to Sec. II.7 and Sec. III.4 for a short summary of our results and conclusions on both subjects and now conclude the thesis with a few more general considerations on the thesis. While in Chapter II we used an analytical approach based on the functional renormalization group, leading to results perturbative in $\epsilon = d_{uc} - d$, in Chapter III we focused on (mostly Bethe ansatz) exactly solvable models for the $d = 1$ case. In both cases the aim was to gain information on universal properties of the underlying renormalization group fixed point, but the approach was completely different. While the functional renormalization group approach mostly ignore the microscopic properties of the model, but rather aims at directly describing the fixed point, the approach based on exactly solvable models is all about finding models whose microscopic properties ensure an exact solvability property. Information of great precision about the KPZ fixed point were later obtained through the large scale analysis of exact results.

Both these methods have their pros and cons. They were used to characterize different observables mostly for technical reasons. While it is an exact method of outstanding interest, studying the statistics of shocks for the directed polymer in $1 + 1d$ with the Bethe ansatz appears very difficult from the technical point of view. Furthermore, exact solvability methods are up to now restricted to the case of $1 + 1$ dimension. In this respect the functional renormalization group approach appears much more versatile. However, in the end, it only leads to results that are perturbative in a dimensional expansion below the upper-critical dimension of the interface. While it would certainly be interesting to obtain the (equivalent of) the Tracy-Widom distribution in an expansion in $\epsilon = 4 - d$, it is clear that the result would be far from the remarkable properties observed in the $d = 1$ case. Those are not only theoretical gems since they are also nowadays measured in experiments.

Overall both these methods permit an advanced understanding of different aspects of the physics of disordered elastic interfaces and of related subjects, making these systems remarkable example of disordered systems for which already existing analytical techniques permit important theoretical progress. While at the quantitative level the

only physics that is accessible through their study is the physics of the universality class of disordered elastic interfaces -which already contains a variety of systems-, at the qualitative level the range of application of ideas emerging from their study might be much broader. In particular, investigating the presence of avalanches in the zero temperature physics of various disordered systems is an interesting goal as it is a neat characterization of the presence of many metastable states in the energy landscape, a property which has a strong influence on many aspects of the physics of disordered systems. This has been done e.g. in amorphous solids at the yielding transition [93], in random field systems [87] or in spin glasses [89], but much work in this direction certainly remains. Even more generally, searching for non-analyticities might be a fruitful angle of approach to the study of various disordered systems, as it has clearly been the case for disordered elastic interfaces.

Appendix A

Paper: Spatial shape of avalanches in the Brownian force model

The following is essentially the article published as

Title: Spatial shape of avalanches in the Brownian force model

Authors: Thimothée Thiery, Pierre Le Doussal, Kay Jörg Wiese

ArXiv: 1504.05342

Journal-Ref: Journal of Statistical Mechanics: Theory and Experiment, Volume 2015, August 2015

Abstract: We study the Brownian force model (BFM), a solvable model of avalanche statistics for an interface, in a general discrete setting. The BFM describes the overdamped motion of elastically coupled particles driven by a parabolic well in independent Brownian force landscapes. Avalanches are defined as the collective jump of the particles in response to an arbitrary monotonous change in the well position (i.e. in the applied force). We derive an exact formula for the joint probability distribution of these jumps. From it we obtain the joint density of local avalanche sizes for stationary driving in the quasi-static limit near the depinning threshold. A saddle-point analysis predicts the spatial shape of avalanches in the limit of large aspect ratios for the continuum version of the model. We then study fluctuations around this saddle point, and obtain the leading corrections to the mean shape, the fluctuations around the mean shape and the shape asymmetry, for finite aspect ratios. Our results are finally confronted to numerical simulations.

A.1 Introduction

A large number of phenomena, as diverse as the motion of domain walls in soft magnets, fluid contact lines on rough surfaces, or strike-slip faults in geophysics, have been described by the model of an elastic interface in a disordered medium [100, 61, 63]. A prominent feature of these systems is that their response to external driving is not smooth, but proceeds discontinuously by jumps called “avalanches”. As a consequence of this ubiquitousness, much effort has been devoted to the study of avalanches, both from a theoretical and an experimental point of view [51, 142, 86, 109]. Despite this activity, there are few exact results for realistic models of elastic interfaces in random media.

An exactly solvable model for a single degree of freedom, representing the center of mass of an interface, was proposed by Alessandro, Beatrice, Bertotti and Montorsi (ABBM) [98, 99] on a phenomenological basis in the context of magnetic noise experiments. It describes a particle driven in a Brownian random force landscape. In [100, 42] it was shown that for an elastic interface with infinite-ranged elastic couplings, the motion of the center of mass has the same statistics as the ABBM model.

In this article, we study a multidimensional generalization of the ABBM model, the Brownian force model (BFM). This model, introduced in [111, 136, 102, 101], was shown to provide the correct mean-field theory describing the full space-time statistics of the velocity in a single avalanche for d -dimensional realistic interfaces close to the depinning transition. Remarkably, restricted to the dynamic of the center of mass, it reproduces the ABBM model. This mean-field description is valid for an interface for $d \geq d_{uc}$ with $d_{uc} = 4$ for short ranged elasticity and $d_{uc} = 2$ for long ranged elasticity.

As shown in [102, 101] the BFM has an exact “solvability property” in any dimension d . It is thus a particularly interesting model to describe avalanche statistics, even beyond its mean-field applicability, i.e. for any dimension d and for arbitrary (monotonous) driving. It allows to calculate the statistics of the spatial structure of avalanches, properties that the oversimplified ABBM model cannot capture. In Ref. [101] some finite wave-vector observables were calculated, demonstrating an asymmetry in the temporal shape. Very recently the distribution of extension of an avalanche has also been calculated [107].

In this article we study a general discrete version of the BFM model, i.e. N points coupled by an elasticity matrix in a random medium, as well as its continuum limit. In the discrete model each point experiences jumps S_i upon driving. We derive an exact formula for the joint probability distribution function (PDF) $P[\{S_i\}]$ of the jumps S_i (the local avalanche sizes) for an arbitrary elasticity matrix. In the limit of small driving this yields a formula for the joint density $\rho[\{S_i\}]$ of local sizes for quasi-static stationary driving near the depinning threshold. This allows us to discuss the “infinite divisibility property” of the BFM avalanche process. The obtained results are rather general and contain the full statistics of the

spatial structure of avalanches. They are, however, difficult to analyze in general since they contain many variables, and thus require computing marginals (i.e. probabilities where one has integrated over most of the variables) from a joint distribution. This is accomplished here in detail for the fully-connected model. We find that in the limit of large N there exist two interesting regimes. The first one corresponds to the usual picture from mean-field depinning models [63, 11], whereas the second one is novel and highlights the intermittent nature of the avalanche motion.

We then analyze the shape of avalanches, first in a discrete setting by considering few degrees of freedom. The probability exhibits an interesting saddle-point structure in phase space. We then study the continuum limit of the model. We find that the spatial shape of avalanches of fixed total size S and extension ℓ , becomes, in the limit of a large aspect ratio S/ℓ^d , dominated by a saddle point. As a result, the avalanche shape becomes deterministic, up to small fluctuations, which vanish in that limit. We calculate the optimal shape of these avalanches. We then analyze the fluctuations around the saddle point. This allows us not only to quantify the shape fluctuations seen in numerical experiments, but also to obtain the mean shape for avalanches with smaller aspect ratios. We test our results with large-scale numerical simulations. While our results are obtained in the special case of an elastic line with local elasticity ($d = 1$) the method can be extended to other dimensions d and more general elasticity. Finally, we discuss the applicability of our results to avalanches in realistic, short-ranged correlated disorder. The outline of this article is as follows: Section A.2 recalls the definition of the BFM model, which is first studied in a discrete setting with general, non-stationary driving. The results of [136, 102, 101] allow us to obtain the Laplace transform of the PDF of local avalanche sizes. Section A.3 contains the derivation of the main result: the full probability distribution of the local avalanche sizes. Section A.4 focuses on the limit of small driving, and how to obtain the avalanche density. Section A.5 contains a detailed analysis of the fully-connected model. Section A.6 studies avalanche shapes for interfaces with a few degrees of freedom. Section A.7 contains one important application of our result, namely the deterministic shape of avalanches with large aspect ratio for an elastic line. Section A.8 analyses the fluctuations around this optimal shape. Section A.9 discusses the application of our results to short-ranged disorder and quasi-static driving. A series of appendices contains details, numerical verifications and some adjunct results. In particular, in A.13, we introduce an alternative method, based on backward Kolmogorov techniques, to calculate the joint local avalanche-size distribution, following a kick in the driving.

A.2 The Brownian force model

A.2.1 Model

We study the over-damped equation of motion in continuous time t of an “interface”, consisting of N points with positions $u_{it} \in \mathbb{R}$, $i = 1, \dots, N$. Each point feels a static random force $F_i(u_{it})$ and is elastically coupled to the other points by a time-independent symmetric elasticity matrix c_{ij} with $\sum_{j=1}^N c_{ij} = 0$. Each particle is driven by an elastic spring of curvature m^2 centered at the time-dependent position w_{it} . The equation of motion reads

$$\eta \partial_t u_{it} = \sum_{j=1}^N c_{ij} u_{jt} - m^2 (u_{it} - w_{it}) + F_i(u_{it}) \quad (\text{A.2.1})$$

for $i = 1 \dots N$. The $F_i(u)$ are N independent Brownian motions (BM) with correlations

$$\overline{[F_i(u) - F_i(u')]^2} = 2\sigma|u - u'| \quad , \quad \overline{F_i(u)F_j(u')} = 0 \text{ for } i \neq j \quad (\text{A.2.2})$$

and $\overline{F_i(u)} = 0$; the overline denotes the average over the random forces $F_i(u)$. For definiteness we consider ¹ a set of one-sided BMs with $u \geq 0$ and $F_i(0) = 0$.

We furthermore suppose that (i) the driving is always non-negative: $\forall t, i, \dot{w}_{it} \geq 0$, and (ii) the elastic energy is convex i.e. $c_{ij} > 0$ for $i \neq j$. Under these assumptions, the Middleton theorem [20] guarantees that if all velocities are non-negative at some initial time: $\exists t_0 \in \mathbb{R} \forall i, \dot{u}_{it_0} \geq 0$, they remain so for all times: $\forall i, \forall t \geq t_0, \dot{u}_{it} \geq 0$.

.1 Some explicit examples of elasticity matrices: Throughout the rest of this article, we sometimes specify the elasticity matrix. The models studied are (where c denotes the elastic coefficient):

1. The fully connected model: $c_{ij} = c(\frac{1}{N} - \delta_{ij})$
2. The elastic line with short-range (SR) elasticity and periodic boundary conditions (PBCs) $c_{ij} = c(\delta_{i,j-1} + \delta_{i-1,j} - 2\delta_{ij})$ with $i + N \equiv i$
3. The elastic line with SR elasticity and free boundary conditions:
 $c_{ij} = c[\delta_{i,j-1} + \delta_{i-1,j} - \delta_{ij}(2 - \delta_{i1} - \delta_{iN})]$
4. The general d -dimensional elastic interface with PBCs, where $i \in \mathbb{Z}^d$ and $c_{ij} = c(f(\|i - j\|) - \delta_{ij} \sum_j f(\|i - j\|))$; here $\|i - j\|$ is the Euclidean distance in \mathbb{Z}^d and $f(r)$ the elastic kernel. Long-ranged elasticity (LR) is usually described by kernels such that $f(r) \sim r^{-(d+\alpha)}$ (i.e. $\sim q^\alpha$ in Fourier).

¹The model can also be studied in a stationary setting, see e.g. [102, 101].

A.2.2 Velocity Theory

Supposing that we start at rest for $t = 0$, $u_{i,t=0} = \dot{u}_{i,t=0} = 0$, then it is more convenient (and equivalent) to study the evolution of the velocity field directly. The equation of motion reads

$$\eta \partial_t \dot{u}_{it} = \sum_{j=1}^N c_{ij} \dot{u}_{jt} - m^2 (\dot{u}_{it} - \dot{w}_{it}) + \sqrt{2\sigma \dot{u}_{it}} \xi_t^i, \quad (\text{A.2.3})$$

where the ξ_t^i are N independent Gaussian white noises, with $\overline{\xi_t^i \xi_{t'}^j} = \delta(t-t') \delta_{ij}$ and $\overline{\xi_t^i} = 0$. Equation (A.2.3) is taken in the Itô sense. Note that we replaced the original quenched noise $\partial_t F_i(u_{it})$ by an annealed one $\sqrt{2\sigma \dot{u}_{it}} \xi_t^i$, making Eq. (A.2.3) a closed equation for the velocity of the interface. The fact that (A.2.1) and (A.2.3) are equivalent (in the sense that disorder averaged observables are the same) is a non-trivial exact property of the BFM model. It was first noted for the ABBM model [98, 99] and extended to the BFM [102, 101]. It originates from the time-change property of the Brownian motion $dB(f(t)) \equiv_{\text{in law}} \sqrt{f'(t)} d\tilde{B}(t)$ for increasing $f(t) = u_t$, valid as a consequence of the Middleton property $\dot{u}_t \geq 0$. A derivation of this property is recalled in A.11.

A.2.3 Avalanche-size observables

In this article we focus on the calculation of avalanche-size observables defined in the following way. Starting from rest at $t = 0$ as previously described, we apply a driving $w_{it} \geq 0$ for $t > 0$ during a finite time interval such that $\int_0^\infty dt \dot{w}_{it} = w_i$ (stopped driving protocol). In response to this driving, the points move and we define the local avalanche size S_i as $S_i = \int_0^\infty dt \dot{u}_{it}$, that is the total displacement of each point. We adopt the vector notation

$$\vec{S} = (S_1, \dots, S_N) \quad , \quad \vec{w} = (w_1, \dots, w_N) . \quad (\text{A.2.4})$$

The S_i 's are random variables whose statistics is encoded in the Laplace transform, also called generating function $G(\vec{\lambda})$, and defined as

$$G(\vec{\lambda}) = \overline{e^{\vec{\lambda} \cdot \vec{S}}} . \quad (\text{A.2.5})$$

The BFM possesses a remarkable ‘‘solvability property’’ that allows us to express this functional as [102, 101]

$$G(\vec{\lambda}) = \overline{e^{\vec{\lambda} \cdot \vec{S}}} = e^{m^2 \sum_{i=1}^N \tilde{u}_i w_i} \quad (\text{A.2.6})$$

in terms of the solution \tilde{u}_i of the ‘‘instanton’’ equation. The latter reads

$$\lambda_i = -\sigma \tilde{u}_i^2 + m^2 \sum_{j=1}^N C_{ij} \tilde{u}_j , \quad (\text{A.2.7})$$

where we have defined the dimensionless matrix

$$C_{ij} = \delta_{ij} - \frac{1}{m^2} c_{ij} , \quad (\text{A.2.8})$$

which contains all elastic and massive terms in the instanton equation. The solution of Eq. (A.2.7) which enters into Eq. (A.2.6) is the unique set of variables \tilde{u}_i continuous in λ_j with the condition that all $\tilde{u}_i = 0$ when all $\lambda_j = 0$. The derivation of this property is recalled in a discrete setting in A.11. The instanton equation thus allows us in principle to express the PDF $P(\vec{S})$ of the local avalanche sizes, as the inverse Laplace transform of $G(\vec{\lambda})$. In the next section we obtain $P(\vec{S})$ directly, without solving (A.2.7), which admits no obvious closed-form solution. We will note $\langle \dots \rangle$ the average of a quantity with respect to the probability P . Note that the PDF $P(\vec{S})$ depends *only on the total driving* $w_i = \int_0^\infty dt \dot{w}_{it}$ and not on the detailed time-dependence of the w_{it} . This is a particularity of the BFM model.

A.2.4 The ABBM model

Before going further into the calculation, let us recall the result of Ref. [102, 101] that the statistical properties of the center of mass of the discrete BFM model is equivalent to that of the ABBM model. To be precise, if we write the *total displacement* (i.e. swept area) $u_t = \sum_i u_{it}$ and total drive $w_t = \sum_i w_{it}$ then, in law, we have

$$\eta \partial_t \dot{u}_t = -m^2 (\dot{u}_t - \dot{w}_t) + \sqrt{2\sigma \dot{u}_t} \xi_t . \quad (\text{A.2.9})$$

Here ξ_t is a Gaussian white noise $\overline{\xi_t \xi_{t'}} = \delta(t-t')$ and $\overline{\xi_t} = 0$.² This equivalence implies that the PDF of the total avalanche size $S = \int_{t=0}^\infty dt \dot{u}_t = \sum_{i=1}^N S_i$ in the discrete BFM model, following an arbitrary stopped driving $\int_0^\infty dt \dot{w}_t = w$, is given by the avalanche-size PDF of the ABBM model [98, 99, 102],

$$P_{\text{ABBM}}(S) = \frac{w}{2\sqrt{\pi S_m} S^{\frac{3}{2}}} \exp\left(-\frac{(S-w)^2}{4SS_m}\right) , \quad S_m = \frac{\sigma}{m^4} . \quad (\text{A.2.10})$$

Here S_m is the large-scale cutoff for avalanche sizes induced by the mass term. This first result on a marginal of the joint distribution $P(\vec{S})$ will provide a useful check of our general formula obtained below for $N > 1$.

²Note that this result uses $\sum_j c_{ij} = 0$ and that the center of mass obeys the same equation with a noise scaled as $N^{-1/2}$ and driving by N^{-1} .

A.3 Derivation of the avalanche-size distribution in the BFM

For simplicity we now switch to dimensionless units. We define

$$v_i = \frac{\sigma}{m^2} \tilde{u}_i \quad , \quad \tilde{w}_i = \frac{w_i}{S_m} \quad , \quad \tilde{\lambda}_i = S_m \lambda_i \quad , \quad \tilde{S}_i = \frac{S_i}{S_m} \quad , \quad (\text{A.3.1})$$

where $S_m = \frac{\sigma}{m^4}$. The instanton equation (A.2.7) now reads

$$\tilde{\lambda}_i = -v_i^2 + \sum_{j=1}^N C_{ij} v_j \quad . \quad (\text{A.3.2})$$

The generating functional is given by

$$G(\vec{\lambda}) = \tilde{G}(\vec{\tilde{\lambda}}) = \overline{e^{\sum_{i=1}^N \tilde{\lambda}_i \tilde{S}_i}} = e^{\sum_{i=1}^N v_i \tilde{w}_i} \quad . \quad (\text{A.3.3})$$

In the following we drop the tildes on dimensionless quantities to lighten notations, and explicitly indicate when we restore units. For the ABBM model, it was possible to explicitly solve the instanton equation for the generating function $G(\lambda)$. The inverse Laplace transform was then computed, leading to (A.2.10). Here this route is hopeless because Eq. (A.3.2) admits no simple closed-form solution. We instead compute directly the probability distribution $P(\vec{S})$ using a change of variables in the inverse Laplace transform (ILT):

$$\begin{aligned} P(\vec{S}) &= \left(\frac{1}{2i\pi}\right)^N \int_{\mathcal{C}} d^N \vec{\lambda} \exp(-\vec{\lambda} \cdot \vec{S}) G(\vec{\lambda}) \\ &= \left(\frac{1}{2i\pi}\right)^N \int_{-i\infty}^{i\infty} dv_1 \cdots \int_{-i\infty}^{i\infty} dv_N \det\left(\frac{\partial \lambda_i}{\partial v_j}\right) \exp\left(-\sum_{i=1}^N (-v_i^2 + \sum_{j=1}^N C_{ij} v_j) S_i + \sum_{i=1}^N v_i w_i\right) , \end{aligned} \quad (\text{A.3.4})$$

where “i” denotes the imaginary unit number to avoid confusion with indexes. The first formula is the ILT where we left unspecified the multi-dimensional contour of integration \mathcal{C} . In the second line we used the expression of λ_i in terms of v_j from (A.3.2), as well as the dimensionless version of (A.2.6). Changing variables from λ_i to v_j , the contours of integration are chosen to obtain a convergent integral, see second line of Eq. (A.3.4). This makes this derivation an educated guess, which however is verified in A.12. We also give another derivation for a special case in A.13. To pursue the derivation, the Jacobian is written using Grassmann variables as

$$\det\left(\frac{\partial \lambda_i}{\partial v_j}\right) = \int \prod_{i=1}^N d\psi_i d\bar{\psi}_i \exp\left(\sum_{i,j=1}^N \bar{\psi}_i (-2v_i \delta_{ij} + C_{ij}) \psi_j\right) \quad . \quad (\text{A.3.5})$$

Reorganizing the order of integrations and changing $v_i \rightarrow iv_i$, we write

$$P(\vec{S}) = \left(\frac{1}{2\pi}\right)^N \prod_{i=1}^N \int d\psi_i d\bar{\psi}_i \prod_{i=1}^N \int_{\mathbb{R}} dv_i \exp\left(-\sum_{i=1}^N (v_i^2 + \sum_{j=1}^N iC_{ij} v_j) S_i + \sum_{i=1}^N iv_i w_i + \sum_{i,j=1}^N \bar{\psi}_i (-2iv_i \delta_{ij} + C_{ij}) \psi_j\right) \quad . \quad (\text{A.3.6})$$

Integrating on v_i leads to

$$P(\vec{S}) = \left(\frac{1}{2\pi}\right)^N \prod_{i=1}^N \int d\psi_i d\bar{\psi}_i (\pi)^{(N/2)} \left(\prod_{i=1}^N S_i\right)^{-\frac{1}{2}} \exp\left(-\frac{1}{4} \sum_{i=1}^N \frac{(w_i - 2\bar{\psi}_i \psi_i - \sum_{j=1}^N C_{ij} S_j)^2}{S_i} + \sum_{i,j=1}^N \bar{\psi}_i C_{ij} \psi_j\right) \quad . \quad (\text{A.3.7})$$

Finally, using $\psi_i^2 = \bar{\psi}_j^2 = 0$, the integration over the Grassmann variables can be expressed as a determinant, leading to our main result

$$\begin{aligned} P(\vec{S}) &= \left(\frac{1}{2\sqrt{\pi}}\right)^N \left(\prod_{i=1}^N S_i\right)^{-\frac{1}{2}} \exp\left(-\frac{1}{4} \sum_{i=1}^N \frac{(w_i - \sum_{j=1}^N C_{ij} S_j)^2}{S_i}\right) \det(M_{ij})_{N \times N} \\ M_{ij} &= C_{ij} + \delta_{ij} \frac{w_i - \sum_{k=1}^N C_{ik} S_k}{S_i} \quad , \quad C_{ij} = \delta_{ij} - \frac{1}{m^2} c_{ij} \quad . \end{aligned} \quad (\text{A.3.8})$$

Here c_{ij} is the elasticity matrix. This is the joint distribution expressed in dimensionless units (A.3.1). The expression in the original units is recovered by substituting $S_i \rightarrow S_i/S_m$, $w_i \rightarrow w_i/S_m$ and $P \rightarrow S_m^N P$ in (A.3.8) while keeping C_{ij} fixed³.

Note that for zero coupling, $c_{ij} = 0$, Eq. (A.3.8) becomes $P(\vec{S}) = \prod_{i=1}^N P_{\text{ABBM}}(S_i)$: the different points are decoupled and one retrieves N independent ABBM models. Non-trivial tests of the formula are performed in A.12. One general

³Note that this formula can be generalized to the case of site-dependent masses and disorder strengths, m_i, σ_i : the expression in the original units is obtained by the substitution $S_i \rightarrow S_i/S_m^i$, $w_i \rightarrow w_i/S_m^i$ and $P \rightarrow \prod_i S_m^i P$ in (A.3.8) with $S_m^i = \frac{\sigma_i}{m_i^4}$ and $C_{ij} = \delta_{ij} - \frac{1}{m_i^2} \frac{\sigma_i m_j^2}{\sigma_j m_i^2} c_{ij}$.

property is that the average local size is $\langle S_i \rangle = \sum_{j=1}^N C_{ij}^{-1} w_j$. This average gives the shape of the interface in the large-driving limit. When $w_i \gg 1$ uniformly in i , it is easy to see by expansion of the above formula that $S_i = \langle S_i \rangle + O(\sqrt{w_i})\eta_i$ where η_i are (correlated) Gaussian random variables.

We show in A.13, using different methods, that when the driving is in the form of kicks, $\dot{w}_{it} = w_i \delta(t)$ ⁴ $P(\vec{S})$ satisfies the exact equation

$$\sum_{\alpha=1}^N \left(-\frac{\partial P}{\partial w_\alpha} \sum_{j=1}^N C_{\alpha j} w_j + \frac{\partial^2 P}{\partial w_\alpha^2} w_\alpha - w_\alpha \frac{\partial P}{\partial S_\alpha} \right) = 0. \quad (\text{A.3.9})$$

We also show that (A.3.8) solves this equation. This alternative derivation support our result (A.3.8) and shed some light on its structure.

Interpretation: Some features of our main result can be understood as follows. Consider the equation of motion (A.2.3). Upon integration from $t = 0$ to $t = \infty$ we obtain

$$0 = \sum_{j=1}^N c_{ij} S_j - m^2 (S_i - w_i) + \int_0^\infty dt \sqrt{2\sigma \dot{u}_{it}} \xi_t^i. \quad (\text{A.3.10})$$

If we could replace the sum of white noises by a gaussian random variable

$$\int_0^\infty dt \sqrt{2\sigma \dot{u}_{it}} \xi_t^i \rightarrow \sqrt{2\sigma} \int_0^\infty dt \dot{u}_{it} \Xi_i = \sqrt{2\sigma S_i} \Xi_i, \quad (\text{A.3.11})$$

then we would obtain (A.3.8), but with a slightly different determinant given by the replacement $\delta_{ij} \rightarrow \frac{1}{2} \delta_{ij}$ in M_{ij} in (A.3.8). However, the replacement (A.3.11) is not legitimate because the variables \dot{u}_{it} are correlated in time. The determinant in (A.3.8) takes care of that correlation.

1 Probability distribution of the shape Even if it is far from being obvious on Eq. (A.3.8), we know from Section A.2.4 that the probability distribution of $S = \sum_{i=1}^N S_i$ is given by (A.2.10) with $\mathbf{w} = \sum_{i=1}^N w_i$. This allows us to define the probability distribution of the shape of an avalanche, given its total size S : Consider $s_1, \dots, s_N \in [0, 1]$ with $s_N = 1 - \sum_{i=1}^{N-1} s_i$, such that $S_i = S s_i$. The probability distribution of the s_i variables, given that the avalanche has a total size $S = \sum_{i=1}^N S_i$ is

$$P(\vec{s}|S) = 2\sqrt{\pi} \frac{S^{N+\frac{1}{2}}}{\mathbf{w}} \exp\left(-\frac{(S-\mathbf{w})^2}{4S}\right) P(S\vec{s}), \quad \sum_{i=1}^N s_i = 1. \quad (\text{A.3.12})$$

A.4 Avalanche densities and quasi-static limit

The goal of this section is to define and calculate avalanche densities. These allow us to describe the intermittent motion of the interface in the regime of small driving, w_i small. The dependence of the PDF, $P_{\vec{w}}(\vec{S})$, on the driving is denoted by a subscript \vec{w} . We first study the jumps of the center of mass described by the ABBM model.

A.4.1 Center of mass: ABBM

For the ABBM model (and for the total size $S = \sum_{i=1}^N S_i$ in the BFM model) the avalanche-size PDF is given by

$$P_{\mathbf{w}}(S) = \frac{\mathbf{w}}{2\sqrt{\pi} S^{\frac{3}{2}}} \exp\left(-\frac{(S-\mathbf{w})^2}{4S}\right), \quad (\text{A.4.1})$$

where $\mathbf{w} = \sum_{i=1}^N w_i$ is the total driving. The limit of small driving \mathbf{w} is very non-uniform. In the sense of distributions, its limit is a delta distribution at $S = 0$,

$$P_{\mathbf{w}}(S) \xrightarrow{\mathbf{w} \rightarrow 0} \delta(S). \quad (\text{A.4.2})$$

However, this hides a richer picture and a separation of scales between typical small avalanches $S \sim \mathbf{w}^2$ and rare large ones $S \sim 1$. If one defines $S = \mathbf{w}^2 s$, the PDF of s has a well-defined $\mathbf{w} \rightarrow 0$ limit given by

$$p_0(s) = \frac{1}{2\sqrt{\pi} s^{\frac{3}{2}}} \exp\left(-\frac{1}{4s}\right), \quad (\text{A.4.3})$$

which is indeed normalized to unity $\int ds p_0(s) = 1$. Hence avalanches of sizes $S \sim \mathbf{w}^2$ are typical ones. However, all positive integer moments of p_0 are infinite. This indicates that these small avalanches, though typical, do not contribute to the

⁴This is sufficient, since we noted above that the result does not depend on the detailed time-dependence of the driving.

moments of P_w , which are finite and controlled by rare but much larger avalanches which we now analyze. In the limit of small w , there remains a probability of order w to observe an avalanche of order 1. For fixed $S = O(1) \gg w^2$ one has

$$P_w(S) = w\rho(S) + O(w^2) \quad , \quad \rho(S) = \frac{1}{2\sqrt{\pi}S^{\frac{3}{2}}} \exp\left(-\frac{S}{4}\right) . \quad (\text{A.4.4})$$

This defines the density (per unit w) of avalanches. These are the ‘‘main’’ avalanches with $S \gg w^2$, which are also called ‘‘quasi-static’’ avalanches (see below and Section A.9). The density is not normalizable because of the divergence at small S , but all its integer moments are finite and contain all the weight in that limit, i.e. $\langle S^n \rangle = w \int dS \rho(S) S^n + O(w^2)$. In particular, $\langle S \rangle = w$ implies $\int dS \rho(S) S = 1$.

We now show that the avalanche density contains more information and controls the moments even for finite w , a property that follows as a consequence of $P_w(S)$ being the PDF of an infinitely divisible process. This is best seen on its Laplace transform

$$G_w(\lambda) = \int dS e^{\lambda S} P_w(S) = e^{wZ(\lambda)} \quad , \quad Z(\lambda) = \frac{1}{2}(1 - \sqrt{1 - 4\lambda}) . \quad (\text{A.4.5})$$

The ‘‘infinite-divisibility property’’ indeed follows: $\forall m$ and $\forall w = w_1 + \dots + w_m$ such that $w_i > 0$

$$G_w(\lambda) = \prod_{i=1}^m G_{w_i}(\lambda) \quad , \quad P_w(S) = (P_{w_1} * \dots * P_{w_m})(S) , \quad (\text{A.4.6})$$

where $*$ denotes the convolution operation. Hence S is a sum of m independent random variables for all m . The ABBM avalanche process can thus be interpreted as a Poisson-type jump process (a Levy process) with jump density $\rho(S)$ [230]. In general the density can be defined as $\rho(S) = \frac{dP_w(S)}{dw} \Big|_{w=0}$ for fixed $S > 0$ (i.e. it does not hold in the sense of distributions), and the relation between $Z(\lambda) := \frac{dG_w(\lambda)}{dw} \Big|_{w=0}$ and ρ is

$$Z(\lambda) = \int dS (e^{\lambda S} - 1) \rho(S) . \quad (\text{A.4.7})$$

The -1 takes care of the divergence at small S . This allows us to write the relation between P_w and ρ , expanding (A.4.5) in powers of w , as

$$\int dS e^{\lambda S} P_w(S) = \sum_{n=0}^{\infty} \frac{w^n}{n!} \int ds_1 \dots ds_n (e^{\lambda s_1} - 1) \dots (e^{\lambda s_n} - 1) \rho(s_1) \dots \rho(s_n) . \quad (\text{A.4.8})$$

Taking derivatives w.r.t. λ , this decomposition shows that the (positive integer) moments of P_w are entirely controlled by ρ , for arbitrary fixed w (beyond the small- w limit). In this sum the term of order w^n can be interpreted as the contribution to the total displacement S of the interface (after a total driving w) of a n -avalanche (quasi-static avalanche) event (of order $O(1)$). The convolution structure in (A.4.8) shows that these events are statistically independent in the ABBM model. In this model however, this interpretation only holds at the level of moments. The accumulation of infinitesimal jumps, manifest in the non-normalizable divergence of ρ at small S prevents us to extend this interpretation to the probability itself, see A.14 for a discussion.

A.4.2 BFM

In the BFM, ‘‘the infinite-divisibility property’’ of the avalanche process is even richer, since avalanches occur at different positions along the interface. Let us define the j -th ‘‘elementary’’ driving which applies only to site j , i.e. $w_i = w_j \delta_{ij}$, and denote the corresponding size-PDF as $P_{w_j}(\vec{S})$. Consider now the PDF for the general driving, $P_{\vec{w}}(\vec{S})$. From the structure of its LT, see (A.3.3), as a product of exponential factors linear in the w_i , this PDF can be written as a convolution for $\vec{w} = (w_1, \dots, w_N)$,

$$P_{\vec{w}}(\vec{S}) = P_{w_1}(\vec{S}) * \dots * P_{w_N}(\vec{S}) . \quad (\text{A.4.9})$$

An avalanche in the BFM can thus be understood as a superposition of N avalanches *independently generated* by each local driving w_j .

As for the ABBM model (center of mass), the structure of the LT of the PDF $P_{w_j}(\vec{S})$ shows that each of these elementary jump processes is infinitely divisible. We define the avalanche density generated by the driving on the j -th point as

$$\rho_j(\vec{S}) := \frac{dP_{\vec{w}}(\vec{S})}{dw_j} \Big|_{\vec{w}=0} = \frac{dP_{w_j}(\vec{S})}{dw_j} \Big|_{w_j=0} , \quad (\text{A.4.10})$$

where as in the previous case, this equality is to be understood point-wise in the \vec{S} variables. Consider the functions v_j of \vec{S} which appear in Eq. (A.3.3) and satisfy Eq. (A.3.2). It is the analogue of $Z(\lambda)$ appearing in (A.4.5) for the ABBM model and we thus conjecture the generalization of (A.4.7),

$$v_j = \int d^N \vec{S} \left(e^{\vec{\lambda} \cdot \vec{S}} - 1 \right) \rho_j(\vec{S}) . \quad (\text{A.4.11})$$

This allows us to write an equation relating $P_{w_j}(\vec{S})$ to $\rho_j(\vec{S})$ similar to (A.4.8) (see A.14). The subtleties linked with the accumulation of small avalanches and the non-normalizability of $\rho_j(\vec{S})$, are the same as in the previous case, which is also reminiscent of the fact that the limit of small driving of $P_{\bar{w}}(\vec{S})$ is very non-uniform, as we now detail. Consider $w_i = w f_i$ with $w \rightarrow 0$ and f_i fixed: the limit of $P_{\bar{w}}(\vec{S})$ is again given (in the sense of distributions) by $\prod_{i=1}^N \delta(S_i)$. More precisely, in this small- w regime, almost all avalanches are $O(w^2)$: $S_i = w_i^2 s_i$ with the s_i distributed according to

$$p_0(\vec{s}) = \prod_{i=1}^N p_0(s_i), \quad (\text{A.4.12})$$

as can be seen from an examination of (A.3.8) in that regime. The PDF p_0 was defined in (A.4.3). One sees that the regime $S_i \sim w^2$ contains all the probability, and that for these very small avalanches the local sizes are statistically independent.

The remaining $O(w)$ probability to observe large avalanches $S_i = O(1)$ is encoded in the densities $\rho_j(\vec{S})$,

$$P_{\bar{w}}(\vec{S}) = \sum_{j=1}^N w_j \rho_j(\vec{S}) + O(w^2). \quad (\text{A.4.13})$$

As before, the positive integer moments are entirely controlled by ρ_j . A more general expression, which illustrates that these large avalanches occur according to a Poisson process, is given in A.14.

We now give exact expressions for these densities. For a general elasticity matrix, the expression of ρ_j is obtained from Eq. (A.3.8), and contains a determinant. Remarkably, one can compute this determinant in various cases, leading to the following result

$$\rho_j(\vec{S}) = \left(\frac{1}{2\sqrt{\pi}} \right)^N \frac{S_j}{\left(\prod_{i=1}^N S_i \right)^{\frac{1}{2}}} K(\vec{S}) \exp \left(-\frac{1}{4} \sum_{i=1}^N \frac{(\sum_{j=1}^N C_{ij} S_j)^2}{S_i} \right), \quad (\text{A.4.14})$$

where $K(\vec{S})$ depends on the chosen elasticity matrix:

- Fully connected model: $K(\vec{S}) = \left(\frac{c}{Nm^2} \right)^{N-1} \frac{(\sum_{i=1}^N S_i)^{N-2}}{\prod_{i=1}^N S_i}$
- Linear chain with periodic boundary conditions: $K(\vec{S}) = \left(\frac{c}{m^2} \right)^{N-1} \sum_{i=1}^N \frac{1}{S_i S_{i+1}}$
- Linear chain with free boundary conditions: $K(\vec{S}) = \left(\frac{c}{m^2} \right)^{N-1} \frac{1}{S_1 S_N}$

.1 PDF of the shape in the small-driving limit As we just detailed, the small-driving limit of $P_{\bar{w}}(\vec{S})$ exhibits a complicated structure due to the accumulation of small avalanches. The situation is very different for the PDF of the shape of the interface conditioned to a given total size $S = O(1)$ (A.3.12). This conditioning naturally introduces a small-scale cutoff that simplifies the small driving limit $w_i = w f_i$ with $w \rightarrow 0$ which reads

$$\rho(\vec{s}|S) = \lim_{w \rightarrow 0} P(\vec{s}|S) = 2\sqrt{\pi} \frac{S^{N+\frac{1}{2}}}{\sum_i f_i} \exp \left(\frac{S}{4} \right) \sum_{j=1}^N f_j \rho_j(S \vec{s}). \quad (\text{A.4.15})$$

This limit holds in the sense of distributions, and $\rho(\vec{s}|S)$ defines a normalized probability distribution. This indicates that the only small-scale divergence present in ρ_j originates from the direction $S_j \sim S \rightarrow 0$ uniformly in j , in agreement with the conjecture (A.4.11).

A.5 Fully-connected model

In this section we use our result (A.3.8) and analyze it for the fully-connected model with uniform driving. Most calculations are reported in A.15, where we also consider driving on a single site, $w_i = w_1 \delta_{i1}$.

.1 Structure of the PDF and marginals In the fully-connected model with homogeneous driving $w_i = w$, it is shown in A.15 that our main result (A.3.8) has the simple structure

$$P(\vec{S}) = \frac{w}{w + cS/N} \prod_{i=1}^N p_{w,S/N}(S_i). \quad (\text{A.5.1})$$

We defined

$$p_{w,z}(S_i) = \frac{w + cz}{2\sqrt{\pi} S_i^{3/2}} \exp \left(-\frac{(w + cz - (1+c)S_i)^2}{4S_i} \right). \quad (\text{A.5.2})$$

For each $w, z > 0$, it is a probability distribution, that corresponds to the (dimensionless, with $m^2 = 1$) PDF of the avalanches of one particle in a Brownian force landscape (ABBM model), interacting with *one parabolic well* through the force $m^2(w - u_i)$ and with *another parabolic well* through the force $c(z - u_i)$. Formula (A.5.1) is thus reminiscent of the

fact that the various sites interact with one another only through the center of mass of the interface. This simple structure permits a direct evaluation of various marginals of (A.5.1) of the type $P(\{S_1, \dots, S_p\}, S)$ (local sizes on $p < N$ sites and total size). This is done in A.15. Here we focus on the joint PDF of the total size S , and the single-site local avalanche size $S_1 < S$. Its explicit form is

$$P(S_1, S) = \frac{w}{2\sqrt{\pi}S_1^{\frac{3}{2}}}(N-1)\frac{w+cS/N}{2\sqrt{\pi}(S-S_1)^{3/2}}\exp\left(-\frac{(w+cS/N-(1+c)S_1)^2}{4S_1}\right) \times \exp\left(-\frac{((N-1)(w+cS/N)-(1+c)(S-S_1))^2}{4(S-S_1)}\right). \quad (\text{A.5.3})$$

Of interest is the participation ratio $s_1 = S_1/S$ of a given site to the total motion. Its average is $\overline{s_1} = 1/N$. Its second moment, conditioned to the total size S , is easily extracted from (A.5.3),

$$\mathbb{E}(s_1^2|S) = \frac{1}{N} - \frac{\sqrt{\pi}(N-1)e^{\frac{(cS+Nw)^2}{4S}}(cS+Nw)\text{erfc}\left(\frac{cS+Nw}{2\sqrt{S}}\right)}{2N^2\sqrt{S}}. \quad (\text{A.5.4})$$

We now study the limit of a large number of sites N in Eq. (A.5.3). There are (at least) two relevant regimes depending on how the driving w scales with N .

.2 First regime: $w = O(1)$ (“many avalanches”): Consider the case $N \rightarrow \infty$ with w fixed. In this case, typical values of $S = \sum_{i=1}^N S_i$ are of order $O(N)$. Consider $\bar{S} = \frac{\sum_{i=1}^N S_i}{N}$ (empirical mean avalanche-size S_i), which is distributed according to

$$P(\bar{S}) = \frac{\sqrt{N}w}{2\sqrt{\pi}\bar{S}^{\frac{3}{2}}}\exp\left(-\frac{N(\bar{S}-w)^2}{4\bar{S}}\right) \rightarrow_{N \rightarrow \infty} \delta(\bar{S}-w). \quad (\text{A.5.5})$$

The joint probability $P(S_1, \bar{S})$, is given by Eq. (A.5.3) (with the change of variable $S \rightarrow N\bar{S}$), and admits the large- N limit

$$P(S_1, \bar{S}) \simeq_{N \rightarrow \infty} \frac{w+c\bar{S}}{2\sqrt{\pi}S_1^{\frac{3}{2}}}\exp\left(-\frac{1}{4}\frac{(w+c\bar{S}-(1+c)S_1)^2}{4S_1}\right)P(\bar{S}) \simeq \frac{w(1+c)}{2\sqrt{\pi}S_1^{\frac{3}{2}}}\exp\left(-\frac{1}{4}\frac{(1+c)^2(w-S_1)^2}{4S_1}\right)\delta(\bar{S}-w). \quad (\text{A.5.6})$$

Hence the jump of the center of mass becomes peaked at $\bar{S} = w$, while the individual sites keep a broader jump distribution. The local avalanche statistics is the same as the one for a particle submitted to the parabolic driving force $m^2(w-u_i)$, and to the elastic force from the center of mass of the interface, $c(\bar{S}-u_i)$. This observation extends to any number of particles $n_{\text{part}} = O(1)$ with respect to N : in the large- N limit, the particles become independently distributed according to the law (A.5.6). This picture is the “mean-field” regime usually studied in fully-connected models [63, 11], and here derived in a rigorous way. Note that in this case, due to a cancellation in (A.5.4), the participation ratio scales as $\mathbb{E}(s_1^2|S) = O(1/N^2)$ which shows that s_1 is typically of order $1/N$.

.3 Second regime: small driving $w = O(1/N)$ (“single avalanche”) We now focus on the regime $w = \hat{w}/N$ with \hat{w} fixed. In this case $S = \sum_{i=1}^N S_i$ is typically of order 1 and is distributed according to

$$P(S) = \frac{\hat{w}}{2\sqrt{\pi}S^{\frac{3}{2}}}\exp\left(-\frac{(S-\hat{w})^2}{4S}\right). \quad (\text{A.5.7})$$

We now compute, using (A.5.3), the joint PDF of S and S_1 in the scaling regime $S_1 = O(1)$ fixed,

$$P(S_1, S) \simeq_{N \rightarrow \infty} \frac{\hat{w}/N}{2\sqrt{\pi}S_1^{\frac{3}{2}}}\exp\left(-\frac{(1+c)^2S_1}{4}\right)\frac{\hat{w}+cS}{2\sqrt{\pi}(S-S_1)^{\frac{3}{2}}}\exp\left(-\frac{1}{4}\frac{(\hat{w}+cS-(1+c)(S-S_1))^2}{4(S-S_1)}\right). \quad (\text{A.5.8})$$

The first factor is reminiscent of the density of avalanches and contains a non-normalizable divergence $\sim S_1^{-3/2}$. However (A.5.3) implies a cutoff on small S_1 of order $\frac{1}{N^2}$. The scaling $w = \hat{w}/N$ allows to isolate single (quasi-static) avalanches (in the interpretation of the BFM avalanche process as a Levy process discussed above) and the factor of $1/N$ is the probability that the site $i = 1$ is part of the avalanche. In this regime, the fluctuations are large and the participation ratio scales as $\mathbb{E}(s_1^2|S) = O(1/N)$.

A.6 Spatial shape in small systems $N = 2, 3$.

In this section we analyze the PDF of the spatial avalanche shape in the small-driving limit, $w_i = w \rightarrow 0$, mostly for $N = 2, 3$. It already exhibits a saddle-point which allows us to discuss the general- N case below. The analysis can be repeated for finite w_i . Similarities and differences give insight into the link between the quasi-static distribution and finite driving. This is done in A.16.

.1 $N=2,3$ We start with $N = 2$, for which the different models we considered are all equivalent. To fix notations, we study the linear chain with PBCs (see Section .1) and $m = 1$. The quasi-static PDF of the shape (A.4.15), conditioned on the total size S , reads

$$\rho(s|S) = \frac{2c}{4\sqrt{\pi}(s(1-s))^{\frac{3}{2}}} e^{-c^2 S \frac{(1-2s)^2}{s(1-s)}}. \quad (\text{A.6.1})$$

We noted $s = s_1 = S_1/S$, the shape variable of the first site. The behavior of this PDF is summarized on Figure A.1. For small S , typical avalanches are mainly distributed on one site. As S increases, the most probable avalanches become more homogeneously distributed over the two sites, and for S larger than $S_c = \frac{3}{8c^2}$, the probability distribution is peaked around $s = \frac{1}{2}$ and the avalanche is extended over the whole system. We call this phenomenon the *shape transition*: For small total size, the most probable avalanches have $\max(s_i) \simeq 1$, whereas for large avalanches $\max(s_i) \simeq 1/N = 1/2$.

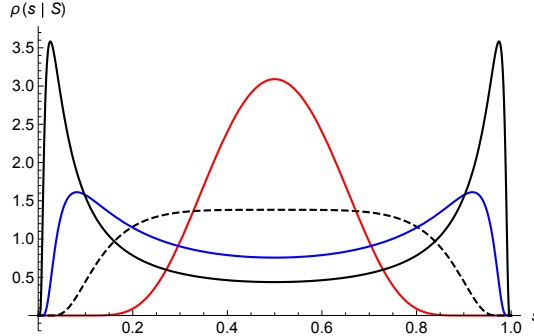


Figure A.1: Shape transition of the quasi-static PDF (A.6.1) for $N = 2$ and $c = 1$ in the linear chain with PBCs. For $S = 0.1S_c$ (black, solid curve) and $S = 0.3S_c$ (blue), the distribution has two symmetric maxima. For $S = 5S_c$, the distribution is peaked around $s = \frac{1}{2}$ (red, upper curve). The transition occurs at $S = S_c = 3/8$ (black, dashed curve).

The case $N = 3$ for a linear chain with PBC is similar. For $S < \frac{1}{c^2}$, the quasi-static density distribution of the shape $\rho(s_1, s_2, s_3 = 1 - s_1 - s_2|S)$ has three symmetric maxima corresponding to avalanches mainly centered on a given site, whereas for $S > \frac{1}{c^2}$ there is only one maximum at $s_i = \frac{1}{3}$. This can be seen on Figure A.2.

.2 General N This study already gives some insight into the structure for generic N : the quasi-static distribution of the shape $\rho(\vec{s}|S)$ exhibits different saddle-points, whose positions and stabilities depend on the value of S . For small S , avalanches are preferentially located on a single site j and $\max(s_i) \simeq 1$. As one increases S , the most probable avalanches are more and more extended. The analytical calculation of the properties of these saddle points is difficult. However, we can generalize the shape transition observed for $N = 2, 3$: The symmetric configuration defined by $\forall i, s_i = \frac{1}{N}$ (a situation corresponding to infinitely extended and uniformly distributed avalanches) is always a saddle-point of translationally invariant models. This saddle-point is only stable for $S > S_c(N)$, which is computed in A.17 for the fully connected model, and for the linear chain with PBC. The result is

$$S_c^{\text{fc}}(N) = \frac{3N}{c^2}, \quad (\text{A.6.2})$$

$$S_c^{\text{PBC}}(N) \sim_{N \rightarrow \infty} \frac{1}{16c^2\pi^4} (N^5 + 12N^4 + O(N^3)).$$

This critical value gives the scaling of the total size above which most probable avalanches are uniformly distributed on all the interface. Below this scaling they adopt a more complex structure (e.g. they are localized on several sites, possess

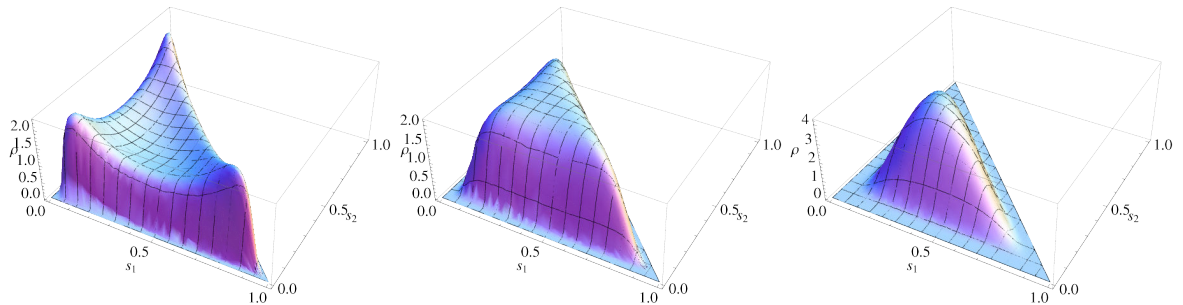


Figure A.2: Shape transition of the quasi-static shape distribution for $N = 3$ and $c = 1$. From left to right: $S = 0.5; 1; 2$.

maxima, etc.). Let us already mention that other saddle-points of the shape PDF are numerically studied in A.19, where the results are compared to the one obtained in the next section for the most probable avalanche shape in a continuum model.

A.7 Continuum limit: avalanches of an elastic line and typical shape of avalanches with large aspect ratio

A.7.1 Avalanche size PDF and density in the continuum limit

We now study the generalization of the previous result to the continuum Brownian-force model with short-ranged elasticity for a line of length L

$$\eta\partial_t\dot{u}_{xt} = \nabla^2 u_{xt} - m^2(\dot{u}_{xt} - \dot{w}_{xt}) + \sqrt{2\sigma\dot{u}_{xt}}\xi_{xt}. \quad (\text{A.7.1})$$

Here ξ_{xt} is a gaussian white noise with $\overline{\xi_{xt}\xi_{x't'}} = \delta(x-x')\delta(t-t')$ and the boundary conditions are either free or periodic. Starting from rest at $t=0$ and imposing a driving $\dot{w}_{xt} \geq 0$ for $t \geq 0$ such that $\int_t \dot{w}_{xt} = w_x$, we note the total displacement of the interface $S_x = \int_{t \geq 0} \dot{u}_{xt}$. The method used in the discrete case can be extended to derive the PDF of avalanches in the continuum. Another route is to consider the continuum model as the appropriate $N \rightarrow \infty$ limit of the discrete model, as is detailed in A.18. Both procedures give the same result, which, for the dimensionless PDF of continuum avalanches, includes a functional determinant

$$P[S_x] \sim \left(\frac{1}{\prod_x S_x} \right)^{\frac{1}{2}} \det(M) \exp\left(-\int_0^L dx \frac{(w_x - S_x + \frac{1}{m^2}\nabla^2 S_x)^2}{4S_x}\right), \quad (\text{A.7.2})$$

$$M(x, y) = -\frac{1}{m^2}(\nabla^2)_{xy} + \delta(x-y) \left(1 + \frac{w_x - S_x + \frac{1}{m^2}\nabla^2 S_x}{S_x}\right).$$

Here ∇^2 is the usual Laplacian, $(\nabla^2)_{xy} = \delta''(x-y)$. Dimensions can be reintroduced as in the discrete case using $S_m = \frac{\sigma\epsilon}{m^4}$. S_m is the avalanche-size scale of the continuum theory. The first factor $(\prod_x S_x)^{\frac{1}{2}}$ also comes from a determinant and could be included in the definition of the operator M .

As in the discrete case, the mean displacement $\langle S_x \rangle$ satisfies $-\nabla^2 \langle S_x \rangle + \langle S_x \rangle = w_x$. For instance, if the driving is only at one point, $w_x = w\delta(x)$, one has $\langle S_x \rangle = \frac{w}{2}e^{-|x|}$. The case of a general w_x is obtained by superposition. This is consistent with the discussion in Section A.4. As in the discrete case, the mean displacement gives the avalanche shape in the limit of large driving (plus an $O(\sqrt{w})$ Gaussian noise).

One can also study the homogeneous quasi-static limit: $w(x) = w \rightarrow 0$ and $S(x) = O(1)$ uniformly in x . Then $P[S] \simeq w\rho[S]$ with $\rho[S]$ the quasi-static density of sizes of continuous avalanches, also obtained as the limit of the discrete ones,

$$\rho[S_x] \sim \frac{(\int_0^L dx S_x) BC[S_x]}{(\prod_x S_x)^{\frac{1}{2}}} \exp\left(-\int_0^L dx \frac{(S_x - \nabla^2 S_x)^2}{4S_x}\right). \quad (\text{A.7.3})$$

From now on we set $m=1$ (by a rescaling of x). The term $BC[S_x]$ depends on the chosen boundary conditions with $BC[S_x] = \int_0^L \frac{dx}{S_x^2}$ (resp. $BC[S] = \frac{1}{S_0 S_L}$) for the periodic case (resp. free case).

.1 Other continuum models Our discrete setting allows us to obtain the avalanche-size PDF of various continuous models, Eq. (A.7.2) being generalizable to an interface of internal dimension d . One may also consider an arbitrary elasticity matrix c_{xy} by changing $\nabla^2 u_x \rightarrow \int dy c_{xy} u_y$. The continuum limit of the formula for the PDF of the shape conditioned to the total size, either at finite w , see Eq. (A.3.12), or for $w \rightarrow 0$ (quasi-static limit), see Eq. (A.4.15), are also easily derived.

A.7.2 Rewriting the probability measure on avalanche sizes

We now wish to determine the most probable shape of quasi-static avalanches, in the limit $L \rightarrow \infty$ ⁵. To render the problem well defined, one needs to specify two scales. A natural choice is the total size $S = \int_x dx S_x$ and the spatial avalanche extension (or length) ℓ , i.e. the size of the support of S_x . While the avalanche-size PDF $P(S)$ is given by the ABBM result (A.2.10), the existence of a finite extension ℓ (i.e. local avalanche sizes being strictly zero outside a finite interval) is non-trivial⁶. Here it naturally arises in the search for saddle-points of the shape PDF: we only found solutions which vanish outside of an interval. This property was also shown recently in [107] where the PDF of the extension $P(\ell)$ is computed.

⁵ In general the shape of avalanches depends on the driving. However, an avalanche following an arbitrary driving (in particular in a quasi-static setting more usual for experiments, see Sec. A.9) in the BFM is a sum of quasi-static avalanches (Sec. A.4), whose spatial structure is, by definition, independent of the driving.

⁶ In a mathematical sense it may be a peculiarity of the BFM in $d=1$ with short range elasticity. Of course rapid decay in space is expected more generally beyond some support region of extension ℓ , and often obtained in numerical simulations.

In the following we study the shape distribution at fixed S and ℓ . We do not take into account the term implementing boundary conditions in (A.7.3) since it should not play a role in the bulk (this hypothesis is explicitly checked on the discrete model in A.19). So we write the density of continuum avalanches S_x as

$$\rho[S] \prod_x dS_x \sim \prod_x \frac{dS_x}{\sqrt{S_x}} \left(\sum_x S_x \right) e^{-\mathcal{H}[S]} \quad , \quad \mathcal{H}[S] = \int_x \frac{[S_x - \nabla^2 S_x]^2}{4S_x} = \int_x \frac{S_x}{4} + \frac{[\nabla^2 S_x]^2}{4S_x} . \quad (\text{A.7.4})$$

To eliminate the factor of $(\prod_x S_x)^{-1/2}$ in the measure, we set

$$S_x = \Phi^2(x) . \quad (\text{A.7.5})$$

The integration $\int_0^\infty \frac{dS_x}{\sqrt{S_x}} = \int_{-\infty}^\infty d\Phi(x)$, thus the integral over $\Phi(x)$ runs from $-\infty$ to ∞ . To further simplify the calculations, we note that the problem is invariant by translation. We thus impose the center of the support to be at $x = 0$. This leads to the definition of the reduced shape $s(x) = \phi^2(x)$

$$S_x = \frac{S}{\ell} s(x/\ell) = \Phi^2(x) = \frac{S}{\ell} \phi^2(x/\ell) \quad , \quad \int_{-\frac{1}{2}}^{\frac{1}{2}} dx \phi^2(x) = 1 \quad , \quad |x| \geq \frac{1}{2} \Rightarrow \phi(x) = 0 . \quad (\text{A.7.6})$$

Note that to study fluctuations around the saddle point it is more convenient to use $\phi(x)$, but the saddle point itself can be obtained equivalently using $s(x)$ or $\phi(x)$. Below we use $\phi(x)$, but also indicate the corresponding formulas for $s(x)$ when these are simpler.

We search for the most probable shape in the limit of small driving, at fixed size S and extension ℓ . The path integral takes the form

$$\prod_x d\phi(x) \exp \left(-\frac{S}{4} - \frac{S}{\ell^4} \mathcal{H}_{\text{el}}[\phi] \right) \quad , \quad \mathcal{H}_{\text{el}}[\phi] = \int_{-\frac{1}{2}}^{\frac{1}{2}} \phi''(x)^2 + \frac{\phi'(x)^4}{\phi(x)^2} + \frac{2\phi'(x)^2 \phi''(x)}{\phi(x)} dx . \quad (\text{A.7.7})$$

The boundary conditions are $\phi(\frac{1}{2}) = \phi(-\frac{1}{2}) = \phi'(\frac{1}{2}) = \phi'(-\frac{1}{2}) = 0$ and

$$\int_{-\frac{1}{2}}^{\frac{1}{2}} dx \phi^2(x) = 1 . \quad (\text{A.7.8})$$

Note the appearance of the factor of $\frac{S}{\ell^4}$ in front of the ‘‘elastic’’ energy.

A.7.3 The saddle point for large aspect ratio S/ℓ^4

The path integral (A.7.7) is for large S/ℓ^4 dominated by a saddle-point. To enforce the constraint (A.7.8), we minimize $\mathcal{H}_{\text{el}}[\phi] - \mathcal{A} \int_{-1/2}^{1/2} dx \phi^2(x)$, with Lagrange multiplier \mathcal{A} , leading to the saddle-point equations ⁷.

$$\mathcal{A} \phi(x) = \frac{1}{2} \frac{\delta \mathcal{H}_{\text{el}}[\phi]}{\delta \phi(x)} = \phi^{(4)}(x) + \frac{5\phi'(x)^4}{\phi(x)^3} - \frac{10\phi'(x)^2 \phi''(x)}{\phi(x)^2} . \quad (\text{A.7.9})$$

In order to find the solution $(\mathcal{A}_0, \phi_0(x))$ of (A.7.9) satisfying the properties written in (A.7.6), we first obtain numerically, using a shooting method, another solution $(\mathcal{A}_1, \phi_1(x))$ of (A.7.9). We impose $\mathcal{A}_1 = 2.5 \times 10^5$, $\phi_1(0) = 1$, $\phi_1'(0) = \phi_1''(0) = 0$, and look for the correct shooting parameter $\phi_1'''(0)$ such that the numerical solution has a support of finite size $[-x_c, x_c]$ with the desired behavior at the boundary, i.e. $\phi_1'(-x_c) = \phi_1(x_c) = 0$. The obtained (unique) solution has the following properties: $\phi_1'''(0) = -276.797090676018$, $x_c = 0.162713$, $\sqrt{\phi_1(x)} \simeq 7.85883(x_c - x)$ for $x \rightarrow x_c$ and $S_1 := \int_{-x_c}^{x_c} \phi_1^2(x) dx = 0.106289$. We now take advantage of rescaling, setting

$$\phi_0(x) := \sqrt{\frac{2x_c}{S_1}} \phi_1(2x_c x) \quad , \quad \text{and } s_0(x) = \phi_0^2(x) . \quad (\text{A.7.10})$$

This function is automatically a solution of (A.7.9) with a different Lagrange multiplier $\mathcal{A}_0 = (2x_c)^4 \mathcal{A}_1$, and the desired properties (A.7.6). By multiplying (A.7.9) by $\phi_0(x)$ and integrating for $x \in [-\frac{1}{2}, \frac{1}{2}]$ (using $\phi_0'(\pm\frac{1}{2}) = 0$), we obtain the relation $\mathcal{H}_{\text{el}}[\phi_0] = \mathcal{A}_0$. Numerically we find

$$\mathcal{E}_0 := \mathcal{H}_{\text{el}}[\phi_0] = \mathcal{A}_0 = (2x_c)^4 \mathcal{A}_1 = 2803.8 \pm 0.2 . \quad (\text{A.7.11})$$

An estimate of the numerical accuracy is given. The error is mostly due to the imprecision in determining x_c .

Alternatively, a variational solution can be used. We make the ansatz

$$\phi_{\text{var}}(x) = \mathcal{N}_c \left(x^2 - \frac{1}{4} \right)^2 \left(1 + \sum_{i=1}^{i_{\text{max}}} c_i \left(x^2 - \frac{1}{4} \right)^i \right) \quad , \quad \text{and } s_{\text{var}}(x) = \phi_{\text{var}}^2(x) . \quad (\text{A.7.12})$$

⁷The saddle point equation has a simpler form in terms of $s(x)$. It reads: $\frac{1}{2}[s''(x)/s(x)]'' - \frac{1}{4}[s''(x)/s(x)]^2 = \mathcal{A}$. Hence $s''(x)/s(x)$ is a Weierstrass function which diverges as $\sim (x \pm x_c)^{-2}$ at the boundaries.

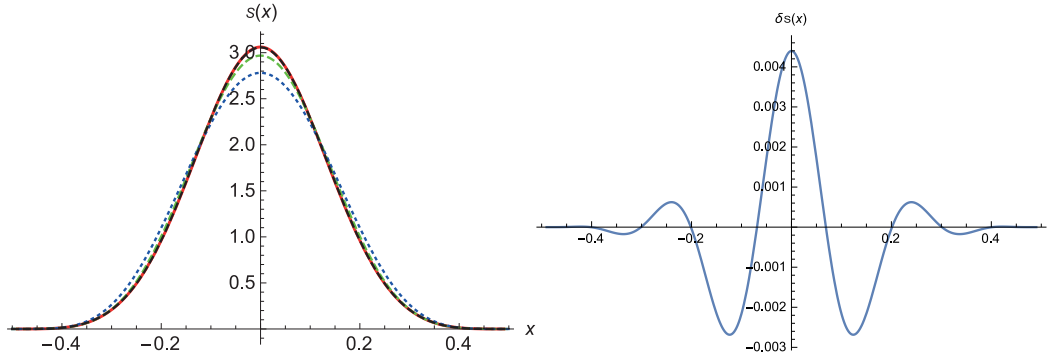


Figure A.3: Left: The function $s_0(x) = \phi_0^2(x)$, as obtained by solving the differential equation (A.7.9) (red solid curve). This is contrasted to the variational ansatz (A.7.12), with one (blue dotted), two (green dashed) and 15 variational parameters (black-dashed, indistinguishable from the solution of the differential equation). Right: Difference between the solution of the differential equation, and the best variational solution.

The behavior at the boundary $x = \pm \frac{1}{2}$ is chosen in agreement with the numerical solution of the saddle-point equation. One can also show that this ansatz leads to an energy which remains finite at the boundary. The \vec{c} -dependent normalization \mathcal{N}_c is chosen s.t. $\int_{-1/2}^{1/2} dx \phi_{\text{var}}(x)^2 = 1$. For a given vector $\vec{c} = \{c_1, \dots, c_{i_{\text{max}}}\}$, one then evaluates $\mathcal{H}[\phi_{\text{var}}]$. Using a Monte Carlo algorithm, the minimum energy is searched by steepest decent in the space of all \vec{c} with given $\int_{-1/2}^{1/2} dx \phi_{\text{var}}(x)^2 = 1$. In Figure A.3 we show that for the shape of the avalanche, this procedure rapidly converges against the solution obtained by solving the differential equation (A.7.9). Our best estimate is for $i_{\text{max}} = 15$, where we find

$$\vec{c} = \{-1.00301, 20.6871, 83.4237, 211.353, -270.898, 179.973, -72.6636, 16.3962, \\ -12.2786, 6.11179, -0.33042, 11.777, 0.750034, -6.77598, -4.56253\} . \quad (\text{A.7.13})$$

This result is compared to the numerical solution of the saddle point on Figure A.3. The energy of this solution gives us, in good agreement with Eq. (A.7.11), the variational bound

$$\mathcal{E}_0 \leq 2803.96 . \quad (\text{A.7.14})$$

In A.19 we confront this result to a study of the optimal shape in a discrete setting. There we also show (see also Figure A.10 below) that this saddle-point is stable. Hence, the reduced shape of an avalanche becomes deterministic in the limit of $S/\ell^4 \gg 1$: $s(x) \xrightarrow{S/\ell^4 \rightarrow \infty} s_0(x) = \phi_0^2(x)$ with probability one. Formula (A.7.7) then shows that \mathcal{E}_0 is measurable in the tail of the distribution of aspect ratios,

$$\text{Proba}(S/\ell^4) \stackrel{S/\ell^4 \gg 1}{\sim} \exp\left(-\mathcal{E}_0 \frac{S}{\ell^4}\right) \quad (\text{A.7.15})$$

with possibly some sub-dominant factors, as e.g. a power-law. This is confronted to numerics below.

A.7.4 Simulations: Protocol and first results

.1 Protocol. Here we describe the simulation used to numerically study the shape of avalanches. We use a discretization with $N = 512$ points of the equation of motion for the velocity in the BFM (A.7.1) using periodic boundary conditions for a system of total size $L = N$. The mass is chosen as $m = 10/L$ in order to get a scale-free statistics for a wide range of events. The other parameters are set to unity, $\eta = \sigma = 1$. The time is discretized using a time-step $dt = 0.01$ and a discretization scheme identical to [231]. Simulations are done via Matlab and results are analyzed using Mathematica. At $t = 0$ the system is at rest and we choose to drive it using a kick of size $\delta w = 100$ on a single site. This is motivated by the fact that we want to study (single) quasi-static avalanches: the value of δw is chosen to be small in adimensioned units $\frac{m}{\sigma} \delta w \simeq 7.4 \cdot 10^{-4}$. Following the discussion of Section A.4 and A.14, we thus know that an avalanche resulting from our driving protocol can either be a “small” avalanche $O(\delta w^2)$ or, with a small probability $p_0 = O(\delta w)$ a quasi-static avalanche of total size $S = O(1)$ (we neglect the $O(\delta w^2)$ probability that several quasi-static avalanches have been triggered). Schematically, we write

$$P(\vec{S}) \simeq (1 - p_0) \delta(\vec{S}) + p_0 \rho_{i_0}(\vec{S}) , \quad (\text{A.7.16})$$

where i_0 is the driven site. Here “ δ ”(\vec{S}) is not a true delta distribution since in the BFM the interface always moves, but it rather denotes the PDF of all the small, non quasi-static avalanches, which is expected to depend highly on the driving. This is made more precise below, and in particular we discuss how we identify the quasi-static avalanches and p_0 from our data set.

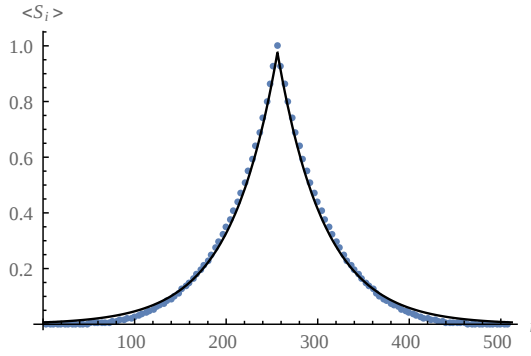


Figure A.4: Measurement of $\langle S_i \rangle$ and comparison with the exact result $\langle S_i \rangle = \frac{mw}{2} e^{-m|i-i_0|}$ with $i_0 = 256$. The total moment is measured as $\langle S \rangle = 99.461$.

We stop the simulation for the rare events when an avalanche reaches the periodic boundary, since we are interested in the distribution of shapes on an infinite line. For every generated avalanche, we numerically compute its shape characteristics S, ℓ (avalanches are indeed observed as having a finite support) and $s(x)$ (discretized with ℓ points). We report results using $n_{\text{it}} = 2 \cdot 10^7$ simulations of a kick. As a first verification, we check on Figure A.4 a coarse-grained information on the spatial structure by measuring the mean local avalanche size. The discrepancy at the boundaries can be attributed to the fact that we stop the simulation when an avalanche reaches the PBCs. This is the only bias expected in our procedure. It is not a problem since for the rest of the article we are interested in observables at large S/ℓ^4 , automatically excluding the largest ℓ .

.2 Consistency check of $\mathcal{E}_0 = 2804$. We predicted above that \mathcal{E}_0 controls the tail of the distribution of aspect-ratios. Numerically, we find that this distribution possesses a power-law part coherent with an exponent of 2 and an exponential cutoff for large S/ℓ^4 with a prefactor coherent with $\mathcal{E}_0 = 2804$: $\text{Proba}(S/\ell^4) \simeq \ell^8/S^2 \exp(-\mathcal{E}_0 S/\ell^4)$ (see left and center of Figure A.5). We also remark that the exponential cutoff function seems to entirely control the PDF of S/ℓ^4 for “massive” avalanches, of extension $\ell \geq 1/m$ (see right of Figure A.5). Obviously this does not constitute a precise measurement of \mathcal{E}_0 , but rather a verification of its non trivial value, which can probably only be understood by studying the complete spatial structure of avalanches as we did.

.3 Identifying quasi-static avalanches. From now on we restrict our numerical results to avalanches of extension $\ell \geq 10$ to obtain a decent spatial resolution. This also allows us to isolate quasi-static avalanches. Avalanches with extension larger than 10 only represents 3.5% of the data. Obviously, this is not a proof that this subset of avalanches only contains quasi-static avalanches, and one needs to check that it has the statistical properties of a set generated by the quasi-static density. One “test” is to study the number $n_{>S_1}$ of avalanches of total size S larger than S_1 , for which the quasi-static hypothesis implies,

$$n_{>S_2} = n_{>S_1} \frac{\int_{S_2}^{\infty} \rho(S) dS}{\int_{S_1}^{\infty} \rho(S) dS}, \quad (\text{A.7.17})$$

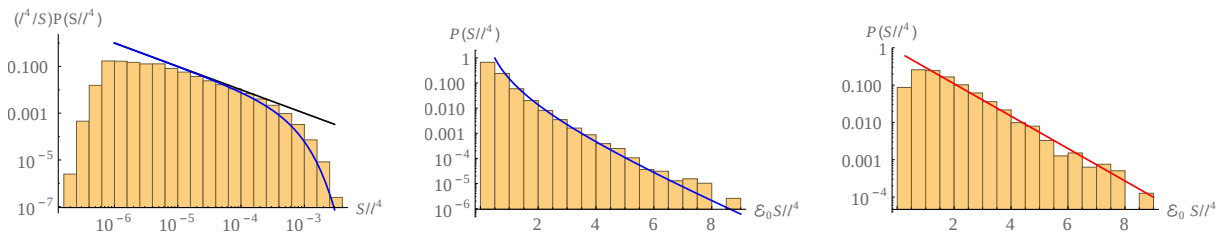


Figure A.5: Different histogram of the PDF of S/ℓ^4 obtained numerically with different binning procedures for the x axis and scale for the y axis. Left: log-log histogram of the full distribution. Center: log histogram of the distribution for aspect ratio $S/\ell^4 \geq 1/5\mathcal{E}_0$. Right: log histogram of the distribution for avalanches of extension $\ell \geq 1/m$. The black line on the left emphasizes the observed power-law behavior $\text{Proba}(S/\ell^4) \sim \ell^8/S^2$. Blue lines are fits using an ansatz of the form $\text{Proba}(S/\ell^4) \sim \ell^8/S^2 \exp(-\mathcal{E}_0 S/\ell^4)$. The red line is a fit using only the cutoff function: $\text{Proba}(S/\ell^4) \sim \exp(-\mathcal{E}_0 S/\ell^4)$.

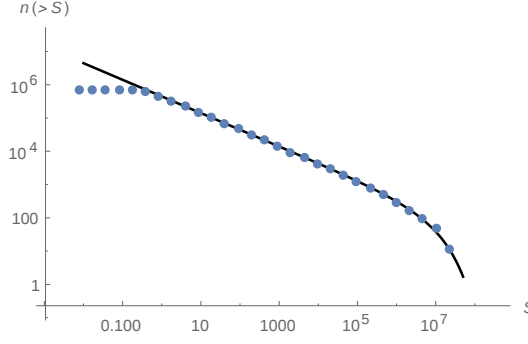


Figure A.6: Left: $n_{>S}$ measured from the datas (blue dots) and compared to the quasi-static prediction ((A.7.17), black line) with $S_2 \rightarrow S$ (S_1 can be chosen anywhere in $[0.5, 10^5]$ and $n_{>S_1}$ is measured from the datas).

where ρ was defined in (A.4.4). Numerically, we find that this relation holds for all S_1, S_2 larger than $S_{\min} = 0.5$ (see Figure A.6). We thus further restrict our set of avalanches to avalanches of total size $S \geq S_{\min}$. Note that though our reduced set of avalanches now only contains 2.7% of the total number of avalanches, it contributes to 99.44% to the first moment $\langle S \rangle$. (This gives a precise sense to Eq. (A.7.16) with $p_0 = 0.027$). We do not further study the other avalanches here, since their characteristics is highly dependent on the chosen driving.

.4 The convergence to the saddle-point. We now check the striking prediction that the shape of avalanches becomes *deterministic* in the limit of large S/ℓ^4 . To this aim, we measure the distance between the optimal shape $s_0(x) = \phi_0^2(x)$ and the simulated shapes $s(x)$ using either the L^1 or the (squared) L^2 canonical norms (see Figure A.7). As expected, we find that the mean value of these quantities at fixed S/ℓ^4 converge to 0 as S/ℓ^4 becomes larger. However, we find that the rate of convergence of these quantities is slower than what is expected from perturbation theory (this is developed in the next section), which predicts for both a convergence as ℓ^4/S . This will be taken into account when comparing the numerical results to the prediction of perturbation theory for the fluctuations around the optimal shape.

.5 The mean shape of avalanches. Finally, we verify on Figure A.8 that the mean shape $\langle s(x) \rangle$ is given by the optimal shape $s_0(x)$ for large S/ℓ^4 . We also explicitly check that the mean-shape decays as $(x \pm 1/2)^4$ close to the boundaries. The agreement is very good, though one can notice that the numerical mean shape is slightly flatter than expected. This observation motivates a study of the fluctuations of the shape around the optimal shape.

A.8 Fluctuations around the saddle point

A.8.1 Field theoretic analysis

We now study the fluctuations around the saddle point $\phi_0(x)$. To this aim, we set

$$\phi(x) = \phi_0(x) + \delta\phi(x) . \quad (\text{A.8.1})$$

Expanding the action yields

$$\mathcal{H}_{\text{el}}[\phi] = \mathcal{E}_0 + 2\mathcal{E}_0 \int_x \phi_0(x) \delta\phi(x) + \mathcal{H}_2[\phi_0, \delta\phi] + \mathcal{H}_3[\phi_0, \delta\phi] + \dots \quad (\text{A.8.2})$$

$$\mathcal{H}_2[\phi_0, \delta\phi] = \int_x \delta\phi(x)^2 \left[\frac{20\phi_0'(x)^2 \phi_0''(x)}{\phi_0(x)^3} - \frac{15\phi_0'(x)^4}{\phi_0(x)^4} \right] + \delta\phi'(x)^2 \frac{10\phi_0'(x)^2}{\phi_0(x)^2} + \delta\phi''(x)^2 \quad (\text{A.8.3})$$

$$\begin{aligned} \mathcal{H}_3[\phi_0, \delta\phi] = & 5 \int_x \delta\phi(x)^2 \delta\phi'(x) \frac{3\phi_0'(x)^3 - \phi_0(x)\phi_0'(x)\phi_0''(x)}{\phi_0(x)^4} - 4\delta\phi(x)\delta\phi'(x)^2 \frac{\phi_0'(x)^2}{\phi_0(x)^3} \\ & + \frac{4}{3} \delta\phi'(x)^3 \frac{\phi_0'(x)}{\phi_0(x)^2} - \frac{1}{3} \delta\phi(x)^3 \frac{\phi_0'''(x)\phi_0'(x) + \phi_0''(x)^2}{\phi_0(x)^3} \end{aligned} \quad (\text{A.8.4})$$

The first term in Eq. (A.8.2) comes from the saddle-point equation (A.7.9) at $\phi = \phi_0$, $\mathcal{A}_0 \phi_0(x) = \frac{1}{2} \frac{\delta \mathcal{H}_{\text{el}}[\phi]}{\delta \phi(x)} |_{\phi(x)=\phi_0(x)}$ together with (A.7.11). We have used our freedom to integrate by part to arrive at these expressions: For $\mathcal{H}_2[\phi_0, \delta\phi]$ we gave a form in which each term is proportional to the square of a $\delta\phi$ -derivative. For the cubic term, which is used in perturbation theory our strategy is different: Since derivatives of $\langle \delta\phi(x)\delta\phi(y) \rangle_{\mathcal{H}_2}$ are numerically unstable, we wrote this expression without a second derivative $\delta\phi''(x)$.

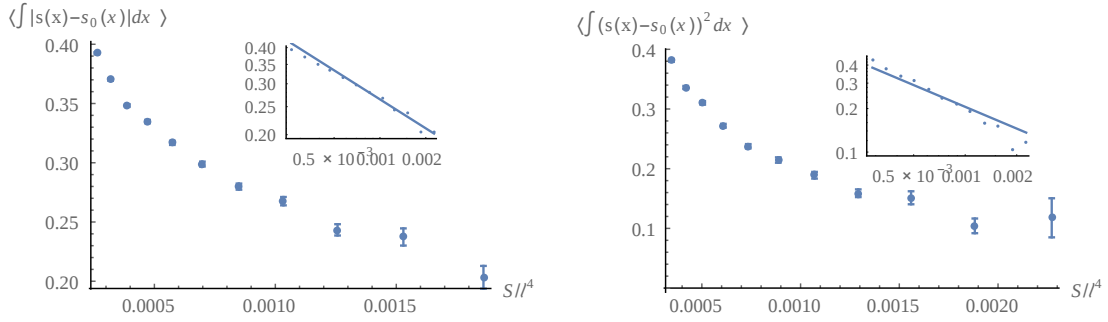


Figure A.7: Left: (resp. Right:) Mean-value at fixed S/ℓ^4 of the L^1 (resp. squared L^2) norm between the optimal shape and the simulated shape $\int_{-1/2}^{1/2} dx |s(x) - s_0(x)|$ (resp. $\int_{-1/2}^{1/2} dx (s(x) - s_0(x))^2$). Inset: log-log plot of the same quantity, fitted with a power-law $(\ell^4/S)^{1/3}$ (resp. $(\ell^4/S)^{1/2}$). Error bars are given using a Gaussian estimate and a numerical measurement of the variance. The fits with power-laws are of low quality, but sufficient to prove that the convergence is slower than ℓ^4/S .

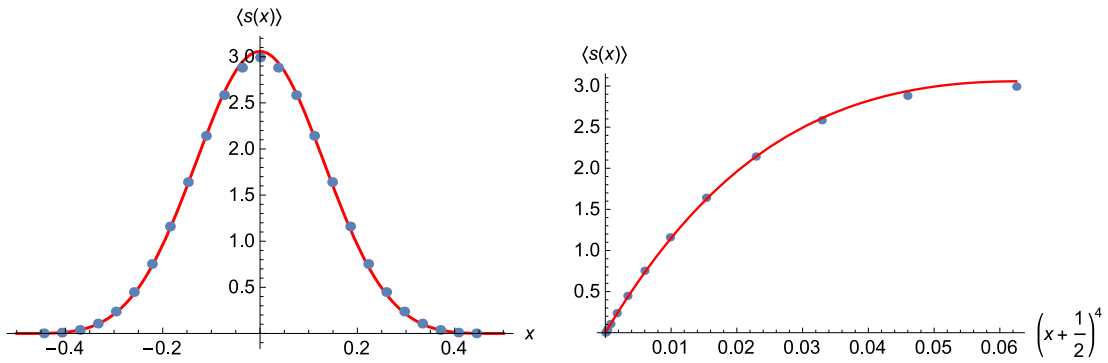


Figure A.8: Left: Mean shape obtained by averaging over the 1000 avalanches with the largest S/ℓ^4 (blue dots, $0.0011 \leq S/\ell^4 \leq 0.0041$), compared to the optimal shape $s_0(x)$ (red line). Right: test of the predicted behavior $s(x) \sim (x + 1/2)^4$ close to the boundaries.

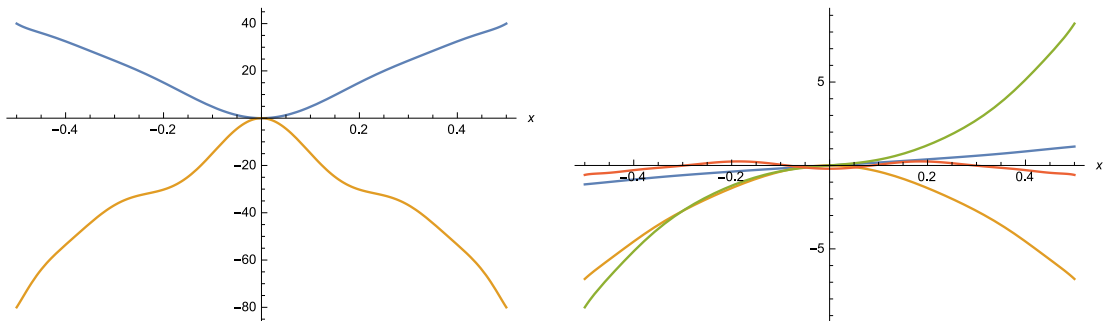


Figure A.9: The coefficients multiplying the different terms in $\mathcal{H}_2[\phi_0, \delta\phi]$ (left) and $\mathcal{H}_3[\phi_0, \delta\phi]$ (right), after replacing $\delta\phi(x) \rightarrow (x^2 - 1/4)^2$ and $\delta\phi'(x) \rightarrow x^2 - 1/4$. This shows that $\delta\phi(x)$ must have the same behavior $\sim (x^2 - 1/4)^2$ as $\phi_0(x)$ at the boundary $x = \pm 1/2$.

To evaluate the coefficients, we use the variational ansatz (A.7.12), with the optimal \bar{c} of Eq. (A.7.13). The plot in Figure A.9 shows that $\delta\phi(x)$ should have the same behavior $\sim (x^2 - 1/4)^2$ as $\phi_0(x)$ at the boundary $x = \pm 1/2$. We therefore make the ansatz

$$\delta\phi(x) = a_0 v_0(x) + \sum_{n=1}^{n_{\max}} \left[a_{2n-1} v_n(x) + a_{2n} u_n(x) \right]. \quad (\text{A.8.5})$$

The basis $u_n(x)$, $v_n(x)$ is constructed using Gram-Schmidt out of

$$\bar{v}_0(x) = \sqrt{\frac{2}{3}} \left[1 + \cos(2\pi x) \right] \quad (\text{A.8.6})$$

$$\bar{v}_n(x) = (-1)^{n+1} \cos(2\pi(n+1)x) + \cos(2\pi x) \quad \text{for } n \geq 1 \quad (\text{A.8.7})$$

$$\bar{u}_n(x) = \frac{(n+1) \sin(2\pi x) + (-1)^{n+1} \sin(2\pi(n+1)x)}{\sqrt{\frac{n^2}{2} + n + 1}}. \quad (\text{A.8.8})$$

This basis is orthonormal. In this basis, the energy $\mathcal{H}_2[\phi_0, \delta\phi]$ can be written as

$$\mathcal{H}_2[\phi_0, \delta\phi] = \frac{1}{2} \int_{x,y} \delta\phi(x) \mathcal{M}(x,y) \delta\phi(y) = \frac{1}{2} \sum_{i,j} \mathcal{M}_{ij} a_i a_j. \quad (\text{A.8.9})$$

This defines \mathcal{M} which we now diagonalize. Its lowest eigenvalue is $\lambda_0 = 2\mathcal{E}_0$, with eigenfunction $\delta\phi_0(x) = \phi_0(x)$. This can be proven with the help of the saddle-point equation (A.7.9). The higher eigenfunctions $\delta\phi_n(x)$ have n knots, see Figure A.10. Since \mathcal{M} is symmetric they form an orthonormal basis. The spectrum is massive (no soft massless modes); we observe that $\ln \lambda_n \simeq 13.1 + 0.256n$, i.e. the eigenvalues grow in geometric progression. This ensures that a truncation at $n_{\max} = 10$ is sufficient for practical purposes.

A delicate problem is to obtain results at fixed $\int_x \phi(x)^2 = 1$. To do so, we write for the expectation value of an observable $\mathcal{O}[\phi]$

$$\begin{aligned} \langle \mathcal{O}[\phi] \rangle &= \frac{1}{\langle 1 \rangle} \int \mathcal{D}[\phi] \mathcal{O}[\phi] \delta\left(\int_x \phi^2(x) - 1\right) \exp\left(-\frac{S}{\ell^4} \left\{ \mathcal{H}_{\text{el}}[\phi_0, \delta\phi] - \mathcal{E}_0 \right\}\right) \\ &= \frac{1}{\langle 1 \rangle} \int \mathcal{D}[\phi] \mathcal{O}[\phi] \delta\left(\int_x \phi^2(x) - 1\right) \\ &\quad \times \exp\left(-\frac{S}{\ell^4} \left\{ \mathcal{H}_2[\phi_0, \delta\phi] - \mathcal{E}_0 \int_x \delta\phi(x)^2 + \mathcal{H}_3[\phi_0, \delta\phi] + \mathcal{H}_4[\phi_0, \delta\phi] + \dots \right\}\right) \end{aligned} \quad (\text{A.8.10})$$

We subtracted the constant \mathcal{E}_0 from the energy in the path integral and used the constraint $\int_x \phi(x)^2 = 1$ to rewrite the linear term appearing in (A.8.2) as a quadratic term: $2\mathcal{E}_0 \int_x \phi_0(x) \delta\phi(x) = -\mathcal{E}_0 \int_x \delta\phi(x)^2$. It ensures that the minimum of the exponential factor at $\delta\phi(x) = 0$ becomes a global saddle point; in addition, the lowest-energy fluctuation $\delta\phi_0$ has zero energy. If we write $\phi(x)$ in the basis of eigenmodes $\delta\phi_n(x)$ of \mathcal{M} , i.e.

$$\phi(x) = \phi_0(x) + \sum_{n=0}^{\infty} a_n \delta\phi_n(x) \equiv (1 + a_0) \phi_0(x) + \sum_{n=1}^{\infty} a_n \delta\phi_n(x), \quad (\text{A.8.11})$$

then

$$\int_x \phi(x)^2 = \int_x \left[\phi_0(x) + \sum_{n=0}^{\infty} a_n \delta\phi_n(x) \right]^2 = (1 + a_0)^2 + \sum_{n=1}^{\infty} a_n^2. \quad (\text{A.8.12})$$

Solving $\int_x \phi(x)^2 = 1$ for a_0 yields

$$a_0 = \sqrt{1 - \sum_{n=1}^{\infty} a_n^2} - 1 \quad \implies \quad a_0 = -\frac{1}{2} \sum_{n=1}^{\infty} a_n^2 + \dots \quad (\text{A.8.13})$$

With this, the path-integral (A.8.10) can be written using equations (A.8.11) and (A.8.13) as

$$\begin{aligned} \langle \mathcal{O}[\phi] \rangle &= \frac{1}{\langle 1 \rangle} \prod_{n=1}^{\infty} da_n \mathcal{O}[\phi] \left(1 - \sum_{n=1}^{\infty} a_n^2\right)^{-\frac{1}{2}} \\ &\quad \times \exp\left(-\frac{S}{\ell^4} \left\{ \sum_{n=1}^{\infty} \frac{\lambda_n - \lambda_0}{2} a_n^2 + \mathcal{H}_3[\phi_0, \delta\phi] + \mathcal{H}_4[\phi_0, \delta\phi] + \dots \right\}\right). \end{aligned} \quad (\text{A.8.14})$$

The factor of $\left(1 - \sum_{n=1}^{\infty} a_n^2\right)^{-\frac{1}{2}}$ comes from the derivative of the δ -function, which has been used to eliminate the integration over a_0 . Note that the Jacobian of the transformation from $\prod_x d\phi(x)$ to $\prod_n da_n$ is $\det(\delta\phi_n(x))_{x \in [-\frac{1}{2}, \frac{1}{2}], n \in \mathbb{N}} = 1$, since the $\delta\phi_n(x)$ are orthonormal.

Hence, to leading order in an expansion in ℓ^4/S , the expectation value of an observable of $\delta\phi(x)$ can be obtained using the decomposition $\delta\phi(x) = \sum_{i=0}^{\infty} a_i \delta\phi_i(x)$, where a_0 is given by (A.8.13) and the a_i are centered Gaussian variables with correlation matrix \mathcal{M}' defined for $i, j \geq 1$ by

$$\langle a_i a_j \rangle_{\mathcal{M}'} := \frac{\ell^4}{S} \frac{\delta_{ij}}{\lambda_i - \lambda_0}. \quad (\text{A.8.15})$$

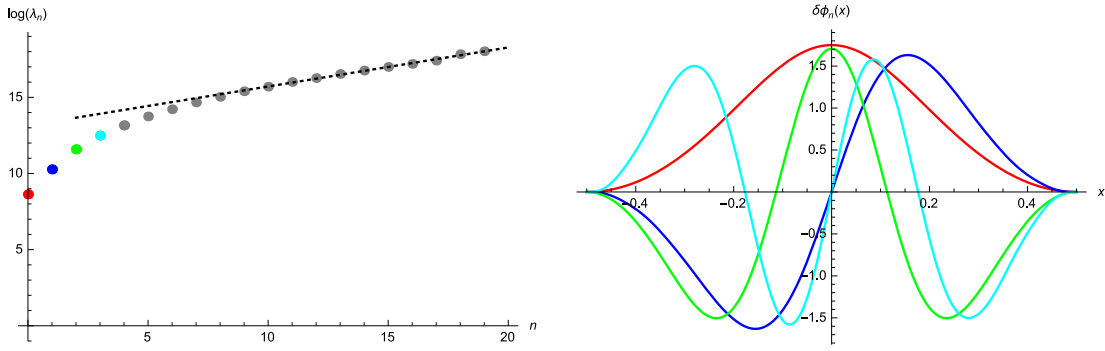


Figure A.10: Left: The spectrum of \mathcal{M} . The smallest eigenvalue is $\lambda_0 = 2\mathcal{E}_0$ (given with precision 10^{-4} for $n_{\max} = 10$). The next two eigenvalues are $\lambda_1 = 5.143\lambda_0$, and $\lambda_2 = 19.20\lambda_0$. Eigenvalues for large modes grow exponentially with the mode, $\ln \lambda_n \simeq 13.1 + 0.256 n$ (black dashed line), showing that the spectrum of fluctuations is massive. The lowest modes are colored in red, blue, orange and cyan. Right: Plot of the first four eigenfunctions in the same colors as the corresponding eigenvalues. $\delta\phi_n(x)$ has n nodes.

One then uses Wick's theorem for expectation values of $\delta\phi$. As an example, the 2-point correlation function is

$$\begin{aligned} \langle \delta\phi(y)\delta\phi(z) \rangle_{\mathcal{H}} &= \sum_{i=0}^{\infty} \sum_{j=0}^{\infty} \langle a_i a_j \rangle_{\mathcal{M}'} \delta\phi_i(y)\delta\phi_j(z) + O\left(\frac{\ell^8}{S^2}\right) \\ &= \frac{\ell^4}{S} \sum_{i=1}^{\infty} \frac{\delta\phi_i(y)\delta\phi_i(z)}{\lambda_i - \lambda_0} + O\left(\frac{\ell^8}{S^2}\right). \end{aligned} \quad (\text{A.8.16})$$

A.8.2 Generating a random configuration, and importance sampling

Our setting allows us to generate a random fluctuation with the measure given by the the leading behaviour of \mathcal{H} for large S/ℓ^4 : Denote by g_n a series of uncorrelated Gaussian random numbers with mean zero and variance 1. Then

$$\delta\phi(x)^{\text{rand}} = \sum_{n=0}^{\infty} a_n \delta\phi_n(x), \quad \text{with} \quad a_n = \sqrt{\frac{\ell^4}{S}} \frac{g_n}{\sqrt{\lambda_n - \lambda_0}} \quad \text{for} \quad n > 0, \quad (\text{A.8.17})$$

and a_0 given by Eq. (A.8.13). In Figure A.11 (left) we show as an example the expectation of $\delta\phi(x)^2$ (solid blue line). This is compared to the average over 500 realizations drawn with the measure (A.8.17), repeated 5 times (the three gray-blue lines, lower set of curves). To illustrate the importance to properly eliminate the mode $\phi_0(x)$, the upper (red) curves are obtained without the constraint on $\int_x \phi^2(x)$, i.e. including fluctuations proportional to $\phi_0(x)$ (with amplitude $\sim 1/\sqrt{\lambda_0}$), and not constraining them by Eq. (A.8.13).

On Figure A.12 we show five realizations for the shape drawn from the measure (A.8.17), and compare this to numerical simulations at the same ratio S/ℓ^4 . The agreement is quite good.

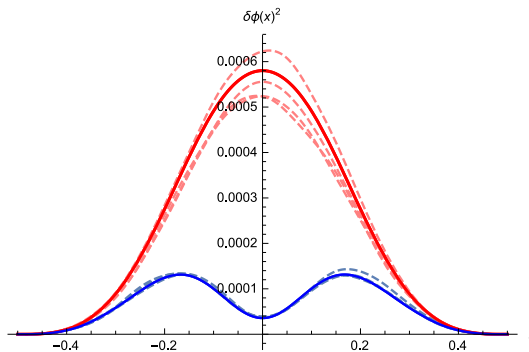


Figure A.11: Left: Plot of the fluctuations $\delta\phi(x)^2$ (blue solid line), and including the mode $\delta\phi_0$ (red solid line). The dashed lines are averages over 500 samples using Eq. (A.8.17), including (top pink) or excluding (bottom, blue-gray) this mode.

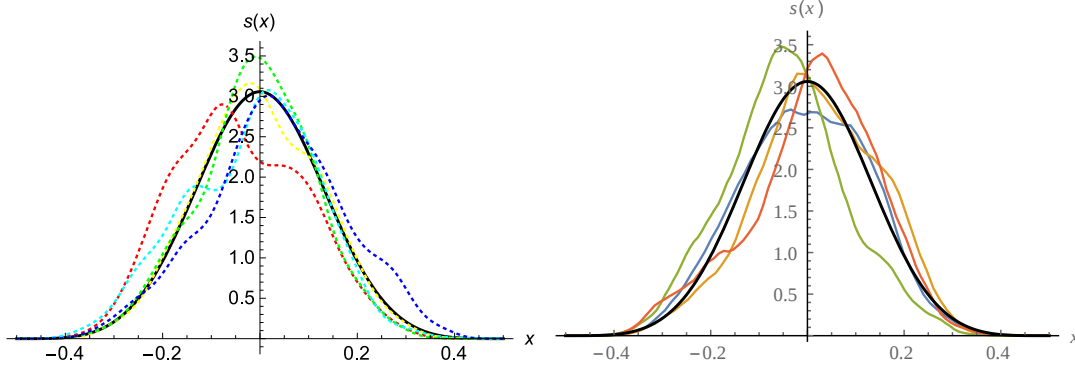


Figure A.12: Left: Plot of the normalized shape $[\phi_0(x) + \sqrt{\frac{\ell^4}{S}} \delta\phi(x)]^2$ for $\frac{\ell^4}{S} = 3 \times 10^{-3}$. Right: The same functions from numerical simulations.

We can use this formulation for an efficient algorithm, known in the literature as *importance sampling* [232]. One writes

$$\begin{aligned} \langle \mathcal{O}[\phi] \rangle &= \frac{1}{\langle 1 \rangle} \left\langle \mathcal{O}[\phi] \left(1 - \sum_{n=1}^{\infty} a_n^2\right)^{-\frac{1}{2}} \exp\left(-\frac{S}{\ell^4} \left\{ \mathcal{H}_3[\phi_0, \delta\phi] + \mathcal{H}_4[\phi_0, \delta\phi] + \dots \right\}\right) \right\rangle_{\mathcal{M}'} \\ &= \frac{1}{\langle 1 \rangle} \left\langle \mathcal{O}[\phi] \left(1 - \sum_{n=1}^{\infty} a_n^2\right)^{-\frac{1}{2}} \exp\left(-\frac{S}{\ell^4} \left\{ \mathcal{H}_{\text{el}}[\phi_0 + \delta\phi] - \mathcal{E}_0 - \sum_{n=1}^{\infty} \frac{\lambda_n - \lambda_0}{2} a_n^2 \right\}\right) \right\rangle_{\mathcal{M}'} . \end{aligned} \quad (\text{A.8.18})$$

In the second line we reintroduced the full Hamiltonian \mathcal{H}_{el} using Eq. (A.8.2). We will compare to simulations below.

A.8.3 The leading correction to the shape at large sizes

For large S/ℓ^4 , the mean shape is given by the optimal shape $s_0(x)$. For smaller S/ℓ^4 , this mean shape becomes flatter, an effect which we now investigate using perturbation theory. Consider

$$\begin{aligned} \langle \delta s(x) \rangle &:= \langle s(x) - \phi_0(x)^2 \rangle \\ &= \left\langle \left(2\phi_0(x)\delta\phi(x) + \delta\phi(x)^2\right) \left(1 - \frac{S}{\ell^4} \mathcal{H}_3[\phi_0, \delta\phi] + \dots\right) \right\rangle_{\mathcal{M}'} \\ &= \frac{\ell^4}{S} \left[\left\langle \delta\phi(x)^2 \right\rangle_{\mathcal{M}'} - 2\phi_0(x) \left\langle \delta\phi(x) \mathcal{H}_3[\phi_0, \delta\phi] \right\rangle_{\mathcal{M}'} \right] + O\left(\frac{\ell^4}{S}\right)^2 . \end{aligned} \quad (\text{A.8.19})$$

The notation $\bar{\mathcal{M}}'$ indicates that all expectation values are taken at $S/\ell^4 = 1$, making the factors of $\frac{S}{\ell^4}$ explicit.

A.8.4 Fluctuations of the shape for large avalanches

We now consider the fluctuations of the shape of an avalanche in perturbation theory:

$$\begin{aligned} \langle \delta s(x)^2 \rangle_c &:= \langle s(x)^2 \rangle - \langle s(x) \rangle^2 \\ &= \left\{ \left\langle \left[\phi_0(x)^2 + 2\phi_0(x)\delta\phi(x) + \delta\phi(x)^2 \right]^2 \left(1 - \frac{S}{\ell^4} \mathcal{H}_3[\phi_0, \delta\phi] + \dots\right) \right\rangle_{\mathcal{M}'} \right. \\ &\quad \left. - \left\langle \left[\phi_0(x)^2 + 2\phi_0(x)\delta\phi(x) + \delta\phi(x)^2 \right] \left(1 - \frac{S}{\ell^4} \mathcal{H}_3[\phi_0, \delta\phi] + \dots\right) \right\rangle_{\mathcal{M}'}^2 \right\} \\ &= 4 \left(\frac{\ell^4}{S} \right) \phi_0(x)^2 \langle \delta\phi(x)^2 \rangle_{\bar{\mathcal{M}}'} + O\left(\frac{\ell^4}{S}\right)^2 . \end{aligned} \quad (\text{A.8.20})$$

Note that the only term which survives is the contraction between one $\delta\phi(x)$ of each factor $s(x)$.

A.8.5 Asymmetry of an avalanche

Another interesting observable is the asymmetry \mathcal{A} of an avalanche, defined by

$$\mathcal{A} := 2 \int_x x \phi^2(x) . \quad (\text{A.8.21})$$

By construction $-1 \leq \mathcal{A} \leq 1$. The asymmetry has mean zero $\langle \mathcal{A} \rangle = 0$, and variance given in perturbation theory by

$$\langle \mathcal{A}^2 \rangle = 16 \left(\frac{\ell^4}{S} \right) \int_{x,y} xy \phi_0(x) \phi_0(y) \langle \delta\phi(x) \delta\phi(y) \rangle_{\bar{\mathcal{M}}'} = 1.1 \times 10^{-5} \left(\frac{\ell^4}{S} \right) . \quad (\text{A.8.22})$$

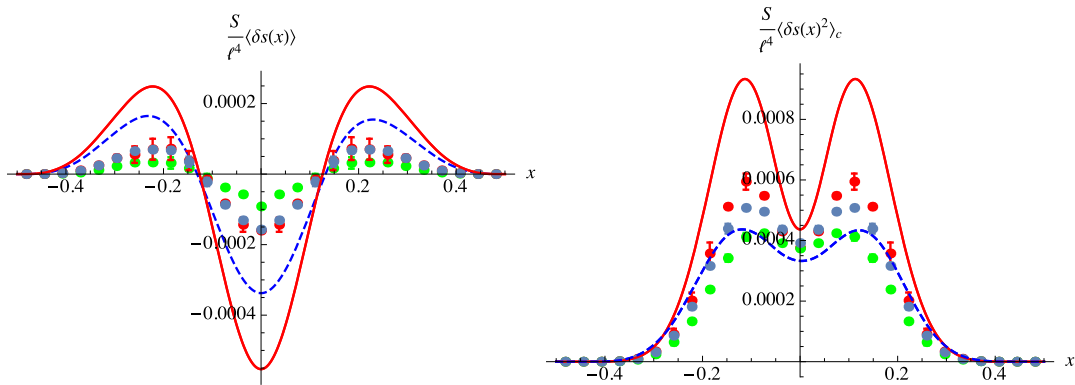


Figure A.13: Left: (resp. Right:) normalized mean shape displacement $\langle S/\ell^4(s(x) - s_0(x)) \rangle$ (resp. shape fluctuations $\langle S/\ell^4(s(x) - s_0(x))^2 \rangle_c$). Red line: result of perturbation theory (A.8.19) (resp. (A.8.20)). Dashed-blue line: result from *importance sampling* using (A.8.18) for $\ell^4/S = 900$. Dots: results from the simulations for avalanches with aspect-ratio $0.9/1800 \leq S/\ell^4 \leq 1.1/1800$ (7023 samples, green), $0.9/900 \leq S/\ell^4 \leq 1.1/900$ (946 samples, blue) and $S/\ell^4 \geq 1.1/1900$ (734 samples, red). We take advantage of the symmetry of the observable $\langle s(x) \rangle \equiv \langle s(-x) \rangle$ to symmetrize the numerical result. We estimate error bars using the difference between the original result and the symmetrized one.

A.8.6 Comparison of the perturbative corrections to the numerics

We had already shown some results of our numerical simulations above. For large S/ℓ^4 , the perturbation theory developed in the preceding section gives the correction $\langle \delta s(x) \rangle$ of the mean shape to the saddle-point solution, as well as the shape fluctuation $\langle \delta s(x)^2 \rangle_c$ around the saddle-point. However, as already pointed out in section A.7.4, the scaling of these quantities with a factor of ℓ^4/S is not seen in the convergence of the numerical simulations to the saddle point, see Figure A.7. This indicates that, even at $S/\ell^4 \approx 10^{-3}$, the simulations are not yet in the perturbative (first-order) scaling regime. Non-linear corrections are still important, and $\frac{S}{\ell^4} \langle \delta s(x) \rangle$ as well as $\frac{S}{\ell^4} \langle \delta s(x)^2 \rangle_c$ still depend on $\frac{S}{\ell^4}$. This is illustrated on Figure A.13.

As can be seen on the left of Figure A.13 (as well as on the left of Figure A.4), corrections to the mean shape are very small, of the order of 10^{-4} , difficult to measure, and at the limit of our simulations. The red solid line is the perturbative result (A.8.19). The points correspond to the same quantity from the numerics with increasing S/ℓ^4 from green over blue-gray to red (see caption for the precise parameters). The dashed blue line is obtained for $S/\ell^4 = 1/900$ via *importance sampling*, see equation (A.8.18)⁸. One remarks that the amplitude is lowered as compared to the perturbative result, in qualitative agreement with the simulations. In view of the difficulty of the numerical simulations, it is very encouraging that at least a qualitative agreement has been obtained, and that *importance sampling* explains why the observed corrections are smaller than the perturbative result, in agreement with intuition: the shape has to remain positive.

The fluctuations around the mean shape, $\frac{S}{\ell^4} \langle \delta s(x)^2 \rangle_c$, are given on the right of Figure A.13 with the same color code as previously. One sees that the numerical results approach the perturbative result for large S/ℓ^4 . In this case, importance sampling predicts fluctuations slightly smaller than our numerical simulations, which converge more quickly towards the perturbative result. We remark that numerically the estimation of $\frac{S}{\ell^4} \langle \delta s(x)^2 \rangle_c$ is less sensitive than the estimation of $\frac{S}{\ell^4} \langle \delta s(x) \rangle$. This may be explained by the fact that only the latter quantity involves non-linearities of \mathcal{H} at dominant order in S/ℓ^4 .

For the asymmetry we find $\frac{S}{\ell^4} \langle \mathcal{A}^2 \rangle = 1.1 \times 10^{-5}$ in perturbation theory, and $5.97 \pm 0.04 \times 10^{-6}$ via exact sampling for $S/\ell^4 = 1/900$. Numerical simulations give $\frac{S}{\ell^4} \langle \mathcal{A}^2 \rangle = (7 \pm 2) \times 10^{-6}$ for the largest avalanches $S/\ell^4 \geq 0.002$ (37 samples), $(5.6 \pm 0.3) \times 10^{-6}$ for the data with $1.1/900 \leq S/\ell^4 \leq 0.002$ (697 samples), $(4.7 \pm 0.2) \times 10^{-6}$ for the data with $0.9/900 \leq S/\ell^4 \leq 1.1/900$ (946 samples) and $(3.05 \pm 0.05) \times 10^{-6}$ for the data with $0.9/1800 \leq S/\ell^4 \leq 1.1/1800$ (7023 samples). Once again we see that the order of magnitude is correctly predicted (an already non-trivial achievement), and that the numerical results get closer to the perturbative one as S/ℓ^4 increases.

From a conceptual point of view it is interesting to note that most of the amplitude of the “double-peak” structure observed on the right of Figure A.13 is due to the first sub-leading mode $\delta\phi_1(x)$ with one node at $x = 0$ (see Fig. A.10). The same holds true for $\langle \mathcal{A}^2 \rangle$.

In conclusion, we have seen that the numerical results agree very well with the theoretical prediction at large S/ℓ^4 , and that the mean shape of avalanches is given by the optimal shape $s_0(x)$ (Figures A.7 and A.8). The consequence for

⁸For $S/\ell^4 = 1/900$, about 44% of the proposed configurations in the importance sampling have a zero-crossing in $s(x)$, and therefore do not contribute. The measured expectation of the weight is $\langle 1 \rangle = 1.61 \pm 0.012$, showing that averages are not dominated by a few configurations.

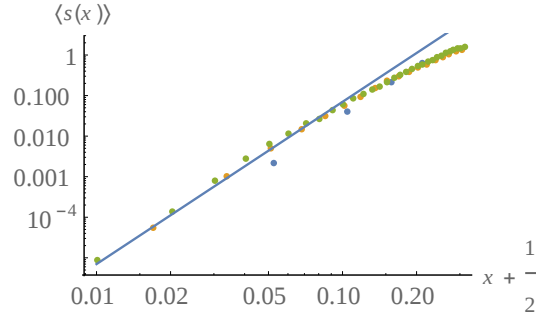


Figure A.14: Log-Log plot of the numerical measurement of the mean shape at fixed ℓ for $\ell = 40$ (blue dots), $\ell = 70$ (orange dots) and $\ell = 100$ (green dots) close to the boundary $-1/2 < x < -1/4$. The first point of each shape was not taken into account to avoid discretization artefacts. As a consequence of the discretization of the simulation, the first visible point of each shape is located at $x = -1/2 + 1/\ell$. The plain line serves as a guide to compare with the behavior $(-1/2 + x)^4$ obtained from the study of the optimal shape at large S/ℓ^4 .

the tail of the PDF of S/ℓ^4 was successfully verified (Figure A.5). For finite S/ℓ^4 , namely fluctuations around the optimal shape, we only got a partial, though already satisfying agreement: The discrepancy with the perturbative results was clearly identified as a consequence of strong non-linearities, even for the largest S/ℓ^4 . This was qualitatively understood by an implementation of *importance sampling*, though the remaining discrepancy raises the question of whether our simulations are sufficiently precise to measure these delicate observables (Figures A.12 and A.13).

A.8.7 The optimal shape beyond extreme value statistics

Before concluding this section, let us mention that though our results on the shape of avalanches were a-priori obtained for the most peaked avalanches (i.e. avalanches with a large aspect ratio of S/ℓ^4 , some of our result extend at least qualitatively to generic avalanches. As an example we show in Figure A.14 that the characteristic decay of the optimal shape near the boundary $s_0(x) \sim (x \pm 1/2)^4$ can still be observed in the decay of the mean shape at fixed ℓ .

In this spirit, we thus encourage experimental and numerical comparison of our results to various, and non-necessary extremal, shape observables.

A.9 Application of our results to realistic interfaces and stationary driving

Up to now we considered avalanches following a stopped driving (see Section A.2). However, as discussed in [136, 101, 102] this setting also yields the densities for the statistics of quasi-static avalanches in the steady state (Middleton state) for stationary driving in the quasi-static limit ($\dot{w}_t = v$ and $v \rightarrow 0^+$). These are the avalanche densities defined in Section A.4, hence the denomination used in this article.

Furthermore, it was shown in Ref. [101], that the BFM is the mean-field theory of an avalanche in the quasi-static limit for an interface in short-ranged disorder with equation of motion

$$\eta_0 \partial_t u_{xt} = \int_y c_{xy} u_{yt} + m^2 (w_{xt} - u_{xt}) + F(x, u_{xt}) . \quad (\text{A.9.1})$$

The disorder-force correlator is given by $\overline{F(x, u)F(x', u')} = \Delta_0(u - u')\delta^d(x - x')$ with $\Delta_0(u)$ a fast decaying function as $|u| \rightarrow \infty$ and c_{xy} a convex elastic kernel. The prediction of the functional renormalization group (FRG) for such systems is that, in the quasi-static limit, when $m \rightarrow 0$ and for $d = d_{uc} - \epsilon$, $\epsilon \geq 0$ ($d_{uc} = 4$ for short-ranged elasticity and more generally $d_{uc} = 2\gamma$ for $g(q) \sim_{q \rightarrow \infty} q^\gamma$), the physics becomes universal in the small- m limit (e.g. independent of microscopic details of the disorder) and entirely controlled by only two relevant couplings, the renormalized friction η_m and the renormalized disorder cumulant $\Delta_m(u)$. The (rescaled and renormalized) second cumulant of the disorder at the fixed point is non-analytic and exhibits a cusp. It is uniformly $O(\epsilon)$, allowing to formulate a controlled perturbative expansion of any observable. For observables associated to a single avalanche, it was shown in [136, 101] that near the upper critical dimension d_{uc} only the behavior of Δ_m near zero, i.e. its cusp, $\Delta_m(u) \simeq_{u \rightarrow 0} -\sigma_m |u|$ plays a role. In this context, the mean-field theory for single-avalanche motion is the BFM studied here, with renormalized parameters $\eta \rightarrow \eta_m$ and $\sigma \rightarrow \sigma_m$. Hence, the avalanche densities derived in Section A.4 are exact for interfaces at their upper critical dimension. They also open the way to a perturbative calculation for $d \leq d_{uc}$. Interestingly, some physical systems described by (A.9.1) are at their upper critical dimension, as e.g. domain walls in certain soft magnets for which $\gamma = 1$ [45].

A.10 Conclusion

In this article we obtained an exact formula for the joint PDF of the local sizes of avalanches in a discrete version of the BFM model. This result is valid for an arbitrary elasticity matrix and arbitrary monotonous driving. This allowed us to derive the densities describing the quasi-static avalanches in the limit of small driving, and to discuss in depth the physical picture underlying this avalanche process. We presented two applications where it was possible to go further in the analytical calculation of detailed physical properties. For the fully connected model we obtained the joint distribution of the local and global jumps. This allowed us to retrieve in a rigorous way the usual large- N limit, as well as a new regime, and finite- N information.

We then presented another application by analyzing the most probable shape of avalanches of a given size and extension, first for systems made of few coupled particles, then in the continuum limit for an elastic line with short-ranged elasticity. Quantitative results for the optimal shape and the fluctuations around it were obtained and compared to a numerical simulation of the model.

Let us conclude by stressing that, since our formula was obtained in a general setting and contains all the spatial statistics of avalanches, it should be possible to extract from it a variety of new information on their spatial structure of direct experimental interest. It would also be interesting to compare our results for the shape of avalanches to other models through simulations or experiments, the BFM being the relevant mean-field theory for various more realistic systems.

Acknowledgments: We acknowledge support from PSL grant ANR-10-IDEX-0001-02-PSL. We thank KITP for hospitality and support in part by NSF Grant No. NSF PHY11-25915.

A.11 Appendix A: Recall of the result for the generating function

For completeness, we recall in this section, the derivation, here in a discrete setting, of the exact result for the generating function of the BFM (A.2.6). Related derivations can be found in [102, 101]. The original equation of motion, including the quenched noise term $\partial_t F_i(u_{it})$ reads

$$\eta \partial_t \dot{u}_{it} = \sum_{j=1}^N c_{ij} \dot{u}_{jt} - m^2 (\dot{u}_{it} - \dot{w}_{it}) + \partial_t F_i(u_{it}) . \quad (\text{A.11.1})$$

We use the dynamical field theory formalism [130, 131] which allows to compute the disorder average of any physical observable $O[\dot{u}]$. We introduce N response fields \tilde{u}_{it} such that disorder averages can be computed as

$$\overline{O[\dot{u}]} = \int \mathcal{D}[\dot{u}, \tilde{u}] O[\dot{u}] e^{-S[\dot{u}, \tilde{u}]} . \quad (\text{A.11.2})$$

The dynamical action splits into a deterministic, quadratic part and a disorder part: $S[\dot{u}, \tilde{u}] = S_0[\dot{u}, \tilde{u}] + S_{\text{dis}}[\dot{u}, \tilde{u}]$, with

$$\begin{aligned} S_0[\dot{u}, \tilde{u}] &= \sum_{i=1}^N \int_t \tilde{u}_{it} \left(\eta \partial_t \dot{u}_{it} - \sum_{j=1}^N c_{ij} \dot{u}_{jt} + m^2 (\dot{u}_{it} - \dot{w}_{it}) \right) \\ &= - \sum_{i=1}^N \int_t m^2 \tilde{u}_{it} \dot{w}_{it} + \sum_i \int_t \dot{u}_{it} \left(-\eta \partial_t \tilde{u}_{it} - \sum_{j=1}^N c_{ij} \tilde{u}_{jt} + m^2 \tilde{u}_{it} \right) \end{aligned} \quad (\text{A.11.3})$$

where in the second line, we made an integration by part assuming \dot{u} vanishes at infinity. The disorder part of the action is

$$S_{\text{dis}}[\dot{u}, \tilde{u}] = \frac{\sigma}{2} \sum_{i=1}^N \int_{tt'} \tilde{u}_{it} \tilde{u}_{it'} \partial_t \partial_{t'} |u_{it} - u_{it'}| , \quad (\text{A.11.4})$$

it contains all the correlation of the Gaussian force (A.2.2). As noted in [102, 101], the action functional can be simplified using the Middleton property recalled in the main text, valid for our setting: $t_2 \geq t_1 \iff u_{it_2} \geq u_{it_1}$ so that

$$\partial_t \partial_{t'} |u_{it} - u_{it'}| = \dot{u}_{it} \partial_{t'} \text{sgn}(t - t') = -2 \dot{u}_{it} \delta(t - t') . \quad (\text{A.11.5})$$

This leads to

$$S_{\text{dis}}[\dot{u}, \tilde{u}] = -\sigma \sum_{i=1}^N \int_t \tilde{u}_{it}^2 \dot{u}_{it} . \quad (\text{A.11.6})$$

It is straightforward to check that the replacement $\partial_t F_i(u_{it}) \rightarrow \sqrt{2\sigma} \dot{u}_{it} \xi_t^i$ used in the main text leads to the same action. This shows that both theories are equivalent for this choice of initial conditions. As written, the action is linear in \dot{u} : this

simplifies the calculation of the generating functional of the velocity field $G[\lambda, w] = e^{\overline{\sum_{i=1}^N \int_t \lambda_{it} \dot{u}_{it}}}$:

$$\begin{aligned} G[\lambda, w] &= \int \mathcal{D}[\dot{u}, \tilde{u}] e^{\sum_{i=1}^N \int_t \lambda_{it} \dot{u}_{it} - S[\dot{u}, \tilde{u}]} \\ &= \int \mathcal{D}[\tilde{u}] e^{m^2 \sum_{i=1}^N \int_t \tilde{u}_{it} \dot{w}_{it}} \prod_{it} \delta \left(\lambda_{it} + \sigma \tilde{u}_{it}^2 + \eta \partial_t \tilde{u}_{it} + \sum_{j=1}^N c_{ij} \tilde{u}_{jt} - m^2 \tilde{u}_{it} \right) \\ &= e^{m^2 \sum_{i=1}^N \int_t \tilde{u}_{it}^\lambda \dot{w}_i(t)}. \end{aligned} \quad (\text{A.11.7})$$

In the last line, the response field \tilde{u}_{it}^λ is solution to the ‘‘instanton’’ equation [136, 102, 101]

$$\lambda_{it} + \sigma \tilde{u}_{it}^2 + \eta \partial_t \tilde{u}_{it} + \sum_{j=1}^N c_{ij} \tilde{u}_{jt} - m^2 \tilde{u}_{it} = 0. \quad (\text{A.11.8})$$

It is imposed by the delta functional. Note that this evaluation involves a w -independent Jacobian, which equals unity since we have supposed the interface to be at rest and stable for $t \leq 0$, so that if $\dot{w}_{it} = 0$ then $\dot{u}_{it} = 0$. The above result is thus correctly normalized. Equation (A.11.8) must in general be supplemented by some boundary conditions, depending on the observable (e.g. if $\lambda_{it} = 0$ for all i and $t > t_1$, we should also have $\tilde{u}_{it} = 0$ for all i and $t > t_1$). Note that a rigorous version (in discrete-time, without path integral) of this result was given in [102]. In the main text we are looking for the statistics of avalanches S_i , which is obtained using constant sources $\lambda_{it} = \lambda_i$, and for which one can look for constant solutions $\tilde{u}_{it} = \tilde{u}_i$ of (A.11.8).

A.12 Appendix B: Tests of the main formula, computation of moments and numerical checks.

We checked (A.3.8) using two methods: the first one consists in solving exactly the instanton equation for small values of N in an expansion in powers of c for a given elasticity matrix. This gives an approximation of the Laplace transform, which can be inverted to give the joint probability distribution up to a certain order in c . This program has been successfully achieved up to $O(c^4)$ for $N = 2$, $O(c^3)$ for $N = 3$ and $O(c^2)$ for $N = 4$. The other method consists in numerically computing various moments of the probability distribution, which can then be compared to the exact results that use the instanton equation (A.3.2): the cumulants are given by

$$\langle S_{i_1} \cdots S_{i_n} \rangle^c = \left(\frac{\partial}{\partial \lambda_{i_1} \cdots \partial \lambda_{i_n}} \ln G(\vec{\lambda}) \right)_{\lambda_i=0} = \sum_{k=1}^N w_k \left(\frac{\partial v_k}{\partial \lambda_{i_1} \cdots \partial \lambda_{i_n}} \right)_{v_i=0} \quad (\text{A.12.1})$$

and these derivatives are numerically computed using $\frac{\partial v_i}{\partial \lambda_j} = J_{ij}^{-1}$ where $J_{ij} = -2v_i \delta_{ij} + C_{ij}$, as seen from (A.3.2).

A.13 Appendix C: Backward Kolmogorov method for a kick driving

In this section, we provide another verification that (A.3.8) is correct when the system is driven by a kick (i.e. $\dot{w}_{it} = w_i \delta(t)$). For simplicity, we directly consider the dimensionless equation of motion

$$\begin{aligned} \partial_t \dot{u}_{it} &= \sum_{j=1}^N c_{ij} \dot{u}_{jt} - \dot{u}_{it} + \dot{w}_{it} + \sqrt{2\dot{u}_{it}} \xi_t^i \\ &=_{t>0} - \sum_{j=1}^N C_{ij} \dot{u}_j + \sqrt{2\dot{u}_{it}} \xi_t^i \end{aligned} \quad (\text{A.13.1})$$

where in the second line we used the definition of C_{ij} (A.2.8) and wrote the equation for $t > 0$ when $\dot{w}_{it} = 0$. For a kick, it is equivalent to consider the equation of motion with $\dot{u}_{it=0} = 0$, or to consider the equation without driving for $t > 0$ (A.13.1) supplemented with the initial condition $\dot{u}_{i,t=0^+} = w_i$. The generating function G is still given by $G(\vec{\lambda}) = e^{\overline{\sum_{i=1}^N \lambda_i \int_0^\infty dt \dot{u}_{it}}}$. For a kick, we can write it as a conditional expectation value on the process without driving (A.13.1): $G(\vec{\lambda}) = \hat{G}(\vec{\lambda}, \vec{w}, 0, \infty)$ where \hat{G} is defined as

$$\hat{G}(\vec{\lambda}, \vec{w}, t_i, t_f) = \mathbb{E} \left(e^{\sum_{i=1}^N \lambda_i \int_{t_i}^{t_f} dt \dot{u}_{it}} \middle| \dot{u}_{it_i} = w_i \right) \quad (\text{A.13.2})$$

where \dot{u}_{it} evolves according to (A.13.1) for all times and $\mathbb{E} \left(\dots \middle| \dot{u}_{it_i} = w_i \right)$ denotes the average on the stochastic process without driving (A.13.1) conditioned to the initial condition $\dot{u}_{it_i} = w_i$. We now derive a partial differential equation (PDE)

fo G , similar to a Backward Kolmogorov equation, using a splitting of $[t_i, t_f]$ into $[t_i, t_i + \delta t] \cup [t_i + \delta t, t_f]$ with δt small:

$$\begin{aligned}\hat{G}(\vec{\lambda}, \vec{w}, t_i, t_f) &= \mathbb{E} \left(e^{\sum_{i=1}^N \lambda_i \int_{t_i+\delta t}^{t_f} dt \dot{u}_{it} + \sum_{i=1}^N \lambda_i \int_{t_i}^{t_i+\delta t} dt \dot{u}_{it}} \Big| \dot{u}_{it_i} = w_i \right) \\ &= \mathbb{E} \left(e^{\sum_{i=1}^N \lambda_i \int_{t_i+\delta t}^{t_f} dt \dot{u}_{it} + \sum_{i=1}^N \lambda_i \delta t w_{it}} \Big| \dot{u}_{it_i} = w_i \right) + o(\delta t)\end{aligned}\quad (\text{A.13.3})$$

Where in (A.13.3) we used that \dot{u}_{it} is continuous. The expectation value in (A.13.3) can now be split in two parts. We can first average over the noise for $t \in [t_i, t_i + \delta t]$, with δt small, or equivalently on the velocity variation $\delta w_i := \dot{u}_{i,t_i+\delta t} - \dot{u}_{i,t_i} = \dot{u}_{i,t_i+\delta t} - w_i$, as obtained from the equation of motion (A.13.1). Secondly, we average over the noise in $[t_i + \delta t, t_f]$ (these are independent) knowing that the velocity at $t_i + \delta t$ is $\dot{u}_{i,t_i+\delta t} = w_i + \delta w_i$, i.e.

$$\begin{aligned}\hat{G}(\vec{\lambda}, \vec{w}, t_i, t_f) &= \mathbb{E}_{\{\delta w_i\}} \left(\mathbb{E} \left(e^{\sum_{i=1}^N \lambda_i \int_{t_i+\delta t}^{t_f} dt \dot{u}_{it}} \Big| \dot{u}_{i,t_i+\delta t_i} = w_i + \delta w_i \right) \Big| \dot{u}_{it_i} = w_i \right) e^{\sum_{i=1}^N \lambda_i \delta t w_{it}} + o(\delta t) \\ &= \mathbb{E}_{\{\delta w_i\}} \left(\hat{G}(\vec{\lambda}, \vec{w} + \delta \vec{w}, t_i + \delta t_i, t_f) \Big| \dot{u}_{it_i} = w_i \right) e^{\sum_{i=1}^N \lambda_i \delta t w_{it}} + o(\delta t)\end{aligned}\quad (\text{A.13.4})$$

The average over $\{\delta w_i\}$ can be computed at first order in δt using Ito's lemma (we use $\overline{\delta w_\alpha} = -\delta t \sum_{j=1}^N C_{\alpha j} w_j$ and $\overline{\delta w_\alpha^2} = 2w_\alpha \delta t + O(\delta t^2)$). This leads to

$$\begin{aligned}\hat{G}(\vec{\lambda}, \vec{w}, t_i, t_f) &= \left(\hat{G} + \sum_{\alpha=1}^N \delta t \left(\frac{\partial \hat{G}}{\partial w_\alpha} \left(-\sum_{j=1}^N C_{\alpha j} w_j \right) + \frac{1}{2} \frac{\partial^2 \hat{G}}{\partial w_\alpha^2} (2w_\alpha) \right) + \delta t \frac{\partial \hat{G}}{\partial t_i} \right) \\ &\quad \times \left(1 + \sum_{i=1}^N \lambda_i \delta t w_{it} \right) + o(\delta t).\end{aligned}\quad (\text{A.13.5})$$

We also expanded the last term at first order in δt . In the r.h.s. of (A.13.5), all generating functions are taken at the same position $\hat{G}(\vec{\lambda}, \vec{w}, t_i, t_f)$. Now the l.h.s. is of order $O(\delta t^0)$ and in the l.h.s., we exactly computed the $O(\delta t)$ term. This shows that the generating function \hat{G} solves the following PDE:

$$-\frac{\partial \hat{G}}{\partial t_i} = \sum_{\alpha=1}^N \left(-\frac{\partial \hat{G}}{\partial w_\alpha} \sum_{j=1}^N C_{\alpha j} w_j + \frac{\partial^2 \hat{G}}{\partial w_\alpha^2} w_\alpha + \lambda_\alpha w_\alpha \right)\quad (\text{A.13.6})$$

which is also equal to $\frac{\partial \hat{G}}{\partial t_f}$ as a consequence of the time translation invariance of the Brownian motion. The initial condition is $\hat{G}(\vec{\lambda}, \vec{w}, t_i, t_i) = 1$.

To study avalanche sizes, we consider the long-time behavior of \hat{G} to obtain $G = \hat{G}(\vec{\lambda}, \vec{w}, t_i, \infty)$. In this case we can assume that \hat{G} reached the stationary state, i.e.

$$\sum_{\alpha=1}^N \left(-\frac{\partial G}{\partial w_\alpha} \sum_{j=1}^N C_{\alpha j} w_j + \frac{\partial^2 G}{\partial w_\alpha^2} w_\alpha + \lambda_\alpha w_\alpha \right) = 0.\quad (\text{A.13.7})$$

This is automatically satisfied if G is given by (A.2.6) and if the \tilde{u}_i satisfy the instanton equation (A.2.7). This provides a connection between the two methods.

An interesting feature of this method is that one can now write a PDE directly for the probability distribution $P(\vec{w}, \vec{S})$ of avalanche sizes in the BFM model following arbitrary (positive) kicks $\dot{w}_{it} = w_i \delta(t)$. This equation reads:

$$\sum_{\alpha=1}^N \left(-\frac{\partial P}{\partial w_\alpha} \sum_{j=1}^N C_{\alpha j} w_j + \frac{\partial^2 P}{\partial w_\alpha^2} w_\alpha - w_\alpha \frac{\partial P}{\partial S_\alpha} \right) = 0.\quad (\text{A.13.8})$$

We need to find a solution which satisfies the following boundary condition:

$$P(\vec{w} = \vec{0}, \vec{S}) = \prod_{i=1}^N \delta(S_i).\quad (\text{A.13.9})$$

Let us now discuss its solution. Inspired by our result (A.3.8), we make the change of variable $P(\vec{w}, \vec{S}) = F(\vec{x}, \vec{S})$ with $\vec{x} = \vec{w} - C \cdot \vec{S}$. The equation for F then takes a very simple form:

$$\sum_{\alpha=1}^N w_\alpha \left(\frac{\partial^2 F}{\partial x_\alpha^2} - \frac{\partial F}{\partial S_\alpha} \right) = 0\quad (\text{A.13.10})$$

where $w_\alpha = x_\alpha + \sum_{j=1}^N C_{\alpha j} S_j$ and we used that C is a symmetric matrix. In this new variables, we write our main result (A.3.8) using the following decomposition:

$$F(\vec{x}, \vec{S}) = \det(M_{ij})_{N \times N} \tilde{F}(\vec{x}, \vec{S}) \quad , \quad M_{ij} = C_{ij} + \delta_{ij} \frac{x_i}{S_i}\quad (\text{A.13.11})$$

$$\tilde{F}(\vec{x}, \vec{S}) = \left(\frac{1}{2\sqrt{\pi}} \right)^N \left(\prod_{i=1}^N S_i \right)^{-\frac{1}{2}} \exp \left(-\frac{1}{4} \sum_{i=1}^N \frac{x_i^2}{S_i} \right).\quad (\text{A.13.12})$$

This decomposition sheds some light on the structure of (A.3.8), here rewritten as F in (A.13.11): it is simple to see that \tilde{F} defined in (A.13.12) already solves (A.13.10), \tilde{F} can indeed be interpreted as the PDF of the position x_i at "time" S_i of N independent particles diffusing from the origin at time $S_i = 0$. However the result $F = \tilde{F}$ would not satisfy the boundary conditions (A.13.9). We now check that the extra factor $\det(M)$ provides the proper solution. In order for (A.13.11) to also solve (A.13.10), the determinant must verify

$$\sum_{\alpha=1}^N w_{\alpha} \left(\frac{\partial^2 \det(M)}{\partial x_{\alpha}^2} \tilde{F} + 2 \frac{\partial \det(M)}{\partial x_{\alpha}} \frac{\partial \tilde{F}}{\partial x_{\alpha}} - \frac{\partial \det(M)}{\partial S_{\alpha}} \tilde{F} \right) = 0. \quad (\text{A.13.13})$$

Using $\frac{\partial \tilde{F}}{\partial x_{\alpha}} = -\frac{x_{\alpha}}{2S_{\alpha}} \tilde{F}$, this implies an equation for $\det(M)$

$$\sum_{\alpha=1}^N w_{\alpha} \left(\frac{\partial^2 \det(M)}{\partial x_{\alpha}^2} - \frac{x_{\alpha}}{S_{\alpha}} \frac{\partial \det(M)}{\partial x_{\alpha}} - \frac{\partial \det(M)}{\partial S_{\alpha}} \right) = 0. \quad (\text{A.13.14})$$

The first term $\frac{\partial^2 \det(M)}{\partial x_{\alpha}^2}$ is equal to 0, since x_{α} only appears in the α -th column of M . The remaining terms vanishes since M depends on x_{α} and S_{α} only through the combination $\frac{x_{\alpha}}{S_{\alpha}}$. This completes the proof that our result (A.3.8) indeed solves the PDE (A.13.8). The boundary condition is now satisfied since $P_{\vec{w}}(\vec{S})$ is a continuous PDF on positive variables and we know (see Section A.3 and A.12) that $\langle S_i \rangle = \sum_{j=1}^N C_{ij}^{-1} w_j$ vanishes when $w_i \rightarrow 0$.

A.14 Appendix D: Poisson-Levy process for normalizable jump densities

.1 Center of mass We already discussed in the main text the infinite divisibility property (A.4.6) of $P_w(S)$. Given this property, one would like to interpret an avalanche S as the sum of n iid elementary avalanches s_i with n drawn from a Poisson distribution and s_i drawn from a given distribution (this defines a Poisson-Levy jump process, see e.g.[230]). This interpretation is valid at the level of the moments of $P_w(S)$ (see (A.4.8)) but we now show that it does not extend to the probability itself. Let us first assume that the jump density ρ appearing in (A.4.8) is normalizable (see also the discussion in [111], Appendix J). Then one can write $\rho(s) = \rho_0 p(s)$ with p a regular function normalized to unity $\int ds p(s) = 1$ and ρ_0 the density of avalanches; i.e. the mean number of quasi-static avalanches occurring in response to the total driving w is $\rho_0 w$. Using the following identity:

$$\begin{aligned} & \int ds_1 \cdots ds_n (e^{\lambda s_1} - 1) \cdots (e^{\lambda s_n} - 1) \rho(s_1) \cdots \rho(s_n) \\ &= \sum_{m=0}^n \frac{(\rho_0 w)^m}{m!} \frac{(-\rho_0 w)^{n-m}}{(n-m)!} \int ds_1 \cdots ds_m e^{\lambda(s_1 + \cdots + s_m)} p(s_1) \cdots p(s_m) \end{aligned} \quad (\text{A.14.1})$$

(A.4.8) can be rewritten as (performing the sum over $n > m$):

$$\int dS e^{\lambda S} P_w(S) = \sum_{m=0}^{\infty} \frac{(\rho_0 w)^m}{m!} e^{-\rho_0 w} \int ds_1 \cdots ds_m e^{\lambda(s_1 + \cdots + s_m)} p(s_1) \cdots p(s_m). \quad (\text{A.14.2})$$

This leads to a formula for the probability, $P_w(S) = \sum_{m=0}^{\infty} \frac{(\rho_0 w)^m}{m!} e^{-\rho_0 w} (p^*)^m(S)$. Here $(p^*)^m$ denotes m convolutions of p with itself, making the interpretation in terms of a Poisson jump process transparent. One can define the "complete" avalanche-size density as

$$\tilde{\rho}(S) = \frac{dP_w(S)}{dw} \Big|_{w=0} = -\rho_0 \delta(S) + \rho(S). \quad (\text{A.14.3})$$

Where here the first equality holds in the sense of distributions. This total density appears as the sum of the regular density $\rho(S)$ (defined in the main text) and of a delta singularity that accounts for the finite probability that the interface does not jump. As a consequence, $\frac{dG_w(\lambda)}{dw} \Big|_{w=0} = Z(\lambda) = \int dS e^{\lambda S} \tilde{\rho}(S) = \int dS (e^{\lambda S} - 1) \rho(S)$. For the ABBM model, the scale invariance of the Brownian motion leads to an accumulation of small avalanches of arbitrary small sizes, leading to $\rho_0 = \infty$ (in particular for any $w > 0$, $P_w(S=0) = e^{-\rho_0 w} \rightarrow 0$) and one can not define $\tilde{\rho}$. The formula $\frac{dG_w(\lambda)}{dw} \Big|_{w=0} = \int dS (e^{\lambda S} - 1) \rho(S)$ is however still valid and allowed us to prove (A.4.8).

.2 Levy Process for the interface The generalization to the interface is immediate: in this case, the LT of $P_{\vec{w}}(\vec{S})$ reads

$$\int d^N \vec{S} e^{\vec{\lambda} \cdot \vec{S}} P_{\vec{w}}(\vec{S}) = e^{\vec{w} \cdot \vec{v}} = \sum_{n=0}^{\infty} \sum_{(i_1, \dots, i_n)} \frac{w_{i_1} \cdots w_{i_n}}{n!} v_{i_1}, \dots, v_{i_n} \quad (\text{A.14.4})$$

where the second sum is for all $(i_1, \dots, i_n) \in \{1, \dots, N\}^n$ and the v_i variables are functions of $\vec{\lambda}$ solutions of (A.3.2). Using our conjecture (A.4.11), we obtain

$$\int d^N \vec{S} e^{\vec{\lambda} \cdot \vec{S}} P_{\vec{w}}(\vec{S}) = \sum_{n=0}^{\infty} \sum_{(i_1, \dots, i_n)} \frac{w_{i_1} \cdots w_{i_n}}{n!} \prod_{l=1}^n d^N \vec{s}_{i_l} (e^{\lambda \vec{s}_{i_l}} - 1) \rho_{i_1}(\vec{s}_{i_1}) \cdots \rho_{i_n}(\vec{s}_{i_n}) \quad (\text{A.14.5})$$

which is the multidimensional generalization of (A.4.8) and shows that the densities $\rho_j(\vec{S})$ entirely control the moments of $P_{\vec{w}}(\vec{S})$. It is also in agreement with the interpretation of an avalanche \vec{S} as a superposition of independent avalanches, as already discussed in the main text.

A.15 Appendix E: Details on the fully connected model

Here we detail the calculations leading to the results of Section A.5, and give some results for the fully-connected model driven by a single site.

.1 Marginals distributions for uniform driving For uniform driving, the matrix C and M entering in (A.3.8) admit the following simple expressions, allowing us to evaluate $\det M$ in a concise way:

$$\begin{aligned} C_{ij} &= (1+c)\delta_{ij} - \frac{c}{N}, \quad M_{ij} = \delta_{ij} \frac{1}{S_i} (w + cS/N) - \frac{c}{N} \\ \det M &= w(w + cS/N)^{N-1} \prod_{i=1}^N \frac{1}{S_i}, \quad S = \sum_{k=1}^N S_k \end{aligned} \quad (\text{A.15.1})$$

This leads to (A.5.1). Various marginals of this PDF can be computed by noting that the Laplace transform of $p_{w,S/N}(s)$ entering into (A.5.1) reads

$$\int_0^\infty ds p_{w,S/N}(s) e^{-ps} = e^{\frac{1}{2}(1+c)(w+cS/N)(1-\sqrt{1+\frac{4p}{(1+c)^2}})}. \quad (\text{A.15.2})$$

We write the joint PDF of local and total size as

$$P(\vec{S}, S) = \delta\left(S - \sum_{i=1}^N S_i\right) P(\vec{S}). \quad (\text{A.15.3})$$

For any $1 \leq m \leq N-1$, the marginal $P(\{S_1, \dots, S_m\}, S)$ can be computed as

$$\begin{aligned} P(\{S_1, \dots, S_m\}, S) &= \frac{w}{w + cS/N} \prod_{i=1}^m p_{w,S/N}(S_i) \int_{\sum_{i=m+1}^N S_i = S - \sum_{i=1}^m S_i} \prod_{i=m+1}^N p_{w,S/N}(S_i) \\ &= \frac{w}{w + cS/N} \prod_{i=1}^m p_{w,S/N}(S_i) p_{(N-m)w, (N-m)S/N}(S - \sum_{i=1}^m S_i). \end{aligned} \quad (\text{A.15.4})$$

Where the multiple convolution of $p_{w,S/N}(s)$ has been easily calculated as a consequence of the simple structure of its Laplace transform. In particular, this leads to the formula (A.5.3) of the main text.

.2 Single-site driving Taking w_i to be non-uniform breaks the permutation invariance $i \leftrightarrow j$ of the problem, making the computation more complicated than for the uniform case. Another solvable case is $w_i = 0$ for $i \neq 1$, for which the PDF (A.3.8) takes the form

$$P(\vec{S}) = \frac{S_1 w_1}{S(w_1 + cS/N)} p_{w_1, S/N}(S_1) \prod_{j=2}^N p_{0, S/N}(S_j). \quad (\text{A.15.5})$$

The computation of marginals involving an integration over some S_j for $j > 1$ is identical to the uniform driving case and leads, for $1 \leq m \leq N-1$, to

$$P(\{S_1, \dots, S_m\}, S) = \frac{S_1 w_1}{S(w_1 + cS/N)} p_{w_1, S/N}(S_1) \prod_{j=2}^m p_{0, S/N}(S_j) p_{0, (N-m)S/N}(S - \sum_{i=1}^m S_i) \quad (\text{A.15.6})$$

In particular, we obtain

$$\begin{aligned} P(S_1, S) &= \frac{w_1}{2\sqrt{\pi} S_1^{\frac{3}{2}}} (N-1) \frac{cS_1/N}{2\sqrt{\pi}(S-S_1)^{3/2}} \exp\left(-\frac{(w_1 + cS/N - (1+c)S_1)^2}{4S_1}\right) \\ &\times \exp\left(-\frac{((N-1)(cS/N) - (1+c)(S-S_1))^2}{4(S-S_1)}\right) \theta(S-S_1). \end{aligned} \quad (\text{A.15.7})$$

In this case $S = \sum_{i=1}^N S_i$ is typically of order 1 and is distributed according to

$$P(S) = \frac{w_1}{2\sqrt{\pi} S^{\frac{3}{2}}} \exp\left(-\frac{(S-w_1)^2}{4S}\right). \quad (\text{A.15.8})$$

The large- N limit now exhibits a single non-trivial regime, with $w_1 = O(N^0)$, and for which (A.15.7) admits the limit

$$P(S_1, S) = \frac{w_1}{2\sqrt{\pi}S_1^{\frac{3}{2}}} \frac{cS_1}{2\sqrt{\pi}(S-S_1)^{3/2}} \exp\left(-\frac{(w_1 - (1+c)S_1)^2}{4S_1}\right) \times \exp\left(-\frac{(cS - (1+c)(S-S_1))^2}{4(S-S_1)}\right) \theta(S-S_1). \quad (\text{A.15.9})$$

Remarkably, in this case one can even integrate over the total size to find the marginal PDF $P(S_1)$ in the large- N limit,

$$P(S_1) = \frac{w_1}{2\sqrt{\pi}S_1^{\frac{3}{2}}} \exp\left(-\frac{(w_1 - (1+c)S_1)^2}{4S_1}\right). \quad (\text{A.15.10})$$

In agreement with the physical intuition, this is the ABBM result for a particle with driving $m^2(w_1 - u)$ and $c(\bar{S} - u)$, as discussed above, and $\bar{S} = 0$, since the center of mass has not moved appreciably.

A.16 Appendix F: Shape for small N at finite driving

Here we briefly discuss what becomes of the shape transition observed in the quasi-static PDF of avalanche shape at fixed total size S of the linear chain with PBCs (see Section A.6) when one is interested in the full PDF for finite $w_i = w$ as given in (A.3.12). For $N = 2$ and $w < \frac{3}{16c}$, there is now an additional regime with two transitions instead of one:

- $S < \frac{-8cw - \sqrt{3}\sqrt{3-16cw}+3}{8c^2}$: the distribution of s is peaked around $\frac{1}{2}$.
- $\frac{-8cw - \sqrt{3}\sqrt{3-16cw}+3}{8c^2} < S < \frac{-8cw + \sqrt{3}\sqrt{3-16cw}+3}{8c^2}$: the distribution possesses two symmetric maxima around $s = \frac{1}{2}$.
- $S > \frac{-8cw + \sqrt{3}\sqrt{3-16cw}+3}{8c^2}$, one retrieves a single maximum at $s = \frac{1}{2}$.

The first regime is new, and was not captured by the study of ρ . For small $w \rightarrow 0$ it corresponds to avalanches smaller than the lower-scale cutoff $S < \frac{4}{3}w^2$, which are not described by ρ as we know from Section A.4. In this regime, the fact that the saddle-point again corresponds to uniform avalanches with $s = 1/2$ is not a consequence of elasticity (as noted in Section A.4, local avalanche sizes are even independent in this limit), but is related to the fast decay of $p_0(s)$ at its lower cutoff (see Section A.4). For larger $w > \frac{3}{16c}$, the intermediate regime disappears, and the most probable avalanches are homogeneously distributed. Indeed, as w increases, the motion of the interface becomes mostly deterministic and the remaining fluctuations become negligible.

The case $N = 3$ is identical. For $w < \frac{1}{4c}$ the finite w probability distribution exhibits the same three different regimes with boundaries 0 , $\frac{1-2cw - \sqrt{1-4cw}}{2c^2}$ and $\frac{1-2cw + \sqrt{1-4cw}}{2c^2}$. The interpretation is identical to $N = 2$.

A.17 Appendix G: Stability of infinite, uniform avalanches.

In this appendix, we compute the value $S_c(N)$ such that avalanches uniformly distributed over all the system, and of total size $S > S_c(N)$ are stable. We do this for the fully-connected model and for the linear chain with PBCs, for which uniform avalanches uniformly distributed are always an extremum of the quasi-static density ρ (for uniform driving $f_i = 1$). As such, $S_c(N)$ is the value of S above which all the eigenvalues of the hessian of the quasi-static distribution at this uniform saddle-point are negative. Since this saddle-point and the elasticity matrix are translationally invariant, the Hessian of the logarithm of the probability at the saddle point is a circular matrix given by

$$H_{\alpha\beta} = \frac{\partial^2 \log \rho(\bar{s}|S)}{\partial s_\alpha \partial s_\beta} \Big|_{s_i=s} = -\frac{S}{2s} (c^2)_{\alpha\beta} + \frac{1}{2s^2} \delta_{\alpha\beta} + h_{\alpha\beta}. \quad (\text{A.17.1})$$

c is the elasticity matrix of the model (here $m^2 = 1$), $s = 1/N$ is the uniform local avalanche size at the saddle-point and $h_{\alpha\beta}$ depends on the chosen model as $h_{\alpha\beta} = -\frac{4}{N^2 s^2} + \frac{1}{N s^2} (4\delta_{\alpha\beta} + \delta_{\alpha,\beta-1} + \delta_{\alpha,\beta+1})$ for the linear chain with periodic boundary conditions, and $h_{\alpha\beta} = -\frac{(N-2)}{(Ns)^2} + \frac{1}{s^2} \delta_{\alpha\beta}$ for the fully connected one. The eigenvalues of these matrices can be computed using a discrete Fourier transformation, showing that they are indexed by a wave-vector $q = \frac{2\pi k}{N}$ with $k = 1, \dots, N-1$. The $q = k = 0$ mode does not intervene since it corresponds to a uniform displacement of the interface, which is forbidden by the fact that we work at fixed S : $\sum_i ds_i = 0$. The eigenvalues of the Hessian are all identical for the fully-connected model: $\lambda_{f.c.} = -\frac{S}{2s} c^2 + \frac{1}{2s^2} + \frac{1}{s^2}$. For the linear model they are given by $\lambda_q = -\frac{2S}{s} [1 - \cos(q)]^2 + \frac{1}{2s^2} + \frac{4}{Ns^2} [4 + 2 \cos(q)]$. In the latter case, the most unstable mode is $q = \frac{2\pi}{N}$, leading to the following critical values

$$S_c^{\text{fc}}(N) = \frac{3N}{c^2}, \quad (\text{A.17.2})$$

$$S_c^{\text{PBC}}(N) = \frac{N}{2c^2(1 - \cos(\frac{2\pi}{N}))^2} \left(\frac{1}{2} + \frac{1}{N} (4 + 2 \cos(\frac{2\pi}{N})) \right) \simeq_{N \rightarrow \infty} \frac{1}{16c^2\pi^4} (N^5 + 12N^4 + O(N^3)). \quad (\text{A.17.3})$$

A.18 Appendix H: Continuum limit

Here we detail the scaling that allows to find the probability distribution of the dimensionless continuum avalanches $P[S_x]$ knowing the probability distribution of the discrete case $P(\vec{S})$. We denote for clarity the continuum field as $u_t(x)$, $x \in [0, L]$, and its N -point discretization as $u_{it} = u_t(i\frac{L}{N})$. We will add indices c and d to distinguish between physical quantities of the continuum and discrete models. An easy way to ensure that the statistic of the discrete case corresponds to the statistic of the continuum one is to compare the different terms in the dynamical action (see A.11) :

- The disorder term: $\sum_{i=1}^N \int_t \sigma_d \tilde{u}_{it}^2 \dot{u}_{it} \equiv \int_0^L dx \int_t \sigma_c \tilde{u}_t(x)^2 \dot{u}_t(x) \simeq \sum_{i=1}^N \frac{L}{N} \sigma_c \int_t \tilde{u}_t(i\frac{L}{N})^2 \dot{u}_t(i\frac{L}{N})$
- The elastic term: $\sum_{i=1}^N \int_t \tilde{u}_{it} c_d (\dot{u}_{i+1t} - 2\dot{u}_{it} + \dot{u}_{i-1t}) \equiv \int_0^L dx \int_t \tilde{u}_t(x) c_c \Delta u_t(x) \simeq \sum_{i=1}^N \frac{L}{N} \int_t \tilde{u}_t(i\frac{L}{N}) c_c \frac{\dot{u}_t((i+1)\frac{L}{N}) - 2\dot{u}_t(i\frac{L}{N}) + \dot{u}_t((i-1)\frac{L}{N})}{\frac{L^2}{N^2}}$
- The driving term: $\sum_{i=1}^N \int_t m_d^2 \tilde{u}_{it} \dot{w}_{it} \equiv \int_0^L dx \int_t m_c^2 \tilde{u}_t(x) \dot{w}_t(x) \simeq \sum_{i=1}^N \frac{L}{N} m_c^2 \int_t \tilde{u}_t(i\frac{L}{N}) \dot{w}_t(i\frac{L}{N})$

This indicates that the quantity of the discrete model should be $m_d^2 = \frac{L}{N} m_c^2$, $c_d = \frac{N}{L} c_c$ and $\sigma_d = \frac{L}{N} \sigma_c$. In particular, the rescaled quantities which appear in the text, in the formula for the dimensionless discrete distributions are $\frac{c_d}{m_d^2} = \frac{N^2}{L^2} \frac{c_c}{m_c^2}$ and $S_m^d = \frac{N}{L} S_m^c$. Note that we will choose everywhere in the main text $c_c = 1$. This implies that the probability distribution of the dimensionless rescaled continuum avalanches denoted by P_c is given in terms of its discrete analog $P \equiv P_d$ given in (A.3.8) as (introducing the explicit dependence in the driving):

$$P_c[S(x), w(x)] = \lim_{N \rightarrow \infty} \left(\frac{L}{N} \right)^N P_d \left(\frac{L}{N} \vec{S}, \frac{L}{N} \vec{w} \right) \quad (\text{A.18.1})$$

where here $\vec{S} = (S(Li/N))_{i=1, \dots, N}$ and $\vec{w} = (w(Li/N))_{i=1, \dots, N}$. This leads to the formula of the main text. Note also that for η -dependent observables, one should choose $\eta_d = \frac{L}{N} \eta_c$.

A.19 Appendix I: Optimal shape in the discrete model

Here we compare the results on the continuum optimal shape with the discrete case. This is not only a consistency check, but also allows us to compare the results of the optimization when we include boundary conditions, and to investigate the stability of the shape. We choose to work on the discrete model with an elastic coefficient set to unity, which corresponds to a N -point approximation of the continuum model with a line of length $L = N$, i.e. the index i of the discrete model is the coordinate of the continuum line (see A.18). In the continuum, the optimal reduced shape s_0 is obtained for total size S and extension ℓ fixed, and contains all the probability when $S/\ell^4 \gg 1$. To compare this result with the discrete model we used two different optimization procedures on the discrete probability. We always impose the total size S and optimize on the shape variables $s_i = S_i/S$ with

1. either the two central points tuned to coincide with the optimal continuum result: we note n_{mid} the integer part of $N/2$ and impose $s_{n_{mid}} = s_{n_{mid}+1} = \frac{1}{\ell} s_0(0.5/\ell)$.
2. either $N - l$ successive shape variables fixed to be small (below we use $s_i = 10^{-5}$)

Procedure (i) is an indirect way to impose the extension by imposing that the avalanche shape is peaked around some region, whereas procedure (ii) is closer to the continuum setting where we directly imposed the finite extension. In both cases we impose $S \gg \ell^4$ to obtain a true maximum. The optimal shape is always found to be symmetric, which allows us to impose this condition to study reasonably large N . The result of the optimization is then compared with the prediction from the continuum theory: $s_i = \frac{S(x=i)}{S} =_{S \gg \ell^4} \frac{1}{\ell} s_0(i/\ell)$. One can then

- Verify that the optimization on ρ (including boundary conditions) or \mathcal{H} alone (defined in the continuum in (A.7.4)) give the same results. It is already obvious for $\ell \ll N$ and Figure A.15 explicitly shows that it is always true for $S \gg \ell^4$, even if $\ell \simeq N$. This validate the hypothesis made in the continuum that boundary conditions do not play a role for large S/ℓ^4 .
- Using an optimization on \mathcal{H} , we can verify that the discrete optimal shape coincides with the continuum one. The results are shown in Figure A.16. One can see that, apart from some discretization artefacts, procedure (ii) give results in agreement with the continuum result. On the other hand, procedure (i) leads to a shape with an effectively larger extension. This is in agreement with the idea that the property that avalanches have a strictly finite extension is only a feature of the continuum limit, as explained in Section A.7.2, and is coherent with the idea that procedure (i) only imposes a "characteristic" extension in the discrete setting.
- Finally, we can study the behavior of the maximum eigenvalue λ_{max} of the Hessian of the discrete Hamiltonian \mathcal{H} at the most probable shape (since the eigenvalues are negative it is the maximum one that is the closest to 0 and that controls the stability of the saddle-point) using procedure (i). The behavior of the eigenvalues of the Hessian with S is trivial: since S can be factorized in front of the Hamiltonian, they are proportional to S . However, in the discrete case, there is no way to see the scaling $\frac{1}{\ell^4}$ emerge from the Hamiltonian. Still, we clearly numerically find (see Figure A.17) that λ_{max} scales with $1/\ell^4$ for $\ell \rightarrow 0$. This thus provides an alternative verification that the saddle-point is stable, and that its stability is controlled by $S/\ell^4 \gg 1$.

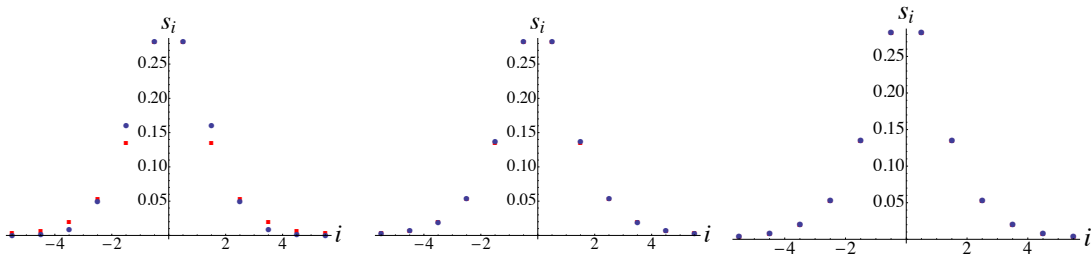


Figure A.15: Comparison between the most probable shape of length $\ell = 10$ with $N = 12$ computed using optimization on \mathcal{H} (blue dots) or ρ (red dots), using procedure (i), and for different total sizes S from left to right: $\frac{S}{\ell^4} = 10^{-2}, 10^{-1}, 1$. The influence of boundary conditions quickly decreases as S/ℓ^4 is increased.

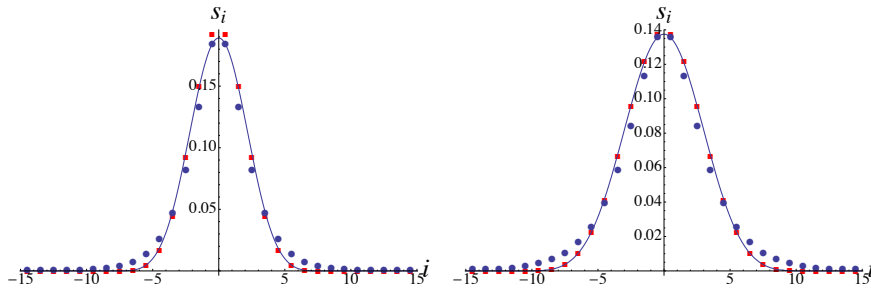


Figure A.16: Most probable shape in the discrete model obtained using numerical optimization on \mathcal{H} with procedure (i) (blue dots) or procedure (ii) (red square) with $N = 30$ and $\ell = 16$ (left) or $\ell = 22$ (right), compared to the continuum saddle-point prediction $s_0(x/\ell)/\ell$ (straight line).

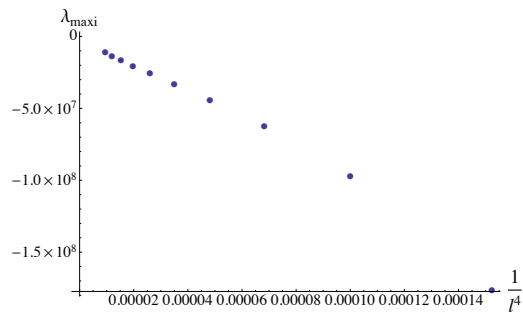


Figure A.17: Maximum eigenvalue of the hessian of the hamiltonian at the numerical optimum as a function of $\frac{1}{\ell^4}$ for large, fixed S with procedure (i).

Appendix B

Paper: Universality in the spatial shape of avalanches

The following is essentially the article published as

Title: Universality in the mean spatial shape of avalanches

Authors: Thimothée Thiery and Pierre Le Doussal

Journal-Ref: EPL (Europhysics Letters), Volume 114, Number 3

Abstract: Quantifying the universality of avalanche observables beyond critical exponents is of current great interest in theory and experiments. Here, we improve the characterization of the spatio-temporal process inside avalanches in the universality class of the depinning of elastic interfaces in random media. Surprisingly, at variance with the temporal shape, the spatial shape of avalanches has not yet been predicted. In part this is due to a lack of an analytically tractable definition: how should the shapes be centered? Here we introduce such a definition, accessible in experiments, and study the *mean spatial shape of avalanches at fixed size centered around their starting point (seed)*. We calculate the associated universal scaling functions, both in a mean-field model and beyond. Notably, they are predicted to exhibit a cusp singularity near the seed. The results are in good agreement with a numerical simulation of an elastic line.

Together with the associated supplemental material published in

ArXiv: 1601.00174

B.1 Letter

Numerous slowly driven non-linear systems exhibit motion which is not smooth in time but rather proceeds discontinuously via jumps extending over a broad range of space and time scales. Developing predictive models of avalanche motion and understanding their universality, or lack thereof, has emerged as an outstanding challenge of modern statistical physics [81]. In condensed matter recent developments have led to distinguish two broad classes, depending on the importance of plastic deformations. In systems such as dislocated solids, metallic glasses, granular media near jamming, plastic deformations play a crucial role and despite recent progresses a theoretical description is still under construction [91, 93, 233, 234]. In many other situations the description by an elastic interface driven in a disordered medium has proved relevant [63, 235, 236, 68]. Examples are domain walls in soft magnets [100, 45], fluid contact lines on rough surfaces [60, 61], strike-slip faults in geophysics [64, 65, 66], fractures in brittle materials [52, 56, 55, 51] or imbibition fronts [69]. This class exhibits a dynamical phase transition - the so-called depinning transition - accompanied by collective avalanche motion. While the microscopic details of the dynamics are specific to each system, the large scale statistical properties of the avalanches are believed to be universal. The most studied quantities in this context are the critical exponents characterizing the scale-free probability distribution function (PDF) of avalanche total sizes S , $P(S) \sim S^{-\tau_S}$ and durations T , $P(T) \sim T^{-\tau_T}$. They are related to the roughness and dynamical exponents, ζ and z , defined at the depinning transition of the interface, using the scaling relations $S \sim \ell^{d+\zeta}$ and $T \sim \ell^z$ with ℓ the lateral extension of the avalanche.

Recent improvements in experimental techniques allow studies of avalanches with higher accuracy and to access new, finer quantities, with the aim of distinguishing more efficiently the different universality classes. This notably includes the direct imaging of the spatio-temporal process of the velocity field inside an avalanche $v(x, t)$ where x denotes the internal coordinate of the (d -dimensional) interface and t is the time since the beginning of the avalanche. A question of great interest is to understand whether and how scaling and universality extend to $v(x, t)$.

Until now the focus was on the center of mass velocity $v_{\text{cm}}(t) \sim \int d^d x v(x, t)$ and the mean temporal shape at fixed duration T , $\langle v_{\text{cm}}(t) \rangle_T$, where here $\langle \rangle_T$ denotes the statistical average over all avalanches of fixed duration T . A scaling analysis suggests, through the sum rule $S = \int dt d^d x v(x, t)$, the existence of a scaling function $f_d^{\text{temp}}(t)$ such that $\langle v_{\text{cm}}(t) \rangle_T = T^{\gamma-1} f_d^{\text{temp}}(t/T)$, where $\gamma = (d + \zeta)/z$. The universality of $f_d^{\text{temp}}(t)$ was shown theoretically and studied experimentally in [143, 142, 237, 144, 145]. The beautiful parabola-shape predicted at mean field level, $f_{\text{temp}}(t) = t(1 - t)$ (and $\gamma = 2$), stimulated the excitement around this observable.

Though very interesting, this observable does not contain information on the remarkable spatial structure of avalanche

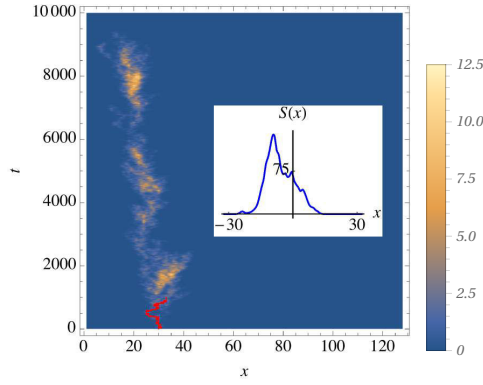


Figure B.1: Density plot of the velocity field $v(x, t)$ inside an avalanche of size $S = 1760$ in the mean-field model (Brownian Force Model) for $d = 1$ discretized with $N = 128$ points. Time is given in machine-time unit. Line in red: backward path produced by the algorithm used to find the seed of the avalanche (see text). Inset: the spatial shape of this avalanche when centered around its starting point.

processes (see for illustration Fig. B.1). A characterization of even the mean spatial shape of avalanches in terms of a simple scaling function is presently lacking. In this Letter we propose and calculate such a scaling function. We consider the mean shape of avalanches at fixed total size S , for which a scaling analysis suggests (in real or in Fourier space $\langle S(q) \rangle_S = \int d^d x e^{iqx} \langle S(x) \rangle_S$)

$$\begin{aligned} \langle S(x) \rangle_S &= S^{1 - \frac{d}{d+\zeta}} f_d\left(\frac{x}{S^{\frac{1}{d+\zeta}}}\right), \\ \langle S(q) \rangle_S &= S \tilde{f}_d(q S^{\frac{1}{d+\zeta}}), \end{aligned} \quad (\text{B.1.1})$$

where $S(x) = \int dt v(x, t)$ is the “local size” at x , $f_d(x)$ and $\tilde{f}_d(q)$ are radial scaling functions (hence x and q as arguments of the scaling functions always denote the norm of the vectors x and q), normalized as $\int d^d x f_d(x) = \tilde{f}_d(q = 0) = 1$, since $S = \int d^d x S(x)$. Here the local size at x , $S(x)$ is the local displacement of the interface between the beginning and the end of an avalanche at the point x , while the total size S is the area swept by the interface during the avalanche. Note that these definitions are not complete: there are various ways of centering an avalanche. Our proposal is to study the spatial structure by *centering the avalanches on their starting points*. Hence in (B.1.1) $\langle \rangle_S$ denotes the statistical average over all avalanches of fixed total size S and starting point $x = 0$. We call this procedure the *seed-centering* which appears natural when one thinks of how an avalanche unfolds following a branching process (see Fig. B.1). Furthermore, it permits analytical treatment and is thus appropriate to compare theory and experiments.

We first calculate the above scaling functions at the level of mean-field. This requires to go beyond the simplest mean-field toy model, the ABBM model [98, 99] which only describes the center of mass motion of the interface. To this aim we consider the Brownian Force Model (BFM), recently introduced as the relevant mean-field theory to describe spatial correlations [111, 102, 101, 1]. For this model, we even compute the full *mean velocity-field inside a seed-centered avalanche of given size S* which in general obeys the scaling form

$$\langle v(x, t) \rangle_S = S^{\frac{\zeta - z}{d+\zeta}} F(t/S^{\frac{z}{d+\zeta}}, x/S^{\frac{1}{d+\zeta}}). \quad (\text{B.1.2})$$

More generally, in this Letter we consider elastic interfaces in the quenched Edward-Wilkinson universality class with short ranged disorder. In this context, the BFM is accurate for $d \geq d_c$, where d_c is the upper critical dimension of the depinning transition, $d_c = 4$ for short-range (SR) elasticity and $d_c = 2$ for the most common long-range (LR) elasticity. In lower dimensions $d < d_c$, correlations play an important role. To take them into account and study this more difficult case, we use the Functional Renormalization Group (FRG) and calculate the scaling functions $f_d(x)$ and $\tilde{f}_d(q)$ perturbatively in $\epsilon = d_c - d$, to one-loop, i.e. $O(\epsilon)$ accuracy (see [114, 127, 126, 116, 129, 117] for background on FRG, and [86, 109, 111, 101] for its application to the study of avalanches). We show that the scaling ansatz (B.1.1) holds and that the scaling functions contain only one non-universal scale ℓ_σ (which is discussed in details below)

$$f_d(x) = \frac{1}{\ell_\sigma^d} \mathcal{F}_d\left(\frac{x}{\ell_\sigma}\right), \quad \tilde{f}_d(q) = \tilde{\mathcal{F}}_d(\ell_\sigma q), \quad (\text{B.1.3})$$

where \mathcal{F}_d and $\tilde{\mathcal{F}}_d$ are fully universal and depend only on the space dimension d and the universality class of the model (i.e. range of elasticity and disorder). The precise model that is the starting point of our theoretical analysis (for elastic interfaces with short-ranged elasticity) is given in (B.1.12). Our conclusions however apply in much greater generality and the details of the model are unimportant (once the range of elasticity and disorder correlation have been set). Indeed, since the scaling functions that we compute are universal and entirely determined by the properties of the FRG fixed point for models in the quenched Edward-Wilkinson universality class, any model in the same universality class leads to the same

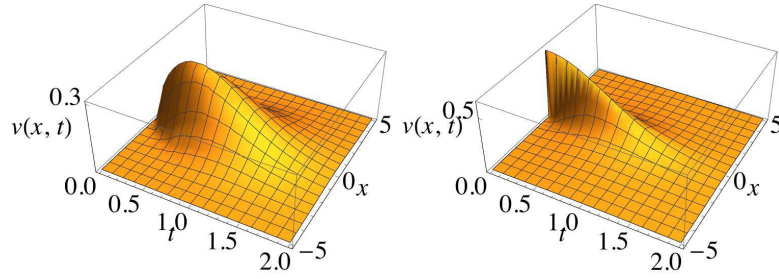


Figure B.2: Plot of the mean-field result for the space-time mean velocity profile inside an avalanche in $d = 1$ for SR (left, see (B.1.4)) and LR elasticity (right, see (B.1.7)).

scaling functions. In the first part of the Letter we thus focus on stating our results, and report the discussion of the model and of the method to the second part. For a generic system, we expect scaling and universality to hold for avalanche of size S in a scaling regime $S_{\min} \ll S \ll S_{\max}$. Note that in (B.1.3), the space variable x is measured in units of $S^{\frac{1}{d+\zeta}}$ (see (B.1.1)). In the original units, the universality in the avalanche shape should hold for both small and large x (compared to $S^{\frac{1}{d+\zeta}}$) as long as $x_{\min} \ll x \ll x_{\max}$ where $x_{\min/\max} \sim S^{\frac{1}{d+\zeta}}_{\min/\max}$. We will start by discussing the exact results obtained for the BFM (defined below, see (B.1.12)). These results are also of interests for the SR disorder universality class as the lowest order terms in the ϵ expansion (i.e. $O(\epsilon^0)$ terms) of the true universal scaling functions.

Results within mean-field: The BFM can be studied analytically in any dimension d . Let us first consider the case of SR elasticity. The exponents are $\tau_S = 3/2$, $\tau_T = z = 2$ and $\zeta = 4 - d$. The scaling function in (B.1.2) admits a very simple expression:

$$F(t, x) = 2te^{-t^2} \frac{1}{(4\pi t)^{d/2}} e^{-x^2/(4t)}, \quad (\text{B.1.4})$$

which is plotted in Fig. B.2. Here we use dimensionless units, the original units can be recovered using $x \rightarrow mx$, $t \rightarrow t/\tau_m$ and $S \rightarrow S/S_m$ where $\tau_m = \eta/m^2$ and $S_m = \sigma/m^4$ and the parameters η, m and σ are those in the equation of motion of the model (B.1.12). Time integration of (B.1.4) confirms for the BFM the general scaling law (B.1.1) and (B.1.3) with $\mathcal{F}_d^{\text{MF}}(x) = \int_0^{+\infty} dt F(t, x)$ and $\ell_\sigma = \sigma^{-1/4}$. The result is simplest in Fourier space and does not depend on the dimension:

$$\tilde{\mathcal{F}}_d^{\text{MF}}(q) = \tilde{\mathcal{F}}^{\text{MF}}(q) = 1 - \frac{\sqrt{\pi} q^2}{2} e^{\frac{q^4}{4}} \text{erfc}\left(\frac{q^2}{2}\right), \quad (\text{B.1.5})$$

where $\text{erfc}(z) = \frac{2}{\sqrt{\pi}} \int_z^{+\infty} e^{-t^2} dt$. In real space, $\mathcal{F}_d^{\text{MF}}(x)$ depends on the dimension and can be expressed using hypergeometric functions [238] with $\mathcal{F}_{d \leq 4}^{\text{MF}}(0) = \frac{2^{-d} \pi^{1-\frac{d}{2}}}{\Gamma(\frac{d}{4}) \sin(\frac{\pi d}{4})}$. Both $\tilde{\mathcal{F}}^{\text{MF}}(q)$ and $\mathcal{F}_{d=1,2}^{\text{MF}}(x)$ are plotted in black in Fig. B.3. A fundamental property of $\tilde{\mathcal{F}}^{\text{MF}}(q)$ is that it possesses an algebraic tail $\tilde{\mathcal{F}}^{\text{MF}}(q) \sim q^{-4}$ at large q , which generates a non-analytic term $\sim |x|^{4-d}$ in the small x expansion of $\mathcal{F}_d^{\text{MF}}(x)$ around the origin. Its behavior at large x is evaluated using a saddle-point on (B.1.4), leading to a stretched exponential decay with a d -independent exponent $4/3$:

$$\mathcal{F}_d^{\text{MF}}(x) \simeq_{x \rightarrow \infty} \frac{2^{-d/2} \pi^{\frac{1}{2}-\frac{d}{2}}}{\sqrt{3}} x^{\frac{2-d}{3}} e^{-\frac{3x^{4/3}}{4}}. \quad (\text{B.1.6})$$

These results easily extend to LR elasticity, in which case $z = 1$, $\zeta = 2 - d$ and the mean shape in Fourier space is obtained replacing $q^2 \rightarrow q$ in (B.1.5). Let us also give here the spatiotemporal shape (B.1.2) for the experimentally most relevant case of $d = 1$, with

$$F(t, x) = \frac{2t^2 e^{-t^2}}{\pi(x^2 + t^2)}. \quad (\text{B.1.7})$$

Results beyond mean-field for SR elasticity: For realistic SR disorder, the BFM is the starting point in the $\epsilon = 4 - d$ expansion. It is most clearly implemented in Fourier space, since the mean-field result for $\tilde{\mathcal{F}}_d(q)$ does not depend on d :

$$\tilde{\mathcal{F}}_d^{\text{SR}}(q) = \tilde{\mathcal{F}}^{\text{MF}}(q) + \delta \tilde{\mathcal{F}}_d(q) + O(\epsilon^2), \quad (\text{B.1.8})$$

with $\delta \tilde{\mathcal{F}}_d(q) = \epsilon \tilde{\mathcal{F}}^{(1)}(q)$. Here $\tilde{\mathcal{F}}^{(1)}(q) = \int_{\mathcal{C}} \frac{d\mu}{2i\pi} e^{\mu} \tilde{H}(\mu, q)$ is obtained as an Inverse Laplace Transform (ILT) $\mu \rightarrow 1$:

$$\begin{aligned} \tilde{H}(\mu, q) = & \frac{4\sqrt{\pi}}{9} \left[\frac{2 - 3\gamma_E}{8} \frac{1}{q^2 + 2\sqrt{\mu}} - \frac{4\sqrt{\mu}}{(q^2 + 2\sqrt{\mu})^2} \right. \\ & \left. \times \left(\frac{q^2 + 9\sqrt{\mu}}{q\sqrt{q^2 + 8\sqrt{\mu}}} \sinh^{-1} \left(\frac{q}{2\sqrt{2\sqrt{\mu}}} \right) - 1 + \frac{3}{16} \ln(4\mu) \right) \right] \end{aligned} \quad (\text{B.1.9})$$

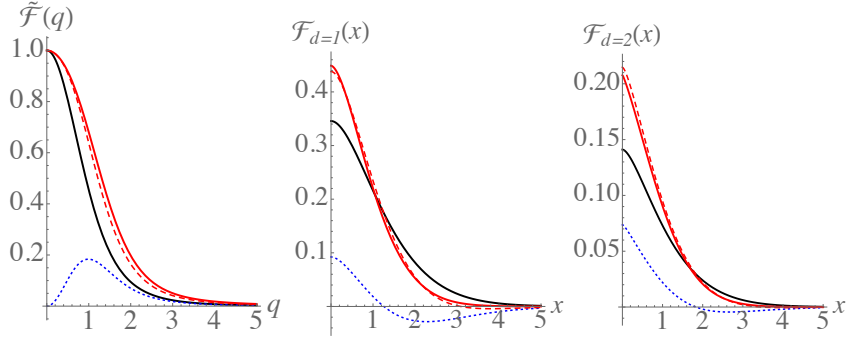


Figure B.3: (color online). Analytical results at MF and $O(\epsilon)$ level for the universal scaling function $\tilde{\mathcal{F}}_{d=1}$ in Fourier space (Left) and \mathcal{F}_d in real space for $d = 1$ (Middle) and $d = 2$ (Right) for SR elasticity. Black lines: tree/mean-field results. Dotted blue lines: universal corrections, $\delta\tilde{\mathcal{F}}_1(q)$ (left, $O(\epsilon)$ correction in Fourier space in $d = 1$), $\delta\mathcal{F}_1(x)$ (middle) and $\delta\mathcal{F}_2(x)$ (right). Red-dashed lines: $O(\epsilon)$ estimate obtained by simply adding the corrections to the MF value. Red lines: improved $O(\epsilon)$ estimate, which, through a re-exponentiation procedure, takes properly into account the modification of exponents (B.1.10) and (B.1.11) (see [238]). Note that the cusp at the origin of the avalanche shape at $O(\epsilon)$ is not obvious in this plot since the non-analyticity is rather small, but it can be emphasized using a log-log scale (and measured in numerics, see Fig. B.5).

where γ_E is Euler's Gamma constant (see [238] for the choice of \mathcal{C}). We then define the correction to the mean shape in real space as the d -dimensional Fourier transform $\delta\mathcal{F}_d(x) = \int \frac{d^d q}{(2\pi)^d} e^{-iqx} \delta\tilde{\mathcal{F}}_d(q)$. Hence, $\mathcal{F}_d^{\text{SR}}(x) = \mathcal{F}_d^{\text{MF}}(x) + \delta\mathcal{F}_d(x) + O(\epsilon^2)$. From the ILT expression (B.1.9) we obtain the following analytical properties of the $O(\epsilon)$ corrections:

- 1) Its large q expansion is $\delta\tilde{\mathcal{F}}_d(q) \simeq_{q \gg 1} \epsilon \frac{8 \log(q) - \gamma_E - 8}{9q^4}$, interpreted as a *change in the tail exponent* $\tilde{\eta}_d$:

$$\tilde{\mathcal{F}}_d(q) \simeq_{q \gg 1} \tilde{A}_d q^{-\tilde{\eta}_d} \quad , \quad \tilde{\eta}_d = 4 - \frac{4\epsilon}{9} + O(\epsilon^2) \quad , \quad (\text{B.1.10})$$

with a universal prefactor $\tilde{A}_d = 2(1 - (2 + \frac{\gamma_E}{4})\frac{2\epsilon}{9})$. In real space this implies, in the expansion of $\mathcal{F}_d(x)$ at small x , a non-analytic term $\sim |x|^{\eta_d}$ with $\eta_d = \tilde{\eta}_d - d = \frac{5\epsilon}{9} + O(\epsilon^2)$. Restoring the S dependence from (B.1.1) this leads to $\langle S(q) \rangle_S \sim_{q \rightarrow +\infty} S^{1 - \frac{\tilde{\eta}_d}{d+\zeta}} q^{-\tilde{\eta}_d}$ and the non-analytic part $\langle S(x) \rangle_S^{n,a} \sim_{x \rightarrow 0} S^{1 - \frac{\tilde{\eta}_d}{d+\zeta}} |x|^{\eta_d}$. Note that in the BFM the value $\tilde{\eta}_d = 4 = d + \zeta$ implies that the large q behavior of $\langle S(q) \rangle_S$ *does not depend on S* . This may seem natural: in the BFM the small scales do not know about the total size of the avalanche. A generalization of this property to the SR disorder case would suggest the guess $\tilde{\eta}_d^{\text{guess}} = d + \zeta$. Our result explicitly shows that this property fails with $\tilde{\eta}_d > d + \zeta$. Hence in the SR disorder case the *large avalanches tend to be more smooth than small avalanches*. Note that the predicted value of η_d is smaller than 2 in all physical dimension: *this non-analytic term should actually dominate the behavior of $\mathcal{F}_d(x)$ around 0* (and thus lead to a cusp singularity). A possible interpretation of this cusp singularity is that around 0 the mean shape of avalanches $\mathcal{F}_d(x)$ is dominated by avalanches whose largest local size is at their seed. This could correspond to the fact that such avalanches occur as a consequence of large fluctuations of the disorder that would pin a specific point of the interface for a long time. These would result in configurations of the interface with a single point well behind the rest of the interface. The depinning of such a point would then trigger an avalanche that is peaked around its seed [239].

- 2) At large x , we obtain that the stretched exponential decay exponent of the mean shape is modified from its MF behavior $\delta^{\text{MF}} = 4/3$:

$$\mathcal{F}_d(x) \sim e^{-Cx^\delta} \quad , \quad \delta = \frac{4}{3} + \frac{2}{27}\epsilon + O(\epsilon^2) \quad , \quad (\text{B.1.11})$$

with a universal prefactor $C = \frac{3}{4} + (\frac{7\sqrt{3}}{36} - 1)\frac{2\epsilon}{9}$. Remarkably, using $\zeta = \epsilon/3 + O(\epsilon^2)$, this agrees to $O(\epsilon)$ with the conjecture $\delta = \frac{d+\zeta}{d+\zeta-1}$ that we justify in [238].

Furthermore, the ILT expression (B.1.9) is easily calculated numerically. The corrections $\delta\tilde{\mathcal{F}}_d(q)$ and $\delta\mathcal{F}_d(x)$ are shown in Fig. B.3, together with the resulting estimates for the functions $\mathcal{F}_d^{\text{SR}}(x)$ and $\tilde{\mathcal{F}}_d^{\text{SR}}(q)$.

Model and method: For SR elasticity, the equation of motion for the interface position $u(x, t)$ (denoted u_{xt}) is

$$\eta \partial_t u_{xt} = \nabla_x^2 u_{xt} - m^2 (u_{xt} - w_t) + F(u_{xt}, x) \quad , \quad (\text{B.1.12})$$

where η is the friction, m is a mass cutoff which suppresses fluctuations beyond the length $\ell_m = 1/m$ and $m^2 w_t$ is the driving force. In the BFM, the random pinning force $F(u, x)$ is an independent Brownian motion in u for each x with $(F(u, x) - F(u', x))^2 = 2\sigma|u - u'|$. For the SR disorder universality class, the second cumulant is $\overline{F(u, x)F(u', x')} =$

$\delta^d(x-x')\Delta_0(u-u')$ with $\Delta_0(u)$ a fast decaying function. Eq. (B.1.12) is analyzed using the dynamical field theory and the FRG [238]. This leads to an expression for $\langle S(x) \rangle_S$ as an ILT: $\langle S(y) \rangle_S \sim LT_{\mu \rightarrow S}^{-1}(\langle \tilde{u}_{x=0}^1 \rangle_\xi) / \rho(S)$ where $\rho(S)$ is the avalanche-size density (previously computed to $O(\epsilon)$ accuracy in [109, 101]) and $\tilde{u}_{x=0}^1$ is the $O(\lambda)$ term taken at $x=0$ of the solution \tilde{u}_x of the following differential equation (here in dimensionless units):

$$-\mu + \lambda\delta(x-y) + (\tilde{u}_x)^2 + \nabla_x^2 \tilde{u}_x - (1 + \xi_x)\tilde{u}_x = 0, \quad (\text{B.1.13})$$

where ξ_x is a white-noise of order $\sqrt{\epsilon}$ and $\langle \cdot \rangle_\xi$ denotes the average over it. For the BFM, the result is thus obtained setting $\xi_x \rightarrow 0$ above. At $O(\epsilon)$ for the SR disorder universality class, it is thus sufficient to solve (B.1.13) perturbatively to second order in ξ_x . Here the fact that we are looking at the local size of avalanches at $x=y$ and whose seed is centered at $x=0$ is encoded in (B.1.13) as the fact that we are computing the value at $x=0$ (seed position) of the solution of (B.1.13) with a delta source $\lambda\delta(x-y)$ (local size position). The seed centering therefore allows analytical treatment here because $\tilde{u}_{x=0}$ only contains the contribution of avalanches starting at 0 (see [238]). Using another type of spatial centering does not allow a similar simple treatment.

In our model (B.1.12), the non-universal scale ℓ_σ in (B.1.3) is $m^{-1}S_m^{-1/(d+\zeta)}$ where S_m is defined from the ratio of the first two moments of the avalanche size distribution, $S_m = \langle S^2 \rangle / (2\langle S \rangle)$, which can be measured in numerics and experiments. Here $\langle \cdot \rangle$ denotes the average with respect to the avalanche size distribution. In cases where the numerical or experimental setup corresponds to our model (as in our simulations, see below), this prediction for ℓ_σ allows unambiguous comparison between our results and the data. In cases where ℓ_σ cannot be predicted, some scale-independent features of the mean-shape still allow comparison with the experiments. This includes the tail exponent of $\tilde{\mathcal{F}}_d(q)$ in (B.1.10), the small and large distance behavior of $\mathcal{F}_d(x)$ in (B.1.11), and the *universal ratios* $c_p = \frac{\int d^d x |x|^{2p} \mathcal{F}_d(x)}{(\int d^d x |x|^p \mathcal{F}_d(x))^2}$. In $d=1$, $(c_1, c_2) \simeq (1.6944, 3.8197)$ for the BFM while $(c_1, c_2) \simeq (1.641 \pm 0.001, 3.43 \pm 0.02)$ for SR disorder to $O(\epsilon)$.

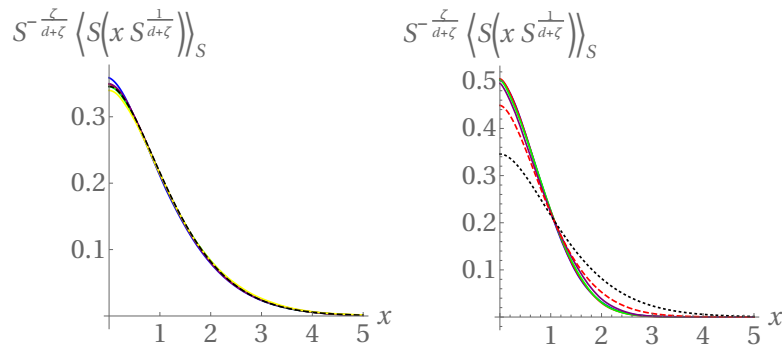


Figure B.4: (color online). Plain lines: rescaled mean shapes of avalanches at fixed size S from the simulation of the BFM model (left) and of the model with SR disorder (right), in $d=1$, for $S=10$ (left only, blue), $S=50$ (right only, blue), $S=10^2$ (red), $S=10^3$ (green), $S=10^4$ (purple) and $S=10^5$ (left only, yellow). Dashed black lines: theoretical MF result. Red dashed line: $O(\epsilon)$ result. No fitting parameter.

Numerical simulations. A convenient choice of SR disorder, amenable to Markovian evolution, is the Gaussian disorder $F(u, x)$ with "Ornstein-Uhlenbeck" (OU) correlator $\Delta_0(u) = \sigma\delta u e^{-|u|/\delta u}$. It is defined by two coupled equations for the velocity $v_{xt} \equiv v(x, t)$ and the force $F(x, t)$ (the first one being the time-derivative of (B.1.12)):

$$\begin{aligned} \eta\partial_t v_{xt} &= \nabla^2 v_{xt} + m^2(\dot{w}_t - v_{xt}) + \partial_t F(x, t), \\ \partial_t F(x, t) &= \sqrt{2\sigma v_{xt} \chi_{xt}} - \frac{v_{xt}}{\delta u} F(x, t), \end{aligned} \quad (\text{B.1.14})$$

with χ_{xt} a centered Gaussian white noise $\overline{\chi_{xt}\chi_{x't'}} = \delta^d(x-x')\delta(t-t')$ and initial condition $v_{xt=0} = F(x, t=0) = 0$. In the stationary regime, this model is equivalent [43, 92] to Eq. (B.1.12) with $\dot{u}_{xt} = v_{xt}$ and $F(x, t) = F(u_{xt}, x)$ and initial condition $u_{xt=0} = 0$. When $1/\delta u = 0$ this model becomes equivalent to the BFM. We discretize time in units dt and space with periodic boundary conditions along x . To measure quasi-static avalanches, we apply a succession of kicks of sizes δw : we impose $v_{xt} = (m^2/\eta)\delta w$ at $t=0^+$ (beginning of the avalanche), iterate (B.1.14) and wait for the interface to stop before applying a new kick [238]. To identify the seed of each avalanche, we record the velocity $v(x, t)$ for the $n_t = 10^3$ first time-steps of the avalanche. We find the position $x_{\max}(n_t)$ of maximum velocity at $t_{n_t} = n_t dt$ (or at the end of the avalanche if it has stopped before), and then successively identify at each time step $t_n < t_{n_t}$ the position $x_{\max}(n)$ defined as the neighbor of $x_{\max}(n+1)$ with the largest velocity at time t_n . $x_{\max}(n=1)$ is identified as the seed of the avalanche. The size of the kicks is chosen small enough so that the probability to trigger several macroscopic and overlapping avalanches is negligible (see [238] for details).

In dimension $d=1$ we use a system of size $L=2048$ discretized with $N=L$ points and a mass $m=10/L$. In Fig. B.4 we show our results for the mean-shape for different values of S and compare with our theoretical predictions using the predicted value of ℓ_σ (deduced from the measurement of S_m), hence with no fitting parameter. The results for the BFM

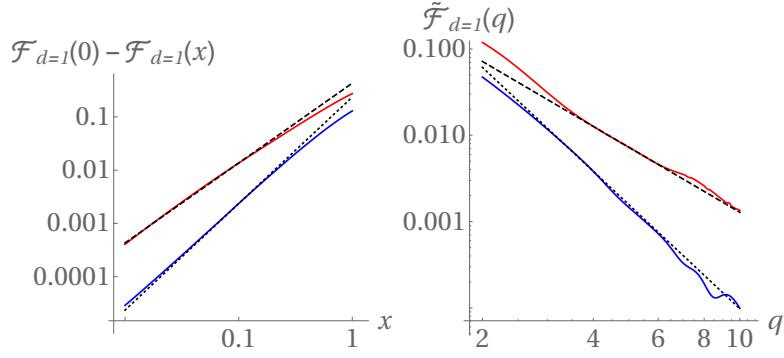


Figure B.5: (color online). Left: (resp. Right:) Log-Log plot of $\mathcal{F}_{d=1}(0) - \mathcal{F}_{d=1}(x)$ (resp. $\tilde{\mathcal{F}}_{d=1}(q)$) numerically obtained in the BFM model (blue) and in the model with SR disorder (red). Dotted lines: guide lines for the BFM result x^2 (left) and $1/q^4$ (right). Dashed lines: $x^{1.5}$ (left) and $1/q^{2.5}$ (right). These results are consistent with (i) the exact result $\tilde{\eta}_{d=1} = 4$ for the BFM (ii) $\tilde{\eta}_{d=1} \simeq 2.5$ for the SR disorder model (in between the guess $\tilde{\eta}_{d=1}^{\text{guess}} = d + \zeta \simeq 2.25$ and our $O(\epsilon)$ prediction $\tilde{\eta}_{d=1} \simeq 8/3 \simeq 2.66$).

are excellent. For the model with SR disorder, the improvement brought by the $O(\epsilon)$ correction is substantial. If one instead uses a measurement of ℓ_σ by e.g. setting the value of the shape at the origin, the agreement with the SR disorder model is, to the naked eye, almost perfect. We also measure properties independent of the value of ℓ_σ : (i) in Fig.B.5 the small x and large q behaviors (ii) the universal ratios c_p . We obtain $(c_1, c_2) \simeq (1.699 \pm 0.003, 3.83 \pm 0.05)$ for the BFM and $(c_1, c_2) \simeq (1.612 \pm 0.004, 3.16 \pm 0.03)$ for the model with SR disorder (error-bars are 3 sigma estimates). The above predictions are in perfect agreement for the BFM, and our $O(\epsilon)$ corrections go in the right direction for the SR disorder case.

To conclude, we introduced an original way of characterizing the mean shape of an avalanche by centering around its seed. We obtained theoretical predictions for this observable and confronted them to numerical simulations. We also proposed a protocol to measure it. We hope that this work stimulates measurements of this quantity in numerical setups and imaging experiments.

B.2 Supplemental Material

We give here a derivation of the results presented in the main text of the letter and details on the numerical simulations.

Dynamical Field Theory Setting

Here we first introduce the formalism used to derive the results presented in the letter.

Equation of motion and dynamical action

As written in the main text, we consider the equation of motion for the over-damped dynamic of an elastic interface of internal dimension d in a quenched random force field and driven by a parabolic well of position w_{xt}

$$\eta \partial_t u_{xt} = \nabla_x^2 u_{xt} - m^2 (u_{xt} - w_{xt}) + F(u_{xt}, x) \quad (\text{B.2.1})$$

where $x \in \mathbb{R}^d$, $t \in \mathbb{R}$, $u_{xt} \in \mathbb{R}$ (the space-time dependence is indicated by subscripts). The elastic-coefficient has been set to unity by a choice of units. In this formulation, the driving force of the parabolic well is $f_{xt} = m^2 (w_{xt} - u_{xt})$. The pinning force $F(u, x)$ is chosen centered, Gaussian with second cumulant $\overline{F(u, x)F(u', x')} = \delta^d(x - x') \Delta_0(u - u')$ (the overline denotes the average over disorder) where $\Delta_0(u)$ is a short-ranged function. Higher cumulants can also exist (i.e. non Gaussian force, and are taken into account in the FRG treatment). Note that here we have written the case of short-ranged (SR) elasticity with an elastic term of the form $\nabla_x^2 u_{xt}$. Other elastic kernels can also be considered, by changing

$$\nabla_x^2 u_{xt} - m^2 u_{xt} \rightarrow \int_{x'} g_{xx'}^{-1} u_{x't} \quad (\text{B.2.2})$$

where $g_{xx'}^{-1}$ is a translationally invariant ($g_{xx'}^{-1} = g_{x-x'}^{-1}$) elastic kernel. In particular, we will consider the following kernel (here written in Fourier space) ($g_q^{-1} = \int_x e^{iqx} g_x^{-1}$, here and throughout the rest of the Supplemental Material $\int_x = \int_{x \in \mathbb{R}^d} d^d x$ and $\int_q = \int_{q \in \mathbb{R}^d} \frac{d^d q}{(2\pi)^d}$)

$$g_q^{-1} = \sqrt{\mu^2 + q^2} \quad (\text{B.2.3})$$

which is known to be relevant in the description of standard long-ranged (LR) elasticity. In this situation, the parameter μ is related to the mass m as $m = \sqrt{\mu}$. In most of the following, we will deal with the SR elasticity case, and explicitly mention when we consider the LR one. Introducing a response field \tilde{u}_{xt} , the generating function of the velocity field

$G[\lambda_{xt}] = \overline{e^{\int_{xt} \lambda_{xt} \dot{u}_{xt}}}$ is computed using the dynamical action formalism for the velocity theory, that is for the time-derivative of (B.2.1) [132, 130]:

$$G[\lambda_{xt}] = \int D[\tilde{u}] D[\dot{u}] e^{\int_{xt} \lambda_{xt} \dot{u}_{xt} + m^2 \int_{xt} \tilde{u}_{xt} \dot{w}_{xt} - S_0 - S_{dis}}$$

$$S_0 = \int_{xt} \tilde{u}_{xt} (\eta \partial_t - \nabla^2 + m^2) \dot{u}_{xt} \quad , \quad S_{dis} = -\frac{1}{2} \int_{xtt'} \tilde{u}_{xt} \tilde{u}_{xt'} \partial_t \partial_{t'} \Delta_0(u_{xt} - u_{xt'}) \quad (\text{B.2.4})$$

The renormalized field theory

As discussed in [101], in the limit of small m , and in the quasi-static limit $\dot{w}_{xt} = v \rightarrow 0^+$, universal quantities associated to the motion inside a single avalanche can be computed in an expansion in $\epsilon = 4 - d$ using an effective action identical to (B.2.4) with the replacement $\Delta_0(u) \rightarrow \Delta(u) = \Delta(0) - \sigma|u| - 4\pi^2 \alpha m^{4-d} u^2 + O(\epsilon^2)$, where σ and $\alpha = O(\epsilon)$ are renormalized quantities. σ is a non-universal parameter whose value is related to the two first moments of the avalanche size distribution through the exact relation $2\sigma/m^4 = \langle S^2 \rangle / \langle S \rangle$. On the other hand α is dimensionless and universal at the FRG fixed point with value $\alpha = -2\epsilon/9 + O(\epsilon^2)$. In terms of the action, this replacement reads $S_{dis} \rightarrow S_{dis}^{eff} = S_{tree} + \delta_{1-loop} S$ with

$$S_{tree} = -\sigma \int_{xt} \tilde{u}_{xt}^2 \dot{u}_{xt} \quad , \quad \delta_{1-loop} S = -4\pi^2 \alpha m^{4-d} \int_{xtt'} \tilde{u}_{xt} \dot{u}_{xt} \tilde{u}_{xt'} \dot{u}_{xt'} \quad (\text{B.2.5})$$

At lowest order in ϵ , the action is $S_{dis}^{eff} = S_{tree}$. Using the renormalized value of σ , it gives the exact result for universal quantities in $d > 4$. In any dimension, this tree/mean-field theory also corresponds to an interface slowly driven in a Brownian force landscape: for each x , $F(u, x)$ is a Brownian in u independent of the others with $(F(u', x) - F(u, x))^2 = 2\sigma|u' - u|$. This is the Brownian Force Model (BFM). The $O(\epsilon)$ corrections around the BFM are easily computed using the fact that $\delta_{1-loop} S$ can also be taken into account by introducing a fictitious Gaussian centered white noise ξ_{xt} with correlations $\langle \xi_x \xi_{x'} \rangle_\xi = 8\pi^2 \alpha m^{4-d} \delta^d(x - x')$ through the identity

$$e^{-S_0 - S_{dis}^{eff}} = \langle e^{-\int_{xt} \tilde{u}_{xt} (\eta \partial_t - \nabla^2 + m^2 + \xi_x) \dot{u}_{xt} - S_{tree}} \rangle_\xi \quad (\text{B.2.6})$$

where $\langle \rangle_\xi$ denotes the average over ξ . One-loop observables are thus rewritten as averaged tree observables in a theory with space-dependent mass $m^2 \rightarrow m^2 + \xi_x$. Since $\xi_x = O(\sqrt{\epsilon})$, the effect of ξ_x can be taken into account perturbatively up to order $O(\xi_x^2)$.

Avalanches observables

Avalanches in non-stationary driving

Let us first introduce our avalanche observables in a non-stationary setting. We refer the reader to [102, 101, 1] for more details on this procedure. We first prepare the interface in its quasi-static stationary state $\dot{w}_{xt} \sim v = 0^+$, then turn the driving off: $\dot{w}_{xt} = 0$ and finally wait for the interface to stop at some metastable position. Supposing we are in such a state at $t = 0$, we apply to the interface a step in the driving force localized at $x = t = 0$, $\dot{f}_{xt} = m^2 \delta w \delta(x) \delta(t)$ (local kick) and let it evolve. Information about the resulting motion of the interface is encoded in the generating functional

$G[\lambda_{xt}] = \overline{e^{\int_{x,t>0} \lambda_{xt} \dot{u}_{xt}}}$. Remarkably, since the action (B.2.5) (written at one-loop in terms of ξ_x (B.2.6)) is linear in \dot{u}_{xt} , the evaluation of $G[\lambda_{xt}]$ through the path-integral formalism simplifies. The integration on the velocity field \dot{u}_{xt} leads to a delta functional and to the result:

$$G[\lambda_{xt}] = \langle e^{m^2 \delta w \tilde{u}_{x=t=0}^{\lambda, \xi}} \rangle_\xi \quad (\text{B.2.7})$$

where $\tilde{u}_{xt}^{\lambda, \xi}$ is the solution of the so-called instanton equation:

$$\partial_t \tilde{u}_{xt} + \nabla^2 \tilde{u}_{xt} - (1 + \xi_x) \tilde{u}_{xt} + \tilde{u}_{xt}^2 + \lambda_{xt} = 0 \quad (\text{B.2.8})$$

here written in dimensionless units using the variables $\tilde{u}_x = \frac{m^2}{\sigma} \hat{u}_{\hat{x}}$, $x = \hat{x}/m$, $t = \frac{\eta}{m^2} \hat{t}$, $\lambda_{xt} = \frac{m^4}{\sigma} \hat{\lambda}_{\hat{x}\hat{t}}$, and omitting the hats in what follows, to lighten notations. The boundary conditions is $\tilde{u}_{xt} = 0$ for $t = +\infty$. Here we will only be interested in single avalanche, defined as the response of the interface to an infinitesimal step in the force. We introduce the generating functional $Z[\lambda_{xt}]$ as (expanding (B.2.7) in δw):

$$\overline{e^{\int_{x,t>0} \lambda_{xt} \dot{u}_{xt}}} - 1 = \delta w Z[\lambda_{xt}] + O(\delta w^2)$$

$$Z[\lambda_{xt}] = m^2 \langle \tilde{u}_{x=t=0}^{\lambda, \xi} \rangle_\xi \quad (\text{B.2.9})$$

In the above expansion, the δw factor just accounts for the probability to trigger an avalanche at $t = x = 0$. Introducing $\rho_{t=x=0}[\dot{u}_{xt}]$, the density of velocity field \dot{u}_{tx} inside an avalanche that starts at $t = x = 0$, we write

$$Z[\lambda_{xt}] = \int D[\dot{u}] \left(e^{\int_{xt} \lambda_{xt} \dot{u}_{xt}} - 1 \right) \rho_{t=x=0}[\dot{u}_{xt}] \quad , \quad (\text{B.2.10})$$

where here this equation can actually be viewed as a definition of the density $\rho_{t=x=0}$. The fact that these definitions indeed correspond to what is usually meant by avalanches in the quasi-static limit is discussed below. This formulation is up to now completely general. Let us now focus on two types of sources: $\lambda_{xt}^1 = (-\mu + \lambda \delta(x - y) \delta(t - s)) \theta(t)$ and

$\lambda_{xt}^2 = (-\mu + \lambda\delta(x-y))\theta(t)$ ($\theta(\cdot)$ denotes the Heaviside theta function). In both cases, the μ variable probes the total size of the avalanche $S = \int_{x,t>0} \dot{u}_{xt}$. In the first case, λ probes the local velocity at $t = s$ and $x = y$ during the avalanche. In the second case, λ probes the local size of the avalanche at $x = y$, $S_y = \int_{t>0} \dot{u}_{yt}$. We write the associated generating function $Z^{(1)}[\lambda_{xt}^1] = Z^{(1)}(\mu, \lambda, y, s)$ and $Z^{(2)}[\lambda_{xt}^2] = Z^{(2)}(\mu, \lambda, y)$. These are obtained through the formula (B.2.9) by solving (B.2.8) which leads to

$$Z^{(1)}(\mu, \lambda, y, s) = \int dS d\dot{u}_{ys} e^{-\mu S + \lambda \dot{u}_{ys}} \rho_{t=x=0}^{(1)}(S, \dot{u}_{ys}) \quad , \quad Z^{(2)}(\mu, \lambda, y) = \int dS dS_y e^{-\mu S + \lambda S_y} \rho_{t=x=0}^{(2)}(S, S_y), \quad (\text{B.2.11})$$

where $\rho_{t=x=0}^{(1)}(S, \dot{u}_{ys})$ (resp. $\rho_{t=x=0}^{(2)}(S, \dot{u}_{ys})$) is the joint density of total size S and velocity field \dot{u}_{ys} (resp. of total size S and local size S_y) for avalanches starting at $t = x = 0$. In practice we will only be interested in computing the mean velocity-field inside avalanche of total size S , $\langle \dot{u}_{ys} \rangle_S$ (resp. the mean local size inside avalanche of total size S , $\langle S_y \rangle_S$). These are computed as

$$\langle \dot{u}_{ys} \rangle_S = \frac{LT_{\mu \rightarrow S}^{-1} \partial_\lambda Z^{(1)}|_{\lambda=0}}{\rho(S)/L^d} \quad , \quad \langle S_y \rangle_S = \frac{LT_{\mu \rightarrow S}^{-1} \partial_\lambda Z^{(2)}|_{\lambda=0}}{\rho(S)/L^d} = \int_{s=0}^{\infty} ds \langle \dot{u}_{ys} \rangle_S \quad (\text{B.2.12})$$

where $LT_{\mu \rightarrow S}^{-1}$ denotes the Inverse Laplace Transform (ILT) operation $LT_{\mu \rightarrow S}^{-1} = \frac{1}{2i\pi} \int_C d\mu e^{\mu S}$ with appropriate contour of integration, and we have introduced $\rho(S)$ the density of avalanches of total size S , previously computed up to one-loop in [109, 111, 101] ($\rho(S)/L^d = \int d\dot{u}_{ys} \rho_{t=x=0}^{(1)}(S, \dot{u}_{ys}) = \int dS_y \rho_{t=x=0}^{(2)}(S, S_y)$ is the density of avalanches of total size S starting at $x = 0$). For the observables we are interested in, we will thus only need to solve (B.2.8) at first order in λ .

Link with the stationary driving

Let us now present here how the precedent approach is linked to avalanches occurring in the quasi-static stationary state of the interface dynamic $\dot{w}_{xt} = v \rightarrow 0^+$. We introduce ρ_0 the mean density of avalanche per unit of driving and $p[\dot{u}_{tx}]$ the (functional) probability of velocity field \dot{u}_{tx} inside an avalanche. At first order in v , the generating function $G[\lambda_{xt}] = e^{\int_{xt} \lambda_{xt} \dot{u}_{xt}}$ can be written as

$$G[\lambda_{xt}] = (1 - \rho_0 v T) + \rho_0 v T \int D[\dot{u}] e^{\int_{xt} \lambda_{xt} \dot{u}_{xt}} p[\dot{u}_{xt}] + O(v^2) = 1 + v T \int D[\dot{u}] \left(e^{\int_{xt} \lambda_{xt} \dot{u}_{xt}} - 1 \right) \rho[\dot{u}_{xt}] + O(v^2) \quad (\text{B.2.13})$$

where we reintroduced $\rho[\dot{u}_{xt}] = \rho_0 p[\dot{u}_{xt}]$ the density of velocity field \dot{u}_{xt} inside an avalanche. The equation (B.2.13) can be seen as a definition of what is meant by avalanches in the quasi-static setting. The time scale T that appears in (B.2.13) should be much larger than the time-scale of avalanche motion (to allow the avalanche to terminate) and much smaller than the typical waiting time between avalanches. This only works if λ_{xt} is also non-zero in a time window smaller than T : this ensures that the measurement made on the velocity-field is also inside a single-avalanche. On the other hand, the small velocity expansion made directly on the action (B.2.4) and compared to (B.2.13) gives

$$G[\lambda_{xt}] = 1 + v \langle m^2 \rangle_{\lambda_{xt}} \longrightarrow \int D[\dot{u}] \left(e^{\int_{xt} \lambda_{xt} \dot{u}_{xt}} - 1 \right) \rho[\dot{u}_{xt}] = \int_{xt} \frac{m^2}{T} \langle \tilde{u}_{xt} \rangle_{\lambda_{xt}}, \quad (\text{B.2.14})$$

where here the average $\langle \cdot \rangle_{\lambda_{xt}}$ refers to the average with respect to the dynamical action (B.2.4) with source λ_{xt} . In the right of (B.2.14), the integral over time and space originates from the fact that we have consider the effect of avalanches starting at any point of the interface, and at any time in the time-window T . From a field-theory point of view, it is then natural to interpret $m^2 \langle \tilde{u}_{x=t=0} \rangle_{\lambda_{xt}}$ as the contribution from avalanches starting at $t = x = 0$ (diagrams entering into $\langle \tilde{u}_{x=t=0} \rangle_{\lambda_{xt}}$ can only have a first non-zero \dot{u}_{xt} at $x = 0$). Furthermore, this is supported by the non-stationary setting in which this interpretation is immediate. In the quasi-static setting we can only a priori consider sources λ_{xt} non-zero in time windows smaller than T to make sure that only one avalanche is taken into account. However, from a practical point of view, when $T \gg \tau_m$ where τ_m is the typical time scale of avalanches, both descriptions give exactly the same result as detailed in [101].

Calculation in the BFM

Mean-velocity field inside an avalanche in the BFM

Here we present the calculations leading to the results Eq.(B.1.4) and Eq.(B.1.7) of the letter for the mean-velocity field inside avalanche of total size S in the BFM $\langle \dot{u}_{ys} \rangle_S$ (denoted $v(y, s)$ in the main text with $y = x$ and $s = t$). We have to solve to first order in λ the instanton equation

$$\partial_t \tilde{u}_{xt} + \nabla^2 \tilde{u}_{xt} - \tilde{u}_{xt} + \tilde{u}_{xt}^2 - \mu + \lambda \delta(x-y) \delta(t-s) = 0. \quad (\text{B.2.15})$$

Note that here, in dimensionless units, time and avalanche size are measured in terms of the natural units of avalanches motion $\tau_m = \eta/m^2$ and $S_m = \sigma/m^4$. The perturbative solution is $\tilde{u}_{xt} = \tilde{u}_{xt}^0 + \tilde{u}_{xt}^1 \lambda + O(\lambda^2)$ with

$$\tilde{u}_x^0 = Z(\mu) = \frac{1}{2} (1 - \kappa^2(\mu)) \quad , \quad \kappa(\mu) = (1 + 4\mu)^{\frac{1}{4}} \quad , \quad \tilde{u}_{qt}^1 = - \int_{t'=+\infty}^t e^{(q^2 + \kappa^2(\mu))(t-t') + i q y} \delta(t' - s) dt' \quad (\text{B.2.16})$$

here written in Fourier space for the $O(\lambda)$ part: $\tilde{u}_{qt}^1 = \int_x e^{i q x} \tilde{u}_{xt}^1$. This immediately gives

$$\tilde{u}_{t=x=0}^1 = \int_q e^{i q y - (q^2 + \kappa^2(\mu))s} \quad (\text{B.2.17})$$

Using the tree result for the avalanche size density $\rho^{\text{MF}}(S) = \frac{L^d}{2\sqrt{\pi}S^{\frac{3}{2}}}e^{-S/4}$ we obtain the mean velocity field inside a single avalanche using (B.2.12) as

$$\langle \dot{u}_{ys} \rangle_S = 2\sqrt{\pi}S^{3/2}e^{S/4}LT_{\mu \rightarrow S}^{-1} \int_q e^{iqy - (q^2 + \sqrt{1+4\mu})s} = 2se^{-\frac{s^2}{S}} \int_q e^{iqy - q^2s} = 2se^{-s^2/S} \frac{1}{(4\pi s)^{d/2}} e^{-y^2/(4s)} \quad (\text{B.2.18})$$

In the notation of the main text, we thus obtain (B.1.4) that we recall here

$$\langle v(x, t) \rangle_S = S^{\frac{2-d}{4}} F(t/S^{1/2}, x/S^{1/4}) \quad , \quad F(t, x) = 2te^{-t^2} \frac{1}{(4\pi t)^{d/2}} e^{-x^2/(4t)} \quad (\text{B.2.19})$$

Extension to LR elasticity

Following the same computation, one obtains for the case of the BFM with long-ranged elasticity (with the kernel (B.2.3))

$$\tilde{u}_{t=x=0} = \int_q e^{iqy - (\sqrt{1+q^2} - 1 + \kappa^2(\mu))s} \quad (\text{B.2.20})$$

And thus

$$\langle \dot{u}_{ys} \rangle_S = 2se^{-\frac{s^2}{S}} \int_q e^{iqy - (\sqrt{1+q^2} - 1)s} \quad (\text{B.2.21})$$

Note that here, the spatio-temporal shape does not satisfy the expected scaling form (B.1.2), $\langle \dot{u}_{ys} \rangle_S = S^{\frac{2-d-1}{2}} F(s/S^{\frac{1}{2}}, y/S^{\frac{1}{2}})$ for all S . This should not be surprising, it is known that the present theory describes scale-invariant avalanches only for $S \ll S_m$ (here $S_m = 1$ in dimensionless units is the large scale cutoff S_{max} mentioned in the main text, and note that in our theory the low-scale cutoff on the scaling regime S_{min} also mentioned in the main text can effectively be taken to 0 for shape observables). The fact that the scaling hypothesis for the mean velocity field holds $\forall S$ in the BFM with short-ranged elasticity is the true surprise. Scaling in the long-ranged model is restored at small S and here

$$F(s, y) = \lim_{S \rightarrow 0} S^{\frac{d-1}{2}} \langle \dot{u}_{S^{\frac{1}{2}}y, S^{\frac{1}{2}}s} \rangle_S = 2se^{-s^2} \int_q e^{iqy - |q|s} \quad (\text{B.2.22})$$

Evaluating this integral in dimension 1 immediately leads to the result (B.1.7).

The mean shape of avalanches in the BFM: results in Fourier space

We now derive the result Eq.(B.1.5) of the letter. Using (B.2.17), we immediately obtain the mean-shape of avalanche in Fourier space in the BFM as

$$\tilde{\mathcal{F}}^{\text{MF}}(q) = \int_{s=0}^{\infty} 2se^{-s^2 - q^2s} = 1 - \frac{\sqrt{\pi}q^2}{2} e^{\frac{q^4}{4}} \text{erfc}\left(\frac{q^2}{2}\right) \quad (\text{B.2.23})$$

i.e. the result (B.1.5) of the main text. Note that here avalanche sizes have been expressed in units of $S_m = \sigma/m^4$ and distances in units of $1/m$. Hence the non-universal scale ℓ_σ of the main text is indeed $\ell_\sigma = \frac{1}{m} S_m^{-1/4} = \sigma^{-1/4}$. Let us give here the large and small momenta behavior of $\tilde{\mathcal{F}}^{\text{MF}}(q)$:

$$\tilde{\mathcal{F}}^{\text{MF}}(q) =_{q \gg 1} \frac{2}{q^4} - \frac{12}{q^8} + \frac{120}{q^{12}} + O\left(\frac{1}{q^{16}}\right) \quad (\text{B.2.24})$$

$$\tilde{\mathcal{F}}^{\text{MF}}(q) =_{q \ll 1} 1 - \frac{\sqrt{\pi}q^2}{2} + \frac{q^4}{2} - \frac{\sqrt{\pi}q^6}{8} + O(q^8) \quad (\text{B.2.25})$$

Extension to LR elasticity

We now compute the mean shape in real space. In particular we obtain the result Eq.(B.1.6) of the letter. The extension of the precedent results to the case of LR elasticity is straightforward. As written in the main text and following the formula (B.2.22), the mean-shape in Fourier space in the scaling regime for LR elasticity is simply obtained from the precedent results by changing $q^2 \rightarrow |q|$:

$$\tilde{\mathcal{F}}^{\text{MF,LR}}(q) = \tilde{\mathcal{F}}^{\text{MF}}(\sqrt{q}). \quad (\text{B.2.26})$$

In particular it now has an algebraic tail at large q with exponent $1/q^2$, $\tilde{\mathcal{F}}^{\text{MF,LR}}(q) \simeq_{q \gg 1} \frac{2}{q^2}$.

The mean shape of avalanches in the BFM: results in real space

In real space, $\mathcal{F}_d^{\text{MF}}(x)$ is most simply obtained by integration of (B.2.19):

$$\mathcal{F}_d^{\text{MF}}(x) = \frac{2}{(4\pi)^{d/2}} \int_0^{+\infty} dt t^{1-d/2} e^{-t^2 - \frac{x^2}{4t}} \quad (\text{B.2.27})$$

This integral can be expressed either as the sum of three series:

$$\mathcal{F}_d^{\text{MF}}(x) = \pi^{1-\frac{d}{2}} \sum_{p=0}^{\infty} (-1)^p 2^{-4p} \left[\frac{a_p}{\sin \frac{d\pi}{4}} x^{4p} - \frac{a_{p+\frac{1}{2}}}{4 \cos \frac{d\pi}{4}} x^{4p+2} + \frac{b_p}{\sin \frac{d\pi}{2}} x^{4-d+4p} \right] \quad (\text{B.2.28})$$

$$a_p = \frac{2^{-d}}{(2p)! \Gamma\left(\frac{d}{4} + p\right)} \quad , \quad b_p = \frac{2^{-3}}{p! \Gamma\left(-\frac{d}{2} + 2p + 3\right)} \quad (\text{B.2.29})$$

or, equivalently, as the sum of three generalized hypergeometric functions (corresponding term by term to the series):

$$\mathcal{F}_d^{\text{MF}}(x) = \frac{1}{8}\pi^{1-\frac{d}{2}} \left(\frac{2^{3-d} \csc\left(\frac{\pi d}{4}\right) {}_0F_2\left(\cdot; \frac{1}{2}, \frac{d}{4}; -\frac{x^4}{64}\right)}{\Gamma\left(\frac{d}{4}\right)} - \frac{2^{1-d} x^2 \sec\left(\frac{\pi d}{4}\right) {}_0F_2\left(\cdot; \frac{3}{2}, \frac{d}{4} + \frac{1}{2}; -\frac{x^4}{64}\right)}{\Gamma\left(\frac{d+2}{4}\right)} \right. \\ \left. + \frac{x^{4-d} \csc\left(\frac{\pi d}{2}\right) {}_0F_2\left(\cdot; \frac{3}{2} - \frac{d}{4}, 2 - \frac{d}{4}; -\frac{x^4}{64}\right)}{\Gamma\left(3 - \frac{d}{2}\right)} \right) \quad (\text{B.2.30})$$

The expressions (B.2.28) and (B.2.30) are adequate for $d = 1, 3$. For $d = 2, 4$ one must first take the limit $d \rightarrow 2, 4$ before evaluating. This is easy to do with mathematica, and we give here only the two leading terms at small x :

$$\mathcal{F}_2^{\text{MF}}(x) = \frac{1}{4\sqrt{\pi}} - \frac{x^2(-4\log(x) - 3\gamma_E + 2 + \log(16))}{16\pi} + O(x^3) \quad (\text{B.2.31})$$

$$\mathcal{F}_4^{\text{MF}}(x) = \frac{-4\log(x) - 3\gamma_E + \log(16)}{16\pi^2} + \frac{x^2}{32\pi^{3/2}} + O(x^3) \quad (\text{B.2.32})$$

For $d < 4$ the value at zero is finite:

$$\mathcal{F}_d^{\text{MF}}(0) = \frac{2^{-d}\pi^{1-\frac{d}{2}}}{\Gamma\left(\frac{d}{4}\right)\sin\left(\frac{\pi d}{4}\right)} \quad (\text{B.2.33})$$

$$\mathcal{F}_1^{\text{MF}}(0) \approx 0.345684 \quad , \quad \mathcal{F}_2^{\text{MF}}(0) \approx 0.141047 \quad , \quad \mathcal{F}_4^{\text{MF}}(0) \approx 0.0813891 \quad (\text{B.2.34})$$

and $\mathcal{F}_d^{\text{MF}}(0)$ diverges as $\frac{1}{4\pi^{2\epsilon}}$ as $d \rightarrow 4^-$ (it has a minimum near $d = 3.2$). For $d > 4$ it diverges near zero as $\mathcal{F}_1^{\text{MF}}(x) \simeq \frac{\pi^{1-\frac{d}{2}} \csc\left(\frac{\pi d}{2}\right)}{8\Gamma\left(3-\frac{d}{2}\right)} x^{4-d}$. The large distance behavior is easily obtained from the saddle-point method on (B.2.27). It yields a stretched exponential decay at large x with exponent $4/3$, independent of d :

$$\mathcal{F}_d^{\text{MF}}(x) \simeq \frac{2^{-d/2}\pi^{\frac{1}{2}-\frac{d}{2}}}{\sqrt{3}} x^{\frac{2-d}{3}} e^{-\frac{3x^{4/3}}{4}} \quad (\text{B.2.35})$$

Extension to LR elasticity

We did not attempt to find expressions for the mean-shape in real space for LR elasticity in any d . In the most experimentally relevant case of $d = 1$ however it takes a simple expression: integrating (B.1.7) from $t = 0$ to $t = \infty$ leads

$$\mathcal{F}_{d=1}^{\text{MF,LR}}(x) = \frac{1}{\sqrt{\pi}} - |x|e^{x^2} \text{erfc}(|x|) \quad (\text{B.2.36})$$

We note in particular the behavior around $x = 0$, $\mathcal{F}_{d=1}^{\text{MF,LR}}(x) =_{x \ll 1} \frac{1}{\sqrt{\pi}} - |x| + O(x^2)$, reminiscent of the $2/q^2$ tail in Fourier space. At large x , the mean-shape now decays algebraically as $\mathcal{F}_{d=1}^{\text{MF,LR}}(x) =_{x \gg 1} \frac{1}{2\sqrt{\pi}x^2} + O(1/x^4)$.

$O(\epsilon)$ corrections

“Brut” corrections

At $O(\epsilon)$ we focus directly on the computation of the mean-shape at fixed size $\langle S_y \rangle_S$. We need to solve

$$\partial_t \tilde{u}_{xt} + \nabla^2 \tilde{u}_{xt} - (1 + \xi_x) \tilde{u}_{xt} + \tilde{u}_{xt}^2 - \mu + \lambda \delta(x - y) = 0 \quad (\text{B.2.37})$$

at order 1 in λ and order 2 in ξ_x . When $\xi_x = 0$ (corresponding to the BFM model) this equation was recently solved exactly [107] to study the joint distribution of total size S and local size S_y in the BFM. Here we will only be interested in its perturbative solution up to first order in λ (to study the mean shape) but up to second order in ξ_x (to study $O(\epsilon)$ corrections). We can look for time-independent solution and use a double expansion $\tilde{u}_x = \sum_{i=0}^1 \sum_{j=0}^2 \tilde{u}_j^i(x)$ where $\tilde{u}_j^i(x) = O(\lambda^i \xi^j)$. The observable of interest is $\mathcal{Z}(\mu, y) = \partial_\lambda Z^{(2)}(\mu, y, \lambda)|_{\lambda=0}$ where $Z^{(2)}$ was introduced in (B.2.9). Using $Z^{(2)}(\mu, y, \lambda) = m^2 \langle \tilde{u}_{x=0} \rangle_\xi$ we obtain (in dimensionless units)

$$\mathcal{Z}(\mu, y) = \mathcal{Z}^{\text{MF}}(\mu, y) + \delta \mathcal{Z}(\mu, y) \quad , \quad \mathcal{Z}^{\text{MF}}(\mu, y) = \tilde{u}_0^1(x=0) \quad , \quad \delta \mathcal{Z}(\mu, y) = \langle \tilde{u}_2^1(x=0) \rangle_\xi \quad (\text{B.2.38})$$

These are most simply expressed in Fourier space $\tilde{\mathcal{Z}}(\mu, q) = \int_x e^{iqy} \mathcal{Z}(\mu, y)$ and we find

$$\tilde{\mathcal{Z}}^{\text{MF}}(\mu, q) = G_q(\mu) = \frac{1}{q^2 + \kappa^2(\mu)} \\ \delta \tilde{\mathcal{Z}}(\mu, q) = 8\pi^2 \alpha (G_q(\mu))^2 \left(\int_p G_p(\mu) (1 + 2Z(\mu)G_{p-q}(\mu))^2 + 2G_0(\mu) \int_p (1 + Z(\mu)G_p(\mu))Z(\mu)G_p(\mu) \right) \quad (\text{B.2.39})$$

where we have introduced the response function $G_q(\mu)$, a dressed version of the elastic kernel $g_q = \frac{1}{m^2 + q^2}$.

Counter-terms

The result for $\delta \tilde{\mathcal{Z}}(\mu, q)$ is not yet complete: the integrals present in (B.2.39) diverge at large q for $d < 4$. This is a usual feature of one-loop computations in field theory. As detailed in [101], when doing a perturbative calculation in (B.2.5), one has to take into account a renormalization of σ and m^2 (the latter being in fact an artifact due to the utilization of

the oversimplified one-loop action (B.2.5)). For clarity let us now denote σ_0 and m_0^2 the parameters used so far in the perturbative calculation. These are renormalized as $\sigma_0 \rightarrow \sigma = \sigma_0 + \delta\sigma$ and $m_0^2 \rightarrow m^2 = m_0^2 + \delta m^2$ with

$$\delta\sigma = 24\pi^2\alpha \int_k g_k^2 \quad , \quad \delta m^2 = -8\pi^2\alpha \int_k g_k \quad (\text{B.2.40})$$

where $g_k = \frac{1}{k^2 + m_0^2}$ is the bare propagator. The parameters entering in (B.2.40) are either the bare parameters or the renormalized parameters (these choices differ from a term of order $O(\epsilon^2)$). The fact that the theory is renormalizable imply that divergences present in (B.2.39) should disappear when expressing the results in terms of renormalized parameters. Let us thus denote $\{K_0\} := \{\sigma_0, m_0^2\}$ the set of important couplings and emphasize the dependance of $\tilde{Z}(\mu, q)$ by momentarily adopting the simple notation $\tilde{Z}(\{K_0\})$. Rewriting the result $\tilde{Z}(\{K_0\})$ in terms of the renormalized coupling $\{K\}$ leads to the definition of the counter-terms $\delta_{c.t.}\tilde{Z}(\{K\})$ as

$$\tilde{Z}(\{K_0\}) = \tilde{Z}(\{K - \delta K\}) = \tilde{Z}^{\text{MF}}(\{K\}) + \delta_{c.t.}\tilde{Z}(\{K\}) + \delta\tilde{Z}(\{K\}) + O(\epsilon^2) \quad (\text{B.2.41})$$

and thus $\delta_{c.t.}\tilde{Z}(\{K\}) = -\frac{\partial\tilde{Z}^{\text{MF}}(\{K\})}{\partial K_\alpha}\delta K_\alpha$. To compute these partial derivatives, we reintroduce the original units of the problem in $\tilde{Z}^{\text{MF}}(\{K\})$:

$$\tilde{Z}^{\text{MF}}(\{K\}) = \frac{e^{iqy}}{q^2 + \sqrt{1 + 4\sigma\mu/m^4}} \quad (\text{B.2.42})$$

The $\frac{m^2}{\sigma}$ comes from the rescaling of \tilde{u} , the m^{-d} from the rescaling of the Fourier Transform and the $\frac{\sigma}{m^{4-d}}$ from the rescaling of λ . Computing the derivatives with respect to σ and m^2 and going back to dimensionless units leads to the following expression for the counter terms:

$$\delta_{c.t.}\tilde{Z}(\mu, q) = 8\pi^2\alpha e^{iqy} G_{q=0}(\mu) G_q(\mu)^2 (6\mu \int_k g_k^2 - \int_k g_k) \quad (\text{B.2.43})$$

It is then easy to check that adding (B.2.43) to (B.2.39) indeed regularizes the result. The computation of the resulting, convergent integrals in $d = 4$ leads to the full result for the one loop correction $\delta\tilde{Z}(\mu, q) \rightarrow \delta\tilde{Z}(\mu, q) + \delta_{c.t.}\tilde{Z}(\mu, q)$ with

$$\delta\tilde{Z}(\mu, q) = \alpha(G_q(\mu))^2 \left(\frac{(1 + 6\mu)\log(1 - 2Z) + 2Z}{2(1 - 2Z)} + 4Z \left(1 + \sinh^{-1}\left(\frac{q}{2\sqrt{1 - 2Z}}\right) \frac{Z - (q^2 + 4(1 - 2Z))}{q\sqrt{q^2 + 4(1 - 2Z)}} \right) \right) \quad (\text{B.2.44})$$

and $Z \equiv Z(\mu)$.

The mean-shape at $O(\epsilon)$: Laplace transform in Fourier

We now obtain the result Eq.(B.1.9) presented in the letter. Using (B.2.12), the mean-shape in Fourier space is computed as $\langle S(q) \rangle_S = \frac{L^d}{\rho^{\text{MF}}(S)} LT_{\mu \rightarrow S}^{-1} (\tilde{Z}^{\text{MF}}(\mu, q))$. To order $O(\epsilon)$, we have $\tilde{Z}(\mu, q) = \tilde{Z}^{\text{MF}}(\mu, q) + \delta\tilde{Z}(\mu, q)$. The density ρ was computed to $O(\epsilon)$ in [111] with the result $\rho(S) = \rho^{\text{MF}}(S) + \delta\rho(S)$ with

$$\delta\rho(S) = \alpha\rho^{\text{MF}}(S) \times \frac{\gamma_E(S - 6) + 4S - 8\sqrt{\pi}\sqrt{S} + (S - 6)\log(S) + 4}{16} \quad (\text{B.2.45})$$

$\langle S(q) \rangle_S$ can thus be computed to $O(\epsilon)$ as

$$\langle S(q) \rangle_S = \frac{L^d}{\rho^{\text{MF}}(S)} LT_{\mu \rightarrow S}^{-1} (\tilde{Z}^{\text{MF}}(\mu, q)) - \frac{L^d\delta\rho(S)}{(\rho^{\text{MF}}(S))^2} LT_{\mu \rightarrow S}^{-1} (\tilde{Z}^{\text{MF}}(\mu, q)) + \frac{L^d}{\rho^{\text{MF}}(S)} LT_{\mu \rightarrow S}^{-1} (\delta\tilde{Z}(\mu, q)) + O(\epsilon^2) . \quad (\text{B.2.46})$$

One can check that the $O(\epsilon^0)$ part of this result allows to retrieve directly the result of the precedent section for the mean-shape (i.e. without computing $\langle v(x, t) \rangle_S$ first), so that everything is consistent. A new difficulty (compared to the BFM case), is that $\langle S(q) \rangle_S$ defined in (B.2.46) does not satisfy the scaling form $\langle S(q) \rangle_S = S\tilde{\mathcal{F}}_d(qS^{\frac{1}{d+\zeta}}) \forall S$. This is natural: the scaling regime of the problem is for $S \ll S_m$ (here $S_m = 1$ in dimensionless units) and the universal shape of avalanches is the one obtained from (B.2.46) as $S \rightarrow 0$. It is thus obtained here as

$$\tilde{\mathcal{F}}_d(q) = \lim_{S \rightarrow 0} \frac{\langle S(qS^{\frac{1}{d+\zeta}}) \rangle_S}{S} \quad (\text{B.2.47})$$

We now compute the ϵ expansion of (B.2.47) using (B.2.46). By definition $\tilde{\mathcal{F}}_d(q) = \tilde{\mathcal{F}}^{\text{MF}}(q) + \delta\tilde{\mathcal{F}}_d(q)$. We also use the one-loop value of $\zeta = \zeta_1\epsilon$ ($\zeta_1 = 1/3$) and obtain

$$\delta\tilde{\mathcal{F}}_d(q) = \lim_{S \rightarrow 0} \epsilon \frac{\zeta_1 - 1}{16} q \log(S) \frac{\partial\tilde{\mathcal{F}}^{\text{MF}}}{\partial q}(q) + L^d \frac{LT_{\mu \rightarrow S}^{-1} \delta\tilde{Z}(\mu, qS^{-\frac{1}{4}})}{S\rho^{\text{MF}}(S)} - \tilde{\mathcal{F}}^{\text{MF}}(q) \frac{\delta\rho(S)}{\rho^{\text{MF}}(S)} \quad (\text{B.2.48})$$

Let us first look at the second term in (B.2.48):

$$\begin{aligned}
 L^d \frac{LT_{\mu \rightarrow S}^{-1} \delta \tilde{\mathcal{Z}}(\mu, qS^{-\frac{1}{4}})}{S \rho^{\text{MF}}(S)} &= \frac{L^d}{S \rho^{\text{MF}}(S)} \int_{c-i\infty}^{c+i\infty} \frac{d\mu}{2i\pi} e^{\mu S} \delta \tilde{\mathcal{Z}}(\mu, qS^{-\frac{1}{4}}) \\
 &= \frac{L^d e^{-S/4}}{S \rho^{\text{MF}}(S)} \int_{c'-i\infty}^{c'+i\infty} \frac{d\mu}{2i\pi S} e^{\mu} \delta \tilde{\mathcal{Z}}(-1/4 + \mu/S, qS^{-\frac{1}{4}}) \\
 &\simeq_{S \ll 1} \alpha LT_{\mu \rightarrow 1}^{-1} \left(H(q, \mu) - \frac{3\sqrt{\pi}}{2} \frac{\sqrt{\mu} \log(S)}{(2\sqrt{\mu} + q^2)^2} + O(S) \right)
 \end{aligned} \tag{B.2.49}$$

Where here from the first to the second line we used a change of variables $\mu \rightarrow -1/4 + \mu/S$ and then took the limit $S \rightarrow 0^+$ of (B.2.44) to define

$$H(q, \mu) = \frac{\sqrt{\mu} \sqrt{\pi} \left(q (6 \log(2\sqrt{\mu}) - 16) \sqrt{8\sqrt{\mu} + q^2} + 16 (9\sqrt{\mu} + q^2) \sinh^{-1} \left(\frac{q}{2\sqrt{2}\sqrt{\mu}} \right) \right)}{2q (2\sqrt{\mu} + q^2)^2 \sqrt{8\sqrt{\mu} + q^2}} \tag{B.2.50}$$

Using similar manipulations, the other terms are inserted inside the ILT using the representation

$$\tilde{\mathcal{F}}^{\text{MF}}(q) = LT_{\mu \rightarrow 1}^{-1} \left(\frac{2\sqrt{\pi}}{2\sqrt{\mu} + q^2} \right), \quad \frac{\partial \tilde{\mathcal{F}}^{\text{MF}}}{\partial q}(q) = LT_{\mu \rightarrow 1}^{-1} \left(\frac{-4\sqrt{\pi}q}{(2\sqrt{\mu} + q^2)^2} \right), \quad \frac{\zeta_1 - 1}{16} = \frac{3\alpha}{16\epsilon} \tag{B.2.51}$$

This representation shows that the $O(\log(S))$ terms present in (B.2.48) cancel and we obtain the result

$$\delta \tilde{\mathcal{F}}_d(q) = \alpha LT_{\mu \rightarrow 1}^{-1} \left(-\frac{\sqrt{\pi}}{8} \frac{(4 - 6\gamma_E)}{(2\sqrt{\mu} + \tilde{q}^2)} + H(q, \mu) \right) \tag{B.2.52}$$

which leads to the result (B.1.9) in the main text. Note that the result satisfies, as required from normalization

$$\tilde{\mathcal{F}}_d(q=0) = 1, \quad \delta \tilde{\mathcal{F}}_d(q=0) = 0 \tag{B.2.53}$$

which can be checked explicitly from the above expressions using that $LT_{\mu \rightarrow 1}^{-1} \frac{\gamma_E + \ln(4\mu)}{\sqrt{\mu}} = 0$. Equivalently, the total shape in Fourier takes the form

$$\tilde{\mathcal{F}}_d(q) = LT_{\mu \rightarrow 1}^{-1} \left(\left(1 + \alpha \frac{3\gamma_E - 2}{8} \right) \frac{2\sqrt{\pi}}{q^2 + 2\sqrt{\mu} + \Sigma(q, \mu)} \right) + O(\alpha^2) \tag{B.2.54}$$

where the "self-energy" correction reads, to lowest order

$$\Sigma(q, \mu) = -4\alpha\sqrt{\mu} \left(\frac{q^2 + 9\sqrt{\mu}}{q\sqrt{q^2 + 8\sqrt{\mu}}} \sinh^{-1} \left(\frac{q}{2\sqrt{2}\sqrt{\mu}} \right) - 1 + \frac{3}{16} \ln(4\mu) \right) \tag{B.2.55}$$

Units and scales: Let us mention here that, since this result was obtained in dimensionless units, the universal scale ℓ_σ appearing in the main text is here given by $\ell_\sigma = \frac{1}{m} \left(\frac{1}{S_m} \right)^{\frac{1}{d+\zeta}}$. S_m can always be measured as $S_m = \frac{\langle S^2 \rangle}{2\langle S \rangle}$ and is exactly given in terms of the parameters of the model by $S_m = \frac{\sigma}{m^4}$. As $m \rightarrow 0$, the dependence of σ on m is universal: $\sigma \sim m^{4-d-\zeta} \sigma^*$ with σ^* a dimensionless number. Thus $\ell_\sigma \simeq (\sigma^*)^{\frac{-1}{d+\zeta}}$. The number σ^* is non-universal and depends on the microscopic disorder. Thus the scale ℓ_σ is non-universal and depends on *microscopic* properties of the disorder. Note also that using (B.2.46) one can also study the dependence of the mean-shape when S gets close to the cutoff avalanche size S_m . This dependence is expected to be non-universal and in our model we find that the amplitude of the $O(\epsilon)$ corrections decrease as S increases close to S_m .

Small and large q expansion of the mean-shape in Fourier space

We now derive the result Eq.(B.1.10) of the letter. The small q expansion of $\delta \tilde{\mathcal{F}}_d(q)$ is obtained from (B.2.52) at any order. The first terms are:

$$\begin{aligned}
 \delta \tilde{\mathcal{F}}_d(q) &\simeq_{q \ll 1} \alpha \left(-\frac{1}{16} \sqrt{\pi} (-3\gamma_E + 1 + \log(4096)) q^2 + \frac{1}{240} (299 - 90\gamma_E) q^4 + \frac{\sqrt{\pi} \alpha (1890\gamma_E - 3121 - 5040 \log(2))}{13440} q^6 \right. \\
 &\quad \left. + \left(\frac{2299}{5040} - \frac{\gamma_E}{8} \right) q^8 + O(q^{10}) \right) \\
 &\simeq_{q \ll 1} \alpha \left(-0.840378 q^2 + 1.02938 q^4 - 0.728437 q^6 + 0.383999 q^8 + O(q^{10}) \right)
 \end{aligned} \tag{B.2.56}$$

For the large q expansion, the expansion at large q of $\delta \tilde{\mathcal{F}}_d(q)$ cannot be naively ILT. However, since we compute the ILT from μ to 1, one can derive the result with respect to μ an arbitrary number of times m to make the ILT convergent before taking the ILT since this just multiplies the end result by an innocent $(-1)^m$ factor). This leads to

$$\begin{aligned}
 \delta \tilde{\mathcal{F}}_d(q) &\simeq_{q \gg 1} \alpha \left(\frac{\frac{\gamma_E}{2} + 4 - 4 \log(q)}{q^4} - \frac{8\sqrt{\pi}}{q^6} + \frac{-48\gamma_E + 23 - 120 \log(q)}{q^8} + \frac{624\sqrt{\pi}}{q^{10}} + O\left(\frac{1}{q^{12}}\right) \right) \\
 &\simeq_{q \gg 1} \alpha \left(\frac{-4 \log(q) + 4.28861}{q^4} - \frac{14.1796}{q^6} + \frac{-120 \log(q) - 4.70635}{q^8} + \frac{1106.01}{q^{10}} + O\left(\frac{1}{q^{12}}\right) \right)
 \end{aligned} \tag{B.2.57}$$

And as explained in the main text, the first term of this expansion is interpreted as a modification of the power-law behavior of $\tilde{\mathcal{F}}_d(q)$, $\tilde{\mathcal{F}}_d(q) \simeq_{q \gg 1} 2(1 + (2 + \frac{\gamma_E}{4})\alpha)q^{-4-2\alpha} + O(\epsilon^2)$.

Dominant non-analyticity at small x

Let us now understand more precisely how the large q behavior of $\tilde{\mathcal{F}}_d(q)$ generates a non-analyticity in $\mathcal{F}_d(x)$ at small x . We consider the effect of a fat tail $q^{-2\beta}$ in a Fourier transform. We write

$$\begin{aligned} \int \frac{d^d q}{(2\pi)^d} \frac{e^{iq_1 x}}{q^{2\beta}} &= \frac{1}{\Gamma(\beta)} \int_{t>0} \frac{dt}{t} t^\beta \int \frac{d^d q}{(2\pi)^d} e^{iq_1 x - q^2 t} = |x|^{2\beta-d} \int dt \frac{2^{-d} \pi^{-\frac{d}{2}} e^{-\frac{1}{4t}} (t)^{\beta-\frac{d}{2}}}{t\Gamma(\beta)} \\ &\sim |x|^{2\beta-d} \frac{2^{-2\beta} \pi^{-\frac{d}{2}} \Gamma(\frac{d}{2} - \beta)}{\Gamma(\beta)} \end{aligned} \quad (\text{B.2.58})$$

The above derivation is formal since e.g. the first integral on q on the left-hand side of (B.2.58) do not converge but we notice that (B.2.58) indeed gives, for $\beta = 2$, the dominant non-analyticity in the expansion (B.2.28) (i.e. the $b_{p=0}$ term). The above calculation indicates that the leading non-analyticity present in the small x expansion of $\mathcal{F}_d(x)$ is a term of the form

$$\mathcal{F}_d^{sing}(x) \simeq 2(1 + (2 + \frac{\gamma_E}{4})\alpha) |x|^{4+2\alpha-d} \frac{2^{-4-2\alpha} \pi^{-d/2} \Gamma(d/2 - 2 - \alpha)}{\Gamma(2 + \alpha)} \quad (\text{B.2.59})$$

Expanding this result in α , it implies the existence of a term

$$\delta\mathcal{F}_d^{sing}(x) \simeq \frac{\alpha}{32} \pi^{-\frac{d}{2}} x^{4-d} \Gamma\left(\frac{d}{2} - 2\right) \left(-4\psi\left(\frac{d}{2} - 2\right) + 8\log(x) + 5\gamma_E + 4 - 8\log(2)\right) \quad (\text{B.2.60})$$

in the small x expansion of $\delta\mathcal{F}_d(x)$ ($\psi = \frac{\Gamma'}{\Gamma}$ is the diGamma function). For $d = 1, 3$ this result correctly gives the dominant non-analyticity in $\delta\mathcal{F}_d(x)$. For $d = 2$, one has to look at the expansion of (B.2.60) around $d = 2$. In doing so, one obtains terms (i) regular in x (proportional to x^2) that diverge as $d \rightarrow 2$: these terms are unimportant and would be cancelled by other regular terms present in $\delta\mathcal{F}_d(x)$, and (ii) a singular term which admit a well defined $d \rightarrow 2$ limit and read:

$$\delta\mathcal{F}_{d=2}^{sing}(x) \simeq \frac{\alpha}{16\pi} (9\gamma_E - 8\log(2) + 4\log(x)) x^2 \log(x). \quad (\text{B.2.61})$$

This term is the dominant non analyticity present in $\delta\mathcal{F}_{d=2}(x)$.

Large x expansion of the mean-shape in real space

We now obtain the modification of the large x behavior of $\mathcal{F}_d(x)$, and derive Eq.(B.1.11) of the letter. The mean shape in real space is obtained by Fourier transform and ILT from (i) the expressions $\tilde{\mathcal{F}}^{MF}(q)$ (B.2.51), $\delta\tilde{\mathcal{F}}_d(q)$ (B.2.52) and the definition of $H(q, \mu)$, (B.2.50), or, equivalently to lowest order in α , (ii) from the expressions (B.2.54, B.2.55). We use the latter here:

$$\mathcal{F}_d(x) = \int \frac{d^d q}{(2\pi)^d} e^{-iq_1 x} \int_{\mathcal{C}} \frac{d\mu}{2i\pi} e^{\mu} \left(\frac{2\sqrt{\pi}c}{q^2 + 2\sqrt{\mu} + \Sigma(q, \mu)} \right), \quad c = (1 + \alpha \frac{3\gamma_E - 2}{8}) \quad (\text{B.2.62})$$

where here the contour \mathcal{C} can be chosen as a wedge around the branch cut $\mu < 0$ of the integrand, such as e.g. $\mathcal{C} = (1 + e^{-\frac{3i\pi}{4}} \mathbb{R}_+) \cup (1 + e^{\frac{3i\pi}{4}} \mathbb{R}_+)$. To compute this radial Fourier transform, we chose $x > 0$ oriented along the first axis. The integration over the other components $q_2 \dots q_d$ depends only on $q = \sqrt{q_2^2 + \dots + q_d^2}$: the change of variable brings out a factor $S_{d-1} = \frac{2(\pi)^{\frac{d-1}{2}}}{\Gamma(\frac{d-1}{2})}$. Performing the rescaling $(q_1, q) \rightarrow \sqrt{2}(q_1, q)$ we obtain the more convenient form

$$\mathcal{F}_d(x/\sqrt{2}) = 2^{\frac{d}{2}} \sqrt{\pi} c \int_{-\infty}^{\infty} \frac{dq_1}{2\pi} \int_0^{\infty} \frac{dq S_{d-1}}{(2\pi)^{d-1}} q^{d-2} e^{-iq_1 x} \int_{\mathcal{C}} \frac{d\mu}{2i\pi} e^{\mu} \frac{1}{q_1^2 + q^2 + \sqrt{\mu} - \frac{\alpha}{2} h(\sqrt{2}\sqrt{q_1^2 + q^2}, \mu)} \quad (\text{B.2.63})$$

where we denote $\Sigma(q, \mu) = -\alpha h(q, \mu)$.

At the mean-field level, i.e. $\alpha = 0$, the integral on q_1 can be performed by closing the contour of integration in the upper half plane (the integrand is then analytic in q_1), and taking into account the contribution of the pole at $q_1(\mu) = i\sqrt{q^2 + \sqrt{\mu}}$. The scaling of this pole with μ , $q_1 \sim \mu^{\frac{1}{4}}$ notably leads to the stretched exponential decay of the shape at large x with exponent $4/3$. Here, at $O(\epsilon)$ we cannot a priori performs this residue calculation since the integrand is non analytic in q_1 . It seems however reasonable to assume that the behavior of $\mathcal{F}_d(x)$ at large $|x|$ will still be dominated by this pole in the integration on q_1 . At first order in $O(\epsilon)$ the position of this pole is shifted as

$$q_1(\mu) \simeq i \left(\sqrt{q^2 + \sqrt{\mu}} - \alpha \frac{\delta q(\mu)}{\sqrt{q^2 + \sqrt{\mu}}} \right), \quad \delta q(\mu) = \frac{1}{4} h(i\sqrt{2}\mu^{1/4}, \mu) = \frac{1}{72} \sqrt{\mu} (27\log(2\sqrt{\mu}) + 14\pi\sqrt{3} - 72) \quad (\text{B.2.64})$$

And for the saddle-point calculation of the integral on q_1 , we can approximate

$$\frac{1}{q_1^2 + q^2 + \sqrt{\mu} - \frac{\alpha}{2} h(\sqrt{2}\sqrt{q_1^2 + q^2}, \mu)} \simeq \frac{1}{(q_1 - q_1(\mu))(q_1 + q_1(\mu) - \frac{\alpha}{2} \Delta q(\mu))} \quad (\text{B.2.65})$$

With

$$\Delta q(\mu) = \sqrt{2}\sqrt{q^2 + \sqrt{\mu}}(\mu)^{-\frac{1}{4}} \partial_1 h(i\sqrt{2}\mu^{\frac{1}{4}}, \mu) = \frac{2i}{27} (13\sqrt{3}\pi - 63) \sqrt{q^2 + \sqrt{\mu}} \quad (\text{B.2.66})$$

| | $\epsilon = 0$ | $\epsilon = 1$ | $\epsilon = 2$ | $\epsilon = 3$ |
|---------------------------|----------------|----------------------|-------------------|-------------------|
| B at $O(\epsilon)$ | $-2/3$ | -0.298 ± 0.002 | 0 | 0.235 ± 0.014 |
| B conjecture | $-2/3$ | -0.2876 ± 0.0001 | 0 | 0.100 ± 0.002 |
| δ at $O(\epsilon)$ | $4/3$ | 1.410 ± 0.002 | 1.49 ± 0.01 | 1.58 ± 0.02 |
| δ conjecture | $4/3$ | 1.4246 ± 0.0002 | 1.570 ± 0.001 | 1.800 ± 0.004 |

Table B.1: Predicted values for the exponents B and δ from the $O(\epsilon)$ calculation, and from the conjecture (B.2.69) (the values are averaged over the two Pade, and the spread is indicated), and compared to the conjecture (B.2.69) using the value of ζ determined numerically in [240] ($\zeta = 0.355 \pm 0.001$ for $d = 3$ and $\zeta = 0.753 \pm 0.002$ for $d = 2$) and [241] ($\zeta = 1.250 \pm 0.005$ in $d = 1$).

(Through rescaling one shows that higher order terms in the series expansion of $h(\sqrt{2}\sqrt{q_1^2 + q^2}, \mu)$ around $q_1 = i\sqrt{q^2 + \sqrt{\mu}}$ do not contribute). Hence we have

$$\begin{aligned}
 \mathcal{F}_d(x/\sqrt{2}) &= c2^{d/2}\sqrt{\pi} \int \frac{d\mu}{2i\pi} e^{\mu} \int_0^{+\infty} \frac{S_{d-1}}{(2\pi)^{d-1}} q^{d-2} dq \frac{2i\pi}{2\pi} \frac{e^{-x\left(\sqrt{q^2+\sqrt{\mu}} - \frac{\alpha\delta q}{\sqrt{q^2+\sqrt{\mu}}}\right)}}{2q_1(\mu) - \frac{\alpha}{2}\Delta q(\mu)} \\
 &\simeq c2^{d/2-1}\sqrt{\pi} \frac{S_{d-1}}{(2\pi)^{d-1}} \int \frac{d\mu}{2i\pi} e^{\mu-x\left(\mu^{\frac{1}{4}} - \alpha\frac{\delta q}{\mu^{\frac{1}{4}}}\right)} \int_0^{+\infty} q^{d-2} \frac{1}{\left(1 - \frac{\alpha}{54}(13\sqrt{3}\pi - 63)\right)\mu^{\frac{1}{4}} - \alpha\frac{\delta q}{\mu^{\frac{1}{4}}}} e^{-x\frac{q^2(\delta q\alpha + \sqrt{\mu})}{2\mu^{3/4}}} \\
 &\simeq c\frac{\pi^{1-\frac{d}{2}}}{\sqrt{2}} \int \frac{d\mu}{2i\pi} e^{\mu-xa\mu^b} \frac{1}{a'\mu^b} \left(\frac{a\mu^b}{x}\right)^{\frac{d-1}{2}}
 \end{aligned} \tag{B.2.67}$$

Where we have used the fact that the dominant behavior of the integral on q is given by $q \simeq 0$, and we have introduced the notation

$$a = 1 + \frac{-14\sqrt{3}\pi + 72 - 9\log(8)}{72}\alpha, \quad b = \frac{1}{4} - \frac{3}{16}\alpha, \quad a' = 1 + \frac{468 - 94\pi\sqrt{3} - 81\log(2)}{216}\alpha \tag{B.2.68}$$

So that $a\mu^b = \mu^{\frac{1}{4}} - \alpha\frac{\delta q}{\mu^{\frac{1}{4}}} + O(\epsilon^2)$ and $a'\mu^b = \left(1 - \frac{\alpha}{54}(13\sqrt{3}\pi - 63)\right)\mu^{\frac{1}{4}} - \alpha\frac{\delta q}{\mu^{\frac{1}{4}}} + O(\alpha^2)$. Note that, using $\zeta = \frac{1}{3}\epsilon$ and $\alpha = -2\epsilon/9$, the $O(\epsilon)$ value of b is consistent with the conjecture $b = \frac{1}{d+\zeta}$ which is quite natural: the exponent b gives the scaling with μ of the pole $q_1(\mu) \sim \mu^b$. We know that momenta inside avalanches of sizes S scale with S as $S^{\frac{-1}{d+\zeta}}$. On the other hand, μ is conjugate to S : $\mu \sim S^{-1}$, hence the conjecture $q_1(\mu) \sim \mu^{\frac{1}{d+\zeta}}$. At large x , the integral on μ can now be evaluated using a saddle-point calculation. It leads to, at first order in ϵ ,

$$\begin{aligned}
 \mathcal{F}_d(x) &\simeq Ax^B e^{-Cx^\delta} \\
 A &= \frac{2^{-d/2}\pi^{\frac{1}{2}-\frac{d}{2}}}{\sqrt{3}} \left(1 + \frac{1}{216}\alpha \left(4\sqrt{3}\pi(27-7d) + 9(13d+9(\gamma_E-8))\right)\right) \\
 B &= -\frac{d-2}{2} \frac{1-2b}{1-b} = \frac{2-d}{3} \left(1 + \frac{1}{2}\alpha\right) \\
 C &= \frac{3}{4} + \alpha \frac{(36-7\sqrt{3}\pi)}{36}, \quad \delta = \frac{1}{1-b} = \frac{4}{3} - \frac{\alpha}{3}
 \end{aligned}$$

Following the conjecture on the value of b we can also conjecture

$$B = -\frac{(d-2)(d+\zeta-2)}{2(d+\zeta-1)}, \quad \delta = \frac{d+\zeta}{d+\zeta-1} \tag{B.2.69}$$

Setting $\alpha = 0$ in the above result, we retrieve the large x behavior of $\mathcal{F}_d^{\text{MF}}(x)$ using here a totally different route. Let us warn the reader that there is some uncertainty on the values of A and B since additional contributions could come from the branch cut in q_1 . The values of C and δ however should be correct. The resulting numerical values of the exponents B and δ are summarized in Table B.1.

Note that (B.2.69) can also be expanded in α and gives the prediction

$$\begin{aligned}
 \delta\mathcal{F}_d(x) \simeq_{x \gg 1} &\alpha \frac{2^{-\frac{d}{2}-3}\pi^{\frac{1}{2}-\frac{d}{2}} e^{-\frac{3}{4}x^{4/3}} x^{\frac{2}{3}-\frac{d}{3}}}{27\sqrt{3}} \left(2\pi\sqrt{3}(-14d+21x^{4/3}+54)\right. \\
 &\left.+ 9\left((-4d+6x^{4/3}+8)\log(x) + 13d-24(x^{4/3}+3) + 9\gamma\right)\right)
 \end{aligned} \tag{B.2.70}$$

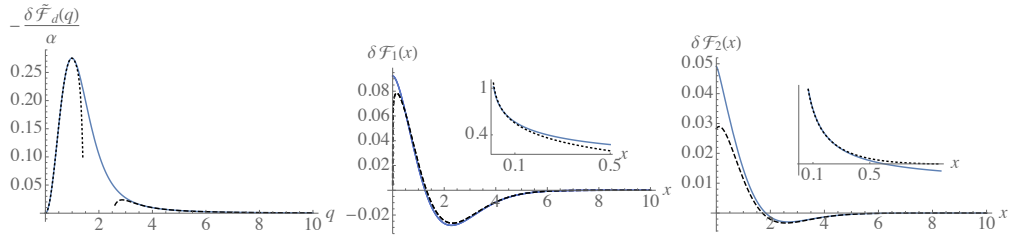


Figure B.6: In blue from left to right: $O(\epsilon)$ correction to the mean-shape in Fourier space divided by $-\alpha$, $-\frac{\delta\tilde{\mathcal{F}}_d(q)}{\alpha}$, in real space in $d = 1$, $\delta\mathcal{F}_1(x)$ and in $d = 2$, $\delta\mathcal{F}_2(x)$. The dotted line on the left is the theoretical small q expansion (B.2.56) up to $O(q^{20})$ and the dashed line is the large q expansion (B.2.57). The dashed line in the middle and on the right are the theoretical large x expansion (B.2.70). Middle inset: plot of $\frac{1}{x^3}(\delta\mathcal{F}_1(x) - \delta\mathcal{F}_1(0) - \frac{a_0}{2}x^2)$ (plain line), compared with the prediction (B.2.60) (dashed line). Right inset: plot of $-\frac{\delta\mathcal{F}_2(x) - \delta\mathcal{F}_2(0) + 0.06x^2}{x^2}$ (plain line), compared with the prediction (B.2.61) (dashed line).

Numerical obtention of the mean shape

We now explain how our analytical results are used to obtain numerically the mean shape computed at $O(\epsilon)$. In particular we explain how we obtain the theoretical curves presented in Fig. B.3 and Fig. B.4 of the letter. The correction $\delta\tilde{\mathcal{F}}_d(q)$ can easily be obtained numerically using a numerical integration on the formula (B.2.52) and choosing a contour of integration for μ as $\mathcal{C} = (1 + e^{-\frac{3i\pi}{4}}\mathbb{R}_+) \cup (1 + e^{\frac{3i\pi}{4}}\mathbb{R}_+)$. The precision of the numerical integration can be tested against the exact results at small and large q , (see Fig. B.6). It can easily be Fourier transformed in any dimension to find the correction $\delta\mathcal{F}_d(x)$:

$$\delta\mathcal{F}_{d=1}(x) = 2 \int_0^\infty \frac{dq}{2\pi} \cos(qx) \delta\tilde{\mathcal{F}}_d(q) \quad , \quad \delta\mathcal{F}_d(x) = \frac{1}{(2\pi)^{\frac{d}{2}} x^{\frac{d-2}{2}}} \int_0^\infty dq J_{\frac{d-2}{2}}(qx) q^{\frac{d}{2}} \delta\tilde{\mathcal{F}}_d(q) \quad (\text{B.2.71})$$

where $J_n(x)$ denotes the Bessel function of the first kind. The large x behavior of these corrections agrees with our prediction (B.2.70), to a surprisingly large extent (see Fig. B.6). Some properties of these corrections are their values at the origin $\delta\mathcal{F}_{d=1}(0) = 0.09227$, $\delta\mathcal{F}_{d=2}(0) = 0.04912$, the position where they cross 0, $x_0 = 1.2567$ ($d = 1$), $x_0 = 1.8286$ ($d = 2$), the position of their minimum and minimal value, $x_{min} = 2.2783$, $\mathcal{F}_1(x_{min}) = -0.02835$, $x_{min} = 2.6634$; $\mathcal{F}_2(x_{min}) = -0.002980$ ($d = 2$). We also investigate the presence of non-analyticities in the form of logarithm in the short-distance behavior of the result. In dimension 1, the correction $\delta\mathcal{F}_1(0)$ has a second derivative at 0 evaluated as $a_0 = \delta\mathcal{F}_1''(0) \simeq -0.512$. By plotting $\frac{1}{x^3}(\delta\mathcal{F}_1(x) - \delta\mathcal{F}_1(0) - \frac{a_0}{2}x^2)$, we shed the light on the non analyticity present in $\delta\mathcal{F}_1(x)$ at small x , which is found to be in very good agreement with (B.2.60) (see Fig. B.6). In dimension 2, the dominant non-analyticity predicted in (B.2.61) compares very well with the plot of $\frac{\delta\mathcal{F}_2(x) - \delta\mathcal{F}_2(0) + 0.06x^2}{x^2}$ at small x (the $0.06x^2$ term is a regular term which was not predicted by our calculations).

Adding naively these corrections to the mean-field result $\mathcal{F}_d(x) = \mathcal{F}_d^{\text{MF}}(x) + \delta\mathcal{F}_d(x)$ then gives a result which suffers from several problems. At large x it becomes slightly negative in $d = 1$ and does not have the right non-analytic behavior at small x . The second problem can be cured by considering the reexponentiated Fourier result

$$\tilde{\mathcal{F}}_d^{\text{reg}}(q) = \tilde{\mathcal{F}}_d^{\text{MF}}(q) \exp\left(\frac{\delta\tilde{\mathcal{F}}_d(q)}{\tilde{\mathcal{F}}_d^{\text{MF}}(q)}\right) \quad (\text{B.2.72})$$

This result is still correct to first order in ϵ and has the advantage of having the correct behavior at large q , $\tilde{\mathcal{F}}_d^{\text{reg}}(q) \simeq 2(1 + (2 + \frac{\gamma_E}{4})\alpha)q^{-4-2\alpha} + O(\epsilon^2)$. It is plotted in plain red in Fig. B.7. Taking the Fourier transform of this result we obtain a function $\mathcal{F}_d^{\text{reg1}}(x)$ which has now the correct behavior at small x but is still slightly negative at large x . On the other hand the function

$$\mathcal{F}_d^{\text{reg2}}(x) = \frac{1}{\mathcal{N}} \exp\left(-\exp\left(\log(-\log(\mathcal{F}_d^{\text{MF}}(x))) + \frac{\delta\mathcal{F}_d(x)}{\mathcal{F}_d^{\text{MF}}(x) \log(\mathcal{F}_d^{\text{MF}}(x))}\right)\right) \quad (\text{B.2.73})$$

where \mathcal{N} is a normalization constant ensuring that $\int d^d x \mathcal{F}_d^{\text{reg2}}(x) = 1$, is correct to $O(\epsilon)$ and takes properly into account the change of exponent in the exponential decay of the shape at $x = \infty$ and is everywhere positive. However, it doesn't have the correct behavior at small x . Since $\mathcal{F}_d^{\text{reg1}}(x)$ and $\mathcal{F}_d^{\text{reg2}}(x)$ intersect themselves at some x_c , we construct the function

$$\mathcal{F}_d^{\text{reg}}(x) = \frac{1}{\mathcal{N}} (r(x)\mathcal{F}_d^{\text{reg1}}(x) + (1 - r(x))\mathcal{F}_d^{\text{reg2}}(x)) \quad (\text{B.2.74})$$

where \mathcal{N} is a normalization factor and $r(x)$ is a function that interpolates smoothly between $r(1) = 1$ and $r(\infty) = 0$ sufficiently fast to obtain a positive result everywhere. Here we have chosen $r(x) = e^{-x^2/xc^2}$ but this choice does not matter drastically since all these functions are close to each others (see Fig. B.7). The result (B.2.74) is still correct to $O(\epsilon)$ and

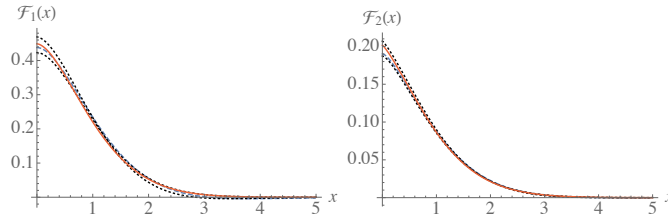


Figure B.7: Different mean shape $\mathcal{F}_d(x)$ correct at $O(\epsilon)$ for $d = 1$ (left) and $d = 2$ (right). Dashed-blue lines: naive result $\mathcal{F}_d(x) = \mathcal{F}_d^{\text{MF}}(x) + \delta\mathcal{F}_d(x)$. Dotted lines: $\mathcal{F}_d^{\text{reg1}}(x)$ (largest at the origin) and $\mathcal{F}_d^{\text{reg2}}(x)$ (smallest at the origin). Red line: regularized result $\mathcal{F}_d^{\text{reg}}(x)$ used for comparison with numerics.

has the right behavior at small and large x . It is plotted for $d = 1$ and $d = 2$ in plain red in (B.7) and used for comparison to numerical simulations.

Universal ratios

Here we compute the universal ratios in dimension 1 and 2 of the various mean-shapes. These are defined as $c_p = \frac{\int d^d x |x|^{2p} \mathcal{F}_d(x)}{(\int d^d x |x|^p \mathcal{F}_d(x))^2}$. In dimension 1 and for p even they are exactly obtained as $c_p = \frac{\bar{\mathcal{F}}_d^{(2p)}(0)}{(\bar{\mathcal{F}}_d^{(p)}(0))^2}$. For p odd and in dimension $d = 2$ one has to rely on direct numerical integration techniques. Fortunately, the exponential decay of the shape at large x (which is known analytically) allows us to obtain an excellent numerical precision, we compute them perturbatively in $O(\epsilon)$ using

$$c_p \simeq \frac{\int d^d x |x|^{2p} \mathcal{F}_d^{\text{MF}}(x)}{(\int d^d x |x|^p \mathcal{F}_d^{\text{MF}}(x))^2} + \alpha \left(\frac{\int d^d x |x|^{2p} \delta\mathcal{F}_d(x)}{(\int d^d x |x|^p \mathcal{F}_d^{\text{MF}}(x))^2} - 2 \frac{\int d^d x |x|^{2p} \mathcal{F}_d^{\text{MF}}(x) \int d^d x |x|^p \delta\mathcal{F}_d(x)}{(\int d^d x |x|^p \mathcal{F}_d^{\text{MF}}(x))^3} \right) \quad (\text{B.2.75})$$

Table B.2 contains our results in $d = 1$ and $d = 2$. The even values in $d = 1$ are exact for both the BFM and (to $O(\epsilon)$) the SR case. The odd values are results of numerical integration. The uncertainty on the numerical integration is evaluated in $d = 1$ by comparing the result obtained using numerical integrations for even ratios to the exact ones. The values in $d = 2$ are results of numerical integrations. We also give for reference in Table B.2 the value of the universal ratios for a Gaussian shape function ($\mathcal{F}_{d=1}^{\text{Gauss}}(x) = \frac{e^{-x^2}}{\sqrt{\pi}}$ and $\mathcal{F}_{d=2}^{\text{Gauss}}(x) = \frac{e^{-x^2}}{\pi}$)

Details on numerical simulations

We now give details on the numerical simulations leading to the results presented in Fig. B.4 and Fig. B.5 in the letter.

Parameters of the simulations

For our simulations we have used $\sigma = 1$ and $dt = 0.02$. The discretization in time is handled using an algorithm similar to the one presented in [231]. The used values of δw and number of simulated kicks n_{kicks} are: $\delta w = 0.1$ and $n_{kicks} = 40 \times 10^6$ for the SR model; $\delta w = 1$ and $n_{kicks} = 100 \times 10^6$ for the BFM model. As discussed in the main text, these simulations are performed in $d = 1$ for a line of size $L = 2048$ discretized with $N = L$ points. For the SR model, δu is chosen as $\delta u = 5\delta w$.

PDF of avalanche sizes and measurement of S_m

The measurement of the PDF $P(S)$ (plotted in Fig. B.8) shows that the avalanche size distribution of both models have a lower cutoff $S_{\delta w} \simeq \frac{(L\delta w)^2}{S_m^{\text{BFM}}}$ where S_m^{BFM} is always given by σ/m^4 . In the BFM model, we observe a scaling regime $P(S) \sim S^{-\tau_S^{\text{BFM}}}$ with $\tau_S^{\text{BFM}} = 3/2 = 2 - \frac{d}{d+\zeta^{\text{BFM}}}$ ($\zeta^{\text{BFM}} = 4 - d$) for $S_{\delta w} \ll S \ll S_m^{\text{BFM}}$. In the SR model, for $S_{\delta w} \leq S \leq S_{\delta u} = S_{\delta u} \simeq (\delta u) \frac{d+\zeta^{\text{BFM}}}{\zeta^{\text{BFM}}}$, the interface does not feel the short-ranged nature of the disorder and we observe a first scaling regime coherent with the BFM, $P(S) \sim S^{-\tau_S^{\text{BFM}}}$. In the SR model, S_m^{SR} is measured as $\langle S^2 \rangle / (2\langle S \rangle)$ with the result $S_m^{\text{SR}} = (1.40 \pm 0.05) \times 10^5$ (statistical uncertainty given with 3 sigma estimation). For $S_{\delta u} \ll S \ll S_m^{\text{SR}}$, we observe a second scaling regime coherent with the known features of the SR fixed point: $P(S) \sim S^{-\tau_S^{\text{SR}}}$ with $\tau_S^{\text{SR}} = 2 - \frac{d}{d+\zeta^{\text{SR}}}$ and our data are consistent with the value of ζ numerically estimated in [241], $\zeta^{\text{SR}} \simeq 1.250 \pm 0.005$ (see Fig. B.8). These measurements allows us to identify the desired scaling regime and compare our simulations with known features of the BFM and SR fixed point.

Details on the search for the seed

Let us now make a few comments on some subtle points and emphasize the importance of the algorithm used in the main text to retrieve the seed of each avalanche. When we apply a uniform kick of size δw to the system, the interface always moves from a small amount. As seen above and in Fig. B.8, avalanches of size much smaller than $S_{\delta w}$ are very unlikely (note that the discretization procedure introduces another sharp, artificial, small scale cutoff on the avalanches size: since each points moves at least during the first iteration of the algorithm with velocity $m^2\delta w/\eta$, the avalanche cannot be smaller than $L^d dt m^2 \delta w/\eta$). After the first iteration, it is actually highly probable that several points along the interface are still moving, each of them being the seed of an avalanche. With a high probability, these small avalanches have sizes of order $S_{\delta w}$ and quickly perish, hence we do not analyze their shapes (they are 'microscopic avalanches'). In the following we

| | c_1 | c_2 | c_3 | c_4 | c_5 | c_6 |
|----------------------|--|---|---|--|--|--|
| Gaussian $d = 1$ | 1.5708 | 3 | 5.8905 | 11.67 | 29.1938 | 46.2 |
| BFM $d = 1$: Theory | 1.6944 | 3.8197 | 9.2703 | 23.3333 | 60.045 | 156.863 |
| SR $d = 1$: Theory | 1.6944 +0.0798 α $\simeq 1.641$ ± 0.001 | 3.8197 +0.6196 α $\simeq 3.43$ ± 0.02 | 9.2703 +2.8 α $\simeq 7.53$ ± 0.16 | 23.3333 +11.4444 α $\simeq 16.6$ ± 0.9 | 60.045 +37 α $\simeq 38.5$ ± 3.7 | 156.863 +138.296 α $\simeq 81$ ± 17 |
| Gaussian $d = 2$ | 1.27324 | 2 | 3.3953 | 6 | 10.865 | 20 |
| BFM $d = 2$: Theory | 1.3734 | 2.5464 | 5.3435 | 12 | 28.1289 | 67.9111 |
| SR $d = 2$: Theory | 1.3734 +0.06482 α $\simeq 1.3449$ ± 0.0002 | 2.5464 +0.4110 α $\simeq 2.369$ ± 0.006 | 5.3435 +1.6647 α $\simeq 4.65$ ± 0.05 | 12 +5.7758 α $\simeq 9.6$ ± 0.2 | 28.1289 +18.6579 α $\simeq 20.8$ ± 0.9 | 67.9111 +58.0856 α $\simeq 45.7$ ± 3.6 |

Table B.2: Prediction for the universal ratios in dimension 1 ($\epsilon = 3$) and 2 ($\epsilon = 2$). Here $\alpha = -2\epsilon/9$. The values displayed are the average over the two Pade and their spread is indicated (as an indication of the uncertainty).

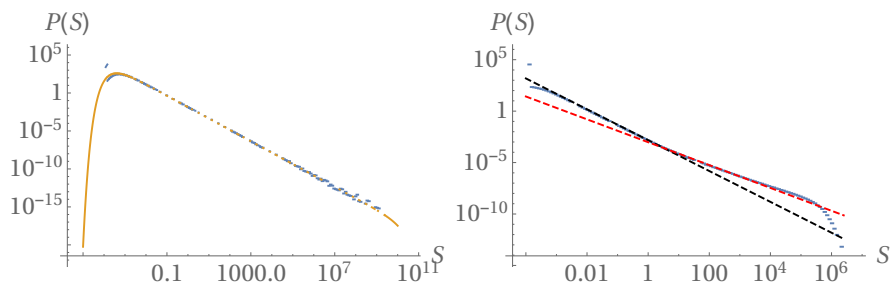


Figure B.8: Blue: Measurement of the avalanche size distribution in the BFM model (left) and the SR model (right). Yellow curve on the left: theoretical prediction for $P(S) = p^{\text{MF}}(S)$ (no scaling parameter). The excess of small avalanches is an artifact due to the discretization and does not affect the statistics of larger avalanches. Black dashed line on the right: power-law $S^{-\tau_S^{\text{BFM}}}$ with $\tau_S^{\text{BFM}} = 3/2$. Red dashed line on the right: power-law $S^{-\tau_S^{\text{SR}}}$ with $\tau_S^{\text{SR}} \simeq 2 - \frac{2}{1+1.250} \simeq 1.11$.

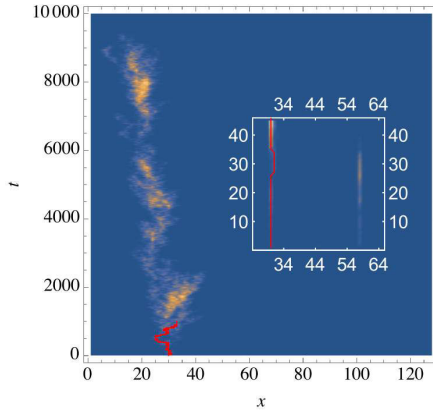


Figure B.9: Density plot of the velocity field $v(x, t)$ inside an avalanche of size $S = 1760$ in the mean-field model (BFM) for $d = 1$ discretized with $N = 128$ points. Line in red: backward path produced by the algorithm to find the seed of the avalanche. The inset illustrates the efficiency of the algorithm to identify, from the set of moving points of the interface just after the kick, the true seed of the observed macroscopic avalanche. In this avalanche (at least) two points (at $x = 32$ and $x = 57$) still moves at $t = 2dt$, but only the point at $x = 32$ is inside the cluster of moving points of the macroscopic avalanche and can be its seed.

are only interested in the shape of avalanches of total size $S > 1 \gg S_{\delta w}$ ('macroscopic avalanches'), which only occur with a small probability. When such an avalanche occurs, since there is a large separation of scales with the small avalanches of order $S_{\delta w}$, we expect its shape to be only very weakly perturbed by the fact that other small avalanches could have been triggered after the kick. We neglect the small probability that more than one macroscopic avalanche have been triggered by the kick. A crucial step is to unambiguously identify, from the set of points still moving during the second iteration of the algorithm, which one is the true seed of the observed macroscopic avalanche. This is what is accomplished by the algorithm explained in the text: after n_t iterations of the algorithm, all the small avalanches triggered at the beginning of the avalanche have already stopped (thus in general n_t has to be chosen sufficiently large). Identifying the maximum velocity inside the avalanche at time n_t , we are sure to have identified a point which is inside the macroscopic avalanche. The algorithm is then devised to run within the history of the avalanche backward in time and always identify a point moving along the interface *which is in the correct cluster of moving points defining the macroscopic avalanche*. This is illustrated in Fig. B.9

Measurement of the mean-shape

We always only measure mean-shape with values of S well inside the desired scaling regime. The binning on the values of the total size S is of 0.05, we construct a grid of total sizes with the values $S_i = 1 \times \left(\frac{1.05}{0.95}\right)^{i-1}$ and avalanches with total size S such that $0.95S_i < S < 1.05S_i$ are rescaled as $S \rightarrow S_i$. The difference between S_m^{SR} and S_m^{BFM} and τ_S^{SR} and τ_S^{BFM} explains the difference between the chosen values of δw and n_{kicks} for each model: these parameters are adjusted so as to give a comparable numerical precision for the measurement of the mean-shape of interest (i.e. large avalanches which provide a good spatial precision - for the same δw , one observes more large avalanches in the SR model than in the BFM model). The shapes are rescaled onto one another using the value of ζ given above and determined numerically in [241]. The fact that they collapse (see Fig. B.4) using this value is another check that our simulations are correct since they appear in agreement with the high-precision simulations performed in [241]. Let us also present here the results analogous to Fig. B.4 in Fourier space: see Fig. B.10.

Measurement of the non-analyticity at small x and fat tail at large q

To measure these observables with a good precision in $d = 1$, we use the models discretized using 2048 points. We first obtain a smooth numerical mean-shape for the BFM and SR model by taking the average of several mean-shapes obtained for various sizes (taken large to obtain a good spatial precision: for the BFM we use 20 shapes with $13575 < S < 100478$, for the SR model we use 10 shapes with $7386 < S < 20095$). The resulting shapes are shown on the left of Fig. B.11. We also plot in Fig. B.12 the difference between the mean shape measured in our numerical simulations of the SR model and the theoretical mean-field result in $d = 1$ and compare it with our theoretical $O(\epsilon)$ predictions. This notably highlights the efficiency of the reexponentiation procedure discussed previously. We then directly study the small x behavior of these shapes, leading to the results presented on the left of Fig. B.5. The study of the large q behavior is more tedious: at large x the mean shapes we obtained start to be dominated by the noise present in our numerical results. This noise blurs the analysis of the large frequency content of the mean-shape. We thus first smooth our results at large x result by using an exponential fit e^{-Cx^δ} with the theoretical value of δ previously obtained exactly for the BFM and using our conjecture (B.2.69) for the SR model (see Table B.1). This fitting procedure is illustrated in Fig. B.11. By Fourier transform, we then obtain the results presented on the right of Fig. B.5.

Measurement of the universal ratios

Here we describe the protocol used to measure the universal ratios. We measure the universal ratios defined in (B.2.75)

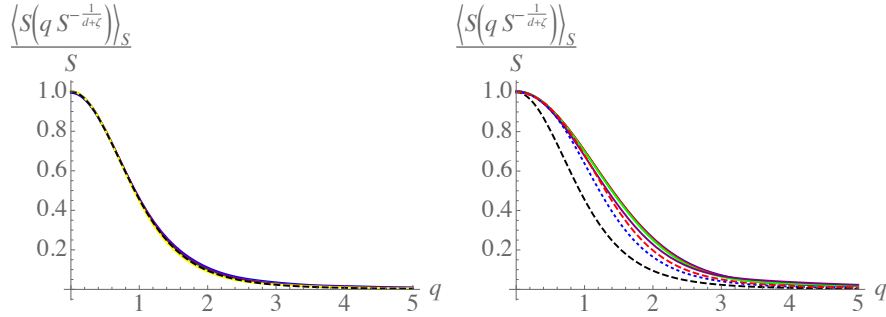


Figure B.10: The mean shape in Fourier space measured in simulations (left: BFM and right: SR), (plain lines, same color code as Fig. B.4) and compared to the theoretical predictions (dashed-black: BFM result, dotted-blue: naive $O(\epsilon)$ result and dashed-red: improved $O(\epsilon)$ result (B.2.72).

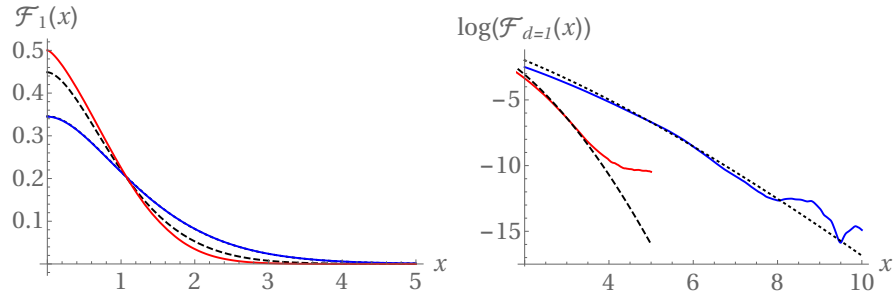


Figure B.11: Left: mean shapes obtained in the simulations of the SR model (red) and of the BFM model (blue) compared with the $O(\epsilon)$ result (dashed, black) and BFM result (dotted black). Right: blue (resp. red) large x behavior of the mean shape measured in the BFM model (resp. SR model). To avoid the noise present at large x to dominate the large q behavior of the mean shape, we smooth our result at large x using an exponential ansatz as explained below.

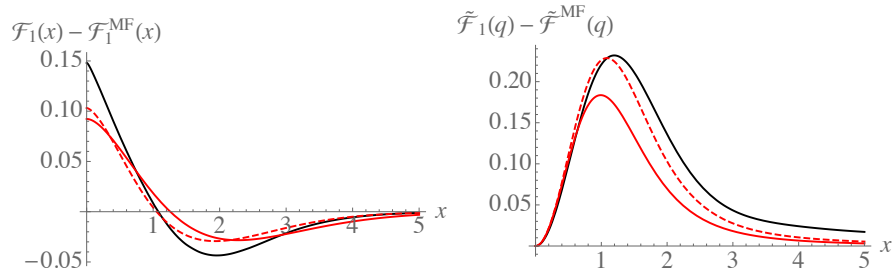


Figure B.12: Left: (resp. Right:) Black line: Difference between the mean shape measured in the numerical simulations of the SR model in real space $\mathcal{F}_1(x)$ (resp. in Fourier space $\tilde{\mathcal{F}}_1(q)$) and the theoretical mean field result $\mathcal{F}_1^{\text{MF}}(x)$ (B.2.30) (resp. $\tilde{\mathcal{F}}_1^{\text{MF}}(q)$ (B.1.5)). Red line: theoretical $O(\epsilon)$ result $\delta\mathcal{F}_1(x)$ (B.2.71) (resp. $\delta\tilde{\mathcal{F}}_1(q)$ (B.2.52)). Red-dashed line: improved (through the reexponentiation procedure) theoretical $O(\epsilon)$ result $\mathcal{F}_1^{\text{reg}}(x) - \mathcal{F}_1^{\text{MF}}(x)$ (B.2.74) (resp. $\tilde{\mathcal{F}}_1^{\text{reg}}(q) - \tilde{\mathcal{F}}_1^{\text{MF}}(q)$ (B.2.72)). The reexponentiation procedure chosen in Fourier space sensibly improves the accuracy of the result. Nevertheless, higher loop corrections will be necessary to account for the remaining difference.

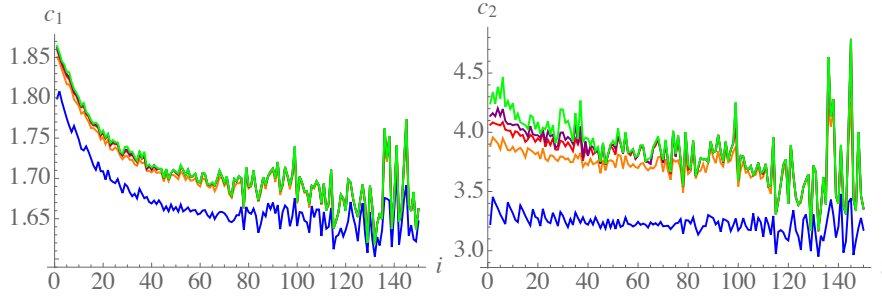


Figure B.13: Universal ratios $c_1(\ell_{cut})$ (left) and $c_2(\ell_{cut})$ (right) measured in the BFM for various cutoff length $\ell_{cut} = 4, 6, 8, 10, 12$ (Blue, Orange, Red, Purple and Green) as a function of the total sizes $S = S_i = 1 \times (\frac{1.05}{0.95})^{i-1}$. For the BFM, as a consequence of these plots, the results presented in Table B.3 are averages on the universal ratios obtained for $S > S_i$ with $i = 60$ and $\ell_{cut} = 8$ to obtain a result that do not depend on ℓ_{cut} and is free of discretization artifacts as explained in the text. A similar procedure is used for the SR model. Note that the important variations observed here for large i are just a consequence of the fact that only a few avalanches with the largest S_i have been measured, hence the statistical uncertainty on the measurements of $c_i(\ell_{cut})$ increases when S_i increases.

using several cutoff length ℓ_{cut} for the integral on x (i.e. we consider different approximations of the universal ratios

$$c_j(\ell_{cut}) = \frac{\int_{-\ell_{cut}}^{\ell_{cut}} dx |x|^{2j} \mathcal{F}_1(x)}{\left(\int_{-\ell_{cut}}^{\ell_{cut}} dx |x|^j \mathcal{F}_1(x) \right)^2}$$

that should converge to the true universal ratios c_j as $\ell_{cut} \rightarrow \infty$). These are measured

on the mean-shape $\mathcal{F}_1(x)$ numerically obtained for each possible total size S_i (see above for the definition of the binning procedure). Using these measurements we make sure that ℓ_{cut} is chosen large enough so that the results are not sensitive to its finite value. We also control discretization artifacts by studying the dependence of the measured universal ratios $c_j(\ell_{cut})$ on the total size S_i : for small S_i , the avalanches extend only over a few sites and the mean shape deduced from them is different from the one of the continuum theory, a difference that is seen in the universal ratios. For large enough S_i , the universal ratios become size independent and we reach the continuum regime. This is illustrated for the two first universal ratios in the BFM model in Fig. B.13. In the end, the universal ratios are measured by performing an average over various, large enough total sizes S_i , leading to the values presented in Table B.3.

| | c_1 | c_2 | c_3 | c_4 | c_5 | c_6 |
|------------------------|-------------------------------|-----------------------------|-----------------------------|----------------------------|----------------------------|-------------------------|
| BFM $d = 1$: Theory | 1.694 | 3.819 | 9.270 | 23.334 | 59.255 | 156.863 |
| SR $d = 1$: Theory | $\simeq 1.641$ ± 0.001 | $\simeq 3.43$ ± 0.02 | $\simeq 7.53$ ± 0.16 | $\simeq 16.6$ ± 0.9 | $\simeq 38.5$ ± 3.7 | $\simeq 81$ ± 17 |
| BFM $d = 1$: Numerics | 1.699 ± 0.003 | 3.83 ± 0.05 | 9.3 ± 0.3 | 23 ± 7 | 59 ± 26 | 143 ± 41 |
| SR $d = 1$: Numerics | 1.612 ± 0.004 | 3.16 ± 0.03 | 6.4 ± 0.3 | 13.6 ± 0.2 | 27 ± 2 | 57 ± 9 |

Table B.3: Universal ratios in dimension 1. First two lines: theoretical result for the BFM and $O(\epsilon)$ theoretical result for the SR universality class. Last two lines: numerical measurement in the simulations of the BFM and SR model. Error-bars for the numerics are 3-sigma estimates. Note that the statistical uncertainty on the numerical measurements of the universal ratios c_j increases with j since these quantities become more and more sensitive to the presence of noise in the large x tail of the measured shapes of avalanches.

Appendix C

Paper: Universal correlations between shocks in the ground state of elastic interfaces in disordered media

The following is essentially the article published as

Title: Universal correlations between shocks in the ground state of elastic interfaces in disordered media

Authors: Thimothée Thiery, Pierre Le Doussal and Kay Jörg Wiese

ArXiv: 1604.05556

Journal-Ref: Phys. Rev. E **94**, 2016

Abstract: The ground state of an elastic interface in a disordered medium undergoes collective jumps upon variation of external parameters. These mesoscopic jumps are called shocks, or static avalanches. Submitting the interface to a parabolic potential centered at w , we study the avalanches which occur as w is varied. We are interested in the correlations between the avalanche sizes S_1 and S_2 occurring at positions w_1 and w_2 . Using the Functional Renormalization Group (FRG), we show that correlations exist for realistic interface models below their upper critical dimension. Notably, the connected moment $\langle S_1 S_2 \rangle^c$ is up to a prefactor *exactly* the renormalized disorder correlator, itself a function of $|w_2 - w_1|$. The latter is the universal function at the center of the FRG; hence correlations between shocks are universal as well. All moments and the full joint probability distribution are computed to first non-trivial order in an ϵ -expansion below the upper critical dimension. To quantify the local nature of the coupling between avalanches, we calculate the correlations of their local jumps. We finally test our predictions against simulations of a particle in random-bond and random-force disorder, with surprisingly good agreement.

C.1 Introduction

The model of an elastic interface in a disordered medium has been put forward as a relevant description for a large number of systems [63, 235, 236, 68]. Examples include domain walls in soft magnets [100, 45], fluid contact lines on a rough surface [59, 61], strike-slip faults in geophysics [64, 66], fracture in brittle materials [52, 56, 51] or imbibition fronts [69]. An important common property of these systems is that their response to an applied field is not smooth but rather proceeds via jumps extending over a broad range of space and time scales. As a consequence, understanding the properties and the universality of avalanche processes has received a lot of attention in the past years [81, 112, 145].

A problem of outstanding interest is to quantify the correlations between successive avalanches. In the context of earthquakes those are linked to the notion of *aftershocks*, whose statistics is characterized through phenomenological laws such as the Omori law [67]. Several mechanisms have been advanced to explain these strong correlations, all involving an additional dynamical variable [146, 147]. For elastic interfaces, correlations between avalanches were yet only studied as a result of such additional degrees of freedom in the interface dynamics, as relaxation processes [148, 149] or memory effects [144]. In this work, we show that even in the absence of such mechanisms, *avalanches in elastic interfaces are generically correlated below their upper critical dimension*. These correlations are universal.

Let us emphasize that the goal of this paper is *not* to understand or explain the aftershock statistics observed in earthquakes, for which additional mechanisms such as those discussed above are necessary. Rather, it is to emphasize that for disordered elastic systems, *except for mean-field models, correlations between avalanches always exist*. A precise quantitative understanding of these correlations is necessary to correctly quantify correlations induced by additional mechanisms. In systems where the description by the standard elastic-interface model is accurate (without additional mechanisms) our results quantify the correlations between avalanches. To our knowledge, these correlations have up to now been ignored in theoretical or experimental work. It would thus be interesting to quantify them better, in order to access universality, or lack thereof, in various avalanche processes.

In this article we study the correlations between the sizes and locations of shocks in the ground state (also called “static avalanches”) of elastic interfaces in disordered media. These static avalanches are close cousins of the (dynamic) avalanches observed in the interface dynamics at depinning. As we discuss below, we expect most of our results to hold

for both classes. Our study is conducted using the Functional Renormalization Group (FRG). Originally introduced as a powerful tool to study the universal properties of the statics and dynamics (at the depinning transition) of elastic interfaces in disordered media [114, 127, 126, 108, 116, 129, 117], the FRG has been recently adapted to the study of avalanches [109, 111, 101, 107, 1, 110]. It has notably led to a rigorous identification of the relevant mean-field theory for the statistics of single avalanches: the Brownian-Force Model (BFM), a multidimensional generalization of the celebrated Alessandro-Beatrice-Bertotti-Montorsi (ABBM) model [98, 99]. Interestingly, the FRG allows to go beyond mean-field theory and to compute in a controlled way avalanche observables in an expansion in $\epsilon = d_{uc} - d$ where d is the interface dimension, and d_{uc} the upper critical dimension of the problem. The latter depends on the range of the elastic interactions, with $d_{uc} = 4$ for short-ranged (SR) elasticity and $d_{uc} = 2$ for the usual long-ranged (LR) elasticity.

The outline of this article is as follows: In section C.2 we summarize our results, preceded by a definition of the relevant observables. In Section C.3 we introduce the model and the observables we are interested in. Section C.4 contains the derivation of the main results presented above. Section C.5 gives an analysis of the correlations between the local shock sizes. Section C.6 presents the results of our numerical analysis of these correlations for a toy model with a single degree of freedom, i.e. $d = 0$. Finally, a series of appendices contains technical derivations.

C.2 Main results

Let us now state our main results. To this aim, we parameterize the position of the interface by the (real, one-component) displacement field $u(x)$, where $x \in \mathbb{R}^d$ is the internal coordinate of the interface. For notational convenience we denote $u(x) \equiv u_x$. The interface is submitted to a quenched random potential $V(u_x, x)$, and to an external parabolic confining field $\frac{m^2}{2}(u_x - w)^2$ centered at w . In a given disorder realization V , upon variation of the external field w , the ground state (i.e. lowest-energy) configuration of the interface, denoted $u_x(w)$, changes discontinuously at a set of discrete locations w_i , according to

$$u_x(w_i^-) \rightarrow u_x(w_i^+) = u_x(w_i^-) + S_x^{(i)}. \quad (\text{C.2.1})$$

The event $(w_i, S_x^{(i)})$ is the i^{th} shock of the interface, w_i is the location of the shock, $S_x^{(i)}$ is its local size at x and $S^{(i)} = \int d^d x S_x^{(i)}$ its total size. The statistical properties associated to one shock were thoroughly analyzed using FRG in [109, 111]. Such properties are encoded in the *shock density* ρ_0 , defined as

$$\rho_0 := \overline{\sum_i \delta(w - w_i)}, \quad (\text{C.2.2})$$

and in the *avalanche-size density*

$$\rho(S) := \overline{\sum_i \delta(w - w_i) \delta(S - S^{(i)})}. \quad (\text{C.2.3})$$

The *shock-size density* $\rho(S)$ is linked to ρ_0 through $\rho_0 = \int dS \rho(S)$. Note that these quantities do not depend on w due to the statistical translational invariance (STS) of the disorder. Considering two points $w < w'$ and sizes $S_1 < S_2$, $\int_w^{w'} d\tilde{w} \int_{S_1}^{S_2} dS \rho(S)$ is the mean number of shocks occurring between w and w' with size $S \in [S_1, S_2]$, while $(w' - w)\rho_0$ is the mean number of shocks (irrespective of their size). Note that throughout the rest of this section we will discuss our results in terms of densities but they can be translated into results for normalized probabilities as we discuss in Sec. C.3.5.

These observables alone do not determine the statistical properties of the sequence $\{(w_i, S^{(i)})\}_{i \in \mathbb{Z}}$ of shocks experienced by the interface in a given environment. In particular, they do not contain any information about the correlations between the shocks. For a given distance $W > 0$, let us therefore introduce the *two-shock density at distance W* ,

$$\rho_2(W) := \overline{\sum_{i \neq j} \delta(w - w_i) \delta(w + W - w_j)}. \quad (\text{C.2.4})$$

This observable scales as *the square of a density*. Thus $\int_{w_1}^{w'_1} dw \int_{w_2}^{w'_2} dw' \rho_2(w' - w)$ counts *the mean number of pairs of shocks* such that the first shock occurs between w_1 and w'_1 , and the second one between w_2 and w'_2 . Equivalently, $\tilde{\rho}_2(W) := \frac{\rho_2(W)}{\rho_0^2}$ is the density of shocks at a distance W from a given shock. These observables contain information about the correlations between shocks. Indeed an uncorrelated sequence of shocks implies $\rho_2(W) = \rho_0^2$ (and thus $\tilde{\rho}_2(W) = \rho_0$). A central question addressed in this work is whether the presence of a shock at a given point decreases ($\rho_2(W) < \rho_0^2$) or increases ($\rho_2(W) > \rho_0^2$) the density of shocks at a distance W .

To measure the correlations between the size of the shocks (and not only their positions) we introduce the *two-shock size density at distance W* ,

$$\rho_W(S_1, S_2) := \overline{\sum_{i \neq j} \delta(w - w_i) \delta(S_1 - S^{(i)}) \delta(w + W - w_j) \delta(S_2 - S^{(j)})}. \quad (\text{C.2.5})$$

It is linked to $\rho_2(W)$ via

$$\rho_2(W) = \int dS_1 dS_2 \rho_W(S_1, S_2). \quad (\text{C.2.6})$$

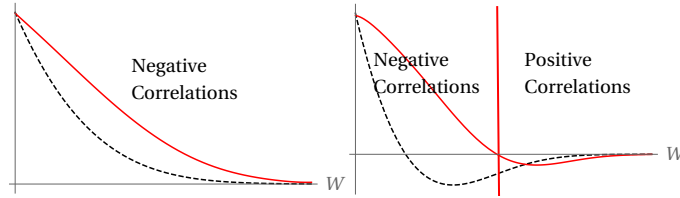


Figure C.1: Cartoons of the typical shape of the renormalized disorder correlator $\Delta(W)$ (black-dashed line) and of its second order derivative $\Delta''(W)$ (red line) for the Random-Field (left) and Random-Bond (right) universality classes (not to scale). Our results predict that the shock sizes are always negatively correlated in the Random-Field universality class, whereas the Random-Bond universality class exhibits a richer structure with negatively (resp. positively) correlated shock sizes at small (resp. large) distances.

Here $\int_{w_1}^{w'_1} dw \int_{w_2}^{w'_2} dw' \int_{S_1}^{S'_1} dS \int_{S_2}^{S'_2} dS' \rho_{w'-w}(S, S')$ counts the mean number of pairs of shocks such that the first shock occurred between w_1 and w'_1 , and the second between w_2 and w'_2 , with sizes between S_1 and S'_1 , resp. S_2 and S'_2 . For this observable, an absence of correlations in the sequence of shocks implies $\rho_W(S_1, S_2) = \rho(S_1)\rho(S_2)$. To investigate the presence of correlations we thus study the *connected two-shock size density* $\rho_W^c(S_1, S_2)$, defined as

$$\rho_W^c(S_1, S_2) := \rho_W(S_1, S_2) - \rho(S_1)\rho(S_2) . \quad (\text{C.2.7})$$

At the level of mean-field theory, i.e. in the BFM model, it is known [111, 1] that the shocks are independent and the process $w \rightarrow u_x(w)$ is a Levy jump process. As a consequence, $\rho_W^c(S_1, S_2) = 0$. On the other hand, for realistic interface models below their upper critical dimension, the shocks are correlated, demanding to go beyond the BFM. This can be seen from the second moment for which we show below the *exact* relation

$$\frac{\langle S_1 S_2 \rangle_{\rho_W^c}}{[\langle S \rangle_\rho]^2} = -\frac{\Delta''(W)}{L^d m^4} . \quad (\text{C.2.8})$$

On the left-hand-side, $\langle \dots \rangle_{\rho_W^c}$ denotes the average with respect to ρ_W^c as defined in Eq. (C.2.7). On the right-hand-side, L is the lateral extension of the system, and m^2 the curvature of the confining potential, which sets the correlation length $L_m := 1/m$ for avalanches in the lateral direction. Finally, $\Delta(W)$ is the renormalized disorder-force correlator, the central object in the FRG treatment of disordered elastic systems: Denoting $u(w)$ the center-of-mass position of the interface, given well-position w , the correlator $\Delta(W)$ is defined as the connected correlation function of the center-of-mass fluctuations of the interface position [123],

$$\Delta(W) := L^d m^4 \overline{[u(w) - w][u(w+W) - (w+W)]^c} . \quad (\text{C.2.9})$$

Up to a universal scaling factor and a single non-universal scale, the function $\Delta(W)$ only depends on the universality class of the problem. It was computed up to two-loop accuracy in Ref. [117] and measured numerically in Ref. [105]. For our purpose it is important that the function $\Delta(W)$ is uniformly of order ϵ , and that its second derivative is non-zero. Thus the correlations (C.2.8) increase when going away from the upper critical dimension, where mean-field theory, or equivalently the BFM is relevant. Indeed, for the BFM $\Delta''(W) = 0$, and the effective disorder force is distributed as a Brownian motion. Beyond mean-field theory, the sequence of shocks is correlated, thus the effective disorder force at large scales has a different statistics than Brownian motion. The sign of these correlations depends on the sign of $\Delta''(W)$, which, in turn, depends on the universality class of the problem. As detailed in Sec. C.3.3, *our results predict qualitatively different correlations depending on the universality class*. The most important static universality classes of non-periodic, short-ranged disorder are the random-bond (RB) universality class, which at the microscopic level has short-ranged potential-potential correlations, and the random-field (RF) universality class, for which the force-force correlations, but not the potential-potential correlations, are short-ranged at the microscopic level. As is summarized in Fig. C.1, for RF-disorder $\Delta''(W) > 0$, and thus avalanches are always anti-correlated. On the other hand, for RB-disorder, avalanches are anti-correlated at short distances W , but positively correlated at larger ones.

To obtain results for higher avalanche-size moments, we use the FRG and the $\epsilon = (d_{uc} - d)$ expansion to show that, to lowest non-trivial order in the expansion,

$$\rho_W^c(S_1, S_2) = -\frac{\Delta''(W)}{L^d m^4} \frac{S_1 S_2}{4S_m^2} \rho(S_1)\rho(S_2) + O(\epsilon^2) . \quad (\text{C.2.10})$$

Here

$$S_m := \frac{\langle S^2 \rangle_\rho}{2\langle S \rangle_\rho} , \quad (\text{C.2.11})$$

where $\langle \dots \rangle_\rho$ denotes the average with respect to ρ as defined in Eq. (C.2.3), is the characteristic size of avalanches, which acts as a large-scale cutoff for the avalanche-size density $\rho(S)$, and $\Delta''(W)$ introduced above is $O(\epsilon)$. Integrating Eq. (C.2.10) times $S_1 S_2$ over S_1 and S_2 , we recover Eq. (C.2.8). Contrary to the latter equation which is exact, relation (C.2.10) is correct only to order ϵ .

As a consequence of Eq. (C.2.10), and its generalizations to higher order, the correlations between avalanches are universal. To make this more transparent, we rewrite Eq. (C.2.10) as

$$\rho_W^c(S_1, S_2) = \frac{1}{(Lm)^d} \frac{L^{2d}}{S_m^4} \mathcal{F}_d \left(\frac{W}{W_{mu}}, \frac{S_1}{S_m}, \frac{S_2}{S_m} \right). \quad (\text{C.2.12})$$

The function \mathcal{F}_d is universal and apart from its three arguments depends only on the spatial dimension. To first order in $d = d_{uc} - \epsilon$, and in the limit of large L and small m , it is given by

$$\mathcal{F}(w, s_1, s_2) \simeq \frac{A_d \tilde{\Delta}^{*''}(w)}{16\pi \sqrt{s_1 s_2}} e^{-(s_1 + s_2)/4} + O(\epsilon^2). \quad (\text{C.2.13})$$

Here A_d is an explicit constant, with $A_{d=4} = 8\pi^2$ for SR elasticity; the scale $W_{mu} \sim m^{-\zeta}$, with ζ the roughness exponent contains a non-universal amplitude. The range of validity of this result is discussed in the main text. The presence of the factor of $1/(Lm)^d$ highlights the fact that the correlations between shocks are local (indeed $N := (Lm)^d$ counts the number of elastically independent regions of the interface). We will analyze this local structure by studying the correlations between the local sizes of the shocks.

To summarize, let us emphasize again our main message namely that for realistic models (beyond mean-field) the sequence of shocks is always correlated.

C.3 Model, shock observables and method

C.3.1 Model

Consider the Hamiltonian for a d -dimensional elastic interface with position $u(x) \equiv u_x \in \mathbb{R}$ ($x \in \mathbb{R}^d$), elastic kernel $g_{xx'}^{-1}$, subjected to a harmonic well centered at w , and to a disorder potential $V(u, x)$:

$$\mathcal{H}[u; w] = \frac{1}{2} \int_{xx'} g_{xx'}^{-1} (u_x - w)(u_{x'} - w) + \int_x V(u_x, x). \quad (\text{C.3.1})$$

Here $\int_x = \int d^d x$ and we assume everywhere that the system is confined in a box of length L with e.g. periodic boundary conditions (the boundary conditions will not play a role in the following). We also assume the existence of a short-scale length cutoff a . The elastic kernel is translationally invariant ($g_{xx'}^{-1} = g_{x-x'}^{-1}$) and defines a convex elastic-energy functional (i.e. $g_{xx'}^{-1} > 0$ for $x \neq x'$). We denote $g_q^{-1} = 1/g_q$ its Fourier transform defined as $g_q^{-1} = \int_q e^{iqx} g_x^{-1}$, where $\int_q = \int \frac{d^d q}{(2\pi)^d}$. A possible choice is the standard short-ranged elasticity defined by

$$g_{xx'}^{-1} = \delta_{xx'} (-\nabla_{x'}^2 + m^2) \quad , \quad \bar{g}_q^{-1} = q^2 + m^2. \quad (\text{C.3.2})$$

Here $\delta_{xx'}$ is the Dirac δ distribution, and the elastic coefficient has been set to one using an appropriate choice of units. Another kernel we consider is

$$g_q^{-1} = (q^2 + \mu^2)^{\frac{\gamma}{2}}, \quad (\text{C.3.3})$$

where $\gamma = 2$ corresponds to the previous case, and $\gamma = 1$ is relevant for long-ranged elasticity, as encountered in fracture and contact-line experiments. For a kernel of the form (C.3.3) we define the mass term as

$$m^2 := g_{q=0}^{-1} = \mu^\gamma. \quad (\text{C.3.4})$$

It is the strength of the harmonic well. For short-ranged elasticity we have

$$\begin{aligned} \mathcal{H}_{\text{el}}[u; w] &:= \frac{1}{2} \int_{xx'} g_{xx'}^{-1} (u_x - w)(u_{x'} - w) \\ &= \frac{1}{2} \int_x (\nabla_x u_x)^2 + m^2 (u_x - w)^2. \end{aligned} \quad (\text{C.3.5})$$

Thus $L_m := m^{-1}$ defines a length scale beyond which different parts of the interface are elastically independent. It also provides a large-scale cutoff in loop integrals encountered in the field theory. For more general kernels (C.3.3) this length scale is $L_\mu := \mu^{-1}$, and we suppose $L_\mu \ll L$, ensuring that boundary conditions do not play a role. The number of elastically independent parts of the interface is $N = (L/L_\mu)^d$. The disordered potential $V(u, x)$ is supposed to be short-ranged in internal space x , and statistically translationally invariant, with a second cumulant

$$\overline{V(u, x)V(u', x')^c} = \delta_{xx'} R_0(u - u'). \quad (\text{C.3.6})$$

The overline $\overline{(\dots)}$ denotes the average over the disorder, and superscript c stands for connected averages. The detailed form of R_0 is, apart from global features that determine the universality class of the problem (see Sec. C.3.3), unimportant. We also consider the force-force cumulant $\Delta_0(u) = -R_0''(u)$ such that $\overline{\partial_u V(u, x)\partial_{u'} V(u', x')^c} = \delta_{xx'} \Delta_0(u - u')$. Introducing

a (finite) temperature T , disorder and thermal averages in this model can efficiently be computed using a replicated field theory. Introducing n replicated fields u_{ax} , $a = 1, \dots, n$, the replicated action reads

$$S[u] = \frac{1}{2T} \sum_a \int_{xx'} g_{xx'}^{-1} (u_{ax} - w)(u_{ax'} - w) - \frac{1}{2T^2} \sum_{a,b} \int_x R_0(u_{ax} - u_{bx}) + \dots \quad (\text{C.3.7})$$

where \dots indicates eventual higher cumulants of the disorder.

C.3.2 The ground state and the scaling limit

As discussed in the introduction, we are interested in the minimal energy configuration of the interface for a given parabolic well position w and disorder realization V (i.e. the $T = 0$ problem). It is defined as the configuration $u_x(w)$, which minimises the energy,

$$u_x(w) := \underset{u_x}{\operatorname{argmin}} \mathcal{H}[u; w]. \quad (\text{C.3.8})$$

We denote

$$u(w) := \frac{1}{L^d} \int_x u_x(w), \quad (\text{C.3.9})$$

the center of mass of the ground-state of the interface. The statistical properties of $u_x(w)$ have been extensively studied in the literature. In particular it is known that the interface is self-affine with a (static) roughness exponent ζ , defined by $[\overline{u_x(w) - u_{x'}(w)}]^2 \sim |x - x'|^{2\zeta}$. This scaling form generally holds in the scaling regime $L_c \ll |x - x'| \ll L_\mu$ where L_c is the Larkin length. The scaling limit is thus obtained for $L_\mu \rightarrow \infty$ or equivalently for $\mu \rightarrow 0$, also equivalent to $m \rightarrow 0$ a regime which is implicit throughout this work. In the FRG treatment of this problem, the ground state statistics is studied using the replicated field theory (C.3.7). The mass term m (or $\mu = m^{2/\gamma}$) can be conveniently used as a control parameter to study the flow of the effective action. As $m \rightarrow 0$ and through a proper rescaling, the effective action approaches a RG fixed point. This fixed point is perturbative in $\epsilon = d_{\text{uc}} - d > 0$ where d_{uc} is the upper critical dimension of the model (for kernels of the form (C.3.3) it is given by $d_{\text{uc}} = 2\gamma$, thus $d_{\text{uc}} = 4$ for short-ranged elasticity and $d_{\text{uc}} = 2$ for long-ranged elasticity). The central object of the theory is the effective disorder correlator $R(u)$, a renormalized version of $R_0(u)$. It appears in the effective action of the theory $\Gamma[u]$, as $R_0(u)$ appears in the bare action $S[u]$ of Eq. (C.3.7) (see the action (C.3.44) below). Remarkably, as shown in Ref. [96], it is related to a physical observable, the renormalized disorder force-force correlator $\Delta(u)$ defined as

$$\Delta(w - w') := L^d m^4 \overline{[u(w) - w][u(w') - w']^c}, \quad (\text{C.3.10})$$

through the relation $\Delta''(u) = -R(u)$. This is the function that appears in the results (C.2.8) and (C.2.10) of the introduction. The RG flow can be equivalently studied on R or Δ . For $m \rightarrow \infty$, the correlator $\Delta(w)$ is equal to the bare force-force correlator: $\Delta(w) \rightarrow_{m \rightarrow \infty} \Delta_0(w)$. In the limit $m \rightarrow 0$ it admits a scaling form

$$\Delta(w) = A_d \mu^{\epsilon - 2\zeta} \tilde{\Delta}(\mu^\zeta w) \quad (\text{C.3.11})$$

where A_d is a dimensionless constant, and we recall $\mu = m^{2/\gamma}$. For kernels of the form (C.3.3), a convenient choice is to take A_d as $A_d = \frac{1}{\epsilon \tilde{I}_2}$ with the dimensionless loop integral $\tilde{I}_2 := \int_q \frac{1}{(1+q^2)^\gamma}$. Note that the combination $\epsilon \tilde{I}_2$ stays finite as $\epsilon \rightarrow 0$. In general

$$A_d^{-1} = \epsilon \tilde{I}_2 = \frac{2}{(2\sqrt{\pi})^d} \frac{\Gamma(\gamma + 1 - d/2)}{\Gamma(\gamma)}, \quad (\text{C.3.12})$$

and for example $\epsilon \tilde{I}_2 =_{\gamma=2; d=4} 1/(8\pi^2)$ and $\epsilon \tilde{I}_2 =_{\gamma=1; d=2} 1/(2\pi)$. As $m \rightarrow 0$, the rescaled disorder correlator $\tilde{\Delta}$ converges to the fixed point of the FRG flow equation $\tilde{\Delta}^*(u)$, which depends only on the universality class.

Let us now recall some important properties of these fixed-point functions.

C.3.3 Properties of $\tilde{\Delta}^*(u)$ and static universality classes

Depending on the properties of the bare disorder correlator $R_0(u)$, the FRG predicts that $\tilde{\Delta}(u)$ converges as $m \rightarrow 0$ to one of the fixed point of the FRG equation. A property of the (zero-temperature) FRG equation is that, for non-periodic disorder, if $\tilde{\Delta}^*(u)$ is a fixed point, $\kappa^2 \tilde{\Delta}^*(u/\kappa)$ also is a fixed point. Hence the fixed point towards which the system flows contains one non-universal class whose value depends on microscopic properties of the disorder. The known fixed points can be regrouped into four main classes¹. Analytic properties of these fixed-point functions are known up to two-loop order, i.e. $O(\epsilon^2)$, see Ref. [117] to which we refer the reader for quantitative results. An important property is that all fixed points exhibit a cusp around 0, $\Delta(u) \simeq \Delta(0) + \Delta'(0^+) |u| + O(u^2)$, related to the presence of avalanches [109, 101]. For our analysis the sign of $(\tilde{\Delta}^*)''(u)$ is crucial as it determines the sign of the correlations. From the exact result (C.2.8) (shown below) we see that for $(\tilde{\Delta}^*)''(W) > 0$ shock sizes at distance W are anti-correlated, whereas for $(\tilde{\Delta}^*)''(W) < 0$ they are positively correlated.

¹There are other classes with different long-range correlations, but we will not study them.

Random-bond: This class has a bare disorder potential $V(x, u)$ distributed with short-ranged correlations in the u direction: The bare disorder correlator $R_0(u)$ decays quickly to 0 as $u \rightarrow \infty$. The most important property for our analysis of the fixed-point function $\tilde{\Delta}_{\text{RB}}^*(u)$ (its typical form is plotted on the right of Fig. C.1) is that $(\tilde{\Delta}_{\text{RB}}^*)''(u) > 0$ at small u and $(\tilde{\Delta}_{\text{RB}}^*)''(u) < 0$ at large u .

Random field: This class has the bare disorder force $F(x, u) = -\partial_u V(x, u)$ distributed with short-ranged correlations. Then the bare force-force correlator $\Delta_0(u)$ is short-ranged and $R_0(u) \simeq_{u \gg 1} -\sigma|u|$ where σ is called the amplitude of the random field. The most important property for our analysis of the fixed point function $\tilde{\Delta}_{\text{RF}}^*(u)$ (its typical form is plotted on the left of Fig. C.1) is that $(\tilde{\Delta}_{\text{RF}}^*)''(u) > 0$ for all x .

Random periodic: This class corresponds to periodic disorder $V(u+1) = V(u)$. As a consequence, $\tilde{\Delta}^*(u)$ is also periodic and $(\tilde{\Delta}^*)''(u) = (\tilde{\Delta}^*)''(0) > 0$ is constant. Though our analysis still applies to this universality class and our results are correct to $O(\epsilon)$, we will not discuss it here. As the shock process is periodic in any dimension, correlations naturally arise from this periodicity (in particular in $d=0$ in the $m \rightarrow 0$ limit only one shock survives per interval).

The Brownian-Force-Model universality class: Finally, the Brownian-Force-Model defined as $\Delta_0(u) = -\sigma|u|$ is also a fixed point of the FRG flow equation and attracts all bare disorder such that $\Delta_0(u) \simeq -\sigma'|u|$ at large u . It models avalanches at the mean-field level. (It resums tree diagrams). In this model shocks are uncorrelated.

Hence, from the perspective of practical applications, the *qualitative* behavior of the correlations between shocks as a function of the distance strongly depends on the universality class of the model (see Fig. C.1).

C.3.4 Shocks observables: Densities

As recalled in the introduction, it is well known that in the limit of small m the (rescaled) ground state $u_x(w)$ is piecewise constant as a function of w . In terms of the sequence of shocks $\{(w_i, S_x^{(i)})\}_{i \in \mathbb{Z}}$ one can write $u_x(w)$ and $u(w)$ as

$$\begin{aligned} u_x(w) &= \sum_i \theta(w - w_i) S_x^{(i)}, \\ u(w) &= \frac{1}{L^d} \sum_i \theta(w - w_i) S^{(i)}, \end{aligned} \quad (\text{C.3.13})$$

where $\theta(x)$ is the Heaviside theta function. We recall the definition of the one and two-shock size-density:

$$\rho(S) = \overline{\sum_i \delta(w - w_i) \delta(S - S^{(i)})}, \quad (\text{C.3.14})$$

$$\begin{aligned} \rho_W(S_1, S_2) &= \\ &= \overline{\sum_{i \neq j} \delta(w - w_i) \delta(S_1 - S^{(i)}) \delta(w + W - w_j) \delta(S_2 - S^{(j)})}. \end{aligned} \quad (\text{C.3.15})$$

These distributions possess a large-scale cutoff which we denote S_m ; the latter diverges for m to 0 as $S_m \sim m^{-d-\zeta}$. Additionally, we suppose that they have a small-scale cutoff S_0 . In the scaling regime, $\rho(S)$ behaves as a power law with a characteristic exponent τ : $\rho(S) \sim S^{-\tau}$ for $S_0 \ll S \ll S_m$. We us also define the connected density

$$\rho_W^c(S_1, S_2) = \rho_W(S_1, S_2) - \rho(S_1)\rho(S_2). \quad (\text{C.3.16})$$

In the first part of this work our goal is to compute $\rho_W^c(S_1, S_2)$ up to first order in ϵ using the FRG.

C.3.5 Shocks observables: Probabilities

One can normalize the above densities to define proper probability distributions as follows:

$$\rho_0 := \int \rho(S) dS, \quad (\text{C.3.17})$$

$$\rho_2(W) := \int \rho_W(S_1, S_2) dS_1 dS_2, \quad (\text{C.3.18})$$

$$P(S) := \frac{\rho(S)}{\rho_0}, \quad (\text{C.3.19})$$

$$P_W(S_1, S_2) := \frac{\rho_W(S_1, S_2)}{\rho_2(W)}. \quad (\text{C.3.20})$$

With this definition, $\rho_0 dw$ is the mean number of avalanches occurring in an interval dw and $\int_{w_1}^{w_2} dw \int_{w_3}^{w_4} dw' \rho_2(w' - w)$ counts the number of pairs of shocks where the first one occurs between w_1 and w_2 and the second between w_3 and w_4 ,

irrespective of their sizes. Given these definitions, $P(S)$ and $P_W(S)$ are normalized probability distribution functions (PDF). $\int_S^{S'} d\tilde{S} P(\tilde{S})$ is the probability, given that a shock has occurred, that its size is between S and S' . $\int_{S_1}^{S'_1} dS \int_{S_2}^{S'_2} dS' P_W(S, S')$ is the probability, given that two shocks occurred at a distance W , that their sizes are between S_1 and S'_1 , and S_2 and S'_2 . Note that a priori the marginal distribution $\int dS_1 P_W(S_1, S_2)$ is different from $P(S_2)$ since it contains the additional information that a shock occurred at a distance W . At the level of these PDFs, the absence of correlations would imply $P_W(S_1, S_2) = P(S_1, S_2)$ and, though in the remaining of the text we will favor the use of densities, our results can be translated to probabilities using Eq. (C.3.20). As discussed in Ref. [109], for an avalanche-size distribution $\rho(S)$ with exponent $\tau > 1$ (which is relevant here), the value of ρ_0 is dominated by the small-scale cutoff S_0 for avalanche sizes, and diverges as $S_0 \rightarrow 0$,

$$\rho_0 = \int_{S_0}^{\infty} \rho(S) dS \sim_{S_0 \rightarrow 0} S_0^{1-\tau}. \quad (\text{C.3.21})$$

Hence, ρ_0 is non-universal. In the same way $\rho_2(W)$ is non-universal, even though its relation with ρ_0 has some universal features as we will show below. We denote by $\langle \dots \rangle_\rho$, $\langle \dots \rangle_{\rho_W}$, $\langle \dots \rangle_{\rho_W^c}$, $\langle \dots \rangle_P$ and $\langle \dots \rangle_{P_W}$ the averages with respect to ρ , ρ_W , ρ_W^c , P and P_W .

C.3.6 Relation between avalanche-size moments and renormalized force cumulants: First moment

The n^{th} cumulant of the renormalized pinning force is defined as

$$m^{2n} \overline{[u(w_1) - w_1] \dots [u(w_n) - w_n]^c} = (-1)^n L^{-(n-1)d} \hat{C}^{(n)}(w_1, \dots, w_n). \quad (\text{C.3.22})$$

By definition $\hat{C}^{(2)}(w_1, w_2) = \Delta(w_1 - w_2)$ as introduced above. By parity invariance of the disorder $m^2 \overline{[u(w) - w]} = 0$, and thus $\hat{C}^{(1)}(w) = 0$.

First cumulant: One immediately gets by inserting Eq. (C.3.13) into $m^2 \overline{[u(w) - w]} = 0$ the exact relation

$$\langle S \rangle_\rho = \rho_0 \langle S \rangle_P = L^d. \quad (\text{C.3.23})$$

Second cumulant: Differentiating with respect to w_1 and w_2 the definition $L^{-d} \Delta(w_1 - w_2) = m^4 \overline{[u(w_1) - w_1][u(w_2) - w_2]}$ with Eq. (C.3.13) inserted, one obtains the relation (33) of [109] (with a corrected misprint $1 \rightarrow -1$). It can be written in the form

$$-\frac{\Delta''(w_1 - w_2)}{L^d m^4} = L^{-2d} \langle S^2 \rangle_\rho \delta(w_1 - w_2) + L^{-2d} \langle S_1 S_2 \rangle_{\rho_{w_2 - w_1}} - 1. \quad (\text{C.3.24})$$

Hence, as pointed out in Ref. [109], the singular part of the second derivative of $\Delta''(w_1 - w_2)$ around $w_2 = w_1$ gives an exact relation between the cusp in the renormalized disorder correlator

$$\sigma := -\Delta'(0^+) = R'''(0^+), \quad (\text{C.3.25})$$

and the second avalanche-size moment,

$$S_m := \frac{\langle S^2 \rangle_\rho}{2 \langle S \rangle_\rho} = \frac{\langle S^2 \rangle_P}{2 \langle S \rangle_P} = \frac{\sigma}{m^4}. \quad (\text{C.3.26})$$

The avalanche size S_m plays the role of a large-scale cutoff for $\rho(S)$. On the other hand, the regular part of Eq. (C.3.24) gives the exact relation

$$L^{-2d} \langle S_1 S_2 \rangle_{\rho_W} = 1 - \frac{\Delta''(W)}{L^d m^4}. \quad (\text{C.3.27})$$

For uncorrelated shocks we would have obtained $L^{-2d} \langle S_1 S_2 \rangle_{\rho_W} = 1$. The correlations thus come from the non-zero value of $\Delta''(W) \neq 0$, a property which is generally expected from the FRG. It is a simple signature of the fact that the effective disordered force felt by the interface at large scale is not Brownian. Note that in terms of the moments of the connected density, the exact relation (C.3.27) reads

$$L^{-2d} \langle S_1 S_2 \rangle_{\rho_W^c} = -\frac{\Delta''(W)}{L^d m^4}. \quad (\text{C.3.28})$$

Let us also write the exact relation (C.3.27) in terms of the probabilities defined in Sec. C.3.5:

$$\frac{\rho_2(W)}{\rho_0^2} \frac{\langle S_1 S_2 \rangle_{P_W}}{(\langle S \rangle_P)^2} = 1 - \frac{\Delta''(W)}{L^d m^4}. \quad (\text{C.3.29})$$

C.3.7 Generating functions

We now introduce the generating functions which encode all the moments of the density $\rho_W(S_1, S_2)$. Let us first recall the generating functions used in the one-shock case:

$$\begin{aligned} Z(\lambda) &= L^{-d} \langle e^{\lambda S} - 1 \rangle_\rho, \\ \hat{Z}(\lambda) &= L^{-d} \langle e^{\lambda S} - \lambda S - 1 \rangle_\rho = Z(\lambda) - \lambda. \end{aligned} \quad (\text{C.3.30})$$

They are related to observables associated with the position as

$$\begin{aligned} Z(\lambda) &= L^{-d} \lim_{\delta \rightarrow 0^+} \overline{\partial_\delta e^{L^d [u(w+\delta) - u(w)]}}, \\ \hat{Z}(\lambda) &= L^{-d} \lim_{\delta \rightarrow 0^+} \overline{\partial_\delta e^{L^d [\hat{u}(w+\delta) - \hat{u}(w)]}}, \end{aligned} \quad (\text{C.3.31})$$

where $\hat{u}(w) := u(w) - w$ is the translated position field. Note that due to STS they are independent of w . These relations were proven in Ref. [111]. For two shocks we introduce

$$Z_W(\lambda_1, \lambda_2) := L^{-2d} \langle (e^{\lambda_1 S_1} - 1)(e^{\lambda_2 S_2} - 1) \rangle_{\rho_W}. \quad (\text{C.3.32})$$

We show in Appendix C.8 that it can be computed as

$$\begin{aligned} Z_W(\lambda_1, \lambda_2) &= \hat{Z}_W(\lambda_1, \lambda_2) + \lambda_2 \hat{Z}(\lambda_1) + \lambda_1 \hat{Z}(\lambda_2) + \lambda_1 \lambda_2 \\ &= \hat{Z}_W(\lambda_1, \lambda_2) + \lambda_2 Z(\lambda_1) + \lambda_1 Z(\lambda_2) - \lambda_1 \lambda_2. \end{aligned} \quad (\text{C.3.33})$$

We used the definition

$$\begin{aligned} \hat{Z}_{w_2-w_1}(\lambda_1, \lambda_2) &:= L^{-2d} \times \\ &\lim_{\delta_1, \delta_2 \rightarrow 0^+} \overline{\partial_{\delta_1, \delta_2} e^{L^d \lambda_1 [\hat{u}(w_1+\delta_1) - \hat{u}(w_1)]} e^{L^d \lambda_2 [\hat{u}(w_2+\delta_2) - \hat{u}(w_2)]}} \end{aligned} \quad (\text{C.3.34})$$

In the following we compute $\hat{Z}_W(\lambda_1, \lambda_2)$ using the FRG through formula (C.3.34). Let us also define the connected generating functions

$$\begin{aligned} Z_W^c(\lambda_1, \lambda_2) &:= L^{-2d} \langle (e^{\lambda_1 S_1} - 1)(e^{\lambda_2 S_2} - 1) \rangle_{\rho_W^c} \\ &= Z_W(\lambda_1, \lambda_2) - Z(\lambda_1)Z(\lambda_2) \\ \hat{Z}_W^c(\lambda_1, \lambda_2) &:= \hat{Z}_W(\lambda_1, \lambda_2) - \hat{Z}(\lambda_1)\hat{Z}(\lambda_2) \end{aligned} \quad (\text{C.3.35})$$

These functions are actually equal: $Z_W^c(\lambda_1, \lambda_2) = \hat{Z}_W^c(\lambda_1, \lambda_2)$ as is easily seen using (C.3.33).

C.3.8 Relation between avalanche-size moments and renormalized force cumulants: Kolmogorov cumulants and chain rule

Using Eq. (C.3.34) and the fact that $\overline{\hat{u}(w)} = 0$, the generating function $\hat{Z}_W(\lambda_1, \lambda_2)$ can be written as

$$\begin{aligned} \hat{Z}_W(\lambda_1, \lambda_2) &= \sum_{n, m=1}^{\infty} \frac{\lambda_1^n \lambda_2^m}{n!m!} \lim_{\delta_1, \delta_2 \rightarrow 0^+} \\ &\frac{L^{(n+m-2)d}}{\delta_1 \delta_2} \overline{[\hat{u}(\delta_1) - \hat{u}(0)]^n [\hat{u}(W + \delta_2) - \hat{u}(W)]^m}. \end{aligned} \quad (\text{C.3.36})$$

In the limit of $\delta_i \rightarrow 0$ we encounter for each (n, m) two types of terms:

$$\begin{aligned} &\overline{[\hat{u}(\delta_1) - \hat{u}(0)]^n [\hat{u}(W + \delta_2) - \hat{u}(W)]^m} = \\ &\overline{[\hat{u}(\delta_1) - \hat{u}(0)]^{n^c} \times [\hat{u}(W + \delta_2) - \hat{u}(W)]^{m^c}} \\ &+ \overline{[\hat{u}(\delta_1) - \hat{u}(0)]^n [\hat{u}(W + \delta_2) - \hat{u}(W)]^{m^c}} + O(\delta_i^3). \end{aligned} \quad (\text{C.3.37})$$

The term in the second line of Eq. (C.3.37) produces the disconnected part of the avalanche moment $\langle S_1^n \rangle \langle S_2^m \rangle$ and thus the disconnected part of the generating function $\hat{Z}_W(\lambda_1, \lambda_2)$, that is $\hat{Z}(\lambda_1)\hat{Z}(\lambda_2)$. The last term on the other hand contributes to $\langle S_1^n S_2^m \rangle_{\rho_W^c}$ and to the connected part of the generating function, $\hat{Z}_W^c(\lambda_1, \lambda_2) = Z_W^c(\lambda_1, \lambda_2)$ which is the true unknown. Introducing the Kolmogorov cumulants

$$\begin{aligned} K_W^{(n, m)}(\delta_1, \delta_2) &:= \\ &L^{(n+m-2)d} \overline{[\hat{u}(\delta_1) - \hat{u}(0)]^n [\hat{u}(W + \delta_2) - \hat{u}(0)]^{m^c}}, \end{aligned} \quad (\text{C.3.38})$$

we can write

$$Z_W^c(\lambda_1, \lambda_2) = \sum_{n, m=1}^{\infty} \frac{\lambda_1^n \lambda_2^m}{n!m!} \lim_{\delta_1, \delta_2 \rightarrow 0^+} \frac{1}{\delta_1 \delta_2} K_W^{(n, m)}(\delta_1, \delta_2), \quad (\text{C.3.39})$$

or, equivalently,

$$\langle S_1^n S_2^m \rangle_{\rho_W^c} = \lim_{\delta_1, \delta_2 \rightarrow 0^+} \frac{1}{\delta_1 \delta_2} K_W^{(n,m)}(\delta_1, \delta_2). \quad (\text{C.3.40})$$

The Kolmogorov cumulants (C.3.38) can be generally extracted from the renormalized force cumulants (C.3.22), as we now explain. Let us introduce²

$$C^{(n,m)}(w_1, \dots, w_n, w_{n+1}, \dots, w_{n+m}) = \frac{L^{(n+m-2)d}}{\hat{u}(w_1) \dots \hat{u}(w_n) \hat{u}(w_{n+1}) \dots \hat{u}(w_{n+m})^c}. \quad (\text{C.3.41})$$

They are trivially linked to the renormalized force cumulants (C.3.22): $C^{(n,m)}(w_1, \dots, w_n, w_{n+1}, \dots, w_{n+m}) = \frac{1}{L^d} (-1/m^2)^{n+m} \hat{C}^{(n+m)}$. Explicit expressions for the lowest cumulants with $n+m \leq 4$ are displayed in Ref. [109], see e.g. Eq. (61) there. In the notation for $C^{(n,m)}$, though the expression is symmetric in w_i , we have highlighted the facts that in the end the n first w_i will be taken around $w=0$, whereas the last m will be around W . Indeed, to obtain $K_W^{(n,m)}(\delta_1, \delta_2)$ from the moments $C^{(n,m)}$, we must successively evaluate $C^{(n,m)}$ with $w_i \rightarrow \delta_1$ minus $C^{(n,m)}$ with $w_i \rightarrow 0$ for each $i=1, \dots, n$, then set $w_i \rightarrow W + \delta_2$ minus $C^{(n,m)}$ with $w_i \rightarrow W$ for each $i=n+1, \dots, n+m$. Ambiguities associated with the possible presence of terms such as $\Delta'(0^\pm)$, are lifted by taking the limit of coinciding points with a given specific ordering of the w_i . Consistency requires that the end result does not depend on the chosen ordering, a property linked to the assumption that all singularities of the field $\hat{u}(w)$ can be modeled by a finite density of dilute shocks (which guarantees e.g. the continuity of \hat{C}). This iterative procedure was called the \mathcal{K} operation in [109].

C.3.9 Strategy of the calculation and validity of the results

In order to compute $\hat{Z}_W(\lambda_1, \lambda_2)$, we must be able to perform disorder averages of moments of the position field at various positions w_i for $i=1, \dots, r$. For example $r=4$ is sufficient in the formulation (C.3.34) and used in Appendix C.10. In the main part of this work we report a calculation of $\hat{Z}_W(\lambda_1, \lambda_2)$ from the study of the moments (C.3.41) and we thus need to keep r arbitrary. We therefore consider the theory for r position fields u_x^i coupled to different parabolic wells centered at positions w_i in the same disordered environment. The Hamiltonian of the problem is

$$\mathcal{H}[\{u\}, \{w\}] = \sum_{i=1}^r \mathcal{H}_{\text{el}}[u^i, w^i] + \sum_{i=1}^r \int_x V(u_x^i, x). \quad (\text{C.3.42})$$

This leads to a replicated action of the form

$$S[u] = \frac{1}{2T} \sum_{a,i} \int_{xx'} g_{xx'}^{-1}(u_{ax}^i - w_i)(u_{ax'}^i - w_i) - \frac{1}{2T^2} \sum_{a,i;b,j} \int_x R_0(u_{ax}^i - u_{bx}^j) + \dots \quad (\text{C.3.43})$$

The effective action of the theory is [109, 111, 96]

$$\Gamma[u] = \frac{1}{2T} \sum_{a,i} \int_{xx'} g_{xx'}^{-1}(u_{ax}^i - w_i)(u_{ax'}^i - w_i) - \frac{1}{2T^2} \sum_{a,i;b,j} \int_x R(u_{ax}^i - u_{bx}^j) + O(\epsilon^2). \quad (\text{C.3.44})$$

Here $R(u) = O(\epsilon)$ is the renormalized disorder correlator already introduced in the previous section, while the neglected terms are higher-order terms in ϵ that can be expressed as loop integrals with higher powers of R . The calculation of observables using the effective action (C.3.44) has been called the *improved tree approximation* [109, 111]. Here we did not specify the number of replicas $a=1, \dots, n_r$. As is usual in replica calculations, the $n_r \rightarrow 0$ limit will be implicit in the following. Since (C.3.44) is the effective action, observables will be computed using a saddle-point calculation, or equivalently in a diagrammatic language, by resumming all tree diagrams generated by the action (C.3.44). This calculation allows to get the lowest order in ϵ for any observable. Let us recall the known results at the improved tree level for $\rho(S)$ and $Z(\lambda)$ as obtained in Refs. [109, 111]:

$$\rho(S) = \frac{L^d}{2\sqrt{\pi} S^{\frac{3}{2}} (S_m)^{\frac{1}{2}}} e^{-\frac{S}{4S_m}}, \quad (\text{C.3.45})$$

$$Z(\lambda) = \lambda + S_m Z(\lambda)^2 = \frac{1}{2S_m} (1 - \sqrt{1 - 4\lambda S_m}). \quad (\text{C.3.46})$$

²Note that those differ from \mathcal{C} introduced in [109] by an additional factor of L^{-d} .

Using (C.3.40) we conclude that

$$L^{-2d} \langle S_1 S_2 \rangle_{\rho_W^c} = -\frac{\Delta''(W)}{L^d m^4}. \quad (\text{C.4.5})$$

This is the exact result (C.3.27), here retrieved diagrammatically within the improved tree approximation. A priori there could be higher-order corrections $O(\epsilon^2)$ on the r.h.s. of (C.4.5), coming from loop diagrams. However, the definition (C.3.10) of $\Delta(u)$ as a physical observable effectively resums an infinite number of loop diagrams. The same diagrams then arise on both sides of Eq. (C.4.5), and the result (C.3.27) is exact.

Second moment: Let us now consider the computation of $\langle S_1^2 S_2 \rangle_{\rho_W^c}$. We first need to compute $C^{(2,1)}(w_1, w_2, w_3)$. Diagrammatically it is given by

$$\begin{aligned} & C^{(2,1)}(w_1, w_2, w_3) \\ &= 2 \text{Sym}_{w_1 \leftrightarrow w_2} \left(\begin{array}{c} w_2 \approx 0 \quad w_1 \approx 0 \quad w_3 \approx W \quad w_3 \approx W \quad w_1 \approx 0 \quad w_2 \approx 0 \quad w_2 \approx 0 \quad w_3 \approx W \quad w_1 \approx 0 \\ \left[\begin{array}{c} \text{---} \text{---} \text{---} \\ \text{---} \text{---} \text{---} \\ \text{---} \text{---} \text{---} \end{array} \right] = \left[\begin{array}{c} \text{---} \text{---} \text{---} \\ \text{---} \text{---} \text{---} \\ \text{---} \text{---} \text{---} \end{array} \right] \\ + \quad \left[\begin{array}{c} \text{---} \text{---} \text{---} \\ \text{---} \text{---} \text{---} \\ \text{---} \text{---} \text{---} \end{array} \right] \\ + \quad \left[\begin{array}{c} \text{---} \text{---} \text{---} \\ \text{---} \text{---} \text{---} \\ \text{---} \text{---} \text{---} \end{array} \right] \end{array} \right) \\ &= \frac{2}{L^d m^8} \text{Sym}_{w_1 \leftrightarrow w_2} \left[\Delta(w_1 - w_2) \Delta'(w_1 - w_3) + \Delta(w_1 - w_3) \Delta'(w_1 - w_2) + \Delta(w_3 - w_2) \Delta'(w_3 - w_1) \right] \end{aligned} \quad (\text{C.4.6})$$

In doing the \mathcal{K} operation to go from $C^{(2,1)}$ to $K_W^{(2,1)}$, these diagrams are not equivalent. At order $\delta_1 \delta_2$ that we are interested in, the first term leads to $4 \frac{\Delta'(0^+)}{m^4} \frac{\Delta''(W)}{L^d m^4} \delta_1 \delta_2$, the second to $2 \frac{\Delta'(0^+)}{m^4} \frac{\Delta''(W)}{L^d m^4} \delta_1 \delta_2$, whereas the third one is of order $O(\delta_1^2 \delta_2)$ and does not contribute. Using Eq. (C.3.40) we conclude that

$$L^{-2d} \langle S_1^2 S_2 \rangle_{\rho_W^c} = 6 \frac{\Delta'(0^+)}{m^4} \frac{\Delta''(W)}{L^d m^4} + O(\epsilon^2). \quad (\text{C.4.7})$$

General rules for diagrams: The last example is rather instructive for the three general rules:

- (i) the only diagrams that contribute to the Kolmogorov cumulant $K_W^{(n,m)}(\delta_1, \delta_2)$ at order $\delta_1 \delta_2$ contain a single double-dashed vertex (that is a single disorder interaction vertex connecting the two disjoint sets of points at $w \approx 0$ and $w \approx W$);
- (ii) this vertex becomes a $\Delta''(W)$ at order $\delta_1 \delta_2$;
- (iii) the other interaction vertices are between (almost) coinciding points, and produce a factor of $\Delta'(0^+)$ at order $\delta_1 \delta_2$.

These rules come from the fact that in the \mathcal{K} operation each external leg produces an additional factor of δ_i (for the n legs at $w_1, \dots, w_n \approx 0$) or δ_2 (for the m legs at $w_{n+1}, \dots, w_{n+m} \approx W$), thus tend to be of higher order in δ_1 and δ_2 . However, from the study of the one-shock case (see Section V.C of [109]), we know the general mechanism to escape this apparent trivialization and to allow that each part of the diagram that connects only coinciding points together brings a single δ_i . In this case, starting from the top of a diagram the δ_i attached to an external leg can be brought to the bottom of the diagram as long as the disorder vertex encountered along the way leads to a $\Delta'(0^+)$ when taking the limit of coinciding points. In such diagrams each vertex linking coinciding points must have two up-going propagators and one entering from below (effectively corresponding to the $\Delta'(0^+)$ cubic vertex of the BFM [101]), except for the vertex at the bottom of the diagram which has only two up-going propagators (see Section V.D. of [109]). This last vertex is the one carrying the remaining factor of δ_1 : being differentiated in the end it also leads to an additional factor of $\Delta'(0^+)$. This explains why the disorder only enters as $\Delta'(0^+)$ in the one-shock improved-tree-theory result (C.3.45). The rule (iii) stated above is a generalization of that property.

In the two-shock case the same mechanism occurs and rule (i) is obvious: a diagram cannot have more than two sets of points separated by a double-dashed line (one around $w \approx 0$ and one around $w \approx W$) since each set contributes a factor of δ_i . For example, in the last diagram of Eq. (C.4.6), each leg is such a set of points, and the diagram is $O(\delta_1^2 \delta_2)$. To explain rule (ii), let us consider one endpoint of a double-dashed line and distinguish three cases. First, if there is no propagator entering from below this point, such as the points at $w \approx W$ in the first and second diagrams of Eq. (C.4.6) and the two points in Eq. (C.4.3), then the δ_i originating from the set of connected points above it end at this vertex, and the vertex is differentiated during the \mathcal{K} operation. Second, if there is a propagator entering from below that point, such as the point at $w_1 \approx 0$ in the first diagram of Eq. (C.4.6), then the δ_i originating from above the vertex continues downward the diagram without modifying the vertex. Third, if there is more than one propagator entering from below the point then the diagram will necessarily be of higher order in δ_i . Combining these three cases, one concludes that the double-dashed-line vertex necessarily corresponds to a $\Delta''(W)$.

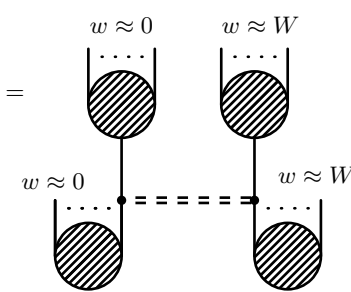
Hence we see that the diagrams contributing to the two-shock moments consist of diagrams reminiscent of the one-shock case (i.e. they contain only $\Delta'(0^+)$ vertices) linked together by an interaction vertex $-\frac{\Delta''(W)}{L^d m^4}$.

C.4.3 Generating function for all moments

Let us now use the above rules and give a diagrammatic computation of $Z_W^c(\lambda_1, \lambda_2) = \hat{Z}_W^c(\lambda_1, \lambda_2)$ defined in Eq. (C.3.35). To this aim, let us first introduce a diagrammatic notation for $Z(\lambda)$ defined in Eq. (C.3.30):

$$Z(\lambda) = \left[\begin{array}{c} \dots \\ \text{---} \text{---} \text{---} \\ \text{---} \text{---} \text{---} \end{array} \right]. \quad (\text{C.4.8})$$

We have emphasized using dots that there is an arbitrary number of external legs at the top of the diagrams summed in Eq. (C.4.8). Using the expansion (C.3.36) and following the rules explained in the previous section, the diagrams entering in $\hat{Z}_W^c(\lambda_1, \lambda_2)$ are made of two trees linked by a single doubled dashed line. It is the sum of all tree diagrams for avalanches at $w = 0$, times all tree diagrams for avalanches at $w = W$, linked together by a single $-\frac{\Delta''(W)}{L^d m^4}$ inserted between any pair of points belonging to each tree. This can be represented as

$$Z_W^c(\lambda_1, \lambda_2) = \hat{Z}_W^c(\lambda_1, \lambda_2)$$

(C.4.9)

The diagrams above the point of insertion of $\Delta''(W)$ on the left are given by $Z(\lambda_1)$. The terms below are all the diagrams in $Z(\lambda_1)$ with an arbitrary external leg selected, that is $\frac{dZ(\lambda_1)}{d\lambda_1}$. A similar contribution arises on the right-hand side. Hence we arrive at the result

$$Z_W^c(\lambda_1, \lambda_2) = -\frac{\Delta''(W)}{L^d m^4} Z(\lambda_1) \frac{dZ(\lambda_1)}{d\lambda_1} Z(\lambda_2) \frac{dZ(\lambda_2)}{d\lambda_2} + O(\epsilon^2)$$
(C.4.10)

In terms of $Z_W(\lambda_1, \lambda_2)$ this result reads

$$Z_W(\lambda_1, \lambda_2) = Z(\lambda_1) Z(\lambda_2) - \frac{\Delta''(W)}{L^d m^4} Z(\lambda_1) \frac{dZ(\lambda_1)}{d\lambda_1} Z(\lambda_2) \frac{dZ(\lambda_2)}{d\lambda_2}$$
(C.4.11)

It is correct to $O(\epsilon)$ if one takes into account the $O(\epsilon)$ corrections to $Z(\lambda)$. Expanding the result (C.4.10) one obtains the moments $\langle S_1^n S_2^m \rangle_{\rho_W^c}$:

$$\langle S_1^n S_2^m \rangle_{\rho_W^c} = -\frac{\Delta''(W)}{L^{3d} m^4} n! m! \times \sum_{p=0}^{n-1} \sum_{q=0}^{m-1} \frac{\langle S^{n-p} \rangle_\rho \langle S^{p+1} \rangle_\rho \langle S^{m-q} \rangle_\rho \langle S^{q+1} \rangle_\rho}{(n-p)! p! (m-q)! q!} + O(\epsilon^2)$$
(C.4.12)

The diagrammatic interpretation of this result is straightforward: to construct an arbitrary diagram contributing to $\langle S_1^n S_2^m \rangle_{\rho_W^c}$, one must first choose $p \leq n-1$ external legs on the left that will be below the point of insertion of $-\frac{\Delta''(W)}{L^d m^4}$ (there must be at least one leg above this point of insertion). In the \mathcal{K} operation, all those points lead to a term that contributes to $\langle S^p \rangle_\rho$. The combinatorial term accounts for the C_p^n possible choices. Note that this result was derived using the heuristic diagrammatic rules developed in the preceding section. We observe that:

- (i) It correctly reproduces the results for the small-order moments (C.4.5) and (C.4.7). We checked that it leads to $\langle S_1^3 S_2 \rangle_{\rho_W^c} = -60 \frac{\Delta''(W)}{L^d m^4} S_m^2$ and $\langle S_1^2 S_2^2 \rangle_{\rho_W^c} = -27 \frac{\Delta''(W)}{L^d m^4} S_m^2$, which can also be derived from the expression for $\hat{C}^{(4)}(w_1, w_2, w_3, w_4)$ given e.g. in formula (61) of Ref. [109].
- (ii) We give in Appendix C.9 an alternative derivation of Eq. (C.4.11) that uses the Carraro-Duchon formalism [230, 111].
- (iii) We give in Appendix C.10 a derivation using a saddle-point calculation within the effective action (C.3.44). This also yields the local structure of correlations studied in Section C.5.

C.4.4 Results for the densities

To infer ρ_W from Eq. (C.4.11), we first note the identity $Z(\lambda) \frac{dZ(\lambda)}{d\lambda} = \frac{1}{2S_m} \frac{d}{d\lambda} (Z(\lambda) - \lambda)$, derived from the self-consistent equation (C.3.45) for $Z(\lambda)$. Differentiating $L^{-d} \int dS (e^{\lambda S} - 1) \rho(S) = Z(\lambda)$ with respect to λ and using $\langle S \rangle_\rho = L^d$ yields

$$L^{-d} \int dS (e^{\lambda S} - 1) S \rho(S) = \frac{d}{d\lambda} [Z(\lambda) - \lambda]$$
(C.4.13)

Finally, using Eqs. (C.3.32) and (C.4.11), we obtain

$$\rho_W(S_1, S_2) = \rho(S_1) \rho(S_2) \left(1 - \frac{\Delta''(W)}{L^d m^4} \frac{S_1 S_2}{4S_m^2} \right)$$
(C.4.14)

This is our main result for the two-shock density, already announced in Eq. (C.2.10) of the introduction. It can be used to extract a variety of physical observables.

Mean number of pairs of shocks: Integrating over S_1 and S_2 , we obtain two equivalent formulas for $\rho_2(W)$:

$$\begin{aligned}\rho_2(W) &= \rho_0^2 - \frac{\Delta''(W)}{L^d m^4} \frac{L^{2d}}{4S_m^2} \\ &= \rho_0^2 \left[1 - \frac{\Delta''(W)}{L^d m^4} \left(\frac{\langle S \rangle_P}{2S_m} \right)^2 \right].\end{aligned}\quad (\text{C.4.15})$$

Hence, although both ρ_0 and $\rho_2(W)$ are non-universal and dominated by the non-universal small avalanche size cutoff S_0 discussed in Sec. C.3.5, the connected density $\rho_2(W) - \rho_0^2$ does not depend on S_0 and is universal.

Normalized probability distribution: The above results allow us to express the probability distribution $P_W(S_1, S_2) = \frac{\rho_W(S_1, S_2)}{\rho_2(W)}$ to $O(\epsilon)$ accuracy as

$$\begin{aligned}P_W(S_1, S_2) &= \\ &P(S_1)P(S_2) \left[1 - \frac{\Delta''(W)}{4S_m^2 L^d m^4} \left(S_1 S_2 - \langle S \rangle_P^2 \right) \right].\end{aligned}\quad (\text{C.4.16})$$

Conditional probability distribution: Another PDF of interest is the conditional probability to have a shock with amplitude S_2 , given that there was a shock of amplitude S_1 at a distance W before. To $O(\epsilon)$ accuracy

$$\begin{aligned}P_W(S_2|S_1) &= \frac{P_W(S_1, S_2)}{\int dS_2 P_W(S_1, S_2)} \\ &= P(S_2) \left[1 - \frac{\Delta''(W) S_1}{4S_m^2 L^d m^4} \left(S_2 - \langle S \rangle_P \right) \right].\end{aligned}\quad (\text{C.4.17})$$

Its mean value, normalized by $\langle S \rangle_P$, is

$$\frac{\langle S_2|S_1 \rangle}{\langle S \rangle_P} = 1 - \frac{\Delta''(W) S_1}{4S_m^2 L^d m^4} \left(2S_m - \langle S \rangle_P \right).\quad (\text{C.4.18})$$

Second shock marginal: The probability for the size S_2 of a second shock at W , given that there was a shock at 0, is

$$\begin{aligned}P_W(S_2) &= \int dS_1 P_W(S_1, S_2) \\ &= P(S_2) \left[1 - \frac{\Delta''(W) \langle S \rangle_P}{4S_m^2 L^d m^4} \left(S_2 - \langle S \rangle_P \right) \right].\end{aligned}\quad (\text{C.4.19})$$

The normalized mean value of the second shock is

$$\frac{\langle S_2 \rangle_W}{\langle S \rangle_P} = 1 - \frac{\Delta''(W) \langle S \rangle_P}{4S_m^2 L^d m^4} \left(2S_m - \langle S \rangle_P \right).\quad (\text{C.4.20})$$

C.4.5 Analysis of the results

Sign of the correlations: As discussed in Sec. C.3.3, the sign of the correlations (positively or negatively correlated shock sizes) solely depends on the sign of $\Delta''(W)$, which depends on the distance W and on the universality class of the problem. The above results thus unveil a rich phenomenology for the correlations as pictured in Fig. C.1.

Range of validity: The result (C.4.10) was obtained in the framework of the ϵ expansion. The results for the connected part of the correlations are by definition the first non-zero terms in this expansion, since they were obtained within the improved tree approximation, and they appear at $O(\epsilon)$. As a perturbative result, it is by definition controlled for $\epsilon \rightarrow 0$. For finite ϵ , the predictions should be accurate as long as the corrections to the mean-field behavior are small. This is worth emphasizing, since the moments $\langle S_1^n S_2^m \rangle_{\rho_W}$ predicted by the formula (C.4.12) become negative for large (n, m) , signaling a breakdown of the improved tree approximation. This is also the case of the two-shock density computed at the improved tree level in Eq. (C.4.14) which becomes negative at large S_i . There the approximation is not controlled anymore since $O(\epsilon)$ corrections are larger than the mean-field result. Let us see when this occurs: using the simple estimate $\Delta''(W) \approx |\Delta'(0^+)|/W_\mu$, where W_μ is the length of order $\mu^{-\zeta}$ on which $\Delta(W)$ decay, see below, and $|\Delta'(0^+)| = m^4 S_m$, the bound $\rho(S_1, S_2) > 0$ is violated if

$$1 \lesssim \frac{S_m}{W_\mu \mu^{-d}} \times \frac{1}{\langle \rangle^d} \times \frac{S_1 S_2}{4S_m^2}.\quad (\text{C.4.21})$$

While the first factor is a dimensionless number of order 1, which vanishes as $O(\epsilon)$ near $d = d_{uc}$, the second vanishes in the thermodynamic limit of $L \rightarrow \infty$. Thus the bound can only be violated if $S_1 S_2 / S_m^2$ compensates this factor. This can

only be achieved if at least one of the avalanches is either system-spanning, or far out in the tail of the distribution, i.e. the bound is only violated for very unlikely events.

Note however that the exact result (C.3.27) is protected from being negative since

$$L^{-2d}\langle S_1 S_2 \rangle_{\rho_W} = 1 - \frac{\Delta''(W)}{L^d m^4} = \overline{\partial_w u(w) \partial_w u(W+w)}, \quad (\text{C.4.22})$$

and $\partial_w u(w)$ is always positive since $u(w)$ is monotonically increasing as a function of w . The latter can be shown rigorously using a stability argument: Writing that $u_x(w)$ is a stable minimum of the Hamiltonian (C.3.1) implies for all x two equations, namely $\frac{\delta \mathcal{H}[u,w]}{\delta u(x)} = 0$, and $\frac{\delta^2 \mathcal{H}[u,w]}{\delta u(x) \delta u(y)} \geq 0$. Specifying the second equation to $x = y$, we obtain

$$m^2 [u_x(w) - w] + \partial_u V(u_x(w), x) = 0, \quad (\text{C.4.23})$$

$$m^2 + \partial_u^2 V(u_x(w), x) \geq 0. \quad (\text{C.4.24})$$

Taking a derivative of Eq. (C.4.23) w.r.t. w , solving for $\partial_w u_x(w)$, and using Eq. (C.4.24) implies

$$\partial_w u_x(w) = \frac{1}{1 + m^{-2} \partial_u^2 V(u_x(w), x)} \geq 0. \quad (\text{C.4.25})$$

Comparison with experiments and numerics: Though our predictions rely on the analysis of the model (C.3.1), they were obtained using FRG and thus we expect Eqs. (C.4.10) and (C.4.12) to be valid for all models in the same universality class. All our results, namely Eq. (C.4.12) and Eqs. (C.4.14)-(C.4.20), contain the combination $\frac{\Delta''(W)}{L^d m^4}$. On one hand it can be used to give a result to order $O(\epsilon)$ in the form of a universal function (see below). On the other hand all quantities entering the r.h.s of these equations can be measured directly in an experiment or in a numerical simulation. Indeed we recall that

$$S_m := \frac{\langle S^2 \rangle_P}{2 \langle S \rangle_P} \equiv \frac{\langle S^2 \rangle_\rho}{2 \langle S \rangle_\rho} \quad (\text{C.4.26})$$

and the combination

$$\frac{\Delta''(W)}{L^d m^4} = \partial_W^2 \overline{[u(w) - w][u(w+W) - w - W]^c} \quad (\text{C.4.27})$$

can both be measured and do not require to know the mass m which might be hard to identify. The computation of this second derivative then gives a precise characterization of the amplitude of the correlations through the exact formula (C.3.28). The accuracy of the ϵ expansion and universality can then be tested against the formulas given in the previous section.

Universal function: Using rescaled quantities we can rewrite our main result as (see Eq. (C.3.11) and Sec. C.3.3)

$$\rho_W^\epsilon(S_1, S_2) = \frac{1}{(L\mu)^d} \frac{L^{2d}}{S_m^4} \mathcal{F}_d \left(\frac{W}{W\mu}, \frac{S_1}{S_m}, \frac{S_2}{S_m} \right) \quad (\text{C.4.28})$$

where the function \mathcal{F}_d is universal and depends only on the space dimension. To first order in $d = d_{\text{uc}} - \epsilon$, it is given by

$$\mathcal{F}(w, s_1, s_2) \simeq \frac{A_d \Delta^{*''}(w)}{16\pi \sqrt{s_1 s_2}} e^{-(s_1 + s_2)/4} + O(\epsilon^2) \quad (\text{C.4.29})$$

in the limit of large L and small μ and A_d was given in Eq. (C.3.12). Here $\Delta^{*''}(w)$ is the universal fixed point of the FRG equation, normalized to $\Delta^*(0) = \epsilon$. Indeed, for small m the rescaled renormalized disorder correlator of the system $\tilde{\Delta}(w)$, appearing in Eq. (C.3.11), is close to one of the fixed points of the FRG equation: $\tilde{\Delta}(w) \simeq \tilde{\Delta}^*(w)$. For non-periodic disorder, the latter can be expressed using one constant κ as $\tilde{\Delta}^*(w) = \kappa^2 \Delta^*(w/\kappa)$ (see Sec. C.3.3). The parameter κ is thus the single non-universal constant in our formula. The scales in Eq. (C.4.28) are then given by

$$W_{mu} \simeq \kappa \mu^{-\zeta}, \quad S_m \simeq A_d \kappa \Delta^{*'}(0^+) \mu^{-(d+\zeta)} \quad (\text{C.4.30})$$

for small μ . With the above normalization, to order ϵ , $\Delta^{*'}(0^+) = \sqrt{\epsilon(\epsilon - 2\zeta)}$ and $\Delta^{*''}(0) = \frac{2\epsilon}{9}$.

Locality: Note that in the result (C.4.28) the amplitude of the correlation is inversely proportional to $N = (L\mu)^d$, the number of elastically independent degrees of freedom of the interface. This is a signature of the local nature of the correlations. For two shocks a distance W apart, there is a probability of order $1/N$ that they occur in the same region of space. To go further into this locality property and to remove this bias we investigate in the next section the correlations between the local shock sizes.

C.5 Local structure of correlations

In this section we analyze the correlations between the local shock sizes. We start by deriving a general formula for the correlations between the local shock sizes measured on an arbitrary subset of the internal space of the interface. To this aim we define

$$S_1^{\phi_1} = \int_x S_{1x} \phi_{1x}, \quad S_2^{\phi_2} = \int_x S_{2x} \phi_{2x}, \quad (\text{C.5.1})$$

where ϕ_1 and ϕ_2 are two arbitrary test functions. Two extreme cases are $\phi_{1x} = 1$: in this case $S_1^{\phi_1} = S_1$, and the observable is the total size studied in the precedent section. The other extreme is $\phi_{1x} = \delta^d(x - x_1)$, for which $S_1^{\phi_1} = S_{1x_1}$ is the local size at $x = x_1$.

C.5.1 Reminder: one-shock case

Here we briefly recall the essential definitions and results given in Refs. [109, 111] on the density and generating function associated to the local one-shock size statistics. For a general test function ϕ we introduce

$$\begin{aligned}\rho^\phi(S^\phi) &:= \overline{\sum_i \delta(S^{(i),\phi} - S^\phi) \delta(w_i - w)}, \\ Z^\phi(\lambda) &:= \frac{1}{\int_x \phi_x} \langle e^{\lambda S^\phi} - 1 \rangle_{\rho^\phi}, \\ \hat{Z}^\phi(\lambda) &:= Z^\phi(\lambda) - \lambda,\end{aligned}\tag{C.5.2}$$

where $\langle \dots \rangle_{\rho^\phi}$ denotes the average with respect to ρ^ϕ . Note that \hat{Z}^ϕ has no linear term, since the first moment of ρ^ϕ is due to STS

$$\langle S^\phi \rangle_{\rho^\phi} = \int_x \phi_x.\tag{C.5.3}$$

The generating function $\hat{Z}^\phi(\lambda)$ is obtained from the replica field theory using the exact relation

$$\hat{Z}^\phi(\lambda) = \frac{1}{\int_x \phi_x} \partial_\delta \overline{e^{\int_x \phi_x [u_x(w+\delta) - u_x(w) - \delta]}} \Big|_{\delta=0+}.\tag{C.5.4}$$

It was shown in Refs. [109, 111] that $Z^\phi(\lambda)$ can be written as

$$Z^\phi(\lambda) = \frac{\int_x Z_x^\phi(\lambda)}{\int_x \phi_x},\tag{C.5.5}$$

where, at the improved-tree-theory level, $Z_x^\phi(\lambda)$ satisfies the following self-consistent equation

$$Z_x^\phi(\lambda) = \lambda \phi_x + \sigma \int_{yy'} g_{x-y} g_{x-y'} Z_y^\phi(\lambda) Z_{y'}^\phi(\lambda).\tag{C.5.6}$$

The quantity $\sigma = -\Delta'(0^+)$ was defined in Eq. (C.3.25).

C.5.2 Two-shock case: Notation and diagrammatic result

Densities and generating functions: Consider

$$\rho_W^{\phi^1 \phi^2}(S_1^{\phi^1}, S_2^{\phi^2}) := \overline{\sum_{i \neq j} \delta(w - w_i) \delta(S_1^{\phi^1} - S^{(i), \phi^1}) \delta(w + W - w_j) \delta(S_2^{\phi^2} - S^{(j), \phi^2})}.$$

The generating functions are

$$Z_W^{\phi^1 \phi^2} := \frac{1}{\int_x \phi_x^1 \int_x \phi_x^2} \left\langle \left(e^{\lambda_1 S_1^{\phi^1}} - 1 \right) \left(e^{\lambda_2 S_2^{\phi^2}} - 1 \right) \right\rangle_{\rho_W^{\phi^1 \phi^2}}\tag{C.5.7}$$

$$\hat{Z}_{w_2 - w_1}^{\phi^1 \phi^2}(\lambda_1, \lambda_2) := \frac{1}{\int_x \phi_x^1 \int_x \phi_x^2} \lim_{\delta_1, \delta_2 \rightarrow 0^+} \partial_{\delta_1, \delta_2} \overline{e^{\int_x \phi_x^1 \lambda_1 [\hat{u}_x(w_1 + \delta_1) - \hat{u}_x(w_1)]} e^{\int_x \phi_x^2 \lambda_2 [\hat{u}_x(w_2 + \delta_2) - \hat{u}_x(w_2)]}},\tag{C.5.8}$$

where $\langle \dots \rangle_{\rho_W^{\phi^1 \phi^2}}$ denotes the average with respect to $\rho_W^{\phi^1 \phi^2}$. The following relation holds

$$\begin{aligned}Z_W^{\phi^1 \phi^2}(\lambda_1, \lambda_2) &= \hat{Z}_W^{\phi^1 \phi^2}(\lambda_1, \lambda_2) + Z^{\phi^1}(\lambda_1) \lambda_2 \\ &\quad + \lambda_1 Z^{\phi^2}(\lambda_2) - \lambda_1 \lambda_2.\end{aligned}\tag{C.5.9}$$

(These relations are a consequence of Appendix C.8). The connected equivalents of the previous definitions are constructed as in the previous section for the correlations between the total sizes; for example

$$\rho_W^{c; \phi^1 \phi^2}(S_1^{\phi^1}, S_2^{\phi^2}) = \rho_W^{\phi^1 \phi^2}(S_1^{\phi^1}, S_2^{\phi^2}) - \rho^{\phi^1}(S_1^{\phi^1}) \rho^{\phi^2}(S_2^{\phi^2}),\tag{C.5.10}$$

and we note $\langle \dots \rangle_{\rho_W^{c; \phi^1 \phi^2}}$ the average w.r.t. $\rho_W^{c; \phi^1 \phi^2}$.

Hence

$$\begin{aligned} \frac{\delta Z_x^\phi}{\lambda \delta \phi_u} &= \delta(x-u) + 2\lambda\sigma \int_y g_{x-y} g_{x-u} \phi_y \\ &+ 2\lambda^2 \sigma^2 \left(2 \int_{yy'z} g_{x-y} g_{x-y'} g_{y-z} g_{y-u} \phi_z \phi_{y'} \right. \\ &\left. + \int_{yyz'} g_{x-y} g_{x-u} g_{y-z} g_{y-z'} \phi_z \phi_{z'} \right) + O(\lambda^3). \end{aligned} \quad (\text{C.5.19})$$

We then obtain from Eq. (C.5.17) the local version of the exact result (C.2.8), namely ⁵

$$\frac{\langle\langle S_1^{\phi_1} S_2^{\phi_2} \rangle\rangle_{\rho_W^c}}{\int_x \phi_x^1 \int_x \phi_x^2} = -\frac{\Delta''(W)}{\int_x \phi_x^1 \int_x \phi_x^2} \int_{zx_1x_2} g_{z-x_1} g_{z-x_2} \phi_{x_1}^1 \phi_{x_2}^2 + O(\epsilon^2). \quad (\text{C.5.20})$$

Let us also give the result for the third-order moment,

$$\begin{aligned} \frac{\langle\langle (S_1^{\phi_1})^2 S_2^{\phi_2} \rangle\rangle_{\rho_W^c}}{\int_x \phi_x^1 \int_x \phi_x^2} &= -\frac{\Delta''(W)}{\int_x \phi_x^1 \int_x \phi_x^2} \sigma \times \\ &\left(4 \int_{zx_1x_2y_1t_1} g_{z-x_1} g_{z-x_2} g_{y_1-t_1} g_{y_1-z} \phi_{x_1}^1 \phi_{t_1}^1 \phi_{x_2}^2 \right. \\ &\left. + 2 \int_{zx_1x_2t_1t_1'} g_{z-x_1} g_{z-x_2} g_{x_1-t_1} g_{x_1-t_1'} \phi_{t_1}^1 \phi_{t_1'}^1 \phi_{x_2}^2 \right) \\ &+ O(\epsilon^2). \end{aligned} \quad (\text{C.5.21})$$

C.5.4 First moment: correlations between the local shock sizes for short-ranged elasticity.

Let us now give the precise form of the first connected moment for an interface with the short-ranged elasticity (C.3.2) and for correlations between the local avalanche sizes at two points x_1 and x_2 . We choose $\phi_x^1 = \delta^d(x-x_1)$ and $\phi_x^2 = \delta^d(x-x_2)$ and note $x = |x_1 - x_2|$ the distance between the two points. Thus $S_1^{\phi_1} = S_{1x_1}$ and $S_2^{\phi_2} = S_{2x_2}$. We obtain

$$\begin{aligned} \langle\langle S_{1x_1} S_{2x_2} \rangle\rangle_{\rho_W^c} &= -\Delta''(W) \int_q e^{iq(x_1-x_2)} g_q g_{-q} \\ &= -\Delta''(W) m^{d-4} 2^{-\frac{d}{2}-1} \pi^{-\frac{d}{2}} (mx)^{2-\frac{d}{2}} K_{2-\frac{d}{2}}(mx) \\ &=_{x=0} -\Delta''(W) 2^{-d} \pi^{-\frac{d}{2}} m^{d-4} \Gamma\left(2 - \frac{d}{2}\right) \\ &\simeq_{x \gg 1/m} -\Delta''(W) 2^{-\frac{d}{2}-\frac{3}{2}} \pi^{\frac{1}{2}-\frac{d}{2}} m^{\frac{d-5}{2}} x^{\frac{3}{2}-\frac{d}{2}} e^{-mx}, \end{aligned} \quad (\text{C.5.22})$$

where $K_n(x)$ denotes a modified Bessel function of the second kind. Note that integrating this formula yields an exact result,

$$\int_{x_1, x_2} \langle\langle S_{1x_1} S_{2x_2} \rangle\rangle_{\rho_W^c} = \langle S_1 S_2 \rangle_{\rho_W^c} = -L^d \frac{\Delta''(W)}{m^4}. \quad (\text{C.5.23})$$

This is equivalent to Eq. (C.3.28), which is *exact*. We thus expect Eq. (C.5.22) to be quite accurate even for large values of ϵ .

As expected, we observe that the amplitude of the correlations decays exponentially beyond the length $L_m = 1/m$. For smaller distances they decay algebraically with an exponent that depends on the dimension:

$$\begin{aligned} &\langle\langle S_{1x_1} S_{2x_1+x} \rangle\rangle_{\rho_W^c} - \langle\langle S_{1x_1} S_{2x_1} \rangle\rangle_{\rho_W^c} \\ &\simeq_{d=1} \frac{\Delta''(W)}{8m} x^2 + O(x^3) \\ &\simeq_{d=2} -\frac{\Delta''(W)}{16\pi} \left[2\gamma_E - 1 + 2 \log(mx/2) \right] x^2 \\ &\simeq_{d=3} \frac{\Delta''(W)}{8\pi} x + O(x^2). \end{aligned} \quad (\text{C.5.24})$$

⁵The result (C.5.20) can simply be turned into an exact one if one introduces the bi-local part of the renormalized disorder correlator $\Delta_{x_2-x_1}(w_1-w_2) = m^4 [u_{x_1}(w_1) - w_1][u_{x_2}(w_2) - w_2]$ (see also [96]) and proceeds as in Sec. C.3.6. The result (C.5.20) can then be understood as the lowest-order approximation of $\Delta_{x_2-x_1}(w)$ in terms of $\Delta(w)$.

Finally, to emphasize the universal nature of Eq. (C.5.22), we note that it can be rewritten, using the notations of Sec. C.4.5 and introducing a new universal scaling function $\mathcal{F}_d^{11}(w, x)$, as

$$\langle\langle S_{1x_1} S_{2x_2} \rangle\rangle_{\rho_W^c} = \mathcal{F}_d^{11}\left(\frac{W}{W_\mu}, m|x_1 - x_2|\right) \quad (\text{C.5.25})$$

$$\begin{aligned} \mathcal{F}_d^{11}(w, x) &= -2^{-\frac{d}{2}-1} \pi^{-\frac{d}{2}} A_d \Delta^{*''}(w) x^{2-\frac{d}{2}} K_{2-\frac{d}{2}}(x) \\ &+ O(\epsilon^2). \end{aligned} \quad (\text{C.5.26})$$

C.5.5 First moment: correlations between the local shock sizes for long-ranged elasticity.

Let us now study the correlations between local avalanche sizes (we choose again $\phi_x^1 = \delta^d(x - x_1)$ and $\phi_x^2 = \delta^d(x - x_2)$ with $|x_1 - x_2| = x$) for the case of long-ranged elasticity using the kernel (C.3.3) with $\gamma = 1$. Then the result for the first connected moment is

$$\begin{aligned} \langle\langle S_{1x_1} S_{2x_2} \rangle\rangle_{\rho_W^c} &= -\Delta''(W) \frac{\mu^{d-2}}{(2\pi)^{\frac{d}{2}}} (\mu x)^{1-\frac{d}{2}} K_{1-\frac{d}{2}}(x\mu) \\ &=_{d=1} \frac{e^{-\mu x}}{2\mu}. \end{aligned} \quad (\text{C.5.27})$$

As the previous formula for short-ranged elasticity, this formula should be rather accurate for the experimentally relevant case of $d = 1$ (in this case $\epsilon = 1$). We again observe an exponential decay of the correlations beyond the length $L_\mu = 1/\mu$. However, here the correlations are constant at small distances, a signature of the long-range nature of the elasticity. As before, the universal nature of this result can be emphasized by introducing a universal scaling function $\mathcal{F}_{d,\text{LR}}^{11}(w, y)$:

$$\begin{aligned} \langle\langle S_{1x_1} S_{2x_2} \rangle\rangle_{\rho_W^c} &= \mathcal{F}_{d,\text{LR}}^{11}\left(\frac{W}{W_\mu}, \mu|x_1 - x_2|\right) \\ \mathcal{F}_d^{11}(w, x) &= -(2\pi)^{-\frac{d}{2}} A_d \Delta^{*''}(w) x^{1-\frac{d}{2}} K_{1-\frac{d}{2}}(x) + O(\epsilon^2), \end{aligned} \quad (\text{C.5.28})$$

where we used the same notations as in Sec. C.4.5.

C.6 Measurement of correlations in simulations of $d = 0$ toy models.

C.6.1 Models and goals

In this section we compare our results with numerical simulations of toy models of a particle in a discrete random potential. The position of the particle can only take integer values $u \in \mathbb{N}$ and its Hamiltonian is

$$\mathcal{H}_V[u; w] = V(u) + \frac{1}{2} m^2 (u - w)^2, \quad (\text{C.6.1})$$

where V is a random potential. We consider two distributions for the random potential mimicking the two non-periodic static universality classes of interfaces models:

RB model: The first model is a toy model for the Random-Bond universality class with short-ranged correlated disorder where the random potentials $V(i)$ at each site $i \in \mathbb{N}$, are chosen as independent, centered and normalized Gaussian random variables.

RF model: The second model is a toy model for the Random-Field universality class where $V(0) = 0$ and for $i \geq 1$, $V(i) = -\sum_{j=1}^i F(j)$; the random forces $F(i)$ at each site $i \in \mathbb{N}$ are chosen as independent, centered and normalized random variables. Thus $V(i)$ is a random walk with Gaussian increments.

In the RB model we choose the mass as $m_{\text{RB}} = 0.01$ and in the RF model as $m_{\text{RF}} = 0.02$. With these parameters, the probability ρ_0 to trigger a shock when moving $w \rightarrow w + 1$ is $\rho_0^{\text{RF}} = (6.959 \pm 0.001) \times 10^{-3}$ and $\rho_0^{\text{RB}} = (9.471 \pm 0.001) \times 10^{-3}$. These small values of the masses ensure that the models efficiently approximate our continuum model in $d = 0$, and that the particle optimizes its energy over a large number of random variables. We perform averages over 10 simulations of environments of size $N = 5 \times 10^8$ sites. We obtain excellent statistics for various observables studied in this work, including $\rho_2(W)$, $\Delta(W)$ measured using Eq. (C.3.10), $\langle S_1 S_2 \rangle_{\rho_W}$ and $\langle S_1^2 S_2 \rangle_{\rho_W}$.

Let us emphasize that these simulations are more a proof of principle to motivate simulations on higher dimensional models and measurements in experiments, than a full test of the results obtained in this article. This said, our simulations allow us to verify the exact result (C.3.27) to a very high accuracy. Second, although $d = 0$ is at a large value of ϵ in the $d = 4 - \epsilon$ expansion, the FRG equation and the associated fixed-point functions for random-field disorder are known to behave quite similarly [97, 117]. For random-bond disorder we expect less universality since $\Delta(u)$ is non-universal in $d = 0$; nevertheless the relations between the correlation and $\Delta(u)$ are interesting to investigate, in particular the sign of the correlations.

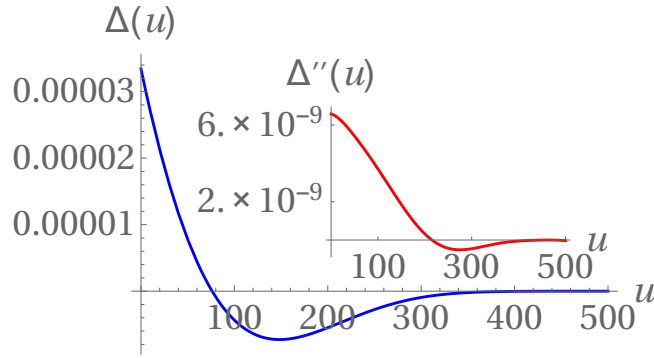


Figure C.2: Renormalized disorder $\Delta(u)$ measured in the $d = 0$ RB toy model. Inset: its second derivative $\Delta''(u)$, computed using a numerical fit of the measured $\Delta(u)$.

C.6.2 Numerical Results: RB model

Using the definition (C.3.10) we measure the renormalized disorder correlator. The result is shown in Fig. C.2. Using an interpolation of the result with a polynomial of degree 10, we obtain a smooth version that is later used to compute its second derivative $\Delta''(u)$ which appears in our analysis as the central object controlling the amplitude of the correlations. Some measured properties are: $\Delta(0) \approx 3.34 \times 10^{-5}$, $\Delta''(0) \approx 6.78 \times 10^{-9}$; $\Delta(76.2) \approx 0$, $\Delta''(215) \approx 0$; the position of the minimum and the value at the minimum: $\Delta(148.2) \approx -7.3 \times 10^{-6}$, $\Delta''(274.4) \approx -5.1 \times 10^{-10}$. This is compared with the measurement of $\langle S_1 S_2 \rangle_{\rho_W}$ using the exact result (C.3.27), see Fig. C.3. We obtain a perfect agreement.

From a qualitative perspective, we note the following:

(i) We observe the predicted crossover from anti-correlated shocks at small distances ($W < 215$) to positively correlated shocks at large distances.

(ii) The correlations are far from being negligible: by definition $\frac{\langle S_1 S_2 \rangle_{\rho_W^c}}{\langle S \rangle_{\rho^2}} > -1$, while we observe $\frac{\langle S_1 S_2 \rangle_{\rho_W^c}}{\langle S \rangle_{\rho^2}} \approx -0.6$, an indication that the shocks in this toy model are strongly correlated.

We now check the predictions obtained using the ϵ expansion. We first measure $\rho_2(W)$ and compare it with the result (C.4.15), see Fig. C.4. We obtain a surprisingly good agreement between the two curves, considering that $\epsilon = 4$. We also measure $\langle S_1^2 S_2 \rangle_{\rho_W}$ and compare it with the result (C.4.7), see Fig. C.5. Here the discrepancy is large for smaller values of W , a fact that can be anticipated since our result predicts $\frac{\langle S_1^2 S_2 \rangle_{\rho_W^c}}{\langle S^2 \rangle_{\rho} \langle S \rangle_{\rho}} < -1$ at small W , which is unphysical. This discrepancy keeps increasing with higher-order moments. However the sign of the correlation, and its value for large W is quite well predicted.

C.6.3 Numerical Results: RF model

In Figs. C.6 to C.9 we show the corresponding results for the RF toy model. They are similar except that as predicted in this type of model the shocks are *always anti-correlated*. The value at the origin of the renormalized disorder correlator and of its second derivative are measured as $\Delta(0) \approx 3.4 \times 10^{-3}$, $\Delta''(0) \approx 9.4 \times 10^{-8}$. Once again we observe that these correlations are large, $\frac{\langle S_1 S_2 \rangle_{\rho_W^c}}{\langle S \rangle_{\rho^2}} \approx -0.6$. We obtain a perfect agreement for the exact result $\langle S_1 S_2 \rangle_{\rho_W}$, see Fig. C.7. The agreement for the $O(\epsilon)$ result for $\rho_2(W)$ (C.4.15) is surprisingly good (see Fig. C.8), whereas the $O(\epsilon)$ approximation breaks down for higher moments at small W such as $\langle S_1^2 S_2 \rangle_{\rho_W^c}$, see Fig. C.9.

C.7 Conclusion

In this paper we shed light on the fact that, for realistic models of elastic interfaces in a random medium below their upper critical dimension, correlations between (static) avalanches should always be expected. To do so we have studied the correlations between the size and location of shocks in the ground state of elastic interfaces in a random potential. We found the exact relation (C.2.8) for the first connected moment that characterizes these correlations in terms of the renormalized disorder correlator, a universal quantity at the center of the FRG treatment of disordered elastic systems. Beyond the first cumulant, higher-order moments (C.4.10), (C.4.12) and the full joint density of shocks (C.4.14) were computed using the FRG at first non-trivial order in the ϵ expansion. The local structure of these correlations was made precise through a study of local shock sizes. The qualitative phenomenology associated with these correlations clearly distinguishes between the Random-Bond and Random-Field universality classes. This was highlighted through a numerical simulation of $d = 0$ toy models.

We expect our results to broadly apply to models in the universality class of the statics of disordered elastic systems. Concerning the dynamics, and avalanches at the depinning transition of elastic interfaces, we expect our results to be equivalently *applicable and accurate*. The derivation of the exact relation (C.2.8) can easily be adapted to the dynamics by

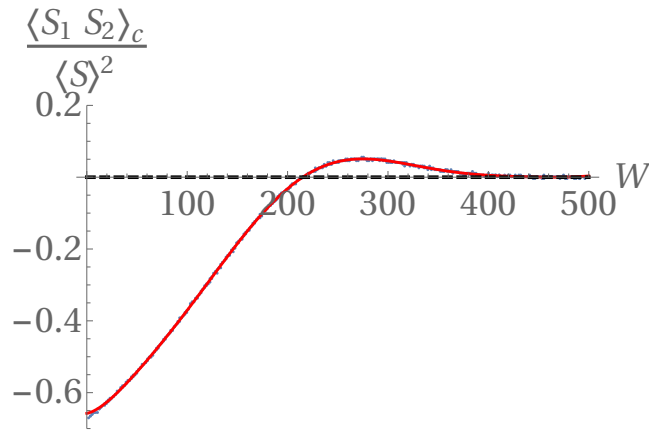


Figure C.3: Comparison between the measurement of the normalized moment $\frac{\langle S_1 S_2 \rangle_{\rho_W^c}}{\langle S \rangle_{\rho}^2}$ (blue dots) and the prediction from the exact result (C.3.27) using the measurement of $\Delta(u)$ (red curve) in the RB toy model. The agreement is perfect as expected.

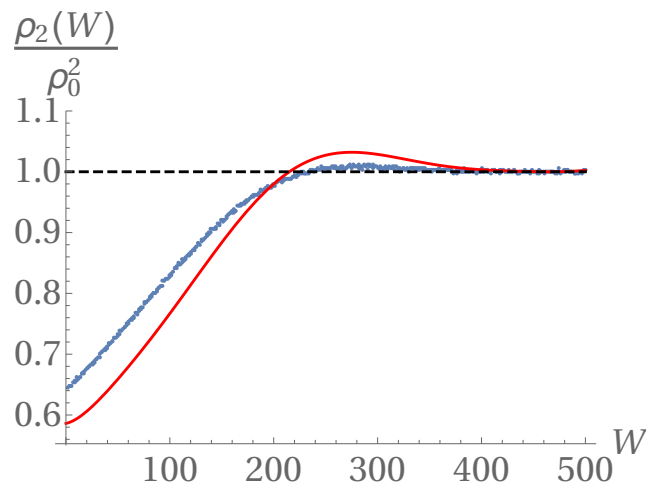


Figure C.4: Comparison between the measurement of $\rho_2(W)$ (blue dots) and the prediction from the $O(\epsilon)$ result (C.4.15) using the measurement of $\Delta(u)$ (red curve) in the RB toy model. We obtain a surprisingly good agreement.

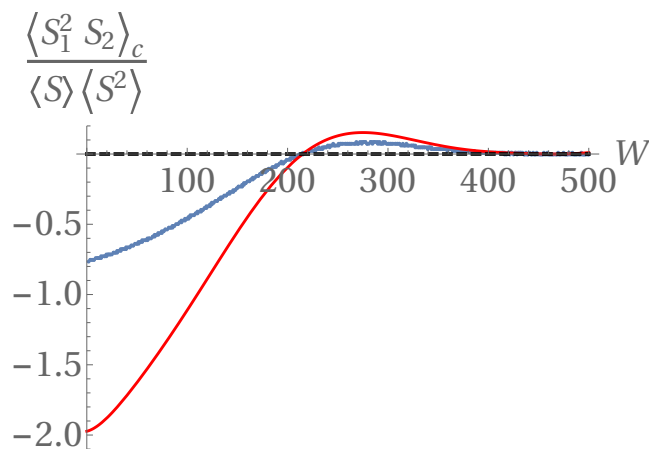


Figure C.5: Comparison between the measurement of the normalized moment $\frac{\langle S_1^2 S_2 \rangle_{\rho_W^c}}{\langle S^2 \rangle_{\rho} \langle S \rangle_{\rho}}$ (blue dots) and the prediction from the exact result (C.3.27) using the measurement of $\Delta(u)$ (red curve) in the RB toy model.

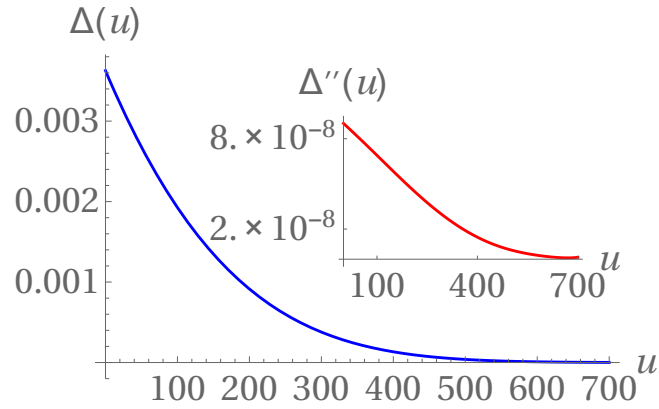


Figure C.6: Renormalized disorder $\Delta(u)$ measured in the $d = 0$ RF toy model. Inset: its second derivative $\Delta''(u)$, computed using a numerical fit of the measured $\Delta(u)$.

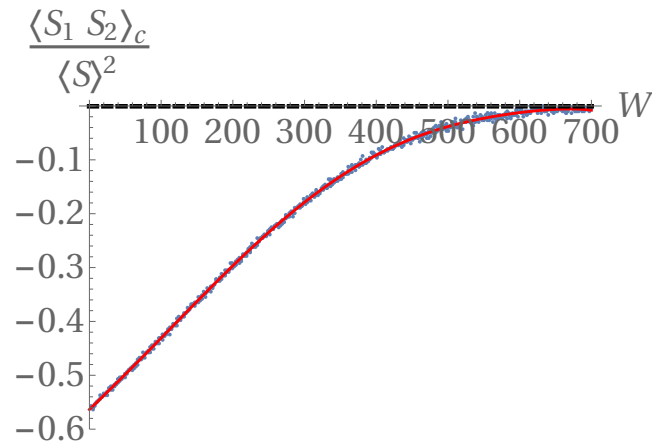


Figure C.7: Comparison between the measurement of the normalized moment $\frac{\langle S_1 S_2 \rangle_{\rho_W^c}}{\langle S \rangle_{\rho}^2}$ (blue dots) and the prediction from the exact result (C.3.27) using the measurement of $\Delta(u)$ (red curve) in the RF toy model. The agreement is perfect as expected.

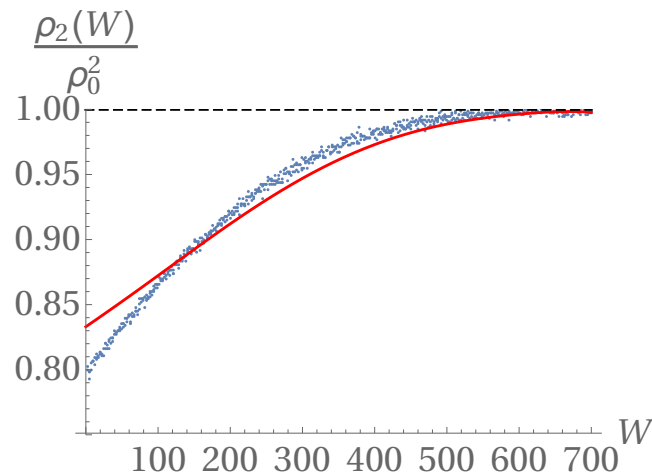


Figure C.8: Comparison between the measurement of $\rho_2(W)$ (blue dots) and the prediction from the $O(\epsilon)$ result (C.4.15) using the measurement of $\Delta(u)$ (red curve) in the RF toy model. The agreement is surprisingly good.

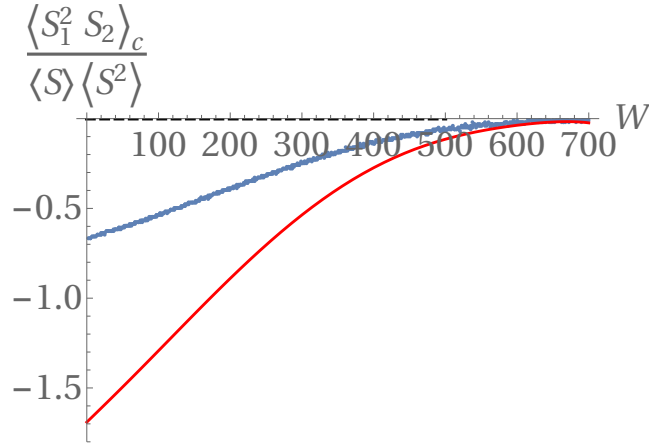


Figure C.9: Comparison between the measurement of the normalized moment $\frac{\langle S_1^2 S_2 \rangle_{\rho}^c}{\langle S^2 \rangle_{\rho} \langle S \rangle_{\rho}}$ (blue dots) and the prediction from the $O(\epsilon)$ result (C.3.27) using the measurement of $\Delta(u)$ (red curve) in the RF toy model.

considering the quasi-static steady-state process of the position field of the interface instead of the position of its ground-state as was done in Ref. [101]. For the results at the improved tree level, it is expected that both theories are equivalent for those observables [101]. The most important difference is that in the dynamics the Random-Bond universality class is unstable, and thus the observed correlations should always be of the Random-Field type (at least as long as the microscopic disorder is short-ranged).

For physical systems where the usual model of elastic interfaces is accurate, our results give a precise description of the correlations. Even if additional mechanisms generating correlations are present, such as in earthquake problems, correlations due to the short-ranged nature of the disorder as described in this work should be included in order to gain a quantitative understanding of the correlations due to these additional mechanisms.

acknowledgments We warmly thank Alexander Dobrinevski for numerous discussions. We acknowledge hospitality from the KITP in Santa Barbara where part of this work was conducted. This research was supported in part by the National Science Foundation under Grant No. NSF PHY11-25915. We acknowledge support from PSL grant ANR-10-IDEX-0001-02-PSL.

C.8 Appendix A: Proof of the identity on generating functions

As in the case of one shock (Appendix A of [109]), the important identity is

$$\begin{aligned} & (\partial_{\delta} + \lambda L^d) e^{\lambda L^d (u(w+\delta) - w - \delta)} = \\ & \sum_i (e^{\lambda S_i} - 1) e^{\lambda L^d [u(w_i^-) - w - \delta]} \delta(w + \delta - w_i) \end{aligned} \quad (\text{C.8.1})$$

By definition $u(w_i^-) = L^{-d} \sum_{j < i} S_j$. Let us consider

$$\begin{aligned} G_{w_1, w_2}(\delta_1, \delta_2) &= (\partial_{\delta_1} + \lambda_1 L^d)(\partial_{\delta_2} + \lambda_2 L^d) \times \\ & e^{\lambda_1 L^d [u(w_1 + \delta_1) - u(w_1) - \delta_1] + \lambda_2 L^d [u(w_2 + \delta_2) - u(w_2) - \delta_2]} \\ &= \sum_{ij} (e^{\lambda_1 S_i} - 1)(e^{\lambda_2 S_j} - 1) e^{\lambda_1 L^d [u(w_i^-) - u(w_1) - \delta_1]} \times \\ & e^{\lambda_2 L^d [u(w_j^-) - u(w_2) - \delta_2]} \delta(w_1 + \delta_1 - w_i) \delta(w_2 + \delta_2 - w_j) \end{aligned} \quad (\text{C.8.2})$$

Taking advantage of the Dirac δ -function, we can replace the $u(w_1)$ inside the exponential by $u(w_i - \delta_1)$ which unambiguously gives $u(w_i^-)$ when one takes the limit of $\delta_1 \rightarrow 0^+$. We thus obtain

$$\begin{aligned} \lim_{\delta_1, \delta_2 \rightarrow 0^+} G_{w_1, w_2}(\delta_1, \delta_2) &= \\ & \sum_{ij} (e^{\lambda_1 S_i} - 1)(e^{\lambda_2 S_j} - 1) \delta(w_1 - w_i) \delta(w_2 - w_j). \end{aligned} \quad (\text{C.8.3})$$

Taking the average over disorder, we obtain by definition of $Z_{w_2 - w_1}(\lambda_1, \lambda_2)$

$$Z_{w_2 - w_1}(\lambda_1, \lambda_2) = \lim_{\delta_1, \delta_2 \rightarrow 0^+} L^{-2d} \overline{G_{w_1, w_2}(\delta_1, \delta_2)}. \quad (\text{C.8.4})$$

On the other hand, developing $(\partial_{\delta_1} + \lambda_1 L^d)(\partial_{\delta_2} + \lambda_2 L^d) = \partial_{\delta_1} \partial_{\delta_2} + L^d \lambda_1 \partial_{\delta_2} + L^d \lambda_2 \partial_{\delta_1} + L^{2d} \lambda_1 \lambda_2$ in the expression of $G_{w_1, w_2}(\delta_1, \delta_2)$ one arrives at Eqs. (C.3.33) and (C.3.34).

C.9 Appendix B: A derivation from the Carraro-Duchon formula

Let us recall the results obtained in Ref. [111], generalizing to arbitrary dimension the result from Ref. [230]. Consider

$$e^{L^d \hat{Z}_t \{\omega_i, w_i\}} := e^{\frac{-L^d}{t} \sum_{i=1}^p \omega_i [u(w_i) - w_i]}, \quad (\text{C.9.1})$$

where $t := \frac{1}{m^2}$. Then, in the improved-tree theory, \hat{Z} solves the differential equation

$$\begin{aligned} \partial_t \hat{Z}_t \{\omega_i, w_i\} &= - \sum_{i=1}^p \frac{\partial}{\partial \omega_i} \hat{Z}_t \{\omega_i, w_i\} \frac{\partial}{\partial w_i} \hat{Z}_t \{\omega_i, w_i\} \\ \hat{Z}_{t=0} \{\omega_i, w_i\} &= \frac{1}{2} \sum_{i,j=1}^p \omega_i \omega_j \Delta(w_i - w_j). \end{aligned} \quad (\text{C.9.2})$$

It further satisfies the STS symmetry relation,

$$\begin{aligned} \hat{Z}_t \{\omega_i, w_i + \delta w\} &= \hat{Z}_t \{\omega_i, w_i\} \\ \sum_i \frac{\partial}{\partial w_i} \hat{Z}_t \{\omega_i, w_i\} &= 0. \end{aligned} \quad (\text{C.9.3})$$

In order to extract the needed information for the two-shock statistics we choose $p = 4$ and the quadruplets $(\omega_1, \omega_2, \omega_3, \omega_4) = (-\omega_1 - \tilde{\omega}, \omega_1, -\omega_2 + \tilde{\omega}, \omega_2)$ and $(w_1, w_2, w_3, w_4) = (0, \delta_1, W, W + \delta_2)$. We then consider (with a slight abuse of notations)

$$\begin{aligned} \tilde{Z}_t(\omega_1, \delta_1, \tilde{\omega}, W, \omega_2, \delta_2) \\ = \hat{Z}_t(-\omega_1 - \tilde{\omega}, 0, \omega_1, \delta_1, -\omega_2 + \tilde{\omega}, W, \omega_2, W + \delta_2) \end{aligned} \quad (\text{C.9.4})$$

Because of the STS the $p = 4$ function \tilde{Z}_t depends only on six variables (and not eight) and satisfies a closed equation. Indeed, using Eqs. (C.9.2) and (C.9.3), one proves that \tilde{Z}_t satisfies the following evolution equation

$$\partial_t \tilde{Z}_t = - \left(\frac{\partial}{\partial \omega_1} \tilde{Z}_t \frac{\partial}{\partial \delta_1} \tilde{Z}_t + \frac{\partial}{\partial \tilde{\omega}} \tilde{Z}_t \frac{\partial}{\partial W} \tilde{Z}_t + \frac{\partial}{\partial \omega_2} \tilde{Z}_t \frac{\partial}{\partial \delta_2} \tilde{Z}_t \right) \quad (\text{C.9.5})$$

We are only interested in a perturbative resolution. Define the expansion

$$\tilde{Z}_t = \sum_{mnp} z_{mnp}^p(t, \omega_1, \omega_2, W) \delta_1^m \delta_2^n \tilde{\omega}^p. \quad (\text{C.9.6})$$

Indeed, this is sufficient to retrieve the generating function $\hat{Z}_W(\lambda_1, \lambda_2) = \hat{Z}_W^{\text{disc}}(\lambda_1, \lambda_2) + \hat{Z}_W^c(\lambda_1, \lambda_2)$ as (compare with the small- δ_i expansion of (C.9.1) and (C.3.34))

$$\begin{aligned} \hat{Z}_W^{\text{disc}}(\lambda_1, \lambda_2) &= z_{10}^0(\omega_1, \omega_2, W) z_{01}^0(\omega_1, \omega_2, W) \\ \hat{Z}_W^c(\lambda_1, \lambda_2) &= L^{-d} z_{11}^0(\omega_1, \omega_2, W). \end{aligned} \quad (\text{C.9.7})$$

On the right-hand side the arguments are $\omega_1 = -t\lambda_1$ and $\omega_2 = -t\lambda_2$. Inserting the expansion (C.9.6) inside Eq. (C.9.5), we obtain the initial conditions:

$$\begin{aligned} z_{00}^0(t=0, \omega_1, \omega_2, W) &= 0 \\ z_{10}^0(t=0, \omega_1, \omega_2, W) &= -\Delta'(0^+) \omega_1^2 \\ z_{01}^0(t=0, \omega_1, \omega_2, W) &= -\Delta'(0^+) \omega_2^2 \\ z_{11}^0(t=0, \omega_1, \omega_2, W) &= -\Delta''(W) \omega_1 \omega_2 \\ z_{00}^1(t=0, \omega_1, \omega_2, W) &= 0. \end{aligned} \quad (\text{C.9.8})$$

Obviously we have $z_{00}^0(t, \omega_1, \omega_2, W) = 0, \forall t$. We also obtain the evolution equation:

$$\begin{aligned} \partial_t z_{10}^0 &= - \left(\frac{\partial}{\partial \omega_1} z_{10}^0 \right) z_{10}^0 - \left(\frac{\partial}{\partial \omega_2} z_{10}^0 \right) z_{01}^0 - z_{00}^1 \frac{\partial}{\partial W} z_{10}^0 \\ \partial_t z_{01}^0 &= - \left(\frac{\partial}{\partial \omega_1} z_{01}^0 \right) z_{10}^0 - \left(\frac{\partial}{\partial \omega_2} z_{01}^0 \right) z_{01}^0 - z_{00}^1 \frac{\partial}{\partial W} z_{01}^0 \\ \partial_t z_{11}^0 &= - \left(\frac{\partial}{\partial \omega_1} z_{11}^0 \right) z_{11}^0 - \left(\frac{\partial}{\partial \omega_1} z_{01}^0 \right) 2z_{20}^0 - \left(\frac{\partial}{\partial \omega_1} z_{11}^0 \right) z_{10}^0 \\ &\quad - \left(\frac{\partial}{\partial \omega_2} z_{11}^0 \right) 2z_{02}^0 - \left(\frac{\partial}{\partial \omega_2} z_{01}^0 \right) z_{11}^0 - \left(\frac{\partial}{\partial \omega_2} z_{11}^0 \right) z_{01}^0 \\ &\quad - z_{00}^1 \frac{\partial}{\partial W} z_{11}^0 - z_{10}^1 \frac{\partial}{\partial W} z_{01}^0 - z_{01}^1 \frac{\partial}{\partial W} z_{10}^0 \\ \partial_t z_{00}^1 &= - \left(\frac{\partial}{\partial \omega_1} z_{00}^1 \right) z_{10}^0 - \left(\frac{\partial}{\partial \omega_2} z_{00}^1 \right) z_{01}^0 - z_{00}^1 \frac{\partial}{\partial W} z_{00}^1 \end{aligned} \quad (\text{C.9.9})$$

As a consequence of the initial conditions (C.9.8), one can look for a solution of Eq. (C.9.9) such that

$$\frac{\partial}{\partial \omega_2} z_{10}^0 = \frac{\partial}{\partial \omega_1} z_{01}^0 = \frac{\partial}{\partial W} z_{10}^0 = \frac{\partial}{\partial W} z_{01}^0 = z_{00}^1 = 0. \quad (\text{C.9.10})$$

Each term has an interpretation in the notations of the main text. z_{10}^0 corresponds to $\hat{Z}(\lambda_1)$ and z_{01}^0 corresponds to $\hat{Z}(\lambda_2)$, which in the present notations reads (see Eqs. (C.3.30) and (C.3.45) and recall $S_m = \sigma/m^4 = \sigma t^2$)

$$z_{10}^0(\omega_i) = \hat{Z}(\lambda_i) = \frac{1 + 2\sigma\omega_i t - \sqrt{1 + 4\sigma\omega_i t}}{2\sigma t^2}. \quad (\text{C.9.11})$$

This is the solution of Eq. (C.9.9) using Eq. (C.9.10). Note that $z_{00}^1 = 0$ can be seen as the signature that diagrams contributing to the avalanche at $w = 0$ and at $w = W$ can be linked only by one vertex $\Delta''(W)$, as observed in the diagrammatics, see Eq. (C.4.9). This is already present in the initial condition (C.9.8). The equation for z_{11}^0 becomes

$$\begin{aligned} \partial_t z_{11}^0 &= -\left(\frac{\partial}{\partial \omega_1} z_{10}^0\right) z_{11}^0 - \left(\frac{\partial}{\partial \omega_1} z_{11}^0\right) z_{10}^0 \\ &\quad - \left(\frac{\partial}{\partial \omega_2} z_{01}^0\right) z_{11}^0 - \left(\frac{\partial}{\partial \omega_2} z_{11}^0\right) z_{01}^0. \end{aligned} \quad (\text{C.9.12})$$

One can check that the result (C.4.10) obtained diagrammatically in the main text, and which in the present notations reads

$$z_{11}^0 = -\frac{\Delta''(W)}{4\sigma^2 t^2} \frac{1 - \sqrt{1 + 4\sigma\omega_1 t}}{\sqrt{1 + 4\sigma\omega_1 t}} \frac{1 - \sqrt{1 + 4\sigma\omega_2 t}}{\sqrt{1 + 4\sigma\omega_2 t}},$$

solves this equation with the initial condition (C.9.8). This demonstrates the equivalence of the two methods and results.

C.10 Appendix C: Saddle-point calculation for the local structure.

C.10.1 Algebraic derivation of Eq. (C.5.17)

In this appendix we prove formula (C.5.17) “from first principles” using a saddle-point calculation on the improved action (C.3.44). This computation is similar to the one presented in Ref. [111] for the calculation of the one-shock density. Here the observable of interest is

$$\begin{aligned} \hat{Z}_W^{\phi^1 \phi^2}(\lambda_1, \lambda_2) &= \frac{1}{\int_x \phi_x^1 \int_x \phi_x^2} \lim_{\delta_1, \delta_2 \rightarrow 0^+} \partial_{\delta_1, \delta_2} G_W(\delta_1, \delta_2) \\ G_W(\delta_1, \delta_2) &= \frac{G_W(\delta_1, \delta_2)}{e^{\int_x \phi_x^1 \lambda_1 (\dot{u}_x(w_1 + \delta_1) - \dot{u}_x(w_1))} e^{\int_x \phi_x^2 \lambda_2 (\dot{u}_x(w_2 + \delta_2) - \dot{u}_x(w_2))}}, \end{aligned} \quad (\text{C.10.1})$$

where $w_2 = w_1 + W$. This observable can be expressed using the improved action $\Gamma[u]$ of the replicated field theory (C.3.44) with $i = 1, \dots, 4$ sets of $a = 1, \dots, n$ replicated position fields \tilde{u}_{ax}^i feeling a parabolic well at position \tilde{w}_i with $\tilde{w}_1 = w_1$, $\tilde{w}_2 = w_1 + \delta_1$, $\tilde{w}_3 = w_1 + W$, $\tilde{w}_4 = w_1 + W + \delta_2$:

$$G_W(\delta_1, \delta_2) = \int \mathcal{D}[u] e^{\int_x \sum_{i=1}^4 \nu_i \psi_x^i (u_{1x}^i - \tilde{w}_i) - \Gamma[u]} \quad (\text{C.10.2})$$

Here and for the rest of this appendix, the $n \rightarrow 0$ limit is implicit. To compute the disorder average we have singled out replica $a = 1$. In order to write the formulas in a compact form, we introduced new variables $\nu_2 = \lambda_1$, $\nu_1 = -\lambda_1$, $\nu_4 = \lambda_2$, $\nu_3 = -\lambda_2$, $\psi_x^1 = \psi_x^2 = \phi_x^1$, $\psi_x^3 = \psi_x^4 = \phi_x^2$. At the improved tree level, the functional integral is evaluated through a saddle-point calculation as

$$G_W(\delta_1, \delta_2) = e^{\int_x \sum_{i=1}^4 \nu_i \psi_x^i (u_{1x}^i - \tilde{w}_i) - \Gamma[u]}, \quad (\text{C.10.3})$$

where the position fields u_{ax}^i solve the saddle-point equation

$$\int_{x'} g_{xx'}^{-1}(u_{ax'}^i - \tilde{w}_i) - \frac{1}{T} \sum_{cj} R'(u_{ax}^i - u_{cx}^j) = T \nu_i \psi_x^i \delta_{a1}. \quad (\text{C.10.4})$$

We are interested in the solution of Eq. (C.10.4) in the $T \rightarrow 0$ limit. As in Ref. [111], we look for a solution that isolates the first replica ($a = 1$) in each set ($i = 1, \dots, 4$) of position fields as

$$u_{ax}^i = u_x^i - (1 - \delta_{a1}) T U_x^i. \quad (\text{C.10.5})$$

Inserting the Ansatz (C.10.5) into (C.10.4) leads to

$$\begin{aligned} \int_{x'} g_{xx'}^{-1}(u_{1x'}^i - \tilde{w}_i) + \sum_j R''(u_{1x}^i - u_{1x}^j) U_x^j &= 0 \\ \int_{x'} g_{xx'}^{-1} U_x^i + \sum_{j \neq i} R'''(u_{1x}^i - u_{1x}^j) U_x^i U_x^j &= \nu_i \psi_x^i. \end{aligned}$$

Being ultimately interested in the computation of (C.10.1), we solve this equation in an expansion in δ_1 and δ_2 as

$$\begin{aligned}
u_x^1 &= \frac{\tilde{w}_1 + \tilde{w}_2}{2} - u_x^{11} \delta_1 + u_x^{12} \delta_2 \\
u_x^2 &= \frac{\tilde{w}_1 + \tilde{w}_2}{2} + u_x^{21} \delta_1 + u_x^{22} \delta_2 \\
u_x^3 &= \frac{\tilde{w}_3 + \tilde{w}_4}{2} + u_x^{31} \delta_1 - u_x^{32} \delta_2 \\
u_x^4 &= \frac{\tilde{w}_3 + \tilde{w}_4}{2} + u_x^{41} \delta_1 + u_x^{42} \delta_2 \\
U_x^i &= U_x^{i0} + U_x^{i1} \delta_1 + U_x^{i2} \delta_2.
\end{aligned} \tag{C.10.6}$$

Using now the definition (C.10.1) we need to perform the following derivatives of (C.10.3), $\partial_{\delta_1} \partial_{\delta_2} = \partial_{\tilde{w}_2} \partial_{\tilde{w}_4}$. Since the fields u_{ax}^i are evaluated at the saddle point, we can differentiate only with respect to the explicit dependence in the \tilde{w}_i . Using the form (C.3.44) for $\Gamma[u]$, these derivatives can be calculated by repeating the identity

$$\partial_{\tilde{w}_i} G_W = \left(-\nu_i \int_x \psi_x^i + \frac{1}{T} \sum_{ai} \int_{xx'} g_{xx'}^{-1} (u_{ax'}^i - \tilde{w}_i) \right) G_W.$$

Using that $\lim_{n \rightarrow 0} \sum_a (u_{ax}^i - \tilde{w}_i) = T U_x^i$ we obtain the following decomposition

$$\hat{Z}_W^{\phi^1 \phi^2}(\lambda_1, \lambda_2) = \hat{Z}^{\phi^1}(\lambda_1) \hat{Z}^{\phi^2}(\lambda_2) + \hat{Z}_W^{c, \phi^1 \phi^2}(\lambda_1, \lambda_2) \tag{C.10.7}$$

with the explicit forms

$$\begin{aligned}
\hat{Z}^{\phi^1}(\lambda_1) &= \frac{\int_x (-\nu_2 \psi_x^2 + \int_{x'} g_{xx'}^{-1} U_{x'}^{20})}{\int_x \psi_x^2} \\
\hat{Z}^{\phi^2}(\lambda_2) &= \frac{\int_x (-\nu_4 \psi_x^4 + \int_{x'} g_{xx'}^{-1} U_{x'}^{40})}{\int_x \psi_x^4}
\end{aligned} \tag{C.10.8}$$

and

$$\begin{aligned}
\hat{Z}_W^{c, \phi^1 \phi^2}(\lambda_1, \lambda_2) &= \frac{1}{\int \psi_x^2 \int \psi_{x'}^4} \int_x \int_{x'} g_{xx'}^{-1} U_{x'}^{22} \\
&= \frac{1}{\int \psi_x^2 \int \psi_{x'}^4} \int_x \int_{x'} g_{xx'}^{-1} U_{x'}^{41}.
\end{aligned} \tag{C.10.9}$$

Although not obvious, these definitions are in agreement with those of the main text. Despite their complexity, the equations satisfied by the u and U variables obey several symmetries. The important ones are $U_x^{10} = -U_x^{20}$ and $U_x^{30} = -U_x^{40}$; $U_x^{11} = -U_x^{21}$ and $U_x^{32} = -U_x^{42}$; $U_x^{12} = -U_x^{22}$ and $U_x^{31} = -U_x^{41}$; $u_x^{11} = u_x^{21}$ and $u_x^{32} = u_x^{42}$; $u_x^{12} = u_x^{22}$ and $u_x^{31} = u_x^{41}$. We also have $U_x^{22} = U_x^{41}$.

Using these symmetries, one finds that U_x^{20} and U_x^{40} satisfy

$$\begin{aligned}
\int_{x'} g_{xx'}^{-1} U_{x'}^{20} &= \sigma (U_x^{20})^2 + \nu_2 \psi_x^2, \\
\int_{x'} g_{xx'}^{-1} U_{x'}^{40} &= \sigma (U_x^{40})^2 + \nu_4 \psi_x^4,
\end{aligned} \tag{C.10.10}$$

where $\sigma = R'''(0^+)$. Note that these are related to the function $Z_x^\phi(\lambda)$ defined in the main text in Eq. (C.5.6) through the relation $Z_x^{\phi^1}(\lambda_1) = \int_{x'} g_{xx'}^{-1} U_{x'}^{20}$. Hence, Eq. (C.10.8) leading to the disconnected part of the result for $\hat{Z}_W^{\phi^1 \phi^2}(\lambda_1, \lambda_2)$ is in agreement with the main text. Let us now introduce two important kernels defined as the functional derivatives $K_2(x, z) = \frac{\delta U_x^{20}}{\nu_2 \delta \psi_x^2}$ and $K_4(x, z) = \frac{\delta U_x^{40}}{\nu_4 \delta \psi_x^4}$. They satisfy

$$\begin{aligned}
\int_{x'} g_{xx'}^{-1} K_2(x', z) - 2\sigma U_x^{20} K_2(x, z) &= \delta(x - z) \\
\int_{x'} g_{xx'}^{-1} K_4(x', z) - 2\sigma U_x^{40} K_4(x, z) &= \delta(x - z)
\end{aligned}$$

and are important building blocks in our calculation. These kernels are symmetric: the kernel of the operator K_2^{-1} is given by $K_2^{-1}(x, x') = g_{xx'}^{-1} - 2\sigma U_{20x} \delta(x - x')$. In particular it is a symmetric function of its arguments, and thus $K_2(x, z)$ also is a symmetric function. The analytic expressions of the functions U_x^{20} and U_x^{40} are hard to obtain in generality. In Ref. [109] they were obtained for avalanches measured on hyperplanes for SR elasticity: $\psi_x^2 = \delta(x_1)$ where x_1 denotes the first coordinate of the d -dimensional variable x . We recall this explicit solution below in Appendix C.10.2.

a Solutions for the u variables

Let us first consider the solution for the u variables. The equations read

$$\begin{aligned}
\int_{x'} g_{xx'}^{-1} \left(\frac{1}{2} - u_{x'}^{11} \right) - 2\sigma U_x^{10} u_x^{11} &= 0 \\
\int_{x'} g_{xx'}^{-1} u_{x'}^{31} &= 2u_x^{11} U_x^{10} R'''(W) \\
\int_{x'} g_{xx'}^{-1} \left(\frac{1}{2} - u_{x'}^{32} \right) - 2\sigma U_x^{30} u_x^{32} &= 0 \\
\int_{x'} g_{xx'}^{-1} u_{x'}^{12} &= 2u_x^{32} U_x^{30} R'''(W)
\end{aligned} \tag{C.10.11}$$

The solutions are expressed in terms of the two kernels as

$$\begin{aligned}
u_x^{11} = u_x^{21} &= -\frac{\sigma}{R'''(W)} u_x^{31} + \frac{1}{2} = -\frac{\sigma}{R'''(W)} u_x^{41} + \frac{1}{2} \\
&= \frac{m^2}{2} \int_z K_2(x, z)
\end{aligned} \tag{C.10.12}$$

$$\begin{aligned}
u_x^{32} = u_x^{42} &= -\frac{\sigma}{R'''(W)} u_x^{12} + \frac{1}{2} = -\frac{\sigma}{R'''(W)} u_x^{22} + \frac{1}{2} \\
&= \frac{m^2}{2} \int_z K_4(x, z)
\end{aligned} \tag{C.10.13}$$

b Solutions for the U variables

For the U variables, the equations read

$$\begin{aligned}
\int_{x'} g_{xx'}^{-1} U_{x'}^{21} - 2\sigma U_x^{20} U_x^{21} - 2R^{(4)}(0) u_x^{11} (U_x^{20})^2 &= 0 \\
\int_{x'} g_{xx'}^{-1} U_{x'}^{42} - 2\sigma U_x^{40} U_x^{42} - 2R^{(4)}(0) u_x^{32} (U_x^{40})^2 &= 0 \\
\int_{x'} g_{xx'}^{-1} U_{x'}^{22} - 2\sigma U_x^{20} U_x^{22} - 2R^{(4)}(W) u_x^{32} U_x^{20} U_x^{40} &= 0 \\
\int_{x'} g_{xx'}^{-1} U_{x'}^{41} - 2\sigma U_x^{40} U_x^{41} - 2R^{(4)}(W) u_x^{11} U_x^{40} U_x^{20} &= 0
\end{aligned} \tag{C.10.14}$$

Its solutions are

$$\begin{aligned}
U_x^{11} &= -U_x^{21} = -2R^{(4)}(0) \int_z K_2(x, z) u_z^{11} (U_z^{20})^2 \\
U_x^{32} &= -U_x^{42} = -2R^{(4)}(0) \int_z K_2(x, z) u_z^{32} (U_z^{40})^2 \\
U_x^{12} &= -U_x^{22} = -2R^{(4)}(W) \int_z K_2(x, z) u_z^{32} U_z^{20} U_z^{40} \\
U_x^{31} &= -U_x^{41} = -2R^{(4)}(W) \int_z K_4(x, z) u_z^{11} U_z^{20} U_z^{40}
\end{aligned} \tag{C.10.15}$$

c Final result

Using Eq. (C.10.9) we obtain

$$\begin{aligned}
\hat{Z}_W^{c; \phi_1, \phi_2}(\lambda_1, \lambda_2) &= \\
&= \frac{1}{\int \psi_x^2 \int \psi_x^4} R^{(4)}(W) m^4 \int_{x', z, z'} K_2(x', z) U_z^{20} U_z^{40} K_4(z', z)
\end{aligned} \tag{C.10.16}$$

Using the above results $U_x^{20} = \int_{x'} g_{xx'} Z_{x'}^{\phi_1}(\lambda_1)$, and $U_x^{40} = \int_{x'} g_{xx'} Z_{x'}^{\phi_2}(\lambda_2)$, as well as $K_2(x, z) = \int_{x'} g_{xx'} \frac{\delta Z_{x'}^{\phi_1}(\lambda_1)}{\lambda_1 \delta \phi_z^1}$ and $K_4(x, z) = \int_{x'} g_{xx'} \frac{\delta Z_{x'}^{\phi_2}(\lambda_2)}{\lambda_2 \delta \phi_z^2}$; remembering that $\psi_x^2 = \phi_x^1$ and $\psi_x^4 = \phi_x^2$, one shows that this formula is equivalent to Eq. (C.5.17).

d Simplified form of the final result

The equivalent results (C.10.16) and (C.5.17) both involve a functional derivative, which is in general a rather complicated object. We can however obtain a simplified formulation. From Eq. (C.10.16) it is clear that it is sufficient to compute, for $i = 1, 2$,

$$\chi_i(x) = \int_z K_i(z, x) = \int_z K_i(x, z) \quad (\text{C.10.17})$$

rather than the full kernel K_i , and using the symmetry of K_i . Integrating Eq. (C.10.11) over z one shows that $\chi_i(x)$ solves the equation

$$\begin{aligned} \int_{x'} g_{xx'}^{-1} \chi_2(x') - 2\sigma U_x^{20} \chi_2(x) &= 1, \\ \int_{x'} g_{xx'}^{-1} \chi_4(x') - 2\sigma U_x^{40} \chi_4(x) &= 1. \end{aligned}$$

Solving these equations (a task a priori simpler than the computation of the functional derivative) then leads to, following (C.10.16),

$$\begin{aligned} \hat{Z}_W^{c;\phi_1,\phi_2}(\lambda_1, \lambda_2) & \\ &= -\frac{1}{\int \phi_x^1 \int \phi_x^2} \Delta''(W) m^4 \int_z \chi_2(z) U_z^{20} U_z^{40} \chi_4(z). \end{aligned} \quad (\text{C.10.18})$$

C.10.2 More explicit solution for avalanches measured on parallel hyperplanes

a Setting

We now obtain more explicit formulas in the case where avalanches are measured on two parallel hyperplanes at a distance $y > 0$ from one another and where the elasticity is short-ranged with kernel (C.3.2). That is, noting for definiteness x_1 the first coordinate of the d -dimensional vector x ,

$$\phi_x^1 = \delta(x_1) \quad , \quad \phi_x^2 = \delta(x_1 - y). \quad (\text{C.10.19})$$

In this case the problem becomes effectively unidimensional and the functions U and χ entering into Eq. (C.10.18) only depend on x_1 , abbreviated as x in the following. Furthermore, by translational invariance we can write

$$\begin{aligned} U_x^{20} &= Y(\lambda_1, x) \quad , \quad \chi_2(x) = \chi(\lambda_1, x) \\ U_x^{40} &= Y(\lambda_2, x - y) \quad , \quad \chi_4(x) = \chi(\lambda_2, x - y). \end{aligned} \quad (\text{C.10.20})$$

These quantities obey the equations

$$\begin{aligned} \left(-\frac{d^2}{dx^2} + m^2\right) Y(\lambda, x) - \sigma (Y(\lambda, x))^2 &= \lambda \delta(x) \\ \left(-\frac{d^2}{dx^2} + m^2\right) \chi(\lambda, x) - 2\sigma Y(\lambda, x) \chi(\lambda, x) &= 1. \end{aligned} \quad (\text{C.10.21})$$

Solving these equations then leads to

$$\begin{aligned} \hat{Z}_W^{c;\phi_1,\phi_2}(\lambda_1, \lambda_2) &= \frac{1}{L^{d-1}} R^{(4)}(W) m^4 \times \\ &\times \int_x \chi(\lambda_1, x) Y(\lambda_1, x) Y(\lambda_2, x - y) \chi(\lambda_2, x - y). \end{aligned} \quad (\text{C.10.22})$$

b Solution for Y

The solution $Y(\lambda, x)$ of equation (C.10.21) is already known in the literature, see Ref. [107] for details. It admits a scaling form

$$Y(\lambda, x) = \frac{m^2}{\sigma} \tilde{Y}\left(\frac{\sigma}{m^3} \lambda, mx\right), \quad (\text{C.10.23})$$

where $\tilde{Y}(\tilde{\lambda}, \tilde{x})$ solves

$$\left(-\frac{d^2}{d\tilde{x}^2} + 1\right) \tilde{Y}(\tilde{\lambda}, \tilde{x}) - (\tilde{Y}(\tilde{\lambda}, \tilde{x}))^2 = \tilde{\lambda} \delta(\tilde{x}). \quad (\text{C.10.24})$$

An explicit solution is

$$\tilde{Y}(\tilde{\lambda}, \tilde{x}) = \frac{6(1 - z^2)e^{-|\tilde{x}|}}{(1 + z + (1 - z)e^{-|\tilde{x}|})^2}, \quad (\text{C.10.25})$$

where $z(\tilde{\lambda})$ is one of the solutions of

$$\tilde{\lambda} = 3z(1 - z^2). \quad (\text{C.10.26})$$

The right solution is uniquely defined from the following properties: it is defined for $\tilde{\lambda} \in] -\infty, \tilde{\lambda}_c = 2/\sqrt{3}[$, decreases from $z(-\infty) = \infty$ to $z_c = z(\tilde{\lambda}_c) = 1/\sqrt{3}$ and approaches 1 as $\tilde{\lambda}$ approaches 0.

c Solution for χ

From the coupled equations (C.10.21), it is seen that $\chi(\lambda, x)$ can be deduced from $Y(\lambda, x)$ as

$$\chi(\lambda, x) = \frac{1}{m^2} - \frac{2\sigma}{m^2} \frac{\partial Y}{\partial m^2}. \quad (\text{C.10.27})$$

Using the scaling form (C.10.23) we obtain

$$\chi(\lambda, x) = \frac{1}{m^2} \tilde{\chi} \left(\tilde{\lambda} = \lambda \frac{\sigma}{m^3}, \tilde{x} = mx \right), \quad (\text{C.10.28})$$

where

$$\tilde{\chi} = 1 - 2\tilde{Y} + 3\tilde{\lambda}\partial_{\tilde{\lambda}}\tilde{Y} - 2\tilde{x}\partial_{\tilde{x}}\tilde{Y}. \quad (\text{C.10.29})$$

d Final scaling form

Combining Eqs. (C.10.22), (C.10.23) and (C.10.28) we can express our result in terms of a universal scaling function $\mathcal{Z}_{\tilde{w}}$ as (we scale $y = \tilde{y}/m$, $\lambda_i = \frac{m^3}{\sigma} \tilde{\lambda}_i$, $W = \tilde{w}/W_\mu$):

$$\begin{aligned} & \hat{Z}_{\tilde{w}/W_\mu}^{c; \phi_1, \phi_2} \left(\frac{m^3}{\sigma} \tilde{\lambda}_1, \frac{m^3}{\sigma} \tilde{\lambda}_2 \right) \\ &= \frac{1}{(Lm)^{d-1}} \frac{1}{(mS_m)^2} \times \hat{\mathcal{Z}}_{\tilde{w}}(\tilde{\lambda}_1, \tilde{\lambda}_2, \tilde{y}) \end{aligned} \quad (\text{C.10.30})$$

The quantities W_μ and S_m are as in Eq. (C.4.30) with here $\mu = m^2$ (SR elasticity) and

$$\begin{aligned} \mathcal{Z}_{\tilde{w}}(\tilde{\lambda}_1, \tilde{\lambda}_2, \tilde{y}) &= A_d \Delta^{*''}(\tilde{w}) \times \\ & \int_{\tilde{x}} \tilde{\chi}(\tilde{\lambda}_1, \tilde{x}) \tilde{Y}(\tilde{\lambda}_1, \tilde{x}) \tilde{Y}(\tilde{\lambda}_2, \tilde{x} - \tilde{y}) \tilde{\chi}(\tilde{\lambda}_2, \tilde{x} - \tilde{y}), \end{aligned} \quad (\text{C.10.31})$$

where \tilde{Y} and $\tilde{\chi}$ are explicit functions given in Eqs. (C.10.25) and (C.10.29). This is our final result; its explicit evaluation is left for the future.

C.11 Appendix D: First moment to one-loop order

In this appendix we give the result for $\langle S_1^2 S_2 \rangle_{\rho_W^c}$ to one-loop accuracy for short-ranged elasticity. Note that since the formula (C.3.27) is exact, it does not receive higher-loop contributions and the first improvement brought to moments of ρ_W^c is for $\langle S_1^2 S_2 \rangle_{\rho_W^c}$. The latter can be obtained from the known formulas (61) and (118) of Ref. [109],

$$\begin{aligned} \hat{C}^{(3)}(w_1, w_2, w_3) &= -\frac{6}{m^2} \text{sym}_{123} \left\{ \Delta'(w_{12}) \Delta(w_{13}) \right\} \\ & - 6I_3 \text{sym}_{123} \left\{ \Delta'(w_{12})^2 \Delta'(w_{13}) + [\Delta(w_{12}) - \Delta(0)] [\Delta'(w_{13}) \Delta''(w_{12}) + \Delta'(w_{12}) \Delta''(w_{13}) \Delta'(w_{23}) \Delta''(w_{13})] \right\}. \end{aligned} \quad (\text{C.11.1})$$

The first line corresponds to the improved tree approximation, sym_{123} denotes the symmetrization over the w_i variables, $I_3 = \int_k \frac{1}{(k^2 + m^2)^3}$, and we have use the shorthand notation $w_{ij} := w_i - w_j$. As explained in the text, this formula is sufficient to obtain $\langle S_1^2 S_2 \rangle_{\rho_W^c}$ using the \mathcal{K} operation. The final result reads

$$L^{-2d} \langle S_1^2 S_2 \rangle_{\rho_W^c} = -6S_m - 4I_3 \frac{S_m}{L^d m^2} \left[\Delta''(0) \Delta''(W) + 3\Delta''(W)^2 + 3\Delta'(W) \Delta'''(W) \right] + O(\epsilon^3). \quad (\text{C.11.2})$$

Appendix D

Paper: Log-Gamma directed polymer with fixed endpoints via the replica Bethe Ansatz

The following is essentially the article published as

Title: Log-Gamma directed polymer with fixed endpoints via the replica Bethe Ansatz

Authors: Thimothée Thiery and Pierre Le Doussal

ArXiv: 1406.5963

Journal-Ref: Journal of Statistical Mechanics: Theory and Experiment, Volume 2014, October 2014

Abstract: We study the model of a discrete directed polymer (DP) on the square lattice with homogeneous inverse gamma distribution of site random Boltzmann weights, introduced by Seppalainen [197]. The integer moments of the partition sum, \overline{Z}^n , are studied using a transfer matrix formulation, which appears as a generalization of the Lieb-Liniger quantum mechanics of bosons to discrete time and space. In the present case of the inverse gamma distribution the model is integrable in terms of a coordinate Bethe Ansatz, as discovered by Brunet. Using the Brunet-Bethe eigenstates we obtain an exact expression for the integer moments of \overline{Z}^n for polymers of arbitrary lengths and fixed endpoint positions. Although these moments do not exist for all integer n , we are nevertheless able to construct a generating function which reproduces all existing integer moments, and which takes the form of a Fredholm determinant (FD). This suggests an analytic continuation via a Mellin-Barnes transform and we thereby propose a FD ansatz representation for the probability distribution function (PDF) of Z and its Laplace transform. In the limit of very long DP, this ansatz yields that the distribution of the free energy converges to the Gaussian unitary ensemble (GUE) Tracy-Widom distribution up to a non-trivial average and variance that we calculate. Our asymptotic predictions coincide with a result by Borodin et al. [218] based on a formula obtained by Corwin et al. [198] using the geometric Robinson-Schensted-Knuth (gRSK) correspondence. In addition we obtain the dependence on the endpoint position and the exact elastic coefficient at large time. We argue the equivalence between our formula and the one of Borodin et al. As we discuss, this provides connections between quantum integrability and tropical combinatorics.

D.1 Introduction

Recently it was realized that methods of integrability in quantum systems could be used to obtain exact solutions for the one dimensional continuum Kardar-Parisi-Zhang equation (KPZ). The KPZ equation [33] is a paradigmatic model for 1D noisy growth processes, encompassing a vast universality class of discrete growth or equivalent models (the so-called KPZ class). The probability distribution function (PDF) of the KPZ height field h at time t was obtained (at one, or several space points) and shown to converge at large t to the universal Tracy-Widom (TW) distributions [37] for the largest eigenvalues of large Gaussian random matrices.

One route, entirely within continuum models, is to use the Cole-Hopf mapping onto the problem of the directed polymer, $h \sim \ln Z$, where h is the height of the KPZ interface, and Z the partition sum (in the statistical mechanics sense) of continuum directed paths in presence of quenched disorder. Using the replica method, the time evolution of the moments \overline{Z}^n maps [201] onto the (imaginary time) quantum evolution of bosons with attractive interactions, the so-called Lieb-Liniger model [202]. This model is integrable via the Bethe Ansatz, which ultimately yields exact expressions for the integer moments \overline{Z}^n of $P(Z)$, the PDF of Z . Although recovering from there the PDF of the KPZ height field requires the use of some heuristics (since the moments actually grow too fast to ensure uniqueness), this method allowed to obtain the Laplace transform of $P(Z)$ (also called generating function) for all the important classes of KPZ initial conditions (droplet, flat, stationary, half-space) [173, 165, 177, 183, 169, 215, 175, 214]. Interestingly, in all the solvable cases, it was obtained as a Fredholm determinant, with various kernels and valid for all times t . Let us also mention the recently observed connection between the continuum model and the sine-Gordon quantum field theory [242].

Another route is to study appropriate discrete models, which, in some limit, reproduce the continuum result. This route is favored in the mathematics community since it does not suffer, in the favorable cases, from the moment problem. In [172, 171, 34], the solution for the continuum KPZ equation with droplet initial conditions was obtained as the weak asymmetry limit of the ASEP. Another integrable discrete model, the q -TASEP, also exhibits such a limit for $q \rightarrow 1$, and

was shown to be part of a broader integrability structure related to Macdonald processes. This allows for rigorous extensions to the other class of KPZ initial conditions, which are under intense current scrutiny [192, 208, 243, 180].

Among the solvable discrete models, are the discrete and semi-discrete directed polymer models. The model studied by Johansson in [159] considers a DP on a square lattice with a geometric distribution of the on-site random potentials, and allows for an exact solution. It is a zero temperature DP model since it focuses on the path with minimal energy (energy being additive along a path), as in the last passage percolation models. Another remarkable solvable model is called the log-gamma polymer and was introduced by Seppalainen [197]. It is a finite temperature model as it focuses on Boltzmann weights (which are multiplicative along a path). Its peculiarity is that the random weights on the sites are distributed according to a so-called inverse gamma distribution, which has a power law fat tail. Such a choice for the quenched disorder leads to remarkable properties: an exact expression for the Laplace transform of $P(Z)$ (the generating function) was obtained by Corwin et al. in [198]. The method is quite involved and uses combinatorics methods known as the gRSK correspondence (a geometric lifting of the Robinson-Schensted-Knuth (RSK) correspondence) also called tropical combinatorics. These involve properties of the $GL(N, R)$ Whittaker functions, which are generalizations of Bessel functions. Later, it was shown by Borodin et al. [218] that this generating function takes the form of a Fredholm determinant. This form allowed them to perform an asymptotic analysis for long DP and to prove again convergence of the PDF of the free energy to the GUE Tracy-Widom distribution. Finally, the O Connel-Yor model of the semi-discrete polymer [191], which leads to an exactly solvable hierarchy, can be obtained as a limit of the log-gamma polymer [198]. It would be of great interest to extend the Bethe Ansatz replica method to the discrete models. Recently, it was discovered by Brunet [244] that eigenfunctions of the replica transfer matrix of the log-gamma polymer on the square lattice can be constructed using a lattice version of the Bethe ansatz. The present paper aims at studying these eigenfunctions, and from them to calculate the generating function for the integer moments $\overline{Z^n}$ of the partition sum of the log-gamma polymer. Here we treat the case of fixed endpoints. The generating function is found to take the form of a Fredholm determinant for all polymer lengths.

This goal may appear hopeless at first sight, since the integer moments $\overline{Z^n}$ cease to exist for $n \geq \gamma$ where γ is the parameter of the model and the exponent of the power law fat tail. However, our generating function reproduces all existing integer moments. Furthermore, it suggests an analytic continuation, inspired from Mellin-Barnes identities, which leads us to a conjecture for the Laplace transform of $P(Z)$ in the form a Fredholm determinant, with an (analytically continued) kernel. We use it to obtain the asymptotic behavior of the PDF of the free energy $\ln Z$ at large polymer lengths. In the limit of a very long DP, it yields convergence to the GUE Tracy-Widom distribution up to non-trivial average and variance that we calculate. Our asymptotic predictions coincide with the result of Borodin et al. [218] obtained by completely different methods (using the formula obtained in [198]). In addition, we obtain the dependence in the end-point position on the lattice, e.g. the exact elastic coefficient at large times. We perform some numerical checks of these results.

A more ambitious goal is then to show that the kernel obtained here is equivalent to the one obtained in Borodin et al. [218]. Most steps of the correspondence are achieved and detailed here. However, the last step involves the use of heuristics, although we present some hints that it is correct.

Of course, as we show, our results also reproduce the ones of the continuum model, both at the level of the Bethe-Ansatz (the Lieb-Linger model) and of the final result, i.e. our kernel reproduces the finite time kernel for the corresponding KPZ/DP continuum model [173, 165]. In yet another limit it also provides a Bethe Ansatz solution to the semi-discrete polymer problem [191].

In general, the present work opens the way to explore the connections between quantum integrability and tropical combinatorics.

The outline of the paper is as follows. In Section D.2 we recall the log-Gamma DP problem introduced by Seppalainen and introduce some useful notations. In Section D.3 we present the ansatz discovered by Brunet. In Section D.4 we detail how this ansatz can be used to recursively compute the integer moments $\overline{Z^n}$, in particular we identify the weighted scalar product that makes the Brunet states orthogonal and (presumably) complete. In Section D.5 we identify a scaling limit that relates the continuum model to the discrete one studied here. In Section D.6 we conjecture a formula for the norm of the Brunet functions that generalizes the Gaudin formula. In Section D.7 we show how the Bethe-Brunet equations are solved in the "thermodynamic" limit. This allows us to find in Section D.8 an explicit formula for $\overline{Z^n}$. In Section D.9 we perform an analytic continuation leading to a conjecture for the Laplace transform of the PDF of Z , as well as a formula for the PDF at fixed length. This is used in Section D.10 to explicitly show the KPZ universality class and convergence of the fluctuations of $\log Z$ to the Tracy-Widom GUE distribution. In Section D.11 we compare our results to those obtained in [218]. Section D.12 summarizes the main conclusions of the paper, and a series of Appendices present some conceptual discussions and technical details.

D.2 Model

D.2.1 Model

The log-Gamma directed polymer (DP) introduced by Seppalainen [197] is defined as follows. Consider the square lattice $(i, j) \in \mathbb{Z}^2$ and the set of directed up-right paths (directed polymers) from $(1, 1)$ to (I, J) . To emphasize the directed nature of the problem, we define (x, t) , with each coordinate running through one diagonal of the square lattice (see Fig. D.1):

$$t = i + j - 2 \quad , \quad x = \frac{i - j}{2} \tag{D.2.1}$$

so that the x (space) coordinate of the points on a line with t (time) even (resp. odd) are integers (resp. half integers). With this definition a directed path contains only jumps from (x, t) to $(x + \frac{1}{2}, t + 1)$ or $(x - \frac{1}{2}, t + 1)$. We define $Z_t(x)$ the

(finite temperature) partition sum of the directed paths from $(0, 0)$ to (x, t) :

$$Z_t(x) = \sum_{\pi: (0,0) \rightarrow (x,t)} \prod_{(x',t') \in \pi} w_{x',t'} \quad (\text{D.2.2})$$

in terms of the Boltzmann weights $w_{x,t} = e^{-V_{x,t}}$ defined on the site of the lattice (the temperature is set to unity). In the simplest (i.e. homogeneous) version of the log-Gamma DP model the $w_{x,t}$ are i.i.d. random variables distributed according to the inverse-Gamma distribution:

$$P(w)dw = \frac{1}{\Gamma(\gamma)} w^{-1-\gamma} e^{-1/w} dw \quad (\text{D.2.3})$$

with parameter $\gamma > 0$. In the following $\overline{(\cdot)}$ denotes the average over $w_{x,t}$ ("disorder average").

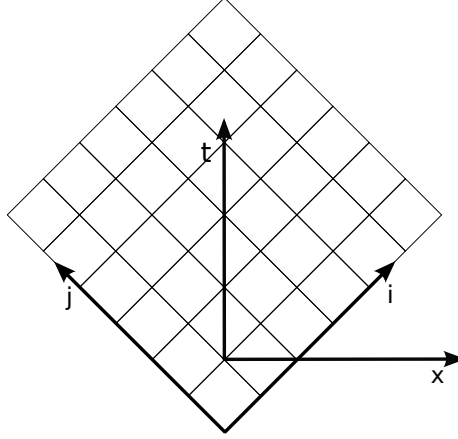


Figure D.1: The two coordinate systems for the square lattice, see (D.2.1). The starting point of the path is $(i = 1, j = 1)$, which corresponds to the origin $(0, 0)$ in the (x, t) coordinates.

Our goal is to calculate the PDF of (minus) the free energy, $\ln Z_t(x)$, equivalently $P(Z_t(x))$. In the spirit of the recent works on the replica Bethe Ansatz approach to the continuum directed polymer, we start by calculating the integer moments $\overline{Z_t(x)^n}$ with $n \in \mathbb{N}$. Clearly these moments do not exist for $n \geq \gamma$, as can be seen already ¹ from the one-site problem $Z_0(0) = w_{0,0} = w$ whose moments are:

$$\overline{w^n} = \frac{\Gamma(\gamma - n)}{\Gamma(\gamma)} \quad (\text{D.2.4})$$

for $n < \gamma$, and diverge for $n \geq \gamma$. This makes a priori the problem of the log-Gamma polymer more difficult to study using replica. However, note that (D.2.4) is valid more generally for $\text{Re}(n) < \gamma$ and possesses a simple analytic continuation to the complex n plane (minus the poles) via the Γ function as given in (D.2.4). For this example, and for more general ones, we show in D.13 how to obtain the Laplace transform e^{-uw} from the integer moments (D.2.4).

This gives some hope to calculate the Laplace transform of $P(Z_t(x))$ with the sole knowledge of its integer moments, via an analytic continuation, in the spirit of D.13. The moment problem was a challenge for the case of the continuum directed polymer due to the too rapid growth of the moments $\overline{Z^n} \sim e^{n^3 t}$. Here, the difficulty is the existence of poles in the moments, however the situation for the analytic continuation appears more favorable.

D.2.2 Rescaled Potential

From now on we restrict ourselves to $\gamma > 1$ and for convenience we normalize the weights so that their first moment is unity. We thus define:

$$w = \frac{1}{\gamma - 1} \tilde{w} = e^{-V} \quad , \quad V = \tilde{V} + V_0 \quad , \quad e^{-V_0} = \frac{1}{\gamma - 1}$$

such that the integer moments become:

$$h_n = \overline{e^{-n\tilde{V}}} = \frac{(\gamma - 1)^n}{(\gamma - 1) \dots (\gamma - n)} = \prod_{k=0}^{n-1} \frac{4}{4 - k\bar{c}} \quad (\text{D.2.5})$$

where we introduced the interaction parameter:

$$\bar{c} = \frac{4}{\gamma - 1} > 0. \quad (\text{D.2.6})$$

In particular, $h_0 = h_1 = 1$.

¹ $Z_t(x)$ always contains the statistically independent factors $w_{0,0}$ and $w_{x,t}$, corresponding to the endpoints.

D.3 Evolution equation and Brunet Bethe ansatz

D.3.1 Evolution equation

The partition sum of the directed polymer defined by (D.2.2) can be calculated recursively as:

$$Z_{t+1}(x) = e^{-V_{x,t}} \left(Z_t(x - \frac{1}{2}) + Z_t(x + \frac{1}{2}) \right) \quad , \quad Z_0(x) = e^{-V_{0,0}} \delta_{x,0} \quad (\text{D.3.1})$$

The moments of the partition sum are conveniently encoded in the "wavefunction" ψ , defined on \mathbb{Z}^n (for t even) and $(\mathbb{Z} + \frac{1}{2})^n$ (for t odd) as

$$\psi_t(x_1, \dots, x_n) = 2^{-nt} e^{V_{0n}(t+1)} \overline{Z_t(x_1) \cdots Z_t(x_n)} \quad (\text{D.3.2})$$

which satisfies the evolution equation

$$\psi_{t+1}(x_1, \dots, x_n) = \frac{1}{2^n} a_{x_1, \dots, x_n} \sum_{(\delta_1, \dots, \delta_n) \in \{-\frac{1}{2}, \frac{1}{2}\}^n} \psi_t(x_1 - \delta_1, \dots, x_n - \delta_n) \quad (\text{D.3.3})$$

where we note:

$$a_{x_1, \dots, x_n} = e^{-\sum_{\alpha=1}^n \tilde{V}_{x_\alpha, t+1}} = \prod_x h_{\sum_{\alpha=1}^n \delta_{x, x_\alpha}} \quad (\text{D.3.4})$$

and h_n defined as in (D.2.5).

D.3.2 Bethe-Brunet Ansatz

Consider the eigenvalue problem:

$$\psi_\mu(x_1, \dots, x_n) = \theta_\mu \frac{1}{2^n} a_{x_1, \dots, x_n} \sum_{(\delta_1, \dots, \delta_n) \in \{-\frac{1}{2}, \frac{1}{2}\}^n} \psi_\mu(x_1 - \delta_1, \dots, x_n - \delta_n) \quad (\text{D.3.5})$$

It was found by Brunet [244] that fully-symmetric solutions ψ_μ of (D.3.5) can be obtained as superpositions of plane waves in a form that generalizes the usual Bethe Ansatz:

$$\psi_\mu(x_1, \dots, x_n) = \sum_{\sigma \in \mathcal{S}_n} A_\sigma \prod_{\alpha=1}^n z_{\sigma(\alpha)}^{x_\alpha} \quad , \quad A_\sigma = \prod_{1 \leq \alpha < \beta \leq n} \left(1 + \frac{\bar{c}}{2} \frac{\text{sgn}(x_\beta - x_\alpha + 0^+)}{t_{\sigma(\alpha)} - t_{\sigma(\beta)}} \right) \quad (\text{D.3.6})$$

with

$$z_\alpha = e^{i\lambda_\alpha} \quad , \quad t_\alpha = i \tan\left(\frac{\lambda_\alpha}{2}\right) = \frac{z_\alpha - 1}{z_\alpha + 1} \quad (\text{D.3.7})$$

These solutions ψ_μ are parametrized by a set of (distinct) complex variables $\{z_1, \dots, z_n\}$. It is convenient to parametrize the z_α in terms of variables λ_α as above, with $-\pi < \text{Re}(\lambda_\alpha) \leq \pi$, which we call rapidities by analogy with the continuum case (see discussion below). The eigenvalue associated with ψ_μ is then given by: ²

$$\theta_\mu = \prod_{i=1}^n z_\alpha^{\frac{1}{2}} \frac{1 + z_\alpha^{-1}}{2} \quad (\text{D.3.8})$$

The property (D.3.5) is easily checked for all x_α distinct, in which case it is similar to the continuum case [202, 210]. The case where there are two coinciding x_α is reminiscent of the matching condition of the continuum case. Verifying the property (D.3.5) for an arbitrary number of coinciding points is non-trivial, and is found to work *only* when the h_n in (D.3.4) have values precisely given by (D.2.5) [244]. Hence this integrability property is a special property of the inverse Gamma distribution ³. Until now the possible values of the z_α remain unspecified. As an intermediate stage in our calculation we impose here for convenience periodic boundary conditions $\psi(x_1, \dots, x_\alpha + L, \dots, x_n) = \psi(x_1, \dots, x_n)$, $\alpha = 1, \dots, n$, i.e. a system of finite number of sites L . This can be satisfied if the rapidities satisfy the generalized Bethe equation [244]:

$$e^{i\lambda_\alpha L} = \prod_{1 \leq \beta \leq n, \beta \neq \alpha} \frac{2t_\alpha - 2t_\beta + \bar{c}}{2t_\alpha - 2t_\beta - \bar{c}} = \prod_{1 \leq \beta \leq n, \beta \neq \alpha} \frac{2 \tan(\frac{\lambda_\alpha}{2}) - 2 \tan(\frac{\lambda_\beta}{2}) - i\bar{c}}{2 \tan(\frac{\lambda_\alpha}{2}) - 2 \tan(\frac{\lambda_\beta}{2}) + i\bar{c}} \quad (\text{D.3.9})$$

for $\alpha = 1, \dots, n$, which are derived exactly as in the continuum case.

²the first factor $\prod_{\alpha=1}^n z_\alpha^{\frac{1}{2}}$ was absent in Brunet's formula due to a different choice of coordinates $x' = x + t/2$.

³there are other solvable cases, by different methods, such as zero temperature model of [159], solved in terms of a determinantal process related to free fermions.

D.4 Time evolution of the moments, symmetric transfer matrix

D.4.1 Symmetric transfer matrix and scalar product

In this section we motivate the introduction of a peculiar weighted scalar product, for which the Brunet functions form an orthogonal set. The Brunet functions diagonalize the evolution equation (D.3.3), which is not encoded by a symmetric transfer operator since the variable a_{x_1, \dots, x_n} depends only on the arrival point. This can be traced to the recursion (D.3.1), which counts the contribution of the disorder only at the points on the line at $t + 1$. Hence the Brunet functions have no reason to form an orthogonal set for the canonical scalar product, and we indeed find that they do not. On the other hand, if we consider the change of function $\tilde{\psi}(x_1, \dots, x_n) = \frac{1}{\sqrt{a_{x_1, \dots, x_n}}} \psi(x_1, \dots, x_n)$, (D.3.3) now reads

$$\tilde{\psi}_{t+1}(x_1, \dots, x_n) = \sqrt{a_{x_1, \dots, x_n}} \sum_{(\delta_1, \dots, \delta_n) \in \{-\frac{1}{2}, \frac{1}{2}\}^n} \sqrt{a_{x_1 - \delta_1, \dots, x_n - \delta_n}} \tilde{\psi}_t(x_1 - \delta_1, \dots, x_n - \delta_n) \quad (\text{D.4.1})$$

The disorder now appears in a symmetric way, and the transformed Brunet functions $\tilde{\psi}_\mu$ naturally appear as eigenvectors of an Hermitian transfer operator, with the same eigenvalue θ_μ as before. This shows that $\theta_\mu \in \mathbb{R}$. Since (D.4.1) involves the evaluation of a function both at integer coordinates and half-odd integer coordinates, this operator acts on the function defined on $\mathbb{Z}^n \oplus (\mathbb{Z} + \frac{1}{2})^n$. It appears more convenient to consider the evolution equation that links t and $t + 2$: this defines the transfer matrix T_n :

$$\tilde{\psi}_{t+2} = T_n \tilde{\psi}_t \quad (\text{D.4.2})$$

which is thus naturally defined as an Hermitian operator on $L^2(\mathbb{Z}^n)$, and for which the Brunet states $\tilde{\psi}_\mu$ are eigenvectors with eigenvalues $e^{-2E_\mu} = \theta_\mu^2 > 0$

$$\theta_\mu^2 = e^{-2E_\mu} = \prod_{\alpha=1}^n \frac{z_\alpha + 2 + z_\alpha^{-1}}{4} = \prod_{\alpha=1}^n \frac{1}{1 - t_\alpha^2} \quad (\text{D.4.3})$$

where the last equation is an equivalent form, using that $z_\alpha = (1 + t_\alpha)/(1 - t_\alpha)$.

To be more precise, we have chosen to work with periodic boundary conditions and we thus consider T_n as an operator that acts on the function defined on $\{0, \dots, L - 1\}^n$, which has dimension L^n . This is only a convenient choice and should have no effect on the results for the case of interest here, i.e. a polymer with a fixed starting point, as long as we consider $t < L$: in this case the polymer does not ever feel the boundary. In the end we will consider the limit $L \rightarrow \infty$ at fixed t , so that the polymer never feels the boundary.

Going back to the original wavefunctions, the above construction partially justifies the claim that the original Brunet states $\{\psi_\mu\}$ given in (D.3.6) form a *complete* basis of the symmetric functions on $\{0, \dots, L - 1\}^n$, and that it is *orthogonal* with respect to the following weighted scalar product

$$\langle \phi, \psi \rangle = \sum_{(x_1, \dots, x_n) \in \{0, \dots, L-1\}^n} \frac{1}{a_{x_1, \dots, x_n}} \phi^*(x_1, \dots, x_n) \psi(x_1, \dots, x_n) \quad (\text{D.4.4})$$

We have not attempted to provide a general proof of this statement (a usually challenging goal when dealing with Bethe Ansatz), however we did explicitly check it for various low values of (L, n) . We will thus proceed by assuming that it is correct.

1 We conclude this section with a minor remark on a special case: if there is a solution of the Brunet equation with $z_i = -1$, then $e^{-2E_\mu} = 0$ and the Brunet state is ill-defined. In fact, it is easy to see that $T\psi_\mu = 0$ if and only if $M\psi_\mu = 0$ with M the transfer matrix without disorder, which can be diagonalized using plane waves. Hence to have a well-defined complete basis, one has to complete the Brunet states with the symmetric plane waves with vanishing eigenvalues that exist when L is even. These additional states do not play any role in the following (since they correspond to zero eigenvalues) but they are important to assess the validity of the completeness property.

D.4.2 Time-evolution of the moments

This formalism allows us to give a simple expression for the moments with arbitrary endpoints:

$$\overline{Z_t(x_1) \cdots Z_t(x_n)} = 2^{nt} \left(\frac{\bar{c}}{4}\right)^{n(t+1)} \psi_t(x_1, \dots, x_n) \quad (\text{D.4.5})$$

Since the Brunet states form a complete basis of the symmetric functions on $\{0, \dots, L - 1\}^n$, which are orthogonal with respect to the scalar product (D.4.4) and since the initial condition

$$\psi_0(x_1, \dots, x_n) = h_n \prod_{\alpha=1}^n \delta_{x_\alpha, 0} \quad (\text{D.4.6})$$

is symmetric in position space, one can write the decomposition of the initial condition on the Brunet-Bethe states as:

$$\psi_0 = \sum_{\mu} \frac{\langle \psi_\mu, \psi_0 \rangle}{\|\psi_\mu\|^2} \psi_\mu = \sum_{\mu} \frac{n!}{\|\psi_\mu\|^2} \psi_\mu \quad (\text{D.4.7})$$

using the explicit expression (D.3.6) for the (un-normalized) eigenstates. The simple iteration of the evolution equation (D.3.3) directly leads to, for all $t \in \mathbb{N}$:

$$\psi_t = \sum_{\mu} \frac{n!}{\|\psi_{\mu}\|^2} (\theta_{\mu})^t \psi_{\mu} \quad (\text{D.4.8})$$

and thus

$$\overline{Z_t(x_1) \cdots Z_t(x_n)} = 2^{nt} \left(\frac{\bar{c}}{4}\right)^{n(t+1)} \sum_{\mu} \frac{n!}{\|\psi_{\mu}\|^2} (\theta_{\mu})^t \psi_{\mu}(x_1, \dots, x_n) \quad (\text{D.4.9})$$

Using that:

$$\psi_{\mu}(x, \dots, x) = n! \left(\prod_{\alpha=1}^n z_{\alpha} \right)^x \quad (\text{D.4.10})$$

for any eigenstate μ given by (D.3.6), we finally obtain the integer moment of the DP with fixed starting point at $(0, 0)$ and endpoint at (x, t) as:

$$\overline{Z_t(x)^n} = 2^{nt} \left(\frac{\bar{c}}{4}\right)^{n(t+1)} \sum_{\mu} \frac{(n!)^2}{\|\psi_{\mu}\|^2} (\theta_{\mu})^t \left(\prod_{\alpha=1}^n z_{\alpha} \right)^x \quad (\text{D.4.11})$$

where we recall θ_{μ} to be given by (D.3.8). Hence the only remaining unknown quantities here are the norm of the Brunet states, and we will now calculate them in the infinite size limit $L \rightarrow \infty$.

Before we do so, let us indicate how the present discrete model recovers the continuum model in some limit, in particular how the discrete space-time quantum mechanics recovers the standard continuum one.

D.5 The continuum/Lieb-Liniger limit

It is interesting to note that the Brunet equations (D.3.9) and the form of the eigenfunctions (D.3.6) tend to those of the Lieb-Liniger model (LL) as given by the standard Bethe ansatz solution if one takes the limit of small λ_i and \bar{c} simultaneously. In such limit, one has $t_i \simeq i \frac{\lambda_i}{2}$.

More precisely, to understand the correspondence between the continuum LL model [202] and the present discrete model, we must reintroduce a lattice spacing a that sets the dimension of the parameters of the continuum case. We define

$$\lambda_{\alpha} = a \lambda_{\alpha}^{LL}, \quad \bar{c} = a \bar{c}^{LL}, \quad x_{\alpha} = \frac{x_{\alpha}^{LL}}{a}, \quad t = \eta \frac{t^{LL}}{a^2} \quad (\text{D.5.1})$$

where we keep temporarily η as a free parameter. At finite size we must also define the periodicity of the LL model, $L^{LL} = aL$.

If one now takes the LL limit defined by $a \rightarrow 0$ with the quantities of the continuum (labelled LL) fixed, one recovers from (D.3.6)-(D.3.7) the usual Bethe wavefunctions for the LL model, with rapidities λ_{α}^{LL} and (attractive) interaction parameter $c^{LL} = -\bar{c}^{LL} < 0$. From (D.3.9) we also recover the usual Bethe equations for the LL model:

$$e^{i\lambda_{\alpha}^{LL} L^{LL}} = \prod_{\beta \neq \alpha} \frac{\lambda_{\alpha}^{LL} - \lambda_{\beta}^{LL} - i\bar{c}^{LL}}{\lambda_{\alpha}^{LL} - \lambda_{\beta}^{LL} + i\bar{c}^{LL}} \quad (\text{D.5.2})$$

The parameter η tunes the correspondence between the LL time and our discrete time t : in the LL case the time-evolution of an eigenfunction μ is encoded through the multiplication by a factor $e^{-E_{\mu}^{LL} t^{LL}} = e^{-\sum_{i=1}^n (\lambda_i^{LL})^2 t^{LL}}$, which should be equal to the LL limit of $(\theta_{\mu})^t$. This implies

$$t^{LL} \sum_{\alpha=1}^n (\lambda_{\alpha}^{LL})^2 = - \lim_{a \rightarrow 0} \eta \frac{t^{LL}}{a^2} \sum_{\alpha=1}^n \log \left(\frac{e^{\frac{ia\lambda_{\alpha}^{LL}}{2}} + e^{-\frac{ia\lambda_{\alpha}^{LL}}{2}}}{2} \right) = \eta t^{LL} \sum_{\alpha=1}^n \frac{(\lambda_{\alpha}^{LL})^2}{8} \quad (\text{D.5.3})$$

If we now follow standard conventions and definitions of the LL model, see e.g. [173, 177], this implicates $\eta = 8$. With this choice, the time-evolution of our wavefunction is consistent with the one of the continuum model.

To further extend the correspondence to the moments of the partition sum, we must compare the formula (D.4.5) with the similar evolution for the LL model (where the wavefunction was simply equal to the moment). The correspondence thus reads:

$$\overline{Z_{t^{LL}}^{LL}(x_1^{LL}) \cdots Z_{t^{LL}}^{LL}(x_n^{LL})}^{V_{LL}} = \lim_{a \rightarrow 0} 2^{-nt} \left(\frac{4}{\bar{c}}\right)^{n(t+1)} \overline{Z_t(x_1) \cdots Z_t(x_n)}^w \quad (\text{D.5.4})$$

$$Z_{t^{LL}}^{LL}(x^{LL}) \equiv_{\text{inlaw}} \lim_{a \rightarrow 0} 2^{-t} \left(\frac{4}{\bar{c}}\right)^{(t+1)} Z_t(x) \quad (\text{D.5.5})$$

where on the right the limit has to be taken using (D.5.1). We have emphasized that averages in the continuum model (LL) are computed for a Gaussian potential V_{LL} , which is distinct from the quenched disorder in the discrete model. The second equation states the equivalence "in law" between the discrete log-gamma DP model in the small lattice spacing limit, and

the continuum DP model ⁴. For a precise definition of the continuum DP model, including V_{LL} , with the same conventions, see e.g. [173, 177].

Note that we have somewhat "reverse-engineered" here, since one can also establish (D.5.4) by directly starting from the evolution equation for the moments (D.3.3), without any knowledge of the Bethe ansatz solution. A similar calculation was performed in [245]. The present considerations thus provide a useful consistency check. Note that the various continuum limits are also discussed in [192], Section 5.

In the following, we note \simeq_{LL} the LL limit, which is the limit of small \mathbf{a} with the scaling (D.5.1). Note that it corresponds to the limit of $\gamma = 1 + 4/(\mathbf{a}\bar{c}_{LL}) \rightarrow \infty$ in the log-gamma DP model.

D.6 Norm of the eigenstates

Here we will guess a general formula for the norm of the eigenstates for the discrete model (the Brunet states). The approach involves some heuristics, but the final formula reproduces all numerical verifications that we performed for small values of n , as it is summarized in D.14. The complete proof of the formula will surely be involved, e.g. as it was the case in the continuum case [210].

Let us recall the formula for the norm for the LL model (with periodic boundary conditions):

$$\|\mu\|_{LL}^2 = n! \prod_{1 \leq \alpha < \beta \leq n} \frac{(\lambda_\alpha^{LL} - \lambda_\beta^{LL})^2 + (\bar{c}^{LL})^2}{(\lambda_\alpha^{LL} - \lambda_\beta^{LL})^2} \det G^{LL} \quad (\text{D.6.1})$$

where G^{LL} is the Gaudin matrix whose entries are:

$$G_{\alpha\beta}^{LL} = \delta_{\alpha\beta} \left(L + \sum_{\gamma=1}^n K(\lambda_\alpha^{LL} - \lambda_\gamma^{LL}) \right) - K(\lambda_\alpha^{LL} - \lambda_\beta^{LL}) \quad (\text{D.6.2})$$

$$K(x) = \frac{-2\bar{c}^{LL}}{x^2 + (\bar{c}^{LL})^2} \quad (\text{D.6.3})$$

A useful remark is that the entries of the Gaudin matrix in the LL case are the derivatives of the logarithm of the LL Bethe equations (D.5.2).

Let us *assume* that this property still holds. From the Brunet-Bethe equations (D.3.9) we can then summarize that in the present case:

$$G_{\alpha\beta} = \frac{1}{i} \frac{\partial}{\partial \lambda_\beta} \left(\log \left(e^{i\lambda_\alpha L} \prod_{j \neq i} \frac{2t_\alpha - 2t_\beta - \bar{c}}{2t_\alpha - 2t_\beta + \bar{c}} \right) \right) \quad (\text{D.6.4})$$

Using that $\partial_{i\lambda_\alpha} t_\alpha = \frac{1-t_\alpha^2}{2}$, this leads to a modified Gaudin matrix:

$$G_{\alpha\beta} = \delta_{\alpha\beta} \left(L + (1-t_\alpha^2) \sum_{\gamma=1}^n \tilde{K}(t_\alpha - t_\gamma) \right) - (1-t_\beta^2) \tilde{K}(t_\alpha - t_\beta) \quad (\text{D.6.5})$$

with

$$\tilde{K}(t) = \frac{-2\bar{c}}{-4t^2 + \bar{c}^2} \quad (\text{D.6.6})$$

And our final conjecture for the norm is:

$$\|\mu\|^2 = n! \prod_{1 \leq \alpha < \beta \leq n} \frac{(2t_\alpha - 2t_\beta)^2 - \bar{c}^2}{(2t_\alpha - 2t_\beta)^2} \det G \quad (\text{D.6.7})$$

where the t_α are given by (D.3.7) and are solutions of the Bethe-Brunet equations (D.3.9). This formula is constructed to coincide with the formula (D.6.1) in the LL limit. It is remarkable, since it could have been constructed without knowing the definition (D.4.4) of our peculiar weighted scalar product, and as such it is another manifestation of the nice properties of integrable systems.

We will now proceed assuming this formula to be correct, and later on the way we will indeed carry more indirect checks of its validity.

D.7 Large L limit

In this section we obtain the string eigenstates in the large L limit, as well as expressions for their eigenvalue (energy), momentum, phase-space contribution and norm.

⁴strictly, this could be considered as a conjecture since both models have an ill-defined moment problem (see however below).

D.7.1 Strings

We now turn to the large L limit where the analysis can be made more precise, and the Bethe-Brunet equations (BBE) can be solved in an asymptotic sense, the crucial point being the existence of string-states. Let us analyze the BBE equations (D.3.9) in the large L limit:

$$e^{i\lambda_\alpha L} = \prod_{\beta \neq \alpha} \frac{2t_\alpha - 2t_\beta + \bar{c}}{2t_\alpha - 2t_\beta - \bar{c}} \quad (\text{D.7.1})$$

where we recall $t_\alpha = i \tan(\frac{\lambda_\alpha}{2})$. The analysis parallels the one of the continuum problem, with a few (important) differences.

If all the λ_α are real, we note $\lambda_\alpha = \hat{k}_\alpha \in \mathbb{R}$ and the t_α are pure imaginary numbers, $t_\alpha = i \frac{k_\alpha}{2}$ with $k_\alpha \in \mathbb{R}$. This situation is very similar to the LL model: the left hand side in (D.7.1) is $e^{i\hat{k}_\alpha L}$ and the quantization of the variables \hat{k}_α is similar to the free momenta quantization, plus corrections of order $O(1/L)$. The momentum variable \hat{k}_α belongs to the first Brillouin zone, $]-\pi, \pi]$, which is natural since we are studying a discrete model. This situation corresponds to 1-strings, also called particles. Note that $k_\alpha = 2 \tan(\hat{k}_\alpha/2)$, and the two quantities become identical only in the LL limit, where both are small (see below).

If however one of the λ_α has an imaginary part δ , which we assume to be positive, the left hand side of the equation tends to zero exponentially as $e^{-\delta L}$. This indicates that there must exist another t_β such that

$$t_\beta = t_\alpha + \frac{\bar{c}}{2} + O(e^{-\delta L}) \quad (\text{D.7.2})$$

or equivalently

$$\tan(\frac{\lambda_\beta}{2}) = \tan(\frac{\lambda_\alpha}{2}) - i \frac{\bar{c}}{2} + O(e^{-\delta L}) \quad (\text{D.7.3})$$

Since $z \rightarrow \tan(z)$ preserves the sign of the imaginary part, we get a new eigenvalue with a lower imaginary part and we can continue the procedure. If the imaginary part of t_γ is negative we get that there must exist γ' such that $t_{\gamma'} = t_\gamma - \frac{\bar{c}}{2} + O(e^{-\delta L})$, and this procedure has to terminate at some point. In fact, as in the Lieb-Liniger case, we believe that it is a general fact that each set of it_α solution to the Brunet equations is self-conjugate, and that in the large-time limit the t_α organize themselves as depicted above.

To conclude, the key idea is that in the large L limit, a set $\{t_\alpha\}$ that solves the Brunet equations is divided into strings such that inside each string the t_α are distant from each other by $\frac{\bar{c}}{2}$. A general eigenstate is given by partitioning n into n_s strings, each string containing m_j particles where the index $j = 1, \dots, n_s$ labels the string. We can thus write all the t_α , $\alpha = 1, \dots, n$, in the form:

$$t_\alpha = t_{j,a} = i \frac{k_j}{2} + \frac{\bar{c}}{4}(m_j + 1 - 2a) + \frac{\delta_{j,a}}{2} \quad (\text{D.7.4})$$

where we introduce an index $a = 1, \dots, m_j$ that labels the rapidity inside a string, and $\delta_{j,a}$ are deviations that fall off exponentially with L . Hence inside the j^{th} string the t variables have the same imaginary part that is denoted by $\frac{k_j}{2}$.

One easily sees that the strings of the present model reproduce the LL strings in the LL limit. For infinite L the correspondence reads:

$$t_\alpha = t_{j,a} \simeq_{LL} a \lambda_{j,a}^{LL} + O(a^3) \quad , \quad \lambda_{j,a}^{LL} = i \frac{k_j^{LL}}{2} + \frac{\bar{c}^{LL}}{4}(m_j + 1 - 2a) \quad (\text{D.7.5})$$

and the variables k_j in (D.7.4) correspond to leading order to the LL string momenta through the scaling $k_j \simeq a k_j^{LL} + O(a^3)$.

Restriction on the multiplicity of the string: there is however an important difference with the case of LL strings. One can see that the mapping between λ_α and t_α is a bijection if $|Re(t_\alpha)| < 1$, i.e. if $\bar{c} < \frac{4}{m-1}$. Since $m \leq n$ this implies $\bar{c} < \frac{4}{n-1}$ or equivalently $n < \gamma$, which is exactly the condition for the moment problem to be well-defined. In the LL limit we have $\gamma \rightarrow \infty$ and one recovers that there are no restriction on m, n .

D.7.2 Eigenvalue of a string: energy

Inserting (D.7.4) into (D.4.3) easily gives that the eigenvalue associated to a string state takes the form of a product:

$$\theta_\mu = \prod_{j=1}^{n_s} \theta_{m_j, k_j} \quad (\text{D.7.6})$$

where the contribution of a single string can be written in several forms ⁵

$$\theta_{m_j, k_j} = \left(\prod_{a=1}^{m_j} \frac{1}{1 - t_{j,a}^2} \right)^{\frac{1}{2}} = \left(\frac{2}{\bar{c}} \right)^{m_j} \left(\frac{1}{\left(\frac{-m_j \bar{c} + \bar{c} - 2i k_j + 4}{2\bar{c}} \right)_{m_j} \left(\frac{-m_j \bar{c} + \bar{c} + 2i k_j + 4}{2\bar{c}} \right)_{m_j}} \right)^{\frac{1}{2}} \quad (\text{D.7.7})$$

$$= \left(\frac{2}{\bar{c}} \right)^{m_j} \left(\frac{\Gamma(-\frac{m_j}{2} + \frac{\gamma}{2} - i \frac{k_j}{\bar{c}}) \Gamma(-\frac{m_j}{2} + \frac{\gamma}{2} + i \frac{k_j}{\bar{c}})}{\Gamma(\frac{m_j}{2} + \frac{\gamma}{2} - i \frac{k_j}{\bar{c}}) \Gamma(\frac{m_j}{2} + \frac{\gamma}{2} + i \frac{k_j}{\bar{c}})} \right)^{\frac{1}{2}} \quad (\text{D.7.8})$$

⁵note that from (D.7.4) $1 - t_a = (1 + t_{m+1-a})^*$ and complex conjugation amounts to change $k \rightarrow -k$.

which are equivalent for integer m . Here $(a)_m = a(a+1)\dots(a+m-1) = \Gamma(a+m)/\Gamma(a)$ is the Pochhammer symbol and we reintroduced $\gamma = 1 + \frac{4}{\bar{c}}$ in the last expression.

Writing $\theta_\mu = e^{-E_\mu}$, one can verify the Lieb-Liniger limit:

$$E_\mu t \simeq_{LL} \sum_{i=1}^{m_j} \left(m_j (k_j^{LL})^2 - \frac{(\bar{c}^{LL})^2}{12} m_j (m_j^2 - 1) \right) t^{LL}. \quad (\text{D.7.9})$$

in two ways. Either the easy way, on the starting expression (first equation in (D.7.7) before summing over a) using (D.7.5) and performing an expansion similar to (D.5.3). A more tedious way is to use the final expression in (D.7.7) after summation over a . This is detailed in D.15, where the next higher order corrections $O(a^2)$ are also given.

D.7.3 Momentum of a string

In the formula (D.4.11) for $\overline{Z}_t(x)$, the temporal dependence appears through the eigenvalue whereas the position dependence appears through the factor $(\prod_\alpha z_\alpha)^x$ which also takes a simple form in string notations: $\prod_\alpha z_\alpha = \prod_{j=1}^{n_s} \prod_{a=1}^{m_j} \frac{1+t_{j,a}}{1-t_{j,a}}$, the contribution of a single string being

$$\prod_{a=1}^{m_j} \frac{1+t_{j,a}}{1-t_{j,a}} = \frac{\Gamma(-\frac{m_j}{2} + \frac{\gamma}{2} - i\frac{k_j}{\bar{c}}) \Gamma(\frac{m_j}{2} + \frac{\gamma}{2} + i\frac{k_j}{\bar{c}})}{\Gamma(\frac{m_j}{2} + \frac{\gamma}{2} - i\frac{k_j}{\bar{c}}) \Gamma(-\frac{m_j}{2} + \frac{\gamma}{2} + i\frac{k_j}{\bar{c}})} \quad (\text{D.7.10})$$

As for the eigenvalue, one can check the Lieb-Liniger limit:

$$\left(\prod_{a=1}^{m_j} \frac{1+t_{j,a}}{1-t_{j,a}} \right)^x \simeq_{LL} e^{im_j k_j^{LL} x^{LL}} \quad (\text{D.7.11})$$

D.7.4 Phase space

The sum over all eigenstates in (D.4.11) can be computed as follows: as in the case of the Lieb-Liniger model [209], regarding the quantization of its center of mass, each string state should be considered as a free particle in the large L limit, with total momentum $K_j = \sum_{a=1}^{m_j} \lambda_{j,a} \in [-m_j\pi, m_j\pi]$ (we choose to restrict the momenta to belong to the first Brillouin zone, since we work on a discrete model). This property allows us to compute the Jacobian and therefore to express sums over Brunet eigenstates: we write

$$e^{iLK_j} = \prod_{a=1}^{m_j} \frac{1+t_{j,a}}{1-t_{j,a}} \quad (\text{D.7.12})$$

where we effectively ignored the interaction with the other strings. We can thus rewrite the sum over string states using (D.7.12) as:

$$\sum_{m_j \text{ string-states}} \rightarrow \frac{L}{2\pi} \int_{-m_j\pi}^{m_j\pi} dK_j \rightarrow \frac{L}{2\pi} \int_{-\infty}^{\infty} dk_j \sum_{a=1}^{m_j} \frac{1}{1-t_{j,a}^2} \quad (\text{D.7.13})$$

which, in comparison with the usual formula for the LL model $\frac{L}{2\pi} m_j \int_{-\infty}^{\infty} dk_j$ has an additional "Jacobian" factor.

D.7.5 Norm of the string states

As in the Lieb-Liniger case, our analogous Gaudin-like formula for the norm (D.6.7) has to be studied carefully in the limit of a large system size to obtain the formula for the norm of the string states. The calculation is detailed in D.16 and we only give here the result that the leading order in L is

$$\|\mu\|^2 = n! L^{n_s} \prod_{1 \leq i < j \leq n_s} \frac{4(k_i - k_j)^2 + \bar{c}^2(m_i + m_j)^2}{4(k_i - k_j)^2 + \bar{c}^2(m_i - m_j)^2} \prod_{j=1}^{n_s} \left[\frac{m_j}{\bar{c}^{m_j-1}} \left(\sum_{a=1}^{m_j} \frac{1}{1-t_{j,a}^2} \right) \prod_{b=1}^{m_j} (1-t_{j,b}^2) \right] \quad (\text{D.7.14})$$

which is the generalization of the Calabrese-Caux formula in the case of the LL model [209]. The LL formula is recovered by setting all $t_j = 0$ in the above result. Note that it should be possible to derive a rigorous proof of this result and of the completeness of the Brunet states in the $L \rightarrow \infty$ limit, where one can use e.g. Plancherel type isomorphism techniques, as was done in [208] for the q -Boson particle system.

D.8 Formula for the integer moments \overline{Z}^n

We now have all the ingredients to compute the moments in the limit of large system size $L \rightarrow \infty$ at fixed t, x . Using the results of the previous section, (D.4.11) can be rewritten as:

$$\begin{aligned} \overline{Z_t(x)^n} &= 2^{nt} \left(\frac{\bar{c}}{4}\right)^{n(t+1)} n! \sum_{n_s=1}^n \frac{1}{n_s!} \sum_{(m_1, \dots, m_{n_s})_n} \prod_{j=1}^{n_s} \int_{-\infty}^{+\infty} \left[\frac{dk_j}{2\pi} \sum_{a=1}^{m_j} \frac{1}{1-t_{j,a}^2} \right] \prod_{1 \leq i < j \leq n_s} \frac{4(k_i - k_j)^2 + \bar{c}^2(m_i - m_j)^2}{4(k_i - k_j)^2 + \bar{c}^2(m_i + m_j)^2} \\ &\prod_{j=1}^{n_s} (\bar{c})^{m_j-1} \frac{1}{m_j \left(\sum_{a=1}^{m_j} \frac{1}{1-t_{j,a}^2} \right) \prod_{b=1}^{m_j} (1-t_{j,b}^2)} \prod_{b=1}^{m_j} \left(\frac{1}{1-t_{j,b}^2} \right)^{t/2} \left(\frac{1+t_{j,b}}{1-t_{j,b}} \right)^x \end{aligned} \quad (\text{D.8.1})$$

where we have used that the sum over states can be written as $\sum_{\mu} = \sum_{n_s=1}^n \frac{1}{n_s!} \sum_{(m_1, \dots, m_{n_s})_n} \sum_{m_j \text{ string-states}}$, where $\sum_{(m_1, \dots, m_{n_s})_n}$ means that we sum over all n_s -uplets (m_1, \dots, m_{n_s}) such that $\sum_{i=1}^{n_s} m_i = n$, and the $n_s!$ factor avoids counting the same string state twice. Note the cancellation in that formula between the phase space Jacobian factor and a similar factor in the norm. The rescaling $k_i \rightarrow \bar{c}k_i$ and the use of the formula for the energy term (D.7.7) and for the momentum term (D.7.12) directly gives our main formula for the integer moments:

$$\begin{aligned} \overline{Z_t(x)^n} &= n! \sum_{n_s=1}^n \frac{1}{n_s!} \sum_{(m_1, \dots, m_{n_s})_n} \prod_{j=1}^{n_s} \int_{-\infty}^{+\infty} \frac{dk_j}{2\pi} \prod_{1 \leq i < j \leq n_s} \frac{4(k_i - k_j)^2 + (m_i - m_j)^2}{4(k_i - k_j)^2 + (m_i + m_j)^2} \\ &\prod_{j=1}^{n_s} \frac{1}{m_j} \left(\frac{\Gamma(-\frac{m_j}{2} + \frac{\gamma}{2} - ik_j)}{\Gamma(\frac{m_j}{2} + \frac{\gamma}{2} - ik_j)} \right)^{\frac{t}{2}+1+x} \left(\frac{\Gamma(-\frac{m_j}{2} + \frac{\gamma}{2} + ik_j)}{\Gamma(\frac{m_j}{2} + \frac{\gamma}{2} + ik_j)} \right)^{\frac{t}{2}+1-x} \end{aligned} \quad (\text{D.8.2})$$

where \bar{c} does not appear explicitly (it appears only via γ). The dependence of this expression on the variables (x, t) suggests to reintroduce the original coordinates of the square lattice $I = \frac{t}{2} + 1 + x$ and $J = \frac{t}{2} + 1 - x$ (see Section D.2 and Figure D.1) and in the following we note $Z(I, J) = Z_{I+J-2}(\frac{I-J}{2})$.

This formula should be valid for arbitrary I, J , and in particular when evaluated for $(I, J) = (1, 1)$, for which it should simplify to $\overline{w^n} = \frac{\Gamma(\gamma-n)}{\Gamma(\gamma)}$. Verifying that property is a quite non trivial check of the procedure (e.g. of the completeness). Although we did not attempt to provide a general proof, we have successfully checked it for various n using Mathematica or the residues theorem (see D.20).

We stress here that this formula is ambiguity-free when the moment problem is well-defined: $m \leq n \leq \gamma$ and should reproduce all existing moments. Very much like what happens for $\overline{w^n}$, it also suggests an analytic continuation, which we use below to derive results on the full probability distribution.

D.9 Generating function

Our goal is to calculate the Laplace transform of the probability distributions of the partition sum:

$$g_{I,J}(u) = \overline{\exp -uZ(I, J)} \quad (\text{D.9.1})$$

However, as it can be seen already for the one-site problem $I = J = 1$, this Laplace transform must contain two pieces: (i) one that comes from the *generating function of the integer moments* and (ii) a second piece, which we will conjecture below from an analytic continuation. The one-site problem and the length 2 polymer are very instructive in that respect and are studied in D.17.

D.9.1 Generating function for the moments

Since we only know the integer moments of the partition sum, we start by computing the contribution in $g_{I,J}(u)$ that comes from the moments, i.e. we define the series:

$$g_{I,J}^{mom}(u) = 1 + \sum_{n=1}^{+\infty} (-1)^n \frac{u^n}{n!} \overline{Z(I, J)^n} \quad (\text{D.9.2})$$

where $\overline{Z(I, J)^n}$ denotes in this expression the right hand side of (D.8.2) for arbitrary integers $n \geq 1$. While this distinction is immaterial for $n < \gamma$, it already implies an analytic continuation since $\overline{Z(I, J)^n}$ does not exist for $n > \gamma$, while the r.h.s. of (D.8.2) does.

We can use the same strategy as in [173], [177]. Since we sum over n , the summations over the n_s and the m_j hidden in the expression (D.8.2) for $\overline{Z(I, J)^n}$ become free summations from 1 to ∞ . Permuting the summations over n and over the m_j leads to

$$g_{I,J}^{mom}(u) = 1 + \sum_{n_s=1}^{+\infty} \frac{1}{n_s!} Z(n_s, u) \quad (\text{D.9.3})$$

with

$$\begin{aligned}
Z(n_s, u) &= \prod_{j=1}^{n_s} \sum_{m_j=1}^{+\infty} \int_{-\infty}^{+\infty} \frac{dk_j}{2\pi} \prod_{1 \leq i < j \leq n_s} \frac{4(k_i - k_j)^2 + (m_i - m_j)^2}{4(k_i - k_j)^2 + (m_i + m_j)^2} \\
&\quad \prod_{j=1}^{n_s} (-1)^{m_j} u^{m_j} \frac{1}{m_j} \prod_{j=1}^{n_s} \left(\frac{\Gamma(-\frac{m_j}{2} + \frac{\gamma}{2} - ik_j)}{\Gamma(\frac{m_j}{2} + \frac{\gamma}{2} - ik_j)} \right)^I \left(\frac{\Gamma(-\frac{m_j}{2} + \frac{\gamma}{2} + ik_j)}{\Gamma(\frac{m_j}{2} + \frac{\gamma}{2} + ik_j)} \right)^J
\end{aligned} \tag{D.9.4}$$

and the sums over the m_j are free.

It is shown in D.18 that this expression has the structure of a determinant, which allows us to express the generating function as a Fredholm determinant:

$$g_{I,J}^{mom}(u) = \text{Det} \left(I + K_{I,J}^{mom} \right) \tag{D.9.5}$$

with the kernel:

$$\begin{aligned}
K_{I,J}^{mom}(v_1, v_2) &= \\
\sum_{m=1}^{\infty} \int_{-\infty}^{+\infty} \frac{dk}{\pi} (-u)^m e^{-2ik(v_1 - v_2) - m(v_1 + v_2)} &\left(\frac{\Gamma(-\frac{m}{2} + \frac{\gamma}{2} - ik)}{\Gamma(\frac{m}{2} + \frac{\gamma}{2} - ik)} \right)^I \left(\frac{\Gamma(-\frac{m}{2} + \frac{\gamma}{2} + ik)}{\Gamma(\frac{m}{2} + \frac{\gamma}{2} + ik)} \right)^J
\end{aligned} \tag{D.9.6}$$

and $K_{I,J}^{mom} : L^2(\mathbb{R}_+) \rightarrow L^2(\mathbb{R}_+)$, so that the two auxiliary integration variables v_1 and v_2 are positive. The sum over m is convergent and the result can be expressed in terms of high order hypergeometric functions ${}_1F_{4t}$ that are meromorphic and well-defined on (almost) all the complex plane, see D.19. One can also verify that, at fixed m , the integral on k also converges: rewriting the Gamma function using the Pochhammer's symbol leads to simple rational fractions.

The main property of this function $g_{I,J}^{mom}(u)$ is that its coefficient $(-u)^n$ in its Taylor expansion in u reproduces $Z(I, J)^n/n!$. In D.20 we verify this property for small values of (I, J) , which is a non trivial test of the completeness of the Bethe-Brunet eigenstates.

D.9.2 Generating function: Laplace transform

By analogy with the simpler cases studied in D.13 and D.17, we now conjecture that the full generating function, i.e. the Laplace transform of $P(Z)$ for the log-gamma polymer, can be computed using a trick inspired by the Mellin-Barnes identity, leading to our main result:

$$g_{I,J}(u) = \overline{\exp -uZ(I, J)} = \text{Det} \left(I + K_{I,J} \right) \tag{D.9.7}$$

$$\begin{aligned}
K_{I,J}(v_1, v_2) &= \int_{-\infty}^{+\infty} \frac{dk}{\pi} \frac{-1}{2i} \int_C \frac{ds}{\sin(\pi s)} u^s e^{-2ik(v_1 - v_2) - s(v_1 + v_2)} \\
&\quad \left(\frac{\Gamma(-\frac{s}{2} + \frac{\gamma}{2} - ik)}{\Gamma(\frac{s}{2} + \frac{\gamma}{2} - ik)} \right)^I \left(\frac{\Gamma(-\frac{s}{2} + \frac{\gamma}{2} + ik)}{\Gamma(\frac{s}{2} + \frac{\gamma}{2} + ik)} \right)^J
\end{aligned} \tag{D.9.8}$$

where $C = a + i\mathbb{R}$ with $0 < a < 1$ (here the sum runs from 1 to infinity) and $K_{I,J} : L^2(\mathbb{R}_+) \rightarrow L^2(\mathbb{R}_+)$ ⁶. Note that the symmetry $I \leftrightarrow J$ is explicit under the change of variable $k \leftrightarrow -k$. We discuss below in Section D.11 the connection between this result, obtained via the Bethe Ansatz, and the previous formula of [218], obtained using a completely different route.

D.9.3 Probability distribution

Before turning to the large-length limit, let us briefly mention that one can directly obtain from (D.9.8) the probability distribution of $\log Z(I, J)$ as a convolution: $\log Z(I, J) = \log Z_0 + \log \tilde{Z}(I, J)$ where $-\log Z_0$ is an independent random variable with a standard (unit) Gumbel distribution and $\tilde{Z}(I, J)$ is distributed according to a probability density $\tilde{P}_{I,J}$ given by

$$\tilde{P}_{I,J}(v) = \frac{1}{2i\pi v} \left(\text{Det}(I + \check{K}_{I,J}^{(1)} - i\check{K}_{I,J}^{(2)}) - \text{Det}(I + \check{K}_{I,J}^{(1)} + i\check{K}_{I,J}^{(2)}) \right) \tag{D.9.9}$$

where $\check{K}_{I,J}^{(j)}$, $j = 1, 2$, are two operators $\check{K}_{I,J}^{(j)} : L^2(\mathbb{R}_+) \rightarrow L^2(\mathbb{R}_+)$ with kernels:

$$\begin{aligned}
\check{K}_{I,J}^{(j)}(v_1, v_2) &= \int_{-\infty}^{+\infty} \frac{dk}{\pi} \frac{-1}{2i} \int_C \frac{ds}{f^{(j)}(\pi s)} v^{-s} e^{-2ik(v_1 - v_2) - s(v_1 + v_2)} \\
&\quad \left(\frac{\Gamma(-\frac{s}{2} + \frac{\gamma}{2} - ik)}{\Gamma(\frac{s}{2} + \frac{\gamma}{2} - ik)} \right)^I \left(\frac{\Gamma(-\frac{s}{2} + \frac{\gamma}{2} + ik)}{\Gamma(\frac{s}{2} + \frac{\gamma}{2} + ik)} \right)^J
\end{aligned} \tag{D.9.10}$$

⁶ Note that for $I = J$ and s, ik on the imaginary axis the ratio of gamma function is a complex number of modulus unity. For $a > 0$ it has modulus smaller than one, decaying to zero for large $|s|, k$. The exponential convergence in s is ensured by the $1/\sin$ but the convergence in k is slower (algebraic).

where $f^{(1)}(x) = \tan x$ and $f^{(2)}(x) = 1$. The derivation of this result is given in D.21.

D.10 Limit of very long polymers and universality

In this section we show how the above formula leads to Tracy-Widom universality and derive explicit expressions for the asymptotic probability distribution of the free energy.

Let us consider the large length limit, for which we find more convenient to use our coordinates (x, t) (see Fig. D.1), and focus first on the scaling $x \sim \varphi t$ with $-\frac{1}{2} < \varphi < \frac{1}{2}$. We define the free energy as:

$$F_t(\varphi) = -\ln Z_t(x = \varphi t) \quad (\text{D.10.1})$$

We thus need to analyze the $t \rightarrow \infty$ limit of $g_{\varphi,t}(u) = \text{Det}(I + K_{\varphi,t})$ with $K_{\varphi,t} : L^2(\mathbb{R}_+) \rightarrow L^2(\mathbb{R}_+)$ defined by its kernel (from (D.9.8)):

$$K_{\varphi,t}(v_1, v_2) = \int_{\mathbb{R}} \frac{dk}{\pi} \frac{-1}{2i} \int_C \frac{ds}{\sin(\pi s)} u^s e^{-2ik(v_1-v_2)-s(v_1+v_2)} \quad (\text{D.10.2})$$

$$\left(\frac{\Gamma(-\frac{s}{2} + \frac{\gamma}{2} - ik)}{\Gamma(\frac{s}{2} + \frac{\gamma}{2} - ik)} \right)^{1+t(\frac{1}{2}+\varphi)} \left(\frac{\Gamma(-\frac{s}{2} + \frac{\gamma}{2} + ik)}{\Gamma(\frac{s}{2} + \frac{\gamma}{2} + ik)} \right)^{1+t(\frac{1}{2}-\varphi)}$$

The behavior of the large length limit is estimated through a saddle-point analysis. We define $G_\varphi(x) = (\frac{1}{2} + \varphi) \log \Gamma(\frac{\gamma}{2} - x) - (\frac{1}{2} - \varphi) \log \Gamma(\frac{\gamma}{2} + x)$ to write the Gamma function factor as

$$\exp \left(t \left(G_\varphi\left(\frac{s}{2} + ik\right) - G_\varphi\left(-\frac{s}{2} + ik\right) \right) + 2 \left(G_0\left(\frac{s}{2} + ik\right) - G_0\left(-\frac{s}{2} + ik\right) \right) \right) \quad (\text{D.10.3})$$

We now use a Taylor expansion around the critical-point $(s, k) = (0, -ik_\varphi)^T$:

$$G_\varphi\left(\frac{s}{2} + ik\right) - G_\varphi\left(-\frac{s}{2} + ik\right) = 0 + G'_\varphi(k_\varphi)s + G''_\varphi(k_\varphi)is\tilde{k} + \frac{G'''_\varphi(k_\varphi)}{6}\left(\frac{s^3}{4} - 3s\tilde{k}^2\right) + O(s^4) \quad (\text{D.10.4})$$

where $\tilde{k} = k + ik_\varphi$ and s are considered to be of the same order (this is indeed the case, see below). It is easy to see that $G'_\varphi(k_\varphi)$ corresponds to the additive part of the free-energy. This is thus the proper saddle-point only if $G''_\varphi(k_\varphi)$ is 0, which implicitly defines k_φ as a function of φ as the solution of the equation:

$$\left(\frac{1}{2} + \varphi\right)\psi'\left(\frac{\gamma}{2} - k_\varphi\right) - \left(\frac{1}{2} - \varphi\right)\psi'\left(\frac{\gamma}{2} + k_\varphi\right) = 0 \quad (\text{D.10.5})$$

where $\psi = \frac{\Gamma'}{\Gamma}$ is the digamma function. The numerical solution k_φ is plotted in D.22. The expansion (D.10.4) indicates that we have to rescale the free-energy as:

$$F_t(\varphi) = c_\varphi t + \lambda_\varphi f_t \quad (\text{D.10.6})$$

where $c_\varphi = -G'_\varphi(k_\varphi)$ is the free-energy per unit length (which is self-averaging at large t) and $\lambda_\varphi = \left(\frac{tG'''_\varphi(k_\varphi)}{8}\right)^{\frac{1}{3}}$ is the scale of the free energy fluctuations, such that f_t is an $O(1)$ random variable. With these definitions, the rescaled generating function of the λ_φ rescaled free energy, $\tilde{g}_{\varphi,t}(z) = \exp(-e^{-\lambda_\varphi(z+f_t)})$, is given by the Fredholm determinant of a rescaled kernel, $\tilde{g}_{\varphi,t}(z) = \text{Det}(I + \tilde{K}_{\varphi,t})$, which is obtained by rescaling $s \rightarrow \frac{s}{\lambda_\varphi}$, $\tilde{k} \rightarrow \frac{\tilde{k}}{\lambda_\varphi}$, as well as $v_i \rightarrow \lambda_\varphi v_i$:

$$\tilde{K}_{\varphi,t}(v_1, v_2) = \int_{\mathbb{R}} \frac{d\tilde{k}}{\pi} \frac{-1}{2i} \int_C \frac{ds}{\lambda_\varphi \sin(\pi \frac{s}{\lambda_\varphi})} e^{-sz - 2i\tilde{k}(v_1-v_2) - s(v_1+v_2) - 4\tilde{k}^2 s + \frac{s^3}{3} + O(\frac{1}{\lambda_\varphi})} \quad (\text{D.10.7})$$

where the $O(\frac{1}{\lambda_\varphi})$ term contains higher order derivatives of G_φ and the expansion of G_0 around k_φ ⁸. The large polymer length limit $\lambda_\varphi \rightarrow \infty$ can be safely taken in this last expression, leading to a kernel \tilde{K}_∞ for which there is more freedom in the choice of the integration contour C : it should only define a convergent integral and passes to the right of zero. The $t \rightarrow \infty$ limit of the rescaled generating function can thus be written as $\lim_{t \rightarrow \infty} \tilde{g}_{\varphi,t}(z) = \text{Prob}(-f < z) = \text{Det}(I + \tilde{K}_\infty)$ with

$$\tilde{K}_\infty(v_1, v_2) = \int_{\mathbb{R}} \frac{d\tilde{k}}{\pi} \int_C \frac{-ds}{2i\pi s} e^{-sz - 2i\tilde{k}(v_1-v_2) - s(v_1+v_2) - 4\tilde{k}^2 s + \frac{s^3}{3}} \quad (\text{D.10.8})$$

which corresponds to the Tracy-Widom GUE distribution. Indeed, the Airy trick $\int_{\mathbb{R}} dy Ai(y) e^{ys} = e^{\frac{s^3}{3}}$ valid for $\text{Re}(s) > 0$, followed by the shift $y \rightarrow y + z + v_1 + v_2 + 4\tilde{k}^2$, the identity $\int_C \frac{ds}{2i\pi s} e^{sy} = \theta(y)$, and the rescaling $\tilde{k} \rightarrow \tilde{k}/2$ give

$$\tilde{K}_\infty(v_1, v_2) = - \int_{\mathbb{R}} \frac{d\tilde{k}}{2\pi} \int_{\mathbb{R}_+} dy Ai(y + z + v_1 + v_2 + \tilde{k}^2) e^{-i\tilde{k}(v_1-v_2)} \quad (\text{D.10.9})$$

⁷this is natural since $\varphi \neq 0$ breaks the symmetry $k \rightarrow -k$ of (D.10.3) while the factor in the exponential remains odd in s .

⁸The extra factor $e^{-2k_\varphi \lambda_\varphi (v_1-v_2)}$ originating from the change of variable has been removed since it is immaterial in the calculation of the Fredholm determinant.

which is one way to define F_2 as in [173] : this kernel indeed corresponds to $Prob(-f_\infty < z) = \det(I + \tilde{K}_\infty) = F_2(2^{-\frac{2}{3}}z)$. Putting everything together, our result for the asymptotic limit reads

$$\lim_{t \rightarrow \infty} Prob\left(\frac{\log Z_t(\varphi t) + tc_\varphi}{\lambda_\varphi} < 2^{\frac{2}{3}}z\right) = F_2(z) \quad (\text{D.10.10})$$

where $F_2(z)$ is the standard GUE Tracy-Widom cumulative distribution function, and the (angle-dependent) constants are determined by the system of equations:

$$0 = \left(\frac{1}{2} + \varphi\right)\psi'\left(\frac{\gamma}{2} - k_\varphi\right) - \left(\frac{1}{2} - \varphi\right)\psi'\left(\frac{\gamma}{2} + k_\varphi\right) \quad (\text{D.10.11})$$

$$c_\varphi = \left(\frac{1}{2} + \varphi\right)\psi\left(\frac{\gamma}{2} - k_\varphi\right) + \left(\frac{1}{2} - \varphi\right)\psi\left(\frac{\gamma}{2} + k_\varphi\right) \quad (\text{D.10.12})$$

$$\lambda_\varphi = \left(-\frac{t}{8} \left(\left(\frac{1}{2} + \varphi\right)\psi''\left(\frac{\gamma}{2} - k_\varphi\right) + \left(\frac{1}{2} - \varphi\right)\psi''\left(\frac{\gamma}{2} + k_\varphi\right) \right)\right)^{\frac{1}{3}} \quad (\text{D.10.13})$$

.1 Central region (i.e. square lattice diagonal): In the special case $\varphi = 0$ the solution is explicit: $k_\varphi = 0$ and the free energy per unit length and the scale of the free-energy fluctuations are given by

$$\lambda_0 = \left(-t \frac{\psi''\left(\frac{\gamma}{2}\right)}{8}\right)^{\frac{1}{3}} \quad c_0 = \psi\left(\frac{\gamma}{2}\right) \quad (\text{D.10.14})$$

For small angle φ one can also compute perturbatively the first correction, which is $k_\varphi = \frac{2\psi'\left(\frac{\gamma}{2}\right)}{\psi''\left(\frac{\gamma}{2}\right)}\varphi + O(\varphi^3)$. This allows to obtain the leading correction to the extensive part of the mean-free energy as a function of the angle, and of the endpoint position, as:

$$tc_\varphi = t\psi\left(\frac{\gamma}{2}\right) - t \frac{2\psi'\left(\frac{\gamma}{2}\right)^2}{\psi''\left(\frac{\gamma}{2}\right)}\varphi^2 + O(\varphi^4) = t\psi\left(\frac{\gamma}{2}\right) - \kappa \frac{x^2}{4t} + \dots \quad (\text{D.10.15})$$

which defines the effective elastic constant κ as (the last equation is valid in the scaling region $x/t \ll 1$)

$$\kappa = \left(-8 \frac{\psi'\left(\frac{\gamma}{2}\right)^2}{\psi''\left(\frac{\gamma}{2}\right)}\right) \quad (\text{D.10.16})$$

We see here that, although the discrete model does not obey an exact statistical tilt symmetry (STS), see e.g. CalabreseLeDoussal2011-flat, this symmetry is recovered at large scale (within this scaling region) with an effective elastic constant originating from the geometrical entropy effect.

.2 Remark on the digamma function The appearance of the digamma function in the mean free energy is natural since, as was noted in [197], a potential $V = -\ln w$ distributed according to a log-Gamma distribution of parameter γ verify $\overline{V^q} = \partial_\gamma^{q-1}\psi(\gamma)$. However, the appearance of the parameter $\frac{\gamma}{2}$ is non-trivial and has to do with the existence of an invariant measure of parameter $\frac{\gamma}{2}$ as was proved in [197] using peculiar boundary conditions. Here we did not use these boundary conditions and this is visible in the fact that $\lim_{\varphi \rightarrow \frac{1}{2}} c_\varphi = \psi(\gamma)$ (see D.22): when one approaches the border of the lattice one retrieves the original parameter γ since there is a single path. The behavior of the above equations is, however, ill-defined in this limit: this is a signature that, at $\varphi = \frac{1}{2}$, the fluctuations of the free-energy become Gaussian and scale as \sqrt{t} (as a simple application of the central limit theorem).

.3 Lieb-Liniger limit We can recover the results of [173, 165, 172, 171] in the continuum (Lieb-Liniger) limit by considering the LL limit (see Section D.5) around the angle zero (since in that limit $x/t \sim a$). Using $\psi(x) \sim_{x \rightarrow \infty} \log x - \frac{1}{2x} - \frac{1}{12x^2} + O(x^{-4})$ and (D.5.4) one can show the following Lieb-Liniger limits:

$$\begin{aligned} \lambda_0 &= \left(-t \frac{\psi''\left(\frac{\gamma}{2}\right)}{8}\right)^{\frac{1}{3}} \simeq_{LL} \left(\frac{\bar{c}_{LL}^2 t_{LL}}{4}\right)^{\frac{1}{3}} \\ c_0 t &\simeq_{LL} \frac{8}{a^2} t_{LL} \ln\left(\frac{2}{a\bar{c}_{LL}}\right) + \frac{\bar{c}_{LL}}{12} t_{LL} + O(a^2) \quad , \quad \kappa \frac{x^2}{4t} \simeq_{LL} \frac{x_{LL}^2}{4t_{LL}} \end{aligned} \quad (\text{D.10.17})$$

where the first term in the extensive part of the mean free energy arises from lattice entropic effect and can be anticipated from (D.5.4). Putting all together, one recovers the result for the one point distribution of the continuum Airy₂ process:

$$\lim_{t_{LL} \rightarrow \infty} Prob\left(\frac{\log Z_{t_{LL}}^{LL}(x_{LL}) + \frac{x_{LL}^2}{4t_{LL}} + \frac{\bar{c}_{LL}}{12} t_{LL}}{\left(\frac{\bar{c}_{LL}^2 t_{LL}}{4}\right)^{\frac{1}{3}}} < 2^{\frac{2}{3}}z\right) = F_2(z) \quad (\text{D.10.18})$$

.4 Numerical results: Using a direct simulation of (D.3.1) with Mathematica, we calculate the partition sum for various lengths and samples of environments. This provides some numerical verifications of the above results. The full check of (D.10.10) is qualitatively satisfying. In Fig D.2 we show the convergence of the two first cumulants of the probability distribution of $F_t(0)$ for $\gamma = 3$ and $t = 2^i$, $i = 1, \dots, 13$. Numerical cumulants are evaluated using $N = 10^5$

samples ($i = 1, \dots, 10$) or $N = 10^4$ ($i = 11, 12, 13$). The mean free energy $\overline{\frac{F_t(0)}{t}}$ quickly converges since the theoretical prediction (D.10.10) already includes a finite size correction. The asymptote is $\psi(\gamma/2) = 0.03649$. The convergence of the rescaled variance $\frac{\text{Var}(F_t(0))}{2^{\frac{4}{3}} \lambda_0^2}$ is slower but in good agreement with the Tracy-Widom asymptotic value 0.813.

We also checked the dependence on φ of the two first rescaled cumulants. In Fig D.3 we show the obtained dependence of $\overline{\frac{F_t(\varphi)}{t}}$ and $\frac{\text{Var}(F_t(\varphi))}{t^{\frac{4}{3}}}$ for $\gamma = 3$ and $t = 4096$. These cumulants are numerically evaluated using 10^4 samples. The theoretical predictions are given by (D.10.10) where k_φ is evaluated as explained in D.22.

.5 Semi-discrete O'Connell-Yor polymer Let us finally mention another interesting asymptotic limit that is briefly discussed in D.23 and that allows us to retrieve the semi-discrete directed polymer model of [191]. This limit is most conveniently studied on the equivalent form (D.11.11) of the Fredholm determinant formula (D.9.8) that is derived in the next section.

D.11 Comparison with other results

.1 Mathematical Results Using the geometric RSK correspondence, it was shown in [198], that the Laplace transform of the partition sum of the polymer with fixed endpoints $(1, 1) \rightarrow (I, J)$ with $I \geq J$ can be expressed as a J-fold integral:

$$\overline{e^{-uZ(I,J)}} = \frac{1}{J!} \int_{(iR)^J} \prod_{j=1}^J \frac{dw_j}{2i\pi} \prod_{j \neq k=1}^J \frac{1}{\Gamma(w_j - w_k)} \left[\prod_{j=1}^J u^{w_j - a} \Gamma[a - w_j]^J \frac{\Gamma(\alpha - w_j)^J}{\Gamma(\gamma)^J} \right] \quad (\text{D.11.1})$$

where $\alpha - a = \gamma > 0$, the parameter of the underlying inverse Gamma distribution. In [218], it was shown that this integral can be expressed as a Fredholm determinant: $\overline{e^{-uZ(I,J)}} = \text{Det}(I + K_{I,J}^{RSK})$ with

$$K_{I,J}^{RSK}(v, v') = \frac{1}{(2\pi i)^2} \int_{l_{\delta_2}} dw \frac{\pi}{\sin(\pi(v-w))} \frac{1}{w-v'} u^{w-v} \left(\frac{\Gamma(\alpha-w)}{\Gamma(\alpha-v)} \right)^I \left(\frac{\Gamma(v-a)}{\Gamma(w-a)} \right)^J \quad (\text{D.11.2})$$

where $0 < \delta_2 < 1$, $0 < \delta_1 < \min\{\delta_2, 1 - \delta_2\}$ and $0 < a < \delta_1$, $\alpha > \delta_2$. Here l_{δ_2} denotes the axis $\text{Re}(z) = \delta_2$ oriented from the bottom to the top. K is the kernel of an operator $L^2(C_{\delta_1}) \rightarrow L^2(C_{\delta_1})$ with C_{δ_1} a positively oriented circle of center 0 and radius δ_1 . The measure of integration on C_{δ_1} is chosen here as the Lebesgue measure, hence the extra factor of $1/(2i\pi)$ as compared to [218] that uses a different convention. The contour for the v, v' integrals is tailored so that only the pole at $v = a$ contributes. Using this expression, they could perform the asymptotic analysis and show that

$$\lim_{N \rightarrow \infty} \text{Proba} \left(\frac{\log(Z(N, N)) + 2N\psi(\frac{\gamma}{2})}{(N)^{\frac{1}{3}}} < (-\psi''(\frac{\gamma}{2}))^{\frac{1}{3}} z \right) = F_2(z) \quad (\text{D.11.3})$$

which is exactly the same result as ours in (D.10.10) for the case of the central region $\varphi = 0$.

.2 Kernels correspondence We now sketch how we find the kernel $K_{I,J}^{RSK}$ and our kernel to be closely related. We start from our result (D.9.8) where $C = a + i\mathbb{R}$ with $0 < a < 1$. The first step is to make the change of variables $s = a + i\tilde{s}$, which allows us to rewrite this kernel as an integral on \mathbb{R}^2 :

$$K_{I,J}(v_1, v_2) = \int_{\mathbb{R}^2} \frac{-dkd\tilde{s}}{2\pi} \frac{1}{\sin(\pi(a+i\tilde{s}))} u^{a+i\tilde{s}} e^{-2ik(v_1-v_2)-(a+i\tilde{s})(v_1+v_2)} \left(\frac{\Gamma(-\frac{a+i\tilde{s}}{2} + \frac{\gamma}{2} - ik)}{\Gamma(\frac{a+i\tilde{s}}{2} + \frac{\gamma}{2} - ik)} \right)^I \left(\frac{\Gamma(-\frac{a+i\tilde{s}}{2} + \frac{\gamma}{2} + ik)}{\Gamma(\frac{a+i\tilde{s}}{2} + \frac{\gamma}{2} + ik)} \right)^J \quad (\text{D.11.4})$$

We now use the change of variables $(k, \tilde{s}) \rightarrow (s_+, s_-)$ with $s_+ = \frac{\tilde{s}}{2} + k$ and $s_- = \frac{\tilde{s}}{2} - k$, this gives

$$K_{I,J}(v_1, v_2) = \int_{\mathbb{R}^2} ds_+ ds_- A(v_1, s_+) B(s_+, s_-) C(s_-, v_2) \quad (\text{D.11.5})$$

where we introduced $\gamma_- = \gamma - a$ and $\gamma_+ = \gamma + a$ and

$$A(v_1, s_+) = e^{-v_1(2is_+ + a)} \quad C(s_-, v_2) = e^{-v_2(2is_- + a)} \quad (\text{D.11.6})$$

$$B(s_+, s_-) = \frac{-1}{2\pi} \frac{1}{\sin(\pi(a+i(s_+ + s_-)))} u^{a+i(s_+ + s_-)} \left(\frac{\Gamma(\frac{\gamma_-}{2} - is_+)}{\Gamma(\frac{\gamma_+}{2} + is_-)} \right)^I \left(\frac{\Gamma(\frac{\gamma_-}{2} - is_-)}{\Gamma(\frac{\gamma_+}{2} + is_+)} \right)^J \quad (\text{D.11.7})$$

The kernel now has the form of a product of operators, hence we can use the identity $\text{Det}(I + ABC) = \text{Det}(I + CAB)$ (from the cyclic property of the trace) to obtain that the Laplace transform $g_{I,J}(u)$ can be expressed as the Fredholm determinant $g_{I,J}(u) = \text{Det}(I + K''_{I,J})$ with $K''_{I,J} = CAB$:

$$K''_{I,J}(v, v') = \int_{\mathbb{R}} ds_+ \int_{\mathbb{R}_+} dv_2 C(v, v_2) A(v_2, s_+) B(s_+, v') \quad (\text{D.11.8})$$

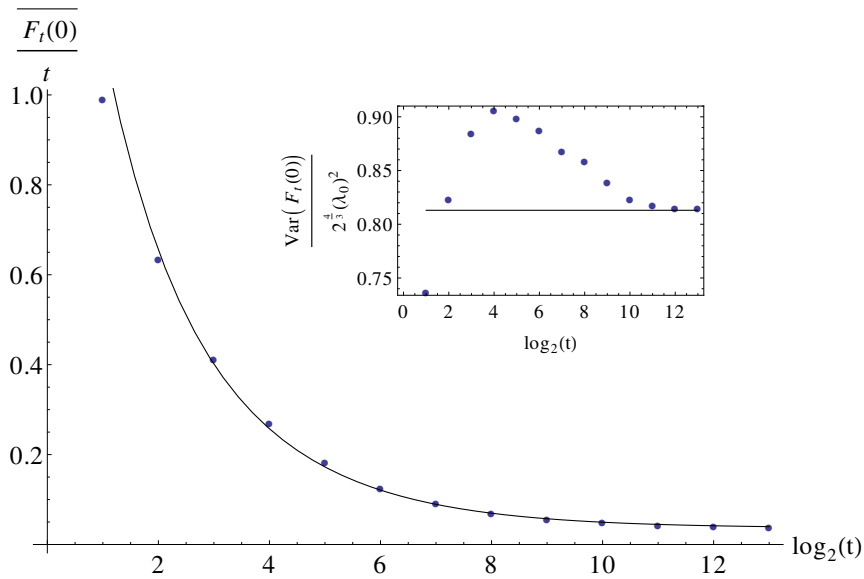


Figure D.2: Convergence of the mean free energy density $\overline{\frac{F_t(0)}{t}}$ (main curve) and of the rescaled variance of the free-energy $\frac{\text{Var}(F_t(0))}{2^{\frac{4}{3}}(\lambda_0)^2}$ (inset) as compared to the theoretical prediction (D.10.10). The blue dots are the numerical results, the black lines are the theoretical predictions of (D.10.10). There are no fitting parameter.

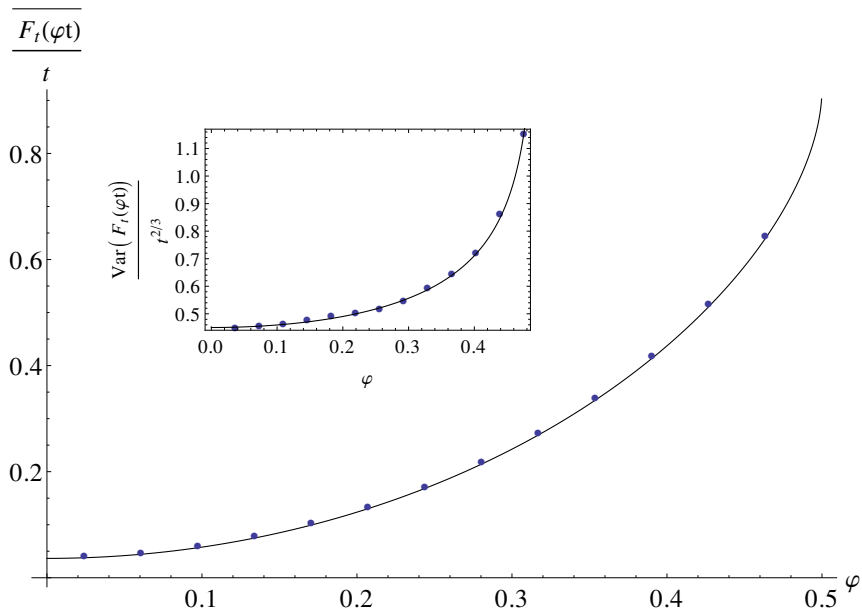


Figure D.3: Dependence on the endpoint position $x = \varphi t$ of the mean free energy density $\overline{\frac{F_t(\varphi t)}{t}}$ (main curve) and of the rescaled variance of the free-energy $\frac{\text{Var}(F_t(\varphi t))}{t^{\frac{2}{3}}}$ (inset), for $t = 4096$. The blue dots are the numerical results, the black lines are the theoretical predictions from (D.10.10). There are no fitting parameter.

where in this expression, the integral on v_2 is straightforward and we find

$$K''_{I,J}(v, v') = \int_R ds_+ \frac{-1}{4\pi(a + i(s_+ + v))} \frac{1}{\sin(\pi(a + i(v' + s_+)))} u^{a+i(v'+s_+)} \left(\frac{\Gamma(\frac{\gamma_-}{2} - is_+)}{\Gamma(\frac{\gamma_+}{2} + iv')} \right)^I \left(\frac{\Gamma(\frac{\gamma_-}{2} - iv')}{\Gamma(\frac{\gamma_+}{2} + is_+)} \right)^J \quad (\text{D.11.9})$$

where now $K''_{I,J} : L^2(R) \rightarrow L^2(R)$. Note that the convergence of the integral over s_+ , a necessary condition to exchange the integrations, is satisfied when $I \geq J$, which we now assume. If $J \geq I$ we would instead write $\text{Det}(I+ABC) = \text{Det}(I+BCA)$, leading to the same kernel with I and J exchanged (and v, v' exchanged which is immaterial in the Fredholm determinant). Using the change of variables $w = a + \frac{\gamma_+}{2} + is_+$ and $z = -iv' + \frac{\gamma_+}{2}$ (it adds a minus sign), the result for $g_{I,J}(u)$ is re-expressed as the Fredholm determinant $g_{I,J}(u) = \text{Det}(I + K'_{I,J})$ with $K'_{I,J} : L^2(\frac{\gamma_+}{2} + i\mathbb{R}) \rightarrow L^2(\frac{\gamma_+}{2} + i\mathbb{R})$ and

$$K'_{I,J}(z, z') = \int_{a+\frac{\gamma_+}{2}+i\mathbb{R}} dw \frac{1}{4\pi(w-z')} \frac{1}{\sin(\pi(w-z))} u^{w-z} \left(\frac{\Gamma(\gamma+a-w)}{\Gamma(\gamma+a-z)} \right)^I \left(\frac{\Gamma(z-a)}{\Gamma(w-a)} \right)^J \quad (\text{D.11.10})$$

In this last expression we have some freedom in the choice of the contours: the evaluation of the Fredholm determinant involves integrals on w and on z that are invariant as long as we translate the contours of integration by the same amount, and that we do not cross the poles located at $w = \gamma + a + n$ and $z = a - n$ for $n \in \mathbb{N}$. We can thus write our final result as $g_{I,J}(u) = \text{Det}(I + K^{BA}_{I,J})$ with $K^{BA}_{I,J} : L^2(a + \tilde{a} + i\mathbb{R}) \rightarrow L^2(a + \tilde{a} + i\mathbb{R})$ defined as the "Bethe ansatz" kernel:

$$K^{BA}_{I,J}(z, z') = \int_{2a+\tilde{a}+i\mathbb{R}} dw \frac{1}{4\pi(w-z')} \frac{1}{\sin(\pi(w-z))} u^{w-z} \left(\frac{\Gamma(\alpha-w)}{\Gamma(\alpha-z)} \right)^I \left(\frac{\Gamma(z-a)}{\Gamma(w-a)} \right)^J \quad (\text{D.11.11})$$

where $\alpha = \gamma + a$, $0 < a < 1$ and $0 < \tilde{a} < \gamma - a$ and $I \geq J$.

.3 The next step to achieve the correspondence would be to deform the contour of integration of z into the circle C_{δ_1} . This seems to be a difficult task since when deforming the contour one a priori encounters an infinite number of poles. However we conjecture that it works and that:

$$\text{Det}(I + K^{BA}_{I,J}) = \text{Det}(I + K^{RSK}_{I,J}) \quad (\text{D.11.12})$$

We verified that identity in some simple cases, e.g. by explicitly computing the u, u^2, u^3 terms (for $t = 0$ and $t = 2$) and the $u^\gamma, u^{\gamma+1}$ terms ($t = 0$ only). A proof may require lifting the model to a higher generalization involving Macdonald processes. Note that in the case of the semi-discrete polymer (see D.23), the equivalence between such small circles and open contours was already proved in [243].

Let us finally mention that this kernel allows to obtain another formula for the probability distribution of $\log Z$ analogous to (D.9.10). More precisely (D.9.10) still holds with $\check{K}_{I,J}^{(j)} \rightarrow \check{K}_{I,J}^{(j),BA}$ where the kernels $\check{K}_{I,J}^{(j),BA}$ are obtained from $K^{BA}_{I,J}$ in (D.11.11) by substituting $\frac{1}{\sin(\pi(w-z))} u^{w-z} \rightarrow v^{z-w} / f^{(j)}(\pi(w-z))$.

.4 Results from the physics literature During the last stage of the redaction of this article, we became aware of a very recent work [222] where zero-range q -boson models with factorized steady state measures and which are integrable via the Bethe ansatz are classified. Although these results were obtained in a different context, there is a clear connection to the ansatz studied here. The main difference is that the stochasticity hypothesis has to be relaxed to get a more general framework that encompasses our model. This is however easily done (work in progress) and the Brunet ansatz then appears as a (singular) limit of this generalized ansatz.

D.12 Conclusion

In this paper we have studied the problem of a directed polymer on the square lattice in presence of log-Gamma distributed quenched random weights. Building up on an earlier work by Brunet, we have shown how the Bethe-Ansatz and integrability techniques could be efficiently used to derive an exact formula for the n -th integer moment of the partition function for fixed endpoints and arbitrary polymer length, (D.8.2), defined for $n < \gamma$. Based on this formula and the observations made in D.13 and D.17, we conjectured a formula for the Laplace transform of the probability distribution of the partition sum. From this: (i) we obtained a formula for the probability distribution of the partition function for any polymer length (D.9.10) (ii) we showed convergence of the free energy distribution to the Tracy-Widom distribution at large time (D.10.10) and derived the normalizing constants and their dependence in the endpoint position (i.e. in the angle with respect to the diagonal of the lattice). Specifically, we obtained the extensive part of the mean free energy, as well as the variance of the fluctuations. From the angle dependence we also obtained the elastic coefficient. We performed numerical simulations of long polymers to check and confirm some of these results with very good agreement. At each stage of the calculation we proved that all of our formulas reduce, in the continuum limit, to the ones for the Lieb-Liniger model, thereby recovering the results for the continuum KPZ model obtained in previous works.

In the last section we showed how these results are related to the previous work of [218]. Our asymptotic limit agrees and extends their result to arbitrary angle, and our Fredholm determinant formula are closely related, with an essential

difference in the contours of integration. This difference seems to be a signature of the method: our integrability techniques naturally give rise to "large" contours formulas, whereas the techniques used in the mathematical context give rise to "small" contours formulas. Although we provided some verifications, the full proof of the equivalence of the two formulas may require considering a regularized, (e.g. q -deformed) version of the log-Gamma model.

.1 This paper thus offers new tools which could be used to explore further the similarities between quantum integrability and tropical combinatorics methods. It also opens the way to other studies on the log-Gamma directed polymer with e.g. other boundary conditions, such as flat (as in [177]) or stationary (as in [197]) and extension to the inhomogeneous model of [198], which are left for future studies.

Acknowledgments:

We want to thank E. Brunet for explaining his results on the eigenstates of this model and fruitful discussions. We are grateful to A. Borodin, P. Calabrese, T. Gueudre, A. M. Povolotsky, J. Quastel, D. Remenik, T. Seppalainen, N. Zygouras for useful discussions. We thank I. Corwin for careful reading of the manuscript and useful remarks. This work is supported by a PSL grant ANR-10-IDEX-0001-02-PSL.

D.13 Appendix A: Analytic continuation: Laplace transform from the moments

In this section, we illustrate the use of the Mellin-Barnes identity to compute the Laplace transform of a probability distribution from its integer moments. In the most favorable cases the Laplace transform of the probability distribution $P(Z)$ of a positive random variable Z , such as a partition sum, can be calculated by a simple re-summation of the integer moments:

$$\overline{e^{-uZ}} := \int_{Z>0} dZ P(Z) e^{-uZ} = \sum_{n=0}^{+\infty} \frac{1}{n!} (-u)^n \overline{Z^n} \quad (\text{D.13.1})$$

Clearly this formula cannot be used when some of the moments do not exist, e.g. when $P(Z)$ has an algebraic tail. In that case however one can use a more general formula in terms of a Mellin-Barnes transform.

The basic identity is the following integral representation of the exponential function:

$$e^{-z} = \int_{-a+i\mathbb{R}} \frac{ds}{2i\pi} \Gamma(-s) z^s = - \int_{-a+i\mathbb{R}} \frac{ds}{2i \sin(\pi s)} \frac{1}{\Gamma(1+s)} z^s \quad (\text{D.13.2})$$

where $a > 0$ and $z > 0$. It allows us to express the Laplace transform of the probability distribution $P(Z)$ as:

$$\begin{aligned} \overline{e^{-uZ}} &= - \int dZ P(Z) \int_{-a+i\mathbb{R}} \frac{ds}{2i \sin(\pi s)} \frac{1}{\Gamma(1+s)} (uZ)^s \\ &= - \int_{-a+i\mathbb{R}} \frac{ds}{2i \sin(\pi s)} \frac{u^s}{\Gamma(1+s)} \overline{Z^s} \end{aligned} \quad (\text{D.13.3})$$

a more general formula, which is valid provided the integral converges. This is the case for instance for the single site problem, i.e. $Z = w$ given by the inverse Gamma distribution, in which case $\overline{w^s} = \Gamma(\gamma - s)/\Gamma(\gamma)$ for $\text{Re}(s) < \gamma$. In fact, in that (trivial) case the formula (D.13.3) is precisely the representation given in [198], see e.g. (D.11.1) setting $I = J = 1$.

In the case where $f(s) = \overline{Z^s}$ is analytic on the positive half-plane $\text{Re}(s) \geq 0$, and satisfies the conditions of Carlson theorem (i) $\exists C, \tau, |f(z)| < C e^{\tau z}$ (ii) $|f(iy)| < C e^{\pi y}$, the integral (D.13.3) converges and we can close the contour on the positive half plane. From the residues of the poles of the $1/\sin$ function one then recovers the formula (D.13.1) (equivalently, going from (D.13.1) to (D.13.3) is nothing but the Mellin-Barnes formula).

D.14 Appendix B: Verifications of the formula for the norm

Here we calculate the norm of the Brunet states in some simple cases, which provide verifications for the general formula given in the text.

D.14.1 finite L

For fixed L one can directly compute the norm of a general 2 particles state with real momenta: $t_i = i \frac{k_i}{2}, k_i \in \mathbb{R}$. Using the formula for the weighted scalar product (D.4.4), one finds:

$$\|\psi_\mu\|^2 = -\bar{c}L \frac{8 + k_1^2 + k_2^2}{(k_1 - k_2)^2} + 2L^2 \frac{(\bar{c}^2 + (k_1 - k_2)^2)}{(k_1 - k_2)^2} \quad (\text{D.14.1})$$

in agreement with the formula (D.6.7) using the modified Gaudin determinant.

D.14.2 in the limit $L \rightarrow +\infty$

Norm of a single n -string In the limit $L \rightarrow \infty$, one can compute explicitly the norm of the state consisting of a single string (see section D.7), i.e. of particle content $m = n \in \mathbb{N}$. Inserting the string decomposition (D.7.4) into the Brunet eigenfunctions (D.3.6), one sees that the single n -string eigenstate takes the simple form:

$$\psi_{n\text{-string}}(x_1, \dots, x_n) = n! z_1^{x_1} \cdots z_n^{x_n} \quad , \quad x_1 \leq \dots \leq x_n \quad (\text{D.14.2})$$

with $z_a = \frac{1+t_a}{1-t_a}$ and where the t_a variables are organized as $t_a = i\frac{k}{2} + \frac{\bar{c}}{4}(m+1-2a)$. For the infinite system one can recursively sum on the variables $y_i = x_i - x_{i-1}$ starting with y_n , carefully using the definition of the scalar product (D.4.4). Let us illustrate the calculation for $n = 2, 3$. One has:

$$\begin{aligned} \|\psi_{2\text{-string}}\|^2 &= \sum_{x_1, x_2} \frac{1}{a_{x_1, x_2}} |\psi_{2\text{-string}}(x_1, x_2)|^2 = 2 \sum_{x_1 < x_2} 4|z_1|^{2x_1} |z_2|^{2x_2} + \frac{4}{h_2} \sum_{x_1} |z_1 z_2|^{2x_1} \\ &\simeq 8L \sum_{y=1}^{+\infty} |z_2|^{2y} + \frac{4L}{h_2} \end{aligned} \quad (\text{D.14.3})$$

using $|z_1 z_2| = 1$ from the Bethe equation. Using that $z_2 = \frac{2-\frac{\bar{c}}{2}+ik}{2+\frac{\bar{c}}{2}-ik}$ one sees that $|z_2| < 1$. Using that $h_2 = 4/(4-\bar{c})$ and performing the sum one finds:

$$\|\psi_{2\text{-string}}\|^2 \simeq_{L \rightarrow \infty} \frac{L(4(4+k^2) - \bar{c}^2)}{2\bar{c}} \quad (\text{D.14.4})$$

in agreement with (D.7.14).

A similar calculation for $n = 3$ is performed using that

$$\sum_{x_1, x_2, x_3} a_{x_1, x_2, x_3}^{-1} |\psi(x_1, x_2, x_3)|^2 = 6 \sum_{x_1 < x_2 < x_3} |\psi(x_1, x_2, x_3)|^2 \quad (\text{D.14.5})$$

$$+ \frac{3}{h_2} \left[\sum_{x_1 < x_3} |\psi(x_1, x_1, x_3)|^2 + \sum_{x_1 < x_2} |\psi(x_1, x_2, x_2)|^2 \right] + \frac{1}{h_3} \sum_{x_1} |\psi(x_1, x_1, x_1)|^2 \quad (\text{D.14.6})$$

Inserting (D.14.2), using that $|z_2| = 1$, $|z_1|^2 = 1/|z_3|^2$ and $|z_3|^2 = \frac{(2-\bar{c}-ik)(2-\bar{c}+ik)}{(2+\bar{c}-ik)(2+\bar{c}+ik)}$ and performing the sums leads to the norm of the 3-string as:

$$\|\psi_{m=n=3}\|^2 \sim_{L \rightarrow \infty} \frac{9L(-16\bar{c}^2 + \bar{c}^4 + 3(4+k^2)^2)}{8\bar{c}^2} \quad (\text{D.14.7})$$

As one can see from this expression, it is hard to guess the general formula. Fortunately one can check that it agrees with the conjecture (D.7.14).

.1 *n 1-strings:* In the case of n particles with $n_s = n$, one easily obtains the norm in the large L limit. In the calculation of $\sum_{x_1, \dots, x_n} \frac{1}{a_{x_1, \dots, x_n}} \psi^*(x_1, \dots, x_n) \psi(x_1, \dots, x_n)$, one only encounters plane waves with real momenta. It is then easy to see that, inserting the form (D.3.6) and expanding both wavefunctions in sum over permutations, only the terms that come from the same permutation in ψ^* and ψ can give a power of L^n . The computation of the other (non-diagonal) terms involve the use of the Bethe equations (D.3.9) and give subdominant powers of L . Also, in that case, the factor a_{x_1, \dots, x_n} can be set to unity to leading order in the large L limit. From there one easily obtains:

$$\|\psi\|^2 = n! L^n \prod_{i < j} \frac{\bar{c}^2 + (k_i - k_j)^2}{(k_i - k_j)^2} + O(L^{n-1}) \quad (\text{D.14.8})$$

which is a consistency check of the first factor in the first formula (D.7.14), and a check of the general norm formula (D.6.7).

D.15 Appendix C: Expansion of the eigenenergy around the LL limit

Consider the expression for the eigenvalue (D.7.7). The LL limit amounts to perform a small \bar{c} expansion at fixed $\tilde{k} = k/\bar{c}$. We can use the expansion of the Pochhammer symbol at large x , $(x)_m = x^m f(x)$ with $f(x) = 1 + \frac{m(m-1)}{2x} + \frac{m(3m^3-10m^2+9m-2)}{24x^2} + O(1/x^3)$, with $x = -\frac{m}{2} + \frac{\gamma}{2} + i\tilde{k}$ and $\gamma = 1 + \frac{4}{\bar{c}}$. Then $\theta_{m,k}^2 = (\frac{2}{\bar{c}}|x|)^2 f(x)f(x^*)$, where x^* is the complex conjugate. Since $\frac{2}{\bar{c}}|x| \rightarrow 1$ as $\bar{c} \rightarrow 0$ one can easily take the logarithm and expanding in \bar{c} , up to $O(\bar{c}^4)$ one finds, up to terms of $O(\bar{c}^6, k^6, \dots)$:

$$-8 \ln \theta_{m,k} = mk^2 + \frac{1}{12}(m-m^3)\bar{c}^2 - \frac{\bar{c}^4 m(3m^4 - 10m^2 + 7)}{1920} + \frac{1}{16}\bar{c}^2 k^2 m(m^2 - 1) - \frac{k^4 m}{8} \quad (\text{D.15.1})$$

This expression is $O(\mathbf{a}^2) + O(\mathbf{a}^4)$ in the LL limit and when combined with the scaling of $t = \frac{tLL}{8\mathbf{a}^2}$ it gives the correct finite LL limit displayed in the text, together with the first correction in \mathbf{a} .

D.16 Appendix D: Norm of strings from modified Gaudin formula in the limit

$$L \rightarrow \infty$$

We start from the formula (D.6.7) for the norm of an eigenstate given in the main text. As in the case of the Lieb-Liniger model, this formula is a-priori singular and the limit should be taken with care for $L \rightarrow +\infty$ when string states appear. Here we follow the strategy of [209]. In that limit we split the n particles into n_s strings of multiplicity m_j :

$$t_{j,a} = i \frac{k_j}{2} + \frac{\bar{c}}{4}(m_j + 1 - 2a) + \frac{\delta_j^{j,a}}{2} \quad (\text{D.16.1})$$

where $j = 1, \dots, n_s$ and $a = 1, \dots, m_j$.

.1 Limit of the prefactor in string notations: The prefactor is most conveniently written as

$$\prod_{1 \leq \alpha < \beta \leq n} \frac{(2t_\alpha - 2t_\beta)^2 - \bar{c}^2}{(2t_\alpha - 2t_\beta)^2} = \prod_{\alpha \neq \beta} \frac{2t_\alpha - 2t_\beta - \bar{c}}{2t_\alpha - 2t_\beta} \quad (\text{D.16.2})$$

We now use the string notations and split the intra-string part from the inter-string part:

$$\begin{aligned} \prod_{\alpha \neq \beta} \frac{2t_\alpha - 2t_\beta - \bar{c}}{2t_\alpha - 2t_\beta} &= \prod_{i \neq j} \prod_{a=1}^{m_i} \prod_{b=1}^{m_j} \frac{i(k_i - k_j) + \frac{\bar{c}}{2}(m_i - m_j - 2(a - b + 1))}{i(k_i - k_j) + \frac{\bar{c}}{2}(m_i - m_j - 2(a - b))} \\ &\quad \prod_{j=1}^{n_s} \prod_{a=1}^{m_j} \prod_{b \neq a} \frac{\bar{c}(a - b + 1) - \delta_j^{(a,b)}}{\bar{c}(a - b)} \end{aligned} \quad (\text{D.16.3})$$

where we denote $\delta_j^{(a,b)} = \delta_{j,a} - \delta_{j,b}$ and keep these strings deviations only where needed for the limit. After some work one finds that the leading term in the expansion in the strings deviations is given by:

$$\prod_{1 \leq i < j \leq n_s} \frac{4(k_i - k_j)^2 + \bar{c}^2(m_i + m_j)^2}{4(k_i - k_j)^2 + \bar{c}^2(m_i - m_j)^2} \prod_{1 \leq j \leq n_s} m_j \left(\frac{1}{\bar{c}}\right)^{m_j-1} \prod_{a=1}^{m_j-1} \delta_j^{(a,a+1)} \quad (\text{D.16.4})$$

.2 Limit of the modified Gaudin determinant: Consider formula (D.6.5) in the main text. As in the Lieb-Liniger case, the determinant is singular and contains terms of the form $K(t_{j,a} - t_{j,a+1}) = K_j^{(a,a+1)} = \frac{1}{\delta_j^{(a,a+1)}} + O(1)$ that become exponentially large. It is easy to see that the leading term in the string deviation is obtained when one computes the determinant as if all string were decoupled: $\det G \sim \prod_{j=1}^{n_s} \det G_j$ where

$$\det G_j = \begin{vmatrix} L + (1 - t_{j,1}^2) \sum_{b \neq 1} K_j^{(1,b)} & -(1 - t_{j,1}^2) K_j^{(1,2)} & \cdots & -(1 - t_{j,1}^2) K_j^{(1,m_j)} \\ -(1 - t_{j,2}^2) K_j^{(1,2)} & L + (1 - t_{j,2}^2) \sum_{b \neq 2} K_j^{(2,b)} & \cdots & -(1 - t_{j,2}^2) K_j^{(2,m_j)} \\ \vdots & \vdots & \ddots & \vdots \\ -(1 - t_{j,m_j}^2) K_j^{(1,m_j)} & -(1 - t_{j,m_j}^2) K_j^{(2,m_j)} & \cdots & L + (1 - t_{j,m_j}^2) \sum_{b \neq m_j} K_j^{(b,m_j)} \end{vmatrix} \quad (\text{D.16.5})$$

This determinant can be handled in the same spirit as in [209]. One starts by adding the first column to the second one, then one adds to the second row the first one multiplied by $\frac{1-t_{j,2}^2}{1-t_{j,1}^2}$. The singular term $K_j^{(1,2)}$ now only appears in the top-left entry and the entry (2,2) now contains $L(1 + \frac{1-t_{j,2}^2}{1-t_{j,1}^2})$. One now iterates this procedure by adding the second column to the third one, and adding to the third row the second one multiplied by $\frac{1-t_{j,3}^2}{1-t_{j,2}^2}$, and the entry (3,3) now contains $L \left(1 + \frac{1-t_{j,3}^2}{1-t_{j,2}^2} \left(1 + \frac{1-t_{j,2}^2}{1-t_{j,1}^2}\right)\right) = L \left(1 + \frac{1-t_{j,3}^2}{1-t_{j,2}^2} + \frac{1-t_{j,2}^2}{1-t_{j,1}^2}\right)$. In the end all the singular terms $K_j^{(a,a+1)}$ are located on the first $m_j - 1$ diagonal entries and the last term contains the leading power in L which is $L(1 - t_{j,m_j}^2) \sum_{b=1}^{m_j} \frac{1}{1-t_{j,b}^2}$. We thus obtain

$$\det G_j \sim L \left(\prod_{a=1}^{m_j-1} (1 - t_{j,a}^2) K_j^{(a,a+1)} \right) (1 - t_{j,m_j}^2) \sum_{b=1}^{m_j} \frac{1}{1 - t_{j,b}^2} \quad (\text{D.16.6})$$

Note that we can do the exact same operation on the full modified Gaudin determinant to explicitly show that the different strings decouple. Taking all the strings into account, we thus arrive to:

$$\det G \sim \prod_{j=1}^{n_s} L \left(\prod_{a=1}^{m_j-1} \frac{1}{\delta_j^{(a,a+1)}} \right) \prod_{a=1}^{m_j} (1 - t_{j,a}^2) \sum_{b=1}^{m_j} \frac{1}{1 - t_{j,b}^2} \quad (\text{D.16.7})$$

The divergent part precisely cancels the vanishing part of the prefactor and leads to the formula of the main text.

D.17 Appendix E: Laplace transform versus moment generating function: some simple cases.

.1 Calculations for the one-site problem $I = J = 1$ In the case of $Z = w$ distributed according to the inverse gamma distribution one can still close the contour in (D.13.3). This coincides with the formula of [198] applied to one site. This leads to the result:

$$\overline{e^{-uZ}} = \sum_{n=0}^{\infty} \frac{(-u)^n}{n!} \frac{\Gamma(\gamma - n)}{\Gamma(\gamma)} + \sum_{n=0}^{\infty} \frac{(-1)^n}{n!} u^{\gamma+n} \frac{\Gamma(-\gamma - n)}{\Gamma(\gamma)} \quad (\text{D.17.1})$$

$$= \frac{2}{\Gamma[\gamma]} u^{\frac{\gamma}{2}} K_{\gamma}(2\sqrt{u}) \quad (\text{D.17.2})$$

One can check that this is an exact formula. Notice that in the expansion, both sums converge separately but just give a part of the total Laplace transform:

$$\sum_{n=0}^{\infty} \frac{(-u)^n}{n!} \frac{\Gamma(\gamma - n)}{\Gamma(\gamma)} = u^{\gamma/2} \Gamma(1 - \gamma) I_{-\gamma}(2\sqrt{u}) \quad (\text{D.17.3})$$

$$\sum_{n=0}^{\infty} \frac{(-1)^n}{n!} u^{\gamma+n} \frac{\Gamma(-\gamma - n)}{\Gamma(\gamma)} = \frac{u^{\gamma/2} \Gamma(-\gamma) \Gamma(\gamma + 1) I_{\gamma}(2\sqrt{u})}{\Gamma(\gamma)}$$

where we used the usual notations for the Bessel functions. This is not apparent, but one can also notice that the sum of the (analytically-continued) moments possesses the symmetry $\gamma \rightarrow 2 - \gamma$, which is also the case for the Fredholm determinant computed in terms of hypergeometric functions computed in D.19. Note however that neither the Laplace transform, nor $P(w)$, possess this symmetry, another manifestation that the integer moments give only a part of the total Laplace transform. The same property holds for the general case of arbitrary t , as discussed below.

.2 Calculation for $t=2$ We now give a non-trivial check of the procedure for a length 2 polymer. Consider the moments of $Z_2(0) = w_{0,0}(w_{-\frac{1}{2},1} + w_{\frac{1}{2},1})w_{0,2}$: they are given for $n < \gamma$ by

$$\overline{Z_2(0)^n} = \sum_{k=0}^n C_n^k \frac{\Gamma(\gamma - n)^2 \Gamma(\gamma - k) \Gamma(\gamma - (n - k))}{\Gamma(\gamma)^4} \quad (\text{D.17.4})$$

Because of the sum over k , it is not straightforward to analytically continue this formula in n . However, if we compute the moment generating function $g_{mom}(u) = \sum_{n=0}^{\infty} (-1)^n \frac{u^n}{n!} \overline{Z_2(0)^n}$, we obtain:

$$g_{mom}(u) = \sum_{k_1 \geq 0, k_2 \geq 0} \frac{(-u)^{k_1+k_2}}{\Gamma(1+k_1)\Gamma(1+k_2)} \frac{\Gamma(\gamma - n)^2 \Gamma(\gamma - k) \Gamma(\gamma - (n - k))}{\Gamma(\gamma)^4} \quad (\text{D.17.5})$$

On this function we can now perform the Mellin-Barnes trick to conjecture a formula for the Laplace transform $g(u) = \overline{e^{-uZ_2(0)}}$:

$$g(u) = \frac{1}{4\pi^2} \int_{-a+i\mathbb{R}} \int_{-a+i\mathbb{R}} dk_1 dk_2 u^{k_1+k_2} \Gamma(-k_1) \Gamma(-k_2) \frac{\Gamma(\gamma - n)^2 \Gamma(\gamma - k) \Gamma(\gamma - (n - k))}{\Gamma(\gamma)^4} \quad (\text{D.17.6})$$

where we used the reflection formula for the Gamma function. This formula is similar to the exact result obtained in [198], and we have numerically verified that the two results coincide. This provides a verification, for $t = 2$, of the general procedure detailed in the text to conjecture the formula (D.9.8) for the Laplace transform for arbitrary t using the Mellin-Barnes trick.

D.18 Appendix F: Generating Function as a Fredholm determinant

We start from the formula (D.9.4) for the partition sum at fixed number of strings. As in [173] we use the following crucial identity:

$$\prod_{1 \leq i < j \leq n_s} \frac{4(k_i - k_j)^2 + (m_i - m_j)^2}{4(k_i - k_j)^2 + (m_i + m_j)^2} = \det \left[\frac{1}{2i(k_i - k_j) + m_i + m_j} \right] \times \prod_{j=1}^{n_s} (2m_j) \quad (\text{D.18.1})$$

Hence we can rewrite (D.9.4) as:

$$\begin{aligned} Z(n_s, u) &= \prod_{j=1}^{n_s} \sum_{m_j=1}^{+\infty} \int \frac{dk_j}{\pi} \det \left[\frac{1}{2i(k_i - k_j) + m_i + m_j} \right] \\ &\times \prod_{j=1}^{n_s} (-u)^{m_j} \prod_{j=1}^{n_s} \left(\frac{\Gamma(-\frac{m_j}{2} + \frac{\gamma}{2} - ik_j)}{\Gamma(\frac{m_j}{2} + \frac{\gamma}{2} - ik_j)} \right)^I \left(\frac{\Gamma(-\frac{m_j}{2} + \frac{\gamma}{2} + ik_j)}{\Gamma(\frac{m_j}{2} + \frac{\gamma}{2} + ik_j)} \right)^J \end{aligned} \quad (\text{D.18.2})$$

The determinant can be written as a sum over permutations σ , and we also introduce the representation $\frac{1}{x} = \int_{R_+} dv e^{-vx}$, which leads to

$$\begin{aligned} Z(n_s, u) &= \sum_{\sigma \in S_n} (-1)^\sigma \prod_{j=1}^{n_s} \sum_{m_j=1}^{+\infty} \int \frac{dk_j}{\pi} \int_{v_j > 0} e^{-v_j(2i(k_j - k_{\sigma(j)} + m_j + m_{\sigma(j)}))} (-u)^{m_j} \\ &\quad \times \prod_{j=1}^{n_s} \left(\frac{\Gamma(-\frac{m_j}{2} + \frac{\gamma}{2} - ik_j)}{\Gamma(\frac{m_j}{2} + \frac{\gamma}{2} - ik_j)} \right)^I \left(\frac{\Gamma(-\frac{m_j}{2} + \frac{\gamma}{2} + ik_j)}{\Gamma(\frac{m_j}{2} + \frac{\gamma}{2} + ik_j)} \right)^J \end{aligned}$$

We then perform the change $\sum_j v_j k_{\sigma(j)} = \sum_j v_{\sigma^{-1}(j)} k_j$ (and the same for $\sum_j v_j m_{\sigma(j)}$) and relabel as $\sigma \rightarrow \sigma^{-1}$, this leads to:

$$\begin{aligned} Z(n_s, u) &= \sum_{\sigma \in S_n} (-1)^\sigma \prod_{j=1}^{n_s} \sum_{m_j=1}^{+\infty} \int \frac{dk_j}{\pi} \int_{v_j > 0} e^{-2ik_j(v_j - v_{\sigma(j)}) - m_j(v_j + v_{\sigma(j)})} (-u)^{m_j} \\ &\quad \left(\frac{\Gamma(-\frac{m_j}{2} + \frac{\gamma}{2} - ik_j)}{\Gamma(\frac{m_j}{2} + \frac{\gamma}{2} - ik_j)} \right)^I \left(\frac{\Gamma(-\frac{m_j}{2} + \frac{\gamma}{2} + ik_j)}{\Gamma(\frac{m_j}{2} + \frac{\gamma}{2} + ik_j)} \right)^J \end{aligned}$$

which has the structure of a determinant:

$$Z(n_s, u) = \prod_{j=1}^{n_s} \int_{v_j > 0} \det[K_{I,J}^{mom}(v_i, v_j)]_{n_s \times n_s} \quad (\text{D.18.3})$$

with the kernel $K_{I,J}^{mom}$ given in (D.9.6). Summation over n_s leads to the Fredholm determinant expression given in the text.

D.19 Appendix G: Moments-kernel in term of hypergeometric functions

We show that the moments-kernel K_{mom} can be exactly expressed in terms of hypergeometric functions by separating the summation over m even and m odd. We restrict to t even and $x = 0$ and define:

$$G_n(k, z) = \sum_{m=1}^{\infty} (-z)^m \left(\frac{\Gamma(-\frac{m}{2} + \frac{\gamma}{2} - ik) \Gamma(-\frac{m}{2} + \frac{\gamma}{2} + ik)}{\Gamma(\frac{m}{2} + \frac{\gamma}{2} - ik) \Gamma(\frac{m}{2} + \frac{\gamma}{2} + ik)} \right)^n = -1 + A_n(k, z^2) - z B_n(k, z^2)$$

with

$$A_n(k, z) = \sum_{m=0}^{\infty} z^m \left(\frac{\Gamma(-m + \frac{\gamma}{2} - ik) \Gamma(-m + \frac{\gamma}{2} + ik)}{\Gamma(m + \frac{\gamma}{2} - ik) \Gamma(m + \frac{\gamma}{2} + ik)} \right)^n \quad (\text{D.19.1})$$

and

$$B_n(k, z) = \sum_{m=0}^{\infty} z^m \left(\frac{\Gamma(-m - \frac{1}{2} + \frac{\gamma}{2} - ik) \Gamma(-m - \frac{1}{2} + \frac{\gamma}{2} + ik)}{\Gamma(m + \frac{1}{2} + \frac{\gamma}{2} - ik) \Gamma(m + \frac{1}{2} + \frac{\gamma}{2} + ik)} \right)^n \quad (\text{D.19.2})$$

Using the Euler reflection formula three times, we obtain:

$$\Gamma(-m + \frac{\gamma}{2} - ik) \Gamma(-m + \frac{\gamma}{2} + ik) = \frac{\Gamma(\frac{\gamma}{2} - ik) \Gamma(1 - \frac{\gamma}{2} + ik) \Gamma(\frac{\gamma}{2} + ik) \Gamma(1 - \frac{\gamma}{2} - ik)}{\Gamma(1 + m - \frac{\gamma}{2} + ik) \Gamma(1 + m - \frac{\gamma}{2} - ik)}$$

This allows to express

$$A_n(k, z) = {}_1F_{4n} \left(\{1\}, \left\{ \left(1 - \frac{\gamma}{2} + ik\right), \left(1 - \frac{\gamma}{2} - ik\right), \left(\frac{\gamma}{2} - ik\right), \left(\frac{\gamma}{2} + ik\right) \right\}_n; z \right) \quad (\text{D.19.3})$$

where we denote:

$$\begin{aligned} &\left\{ \left(1 - \frac{\gamma}{2} + ik\right), \left(1 - \frac{\gamma}{2} - ik\right), \left(\frac{\gamma}{2} - ik\right), \left(\frac{\gamma}{2} + ik\right) \right\}_n = \\ &\bigoplus_{i=1}^n \left\{ \left(1 - \frac{\gamma}{2} + ik\right), \left(1 - \frac{\gamma}{2} - ik\right), \left(\frac{\gamma}{2} - ik\right), \left(\frac{\gamma}{2} + ik\right) \right\} \end{aligned} \quad (\text{D.19.4})$$

The same type of calculation leads to

$$\begin{aligned} B_n(k, z) &= \left(\frac{4}{(\gamma - 1)^2 + 4k^2} \right)^n \\ &{}_1F_{4n} \left(\{1\}, \left\{ \left(\frac{3}{2} - \frac{\gamma}{2} + ik\right), \left(\frac{3}{2} - \frac{\gamma}{2} - ik\right), \left(\frac{1}{2} + \frac{\gamma}{2} - ik\right), \left(\frac{1}{2} + \frac{\gamma}{2} + ik\right) \right\}_n; z \right) \end{aligned} \quad (\text{D.19.5})$$

And this allows to express K_{mom} in (D.9.6) as:

$$K^{mom}(v_1, v_2) = \int_{\mathbb{R}} \frac{dk}{\pi} e^{-2ik(v_1 - v_2)} \left(-1 + A_{\frac{t}{2}+1}(k, u^2 e^{-2(v_1 + v_2)}) - u e^{-(v_1 + v_2)} B_{\frac{t}{2}+1}(k, u^2 e^{-2(v_1 + v_2)}) \right) \quad (\text{D.19.6})$$

The interesting feature is that on this result, the symmetry $\gamma \rightarrow 2 - \gamma$ holds. Since we know that the Laplace transform cannot have this symmetry, this shows once again that it cannot be equal to the moment generating function.

D.20 Appendix H: Some verifications of the various kernels

For t even and $x = 0$ (centered arrival point), the kernel (D.9.6) takes the form

$$K_t^{mom}(v_1, v_2) = \sum_{m=1}^{\infty} \int_{-\infty}^{+\infty} \frac{dk}{\pi} (-1)^m u^m e^{-2ik(v_1-v_2)-m(v_1+v_2)} \left(\frac{\Gamma(-\frac{m}{2} + \frac{\gamma}{2} - ik)\Gamma(-\frac{m}{2} + \frac{\gamma}{2} + ik)}{\Gamma(\frac{m}{2} + \frac{\gamma}{2} - ik)\Gamma(\frac{m}{2} + \frac{\gamma}{2} + ik)} \right)^{\frac{t}{2}+1} \quad (\text{D.20.1})$$

The integration over k can be performed by noting that there are two series of poles $ik = \pm(-p + \frac{m-\gamma}{2})$, $p \in \mathbb{N}$, in the gamma functions (the use of the residues formula here is legitimate, since, as in the main text, one can easily rewrite the quotient of Gamma functions as a rational fraction).

Consider $t = 0$. Let us consider for now only the terms $m < \gamma$, our goal will be to recover the moments $n < \gamma$ from the Fredholm determinant. The integral over k can be performed by closing the contour on the side $ik > 0$ or $ik < 0$ depending on the sign of $v_1 - v_2$ leading to:

$$K_{t=0}^{mom}(v_1, v_2) = 2 \sum_{m=1}^{\infty} \sum_{p=0}^{m-1} \frac{(-1)^p}{p!} \frac{\Gamma(\gamma + p - m)}{\Gamma(m - p)\Gamma(\gamma + p)} (-u)^m e^{-(2p+\gamma-m)|v_1-v_2|-m(v_1+v_2)}$$

since for $m < \gamma$ one picks either the first series of poles $ik > 0$ or the second.

Here at $t = 0$, we want to check that:

$$\text{Det}(I + K_{t=0}^{mom})|_{(-u)^n} = n!\Gamma(\gamma - n)/\Gamma(\gamma) \quad (\text{D.20.2})$$

We can use the expansion:

$$\begin{aligned} \text{Det}(I + K) &= e^{\ln(I+K)} = 1 + K + \frac{1}{2}((K)^2 - K^2) \\ &+ \frac{1}{6}((K)^3 - 3KK^2 + 2K^3) + \dots \end{aligned} \quad (\text{D.20.3})$$

we now denote $K = \sum_m K_m$ and check up to order 3 or 4 ..

The same reasoning can be applied to the different kernels obtained from this one in the text. One can check that (D.9.8) and (D.11.11) indeed give the moments of the distribution (checked at $t = 0$ and $t = 2$). One can also check that the first non-analytic terms in the Laplace transform of the probability distribution at $t = 0$ are reproduced. For that one starts from (D.11.11) and explicitly calculate the integral over w using residues

$$\begin{aligned} K_{1,1}^{BA}(z, z') &= \frac{1}{2\pi i} \sum_{n_1=1}^{\infty} \frac{(-u)^{n_1}}{z + n_1 - z'} \frac{\Gamma(\alpha - z - n_1)\Gamma(z - a)}{\Gamma(z + n_1 - a)\Gamma(\alpha - z)} \\ &+ \frac{1}{2\pi i} \sum_{n_2=0}^{\infty} \frac{\pi}{\sin(\pi(z - \alpha - n_2))} \frac{(-1)^{n_2}}{n_2!} \frac{u^{\alpha+n_2-z}}{\alpha + n_2 - z'} \frac{\Gamma(z - a)}{\Gamma(\alpha + n_2 - a)\Gamma(\alpha - z)} \end{aligned} \quad (\text{D.20.4})$$

Using this expansion allows to recover the first terms in D.17.3 and in particular the non analytic terms $\frac{(-1)^n}{n!} u^{\gamma+n} \frac{\Gamma(-\gamma-n)}{\Gamma(\gamma)}$ (we checked it for $n = 0, 1$). The various traces can be computed using the residues theorem. Integer powers of u come from the first part of the expansion and from the poles of the sine function in the second part, whereas non-integer powers of u come from the poles of the Gamma function in the second part. The fact that we can extract the correct integer moments from the kernels is a consistency check of the procedure. On the other hand, being able to retrieve the non analyticity is another sign that the Mellin-Barnes trick indeed provides the correct analytic continuation.

D.21 Appendix I: Probability distribution at any time

Starting from the expression for the generating function $g_{I,J}(u) = \overline{e^{-uZ(I,J)}}$ and writing formally $Z(I, J)$ as the product of a variable Z_0 with an exponential distribution: $P_0(Z_0) = e^{-Z_0}$ (i.e. $\log Z_0$ has a unit Gumbel distribution), and a new positive random variable $\tilde{Z}(I, J)$ distributed according to $\tilde{P}_{I,J}$, one has

$$g_{I,J}(u) = \overline{e^{-uZ_0\tilde{Z}(I,J)}} = \int dZ_0 e^{-uZ_0\tilde{Z}(I,J)} e^{-Z_0} = \frac{1}{1 + u\tilde{Z}(I,J)} = \int d\tilde{Z} \frac{1}{1 + u\tilde{Z}} \tilde{P}_{I,J}(\tilde{Z}) \quad (\text{D.21.1})$$

Assuming an analytic continuation, we write

$$g_{I,J}\left(\frac{1}{-v - i\epsilon}\right) = \int d\tilde{Z} \frac{-v}{\tilde{Z} - v - i\epsilon} \tilde{P}_{I,J}(\tilde{Z}) \quad (\text{D.21.2})$$

And the limit $\epsilon \rightarrow 0^+$ allows to extract the probability distribution $\tilde{P}_{I,J}$ as

$$\tilde{P}_{I,J}(v) = \frac{1}{2i\pi v} \lim_{\epsilon \rightarrow 0^+} \left(g_{I,J}\left(\frac{1}{-v + i\epsilon}\right) - g_{I,J}\left(\frac{1}{-v - i\epsilon}\right) \right) \quad (\text{D.21.3})$$

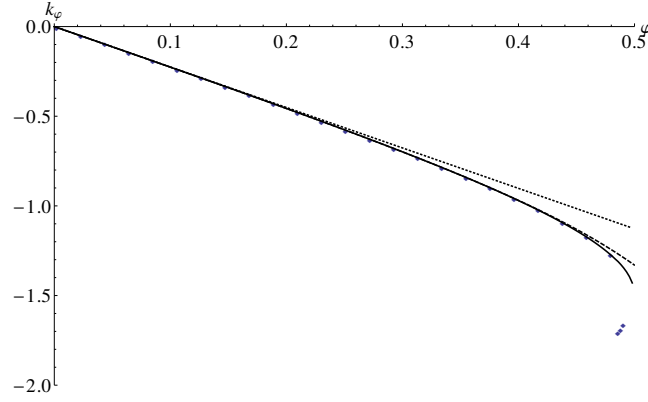


Figure D.4: Saddle-point position k_φ as a function of φ for $\gamma = 3$. The dotted-line is the approximation to lowest order in φ , i.e. $k_\varphi \sim \varphi$ (STS). The losanges are the numerical solution. The dashed line is a high order perturbative approximation and the solid line is the final result that uses the non-analytic behaviour near $\varphi = \frac{1}{2}$. The additional points below arise from numerical artefacts.

Using (D.9.8), we write $g_{I,J}(\frac{1}{-v \pm i\epsilon}) = \text{Det}(I + \tilde{K}_{I,J}^\pm)$ with

$$\tilde{K}_{I,J}^\pm(v_1, v_2) = \int_{-\infty}^{+\infty} \frac{dk}{\pi} \frac{-1}{2i} \int_{\mathcal{C}} \frac{ds}{\sin(\pi s)} \left(\frac{1}{-v \pm i\epsilon} \right)^s e^{-2ik(v_1 - v_2) - s(v_1 + v_2)} \quad (\text{D.21.4})$$

$$\left(\frac{\Gamma(-\frac{s}{2} + \frac{\gamma}{2} - ik)}{\Gamma(\frac{s}{2} + \frac{\gamma}{2} - ik)} \right)^I \left(\frac{\Gamma(-\frac{s}{2} + \frac{\gamma}{2} + ik)}{\Gamma(\frac{s}{2} + \frac{\gamma}{2} + ik)} \right)^J$$

Using the principal determination of the logarithm, and since v has to be positive, we have

$$\lim_{\epsilon \rightarrow 0^+} \left(\frac{1}{-v \pm i\epsilon} \right)^s = \exp(-s \log(v) \mp i\pi s) \quad (\text{D.21.5})$$

Finally, writing $e^{\mp i\pi s} = \cos(\pi s) \mp i \sin(\pi s)$ leads to the formula of the main text.

D.22 Appendix J: Saddle point position

The numerical resolution of the saddle-point equation (D.10.5), i.e.:

$$\frac{\frac{1}{2} + \varphi}{\frac{1}{2} - \varphi} = \frac{\psi'(\frac{\gamma}{2} - k_\varphi)}{\psi'(\frac{\gamma}{2} + k_\varphi)} \quad (\text{D.22.1})$$

is complicated by the divergence near $\varphi = \frac{1}{2}$. In fact there is a solution such that the argument of the ψ' function remains positive. Since $\lim_{x \rightarrow 0^+} \psi'(x) = +\infty$ it is easy to see that $\lim_{\varphi \rightarrow \frac{1}{2}} k_\varphi = -\frac{\gamma}{2}$. Explicitly, the leading behavior of k_φ is

$$k_\varphi \simeq_{\varphi \rightarrow \frac{1}{2}} -\frac{\gamma}{2} + \left(\frac{\frac{1}{2} - \varphi}{\psi'(\gamma)} \right)^{\frac{1}{2}} + \dots \quad (\text{D.22.2})$$

This divergence makes the numerical solution fail around $\varphi = \frac{1}{2}$: k_φ crosses the singularity at $-\frac{\gamma}{2}$. On the other hand, the non-analyticity makes a perturbative calculation inefficient close to this point. The most accurate determination appears to be a fit between the numerical result and the known non analyticity, which is what was used for Fig. D.2 and D.3 in the text. Fig D.4 summarize the situation.

D.23 Appendix K: The semi-directed random polymer

The semi-directed random polymer was introduced by O'Connell and Yor in [190, 191]. In [193] it was argued that it constitutes a universal scaling limit for polymer restricted to stay close to the boundary (with proper rescaling of the temperature or in our case, of the parameter of the inverse-gamma distribution). In the simplest case (no drift, temperature and total polymer length t set to unity) it is defined as the partition sum

$$Z_N^{s.d.} = \int_{0 < s_1 < \dots < s_{N-1} \leq 1} e^{B_1(s_1) + (B_2(s_2) - B_2(s_1)) + \dots + (B_N(1) - B_N(s_{N-1}))} \quad (\text{D.23.1})$$

where $B_j(s)$ are N independent standard Brownian motions. In [198], it was shown that this model could be obtained as the following scaling limit of the log-Gamma polymer: $Z_N^{s,d} \underset{\text{in law}}{\sim} \lim_{n \rightarrow \infty} e^{n \log(n) - \frac{1}{2}} Z(n, N)|_{\gamma=n}$. Here we show how this scaling limit naturally appears and we obtain a Fredholm-Determinant formula for the Laplace transform of the semi-directed polymer partition sum. Starting from (D.11.11) we need to analyze the large n limit of $\text{Det}(I + K_{n,N}^{BA})$ where

$$K_{n,N}^{BA}(z, z') = \int_{a+i\mathbb{R}} ds \frac{1}{4\pi(s+z-z')} \frac{1}{\sin(\pi s)} u^s \left(\frac{\Gamma(z)}{\Gamma(z+s)} \right)^N \left(\frac{\Gamma(n-z-s)}{\Gamma(n-z)} \right)^n \tag{D.23.2}$$

and $z, z' \in \tilde{a} + i\mathbb{R}$. We have defined $s = w - z$ and renamed $z - a \rightarrow z$. Here the factor $\left(\frac{\Gamma(n-z-s)}{\Gamma(n-z)} \right)^n$ takes a simple form in the large n limit:

$$\left(\frac{\Gamma(n-z-s)}{\Gamma(n-z)} \right)^n = \exp \left(n \left(-s\psi(n) + \frac{1}{2}\psi'(n)(2sz + s^2) + O\left(\frac{1}{n^2}\right) \right) \right) \tag{D.23.3}$$

where use that $\psi^{(k)}(n) = O\left(\frac{1}{n^k}\right)$ for $n \rightarrow \infty$. Using $\psi(n) =_{n \rightarrow \infty} \log(n) - \frac{1}{2n} + O\left(\frac{1}{n^2}\right)$ and $\psi'(n) =_{n \rightarrow \infty} \frac{1}{n} + O\left(\frac{1}{n^2}\right)$, we thus arrive at:

$$\left(\frac{\Gamma(n-z-s)}{\Gamma(n-z)} \right)^n \underset{n \rightarrow \infty}{\sim} \exp \left(-s(n \log n - \frac{1}{2}) + sz + \frac{1}{2}s^2 \right) \tag{D.23.4}$$

The first term indeed imposes to rescale the partition sum as $\hat{Z}(n, N) = e^{n \log(n) - \frac{1}{2}} Z(n, N)$ so that the laplace transform of $\hat{Z}(n, N)$, $\hat{g}_{n,N} = \exp -u\hat{Z}(n, N)$ has a well-defined $n \rightarrow \infty$ limit given by a Fredholm determinant, with:

$$\lim_{n \rightarrow +\infty} \hat{g}_{n,N} = \text{Det}(I + \hat{K}_N) \tag{D.23.5}$$

$$\hat{K}_N(z, z') = \int_{a+i\mathbb{R}} ds \frac{1}{4\pi(s+z-z')} \frac{1}{\sin(\pi s)} u^s \left(\frac{\Gamma(z)}{\Gamma(z+s)} \right)^N e^{sz + \frac{1}{2}s^2} \tag{D.23.6}$$

and $z, z' \in \tilde{a} + i\mathbb{R}$. We recall $0 < a < 1$ and $0 < \tilde{a}$ (in the limit). This result is identical to Theorem 3 of [218] for the case of zero drift and $t = 1$ (see also Theorem 1.5 in [34]) apart from the (now usual) difference of contours. There z, z' belong to a small circle around 0, while the s contour is the same. A similar (large-contour) formula can be found in Theorem 1.17. of [243]. There (for our case), the contour of integration on z is a wedge $C_{\alpha,\phi} = \{\alpha + e^{i(\pi+\phi)}\mathbb{R}_+\} \cup \{\alpha + e^{i(\pi-\phi)}\mathbb{R}_+\}$ where $\alpha > 0$ and $0 < \phi < \pi/4$, and the contour of integration on s , D_z , is z -dependent and given by straight-lines joining $R(z) - i\infty$ to $R(z) - id$ to $\frac{1}{2} - id$ to $\frac{1}{2} + id$ to $R(z) + id$ to $R(z) + i\infty$, where $R(z) = -\text{Re}(z) + \alpha + 1$ and $d > 0$ is small enough so that to ensure that $z + D_z$ do not intersect $C_{\alpha,\phi}$. These contours are more involved but are similarly located as ours with respect to the poles of the integrand.

Appendix E

Paper: On integrable directed polymer models on the square lattice

The following is essentially the article published as

Title: On integrable directed polymer models on the square lattice

Authors: Thimothée Thiery and Pierre Le Doussal

ArXiv: 1506.05006

Journal-Ref: Journal of Physics A: Mathematical and Theoretical, Volume 48, Number 46

Abstract: In a recent work Povolotsky [222] provided a three-parameter family of stochastic particle systems with zero-range interactions in one dimension which are integrable by coordinate Bethe ansatz. Using these results we obtain the corresponding condition for integrability of a class of directed polymer models with random weights on the square lattice. Analyzing the solutions we find, besides known cases, a new two-parameter family of integrable DP model, which we call *the Inverse-Beta polymer*, and provide its Bethe ansatz solution.

E.1 Introduction and main results

E.1.1 overview

There is considerable recent interest in exact solutions for models in the universality class of the 1D stochastic growth Kardar-Parisi-Zhang equation (KPZ) [33]. Models in the KPZ class share the same large time statistics, also found to be related to the universal statistics of large random matrices [37]. Methods developed in the context of quantum integrability are exploited and broadly extended to solve a variety of 1D stochastic models. The Bethe ansatz solution of the attractive delta Bose gas (the Lieb-Liniger model [202, 209]) was combined with the replica method [201], to obtain exact solutions for the KPZ equation directly in the continuum and at arbitrary time, for the main classes of initial conditions (droplet, flat, stationary, half-space) [173, 165, 177, 183, 169, 215, 175, 214, 242]. The Cole-Hopf mapping $h \sim \ln Z$ is used, where h is the height of the KPZ interface and Z the partition sum of a directed polymer in a random potential (DP). Hence in the continuum, studying KPZ growth is equivalent to studying the DP model, an equilibrium statistical mechanics problem with quenched disorder. The time in KPZ growth becomes the length of the polymer t . The replica Bethe ansatz (RBA) method then allows to calculate the integer moments $\overline{Z^n}$ and, from them, to retrieve the probability distribution function (PDF) of Z . Since the last step is non-rigorous because of the fast growth of these moments, the mathematical community has concentrated on the exact solution of discrete models, which in favorable cases, do not suffer from the moment growth problem. Discrete models, such as the PNG growth model [39, 246], the TASEP and ASEP particle transport model [226] and discrete DP models [159, 190] played a pioneering role in unveiling the universal statistics of the KPZ class at large time (the Airy processes). Recently they have been considerably generalized, unveiling a very rich underlying "stochastic integrability" structure [192, 222, 191, 208, 243, 208, 34, 247]. Since in suitable limits (e.g. ASEP with weak asymmetry, q -TASEP with $q \rightarrow 1$, semi-discrete DP) they converge to the continuum KPZ equation, they also led to some recent rigorous results for KPZ at arbitrary time [172, 171, 34, 185, 180].

Besides their interest in relation to KPZ growth, directed polymers are also important in a variety of fields. This includes optimization and glasses [248, 249], vortex lines in superconductors [235], domain walls in magnets [29], disordered conductors [250], Burgers equation in fluid mechanics [194], exploration-exploitation tradeoff in population dynamics and economics [251] and in biophysics [252, 253]. In some situations (heavy tailed disorder) they exhibit anomalous (non-standard KPZ) scaling [13, 14]. Apart from models on trees, exactly solvable models of DP (e.g. on regular lattices) remain, however, exceedingly rare. We will present in this paper a new solvable DP model.

On the square lattice a few remarkable solvable DP models have been found. The first that was discovered is at zero temperature $T = 0$ (i.e. it amounts to find the minimal energy path, energies being additive along a path), with a geometric distribution (of parameter $q < 1$) of on-site random potentials [159]. The second that was discovered, called the log-Gamma polymer [197], is a finite temperature model (as it focuses on Boltzman weights, which are multiplicative along a path), with a so-called inverse gamma distribution for the on-site random weights, with parameter γ . This weight distribution

has the peculiarity of exhibiting a fat tail $P(w) \sim w^{-1+\gamma}$. These models are not unrelated: in the limit $\gamma \rightarrow 0$ (so-called zero temperature) the log-Gamma converges to the $q \rightarrow 1$ limit of the Johansson model (i.e. with exponentially distributed on-site weights) [198]. They were both proved to belong to the KPZ class, with convergence of the free energy PDF to the GUE Tracy Widom distribution. The Johansson model was solved as a determinantal process [159]. The log-Gamma model was solved using the gRSK correspondence (a geometric lifting of the Robinson-Schensted-Knuth (RSK) correspondence) leading finally to an expression for the Laplace transform of $P(Z)$ as a Fredholm determinant [198, 218].

Recently, we provided a solution of the log-Gamma polymer using replicas and the coordinate Bethe ansatz, closer in spirit to the integrability methods used to solve KPZ [4]. As in the continuum, this replica Bethe ansatz approach consists in computing the moments of the partition sum of the DP using a transfer matrix (i.e. recursive) formulation of the problem. This formulation can formally be interpreted as a discrete-time quantum mechanical model of interacting Bosons. Such a connection between discrete-time particle models and lattice DP was also noted, and exploited in [219] to unveil and study a new integrable DP model with Gamma distributed Boltzmann weights, called the ‘‘Strict-Weak’’ DP model, as the $q \rightarrow 1$ limit of the discrete time q -TASEP model [254]. In parallel, this DP model was also solved using the gRSK correspondence in [220].

In a recent seminal work, Povolotsky [222] provided a three parameter family of discrete-time stochastic interacting particles systems with zero range interactions (‘‘zero-range processes’’ (ZRP)) called the (q, μ, ν) -Boson process and integrable by coordinate Bethe ansatz. This led to further rigorous work on this class of particle model and on a dual model, termed the q -Hahn TASEP, which eventually allowed to unify integrability properties of ASEP and q -TASEP, a long-standing goal [208, 208, 34]. On the directed polymer side, this work also led to the discovery of a new integrable model, called the ‘‘Beta’’ polymer, introduced and studied in [224]. There the model was solved as a $q \rightarrow 1$ limit of the (q, μ, ν) -Boson (in analogy with the Strict-Weak case), but the authors also already provided a direct replicas Bethe ansatz solution of the model.

The aim of the present paper is to explore more systematically the consequences of Povolotsky’s work to directly search for, and attempt to classify, the corresponding family of integrable DP models. Integrability then leads to a constraint on the integer moments of the Boltzmann weights distributions, and we search for solutions in terms of PDF of bond and site disorder.

We find that there are two main solutions, the first one corresponding to the Beta polymer[224]. The second however is new and corresponds to weights v on horizontal bonds, and u on vertical bonds of the square lattice, with the following PDF: u , is distributed according to:

$$\tilde{p}_{\gamma, \beta}(u) = \frac{\Gamma(\gamma + \beta)}{\Gamma(\gamma)\Gamma(\beta)} \frac{1}{u^{1+\gamma}} \left(1 - \frac{1}{u}\right)^{\beta-1}, \quad u \in [1, +\infty[\quad , \gamma, \beta > 0 \quad (\text{E.1.1})$$

The weights are correlated on bonds which share a top/right site (see Fig. E.1), with $v = u - 1 \in [0, +\infty[$ but otherwise uncorrelated. Given the form of (E.1.1) we call our new model the Inverse-Beta polymer¹.

We will provide in this paper the coordinate Bethe ansatz solution to this model, as well as some explicit integral representation and Fredholm determinant formulas for its Laplace transform. It is interesting to note that for $\beta \rightarrow +\infty$ this model, under suitable rescaling, converges to the log-Gamma polymer (see below). Hence it can be considered as a generalization of the log-Gamma polymer.

E.1.2 Main results and outline of the paper

The first result of this paper, obtained in Section E.2, are some general conditions for a finite temperature model of directed polymer on the square lattice to be integrable using the coordinate Bethe ansatz. The only hypothesis are that Boltzmann weights on horizontal edges and vertical edges can be correlated only if they share the same top or right site (an example of short-range correlations), and that they are homogeneously distributed. Within this framework, in Section E.3, we attempt a classification of integrable DP models, retrieve the known integrable models and introduce a new one, the Inverse-Beta polymer, whose Boltzmann weights are distributed as (E.1.1). This model has two parameters $\gamma, \beta > 0$ and contains the log-Gamma and Strict-Weak polymers as scaling limits. More precisely, we show that the partition sum $Z_t(x)$ of the Inverse-Beta model (see Section E.2.1 for the definition) converges in law to the partition sum of the log-Gamma (resp. Strict-Weak) polymer $Z_t^{LG}(x)$ (resp. $Z_t^{SW}(x)$) as

$$\lim_{\beta \rightarrow \infty} \frac{1}{\beta^t} Z_t(x) \sim Z_t^{LG}(x) \quad , \quad \lim_{\gamma \rightarrow \infty} \gamma^x Z_t(x) \sim Z_t^{SW}(x) . \quad (\text{E.1.2})$$

In Section E.4 we use the coordinate Bethe ansatz to study the Inverse-Beta polymer with point-to-point boundary conditions. We obtain an exact result for the integer moments of the partition sum $\overline{Z}_t(x)^n$ (E.4.18), defined for $n < \gamma$. Using this result, we conjecture the formula (E.4.27) that expresses the Laplace transform of $Z_t(x)$ as a Fredholm determinant $e^{-uZ_t(x)} = \text{Det}(I + K_{t,x})$ with

$$K_{t,x}(v_1, v_2) = \int_{-\infty}^{+\infty} \frac{dk}{\pi} \frac{-1}{2i} \int_C \frac{ds}{\sin(\pi s)} u^s e^{-2ik(v_1 - v_2) - s(v_1 + v_2)} \quad (\text{E.1.3})$$

$$\left(\frac{\Gamma(-\frac{s}{2} + \frac{\gamma}{2} - ik)}{\Gamma(\frac{s}{2} + \frac{\gamma}{2} - ik)} \right)^{1+x} \left(\frac{\Gamma(-\frac{s}{2} + \frac{\gamma}{2} + ik)}{\Gamma(\frac{s}{2} + \frac{\gamma}{2} + ik)} \right)^{1-x+t} \left(\frac{\Gamma(\beta + ik + \frac{\gamma}{2} + \frac{s}{2})}{\Gamma(\beta + ik + \frac{\gamma}{2} - \frac{s}{2})} \right)^t$$

¹Note that a nomenclature based on the names of the weight distributions, the log-Gamma polymer could be called the Inverse-Gamma polymer, and the Strict-Weak the Gamma polymer. Alternatively our model could be called the log-Beta polymer.

where $C = a + i\mathbb{R}$ with $0 < a < \min(1, \gamma)$ and $K_{t,x} : L^2(\mathbb{R}_+) \rightarrow L^2(\mathbb{R}_+)$. Alternatively, we obtain an equivalent Fredholm determinant for the same quantity with a different kernel (which contains notably one less integral) in (E.4.28). By analogy with a known formula for the log-Gamma polymer, we also conjecture a n-fold integral formula (E.4.29) for the Laplace transform

$$\overline{e^{-uZ_t(x)}} = \frac{1}{J!} \int_{(i\mathbb{R})^J} \prod_{j=1}^J \frac{dw_j}{2i\pi} \prod_{j \neq k=1}^J \frac{1}{\Gamma(w_j - w_k)} \left(\prod_{j=1}^J u^{w_j - a} \Gamma[a - w_j]^J \left(\frac{\Gamma(\gamma + a - w_j)}{\Gamma(\gamma)} \right)^I \left(\frac{\Gamma(w_j - a + \beta)}{\Gamma(\beta)} \right)^{I+J-2} \right), \quad (\text{E.1.4})$$

with $0 < a < \min(1, \gamma)$, valid for $\text{Re}(u) > 0$, $1 \leq J \leq I$ and where $x = I - 1$ and $t = I + J - 2$. Using an asymptotic analysis of our Fredholm determinant formulas, we show in Section E.4.3 the KPZ universality of the model for polymers of large length $t \rightarrow \infty$ with an arbitrary angle $\varphi \in] -1/2, 1/2\hat{a}[$ with respect to the diagonal. More precisely, we show

$$\lim_{t \rightarrow \infty} \text{Prob} \left(\frac{\log Z_t((1/2 + \varphi)t) + tc_\varphi}{\lambda_\varphi} < 2^{\frac{2}{3}} z \right) = F_2(z) \quad (\text{E.1.5})$$

where $F_2(z)$ is the standard GUE Tracy-Widom cumulative distribution function, $\lambda_\varphi \sim t^{1/3}$ and the (φ -dependent) constants are determined by a system of equations (E.4.38) that involves the digamma function ψ . As a particular case we study these characteristic constants for long polymers with the ‘optimal angle’ $\varphi = \varphi^*$ (in the sense that the mean free energy c_φ is minimal for this angle) and find explicit expressions as

$$\begin{aligned} \varphi^* &= -\frac{1}{2} \frac{\psi'(\beta + \gamma/2)}{\psi'(\gamma/2)} < 0 \\ c_{\varphi^*} &= \psi(\gamma/2) - \psi(\beta + \gamma/2) \\ \lambda_{\varphi^*} &= \left(\frac{t}{8} (\psi''(\beta + \gamma/2) - \psi''(\gamma/2)) \right)^{1/3}. \end{aligned} \quad (\text{E.1.6})$$

Finally, in Section (E.4.4) we study a two parameters zero temperature DP model that we obtain as the limit $\gamma = \epsilon\gamma'$ and $\beta = \epsilon\beta'$ with $\epsilon \rightarrow 0$ of the Inverse-Beta polymer. This study is close in spirit to the one made in [224] where the zero temperature limit of the Beta polymer is studied, but the models are qualitatively very different. The energy of this model are distributed as $(\mathcal{E}'_u, \mathcal{E}'_v) = (-\zeta E_{\gamma'}, (1 - \zeta) E_{\beta'} - \zeta E_{\gamma'})$ where $(\mathcal{E}'_u, \mathcal{E}'_v)$ are the energies on vertical and horizontal edges, ζ is a Bernoulli random variable of parameter $p = \beta' / (\gamma' + \beta')$ and $E_{\gamma'}$ and $E_{\beta'}$ are exponential random variables of parameter $\gamma' > 0$ and $\beta' > 0$, independent of ζ . This model generalizes the known zero temperature limit of the log-Gamma directed polymer and we obtain exact results for the cumulative distribution of the optimal energy, noted $\mathfrak{E}_{(t,x)}$, of this zero temperature model $\text{Prob}(\mathfrak{E}_{(t,x)} > r)$. In particular we obtain a Fredholm determinant formula (E.4.57) $\text{Prob}(\mathfrak{E}_{(t,x)} > r) = \text{Det}(I + K_{t,x}^{T=0})$ with

$$K_{t,x}^{T=0}(v_1, v_2) = - \int_{-\infty}^{+\infty} \frac{dk}{\pi} \int_C \frac{ds}{2i\pi s} e^{sr - 2ik(v_1 - v_2) - s(v_1 + v_2)} \left(\frac{\frac{s}{2} + \frac{\gamma'}{2} - ik}{-\frac{s}{2} + \frac{\gamma'}{2} - ik} \right)^{1+x} \left(\frac{\frac{s}{2} + \frac{\gamma'}{2} + ik}{-\frac{s}{2} + \frac{\gamma'}{2} + ik} \right)^{1-x+t} \left(\frac{\beta' + ik + \frac{\gamma'}{2} - \frac{s}{2}}{\beta' + ik + \frac{\gamma'}{2} + \frac{s}{2}} \right)^t. \quad (\text{E.1.7})$$

where $\tilde{C} = a + i\mathbb{R}$ with $0 < a < \gamma'$ and $K_{t,x}^{T=0} : L^2(\mathbb{R}_+) \rightarrow L^2(\mathbb{R}_+)$. We also conjecture an equivalent n-fold integral formula (E.4.59)

$$\text{Prob}(\mathfrak{E}_{(t,x)} > r) = \frac{1}{J!} \int_{(i\mathbb{R})^J} \prod_{j=1}^J \frac{dw_j}{2i\pi} \prod_{j \neq k=1}^J (w_j - w_k) \prod_{j=1}^J \frac{e^{r(w_j - a)}}{(a - w_j)^J} \left(\frac{\gamma'}{\gamma' + a - w_j} \right)^I \left(\frac{\beta'}{w_j - a + \beta'} \right)^{I+J-2}. \quad (\text{E.1.8})$$

with $0 < a < \gamma'$. Using our exact results, we conclude this section by showing the KPZ universality of the zero temperature model in (E.4.64). In the case $\beta' / \gamma' \rightarrow \infty$ the model maps onto the Johansson DP model with an exponential distribution and we show that our solution reproduces all the (non trivial) angle dependent normalizing constants in the statement of convergence to the GUE Tracy Widom distribution.

A series of appendices also contains additional discussions and some technical details separated from the main text for clarity.

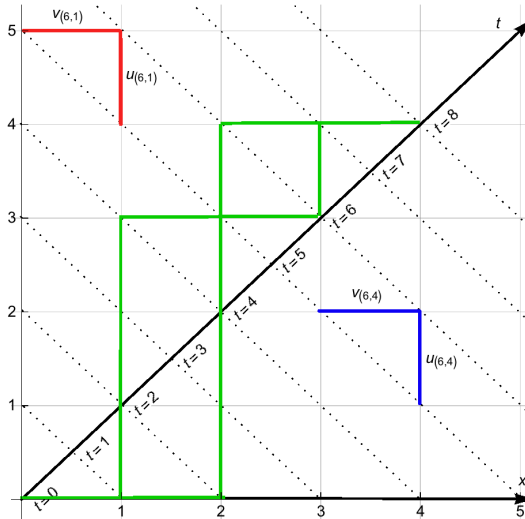


Figure E.1: General scheme for the models of directed polymer studied here. Blue (resp. Red) : couple of correlated Boltzmann weight on edges arriving at $(t = 6, x = 1)$ (resp. $(t = 6, x = 4)$). Green: two admissible (i.e. up/right) paths for polymers with starting point $(0, 0)$ and endpoint $(8, 4)$.

E.2 Directed Polymers on the square Lattice: Replica method and integrability

E.2.1 Definition of the model

We consider the square lattice \mathbb{Z}^2 with coordinates (t, x) with x the usual horizontal coordinate and t a coordinate² running through the diagonal of \mathbb{Z}^2 as depicted in Fig. E.1. We will also sometime use the usual euclidean coordinates (I, J) on \mathbb{Z}^2 with $x = I - 1$ and $t = I + J - 2$. The first quadrant is thus $I, J \geq 1$ and $x, t \geq 0$. A directed polymer model on \mathbb{Z}^2 is defined by the partition sum

$$Z_t(x) = \sum_{\pi: (0,0) \rightarrow (t,x)} \prod_{e \in \pi} w_e \quad (\text{E.2.1})$$

where the sum is on all directed (i.e. up/right) paths with fixed starting point $(0, 0)$ (corresponding to $(I, J) = (1, 1)$) and endpoint (t, x) , and the product is on all edges $e = (t', x') \rightarrow (t' + 1, x')$ or $e = (t', x') \rightarrow (t' + 1, x' + 1)$ visited by π . Here for definiteness we consider a directed polymer model with fixed endpoints, but the model can be generalized to other boundary conditions. We also restrict ourselves to models with on-links Boltzmann weights w_e . Obviously, by redefining the weights w_e , one can also include on-sites Boltzmann weights so that this hypothesis is non restrictive. The Boltzmann weights are positive random variables $w_e \in \mathbb{R}_+$. We will generally note u (resp. v) the Boltzmann weights on vertical (resp. horizontal) edges:

$$\begin{aligned} w_e &= u_{t,x} \text{ if } e = (t-1, x) \rightarrow (t, x), \\ w_e &= v_{t,x} \text{ if } e = (t-1, x-1) \rightarrow (t, x). \end{aligned} \quad (\text{E.2.2})$$

We will consider the class of models with the following structure of local correlations, which naturally emerges in the integrable family we are studying: the weights on edges arriving at different sites are statistically independent, but the weights of two edges arriving at the same site are correlated. Thus the model is defined by a (common) joint PDF for the weights of the type $(u_{t,x}, v_{t,x})$, denoted $p(u, v)$ (see Fig. E.1). The pairs $(u_{t,x}, v_{t,x})$ are chosen independently from site to site. In the following, the overline $\overline{(\cdot)}$ denotes the average of a quantity over all realizations for the $(u_{t,x}, v_{t,x})$.

E.2.2 The replica method and the coordinate Bethe Ansatz.

In general, one is interested in computing the PDF of $Z_t(x)$ or of its logarithm $\log Z_t(x)$. The replica method consists in first studying the equal-time moments of $Z_t(x)$: for $n \in \mathbb{N}$ and whenever they exist, one defines

$$\psi_t(x_1, \dots, x_n) = \overline{Z_t(x_1) \dots Z_t(x_n)}. \quad (\text{E.2.3})$$

²Note that the (t, x) coordinates of the present paper do not coincide with the ones of [4] that we denote (T, X) . To compare formulas, one can use $t = T$ and $x = t/2 + X$.

In the general case these moments are only defined for $n \leq n_{\max}$, because of possible fat-tail in the distribution of Boltzmann weights, such that $\overline{u^{n_1} v^{n_2}}$ are finite for $n_1 + n_2 \leq n_{\max}$ but are infinite for some (n_1, n_2) with $n_1 + n_2 > n_{\max}$. In the log-Gamma case one has $n_{\max} = \lfloor \gamma^- \rfloor$ whereas in the Beta polymer case $n_{\max} = \infty$. Obtaining the PDF of $Z_t(x)$ from the knowledge of the moments is usually non-trivial, especially when $n_{\max} < \infty$. In this case the procedure is non-rigorous and one has to perform some analytical continuation as in the log-Gamma case. In most of this section we will not discuss this issue and only focus on computing the moments for $n \leq n_{\max}$, which is a well-defined problem. The problem of computing ψ_t is manageable thanks to a the recursive formulation of (E.2.1):

$$\begin{aligned} Z_{t=0}(x) &= \delta_{x,0} \\ Z_{t+1}(x) &= u_{t+1,x} Z_t(x) + v_{t+1,x} Z_t(x-1). \end{aligned} \quad (\text{E.2.4})$$

This can be translated to a recursive (i.e. transfer matrix) equation for ψ_t :

$$\begin{aligned} \psi_{t=0}(x_1 \dots, x_n) &= \delta_{x_1,0} \dots \delta_{x_n,0} \\ \psi_{t+1}(x_1 \dots, x_n) &= \sum_{\{\delta_1, \dots, \delta_n\} \in \{0,1\}^n} a_{x_1, \dots, x_n}^{\delta_1, \dots, \delta_n} \psi_t(x_1 - \delta_1, \dots, x_n - \delta_n) = (T_n \psi_t)(x_1 \dots, x_n) \\ a_{x_1, \dots, x_n}^{\delta_1, \dots, \delta_n} &= \prod_{y \in \mathbb{Z}} (u)^{\sum_{i=1}^n \delta_{x_i, y} \delta_{\delta_i, 0}} (v)^{\sum_{i=1}^n \delta_{x_i, y} \delta_{\delta_i, 1}}. \end{aligned} \quad (\text{E.2.5})$$

Where we used the statistical independence of the Boltzmann weights ending at different sites and the definition of (u, v) . Note that the evolution equation (E.2.5) is symmetric by exchange $x_i \leftrightarrow x_j$. Therefore, since the initial condition is also fully symmetric, if one is able to find all the symmetric eigenfunctions ψ_μ of T_n , i.e. a complete basis of symmetric functions such that $T_n \psi_\mu = \Lambda_\mu \psi_\mu$, the problem is essentially solved. In the already known models, it was possible to find the eigenfunctions of T_n in the form of the coordinate Bethe Ansatz. More precisely, in the sector $W_n = \{x_1 \leq \dots \leq x_n\}$ (this defines the Weyl chamber), one looks for eigenfunctions of the form

$$\begin{aligned} \psi_\mu(x_1, \dots, x_n) &= \tilde{\psi}_\mu(x_1, \dots, x_n) \text{ if } x_1 \leq \dots \leq x_n \\ \tilde{\psi}_\mu(x_1, \dots, x_n) &= \sum_{\sigma \in S_n} A_\sigma \prod_{i=1}^n z_{\sigma(i)}^{x_i} \end{aligned} \quad (\text{E.2.6})$$

where the sum runs over all permutations of $\{1, \dots, n\}$, and the variables A_σ and z_i are complex numbers. The wave function $\psi_\mu(x_1, \dots, x_n)$ is deduced in the other sectors by using that it is fully symmetric function of its arguments. As one can guess, this form of eigenfunction is restrictive and it can only works if the variables $a_{x_1, \dots, x_n}^{\delta_1, \dots, \delta_n}$, or equivalently the integer moments $\overline{u^{n_1} v^{n_2}}$ for $(n_1, n_2) \in \mathbb{N}^2$ obey a particular structure. Thus one can hope to classify the models that are solvable by the coordinate Bethe Ansatz. In fact, (E.2.5) is reminiscent of the equations usually considered in the study of zero-range stochastic particle systems, for which a classification was proposed in [222] and latter extended in [247]. In the next section we follow the route of [222] and adapt it to our setting to deduce a classification of integrable directed polymers models³.

E.2.3 The constraint of integrability on integer moments.

If one can diagonalize the evolution equation (E.2.5) using the Bethe Ansatz (E.2.6), then in the sector $\overset{\circ}{W}_n = \{x_1 < \dots < x_n\}$ (i.e. the interior of the Weyl chamber where all particles sit on distinct sites and do not interact), one must have

$$\begin{aligned} \Lambda_\mu \psi_\mu(x_1, \dots, x_n) &= (T_n \psi_\mu)(x_1, \dots, x_n) \\ \Lambda_\mu \tilde{\psi}_\mu(x_1, \dots, x_n) &= \sum_{\{\delta_1, \dots, \delta_n\} \in \{0,1\}^n} (\bar{u})^{n - \sum_{i=1}^n \delta_i} (\bar{v})^{\sum_{i=1}^n \delta_i} \tilde{\psi}_\mu(x_1 - \delta_1, \dots, x_n - \delta_n) \\ &= \prod_{i=1}^n (\bar{u} + \bar{v} z_i^{-1}) \tilde{\psi}_\mu(x_1, \dots, x_n), \end{aligned} \quad (\text{E.2.7})$$

and this already imposes the eigenvalue to be $\Lambda_\mu = \prod_{i=1}^n (\bar{u} + \bar{v} z_i^{-1})$. Note that this is a direct consequence of the weights having zero-range interaction: in the $\overset{\circ}{W}_n$ sector, the operator T_n just acts as a (biased) diffusion operator on the one-dimensional line. Let us now look at what happens when exactly two particles are at the same position: $x_1 < \dots < x_i = x_{i+1} < \dots < x_n$. In this case, the evolution equation reads

$$\begin{aligned} \Lambda_\mu \psi_\mu(x_1, \dots, x_n) &= \sum_{\{\delta_1, \dots, \delta_n\} - \{\delta_i, \delta_{i+1}\} \in \{0,1\}^{n-2}} (\bar{u})^{n-2 - \sum_{j=1, j \neq i, i+1}^n \delta_j} (\bar{v})^{\sum_{j=1, j \neq i, i+1}^n \delta_j} (\bar{u}^2 \psi_\mu(x_1 - \delta_1, \dots, x_i, x_i, \dots, x_n - \delta_n)) \\ &+ 2\bar{u}\bar{v} \psi_\mu(x_1 - \delta_1, \dots, x_i - 1, x_i, \dots, x_n - \delta_n) + \bar{v}^2 \psi_\mu(x_1 - \delta_1, \dots, x_i - 1, x_i - 1, \dots, x_n - \delta_n), \end{aligned} \quad (\text{E.2.8})$$

³Note that the extension of [247] of the classification of [222] corresponds to stochastic particles systems with non-simultaneous updates. Hence the classification of [222] is sufficient in our context.

Where we used the symmetry of ψ_μ to express each terms with coordinates in the Weyl chamber W_n . However, the left-hand side of (E.2.8) is already constrained to be equal to the right-hand side (last line) of (E.2.7) even for $x_i = x_{i+1}$ because the eigenvalue Λ_μ is entirely determined by (E.2.7). For this equality to hold $\forall x_1 < \dots < x_i = x_{i+1} < \dots < x_n$ for an eigenfunction of the form (E.2.6) one must have, rewriting (E.2.8) in terms of $\tilde{\psi}_\mu$,

$$\begin{aligned} & \overline{u^2} \tilde{\psi}_\mu(x_1 - \delta_1, \dots, x_i, x_i, \dots, x_n - \delta_n) + 2\overline{uv} \tilde{\psi}_\mu(x_1 - \delta_1, \dots, x_i - 1, x_i, \dots, x_n - \delta_n) \\ & + \overline{v^2} \tilde{\psi}_\mu(x_1 - \delta_1, \dots, x_i - 1, x_i - 1, \dots, x_n - \delta_n) \\ = & (\overline{v})^2 \tilde{\psi}_\mu(x_1 - \delta_1, \dots, x_i - 1, x_i - 1, \dots, x_n - \delta_n) + (\overline{v})(\overline{u}) \tilde{\psi}_\mu(x_1 - \delta_1, \dots, x_i - 1, x_i, \dots, x_n - \delta_n) \\ & + (\overline{u})(\overline{v}) \tilde{\psi}_\mu(x_1 - \delta_1, \dots, x_i, x_i - 1, \dots, x_n - \delta_n) + (\overline{u})^2 \tilde{\psi}_\mu(x_1 - \delta_1, \dots, x_i, x_i, \dots, x_n - \delta_n). \end{aligned} \quad (\text{E.2.9})$$

Notice that the third term in the right-hand side in (E.2.9) involves coordinates outside of the Weyl chamber and is thus not a physical term. For the two particles problem to be solved, it must have the value

$$\begin{aligned} \tilde{\psi}_\mu(x_i, x_i - 1) &= \mathbf{a} \tilde{\psi}_\mu(x_i, x_i) + \mathbf{b} \tilde{\psi}_\mu(x_i - 1, x_i) + \mathbf{c} \tilde{\psi}_\mu(x_i - 1, x_i - 1) \\ \mathbf{a} &= \frac{\overline{u^2} - (\overline{u})^2}{(\overline{u})(\overline{v})} \quad \mathbf{b} = \frac{2\overline{uv} - (\overline{u})(\overline{v})}{(\overline{u})(\overline{v})} \quad \mathbf{c} = \frac{\overline{v^2} - (\overline{v})^2}{(\overline{u})(\overline{v})}, \end{aligned} \quad (\text{E.2.10})$$

where here, for clarity, we did not write the other particles positions. For obvious reasons, (E.2.10) is called the two-particles boundary condition. It is also a consequence of the short-ranged nature of the correlations between Boltzmann weights that the two-particles evolution equation can simply be interpreted as a two particles boundary conditions. In terms of the Bethe Ansatz (E.2.6), it imposes the quotient of two amplitudes A_σ related to each other by a permutation to be given by

$$S(z_i, z_j) := \frac{A_{\dots j i \dots}}{A_{\dots i j \dots}} = -\frac{\mathbf{c} + \mathbf{b}z_j + \mathbf{a}z_i z_j - z_i}{\mathbf{c} + \mathbf{b}z_i + \mathbf{a}z_i z_j - z_j}. \quad (\text{E.2.11})$$

Where this defines the S matrix. This can be solved as

$$A_\sigma = \epsilon(\sigma) \prod_{1 \leq i < j \leq n} \frac{\mathbf{c} + \mathbf{b}z_{\sigma(i)} + \mathbf{a}z_{\sigma(i)}z_{\sigma(j)} - z_{\sigma(j)}}{\mathbf{c} + \mathbf{b}z_i + \mathbf{a}z_i z_j - z_j}. \quad (\text{E.2.12})$$

As a consequence, up to a multiplicative factor, the form of the Bethe Ansatz is now entirely specified and something special has to happen if it also solves the m particles problem (case where m particles are at the same position) for arbitrary $2 \leq m \leq n$. Indeed, for arbitrary m , one can repeat the same analysis and check that the ansatz (E.2.6) works, i.e. that the evolution equation with m particles at the same position (generalization of (E.2.8)) can be transformed into the free evolution equation (generalization of (E.2.9)) by only applying (E.2.10) recursively. Schematically, this is conveniently encoded in a non-commutative algebras with two generators (A, B) such that

$$BA = \mathbf{a}A^2 + \mathbf{b}AB + \mathbf{c}B^2, \quad (\text{E.2.13})$$

which encodes what happen when one transforms a forbidden term of the form $\tilde{\psi}_\mu(\dots, x_i, x_i - 1 \dots)$ into a sum of terms with coordinates in the Weyl chamber. In this language, the model is indeed integrable with the coordinate Bethe Ansatz (E.2.6) if and only if

$$(\overline{u}A + \overline{v}B)^m = \sum_{n_1=0}^m \overline{u^{n_1} v^{m-n_1}} C_m^{n_1} A^{n_1} B^{m-n_1}. \quad (\text{E.2.14})$$

Where the right-hand side represents the true evolution equation that only contains terms in the Weyl chamber, i.e. in this language, that only contains ordered words of the form $A^{n_1} B^{n_2}$, and the left hand side is the formal free evolution equation, which contains various terms outside the Weyl chamber, i.e. wrongly ordered words. The right-hand side of (E.2.14) can be computed using the formula appearing in [222]. In the context of this paper, only models satisfying the ‘‘stochasticity hypothesis’’, $\mathbf{a} + \mathbf{b} + \mathbf{c} = 1$ (corresponding to a conservation of probability) were considered. Here in general, this hypothesis has to be relaxed and $\mathbf{a} + \mathbf{b} + \mathbf{c} \neq 1$. This is easily done by a scale transformation⁴, i.e. we introduce new parameters $(\rho, \mathbf{a}', \mathbf{b}', \mathbf{c}')$ and generators (A', B') , such that

$$\mathbf{a} = \mathbf{a}'\rho \quad , \quad \mathbf{b} = \mathbf{b}' \quad , \quad \mathbf{c} = \frac{\mathbf{c}'}{\rho} \quad (\text{E.2.15})$$

$$A = \frac{A'}{\rho} \quad , \quad B = B' \quad , \quad B'A' = \mathbf{a}'A'^2 + \mathbf{b}'A'B' + \mathbf{c}'B'^2 \quad (\text{E.2.16})$$

⁴We thank A.M. Povolotsky for this remark.

where ρ is chosen such that $a' + b' + c' = 1$, in which case we can use the results of Ref. [222] in terms of the new generators (A', B') and parameters (a', b', c') (called there (A, B) and α, β, γ). We obtain

$$\begin{aligned} (\bar{u}A + \bar{v}B)^m &= \left(\frac{\bar{u}}{\rho}A' + \bar{v}B'\right)^m \\ &= \left(\frac{\bar{u}}{\rho} + \bar{v}\right)^m (pA' + (1-p)B')^m \\ &= \left(\frac{\bar{u}}{\rho} + \bar{v}\right)^m \sum_{n_1=0}^m \phi_{q,\mu,\nu}(n_1|m)(A')^{n_1}(B')^{m-n_1} \\ &= \left(\frac{\bar{u}}{\rho} + \bar{v}\right)^m \sum_{n_1=0}^m \rho^{n_1} \phi_{q,\mu,\nu}(n_1|m)A^{n_1}B^{m-n_1} \end{aligned} \tag{E.2.17}$$

where we used the same notations introduced in Ref. [222] for the three parameters of the model q, μ, ν and the auxiliary parameter p , so that

$$\begin{aligned} p &= \frac{\bar{u}}{\bar{u} + \rho\bar{v}} \quad , \quad a' = \frac{\nu(1-q)}{1-q\nu} \quad , \quad b' = \frac{q-\nu}{1-q\nu} \quad , \quad c' = \frac{1-q}{1-q\nu} \quad , \quad \mu = p + \nu(1-p) \\ \phi_{q,\mu,\nu}(n_1|m) &= \mu^{n_1} \frac{(\frac{\nu}{\mu}; q)_{n_1}(\mu; q)_{m-n_1}}{(\nu; q)_m} \frac{(q; q)_m}{(q; q)_{n_1}(q; q)_{m-n_1}} \end{aligned} \tag{E.2.18}$$

from equations (8) and (26-27) in Ref. [222]. The q -Pochhammer symbol (used extensively below) is defined as, for $n > 0$:

$$(a; q)_n = \prod_{k=0}^{n-1} (1 - aq^k) \quad , \quad (a; q)_{-n} = \prod_{k=1}^n (1 - aq^{-k})^{-1} \tag{E.2.19}$$

and $(a; q)_0 = 1$. For given parameters q, μ, ν the first equation in (E.2.18) fixes the scale factor ρ as a function of \bar{u}/\bar{v} .

Comparing this equation with (E.2.14) one sees that one must have, $\forall (n_1, n_2)$ such that $n_1 + n_2 \leq n_{\max}$,

$$\frac{\bar{u}^{n_1}\bar{v}^{n_2}}{p} = \left(\frac{\bar{u}}{p}\right)^{n_1} \left(\frac{\bar{v}}{1-p}\right)^{n_2} (\mu)^{n_1} \frac{(\frac{\nu}{\mu}; q)_{n_1}(\mu; q)_{n_2}}{(\nu; q)_{n_1+n_2}} \frac{(q; q)_{n_1+n_2}}{(q; q)_{n_1}(q; q)_{n_2}} \frac{1}{C_{n_1+n_2}^{n_1}} \tag{E.2.20}$$

We can now explicitly check that for $(n_1, n_2) = (1, 0), (0, 1)$ the r.h.s gives \bar{u} and \bar{v} and that for $(n_1, n_2) = (2, 0), (1, 1), (0, 2)$ it yields second moments compatible with all relations (E.2.10) and (E.2.15), (E.2.18). Thanks to the above construction based on Ref. [222] we know that it solves the integrability constraint for all higher positive integer moments with $n_1 + n_2 \leq n_{\max}$.

In this expression, the power-law parts are unimportant (they can be absorbed into a rescaling of the Boltzmann weights which cannot break the integrability of the model). We can now reverse the construction and study a polymer model defined with weights with moments given by

$$\frac{\bar{u}^{n_1}\bar{v}^{n_2}}{u^{n_1}v^{n_2}} = \frac{(\frac{\nu}{\mu}; q)_{n_1}(\mu; q)_{n_2}}{(\nu; q)_{n_1+n_2}} \frac{(q; q)_{n_1+n_2}}{(q; q)_{n_1}(q; q)_{n_2}} \frac{1}{C_{n_1+n_2}^{n_1}} := \psi_{q,\mu,\nu}(n_1, n_2) \tag{E.2.21}$$

where $(q, \mu, \nu) \in \mathbb{R}^3$ to obtain real Boltzmann weights. This model is automatically integrable, and with the hypothesis that we made, it is the only form for the moments that leads to integrability. However, we now need to check if this DP model really exists, namely that (E.2.21) corresponds to the moments of a PDF $p(u, v)$.

Let us now define the moment problem that we must now solve. We are interested in finding a joint PDF $p(u, v)$ with positive integer moments given by (E.2.21) and random variables (u, v) living in one of the four quadrants $(\mathbb{R}^{\pm}, \mathbb{R}^{\pm})$. Indeed, if that is the case we automatically find, using a change of the type $(u, v) \rightarrow (\pm u, \pm v)$, positive random variables with moments given by (E.2.21) (eventually multiplied by additional power laws $(\pm 1)^{n_1}(\pm 1)^{n_2}$ which do not spoil integrability). Since we extend our search to also include polymer models with $n_{\max} < \infty$, we will generally look for PDF with moments given by (E.2.21) for $n_1 + n_2 \leq n_{\max}$ for some n_{\max} . Note that if $n_{\max} < \infty$, this replica Bethe ansatz method allows us to compute a-priori only a few integer moments of $Z_t(x)$. The ultimate goal of computing the PDF from this knowledge is not a mathematically well-posed problem. Fortunately, as e.g. in the case of the log-Gamma polymer (see [4] for more details on this issue), and in the case of the Inverse-Beta polymer studied below in this paper, the situation turns out to be more favorable. Indeed in these cases, though $n_{\max} < \infty$, the complex moments $\bar{u}^{n_1}\bar{v}^{n_2}$ of the PDF $p(u, v)$ exist for (n_1, n_2) in a large domain of the complex plane \mathbb{C} . These are given by an analytical continuation of (E.2.21) and allow, using a Mellin-Barnes type contour integral formula, to recover the Laplace transform of $p(u, v)$ in a rigorous manner. In this paper and as in the log-Gamma case, we adapt this observation to conjecture a formula for the LT of $Z_t(x)$ by using an analytical continuation of the formula for the integer moments that we compute using the replicas Bethe ansatz.

The search of such a PDF $p(u, v)$ with moments given by (E.2.21) is in general a difficult task. Notice however that it is sufficient to examine the case $|q| \leq 1$. Indeed, using that $(\frac{1}{a}; \frac{1}{q})_n = (-a)^{-n} q^{-\frac{n(n-1)}{2}} (a; q)_n$ one easily sees on (E.2.21) that the simultaneous change $q \rightarrow 1/q, \mu \rightarrow 1/\mu$ and $\nu \rightarrow 1/\nu$ in $\psi_{q,\mu,\nu}(n_1, n_2)$ just multiplies it by power-law terms, easily absorbed in rescaling of the variables (u, v) and which cannot break the integrability of the model.

E.3 Integrable polymer models

E.3.1 The $|q| < 1$ case.

Without loss of generality we restrict ourselves in the following to $|q| < 1$, and we further restrict to $q, \mu, \nu \in \mathbb{R}$.

We now consider the case where the moments exist at least up to the second moments (i.e. $n_{\max} \geq 2$). Let us consider the random variable $z_x = u + xv$, $x \in \mathbb{R}$. A simple calculation from (E.2.21) gives that its variance is:

$$\overline{z_x^2} - \overline{z_x}^2 = \frac{(\mu - 1)(1 - q)(\mu - \nu)(\mu x - 1)(\mu x - \nu)}{\mu^2(\nu - 1)^2(\nu q - 1)} \quad (\text{E.3.1})$$

Under our assumptions this expression must be positive. Since the polynomial in x changes sign at $x = \frac{\nu}{\mu}$ and $x = \frac{1}{\mu}$ this clearly rules out the generic case for $q < 1, \mu, \nu$.

We must thus look for degenerations with $\nu/\mu = 1/\mu$ so that the variance of z_x can eventually be positive $\forall x$. The various cases are studied systematically in Appendix E.6 where we show that the only possibility for the existence of such a PDF is in the $q \rightarrow 1$ limit which we now study in details. Moreover, we also show there that the limit $q \rightarrow 1$ and $\mu, \nu \rightarrow 1$ at the same speed than q , contains all the interesting cases.

Finally, note that the above considerations do not rule out completely the existence of an integrable polymer model with $q < 1$ since it could correspond to a model with $n_{\max} < 2$. From the discussion of the previous Section, this would involve however an exhaustive study of the possible analytical continuations of (E.2.21) which goes beyond the present work.

E.3.2 The $q \rightarrow 1$ limit

a Form of the moments.

Let us now discuss the $q \rightarrow 1$ limit. We use that at fixed n, a , $(q^a; q)_n \simeq_{q \rightarrow 1} (1 - q)^n (a)_n$, where $(a)_n = a(a+1)\dots(a+n-1)$ is the standard Pochhammer symbol. This is easily seen setting $q = e^{-\epsilon}$ and taking $\epsilon \rightarrow 0$. The ratio $\frac{(q; q)_n}{(q; q)_m (q; q)_{n-m}}$ thus tends to the standard binomial coefficient C_n^m .

To obtain a meaningful limit we scale $\nu = q^{\alpha+\beta}$, $\mu = q^\beta$. In this case, one gets as $q \rightarrow 1$:

$$\overline{u^{n_1} v^{n_2}} = (\epsilon_1)^{n_1} (\epsilon_2)^{n_2} \frac{(\alpha)_{n_1} (\beta)_{n_2}}{(\alpha + \beta)_{n_1 + n_2}}, \quad (\text{E.3.2})$$

where we have added two power law terms with $(\epsilon_1, \epsilon_2) \in \{-1, 1\}^2$. We were allowed to do it if we start to examine the moment problem for real variables. These two additional parameters are then tuned so that (u, v) are positive random variables. Since they are a-priori arbitrary we must examine all cases. Other interesting limits can also be considered but they can all be obtained from (E.3.2) as a new limit (see Appendix E.6). Note that (E.3.2) implies, $\forall n \in \mathbb{N}$,

$$\overline{(u/\epsilon_1 + v/\epsilon_2)^n} = \sum_{n_1=0}^n C_n^{n_1} \frac{(\alpha)_{n_1} (\beta)_{n-n_1}}{(\alpha + \beta)_n} = 1, \quad (\text{E.3.3})$$

so that, except maybe in some marginal cases discussed in Appendix E.7, this implies that u and v are correlated as $\epsilon_2 u + \epsilon_1 v = \epsilon_1 \epsilon_2$. In Appendix E.7, we initiate a more systematic study of all possible cases as ϵ_i are varied.

b The Beta Polymer and the Strict-Weak limit

The case of $(\epsilon_1, \epsilon_2) = (1, 1)$, $\alpha > 0$ and $\beta > 0$ indeed corresponds to the moments of two positive random variables. In this case, one has $v = 1 - u$ and $u \in [0, 1]$ is distributed according to Beta random variable:

$$\begin{aligned} u \sim \text{Beta}(\alpha, \beta) &\iff p_{\alpha, \beta}(u) = \frac{\Gamma(\alpha + \beta)}{\Gamma(\alpha)\Gamma(\beta)} u^{\alpha-1} (1-u)^{\beta-1} \hat{\mathbb{A}} \hat{\mathbb{A}} \\ v = 1 - u \quad , \quad \overline{u^{n_1} v^{n_2}} &= \frac{(\alpha)_{n_1} (\beta)_{n_2}}{(\alpha + \beta)_{n_1 + n_2}}. \end{aligned} \quad (\text{E.3.4})$$

Where from now on \sim means distributed as or the equivalence in probability. Note that Beta distributions satisfy $\text{Beta}(\alpha, \beta) \sim 1 - \text{Beta}(\beta, \alpha)$, and that in the Beta polymer model, interverting horizontal and vertical edges amounts to permute α and β .

Note that for this distribution of (u, v) , the formula for the moments (E.3.4) can be extended to the complex moments and admits a more general expression as

$$\overline{u^{s_1} v^{s_2}} = \frac{\Gamma(\alpha + \beta) \Gamma(\alpha + s_1) \Gamma(\beta + s_2)}{\Gamma(\alpha) \Gamma(\beta) \Gamma(\alpha + \beta + s_1 + s_2)} \quad (\text{E.3.5})$$

which is valid for arbitrary complex numbers $(s_1, s_2) \in \mathbb{C}^2$ in the domain $\text{Re}(s_1) > -\alpha$ and $\text{Re}(s_2) > -\beta$. The corresponding Directed Polymer model was introduced and studied in [224]. As already observed there, this model also contains the Strict-Weak polymer model introduced in [219] as a limit $\beta \rightarrow \infty$:

$$\begin{aligned} \lim_{\beta \rightarrow \infty} \overline{(\beta u)^{n_1} v^{n_2}} &= (\alpha)_{n_2} = \frac{\Gamma(\alpha + n_1)}{\Gamma(\alpha)} \\ (\beta u, v) \sim (\beta \text{Beta}(\alpha, \beta), (1 - \text{Beta}(\alpha, \beta))) &\sim_{\beta \rightarrow \infty} (\text{Gamma}(\alpha), 1), \end{aligned} \quad (\text{E.3.6})$$

which corresponds to a Strict-Weak polymer model with random Boltzmann weights on *vertical edges* distributed according to a Gamma distribution of parameter $\alpha > 0$, more precisely the rescaled Boltzmann weight $u' = \beta u$ is distributed according to a PDF $p_\alpha(u')$ such that

$$u' \sim \text{Gamma}(\alpha) \iff p_\alpha(u') = \frac{1}{\Gamma(\alpha)} (u')^{-1+\alpha} e^{-u'} . \quad (\text{E.3.7})$$

A second, and completely symmetric, Strict-Weak DP limit exists for $\alpha \rightarrow \infty$ at fixed β , with random $\text{Gamma}(\beta)$ weights on horizontal edges.

c The Inverse-Beta polymer

We now investigate the case $(\epsilon_1, \epsilon_2) = (1, -1)$ with $\beta > 0$ and $\alpha + \beta < 1$, and for convenience let us introduce the parameter γ as:

$$\gamma := 1 - (\alpha + \beta) \quad (\text{E.3.8})$$

In this case, a solution to the moment problem (E.3.2) is given by $v = u - 1$ (in agreement with the general argument proposed above) and $u \in [1, +\infty[$ distributed as

$$\begin{aligned} \tilde{p}_{\gamma, \beta}(u) &= \frac{\Gamma(\gamma + \beta)}{\Gamma(\gamma)\Gamma(\beta)} \frac{1}{u^{1+\gamma}} \left(1 - \frac{1}{u}\right)^{\beta-1} , \quad v = u - 1 , \quad u \in [1, +\infty[, \gamma > 0 \\ \overline{u^{n_1} v^{n_2}} &= (-1)^{n_2} \frac{(\alpha)_{n_1} (\beta)_{n_2}}{(\alpha + \beta)_{n_1 + n_2}} \text{ for } n_1 \leq 1 - \alpha = \gamma + \beta , \quad n_1 + n_2 \leq 1 - (\alpha + \beta) = \gamma . \end{aligned} \quad (\text{E.3.9})$$

In this case the moments problem (E.3.2) is indeed truly solved only for $n_1 + n_2 \leq \gamma$ since the moments cease to exist beyond this bound, due to divergence for large values of u, v . However there is a more general expression of the moments for complex $(s_1, s_2) \in \mathbb{C}^2$ with $\text{Re}(s_1 + s_2) \leq \gamma$ and $\text{Re}(s_2) > -\beta$

$$\overline{u^{s_1} v^{s_2}} = \frac{\Gamma(\gamma + \beta)}{\Gamma(\gamma)\Gamma(\beta)} \frac{\Gamma(\gamma - s_1 - s_2)\Gamma(\beta + s_2)}{\Gamma(\gamma + \beta - s_1)} . \quad (\text{E.3.10})$$

Using the analytical continuation of the Gamma function to the full complex plane, one thus see, using (E.3.10), that the moment problem (E.3.2) is indeed solved in an analytical continuation sense. This situation is very similar to the case of the log-Gamma polymer which the present model generalizes, as we show below. Note that for the present model, the variable $1/u$ is distributed according to a Beta distribution of parameters γ and β , $1/u \sim \text{Beta}(\gamma, \beta)$ and for this reason we call this model *the Inverse-Beta polymer*. This observation renders the proof of the convergence of this model to the log-Gamma polymer immediate. Indeed, one has

$$\begin{aligned} \lim_{\beta \rightarrow \infty} \overline{\left(\frac{u}{\beta}\right)^{n_1} \left(\frac{v}{\beta}\right)^{n_2}} \tilde{\text{A}}\tilde{\text{A}} &= \frac{\Gamma(\gamma - (n_1 + n_2))}{\Gamma(\gamma)} \\ \left(\frac{u}{\beta}, \frac{v}{\beta}\right) &\sim \left(\frac{1}{\beta \text{Beta}(\gamma, \beta)}, \frac{1 - \text{Beta}(\gamma, \beta)}{\beta \text{Beta}(\gamma, \beta)}\right) \sim_{\beta \rightarrow \infty} \frac{(1, 1)}{\text{Gamma}(\gamma)} . \end{aligned} \quad (\text{E.3.11})$$

And this limit thus corresponds to a model of polymer with on sites Boltzmann weights (since the weights on neighboring links are equals in the limit) distributed according to an inverse Gamma distribution, i.e. the log-Gamma polymer. This analysis thus unveil a natural duality between known integrable directed polymer models, as can be seen comparing (E.3.6) and (E.3.11). However, more surprisingly, this model also contains the Strict-Weak polymer model as a limit. Indeed, one has

$$\begin{aligned} \lim_{\gamma \rightarrow \infty} \overline{u^{n_1} (\gamma v)^{n_2}} &= \frac{\Gamma(\beta + n_2)}{\Gamma(\beta)} \\ (u, \gamma v) &\sim \left(\frac{1}{\text{Beta}(\gamma, \beta)}, \frac{\gamma(1 - \text{Beta}(\gamma, \beta))}{\text{Beta}(\gamma, \beta)}\right) \sim_{\gamma \rightarrow \infty} (1, \text{Gamma}(\beta)) \end{aligned} \quad (\text{E.3.12})$$

which corresponds to a Strict-Weak polymer model with Boltzmann weights on *horizontal edges* distributed with a Gamma distribution of parameter $\beta > 0$. In terms of the partition sum, the convergence of the Inverse-Beta model to the log-Gamma and Strict-Weak (E.1.2) is easily obtained using (E.3.11) and (E.3.12). Note that one can formally take a limit on the moments of the Beta polymer to obtain the moments of the log-Gamma polymer. Indeed, taking on the moments appearing in (E.3.4) $\alpha + \beta = 1 - \gamma$ fixed and letting $\alpha \rightarrow \infty$, one obtain

$$\lim_{|\alpha|, |\beta| \rightarrow \infty, \alpha + \beta = 1 - \gamma} \overline{\left(\frac{u}{-\alpha}\right)^{n_1} \left(\frac{v}{-\beta}\right)^{n_2}} = \frac{(-1)^{n_1 + n_2}}{(1 - \gamma)_{n_1 + n_2}} = \frac{\Gamma(\gamma - (n_1 + n_2))}{\Gamma(\gamma)} . \quad (\text{E.3.13})$$

But in doing so, the parameters α and β passes through region where the PDF $\text{Beta}(\alpha, \beta)$ is not normalizable and the convergence of the Beta to the log-Gamma polymer thus does not hold in probability. The situation and relations between this different polymer models is summarized in Fig. E.2. Notice that parts of this scheme remain empty, and there still remains some room for new integrable models with moments of the form (E.3.2). In Appendix E.7 we attempt a first step in this direction by studying different analytical continuations of (E.3.2),

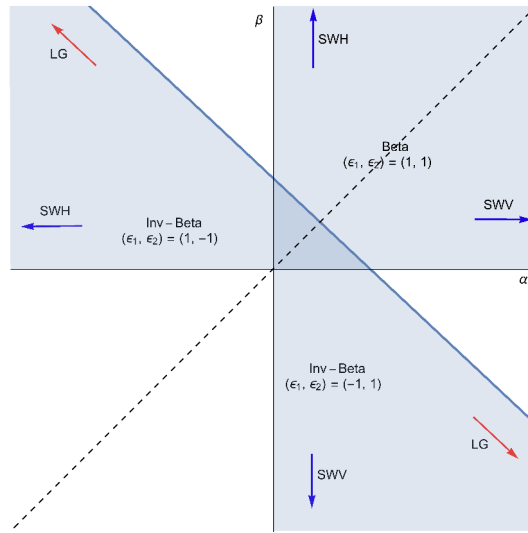


Figure E.2: Duality between polymers models in the (α, β) plane. The dashed line represents the axe of symmetry $\alpha \leftrightarrow \beta$, or equivalently the symmetry between vertical and horizontal edges. The blue line indicates the line $\alpha + \beta = 1$ or equivalently $\gamma = 1 - (\alpha + \beta) = 0$. Limiting polymer models are indicated by red arrows for the log-Gamma (LG) and blue arrows for the Strict-Weak (with weights either on horizontal edges (SWH) or vertical edges (SWV)). We also emphasize the values of (ϵ_1, ϵ_2) which corresponds to the polymer considered. Notice that the region $\alpha > 0, \beta > 0$ and $\gamma < 1$ is a region of coexistence of the Inverse-Beta and the Beta polymer, only distinguished by the value of (ϵ_1, ϵ_2) .

E.4 Study of the Inverse-Beta Polymer

We now turn to the analysis of the Inverse-Beta polymer. In Section E.4.1 we use the Bethe ansatz solvability of the model to obtain formulas for the firsts (i.e. those that exist) integer moments of the partition sum of the model. In Section E.4.2 we use the prescription already used in [4] for the log-Gamma polymer to conjecture a formula for the Laplace transform of the partition sum from the knowledge of its moments. Based on this conjecture, we show in Section E.4.3 the KPZ universality of the model. Finally, we study in Section E.4.4 a zero temperature model associated to the Inverse-Beta polymer.

E.4.1 Moments Formula and Coordinate Bethe Ansatz

a Coordinate Bethe Ansatz

The moments of the Boltzmann weights of the Inverse-Beta polymer read (in the following we keep the notations and coordinates introduced in the general setting of the precedent section)

$$\frac{1}{u^{n_1} v^{n_2}} = (-1)^{n_2} \frac{(\alpha)_{n_1} (\beta)_{n_2}}{(\alpha + \beta)_{n_1 + n_2}}. \quad (\text{E.4.1})$$

where $\alpha < 0, \beta > 0$ and $\alpha + \beta < 1$. As we showed in Section E.3.2, this model is integrable using a coordinate Bethe ansatz Eq. (E.2.6) with a two body S -matrix $S(z_i, z_j)$ given by (E.2.11). Its parameters are calculated from the second moment equation Eq. (E.2.10) and their definition (E.4.1), leading to:

$$\mathbf{a} = \mathbf{c} = -\frac{1}{1 + \alpha + \beta} = \frac{1}{\gamma - 2}, \quad \mathbf{b} = \frac{-1 + \alpha + \beta}{1 + \alpha + \beta} = \frac{\gamma}{\gamma - 2}, \quad \gamma = 1 - (\alpha + \beta) \quad (\text{E.4.2})$$

where we have recalled the definition of the parameter γ . We now introduce

$$\bar{c} = \frac{4}{\gamma - 1} = -\frac{4}{\alpha + \beta} \\ z_j = e^{i\lambda_j}, \quad t_j = i \tan\left(\frac{\lambda_j}{2}\right) = \frac{z_j - 1}{z_j + 1}, \quad z_j = \frac{1 + t_j}{1 - t_j}. \quad (\text{E.4.3})$$

In the following we suppose $\bar{c} > 0$, i.e. $\gamma > 1$. As in the log-Gamma case, this is only a technical assumption that allows us to use the coordinate Bethe ansatz to compute the $n < \gamma$ first moments of the partition sum, and we will specify when the

validity of some results extends to $\gamma < 1$. Using these notations, it is a simple exercise to check that the S -matrix of the Inverse-Beta polymer can be expressed as

$$S(z_i, z_j) = \frac{2t_j - 2t_i + \bar{c}}{2t_j - 2t_i - \bar{c}}. \quad (\text{E.4.4})$$

Remarkably, it is equal to the S -matrix of the log-Gamma polymer studied in our previous work [4]. Hence, the Bethe eigenfunctions of this model can be taken as the one already introduced for the log-Gamma polymer, namely

$$\tilde{\psi}_\mu(x_1, \dots, x_n) = \sum_{\sigma \in S_n} A_\sigma \prod_{\alpha=1}^n z_{\sigma(\alpha)}^{x_\alpha}, \quad A_\sigma = \prod_{1 \leq \alpha < \beta \leq n} \left(1 + \frac{\bar{c}}{2(t_{\sigma(\alpha)} - t_{\sigma(\beta)})}\right). \quad (\text{E.4.5})$$

Note that it only differs from the solution (E.2.12) proposed in [222] by a global multiplicative constant. Following the same approach than in [4], we now study the model using periodic boundary conditions and look for eigenstates of the transfer matrix such that $\psi_\mu(x_1, \dots, x_j + L, \dots, x_n) = \psi(x_1, \dots, x_n)$. This imposes the Bethe equations

$$e^{i\lambda_i L} = \prod_{1 \leq j \leq n, j \neq i} \frac{2t_i - 2t_j + \bar{c}}{2t_i - 2t_j - \bar{c}}, \quad i = 1, \dots, n \quad (\text{E.4.6})$$

Note that this is only a convenient choice and should have no effects on $Z_t(x)$ as long as $t < L$ as discussed there. We will now recall some useful properties of the eigenstates (E.4.5) that were obtained [4] and generalize some of them.

b Recall of some properties of the eigenstates

b.1 A weighted scalar product The eigenfunctions (E.4.5) form a basis of the set of periodic functions of n variables on \mathbb{N}^n . They are orthogonal with respect to the following scalar product

$$\langle \phi, \psi \rangle = \sum_{(x_1, \dots, x_n) \in \{0, \dots, L-1\}^n} \frac{1}{\prod_x h_{\sum_{\alpha=1}^n \delta_{x, x_\alpha}}} \phi^*(x_1, \dots, x_n) \psi(x_1, \dots, x_n), \quad h_n = \prod_{k=0}^{n-1} \frac{4}{4 - k\bar{c}} = (\gamma - 1)^n \frac{\Gamma(\gamma - n)}{\Gamma(\gamma)}. \quad (\text{E.4.7})$$

b.2 The string solution In the large L limit, the solutions of the Bethe equations (E.4.6) organized themselves into strings. Each set $\{t_\alpha\}$ that solve (E.4.6) is given by partitioning n into n_s strings, each string containing m_j particles where the index $j = 1, \dots, n_s$ labels the string. Inside a string, the t_α are given by (we use the notations of [4]):

$$t_\alpha = t_{j,a} = i \frac{k_j}{2} + \frac{\bar{c}}{4}(m_j + 1 - 2a) + \frac{\delta_{j,a}}{2} \quad (\text{E.4.8})$$

where we introduced an index $a = 1, \dots, m_j$ that labels the rapidities inside a string, $\frac{k_j}{2} \in \mathbb{R}$ denotes their common imaginary part and $\delta_{j,a}$ are deviations that fall off exponentially with L . In the large L limit, the strings behave as independent free particles with total momentum $K_j = \sum_{a=1}^{m_j} \lambda_{j,a} \in [-m_j\pi, m_j\pi]$. In particular, in the large L limit, the sum over all eigenstates can be computed as

$$\sum_{m_j \text{ string-states}} \rightarrow \frac{L}{2\pi} \int_{-m_j\pi}^{m_j\pi} dK_j \rightarrow \frac{L}{2\pi} \int_{-\infty}^{\infty} dk_j \sum_{a=1}^{m_j} \frac{1}{1 - t_{j,a}^2}. \quad (\text{E.4.9})$$

We will also need the norm of an eigenstate composed of strings in the large L limit. This was computed in [4].

$$\|\mu\|^2 = n! L^{n_s} \prod_{1 \leq i < j \leq n_s} \frac{4(k_i - k_j)^2 + \bar{c}^2(m_i + m_j)^2}{4(k_i - k_j)^2 + \bar{c}^2(m_i - m_j)^2} \prod_{j=1}^{n_s} \left[\frac{m_j}{\bar{c}^{m_j-1}} \left(\sum_{a=1}^{m_j} \frac{1}{1 - t_{j,a}^2} \right) \prod_{b=1}^{m_j} (1 - t_{j,b}^2) \right] \quad (\text{E.4.10})$$

b.3 Energy-momentum of the strings Although the eigenfunctions are the same as the one for the log-Gamma polymer, the *eigenvalues* are different. The eigenvalue of the transfer matrix T_n associated to an eigenstate ψ_μ was given in (E.2.7) as $\Lambda_\mu = \prod_{i=1}^n (\bar{u} + \bar{v}z_i^{-1})$ and depends only on the first moments of the weights. Inserting their values from (E.4.1) and taking into account that for a string state, it is a product of string contributions, we obtain $\Lambda_\mu = \prod_{j=1}^{n_s} \Lambda_j$ with:

$$\begin{aligned} \Lambda_j &= \prod_{a=1}^{m_j} \left(\frac{\alpha}{\alpha + \beta} - \frac{\beta}{\alpha + \beta} \frac{1 - t_{j,a}}{1 + t_{j,a}} \right) = \frac{\left(-\beta - \frac{ik_j}{\bar{c}} - \frac{\gamma}{2} - \frac{m_j}{2} + 1 \right)_{m_j}}{\left(-\frac{ik_j}{\bar{c}} - \frac{\gamma}{2} - \frac{m_j}{2} + 1 \right)_{m_j}} \\ &= \frac{\Gamma\left(\beta + \frac{ik_j}{\bar{c}} + \frac{\gamma}{2} + \frac{m_j}{2}\right) \Gamma\left(\frac{ik_j}{\bar{c}} + \frac{\gamma}{2} - \frac{m_j}{2}\right)}{\Gamma\left(\beta + \frac{ik_j}{\bar{c}} + \frac{\gamma}{2} - \frac{m_j}{2}\right) \Gamma\left(\frac{ik_j}{\bar{c}} + \frac{\gamma}{2} + \frac{m_j}{2}\right)}. \end{aligned} \quad (\text{E.4.11})$$

Where, in the second line, we have rewritten the Pochhammer symbols using Gamma functions, an identity valid for integer m_j .

Another important quantity is the eigenvalue associated to the action of the unit translation operator on a string state, defined as

$$\prod_{a=1}^{m_j} z_{j,a} = \prod_{a=1}^{m_j} \frac{1+t_{j,a}}{1-t_{j,a}} = \frac{\Gamma(-\frac{m_j}{2} + \frac{\gamma}{2} - i\frac{k_j}{c})\Gamma(\frac{m_j}{2} + \frac{\gamma}{2} + i\frac{k_j}{c})}{\Gamma(\frac{m_j}{2} + \frac{\gamma}{2} - i\frac{k_j}{c})\Gamma(-\frac{m_j}{2} + \frac{\gamma}{2} + i\frac{k_j}{c})}, \quad (\text{E.4.12})$$

an expression identical to the one obtained in [4]. Finally, we will also need

$$\left(\prod_{a=1}^{m_j} \frac{1}{1-t_{j,a}^2} \right) = \left(\frac{2}{\bar{c}} \right)^{2m_j} \left(\frac{\Gamma(-\frac{m_j}{2} + \frac{\gamma}{2} - i\frac{k_j}{c})\Gamma(-\frac{m_j}{2} + \frac{\gamma}{2} + i\frac{k_j}{c})}{\Gamma(\frac{m_j}{2} + \frac{\gamma}{2} - i\frac{k_j}{c})\Gamma(\frac{m_j}{2} + \frac{\gamma}{2} + i\frac{k_j}{c})} \right). \quad (\text{E.4.13})$$

c Moments formula

We have now all the ingredients to compute the integer moments of the partition sum. As will appear clearly in the following, it is convenient to start with an initial condition

$$Z_{t=0}(x) = w_{0,0}\delta_{x,0}, \quad (\text{E.4.14})$$

where $w_{0,0}$ is Boltzmann weight, statistically independent of the others, and distributed with an inverse Gamma distribution of parameter γ . The problem with initial condition $Z_{t=0}(x) = \delta_{x,0}$ is obviously simply connected to this one and the details of the relations are given in Appendix E.8. In terms of the wave-function $\psi_t(x_1, \dots, x_n)$, the initial conditions reads $\psi_{t=0}(x_1, \dots, x_n) = \frac{\Gamma(\gamma-n)}{\Gamma(\gamma)} \prod_{i=1}^n \delta_{x_i,0}$ and we use the scalar product (E.4.7) to decompose it on the Bethe eigenstates. Using this decomposition we obtain

$$\psi_t(x_1, \dots, x_n) = \sum_{\mu} \frac{\Gamma(\gamma-n)n!}{\Gamma(\gamma)h_n \|\psi_{\mu}\|^2} (\Lambda_{\mu})^t \psi_{\mu}(x_1, \dots, x_n). \quad (\text{E.4.15})$$

In particular,

$$\overline{Z_t(x)^n} = \sum_{\mu} \frac{\Gamma(\gamma-n)(n!)^2}{\Gamma(\gamma)h_n \|\psi_{\mu}\|^2} (\Lambda_{\mu})^t \left(\prod_{\alpha=1}^n z_{\alpha} \right)^x. \quad (\text{E.4.16})$$

Replacing in this expression each terms by its value in the large L limit, one obtains:

$$\begin{aligned} \overline{Z_t(x)^n} &= \frac{\Gamma(\gamma-n)(n!)^2}{\Gamma(\gamma)h_n} \sum_{n_s=1}^n \frac{1}{n_s!} \sum_{(m_1, \dots, m_{n_s})_n} \prod_{j=1}^{n_s} \int_{-\infty}^{+\infty} \frac{dk_j}{2\pi} \sum_{a=1}^{m_j} \frac{1}{1-t_{j,a}^2} \frac{1}{n!} \prod_{1 \leq i < j \leq n_s} \frac{4(k_i - k_j)^2 + \bar{c}^2(m_i - m_j)^2}{4(k_i - k_j)^2 + \bar{c}^2(m_i + m_j)^2} \\ &\prod_{j=1}^{n_s} (\bar{c})^{m_j-1} \frac{1}{m_j (\sum_{a=1}^{m_j} \frac{1}{1-t_{j,a}^2}) \prod_{b=1}^{m_j} (1-t_{j,b}^2)} (\Lambda_j)^t \prod_{b=1}^{m_j} \left(\frac{1+t_{j,b}}{1-t_{j,b}} \right)^x. \end{aligned} \quad (\text{E.4.17})$$

Where we have written the sum over all eigenstates as $\sum_{\mu} = \sum_{n_s=1}^n \frac{1}{n_s!} \sum_{(m_1, \dots, m_{n_s})_n} \sum_{m_j \text{ string-states}}$, where $\sum_{(m_1, \dots, m_{n_s})_n}$ means summing over all n_s -uplets (m_1, \dots, m_{n_s}) such that $\sum_{i=1}^{n_s} m_i = n$, and the $n_s!$ factor avoids multiple counting of a same string state. Rearranging this formula and rescaling $k \rightarrow \bar{c}k$, we finally obtain:

$$\begin{aligned} \overline{Z_t(x)^n} &= n! \sum_{n_s=1}^n \frac{1}{n_s!} \sum_{(m_1, \dots, m_{n_s})_n} \prod_{j=1}^{n_s} \int_{-\infty}^{+\infty} \frac{dk_j}{2\pi} \prod_{1 \leq i < j \leq n_s} \frac{4(k_i - k_j)^2 + (m_i - m_j)^2}{4(k_i - k_j)^2 + (m_i + m_j)^2} \\ &\prod_{j=1}^{n_s} \frac{1}{m_j} \left(\frac{\Gamma(-\frac{m_j}{2} + \frac{\gamma}{2} - ik_j)}{\Gamma(\frac{m_j}{2} + \frac{\gamma}{2} - ik_j)} \right)^{1+x} \left(\frac{\Gamma(-\frac{m_j}{2} + \frac{\gamma}{2} + ik_j)}{\Gamma(\frac{m_j}{2} + \frac{\gamma}{2} + ik_j)} \right)^{1-x+t} \left(\frac{\Gamma(\beta + ik_j + \frac{\gamma}{2} + \frac{m_j}{2})}{\Gamma(\beta + ik_j + \frac{\gamma}{2} - \frac{m_j}{2})} \right)^t, \end{aligned} \quad (\text{E.4.18})$$

valid for $n < \gamma$. The convergence of the various integrals is algebraic, the integrand being $O(1/k_j^{2m_j})$ as can be checked by rewriting the quotient of Gamma functions as Pochhammer symbols. This formula was checked using direct numerical integrations for low values of $t \leq 2$, $x \leq 2$ and $n \leq 2$. The case $t = 0$ is already non-trivial since it confirms the completeness of the eigenstates. Note that if one chooses the initial condition $Z_{t=0}(x=0) = \delta_{x,0}$, then $\overline{Z_t(x)^n}$ is trivially given by (E.4.18) with an additional factor of $\Gamma(\gamma)/\Gamma(\gamma-n)$ in front.

Degenerations towards the log-Gamma and Strict-Weak polymers: Since the Inverse-Beta polymer contains the log-Gamma polymer and the Strict-Weak polymer as limits (see (E.3.11) and (E.3.12)), (E.4.18) also contains moments formula for the Strict-Weak and log-Gamma cases as we show now.

- The moments of the log-Gamma polymer are obtained as the limit $\overline{(Z_t^{LG}(x))^n} = \lim_{\beta \rightarrow \infty} \frac{1}{\beta^{nt}} \overline{Z_t(x)^n}$, where $Z_t^{LG}(x)$ is the partition sum of the log-Gamma polymer. Indeed, the factor $\frac{1}{\beta^{nt}}$ exactly cancels the divergence of the last quotient of Gamma functions in (E.4.18), leading to the formula (54) of [4]. Let us recall that the present coordinates are $t = T$ and $x = t/2 + X$ as a function of those, T, X (but denoted there t, x) of that work.

- We now obtain a moment formula for the Strict-Weak polymer with initial condition $Z_t^{SW}(x=0) = \delta_{x,0}$, following (E.3.12), we consider the limit $\overline{(Z_t^{SW}(x))^n} = \lim_{\gamma \rightarrow \infty} \frac{\Gamma(\gamma)}{\Gamma(\gamma-n)} \gamma^{nx} \overline{Z_t(x)^n}$. In this case, the point-wise limit of the integrand cannot be taken as simply and we need to first perform the change of variables $k_j \rightarrow k_j + i\frac{\gamma}{2}$. We obtain

$$\begin{aligned} \overline{(Z_t^{SW}(x))^n} &= \lim_{\gamma \rightarrow \infty} \frac{\Gamma(\gamma)}{\Gamma(\gamma-n)} \gamma^{nx} n! \sum_{n_s=1}^n \frac{1}{n_s!} \sum_{(m_1, \dots, m_{n_s})_n} \prod_{j=1}^{n_s} \int_{L^n} \frac{dk_j}{2\pi} \prod_{1 \leq i < j \leq n_s} \frac{4(k_i - k_j)^2 + (m_i - m_j)^2}{4(k_i - k_j)^2 + (m_i + m_j)^2} \\ &\prod_{j=1}^{n_s} \frac{1}{m_j} \left(\frac{\Gamma(-\frac{m_j}{2} + \gamma - ik_j)}{\Gamma(\frac{m_j}{2} + \gamma - ik_j)} \right)^{1+x} \left(\frac{\Gamma(-\frac{m_j}{2} + ik_j)}{\Gamma(\frac{m_j}{2} + ik_j)} \right)^{1-x+t} \left(\frac{\Gamma(\beta + ik_j + \frac{m_j}{2})}{\Gamma(\beta + ik_j - \frac{m_j}{2})} \right)^t. \end{aligned} \quad (\text{E.4.19})$$

Where $L = -i\frac{\gamma}{2} + \mathbb{R}$. Since the integral over k_j quickly converges as $O(1/k_j^{2m_j})$, we can now close the different contours of integrations on the upper half plane before taking the limit $\gamma \rightarrow \infty$. This leads to:

$$\begin{aligned} \overline{(Z_t^{SW}(x))^n} &= n! \sum_{n_s=1}^n \frac{1}{n_s!} \sum_{(m_1, \dots, m_{n_s})_n} \prod_{j=1}^{n_s} \int_{\tilde{L}^n} \frac{dk_j}{2\pi} \prod_{1 \leq i < j \leq n_s} \frac{4(k_i - k_j)^2 + (m_i - m_j)^2}{4(k_i - k_j)^2 + (m_i + m_j)^2} \\ &\prod_{j=1}^{n_s} \frac{1}{m_j} \left(\frac{\Gamma(-\frac{m_j}{2} + ik_j)}{\Gamma(\frac{m_j}{2} + ik_j)} \right)^{1-x+t} \left(\frac{\Gamma(\beta + ik_j + \frac{m_j}{2})}{\Gamma(\beta + ik_j - \frac{m_j}{2})} \right)^t, \end{aligned} \quad (\text{E.4.20})$$

where \tilde{L} is an horizontal line that stays below all the poles of the integrand. This formula is formal because the resulting integral does not converge, but one must remember that we have formally already closed the contours of integrations. Computing the integral on k_i thus just amounts at taking the sum over the residues of all the poles of the integrands except those of the type $k_i = k_j - iA$ where $A > 0$ (since the contours have been closed on the upper half-plane).

E.4.2 Fredholm determinant formulas and KPZ universality

In this section, we use the formula (E.4.18) to obtain the Laplace transform of the distribution of $Z_t(x)$,

$$g_{t,x}(u) = \overline{\exp(-uZ_t(x))}. \quad (\text{E.4.21})$$

The issue of obtaining this generating function from the sole knowledge of the integer moments of the partition sum was thoroughly discussed in [4] and here we follow the same route.

a The moment generating function

We start by computing the moment generating function

$$g_{t,x}^{mom}(u) = \sum_{n=0}^{\infty} \frac{(-u)^n}{n!} \overline{Z_t(x)^n}. \quad (\text{E.4.22})$$

where $u > 0$. Here, though $\overline{Z_t(x)^n}$ is only defined for $n \leq \gamma$, the right hand side of formula (E.4.18) is well defined for $n \in \mathbb{N}$ (except if $\gamma \in \mathbb{N}$) and we take advantage of this analytical continuation to perform the sum (E.4.22). Note that this object has no reason to correspond to the Laplace transform of $Z_t(x)$ but⁵, as in the log-Gamma case, we will use it to conjecture a formula for the true Laplace transform $g_{t,x}(u)$ defined in (E.4.21). Since we perform the sum over $n \in \mathbb{N}$, the constrained sum appearing in (E.4.18) becomes free summation and one can write

$$g_{t,x}^{mom}(u) = 1 + \sum_{n_s=1}^{+\infty} \frac{1}{n_s!} Z(n_s, u) \quad (\text{E.4.23})$$

where

$$\begin{aligned} Z(n_s, u) &= \prod_{j=1}^{n_s} \sum_{m_j=1}^{+\infty} \int_{-\infty}^{+\infty} \frac{dk_j}{2\pi} \prod_{1 \leq i < j \leq n_s} \frac{4(k_i - k_j)^2 + (m_i - m_j)^2}{4(k_i - k_j)^2 + (m_i + m_j)^2} \\ &\prod_{j=1}^{n_s} \frac{(-u)^{m_j}}{m_j} \left(\frac{\Gamma(-\frac{m_j}{2} + \frac{\gamma}{2} - ik_j)}{\Gamma(\frac{m_j}{2} + \frac{\gamma}{2} - ik_j)} \right)^{1+x} \left(\frac{\Gamma(-\frac{m_j}{2} + \frac{\gamma}{2} + ik_j)}{\Gamma(\frac{m_j}{2} + \frac{\gamma}{2} + ik_j)} \right)^{1-x+t} \left(\frac{\Gamma(\beta + ik_j + \frac{\gamma}{2} + \frac{m_j}{2})}{\Gamma(\beta + ik_j + \frac{\gamma}{2} - \frac{m_j}{2})} \right)^t \end{aligned} \quad (\text{E.4.24})$$

In this formula and following [4], one recognizes the structure of a Fredholm determinant

$$g_{t,x}^{mom}(u) = \text{Det} \left(I + K_{t,x}^{mom} \right) \quad (\text{E.4.25})$$

⁵And indeed it is not, a simple reason being that, just as the Laplace transform of the PDF $\tilde{p}_{\gamma,\beta}$ of the Boltzmann weights of the Inverse-Beta polymer (see (E.3.9)), the Laplace transform of $Z_t(x)$ is not an analytic function. See also Appendix E.9 for more details on this question.

with the kernel:

$$K_{t,x}^{mom}(v_1, v_2) = \sum_{m=1}^{\infty} \int_{-\infty}^{+\infty} \frac{dk}{\pi} (-u)^m e^{-2ik(v_1-v_2)-m(v_1+v_2)} \quad (\text{E.4.26})$$

$$\left(\frac{\Gamma(-\frac{m_j}{2} + \frac{\gamma}{2} - ik_j)}{\Gamma(\frac{m_j}{2} + \frac{\gamma}{2} - ik_j)} \right)^{1+x} \left(\frac{\Gamma(-\frac{m}{2} + \frac{\gamma}{2} + ik)}{\Gamma(\frac{m}{2} + \frac{\gamma}{2} + ik)} \right)^{1-x+t} \left(\frac{\Gamma(\beta + ik + \frac{\gamma}{2} + \frac{m}{2})}{\Gamma(\beta + ik + \frac{\gamma}{2} - \frac{m}{2})} \right)^t$$

and $K_{t,x}^{mom} : L^2(\mathbb{R}_+) \rightarrow L^2(\mathbb{R}_+)$, so that the two auxiliary integration variables v_1 and v_2 are positive⁶.

b The Laplace transform as a Fredholm determinant

We now use the same prescription used in [4] to obtain a conjecture for the Laplace transform $g_{t,x}(u)$ from the moment generating function $g_{t,x}^{mom}(u)$. It consists in rewriting the sum over m in the Kernel $K_{t,x}^{mom}$ as a Mellin-Barnes integral. In Appendix E.9 we also show how this type of manipulation efficiently works on a simpler object, namely the Laplace transform of the PDF $\tilde{p}_{\gamma,\beta}$ defined in (E.3.9). We thus conjecture, $g_{t,x}(u) = \text{Det}(I + K_{t,x})$ with

$$K_{t,x}(v_1, v_2) = \int_{-\infty}^{+\infty} \frac{dk}{\pi} \frac{-1}{2i} \int_C \frac{ds}{\sin(\pi s)} u^s e^{-2ik(v_1-v_2)-s(v_1+v_2)} \quad (\text{E.4.27})$$

$$\left(\frac{\Gamma(-\frac{s}{2} + \frac{\gamma}{2} - ik)}{\Gamma(\frac{s}{2} + \frac{\gamma}{2} - ik)} \right)^{1+x} \left(\frac{\Gamma(-\frac{s}{2} + \frac{\gamma}{2} + ik)}{\Gamma(\frac{s}{2} + \frac{\gamma}{2} + ik)} \right)^{1-x+t} \left(\frac{\Gamma(\beta + ik + \frac{\gamma}{2} + \frac{s}{2})}{\Gamma(\beta + ik + \frac{\gamma}{2} - \frac{s}{2})} \right)^t$$

where $C = a + i\mathbb{R}$ with $0 < a < \min(1, \gamma)$ and $K_{t,x} : L^2(\mathbb{R}_+) \rightarrow L^2(\mathbb{R}_+)$. As in the log-Gamma case, we expect this formula to be also valid for $0 < \gamma < 1$. Note that in going from (E.4.26) to (E.4.27) we have to choose an analytical continuation to go from $m \in \mathbb{N}$ to $s \in \mathbb{C}$. Here the chosen analytical continuation is the most natural one in the sense that it generalizes the one used for the log-Gamma polymer in [4], and also mimics the calculation of Appendix E.9. This Kernel is the one that is naturally obtained from the Bethe Ansatz and its structure is reminiscent of the string solution: the integral over s encodes for the contributions of the different types of strings, whereas the integral over k is the summation on the momenta of the strings. As shown in [4] (section 11), it is also possible to rewrite $g_{t,x}(u)$ as the Fredholm determinant of another Kernel which contains one less integral. Since the proof is strictly analogous to the case of the log-Gamma polymer, we only give here the final result: we also have $g_{t,x}(u) = \text{Det}(I + K_{t,x}^{BA})$ where

$$K_{t,x}^{BA}(z, z') = \int_{2a+\tilde{a}+i\mathbb{R}} dw \frac{1}{4\pi(w-z')} \frac{1}{\sin(\pi(w-z))} u^{w-z}$$

$$\left(\frac{\Gamma(\gamma + a - w)}{\Gamma(\gamma + a - z)} \right)^{1+x} \left(\frac{\Gamma(z - a)}{\Gamma(w - a)} \right)^{1-x+t} \left(\frac{\Gamma(w - a + \beta)}{\Gamma(z - a + \beta)} \right)^t \quad (\text{E.4.28})$$

where $K_{t,x}^{BA} : L^2(a + \tilde{a} + i\mathbb{R}) \rightarrow L^2(a + \tilde{a} + i\mathbb{R})$ $0 < a < \min(1, \gamma)$ and $0 < \tilde{a} < \gamma - a$. Note that here this formula should be valid for arbitrary x , whereas for the log-Gamma polymer the analogous formula was only valid for $2x \leq t$ (with a mirror formula for the other case)⁷. This formula is a large contour formula and an analogous small contour formula should also exist, as in the log-Gamma polymer. Let us also mention here that, following the same procedure that led in the log-Gamma case to formula (63) and (64) of [4], it is possible to directly obtain from (E.4.27) or (E.4.28) formulas for the PDF of $\log Z_t(x)$ as differences of two Fredholm determinants.

c The Laplace transform as a n-fold integral

In [218], a formula giving an identity between a certain class of Fredholm determinant with Kernels similar to the one in (E.4.28) and a class of n-fold contour integrals was given (Theorem 2). Though the explicit form of (E.4.28) explicitly breaks the hypothesis under which this formula was proven, an analogous formula should also exist in a more general setting. Guided by this belief, we conjecture the following formula for the Laplace transform:

$$\overline{e^{-uZ_t(x)}} = \frac{1}{J!} \int_{(i\mathbb{R})^J} \prod_{j=1}^J \frac{dw_j}{2i\pi} \prod_{j \neq k=1}^J \frac{1}{\Gamma(w_j - w_k)}$$

$$\left(\prod_{j=1}^J u^{w_j - a} \Gamma[a - w_j] \left(\frac{\Gamma(\gamma + a - w_j)}{\Gamma(\gamma)} \right)^I \left(\frac{\Gamma(w_j - a + \beta)}{\Gamma(\beta)} \right)^{I+J-2} \right), \quad (\text{E.4.29})$$

with $0 < a < \min(1, \gamma)$, valid for $\text{Re}(u) > 0$, $1 \leq J \leq I$ and where $x = I - 1$ and $t = I + J - 2$. This can be seen as a modification to our model of the formula given in [198] (Theorem 3.8), and also stated in [218] (Proposition 1.4), for the log-Gamma polymer. Since ours is merely a conjecture, we have tested it numerically against direct numerical computations of the Laplace transform for various u , β and γ and for $J = 1$, $I = 1, 2, 3$ and $J = 2$, $I = 2$.

⁶Note that this FD structure would have been broken by the initial condition $Z_{t=0}(x) = \delta_{x=0}$. (In which case (E.4.24) contains a non factorizable term of the form $\Gamma(\gamma)/\Gamma(\gamma - \sum_{i=1}^{n_s} m_i)$).

⁷Convergence of the w integral is checked using that $|\Gamma(x + iy)| \simeq \sqrt{2\pi}|y|^{x-\frac{1}{2}} e^{-\frac{\pi}{2}|y|}$.

d Degeneration towards the log-Gamma polymer.

The results of the last three paragraphs for the Laplace transforms of Z are easily seen to degenerate into the usual results for the log-Gamma polymer as $\beta \rightarrow +\infty$ using that $\exp(-uZ_t^{LG}(x)) = \lim_{\beta \rightarrow \infty} \exp(-\frac{u}{\beta t} Z_t(x))$. For example, taking the limit on formula (E.4.27), this introduces a term $\exp(-st \log(\beta))$ in the Kernel that exactly cancels the divergence of the last quotient of Gamma functions, and similarly for the other formula.

E.4.3 The large length limit and the KPZ universality.

We now study the limit of polymers of large length $t \gg 1$ for polymers with fixed endpoints $(0, 0)$ and $(t, x) = (t, (1/2 + \varphi)t)$ where $\varphi \in [-1/2, 1/2]$ represents the average angle of the path measured from the diagonal of the square lattice. The large t behavior of (E.4.27) is estimated through a saddle-point analysis similar to the one in [4] to which we refer for details. We define

$$G_\varphi(y) = \left(\frac{1}{2} + \varphi\right) \log \Gamma\left(\frac{\gamma}{2} - y\right) - \left(\frac{1}{2} - \varphi\right) \log \Gamma\left(\frac{\gamma}{2} + y\right) + \log \Gamma\left(\beta + \frac{\gamma}{2} + y\right). \quad (\text{E.4.30})$$

So that the leading behavior of the product of Gamma functions appearing in (E.4.27) is

$$(\Gamma\Gamma)^t := \exp\left(t\left(G_\varphi\left(\frac{s}{2} + ik\right) - G_\varphi\left(-\frac{s}{2} + ik\right)\right)\right). \quad (\text{E.4.31})$$

We now look for the critical point $(s, k) = (0, -ik_\varphi)$ such that $G_\varphi''(k_\varphi)$ is 0. This defines implicitly k_φ as

$$\left(\frac{1}{2} + \varphi\right) \psi'\left(\frac{\gamma}{2} - k_\varphi\right) - \left(\frac{1}{2} - \varphi\right) \psi'\left(\frac{\gamma}{2} + k_\varphi\right) + \psi'\left(\beta + \frac{\gamma}{2} + k_\varphi\right) = 0. \quad (\text{E.4.32})$$

Where $\psi = \frac{\Gamma'}{\Gamma}$ is the diGamma function. Expanding (E.4.31) around this critical point, one obtain

$$(\Gamma\Gamma)^t = \exp\left(t\left(G_\varphi'(k_\varphi)s + \frac{G_\varphi'''(k_\varphi)}{6}\left(\frac{s^3}{4} - 3s\tilde{k}^2\right) + O(s^4)\right)\right) \quad (\text{E.4.33})$$

where $\tilde{k} = k + ik_\varphi$ and s are considered to be of the same order (this is consistent with the rest of the calculation, see below). The linear term $G_\varphi'(k_\varphi)$ corresponds to an additive constant in the limiting free energy, whereas the cubic term sets the scale of the free-energy fluctuations. To pursue the asymptotic analysis, we define

$$\begin{aligned} F_t(\varphi) &= -\log Z_t(x = (1/2 + \varphi)t) = c_\varphi t + \lambda_\varphi f_t(\varphi) \\ c_\varphi &= -G_\varphi'(k_\varphi) \quad , \quad \lambda_\varphi = \left(\frac{tG_\varphi'''(k_\varphi)}{8}\right)^{\frac{1}{3}} \\ \tilde{g}_{t,\varphi}(z) &= \overline{\exp(-e^{-\lambda_\varphi(z + f_t(\varphi))})} \end{aligned} \quad (\text{E.4.34})$$

Where $F_t(\varphi)$ is the free-energy of the directed polymer and $\tilde{g}_{t,\varphi}(z)$ is a rescaled Laplace transform which has a proper $t \rightarrow \infty$ limit for fixed $z \in \mathbb{R}$. Indeed, since $g_{t,x=(1/2+\varphi)t}(u)$ can be written $\overline{\exp(-e^{\log(u) - F_t(\varphi)})}$, one has the identity $\tilde{g}_{t,\varphi}(z) = g_{t,x=(1/2+\varphi)t}(u = e^{c_\varphi t - \lambda_\varphi z})$. Rescaling $s \rightarrow s/\lambda_\varphi$, $\tilde{k} \rightarrow \frac{\tilde{k}}{\lambda_\varphi}$, $v_i \rightarrow \lambda_\varphi v_i$ and inserting $u = e^{c_\varphi t - \lambda_\varphi z}$, as well as the expansion (E.4.33), into (E.4.27), one obtains $\tilde{g}_{t,\varphi}(z) = \text{Det}(I + \tilde{K}_{t,\varphi}(v_1, v_2))^8$

$$\tilde{K}_{t,\varphi}(v_1, v_2) = \int_{\mathbb{R}} \frac{d\tilde{k}}{\pi} \frac{1}{2i} \int_C \frac{ds}{\lambda_\varphi \sin(\pi \frac{s}{\lambda_\varphi})} e^{-sz - 2i\tilde{k}(v_1 - v_2) - s(v_1 + v_2) - 4\tilde{k}^2 s + \frac{s^3}{3} + O(\frac{1}{\lambda_\varphi})} \quad (\text{E.4.35})$$

where $\tilde{K}_{t,\varphi} : L^2(\mathbb{R}_+) \rightarrow L^2(\mathbb{R}_+)$. The large polymer length limit $\lambda_\varphi \rightarrow \infty$ can be safely taken in this last expression, leading to a kernel \tilde{K}_∞ for which there is more freedom in the choice of the integration contour C : it should only define a convergent integral and passes to the right of zero. The $t \rightarrow \infty$ limit of the rescaled generating function can thus be written as $\lim_{t \rightarrow \infty} \tilde{g}_{t,\varphi}(z) = \text{Prob}(-f < z) = \text{Det}(I + \tilde{K}_\infty)$ where $\tilde{K}_\infty : L^2(\mathbb{R}_+) \rightarrow L^2(\mathbb{R}_+)$ is given by

$$\tilde{K}_\infty(v_1, v_2) = - \int_{\mathbb{R}} \frac{d\tilde{k}}{2\pi} \int_{\mathbb{R}_+} dy Ai(y + z + v_1 + v_2 + \tilde{k}^2) e^{-i\tilde{k}(v_1 - v_2)} \quad (\text{E.4.36})$$

where we used the Airy trick $\int_{\mathbb{R}} dy Ai(y) e^{ys} = e^{\frac{s^3}{3}}$ valid for $\text{Re}(s) > 0$, followed by the shift $y \rightarrow y + z + v_1 + v_2 + 4\tilde{k}^2$, the identity $\int_C \frac{ds}{2i\pi s} e^{sy} = \theta(y)$, and the rescaling $\tilde{k} \rightarrow \tilde{k}/2$. As in [4], this kernel corresponds to the Tracy-Widom GUE distribution as $\text{det}(I + \tilde{K}_\infty) = F_2(2^{-\frac{2}{3}}z)$ where $F_2(z)$ is the standard GUE Tracy-Widom cumulative distribution function. We have thus shown

$$\lim_{t \rightarrow \infty} \text{Prob}\left(\frac{\log Z_t((1/2 + \varphi)t) + tc_\varphi}{\lambda_\varphi} < 2^{\frac{2}{3}}z\right) = F_2(z) \quad (\text{E.4.37})$$

⁸ The extra factor $e^{-2k_\varphi \lambda_\varphi (v_1 - v_2)}$ originating from the change of variable has been removed since it is immaterial in the calculation of the Fredholm determinant.

where the (φ -dependent) constants are determined by the system of equations:

$$0 = \left(\frac{1}{2} + \varphi\right)\psi'\left(\frac{\gamma}{2} - k_\varphi\right) - \left(\frac{1}{2} - \varphi\right)\psi'\left(\frac{\gamma}{2} + k_\varphi\right) + \psi'(\beta + \frac{\gamma}{2} + k_\varphi) \quad (\text{E.4.38})$$

$$c_\varphi = \left(\frac{1}{2} + \varphi\right)\psi\left(\frac{\gamma}{2} - k_\varphi\right) + \left(\frac{1}{2} - \varphi\right)\psi\left(\frac{\gamma}{2} + k_\varphi\right) - \psi(\beta + \frac{\gamma}{2} + k_\varphi) \quad (\text{E.4.39})$$

$$\lambda_\varphi = \left(-\frac{t}{8} \left(\left(\frac{1}{2} + \varphi\right)\psi''\left(\frac{\gamma}{2} - k_\varphi\right) + \left(\frac{1}{2} - \varphi\right)\psi''\left(\frac{\gamma}{2} + k_\varphi\right) - \psi''(\beta + \frac{\gamma}{2} + k_\varphi) \right)\right)^{\frac{1}{3}}. \quad (\text{E.4.40})$$

Angle of maximal probability The free energy per unit length c_φ is maximal in the direction defined by the angle φ^* such that $\frac{\partial}{\partial \varphi} c_\varphi|_{\varphi=\varphi^*} = 0$. It is easily seen from (E.4.38) that it is realized for $k_\varphi = 0$, and φ^* is thus given by

$$\varphi^* = -\frac{1}{2} \frac{\psi'(\beta + \gamma/2)}{\psi'(\gamma/2)} < 0, \quad (\text{E.4.41})$$

and the optimal energy per unit length is thus

$$c^* = c_{\varphi^*} = \psi(\gamma/2) - \psi(\beta + \gamma/2). \quad (\text{E.4.42})$$

The amplitude of the fluctuations in the direction φ^* are

$$\begin{aligned} \lambda_{\varphi^*} &= \left(\frac{t}{8}(\psi''(\beta + \gamma/2) - \psi''(\gamma/2))\right)^{1/3} \\ &\simeq_{\beta \rightarrow 0} \left(\frac{t}{8}\psi'''(\gamma/2)\beta\right) \\ &\simeq_{\beta \rightarrow \infty} \left(-\frac{t}{8}\psi''(\gamma/2)\right). \end{aligned} \quad (\text{E.4.43})$$

And one recognizes the usual log-Gamma result for $\varphi = 0$. In the log-Gamma limit $\beta \rightarrow \infty$, one recovers $\varphi^* = 0$, but the parameter $\beta > 0$ biases the DP towards the vertical direction. More precisely,

$$\begin{aligned} \varphi^* &\simeq_{\beta \rightarrow 0} -\frac{1}{2} - \frac{\psi''(\gamma/2)}{\psi'(\gamma/2)}\beta + O(\beta^2) \\ \varphi^* &\simeq_{\beta \rightarrow \infty} -\frac{1}{2\psi'(\gamma/2)\beta} + O(1/\beta^2). \end{aligned} \quad (\text{E.4.44})$$

For small displacement around this optimum direction $\varphi = \varphi^* + \delta\varphi$, one retrieves an isotropic continuum limit characterized by an elastic coefficient κ such that $c_\varphi \simeq c_{\varphi^*} - \frac{1}{4}\kappa\delta\varphi^2$. One easily find using (E.4.38):

$$\kappa = -8 \frac{(\psi'(\gamma/2)\tilde{\Delta}\tilde{\Delta})^2}{\psi''(\gamma/2) - \psi''(\beta + \gamma/2)}, \quad (\text{E.4.45})$$

which generalizes the known result for the log-Gamma.

Degeneration towards the log-Gamma and Strict-Weak polymers.

- The Laplace transform of the partition sum of the log-Gamma polymer is obtained as $\overline{\exp(-uZ_t^{LG}(x))} = \lim_{\beta \rightarrow \infty} \overline{\exp(-\frac{u}{\beta t}Z_t(x))}$. This amounts to change $u^s \rightarrow u^s \exp(-ts \log(\beta))$ in the above formulas. For large β we use the limits $\psi'(x) \rightarrow_{x \rightarrow \infty} 0$, $\psi''(x) \rightarrow_{x \rightarrow \infty} 0$ and $\psi(x) = \log(x) - \frac{1}{2x} + O(\frac{1}{x^2})$. It is then easily seen that the presence of β do not change the position of k_φ in this limit nor the amplitudes of the fluctuations λ_φ , whereas c_φ receives a contribution proportional to $-\log(\beta)$ which exactly cancels the rescaling of the partition sum. This shows that the system of equation (E.4.38) converges to the one of the log-Gamma.
- In the case of the Strict-Weak polymer, the rescaling of the partition sum introduces a term that amounts to change $u^s \rightarrow u^s \exp(sx \log(\gamma)) = \exp(s(1/2 + \varphi) \log(\gamma))$ in the above formulas. This suggest to look for a solution of the form $k_\varphi = -\frac{\gamma}{2} + k_\varphi^{SW}$. The system of equation (E.4.38) then converges to

$$0 = -\left(\frac{1}{2} - \varphi\right)\psi'(k_\varphi^{SW}) + \psi'(\beta + k_\varphi^{SW}) \quad (\text{E.4.46})$$

$$c_\varphi^{SW} = \left(\frac{1}{2} - \varphi\right)\psi(k_\varphi^{SW}) - \psi(\beta + k_\varphi^{SW}) \quad (\text{E.4.47})$$

$$\lambda_\varphi^{SW} = \left(-\frac{t}{8} \left(\left(\frac{1}{2} - \varphi\right)\psi''(k_\varphi^{SW}) - \psi''(\beta + k_\varphi^{SW}) \right)\right)^{\frac{1}{3}}, \quad (\text{E.4.48})$$

so that we retrieve the result of [219] for the Strict-Weak polymer case (the precise correspondence with their notations reads $\kappa = 1/(1/2 - \varphi)$, $\bar{t} = k_\varphi$, $k = \beta$, $\bar{f}_{k,\kappa} = -\kappa c_\varphi^{SW}$ and $\bar{g}_{k,\kappa} = \frac{8}{t(1/2 - \varphi)}(\lambda_\varphi)^3$).

E.4.4 A low temperature limit.

a Definition of the zero temperature model

In this section we study the limit $\gamma = \epsilon\gamma'$ and $\beta = \epsilon\beta'$ of the model with $\epsilon \rightarrow 0$ (hence, $\alpha \rightarrow 1$). As we show now, this model converges to a zero temperature problem.

The analysis is similar to [224]. There (Lemma 4.1) it was shown that for a random variable z chosen with a $Beta(\alpha = \epsilon a, \beta = \epsilon b)$ distribution, the joint PDF of the pair $(-\epsilon \ln z, -\epsilon \ln(1-z))$ converges in law to $(\xi E_a, (1-\xi)E_b)$ as $\epsilon \rightarrow 0$ where ξ a Bernoulli random variable (i.e. $\xi = 0, 1$ with probabilities $p = b/(a+b), 1-p$) and E_a, E_b exponential random variables of parameters a and b respectively (i.e. $p(E) = ae^{-aE}\theta(E)$) statistically independent from ξ . Note that the correlations between E_a and E_b are unimportant since they are multiplied by ξ and $1-\xi$ which cannot be non-zero simultaneously. The occurrence of the Bernoulli variable is intuitively understood since in that limit $p(u)$ exhibits two peaks, one near $u = 0$ and one near $u = 1$ with weights p and $1-p$, and the exponential distributions arise by zooming-in on these peaks and rescaling (u for the first peak, $v = 1-u$ for the other peak).

Since in the Inverse-Beta model $1/u$ is distributed as a $Beta(\gamma, \beta)$ random variable, we immediately obtain that the rescaled random energies of the model $(\mathcal{E}_u, \mathcal{E}_v) = (-\epsilon \log(u), -\epsilon \log(v))$ converge in probability to

$$(-\epsilon \log(u), -\epsilon \log(v)) \sim_{\epsilon \rightarrow 0} (-\zeta E_{\gamma'}, (1-\zeta)E_{\beta'} - \zeta E_{\gamma'}) = (\mathcal{E}'_u, \mathcal{E}'_v), \quad (\text{E.4.49})$$

where ζ is a Bernoulli random variable of parameter $p = \beta' / (\gamma' + \beta')$, $E_{\gamma'}$ and $E_{\beta'}$ are exponential random variables of parameter $\gamma' > 0$ and $\beta' > 0$, independent of ζ . Equivalently one can choose:

$$(\mathcal{E}'_u, \mathcal{E}'_v) = (0, E_{\beta'}) \quad , \quad \text{with proba } 1-p \quad (\text{E.4.50})$$

$$(\mathcal{E}'_u, \mathcal{E}'_v) = (-E_{\gamma'}, 1) \quad , \quad \text{with proba } p \quad (\text{E.4.51})$$

i.e. a model where disorder is chosen randomly either on the site or on the pair of edges arriving at it, with a penalty for the horizontal edge. The two cases corresponds to two peaks near $(u, v) = (1, 0)$ and $(u, v) = (+\infty, +\infty)$ in their distribution in that limit. In terms of the partition sum of the polymer, the limit reads

$$\begin{aligned} -\epsilon \log(Z_t(x)) &= -\epsilon \log\left(\sum_{\pi: (0,0) \rightarrow (t,x)} \exp\left(\sum_{e \in \pi} \log(w_e)\right)\right) \\ &= -\epsilon \log\left(\sum_{\pi: (0,0) \rightarrow (t,x)} \exp\left(-\frac{1}{\epsilon} \sum_{e \in \pi} E_e\right)\right) \\ &\sim_{\epsilon \rightarrow 0} \min_{\pi: (0,0) \rightarrow (t,x)} \sum_{e \in \pi} \mathcal{E}'_e \quad := \mathfrak{E}_{(t,x)}. \end{aligned} \quad (\text{E.4.52})$$

which justifies the name zero temperature limit: the rescaled free energy of the original model converges in probability to the minimal energy $\mathfrak{E}_{(t,x)}$ for the set of all polymers with starting points $(0, 0)$ and ending points (t, x) in the random environment with energies \mathcal{E}'_e distributed according to (E.4.49).

Degeneration to the Exponential (i.e. $q = 1$) Johansson model: In the so-called log-Gamma limit, i.e. $\beta' \rightarrow +\infty$, one obtains $p = 1$ hence:

$$(\mathcal{E}'_u, \mathcal{E}'_v) = (-E_{\gamma'}, 1) \quad (\text{E.4.53})$$

i.e. the on-site exponential distribution model of parameter γ , also identical to the $q \rightarrow 1$ limit of the Johansson model, studied in [159]. Note that the extra weight w_{00} at the origin which we included, allows to precisely recover the Johansson polymer model (with an exponential variable also on the site $x = t = 0$). To make contact with the notations of [159] we have $\mathfrak{E}_{(t,x)} = -H(M, N)$ with $M = I = 1 + x$ and $N = J = 1 + t - x$.

Degeneration to the zero-temperature limit of the Strict-Weak model: In the limit $\gamma' \rightarrow \infty$ one obtains $p = 0$ hence:

$$(\mathcal{E}'_u, \mathcal{E}'_v) = (0, E_{\beta'}) \quad (\text{E.4.54})$$

This model can be interpreted as a discretization of a zero temperature version of the semi-discrete polymer model where one replaces the set of independent Brownian motions by a set of independent random walks.

b Fredholm determinant formula for the zero temperature model

In order to obtain a Fredholm determinant for the zero temperature model starting from our expressions for $g_{tx}(u) = \overline{\exp(-uZ_t(x))}$, we rescale u as $u = \exp(r/\epsilon)$ with $r \in \mathbb{R}$ fixed. Indeed, one then has

$$\begin{aligned} g_{tx}(-\exp(r/\epsilon)) &= \overline{\exp\left(-\exp\frac{1}{\epsilon}(r + \epsilon \log Z_t(x))\right)} \\ &\rightarrow_{\epsilon \rightarrow 0} \overline{\theta(-r + \mathfrak{E}_{(t,x)})} \\ &= \text{Prob}(\mathfrak{E}_{(t,x)} > r). \end{aligned} \quad (\text{E.4.55})$$

We can thus directly write a Fredholm determinant formula for $Prob(\mathfrak{E}_{(t,x)} > r)$ by inserting $u = \exp(r/\epsilon)$ in (E.4.27). The point-wise $\epsilon \rightarrow 0$ limit of the Kernel is taken using a rescaling $s \rightarrow \epsilon s$, $a \rightarrow \epsilon a$ (so that the contour \mathcal{C} do not crosses poles when we take the limit), $k \rightarrow \epsilon k$ and $v_i \rightarrow v_i/\epsilon$ and using

$$\frac{\epsilon}{\sin(\pi\epsilon s)} \rightarrow_{\epsilon \rightarrow 0} \frac{1}{\pi s} \quad , \quad \Gamma(\epsilon x) \simeq_{\epsilon \rightarrow 0} \frac{1}{\epsilon x} + O(1) . \quad (\text{E.4.56})$$

We thus obtain $Prob(\mathfrak{E}_{(t,x)} > r) = \text{Det}(I + K_{tx}^{T=0})$ with

$$K_{t,x}^{T=0}(v_1, v_2) = - \int_{-\infty}^{+\infty} \frac{dk}{\pi} \int_{\mathcal{C}} \frac{ds}{2i\pi s} e^{sr - 2ik(v_1 - v_2) - s(v_1 + v_2)} \quad (\text{E.4.57})$$

$$\left(\frac{\frac{s}{2} + \frac{\gamma'}{2} - ik}{-\frac{s}{2} + \frac{\gamma'}{2} - ik} \right)^{1+x} \left(\frac{\frac{s}{2} + \frac{\gamma'}{2} + ik}{-\frac{s}{2} + \frac{\gamma'}{2} + ik} \right)^{1-x+t} \left(\frac{\beta' + ik + \frac{\gamma'}{2} - \frac{s}{2}}{\beta' + ik + \frac{\gamma'}{2} + \frac{s}{2}} \right)^t .$$

where now $\tilde{C} = a + i\mathbb{R}$ with $0 < a < \gamma'$ and $K_{t,x}^{T=0} : L^2(\mathbb{R}_+) \rightarrow L^2(\mathbb{R}_+)$. Using the same type of rescaling as above, we also obtain an analogous expression to (E.4.28) as $Prob(\mathfrak{E}_{(t,x)} > r) = \text{Det}(I + K_{tx}^{BA,T=0})$ where

$$K_{t,x}^{BA,T=0}(z, z') = \int_{2a+\tilde{a}+i\mathbb{R}} dw \frac{1}{4\pi(w-z')} \frac{1}{\pi(w-z)} e^{r(w-z)} \left(\frac{\gamma' + a - z}{\gamma' + a - w} \right)^{1+x} \left(\frac{w-a}{z-a} \right)^{1-x+t} \left(\frac{z-a+\beta'}{w-a+\beta'} \right)^t \quad (\text{E.4.58})$$

where : $K_{t,x}^{BA,T=0} : L^2(a + \tilde{a} + i\mathbb{R}) \rightarrow L^2(a + \tilde{a} + i\mathbb{R})$ $0 < a < \gamma'$ and $0 < \tilde{a} < \gamma' - a$.

We also immediately obtain a formula analogous to our conjecture (E.4.29) as a *conjecture for the $T = 0$ model*: for $I \geq J$

$$Prob(\mathfrak{E}_{(t,x)} > r) = \frac{1}{J!} \int_{(i\mathbb{R})^J} \prod_{j=1}^J \frac{dw_j}{2i\pi} \prod_{j \neq k=1}^J (w_j - w_k) \prod_{j=1}^J \frac{e^{r(w_j - a)}}{(a - w_j)^J} \left(\frac{\gamma'}{\gamma' + a - w_j} \right)^I \left(\frac{\beta'}{w_j - a + \beta'} \right)^{I+J-2} \quad (\text{E.4.59})$$

with $0 < a < \gamma'$.

Limit to the Johansson model: For $\beta'/\gamma' = +\infty$ one thus finds a formula for the DP model of Johansson (i.e. with independent exponentially distributed on-site energies). It is then interesting to compare our formula with the one obtained in [159] (formula (1.18), which reads (for $r < 0$), $I \geq J \geq 1$):

$$Prob(-\mathfrak{E}_{(t,x)} < -r) = \frac{1}{Z'_{IJ}} \int_{[0, -r]^J} \prod_{j=1}^J dx_j \prod_{1 \leq i < j \leq J} (x_i - x_j)^2 \prod_{j=1}^N x_j^{I-J} e^{-x_j} \quad (\text{E.4.60})$$

which coincides with the CDF of the largest eigenvalue of the Laguerre Unitary Ensemble (LUE) of random matrices (the constant Z'_{IJ} simply ensures the normalisation to unity of the measure on $(\mathbb{R}^+)^J$).

c Asymptotic analysis and KPZ universality for the zero temperature model

We now study the large length limit of the zero temperature model: $t \rightarrow \infty$ and $x = (1/2 + \varphi)t$. The analysis is similar to the one made for the finite temperature model and here we only give the main steps. As before, the $t \rightarrow \infty$ limit is dominated by a saddle point. The dominating term in the Fredholm determinant (E.4.57) now reads $\exp(t(\tilde{G}_\varphi(\frac{s}{2} + ik) - \tilde{G}_\varphi(-\frac{s}{2} + ik)))$ with

$$\tilde{G}_\varphi(y) = -\left(\frac{1}{2} + \varphi\right) \log\left(\frac{\gamma'}{2} - y\right) + \left(\frac{1}{2} - \varphi\right) \log\left(\frac{\gamma'}{2} + y\right) - \log\left(\beta' + \frac{\gamma'}{2} + y\right) . \quad (\text{E.4.61})$$

Note that with the contour previously chosen the arguments of \tilde{G}_φ stay away from the branch cut of the logarithm. As before we look for a critical point, $(s, k) = (0, -i\tilde{k}_\varphi)$ such that $\tilde{G}_\varphi''(\tilde{k}_\varphi) = 0$. This defines \tilde{k}_φ as

$$\frac{(\frac{1}{2} + \varphi)}{(\frac{\gamma'}{2} - \tilde{k}_\varphi)^2} - \frac{(\frac{1}{2} - \varphi)}{(\frac{\gamma'}{2} + \tilde{k}_\varphi)^2} + \frac{1}{(\beta' + \frac{\gamma'}{2} + \tilde{k}_\varphi)^2} = 0 . \quad (\text{E.4.62})$$

Note that this equation as in general several solutions, but the only physical one must have $|\tilde{k}_\varphi| \tilde{\Lambda} < \gamma'/2$ to truly dominate the integration. To this point, we can now follow the exact same steps as before by taking

$$r = t\tilde{c}_\varphi - \tilde{\lambda}_\varphi \tilde{z}$$

$$\tilde{c}_\varphi = -\tilde{G}_\varphi'(\tilde{k}_\varphi) \quad , \quad \tilde{\lambda}_\varphi = \left(\frac{t\tilde{G}_\varphi'''(\tilde{k}_\varphi)}{8} \right)^{\frac{1}{3}} \quad (\text{E.4.63})$$

and using the same rescalings in (E.4.57). In the large length limit, this leads to

$$\lim_{t \rightarrow \infty} Prob \left(\frac{\mathfrak{E}_{(t,x=(1/2+\varphi)t)} - t\tilde{c}_\varphi}{\tilde{\lambda}_\varphi} > -2^{\frac{2}{3}} \tilde{z} \right) = F_2(\tilde{z}) \quad (\text{E.4.64})$$

with

$$\tilde{c}_\varphi = -\frac{(\frac{1}{2} + \varphi)}{\frac{\gamma'}{2} - \tilde{k}_\varphi} - \frac{(\frac{1}{2} - \varphi)}{\frac{\gamma'}{2} + \tilde{k}_\varphi} + \frac{1}{\beta' + \frac{\gamma'}{2} + \tilde{k}_\varphi} \quad (\text{E.4.65})$$

$$0 = \frac{(\frac{1}{2} + \varphi)}{(\frac{\gamma'}{2} - \tilde{k}_\varphi)^2} - \frac{(\frac{1}{2} - \varphi)}{(\frac{\gamma'}{2} + \tilde{k}_\varphi)^2} + \frac{1}{(\beta' + \frac{\gamma'}{2} + \tilde{k}_\varphi)^2} \quad (\text{E.4.66})$$

$$\tilde{\lambda}_\varphi = \left(\frac{t}{8} \left(\frac{(1+2\varphi)}{(\frac{\gamma'}{2} - \tilde{k}_\varphi)^3} + \frac{(1-2\varphi)}{(\frac{\gamma'}{2} + \tilde{k}_\varphi)^3} - \frac{2}{(\beta' + \frac{\gamma'}{2} + \tilde{k}_\varphi)^3} \right) \right)^{\frac{1}{3}}. \quad (\text{E.4.67})$$

Note that this result is coherent with the one obtained at finite temperature (E.4.37) and (E.4.38) and can be obtained from it by scaling $\gamma = \epsilon\gamma'$, $\beta = \epsilon\beta'$ and $k_\varphi = \epsilon\tilde{k}_\varphi$.

Angle of optimal energy The angle of minimum energy $\tilde{\varphi}^*$ of the model is obtained by solving $\frac{\partial}{\partial \varphi} \tilde{c}_\varphi = 0$. This imposes $\tilde{k}_\varphi = 0$ and, using (E.4.65), we thus obtain

$$\varphi^* = -\frac{\gamma'^2}{8} \frac{1}{(\beta' + \frac{\gamma'}{2})^2} < 0. \quad (\text{E.4.68})$$

As for the finite temperature model, we thus retrieve that $\beta' > 0$ biases the DP towards the vertical direction. For $\beta' \rightarrow 0$ we obtain once again $\varphi^* = -\frac{1}{2}$. The optimal energy per unit length, and the scaling parameter $\tilde{\lambda}_{\varphi^*}$ at the optimal angle are respectively

$$\tilde{c}_{\varphi^*} = -\frac{2\beta'}{\gamma'(\beta' + \frac{\gamma'}{2})}, \quad \tilde{\lambda}_{\varphi^*} = \left(\frac{2}{(\gamma')^3} - \frac{2}{(\gamma' + 2\beta')^3} \right)^{\frac{1}{3}} t^{\frac{1}{3}} \quad (\text{E.4.69})$$

recovering the results for the Johansson model:

In the limit $\beta' = +\infty$ the above equations (E.4.65) can be solved explicitly. One finds $\tilde{k}_\varphi = -\frac{\gamma'}{4\varphi}(1 - \sqrt{1 - 4\phi^2})$, where we have chosen the root which vanished at the optimal angle $\varphi^* = 0$ (i.e. the diagonal which is a symmetry axis in this case). This yields:

$$\tilde{c}_\varphi = -\frac{1}{\gamma'}(1 + \sqrt{1 - 4\phi^2}), \quad \tilde{\lambda}_\varphi = \frac{1}{\gamma'} t^{\frac{1}{3}} \left(\frac{8\varphi^4}{(1 - \sqrt{1 - 4\phi^2})^2 \sqrt{1 - 4\phi^2}} \right)^{\frac{1}{3}} \quad (\text{E.4.70})$$

We can now compare with Johansson result (formula 1.22 in [159]) which reads (for $\gamma' = 1$):

$$H(gJ, J) \simeq_{J \rightarrow +\infty} (1 + \sqrt{g})^2 J + g^{-1/6} (1 + \sqrt{g})^{4/3} J^{1/3} \chi_2 \quad (\text{E.4.71})$$

where χ_2 is a Tracy-Widom GUE random variable (of CDF given by F_2). With a little bit of algebra one can check that this is exactly equivalent to our result, namely:

$$\mathfrak{E}_{(t, x=(1/2+\varphi)t)} \simeq_{t \rightarrow +\infty} t \tilde{c}_\varphi - 2^{2/3} \lambda_\varphi \chi_2 \quad (\text{E.4.72})$$

with $\mathfrak{E}_{(t, x=(1/2+\varphi)t)} = -H(gJ, J)$, taking into account that $J = 1 + t - x \simeq (\frac{1}{2} - \phi)t$, hence $g = \frac{1+2\varphi}{1-2\varphi}$.

E.5 Conclusion

In this paper we attempted a classification of finite temperature directed polymer models on the square lattice with homogeneously distributed random Boltzmann weights and a certain type of short-range correlations (Section E.2.1), for which the moments of the partition sum $Z_t(x)$ can be calculated via a coordinate Bethe ansatz. Following the pioneering work of [222], we obtained a rigorous expression (E.2.21) that constrains the possible forms for the moments of the underlying distribution of weights. We discussed in details the possibilities of finding PDF's with the appropriate moments (E.2.21) and, though the classification is still not complete, we were able to exclude a large number of cases. In cases where the moment problem has a solution, we retrieved all the previously known finite temperature integrable DP models (Section E.3.2), and introduced a new one, the Inverse-Beta polymer, which appears as a natural two parameters generalization of the log-Gamma polymer, but also contains the Strict-Weak polymer as a limit. Using the Bethe ansatz, we obtained an integral formula for the moments of the partition sum (E.4.18) of the Inverse-Beta polymer, with point-to-point boundary conditions. Along this route, most of the tools developed in [4] for the Bethe ansatz solution of the log-Gamma polymer proved very useful and were generalized.

Starting from the moments formula and using analytical continuations, we obtained two equivalent Fredholm determinant formulas for the Laplace transform of the PDF of the partition sum (E.4.27) and (E.4.28), and conjectured a n-fold integral formula (E.4.29) for the same object, which generalizes a known formula for the log-Gamma polymer obtained in [198] in the framework of the gRSK correspondence. Using our Fredholm determinant formulas and an asymptotic analysis in the limit of large polymer length, we were able to obtain the KPZ universality of the model (critical exponents and Tracy-Widom GUE free-energy fluctuations) (E.4.37) and as well as exact implicit expressions for the mean free energy and

the amplitude of fluctuations as a function of the polymer orientation w.r.t. the diagonal. As an application we obtained an exact expression for the optimal angle which minimizes the free-energy of the polymer (E.4.41).

In Section E.4.4 we introduced a zero-temperature DP model as a limit of the Inverse-Beta polymer, which generalizes the previously known zero-temperature limit of the log-Gamma polymer. Using the exact formulas obtained for the Inverse-Beta polymer, we showed analogous formulas for this zero-temperature model. In particular we obtained exact formulas (Fredholm determinant and n-fold integrals) for the cumulative distribution of optimal energy of the model (E.4.57), (E.4.58) and (E.4.59). Using an asymptotic analysis, we showed the KPZ universality (E.4.64) of the model. Our formula compare successfully with some results obtained by Johansson in his pioneering study of the Exponential zero-temperature polymer [159], a particular case of our zero-temperature model.

We believe that the present work could be used as a guide for future research of new integrable DP models. In addition, we once again showed that the replica Bethe ansatz method is a valuable and versatile tool for the analysis of such DP models. In particular, some results of this paper could prove useful and adaptable to the analysis of the model with different boundary conditions.

For future works on the Inverse-Beta polymer, it should be very interesting to obtain a solution of this model using the gRSK correspondence or a generalization of the latter (as in the recent work [221]). Our conjecture (E.4.29) could be proven (or invalidated) using these techniques. In addition, we know that an inhomogeneous version of the log-Gamma polymer was amenable to analytical treatment in the framework of the gRSK correspondence, and it is thus likely that an inhomogeneous version of the Inverse-Beta model should also exist.

For future works on the classification of directed polymer models, various directions of research remain. The most direct one is to understand if some integrable models remain to be found to fill the left voids in Fig. E.2 (as e.g. our proposal of Appendix E.7). Other directions would be to extend this framework to introduce inhomogeneous models, or different disorder correlations. The precise implications of our classification of finite temperature DP model for possible zero temperature integrable DP models remain to be elucidated. Indeed all the models we found in our framework admit a zero temperature limit. For example, the zero temperature limit of the log-Gamma model is the $q \rightarrow 1$ limit (beware that this q is a priori different from the one used in Section E.3) of the zero temperature model of Johansson [159], i.e. the Exponential zero-T model (as was pointed out in [198]). However, at this stage, our framework seems to miss the $q \neq 1$ case of the Johansson model. A natural question is then to understand if a finite temperature integrable DP model sits above the Johansson model $\forall q$, and whether the zero temperature model studied in this paper admits a $q \neq 1$ generalization. Since Johansson's model is determinantal, a related outstanding question is to obtain a deeper and more systematic understanding of the relations between Bethe ansatz solvable models and determinantal processes which seem to often occur as limit cases of the former.

We are very grateful to G. Barraquand, I. Corwin and A.M. Povolotsky for very useful remarks and discussions. We gratefully acknowledge hospitality and support from Galileo Galilei Institute (program "Statistical Mechanics, Integrability and Combinatorics) where part of this work was conducted.

E.6 Appendix A: The $|q| < 1$ case: study of degenerations.

Here we study in details the possible degenerations of the parameters (q, ν, μ) that would eventually lead to a PDF $p(u, v)$ such that the moments of u and v are given by (E.2.21) and $n_{\max} \geq 2$. As in the main text, we restrict to the domain $|q| < 1$ and consider the random variable $z_x = u + xv$, $x \in \mathbb{R}$. Its variance is:

$$\frac{\overline{z_x^c}}{z_x^c} = \frac{(\mu - 1)(1 - q)(\mu - \nu)(\mu x - 1)(\mu x - \nu)}{\mu^2(\nu - 1)^2(\nu q - 1)} \quad (\text{E.6.1})$$

which must be positive. Since the polynomial in x changes sign at $x = \frac{\nu}{\mu}$ and $x = \frac{1}{\mu}$ one must look for cases where $\frac{\nu}{\mu} = \frac{1}{\mu}$. The different cases to investigate are thus $\nu = 1$, $|\mu| = \infty$, $\mu = 0$ and a combination of these cases. It is instructive to look at the variance for $x = 1$:

$$\frac{\overline{z_1^c}}{z_1^c} = \frac{(\mu - 1)^2(1 - q)(\mu - \nu)^2}{\mu^2(\nu - 1)^2(\nu q - 1)} \quad (\text{E.6.2})$$

One sees that the positivity of the variance implies $q\nu > 1$, as long as we do not consider degenerations $\mu \rightarrow 1$, $\mu \rightarrow \nu$, or $q \rightarrow 1$ (in which case the variance of z_1 may vanish and the condition may disappear).

- If $\nu \rightarrow 1$, it is easy to see from the variance of z_1 that there must be at least one additional degeneration, either (i) $\mu \rightarrow 1$ or (ii) $q \rightarrow 1$ (iii) both $q \rightarrow 1$ and $\mu \rightarrow 1$. The first one can be ruled out as follows: setting $\mu = 1 + a\epsilon$ and $\nu = 1 + b\epsilon$ with $\epsilon \rightarrow 0$, one finds that the variance is $\frac{\overline{z_x^c}}{z_x^c} = \frac{a(b-a)}{b^2}(1-x)^2$ and that from (E.2.21) the marginals have integer moments $\overline{u^n} = 1 - \frac{a}{b}$ and $\overline{v^n} = \frac{a}{b}$ for all $n \geq 1$. This implies that $u + v = 1$ and $v = 0, 1$ with probability $\frac{a}{b}$, which then predicts joints moments different from the ones obtained from (E.2.21) in that limit, hence no joint PDF exists in case (i). The case (ii) and (iii) both imply a $q \rightarrow 1$ limit which we discuss in the end of this appendix.
- If $|\mu| \rightarrow \infty$. In this case, looking at the original moments (E.2.21), we see that we must scale $v \rightarrow v/\mu$ to obtain a well defined random variable. We define $(u', v') = (u, v/\mu)$. In the limit $\mu \rightarrow \infty$, the moments are

$$\frac{\overline{u'^{n_1} v'^{n_2}}}{u'^{n_1} v'^{n_2}} = \frac{(-1)^{n_2} q^{\frac{n_2(n_2-1)}{2}}}{(\nu; q)_{n_1+n_2}} \frac{(q; q)_{n_1+n_2}}{(q; q)_{n_1} (q; q)_{n_2}} \frac{1}{C_{n_1+n_2}^{n_1}} \quad (\text{E.6.3})$$

we now define the random variable $z'_x = u' + xv'$ and compute its variance:

$$\overline{(z'_x)^2}^c = \frac{(1-q)(x-1)(x-\nu)}{(\nu-1)^2(\nu q-1)} \quad (\text{E.6.4})$$

which must also be positive for all x . However, this polynomial changes sign at $x=1$ and $x=\nu$ so we must have $\nu=1$. Since the constraint $q\nu > 1$ still holds and $q < 1$, the only possibility is to have $q \rightarrow 1$ as well, a case discussed below.

- If $\mu = 0$, looking at (E.2.21), we see that we must now rescale (u, v) as $(u', v') = (\mu u, v)$ and we obtain

$$\overline{u'^{n_1} v'^{n_2}} = \frac{(-1)^{n_1} q^{\frac{n_1(n_1-1)}{2}}}{(\nu; q)_{n_1+n_2}} \frac{(q; q)_{n_1+n_2}}{(q; q)_{n_1} (q; q)_{n_2}} \frac{1}{C_{n_1+n_2}^{n_1}} \quad (\text{E.6.5})$$

i.e. this is a case identical to the previous one, and we also conclude that we must have $q \rightarrow 1$.

Let us now discuss all the possibilities in the $q \rightarrow 1$ limit. Taking the limit directly on (E.2.21), one obtains

$$\overline{u^{n_1} v^{n_2}} = \frac{(1-\nu/\mu)^{n_1} (1-\mu)^{n_2}}{(1-\nu)^{n_1+n_2}} \quad (\text{E.6.6})$$

where we used that at fixed n, a , $(q^a; q)_n \simeq_{q \rightarrow 1} (1-q)^n (a)_n$, where $(a)_n = a(a+1)\dots(a+n-1)$, and here we took $a=1$. Obviously, the limit we took only works if ν, μ and ν/μ are all different from 1, but it also encompasses other limits such that the $\mu \rightarrow \infty$ and $q \rightarrow 1$ case discussed when analyzing (E.6.3). The moments (E.6.6) correspond to deterministic weights $u = \frac{1-\nu/\mu}{1-\nu}$ and $v = \frac{1-\mu}{1-\nu}$. These models are obviously integrable, but trivial.

We must thus study the $q \rightarrow 1$ limit with at least one of those parameters that goes to 1. The question of the speed of the convergence then arises. In general, taking $q = 1 - \epsilon$ and $a = 1 - a'\epsilon^\zeta$ with $\zeta > 0$, one has $(a; q)_n \simeq_{q \rightarrow 0} \epsilon^n (a')_n$ (if $\zeta = 1$), $(a; q)_n \simeq_{q \rightarrow 0} \epsilon^\zeta a'^\zeta \epsilon^{n-1} (n-1)!$ (if $\zeta > 1$ and $n \geq 1$) and $(a; q)_n \simeq_{q \rightarrow 0} \epsilon^{n\zeta} (a')^n$ (if $\zeta < 1$). The possibility of using $\zeta < 1$ for the convergence of μ and/or ν (slow convergence compared to q) is uninteresting since it leads to pure power-laws. The possibility of using $\zeta > 1$ (fast convergence compared to q) is also uninteresting since one cannot rescale (u, v) to obtain well-defined moments in the $\epsilon \rightarrow 0$ limit. In the following, we thus only consider the possibility of convergence of the parameters *at the same speed* than q . Let us first examine the cases where only one of those parameters goes to 1. We obtain

- If $\mu = q^\beta$ and $\nu \neq 1$,

$$\overline{u^{n_1} v^{n_2}} = (\beta)_{n_2} \times \text{power-laws} \quad (\text{E.6.7})$$

- If $\nu = q^{\alpha+\beta}$ and $\mu \neq 1$,

$$\overline{u^{n_1} v^{n_2}} = \frac{1}{(\alpha+\beta)_{n_1+n_2}} \times \text{power-laws} \quad (\text{E.6.8})$$

- If $\nu/\mu = q^\alpha$, $\nu \neq 1$ and $\mu \neq 1$,

$$\overline{u^{n_1} v^{n_2}} = (\alpha)_{n_1} \times \text{power-laws} \quad (\text{E.6.9})$$

where we have not written the precise form of the unimportant power-law terms. As discussed in the main text (Section E.3.2), these cases indeed correspond to proper PDF's and known integrable models for some range of parameters α, β . The first and third ones correspond to the moments of the Strict-Weak polymers, the second one corresponds to the moments of the log-Gamma polymer. Notice however that these models can all be obtained as limits of the case $(q, \mu, \nu) \rightarrow (1, 1, 1)$. Indeed, taking $\mu = q^\beta$, $\nu = q^{\alpha+\beta}$ and $q \rightarrow 1$, we obtain

$$\overline{u^{n_1} v^{n_2}} = \frac{(\alpha)_{n_1} (\beta)_{n_2}}{(\alpha+\beta)_{n_1+n_2}}. \quad (\text{E.6.10})$$

Taking appropriate limits on this last formula, we can retrieve the three precedent cases. For example the limit $\beta \rightarrow \infty$ of (E.6.10) leads to, rescaling u as βu , $\overline{(\beta u)^{n_1} v^{n_2}} = (\alpha)_{n_1}$, and we obtain the moments of the third case. Taking a similar limit $|\alpha|, |\beta| \rightarrow \infty$ with $\alpha + \beta$ fixed, we obtain the second case.

Hence, in this sense, the most general limit of (E.2.21) that can lead to distributions with a well-defined variance is the $(q, \mu, \nu) \rightarrow (1, 1, 1)$ limit. This limit is studied in details in Section E.3.2.

E.7 Appendix B: A more systematic study of analytical continuations of moments.

Starting with a polymer model with moments given by

$$\overline{u^{n_1} v^{n_2}} = (\epsilon_1)^{n_1} (\epsilon_2)^{n_2} \frac{(\alpha)_{n_1} (\beta)_{n_2}}{(\alpha+\beta)_{n_1+n_2}}, \quad (\text{E.7.1})$$

where (α, β) are arbitrary, $(\epsilon_1, \epsilon_2) \in \{-1, 1\}^2$, we look for distributions $p(u, v)$ such that (E.7.1) corresponds to the moments of positive random variables. It is natural, in agreement with the examples of the Beta and Inverse-Beta polymers studied in the text, to analytically continue (E.7.1) to $(n_1, n_2) = (s_1, s_2) \in \mathbb{C}^2$. Obviously there is an infinite number of possible analytical continuations and here we only study arguably the most natural ones (using Euler inversion formula $\Gamma(x)\Gamma(1-x) = \pi/\sin(\pi x)$ and $(-1)^n = \sin(\pi(x+n))/\sin(\pi x)$ for integer n), which we now enumerate.

- First type, $(\epsilon_1, \epsilon_2) = (1, 1)$:

$$\overline{u^{s_1}v^{s_2}} = \frac{\Gamma(\alpha + \beta) \Gamma(\alpha + s_1)\Gamma(\beta + s_2)}{\Gamma(\alpha)\Gamma(\beta) \Gamma(\alpha + \beta + s_1 + s_2)}. \quad (\text{E.7.2})$$

- Second type $(\epsilon_1, \epsilon_2) = (1, -1)$:

$$\overline{u^{s_1}v^{s_2}} = \frac{\Gamma(1 - \alpha)}{\Gamma(1 - \alpha - \beta)\Gamma(\beta)} \frac{\Gamma(1 - \alpha - \beta - s_1 - s_2)\Gamma(\beta + s_2)}{\Gamma(1 - \alpha - s_1)}. \quad (\text{E.7.3})$$

- Third type $(\epsilon_1, \epsilon_2) = (-1, -1)$:

$$\overline{u^{s_1}v^{s_2}} = \frac{1}{\Gamma(\alpha)\Gamma(\beta)\Gamma(1 - \alpha - \beta)} \Gamma(\alpha + s_1)\Gamma(\beta + s_2)\Gamma(1 - \alpha - \beta - s_1 - s_2). \quad (\text{E.7.4})$$

- Fourth type, $(\epsilon_1, \epsilon_2) = (-1, 1)$:

$$\overline{u^{s_1}v^{s_2}} = \frac{\Gamma(\alpha + \beta)\Gamma(1 - \alpha)}{\Gamma(\beta)} \frac{\Gamma(\beta + s_2)}{\Gamma(1 - \alpha - s_1)\Gamma(\alpha + \beta + s_1 + s_2)}. \quad (\text{E.7.5})$$

- Fifth type $(\epsilon_1, \epsilon_2) = (-1, -1)$:

$$\overline{u^{s_1}v^{s_2}} = \Gamma(\alpha + \beta)\Gamma(1 - \alpha)\Gamma(1 - \beta) \frac{1}{\Gamma(1 - \alpha - s_1)\Gamma(1 - \beta - s_2)\Gamma(\alpha + \beta + s_1 + s_2)}. \quad (\text{E.7.6})$$

- Sixth type $(\epsilon_1, \epsilon_2) = (1, 1)$:

$$\overline{u^{s_1}v^{s_2}} = \frac{\Gamma(1 - \alpha)\Gamma(1 - \beta)}{\Gamma(1 - \alpha - \beta)} \frac{\Gamma(1 - \alpha - \beta - s_1 - s_2)}{\Gamma(1 - \alpha - s_1)\Gamma(1 - \beta - s_2)}. \quad (\text{E.7.7})$$

a First type

Let us first consider the first type of analytical continuation (E.7.2). Assuming it to be valid on the full complex plane, the distribution $p(u, v)$ can be directly obtained as an ILT

$$p(u, v) = \frac{1}{N_{\alpha, \beta}} \int_{\mathcal{C}_1} \frac{ds_1}{2i\pi} \int_{\mathcal{C}_2} \frac{ds_2}{2i\pi} u^{-1-s_1} v^{-1-s_2} \frac{\Gamma(\alpha + s_1)\Gamma(\beta + s_2)}{\Gamma(\alpha + \beta + s_1 + s_2)} \quad (\text{E.7.8})$$

where $N_{\alpha, \beta}^{-1} = \frac{\Gamma(\alpha + \beta)}{\Gamma(\alpha)\Gamma(\beta)}$ is a normalization factor, and different contours \mathcal{C}_i can be considered. Here we first consider the most natural choices: vertical lines passing through the right of all the poles of the integrands located at $s_1 = -\alpha - m_1$ and $s_2 = -\beta - m_2$ with $(m_1, m_2) \in \mathbb{N}^2$, e.g. $s_1 = -\alpha + 1 + iy_1$ and $s_2 = -\beta + 1 + iy_2$ with $(y_1, y_2) \in \mathbb{R}^2$. We first consider the integration on s_2 . If $v > 1$, the contour can be closed to the right, giving 0 as a result. On the other hand, if $v < 1$, the contour can only be closed to the left and all the poles of s_2 contribute. This shows

$$p(u, v) = \theta(0 < v < 1) \frac{1}{N_{\alpha, \beta}} \int_{\mathcal{C}_1} \frac{ds_1}{2i\pi} u^{-1-s_1} \sum_{m_2=0}^{\infty} v^{-1+\beta+m_2} \frac{(-1)^{m_2}}{m_2!} \frac{\Gamma(\alpha + s_1)}{\Gamma(\alpha + s_1 - m_2)}. \quad (\text{E.7.9})$$

In this expression, one recognizes the Taylor expansion

$$(1 - v)^\eta = \sum_{k=0}^{\infty} (-v)^k \frac{\Gamma(\eta + 1)}{\Gamma(1 + k)\Gamma(\eta - k + 1)} = \sum_{k=0}^{\infty} \frac{(-v)^k}{k!} \frac{\Gamma(\eta + 1)}{\Gamma(\eta - k + 1)}, \quad (\text{E.7.10})$$

with $\eta = \alpha + s_1 - 1$, and the convergence is here assured by the fact that $v < 1$. We thus get

$$p(u, v) = \theta(0 < v < 1) \frac{1}{N_{\alpha, \beta}} \int_{\mathcal{C}_1} \frac{ds_1}{2i\pi} u^{-1-s_1} v^{-1+\beta} (1 - v)^{\alpha + s_1 - 1}. \quad (\text{E.7.11})$$

And one now recognizes the integral representation of the Dirac δ distribution: $\int_{\mathcal{C}_1} \frac{ds_1}{2i\pi} w^s = \delta(w - 1)$, and

$$\begin{aligned} p(u, v) &= \theta(0 < v < 1) \frac{1}{N_{\alpha, \beta}} u^{-1} v^{-1+\beta} (1 - v)^{\alpha-1} \delta\left(\frac{1-v}{u} - 1\right) \\ &= \theta(0 < u < 1) \frac{\Gamma(\alpha + \beta)}{\Gamma(\alpha)\Gamma(\beta)} u^{-1+\alpha} v^{-1+\beta} \delta(u + v - 1). \end{aligned} \quad (\text{E.7.12})$$

Which is exactly the Beta distribution of the Beta polymer, and the normalizability condition imposes $\alpha > 0$ and $\beta > 0$.

b Second type

Introducing as in the main text $\gamma = 1 - \alpha - \beta$, we now study E.7.3, which reads in these variables:

$$\overline{u^{s_1} v^{s_2}} = \frac{\Gamma(\gamma + \beta)}{\Gamma(\gamma)\Gamma(\beta)} \frac{\Gamma(\gamma - s_1 - s_2)\Gamma(\beta + s_2)}{\Gamma(\gamma + \beta - s_1)}. \quad (\text{E.7.13})$$

We follow the same step as before

$$p(u, v) = \frac{1}{\tilde{N}_{\gamma, \beta}} \int_{\mathcal{C}_1} \frac{ds_1}{2i\pi} \int_{\mathcal{C}_2} \frac{ds_2}{2i\pi} u^{-1-s_1} v^{-1-s_2} \frac{\Gamma(\gamma - s_1 - s_2)\Gamma(\beta + s_2)}{\Gamma(\gamma + \beta - s_1)} \quad (\text{E.7.14})$$

where $\tilde{N}_{\gamma, \beta}^{-1} = \frac{\Gamma(\gamma + \beta)}{\Gamma(\gamma)\Gamma(\beta)}$. The contours \mathcal{C}_1 and \mathcal{C}_2 are chosen so as to avoid the poles $s_1 = \gamma - s_2 + m_1$ and $s_2 = -\beta - m_2$ for $(m_1, m_2) \in \mathbb{N}^2$, e.g. we choose $s_2 = -\beta + 1 + iy_2$ and $s_1 = \gamma + \beta - 2 + iy_2$ with $(y_1, y_2) \in \mathbb{R}^2$. Integrating first on s_1 and following the same steps as before, we now obtain

$$\begin{aligned} p(u, v) &= \theta(1 < u) \frac{1}{\tilde{N}_{\gamma, \beta}} \int_{\mathcal{C}_2} \frac{ds_2}{2i\pi} v^{-1-s_2} \sum_{m_1=0}^{\infty} \frac{(-1)^{m_1}}{m_1!} u^{-1-\gamma+s_2-m_1} \frac{\Gamma(\beta + s_2)}{\Gamma(\beta + s_2 - m_1)} \\ &= \frac{\theta(1 < u)}{\tilde{N}_{\gamma, \beta}} \int_{\mathcal{C}_2} \frac{ds_2}{2i\pi} v^{-1-s_2} u^{-1-\gamma+s_2} \left(1 - \frac{1}{u}\right)^{\beta+s_2-1} \\ &= \frac{\theta(1 < u)}{\tilde{N}_{\gamma, \beta}} v^{-1} u^{-1-\gamma} \left(1 - \frac{1}{u}\right)^{\beta-1} \delta\left(\frac{u}{v}\left(1 - \frac{1}{u}\right) - 1\right) \\ &= \frac{\theta(1 < u)}{\tilde{N}_{\gamma, \beta}} u^{-1-\gamma} \left(1 - \frac{1}{u}\right)^{\beta-1} \delta(v - 1 + u) \end{aligned}$$

We thus obtain the same distribution as before, which is indeed normalizable for $\gamma > 0$ and $\beta > 0$. Note the interesting fact that, though the moments of the distribution only exist for $n_1 + n_2 < \gamma$, the analytical continuation of the moments offered by the Gamma function allows us to retrieve the distribution. Though non-rigorous it gives some insight to understand why the replica method developed in this paper to retrieve the PDF of the partition sum of the associated polymer model works. This is also in agreement with Appendix E.9

c Third type

For the third type (E.7.4), it seems difficult to compute the involved integrals in full generality since they depend on the precise position of the poles. However, we now directly exhibit some examples that define proper distributions for $1 - (\alpha + \beta) = \gamma > 0$. We take $u = \tilde{u}w, v = \tilde{v}w$ with \tilde{u}, \tilde{v} and w independent random variables distributed with PDF

$$\begin{aligned} p_w(w) &= \frac{1}{\Gamma(\gamma)} w^{-1-\gamma} e^{-1/w} \\ p_u(u) &= \frac{1}{\Gamma(\alpha)} u^{-1+\alpha} \left(e^{-u} - \left(\sum_{k=0}^{\lfloor -\alpha \rfloor} \frac{u^k}{k!} \right) \right) \\ p_v(v) &= \frac{1}{\Gamma(\beta)} u^{-1+\beta} \left(e^{-u} - \left(\sum_{k=0}^{\lfloor -\beta \rfloor} \frac{u^k}{k!} \right) \right) \end{aligned} \quad (\text{E.7.15})$$

Where $\lfloor \cdot \rfloor$ denotes the integer part, and the sum appearing in p_u (resp. p_v) is present only if $\alpha < 0$ (resp. $\beta < 0$) and regularizes the eventual divergences near the origin. These distributions are singular and only have a few integer moments, but their complex moments $\overline{u^{s_1} v^{s_2}}$ do exist on a domain $\text{Re}(s_1 + s_2) \leq \gamma$, supplemented by the condition $|\text{Re}(s_1)| < 1/2$ (resp. $|\text{Re}(s_2)| < 1/2$) if $\alpha < 0$ (resp. $\beta < 0$), and are there given by (E.7.4). As in the log-Gamma and Inverse-Beta cases, these moments can be analytically continued to the full complex plane, opening a way for a Bethe ansatz solution of this kind of model. In terms of contours integrals, p_u can be obtained using the same technique as before with $u^s = \Gamma(\alpha + s_1)/\Gamma(\alpha)$, but always choosing a contour of integration as a vertical line passing by the origin (and eventually separating the poles of the integrand). It would be of great interests to understand if one can obtain exact results for a polymer model defined with these types of weights (e.g. the PDF of $\log Z_t(x)$) using analytical continuations of other known results. This is left for future work. Notice that these models could well be good candidates to fill the void left in the down-left quarter of Fig. E.2.

d Other types

For the other types, one intuitively see that they “lack of poles” in the complex plane $(s_1, s_2) \in \mathbb{C}^2$ to obtain a meaningful result after Laplace inversion, and the corresponding integrals diverge. For the fourth (E.7.5) and fifth cases (E.7.6), another argument goes in the same direction. Writing schematically $\overline{u^{s_1} v^{s_2}} = f(s_1, s_2)$, we have

$$\overline{(\ln u)^2}^c = \frac{\partial^2}{\partial s_1^2} f|_{s_1=s_2=0} \quad , \quad \overline{(\ln v)^2}^c = \frac{\partial^2}{\partial s_2^2} f|_{s_1=s_2=0} \quad , \quad (\text{E.7.16})$$

where $\overline{(\cdot)^2}^c$ denotes the variance. Applying this formula on (E.7.5) and (E.7.6) always leads to negative results which is incompatible with $\ln u$ having a PDF with a second moment. We do not consider here the possibility of such very singular distributions.

For the sixth type (E.7.7), there remains small windows of parameters for which both $\overline{(\ln u)^2}^c$ and $\overline{(\ln v)^2}^c$ are positive simultaneously, so that this argument is inconclusive. We do not investigate further the possibility of the existence of another integrable model here.

E.8 Appendix C: Effect of an additional inverse Gamma weight at the starting point

Consider the two partition sums, one, noted $Z_t(x)$ and studied in the text, in presence of the additional inverse Gamma random variable w_{00} on the site $x = t = 0$, and the other one, $\tilde{Z}_t(x)$, in absence of such a weight (which in a sense is the true point to point problem). Clearly one has:

$$Z_t(x) = w_{00}\tilde{Z}_t(x) \quad (\text{E.8.1})$$

for any x, t where w_{00} and $\tilde{Z}_t(x)$ are uncorrelated random variables.

There are various ways to express one problem into the other. Let us use here the shorthand notation $Z \equiv Z_t(x)$ and $\tilde{Z} \equiv \tilde{Z}_t(x)$. The moments are related as:

$$\overline{Z^s} = \frac{\Gamma(\gamma - s)}{\Gamma(\gamma)} \overline{\tilde{Z}^s} \quad (\text{E.8.2})$$

And the Laplace transforms as:

$$\overline{e^{-uZ}} = \overline{e^{-uw_{00}\tilde{Z}}} = \frac{2}{\Gamma(\gamma)} \overline{(u\tilde{Z})^{\gamma/2} K_{\gamma}(2\sqrt{u\tilde{Z}})} \quad (\text{E.8.3})$$

Since the l.h.s. is known explicitly as a Fredholm determinant, we see that to obtain $P(\tilde{Z})$ one needs to invert a modified type of Laplace transform involving Bessel functions.

There is also a useful relation between the CDF's. Let us define the CDF of $\ln Z$, as $F(y) = \text{Prob}(\ln Z < y)$, and the one of $\ln \tilde{Z}$, as $\tilde{F}(y) = \text{Prob}(\ln \tilde{Z} < y)$. Clearly

$$F(y) = \text{Prob}(\ln Z < y) = \langle \text{Prob}(\ln \tilde{Z} < y - \ln w_{00}) \rangle_{w_{00}} = \langle \tilde{F}(y - \ln w_{00}) \rangle_{w_{00}} = \langle e^{-\ln w_{00} \partial_y} \rangle_{w_{00}} \tilde{F}(y) \quad (\text{E.8.4})$$

$$= \frac{\Gamma(\gamma + \partial_y)}{\Gamma(\gamma)} \tilde{F}(y) \quad (\text{E.8.5})$$

Hence, knowing $F(y)$ from Fredholm determinants, one can obtain the CFD $\tilde{F}(y)$ as:

$$\tilde{F}(y) = \frac{\Gamma(\gamma)}{\Gamma(\gamma + \partial_y)} F(y) \quad (\text{E.8.6})$$

an operator which can be interpreted in the sense of a Taylor expansion w.r.t. ∂_y . At fixed γ in the large time limit studied in E.4.3, the rescaling (E.4.34) renders the term ∂_y smaller by $t^{-1/3}$. Defining as in (E.4.37)

$$F_{res}(z) = \text{Prob}\left(2^{-\frac{2}{3}} \frac{\log Z + tc_{\varphi}}{\lambda_{\varphi}} < z\right) = F(y = 2^{2/3} \lambda_{\varphi} z - tc_{\varphi}) \quad (\text{E.8.7})$$

and similarly for $\tilde{F}_{res}(z)$ w.r.t. $\log \tilde{Z}$, we obtain:

$$\tilde{F}_{res}(z) = \frac{\Gamma(\gamma)}{\Gamma(\gamma + 2^{-2/3} \lambda_{\varphi}^{-1} \partial_z)} F_{res}(z) \quad (\text{E.8.8})$$

a relation exact for all t , but which for $t \rightarrow +\infty$ shows that the effect of the operator ∂_y becomes negligible in the scaling variable z (we recall that $\lambda_{\varphi} \sim t^{1/3}$). The rescaled CDF's are thus the same, a very intuitive result: the large-length is insensitive to such a change in the energy of the first site. The formula allows to calculate the subleading corrections.

In the $T = 0$ limit the formula (E.8.6) simplifies. Defining $F_{T=0}(r) = \text{Prob}(\mathfrak{E}_{(t,x)} > r)$ and similarly for $\tilde{F}_{T=0}(r)$ in presence of the additional exponentially distributed energy random variable at site $(x, t) = (0, 0)$, we obtain from the definition (E.4.52):

$$\tilde{F}_{T=0}(r) = \left(1 - \frac{1}{\gamma'} \partial_r\right) F_{T=0}(r) \quad (\text{E.8.9})$$

valid for arbitrary t . At large time the same argument on the rescaled variable \tilde{z} again shows the derivative term to be negligible.

Finally note that such relations have been studied also in the context of stationary models in the KPZ class [183, 185] where it seems also mandatory to add an inverse Gamma variable at the origin in order to obtain a FD representation. Its occurrence in a point to point problem is, to our knowledge, new.

E.9 Appendix D: Laplace transform Vs Moment Generating function: recall

In this appendix we briefly recall the idea, discussed in [4] and to which we refer for more details, that leads to the conjecture (E.4.27). It is best illustrated on the simple problem of obtaining the Laplace transform of (E.1.1):

$$\begin{aligned} g(\lambda) &= \overline{e^{-\lambda u}} = \frac{\Gamma(\gamma + \beta)}{\Gamma(\gamma)\Gamma(\beta)} \int_1^{+\infty} du e^{-\lambda u} \frac{1}{u^{1+\gamma}} \left(1 - \frac{1}{u}\right)^{\beta-1} \\ \overline{e^{-\lambda u}} &= \frac{\Gamma(\gamma + \beta)}{\Gamma(\gamma)\Gamma(\beta)} \int_1^{+\infty} du \sum_{n=0}^{\infty} \frac{(-\lambda)^n}{n!} u^n \frac{1}{u^{1+\gamma}} \left(1 - \frac{1}{u}\right)^{\beta-1} \end{aligned} \quad (\text{E.9.1})$$

In this formula, it is obvious that one cannot invert the sum and integrals sign because the different terms converge only if $n < \gamma$. In which case

$$\frac{\Gamma(\gamma + \beta)}{\Gamma(\gamma)\Gamma(\beta)} \int_1^{+\infty} du \frac{(-\lambda)^n}{n!} u^n \frac{1}{u^{1+\gamma}} \left(1 - \frac{1}{u}\right)^{\beta-1} = \frac{(-\lambda)^n}{n!} \frac{\Gamma(\gamma + \beta)\Gamma(\gamma - n)}{\Gamma(\gamma + \beta - n)\Gamma(\gamma)}. \quad (\text{E.9.2})$$

Note however that, using the analytical continuation of the Gamma function, the right hand side of (E.9.1) also makes sense for $n > \gamma$. We can thus consider the object, called the ‘‘moment generating function’’ defined as

$$g_{mom}(\lambda) = \sum_{n=0}^{\infty} \frac{(-\lambda)^n}{\Gamma(1+n)} \frac{\Gamma(\gamma + \beta)\Gamma(\gamma - n)}{\Gamma(\gamma + \beta - n)\Gamma(\gamma)}. \quad (\text{E.9.3})$$

The question is now to understand how (E.9.3) and (E.9.1) are related. Let us now rewrite (E.9.1) using an integral representation of the exponential as

$$\begin{aligned} g(\lambda) &= \frac{\Gamma(\gamma + \beta)}{\Gamma(\gamma)\Gamma(\beta)} \int_1^{+\infty} du (-1) \int_{\mathcal{C}} \frac{ds}{2i \sin(\pi s)} \frac{\lambda^s}{\Gamma(1+s)} u^s \frac{1}{u^{1+\gamma}} \left(1 - \frac{1}{u}\right)^{\beta-1} \\ &= -\frac{\Gamma(\gamma + \beta)}{\Gamma(\gamma)\Gamma(\beta)} \int_{\mathcal{C}} \frac{ds}{2i \sin(\pi s)} \frac{\lambda^s}{\Gamma(1+s)} \int_1^{+\infty} u^s \frac{1}{u^{1+\gamma}} \left(1 - \frac{1}{u}\right)^{\beta-1} \\ &= -\int_{\mathcal{C}} \frac{ds}{2i \sin(\pi s)} \frac{\lambda^s}{\Gamma(1+s)} \frac{\Gamma(\gamma + \beta)\Gamma(\gamma - s)}{\Gamma(\gamma + \beta - s)\Gamma(\gamma)} \end{aligned} \quad (\text{E.9.4})$$

where here the contour of integration \mathcal{C} is a vertical line $\mathcal{C} = -a + i\mathbb{R}$ with $0 < a < 1$. In this way, one can invert the different integrals and the results only contains complex moments $\overline{u^s}$ in a region where they are defined. The relation between $g(\lambda)$ and $g_{mom}(\lambda)$ now appears clearly by comparing (E.9.3) and (E.9.4): $g(\lambda)$ can formally be obtained by rewriting the sum appearing in $g_{mom}(\lambda)$ as a Mellin-Barnes transform. Note that when closing the contour of integration \mathcal{C} on the $Re(s) > 0$ half-plane in E.9.4, one obtains two types of poles. A first series coming from the sine function that reproduces the series that defines $g_{mom}(\lambda)$, as well as a second series of terms of the form $\lambda^{\gamma+n}$ with $n \in \mathbb{N}$ coming from the poles of $\Gamma(\gamma - s)$: $g(\lambda)$ is not an analytic function of λ . Rewriting the sum appearing in $g_{mom}(\lambda)$ as a Mellin-Barnes integral thus allows us in some way to retrieve the missing, non-analytic terms that are present in the Laplace transform. In the main text we use the same prescription to go from a Fredholm determinant formula for $g_{t,x}^{mom}(u)$ to a formula for $g_{t,x}(u)$ by rewriting the sum over m appearing in the expression of the kernel (E.4.26) as a Mellin-Barnes type integral in (E.4.27). Notice that in (E.4.26), the sum over m runs from 1 to ∞ , and the associated integral written in (E.4.27) is thus chosen as a line that passes through the right of 0 (a trivial modification of the case studied here), and to the left of γ to avoid crossing a pole.

Appendix F

Paper: Exact solution for a random walk in a time-dependent 1D random environment: the point-to-point Beta polymer

The following is essentially the article published as

Title: Exact solution for a random walk in a time-dependent 1D random environment: the point-to-point Beta polymer

Authors: Thimothée Thiery and Pierre Le Doussal

ArXiv: 1605.07538

Abstract: We consider the Beta polymer, an exactly solvable model of directed polymer on the square lattice, introduced by Barraquand and Corwin (BC) in [224]. We study the statistical properties of its point to point partition sum. The problem is equivalent to a model of a random walk in a time-dependent (and in general biased) 1D random environment. In this formulation, we study the sample to sample fluctuations of the transition probability distribution function (PDF) of the random walk. Using the Bethe ansatz we obtain exact formulas for the integer moments, and Fredholm determinant formulas for the Laplace transform of the directed polymer partition sum/random walk transition probability. The asymptotic analysis of these formulas at large time t is performed both (i) in a diffusive vicinity, $x \sim t^{1/2}$, of the optimal direction (in space-time) chosen by the random walk, where the fluctuations of the PDF are found to be Gamma distributed; (ii) in the large deviations regime, $x \sim t$, of the random walk, where the fluctuations of the logarithm of the PDF are found to grow with time as $t^{1/3}$ and to be distributed according to the Tracy-Widom GUE distribution. Our exact results complement those of BC for the cumulative distribution function of the random walk in regime (ii), and in regime (i) they unveil a novel fluctuation behavior. We also discuss the crossover regime between (i) and (ii), identified as $x \sim t^{3/4}$. Our results are confronted to extensive numerical simulations of the model.

F.1 Introduction and main results

F.1.1 Overview

Random walks in random media is a subject of great interest in physics and mathematics. A lot of works have been devoted to the case of time-independent quenched media especially in the context of anomalous diffusion (see [255] for a review, [256, 257]). The case of a time-dependent random medium, with short range correlations both in space and time, has attracted less attention in physics in this context, mainly since diffusive behavior of the walk at large time is expected in that case. However the problem is still non-trivial and can exhibit interesting properties. For example, the trajectories of a set of identical walkers diffusing independently in the *same realization* of the random environment, exhibit non-trivial space-time correlations, e.g. typically they tend to stick together. This, and other properties, such as large deviations, have been studied recently in mathematics [258, 259, 227, 260]. On the other hand, there has been much work of the problem of directed polymers (DP), i.e. the statistical mechanics of directed paths in a short-range correlated random potential pioneered in [249]. In this framework, recent outstanding progresses have been achieved, notably thanks to the discovery of exactly solvable models on a square lattice in $D = 1 + 1$ dimension. This has allowed to put forward a remarkable universality in the DP problem, connected to the 1D Kardar-Parisi-Zhang (KPZ) universality class [33] (for review see e.g. [151, 34, 35]), in particular the emergence of the universal Tracy-Widom distributions [37] in the large scale fluctuations of the DP free energy. These integrable models include last passage percolation with geometric weights [159], the so-called log-Gamma polymer [197, 4, 198, 218], the Strict-Weak polymer [219, 220], the Inverse-Beta polymer [5], the Bernoulli-Geometric polymer [7] and the Beta polymer [224]. Among those the Beta polymer, introduced and first studied by Barraquand and Corwin (BC)¹, has the peculiarity that it can also be interpreted as a random walk in a time

¹Note that random walk in time-dependent Beta distributed random environment already appeared in [261]. There the authors notably considered the Beta-TDRWRE on the discrete circle $\mathbb{Z}/(N\mathbb{Z})$ and showed the large scale $N \rightarrow \infty$ convergence of the process defined by the motion of independent

dependent random environment (TD-RWRE). This is due to a very specific choice of local weight which satisfies conservation of probability. The connection between DPs and TD-RWRE was already remarked in [262], and more generally we note that the interpretation of statistical mechanics models on special varieties in parameter space in terms of a stochastic process has been previously used in other contexts (for review see e.g. [263, 264] and references therein). The Beta polymer provides a remarkable first example of an exactly solvable TD-RWRE. We note however that extracting physical properties from the exact solution still represents a technical challenge, as is often the case in integrable systems. Thus the existence of an integrable model of TD-RWRE is far from being the end of the story, and we expect a variety of interesting result to come in the future from the analysis of the Beta polymer.

The goal of this paper is indeed to pursue this program by obtaining exact results on the sample to sample fluctuations of the probability distribution function (PDF) of the random walk in a given environment, equivalent to the point to point polymer partition sum. We thus complement the results of BC in [224], where the statistics of the half-line to point DP partition sum was studied, equivalent to the cumulative distribution function (CDF) of the random walk (note that it far from trivial to relate the two observables). More precisely in [224] it was notably shown that in the large deviations regime of the RWRE, the fluctuations of the logarithm of the CDF of the random walk scale as $t^{1/3}$ and are distributed according to the Tracy-Widom GUE distribution. Here we will study the fluctuations of the PDF of the random walk (RW) both in the large deviations regime (close in spirit to the results obtained in [224] for the CDF fluctuations) *and* in the diffusive regime around the optimal direction chosen by the RWRE.

F.1.2 Main results and outline of the paper

We recall in Sec. F.2 the definition of the Beta polymer model with parameters $\alpha, \beta > 0$ and introduce our notations for the point to point partition sum, $Z_t(x)$. The latter refers to the partition sum for directed polymers of length $t \in \mathbb{N}$, with starting point $x = 0$ and endpoint $x \in \mathbb{N}$ (see Fig.F.2 for the coordinate system used in this work). Thanks to the interpretation of the Beta polymer as a random walk in a random environment (RWRE), as detailed below, this point to point partition sum can also be interpreted as a transition probability distribution function (PDF) for a directed RWRE where time is reversed and the starting point (resp. endpoint) of the polymer is the endpoint (resp. starting point) of the RW. Our results can thus be interpreted, and are of interest, using both interpretations. In Sec. F.3 we use the coordinate Bethe ansatz to obtain an exact formula (F.3.27) for the integer moments of the partition sum:

$$\overline{Z_t(x)^n} = (-1)^n \frac{\Gamma(\alpha + \beta + n)}{\Gamma(\alpha + \beta)} \prod_{j=1}^n \int_{-\infty}^{+\infty} \frac{dk_j}{2\pi} \prod_{1 \leq i < j \leq n} \frac{(k_i - k_j)^2}{(k_i - k_j)^2 + 1} \prod_{j=1}^n \frac{(ik_j + \frac{\beta - \alpha}{2})^t}{(ik_j + \frac{\alpha + \beta}{2})^{1+x} (ik_j - \frac{\alpha + \beta}{2})^{1-x+t}}. \quad (\text{F.1.1})$$

Where here and throughout the rest of the paper the overline $\overline{(\cdot)}$ represents the average over the random environment. Using this formula we obtain in Sec. F.4 a Fredholm determinant formula (F.4.12) for the Laplace transform of the partition sum:

$$\overline{e^{-uZ_t(x)}} = \frac{1}{\Gamma(\alpha + \beta)} \int_0^{+\infty} dw w^{-1+\alpha+\beta} e^{-w} g_{t,x}(uw) \quad , \quad g_{t,x}(u) = \text{Det} \left(I + u \hat{K}_{t,x}(q_1, q_2) \right) \quad (\text{F.1.2})$$

with

$$\hat{K}_{t,x}(q_1, q_2) = -\frac{2}{\pi} \frac{(1 + iq_1(\alpha - \beta))^{t-x}}{(1 + iq_1(\alpha + \beta))^{1+t-x}} \frac{(1 + iq_2(\alpha - \beta))^x}{(1 - iq_2(\alpha + \beta))^{1+x}} \frac{1}{2 + i(q_1^{-1} - q_2^{-1})}, \quad (\text{F.1.3})$$

where $K_{t,x} : L^2(\mathbb{R}) \rightarrow L^2(\mathbb{R})$. We also obtain other, equivalent Fredholm determinant formulas (F.4.7) and (F.4.10). The asymptotic behavior of these results at large t in a given direction $x = (1/2 + \varphi)t$ with $-1/2 < \varphi < 1/2$ is found to drastically depends on the chosen angle φ as we now detail.

We show that there exists an *optimal angle*, $\varphi_{opt} := \frac{\beta - \alpha}{2(\beta + \alpha)}$, defined as the only angle for which $\overline{Z_t(x = (1/2 + \varphi)t)}$ decreases algebraically and not exponentially. It corresponds to the center of the Gaussian regime in the RWRE interpretation, i.e. the expected direction in space-time chosen by the RW.

In a diffusive vicinity around the optimal angle, we show in Sec. F.4 that the fluctuations of an appropriately rescaled partition sum are Gamma distributed. More precisely we show that the rescaled spatial process defined as,

$$\mathcal{Z}_t(\kappa) = \alpha \sqrt{2\pi r t} e^{\frac{(r+1)^2}{2r} \kappa^2} Z_t \left(x = \left(\frac{1}{2} + \varphi_{opt}(r) \right) t + \kappa \sqrt{t} \right), \quad (\text{F.1.4})$$

with $r = \beta/\alpha$, converges at fixed t , in the large time limit to a *process, constant in κ , with marginal distribution a Gamma distribution with parameter $\alpha + \beta$*

$$\mathcal{Z}_\infty(\kappa) \sim \text{Gamma}(\alpha + \beta). \quad (\text{F.1.5})$$

Let us mention here that we first found this result at the level of one-point observables (i.e. at fixed κ , $\mathcal{Z}_\infty(\kappa) \sim \text{Gamma}(\alpha + \beta)$) using (F.1.1) and (F.1.3), and were later able to extend it to multi-point correlations in this diffusive regime using results by BC [265]. Note that these results would not be expected from the naive application of usual KPZ universality to the point-to-point Beta polymer. This breaking of KPZ universality is due to the RWRE nature of the Beta polymer. Finally,

random walkers in the same environment to so-called Brownian sticky flows on the unit circle.

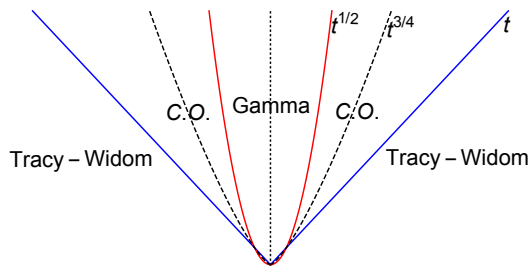


Figure F.1: The different regimes of sample to sample fluctuations of the PDF in the Beta TDRWRE problem around the optimal direction (indicated by a dotted line) for different scaling of the deviation with respect to the optimal direction $\hat{x} = x - (1/2 + \varphi_{opt})t$. In the diffusive regime $\hat{x} \sim \sqrt{t}$ the fluctuations of the PDF are Gamma distributed. In the large deviations regime $\hat{x} \sim t$, fluctuations of the logarithm of the PDF are distributed according to the GUE Tracy-Widom distribution with exponents in agreement with the usual KPZ universality expected in point to point directed polymers problem. These two regimes are connected by a cross-over regime (C.O.) at a scale $\hat{x} \sim t^{3/4}$.

let us also mention that, from the RWRE point of view, although the above results only apply in a diffusive vicinity of a single space-time direction, this spatial region actually contains all the probability in the large time limit.

For all other directions $\varphi \neq \varphi_{opt}$ we find in Sec. F.5 that the fluctuations of an appropriately rescaled free-energy are described by the Tracy-Widom GUE distribution. More precisely we show using a non-rigorous approach that

$$\lim_{t \rightarrow \infty} Prob \left(\frac{\log Z_t((1/2 + \varphi)t) + tc_\varphi}{\lambda_\varphi} < 2^{\frac{2}{3}} z \right) = F_2(z) , \tag{F.1.6}$$

where F_2 is the cumulative distribution function (CDF) of the GUE Tracy-Widom distribution and the parameters c_φ and $\lambda_\varphi \sim t^{\frac{1}{3}}$ are given by the solutions of a system of transcendental equations in (F.5.15). This regime of fluctuations is the one expected from KPZ universality for point to point directed polymers. In the RWRE interpretation, it corresponds to the fluctuations of the PDF in the large deviations regime. A similar result was proved in [224] for the case of the half line to point Beta polymer problem, corresponding to the CDF in the RWRE picture. Quite remarkably we find that (F.1.6) is formally exactly equivalent to the result of [224] if one replaces the half line to point partition sum by the point to point partition sum. In the RWRE picture this shows that the fluctuations of the PDF and of the CDF in the large deviations regime are identical up to order $O(t^{1/3})$ included.

Using the above results, we also briefly discuss in Sec. F.5 the crossover between the two regimes (F.1.5) and (F.1.6) and identify the crossover scale as associated with deviations of order $O(t^{3/4})$ around the optimal direction (see Fig. F.1 for a summary of the different regimes). Finally in Sec. F.6, we compare our results with the approach used by BC [224, 265] and check in Sec.F.7 our results using extensive numerical simulations of the Beta polymer. Two appendix contain technical details.

F.2 Model and earlier work

F.2.1 The Beta polymer

Let us now define the point to point Beta polymer problem. We consider the square lattice with coordinates (t, x) as in Fig. F.2: x is just a regular (euclidean) coordinate along the horizontal axis whereas t goes along the diagonal of the square lattice. On each vertex (i.e. site) of the square lattice lives a random variable (RV) $b_{t,x} \in [0, 1]$ that is distributed as a Beta RV with parameters $\alpha, \beta > 0$. That is,

$$b_{t,x} \sim b \sim Beta(\alpha, \beta) \quad , \quad P_{\alpha, \beta}^{Beta}(b)db = \frac{\Gamma(\alpha + \beta)}{\Gamma(\alpha)\Gamma(\beta)} b^{-1+\alpha} (1 - b)^{-1+\beta} db , \tag{F.2.1}$$

where here $P_{\alpha, \beta}^{Beta}$ is the probability distribution function (PDF) of b , Γ is the Euler's Gamma function and \sim means 'distributed as'. We suppose that the different RV on different vertex are uncorrelated. To each vertex (t, x) and RV $b_{t,x}$ we associate two random Boltzmann weights w_e on the vertical and horizontal edges arriving at t, x as

$$\begin{aligned} w_e &:= u_{t,x} = b_{t,x} & \text{if } e = (t - 1, x) \rightarrow (t, x) \text{ is the vertical edge leading to } (t, x) , \\ w_e &:= v_{t,x} = 1 - b_{t,x} & \text{if } e = (t - 1, x - 1) \rightarrow (t, x) \text{ is the horizontal edge leading to } (t, x) . \end{aligned} \tag{F.2.2}$$

Hence in the Beta polymer, the Boltzmann weights live on the edges (i.e. bonds) of the square lattice and are correlated only when the edges lead to the same site. Noting generally u (resp. v) the Boltzmann weights on vertical (resp. horizontal)

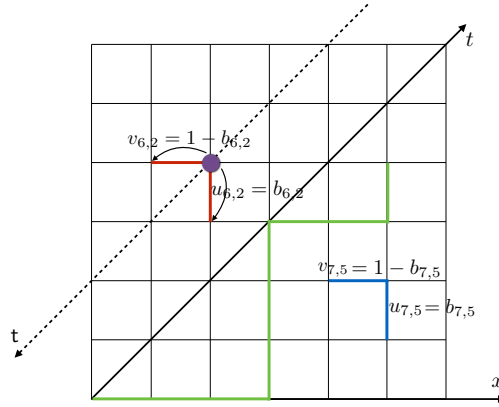


Figure F.2: The Beta polymer and its RWRE interpretation. The random Boltzmann weights live on the edges of the lattice. Blue and Red: two couples of Boltzmann weights. Boltzmann weights leading at the same vertex are correlated: the vertical one u is a Beta RV b , whereas the horizontal one v is $1 - u$. Green: one admissible directed polymer path from $(t, x) = (0, 0)$ to $(t, x) = (9, 5)$. In the RWRE interpretation, a particle (purple dot above) performs a directed random walk in time $t = -t$ and the Boltzmann weights are used as hopping probabilities.

edge and v , we have $u + v = 1$ and $u \sim \text{Beta}(\alpha, \beta)$. Given a random environment defined by a drawing of the Boltzmann weights on each edge of the square lattice, the partition sum of the point to point Beta polymer with starting point $(0, 0)$ and endpoint (t, x) is defined as

$$Z_t(x) = \sum_{\pi: (0,0) \rightarrow (t,x)} \prod_{e \in \pi} w_e. \quad (\text{F.2.3})$$

Where here the sum is over all directed (up/right) paths π from $(0, 0)$ to (t, x) : such a path can only jump to the right following the edge $(t, x) \rightarrow (t + 1, x + 1)$ (in which case the encountered Boltzmann weight is $v_{t+1, x+1}$) or upward following the edge $(t, x) \rightarrow (t + 1, x)$ (in which case the encountered Boltzmann weight is $u_{t+1, x}$). Equivalently, the partition sum can be defined recursively as for $t \geq 0$,

$$\begin{aligned} Z_{t+1}(x) &= u_{t+1, x} Z_t(x) + v_{t+1, x} Z_t(x - 1) \\ Z_{t=0}(x) &= \delta_{x, 0}. \end{aligned} \quad (\text{F.2.4})$$

F.2.2 Relation to a random walk in a random environment

As already noticed in [224], given a random environment specified by a drawing of the $(u_{tx}, v_{tx} = 1 - u_{tx})$, the partition sum of the point to point Beta polymer can also be interpreted as a transition probability for a directed random walk (RW) in the same random environment. We now recall the construction. Let us first introduce a new time coordinate t as

$$t = -t. \quad (\text{F.2.5})$$

And let us also note

$$p_{t,x} = u_{t,x} \in [0, 1]. \quad (\text{F.2.6})$$

A random walk in the Beta distributed random environment is then defined as follows: we note X_t the position of a particle at time t . The particle then performs a RW on \mathbb{Z} with the following transition probabilities

$$\begin{aligned} X_t \rightarrow X_{t+1} &= X_t \text{ with probability } p_{t, X_t} = u_{t=-t, X_t}, \\ X_t \rightarrow X_{t+1} &= X_t - 1 \text{ with probability } 1 - p_{t, X_t} = v_{t=-t, X_t}. \end{aligned} \quad (\text{F.2.7})$$

Hence, the correlations between the Boltzmann weights in the Beta polymer, $u + v = 1$, allows to define a RW² on \mathbb{Z} in a time-dependent random environment defined in terms of the hopping probabilities $p_{t,x}$ (see Fig. F.2). In the RWRE

²Note that with this choice of coordinates, at each time step $t \rightarrow t + 1$ the particle either stays at the same position (with probability $p_{t,x}$), or decreases by one unity (with probability $1 - p_{t,x}$). Alternatively one obtains a more symmetric formulation using the coordinate $\tilde{x} = -t + 2x = t + 2x$ and noting $\tilde{p}_t(\tilde{x}) = p_{t,x=\frac{\tilde{x}-t}{2}}$ and $\tilde{X}_t = t + 2X_t$. The particle then performs a RW on \mathbb{Z} and, at each time step $t \rightarrow t + 1$, the particle either jump by one unity to the right (i.e. $\tilde{X}_{t+1} = \tilde{X}_t - 1$ with probability $\tilde{p}_t(\tilde{X}_t)$) or to the left (i.e. $\tilde{X}_{t+1} = \tilde{X}_t + 1$ with probability $1 - \tilde{p}_t(\tilde{X}_t)$).

language, the partition sum of the Beta polymer is

$$Z_t(x) = P(X_0 = 0 | X_{t=-t} = x), \quad (\text{F.2.8})$$

the probability, given that a particle starts at position x at time $t = -t \leq 0$, that it arrives at position 0 at time $t = t = 0$. In this language, the recursion equation for the polymer partition sum (F.2.4) reads:

$$\begin{aligned} P(X_0 = 0 | X_{t-1} = x) &= p_{t-1x} P(X_0 = 0 | X_t = x) + (1 - p_{t-1x}) P(X_0 = 0 | X_t = x - 1) \\ P(0, 0 | 0, x) &= \delta_{x,0}. \end{aligned} \quad (\text{F.2.9})$$

This equation thus relates the probability for a RW to arrive at the same point starting from different, neighboring points. As such it can be thought of as a Backward equation for the probability $P(X_0 = 0 | X_t = x)$. Note that the starting point of the polymer corresponds in this language to the endpoint of the RW and vice-versa. In the rest of the paper, following this mapping, we will sometimes refer to the random walk in a random environment (RWRE) interpretation of the Beta polymer.

Remark: The RW defined above is a random walk in a one dimensional (\mathbb{Z}) time-dependent random environment. Equivalently, it can be thought of as a directed random walk in a two-dimensional (\mathbb{Z}^2) quenched static random environment.

F.2.3 Relation to the problem and notations of Barraquand-Corwin

The Beta polymer and its RWRE interpretation were introduced in [224] where the half-line to point problem was considered. The half-line to point partition sum can be defined recursively as

$$\begin{aligned} Z_{t+1}^{HL}(x) &= u_{t+1x} Z_t^{HL}(x) + v_{t+1x} Z_t^{HL}(x - 1) \\ Z_{t=0}^{HL}(x) &= \theta(x), \end{aligned} \quad (\text{F.2.10})$$

where θ is the Heaviside function ($\theta(0) = 1$), and the random environment encoded in the variables (u_{tx}, v_{tx}) is the same as before. In the RWRE language,

$$Z_t^{HL}(x) = P(X_0 \geq 0 | X_{t=-t} = x) \quad (\text{F.2.11})$$

is the probability that the particle arrives at a position larger than 0 at time $t = 0$, knowing it started from a position x at time $t = -t \leq 0$. Hence it is the CDF of the RWRE while the point to point is the PDF, with respect to the arrival point X_0 .

Let us now give here a dictionary between this paper and Ref. [224]. In the latter, the half-line to point partition sum was denoted as $\tilde{Z}(t, n)$. t represents the length of the path and corresponds to our t variable. At each step n can either stay identical or increase by one unit. When n stays constant the polymer encounters a Boltzmann weight distributed as $1 - \text{Beta}(\alpha, \beta)$, whereas when n increases the polymer encounters a Boltzmann weight distributed as $1 - \text{Beta}(\alpha, \beta)$. The parameters α and β are also parametrized as $\mu = \alpha$ and $\nu = \alpha + \beta$. Finally, the initial condition in [224] is $\tilde{Z}(t = 0, n) = \theta(x - 1)$. From this we conclude that the results obtained in [224] for $\tilde{Z}(t, n)$ identify to results for $Z_t^{HL}(x)$ in our notations by either correspondences

$$\begin{aligned} (n, \alpha, \beta) &\rightarrow (x + 1, \alpha, \beta) \\ \text{or,} & \\ (n, \alpha, \beta) &\rightarrow (t - x + 1, \beta, \alpha). \end{aligned} \quad (\text{F.2.12})$$

These two choices being related by a reflection along the diagonal of the square lattice.

F.3 Bethe Ansatz solution of the Beta polymer

In this section we compute the integer moments of the point-to-point Beta polymer using the replica Bethe Ansatz. The following differs from the results of [224] by two aspects:

(i) The boundary conditions are different: in [224] the chosen boundary conditions were polymers with one end fixed and one end free on a half-line (half-line to point problem, see also Sec. F.2.3).

(ii) In [224] the replica Bethe Ansatz solution of the model was made directly on the infinite line, naturally leading to a so-called nested contour integral formula for the moments of the Beta polymer. Here, as in [5, 4, 173, 165], we use a different strategy by imposing to the Bethe eigenfunctions artificial boundary conditions on a line of length L , and studying the solutions of the associated Bethe equations in the limit $L \rightarrow \infty$. In doing so we obtain moments formulas with all integrals on the same contour, and unveil the repulsive nature of the model, a physical aspect that distinguish further this model from the log-Gamma and Inverse-Beta polymer.

F.3.1 Bethe ansatz on a line with periodic boundary conditions

The moments of the Beta polymer random Boltzmann weights are obtained from (F.2.1) and (F.2.2) as

$$\frac{u^{n_1} v^{n_2}}{(\alpha + \beta)_{n_1 + n_2}} = \frac{(\alpha)_{n_1} (\beta)_{n_2}}{(\alpha + \beta)_{n_1 + n_2}}, \quad (\text{F.3.1})$$

where here and throughout the rest of the paper the overline $\overline{(\)}$ denotes the average over disorder. We consider, for $n \geq 1$,

$$\psi_t(x_1, \dots, x_n) := \overline{Z_t(x_1) \cdots Z_t(x_n)}, \quad (\text{F.3.2})$$

which is a symmetric function of its arguments. Using the recursion (F.2.4), one shows [5] that ψ_t satisfies a linear recursion relation of the form

$$\psi_{t+1}(x_1, \dots, x_n) = (T_n \psi_t)(x_1, \dots, x_n), \quad (\text{F.3.3})$$

where T_n is a linear operator called the transfer matrix. The precise form of T_n was given in Eq.(13) of [5] for arbitrary moments $\overline{u^{n_1} v^{n_2}}$. The latter is unimportant for our purpose and we will only use here one of the conclusion of [5]: the symmetric eigenfunctions of the transfer matrix, that are the symmetric solutions of the spectral problem

$$T_n \psi_\mu = \tilde{\Lambda}_\mu \psi_\mu, \quad (\text{F.3.4})$$

can be obtained using a coordinate Bethe ansatz, with for $x_1 \leq \dots \leq x_n$, $\psi_\mu(x_1, \dots, x_n) = \tilde{\psi}_\mu(x_1, \dots, x_n) := \sum_{\sigma \in S_n} A_\sigma \prod_{i=1}^n z_i^{x_{\sigma(i)}}$, and the other sectors obtained using that the function is fully symmetric. The sum is over all permutations of the n variables z_i which parameterize the eigenstates. We note that this fact was also already known from [224]. In the notations of [5], (see Eq. (18) and (19) there) the S -matrix $S(z_i, z_j)$ is given by $S(z_i, z_j) = -\frac{c+bz_j+az_i z_j - z_i}{c+bz_i+az_i z_j - z_j}$ with

$$\mathbf{a} = \frac{\overline{u^2} - (\overline{u})^2}{(\overline{u})(\overline{v})} = \frac{1}{1 + \alpha + \beta}, \quad \mathbf{b} = \frac{2\overline{uv} - (\overline{u})(\overline{v})}{(\overline{u})(\overline{v})} = \frac{-1 + \alpha + \beta}{1 + \alpha + \beta}, \quad \mathbf{c} = \frac{\overline{v^2} - (\overline{v})^2}{(\overline{u})(\overline{v})} = \frac{1}{1 + \alpha + \beta}. \quad (\text{F.3.5})$$

We note that $\mathbf{a} + \mathbf{b} + \mathbf{c} = 1$ which is the hallmark of a stochastic model with conservation of probability. Here the moment problem corresponds to a zero-range process as in [222]. We recall that the Bethe ansatz solvability of the two particles problem imposes that the quotient of two amplitudes A_σ related to each other by the transposition of $i \leftrightarrow j$ is $\frac{A_{\dots j i \dots}}{A_{\dots i j \dots}} = S(z_i, z_j)$. Let us now introduce

$$c = \frac{4}{\alpha + \beta} > 0$$

$$z_j = e^{i\lambda_j}, \quad \tilde{t}_j = -i \cot\left(\frac{\lambda_j}{2}\right) = \frac{z_j + 1}{z_j - 1}, \quad z_j = -\frac{1 + \tilde{t}_j}{1 - \tilde{t}_j}. \quad (\text{F.3.6})$$

Using these notations, the S -matrix of the Beta polymer reads

$$S(z_i, z_j) = \frac{2\tilde{t}_j - 2\tilde{t}_i - c}{2\tilde{t}_j - 2\tilde{t}_i + c}. \quad (\text{F.3.7})$$

It has a structure very similar the one of the Inverse-Beta and log-Gamma polymer [5, 4] that we recall here for comparison (see Eq. (45) and (46) in [5]):

$$S^{IB}(z_i, z_j) = \frac{2t_j - 2t_i + \bar{c}}{2t_j - 2t_i - \bar{c}}, \quad t_j = i \tan\left(\frac{\lambda_j}{2}\right) = \frac{z_j - 1}{z_j + 1}. \quad (\text{F.3.8})$$

That is, the S -matrix of the Beta polymer (F.3.7) is identical to the S -matrix of the Inverse-Beta polymer (F.3.8) with the change $\bar{c} > 0 \rightarrow -c$ with $c > 0$ and $t_j \rightarrow \tilde{t}_j$. We will see in the following that this change is responsible for the emergence of a repulsive property of the Bethe ansatz for the Beta polymer. Here $c > 0$ can be interpreted as a repulsive interaction parameter, while in the Inverse-Beta case $\bar{c} > 0$ was interpreted as an attractive interaction parameter. Apart from this, the similarity between the Bethe ansatz applied to the Inverse-Beta and Beta polymer will help us in finding the Bethe ansatz solution of the Beta polymer using the changes $\bar{c} \rightarrow -c$ and $t_i \rightarrow \tilde{t}_i$ (since the S -matrix completely controls the form of the Bethe eigenfunction up to a multiplicative constant). In particular, by analogy with the notations used for the Inverse-Beta polymer (see Eq.(47) in [5]) we will write the Bethe eigenfunctions of the present model as

$$\tilde{\psi}_\mu(x_1, \dots, x_n) = \sum_{\sigma \in S_n} \tilde{A}_\sigma \prod_{\alpha=1}^n z_{\sigma(\alpha)}^{x_\alpha}, \quad \tilde{A}_\sigma = \prod_{1 \leq \alpha < \beta \leq n} \left(1 - \frac{c}{2(\tilde{t}_{\sigma(\alpha)} - \tilde{t}_{\sigma(\beta)})}\right). \quad (\text{F.3.9})$$

Imposing periodic boundary conditions on a line of length L , i.e. $\psi_\mu(x_1, \dots, x_j + L, \dots, x_n) = \psi(x_1, \dots, x_n)$ (which is immaterial [5] in the computation of moments as long as $t < L$) leads to Bethe equations of the form (see Eq. (48) of [5]):

$$e^{i\lambda_i L} = \prod_{1 \leq j \leq n, j \neq i} \frac{2\tilde{t}_i - 2\tilde{t}_j - c}{2\tilde{t}_i - 2\tilde{t}_j + c}. \quad (\text{F.3.10})$$

F.3.2 Resolution of the Bethe equations in the large L limit: repulsion and free particles

In the large L limit, contrary to the case of the log-Gamma and the Inverse-Beta polymer, the Bethe roots λ_α of this model are all real and are distributed as for a model of free particles. The particles do not form bound states, also called strings in the Bethe ansatz literature. In this sense the moment problem of the Beta polymer is similar to the repulsive phase of the Lieb-Liniger (LL) model ³, while the moment problems of the Inverse-Beta polymer (see [5]), the log-Gamma polymer

³at this stage this is only a formal similarity. In fact we have not found a continuum limit of the Beta polymer which would identify to the repulsive LL model.

(see [4]) and the continuum directed polymer (see [173]) were similar to the attractive phase. To see this explicitly, let us use a proof by contradiction and consider the possibility of forming a 2-string. The logarithm of the Bethe equation for two particles ($n = 2$ of (F.3.10)) is:

$$\begin{aligned}\lambda_1 &= \frac{2\pi I_1}{L} - \frac{i}{L} \left(\log(2(\tilde{t}_1 - \tilde{t}_2) - c) - \log(2(\tilde{t}_1 - \tilde{t}_2) + c) \right) , \\ \lambda_2 &= \frac{2\pi I_2}{L} - \frac{i}{L} \left(\log(2(\tilde{t}_2 - \tilde{t}_1) - c) - \log(2(\tilde{t}_2 - \tilde{t}_1) + c) \right) .\end{aligned}\tag{F.3.11}$$

Note that $Im(\lambda_1) + Im(\lambda_2) = 0$ (a property related to the translational invariance of model). Let us consider the possibility of having $Im(\lambda_1) \neq 0$ in the large L limit. Since everything on the right hand side of (F.3.11) is proportional to $1/L$, this means that the \tilde{t}_i variables must flow exponentially fast to the singularity of the logarithm at 0. Let us e.g. suppose

$$2(\tilde{t}_1 - \tilde{t}_2) - c = O(e^{-\delta L})\tag{F.3.12}$$

with $\delta > 0$. Taking the large L limit of (F.3.11), we obtain

$$-Im(\lambda_2) = Im(\lambda_1) \simeq_{L \rightarrow \infty} -\frac{1}{L}(-\delta L) = +\delta > 0 ,\tag{F.3.13}$$

consistency with (F.3.12) in the $L \rightarrow \infty$ limit thus implies

$$-2i(\cot(Re(\lambda_1) + i\delta) - \cot(Re(\lambda_2) - i\delta)) = c > 0.\tag{F.3.14}$$

However, this last equality cannot be satisfied since $c > 0$ and the imaginary part of $\cot(x + iy)$ has a sign opposite to the sign of y . Hence it is impossible to form a bound state of two particles and c can be interpreted as a repulsive interaction parameter. Generalizing this phenomenon to arbitrary n , the large- L limit of the Bethe equations is particularly simple, namely

$$\lambda_i = \frac{2\pi I_i}{L} + O\left(\frac{1}{L^2}\right).\tag{F.3.15}$$

That is, to first order in $1/L$ the particles behave as free particles as already announced. In the following we will parametrize the particle quasi-momentas by the \tilde{t}_i variables. These are pure imaginary numbers that we write (to maintain the analogy with [5], see Eq.(50) there):

$$\tilde{t}_\alpha = i\frac{k_\alpha}{2} \quad , \quad k_\alpha \in \mathbb{R} .\tag{F.3.16}$$

Interpretation of the repulsive nature of the model:

One interpretation of the repulsive nature of the model can be traced back to the relation

$$u + v = 1\tag{F.3.17}$$

that holds in this model for Boltzmann weight for edges arriving on the same vertex. In this model, if it is favorable for the polymer to travel through the edge carrying the disorder u , then it means that u is large. Hence v must be small and it is not favorable for the polymer to travel through the edge carrying v . Consider now two replicas (second moment problem). Clearly the transition $(x - 1, x) \rightarrow (x, x)$ for these two replica is not favorable. This can be interpreted as a nearest neighbor repulsion for these two replicas (i.e particles). Of course the transition $(x - 1, x - 1) \rightarrow (x, x)$ remains favorable (on site attraction). The balance between the two processes however seems to favor the repulsive nature of the model. In the Inverse-Beta (resp. Log-Gamma) polymer, (F.3.17) is replaced by $v - u = 1$ (resp. $v = u$) and the model is attractive.

Another way to see this is through the fact that (F.3.17) precisely permits to interpret the Beta polymer as a RWRE (in this language (F.3.17) is the conservation of probability on each vertex). In this interpretation time is reversed (see Sec. F.2.2) and if two particles stay together at time t in the random environment, then they are more likely to stay on the same site at time $t + 1$ and the transition $(x, x) \rightarrow (x, x - 1)$ is not favored. The attraction between particles in the RWRE language becomes a repulsion in the polymer language when time is reversed.

F.3.3 Bethe ansatz toolbox

Scalar product and norm in the large L limit

Using the already discussed analogy between the Bethe ansatz for the Inverse-Beta and Beta polymer, we easily conclude from Eq.(49) of [5] that the eigenfunctions of the Beta polymer are orthogonal with respect to the following weighted scalar product:

$$\begin{aligned}\langle \phi, \psi \rangle &= \sum_{(x_1, \dots, x_n) \in \{0, \dots, L-1\}^n} \frac{1}{\prod_x \tilde{h}_{\sum_{\alpha=1}^n \delta_{x, x_\alpha}}} \phi^*(x_1, \dots, x_n) \psi(x_1, \dots, x_n) , \\ \tilde{h}_n &= \prod_{k=0}^{n-1} \frac{4}{4 + kc} = (\alpha + \beta)^n \frac{\Gamma(\alpha + \beta)}{\Gamma(\alpha + \beta + n)} .\end{aligned}\tag{F.3.18}$$

We also obtain the formula for the norm of a general eigenstate of n particles in the large L limit (see Eq.(52) of [5], here adapted for the only relevant case here, that is for the case without string states)

$$\|\mu\|^2 = \langle \tilde{\psi}_\mu, \tilde{\psi}_\mu \rangle = n!L^n \prod_{1 \leq i < j \leq n} \frac{(k_i - k_j)^2 + c^2}{(k_i - k_j)^2} + O(L^{n-1}). \quad (\text{F.3.19})$$

Quantization in the large L limit

The model being repulsive, the sum over eigenstates is computed using the free-particle quantization (similar to Eq.(51) of [5]):

$$\sum_{\lambda_\alpha} = \frac{L}{2\pi} \int_{-\pi}^{\pi} d\lambda_\alpha = \frac{L}{2\pi} \int_{-\infty}^{\infty} \frac{4dk_\alpha}{4 + k_\alpha^2}. \quad (\text{F.3.20})$$

Energy-momentum

We will also need the eigenvalue associated with the unit translation-operator on the lattice:

$$\prod_{\alpha=1}^n z_\alpha = \prod_{\alpha=1}^n \frac{2 + ik_\alpha}{-2 + ik_\alpha}, \quad (\text{F.3.21})$$

as well as the eigenvalue associated with the translation in time $\tilde{\Lambda}_\mu = \prod_{i=1}^n (\bar{u} + \bar{v}z_i^{-1})$ which gives

$$\tilde{\Lambda}_\mu = \prod_{\alpha=1}^n \left(\frac{\alpha}{\alpha + \beta} + \frac{\beta}{\alpha + \beta} (-1)^{\frac{1 - \tilde{t}_\alpha}{1 + \tilde{t}_\alpha}} \right) = \prod_{\alpha=1}^n \left(\frac{2(\alpha - \beta) + i(\alpha + \beta)k_\alpha}{2(\alpha + \beta) + i(\alpha + \beta)k_\alpha} \right). \quad (\text{F.3.22})$$

F.3.4 A large contour-type moment formula

We have now all the ingredients to compute the integer moments of the partition sum. The initial condition is:

$$Z_{t=0}(x) = \delta_{x,0} \implies \psi_{t=0}(x_1, \dots, x_n) = \prod_{i=1}^n \delta_{x_i,0}. \quad (\text{F.3.23})$$

We use the scalar product (F.3.18) to decompose it onto the Bethe eigenstates:

$$\psi_t(x_1, \dots, x_n) = \sum_{\mu} \frac{n!}{\tilde{h}_n \|\psi_\mu\|^2} (\tilde{\Lambda}_\mu)^t \psi_\mu(x_1, \dots, x_n). \quad (\text{F.3.24})$$

In particular,

$$\overline{Z_t(x)^n} = \sum_{\mu} \frac{(n!)^2}{\tilde{h}_n \|\psi_\mu\|^2} (\tilde{\Lambda}_\mu)^t \left(\prod_{\alpha=1}^n z_\alpha \right)^x. \quad (\text{F.3.25})$$

Replacing in this expression each terms by its value in the large L limit, one obtains:

$$\begin{aligned} \overline{Z_t(x)^n} &= \frac{L^n}{(2\pi)^n} \frac{1}{n!} \prod_{i=1}^n \int_{-\infty}^{+\infty} \frac{4dk_i}{4 + k_i^2} \frac{(n!)^2}{(\alpha + \beta)^n} \frac{\Gamma(\alpha + \beta + n)}{\Gamma(\alpha + \beta)} \frac{1}{n!L^n} \prod_{1 \leq i < j \leq n} \frac{(k_i - k_j)^2}{(k_i - k_j)^2 + c^2} \\ &\quad \prod_{j=1}^n \left(\frac{2(\alpha - \beta) + i(\alpha + \beta)k_j}{2(\alpha + \beta) + i(\alpha + \beta)k_j} \right)^t \left(\frac{2 + ik_j}{-2 + ik_j} \right)^x. \end{aligned} \quad (\text{F.3.26})$$

Rescaling $k \rightarrow -\frac{4}{\alpha + \beta}k = -ck$ and rearranging, we obtain

$$\overline{Z_t(x)^n} = (-1)^n \frac{\Gamma(\alpha + \beta + n)}{\Gamma(\alpha + \beta)} \prod_{j=1}^n \int_{-\infty}^{+\infty} \frac{dk_j}{2\pi} \prod_{1 \leq i < j \leq n} \frac{(k_i - k_j)^2}{(k_i - k_j)^2 + 1} \prod_{j=1}^n \frac{(ik_j + \frac{\beta - \alpha}{2})^t}{(ik_j + \frac{\alpha + \beta}{2})^{1+x} (ik_j - \frac{\alpha + \beta}{2})^{1-x+t}}. \quad (\text{F.3.27})$$

Which is our main result for the positive integer moments of the point-to-point partition sum of the Beta polymer. Let us now make a remark and introduce a more general formula.

Remark and multi-points moment formula

Let us first note that the formula (F.3.27) has a different structure compared to other formulas obtained using the replica Bethe ansatz on other exactly solvable models of DP (by this we mean using the same replica Bethe ansatz as the one used in this paper, i.e. using periodic boundary conditions and solving the Bethe equations in the large L limit as e.g. in [5, 4, 173, 165]). Indeed, in other cases, one obtains a formula which contains a discrete summation over strings configurations, corresponding to the sum over all eigenstates of an attractive quantum problem (see e.g. Eq.(60) of [5]) and that is expressed as the sum of different n_s -dimensional integrals with $1 \leq n_s \leq n$. Here the repulsive nature of the model leads to a simpler formula since the n^{th} moment is expressed as a *single* n -dimensional integral. We note however that such type of moments formulas already appeared in the literature. In a more general context (see e.g. in the context of Macdonald processes [192]), it is usual to encounter moments formulas of one of the following three types:

1. The first type consists in expressing the n^{th} moments of an observable of a stochastic process as one n -dimensional nested-contours integral with n contours chosen to avoid some poles of the integrand and arranged in a so-called nested fashion (see Fig. F.3 at the end of the paper for an example). In the following we will refer to this type of formula as the nested-contours type.
2. In the second type of formula all the contours of the nested-contours integral formula are deformed onto the largest one. If there are no poles encountered along this deformation, one then obtains a formula with n integrals on the same contour as in (F.3.27). In the following we will refer to this type of formula as the large-contours type
3. In the third type of formula all the contours of the nested contours integral formula are deformed onto the smallest one. In doing this operation, one generally encounters multiple poles of the integrand and one has to keep track of the resulting residues. This process of “book-keeping” residues then lead to formula for the n^{th} moment as a sum of n_s -dimensional integrals with $1 \leq n_s \leq n$ integration variables on one contour, corresponding to the summation over strings configurations evoked above. In the following we will refer to this type of formula as the small-contours or string type.

The specificity of the replica Bethe ansatz applied to the Beta polymer case is thus the fact that we directly obtained a large-contours formula for the moments (see (F.3.27)), rather than a string type formula as could have been naively expected. For the Beta-polymer half-line to point problem considered in [224], Barraquand and Corwin obtained directly a nested contour integral formula for the moments of the partition sum. They also adapted their approach to study the moments of the point-to-point problem and obtained a nested-contours integral formula for the moments $Z_t(x)^n$ which was recently brought to our attention by them [265]. We show in Sec. F.6 how their work compares to ours. In particular we establish the equivalence between our formula (F.3.27) and a nested-contours type formula. Before going further, let us also mention here that with their approach it is also possible to derive rigorously another formula of type 2 valid for the *multi-points moments* of the partition sum that we now display: if $0 \leq x_1 \leq \dots \leq x_n$, then,

$$\overline{Z_t(x_1) \cdots Z_t(x_n)} = (-1)^n \frac{\Gamma(\alpha + \beta + n)}{\Gamma(\alpha + \beta)} \prod_{j=1}^n \int_{\mathbb{R}} \frac{dk_j}{2\pi} \prod_{1 \leq i < j \leq n} \frac{k_i - k_j}{k_i - k_j + i} \prod_{j=1}^n \frac{(ik_j + \frac{\beta - \alpha}{2})^t}{(ik_j + \frac{\alpha + \beta}{2})^{1+x_j} (ik_j - \frac{\alpha + \beta}{2})^{1-x_j+t}} \quad (\text{F.3.28})$$

This formula will be used below to extract interesting information about the correlations of the fluctuations in the diffusive regime.

F.4 Cauchy-type Fredholm determinant formula for the Laplace transform and asymptotic analysis in the optimal direction of the RWRE

F.4.1 The issue of the first site

In the following we will consider the sequence, with $n \in \mathbb{N}$

$$Z_n = \frac{\Gamma(\alpha + \beta)}{\Gamma(\alpha + \beta + n)} \overline{Z_t(x)^n}, \quad (\text{F.4.1})$$

and the associated generating function

$$g_{t,x}(u) = \sum_{n=0}^{\infty} \frac{(-u)^n}{n!} Z_n, \quad (\text{F.4.2})$$

the reason being that only the latter can be simply expressed as a Fredholm determinant. Note that the sum in (F.4.2) converges since $0 < Z_n < \overline{Z_t(x)^n}$ and $0 < Z_t(x) < 1$ (since $Z_t(x)$ can be interpreted as a probability, see Sec. F.2.2). The situation here is also quite different compared to other exactly solvable models of DP: in the continuum case the growth of the moment is too fast to obtain a convergent generating function, while in the log-Gamma and Inverse-Beta case only a finite number of moments exist. Here all the moments exist and do determine the PDF of $Z_t(x)$. Note that it is a priori not clear whether Z_n are the moments of a (positive or not) random variable $\tilde{Z}_t(x)$ (one can e.g. check that this is not the case at $t = 0$). If it is the case, then $Z_t(x)$ is given in law by the product $w_{00} \tilde{Z}_t(x)$ where w_{00} is a random variable (independent of $\tilde{Z}_t(x)$) distributed as

$$w_{00} \sim \text{Gamma}(\alpha + \beta) \quad , \quad P_{w_{00}}(w) = \frac{1}{\Gamma(\alpha + \beta)} w^{-1+\alpha+\beta} e^{-w} \theta(w) \quad , \quad \int dw w^n P_{w_{00}}(w) = \frac{\Gamma(\alpha + \beta + n)}{\Gamma(\alpha + \beta)}, \quad (\text{F.4.3})$$

where $P_{w_{00}}(w)$ is the PDF of w_{00} . Note that the situation is here also different compared to the Inverse-Beta case. In the latter, one needs to add a Boltzmann weight on the first site to obtain a partition sum whose Laplace transform can be expressed as a Fredholm determinant [5]. Here we are formally removing a Boltzmann weight on the first site. In any case the Laplace transform of the original partition sum can be obtained from $g_{t,x}(u)$ using

$$\overline{e^{-u Z_t(x)}} = \langle g_{t,x}(u w_{00}) \rangle_{w_{00}} = \int_0^{+\infty} dw g_{t,x}(uw) P_{w_{00}}(w). \quad (\text{F.4.4})$$

Note that alternatively, using the Hypergeometric function defined $\forall u \in \mathbb{C}$ by ${}_0F_1(\alpha + \beta; u) = \sum_{n=0}^{\infty} \frac{\Gamma(\alpha + \beta)}{\Gamma(\alpha + \beta + n)} \frac{(-u)^n}{n!}$, the generating function $g_{t,x}(u)$ can be rewritten as

$$g_{t,x}(u) = \overline{{}_0F_1(\alpha + \beta; -u Z_t(x))}. \quad (\text{F.4.5})$$

F.4.2 Cauchy type Fredholm determinant formulas

Starting from (F.3.27), it can be shown (see Appendix F.9) that the generating function $g_{t,x}(u)$ can be written as a Fredholm determinant:

$$g_{t,x}(u) = \text{Det}(I + uK_{t,x}), \quad (\text{F.4.6})$$

with the kernel:

$$K_{t,x}(v_1, v_2) = \int_{-\infty}^{+\infty} \frac{dk}{\pi} e^{-2ik(v_1-v_2)-(v_1+v_2)} \frac{(ik + \frac{\beta-\alpha}{2})^t}{(ik + \frac{\alpha+\beta}{2})^{1+x}(ik - \frac{\alpha+\beta}{2})^{1-x+t}}, \quad (\text{F.4.7})$$

and $K_{t,x} : L^2(\mathbb{R}_+) \rightarrow L^2(\mathbb{R}_+)$. Note that the integral on k defining (F.4.7) converges $\forall(t, x) \in \mathbb{N}^2$ (at large k the integrand decays as $1/k^2$). We can also write a simpler expression for the Kernel, writing (F.4.7) as a product of operators

$$\begin{aligned} K_{I,J}(v_1, v_2) &= \int_p A(v_1, p) B(p, v_2) \\ A(v_1, p) &= -\frac{2}{\pi} \theta(v_1) e^{-v_1(1+ip)} \frac{(p + i(\alpha - \beta))^{I-1}}{(p - i(\alpha + \beta))^I} \\ B(p, v_2) &= \theta(v_2) e^{-v_2(1-ip)} \frac{(p + i(\alpha - \beta))^{J-1}}{(p + i(\alpha + \beta))^J} \end{aligned} \quad (\text{F.4.8})$$

where we have reintroduced the euclidean coordinate of the square lattice $I = 1 + x$ and $J = 1 + t - x$ (in this coordinate system the starting point of the polymer is $(I, J) = (1, 1)$) and performed the change of variables $k = p/2$. We then use $\text{Det}(I + AB) = \text{Det}(I + BA)$, leading to

$$g_{I,J}(u) = \text{Det}(I + u\tilde{K}_{I,J}) \quad (\text{F.4.9})$$

with the kernel:

$$\begin{aligned} \tilde{K}_{I,J}(p_1, p_2) &= \int_v B(p_1, v) A(v, p_2) \\ &= \int_{v>0} e^{-v(1-ip_1)} \frac{(p_1 + i(\alpha - \beta))^{J-1}}{(p_1 + i(\alpha + \beta))^J} \times \left(-\frac{2}{\pi}\right) e^{-v(1+ip_2)} \frac{(p_2 + i(\alpha - \beta))^{I-1}}{(p_2 - i(\alpha + \beta))^I} \\ &= -\frac{2}{\pi} \frac{(p_1 + i(\alpha - \beta))^{J-1}}{(p_1 + i(\alpha + \beta))^J} \frac{(p_2 + i(\alpha - \beta))^{I-1}}{(p_2 - i(\alpha + \beta))^I} \frac{1}{2 + i(p_2 - p_1)} \end{aligned} \quad (\text{F.4.10})$$

and $\tilde{K}_{I,J} : L^2(\mathbb{R}) \rightarrow L^2(\mathbb{R})$. Performing the change of variables $p \rightarrow 1/q$ this is also equivalent to

$$g_{I,J}(u) = \text{Det}(I + u\hat{K}_{I,J}) \quad (\text{F.4.11})$$

with the kernel $\hat{K}_{I,J} : L^2(\mathbb{R}) \rightarrow L^2(\mathbb{R})$:

$$\hat{K}_{I,J}(q_1, q_2) = -\frac{2}{\pi} \frac{(1 + iq_1(\alpha - \beta))^{J-1}}{(1 + iq_1(\alpha + \beta))^J} \frac{(1 + iq_2(\alpha - \beta))^{I-1}}{(1 - iq_2(\alpha + \beta))^I} \frac{1}{2 + i(q_2^{-1} - q_1^{-1})} \quad (\text{F.4.12})$$

A final expression which will be preferred in the following. We will also equivalently use the coordinate system (t, x) and the notation $\hat{K}_{t,x} = \hat{K}_{I=1+x, J=1+t-x}$. In Appendix F.10 we use the above Fredholm determinant formulas to obtain a formula for the PDF of $Z_t(x)$.

Remark:

Note that the formulas (F.4.6), (F.4.9) and (F.4.11) have the distinctive feature that the Laplace transform variable u simply multiplies the kernel inside the Fredholm determinant. This should be contrasted with formulas obtained using similar replica Bethe ansatz calculations for other exactly solvable directed polymers models: in these other cases the Laplace transform variable u appears inside the kernel in a non-trivial manner. In a more general context, (see e.g. [192]) this appears as a simple consequence of the fact that the moments formula we obtained is a so-called large-contours type formula (see the discussion in F.3.4). Indeed, it is known in the literature that such formulas lead after summation to Fredholm determinant formulas with the variable u appearing in front of the kernel (usually referred to as Cauchy-type formulas). In this context, the other usually encountered Fredholm determinant formulas are known as Mellin-Barnes type formulas and are obtained after summation of small contours moments formulas (see F.3.4).

It is usually assumed that performing the asymptotic analysis on Cauchy-type formulas is extremely difficult (see in particular the work of Tracy and Widom on the ASEP [225, 226] on which we will comment more later). We will however see in the following that our Cauchy-type formula (F.4.12) is well suited to perform the asymptotic analysis in a specific spatial direction (which will actually turn out to be the optimal direction chosen by the RWRE). In the other directions however, this will not be the case and we will first obtain an alternative Fredholm determinant formula for $g_{t,x}(u)$ of the Mellin-Barnes type in order to carry out the asymptotics.

F.4.3 Asymptotic analysis of the first-moment: definition of the optimal direction and of the asymptotic regimes

Let us now perform an asymptotic analysis in the large time limit with

$$t \gg 1 \quad , \quad x = (1/2 + \varphi)t \quad , \quad (\text{F.4.13})$$

i.e. $I = 1 + x = 1 + (1/2 + \varphi)t$ and $J = 1 + t - x = 1 + (1/2 - \varphi)t$. We first consider the trace of $\hat{K}_{t,x}$, or equivalently Z_1 :

$$-Z_1 = \text{Tr}(\hat{K}_{t,x}) = \frac{-1}{\pi} \int dq \frac{(1 + iq(\alpha - \beta))^t}{(1 - iq(\alpha + \beta))^{1+x}(1 + iq(\alpha + \beta))^{1+t-x}}. \quad (\text{F.4.14})$$

Note that this integral can be performed exactly, the result being, as expected, $Z_1 = \frac{1}{\alpha + \beta} \overline{Z_t(x)} = \frac{\alpha^{t-x} \beta^x}{(\alpha + \beta)^{t+1}} C_t^x$ where C_t^x is the binomial coefficient. Note that in terms of RWRE, the mean value of the partition sum is the mean value of the PDF transition probability. The latter can also be interpreted as the PDF of a RW in an averaged environment: the *annealed* PDF, defined as

$$\mathbb{P}_{\text{ann}}(X_0 = 0 | X_{-t} = x) := \overline{\mathbb{P}(X_0 = 0 | X_{-t} = x)} = \overline{Z_t(x)} \quad (\text{F.4.15})$$

is the transition PDF for a RW defined as in (F.2.9) with $p_{t,x}$ replaced by its average: $p_{t,x} \rightarrow \overline{p_{t,x}} = \bar{u} = \alpha/(\alpha + \beta)$. Note also that by translational invariance of the averaged environment we have $\mathbb{P}_{\text{ann}}(X_0 = 0 | X_{-t} = x) = \mathbb{P}_{\text{ann}}(X_t = -x | X_0 = 0) = \overline{Z_t(x)}$. The asymptotic analysis could easily be performed on this exact formula but the goal here is to understand how the properties of the asymptotic regime emerge from the integral formula (F.4.14). A simple calculation shows that the integral on q in (F.4.14) is dominated by a saddle-point at

$$q_{sp} = -\frac{i(r(2\varphi - 1) + 2\varphi + 1)}{\alpha(r + 1)(r(2\varphi - 1) - 2\varphi - 1)} \quad (\text{F.4.16})$$

where we introduced the asymmetry ratio

$$r = \beta/\alpha \in \mathbb{R}_+. \quad (\text{F.4.17})$$

We obtain

$$\begin{aligned} Z_1 &= \frac{1}{\pi} \left(\frac{2r \left(\frac{r-2r\varphi}{2\varphi+1} \right)^\varphi}{(r+1)\sqrt{r-4r\varphi^2}} \right)^t \int dq \frac{1}{1 + \alpha^2(1+r)^2 q_{sp}^2} e^{t(q-q_{sp})^2 \frac{\alpha^2(r+1)^2(-2r\varphi+r+2\varphi+1)^4}{32r^2(4\varphi^2-1)} + tO((q-q_{sp})^3)} \\ &= \frac{1}{\alpha(1+r)} \sqrt{\frac{2}{\pi t(1-4\varphi^2)}} \left(\frac{2}{\sqrt{1-4\varphi^2}} \left(\frac{1-2\varphi}{2\varphi+1} \right)^\varphi \frac{r^{(1/2+\varphi)}}{1+r} \right)^t (1 + O(1/\sqrt{t})). \end{aligned} \quad (\text{F.4.18})$$

where from the first to the second line we rescaled $q - q_{sp} \rightarrow (q - q_{sp})/\sqrt{t}$. Note that $|q_{sp}| < 1/(\alpha + \beta) = 1/(\alpha(1+r))$ and the implicit deformation of contours in (F.4.18) is legitimate. We thus obtain that the first moment $\overline{Z_t(x)} = (\alpha + \beta)Z_1$ decays exponentially with time at a rate $\log(\psi_r(\varphi))$ where $\psi_r(\varphi) = \frac{2}{\sqrt{1-4\varphi^2}} \left(\frac{1-2\varphi}{2\varphi+1} \right)^\varphi \frac{r^{(1/2+\varphi)}}{1+r}$. Note that $\psi_r(\varphi)$ is always smaller than 1 except at its maximum, the optimal angle, defined by

$$\varphi_{opt}(r) = \frac{r-1}{2(r+1)} \in]-1/2, 1/2[, \quad (\text{F.4.19})$$

for which $\psi_r(\varphi_{opt}) = 1$ and $q_{sp} = 0$. In this specific direction $\overline{Z_t(x)}$ actually decreases only algebraically as

$$Z_1 = \frac{1}{\alpha + \beta} \overline{Z_t(x)} \simeq_{\varphi=\varphi_{opt}} \frac{1}{\alpha\sqrt{2\pi r t}} (1 + O(1/\sqrt{t})). \quad (\text{F.4.20})$$

In terms of RWRE, we thus have that the annealed PDF (F.4.15) decreases exponentially in all directions, except in the direction φ_{opt} where $\mathbb{P}_{\text{ann}}(X_t = -x | X_0 = 0) \simeq \frac{(1+r)}{\sqrt{2\pi r t}} (1 + O(1/\sqrt{t}))$. The optimal angle thus appears as the most probable space-time direction taken by a RW in an averaged environment. Let us now show that it is at the center of a region where $\mathbb{P}_{\text{ann}}(X_t = -x | X_0 = 0)$ is a Gaussian distribution. To see this explicitly, let us now consider a diffusive perturbation around the optimal direction as

$$x = \left(\frac{1}{2} + \varphi_{opt}(r) \right) t + \kappa\sqrt{t}. \quad (\text{F.4.21})$$

Inserting this scaling in (F.4.14), it is easily seen that the large time behavior of $Z_1 = -\text{Tr}(\hat{K}_{t,x})$ is still controlled by the same-saddle point around $q_{sp} = 0$. We now obtain, rescaling again $q \rightarrow q/\sqrt{t}$,

$$\begin{aligned} Z_1 &= -\text{Tr}(\hat{K}_{t,x}) = \int_{\mathbb{R}} \frac{dq}{\pi\sqrt{t}} \frac{1}{1 + \alpha^2(1+r)^2 \frac{q^2}{t}} e^{-2r\alpha^2 q^2 + 2i((1+r)\alpha\kappa q + O(\frac{1}{\sqrt{t}}))} \\ &= \frac{1}{\alpha\sqrt{2\pi r t}} e^{-\frac{(r+1)^2}{2r}\kappa^2} \left(1 + O\left(\frac{1}{\sqrt{t}}\right) \right). \end{aligned} \quad (\text{F.4.22})$$

Or equivalently, in terms of the annealed PDF,

$$x = \left(\frac{1}{2} + \varphi_{opt}(r) \right) t + \kappa\sqrt{t} \implies \mathbb{P}_{\text{ann}}(X_t = -x | X_0 = 0) = \frac{(1+r)}{\alpha\sqrt{2\pi r t}} e^{-\frac{(r+1)^2}{2r}\kappa^2} \left(1 + O\left(\frac{1}{\sqrt{t}}\right) \right). \quad (\text{F.4.23})$$

And the annealed PDF, that is the transition PDF of the RW in an averaged environment, is in the large time limit in the diffusive scaling (F.4.21) Gaussian distributed with a diffusion coefficient $D_{\text{ann}} = \frac{r}{2(r+1)^2}$. Note that this spatial

region actually contains all the probability in the large time limit. Note also that (F.4.23) can be seen as a consequence of the central limit theorem in an averaged environment. Finally, note that the saddle-point position q_{sp} (see (F.4.16)) is 0 only in the optimal direction. Following the change of variables from the quasi-momentas λ of the particles in the Bethe wavefunction (F.3.9) to the variable q in the kernel (F.4.12), we note that $q \sim 0$ corresponds to $\lambda \sim 0$.

In the following we will refer to the regime described by the scaling (F.4.21) as the Gaussian regime, or, to avoid confusion with other sources of randomness, as the diffusive vicinity of the optimal direction. Indeed, although the scaling (F.4.21) corresponds to the Gaussian regime for the RW in an averaged environment (see (F.4.23)), in the following we will be interested in the sample to sample fluctuations of the RWRE PDF. As we will show these fluctuations will turn out to be Gamma (and not Gaussian) distributed. The other regime described by the scaling (F.4.13) with $\varphi \neq \varphi_{opt}$ will be referred to, using the RWRE language, as the large deviations regime. Let us now investigate the consequences of the existence of the saddle-point (F.4.16) beyond the first moment, i.e. on the full Fredholm determinant.

F.4.4 Asymptotic analysis in the diffusive vicinity of the optimal direction on the Cauchy-type Fredholm determinant

The saddle-point performed on the trace of the kernel (F.4.12) is under control for arbitrary φ . A natural question is now to understand whether one can use the same saddle-point on the full Fredholm determinant (57) and (F.4.12). In most cases (more precisely that is whenever $q_{sp} \neq 0$) the answer is negative. Indeed, if $q_{sp} \neq 0$, $Im(q_{sp}) \neq 0$ and the evaluation of e.g. the $Tr(\hat{K} \circ \hat{K})$ term (or equivalently Z_2) using the saddle point involves a shift of the integrals on q to ensure that the contour of integration on q , initially equal to \mathbb{R} , passes upon the saddle-point at q_{sp} . However the presence of the term $\frac{1}{2+i(q_2^{-1}-q_1^{-1})}$ present in (F.4.12) forbids that shift and we cannot use the saddle-point (i.e. it is impossible to deform the contours of integrations without crossing poles). If one tries to perform the saddle-point analysis on the form of the kernel (F.4.10) the difficulty is different: the trace is still dominated by the saddle point at $p_{sp} = \frac{1}{q_{sp}}$ and it seems a priori easy to shift all contours of integrations to avoid crossing the poles of the term $\frac{1}{2+i(p_2-p_1)}$ (using a simple translation of all contours). However in this case $|Im(p_{sp})| > (\alpha + \beta)$ so that the difficulty is now to avoid crossing the pole at $p = \pm i(\alpha + \beta)$. One way to do so is to try to close the contours of integration on the upper half plane, but in this case one inevitably crosses the poles of the term $\frac{1}{2+i(p_2-p_1)}$. This difficulty thus appears as a true property of the asymptotic analysis of the kernels (F.4.7), (F.4.10), (F.4.12): the saddle-point suggested by the study of the trace cannot be used for higher order terms. We will come back to this point in Section F.5.

In the optimal direction however (and in its diffusive vicinity (F.4.21)), we noticed that $q_{sp} = 0$. In this case there is no shift to perform and *all the terms (corresponding to all the moments) in the series expansion of the Fredholm determinant can be evaluated using the saddle-point*, as we will see below. We thus now write

$$x = \left(\frac{1}{2} + \varphi_{opt}(r)\right)t + \kappa\sqrt{t}, \quad (\text{F.4.24})$$

and consider the saddle point at $q_{sp} = 0$ for the evaluation of the Fredholm determinant, using the expansion

$$\begin{aligned} \text{Det}(I + u\hat{K}) &= e^{\ln(I+u\hat{K})} = 1 + u\hat{K} + \frac{u^2}{2}((\hat{K})^2 - \hat{K} \circ \hat{K}) \\ &+ \frac{u^3}{3!}((\hat{K})^3 - 3\hat{K}\hat{K} \circ \hat{K} + 2\hat{K} \circ \hat{K} \circ \hat{K}) + \dots \end{aligned} \quad (\text{F.4.25})$$

In this expansion, all the terms that involve powers of the Kernel, such as $\hat{K} \circ \hat{K}$ and $\hat{K} \circ \hat{K} \circ \hat{K}$ contain terms such as $\frac{q_1 q_2}{q_1 q_2 + (q_2 - q_1)}$. Using the saddle-point and rescaling $q_i \rightarrow q_i/\sqrt{t}$, these terms bring out additional factors of $1/\sqrt{t}$ and are subdominant. Hence we have

$$\begin{aligned} \text{Det}(I + u\hat{K}) &= 1 + u\hat{K} + \frac{u^2}{2}(\hat{K})^2 + \frac{u^3}{3!}(\hat{K})^3 + \dots + O(1/\sqrt{t}) \\ &= e^{u\hat{K}} + O(1/\sqrt{t}) \end{aligned} \quad (\text{F.4.26})$$

If one rescales u as $u = \alpha\sqrt{2\pi r t e^{\frac{(r+1)^2}{2r}\kappa^2}} \tilde{u}$ such that $uZ_1 = -u\hat{K} \simeq_{t \rightarrow \infty} \tilde{u} = O(1)$, then we obtain the following convergence (that holds at each order in the expansion in \tilde{u}):

$$g_{t,x}(\alpha\sqrt{2\pi r t e^{\frac{(r+1)^2}{2r}\kappa^2}} \tilde{u}) = \text{Det}(I + \alpha\sqrt{2\pi r t e^{\frac{(r+1)^2}{2r}\kappa^2}} \tilde{u}\hat{K}) \simeq_{t \gg 1} e^{-\tilde{u}} + O(1/\sqrt{t}). \quad (\text{F.4.27})$$

Note here that the relatively slow growth of moments shows that the convergence in moments imply the convergence of Laplace transform, and hence in distribution. Let us now define for convenience a rescaled partition sum as

$$\mathcal{Z}_t(\kappa) = \alpha\sqrt{2\pi r t e^{\frac{(r+1)^2}{2r}\kappa^2}} Z_t \left(\left(\frac{1}{2} + \varphi_{opt}(r)\right)t + \kappa\sqrt{t} \right). \quad (\text{F.4.28})$$

We thus find that, using (F.4.4),

$$\overline{e^{-\tilde{u}\mathcal{Z}_t(\kappa)}} = \langle g_{t,x}(\alpha\sqrt{2\pi r t e^{\frac{(r+1)^2}{2r}\kappa^2}} \tilde{u}w_{00}) \rangle_{w_{00}} = \langle e^{-\tilde{u}w_{00}} \rangle_{w_{00}} + O(1/\sqrt{t}) \quad (\text{F.4.29})$$

i.e.

$$\mathcal{Z}_{t=\infty}(\kappa) \sim \text{Gamma}(\alpha + \beta) , \quad (\text{F.4.30})$$

and corrections are of order $O(1/\sqrt{t})$. The form of the Gamma distribution was recalled in (F.4.3). The rescaled partition sum (F.4.28) is thus distributed as a Gamma random variable in the large t limit at fixed κ . Using the convergence in law (F.4.30), we obtain that the positive integer moments of the partition sum are

$$x = \left(\frac{1}{2} + \varphi_{opt}(r)\right)t + \kappa\sqrt{t} \implies \overline{Z_t(x)^n} = \frac{\Gamma(\alpha + \beta + n)}{\Gamma(\alpha + \beta)} \frac{e^{-n \frac{(r+1)^2 \kappa^2}{2r}}}{(\alpha\sqrt{2\pi r t})^n} + O(1/(\sqrt{t})^{n+1}) . \quad (\text{F.4.31})$$

Using again (F.4.30), we obtain the first two moments of the directed polymer free-energy at large t in the diffusive scaling (F.4.24):

$$\begin{aligned} \overline{\log \left(Z_t \left(\left(\frac{1}{2} + \varphi_{opt}(r) \right) t + \kappa\sqrt{t} \right) \right)} &= -\frac{1}{2} \log(2\pi r t) - \log(\alpha) + \psi(r\alpha + \alpha) - \frac{(r+1)^2}{2r} \kappa^2 + O(1/\sqrt{t}) \\ \overline{\log \left(Z_t \left(\left(\frac{1}{2} + \varphi_{opt}(r) \right) t + \kappa\sqrt{t} \right) \right)^c} &= \psi'(\alpha + \alpha r) + O(1/\sqrt{t}) , \end{aligned} \quad (\text{F.4.32})$$

where $\psi = \Gamma'/\Gamma$ is the diGamma function and $\overline{(\)^c}$ denotes the connected average over disorder. Those results are quite different from what could naively be expected from the usual KPZ universality. Notably we find that here the free-energy is not extensive and its fluctuations are of order 1 and not $t^{1/3}$. These unusual results (in the context of directed polymers) are linked to the fact that the Beta polymer is also a RWRE. We note that all the fluctuations of the free-energy (which are small) are entirely due to the presence of the fictitious Boltzmann weight w_{00} whose distribution is subtly encoded in the algebraic content of the model (that is it comes out of the structure of the Bethe ansatz). The question of the universality of this behavior for TD-RWRE in other type of random environments deserves further investigations in the future.

F.4.5 Multi-point correlations in a diffusive vicinity of the optimal direction

We now go further and study the asymptotic limit for multi-point correlations in a diffusive vicinity of the optimal direction. We consider the formula for the multi-points moments (F.3.28) with, for $i = 1, \dots, n$

$$x_i = \left(\frac{1}{2} + \varphi_{opt}(r)\right)t + \kappa_i\sqrt{t} \quad , \quad \kappa \in \mathbb{R} \quad , \quad t \rightarrow \infty , \quad (\text{F.4.33})$$

and here $\kappa_1 \leq \dots \leq \kappa_n$ for formula (F.3.28) to apply. As before, let us first perform the change of variables $k_j \rightarrow 1/2q_j$. We obtain a formula equivalent to (F.3.28) as

$$\overline{Z_t(x_1) \cdots Z_t(x_n)} = \frac{\Gamma(\alpha + \beta + n)}{\Gamma(\alpha + \beta)} \prod_{j=1}^n \int_{\mathbb{R}} \frac{dq_j}{\pi} \prod_{1 \leq i < j \leq n} \frac{q_j - q_i}{q_j - q_i + 2iq_i q_j} \prod_{j=1}^n \frac{(q_j - i(\beta - \alpha))^t}{(q_j - i(\alpha + \beta))^{1+x_j} (q_j + i(\alpha + \beta))^{1-x_j+k}} \quad (\text{F.4.34})$$

Using the same saddle-point calculation around $q \simeq 0$ we now obtain, changing $q_j \rightarrow q_j/\sqrt{t}$ in (F.4.34),

$$\begin{aligned} \overline{Z_t(x_1) \cdots Z_t(x_n)} &= \frac{\Gamma(\alpha + \beta + n)}{\Gamma(\alpha + \beta)} \prod_{j=1}^n \int_{\mathbb{R}} \frac{dq_j}{\pi\sqrt{t}} \prod_{1 \leq i < j \leq n} \frac{q_j - q_i}{q_j - q_i + \frac{2i}{\sqrt{t}} q_i q_j} \\ &\quad \times \prod_{j=1}^n \frac{1}{1 + \alpha^2(1+r)^2 \frac{q_j^2}{t}} e^{-2r\alpha^2 q_j^2 + 2i((1+r)\alpha\kappa_j q + O(\frac{1}{\sqrt{t}}))} \\ \overline{Z_t(x_1) \cdots Z_t(x_n)} &= \frac{\Gamma(\alpha + \beta + n)}{\Gamma(\alpha + \beta)} \left(\frac{1}{\alpha\sqrt{2\pi r t}} \right)^n e^{-\frac{(r+1)^2}{2r} \sum_{j=1}^n \kappa_j^2} + O\left(\frac{1}{(\sqrt{t})^{n+1}}\right) \end{aligned} \quad (\text{F.4.35})$$

As before, taking into account the interactions between particles (encoded in the $\prod_{1 \leq i < j \leq n} \frac{q_j - q_i}{q_j - q_i + 2iq_i q_j}$ term) just leads to $O(1/\sqrt{t})$ corrections to this leading behavior. Hence we now obtain that in the diffusive vicinity of the optimal direction, the rescaled spatial process defined in (F.4.28) converges in the large time limit to a *constant process with marginal distribution a Gamma distribution*

$$\mathcal{Z}_{\infty}(\kappa) \sim \text{Gamma}(\alpha + \beta) , \quad (\text{F.4.36})$$

where here the equality now holds in the sense of the full spatial process, extending the one-point result (F.4.30). The fact that all different rescaled partition sum in (F.4.28) share the same fluctuations suggests that these fluctuations are not influenced by the last edges visited by the typical polymer path. Correspondingly, in the RWRE language, the fluctuations of the probability to arrive at the site $(0,0)$ starting from infinity in a diffusive vicinity of the optimal direction are Gamma distributed and not sensitive to the first edges visited by the RWRE.

On the other hand, for a fixed starting point, the probability for the RW to arrive at different end points in the diffusive regime are all distributed as Gamma random variables from (F.4.30), but these Gamma random variables are a priori different, and we now show that they must be. Indeed, applying a general theorem from [259] to the Beta TD-RWRE, we

know that for a given environment, with probability 1 (here probability refers to the disorder distribution), the random walk rescaled diffusively converges to a Gaussian distributed RV with a quenched diffusion coefficient equal to the annealed diffusion coefficient $D_{quenched} = D_{ann} = \frac{r}{2(r+1)^2}$. That is, with probability 1, we have

$$\mathbb{P} \left(\frac{X_t + (1/2 + \varphi_{opt}(r))t}{\sqrt{t}} \in [\kappa, \kappa + d\kappa] | X_0 = 0 \right) \sim_{t \rightarrow \infty, d\kappa \ll 1} \frac{(\alpha + \beta)}{\alpha\sqrt{2\pi r}} e^{-\frac{(r+1)^2}{2r}\kappa^2} d\kappa. \quad (\text{F.4.37})$$

(Here the apparent change of sign comes from (F.2.8)). In (F.4.37) the disordered environment seems erased and no traces of Gamma fluctuations are found in the diffusive region. This result however only concerns the probability for a RW to arrive in a vicinity of order \sqrt{t} of a given point, while our result (F.4.36) really gives the probability to arrive at one point. This means that the Gamma RVs at each arrival points must be different in some way so that, when summing their contribution in a width of order \sqrt{t} , they are effectively averaged out to lead to (F.4.37) (here the $\alpha + \beta$ in the numerator is now interpreted as $\bar{Z}_\infty(\kappa)$). Our result is thus not inconsistent with the general result of [259] if this averaging can take place [266]. Note finally that the Gamma variables on different end points can still be correlated, but only on a width of order t^δ with $\delta < 1/2$.

We have thus now obtained a rather complete understanding of the fluctuations of the partition sum of the Beta polymer / RWRE transition probability in a diffusive vicinity of the optimal direction. Let us now investigate the large deviations regimes.

F.5 Asymptotic analysis in the large deviations regime: KPZ universality

In this section we show how the usual KPZ universality is hidden in the Beta polymer in the large time limit in all directions $\varphi \neq \varphi_{opt}$. In most of this section we use heuristic arguments that will be supported in the next section (see Sec. F.6) by using results of BC.

F.5.1 Recall of the results of Barraquand-Corwin

Let us first recall the results of [224] that will be of interest in the following. In the half-line to point problem, one shows that, in any direction $\varphi < \varphi_{opt}(r)$,

$$\lim_{t \rightarrow \infty} \text{Proba} \left(\frac{\log Z_t^{HL}((1/2 + \varphi)t) + I(\varphi)t}{t^{1/3}\sigma(\varphi)} \leq y \right) = F_2(y) \quad (\text{F.5.1})$$

where F_2 is the cumulative distribution function of the Tracy-Widom GUE distribution. This was rigorously proven for the case of $\alpha = \beta = 1$ (a technical argument) and presented in [224] as Theorem 1.15. The constants $I(\varphi)$ and $\sigma(\varphi)$ are solution of a system of transcendental equations which reads (we now introduce the notations of [224], parametrizing $\varphi = -\frac{x(\theta)}{2}$, and θ implicitly given by the first equation below)

$$\begin{aligned} x(\theta) &= \frac{\psi'(\theta + \alpha + \beta) + \psi'(\theta) - 2\psi'(\theta + \alpha)}{\psi'(\theta) - \psi'(\theta + \alpha + \beta)} \\ I(\theta) &= \frac{\psi'(\theta + \alpha + \beta) - \psi'(\theta + \alpha)}{\psi'(\theta) - \psi'(\theta + \alpha + \beta)} (\psi(\theta + \alpha + \beta) - \psi(\theta)) + \psi(\theta + \alpha + \beta) - \psi(\theta + \alpha) \\ 2\sigma(\theta)^3 &= \psi''(\theta + \alpha) - \psi''(\alpha + \beta + \theta) + \frac{\psi'(\alpha + \theta) - \psi'(\alpha + \beta + \theta)}{\psi'(\theta) - \psi'(\alpha + \beta + \theta)} (\psi''(\alpha + \beta + \theta) - \psi''(\theta)) . \end{aligned} \quad (\text{F.5.2})$$

Where $\psi = \Gamma'/\Gamma$ is the diGamma function. Here the assumption $\varphi < \varphi_{opt}(r)$ ensures here that one looks at a direction in the large deviations regime of the cumulative distribution of the RW. With the notations of Sec. F.2.2: $Z_t^{HL}((1/2 + \varphi)t) = \mathbb{P}(X_0 \geq 0 | X_{t=-t} = (1/2 + \varphi)t)$ and if $\varphi \geq \varphi_{opt}(r)$ the probability that the Random walk arrives on the half-line $x \geq 0$ remains finite as $t \rightarrow \infty$. If $\varphi < \varphi_{opt}(r)$ it decreases exponentially as a function of t with a rate function given by $I(\theta)$, corresponding to the extensive part of the free-energy in the polymer language. For our purpose we note, as already emphasized in [224], that this result also implies that for $\varphi < \varphi_{opt}(r)$ (using that under mild assumptions satisfied here the large deviation rate function of the CDF in a RWRE problem is the same as the one of the PDF, see [227])

$$\lim_{t \rightarrow \infty} \frac{\log Z_t((1/2 + \varphi)t)}{t} =_{a.s.} -I(x(\theta)) , \quad (\text{F.5.3})$$

where as in (F.5.2) $x(\theta) = -2\varphi$. That is the point to point free energy of the Beta polymer is the same as the half line to point free energy in the large deviations regime. Note that the point-to-point free-energy in the region $\varphi > \varphi_{opt}(r)$ can be obtained by using the symmetry $(x, \alpha, \beta) \rightarrow (t - x, \beta, \alpha)$, which amounts at using the result (F.5.2) for $\varphi > \varphi_{opt}(r)$ and $(\alpha, \beta) \rightarrow (\beta, \alpha)$.

A first challenge in the following will thus be to retrieve using our formulas the result (F.5.3), and to extend it to obtain a description of the fluctuations of the $\log Z_t(x)$ in the large deviations regime as well.

F.5.2 An inherent difficulty and a puzzle

In this section we put forward an issue that one encounters if one tries to perform the asymptotic analysis $x = (1/2 + \varphi)t$ and $t \gg 1$ of $g_{t,x}(u)$ in a direction $\varphi \neq \varphi_{opt}(r)$ using one of the Fredholm determinant expression derived in Sec. F.4.2, e.g. using the kernel (F.4.12). The problem can be formulated as follows: on one hand we have

$$g_{t,x}(u) = \text{Det} \left(I + u \hat{K}_{t,x} \right) . \quad (\text{F.5.4})$$

Starting from this expression, the most natural idea is to perform an asymptotic analysis by rescaling u in some way while keeping the Fredholm determinant structure in (F.5.4) intact. Following the computation of Sec. F.4.3, we know that imposing the rescaling on u to be such that the trace of the kernel converges implies

$$u \sim \sqrt{t} \left(\frac{2}{\sqrt{1-4\varphi^2}} \left(\frac{1-2\varphi}{2\varphi+1} \right)^\varphi \frac{r^{(1/2+\varphi)}}{1+r} \right)^{-t} . \quad (\text{F.5.5})$$

On the other hand however, we know that we want to obtain (F.5.3) in the large time limit. This result suggests that the leading part of the proper rescaling of u should be

$$u \sim e^{I(\theta)t+o(t)} , \quad (\text{F.5.6})$$

in order to properly take into account the non-zero free-energy of the DP. The two scalings (F.5.5) and (F.5.6) are not mutually consistent. The rescaling (F.5.5) ensures the convergence of the trace of the kernel, as a result of the saddle-point that controls the trace (see Sec. F.4.3), but cannot be used for higher order terms in the Fredholm determinant (see Sec. F.4.4) and is in apparent contradiction with the free-energy (F.5.3). The rescaling (F.5.6) on the other hand does not ensure the convergence of the trace. The series expansion in u defined by the Fredholm determinant expression (F.5.4) thus does not appear well suited to perform the asymptotic analysis. As we will see in the following, the way out of this dilemma will be to recast this series expansion as, schematically

$$\text{Det}(I + u \hat{K}_{t,x}) = \text{Det}(I + \check{K}_{t,x}(u)) , \quad (\text{F.5.7})$$

i.e. finding a new Fredholm determinant expression for $g_{t,x}(u)$ where u appears non-trivially in the expression of the kernel $\check{K}_{t,x}(u)$. It is interesting to note that the first Cauchy-Type Fredholm determinant formula that appeared in the literature around KPZ was in the work of Tracy and Widom on the ASEP [225]. There it was also emphasized that the asymptotic analysis of this type of formula was extremely difficult, and the solution was later found in [226] and involved a transformation of Fredholm determinants similar as (F.5.7). On the other hand in our case it is interesting to note that the Cauchy-type Fredholm determinant formula did appear very well suited to perform the asymptotic analysis in the diffusive regime of the TD-RWRE.

F.5.3 A formal formula for the moments of the Beta polymer in terms of strings

From other studies on other exactly solvable models of directed polymer and related models (see also the discussion in Sec. F.4.2), we know that alternative Fredholm determinant formulas can be obtained by starting from strings-type/small-contours moments formulas for $\overline{Z_t(x)^n}$. In Appendix F.11 we explain how one can use the known relations between different exactly solvable models of directed polymers on the square lattice to arrive at the following conjecture

$$\begin{aligned} \overline{(Z_t(x))^n} \text{ " = " } & \frac{\Gamma(\alpha + \beta + n)}{\Gamma(\alpha + \beta)} n! \sum_{n_s=1}^n \frac{1}{n_s!} \sum_{(m_1, \dots, m_{n_s})_n} \prod_{j=1}^{n_s} \int_{L^n} \frac{dk_j}{2\pi} \prod_{1 \leq i < j \leq n_s} \frac{4(k_i - k_j)^2 + (m_i - m_j)^2}{4(k_i - k_j)^2 + (m_i + m_j)^2} \\ & \prod_{j=1}^{n_s} \frac{1}{m_j} \left(\frac{\Gamma(-\frac{m_j}{2} + \alpha + \beta + ik_j)}{\Gamma(\frac{m_j}{2} + \alpha + \beta + ik_j)} \right)^{1+x} \left(\frac{\Gamma(-\frac{m_j}{2} + ik_j)}{\Gamma(\frac{m_j}{2} + ik_j)} \right)^{1-x+t} \left(\frac{\Gamma(\beta + ik_j + \frac{m_j}{2})}{\Gamma(\beta + ik_j - \frac{m_j}{2})} \right)^t . \end{aligned} \quad (\text{F.5.8})$$

where here $\sum_{(m_1, \dots, m_{n_s})_n}$ means summing over all n_s -uplets (m_1, \dots, m_{n_s}) such that $\sum_{i=1}^{n_s} m_i = n$. In this formula the integration $\int_L \frac{dk_j}{2\pi}$ is actually not a real integration (hence the presence of quotes around the equality sign) as we now detail. This formula is only valid in the sense of a specific residue expansion of the integrand. It consists in recursively taking, always with a plus sign, starting with the integration over k_{n_s} and then iterating up to k_1 , the residues of the integrand coming from the $\Gamma(-\frac{m_j}{2} + ik_j)/\Gamma(\frac{m_j}{2} + ik_j)$ term as well as the residue at $k_j = k_l + \frac{i}{2}(m_l + m_j)$ and iterating. Note that when one takes the residue at $k_j = k_l + \frac{i}{2}(m_l + m_j)$, it creates new residues for the "integration" on k_l in the term $\Gamma(-\frac{m_j}{2} + ik_j)/\Gamma(\frac{m_j}{2} + ik_j)$. Note also that the position of these residues do not depend on α and β , permitting an easy implementation using e.g. Mathematica.

This formula is strictly speaking a conjecture, and only arises from an educated guess (see Appendix F.11). Its validity was tested against direct checks for small values of x, t and n . Unfortunately, we could not find a contour of integration L which makes this formula correct as a true contour integral formula. From the discussion in Sec. F.3.4 we know that the correct way to find such a formula is first to use a nested contour integral representation of $\overline{(Z_t(x))^n}$. This is done in Sec. F.6 where we obtain a formula similar to this one.

F.5.4 A formal Fredholm determinant and KPZ universality

The formal formula (F.5.8) is very close to the formula (60) obtained in [5] for the Inverse-Beta polymer. (See Appendix F.11 for the comparison). As such, we can follow the same steps as done in [5] and obtain a new Fredholm determinant formula $g_{t,x}(u) = \text{Det}(I + \check{K}_{t,x})$ with

$$\check{K}_{t,x}(v_1, v_2) = \int_L \frac{dk-1}{\pi} \frac{1}{2i} \int_C \frac{ds}{\sin(\pi s)} u^s e^{-2ik(v_1-v_2)-s(v_1+v_2)} \quad (\text{F.5.9})$$

$$\left(\frac{\Gamma(-\frac{s}{2} + \alpha + \beta + ik)}{\Gamma(\frac{s}{2} + \alpha + \beta + ik)} \right)^{1+x} \left(\frac{\Gamma(-\frac{s}{2} + ik)}{\Gamma(\frac{s}{2} + ik)} \right)^{1-x+t} \left(\frac{\Gamma(\beta + ik + \frac{s}{2})}{\Gamma(\beta + ik - \frac{s}{2})} \right)^t.$$

As before, this formula is formal since the integration on L is actually not an integration. A similar (but not formal) formula can be derived using an approach based on nested contour integrals (see Sec. F.6). Let us however ignore this for now and try to perform a saddle-point analysis on (F.5.9) by sending $t \rightarrow \infty$ with $x = (1/2 + \varphi)t$ and proceed as if (F.5.9) was well defined using a true integration. The analysis is then strictly similar to the one made in [5] from which we borrow the notations and to which we refer the reader for more details. The ‘‘integration’’ in (F.5.9) is dominated in the large t limit by the factor

$$\exp \{t (G_\varphi(ik + s/2) - G_\varphi(ik - s/2))\}, \quad (\text{F.5.10})$$

where

$$G_\varphi(x) = \log \Gamma(\beta + x) - (1/2 - \varphi) \log \Gamma(x) - (1/2 + \varphi) \log \Gamma(\alpha + \beta + x). \quad (\text{F.5.11})$$

We look for a cubic saddle-point at $(s, k) = (0, -ik_\varphi)$. Its position is implicitly defined by

$$\psi'(\beta + k_\varphi) - \left(\frac{1}{2} - \varphi\right) \psi'(k_\varphi) - \left(\frac{1}{2} + \varphi\right) \psi'(\alpha + \beta + k_\varphi) \quad (\text{F.5.12})$$

With the same notations as in [5] we define a rescaled free energy $f_t(\varphi)$ as

$$F_t(\varphi) = -\log Z_t(x = (1/2 + \varphi)t) = c_\varphi t + \lambda_\varphi f_t(\varphi)$$

$$c_\varphi = -G'_\varphi(k_\varphi) \quad , \quad \lambda_\varphi = \left(\frac{t G''_\varphi(k_\varphi)}{8} \right)^{\frac{1}{3}}. \quad (\text{F.5.13})$$

Following the exact same steps as in [5] (see also Appendix C there for a discussion that can be adapted to our setting to consider the effect of the additional weight w_{00} introduced in Sec. F.4.1) we obtain

$$\lim_{t \rightarrow \infty} \text{Prob} \left(\frac{\log Z_t((1/2 + \varphi)t) + t c_\varphi}{\lambda_\varphi} < 2^{\frac{2}{3}} z \right) = F_2(z), \quad (\text{F.5.14})$$

where F_2 is the cumulative distribution function of the Tracy-Widom GUE distribution and the parameters c_φ and $\lambda_\varphi \sim t^{\frac{1}{3}}$ are given by (F.5.13) with

$$\varphi = \frac{\psi'(\beta + k_\varphi) - \frac{1}{2} (\psi'(k_\varphi) + \psi'(\alpha + \beta + k_\varphi))}{\psi'(\alpha + \beta + k_\varphi) - \psi'(k_\varphi)}$$

$$c_\varphi = -G'_\varphi(k_\varphi) = \left(\varphi + \frac{1}{2} \right) \psi(k_\varphi + \alpha + \beta) - \psi(k_\varphi + \beta) + \left(\frac{1}{2} - \varphi \right) \psi(k_\varphi)$$

$$\frac{8\lambda_\varphi^3}{t} = G''_\varphi(k_\varphi) = - \left(\varphi + \frac{1}{2} \right) \psi''(k_\varphi + \alpha + \beta) + \psi''(k_\varphi + \beta) - \left(\frac{1}{2} - \varphi \right) \psi''(k_\varphi). \quad (\text{F.5.15})$$

The above system of equations is expected to be valid for $\varphi_{opt}(r) = \frac{\beta-\alpha}{2(\alpha+\beta)} < \varphi < 1/2$, a limitation which is not visible from our formal derivation but that we now explain. A first hint is to consider the limit $\varphi = \pm 1/2$. In the limit $\varphi \rightarrow -\frac{1}{2}$, $Z_t = \prod_{i=1}^t u_i$, the product of t independent u variables. In the limit $\varphi \rightarrow -\frac{1}{2}$, $Z_t = \prod_{i=1}^t v_i$. This implies $-\overline{\log Z_t(0)}/t = \psi(\alpha + \beta) - \psi(\alpha)$ and $-\overline{\log Z_t(t)}/t = \psi(\alpha + \beta) - \psi(\beta)$. The second limit is correctly reproduced by (F.5.15) using $k_\varphi \rightarrow_{\varphi \rightarrow 1/2-} 0^+$, whereas the first one is not. Furthermore, the two first equations in (F.5.15) (i.e. those that determines the extensive part of the free-energy) are also equivalent to the two first equations in (F.5.2) using the symmetry $(\varphi, \alpha, \beta) \rightarrow (-\varphi, \beta, \alpha)$ on (F.5.2) with the identification $\theta = k_\varphi$, $I(\theta) = -G'_\varphi(k_\varphi)$. To see this more explicitly rewrite c_φ in (F.5.15) as

$$c_\varphi = -G'_\varphi(k_\varphi) = \left(\varphi + \frac{1}{2} \right) \psi(k_\varphi + \alpha + \beta) - \psi(k_\varphi + \beta) + \left(\frac{1}{2} - \varphi \right) \psi(k_\varphi)$$

$$= (\varphi - 1/2) (\psi(k_\varphi + \alpha + \beta) - \psi(k_\varphi)) + \psi(k_\varphi + \alpha + \beta) - \psi(k_\varphi + \beta)$$

$$c_\varphi = -G'_\varphi(k_\varphi) = \frac{\psi'(\alpha + \beta + k_\varphi) - \psi'(\beta + k_\varphi)}{\psi'(k_\varphi) - \psi'(\alpha + \beta + k_\varphi)} (\psi(k_\varphi + \alpha + \beta) - \psi(k_\varphi)) + \psi(k_\varphi + \alpha + \beta) - \psi(k_\varphi + \beta) \quad (\text{F.5.16})$$

where from the first to the second line we have only rearranged the terms, and from the second to the last we have inserted φ as given by (F.5.15). Applying the identification mentioned above shows the identity between the two first equations in (F.5.2) and those in (F.5.15).

This fact was expected since the extensive part of the free-energy should be the same in the half-line (in the large deviation regime) and in the point-to-point Beta polymer problem. The condition of validity of (F.5.2), $\varphi < \varphi_{opt}(r)$, then becomes our condition of validity after applying the symmetry.

The new, non-trivial predictions from our formal computations are that

- The fluctuations of the free-energy in the point-to-point Beta polymer problem are also of the GUE Tracy-Widom type with the characteristic $t^{1/3}$ scaling.
- The non-universal constant in front of these fluctuations are exactly the same in the point-to-point and in the half-line to point problem. To see this, notice that the third line of (F.5.15) is also equivalent to the third line of (F.5.2) using the identification $2\sigma(\theta)^3 = G'''(\varphi)$.

The first prediction could have been expected from the KPZ universality of directed polymer problem, a paradigm which however appears dangerous to apply in the Beta polymer as we saw from the study of the fluctuations in the optimal direction. The second is interesting from the RWRE point of view. Indeed, although it is known on general grounds (see [227]) that the large deviations rate functions of the PDF and CDF of a TD-RWRE are identical, a similar identity for the *fluctuations* of the logarithm of the PDF and CDF is to our knowledge not known. Here, in the particular example of the Beta TD-RWRE, we have showed that these fluctuations are identical up to order $t^{1/3}$ included. It would be interesting to understand if this holds more generally for other TD-RWRE.

F.5.5 Crossover between Gamma and Tracy-Widom fluctuations

Let us now use our results (F.4.32) and (F.5.15) to try to gain some information on the crossover between the diffusive regime and the large deviations regime of the RW. Let us first see how both regimes are connected and study the behavior of (F.5.15) around the optimal angle: $\varphi = \varphi_{opt}(r) + \delta\varphi$. Expanding in $\delta\varphi > 0$, the solution of (F.5.15) reads

$$\begin{aligned} k_\varphi &\simeq \frac{\alpha r}{(r+1)\delta\varphi} + \left(\frac{1}{2} - \alpha r\right) + O(\delta\varphi) \\ -G'_\varphi(k_\varphi) &\simeq \frac{(1+r)^2}{2r}\delta\varphi^2 + \frac{(r-1)(r+1)^3}{6r^2}\delta\varphi^3 + O(\delta\varphi^4) \\ G'''_\varphi(k_\varphi) &= \frac{(r+1)^4}{\alpha^2 r^3} \left(\delta\varphi^4 + \frac{r^2-1}{r}\delta\varphi^5 + O(\delta\varphi^6) \right). \end{aligned} \quad (\text{F.5.17})$$

Hence, at fixed, small angle around the optimal position, $\varphi = \varphi_{opt}(r) + \delta\varphi$, we conclude from (F.5.13) that

$$\begin{aligned} \log Z_t(x) &\simeq -\frac{(1+r)^2}{2r}t\delta\varphi^2 + \left(\frac{(r+1)^4}{2\alpha^2 r^3}\right)^{\frac{1}{3}} t^{\frac{1}{3}}\delta\varphi^{\frac{4}{3}}\chi_{GUE}, \\ x &= \left(\frac{1}{2} + \varphi_{opt}(r) + \delta\varphi\right)t, \quad t \gg 1. \end{aligned} \quad (\text{F.5.18})$$

Where χ_{GUE} is a RV which is distributed with the GUE Tracy-Widom distribution. On the other hand, we know from Sec. F.4.5 that, on a diffusive scale around the optimal direction,

$$\begin{aligned} \log Z_t(x) &\simeq -\log(\alpha) - \frac{1}{2}\log(2\pi r t) - \frac{(1+r)^2}{2r}\kappa^2 + \log\chi_{\alpha+\beta}, \\ x &= \left(\frac{1}{2} + \varphi_{opt}(r)\right)t + \kappa\sqrt{t}, \quad t \gg 1. \end{aligned} \quad (\text{F.5.19})$$

Where $\chi_{\alpha+\beta}$ is a RV distributed with a Gamma distribution of parameter $\alpha + \beta$. Introducing the coordinate $\hat{x} = x - (\frac{1}{2} + \varphi_{opt}(r))t$ and changing $\delta\varphi \rightarrow \hat{x}/t$ in (F.5.18) and $\kappa \rightarrow \hat{x}/\sqrt{t}$ in (F.5.19), one sees that both regimes are connected by the angle-dependent term in the extensive part of the free-energy $-\frac{(1+r)^2}{2r}t\delta\varphi^2 = -\frac{(1+r)^2}{2r}\kappa^2 = -\frac{(1+r)^2}{2r}\frac{\hat{x}^2}{t}$. Though the following is non-rigorous, it thus appears reasonable to schematically give a more complete picture of fluctuations at large t around the central region as

$$\begin{aligned} \log Z_t(x) &\simeq -\frac{1}{2}\log(2\pi\alpha\beta t) - \frac{(\alpha+\beta)^2}{2\alpha\beta}\frac{\hat{x}^2}{t} + \log\chi_{\alpha+\beta} + \left(\frac{(\alpha+\beta)^4}{2\alpha^3\beta^3}\right)^{\frac{1}{3}}\frac{\hat{x}^{\frac{4}{3}}}{t}\chi_{GUE} \\ x &= \left(\frac{1}{2} + \varphi_{opt}(r)\right)t + \hat{x}, \quad t \gg 1, \quad \hat{x} = o(t). \end{aligned} \quad (\text{F.5.20})$$

The latter being exact at large time in the central region $\hat{x} = O(1)$ and including the diffusive regime $\hat{x} \sim \sqrt{t}$, as well as in the beginning of the large deviations regime $\hat{x} = \delta\varphi t$ with $\delta\varphi \ll 1$. In between, in the crossover region $\sqrt{t} \ll \hat{x} \ll t$ the fluctuations should be an interpolation between Gamma and Tracy-Widom fluctuations and the above picture is too simple. Equating the amplitude of these two sources of fluctuations, it predicts the existence of a cross-over scale where the competition between Tracy-Widom and Gamma type fluctuations is maximal as

$$\hat{x}_{c.o.} \sim t^{\frac{3}{4}}. \quad (\text{F.5.21})$$

As summarized in Fig. F.1. A way to formalize the identification of this crossover scale is to introduce an (a priori unknown) scaling function involving e.g. the second cumulant of the fluctuations, as

$$\overline{(\log Z_t(x))^{2^c}}^{1/2} = t^\gamma f\left(\frac{\hat{x}}{t^\delta}\right) \quad (\text{F.5.22})$$

for $\hat{x} = o(t)$, where $\frac{1}{2} < \delta < 1$. Imposing the matching conditions on the two above mentioned regimes we obtain

$$t^\gamma f\left(y = \frac{\hat{x}}{t^\delta}\right) \simeq_{y \rightarrow 0} \psi'(\alpha + \beta) \quad (\text{F.5.23})$$

$$t^\gamma f\left(y = \frac{\hat{x}}{t^\delta}\right) \simeq_{y \rightarrow +\infty} \left(\frac{(\alpha + \beta)^4}{2\alpha^3\beta^3}\right)^{\frac{1}{3}} \frac{\hat{x}^{\frac{4}{3}}}{t} \sqrt{\text{Var}(\chi_{GUE})} \quad (\text{F.5.24})$$

This implies $\gamma = 0$ and $\delta = 3/4$ recovering (F.5.21). A more precise characterization of the fluctuations in this regime and of the scaling function remains to be obtained. Note that since the formula $\log Z_t(x) - \log Z_t(0) \simeq -\frac{(\alpha+\beta)^2}{2\alpha\beta} \frac{\hat{x}^2}{t}$ was found to hold in both regimes, it is also expected to hold in the crossover regime. Hence in this regime, writing $\hat{x} = \omega t^{\frac{3}{4}}$, with a fixed ω , we expect that $\overline{\log Z_t(x)} \simeq -\frac{\sqrt{i(r+1)^2\omega^2}}{2r}$ at large t .

F.6 Nested-Contour integral formulas for the point-to-point problem

During the late stages of redaction of this work, we were informed [265] by Guillaume Barraquand and Ivan Corwin of the existence of a nested contour integral formula for the multi-points moments of the Beta polymer, from which (F.3.28) was derived. This approach also allows to obtain other moments formulas and Fredholm determinant formulas which partially justify the heuristic approach used in the last section. The goal of this section is to make the link between our formulas and theirs.

F.6.1 Alternative moments formulas

A nested contour integral formula:

Let us start from the moments formula (F.3.27) that we now recall for readability of the reasoning:

$$\overline{Z_t(x)^n} = (-1)^n \frac{\Gamma(\alpha + \beta + n)}{\Gamma(\alpha + \beta)} \prod_{j=1}^n \int_{-\infty}^{+\infty} \frac{dk_j}{2\pi} \prod_{1 \leq i < j \leq n} \frac{(k_i - k_j)^2}{(k_i - k_j)^2 + 1} \prod_{j=1}^n \frac{(ik_j + \frac{\beta - \alpha}{2})^t}{(ik_j + \frac{\alpha + \beta}{2})^{1+x} (ik_j - \frac{\alpha + \beta}{2})^{1-x+t}}. \quad (\text{F.6.1})$$

We first note that the first part of the integrand in (F.6.1), i.e. the interaction term between particles, can be rewritten as:

$$\prod_{1 \leq i < j \leq n} \frac{(k_i - k_j)^2}{(k_i - k_j)^2 + 1} = \frac{1}{n!} \sum_{\sigma \in S_n} \prod_{1 \leq i < j \leq n} \frac{k_{\sigma(i)} - k_{\sigma(j)}}{k_{\sigma(i)} - k_{\sigma(j)} + i}. \quad (\text{F.6.2})$$

where S_n is the group of permutation of $\{1, \dots, n\}$. This identity is shown in App. F.12. Inserting (F.6.2) in (F.6.1), using that the second part of the integrand

$$\prod_{j=1}^n \frac{(ik_j + \frac{\beta - \alpha}{2})^t}{(ik_j + \frac{\alpha + \beta}{2})^{1+x} (ik_j - \frac{\alpha + \beta}{2})^{1-x+t}} \quad (\text{F.6.3})$$

is symmetric by exchange $k_i \leftrightarrow k_j$, relabelling $k_{\sigma(i)} \rightarrow k_i$, and using that the number of elements of S_n is $n!$ we obtain:

$$\overline{Z_t(x)^n} = (-1)^n \frac{\Gamma(\alpha + \beta + n)}{\Gamma(\alpha + \beta)} \prod_{j=1}^n \int_{-\infty}^{+\infty} \frac{dk_j}{2\pi} \prod_{1 \leq i < j \leq n} \frac{k_i - k_j}{k_i - k_j + i} \prod_{j=1}^n \frac{(ik_j + \frac{\beta - \alpha}{2})^t}{(ik_j + \frac{\alpha + \beta}{2})^{1+x} (ik_j - \frac{\alpha + \beta}{2})^{1-x+t}}. \quad (\text{F.6.4})$$

Let us now make the change of variables $k_j = -i(z_j + \frac{\alpha + \beta}{2})$. We obtain

$$\overline{Z_t(x)^n} = \frac{\Gamma(\alpha + \beta + n)}{\Gamma(\alpha + \beta)} \prod_{j=1}^n \int_L \frac{dz_j}{2\pi i} \prod_{1 \leq i < j \leq n} \frac{z_i - z_j}{z_i - z_j - 1} \prod_{j=1}^n \frac{(z_j + \beta)^t}{(z_j + \alpha + \beta)^{1+x} (z_j)^{1-x+t}}, \quad (\text{F.6.5})$$

where here the contour $L = -\frac{\alpha + \beta}{2} + i\mathbb{R}$ is oriented from top to down. Note that the poles of the integrand are now located at $z_j = 0$, $z_j = -(\alpha + \beta) < 0$ and $z_j = z_i - 1$ if $i < j$. Apart from these, the integrand being analytic in z_n , and decaying as $1/z_n^2$ at infinity, the contour of integration on z_n can be transformed into \mathcal{C}_n , a small, positively oriented, circle around 0 and that excludes $-(\alpha + \beta)$. Note that this transformation of contour is only possible because we have eliminated the poles at $z_j = z_i + 1$ for $j < i$ that would have arose if one had performed the change of variable $k_j \rightarrow z_j$ directly on (F.6.1) and not on (F.6.4). At this point, one can now recursively close all contours in a so-called nested manner so that, $\forall i < j$, \mathcal{C}_i is

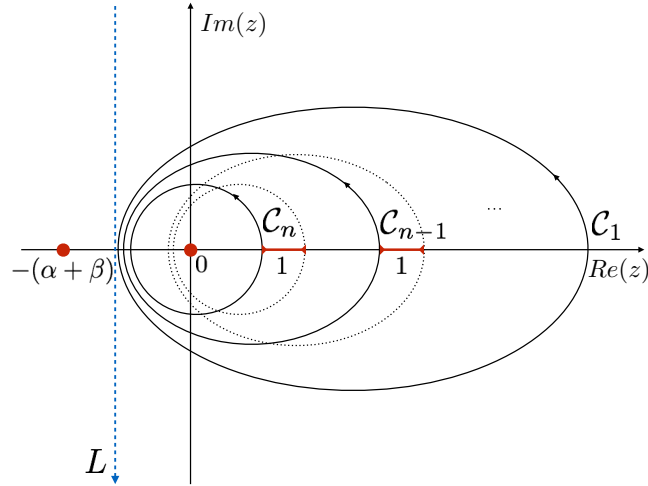


Figure F.3: The different contours involved in (F.6.6) and (F.6.8). In (F.6.6) the n variables z_i are integrated on the vertical line L which is oriented from top to down (dotted blue above). In (F.6.8) the z_i variables are integrated on different contours \mathcal{C}_i organized in a nested fashion as explained in the text. In the above picture the red colour is used to emphasize the important properties of the nested contours: they enclose 0 but not $-(\alpha + \beta)$, and are such that the contour $\mathcal{C}_{j+1} + 1$ (dotted contours above) is inside $\mathcal{C}_j \forall j = 2, \dots, n$.

positively oriented, contains $\mathcal{C}_j + 1$ (to avoid the pole at $z_j = z_i - 1$ for $i < j$) and excludes $-(\alpha + \beta)$ and 0 (see Fig. F.3). We thus obtain

$$\overline{Z_t(x)^n} = \frac{\Gamma(\alpha + \beta + n)}{\Gamma(\alpha + \beta)} \prod_{j=1}^n \int_{\mathcal{C}_j} \frac{dz_j}{2\pi i} \prod_{1 \leq i < j \leq n} \frac{z_i - z_j}{z_i - z_j - 1} \prod_{j=1}^n \frac{(z_j + \beta)^t}{(z_j + \alpha + \beta)^{1+x} (z_j)^{1-x+t}}. \quad (\text{F.6.6})$$

This formula is almost identical to the formula obtained in Proposition 3.4 of [224] for the moments of the partition sum in the half-line to point Beta polymer problem, using $n_j = t - x + 1$ and $\beta \leftrightarrow \alpha$. Actually, suppressing the first factor of Gamma function in (F.6.6) and changing

$$\prod_{j=1}^n \frac{(z_j + \beta)^t}{(z_j + \alpha + \beta)^{1+x} (z_j)^{1-x+t}} \rightarrow \prod_{j=1}^n \frac{(z_j + \beta)^t}{(z_j + \alpha + \beta)^x (z_j)^{1-x+t}}, \quad (\text{F.6.7})$$

one obtains exactly the same formula. Hence, from a computational point of view, the half-line to point problem and the point to point problem appears extremely similar for the Beta polymer. This interesting fact and the formula (F.6.6) was first pointed out to us by BC [265]. In the end it appears that it is this similarity between the half-line to point and the point to point problem that is responsible for the fact that both problems have exactly the same fluctuations in the large deviations regime (see the discussion below (F.5.15)).

Multi-points formulas:

Interestingly, using the techniques used in [224] it is also possible to obtain a formula for the multi-point moments of the partition sum of the point-to-point Beta polymer as

$$\overline{Z_t(x_1) \cdots Z_t(x_n)} = \frac{\Gamma(\alpha + \beta + n)}{\Gamma(\alpha + \beta)} \prod_{j=1}^n \int_{\mathcal{C}_j} \frac{dz_j}{2\pi i} \prod_{1 \leq i < j \leq n} \frac{z_i - z_j}{z_i - z_j - 1} \prod_{j=1}^n \frac{(z_j + \beta)^t}{(z_j + \alpha + \beta)^{1+x_j} (z_j)^{1-x_j+t}}, \quad (\text{F.6.8})$$

where the contours are the same nested contours as those used in (F.6.6) and here $0 \leq x_1 \leq x_2 \leq \dots \leq x_n$. The existence of this formula was pointed out to us by BC [265]. From this formula, successively un-nesting the contours from the \mathcal{C}_i to the L in an opposite manner as what was just done (see Fig. F.3), and performing the change of variables $z_j = ik_j - \frac{\alpha + \beta}{2}$, we obtain the formula (F.3.28) that was extensively discussed above.

Moment formula for the Beta polymer in terms of strings

Finally, it is also possible to obtain a formula for the moments of the point-to-point Beta polymer problem using a decomposition into strings. Proving this formula involves successively shrinking the contours \mathcal{C}_i in (F.6.6) on \mathcal{C}_n and keeping track of all the residues encountered in the calculation. This procedure is actually quite tedious but the steps being exactly similar as those performed in [224] we can easily adapt them to obtain ⁴

⁴following the above remarks, (F.6.9) is an adaptation of Proposition 3.6. of [224] with an incorrect minus sign in the determinant there, which has been corrected here

$$\begin{aligned} \overline{Z_t(x)^n} &= \frac{\Gamma(\alpha + \beta + n)}{\Gamma(\alpha + \beta)} n! \sum_{n_s=1}^n \frac{1}{n_s!} \sum_{(m_1, \dots, m_{n_s})_n} \prod_{j=1}^{n_s} \int_{\mathcal{C}^n} \frac{dz_j}{2i\pi} \det \left(\frac{1}{z_i + m_i - z_j} \right)_{n_s \times n_s} \\ &\quad \prod_{j=1}^{n_s} \left(\frac{\Gamma(z_j + \alpha + \beta)}{\Gamma(z_j + \alpha + \beta + m_j)} \right)^{1+x} \left(\frac{\Gamma(z_j)}{\Gamma(z_j + m_j)} \right)^{1-x+t} \left(\frac{\Gamma(z_j + \beta + m_j)}{\Gamma(z_j + \beta)} \right)^t, \end{aligned} \quad (\text{F.6.9})$$

where \mathcal{C} is a small circle around 0 of radius $r < 1/2$, excluding $-(\alpha + \beta)$ and as in (F.5.8) $\sum_{(m_1, \dots, m_{n_s})_n}$ means summing over all n_s -uplets (m_1, \dots, m_{n_s}) such that $\sum_{i=1}^{n_s} m_i = n$. We note that performing in this formula the shifts $z_j = ik_j - \frac{\alpha + \beta}{2} - m_j/2$, we obtain, using

$$\det \left[\frac{1}{i(k_i - k_j) + (m_i + m_j)/2} \right]_{n_s \times n_s} = \prod_{i=1}^{n_s} \frac{1}{m_i} \prod_{1 \leq i < j \leq n_s} \frac{4(k_i - k_j)^2 + (m_i - m_j)^2}{4(k_i - k_j)^2 + (m_i + m_j)^2} \quad (\text{F.6.10})$$

exactly the integrand inside formula (F.5.8), with the difference that here all contours of integrations are well specified and are *different* for each k_i . It does not seem possible to deform all these contours of integrations onto a single contour L (one would encounter many poles in doing so) as suggested in the formal formula (F.5.8) and this explain why we could only find a formal formula. The formula (F.6.9) thus appears as the correct interpretation of (F.5.8) as a contour integral.

F.6.2 Mellin-Barnes type Fredholm determinant

Finally, following the same steps as in [224] for the half-line to point problem, we obtain from (F.6.9) another Fredholm determinant formula $g_{t,x}(u) = \text{Det} (I + K_{t,x}^{MB})$ defined in (F.4.2) with the kernel ⁵

$$K_{t,x}^{MB}(v, v') = \frac{1}{(2\pi i)^2} \int_{1/2 - i\infty}^{1/2 + i\infty} \frac{\pi ds}{\sin(\pi s)} (u)^s \left(\frac{\Gamma(v + \alpha + \beta)}{\Gamma(v + \alpha + \beta + s)} \right)^{1+x} \left(\frac{\Gamma(v)}{\Gamma(v + s)} \right)^{1-x+t} \left(\frac{\Gamma(v + \beta + s)}{\Gamma(v + \beta)} \right)^t \frac{1}{v' - v - s}, \quad (\text{F.6.11})$$

where $(v, v') \in \mathcal{C}_0^2$, with \mathcal{C}_0 a small circle around 0 of radius $r < 1/4$ excluding $-(\alpha + \beta)$ and -1 . This formula is valid for $u \in \mathbb{C} \setminus \mathbb{R}_-$. Repeating the saddle-point analysis on this kernel would lead to the same result (F.5.15) as the one found heuristically earlier.

F.7 Numerical results

In this section we verify numerically some of the results obtained in the paper. All the results presented in the following are based on numerical simulations of the Beta polymer with parameters $\alpha = \beta = 1$. Using a transfer matrix type algorithm, we compute numerically the partition sum for 5×10^5 different random environments. For each random environment, we store the value of the partition sum for different polymers length t from $t = 90$ to $t = 2048$ with a power-law type binning as $t = t_i = \lfloor 128\sqrt{2}^{i/10} \rfloor$ with $i = 1, \dots, 10$, and for different positions. The studied positions are chosen as $x = \lfloor t/2 + \hat{x} \rfloor$ with either $\hat{x} = \kappa_i t^{\frac{2}{3}}$ with $\kappa_i = 3i/20$ and $i = 0, \dots, 20$ (to study the diffusive regime around the optimal direction $\varphi_{opt}(1) = 0$) or $\hat{x} = \varphi_i t$ with $\varphi_i = i/40$ with $i = 0, \dots, 20$ (to study the large deviations regime of the TD-RWRE).

F.7.1 In the diffusive regime.

One-point

Let us first focus on one-point statistics of the rescaled spatial process at finite time $Z_t(\kappa)$ (see (F.4.28)). Using the simulations described previously, we obtain numerical approximations of its PDF for different times t_i and diffusion parameters κ_j , and compare it to the infinite time prediction (F.4.36) which we recall here (for the choice $\alpha = \beta = 1$): $Z_\infty(\kappa)$ is distributed as $Z \sim \text{Gamma}(2)$. The PDF of Z is thus (see (F.4.3) for the PDF of a Gamma RV with parameter $\alpha + \beta$)

$$P_{\text{Gamma}(2)}(Z) = Z e^{-Z}. \quad (\text{F.7.1})$$

In Fig. F.4 we compare the numerically obtained PDF for $t = 2048$ and $\kappa = 0$ (i.e. exactly in the central region) in log and linear scale. The agreement is excellent. In Fig. F.5 we show how this result vary as a function of the diffusion constant κ and the time t . As a function of the diffusivity constant κ . Important deviations from the asymptotic behavior start to appear only for $\kappa \geq \kappa_7 \simeq 0.95$. To compare this value, note that the mean value of $Z_t(\kappa\sqrt{t})$ is theoretically predicted to converge to a gaussian form with

$$\overline{Z_t(\kappa\sqrt{t})} \simeq \frac{1}{\sigma\sqrt{2\pi t}} e^{-\frac{\kappa^2}{2\sigma^2}}, \quad \sigma = 1/2. \quad (\text{F.7.2})$$

Hence $\kappa_7/\sigma \simeq 1.9$ and in terms of probability in the RWRE picture, more than 94% of the accessible positions of the particles appear very well-described by our asymptotic result for $t = 2048$.

⁵similarly (F.6.11) is an adaptation of Theorem 1.12. of [224] with the minus sign missprint there signaled above corrected here as well

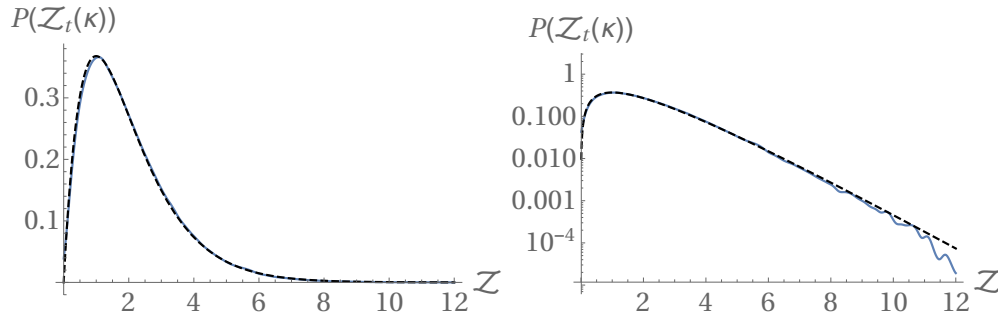


Figure F.4: Left: Blue line: Empirical PDF of $\mathcal{Z}_{t=2048}(0)$ obtained from the numerical simulations. Black-dashed line: PDF of a $\text{Gamma}(2)$ distributed RV (F.7.1). Right: Same figure in a logarithmic scale. There are no fitting parameters.

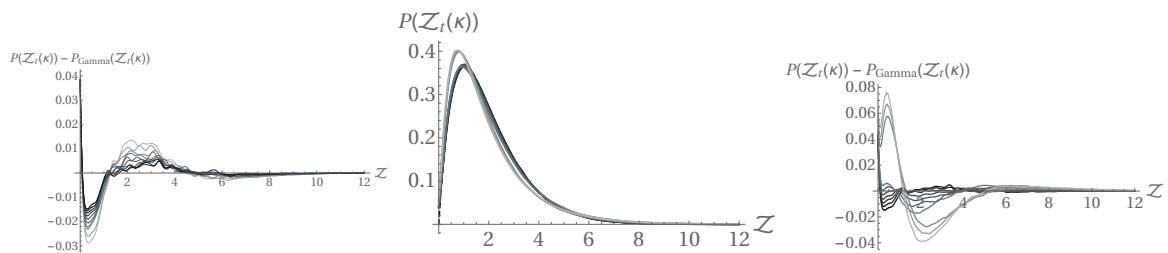


Figure F.5: Left: Difference between the empirical PDF of $\mathcal{Z}_{t_i}(0)$ and the PDF of a $\text{Gamma}(2)$ distributed RV (F.7.1) for $i = 1, \dots, 10$ (from light gray to black). Middle: Empirical PDF of $\mathcal{Z}_{t=2048}(\kappa_i)$ for $i = 0, \dots, 9$ (from black to light gray) together with the PDF of a $\text{Gamma}(2)$ distributed RV (F.7.1) (black-dashed line). Right: Difference between the empirical PDF of $\mathcal{Z}_{t=2048}(\kappa_i)$ and the PDF of a $\text{Gamma}(2)$ distributed RV (F.7.1) for $i = 0, \dots, 9$ (from black to light gray). There are no fitting parameters.

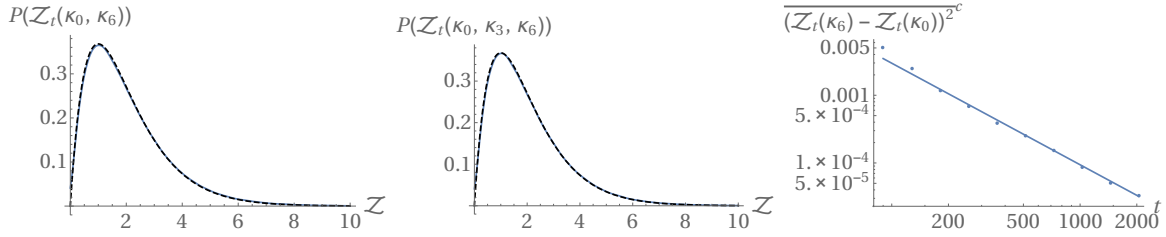


Figure F.6: Left (resp. Middle): Blue line: Empirical PDF of $\mathcal{Z}_{t=2048}(\kappa_0, \kappa_6)$ (resp. $\mathcal{Z}_{t=2048}(\kappa_0, \kappa_3, \kappa_6)$). Black-dashed line: PDF of a $Gamma(2)$ distributed RV (F.7.1) (here there are no fitting parameters.). Right: Blue dots: Empirical variance $(\mathcal{Z}_t(\kappa_6) - \mathcal{Z}_t(\kappa_0))^{2^c}$ obtained from numerical simulations in a log-log scale. The blue line corresponds to a power-law decay as $1/t^{3/2}$.

Multi-points

Let us now verify some of the predictions of our results for the multi-points correlations in the diffusive regime. The prediction (F.4.36) is that, up to $O(1/\sqrt{t})$ deviations, $\mathcal{Z}_t(\kappa)$ converges to a constant process with marginal distribution $\mathcal{Z}_\infty \sim Gamma(2)$. We show here the verification of two consequences of this result. The first one is that, at fixed $\kappa^{(1)}, \dots, \kappa^{(n)}$ for n arbitrary, the RV $\mathcal{Z}_t(\kappa^{(1)}, \dots, \kappa^{(n)}) = (\mathcal{Z}_t(\kappa^{(1)}) \cdots \mathcal{Z}_t(\kappa^{(n)}))^{1/n}$ converges to a $Gamma(2)$ distributed RV. In Fig. F.6 we compare this prediction with the numerically obtained PDF of $\mathcal{Z}_t(\kappa^{(1)}, \dots, \kappa^{(n)})$ for $n = 2$ with $\kappa^{(1)} = \kappa_0$ and $\kappa^{(2)} = \kappa_6$ and $n = 3$ with $\kappa^{(1)} = \kappa_0$, $\kappa^{(2)} = \kappa_3$ and $\kappa^{(3)} = \kappa_6$ and $t = 2048$ and obtain an excellent agreement. Another implication of this result is that the variance $(\mathcal{Z}_t(\kappa^{(1)}) - \mathcal{Z}_t(\kappa^{(2)}))^{2^c}$ must, for arbitrary $\kappa^{(1)}$ and $\kappa^{(2)}$, decay to 0 at large t faster than $1/\sqrt{t}$ (since corrections to (F.4.36) are $O(1/\sqrt{t})$). We show in Fig. F.6 that this is the case for $\kappa^{(1)} = \kappa_0$ and $\kappa^{(2)} = \kappa_7$ and actually measure a faster decay as $1/t^{3/2}$.

F.7.2 In the large deviations regime.

In the ballistic regime we check the result (F.5.14) and (F.5.15). As a function of the angle φ the predictions are notably that, noting $F_t(\varphi) = -\log Z_t(\varphi)$ the free-energy of the DP,

$$\frac{F_t(\varphi)}{t} \xrightarrow{t \rightarrow \infty} c_\varphi, \quad \frac{(F_t(\varphi))^{2^c}}{8^{\frac{1}{3}} \lambda_\varphi^2} \xrightarrow{t \rightarrow \infty} Var(\chi_{GUE}) \quad (F.7.3)$$

where $Var(\chi_{GUE}) \simeq 0.813$ is the variance of the Tracy-Widom GUE distribution and in the case $\alpha = \beta = 1$ studied here the parameters c_φ and λ_φ given implicitly by (F.5.15) admits simple expressions (those were already obtain in [224] for the half-line to point problem):

$$c_\varphi = 1 - \sqrt{1 - 4\phi^2}, \quad \lambda_\varphi = \left(\frac{1}{8} \frac{2 \left(1 - \sqrt{1 - 4\phi^2}\right)^2}{\sqrt{1 - 4\phi^2}} \right)^{\frac{1}{3}} t^{\frac{1}{3}}. \quad (F.7.4)$$

These predictions are checked in Fig. F.7 and Fig. F.8 where we show both the dependence of these results on t (hence the convergence to the infinite time prediction) and on the angle at fixed $t = 2048$. The results are satisfying, though the convergence of the variance is slow as one approaches the optimal angle $\varphi = 0$ where the Gamma-type fluctuations studied previously slowly start to dominate for finite time observations.

We now check the prediction (F.5.14) for the full distribution of fluctuations that we now recall: it is predicted that the rescaled free-energy

$$\hat{f}_t(\varphi) = -\frac{-F_t(\varphi) + tc_\varphi}{2^{\frac{2}{3}} \lambda_\varphi}, \quad (F.7.5)$$

converges as $t \rightarrow \infty$ to $-\chi_{GUE}$ where χ_{GUE} is a RV distributed with the GUE Tracy-Widom distribution. This prediction is checked in Fig. F.8 for $t = 2048$ and $\varphi = \varphi_{13}$ by directly comparing the numerically obtained distribution of $-\hat{f}_{t=2918}(\varphi_{13})$ with the PDF of the GUE TW distribution. The agreement is satisfying. We also show in Fig. F.9 the convergence of the rescaled free-energy to the GUE Tracy-Widom distribution as a function of t .

F.8 Conclusion

In this paper we obtained using the Bethe ansatz, based on the results of [5], exact formulas for the statistical properties of the point to point partition sum of the Beta polymer, or equivalently for the PDF of a directed random walk in a Beta

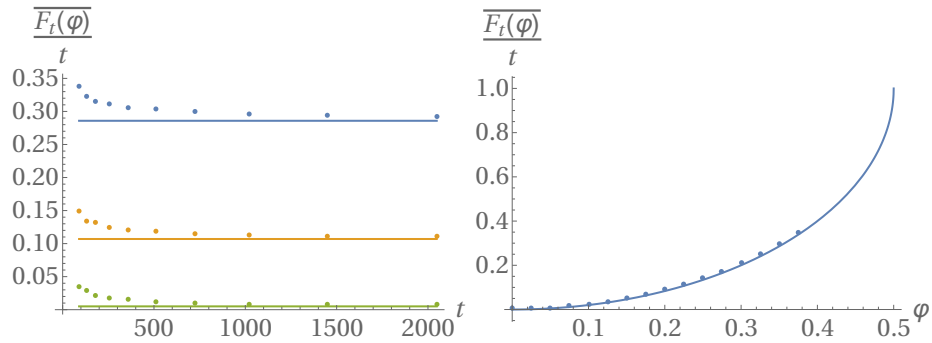


Figure F.7: Left: Dots: Empirical mean value $\overline{F_t(\varphi_i t)}/t$ as a function of t for $i = 2, 9, 14$ (green, orange and blue). Lines: asymptotic prediction (F.7.3). Right: Dots: Empirical mean value $\overline{F_{t=2048}(\varphi t)}/t$ as a function of φ . Line: asymptotic prediction (F.7.3). The numerical values for $\varphi \geq 0.4$ are not obtained due to numerical errors caused by the difficulty of dealing both with 'large' ($\sim 1/\sqrt{t}$) values of the partition sum at small φ and exponentially small ($\sim e^{-c\varphi t}$) values of the partition sum at large φ that are simply set to 0 by the algorithm. There are no fitting parameters..

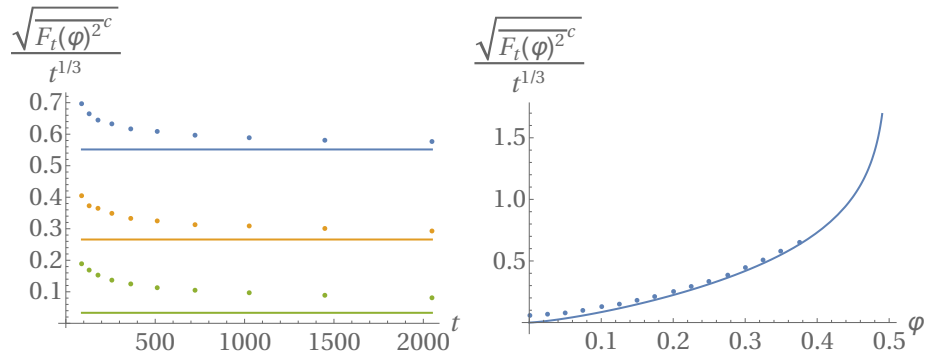


Figure F.8: Left: Dots: Empirical normalized standard deviation $\sqrt{F_t(\varphi_i t)^{2c}}/t^{1/3}$ as a function of t for $i = 2, 9, 14$ (green, orange and blue). Lines: asymptotic prediction (F.7.3). Right: Dots: Empirical normalized standard deviation $\sqrt{F_{t=2048}(\varphi_i t)^{2c}}/t^{1/3}$ as a function of φ . Line: asymptotic prediction (F.7.3). The numerical values for the largest values of φ are not obtained due to numerical errors, see Fig. F.7. There are no fitting parameters.

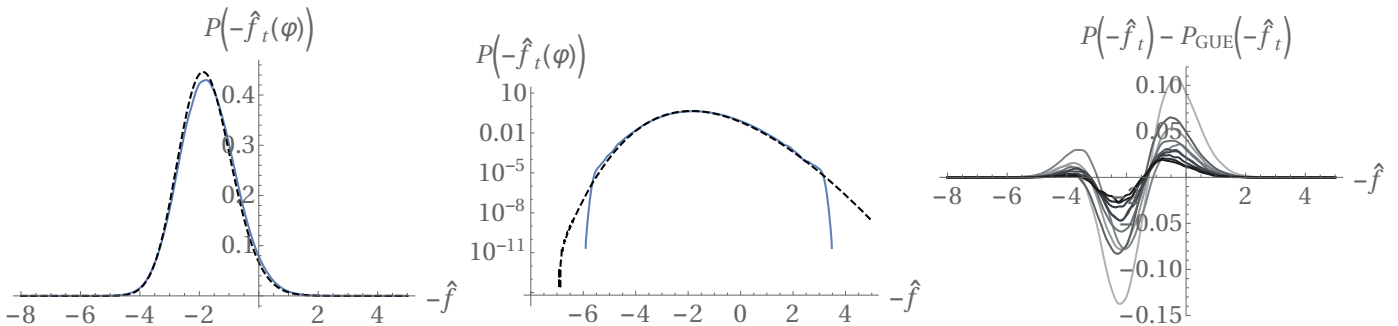


Figure F.9: Left : Blue line: Empirical PDF of $-\hat{f}_{t=2048}(\varphi_{13})$. Black-dashed line: PDF of a GUE Tracy-Widom distributed RV. Middle: same as left in a logarithmic scale. Right: Difference between the empirical PDF of $-\hat{f}_{t_i}(\varphi_{13})$ and the PDF of a GUE Tracy-Widom distributed RV for $i = 1, \dots, 10$ (from light-gray to black). There are no fitting parameters.

distributed random environment. These results complement the results of [224] where the half line to point partition sum, or equivalently the CDF of the RWRE, were considered and a different type of Bethe ansatz approach was used.

We first obtained in Sec. F.3 an exact formula for the moments of the point to point partition sum (F.3.27). This formula was derived using the Bethe ansatz with periodic boundary conditions on a line of length $L \rightarrow \infty$. This procedure highlighted the repulsive nature of the model, an interesting property that distinguishes this model from other exactly solvable models of directed polymers, and which was related to the RWRE interpretation of the model. Based on this formula we obtained in Sec. F.4 Cauchy-type Fredholm determinant formulas for the Laplace transform of the partition sum (F.4.7), (F.4.10), (F.4.12). Using these formulas we obtained asymptotic results for the PDF of the partition sum of the DP in the large time limit in the diffusive regime around the optimal direction of the RWRE. In this regime we showed that the distribution of a rescaled partition sum (F.4.28) converges to a Gamma distribution (F.4.30). This result was then extended to multi-point correlations (F.4.36). We therefore obtained a complete picture of the fluctuations in the diffusive regime around the optimal direction, the spatial region which, in the RWRE language, actually asymptotically contains all the probability. The results in this regime of fluctuations are qualitatively new, as they are different from the KPZ scaling unveiled in BC [224], and they open new perspectives in the study of RWRE.

We then obtained in Sec. F.5 an alternative formula for the moments of the partitions sum of the Beta polymer (F.5.8) expressed in terms of residues calculations. This formula allowed us to formally perform the asymptotic analysis in other directions (thus in the large deviations regime of the RWRE). There we showed that the fluctuations of the free energy of the polymer scale as $t^{1/3}$ and are distributed with the Tracy-Widom GUE distribution (F.5.14), a result expected from KPZ universality for point to point directed polymers. Interestingly we found that this result was formally equivalent to the result of [224] for the half line to point partition sum and therefore showed that the fluctuations of the PDF and of the CDF in the RWRE picture are identical up to $O(t^{1/3})$ included. Based on our results in both the large deviations regime and the optimal direction regime, we also discussed the very interesting crossover regime between them, and identified the crossover scale $x \sim t^{3/4}$.

In Sec. F.6 we discussed the relations between our approach and the approach of BC [224, 265] and justified a posteriori some results obtained using formal computations in Sec. F.5. Finally in Sec. F.7 we checked our main results using numerical simulations.

For future works it would be interesting to obtain a better understanding of the crossover regime between Gamma and Tracy-Widom fluctuations in this model. Another interesting aspect would be to understand the universality of our conclusions. In this spirit this work, together with [224], provides tools and results to analyze an exactly solvable model of RWRE which could serve as a testbed for future works on the subject.

We are very grateful to G. Barraquand and I. Corwin for useful remarks and discussions and for sharing their results with us. We also thank them for useful comments on a preliminary version of this manuscript. We acknowledge hospitality from the KITP in Santa Barbara where part of this work was conducted. This research was supported in part by the National Science Foundation under Grant No. NSF PHY11-25915. We acknowledge support from PSL grant ANR-10-IDEX-0001-02-PSL.

F.9 Appendix A: Fredholm determinant formula

In this appendix we show how to obtain the Fredholm determinant formula (F.4.7) starting from the moment formula (F.3.27). It is based on the following Cauchy determinant identity:

$$\prod_{1 \leq i < j \leq n} \frac{(k_i - k_j)^2}{(k_i - k_j)^2 + 1} = \det \left[\frac{1}{i(k_i - k_j) + 1} \right]_{n \times n}. \quad (\text{F.9.1})$$

This allows to rewrite $g_{t,x}(u)$ as, absorbing a factor 2 in the determinant,

$$\begin{aligned} g_{t,x}(u) &= \sum_{n=0}^{\infty} \frac{u^n}{n!} \prod_{j=1}^n \int_{\mathbb{R}} \frac{dk_j}{\pi} \det \left[\frac{1}{2i(k_i - k_j) + 2} \right]_{n \times n} \prod_{j=1}^n \frac{(ik_j + \frac{\beta - \alpha}{2})^t}{(ik_j + \frac{\alpha + \beta}{2})^{1+x} (ik_j - \frac{\alpha + \beta}{2})^{1-x+t}} \\ &= \sum_{\sigma \in S_n} (-1)^{|\sigma|} \sum_{n=0}^{\infty} \frac{u^n}{n!} \prod_{j=1}^n \int_{\mathbb{R}} \frac{dk_j}{\pi} \int_{v_j > 0} e^{-2v_j(i(k_j - k_{\sigma(j)}) + 1)} \frac{(ik_j + \frac{\beta - \alpha}{2})^t}{(ik_j + \frac{\alpha + \beta}{2})^{1+x} (ik_j - \frac{\alpha + \beta}{2})^{1-x+t}} \end{aligned} \quad (\text{F.9.2})$$

where from the first to second line we have rewritten the determinant as a sum over permutations and used the identity $1/z = \int_{v>0} e^{-vz}$, valid for $\text{Re}(z) > 0$. We then perform the change $\sum_j v_j k_{\sigma(j)}$ and relabel as $\sigma \rightarrow \sigma^{-1}$ to obtain

$$\begin{aligned} g_{t,x}(u) &= \sum_{\sigma \in S_n} (-1)^{|\sigma|} \sum_{n=0}^{\infty} \frac{u^n}{n!} \prod_{j=1}^n \int_{\mathbb{R}} \frac{dk_j}{\pi} \int_{v_j > 0} e^{-2ik_j(v_j - v_{\sigma(j)}) - (v_j + v_{\sigma(j)})} \frac{(ik_j + \frac{\beta - \alpha}{2})^t}{(ik_j + \frac{\alpha + \beta}{2})^{1+x} (ik_j - \frac{\alpha + \beta}{2})^{1-x+t}} \\ &= \sum_{n=0}^{\infty} \frac{u^n}{n!} \prod_{j=1}^n \int_{\mathbb{R}} \frac{dk_j}{\pi} \int_{v_j > 0} \det \left[\frac{e^{-2ik_j(v_j - v_i) - (v_j + v_i)}}{(ik_j + \frac{\alpha + \beta}{2})^{1+x} (ik_j - \frac{\alpha + \beta}{2})^{1-x+t}} \right]_{n \times n}, \end{aligned} \quad (\text{F.9.3})$$

and the last expression is exactly the Fredholm determinant expression associated with the kernel (F.4.7).

F.10 Appendix B: Probability distribution of $Z_t(x)$ for finite polymers lengths.

In this section we obtain, at least a formal level, a formula for the PDF of $Z_t(x)$ for arbitrary $(t, x) \in \mathbb{N}^2$. To do so, let us assume that $Z_t(x)$ can be written as the product of 3 independent ‘random variables’:

$$Z_t(x) = Z_1 Z_2 Z_3(t, x) . \quad (\text{F.10.1})$$

Where (i) Z_1 is distributed as an exponential distribution, i.e. its positive integer moments are $\overline{Z_1^n} = n!$; (ii) Z_2 is distributed as a Gamma variable with parameters $\alpha + \beta$, i.e. its moments are $\overline{Z_2^n} = \Gamma(\alpha + \beta + n)/\Gamma(\alpha + \beta)$; (iii) Z_3 is distributed according to an unknown density (which might not be a PDF) $P(Z_3)$ that we determine self-consistently below. Using the definition of $g_{t,x}(u)$ in (F.4.2), we obtain

$$g_{t,x}(u) = \sum_{n=0}^{\infty} \frac{(-u)^n \Gamma(\alpha + \beta)}{n! \Gamma(\alpha + \beta + n)} \overline{Z_t(x)^n} = \sum_{n=0}^{\infty} (-u)^n \overline{(Z_3(t, x))^n} = \int dZ_3 P(Z_3) \frac{1}{1 + u Z_3} . \quad (\text{F.10.2})$$

Assuming an analytical continuation of $g_{t,x}(u)$ we write,

$$g_{t,x} \left(\frac{1}{-v - i\epsilon} \right) = \int dZ_3 P(Z_3) \frac{-v}{Z_3 - v - i\epsilon} . \quad (\text{F.10.3})$$

And we obtain

$$P(Z_3) = \frac{1}{2i\pi v} \lim_{\epsilon \rightarrow 0^+} \left(g_{t,x} \left(\frac{1}{-v + i\epsilon} \right) - g_{t,x} \left(\frac{1}{-v - i\epsilon} \right) \right) . \quad (\text{F.10.4})$$

Hence, using the Fredholm determinant formulas for $g_{t,x}(u)$ (F.4.6), (F.4.9), (F.4.11) or also (F.6.11), one obtains $P(Z_3)$ by computing the limit (F.10.4). The distribution of $Z_t(x)$ is then obtained using (F.10.1).

F.11 Appendix C: Obtention of formula (F.5.8).

In this appendix we detail the heuristic reasoning that led to formula (F.5.8). It is based on the comparison of two equivalent formulas for the moments of the Strict-Weak polymer that we obtain in the first part of the Appendix. These formulas are obtained using either the fact that the Strict-Weak polymer can be obtained as a limit of the Inverse-Beta polymer or as a limit of the presently studied Beta polymer. More precisely, in the following we will use that,

$$Z_t^{SW}(x) = \lim_{\gamma \rightarrow \infty} \gamma^x Z_t^{IB}(x) , \quad (\text{F.11.1})$$

$$Z_t^{SW}(x) = \lim_{\alpha \rightarrow \infty} Z_t(x) . \quad (\text{F.11.2})$$

Where here,

1. $Z_t^{SW}(x)$ is the point-to-point partition sum of the so-called Strict-Weak polymer with disorder on horizontal weights only. It is a model defined similarly to the Beta polymer with $u = 1$ and $v \sim \text{Gamma}(\beta)$. We refer the reader to [219, 220] for more details on this model.
2. $Z_t^{IB}(x)$ is the point-to-point partition sum of the Inverse-Beta polymer with the same conventions as those of [5] and parameter $\gamma > 0$. We refer the reader to [5] for more details on this model, in particular the proof of the limit (F.11.1).
3. $Z_t(x)$ is the point-to-point partition sum of the Beta polymer studied in this paper. We refer the reader to [224] for the proof of the limit (F.11.2).

Using these two limits, we will obtain two equivalent formulas for $\overline{(Z_t^{SW}(x))^n}$ that will suggest a correspondence between two different types of residues expansion.

F.11.1 Two equivalent formulas for the Strict-Weak polymer

a From the Inverse-Beta to the Strict-Weak

In [5] we obtained a formal expression for the moments of the Strict-Weak polymer with horizontal weights. We recall here the full discussion for completeness. Starting from the moment formula of the Inverse-Beta polymer

$$\begin{aligned} \overline{Z_t^{IB}(x)^n} &= \frac{\Gamma(\gamma)}{\Gamma(\gamma - n)} n! \sum_{n_s=1}^n \frac{1}{n_s!} \sum_{(m_1, \dots, m_{n_s})_n} \prod_{j=1}^{n_s} \int_{-\infty}^{+\infty} \frac{dk_j}{2\pi} \prod_{1 \leq i < j \leq n_s} \frac{4(k_i - k_j)^2 + (m_i - m_j)^2}{4(k_i - k_j)^2 + (m_i + m_j)^2} \\ &\quad \prod_{j=1}^{n_s} \frac{1}{m_j} \left(\frac{\Gamma(-\frac{m_j}{2} + \frac{\gamma}{2} - ik_j)}{\Gamma(\frac{m_j}{2} + \frac{\gamma}{2} - ik_j)} \right)^{1+x} \left(\frac{\Gamma(-\frac{m_j}{2} + \frac{\gamma}{2} + ik_j)}{\Gamma(\frac{m_j}{2} + \frac{\gamma}{2} + ik_j)} \right)^{1-x+t} \left(\frac{\Gamma(\beta + ik_j + \frac{\gamma}{2} + \frac{m_j}{2})}{\Gamma(\beta + ik_j + \frac{\gamma}{2} - \frac{m_j}{2})} \right)^t , \end{aligned} \quad (\text{F.11.3})$$

We obtain a moment formula for the Strict-Weak polymer with initial condition $Z_t^{SW}(x=0) = \delta_{x,0}$ using the limit $\overline{(Z_t^{SW}(x))^n} = \lim_{\gamma \rightarrow \infty} \gamma^{nx} \overline{Z_t^{IB}(x)^n}$. The point-wise limit of the integrand cannot be simply taken and we need to first perform the change of variables $k_j \rightarrow k_j + i\frac{\gamma}{2}$. We obtain

$$\begin{aligned} \overline{(Z_t^{SW}(x))^n} &= \lim_{\gamma \rightarrow \infty} \frac{\Gamma(\gamma)}{\Gamma(\gamma - n)} \gamma^{nx} n! \sum_{n_s=1}^n \frac{1}{n_s!} \sum_{(m_1, \dots, m_{n_s})_n} \prod_{j=1}^{n_s} \int_{L^n} \frac{dk_j}{2\pi} \prod_{1 \leq i < j \leq n_s} \frac{4(k_i - k_j)^2 + (m_i - m_j)^2}{4(k_i - k_j)^2 + (m_i + m_j)^2} \\ &\prod_{j=1}^{n_s} \frac{1}{m_j} \left(\frac{\Gamma(-\frac{m_j}{2} + \gamma - ik_j)}{\Gamma(\frac{m_j}{2} + \gamma - ik_j)} \right)^{1+x} \left(\frac{\Gamma(-\frac{m_j}{2} + ik_j)}{\Gamma(\frac{m_j}{2} + ik_j)} \right)^{1-x+t} \left(\frac{\Gamma(\beta + ik_j + \frac{m_j}{2})}{\Gamma(\beta + ik_j - \frac{m_j}{2})} \right)^t. \end{aligned} \quad (\text{F.11.4})$$

Where $L = -i\frac{\gamma}{2} + \mathbb{R}$. Since the integral over k_j quickly converges as $O(1/k_j^{2m_j})$, we can now close the different contours of integrations on the upper half plane before taking the limit $\gamma \rightarrow \infty$. This leads to:

$$\begin{aligned} \text{form1} := \overline{(Z_t^{SW}(x))^n} &= n! \sum_{n_s=1}^n \frac{1}{n_s!} \sum_{(m_1, \dots, m_{n_s})_n} \prod_{j=1}^{n_s} \int_{\tilde{L}^n} \frac{dk_j}{2\pi} \prod_{1 \leq i < j \leq n_s} \frac{4(k_i - k_j)^2 + (m_i - m_j)^2}{4(k_i - k_j)^2 + (m_i + m_j)^2} \\ &\prod_{j=1}^{n_s} \frac{1}{m_j} \left(\frac{\Gamma(-\frac{m_j}{2} + ik_j)}{\Gamma(\frac{m_j}{2} + ik_j)} \right)^{1-x+t} \left(\frac{\Gamma(\beta + ik_j + \frac{m_j}{2})}{\Gamma(\beta + ik_j - \frac{m_j}{2})} \right)^t, \end{aligned} \quad (\text{F.11.5})$$

where \tilde{L} is an horizontal line that stays below all the poles of the integrand. This formula is formal because the resulting integral does not converge, but one must remember that we have formally already closed the contours of integrations. Computing the integral on k_i thus just amounts at taking the sum over the residues of all the poles of the integrand with a plus sign except those of the type $k_i = k_j - iA$ where $A > 0$ (since the contours have been closed on the upper half-plane).

b From the Beta to the Strict-Weak

We now obtain an alternative formula for $\overline{(Z_t^{SW}(x))^n}$, starting instead from the moment of the Beta polymer:

$$\overline{Z_t(x)^n} = (-1)^n \frac{\Gamma(\alpha + \beta + n)}{\Gamma(\alpha + \beta)} \prod_{j=1}^n \int_{-\infty}^{+\infty} \frac{dk_j}{2\pi} \prod_{1 \leq i < j \leq n} \frac{(k_i - k_j)^2}{(k_i - k_j)^2 + 1} \prod_{j=1}^n \frac{(ik_j + \frac{\beta - \alpha}{2})^t}{(ik_j + \frac{\alpha + \beta}{2})^{1+x} (ik_j - \frac{\alpha + \beta}{2})^{1-x+t}} \quad (\text{F.11.6})$$

And we use $\overline{(Z_t^{SW}(x))^n} = \lim_{\alpha \rightarrow \infty} \alpha^{nx} \overline{Z_t(x)^n}$. As before, the point-wise limit of the integrand cannot be taken and we need to take first $k_j = -i(\alpha + \beta)/2 + k'_j$ where $k'_j \in i(\alpha + \beta)/2 + \mathbb{R}$, successively close all the contours on the lower-half-plane and finally take the $\alpha \rightarrow \infty$ limit. In this way we obtain again a formal formula as

$$\text{form2} := \overline{(Z_t^{SW}(x))^n} = (-1)^n \prod_{j=1}^n \int_{L'} \frac{dk_j}{2\pi} \prod_{1 \leq i < j \leq n} \frac{(k_i - k_j)^2}{(k_i - k_j)^2 + 1} \prod_{j=1}^n \frac{(ik_j + \beta)^t}{(ik_j)^{1-x+t}} \quad (\text{F.11.7})$$

now L' is a straight line that stays above all the poles of the integrand. This is again true only in a formal sense given by residues calculation (since we have already closed all the contours on the lower half plane): computing the formal integral on k_i in (F.11.7) amounts at taking the sum over the residues of all the poles of the integrand with a minus sign except those of the type $k_i = k_j + i$.

F.11.2 A formal formula for the moments of the Beta polymer.

We now give the reasoning that leads to (F.5.8). The comparison of the two formal formulas (F.11.5) and (F.11.7) for the moments of the Strict-Weak polymer shows that there is a correspondence between two types of residues calculation.

Let us now do two remarks:

(i) We first note that in going from (F.11.7) to (F.11.5) the product terms in the integrand are formally changed as

$$ik_j + X \rightarrow \frac{\Gamma(ik_j + X + \frac{m_j}{2})}{\Gamma(ik_j + X - \frac{m_j}{2})}. \quad (\text{F.11.8})$$

(ii) We note that the difference between the formula for the moments of the Beta polymer and (F.11.7) is only that, for the moments of the Beta polymer, an additional

$$\prod_{j=1}^n \left(\frac{1}{ik_j + (\alpha + \beta)} \right)^{1+x} \quad (\text{F.11.9})$$

term is present in the product terms of the integrand. Furthermore, note that it is possible to evaluate the formula for $(Z_t(x))^n$ using only the residues taken into account in (F.11.7) and not those coming from (F.11.9).

The idea beneath (F.5.8) is thus just to add in (F.11.5) the equivalent of (F.11.9) in the product term of the integrand following the rule (F.11.8). That is we add to (F.11.5) the term

$$\prod_{j=1}^{n_s} \left(\frac{\Gamma\left(ik_j + (\alpha + \beta) - \frac{m_j}{2}\right)}{\Gamma\left(ik_j + (\alpha + \beta) + \frac{m_j}{2}\right)} \right)^{1+x}. \quad (\text{F.11.10})$$

And the residues taken into account in the calculation of (F.5.8) are exactly those taken into account in (F.11.5). Note that (F.5.8) can almost be obtained from the formula for the moments of the Inverse-Beta polymer (F.11.3) by using Euler's reflection formula on the first factor of Gamma function and putting $\gamma = 1 - \alpha - \beta$. In doing so however one obtains an additional unwanted $(-1)^m$ term.

F.12 Appendix D: Proof of a symmetrization identity

In this appendix we prove the formula (F.6.2) used in the main text. Let us show that, $\forall n \in \mathbb{N}$, $n \geq 2$ and $\forall (k_1, \dots, k_n) \in \mathbb{C}^n$

$$\frac{1}{n!} \sum_{\sigma \in S_n} \prod_{1 \leq i < j \leq n} \frac{k_{\sigma(i)} - k_{\sigma(j)}}{k_{\sigma(i)} - k_{\sigma(j)} + i} = \prod_{1 \leq i < j \leq n} \frac{(k_i - k_j)^2}{(k_i - k_j)^2 + 1}. \quad (\text{F.12.1})$$

We proceed by recurrence on n and prove (F.12.1) $\forall (k_1, \dots, k_n) \in \mathbb{C}^n$ distincts: this is sufficient since (F.12.1) is trivially true whenever two k_i are equal. The identity (F.12.1) is trivial for $n = 2$. Let us now see how the identity for some $n \geq 2$ imply the identity for $n + 1$. Since any permutation $\sigma \in S_{n+1}$ can be written in a unique way for some $m \in \{1, \dots, n+1\}$ as $\sigma = \tau_{m,n+1} \circ \bar{\sigma}$ with $\bar{\sigma}$ a permutation of S_{n+1} such that $\bar{\sigma}(n+1) = n+1$ (thus equivalent to a permutation of S_n) and $\tau_{m,n+1}$ the transposition $m \leftrightarrow n+1$ we have

$$\begin{aligned} & \frac{1}{(n+1)!} \sum_{\sigma \in S_{n+1}} \prod_{1 \leq i < j \leq n+1} \frac{k_{\sigma(i)} - k_{\sigma(j)}}{k_{\sigma(i)} - k_{\sigma(j)} + i} \\ &= \frac{1}{(n+1)!} \sum_{m=1}^{n+1} \sum_{\bar{\sigma} \in S_{n+1} | \bar{\sigma}(n+1)=n+1} \prod_{1 \leq i < j \leq n} \frac{k_{\tau_{m,n+1} \circ \bar{\sigma}(i)} - k_{\tau_{m,n+1} \circ \bar{\sigma}(j)}}{k_{\tau_{m,n+1} \circ \bar{\sigma}(i)} - k_{\tau_{m,n+1} \circ \bar{\sigma}(j)} + i} \prod_{i=1}^n \frac{k_{\tau_{m,n+1} \circ \bar{\sigma}(i)} - k_{\tau_{m,n+1} \circ \bar{\sigma}(n+1)}}{k_{\tau_{m,n+1} \circ \bar{\sigma}(i)} - k_{\tau_{m,n+1} \circ \bar{\sigma}(n+1)} + i} \\ &= \frac{1}{(n+1)!} \sum_{m=1}^{n+1} \sum_{\bar{\sigma} \in S_{n+1} | \bar{\sigma}(n+1)=n+1} \prod_{1 \leq i < j \leq n} \frac{k_{\tau_{m,n+1} \circ \bar{\sigma}(i)} - k_{\tau_{m,n+1} \circ \bar{\sigma}(j)}}{k_{\tau_{m,n+1} \circ \bar{\sigma}(i)} - k_{\tau_{m,n+1} \circ \bar{\sigma}(j)} + i} \prod_{i=1, i \neq m}^{n+1} \frac{k_i - k_m}{k_i - k_m + i} \\ &= \frac{n!}{(n+1)!} \sum_{m=1}^{n+1} \prod_{1 \leq i < j \leq n} \frac{(k_{\tau_{m,n+1}(i)} - k_{\tau_{m,n+1}(j)})^2}{(k_{\tau_{m,n+1}(i)} - k_{\tau_{m,n+1}(j)})^2 + 1} \prod_{i=1, i \neq m}^{n+1} \frac{k_i - k_m}{k_i - k_m + i} \quad (\text{F.12.2}) \\ &= \frac{1}{n+1} \sum_{m=1}^{n+1} \prod_{1 \leq i < j \leq n} \frac{(k_{\tau_{m,n+1}(i)} - k_{\tau_{m,n+1}(j)})^2}{(k_{\tau_{m,n+1}(i)} - k_{\tau_{m,n+1}(j)})^2 + 1} \prod_{i=1}^{m-1} \frac{k_i - k_m}{k_i - k_m + i} \prod_{i=m+1}^{n+1} \frac{k_m - k_i}{k_m - k_i - i} \\ &= \frac{1}{n+1} \sum_{m=1}^{n+1} \prod_{1 \leq i < j \leq n} \frac{(k_{\tau_{m,n+1}(i)} - k_{\tau_{m,n+1}(j)})^2}{(k_{\tau_{m,n+1}(i)} - k_{\tau_{m,n+1}(j)})^2 + 1} \prod_{i=1}^{m-1} \frac{(k_i - k_m)^2}{(k_i - k_m)^2 + 1} \prod_{i=m+1}^{n+1} \frac{(k_m - k_i)^2}{(k_m - k_i)^2 + 1} \\ &\quad \times \prod_{i=1}^{m-1} \frac{k_i - k_m - i}{k_i - k_m} \prod_{i=m+1}^{n+1} \frac{k_m - k_i + i}{k_m - k_i} \\ &= \frac{1}{n+1} \sum_{m=1}^{n+1} \prod_{1 \leq i < j \leq n+1} \frac{(k_i - k_j)^2}{(k_i - k_j)^2 + 1} \prod_{i=1}^{m-1} \frac{k_i - k_m - i}{k_i - k_m} \prod_{i=m+1}^{n+1} \frac{k_m - k_i + i}{k_m - k_i} \\ &= \left(\prod_{1 \leq i < j \leq n+1} \frac{(k_i - k_j)^2}{(k_i - k_j)^2 + 1} \right) \psi(k_1, \dots, k_{n+1}) \quad (\text{F.12.3}) \end{aligned}$$

Where in (F.12.3) we have used the recursion hypothesis and we have defined

$$\psi(k_1, \dots, k_{n+1}) = \frac{1}{n+1} \sum_{m=1}^{n+1} \prod_{i=1}^{m-1} \frac{k_i - k_m - i}{k_i - k_m} \prod_{i=m+1}^{n+1} \frac{k_m - k_i + i}{k_m - k_i}. \quad (\text{F.12.4})$$

Note also that in the above derivation we have taken the liberty to write products on empty set: such a product is obviously interpreted as 1. To show (F.12.1) it remains to show that ψ is constant and equal to 1 $\forall (k_1, \dots, k_{n+1}) \in \mathbb{C}^{n+1}$ distincts. Let us first show that $\psi(k_1, \dots, k_{n+1})$ is analytic in k_1 on \mathbb{C} . The only thing to do is to prove that $\forall j \in \{2, \dots, n+1\}$, the residue of $\psi(k_1, \dots, k_n + 1)$ at $k_1 = k_j$ is actually 0. It is obvious that the possible pole at $k_1 = k_j$ is at most of order

1. Let us thus write $k_1 = k_j + \delta k$ and focus on the term of order $1/\delta k$ in (F.12.4). These terms only come from the term $m = 1$ and $m = j$ in the sum over m . We obtain

$$\begin{aligned}
\psi(k_j + \delta k, \dots, k_{n+1}) &= \frac{1}{n+1} \left(\prod_{i=2}^{n+1} \frac{k_j + \delta k - k_i + i}{k_j + \delta k - k_i} + \frac{k_j + \delta k - k_j - i}{k_j + \delta k - k_j} \prod_{i=2}^{j-1} \frac{k_i - k_j - i}{k_i - k_j} \prod_{i=j+1}^{n+1} \frac{k_j - k_i + i}{k_j - k_i} \right) + O(1) \\
&= \frac{i}{n+1} \left(\prod_{i=2, i \neq j}^{n+1} \frac{k_j - k_i + i}{k_j - k_i} - \prod_{i=2}^{j-1} \frac{k_i - k_j - i}{k_i - k_j} \prod_{i=j+1}^{n+1} \frac{k_j - k_i + i}{k_j - k_i} \right) \frac{1}{\delta k} + O(1) \\
&= O(1) .
\end{aligned} \tag{F.12.5}$$

Where again we have used the convention that a product on an empty set is 1. Hence $\psi(k_j + \delta k, \dots, k_{n+1})$ has no poles and is analytic on \mathbb{C} . Finally, it is obvious that

$$\lim_{|k_1| \rightarrow \infty} \psi(k_1, \dots, k_{n+1}) = 1 . \tag{F.12.6}$$

Hence, $\psi(k_1, \dots, k_{n+1})$ is analytic and is necessarily bounded. It is thus constant and equal to its limit as $|k_1| \rightarrow \infty$ and thus $\psi(k_1, \dots, k_{n+1}) = 1 \forall (k_1, \dots, k_{n+1}) \in \mathbb{C}^{n+1}$. This terminates the proof of (F.12.1).

Appendix G

Paper: Stationary measures for two dual families of finite and zero temperature models of directed polymers on the square lattice

The following is essentially the article published as

Title: Stationary measures for two dual families of finite and zero temperature models of directed polymers on the square lattice

Authors: Thimothée Thiery

ArXiv: 1604.07995

Journal-Ref: Journal of Statistical Physics, 2016

Abstract: We study the recently introduced Inverse-Beta polymer, an exactly solvable, anisotropic finite temperature model of directed polymer on the square lattice, and obtain its stationary measure. In parallel we introduce an anisotropic zero temperature model of directed polymer on the square lattice, the Bernoulli-Geometric polymer, and obtain its stationary measure. This new exactly solvable model is dual to the Inverse-Beta polymer and interpolates between models of first and last passage percolation on the square lattice. Both stationary measures are shown to satisfy detailed balance. We also obtain the asymptotic mean value of (i) the free-energy of the Inverse-Beta polymer; (ii) the optimal energy of the Bernoulli-Geometric polymer. We discuss the convergence of both models to their stationary state. We perform simulations of the Bernoulli-Geometric polymer that confirm our results.

G.1 Introduction

The directed polymer (DP) problem, i.e. the statistical mechanics problem of directed paths in a random environment, has been the subject of intense studies both from the physics and mathematics community (see e.g. [40, 201] for early physics work). The DP is a classical example of equilibrium statistical mechanics of disordered systems, but its importance goes well beyond this field, notably because of its connection with the Kardar-Parisi-Zhang (KPZ) universality class [33] (for recent reviews see [151, 35, 34]). In the field of DPs in dimension $1 + 1$, important progresses have been possible thanks to the existence of models with *exact solvability properties*, that is models for which, for one or several reasons, exact computations are possible. Examples of such properties include notably Bethe ansatz (BA) integrability, existence of combinatorial mappings (Robinson-Schensted-Knuth (RSK) correspondence and geometric RSK (gRSK) correspondence) and the exact solvability property (ESP) which is the focus of this work, *an exactly known stationary measure* (SM). A given model can have one or several of those properties. The continuum directed polymer is BA solvable [201] and its SM is also known: starting from an initial condition such that the free-energy of the DP performs a Brownian motion, it remains so at all time [248, 195]. Geometric and exponential last passage percolation are exactly solvable using the RSK correspondence [159], can also be mapped (see e.g. [160]) onto the totally asymmetric exclusion process (TASEP), which is exactly solvable by BA, and its SM is also exactly known. The first discovered exactly solvable model of DP on the square lattice at finite temperature, the Log-Gamma polymer, was introduced because of the possibility of writing down exactly its SM [197]. It was later shown that the model was exactly solvable using the gRSK correspondence [198] and also the BA [4]. The shortly after introduced Strict-Weak polymer also enjoy all three properties [219, 220] while for the recently discovered Beta [224, 6] and Inverse-Beta polymer [5] only BA solvability has been shown (although a work on the SM of the Beta polymer is currently in preparation [267]).

The links between these different types of ESPs are not yet understood. As such the discovery of an ESP in a model is of great interest, even when the model already has one known ESP. This is true from a mathematical point of view since these properties are signs of a rich underlying mathematical structure, but it is also important from the perspective of calculating relevant physical observables since each ESP has interesting applications. In particular, although most of the recent focus in exactly solvable models of DP has been on the derivation of exact distribution of fluctuations of the free-energy at large scale, an information which is not contained in the SM and for which RSK/gRSK correspondence [159, 218, 220] and BA

solvability [173, 165, 6, 5, 224, 4] are more adapted, the exact knowledge of the SM is of great interest. The SM indeed contains information on the multi-point correlations of the DP free-energy at large scale. These are notoriously hard to obtain using other analytical techniques. More generally the SM allows to study different questions in a complementary fashion to other ESPs. An important historical example of application of the knowledge of the SM of the continuum DP can be found in [248, 195]: together with the Galilean invariance, it provided the first (and probably still the simplest) derivation of the critical exponents of the KPZ universality class. More recently in the Log-Gamma case, the SM was e.g. used to obtain a rigorous derivation of the critical exponents of the DP [197], or also to derive a precise characterization of the localization properties of the DP [229].

The goal of this paper is twofold. First we obtain the stationary measure of the recently discovered Inverse-Beta polymer. In a few words in the stationary state the free-energy of the DP performs a random walk with Inverse-Beta distributed increments, thus generalizing in a discrete setting the stationary measure of the continuum DP. The existence of this stationary measure is rather natural since the Inverse-Beta polymer is an anisotropic finite temperature model (with two parameters $\gamma, \beta > 0$) of DP on the square lattice which in different limits converges in law to the Log-Gamma ($\beta \rightarrow \infty$, the isotropic limit) and Strict-Weak polymer ($\gamma \rightarrow \infty$, the strongly anisotropic limit). These two models possess an exactly known SM that we will generalize to the Inverse-Beta polymer, and our approach will have a strong methodological and conceptual overlap with the one used by Seppäläinen in [197]. Secondly we introduce a new anisotropic 0 temperature model of DP on the square lattice (with two parameters $q, q' \in [0, 1]$), which we call the Bernoulli-Geometric polymer, and obtain exactly its stationary measure. This model interpolates between the exactly solvable geometric *first* passage percolation problem studied in [216] (in the $q \rightarrow 0$ limit) and the geometric *last* passage percolation problem e.g. studied in [159] (in the $q' \rightarrow 0$ limit). The existence of this model was already suggested in [5] following the fact that a 0 temperature limit ($\gamma = \epsilon\gamma', \beta = \epsilon\beta'$ and $\epsilon \rightarrow 0$) of the Inverse-Beta polymer gave an anisotropic generalization of *exponential* last passage percolation. Since (isotropic) last passage percolation is exactly solvable both for geometric and exponential distribution of random waiting times (the exponential case being the limit $q = 1 - \gamma'\epsilon$ with $\epsilon \rightarrow 0$ of the geometric case), it was rather natural to conjecture that an exactly solvable anisotropic generalization of *geometric* last passage percolation should exist. This motivated the search for such a model. The Bernoulli-Geometric polymer introduced in this paper appears as this missing model, and we thus complement the rich universe of exactly solvable models of DP on the square lattice (see Fig. G.1). For the finite temperature case in particular, the only known model not present in this framework is the Beta polymer, which somehow lives in a different class since it has the peculiarity of also being a model of random walk in a random environment [224, 6].

Before we give the main results of the paper and define the Inverse-Beta and Bernoulli-Geometric polymers in Sec. G.3, let us start by explaining more precisely the general question that is tackled in this article on a simpler model.

G.2 Recall: stationary measure of the Log-Gamma polymer

In this section for pedagogical purposes we recall the stationary measure of the Log-Gamma polymer. The results that we obtain on the stationary measure of the Inverse-Beta polymer can be seen as a generalization of the known results presented in this section to a richer model, and we believe it can be useful for non-specialists to first recall here those simpler results. Specialists on the other hand are encouraged to jump directly to Sec. G.3.

Let us first consider the case of an abstract, homogeneous model of directed polymer on the square lattice with on-site disorder: the random environment is defined by drawing random Boltzmann weights $W_{x_1, x_2} > 0$ at each point (x_1, x_2) of \mathbb{N}^2 . Boltzmann weights on different lattice sites are supposed to be independent and homogeneously distributed as a positive random variable (RV) W with a probability distribution function $P_W(W)$. The partition sum of DP with starting point $(x_1, x_2) = (0, 0)$ and endpoint $(x_1, x_2) \in \mathbb{N}^2$ is defined by

$$Z_{x_1, x_2} := \sum_{\pi: (0,0) \rightarrow (x_1, x_2)} \prod_{(x'_1, x'_2) \in \pi} W_{x'_1, x'_2}, \quad (\text{G.2.1})$$

where the sum $\sum_{\pi: (0,0) \rightarrow (x_1, x_2)}$ is over all directed paths, also called up-right paths, from $(0, 0)$ to (x_1, x_2) . Those are the paths such that the only jumps allowed are to the right, i.e. as $(x_1, x_2) \rightarrow (x_1 + 1, x_2)$ or upward, i.e. as $(x_1, x_2) \rightarrow (x_1, x_2 + 1)$ (see Fig. G.2). For a given model of DP, one would like e.g. to characterize the asymptotic properties of Z_{x_1, x_2} in the limit of long polymers $t = x_1 + x_2 \rightarrow \infty$. In this paper we focus on the horizontal and vertical ratios of partition sums defined as

$$U_{x_1, x_2} := \frac{Z_{x_1, x_2}}{Z_{x_1-1, x_2}}, \quad V_{x_1, x_2} := \frac{Z_{x_1, x_2}}{Z_{x_1, x_2-1}}. \quad (\text{G.2.2})$$

Introducing the variables $t = x_1 + x_2$ (the length of the polymers) and $x = x_1$ and the notations $U_t(x) := U_{x, t-x}$ and $V_t(x) := V_{x, t-x}$, we are interested in obtaining the distribution of these RVs in the limit of long polymers in a given direction. That is, for a given $\varphi \in]-1/2, 1/2[$ (see Fig. G.2) and $\forall T \in \mathbb{N}^*, X \in \mathbb{N}^*$, we are interested in the set of RVs

$$\left(\tilde{U}_{t'}(x'), \tilde{V}_{t'}(x') \right)_{t' \in [0, T], x' \in [-X, X]} := \lim_{t \rightarrow \infty} \left(U_{t+t'}((1/2 + \varphi)t + x'), V_{t+t'}((1/2 + \varphi)t + x') \right)_{t' \in [0, T], x' \in [-X, X]}. \quad (\text{G.2.3})$$

The only known finite temperature model of DP on \mathbb{Z}^2 with on-site disorder (i.e. defined as above) for which characterizing exactly the properties of the asymptotic process $(\tilde{U}_{t'}(x'), \tilde{V}_{t'}(x'))_{t' \in [0, T], x' \in [-X, X]}$ is possible is the Log-Gamma polymer. In this case, the random Boltzmann weights are distributed as the inverse of a gamma random variable: $W \sim \text{Gamma}(\gamma)^{-1}$. Here \sim means ‘distributed as’ and we recall that a RV x is gamma distributed with parameter $\alpha > 0$ if its PDF is

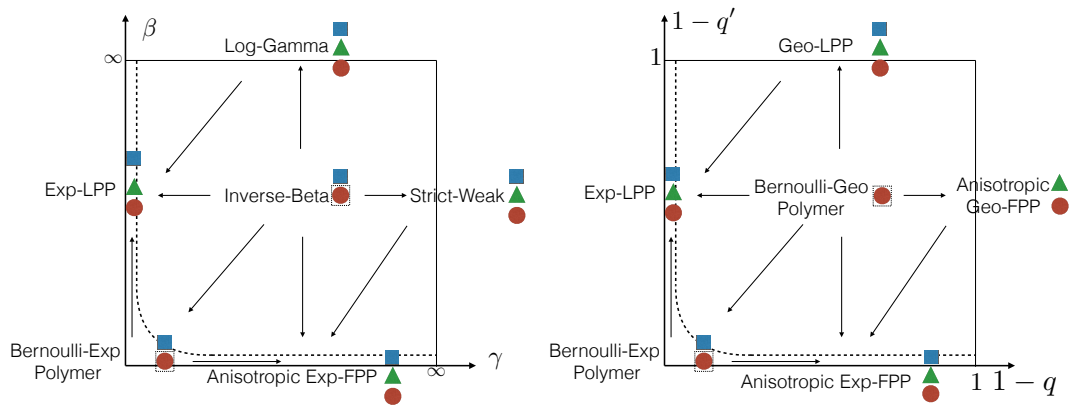


Figure G.1: The Inverse-Beta polymer is at the center of a large class of finite temperature exactly solvable models of DP on the square lattice with continuous random energies (left), but also admits zero-temperature limiting models (‘below the dashed-line’, in the limit $\min(\gamma, \beta) \rightarrow 0$). Conversely, the Bernoulli-Geometric polymer introduced in this paper is at the center of a large class of zero-temperature models of DP on the square lattice with discrete random energies (left), but it also admits limiting models with continuous energies (‘below the dashed-line’, in the limit $\max(q, q') \rightarrow 1$), which coincide with the limiting zero-temperature models of the Inverse-Beta polymer. Arrows indicate the possibility of taking a limit from one model to another. The models shown in this picture are defined in Sec. G.3, Sec. G.4.4 and Sec. G.5.2. Different known exact solvability properties of the various models are here indicated by blue squares for BA solvability, green triangles for RSK or gRSK solvability and by red dots for exactly known stationary measures. The red dots enclosed by a dashed-line (as well as the definition of the Bernoulli-Geometric polymer) are some of the results of this work.

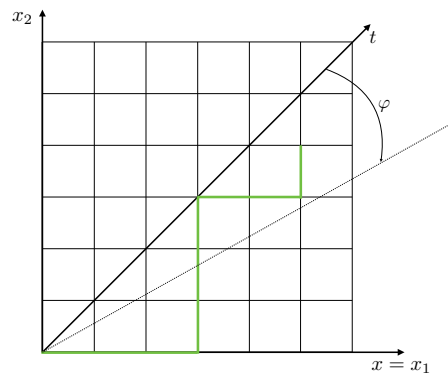


Figure G.2: A model of directed polymer on \mathbb{Z}^2 . Green: an admissible (i.e. up/right) polymer path of length $t = 9$ with starting point $(0, 0)$ and endpoint $(x_1, x_2) = (5, 4)$. We are interested in the stationarity properties that are reached in the limit of long polymers in a given direction φ .

$p(x) = \frac{1}{\Gamma(\alpha)} x^{-1+\alpha} e^{-x} \theta(x)$ (Γ is the Euler's gamma function and θ is the Heaviside theta function). For this special choice of distribution, although it is not mathematically fully proven, the (mathematically rigorous) results of [197, 268] lead to the conjecture that in this case

At fixed $t' \in [0, T]$ the variables $(\tilde{U}_{t'}(x'))_{x' \in [-X, X]}$ and $(\tilde{V}_{t'}(x'))_{x' \in [-X, X]}$ are all independent and distributed as $\tilde{U}_{t'}(x') \sim \text{Gamma}(\gamma - \lambda)^{-1}$ and $\tilde{V}_{t'}(x') \sim \text{Gamma}(\lambda)^{-1}$. The additional parameter $\lambda \in]0, \gamma[$ depends on φ and is the solution of the equation $0 = -(1/2 + \varphi)\psi'(\gamma - \lambda) + (1/2 - \varphi)\psi'(\lambda)$, where $\psi(x) = \Gamma'(x)/\Gamma(x)$ is the digamma function.

An additional property of reversibility of the process is known from [197]. These properties rely on a non trivial property of gamma distributions (see Lemma 3.2 in [197]). Moreover, Lemma 3.2 of [197] also suggests that the Log-Gamma polymer is the only model with on-site disorder for which it is possible to obtain exactly the stationary measure. One of the purposes of this paper is to show that it is also possible to obtain exactly the stationary measure in the Inverse-Beta polymer, an anisotropic finite temperature model of DP on \mathbb{Z}^2 with on-edge disorder that generalizes both the Log-Gamma and Strict-Weak models. We also obtain similar results for the Bernoulli-Geometric polymer, a related zero temperature model that we introduce in this paper.

G.3 Overview: definitions, main results and outline

G.3.1 Definitions of the models of directed polymers

a General notations

All the models of DPs considered in this paper live on the square lattice \mathbb{Z}^2 . We will consider two coordinate systems on \mathbb{Z}^2 , the usual Euclidean coordinates $(x_1, x_2) \in \mathbb{Z}^2$ and the (t, x) coordinates $t = x_1 + x_2$ and $x = x_1$ (see Fig.G.3). The variable t will often corresponds to the length of the polymers. To avoid confusion, an arbitrary real function on the lattice, $f : (x_1, x_2) \in \mathbb{Z}^2 \rightarrow f(x_1, x_2) \in \mathbb{R}$ will be denoted either as $f_{x_1, x_2} := f(x_1, x_2)$, or as $f_t(x) = f(x_1 = x, x_2 = t - x)$. The random environment will live on the *edges* of \mathbb{Z}^2 and we will generally note by e an edge of \mathbb{Z}^2 .

b Finite temperature models: The Inverse-Beta polymer(s)

We now define three versions of the Inverse-Beta (IB) polymer. The first is the usual point to point IB polymer introduced in [5]. Its partition sum will be noted Z_{x_1, x_2} . The second is the IB polymer with boundaries, a model which possesses a stationarity property and whose definition is original to this work. Its partition sum will be noted \hat{Z}_{x_1, x_2} . The third model is the IB polymer with a stationary initial condition, with partition sum \check{Z}_{x_1, x_2} , which also possesses a stationary property and whose definition is original to this work. It is intimately linked with the IB polymer with boundaries and is closer in spirit to the stationary models considered for the continuum DP. The first model will be defined by choosing *two* parameters $(\gamma, \beta) \in \mathbb{R}_+^2$ (henceforth referred to as the bulk parameters). The others have one additional parameter $\lambda \in]0, \gamma[$, which will specify one stationary measure among a family of stationary measures at fixed (γ, β) (henceforth referred to as the stationarity or boundary parameter). Throughout this work the use of the hat and check notations will permit to distinguish between quantities associated to each model.

Definition G.3.1. The point to point IB polymer We recall here the definition of the point to point IB polymer partition sum as studied using Bethe ansatz in [5]. To each vertex $(x_1, x_2) \in \mathbb{Z}^2$ of the square lattice is associated a random variable $W_{x_1, x_2} \in \mathbb{R}_+$. The set of RVs $\{W_{x_1, x_2}, (x_1, x_2) \in \mathbb{Z}^2\}$ consists of independent, identically distributed (iid) RVs distributed as $W \sim \frac{1}{B} - 1$ where $B \in [0, 1]$ is a Beta RV of parameters γ and $\beta > 0$. The PDF $P(B)$ of a Beta random variable is

$$B \sim \text{Beta}(\gamma, \beta) \iff P(B) = \frac{\Gamma(\gamma + \beta)}{\Gamma(\gamma)\Gamma(\beta)} B^{\gamma-1} (1-B)^{\beta-1} \theta(B) \theta(1-B), \quad (\text{G.3.1})$$

where here and throughout the rest of the paper \sim means 'distributed as', Γ is the Euler's gamma function and θ is the Heaviside theta function. Given a random environment specified by a drawing of W_{x_1, x_2} at each vertex $(x_1, x_2) \in \mathbb{Z}^2$, we associate to each edge of the square lattice e a random Boltzmann weight (BW) $w(e)$ as follows. The random BWs $w(e)$ on horizontal (resp. vertical) edges will be denoted by the letter u (resp. v) and indexed by the vertex to which they lead (see left of Fig. G.3 and beware that we use here the opposite convention compared to [5]), and given in terms of W_{x_1, x_2} by

$$\begin{aligned} w((x_1 - 1, x_2) \rightarrow (x_1, x_2)) &= u_{x_1, x_2} = W_{x_1, x_2} > 0, \\ w((x_1 - 1, x_2) \rightarrow (x_1, x_2)) &= v_{x_1, x_2} = W_{x_1, x_2} + 1 > 1. \end{aligned} \quad (\text{G.3.2})$$

Hence in this model the BWs on different edges are correlated if and only if they lead to the same vertex, since in this case $v = u + 1$, and the vertical direction is always favored compared to the horizontal one. The model is thus anisotropic. It interpolates between two other known exactly solvable models of DP on \mathbb{Z}^2 : the Log-Gamma polymer (isotropic $\beta \rightarrow \infty$ limit) and the Strict-Weak polymer ($\gamma \rightarrow \infty$ limit, see Sec. G.4.4). Let us write here for clarity the PDF of W , noted $P_W(W)$:

$$W \sim \frac{1}{\text{Beta}(\gamma, \beta)} - 1 > 0 \quad , \quad P_W(W) = \frac{\Gamma(\gamma + \beta)}{\Gamma(\gamma)\Gamma(\beta)} \left(1 - \frac{1}{W+1}\right)^{\beta-1} \left(\frac{1}{W+1}\right)^{\gamma+1} \theta(W). \quad (\text{G.3.3})$$

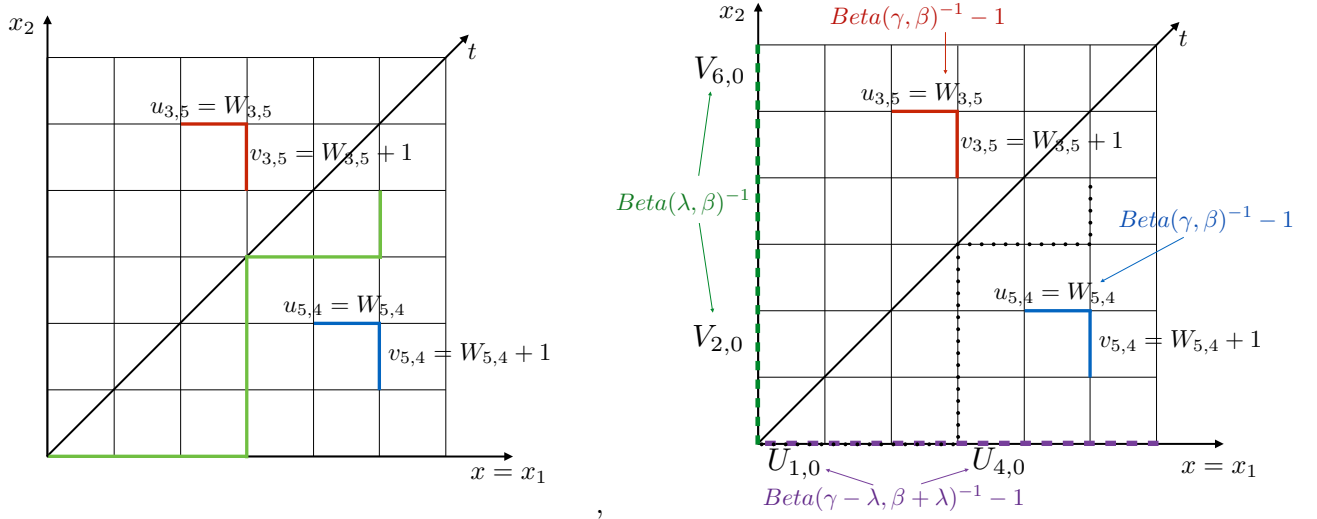


Figure G.3: Left: The point to point Inverse-Beta polymer. Blue (resp. Red) : couple of correlated Boltzmann weights on edges arriving at $(x_1, x_2) = (5, 4)$ (resp. $(x_1, x_2) = (3, 4)$). Green: an admissible (i.e. up/right) polymer path of length $t = 9$ with starting point $(0, 0)$ and endpoint $(x_1, x_2) = (5, 4)$. Right: The Inverse-Beta polymer with boundaries. The Boltzmann weights in the bulk (blue and red) are the same as in the model without boundaries and are distributed as in (G.3.3). The random Boltzmann weights on the vertical (dashed-green) and horizontal (dashed-purple) boundaries are distributed as in (G.3.7). The dotted line represents a possible polymer path from $(x_1, x_2) = (0, 0)$ to $(x_1, x_2) = (5, 4)$.

Given a random environment, the partition sum of the point-to-point IB polymer with starting point $(0, 0)$ and endpoint $(x_1 \geq 0, x_2 \geq 0)$ is defined as

$$Z_{x_1, x_2} = \sum_{\pi: (0,0) \rightarrow (x_1, x_2)} \prod_{e \in \pi} w(e), \quad (\text{G.3.4})$$

where here and throughout the rest of this work the sum $\sum_{\pi: (0,0) \rightarrow (x_1, x_2)}$ is over all directed paths, also called up-right paths, from $(0, 0)$ to (x_1, x_2) . Those are the paths such that the only jumps allowed are either to the right, i.e. as $(x_1, x_2) \rightarrow (x_1 + 1, x_2)$, or upward, i.e. as $(x_1, x_2) \rightarrow (x_1, x_2 + 1)$ (see Fig. G.3). Equivalently, using the (t, x) coordinate system the partition sum $Z_t(x) = Z_{x, t-x}$ is defined recursively as, for $t \geq 0$,

$$\begin{aligned} Z_t(x) &= u_t(x)Z_{t-1}(x-1) + v_t(x)Z_{t-1}(x) \quad \text{for } t \geq 1 \\ Z_{t=0}(x) &= \delta_{x,0}, \end{aligned} \quad (\text{G.3.5})$$

where $\delta_{i,j}$ is the Kronecker delta symbol. Following (G.3.5), the length of the polymers t will also be thought of as a time-like variable, (G.3.5) being then thought of as a Markov process. The latter is a discrete version of the stochastic-heat-equation satisfied by the partition sum of the continuum DP.

Definition G.3.2. The IB polymer with boundaries We define a second version of the IB polymer by changing the BWs on the boundaries of \mathbb{N}^2 . The random BWs are now denoted by $\hat{w}(e)$ and given by

$$\begin{aligned} \hat{w}((x_1 - 1, x_2) \rightarrow (x_1, x_2)) &= u_{x_1, x_2} = W_{x_1, x_2} > 0 \quad , \quad \text{if } x_2 \geq 1, \\ \hat{w}((x_1, x_2 - 1) \rightarrow (x_1, x_2)) &= v_{x_1, x_2} = W_{x_1, x_2} + 1 > 1 \quad , \quad \text{if } x_1 \geq 1, \\ \hat{w}((x_1 - 1, 0) \rightarrow (x_1, 0)) &= U_{x_1, 0}, \\ \hat{w}((0, x_2 - 1) \rightarrow (0, x_2)) &= V_{0, x_2}. \end{aligned} \quad (\text{G.3.6})$$

Here the random BWs in the bulk $u_{x_1, x_2} = W_{x_1, x_2}$ and $v_{x_1, x_2} = W_{x_1, x_2} + 1$ for $x_1, x_2 \geq 1$ are distributed as before (see (G.3.2)), and the BWs on the boundaries are all independent and distributed as $U_{x_1, 0} \sim U$ and $V_{0, x_2} \sim V$ where

$$\begin{aligned} U &\sim \frac{1}{\text{Beta}(\gamma - \lambda, \beta + \lambda)} - 1 > 0 \quad , \quad P_U(U) = \frac{\Gamma(\gamma + \beta)}{\Gamma(\gamma - \lambda)\Gamma(\beta + \lambda)} \left(1 - \frac{1}{U+1}\right)^{\beta + \lambda - 1} \left(\frac{1}{U+1}\right)^{\gamma - \lambda + 1} \theta(U), \\ V &\sim \frac{1}{\text{Beta}(\lambda, \beta)} > 1 \quad , \quad P_V(V) = \frac{\Gamma(\lambda + \beta)}{\Gamma(\lambda)\Gamma(\beta)} \left(1 - \frac{1}{V}\right)^{\beta - 1} \left(\frac{1}{V}\right)^{\lambda + 1} \theta(V - 1). \end{aligned} \quad (\text{G.3.7})$$

Here $0 < \lambda < \gamma$ is an additional parameter and we have written explicitly the PDF $P_U(U)$ and $P_V(V)$ of U and V that easily follow from (G.3.1). In the following we will refer to λ as the boundary or stationarity parameter. We consider again

the partition sum for polymers with starting point $(0, 0)$ and endpoint $(x_1 \geq 0, x_2 \geq 0)$, defined as

$$\hat{Z}_{x_1, x_2} = \sum_{\pi: (0,0) \rightarrow (x_1, x_2)} \prod_{e \in \pi} \hat{w}(e). \quad (\text{G.3.8})$$

Definition G.3.3. The IB polymer with stationary initial condition We define a third version of the IB polymer. Following the recursion equation (G.3.5), we define the DP partition sum $\check{Z}_t(x)$ for $t \geq -1$ and $x \in \mathbb{Z}$ as

$$\check{Z}_t(x) = u_t(x)\check{Z}_{t-1}(x-1) + v_t(x)\check{Z}_{t-1}(x) \quad \text{for } t \geq 1 \quad (\text{G.3.9})$$

and with the initial condition

$$\check{Z}_0(0) = 1, \quad \frac{\check{Z}_0(x)}{\check{Z}_{-1}(x-1)} = U(x), \quad \frac{\check{Z}_0(x)}{\check{Z}_{-1}(x)} = V(x) \quad \text{for } x \in \mathbb{Z}. \quad (\text{G.3.10})$$

Where $(U(x))_{x \in \mathbb{Z}}$ and $(V(x))_{x \in \mathbb{Z}}$ are two sets of iid RVs distributed as $U(x) \sim U$ and $V(x) \sim V$ with U, V distributed as (G.3.7), while the RVs $(u_t(x), v_t(x))$ are distributed as before (G.3.2). The definition of $Z_t(x)$ for $t = -1$ is for future notational convenience and for what concerns $Z_t(x)$ for $t \geq 0$ it is equivalent to set the initial condition as $\check{Z}_0(x+1)/\check{Z}_0(x) = U(x+1)/V(x)$. This model is analogous to the point to Brownian continuum DP.

c Zero temperature models: The Bernoulli-Geometric polymer(s)

We now define as previously for the Inverse-Beta polymer three versions of the Bernoulli-Geometric (BG) polymer: the point to point BG polymer, the BG polymer with boundaries and the BG polymer with stationary initial condition. The first model will be defined by choosing *two* ('bulk') parameters $(q, q') \in [0, 1]^2$. The others have one additional ('boundary' or 'stationarity') parameter $q_b \in]q, 1[$, which will specify one stationary measure among a family of stationary measures at fixed (q, q') . All definitions of this section are to our knowledge original to this work. Here and throughout the paper the similarities between these models and the IB polymers will be highlighted using similar notations, with the convention that we reserve sans-serif letters for the BG polymers. The connection between the IB and BG polymers, which was the main motivation for introducing the BG polymer, was already mentioned in the introduction. It will be made more precise in Sec. G.5.2.

Definition G.3.4. The point to point Bernoulli-Geometric polymer We now define the Bernoulli-Geometric polymer. We assign to each edge e of \mathbb{Z}^2 a discrete random energy $\mathcal{E}(e) \in \mathbb{Z}$. Depending on whether the edge is horizontal or vertical, the random energies are drawn from different probability distributions. Let us introduce the notation

$$\begin{aligned} \mathcal{E}((x_1, x_2) \rightarrow (x_1 + 1, x_2)) &= u_{x_1+1, x_2}, \\ \mathcal{E}((x_1, x_2) \rightarrow (x_1, x_2 + 1)) &= v_{x_1, x_2+1}, \end{aligned} \quad (\text{G.3.11})$$

hence u (resp. v) denotes a random energy on an horizontal (resp. vertical) edge. We suppose that *couples* of random variables indexed by the endpoint of the edges $(u_{x_1, x_2}, v_{x_1, x_2})$ are iid RVs distributed as $(u_{x_1, x_2}, v_{x_1, x_2}) \sim (u, v)$ where the couple (u, v) is distributed as

$$\begin{aligned} u &\sim (1 - \zeta_{uv})(1 + G_{q'}) - \zeta_{uv}G_q \in \mathbb{Z}, \\ v &\sim -\zeta_{uv}G_q \in \mathbb{Z}_-, \end{aligned} \quad (\text{G.3.12})$$

where $0 < q < 1$ and $0 < q' < 1$ are the two parameters of the models and $G_q, G_{q'}$ and ζ_{uv} are independent RVs distributed as follows. $G_q \in \mathbb{N}$ and $G_{q'} \in \mathbb{N}$ are geometric RVs with parameters q and q' with the convention

$$\text{Proba}(G_q = k \in \mathbb{N}) = (1 - q)q^k, \quad (\text{G.3.13})$$

and similarly for $G_{q'}$ with the exchange $q \rightarrow q'$. $\zeta_{uv} \in \{0, 1\}$ is a Bernoulli RV with parameter p_{uv} given by

$$p_{uv} = \frac{1 - q'}{1 - qq'} \in]0, 1[, \quad (\text{G.3.14})$$

and thus

$$\text{Proba}(\zeta_{uv} = 1) = p_{uv}, \quad \text{Proba}(\zeta_{uv} = 0) = 1 - p_{uv}. \quad (\text{G.3.15})$$

As such, $u \geq v$ (equality occurring whenever $\zeta_{uv} = 1$) and note that $u \in \mathbb{Z}$ can be positive or negative while $v \in \mathbb{Z}_-$ is always negative (or zero). u and v are correlated RVs since they are both functions of the same Bernoulli RV ζ_{uv} . Note that one can also add correlations between G_q and $G_{q'}$: since $\zeta_{uv} \in \{0, 1\}$ one easily shows that correlations between G_q and $G_{q'}$ do not affect the PDF of (u, v) . The latter can be written as

$$\begin{aligned} \text{Proba}(u = k_u \in \mathbb{Z}, v = k_v \in \mathbb{Z}_-) &= p_{uv}\delta(k_u = k_v)\delta(k_v \leq 0)(1 - q)q^{-k_v} \\ &\quad + (1 - p_{uv})\delta(k_v = 0)\delta(k_u \geq 1)(1 - q')(q')^{k_u - 1}, \end{aligned} \quad (\text{G.3.16})$$

where here and throughout the rest of the paper the symbol δ is used to denote the indicator function of the set specified inside the δ . Finally, given a random environment specified by a drawing of the random energies $(u_{x_1, x_2}, v_{x_1, x_2})$, we are interested in the optimal energy to go from the origin $(0, 0)$ to the point (x_1, x_2)

$$E_{x_1, x_2} = \min \left\{ \mathcal{E}(\pi) = \sum_{e \in \pi} \mathcal{E}(e), \pi : (0, 0) \rightarrow (x_1, x_2) \right\}. \quad (\text{G.3.17})$$

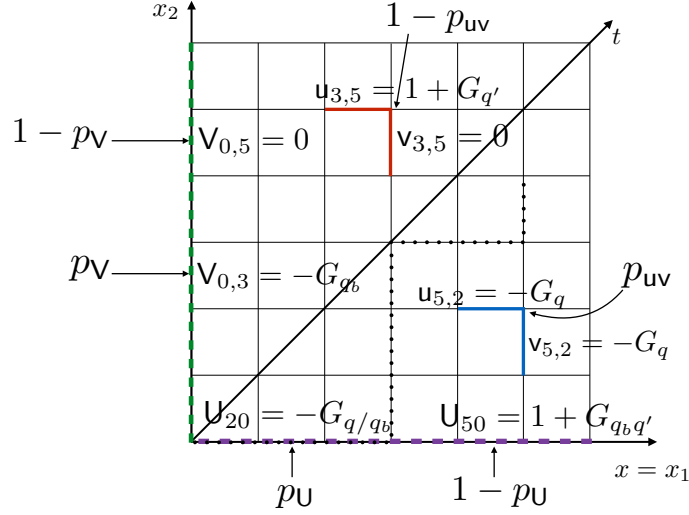


Figure G.4: The Bernoulli-Geometric polymer with boundaries. In the bulk the couple of energies on the edges (u,v) are taken with probability p_{uv} (resp. $(1-p_{uv})$) as $(u,v) = (-G_q, -G_q)$ (blue edges above) (resp. $(u,v) = (1+G_{q'}, 0)$ (red edges above)). The energies on the horizontal boundary U (dashed-purple) are taken with probability p_U (resp. $1-p_U$) as $U = -G_{q/q_b}$ (resp. $U = 1+G_{q_b q'}$). The energies on the vertical boundary V (dashed-green) are taken with probability p_V (resp. $1-p_V$) as $V = -G_{q_b}$ (resp. $U = 1+G_{q_b q'}$). The dotted line represents a possible polymer path from $(x_1, x_2) = (0, 0)$ to $(x_1, x_2) = (5, 4)$.

Where as before the minimization is over up-right paths. Assigning for convention the value $E_{x_1, x_2} = +\infty$ for vertices (x_1, x_2) with either $x_1 < 0$ or $x_2 < 0$, the model can also be recursively defined as, using the (t, x) coordinates

$$\begin{aligned} E_t(x) &= \min(E_{t-1}(x-1) + u_t(x), E_{t-1}(x) + v_t(x)) \text{ for } t \geq 1, \\ E_{t=0}(0) &= 0 \text{ and } E_{t=0}(x) = +\infty \text{ for } x \neq 0. \end{aligned} \quad (\text{G.3.18})$$

The definition of this model is, to our knowledge, original to this work. The model can be defined for any value of the parameter $p_{uv} \in [0, 1]$, but it is only for the value given by (G.3.14) that we can write down exactly its stationary measure. This precise value thus makes the model special, in the sense that it possesses an ESP. In this model the parameters q and q' do not play symmetric roles: q' can be thought of as an anisotropy parameter which favors the vertical edges by sometimes (with probability $1-p_{uv} = q' \frac{1-q}{1-qq'}$) putting a penalty on horizontal edges. Two important limits are an isotropic limit of the model which is obtained by setting $q' \rightarrow 0$, and an anisotropic limit which is obtained for $q \rightarrow 0$. In the isotropic limit $p_{uv} = 1$ and the model corresponds to a problem of last passage percolation, while in the anisotropic limit $p_{uv} = 0$ and the model corresponds to a problem of first passage percolation (see Sec. G.5.2). More generally the Bernoulli-Geometric polymer thus mixes an optimization problem of the first-passage type with an optimization problem of the last-passage type. In this interpretation p_{uv} is a mixing parameter which must have the precise value (G.3.14) for the model to be exactly solvable. Interesting continuous limits are also obtained by letting $q, q' \rightarrow 1$. There the model converges to the zero temperature limit of the Inverse-Beta polymer. This will be further discussed in Sec. G.5.2.

Definition G.3.5. The BG polymer with boundaries We now consider the BG model previously defined and change the distribution of energies on the boundaries of \mathbb{N}^2 . In the model with boundaries the energy on the edges $\hat{E}(e)$ are distributed as

$$\begin{aligned} \hat{E}((x_1, x_2) \rightarrow (x_1+1, x_2)) &= u_{x_1+1, x_2} \text{ if } x_2 \geq 1, \\ \hat{E}((x_1, x_2) \rightarrow (x_1, x_2+1)) &= v_{x_1, x_2+1} \text{ if } x_1 \geq 1, \\ \hat{E}((x_1, 0) \rightarrow (x_1+1, 0)) &= U_{x_1+1, 0}, \\ \hat{E}((0, x_2) \rightarrow (0, x_2+1)) &= V_{0, x_2+1}. \end{aligned} \quad (\text{G.3.19})$$

Where here the random energies in the bulk $(u_{x_1, x_2}, v_{x_1, x_2})|_{x_1, x_2 \geq 1} \sim (u, v)$ are distributed as before with parameters $0 < q < 1$ and $0 < q' < 1$, see (G.3.12) and (G.3.16). The random energies on the edges of \mathbb{N}^2 , $U_{x_1 \geq 1, 0}$ and $V_{0, x_2 \geq 1}$ are independent from the random energies in the bulk and from each other. They are distributed as $U_{x_1, 0} \sim U$ and $V_{0, x_2} \sim V$ where

$$\begin{aligned} U &\sim (1-\zeta_U)(1+G_{q_b q'}) - \zeta_U G_{q/q_b} \in \mathbb{Z}, \\ V &\sim -\zeta_V G_{q_b} \in \mathbb{Z}_-. \end{aligned} \quad (\text{G.3.20})$$

Here $q < q_b < 1$ is a new parameter, G_{q_b} , G_{q/q_b} and $G_{q_b q'}$ are independent geometric RVs distributed as in (G.3.13), while ζ_U and ζ_V are Bernoulli RVs with parameter p_U and p_V distributed as in (G.3.15) with

$$p_U = \frac{1 - q_b q'}{1 - q q'} \quad , \quad p_V = \frac{1 - q'}{1 - q_b q'} . \quad (\text{G.3.21})$$

We can also directly write the probability distribution of U and V as

$$\begin{aligned} \text{Proba}(U = k_U \in \mathbb{Z}) &= p_U \delta(k_U \leq 0) (1 - q/q_b) (q/q_b)^{-k_U} \\ &\quad + (1 - p_U) \delta(k_U \geq 1) (1 - q_b q') (q_b q')^{k_U - 1} , \\ \text{Proba}(V = k_V \in \mathbb{Z}_-) &= p_V \delta(k_V \leq 0) (1 - q_b) (q_b)^{-k_V} + (1 - p_V) \delta(k_V = 0) . \end{aligned} \quad (\text{G.3.22})$$

Given a random environment specified by a drawing of the bulk and edges random energies we are interested in the optimal energy to go from the origin $(0, 0)$ to the point (x_1, x_2)

$$\hat{E}_{x_1, x_2} = \min \left\{ \hat{\mathcal{E}}(\pi) = \sum_{e \in \pi} \hat{\mathcal{E}}(e), \pi : (0, 0) \rightarrow (x_1, x_2) \right\} . \quad (\text{G.3.23})$$

Definition G.3.6. The BG polymer with stationary initial condition We define a third version of the BG polymer. Following the recursion equation (G.3.18), we define the DP optimal energy $\check{E}_t(x)$ for $t \geq -1$ and $x \in \mathbb{Z}$ as

$$\check{E}_t(x) = \min \left(\check{E}_{t-1}(x-1) + u_t(x), \check{E}_{t-1}(x) + v_t(x) \right) \quad \text{for } t \geq 1 \quad (\text{G.3.24})$$

and with the initial condition $\check{E}_t(0) = 1$ and

$$\check{E}_0(x) - \check{E}_{-1}(x-1) = U(x) \quad , \quad \check{E}_0(x) - \check{E}_{-1}(x) = V(x) \quad \text{for } x \in \mathbb{Z} . \quad (\text{G.3.25})$$

Where $(U(x))_{x \in \mathbb{Z}}$ and $(V(x))_{x \in \mathbb{Z}}$ are two sets of iid RVs distributed as $U(x) \sim U$ and $V(x) \sim V$ with U, V distributed as (G.3.20), while the RVs $(u_t(x), v_t(x))$ are distributed as before (G.3.12).

G.3.2 Stationarity and reversibility properties

In this section we now state the stationarity properties of the models previously defined. These properties will be shown rigorously in Sec. G.4 and Sec. G.5¹. Let us first define the notion of down-right paths.

Definition G.3.7. A down-right path of length $N \in \mathbb{N}^*$ on \mathbb{Z}^2 is as sequence of vertices of \mathbb{Z}^2 $(x_1(i), x_2(i))_{i=0, \dots, N}$ such that jumps are either downward: $(x_1(i+1), x_2(i+1)) = (x_1(i), x_2(i)) - (0, 1)$, or are to the right: $(x_1(i+1), x_2(i+1)) = (x_1(i), x_2(i)) + (1, 0)$. The set of edges crossed by the path π_{dr} is $\{(x_1(i), x_2(i)) \rightarrow (x_1(i+1), x_2(i+1)), i = 0, \dots, N-1\}$.

a Stationarity and reversibility in the IB polymer with boundaries and stationary initial condition

Let us introduce, for $x_1, x_2 \geq 0$ and $(x_1, x_2) \neq (0, 0)$, the ratios of partition sum on the horizontal and vertical edges leading to (x_1, x_2) in the model with boundaries:

$$\hat{U}_{x_1, x_2} := \frac{\hat{Z}_{x_1, x_2}}{\hat{Z}_{x_1-1, x_2}} \quad , \quad \hat{V}_{x_1, x_2} := \frac{\hat{Z}_{x_1, x_2}}{\hat{Z}_{x_1, x_2-1}} . \quad (\text{G.3.26})$$

We will refer to these RVs as living on the edges of \mathbb{N}^2 : \hat{U}_{x_1, x_2} (resp. \hat{V}_{x_1, x_2}) is thought of as living on the horizontal (resp. vertical) edge leading to (x_1, x_2) . Note that on the boundaries these ratios coincide with the boundary weights in the IB polymer with boundaries: $\hat{U}_{x_1, 0} = U_{x_1, 0}$ and $\hat{V}_{0, x_2} = V_{0, x_2}$. Similarly in the model with stationary initial condition we define, for $t \geq 0$ and $x \in \mathbb{Z}$:

$$\check{U}_t(x) := \frac{\check{Z}_t(x)}{\check{Z}_{t-1}(x-1)} \quad , \quad \check{V}_t(x) := \frac{\check{Z}_t(x)}{\check{Z}_{t-1}(x)} . \quad (\text{G.3.27})$$

The following four properties hold:

Proposition G.3.1. Stationarity property of the IB polymer with boundaries For all down-right path on \mathbb{N}^2 , the RVs \hat{U}_{x_1, x_2} and \hat{V}_{x_1, x_2} that live on the edges crossed by the down-right path are independent and distributed as $\hat{U}_{x_1, x_2} \sim U$ and $\hat{V}_{x_1, x_2} \sim V$ with U and V distributed as in (G.3.7). In particular, since each edge of \mathbb{N}^2 belongs to at least one down-right path, the RVs \hat{U}_{x_1, x_2} and \hat{V}_{x_1, x_2} are all distributed as U and V in (G.3.7).

Proposition G.3.2. Stationarity property of the IB polymer with stationary initial condition The process $(\check{U}_t(x), \check{V}_t(x))_{t \in \mathbb{N}, x \in \mathbb{Z}}$ is stationary: $\forall t \in \mathbb{N}$ fixed, the RVs $(\check{U}_t(x))_{x \in \mathbb{Z}}$ and $(\check{V}_t(x))_{x \in \mathbb{Z}}$ are independent and distributed as $\check{U}_t(x) \sim U$ and $\check{V}_t(x) \sim V$ with U and V distributed as in (G.3.7).

¹throughout the paper we will pay attention to emphasize the degree of rigor with which each result is shown, and in particular only fully rigorous results will be stated as Propositions

Proposition G.3.3. Reversibility of the stationary process *Considering a finite time interval of duration $T \in \mathbb{N}^*$ and the time-reversed coordinates and time reversed process variables defined by*

$$t_R = T - t - 1 \quad , \quad x_R = -x \quad (G.3.28)$$

$$\check{U}_{t_R}^R(x_R) = \check{U}_{t=T-t_R}(x = -x_R + 1) \quad , \quad \check{V}_{t_R}^R(x_R) = \check{V}_{t=T-t_R}(x = -x_R) \quad , \quad (G.3.29)$$

we have the identity in law

$$(\check{U}_t(x), \check{V}_t(x))_{t=0, \dots, T; x \in \mathbb{Z}} \sim (\check{U}_{t_R}^R(x_R), \check{V}_{t_R}^R(x_R))_{t_R=0, \dots, T; x_R \in \mathbb{Z}} \quad . \quad (G.3.30)$$

Proposition G.3.4. Equivalence between models with boundaries and stationary initial condition *We have*

$$(\check{Z}_t(x))_{(t,x) \in \mathbb{N}^2} \sim (\hat{Z}_t(x))_{(t,x) \in \mathbb{N}^2} \quad . \quad (G.3.31)$$

The model with boundary conditions can thus be seen as an efficient way to study the model with stationary initial condition in the upper-right quadrant of \mathbb{Z}^2 .

b Stationarity and reversibility in the BG polymer with boundaries and stationary initial condition

Conversely, let us introduce in the BG polymer with boundaries, for $x_1, x_2 \geq 0$ and $(x_1, x_2) \neq (0, 0)$, the differences of optimal energies on the horizontal and vertical edges leading to (x_1, x_2) :

$$\hat{U}_{x_1, x_2} := \hat{E}_{x_1, x_2} - \hat{E}_{x_1-1, x_2} \quad , \quad \hat{V}_{x_1, x_2} := \hat{E}_{x_1, x_2} - \hat{E}_{x_1, x_2-1} \quad . \quad (G.3.32)$$

And similarly, in the model with stationary initial condition, for $t \geq 0$ and $x \in \mathbb{Z}$:

$$\check{U}_t(x) = \check{E}_t(x) - \check{E}_{t-1}(x-1) \quad , \quad \check{V}_t(x) = \check{E}_t(x) - \check{E}_{t-1}(x) \quad . \quad (G.3.33)$$

The following four properties hold:

Proposition G.3.5. Stationarity property of the BG polymer with boundaries *For all down-right path on \mathbb{N}^2 , the RVs \hat{U}_{x_1, x_2} and \hat{V}_{x_1, x_2} that live on the edges crossed by the down-right path are independent and distributed as $\hat{U}_{x_1, x_2} \sim \mathbf{U}$ and $\hat{V}_{x_1, x_2} \sim \mathbf{V}$ with \mathbf{U} and \mathbf{V} distributed as in (G.3.20). In particular, since each edge of \mathbb{N}^2 belongs to at least one down-right path, the RVs \hat{U}_{x_1, x_2} and \hat{V}_{x_1, x_2} are all distributed as \mathbf{U} and \mathbf{V} in (G.3.20).*

Proposition G.3.6. Stationarity property of the model with stationary initial condition *The process $(\check{U}_t(x), \check{V}_t(x))_{t \in \mathbb{N}, x \in \mathbb{Z}}$ is stationary: $\forall t \in \mathbb{N}$ fixed, the RVs $(\check{U}_t(x))_{x \in \mathbb{Z}}$ and $(\check{V}_t(x))_{x \in \mathbb{Z}}$ are independent and distributed as $\check{U}_t(x) \sim \mathbf{U}$ and $\check{V}_t(x) \sim \mathbf{V}$ with \mathbf{U} and \mathbf{V} distributed as in (G.3.20).*

Proposition G.3.7. Reversibility of the stationary process *Considering a finite time interval of duration $T \in \mathbb{N}^*$ and the time-reversed coordinates (G.3.28), the time reversed process is defined as*

$$\check{U}_{t_R}^R(x_R) = \check{U}_{t=T-t_R}(x = -x_R + 1) \quad , \quad \check{V}_{t_R}^R(x_R) = \check{V}_{t=T-t_R}(x = -x_R) \quad , \quad (G.3.34)$$

and we have the identity in law

$$(\check{U}_t(x), \check{V}_t(x))_{t=0, \dots, T; x \in \mathbb{Z}} \sim (\check{U}_{t_R}^R(x_R), \check{V}_{t_R}^R(x_R))_{t_R=0, \dots, T; x_R \in \mathbb{Z}} \quad . \quad (G.3.35)$$

Proposition G.3.8. Equivalence between models with boundaries and stationary initial condition *We have*

$$(\check{E}_t(x))_{(t,x) \in \mathbb{N}^2} \sim (\hat{E}_t(x))_{(t,x) \in \mathbb{N}^2} \quad . \quad (G.3.36)$$

G.3.3 Quenched free-energy in point to point models without boundaries

Using the stationary properties stated above, we obtain in Sec.G.6.2 asymptotic results for the mean quenched free-energy/optimal energy in the direction $(s_1, s_2) \in \mathbb{R}_+^2$ in the point to point IB/BG polymer. These quantities are defined as

$$f_{\text{IB}}(s_1, s_2) := \lim_{N \rightarrow \infty} \frac{-\overline{\log Z_{Ns_1, Ns_2}}}{N} \quad , \quad f_{\text{BG}}(s_1, s_2) := \lim_{N \rightarrow \infty} \frac{\overline{E_{Ns_1, Ns_2}}}{N} \quad . \quad (G.3.37)$$

Where here and throughout the paper the overline $\overline{(\cdot)}$ denotes the average over the random environment. For a fixed direction $(s_1, s_2) \in \mathbb{R}_+^2$ and bulk parameters $(\gamma, \beta)/(q, q')$, our results involves the solution of a saddle-point equation for a boundary parameter $\lambda = \lambda^*(s_1, s_2)/q_b = q_b^*(s_1, s_2)$. Based on some unproven ‘natural’ assumptions of convexity and regularity for $f_{\text{IB}}(s_1, s_2)$ and $f_{\text{BG}}(s_1, s_2)$ we obtain:

$$f_{\text{IB}}(s_1, s_2) = s_1 (-\psi(\beta + \lambda^*) + \psi(\gamma - \lambda^*)) + s_2 (-\psi(\beta + \lambda^*) + \psi(\lambda^*)) \quad , \quad (G.3.38)$$

$$0 = s_1 (-\psi'(\beta + \lambda^*) - \psi'(\gamma - \lambda^*)) + s_2 (-\psi'(\beta + \lambda^*) + \psi'(\lambda^*)) \quad , \quad (G.3.39)$$

where $\psi = \Gamma'/\Gamma$ is the diGamma function and with the condition $0 < \lambda^*(s_1, s_2) < \gamma$ for the IB polymer, and

$$f_{\text{BG}}(s_1, s_2) = -\frac{(q - (q_b^*)^2 q')}{(q - q_b^*)(q_b^* q' - 1)} s_1 + \frac{q_b^* (q' - 1)}{(q_b^* - 1)(q_b^* q' - 1)} s_2, \quad (\text{G.3.40})$$

$$(q_b^* - 1)^2 \left(q (q_b^*)^2 (q')^2 + (q^2 - 4q_b^* q + (q_b^*)^2) q' + q \right) s_1 - (q - q_b^*)^2 (q' - 1) ((q_b^*)^2 q' - 1) s_2 = 0, \quad (\text{G.3.41})$$

with the condition $q < q_b^*(s_1, s_2) < 1$ for the BG polymer.

Note that while (G.3.39) is a transcendental equation for $\lambda^*(s_1, s_2)$, (G.3.41) is a quartic equation for $q_b^*(s_1, s_2)$, which can be solved explicitly using radicals. These results cannot be considered as mathematical theorems since they rely on unproven assumptions (which could likely be proven by other means). Still, their derivation is very close to a mathematical proof. We note that the result (G.3.38) for $f_{\text{IB}}(s_1, s_2)$ coincides with the result obtained in Eq.(79)-(81) in [5]² using non-rigorous replica calculations, and the above result thus gives a close to rigorous confirmation of one conjecture of [5].

Optimal angles

Of interest are the *optimal angles* $\varphi_{\text{opt}} \in]-1/2, 1/2[$, the ‘angles’ for which the mean quenched free-energy/optimal energy *per unit length* in the direction $\varphi \in]-1/2, 1/2[$, defined as

$$f_{\text{IB}}^{\text{p.u.l.}}(\varphi) = f_{\text{IB}}(1/2 + \varphi, 1/2 - \varphi) \quad , \quad f_{\text{BG}}^{\text{p.u.l.}}(\varphi) = f_{\text{BG}}(1/2 + \varphi, 1/2 - \varphi), \quad (\text{G.3.42})$$

are maximum. These quantities are non-trivial in these anisotropic models and we obtain the explicit formulas

$$\varphi_{\text{opt}}^{\text{IB}} = -\frac{1}{2} \frac{\psi'(\beta + \gamma/2)}{\psi'(\gamma/2)} \leq 0 \quad , \quad \varphi_{\text{opt}}^{\text{BG}} = -\frac{(\sqrt{q} - 1)^2 q'}{2(\sqrt{q}q' - 1)^2} \leq 0. \quad (\text{G.3.43})$$

These angles would correspond to the mean direction chosen by the polymer for a point to line polymer problem. The formula for $\varphi_{\text{opt}}^{\text{IB}}$ was already given in Eq.(83) of [5].

G.3.4 Convergence of point to point models to their stationary state

Finally, based on the upon results, we *conjecture* that the following limits in law holds: $\forall (L_u, L_v) \in \mathbb{N}^2$ and $(s_1, s_2) \in \mathbb{R}_+^2$

$$\lim_{N \rightarrow \infty} \left(\frac{Z_{N s_1 + x_1, N s_2 + x_2}}{Z_{N s_1, N s_2}} \right)_{0 \leq x_1 \leq L_u, 0 \leq x_2 \leq L_v} \sim (\hat{Z}_{x_1, x_2})_{0 \leq x_1 \leq L_u, 0 \leq x_2 \leq L_v} \quad (\text{G.3.44})$$

$$\lim_{N \rightarrow \infty} (E_{N s_1 + x_1, N s_2 + x_2} - E_{N s_1, N s_2})_{0 \leq x_1 \leq L_u, 0 \leq x_2 \leq L_v} \sim (\hat{E}_{x_1, x_2})_{0 \leq x_1 \leq L_u, 0 \leq x_2 \leq L_v} \quad (\text{G.3.45})$$

where the left hand sides of these limits involve the point to point partition sum/optimal energy in the IB/BG polymer, and the right hand sides involve the corresponding quantities in the models with boundaries with boundary parameters $\lambda = \lambda^*(s_1, s_2)$ and $q_b = q_b^*(s_1, s_2)$, the solutions of the equations (G.3.39) and (G.3.41).

G.3.5 Outline and some additional results not presented here

The outline of the remaining of this manuscript is as follows. In Sec. G.4 and G.5 we prove the stationarity and reversibility properties of the Inverse-Beta and Bernoulli-Geometric polymers of Sec. G.3.2, and discuss the connections between our work and previous works. In Sec. G.6.1 we obtain results for the asymptotic mean quenched free-energy and mean optimal energy in the IB and BG polymers with boundaries, and using these results we obtain in Sec. G.6.2 the corresponding formulas (G.3.38)-(G.3.40) for the point to point models. In Sec. G.6.3 we discuss the conjectures for the convergence of both models to their stationary measure (G.3.44)-(G.3.45). In Sec. G.6.4 we briefly discuss the nature of the fluctuations of the free-energy in the models with boundaries. Finally in Sec. G.7 we perform some simulations of the BG polymer and check our result and conjecture (G.3.40) and (G.3.45) for this newly introduced model.

G.4 Finite-temperature model: stationary measure of the Inverse-Beta polymer

In this section we show the stationarity properties of the IB polymer of Sec. a. We follow closely the approach developed by Seppäläinen for the case of the Log-Gamma polymer [197] and adapt it to the Inverse-Beta polymer. We also discuss the connection between our work and previous works.

²there $c_\varphi = f_{\text{IB}}(1/2 + \varphi, 1/2 - \varphi)$ for $\varphi \in]-1/2, 1/2[$ and the equivalent of λ^* there is the saddle-point parameter $k_\varphi = \gamma/2 + \lambda^*$

G.4.1 Stationary property of the model with boundaries

We begin by showing the stationarity property Prop. G.3.1 of the IB model with boundaries (see Def. G.3.2). First, note that in the bulk of \mathbb{N}^2 , i.e. for $x_1, x_2 \geq 1$, the partition sum \hat{Z}_{x_1, x_2} satisfies the bulk recursion

$$\hat{Z}_{x_1, x_2} = u_{x_1, x_2} \hat{Z}_{x_1-1, x_2} + v_{x_1, x_2} \hat{Z}_{x_1, x_2-1} \quad \text{for } x_1, x_2 \geq 1. \quad (\text{G.4.1})$$

This implies that the vertical and horizontal ratios of partition sums \hat{U}_{x_1, x_2} and \hat{V}_{x_1, x_2} defined in (G.3.26) satisfy the following recursion relation, valid for $x_1, x_2 \geq 1$,

$$\hat{U}_{x_1, x_2} = \phi^{(1)}(\hat{U}_{x_1, x_2-1}, \hat{V}_{x_1-1, x_2}, W_{x_1, x_2}) \quad , \quad \hat{V}_{x_1, x_2} = \phi^{(2)}(\hat{U}_{x_1, x_2-1}, \hat{V}_{x_1-1, x_2}, W_{x_1, x_2}), \quad (\text{G.4.2})$$

where $\phi^{(i)}$ denotes the i^{th} component of the image of the *stationarity-reversibility map* ϕ that we now define.

Definition G.4.1. The stationarity-reversibility map is the function $\phi : (U, V, W) \in (\mathbb{R}^*)^3 \rightarrow (U', V', W') \in (\mathbb{R}^*)^3$ defined by

$$U' = W + (W + 1)\frac{U}{V} \quad , \quad V' = W\frac{V}{U} + W + 1 \quad , \quad W' = \frac{U(V-1)}{U+V}. \quad (\text{G.4.3})$$

It has the following properties:

Proposition G.4.1. Stationarity *If (U, V, W) are three independent RVs distributed as in (G.3.7) and (G.3.3), then $(U', V', W') := \phi(U, V, W)$ are three independent RVs distributed as in (G.3.7) and (G.3.3).*

Proposition G.4.2. Reversibility *ϕ is an involution, i.e. $\phi \circ \phi = Id$.*

These properties are proved in Appendix. G.9. Based on the above properties of ϕ , the stationarity property of the model with boundary conditions Prop. G.3.1 is proved by induction on the set of down-right paths (see Def. G.3.7) on \mathbb{N}^2 . We first need a definition:

Definition G.4.2. Down-left to top-right transformation on down-right paths A down-right path π_{dr_2} is a ‘down-left to top-right’ (henceforth: DLTR) transformed down-right path of a down-right path π_{dr_1} if π_{dr_2} can be obtained from π_{dr_1} by a transformation where edges of π_{dr_1} forming a down-left corner, i.e. of the form $(x_1, x_2) \rightarrow (x_1, x_2-1) \rightarrow (x+1, x_2-1)$, are replaced in π_{dr_2} by the two edges forming the corresponding top-right corner $(x_1, x_2) \rightarrow (x_1+1, x_2) \rightarrow (x_1+1, x_2-1)$ (see Fig. G.5).

Let us now give the proof of the stationarity property Prop. G.3.1 of the model with boundary conditions. First, note that the stationarity property is trivially true for the down-right paths that follow exactly the boundaries of \mathbb{N}^2 (since on these down-right paths the RVs \hat{U}_{x_1, x_2} and \hat{V}_{x_1, x_2} are just the random Boltzmann weights on the boundaries $U_{x_1, 0}$ and V_{0, x_2} which are independent and distributed as (G.3.7)). Let us now suppose that the stationarity property Prop. G.3.1 is true for a down right path π_{dr_1} such that π_{dr_1} contains one couple of edges of the form $(x_1, x_2) \rightarrow (x_1, x_2-1) \rightarrow (x+1, x_2-1)$ (i.e. it contains two edges forming a down-left corner, see Fig. G.5). The vertical edge then carries the RV \hat{V}_{x_1, x_2} and the horizontal edge carries the RV \hat{U}_{x_1+1, x_2-1} . Applying the induction (G.4.2) on this couple of edges, we obtain the couple of RVs $(\hat{U}_{x_1+1, x_2}, \hat{V}_{x_1+1, x_2})$. These RVs, complemented by the other RVs $\hat{U}_{x'_1, x'_2}$ and $\hat{V}_{x'_1, x'_2}$ that live on π_{dr_1} and were left untouched by this induction, now live on a down right path π_{dr_2} defined such that the edges visited by π_{dr_2} are exactly those visited by π_{dr_1} except for the couple of edges $(x_1, x_2) \rightarrow (x_1, x_2-1) \rightarrow (x+1, x_2-1)$ that is replaced by $(x_1, x_2) \rightarrow (x_1+1, x_2) \rightarrow (x_1+1, x_2-1)$ (see Fig. G.5). Using the stationarity property of ϕ Prop. G.4.1 one concludes that those RVs satisfy the stationarity property Prop. G.3.1. Hence the DLTR transformation on down-right paths conserves the stationarity property, and we will generally think of the variables (U, V) (resp. (U', V')) in (G.4.3) as living on down-left (resp. top right) corners (see Fig. G.5). Finally, since any down-right path on \mathbb{N}^2 can be obtained from a down-right path that follows exactly the edges of \mathbb{N}^2 by a sequence of DLTR transformations, the stationarity property holds for any down-right path on \mathbb{N}^2 . In this sense, the stationarity property of the model with boundaries can be thought of as a *propagation of boundary conditions*.

G.4.2 Stationarity property of the model with stationary initial condition

We now consider the IB with stationary initial condition defined in Def. G.3.3. Similarly as before, the horizontal and vertical ratios of partition sums $\check{U}_t(x)$ and $\check{V}_t(x)$ (defined in (G.3.27)) satisfy the following recursion equation, valid for $t \geq 0$ and $x \in \mathbb{Z}$

$$\check{U}_{t+1}(x) = \phi^{(1)}(\check{U}_t(x), \check{V}_t(x-1), W_{t+1}(x)) \quad , \quad \check{V}_{t+1}(x) = \phi^{(2)}(\check{U}_t(x), \check{V}_t(x-1), W_{t+1}(x)). \quad (\text{G.4.4})$$

In this model, the stationary initial condition (G.3.10) is designed to provide an initial down right path on \mathbb{Z}^2 ,

$$\pi_{dr}^{(0)} = \{(x_1, x_2) = (m, -m) \rightarrow (m, -m-1) \rightarrow (m+1, -m-1), m \in \mathbb{Z}\} \quad (\text{G.4.5})$$

on which the variable $\check{U}_t(x)$ and $\check{V}_t(x)$ defined in (G.3.27) are all independent and distributed as in (G.3.7), (see Fig. G.6). Starting from this initial down-right path and successively applying DLTR transformations as described previously, one obtains the following improved (compared to Prop. G.3.2) stationarity property.

Proposition G.4.3. Improved Stationarity property of the model with stationary initial condition *On each down-right path π_{dr} on \mathbb{Z}^2 that can be obtained from $\pi_{dr}^{(0)}$ by a sequence of DLTR transformations, the variables $\check{U}_t(x)$ and $\check{V}_t(x)$ that live on π_{dr} are independent and distributed as in (G.3.7).*

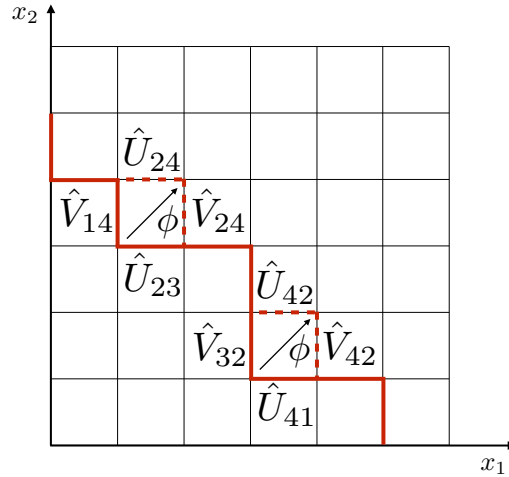


Figure G.5: Red: a down-right path on \mathbb{N}^2 . Red-dashed: a new possible down-right path obtained from the first one by transforming two down-left corners into two top-rights ones (resulting from two down-left to top-right transformations, see Def. G.4.2). The RVs \hat{U}_{x_1, x_2} and \hat{V}_{x_1, x_2} on the new down-right path are either the same as for the first path, or obtained from those on the first path using the stationarity-reversibility map ϕ through the induction (G.4.2).

For concreteness let us highlight some down-right paths that can be obtained from $\pi_{dr}^{(0)}$ using DLTR transformations (see left of Fig. G.6) and prove the properties Prop. G.3.2 and Prop. G.3.4. These includes

1) For all $t \geq 1$ the down-right path

$$\pi_{dr}^{(t)} = \{(x_1, x_2) = (t + m, -m) \rightarrow (t + m, -m - 1) \rightarrow (t + m + 1, -m - 1), m \in \mathbb{Z}\} \quad (\text{G.4.6})$$

In particular this implies the stationarity property Prop. G.3.2. Note that this shows that in the model with stationary initial condition, for all $t \geq 1$, the RVs $\{\check{Y}_t(x) := \check{Z}_t(x+1)/\check{Z}_t(x), x \in \mathbb{Z}\}$ are iid and distributed as U/V with U and V distributed as in (G.3.7). This stationarity property for the $\check{Y}_t(x)$ variables has the advantage of only involving partition sums at the same time coordinate t . It is trivially implied by the stronger property of stationarity of $\check{U}_t(x)$ and $\check{V}_t(x)$ on down-right paths and we will focus on the latter in the following.

2) The boundary of \mathbb{N}^2 , which is itself a down-right path, can also be obtained from $\pi_{dr}^{(0)}$. This shows that on the boundaries of \mathbb{N}^2 , the partition sums in the IB polymer with stationary initial condition \check{Z}_{x_1, x_2} and in the model with boundary conditions \hat{Z}_{x_1, x_2} are equivalent in law. Since the partition sums in these models in the remaining of \mathbb{N}^2 are uniquely determined by their values on the boundaries and by the random BWs in the bulk of \mathbb{N}^2 , which coincide in both models, we obtain Prop. G.3.4, i.e. $(\check{Z}_{x_1, x_2})_{(x_1, x_2) \in \mathbb{N}^2} \sim (\hat{Z}_{x_1, x_2})_{(x_1, x_2) \in \mathbb{N}^2}$.

Remarks

- The condition $\check{Z}_0(0) = 1$ in the initial condition (G.3.10) is arbitrary and could be replaced by any other constant or RV as long as it is independent of the variable $U(x)$ and $V(x)$. The equality in law between the model with stationary initial condition in the upper right quadrant and the model with boundary conditions then more generally reads $(\check{Z}_{x_1, x_2}/\check{Z}_{0,0})_{(x_1, x_2) \in \mathbb{N}^2} \sim (\hat{Z}_{x_1, x_2})_{(x_1, x_2) \in \mathbb{N}^2}$.
- Here we have thus obtained a family (indexed by λ) of stationary measures for the Inverse-Beta polymer. These correspond to discrete random walks at fixed t as a function of x for the free energy $-\log \check{Z}_t(x)$. We will see in the following that these random walks have generally a non-zero drift, except in the ‘equilibrium case’ $\lambda = \gamma/2$. This discrete stationary measure is thus a natural generalization of the stationary measure of the continuum DP, or equivalently of the 1 dimensional KPZ equation [248, 195]. Note also that as in the continuum case, the stationary measure only concerns quotients of partition sums/differences of free-energies and the one-point distribution of $\check{Z}_t(0)$ is not stationary. Hence the full process $(\check{Z}_t(x))_{t=0, \dots, T; x \in \mathbb{Z}}$, which can be equivalently parametrized by the couple $(\check{Z}_t(x=0), (\check{U}_t(x), \check{V}_t(x))_{t=0, \dots, T; x \in \mathbb{Z}})$ is not stationary, but the process we are studying however $(\check{U}_t(x), \check{V}_t(x))_{t=0, \dots, T; x \in \mathbb{Z}}$, is a marginal of the latter and is stationary.

G.4.3 Reversibility of the stationary measure: detailed balance property

We now discuss the reversibility of the stationary process. We first study reversibility at the level of a DLTR transformation on down-right paths, then at the level of the process $(\check{U}_t(x), \check{V}_t(x))_{x \in \mathbb{Z}}$ and prove the property Prop. G.3.3.

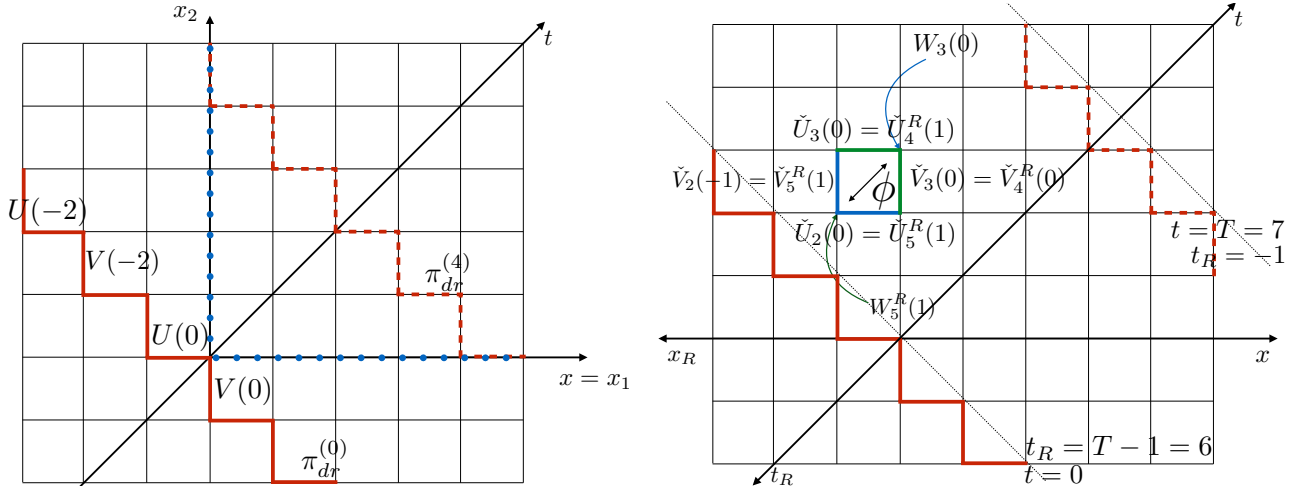


Figure G.6: Left: Stationary measure of the Inverse-Beta polymer with stationary initial condition. The initial down right path $\pi_{dr}^{(0)}$ on which the initial condition is defined carries RVs $\check{U}_{t=0}(x) = U(x)$ and $\check{V}_{t=0}(x) = V(x)$ for which the stationarity property holds. Any down-right paths obtained from $\pi_{dr}^{(0)}$ by down-left to top-right transformations then carries RVs $\check{U}_t(x)$ and $\check{V}_t(x)$ such that the stationarity property holds. These include e.g. all down-right paths $\pi_{dr}^{(t)}$ for $t \geq 0$ (such as $\pi_{dr}^{(4)}$ in dashed-red above) and the boundaries of \mathbb{N}^2 (in dotted blue above). Right: Illustration of the symmetry between the forward and time-reversed process for $T = 7$. In the time evolution of the forward process, the RVs $\check{U}_2(0)$ and $\check{V}_2(-1)$ (on the blue edges above) are transformed using ϕ into the RVs $\check{U}_3(0)$ and $\check{V}_3(0)$ (on the green edges above) using the random Boltzmann weight $W_3(0)$. From this evolution one stores, using ϕ the random Boltzmann weights $W_5^R(1)$ later used in the time evolution of the backward process where the RVs $\check{U}_4^R(1)$ and $\check{V}_4^R(0)$ (on the green edges above) are evolved using ϕ into the RVs $\check{U}_5^R(1)$ and $\check{V}_5^R(1)$.

a At the level of a down-left to top-right transformation

We now show a detailed-balance property for the stationary measure, namely that, if (U, V, W) are distributed as in (G.3.7) and (G.3.3) and $(U', V', W') = \phi(U, V, W)$, then the PDF of the couples of couples of RVS $P((U', V'); (U, V))$ is symmetric by exchange $(U, V) \leftrightarrow (U', V')$. Indeed, let us consider $((U', V'); (U, V))$ fixed and note $P_{stat}(U, V, W) = P_U(U)P_V(V)P_W(W)$ the stationary PDF of the triplet of RVs in (G.4.3) (see (G.3.3) and (G.3.7) for the expressions of $P_U(U)$, $P_V(V)$ and $P_W(W)$). We have

$$\begin{aligned} P((U', V'); (U, V)) &= \int dW \delta(U' - \phi^{(1)}(U, V, W)) \delta(V' - \phi^{(2)}(U, V, W)) P_{stat}(U, V, W) \\ &= \int dW \int dU'' dV'' dW'' \delta(U' - \phi^{(1)}(U, V, W)) \delta(V' - \phi^{(2)}(U, V, W)) \end{aligned} \quad (\text{G.4.7})$$

$$\begin{aligned} &\delta^{(3)}((U, V, W) - \phi(U'', V'', W'')) P_{stat}(U'', V'', W'') \\ &= \int dW \int dU'' dV'' dW'' \delta(U' - U'') \delta(V' - V'') \end{aligned} \quad (\text{G.4.8})$$

$$\begin{aligned} &\delta^{(3)}((U, V, W) - \phi(U'', V'', W'')) P_{stat}(U'', V'', W'') \\ &= \int dW'' \delta(U - \phi^{(1)}(U'', V'', W'')) \delta(V - \phi^{(2)}(U'', V'', W'')) P_{stat}(U'', V'', W'') \end{aligned}$$

$$\implies P((U', V'); (U, V)) = P((U, V); (U', V')) \quad (\text{G.4.9})$$

which is the desired detailed balance property. Here we have successively used that ϕ preserves the PDF $P_{stat}(U, V, W)$ (in (G.4.7)) and that ϕ is an involution (in (G.4.8)). This property can also be rewritten in the more usual form, using that $P((U', V'); (U, V)) = P((U', V')|(U, V))P_{stat}(U, V)$, with $P_{stat}(U, V) = P_U(U)P_V(V)$ the stationary PDF of the couple of RVs (U, V) ,

$$\frac{P((U', V')|(U, V))}{P((U, V)|(U', V'))} = \frac{P_{stat}(U', V')}{P_{stat}(U, V)}. \quad (\text{G.4.10})$$

From a more pragmatcal point of view, the above detailed balance property can also be proven using direct calculations. One easily obtains from (G.4.3) and (G.3.7) that

$$P((U', V')|(U, V)) = \frac{\Gamma(\gamma + \beta)}{\Gamma(\gamma)\Gamma(\beta)} \frac{\left(V \left(-\frac{U-VU'}{VU'+V} \right)^\beta \left(\frac{U+V}{VU'+V} \right)^\gamma \right)}{(VU' - U)} \delta \left(V' - \frac{U'V}{U} \right) \theta(U > 0) \theta(V > 1), \quad (\text{G.4.11})$$

and Eq. (G.4.10) can then directly be checked.

b At the level of the full space-time process

We now give two proofs of the property Prop. G.3.2, with the first only relying on the detailed balance property (G.4.10) and which will be useful for the BG polymer case. We remind the reader that on a finite time interval $t \in [0, T]$ with $T \in \mathbb{N}^*$, the time-reversed coordinates are defined as (see (G.3.28)) $t_R = T - t - 1$ and $x_R = -x$. The stationary forward process is defined by drawing a random environment $(W_t(x))_{t=1, \dots, T, x \in \mathbb{Z}}$ according to (G.3.3), an initial condition $(\check{U}_{t=0}(x), \check{V}_{t=0}(x))$ according to the stationary measure (G.3.7), and let it deterministically evolve using (G.4.4). The time-reversed process was defined for $t_R \in [0, T]$ in (G.3.29) as

$$\check{U}_{t_R}^R(x_R) = \check{U}_{t=T-t_R}(x = -x_R + 1) \quad , \quad \check{V}_{t_R}^R(x_R) = \check{V}_{t=T-t_R}(x = -x_R). \quad (\text{G.4.12})$$

Let us first comment on this definition. First note the shift by one unity of the x coordinate in the definition of $\check{U}_{t_R}^R(x_R)$ compared to $\check{V}_{t_R}^R(x_R)$. The reason for this is that, in the forward evolution, ϕ mixes up RVs (U, V) living on edges leading to different vertices (forming a down-left corner) and creates RVs (U', V') living on edges leading to the same vertex (forming a top-right corner) (see (G.4.4)). In the time-reversed process the U' and V' RVs are then reinterpreted as living on edges leading to different vertices (forming a down-left corner in the (t_R, x_R) coordinates) whereas the RVs U and V live on edges leading to the same vertex (forming a top-right corner in the (t_R, x_R) coordinates). The shift by one unity of the t coordinate in the definition of $\check{U}_{t_R}^R(x_R)$ and $\check{V}_{t_R}^R(x_R)$ (compared to (G.3.28)) ensures that the final values at $t = T$ of the forward process are initial values at $t_R = 0$ for the backward process. This is illustrated on the right of Fig. G.6. Introducing these notations permits to rewrite the detailed balance condition (G.4.9) as

$$\begin{aligned} P((\check{U}_{t+1}^R(x), \check{V}_{t+1}^R(x)), (\check{U}_t(x), \check{V}_t(x-1))) &= P((\check{U}_t(x), \check{V}_t(x-1)), (\check{U}_{t+1}^R(x), \check{V}_{t+1}^R(x))) \\ &= P((\check{U}_{t_R+1}^R(x_R), \check{V}_{t_R+1}^R(x_R)), (\check{U}_{t_R}^R(x_R), \check{V}_{t_R}^R(x_R-1))) \end{aligned} \quad (\text{G.4.13})$$

(here we used that the process is homogeneous and stationary). Using inductively (G.4.13) (and using that the measure is stationary and that the RVs $\check{U}_t(x)$ and $\check{V}_t(x)$ at different position x are independent) shows the equality in law stated in Prop. G.3.3 between the forward and time-reversed process. Another way to understand this reversibility property is to explicitly construct a random environment in which the reversed process performs a forward evolution. In this case we use the stronger (compared to the detailed balance property (G.4.9)) property of reversibility of ϕ Prop. G.4.2:

1. Start from a drawing of a random environment $(W_t(x))_{t=1,\dots,T,x \in \mathbb{Z}}$ distributed as in (G.3.3) and of the variables $(\check{U}_{t=0}(x), \check{V}_{t=0}(x))$ distributed according to the stationary measure (G.3.7).
2. Evolve $(\check{U}_t(x), \check{V}_t(x))$ from $t = 0$ to $t = T$ according to (G.4.4). At each time step, store also a new disorder RV as, for $1 \leq t_r \leq T$,

$$W_{t_r}^R(x_R) = \phi^{(3)}(\check{U}_t(x), \check{V}_t(x-1), W_{t+1}(x))|_{t=T-t_r, x=-x_R+1}. \quad (\text{G.4.14})$$

3. Then, using that ϕ is an involution (Prop. G.4.2) shows that the backward process satisfies

$$\check{U}_{t_r+1}^R(x_R) = \phi^{(1)}(\check{U}_{t_r}^R(x), \check{V}_{t_r}^R(x-1), W_{t_r+1}^R(x)) \quad , \quad \check{V}_{t_r+1}^R(x) = \phi^{(2)}(\check{U}_{t_r}^R(x), \check{V}_{t_r}^R(x_R-1), W_{t_r+1}^R(x_R)) \quad , \quad (\text{G.4.15})$$

that is, the backward process satisfies a forward evolution in the random environment $W_{t_r}^R(x_R)$, which is, using the properties of ϕ , a legitimate Inverse-Beta random environment (i.e. the $W_{t_r}^R(x_R)$ are independent and distributed as (G.3.3) and are independent of the stationary initial condition $(\check{U}_{t_r=0}^R(x_R), \check{V}_{t_r=0}^R(x_R))$).

This shows in a more constructive fashion that the backward process is indistinguishable from a forward process and that the equality in law (G.3.30) holds. This procedure is illustrated on the right of Fig. G.6. Note finally that if the RVs in the reversed process are interpreted as quotients of time-reversed partition sums $\check{Z}_{t_r}^R(x_R)$, we must have by definition

$$\begin{aligned} \check{U}_{t_r}^R(x_R) &= \frac{\check{Z}_{t_r}^R(x_R)}{\check{Z}_{t_r-1}^R(x_R-1)} = \check{U}_{T-t_r}(-x_R+1) = \frac{\check{Z}_{T-t_r}(-x_R+1)}{\check{Z}_{T-t_r-1}(-x_R)} \quad , \\ \check{V}_{t_r}^R(x_R) &= \frac{\check{Z}_{t_r}^R(x_R)}{\check{Z}_{t_r-1}^R(x_R)} = \check{V}_{T-t_r}(-x_R) = \frac{\check{Z}_{T-t_r}(-x_R)}{\check{Z}_{T-t_r-1}(-x_R)} \quad , \end{aligned} \quad (\text{G.4.16})$$

and an appropriate definition of $\check{Z}_{t_r}^R(x_R)$ is thus

$$\check{Z}_{t_r}^R(x_R) := \frac{1}{\check{Z}_{T-t_r-1}(-x_R)}. \quad (\text{G.4.17})$$

Alternatively one can multiply this definition by a constant term as $\check{Z}_{t_r}^R(x_R) := \check{Z}_{T-1}(0)/\check{Z}_{T-t_r-1}(-x_R)$ to ensure the initial condition $\check{Z}_{t_r}^R(0) = 1$ as well. In this case one has in law $(\check{Z}_t(x))_{t=0,\dots,T;x \in \mathbb{Z}} \sim (\check{Z}_{t_r}^R(x_R))_{t_r=0,\dots,T;x_R \in \mathbb{Z}}$.

G.4.4 Relation to other models

In this section we explicitly consider the implication of our results for the Log-Gamma and Stric-Weak polymers, two exactly solvable models of DPs on \mathbb{Z}^2 that can be obtained as limits of the IB polymer. We will not discuss here the 0 temperature limits $(\gamma, \beta) \rightarrow (0, 0)$, whose discussion is reported to Sec. G.5.2. We will use here the language of polymers with boundaries to discuss the stationary measures.

a Limit to the Log-Gamma polymer

In [5] it was shown that the point-to-point partition-sum of the Inverse-Beta polymer (without boundaries) converges to the partition-sum of the Log-Gamma polymer as

$$\lim_{\beta \rightarrow \infty} \frac{Z_{x_1, x_2}}{\beta^{x_1+x_2}} = Z_{x_1, x_2}^{LG} \quad , \quad (\text{G.4.18})$$

where the limit holds in law and Z_{x_1, x_2}^{LG} is the partition sum of the Log-Gamma polymer. The latter is defined as in Def. G.3.1 but in this case the random variables are distributed as $u^{LG} = v^{LG}$ and $(u^{LG})^{-1}$ is distributed as a Gamma distribution with parameter $\gamma > 0^3$. At the level of the random Boltzmann weights the convergence in law reads

$$\left(\frac{u}{\beta}, \frac{v}{\beta} \right) \sim \left(\frac{1 - \text{Beta}(\gamma, \beta)}{\beta \text{Beta}(\gamma, \beta)}, \frac{1}{\beta \text{Beta}(\gamma, \beta)} \right) \sim_{\beta \rightarrow \infty} (u^{LG}, v^{LG}) \sim \frac{(1, 1)}{\text{Gamma}(\gamma)}. \quad (\text{G.4.19})$$

In the same way, using (G.3.7), (G.3.3), a stationary Log-Gamma polymer with boundaries is obtained as

$$\begin{aligned} \hat{Z}_{x_1, x_2}^{LG} &= \lim_{\beta \rightarrow \infty} \frac{\check{Z}_{x_1, x_2}}{\beta^{x_1+x_2}} \quad , \\ U^{LG} &= \lim_{\beta \rightarrow \infty} \frac{U}{\beta} \sim (\text{Gamma}(\gamma - \lambda))^{-1} \quad , \\ V^{LG} &= \lim_{\beta \rightarrow \infty} \frac{V}{\beta} \sim (\text{Gamma}(\lambda))^{-1} \quad , \\ W^{LG} &= \lim_{\beta \rightarrow \infty} \frac{W}{\beta} \sim (\text{Gamma}(\gamma))^{-1} \quad , \end{aligned} \quad (\text{G.4.20})$$

(all these limits hold in law). Here \hat{Z}_{x_1, x_2}^{LG} is the partition sum of the Log-Gamma polymer with boundaries defined as for the IB polymer with boundaries (see Def G.3.2) with random BWs distributed as $U_{x_1, 0} \sim U^{LG}$, $V_{0, x_2} \sim V^{LG}$ and $u_{x_1, x_2} = v_{x_1, x_2} \sim W^{LG}$. This is the same model as introduced in [197] and our results of stationarity in the IB polymer imply the results Lemma 3.2 and Theorem 3.3 of [197].

³Here $u^{LG} = v^{LG}$ means that the random Boltzmann weights can equally well be interpreted as living on the vertices of the square lattice

b Limit to the Strict-Weak polymer

In [5] it was shown that the point-to-point partition-sum of the Inverse-Beta polymer converges to the partition-sum of the Strict-Weak polymer without boundaries as

$$\lim_{\gamma \rightarrow \infty} \gamma^{x_1} Z_{x_1, x_2} = Z_{x_1, x_2}^{SW}, \quad (\text{G.4.21})$$

where the limit holds in law and Z_{x_1, x_2}^{SW} is the partition sum of the Strict-Weak polymer. It is defined as in Def. G.3.1 but in this case the random variables are distributed as $v^{SW} = 1$ and u^{SW} is distributed with a Gamma distribution of parameter $\beta > 0$. At the level of the random Boltzmann weights the convergence in law reads

$$(\gamma u, v) \sim \left(\frac{\gamma(1 - \text{Beta}(\gamma, \beta))}{\text{Beta}(\gamma, \beta)}, \frac{1}{\text{Beta}(\gamma, \beta)} \right) \sim_{\gamma \rightarrow \infty} (u^{SW}, v^{SW}) \sim (\text{Gamma}(\beta), 1). \quad (\text{G.4.22})$$

A stationary Strict-Weak polymer with boundaries is similarly obtained as, using (G.3.7) and (G.3.3),

$$\begin{aligned} \hat{Z}_{x_1, x_2}^{SW} &= \lim_{\gamma \rightarrow \infty} \gamma^{x_1} \hat{Z}_{x_1, x_2}, \\ U^{SW} &= \lim_{\gamma \rightarrow \infty} \gamma U \sim \text{Gamma}(\beta + \lambda), \\ V^{SW} &= \lim_{\gamma \rightarrow \infty} V \sim (\text{Beta}(\lambda, \beta))^{-1}, \\ W^{SW} &= \lim_{\gamma \rightarrow \infty} \gamma W \sim \text{Gamma}(\beta), \end{aligned} \quad (\text{G.4.23})$$

(all these limits hold in law). Here \hat{Z}_{x_1, x_2}^{SW} is the partition sum of the stationary Strict-Weak polymer with boundaries defined as for the IB polymer with boundaries with random BWs distributed as $U_{x_1, 0} \sim U^{SW}$, $V_{0, x_2} \sim V^{SW}$, $u_{x_1, x_2} \sim W^{LG}$ and $v_{x_1, x_2} = 1$. It satisfies stationarity and reversibility properties inherited from those of the IB polymer (see Sec. a). We note that this stationary Strict-Weak polymer with boundaries differs from the one considered in [219]. Indeed, the admissible paths considered in [219] differ from ours, and so does the stationarity property there obtained which involve ratios of partition sums slightly different from ours (see Definition 6.1, Proposition 6.2 and Lemma 6.3 in [219]). While these two stationary process are different, we note that the ESPs that underly them are different incarnations of the Beta-Gamma algebra of RVs.

G.5 Zero temperature model: Stationary measure of the Bernoulli-Geometric polymer

In this section we obtain the stationarity properties of the BG polymer with boundary conditions and stationary initial condition stated in Sec. b and discuss the link between our results and previous results on other models. Thanks to the notations we used, the proof of these properties will be (almost) completely analogous to the finite temperature case and we will thus give much less details in this section.

G.5.1 Stationarity properties of the Bernoulli-Geometric polymer

Let us first focus on the case of the BG polymer with boundaries defined in Def. G.3.5. In the bulk of \mathbb{N}^2 , the optimal energy in the BG polymer with boundaries satisfies the following recursion equation

$$\hat{E}_{x_1, x_2} = \min \left(\hat{E}_{x_1-1, x_2} + u_{x_1, x_2}, \hat{E}_{x_1, x_2-1} + v_{x_1, x_2} \right) \text{ for } (x_1, x_2) \in (\mathbb{N}^*)^2. \quad (\text{G.5.1})$$

This implies the bulk recursion equation for the horizontal and vertical differences of optimal energies (see (G.3.32))

$$\hat{U}_{x_1, x_2} = \phi_{T=0}^{(1)} \left(\hat{U}_{x_1, x_2-1}, \hat{V}_{x_1-1, x_2}, u_{x_1, x_2}, v_{x_1, x_2} \right), \quad \hat{V}_{x_1, x_2} = \phi_{T=0}^{(2)} \left(\hat{U}_{x_1, x_2-1}, \hat{V}_{x_1-1, x_2}, u_{x_1, x_2}, v_{x_1, x_2} \right). \quad (\text{G.5.2})$$

where we have introduced the $T = 0$ stationarity map that we now define.

Definition G.5.1. The $T = 0$ stationarity map $\phi_{T=0}$ is the function $\phi_{T=0} : (\mathbf{U}, \mathbf{V}, \mathbf{u}, \mathbf{v}) \in \mathbb{Z}^4 \rightarrow (\mathbf{U}', \mathbf{V}') \in \mathbb{Z}^2$ defined by

$$\mathbf{U}' = \min(\mathbf{u}, \mathbf{v} + \mathbf{U} - \mathbf{V}) \quad , \quad \mathbf{V}' = \min(\mathbf{u} + \mathbf{V} - \mathbf{U}, \mathbf{v}) = \mathbf{U}' + \mathbf{V} - \mathbf{U}. \quad (\text{G.5.3})$$

It has the following properties (below and throughout the rest of the paper \perp means ‘independent of’):

Proposition G.5.1. Stationarity *If $\mathbf{U}, \mathbf{V}, \mathbf{u}$ and \mathbf{v} are RVs distributed as in (G.3.12) and (G.3.20) with $\mathbf{U} \perp \mathbf{V} \perp (\mathbf{u}, \mathbf{v})$, then the RVs \mathbf{U}', \mathbf{V}' in (G.5.3) are distributed as in (G.3.20) with $\mathbf{U}' \perp \mathbf{V}'$.*

Proposition G.5.2. Detailed balance *If $\mathbf{U}, \mathbf{V}, \mathbf{u}$ and \mathbf{v} are RVs distributed as in (G.3.12) and (G.3.20) with $\mathbf{U} \perp \mathbf{V} \perp (\mathbf{u}, \mathbf{v})$ and \mathbf{U}' and \mathbf{V}' are given by (G.5.3), then*

$$\text{Proba} \left((\mathbf{U}', \mathbf{V}') = (k_{U'}, k_{V'}), (\mathbf{U}, \mathbf{V}) = (k_U, k_V) \right) = \text{Proba} \left((\mathbf{U}', \mathbf{V}') = (k_U, k_V), (\mathbf{U}, \mathbf{V}) = (k_{U'}, k_{V'}) \right). \quad (\text{G.5.4})$$

These two properties are proved in Appendix G.10. Thanks to the existence of these properties and of the induction (G.5.2), the stationarity properties of the BG polymer with boundaries (and similarly of the BG polymer with stationary initial condition) then easily follow as in the previous section by induction on down-right paths.

Remarks

- Note that contrary to the stationarity-reversibility map ϕ defined for the Inverse-Beta polymer in Def. G.4.1, the stationarity map of the $\phi_{T=0}$ model is not an involution. We were not able to extend as before $\phi_{T=0}$ to an involution $\tilde{\phi}_{T=0} : (\mathbf{U}, \mathbf{V}, \mathbf{u}, \mathbf{v}) \rightarrow (\mathbf{U}', \mathbf{V}', \mathbf{u}', \mathbf{v}')$ that conserves the PDF and the independence of \mathbf{U}, \mathbf{V} and of the couple (\mathbf{u}, \mathbf{v}) . We believe this is related to the fact that the recursion equation (G.5.2) ‘loses some memory’, in the sense that if \mathbf{u}_{x_1, x_2} in (G.5.2) is too large, its value cannot be inferred from the sole knowledge of \mathbf{U}_{x_1, x_2} and \mathbf{V}_{x_1, x_2} . Nevertheless, we were still able to prove the detailed balance property (G.5.4), which is sufficient to prove the reversibility property of the stationary process Prop. G.3.7 in the BG polymer with stationary initial condition as for the IB polymer with stationary initial condition: the only difference is that we do not have the explicit construction of the random environment in which the backward process (G.3.34) satisfies a forward evolution equation.
- Sets of random variables satisfying a stationarity property similar to the one of the stationarity map (G.4.3) have played over the years an important role in the theory of queuing systems since they also provide in this framework models with an exact solvability property. The first occurrence of a property of this type in this context is due to Burke for the case of exponentially distributed RVs [199]. Since then such properties have been designated as Burke properties. Examples of sets of RVs for which Burke properties have been shown notably include systems of Geometric variables [216] and more recently mixture of Bernoulli and Geometric variables very similar to the ones considered here [269]. The exact solvability property studied in [269] does not however seem trivially connected to the one studied here. From the technical point of view we note that it involves 4 independent Geometric RVs (while our property involves 5), and more conceptually the model studied in [269] naturally corresponds to a problem of first passage percolation, while our model interpolates between problems of first and last passage percolation (see Sec. G.5.2).

G.5.2 Relation to other models

Let us now discuss the relations between this model and other known models. We discuss this in the framework of the model with boundaries in order to obtain the stationary measure of the limiting model as well. In the following we will only study the limits at the level of the random energies $(\mathbf{u}, \mathbf{v}, \mathbf{U}, \mathbf{V})$. Each limit can be used to define a model equivalent to the BG polymer with boundaries (see Def. G.3.5) with different distributions of energies in the bulk and on the boundaries and a stationarity property on down-right paths.

a $q' \rightarrow 0$ limit: last passage percolation with geometric waiting times

An isotropic limit of the model is obtained by letting $q' \rightarrow 0$. In this case the random energies that enters into the definition of the model with boundaries are distributed as

$$\begin{aligned} \mathbf{u}^{gLPP} &= \mathbf{v}^{gLPP} = -G_q , \\ \mathbf{U}^{gLPP} &= -G_{q/q_b} , \\ \mathbf{V}^{gLPP} &= -G_{q_b} . \end{aligned} \tag{G.5.5}$$

This model exactly corresponds to geometric last passage percolation as e.g. studied in [159] for the case without boundaries (note that $\mathbf{u}^{gLPP} = \mathbf{v}^{gLPP}$ implies that the bulk random energies can be interpreted as living on the vertices of \mathbb{N}^2). Indeed, note that while the random energies in the Bernoulli-Geometric polymer can generally be both positive and negative, in this limit the energies are always negative and the energy-minimization problem can be reinterpreted as a maximization problem of the last passage time. The latter is given by $\mathbf{T}_{x_1, x_2} := -\mathbf{E}_{x_1, x_2} = \max \left\{ \sum_{e \in \pi} \mathbf{t}_e, \pi : (0, 0) \rightarrow (x_1, x_2) \right\}$, where the random waiting times on the edges are the opposite of the random energies, $\mathbf{t}_e := -\mathcal{E}(e) \geq 0$. This model was denoted Geo-LPP in Fig. G.1.

b $q \rightarrow 0$ limit: a first passage percolation problem with Geometric waiting times

An anisotropic limit is obtained by letting $q \rightarrow 0$ with q' fixed. We obtain

$$\begin{aligned} (\mathbf{u}^{bgFPP}, \mathbf{v}^{bgFPP}) &= ((1 - \xi_{uv})(1 + G_{q'}), 0) , \\ \mathbf{U}^{bgFPP} &= (1 - \xi_U)(1 + G_{q_b q'}) , \\ \mathbf{V}^{bgFPP} &= -\xi_V G_{q_b} . \end{aligned} \tag{G.5.6}$$

with now $p_{uv} = 1 - q'$, $p_U = 1 - q_b q'$ and $p_V = \frac{1 - q'}{1 - q_b q'}$. Note that in this limit the energies on the (bulk) edges are either 0 (for vertical edges) or positive. Note also that we can replace the bulk energies on horizontal edges by a simple geometric RV since we have the equality in law $(1 - \xi_{uv})(1 + G_{q'}) \sim G_{q'}$. In this limit the optimal energy \mathbf{E}_{x_1, x_2} is thus always the sum of positive terms and the model is naturally interpreted as a model of first passage percolation. Here the first passage time is $\mathbf{T}_{x_1, x_2} := +\mathbf{E}_{x_1, x_2} = \min \left\{ \sum_{e \in \pi} \mathbf{t}_e, \pi : (0, 0) \rightarrow (x_1, x_2) \right\}$, where the random waiting times on the edges are equal to the random energies, $\mathbf{t}_e := +\mathcal{E}(e) \geq 0$. This model was denoted Anisotropic Geo-FPP in Fig. G.1. This model was already studied in the language of queuing system in [216] where the authors obtained an analogue Burke property and also showed that the model could be solved exactly using the RSK correspondence.

c Continuous limit of the Bernoulli-Geometric polymer and $T = 0$ limit of the Inverse-Beta polymer

We now discuss the exponential/continuous limit. It is obtained by letting $\epsilon \rightarrow 0^+$ with

$$q = 1 - \gamma' \epsilon \quad , \quad q' = 1 - \beta' \epsilon \quad , \quad q_b = 1 - (\gamma' - \lambda') \epsilon \quad , \quad (\text{G.5.7})$$

where $\gamma', \beta' > 0$ and $0 < \lambda' < \gamma'$ (to ensure $q_b > q$) are three parameters. In this limit the energies have to be rescaled by ϵ and converge in law to exponentially distributed random variables as

$$\begin{aligned} (\mathbf{u}^{B-Exp}, \mathbf{v}^{B-Exp}) &= \epsilon(\mathbf{u}, \mathbf{v}) \rightarrow_{\epsilon \rightarrow 0} ((1 - \zeta_{uv})E_{\beta'} - \zeta_{uv}E_{\gamma'}, -\zeta_{uv}E_{\gamma'}) \\ \mathbf{U}^{B-Exp} &= \epsilon \mathbf{U} \rightarrow_{\epsilon \rightarrow 0} (1 - \zeta_U)E_{\beta'+\lambda'} - \zeta_U E_{\gamma'-\lambda'} \\ \mathbf{V}^{B-Exp} &= \epsilon \mathbf{V} \rightarrow_{\epsilon \rightarrow 0} -\zeta_V E_{\lambda'} \end{aligned} \quad (\text{G.5.8})$$

where ζ_{uv} , ζ_U and ζ_V are Bernoulli RVs with parameters $p_{uv} = \frac{\beta'}{\beta'+\gamma'}$, $p_U = \frac{\beta'+\lambda'}{\beta'+\gamma'}$ and $p_V = \frac{\beta'}{\beta'+\lambda'}$ and $E_{\gamma'}$, $E_{\beta'}$, $E_{\gamma'-\lambda'}$, $E_{\lambda'}$ and $E_{\beta'+\lambda'}$ denote exponentially distributed RVs. Let us recall here that the PDF of an exponentially distributed RV is

$$E_\alpha \sim Exp(\alpha) \quad , \quad p(E_\alpha) = \alpha e^{-\alpha E_\alpha} \quad . \quad (\text{G.5.9})$$

The optimal energy in this model has to be scaled accordingly as

$$\hat{\mathbf{E}}_{x_1, x_2}^{B-Exp} = \lim_{\epsilon \rightarrow 0} \epsilon \hat{\mathbf{E}}_{x_1, x_2} \quad , \quad (\text{G.5.10})$$

and the results previously obtained in the BG polymer with boundaries also apply to this model using the now exponentially distributed weights (G.5.8). We call this model the Bernoulli-Exponential polymer with boundaries (denoted as Bernoulli-Exp in Fig. G.1). This model can also be obtained from the IB polymer with boundaries using $\gamma = \epsilon\gamma'$, $\beta = \epsilon\beta'$, $\lambda = \epsilon\lambda'$ and scaling the energies as

$$\begin{aligned} (\mathbf{u}^{B-Exp}, \mathbf{v}^{B-Exp}) &= -\epsilon(\log u, \log v) \rightarrow_{\epsilon \rightarrow 0} ((1 - \zeta_{uv})E_{\beta'} - \zeta_{uv}E_{\gamma'}, -\zeta_{uv}E_{\gamma'}) \quad , \\ \mathbf{U}^{B-Exp} &= -\epsilon \log U \rightarrow_{\epsilon \rightarrow 0} (1 - \zeta_U)E_{\beta'+\lambda'} - \zeta_U E_{\gamma'-\lambda'} \quad , \\ \mathbf{V}^{B-Exp} &= -\epsilon \log V \rightarrow_{\epsilon \rightarrow 0} -\zeta_V E_{\lambda'} \quad , \\ \hat{\mathbf{E}}_{x_1, x_2}^{B-Exp} &= \lim_{\epsilon \rightarrow 0} -\epsilon \log \hat{Z}_{x_1, x_2} \quad . \end{aligned} \quad (\text{G.5.11})$$

Here the convergence in law of the logarithm of the random Boltzmann weights of the Inverse-Beta polymer to a mixture of Bernoulli and exponential distributions was shown in [5]. We refer the reader to [5] for the Bethe ansatz study of this polymer model (without boundary conditions) where the authors notably obtain the full distribution of the optimal energy and show Tracy-Widom GUE asymptotic limit. The Bernoulli-Exponential polymer with boundaries has stationarity properties inherited from the stationarity properties of the IB polymer with boundaries, and was first introduced using the limit (G.5.11). *The definition of the Bernoulli-Geometric polymer with boundaries Def. G.3.5 was found by trial and error as a discretization of the Bernoulli-Exponential polymer with boundaries which conserves these stationarity properties* (see in particular Appendix G.10).

Isotropic limit: Exponential last passage percolation

Note that the Bernoulli-Exponential polymer (G.5.8) admits an isotropic limit $\beta' \rightarrow \infty$ which converges to exponential last passage percolation: in this limit

$$\begin{aligned} \mathbf{u}^{eLPP} &= \mathbf{v}^{eLPP} = -E_{\gamma'} \quad , \\ \mathbf{U}^{eLPP} &= -E_{\lambda'} \quad , \\ \mathbf{V}^{eLPP} &= -E_{\gamma'-\lambda'} \quad . \end{aligned} \quad (\text{G.5.12})$$

This model can also be obtained from the continuum limit ($(q, q_b) = (1 - \epsilon\gamma', 1 - \epsilon\lambda')$, $\epsilon \rightarrow 0$) of geometric last passage percolation (G.5.5), or also directly as the zero-temperature limit ($(\gamma, \lambda) = \epsilon(\gamma', \lambda')$ with $\epsilon \rightarrow 0$) of the Log-Gamma polymer (G.4.20), and was denoted Exp-LPP in Fig. G.1. The first occurrence of this stationary model in the literature was in the language of queuing system and is due to Burke in [199]. Here again $\mathbf{u}^{eLPP} = \mathbf{v}^{eLPP}$ implies that the random energies can be interpreted as living on the sites of \mathbb{N}^2 .

Anisotropic limit: anisotropic Exponential first passage percolation

One can also consider an anisotropic limit $\gamma' \rightarrow \infty$ of the Bernoulli-Exponential polymer (G.5.8) to obtain a first passage percolation problem with exponential waiting times:

$$\begin{aligned} (\mathbf{u}^{eFPP}, \mathbf{v}^{eFPP}) &= (E_{\beta'}, 0) \\ \mathbf{U}^{eFPP} &= E_{\beta'+\lambda'} \\ \mathbf{V}^{eFPP} &= -\zeta_V E_{\lambda'} \quad . \end{aligned} \quad (\text{G.5.13})$$

This model can also be obtained from the continuum limit ($(q', q_b) = (1 - \epsilon\beta', 1 - \epsilon\lambda')$, $\epsilon \rightarrow 0$) limit of (G.5.5), or also as the zero temperature limit ($(\beta, \lambda) = \epsilon(\beta', \lambda')$ with $\epsilon \rightarrow 0$) of the Strict-Weak polymer (G.4.23). As for its geometric counterpart (G.5.5) this model was studied in [216]. It was noted Anisotropic Exp-FPP in Fig. G.1.

G.6 Quenched free-energy, Angle-Boundary parameter equivalence and convergence to the stationary state of point to point models

In this section we first obtain in Sec. G.6.1 preliminary results on the mean optimal energy in the BG polymer with boundaries and the mean free-energy in the IB polymer with boundaries. In Sec. G.6.2 we use these results to obtain the mean quenched optimal energy/free-energy in models without boundaries (Eq. (G.3.38) and (G.3.40)). In Sec. G.6.3 we will discuss the convergence of point to point models to their stationary state (see Sec. G.3.4). Finally in Sec. G.6.4 we will comment on free-energy fluctuations and optimal path properties in models with boundaries.

Let us first collect here some definitions for the mean energies of bulk and boundaries random Boltzmann weights/energies in these models. Below and as before u, v, U, V and u, v, U, V denote RVs distributed as in Def. G.3.2 and Def. G.3.5. We define

$$\begin{aligned}
f_U^{\gamma, \beta}(\lambda) &:= -\overline{\log U} = -\psi(\beta + \lambda) + \psi(\gamma - \lambda) & f_U^{q, q'}(q_b) &:= \bar{U} = \frac{q_b^2 q' - q}{(q_b - q)(1 - q_b q')}, \\
f_V^{\gamma, \beta}(\lambda) &:= -\overline{\log V} = -\psi(\beta + \lambda) + \psi(\lambda) & f_V^{q, q'}(q_b) &:= \bar{V} = -\frac{1 - q'}{1 - q_b q'} \frac{q_b}{1 - q_b}, \\
f_u^{\gamma, \beta} &:= -\overline{\log u} = -\psi(\beta) + \psi(\gamma) & f_u^{q, q'} &:= \bar{u} = \frac{q' - q}{(1 - q)(1 - q')}, \\
f_v^{\gamma, \beta} &:= -\overline{\log v} = -\psi(\beta + \gamma) + \psi(\gamma) & f_v^{q, q'} &:= \bar{v} = -\frac{1 - q'}{1 - q q'} \frac{q}{1 - q},
\end{aligned} \tag{G.6.1}$$

where $\psi = \frac{\Gamma'}{\Gamma}$ is the diGamma function. A key property of models with boundaries, that will notably play a crucial role in the remaining of this section, is that boundaries are attractive.

Indeed it follows from the fact that ψ is strictly increasing and concave that $f_U^{\gamma, \beta}(\lambda) \leq f_u^{\gamma, \beta}$ (equality for $\lambda \rightarrow 0$), $f_V^{\gamma, \beta}(\lambda) \leq f_v^{\gamma, \beta}$, (equality for $\lambda \rightarrow \gamma$). Furthermore, when $\lambda \rightarrow 0$ (resp. $\lambda \rightarrow \gamma$), $f_V^{\gamma, \beta}(\lambda) \rightarrow -\infty$ (resp. $f_U^{\gamma, \beta}(\lambda) \rightarrow -\infty$) and the vertical (resp. horizontal) boundary becomes infinitely attractive. Note also that $f_V^{\gamma, \beta}(\lambda)$ increases with λ while $f_U^{\gamma, \beta}(\lambda)$ decays with λ . Finally note that for $0 < \lambda < \gamma/2$ (resp. $\gamma/2 < \lambda < \gamma$), $f_V^{\gamma, \beta}(\lambda) < f_U^{\gamma, \beta}(\lambda)$ (resp. $f_U^{\gamma, \beta}(\lambda) < f_V^{\gamma, \beta}(\lambda)$) and the vertical (resp. horizontal) boundary is the most attractive. Both boundaries have the same mean energy for $\lambda = \gamma/2$, i.e. $f_U^{\gamma, \beta}(\gamma/2) = f_V^{\gamma, \beta}(\gamma/2)$, a special case referred to as the equilibrium situation in the rest of the paper. Similarly, note that for $q < q_b < 1$, $f_U^{q, q'}(q_b) < f_u^{q, q'}$, $f_V^{q, q'}(q_b) < f_v^{q, q'}$. Note also that $f_U^{q, q'}(q_b)$ increases when q_b increases with $f_U^{q, q'}(q_b) \rightarrow_{q_b \rightarrow q^+} -\infty$ and $f_U^{q, q'}(q_b) \rightarrow_{q_b \rightarrow 1^-} f_u^{q, q'}$, while $f_V^{q, q'}(q_b)$ decays when q_b increases with $f_V^{q, q'}(q_b) \rightarrow_{q_b \rightarrow q^+} f_v^{q, q'}$ and $f_V^{q, q'}(q_b) \rightarrow_{q_b \rightarrow 1^-} -\infty$. Finally $f_U^{q, q'}(q_b) < f_v^{q, q'}(q_b)$ for $q_b < \sqrt{q}$, $f_U^{q, q'}(q_b) > f_v^{q, q'}(q_b)$ for $q_b > \sqrt{q}$ and in the ‘equilibrium case’ $q_b = \sqrt{q}$ we have $f_U^{q, q'}(\sqrt{q}) = f_v^{q, q'}(\sqrt{q})$.

G.6.1 Free-energy in models with boundaries

Bernoulli-Geometric polymer

Let us first focus on the Bernoulli-Geometric polymer with boundaries defined in Def. G.3.5 and write the optimal energy \hat{E}_{x_1, x_2} for $(x_1, x_2) \in \mathbb{N}^2$ as,

$$\hat{E}_{x_1, x_2} = \sum_{i=0}^{x_1} \hat{U}_{i,0} + \sum_{j=0}^{x_2} \hat{V}_{x_1, j}. \tag{G.6.2}$$

Note that this decomposition does not follow a down-right path and the variables \hat{U}_{x_1, x_2} and \hat{V}_{x_1, x_2} in the two sums are correlated. Each one however is distributed as $\hat{U}_{i,0} \sim U$ and $\hat{V}_{x_1, j} \sim V$ as in (G.3.20). Hence we obtain, $\forall (x_1, x_2) \in \mathbb{N}^2$,

$$\overline{\hat{E}_{x_1, x_2}} = x_1 f_U^{q, q'}(q_b) + x_2 f_V^{q, q'}(q_b), \tag{G.6.3}$$

where $f_U^{q, q'}(q_b)$ and $f_V^{q, q'}(q_b)$ were given in (G.6.1). In particular the mean optimal energy in the direction (s_1, s_2) is, for $(s_1, s_2) \in \mathbb{R}_+^2$,

$$\hat{f}_{\text{BG}}(s_1, s_2, q_b) := \lim_{N \rightarrow \infty} \frac{1}{N} \overline{\hat{E}_{N s_1, N s_2}} = s_1 f_U^{q, q'}(q_b) + s_2 f_V^{q, q'}(q_b). \tag{G.6.4}$$

We can also consider the mean optimal energy per-unit-length in a direction $-1/2 < \varphi < 1/2$ as $\hat{f}_{\text{BG}}^{\text{p.u.l.}}(\varphi, q_b) := \lim_{t \rightarrow \infty} \frac{1}{t} \overline{\hat{E}_t(x = (1/2 + \varphi, 1/2 + \varphi), 1/2 - \varphi, q_b)}$, with conversely $\hat{f}_{\text{BG}}(s_1, s_2, q_b) = (s_1 + s_2) \hat{f}_{\text{BG}}^{\text{p.u.l.}}(\frac{s_1 - s_2}{2(s_1 + s_2)}, q_b)$. Note that from (G.6.4), it is clear that the mean optimal energy per-unit-length $\hat{f}_{\text{BG}}^{\text{p.u.l.}}(\varphi, q_b)$ is linear in φ . Furthermore, note that in the special case $q_b = \sqrt{q}$ (referred to as the equilibrium case earlier), $f_U^{q, q'}(q_b) = f_V^{q, q'}(q_b)$ and $\hat{f}_{\text{BG}}^{\text{p.u.l.}}(\varphi, q_b)$ does not depend on φ . We will come back to this point later.

Inverse-Beta polymer

In the same way, in the case of the Inverse-Beta polymer with boundaries, $\forall (x_1, x_2) \in \mathbb{N}^2$, $-\log \hat{Z}_{x_1, x_2} = -\sum_{i=0}^{x_1} \log \hat{U}_{i,0} -$

$\sum_{j=0}^{x_2} \log \hat{V}_{x_1, j}$. We thus have $-\overline{\log \hat{Z}_{x_1, x_2}} = x_1 f_U^{\gamma, \beta}(\lambda) + x_2 f_V^{\gamma, \beta}(\lambda)$, implying that the mean quenched free-energy in the direction $(s_1, s_2) \in \mathbb{R}_+^2$ is

$$\hat{f}_{\text{IB}}(s_1, s_2, \lambda) := - \lim_{N \rightarrow \infty} \frac{1}{N} \overline{\log \hat{Z}_{Ns_1, Ns_2}} = s_1 f_U^{\gamma, \beta}(\lambda) + s_2 f_V^{\gamma, \beta}(\lambda). \quad (\text{G.6.5})$$

And the free-energy per-unit-length in the direction $\varphi \in]-1/2, 1/2[$, $\hat{f}_{\text{IB}}^{\text{p.u.l.}}(\varphi, \lambda) := - \lim_{t \rightarrow \infty} \frac{1}{t} \overline{\log \hat{Z}_{t(1/2+\varphi), t(1/2-\varphi)}} = \hat{f}_{\text{IB}}(1/2 + \varphi, 1/2 - \varphi, \lambda)$ with conversely $\hat{f}_{\text{IB}}(s_1, s_2, \lambda) = (s_1 + s_2) \hat{f}_{\text{IB}}^{\text{p.u.l.}}(\frac{s_1 - s_2}{2(s_1 + s_2)}, \lambda)$. As before, note from (G.6.5) that $\hat{f}_{\text{IB}}^{\text{p.u.l.}}(\varphi, \lambda)$ is generally linear in φ , with the special case that it is constant in the equilibrium situation $\lambda = \gamma/2$.

G.6.2 Free-energy in models without boundaries

a Bernoulli-Geometric polymer

The first part of this section is devoted to the derivation of the formula (G.3.40) for $f(s_1, s_2)$. We believe it to be rather instructive and the main ideas are summarized in Fig. G.7. Furthermore we introduce in this derivation several elements which will be important in Sec. G.6.3. The ideas used in this derivation are close in spirit to those used in

Derivation of a formula for $f_{\text{BG}}(s_1, s_2)$

Let us now consider again the Bernoulli-Geometric model with boundaries defined in Def. G.3.5. $\forall (x_1, x_2) \in (\mathbb{N}^*)^2$ we write the decomposition

$$\hat{E}_{x_1, x_2} = \min \left\{ \min_{i \in [1, x_1]} \left(\sum_{j=1}^i \hat{U}_{j,0} + \mathbf{v}_{i,1} + \mathbf{E}_{x_1, x_2}^{i,1} \right), \min_{i \in [1, x_2]} \left(\sum_{j=1}^i \hat{V}_{0,j} + \mathbf{u}_{1,i} + \mathbf{E}_{x_1, x_2}^{1,i} \right) \right\}, \quad (\text{G.6.6})$$

where we have introduced $\forall (x_1, x_2, x'_1, x'_2) \in (\mathbb{N}^*)^4$ with $x'_1 \leq x_1$ and $x'_2 \leq x_2$, the minimal energy to go from (x'_1, x'_2) to (x_1, x_2)

$$\hat{E}_{x_1, x_2}^{x'_1, x'_2} = \min \left\{ \hat{\mathcal{E}}(\pi) = \sum_{e \in \pi} \hat{\mathcal{E}}(e), \pi : (x'_1, x'_2) \rightarrow (x_1, x_2) \right\}. \quad (\text{G.6.7})$$

Note that an up-right path from (x'_1, x'_2) to (x_1, x_2) cannot pass upon an edge on the boundary of \mathbb{N}^2 . Hence the random energies encountered along the way are only of the bulk type and thus $\hat{E}_{x_1, x_2}^{x'_1, x'_2}$ corresponds to an optimal energy in a model without boundaries. More precisely we have the equality in law, using the statistical translational invariance of the disorder,

$$\hat{E}_{x_1, x_2}^{x'_1, x'_2} \sim \mathbf{E}_{x_1 - x'_1, x_2 - x'_2}, \quad (\text{G.6.8})$$

where here \mathbf{E}_{x_1, x_2} denotes the optimal energy in the point to point Bernoulli-Geometric model as defined in Def. G.3.4. Using (G.6.6), the definitions (G.6.4) and (G.3.37) and the equality in law (G.6.8) we obtain, scaling $i \sim Nr$ in (G.6.6),

$$\begin{aligned} \hat{f}_{\text{BG}}(s_1, s_2, q_b) &= s_1 f_U^{q, q'}(q_b) + s_2 f_V^{q, q'}(q_b) \\ &= \min \left\{ \inf_{0 \leq r \leq s_1} (r f_U^{q, q'}(q_b) + f_{\text{BG}}(s_1 - r, s_2)), \inf_{0 \leq r \leq s_2} (r f_V^{q, q'}(q_b) + f_{\text{BG}}(s_1, s_2 - r)) \right\}. \end{aligned} \quad (\text{G.6.9})$$

The goal is now to ‘invert’ (G.6.9) to obtain $f_{\text{BG}}(s_1, s_2)$. Let us fix $s_1, s_2 > 0$ and study the properties of (G.6.9) as a function of $q_b \in [q, 1]$. Note that in the limit $q_b \rightarrow 1$, $f_V^{q, q'}(q_b) \rightarrow -\infty$ while other quantities stay bounded. As a consequence $\hat{f}_{\text{BG}}(s_1, s_2, q_b) \sim s_2 f_V^{q, q'}(q_b)$ and the minimum in the right hand side of (G.6.9) is attained in the second inf with $r \rightarrow s_2$. Conversely, in the limit $q_b \rightarrow q$, $f_U^{q, q'}(q_b) \rightarrow -\infty$ while other quantities stay bounded, and thus $\hat{f}_{\text{BG}}(s_1, s_2, q_b) \sim s_1 f_U^{q, q'}(q_b)$ and the minimum in the right hand side of (G.6.9) is attained in the first inf with $r \rightarrow s_1$. From this it is clear that there exists a constant $q_{s_1, s_2} \in]q_b, 1[$ such that

$$\begin{aligned} s_1 f_U^{q, q'}(q_b) + s_2 f_V^{q, q'}(q_b) &= \theta(q_{s_1, s_2} - q) \inf_{0 \leq r \leq s_1} (r f_U^{q, q'}(q_b) + f_{\text{BG}}(s_1 - r, s_2)) \\ &\quad + \theta(q - q_{s_1, s_2}) \inf_{0 \leq r \leq s_2} (r f_V^{q, q'}(q_b) + f_{\text{BG}}(s_1, s_2 - r)). \end{aligned} \quad (\text{G.6.10})$$

Let us implicitly define two functions $r_1 : q_b \in [q, q_{s_1, s_2}] \rightarrow r_1(q_b) \in [0, s_1]$ and $r_2 : q_b \in [q_{s_1, s_2}, 1] \rightarrow r_2(q_b) \in [0, s_2]$ such that

$$\begin{aligned} s_1 f_U^{q, q'}(q_b) + s_2 f_V^{q, q'}(q_b) &= \theta(q_{s_1, s_2} - q_b) (r_1(q_b) f_U^{q, q'}(q_b) + f_{\text{BG}}(s_1 - r_1(q_b), s_2)) \\ &\quad + \theta(q_b - q_{s_1, s_2}) (r_2(q_b) f_V^{q, q'}(q_b) + f_{\text{BG}}(s_1, s_2 - r_2(q_b))). \end{aligned} \quad (\text{G.6.11})$$

They satisfy $r_1(q_b) \rightarrow_{q_b \rightarrow q} s_1$, $r_2(q_b) \rightarrow_{q_b \rightarrow 1} s_2$ and are such that

$$\begin{aligned} \forall q_b \in]q, q_{s_1, s_2}[\quad , \quad f_U^{q, q'}(q_b) - \partial_1 f_{\text{BG}}(s_1 - r_1(q_b), s_2) &= 0, \\ \forall q_b \in]q_{s_1, s_2}, 1[\quad , \quad f_V^{q, q'}(q_b) - \partial_2 f_{\text{BG}}(s_1, s_2 - r_2(q_b)) &= 0. \end{aligned} \quad (\text{G.6.12})$$

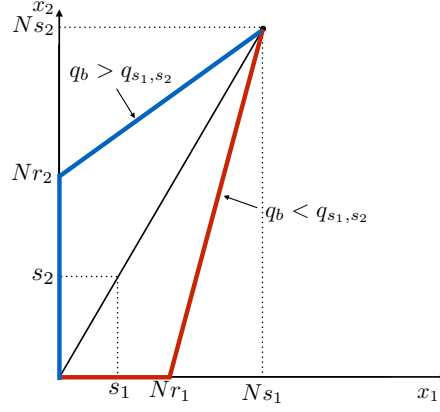


Figure G.7: Cartoon of the notations used in the derivation of (G.6.16). At large N in a fixed direction (s_1, s_2) and varying the boundary parameter q_b , the optimal polymer path sticks to the horizontal (resp. vertical) boundary for Nr_1 (resp. Nr_2) steps for $q_b < q_{s_1, s_2}$ (resp. for $q_b > q_{s_1, s_2}$). We show that r_1 decreases from s_1 to 0 (resp. r_2 increases from 0 to s_2) when q_b increases from q to q_{s_1, s_2} (resp. from q_{s_1, s_2} to 1). We show that $q_{s_1, s_2} = q_b^*(s_1, s_2)$ the solution of the saddle-point equation $\frac{\partial}{\partial q_b} \hat{f}_{\text{BG}}(s_1, s_2, q_b)|_{q_b=q_b^*(s_1, s_2)} = 0$ and that for this boundary parameter in the direction (s_1, s_2) we have the identity $f_{\text{BG}}(s_1, s_2) = \hat{f}_{\text{BG}}(s_1, s_2, q_b^*(s_1, s_2))$.

Differentiating these equations with respect to q_b , we obtain

$$\begin{aligned} \forall q_b \in]q, q_{s_1, s_2}[\quad , \quad (f_{\text{U}}^{q, q'})'(q_b) + \partial_1^2 f_{\text{BG}}(s_1 - r_1(q_b), s_2) r_1'(q_b) &= 0 \quad , \\ \forall q_b \in]q_{s_1, s_2}, 1[\quad , \quad (f_{\text{V}}^{q, q'})'(q_b) + \partial_2^2 f_{\text{BG}}(s_1, s_2 - r_2(q_b)) r_2'(q_b) &= 0 \quad . \end{aligned} \quad (\text{G.6.13})$$

From this and using the fact that $f_{\text{U}}^{q, q'}(q_b)$ (resp. $f_{\text{V}}^{q, q'}(q_b)$) is strictly increasing (resp. decreasing) as a function of q_b and assuming that $f(s_1, s_2)$ is a strictly convex function, we obtain that $r_1(q_b)$ (resp. $r_2(q_b)$) should be strictly decreasing (resp. increasing) on $]q, q_{s_1, s_2}[$ (resp. $]q_{s_1, s_2}, 1[$). Note now that $\hat{f}_{\text{BG}}(s_1, s_2, q_b) = s_1 f_{\text{U}}^{q, q'}(q_b) + s_2 f_{\text{V}}^{q, q'}(q_b)$ is a concave function of q_b on $]q, 1[$ with a single maximum at some $q_b^* \in]q, 1[$. In particular $s_1 f_{\text{U}}^{q, q'}(q_b) + s_2 f_{\text{V}}^{q, q'}(q_b)$ is not constant on any sub-interval and hence both $r_1(q_b)$ and $r_2(q_b)$ cannot be constant on any subinterval either. Combined with the fact that $r_1(q_b)$ is strictly decreasing, this shows that $r_1(q_b) > 0 \quad \forall q_b < q_{s_1, s_2}$. In the same way $r_2(q_b) > 0 \quad \forall q_b > q_{s_1, s_2}$. Let us now differentiate (G.6.11) with respect to q_b for $q_b \neq q_{s_1, s_2}$ and use the saddle-point equation (G.6.12), we obtain

$$s_1 (f_{\text{U}}^{q, q'})'(q_b) + s_2 (f_{\text{V}}^{q, q'})'(q_b) = \theta(q_{s_1, s_2} - q_b) r_1(q_b) (f_{\text{U}}^{q, q'})'(q_b) + \theta(q_b - q_{s_1, s_2}) r_2(q_b) (f_{\text{V}}^{q, q'})'(q_b). \quad (\text{G.6.14})$$

In particular this shows that $\frac{\partial}{\partial q_b} \hat{f}_{\text{BG}}(s_1, s_2, q_b) = s_1 (f_{\text{U}}^{q, q'})'(q_b) + s_2 (f_{\text{V}}^{q, q'})'(q_b)$ is not 0 $\forall q_b \neq q_{s_1, s_2}$. Since we know that $\frac{\partial}{\partial q_b} \hat{f}_{\text{BG}}(s_1, s_2, q_b) = 0$ for $q_b = q_b^*$ we necessarily obtain

$$q_{s_1, s_2} = q_b^* \quad \text{and} \quad 0 = \lim_{q_b \rightarrow (q_b^*)^-} r_1(q_b) (f_{\text{U}}^{q, q'})'(q_b) = \lim_{q_b \rightarrow (q_b^*)^+} r_2(q_b) (f_{\text{V}}^{q, q'})'(q_b). \quad (\text{G.6.15})$$

And hence $\lim_{q_b \rightarrow (q_b^*)^-} r_1(q_b) = \lim_{q_b \rightarrow (q_b^*)^+} r_2(q_b) = 0$.

Final formula for $f_{\text{BG}}(s_1, s_2)$

Using finally by continuity (G.6.11) for $q_b \rightarrow q_b^*$ we obtain our final result for the optimal energy of the model without boundaries: $\forall (s_1, s_2) \in \mathbb{R}_+^2$,

$$\begin{aligned} f_{\text{BG}}(s_1, s_2) &= \hat{f}_{\text{BG}}(s_1, s_2, q_b = q_b^*(s_1, s_2)) \quad , \\ \frac{\partial}{\partial q_b} \hat{f}_{\text{BG}}(s_1, s_2, q_b)|_{q_b=q_b^*(s_1, s_2)} &= 0 \quad . \end{aligned} \quad (\text{G.6.16})$$

Using (G.6.1) and (G.6.4), these formal formulas are rewritten more explicitly in (G.3.40).

Free-energy per-unit-length, optimal angle and the equilibrium case

The free-energy per-unit-length in the direction $\varphi \in]-1/2, 1/2[$, $f_{\text{BG}}^{\text{p.u.l.}}(\varphi) = f_{\text{BG}}(1/2 + \varphi, 1/2 - \varphi)$ is similarly given by

$$f_{\text{BG}}^{\text{p.u.l.}}(\varphi) = (1/2 + \varphi) f_{\text{U}}^{q, q'}(q_b^*(\varphi)) + (1/2 - \varphi) f_{\text{V}}^{q, q'}(q_b^*(\varphi)) \quad (\text{G.6.17})$$

$$0 = (1/2 + \varphi) \partial_{q_b} f_{\text{U}}^{q, q'}(q_b^*(\varphi)) + (1/2 - \varphi) \partial_{q_b} f_{\text{V}}^{q, q'}(q_b^*(\varphi)) \quad (\text{G.6.18})$$

It is plotted in Fig. G.8 for various values of q, q' . $f_{\text{BG}}^{\text{p.u.l.}}(\varphi)$ reaches its minimum at the angle $\varphi_{\text{opt}}^{\text{BG}}$ such that, using the saddle-point structure, in (G.6.17)-(G.6.18)

$$\frac{\partial f_{\text{BG}}^{\text{p.u.l.}}(\varphi)}{\partial \varphi} = 0 = f_{\text{U}}^{qq'}(q_b^*(\varphi_{\text{opt}}^{\text{BG}})) - f_{\text{V}}^{qq'}(q_b^*(\varphi_{\text{opt}}^{\text{BG}})). \quad (\text{G.6.19})$$

And using (G.6.1) this shows that $f_{\text{BG}}^{\text{p.u.l.}}(\varphi)$ is minimum when $q_b^*(\varphi) = \sqrt{q}$, the boundary parameter already referred to as the equilibrium boundary parameter. The optimal angle is thus obtained using (G.6.18) with $q_b = \sqrt{q}$ and one obtains (G.3.43).

Last-Passage-Percolation limit

In the isotropic case $q' = 0$ case we easily obtain from the above formulas, using $\hat{f}_{\text{BG}}(s_1, s_2, q_b)|_{q'=0} = \frac{q}{q-q_b} s_1 + \frac{q_b}{q_b-1} s_2$ and that the quartic equation for q_b^* in (G.3.40) becomes a simpler quadratic equation, that

$$f_{\text{BG}}(s_1, 1)|_{q'=0} = \frac{s_1 q + 2\sqrt{s_1 q} + q}{q-1}, \quad f_{\text{BG}}^{\text{p.u.l.}}(\varphi)|_{q'=0} = \frac{(1-2\phi)\sqrt{\frac{2q\phi+q}{1-2\phi}} + q}{q-1}. \quad (\text{G.6.20})$$

This reproduces the already known result first obtained by Johansson using the RSK correspondence (see Theorem 1.1 in [159] with there $s_1 = \gamma$). The function $f_{\text{BG}}^{\text{p.u.l.}}(\varphi)|_{q'=0}$ is plotted in black-dashed on the left of Fig. G.8 for $q = 0.5$.

First-Passage-Percolation limit

As discussed in Sec.G.5.2, the $q \rightarrow 0$ limit of the model is a model of first passage percolation with Bernoulli-Geometric waiting times on horizontal edges only (see (G.5.5)). Taking the limit $q \rightarrow 0$ of the above formulas is less straightforward than in the last-passage-percolation limit. Indeed in this limit $\hat{f}_{\text{BG}}^{\text{p.u.l.}}(s_1, s_2, q_b)|_{q=0} = -\frac{q_b q'}{q_b q' - 1} s_1 + \frac{q_b (q' - 1)}{(q_b - 1)(q_b q' - 1)} s_2$, and though $\hat{f}_{\text{BG}}^{\text{p.u.l.}}(s_1, s_2, q_b)|_{q=0}$ is still concave as a function of q_b , $\lim_{q_b \rightarrow 0} \hat{f}(s_1, s_2, q_b)|_{q=0} = 0 > -\infty$ and one of the important element in the derivation of (G.6.16) does not hold anymore. One can however repeat a similar derivation and obtain that, at fixed q' and as a function of φ , $\hat{f}_{\text{BG}}^{\text{p.u.l.}}(\varphi, q_b)|_{q=0} = \hat{f}_{\text{BG}}(1/2 + \varphi, 1/2 - \varphi, q_b)|_{q=0}$ reaches its maximum on $q_b = [0, 1]$ at $q_b = 0$ for $\varphi \leq \varphi_{q'} := 1/2 - q'$. In those cases $f_{\text{BG}}^{\text{p.u.l.}}(\varphi)|_{q=0} = \hat{f}_{\text{BG}}^{\text{p.u.l.}}(\varphi, 0)|_{q=0} = 0$. For $\varphi > \varphi_{q'}$ on the other hand $\hat{f}_{\text{BG}}^{\text{p.u.l.}}(\varphi, q_b)|_{q=0}$ reaches its maximum on $q_b = q_b^* \in]0, 1[$ at some q_b^* solution of the quadratic equation $\partial_{q_b} \hat{f}_{\text{BG}}^{\text{p.u.l.}}(\varphi, q_b)|_{q=0} = 0$ and in those cases $f_{\text{BG}}^{\text{p.u.l.}}(\varphi)|_{q=0} = \hat{f}_{\text{BG}}^{\text{p.u.l.}}(\varphi, q_b^*)|_{q=0} > 0$. Solving the resulting quadratic equation one obtains that $f_{\text{BG}}^{\text{p.u.l.}}(\varphi)|_{q=0}$ is given by the non-analytic form

$$f_{\text{BG}}^{\text{p.u.l.}}(\varphi)|_{q=0} = \theta \left(\varphi - \left(\frac{1}{2} - q' \right) \right) \frac{\left(2\sqrt{2}\sqrt{(1-2\varphi)q'} - 2q' + 2\varphi - 1 \right)}{2(q' - 1)} \geq 0. \quad (\text{G.6.21})$$

This formula can also easily be obtained by first solving explicitly the quartic equation in (G.3.40) and then taking the limit $q \rightarrow 0$. A ‘natural’ way to interpret this non-analytic behavior is the existence of a percolation threshold. Indeed, the optimal energy E_{x_1, x_2} is equal to 0 iff there exist a path from $(0, 0)$ to (x_1, x_2) such that all the Bernoulli variables ξ_{uv} on the horizontal edges encountered by the path are 0 (which occurs for each edge with probability q' , see (G.5.5)). When $(x_1, x_2) = t(1/2 - \varphi, 1/2 + \varphi)$ with $t \rightarrow \infty$ and for $\varphi = -1/2$ it is trivial that this occurs with probability 1, and an interesting question is whether there exist a critical angle φ_c up to which this still occurs with probability 1. In the region $\varphi \geq \varphi_{q'}$ this is clearly not the case since $f_{\text{BG}}^{\text{p.u.l.}}(\varphi)|_{q=0} > 0$. In the region $\varphi \leq \varphi_{q'}$, $f_{\text{BG}}^{\text{p.u.l.}}(\varphi)|_{q=0} = 0$ and a natural guess would be $\varphi_c = \varphi_{q'}$, although we cannot simply rule out here the possibility that the optimal path encounters a non-extensive number (i.e. $o(t)$) of edges such that $\xi_{uv} \neq 0$. Around $\varphi_{q'}$ we obtain, for $\delta\varphi > 0$, a quadratic behavior $f_{\text{BG}}^{\text{p.u.l.}}(\varphi_{q'} + \delta\varphi)|_{q=0} \simeq \frac{1}{4q'} \frac{\delta\varphi^2}{1-q'} + O(\delta\varphi^3)$. The function $f_{\text{BG}}^{\text{p.u.l.}}(\varphi)|_{q=0}$ is plotted in black-dashed on the right of Fig. G.8 for $q' = 0.7$.

b Inverse-Beta polymer

Let us now consider the IB polymer with boundaries defined in Def. G.3.2. $\forall (x_1, x_2) \in (\mathbb{N}^*)^2$, we write,

$$\hat{Z}_{x_1, x_2} = \sum_{i=1}^{x_1} \prod_{j=1}^i \hat{U}_{j,0} v_{i,1} \hat{Z}_{x_1, x_2}^{i,1} + \sum_{i=1}^{x_2} \prod_{j=1}^i \hat{V}_{0,j} u_{i,1} \hat{Z}_{x_1, x_2}^{1,i}, \quad (\text{G.6.22})$$

where we have introduced $\forall (x_1, x_2, x'_1, x'_2) \in (\mathbb{N}^*)^4$ with $x'_1 \leq x_1$ and $x'_2 \leq x_2$, the partition sum for polymers with starting point (x'_1, x'_2) and (x_1, x_2) , $\hat{Z}_{x_1, x_2}^{x'_1, x'_2} = \sum_{\pi: (x'_1, x'_2) \rightarrow (x_1, x_2)} \prod_{e \in \pi} \hat{w}(e)$. Since the Boltzmann weights taken into account in this partition sum are all bulk-type weights, we have the equality in law $\hat{Z}_{x_1, x_2}^{x'_1, x'_2} \sim Z_{x_1 - x'_1, x_2 - x'_2}$ where Z_{x_1, x_2} is the partition sum of the point to point IB polymer as defined in Def. G.3.1. The decomposition in (G.6.22) expresses the partition sum \hat{Z}_{x_1, x_2} as a sum of $x_1 + x_2$ positive terms. Hence we have the two inequalities

$$\begin{aligned} -\log \hat{Z}_{x_1, x_2} &\geq -\log \left((x_1 + x_2) \max \left\{ \max_{i \in [0, x_1]} \prod_{j=1}^i \hat{U}_{0,j} v_{1,i} \hat{Z}_{x_1, x_2}^{1,i}, \max_{i \in [0, x_2]} \prod_{j=1}^i \hat{V}_{j,0} u_{i,1} \hat{Z}_{x_1, x_2}^{i,1} \right\} \right) \\ -\log \hat{Z}_{x_1, x_2} &\leq -\log \left(\max \left\{ \max_{i \in [0, x_1]} \prod_{j=1}^i \hat{U}_{0,j} v_{1,i} \hat{Z}_{x_1, x_2}^{1,i}, \max_{i \in [0, x_2]} \prod_{j=1}^i \hat{V}_{j,0} u_{i,1} \hat{Z}_{x_1, x_2}^{i,1} \right\} \right). \end{aligned} \quad (\text{G.6.23})$$

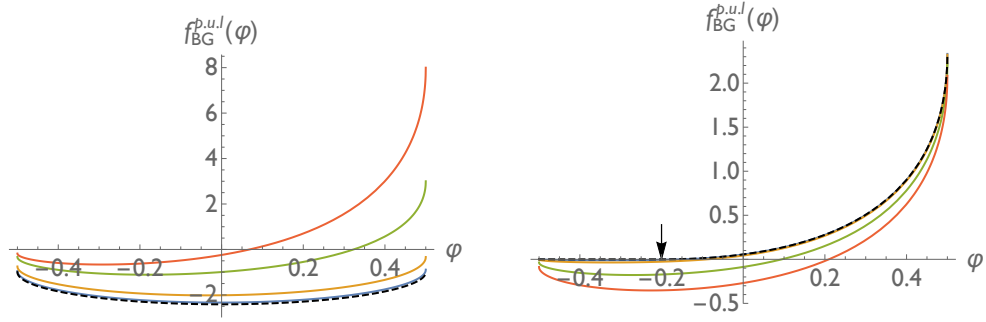


Figure G.8: Left: Optimal energy per-unit-length $f_{\text{BG}}^{\text{p.u.l.}}(\varphi)$ in the point to point BG polymer (G.6.17) for $q = 0.5$ and $q' = 0.1, 0.4, 0.8, 0.9$ (plain lines, blue, orange, green and red) and in the last passage percolation limit $q' \rightarrow 0$ (black dashed line) (G.6.20). Right: Optimal energy per-unit-length $f_{\text{BG}}^{\text{p.u.l.}}(\varphi)$ in the point to point BG polymer (G.6.17) for $q' = 0.7$ and $q' = 0.001, 0.01, 0.1, 0.2$ (plain lines, blue, orange, green and red) and in the first passage percolation limit $q \rightarrow 0$ (black dashed line) (G.6.21). The arrow indicates the percolation threshold of the $q \rightarrow 0$ limit $\varphi_{q'=0.7} = -0.2$.

Taking average values in (G.6.23), scaling $(x_1, x_2) = N(s_1, s_2)$ and $i \sim Nr$ with $N \gg 1$ and using the definitions (G.6.5), (G.6.1) and (G.3.37) we obtain

$$\begin{aligned} \hat{f}_{\text{IB}}(s_1, s_2, \lambda) &= s_1 f_U^{\gamma, \beta}(\lambda) + s_2 f_V^{\gamma, \beta}(\lambda) \\ &= \min \left\{ \inf_{0 \leq r \leq s_1} (r f_U^{\gamma, \beta}(\lambda) + f_{\text{IB}}(s_1 - r, s_2)), \inf_{0 \leq r \leq s_2} (r f_V^{\gamma, \beta}(\lambda) + f_{\text{IB}}(s_1, s_2 - r)) \right\}. \end{aligned} \quad (\text{G.6.24})$$

Note that this equation has the exact same structure as the equation (G.6.9) relating the optimal energies in the Bernoulli-Geometric polymer with and without boundaries. Furthermore, the functions $\hat{f}_{\text{IB}}(s_1, s_2, \lambda)$, $f_U^{\gamma, \beta}(\lambda)$ and $f_V^{\gamma, \beta}(\lambda)$ have similar analytical properties as a function of λ than the mean optimal energies for the BG polymer (see (G.6.1)). We can thus repeat the precedent derivation, and, using that $\hat{f}_{\text{IB}}(s_1, s_2, \lambda)$ is a concave function of λ on $]0, \gamma[$ with a unique maximum $\lambda^* \in]0, \gamma[$, we obtain for the point to point IB polymer, $\forall (s_1, s_2) \in \mathbb{R}_+^2$

$$\begin{aligned} f_{\text{IB}}(s_1, s_2) &= \hat{f}_{\text{IB}}(s_1, s_2, \lambda^*(s_1, s_2)) \\ \partial_\lambda f_{\text{IB}}(s_1, s_2, \lambda)|_{\lambda=\lambda^*(s_1, s_2)} &= 0, \end{aligned} \quad (\text{G.6.25})$$

with $\lambda^*(s_1, s_2) \in]0, \gamma[$. Using the formulas (G.6.1) and (G.6.5) we obtain (G.3.38). The derivation of the formula (G.3.43) for the optimal angle $\varphi_{\text{opt}}^{\text{IB}}$ is identical to the BG polymer case.

G.6.3 Convergence to the stationary measures

We now discuss the conjectures (G.3.44) and (G.3.45) using heuristic arguments. We note that making rigorous and extending the picture discussed in this section is an active research area (focusing on the existence and characterization of so-called Busemann functions and stationary cocycles), see e.g. [270] for problems of directed last passage percolation (including a discussion of the exactly solvable geometric case), [271] for undirected first passage percolation and [268] for the Log-Gamma polymer. We discuss the conjecture for the BG polymer (G.3.45), the argument for the IB polymer being, at the level of rigor of this section, identical. In the following and until the end of the paper we will heavily use the notation $q_b^*(s_1, s_2)$ to denote the solution of the saddle-point equation (G.6.16), or alternatively the notation $q_b^*(\varphi)$ to denote the solution of the saddle-point equation (G.6.18).

Let us thus again consider the optimal energy E_{x_1, x_2} in the point to point BG polymer defined in Def. G.3.4. Let us suppose that, given an arbitrary direction $(s_1, s_2) \in \mathbb{R}_+^2$ and fixing a total horizontal and vertical length $L_u \geq 1$ and $L_v \geq 1$, the difference of optimal energies in the rectangle delimited by the points $(Ns_1, Ns_2) \rightarrow (Ns_1 + L_u, Ns_2) \rightarrow (Ns_1 + L_u, Ns_2 + L_v) \rightarrow (Ns_1, Ns_2 + L_v) \rightarrow (Ns_1, Ns_2)$ converges to a well defined ensemble of RVs. That is

$$(E_{Ns_1+x_1, Ns_2+x_2} - E_{Ns_1, Ns_2})_{0 \leq x_1 \leq L_u, 0 \leq x_2 \leq L_v} \sim_{N \rightarrow \infty} (\tilde{E}_{x_1, x_2})_{0 \leq x_1 \leq L_u, 0 \leq x_2 \leq L_v}. \quad (\text{G.6.26})$$

Where the \tilde{E}_{x_1, x_2} are $O(1)$ RVs. It is clear that if the above convergence holds, the difference of horizontal and vertical energies $\tilde{U}_{x_1, x_2} := \tilde{E}_{x_1, x_2} - \tilde{E}_{x_1-1, x_2}$ and $\tilde{V}_{x_1, x_2} := \tilde{E}_{x_1, x_2} - \tilde{E}_{x_1, x_2-1}$ should be homogeneously distributed. In other words their distributions should be invariant by induction using the stationarity map $\phi_{T=0}$ (G.5.3). It is thus natural to identify the RVs \tilde{E}_{x_1, x_2} with the optimal energies \hat{E}_{x_1, x_2} in the BG polymer with boundaries. We however need to specify

self-consistently the value of the boundary parameter q_b . To do so, let us evaluate the mean value $\overline{\hat{E}_{x_1, x_2}}$ as

$$\begin{aligned} \overline{\hat{E}_{x_1, x_2}} &= \overline{E_{N s_1 + x_1, N s_2 + x_2}} - \overline{E_{N s_1, N s_2}} \\ &\simeq N f_{\text{BG}}(s_1 + x_1/N, s_2 + x_2/N) - N f_{\text{BG}}(s_1, s_2) \\ &\simeq x_1 \partial_1 f_{\text{BG}}(s_1, s_2) + x_2 \partial_2 f_{\text{BG}}(s_1, s_2) \\ &\simeq x_1 f_U^{q, q'}(q_b^*(s_1, s_2)) + x_2 f_V^{q, q'}(q_b^*(s_1, s_2)) \\ &\simeq \overline{\hat{E}_{x_1, x_2}} \text{ if } q_b = q_b^*(s_1, s_2), \end{aligned} \quad (\text{G.6.27})$$

where we used the definition (G.3.37), the result (G.6.16), the saddle-point equation in (G.6.16) to compute the derivatives $\partial_i f$ and (G.6.3). This calculation thus suggests that we have the equality in law, already given in (G.3.45)

$$(\overline{E_{N s_1 + x_1, N s_2 + x_2}} - \overline{E_{N s_1, N s_2}})_{0 \leq x_1 \leq L_u, 0 \leq x_2 \leq L_v} \sim_{N \rightarrow \infty} (\hat{E}_{x_1, x_2})_{0 \leq x_1 \leq L_u, 0 \leq x_2 \leq L_v} \text{ with } q_b = q_b^*(s_1, s_2). \quad (\text{G.6.28})$$

That is we relate the differences of energies in a specific direction at large length in the model without boundaries with the optimal energy in the model with boundaries with a specific boundary parameter. Note that this result fails if one starts to scale the length of the rectangles with N . This is obvious if one scales $L_u \sim N$, but the result is also expected to fail for the smaller scaling $L_u \sim N^{2/3}$. Indeed the exponent $2/3$ is the known rugosity exponent of directed polymer in $d = 1 + 1$ and should correspond to the typical scale at which correlations between energy differences appear.

Let us now reinterpret following this picture some properties of the IB model with boundaries. Following the convergence in law (G.6.28), the optimal energies $\hat{E}_t(x)$ in the model with boundaries with parameter $q_b = q_b^*(\varphi^0)$ with $\varphi^0 \in]-1/2, 1/2[$, are thus interpreted as the difference of energies in the model without boundaries when the polymer starts from infinity in the direction with angle φ^0 (see Fig. G.9). In this interpretation the linear dependence of the free-energy per-unit-length in the model with boundaries $\hat{f}_{\text{BG}}^{\text{p.u.1.}}(\varphi, q_b = q_b^*(\varphi^0))$ as a function of φ is natural since the model with boundaries is obtained by ‘zooming in’ on a specific region of the model without boundaries in the direction $\varphi = \varphi^0$. One easily checks using calculations similar to those of (G.6.27) that $\hat{f}_{\text{BG}}^{\text{p.u.1.}}(\varphi, q_b = q_b^*(\varphi^0)) = f_{\text{BG}}^{\text{p.u.1.}}(\varphi^0) + (\varphi - \varphi^0) \partial_\varphi f_{\text{BG}}^{\text{p.u.1.}}(\varphi)|_{\varphi=\varphi^0}$. In particular, as we already saw, the direction of optimal energy for the model without boundaries $\varphi^0 = \varphi_{\text{opt}}^0$ (such that $\partial_\varphi f_{\text{BG}}^{\text{p.u.1.}}(\varphi)|_{\varphi=\varphi_{\text{opt}}^0} = 0$) corresponds to the equilibrium boundary parameter $q_b = \sqrt{q}$ for which the optimal energy in the model with boundaries $\hat{f}_{\text{BG}}^{\text{p.u.1.}}(\varphi, q_b)$ is constant: there the model with boundaries is obtained by ‘zooming in’ on the region of optimal energy of the model without boundaries.

G.6.4 A remark on optimal paths and energy fluctuations in models with boundaries

Let us now briefly discuss some asymptotic properties of the model with boundaries. For concreteness we will consider the Bernoulli-Geometric polymer but the discussion can be easily adapted to the Inverse-Beta case. We suppose that the boundary parameter q_b corresponds to a direction φ^0 for which $q_b = q_b^*(\varphi^0)$, the solution of the saddle-point-equation (G.6.18). As we saw before in (G.6.28) the optimal energies $\hat{E}_{x_1, x_2} = \hat{E}_{t=(x_1+x_2)}(x = x_1)$ in the model with boundaries on a finite domain are naturally interpreted as the asymptotic limit of the difference of energies of the model without boundaries in the direction φ^0 . That is, for $T \gg 1$ and $(t, x) \in \mathbb{N}^2$ fixed we have

$$\hat{E}_t(x) \sim E_{T+t}((1/2 + \varphi_0)T + x) - E_T((1/2 + \varphi_0)T). \quad (\text{G.6.29})$$

As such, asymptotic properties of optimal energies of the model with boundaries in a direction φ , $\hat{E}_t(x = (1/2 + \varphi)t)$ with $t \gg 1$, are to be interpreted with caution for the model without boundaries since (G.6.29) is a priori valid only for t fixed and $T \rightarrow \infty$. With this in mind, let us now discuss the properties of the energy fluctuations and of the optimal path in the model with boundaries.

Let us first comment on some elements that appeared in the proof of (G.6.16) in Sec. G.6.2. There we defined, for a fixed direction $(s_1, s_2) = (1/2 + \varphi, 1/2 - \varphi)$ and varying the boundary parameter q_b , two functions $r_1^\varphi(q_b)$ and $r_2^\varphi(q_b)$ (here we emphasize the dependence on φ of these quantities by superscript). These two functions correspond to the average length divided by t spent by the optimal polymer path on the horizontal (for $r_1^\varphi(q_b)$) or vertical (for $r_2^\varphi(q_b)$) boundary of \mathbb{N}^2 . Hence for $q_b < q_b^*(\varphi)$ we saw that the polymer spends on average a macroscopic amount of his time ($\sim r_1^\varphi(q_b)t$) on the horizontal boundary, while for $q_b > q_b^*(\varphi)$ the polymer spends on average a macroscopic amount of his time ($\sim r_2^\varphi(q_b)t$) on the vertical boundary.

Conversely, fixing now $q_b = q_b^*(\varphi^0)$ for some $\varphi^0 \in]-1/2, 1/2[$, and varying φ , for $\varphi > \varphi^0$ (resp. $\varphi < \varphi^0$), the optimal polymer path spends on average a macroscopic amount of time $\sim \tilde{r}_1^{\varphi^0}(\varphi)t$ (resp. $\tilde{r}_2^{\varphi^0}(\varphi)t$) on the horizontal (resp. vertical) boundary with $\tilde{r}_1^{\varphi^0}(\varphi) = r_1^\varphi(q_b = q_b^*(\varphi^0))$ (resp. $\tilde{r}_2^{\varphi^0}(\varphi) = r_2^\varphi(q_b = q_b^*(\varphi^0))$). Hence, for $\varphi > \varphi^0$ (resp. $\varphi < \varphi^0$), the optimal energy $\hat{E}_t(x = (1/2 + \varphi)t)$ contains a sum of order t terms of iid distributed RVs of the U type (resp. of the V type) and one thus expects the fluctuations of $\hat{E}_t(x = (1/2 + \varphi)t)$ to scale as \sqrt{t} . Thus, in any direction $\varphi \neq \varphi^0$, one does not observe fluctuations of order $t^{1/3}$ as could have naively been expected from KPZ universality, the reason being that the polymer is then typically pinned by one of the two attractive boundaries for a macroscopic (i.e. of order t) amount of time.

An important question is then to understand how the fluctuations of $\hat{E}_t(x = (1/2 + \varphi)t)$ scale with t when $\varphi = \varphi^0$. In [197] Seppäläinen showed in the Log-Gamma polymer case that these fluctuations scale with the characteristic exponent $t^{1/3}$ as expected from KPZ universality, and a typical polymer path then only spend a time of order $t^{2/3}$ on one of the two

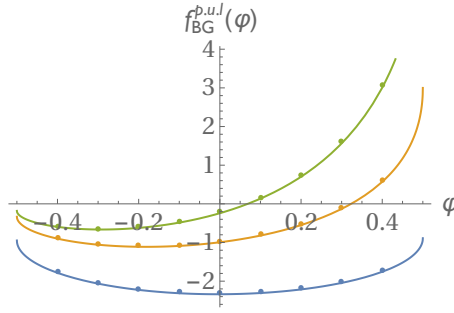


Figure G.10: Comparison between the exact result for the mean asymptotic optimal energy per-unit-length in the Bernoulli-Geometric polymer $f_{\text{BG}}^{\text{p,u,l}}(\varphi)$ (see (G.6.17)) for $q = 0.5$ and $q' = q_1 = 0.1$ (blue line), $q' = q_2 = 0.8$ (orange line) and $q' = q_3 = 0.9$ (green line) and the numerically obtained value $\overline{E}_{t_6}((1/2 + \varphi_k)t_6)/t_6$ for each set of parameters and each angle φ_k (dots, same color code).

G.7 Numerical results for the zero-temperature model

In this section we report results of numerical simulations of the point to point Bernoulli-Geometric polymer (without boundaries, see Def. G.3.4) for three sets of parameters. For each set we have $q = 0.5$ and we vary the anisotropy parameter: we consider an almost isotropic case $q'_1 = 0.1$ and two strongly anisotropic cases $q'_2 = 0.8$ and $q'_3 = 0.9$. For each set we perform 2×10^5 simulations of independent random environments of size 2048×2048 . For each random environment we measure using a transfer matrix algorithm the optimal energy and horizontal and vertical energy differences $E_{t_j}((1/2 + \varphi_k)t_j)$, $U_{t_j}((1/2 + \varphi_k)t_j) := E_{t_j}((1/2 + \varphi_k)t_j) - E_{t_j-1}((1/2 + \varphi_k)t_j - 1)$ and $V_{t_j}((1/2 + \varphi_k)t_j) := E_{t_j}((1/2 + \varphi_k)t_j) - E_{t_j-1}((1/2 + \varphi_k)t_j)$ for different times $t_j = 2^{j+5}$ with $j = 1, \dots, 6$ (hence $t_1 = 64$ and $t_6 = 2048$) and different angle parameters $\varphi_k = -0.4 + \frac{k-1}{10}$ with $k = 1, \dots, 9$.

We first compare in Fig.G.10 for each set of parameters our exact result for the asymptotic value of the mean optimal energy per-unit-length (G.6.17) with the numerically obtained value $\overline{E}_{t_j}((1/2 + \varphi_k)t_j)/t_j$ for $j = 6$ (i.e. polymers of length $t = t_6 = 2048$ for each set of parameters and each angle φ_k). We obtain an excellent agreement.

We then check our conjecture (G.3.45). The latter notably implies, combined with Prop. G.3.1, that the differences of horizontal and vertical energies in a given direction, $U_{t_j}((1/2 + \varphi_k)t_j)$ and $V_{t_j}((1/2 + \varphi_k)t_j)$, converge to independent random variables distributed as U and V in (G.3.22), with for each φ_k the boundary parameter q_b chosen as $q_b = q_b^*(\varphi_k)$, the solution of the saddle-point equation (G.3.41) with $(s_1, s_2) = (1/2 - \varphi_k, 1/2 + \varphi_k)$. In Fig.G.11 we analyze the numerical results for the set of parameters with $q' = q'_3 = 0.9$. We first obtain numerically the PDF of horizontal and vertical differences of optimal energies $U_{t_6}((1/2 + \varphi_8)t_6)$, $V_{t_6}((1/2 + \varphi_8)t_6)$ for an angle $\varphi = \varphi_8 = 0.3$ and polymers of length $t = t_6 = 2048$, and compare it with our asymptotic prediction (G.3.22) (the appropriate boundary parameter is there found to be $q_b^* \simeq 0.922824$). We obtain an excellent agreement. To check the independence of the RVs, we estimate numerically the normalized covariance $\frac{U_{t_j}((1/2 + \varphi_8)t_j)V_{t_j}((1/2 + \varphi_8)t_j)^c}{U_{t_j}((1/2 + \varphi_8)t_j) \times V_{t_j}((1/2 + \varphi_8)t_j)}$ and study its behavior as a function of t . Although fluctuations are large, the normalized covariance clearly decays to 0 with increasing t , a signature of the independence of the RVs. In Fig.G.12 we report similarly satisfying results for the set of parameters with $q' = 0.8$ and in the direction $\varphi = \varphi_2 = -0.3$ (there the appropriate boundary parameter is found to be $q_b^* \simeq 0.667665$).

G.8 Conclusion

In this paper we have obtained the stationary measure of the Inverse-Beta polymer, an exactly solvable, anisotropic finite temperature model of DP on the square lattice recently introduced in [5]. As we discussed, the stationary model can be either studied on \mathbb{Z}^2 with a random initial condition for the polymer such that the free-energy of the DP performs a random walk with inverse-beta distributed increments, or also conveniently in a model on the upper-right quadrant \mathbb{N}^2 with special boundary conditions. This thus confers to the IB polymer a second exact solvability property that complements the coordinate Bethe ansatz solvability shown in [5].

In parallel we introduced a new model of zero temperature DP on the square lattice, the Bernoulli-Geometric polymer. It is obtained by appropriately discretizing the distributions of random energies of the zero temperature limit of the Inverse-Beta polymer from Bernoulli-Exponential distributions to Bernoulli-Geometric distributions. This model is thus canonically dual to the IB polymer. In two different limits the model becomes either a first passage percolation problem, or a last passage percolation problem. We showed that its stationary measure could be exactly obtained, thus conferring to this new model at least one exact solvability property.

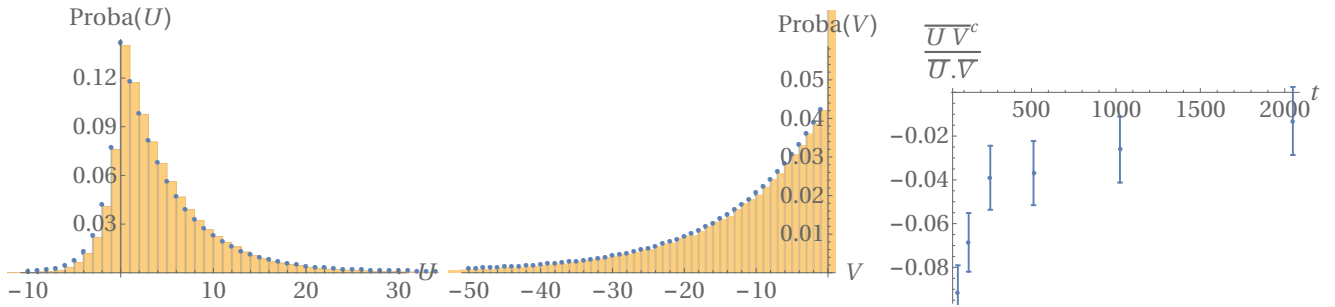


Figure G.11: Left: (resp. Middle:) Comparison between the numerically obtained PDF of $U_{t_6}((1/2 + \varphi_8)t_6)$ (resp. $V_{t_6}((1/2 + \varphi_8)t_6)$) in the simulations with parameters $q = 0.5$, $q' = 0.9$ (yellow histogram) and the PDF of U (resp. V) given in (G.3.22) with $q_b = q_b^* \simeq 0.922824$ (blue dots). Right: numerically obtained normalized covariance $\frac{\overline{U_{t_j}((1/2+\varphi_8)t_j)V_{t_j}((1/2+\varphi_8)t_j)^c}}{\overline{U_{t_j}((1/2+\varphi_8)t_j) \times V_{t_j}((1/2+\varphi_8)t_j)}}$ in the simulations with parameters $q = 0.5$, $q' = 0.9$ as a function of t_j (blue dots). Error bars are 3-sigma Gaussian estimates.

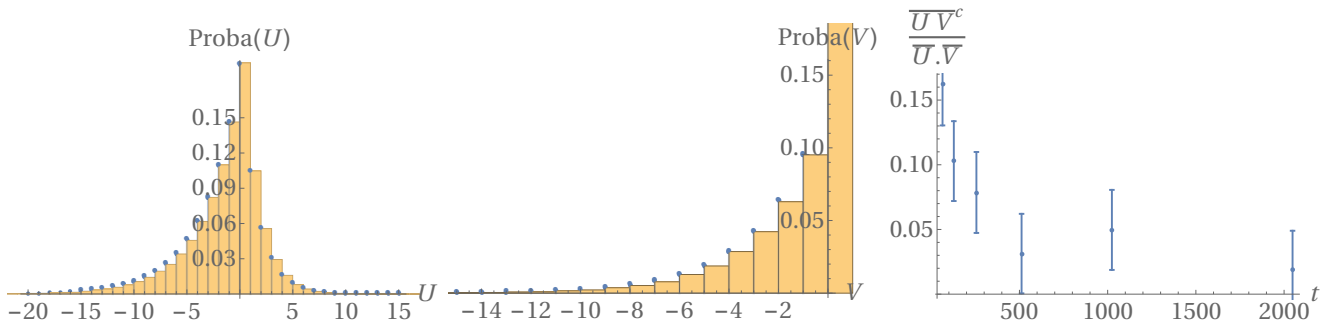


Figure G.12: Left: (resp. Middle:) Comparison between the numerically obtained PDF of $U_{t_6}((1/2 + \varphi_2)t_6)$ (resp. $V_{t_6}((1/2 + \varphi_2)t_6)$) in the simulations with parameters $q = 0.5$, $q' = 0.8$ (yellow histogram) and the PDF of U (resp. V) given in (G.3.22) with $q_b = q_b^* \simeq 0.667665$ (blue dots). Right: numerically obtained normalized covariance $\frac{\overline{U_{t_j}((1/2+\varphi_2)t_j)V_{t_j}((1/2+\varphi_2)t_j)^c}}{\overline{U_{t_j}((1/2+\varphi_2)t_j) \times V_{t_j}((1/2+\varphi_2)t_j)}}$ in the simulations with parameters $q = 0.5$, $q' = 0.8$ as a function of t_j (blue dots). Error bars are 3-sigma Gaussian estimates.

We also showed that the two stationary measures are reversible and satisfy detailed balance. We obtained the mean quenched free-energy (resp. optimal energy) in the IB (resp. BG) polymer. For the IB polymer, the obtained result (G.3.38) coincides with a previously obtained result of [5], therefore confirming the validity of the non-rigorous approach of [5], while in the BG polymer case, (G.3.40) is genuinely new. In both cases, these results allowed us to discuss the convergence of each model to their stationary measure. Finally in Sec. G.7 we reported the results of numerical simulations of the BG polymer and compared them with a very good agreement to our results.

Many possible research directions remain for the future. One interesting direction would be to understand if the models studied in this paper possess other exact solvability properties. Indeed for both models it is not clear whether or not combinatorial mappings similar to RSK and gRSK correspondences could be developed, although they both interpolate between models for which these correspondences can be applied (gRSK at finite temperature [198, 220] and RSK at 0 temperature [159, 216]). The question of the Bethe ansatz solvability of these models is also interesting. For the IB polymer it was shown in [5] that the moment problem is exactly solvable by coordinate BA but another BA solvability could exist. Indeed in the Log-Gamma case it was shown in [4] that the moment problem was BA solvable, but it is also known that the partition sum of the Log-Gamma polymer can be interpreted [221] as an observable of a BA solvable interacting particles system on \mathbb{Z} , the q-Push TASEP [272, 247]. The same is true for the Strict-Weak polymer which can be mapped onto an observable of the q-TASEP [219]. Exhibiting a similar mapping for the IB polymer case remains an open question. For the BG polymer introduced in this paper the question of BA solvability is also open. We note that in the isotropic limit of the model, i.e. last passage percolation with geometric weights, the optimal energy can be interpreted as waiting times of the TASEP with geometric waiting times and step initial condition, which can be solved by BA. Furthermore, we note that a version of the q-TASEP with Bernoulli and Geometric waiting times was already considered in [254] where the authors notably proved BA solvability. Although it is not clear how to map the optimal energies in the BG polymer to the waiting times of an interacting particles system (since the random energies can be both positive and negative), this could be an interesting approach.

Another interesting direction of research would be to understand how to obtain more systematically models of directed polymers with exact solvability properties and how to classify them. For the case of Bethe ansatz solvability of the moment problem for models of DPs at finite temperature, this was already mostly accomplished in [5]. The question remains open for BA solvability of models at zero temperature and for other type of exact solvability properties such as the possibility of writing down the stationary measure exactly. If this was accomplished it would be interesting to see whether or not the two classes coincide. We note that in the related context of zero-range-processes (ZRP) with simultaneous updates, it was recently shown that all BA solvable models have factorizable steady-states, but the converse is not true [222]. For the DP case, a step in this direction was already made since in [197] it was shown that the Log-Gamma was the unique model at finite temperature with *on site* disorder for which it is possible to write down exactly the SM, and the Log-Gamma also appeared as the unique finite temperature model with on site disorder exactly solvable by BA in the classification of [5]. More generally it would be interesting to gain a better understanding of the links between different exact solvability properties.

This paper would have never existed without the numerous discussions I had with Timo Seppäläinen, discussions during which he kindly took the time to explain to me the techniques and results developed and obtained by him and his coworkers for the Log-Gamma polymer. These were a great source of inspiration for this work. He also took an active part during the first stages of research on the stationary measure of the Inverse-Beta polymer and shared with me related new results on the Beta polymer [267]. I warmly thank him for that. I am also grateful to Guillaume Barraquand for many discussions and remarks on the existing mathematical literature, as well as to Francis Comets, Ivan Corwin, Thomas Gueudré, Vivien Lecomte, Jeremy Quastel and Leonid Petrov for interesting discussions. Last but not least, I would like to warmly thank Pierre Le Doussal who introduced me and taught me most of the things I know on this topic through multiple discussions and collaborations on related subjects. I also thank him for useful comments on a first version of this manuscript. I acknowledge the KITP in Santa Barbara for hospitality during the first stages of redaction of this work. This research was supported in part by the National Science Foundation under Grant No. NSF PHY11-25915.

G.9 Appendix A: Proof of the properties of the finite temperature reversibility-stationarity map

In this appendix we prove Prop. G.4.1, Prop. G.4.2 being trivial. We thus consider three independent random variables (U, V, W) distributed as in (G.3.7) and (G.3.3) and consider the RVs $(U', V', W') = \phi(U, V, W)$ as given in (G.4.3). The Jacobian of the transformation $(U, V, W) \rightarrow (U', V', W')$ is easily computed as, schematically,

$$\det \left(\frac{\partial \phi(U, V, W)}{\partial (U, V, W)} \right) = -\frac{UW + U + VW}{UV} < 0. \quad (\text{G.9.1})$$

The PDF of the triplet (U', V', W') is then directly evaluated as

$$P(U', V', W') = P_U(\phi^{(1)}(U', V', W')) P_V(\phi^{(1)}(U', V', W')) P_W(\phi^{(1)}(U', V', W')) \times \frac{UV}{UW + U + VW}. \quad (\text{G.9.2})$$

Where we introduced the PDF of the independent RVs (U, V, W) as noted in (G.3.7) and (G.3.3) and used the fact that ϕ is an involution. It is then directly checked that

$$P(U', V', W') = P_U(U') P_V(V') P_W(W'), \quad (\text{G.9.3})$$

hence showing that U' , V' and W' are independent and distributed as $U' \sim U$, $V' \sim V$ and $W' \sim W$.

G.10 Appendix B: Proof of the properties of the zero temperature stationarity map

In this Appendix we prove Prop. G.5.1 and Prop. G.5.2. Let us first prove the detailed balance property Prop. G.5.2b. We thus consider $U \perp V \perp (u, v)$ distributed as in (G.3.12) and (G.3.20). Let us first compute the conditional probability

$$\Psi(k_{U'}, k_{V'}, k_U, k_V) := \text{Proba} \left(((U', V') = (k_{U'}, k_{V'}) | (U, V) = (k_U, k_V)) \right) \quad (\text{G.10.1})$$

where $k_U \in \mathbb{N}$, $k_V \in \mathbb{Z}_-$, $U' = \min(u, v + U - V)$ and $V' = \min(u + V - U, v) = U' + V - U$. We have

$$\begin{aligned} \Psi(k_{U'}, k_{V'}, k_U, k_V) = & p_{uv} \sum_{G_q=0}^{\infty} (1-q)(q)^{G_q} \delta(k_{U'} = \min(-G_q, -G_q + k_U - k_V)) \delta(k_{V'} = k_{U'} + k_V - k_U) \\ & + (1-p_{uv}) \sum_{G'_q=0}^{\infty} (1-q')(q')^{G'_q} \delta(k_{U'} = \min(1 + G'_q, k_U - k_V)) \delta(k_{V'} = k_{U'} + k_V - k_U) \\ & p_{uv} \sum_{G_q=0}^{\infty} (1-q)(q)^{G_q} \delta(k_{U'} = -G_q) \delta(k_U > k_V) \delta(k_{V'} = k_{U'} + k_V - k_U) \\ & + p_{uv} \sum_{G_q=0}^{\infty} (1-q)(q)^{G_q} \delta(k_{U'} = -G_q + k_U - k_V) \delta(k_U \leq k_V) \delta(k_{V'} = k_{U'} + k_V - k_U) \\ & + (1-p_{uv}) \sum_{G'_q=0}^{\infty} (1-q')(q')^{G'_q} \delta(k_{U'} = 1 + G'_q) \delta(k_U - k_V > 1 + G'_q) \delta(k_{V'} = k_{U'} + k_V - k_U) \\ & + (1-p_{uv}) \sum_{G'_q=0}^{\infty} (1-q')(q')^{G'_q} \delta(k_{U'} = k_U - k_V) \delta(k_U - k_V \leq 1 + G'_q) \delta(k_{V'} = k_{U'} + k_V - k_U), \end{aligned} \quad (\text{G.10.2})$$

i.e.

$$\begin{aligned} \Psi(k_{U'}, k_{V'}, k_U, k_V) = & p_{uv}(1-q)(q)^{-k_{U'}} \delta(k_{U'} \leq 0) \delta(k_U > k_V) \delta(k_{V'} = k_{U'} + k_V - k_U) \\ & + p_{uv}(1-q)(q)^{-k_{U'} + k_U - k_V} \delta(-k_{U'} + k_U - k_V \geq 0) \delta(k_U \leq k_V) \delta(k_{V'} = k_{U'} + k_V - k_U) \\ & + (1-p_{uv})(1-q')(q')^{k_{U'} - 1} \delta(k_{U'} \geq 1) \delta(k_U - k_V > k_{U'}) \delta(k_{V'} = k_{U'} + k_V - k_U) \\ & + (1-p_{uv})(q')^{k_U - k_V - 1} \delta(k_{U'} = k_U - k_V) \delta(k_{U'} \geq 1) \delta(k_{V'} = k_{U'} + k_V - k_U) \\ & + (1-p_{uv}) \delta(k_{U'} = k_U - k_V) \delta(k_{U'} \leq 0) \delta(k_{V'} = k_{U'} + k_V - k_U). \end{aligned} \quad (\text{G.10.3})$$

Using this last expression and the expression of $\text{Proba}((U, V) = (k_U, k_V))$ given in (G.3.22), we obtain

$$\begin{aligned} \tilde{\Psi}(k_{U'}, k_{V'}, k_U, k_V) & := \text{Proba} \left(((U', V') = (k_{U'}, k_{V'}), (U, V) = (k_U, k_V)) \right) \\ & = \Psi(k_{U'}, k_{V'}, k_U, k_V) \text{Proba}((U, V) = (k_U, k_V)) \\ & = \Psi(k_{U'}, k_{V'}, k_U, k_V) \times \\ & \quad \left(p_U \delta(k_U \leq 0) (1-q/q_b) (q/q_b)^{-k_U} + (1-p_U) \delta(k_U \geq 1) (1-q_b q') (q_b q')^{k_U - 1} \right) \times \\ & \quad \left(p_V \delta(k_V \leq 0) (1-q_b) (q_b)^{-k_V} + (1-p_V) \delta(k_V = 0) \right) \end{aligned} \quad (\text{G.10.4})$$

and it is then straightforward (although technically complicated due to the large number of terms) to check the detailed balance property Prop. G.5.2. Namely one shows that the equality

$$\tilde{\Psi}(k_{U'}, k_{V'}, k_U, k_V) = \tilde{\Psi}(k_U, k_V, k_{U'}, k_{V'}) \quad (\text{G.10.5})$$

holds. Let us emphasize here that this property is rather special: the fact that (G.10.5) works requires a large number of cancellation between terms that are made possible by the choice of only three parameters $p_U = \frac{1-q_b q'}{1-q q'}$, $p_V = \frac{1-q'}{1-q_b q'}$ and $p_{uv} = \frac{1-q'}{1-q q'}$, a characteristic sign of the existence of exact solvability properties for the model. Finally, summing (G.10.5) on $k_{U'}$ and $k_{V'}$ gives the stationarity property Prop. G.5.1:

$$\text{Proba}((U, V) = (k_U, k_V)) = \text{Proba}((U', V') = (k_U, k_V)). \quad (\text{G.10.6})$$

Bibliography

- [1] T. Thiery, P. Le Doussal, et K. J. Wiese, “Spatial shape of avalanches in the brownian force model,” *Journal of Statistical Mechanics: Theory and Experiment* **2015**, P08019 (2015). URL : <http://stacks.iop.org/1742-5468/2015/i=8/a=P08019>. (document), II.1, b, b, e, II.6, II.6.1, II.6.2, II.6.2, II.4, II.6.2, B.1, B.2, C.1, C.2
- [2] T. Thiery et P. Le Doussal, “Universality in the mean spatial shape of avalanches,” *ArXiv e-prints* (2016). (document), II.1, b, II.6, II.6.1, II.6.3, II.5, II.6, II.6.3, II.6.3, II.6.3, II.6.3, II.6.3, II.7, II.8, III.3.4, III.3.4
- [3] T. Thiery, P. Le Doussal, et K. Jörg Wiese, “Universal correlations between shocks in the ground state of elastic interfaces in disordered media,” *ArXiv e-prints* (2016). (document), II.1, II.6, II.6.1, II.6.4, II.9, II.6.4, II.6.4, II.6.4, II.10, II.6.4, II.11, II.12
- [4] T. Thiery et P. Le Doussal, “Log-gamma directed polymer with fixed endpoints via the replica Bethe Ansatz,” *Journal of Statistical Mechanics: Theory and Experiment* **10**, 10018 (2014). (document), b, III.3.1, III.3.2, III.3.2, III.3.2, III.3.2, III.3.2, III.3.2, 10, III.3.3, E.1.1, 2, E.2.3, E.4, a, a, a, b.2, b.2, b.3, c, E.4.2, a, b, b, b, E.4.3, E.4.3, E.5, E.9, F.1.1, F.3, F.3.1, F.3.2, F.3.4, G.1, G.8
- [5] T. Thiery et P. Le Doussal, “On integrable directed polymer models on the square lattice,” *Journal of Physics A Mathematical General* **48**, 465001 (2015). (document), III.3.1, III.3.3, III.4, III.3.3, III.3.3, III.3.3, III.3.3, III.3.3, III.5, III.3.3, III.3.3, III.3.4, III.3.5, III.3.5, III.3.5, III.3.5, III.4, F.1.1, F.3, F.3.1, F.3.1, F.3.1, F.3.1, F.3.1, F.3.1, F.3.1, F.3.1, F.3.2, F.3.2, F.3.3, F.3.3, F.3.3, F.3.3, F.3.4, F.4.1, F.5.4, F.5.4, F.5.4, F.5.4, F.8, 2, a, G.1, b, G.3.1, G.3.1, G.3.3, G.3.3, a, b, c, G.8
- [6] T. Thiery et P. Le Doussal, “Exact solution for a random walk in a time-dependent 1D random environment: the point-to-point Beta polymer,” *ArXiv e-prints* (2016). (document), III.3.1, III.3.4, III.6, III.3.4, III.3.4, III.3.4, III.3.4, G.1
- [7] T. Thiery, “Stationary measures for two dual families of finite and zero temperature models of directed polymers on the square lattice,” *ArXiv e-prints* (2016). (document), III.3.1, III.3.5, 12, III.3.5, III.3.5, 13, III.3.5, III.8, III.3.5, F.1.1

- [8] L. Balents, “Glassy phases and dynamics of randomly pinned elastic media,” (1996). URL : <http://online.kitp.ucsb.edu/online/lnotes/balents/bignotes.html>. I
- [9] P. Chauve, “Dynamique des systèmes élastiques désordonnés,” PhD thesis, Université Paris XI Orsay (2000). I, a, a
- [10] T. Giamarchi, A. B. Kolton, et A. Rosso, “Dynamics of Disordered Elastic Systems,” dans “Jamming, Yielding, and Irreversible Deformation in Condensed Matter,” , vol. 688 de *Lecture Notes in Physics, Berlin Springer Verlag*, M. C. Miguel et M. Rubi, édés. (2006), vol. 688 de *Lecture Notes in Physics, Berlin Springer Verlag*, p. 91–108. I
- [11] D. Fisher, “Sliding charge-density waves as a dynamical critical phenomena,” *Phys. Rev.* **B 31**, 1396–1427 (1985). I.1.3, b, A.1, .2
- [12] A. Fedorenko, P. Le Doussal, et K. Wiese, “Statics and dynamics of elastic manifolds in media with long-range correlated disorder,” *Phys. Rev. E* **74**, 061109 (2006). I.1.3, I.2.3
- [13] G. Biroli, J.-P. Bouchaud, et M. Potters, “Extreme value problems in random matrix theory and other disordered systems,” *Journal of Statistical Mechanics: Theory and Experiment* **2007**, P07019 (2007). URL : <http://stacks.iop.org/1742-5468/2007/i=07/a=P07019>. I.2.3, E.1.1
- [14] T. Gueudre, P. Le Doussal, J.-P. Bouchaud, et A. Rosso, “Ground-state statistics of directed polymers with heavy-tailed disorder,” **91**, 062110 (2015). I.2.3, E.1.1
- [15] A. Larkin, *Sov. Phys. JETP* **31**, 784 (1970). b, a
- [16] K. Efetov et A. Larkin, *Sov. Phys. JETP* **45**, 1236 (1977). b, a
- [17] G. Parisi et N. Sourlas, “Random magnetic fields, supersymmetry, and negative dimensions,” *Phys. Rev. Lett.* **43**, 744–5 (1979). b, a
- [18] P. Chauve et P. Le Doussal, “Exact multilocal renormalization group and applications to disordered problems,” *Phys. Rev. E* **64**, 051102/1–27 (2001). b, a
- [19] P. Hohenberg et B. Halperin, “Theory of dynamical critical phenomena,” *Rev. Mod. Phys.* **49**, 435 (1977). a
- [20] A. Middleton, “Asymptotic uniqueness of the sliding state for charge-density waves,” *Phys. Rev. Lett.* **68**, 670–673 (1992). a, II.2.3, a, a, A.2.1
- [21] H. Leschhorn et L.-H. Tang, “Avalanches and correlations in driven interface depinning,” *Phys. Rev. E* **49**, 1238–1245 (1994). URL : <http://link.aps.org/doi/10.1103/PhysRevE.49.1238>. a
- [22] T. Nattermann, “Interface roughening in systems with quenched random impurities,” *EPL (Europhysics Letters)* **4**, 1241 (1987). URL : <http://stacks.iop.org/0295-5075/4/i=11/a=005>. c, a

- [23] L. B. Ioffe et V. M. Vinokur, “Dynamics of interfaces and dislocations in disordered media,” *Journal of Physics C: Solid State Physics* **20**, 6149 (1987). URL : <http://stacks.iop.org/0022-3719/20/i=36/a=016>. c
- [24] T. Nattermann, Y. Shapir, et I. Vilfan, “Interface pinning and dynamics in random systems,” *Phys. Rev. B* **42**, 8577–8586 (1990). URL : <http://link.aps.org/doi/10.1103/PhysRevB.42.8577>. c
- [25] M. V. Feigel'man, V. B. Geshkenbein, A. I. Larkin, et V. M. Vinokur, “Theory of collective flux creep,” *Phys. Rev. Lett.* **63**, 2303–2306 (1989). URL : <http://link.aps.org/doi/10.1103/PhysRevLett.63.2303>. c
- [26] P. Chauve, T. Giamarchi, et P. Le Doussal, “Creep via dynamical functional renormalization group,” *Europhys. Lett.* **44**, 110–115 (1998). c, a
- [27] P. Chauve, T. Giamarchi, et P. Le Doussal, “Creep and depinning in disordered media,” *Phys. Rev. B* **62**, 6241–67 (2000). c
- [28] A. Kolton, A. Rosso, et T. Giamarchi, “Creep motion of an elastic string in a random potential,” *Phys. Rev. Lett.* **94**, 047002 (2005). c
- [29] S. Lemerle, J. Ferré, C. Chappert, V. Mathet, T. Giamarchi, et P. Le Doussal, “Domain wall creep in an Ising ultrathin magnetic film,” *Phys. Rev. Lett.* **80**, 849 (1998). c, a, E.1.1
- [30] E. Agoritsas, R. García-García, V. Lecomte, L. Truskinovsky, et D. Vandembroucq, “Driven interfaces: from flow to creep through model reduction,” *ArXiv e-prints* (2016). c
- [31] E. A. Jagla, “Scaling theory of thermal rounding phenomena in depinning and related transitions,” *ArXiv e-prints* (2016). c
- [32] E. E. Ferrero, L. Foini, T. Giamarchi, A. B. Kolton, et A. Rosso, “Spatio-temporal patterns in ultra-slow domain wall creep dynamics,” *ArXiv e-prints* (2016). c, c, II.7
- [33] M. Kardar, G. Parisi, et Y.-C. Zhang, “Dynamic scaling of growing interfaces,” *Phys. Rev. Lett.* **56**, 889–892 (1986). b, c, a, D.1, E.1.1, F.1.1, G.1
- [34] I. Corwin, “The kardar-parisi-zhang equation and universality class,” *Random Matrices: Theory and Applications* **01**, 1130001 (2012). URL : <http://www.worldscientific.com/doi/abs/10.1142/S2010326311300014>. c, c, c, III.1, d, III.1.2, f, D.1, D.23, E.1.1, F.1.1, G.1
- [35] T. Halpin-Healy et K. A. Takeuchi, “A KPZ Cocktail-Shaken, not Stirred...” *Journal of Statistical Physics* **160**, 794–814 (2015). c, III.1, F.1.1, G.1
- [36] J. Quastel et H. Spohn, “The One-Dimensional KPZ Equation and Its Universality Class,” *Journal of Statistical Physics* **160**, 965–984 (2015). c, III.1

- [37] C. A. Tracy et H. Widom, “Level-spacing distributions and the Airy kernel,” *Physics Letters B* **305**, 115–118 (1993). c, 1, e, D.1, E.1.1, F.1.1
- [38] C. A. Tracy et H. Widom, “On orthogonal and symplectic matrix ensembles,” *Communications in Mathematical Physics* **177**, 727–754 (1996). c, 2, III.1.2
- [39] J. Baik et E. Rains, “Limiting distributions for a polynuclear growth model with external sources,” *ArXiv Mathematics e-prints* (2000). c, 3, E.1.1
- [40] D. A. Huse et C. L. Henley, “Pinning and roughening of domain walls in Ising systems due to random impurities,” *Phys. Rev. Lett.* **54**, 2708–2711 (1985). a, G.1
- [41] H. Ji et M. O. Robbins, “Transition from compact to self-similar growth in disordered systems: Fluid invasion and magnetic-domain growth,” *Phys. Rev. A* **44**, 2538–2542 (1991). URL : <http://link.aps.org/doi/10.1103/PhysRevA.44.2538>. a
- [42] F. Colaiori, “Exactly solvable model of avalanches dynamics for barkhausen crackling noise,” *Advances in Physics* **57**, 287 (2008). URL : [doi:10.1080/00018730802420614](https://doi.org/10.1080/00018730802420614). a, b, d, II.6.1, A.1
- [43] A. Dobrinevski, “Field theory of disordered systems – avalanches of an elastic interface in a random medium,” *arXiv:1312.7156* (2013). a, b, II.2.3, b, a, c, 8, II.6.1, B.1
- [44] H. Barkhausen, “No Title,” *Phys. Z.* **20**, 401–403 (1919). a
- [45] G. Durin et S. Zapperi, “Scaling exponents for Barkhausen avalanches in polycrystalline and amorphous ferromagnets,” *Phys. Rev. Lett.* **84**, 4705–4708 (2000). a, a, b, II.7, A.9, B.1, C.1
- [46] G. Durin et S. Zapperi, “The Barkhausen effect,” dans “The Science of Hysteresis,” , G. Bertotti et I. Mayergoyz, éd. (Amsterdam, 2006), p. 51. URL : <http://arxiv.org/abs/cond-mat/0404512>. a, a
- [47] P. Cizeau, S. Zapperi, G. Durin, et H. Stanley, “Dynamics of a Ferromagnetic Domain Wall and the Barkhausen Effect,” *Phys. Rev. Lett.* **79**, 4669–4672 (1997). URL : <http://link.aps.org/doi/10.1103/PhysRevLett.79.4669>. a
- [48] D. Bonamy, “Intermittency and roughening in the failure of brittle heterogeneous materials,” *Journal of Physics D: Applied Physics* **42**, 214014 (2009). URL : <http://stacks.iop.org/0022-3727/42/i=21/a=214014>. b
- [49] J. Schmittbuhl, S. Roux, J.-P. Vilotte, et K. Jorgen Måløy, “Interfacial crack pinning: Effect of nonlocal interactions,” *Phys. Rev. Lett.* **74**, 1787–1790 (1995). URL : <http://link.aps.org/doi/10.1103/PhysRevLett.74.1787>. b
- [50] S. Ramanathan, D. Ertaş, et D. S. Fisher, “Quasistatic crack propagation in heterogeneous media,” *Phys. Rev. Lett.* **79**, 873–876 (1997). URL : <http://link.aps.org/doi/10.1103/PhysRevLett.79.873>. b

- [51] D. Bonamy, S. Santucci, et L. Ponson, “Crackling dynamics in material failure as the signature of a self-organized dynamic phase transition,” *Phys. Rev. Lett.* **101**, 045501 (2008). URL : <http://link.aps.org/abstract/PRL/v101/e045501>. b, A.1, B.1, C.1
- [52] L. Ponson, “Depinning transition in failure of inhomogeneous brittle materials,” *Phys. Rev. Lett.* **103**, 055501 (2009). b, B.1, C.1
- [53] J. Schmittbuhl et K. Måløy, “Direct observation of a self-affine crack propagation,” *Phys. Rev. Lett.* **78**, 3888–91 (1997). b
- [54] A. Delaplace, J. Schmittbuhl, et K. J. Måløy, “High resolution description of a crack front in a heterogeneous plexiglas block,” *Phys. Rev. E* **60**, 1337–1343 (1999). URL : <http://link.aps.org/doi/10.1103/PhysRevE.60.1337>. b
- [55] L. Laurson, S. Santucci, et S. Zapperi, “Avalanches and clusters in planar crack front propagation,” *Phys. Rev. E* **81**, 046116 (2010). URL : <http://link.aps.org/doi/10.1103/PhysRevE.81.046116>. b, B.1
- [56] S. Santucci, M. Grob, R. Toussaint, J. Schmittbuhl, A. Hansen, et K. J. Maløy, “Fracture roughness scaling: A case study on planar cracks,” *EPL (Europhysics Letters)* **92**, 44001 (2010). URL : <http://stacks.iop.org/0295-5075/92/i=4/a=44001>. b, B.1, C.1
- [57] K. Tallakstad, R. Toussaint, S. Santucci, J. Schmittbuhl, et K. Måløy, “Local dynamics of a randomly pinned crack front during creep and forced propagation: An experimental study,” *Phys. Rev. E* **83**, 046108 (2011). URL : <http://link.aps.org/doi/10.1103/PhysRevE.83.046108>. b
- [58] E. Schäffer et P.-z. Wong, “Contact line dynamics near the pinning threshold: A capillary rise and fall experiment,” *Phys. Rev. E* **61**, 5257–5277 (2000). URL : <http://link.aps.org/doi/10.1103/PhysRevE.61.5257>. c
- [59] S. Moulinet, C. Guthmann, et E. Rolley, “Roughness and dynamics of a contact line of a viscous fluid on a disordered substrate,” *Eur. Phys. J. E* **8**, 437–443 (2002). c, C.1
- [60] S. Moulinet, C. Guthmann, et E. Rolley, “Dissipation in the dynamics of a moving contact line: effect of the substrate disorder,” *Eur. Phys. J. B* **37**, 127–136 (2004). c, B.1
- [61] P. Le Doussal, K. Wiese, S. Moulinet, et E. Rolley, “Height fluctuations of a contact line: A direct measurement of the renormalized disorder correlator,” *EPL* **87**, 56001 (2009). c, a, b, II.6.1, A.1, B.1, C.1
- [62] P. L. Doussal, K. Wiese, E. Raphael, et R. Golestanian, “Can non-linear elasticity explain contact-line roughness at depinning?” *Phys. Rev. Lett.* **96**, 015702 (2006). c
- [63] D. Fisher, “Collective transport in random media: From superconductors to earthquakes,” *Phys. Rep.* **301**, 113–150 (1998). c, A.1, .2, B.1, C.1

- [64] Y. Ben-Zion et J. Rice, “Earthquake failure sequences along a cellular fault zone in a three-dimensional elastic solid containing asperity and nonasperity regions,” *Journal of Geophysical Research* **98**, 14109–14131 (1993). URL : <http://citeseerx.ist.psu.edu/viewdoc/download?doi=10.1.1.161.5821&rep=rep1&type=pdf>. c, B.1, C.1
- [65] Y. Ben-Zion et J. Rice, “Dynamic simulations of slip on a smooth fault in an elastic solid,” *Journal of Geophysical Research* **102**, 17–17 (1997). URL : http://earth.usc.edu/~ybz/pubs_recent/BZR_JGR97/BZR_JGR97.pdf. c, B.1
- [66] D. S. Fisher, K. Dahmen, S. Ramanathan, et Y. Ben-Zion, “Statistics of earthquakes in simple models of heterogeneous faults,” *Phys. Rev. Lett.* **78**, 4885–4888 (1997). URL : <http://link.aps.org/doi/10.1103/PhysRevLett.78.4885>. c, B.1, C.1
- [67] F. Omori, “On the aftershocks of earthquakes,” *Journal of the College of Science, Imperial University of Tokyo* **7**, 111–200. c, II.6.1, C.1
- [68] T. Giamarchi et P. Le Doussal, “Statics and dynamics of disordered elastic systems,” dans “Spin glasses and random fields,” , A. Young, éd. (World Scientific, Singapore, 1997). c, B.1, C.1
- [69] R. Planet, S. Santucci, et J. Ortín, “Avalanches and non-gaussian fluctuations of the global velocity of imbibition fronts,” *Phys. Rev. Lett.* **102**, 094502 (2009). URL : <http://link.aps.org/doi/10.1103/PhysRevLett.102.094502>. c, B.1, C.1
- [70] M. Alava, M. Rost, et M. Dubé, “Imbibition in disordered media,” *Advances in Physics* **53**, 83–175 (2004). c
- [71] A.-L. Barabási et H. E. Stanley, *Fractal Concepts in Surface Growth* (Cambridge University Press, 1995). URL : <http://dx.doi.org/10.1017/CB09780511599798>, cambridge Books Online. I.4.2
- [72] T. Halpin-Healy et Y.-C. Zhang, “Kinetic roughening phenomena, stochastic growth, directed polymers and all that,” *Phys. Rep.* **254**, 215–415 (1995). I.4.2
- [73] J. ichi Wakita, H. Itoh, T. Matsuyama, et M. Matsushita, “Self-affinity for the growing interface of bacterial colonies,” *Journal of the Physical Society of Japan* **66**, 67–72 (1997). URL : <http://dx.doi.org/10.1143/JPSJ.66.67>. a
- [74] M. A. C. Huergo, M. A. Pasquale, P. H. González, A. E. Bolzán, et A. J. Arvia, “Growth dynamics of cancer cell colonies and their comparison with noncancerous cells,” *Phys. Rev. E* **85**, 011918 (2012). URL : <http://link.aps.org/doi/10.1103/PhysRevE.85.011918>. a
- [75] M. Myllys, J. Maunuksela, M. Alava, T. Ala-Nissila, J. Merikoski, et J. Timonen, “Kinetic roughening in slow combustion of paper,” *Phys. Rev. E* **64**, 036101 (2001). URL : <http://link.aps.org/doi/10.1103/PhysRevE.64.036101>. b

- [76] K. A. Takeuchi et M. Sano, “Universal Fluctuations of Growing Interfaces: Evidence in Turbulent Liquid Crystals,” *Physical Review Letters* **104**, 230601 (2010). c
- [77] K. A. Takeuchi, M. Sano, T. Sasamoto, et H. Spohn, “Growing interfaces uncover universal fluctuations behind scale invariance,” *Scientific Reports* **1**, 34 (2011). c
- [78] K. A. Takeuchi et M. Sano, “Evidence for Geometry-Dependent Universal Fluctuations of the Kardar-Parisi-Zhang Interfaces in Liquid-Crystal Turbulence,” *Journal of Statistical Physics* **147**, 853–890 (2012). c
- [79] K. A. Takeuchi, “Crossover from Growing to Stationary Interfaces in the Kardar-Parisi-Zhang Class,” *Physical Review Letters* **110**, 210604 (2013). c
- [80] K. A. Takeuchi, “Experimental approaches to universal out-of-equilibrium scaling laws: turbulent liquid crystal and other developments,” *Journal of Statistical Mechanics: Theory and Experiment* **1**, 01006 (2014). c
- [81] J. Sethna, K. Dahmen, et C. Myers, “Crackling noise,” *Nature* **410**, 242–250 (2001). II.1, B.1, C.1
- [82] P. Bak, C. Tang, et K. Wiesenfeld, “Self-organized criticality - an explanation of $1/f$ noise,” *Phys. Rev. Lett.* **59**, 381–384 (1987). II.1
- [83] S. Manna, “Two-state model of self-organized critical phenomena,” *J. Phys. A* **24**, L363–L369 (1991). II.1
- [84] D. Dhar, “The Abelian sandpile and related models,” *Physica A* **263**, 4 (1999). URL : <http://www.citebase.org/abstract?id=oai:arXiv.org:cond-mat/9808047>. II.1
- [85] G. Pruessner, *Self-Organised Criticality: Theory, Models and Characterisation* (Cambridge University Press, 2012). II.1
- [86] K. Dahmen et J. Sethna, “Hysteresis, avalanches, and disorder-induced critical scaling: A renormalization-group approach,” *Phys. Rev. B* **53**, 14872–14905 (1996). II.1, A.1, B.1
- [87] G. Tarjus, M. Baczyk, et M. Tissier, “Avalanches and dimensional reduction breakdown in the critical behavior of disordered systems,” *Physical review letters* **110**, 135703 (2013). II.1, III.4
- [88] G. Tarjus et M. Tissier, “Avalanches and perturbation theory in the random-field ising model,” *Journal of Statistical Mechanics: Theory and Experiment* **2016**, 023207 (2016). URL : <http://stacks.iop.org/1742-5468/2016/i=2/a=023207>. II.1
- [89] P. Le Doussal, M. Müller, et K. J. Wiese, “Avalanches in mean-field models and the Barkhausen noise in spin-glasses,” *EPL (Europhysics Letters)* **91**, 57004 (2010). II.1, III.4

- [90] P. Le Doussal, M. Müller, et K. J. Wiese, “Equilibrium avalanches in spin glasses,” **85**, 214402 (2012). II.1
- [91] M. Müller et M. Wyart, “Marginal stability in structural, spin, and electron glasses,” *Annual Review of Condensed Matter Physics* **6**, 177–200 (2015). URL : <http://dx.doi.org/10.1146/annurev-conmatphys-031214-014614>. II.1, B.1
- [92] P. L. Doussal et K. Wiese, “An exact mapping of the stochastic field theory for Manna sandpiles to interfaces in random media,” *Phys. Rev. Lett.* **114**, 110601 (2014). II.1, B.1
- [93] J. Lin, E. Lerner, A. Rosso, et M. Wyart, “Scaling description of the yielding transition in soft amorphous solids at zero temperature,” *Proceedings of the National Academy of Sciences* **111**, 14382–14387 (2014). URL : <http://www.pnas.org/content/111/40/14382.abstract>. II.1, III.4, B.1
- [94] Y. G. Sinai, “The limiting behavior of a one-dimensional random walk in a random medium,” *Theory of Probability & Its Applications* **27**, 256–268 (1983). URL : <http://dx.doi.org/10.1137/1127028>. II.2.1
- [95] S. Kida, “Asymptotic properties of burgers turbulence,” *Journal of Fluid Mechanics* **93**, 337–377 (1979). URL : http://journals.cambridge.org/article_S0022112079001932. II.2.1
- [96] P. Le Doussal, “Exact results and open questions in first principle functional RG,” *Annals of Physics* **325**, 49–150 (2009). II.2.1, a, a, b, b, b, c, d, d, 3, a, b, C.3.2, C.3.9, 5
- [97] P. Le Doussal et K. J. Wiese, “Driven particle in a random landscape: disorder correlator, avalanche distribution and extreme value statistics of records,” *Phys. Rev. E* **79**, 051105 (2009). II.2.2, a, II.6.1, C.6.1
- [98] B. Alessandro, C. Beatrice, G. Bertotti, et A. Montorsi, “Domain-wall dynamics and barkhausen effect in metallic ferromagnetic materials. i. theory,” *Journal of Applied Physics* **68** (1990). b, b, A.1, A.2.2, A.2.4, B.1, C.1
- [99] B. Alessandro, C. Beatrice, G. Bertotti, et A. Montorsi, “Domain-wall dynamics and barkhausen effect in metallic ferromagnetic materials. ii. experiments,” *Journal of Applied Physics* **68** (1990). b, A.1, A.2.2, A.2.4, B.1, C.1
- [100] S. Zapperi, P. Cizeau, G. Durin, et H. E. Stanley, “Dynamics of a ferromagnetic domain wall: Avalanches, depinning transition, and the Barkhausen effect,” *Phys. Rev. B* **58**, 6353–6366 (1998). b, d, A.1, B.1, C.1
- [101] P. Le Doussal et K. J. Wiese, “Avalanche dynamics of elastic interfaces,” *Phys. Rev. E* **88**, 022106 (2013). URL : <http://link.aps.org/doi/10.1103/PhysRevE.88.022106>. b, c, c, c, 8, d, d, d, d, e, e, II.6.1, A.1, 1, A.2.2, A.2.3, A.2.4, A.9, A.9, A.11, A.11, A.11, B.1, B.1, B.1, B.2, B.2, B.2, B.2, B.2, C.1, C.3.3, C.4.2, C.7

- [102] A. Dobrinevski, P. Le Doussal, et K. J. Wiese, “Non-stationary dynamics of the Alessandro-Beatrice-Bertotti-Montorsi model,” *Phys. Rev. E* **85**, 031105 (2012). b, d, d, d, e, II.6.1, A.1, 1, A.2.2, A.2.3, A.2.4, A.2.4, A.9, A.11, A.11, A.11, A.11, B.1, B.2
- [103] G. Bertotti, G. Durin, et A. Magni, “Scaling aspects of domain wall dynamics and barkhausen effect in ferromagnetic materials,” *Journal of Applied Physics* **75** (1994). b, II.6.1
- [104] C. W. Gardiner, *Handbook of stochastic methods for physics, chemistry and the natural sciences*, vol. 13 de *Springer Series in Synergetics* (Springer-Verlag, Berlin, 2004), 3è éd. b, II.6.2, a
- [105] A. A. Middleton, P. Le Doussal, et K. J. Wiese, “Measuring functional renormalization group fixed-point functions for pinned manifolds,” *Phys. Rev. Lett.* **98**, 155701 (2007). a, a, C.2
- [106] P. Le Doussal, A. Middleton, et K. Wiese, “Statistics of static avalanches in a random pinning landscape,” *Phys. Rev. E* **79**, 050101 (R) (2009). URL : <http://www.phys.ens.fr/~wiese/abstracts/stat-avalanche-PRL.html>. a, II.6.1
- [107] M. Delorme, P. Le Doussal, et K. Wiese, “Distribution of joint local and total size and of extension for avalanches in the Brownian force model,” *ArXiv e-prints* (2016). b, II.6.1, A.1, A.7.2, B.2, C.1, b
- [108] O. Narayan et D. S. Fisher, “Threshold critical dynamics of driven interfaces in random media,” *Phys. Rev. B* **48**, 7030–42 (1993). b, a, a, II.6.1, C.1
- [109] P. Le Doussal et K. J. Wiese, “Size distributions of shocks and static avalanches from the functional renormalization group,” *Phys. Rev. E* **79**, 051106 (2009). b, c, b, b, b, b, II.6.1, A.1, B.1, B.1, B.2, C.1, C.2, C.3.3, C.3.5, C.3.6, C.3.6, C.3.8, C.3.9, C.3.9, 2, C.4.1, C.4.2, C.4.3, C.5.1, C.5.1, C.8, C.10.1, C.11
- [110] A. Dobrinevski, P. Le Doussal, et K. Wiese, “Avalanche shape and exponents beyond mean-field theory,” *EPL* **108**, 66002 (2014). b, II.6.1, C.1
- [111] P. Le Doussal et K. J. Wiese, “First-principle derivation of static avalanche-size distribution,” *Phys. Rev. E* **85**, 061102 (2012). URL : <http://pre.aps.org/abstract/PRE/v85/i6/e061102>. c, b, b, b, b, b, d, d, d, II.6.1, A.1, .1, B.1, B.1, B.2, B.2, C.1, C.2, C.2, C.3.7, C.3.9, C.3.9, C.4.3, C.5.1, C.5.1, C.9, C.10.1, C.10.1
- [112] L. E. Aragón, A. B. Kolton, P. L. Doussal, K. J. Wiese, et E. A. Jagla, “Avalanches in tip-driven interfaces in random media,” *EPL (Europhysics Letters)* **113**, 10002 (2016). URL : <http://stacks.iop.org/0295-5075/113/i=1/a=10002>. b, b, C.1
- [113] M. Paczuski et S. Boettcher, “Universality in sandpiles, interface depinning, and earthquake models,” *Phys. Rev. Lett.* **77**, 111 (1996). URL : <http://link.aps.org/doi/10.1103/PhysRevLett.77.111>. b, b

- [114] D. S. Fisher, “Interface fluctuations in disordered systems: $5 - \epsilon$ expansion and failure of dimensional reduction,” *Phys. Rev. Lett.* **56** (1986). URL : <http://link.aps.org/doi/10.1103/PhysRevLett.56.1964>. a, d, d, 1, B.1, C.1
- [115] L. Balents, J. Bouchaud, et M. Mézard, “The large scale energy landscape of randomly pinned objects,” *J. Phys. I (France)* **6**, 1007–20 (1996). a
- [116] P. Chauve, P. Le Doussal, et K. Wiese, “Renormalization of pinned elastic systems: How does it work beyond one loop?” *Phys. Rev. Lett.* **86**, 1785–1788 (2001). a, d, d, d, d, 2, 3, 4, B.1, C.1
- [117] P. Le Doussal, K. J. Wiese, et P. Chauve, “Functional renormalization group and the field theory of disordered elastic systems,” *Phys. Rev. E* **69**, 026112 (2004). a, B.1, C.1, C.2, C.3.3, C.6.1
- [118] G. Schehr et P. Le Doussal, “Exact multilocal renormalization of the effective action: Application to the random sine gordon model statics and nonequilibrium dynamics,” *Phys. Rev. E* **68**, 046101 (2003). URL : <http://link.aps.org/doi/10.1103/PhysRevE.68.046101>. a, c
- [119] L. Balents et P. L. Doussal, “Thermal fluctuations in pinned elastic systems: field theory of rare events and droplets,” *Annals of Physics* **315**, 213–303 (2005). a
- [120] K. Wiese, “Why one needs a functional renormalization group to survive in a disordered world,” *Pramana* **64**, 817–827 (2005). a
- [121] K. Wiese et P. L. Doussal, “Functional renormalization for disordered systems: Basic recipes and gourmet dishes,” *Markov Processes Relat. Fields* **13**, 777–818 (2007). a
- [122] B. Delamotte, “An Introduction to the Nonperturbative Renormalization Group,” dans “Lecture Notes in Physics, Berlin Springer Verlag,” , vol. 852 de *Lecture Notes in Physics, Berlin Springer Verlag*, J. Polonyi et A. Schwenk, édés. (2012), vol. 852 de *Lecture Notes in Physics, Berlin Springer Verlag*, p. 49. b
- [123] P. Le Doussal, “Finite temperature Functional RG, droplets and decaying Burgers turbulence,” *Europhys. Lett.* **76**, 457–463 (2006). b, a, C.2
- [124] C. Wetterich, “Exact evolution equation for the effective potential,” *Physics Letters B* **301**, 90 – 94 (1993). URL : <http://www.sciencedirect.com/science/article/pii/037026939390726X>. c
- [125] T. R. Morris, “The exact renormalization group and approximate solutions,” *International Journal of Modern Physics A* **9**, 2411–2449 (1994). c
- [126] O. Narayan et D. S. Fisher, “Critical behavior of sliding charge-density waves in 4-epsilon dimensions,” *Phys. Rev. B* **46**, 11520–49 (1992). a, B.1, C.1

- [127] T. Nattermann, S. Stepanow, L.-H. Tang, et H. Leschhorn, “Dynamics of interface depinning in a disordered medium,” *J. Phys. II (France)* **2**, 1483–8 (1992). a, B.1, C.1
- [128] H. Leschhorn, T. Nattermann, S. Stepanow, et L.-H. Tang, “Driven interface depinning in a disordered medium,” *Annalen der Physik* **509**, 1–34 (1997). a
- [129] P. Le Doussal, K. J. Wiese, et P. Chauve, “2-loop functional renormalization group analysis of the depinning transition,” *Phys. Rev. B* **66**, 174201 (2002). a, b, c, c, c, c, c, B.1, C.1
- [130] P. Martin, E. Siggia, et H. Rose, “Statistical dynamics of classical systems,” *Phys. Rev. A* **8**, 423–437 (1973). a, A.11, B.2
- [131] H.-K. Janssen, “On a lagrangean for classical field dynamics and renormalization group calculations of dynamical critical properties,” *Zeitschrift für Physik B Condensed Matter* **23**, 377–380 (1976). URL : <http://dx.doi.org/10.1007/BF01316547>. a, A.11
- [132] H. Janssen, “On the renormalized field theory of nonlinear critical relaxation,” dans “From Phase Transitions to Chaos,” (World Scientific, Singapore, 1992), *Topics in Modern Statistical Physics*, p. 68–117. a, B.2
- [133] U. Täuber, *Critical Dynamics: A Field Theory Approach to Equilibrium and Non-Equilibrium Scaling Behavior* (Cambridge University Press, 2014). a
- [134] A. Rosso, P. Le Doussal, et K. Wiese, “Numerical calculation of the functional renormalization group fixed-point functions at the depinning transition,” *Phys. Rev. B* **75**, 220201 (2007). c
- [135] B. Delamotte, “A Hint of renormalization,” *Am. J. Phys.* **72**, 170–184 (2004). c
- [136] P. Le Doussal et K. J. Wiese, “Distribution of velocities in an avalanche,” *EPL* **97**, 46004 (2012). URL : <http://www.phys.ens.fr/~wiese/pdf/ep114307-offprints.pdf>. d, e, II.6.1, A.1, A.9, A.9, A.11
- [137] M. LeBlanc, L. Angheluta, K. Dahmen, et N. Goldenfeld, “Universal fluctuations and extreme statistics of avalanches near the depinning transition,” *Phys. Rev. E* **87**, 022126 (2013). URL : <http://link.aps.org/doi/10.1103/PhysRevE.87.022126>. II.6.1
- [138] M. LeBlanc, L. Angheluta, K. Dahmen, et N. Goldenfeld, “Distribution of maximum velocities in avalanches near the depinning transition,” *Phys. Rev. Lett.* **109**, 105702 (2012). URL : <http://link.aps.org/doi/10.1103/PhysRevLett.109.105702>. II.6.1
- [139] A. Rosso, P. Le Doussal, et K. Wiese, “Avalanche-size distribution at the depinning transition: A numerical test of the theory,” *Phys. Rev. B* **80**, 144204 (2009). II.6.1

- [140] A. Baldassarri, F. Colaiori, et C. Castellano, “Average shape of a fluctuation: Universality in excursions of stochastic processes,” *Phys. Rev. Lett.* **90**, 060601 (2003). URL : <http://link.aps.org/doi/10.1103/PhysRevLett.90.060601>. II.6.1
- [141] F. Colaiori, S. Zapperi, et G. Durin, “Shape of a Barkhausen pulse,” *Journal of Magnetism and Magnetic Materials* **272-276**, E533–E534 (2004). URL : <http://linkinghub.elsevier.com/retrieve/pii/S0304885303025423>. II.6.1
- [142] S. Papanikolaou, F. Bohn, R. Sommer, G. Durin, S. Zapperi, et J. Sethna, “Universality beyond power laws and the average avalanche shape,” *Nature Physics* **7**, 316–320 (2011). URL : <http://dx.doi.org/10.1038/nphys1884>. II.6.1, A.1, B.1
- [143] S. Zapperi, C. Castellano, F. Colaiori, et G. Durin, “Signature of effective mass in crackling-noise asymmetry,” *Nat Phys* **1**, 46–49 (2005). URL : <http://dx.doi.org/10.1038/nphys101>. II.6.1, B.1
- [144] A. Dobrinevski, P. Le Doussal, et K. J. Wiese, “Statistics of avalanches with relaxation and barkhausen noise: A solvable model,” *Phys. Rev. E* **88**, 032106 (2013). URL : <http://link.aps.org/doi/10.1103/PhysRevE.88.032106>. II.6.1, II.7, B.1, C.1
- [145] G. Durin, F. Bohn, M. A. Correa, R. L. Sommer, P. Le Doussal, et K. J. Wiese, “Quantitative scaling of magnetic avalanches,” *ArXiv e-prints* (2016). II.6.1, B.1, C.1
- [146] R. Burridge et L. Knopoff, “Model and theoretical seismicity,” *Bulletin of the Seismological Society of America* **57**, 341–371 (1967). II.6.1, C.1
- [147] E. Jagla et A. Kolton, “The mechanisms of spatial and temporal earthquake clustering,” *arXiv:0901.1907* (2009). II.6.1, C.1
- [148] E. A. Jagla, F. P. Landes, et A. Rosso, “Viscoelastic effects in avalanche dynamics: A key to earthquake statistics,” *Phys. Rev. Lett.* **112**, 174301 (2014). URL : <http://link.aps.org/doi/10.1103/PhysRevLett.112.174301>. II.6.1, C.1
- [149] E. A. Jagla, “Aftershock production rate of driven viscoelastic interfaces,” *Phys. Rev. E* **90**, 042129 (2014). URL : <http://link.aps.org/doi/10.1103/PhysRevE.90.042129>. II.6.1, C.1
- [150] J. Quastel, “Introduction to KPZ,” *Current Developments in Mathematics* (2011). III.1
- [151] H. Spohn, “The Kardar-Parisi-Zhang equation - a statistical physics perspective,” *ArXiv e-prints* (2016). III.1, F.1.1, G.1
- [152] M. Hairer, “Solving the KPZ equation.” *Ann. Math. (2)* **178**, 559–664 (2013). a
- [153] J. Imbrie et T. Spencer, “Diffusion of directed polymers in a random environment,” *J. Stat. Phys.* **52**, 609 (1988). b

- [154] E. Bolthausen, “A note on the diffusion of directed polymers in a random environment,” *Comm. Math. Phys.* **123**, 529–534 (1989). URL : <http://projecteuclid.org/euclid.cmp/1104178982>. b
- [155] F. Comets, T. Shiga, N. Yoshida *et al.*, “Probabilistic analysis of directed polymers in a random environment: a review,” *Advanced Studies in Pure Mathematics* **39**, 115–142 (2004). b
- [156] F. Comets, T. Shiga, et N. Yoshida, “Directed polymers in a random environment: path localization and strong disorder,” *Bernoulli* **9**, 705–723 (2003). b
- [157] J. M. Hammersley et D. Welsh, “First-passage percolation, subadditive processes, stochastic networks, and generalized renewal theory,” dans “Bernoulli 1713 Bayes 1763 Laplace 1813,” (Springer, 1965), p. 61–110. c
- [158] J. B. Martin, “Last-passage percolation with general weight distribution,” URL : <http://www.stats.ox.ac.uk/~martin/papers/lppssurvey.ps.gz>. c, c
- [159] K. Johansson, “Shape fluctuations and random matrices,” *Communications in mathematical physics* **209**, 437–476 (2000). c, III.1.2, c, a, III.3.1, III.3.5, D.1, 3, E.1.1, a, b, c, E.5, F.1.1, G.1, a, a, G.8
- [160] T. Kriecherbauer et J. Krug, “A pedestrian’s view on interacting particle systems, KPZ universality, and random matrices,” *ArXiv e-prints* (2008). d, a, G.1
- [161] I. Corwin, J. Quastel, et D. Remenik, “Renormalization fixed point of the KPZ universality class,” *ArXiv e-prints* (2011). III.1.2, III.1.2
- [162] M. Praehofer et H. Spohn, “Scale Invariance of the PNG Droplet and the Airy Process,” *ArXiv Mathematics e-prints* (2001). 1, III.1.2
- [163] T. Sasamoto, “Spatial correlations of the 1d kpz surface on a flat substrate,” *Journal of Physics A: Mathematical and General* **38**, L549 (2005). URL : <http://stacks.iop.org/0305-4470/38/i=33/a=L01>. 2, III.1.2
- [164] J. Quastel et D. Remenik, *Topics in Percolative and Disordered Systems* (Springer New York, New York, NY, 2014), chap. Airy Processes and Variational Problems, p. 121–171. URL : http://dx.doi.org/10.1007/978-1-4939-0339-9_5. III.1.2
- [165] V. Dotsenko, “Bethe ansatz derivation of the tracy-widom distribution for one-dimensional directed polymers,” *EPL (Europhysics Letters)* **90**, 20003 (2010). URL : <http://stacks.iop.org/0295-5075/90/i=2/a=20003>. III.1.2, III.2.3, e, e, f, D.1, .3, E.1.1, F.3, F.3.4, G.1
- [166] V. Dotsenko, “On two-time distribution functions in (1+1) random directed polymers,” *ArXiv e-prints* (2016). III.1.2, f
- [167] K. Johansson, “Two time distribution in Brownian directed percolation,” *ArXiv e-prints* (2015). III.1.2

- [168] P. L. Ferrari et H. Spohn, “On time correlations for KPZ growth in one dimension,” ArXiv e-prints (2016). III.1.2
- [169] T. Gueudré et P. Le Doussal, “Directed polymer near a hard wall and KPZ equation in the half-space,” EPL (Europhysics Letters) **100**, 26006 (2012). III.1.2, f, D.1, E.1.1
- [170] J. Baik, P. Deift, et K. Johansson, “On the Distribution of the Length of the Longest Increasing Subsequence of Random Permutations,” ArXiv Mathematics e-prints (1998). III.1.2
- [171] G. Amir, I. Corwin, et J. Quastel, “Probability Distribution of the Free Energy of the Continuum Directed Random Polymer in 1+1 dimensions,” ArXiv e-prints (2010). III.1.2, D.1, .3, E.1.1
- [172] T. Sasamoto et H. Spohn, “Exact height distributions for the KPZ equation with narrow wedge initial condition,” Nuclear Physics B **834**, 523–542 (2010). III.1.2, D.1, .3, E.1.1
- [173] P. Calabrese, P. Le Doussal, et A. Rosso, “Free-energy distribution of the directed polymer at high temperature,” EPL (Europhysics Letters) **90**, 20002 (2010). III.1.2, III.1.3, III.2.3, e, e, e, f, D.1, D.5, D.5, D.9.1, D.10, .3, D.18, E.1.1, F.3, F.3.2, F.3.4, G.1
- [174] K. Johansson, “Discrete polynuclear growth and determinantal processes,” Communications in Mathematical Physics **242**, 277–329 (2003). URL : <http://dx.doi.org/10.1007/s00220-003-0945-y>. III.1.2
- [175] S. Prolhac et H. Spohn, “The one-dimensional KPZ equation and the Airy process,” Journal of Statistical Mechanics: Theory and Experiment **3**, 03020 (2011). III.1.2, f, D.1, E.1.1
- [176] J. Baik et E. M. Rains, “The asymptotics of monotone subsequences of involutions,” Duke Math. J. **109**, 205–281 (2001). URL : <http://dx.doi.org/10.1215/S0012-7094-01-10921-6>. III.1.2
- [177] P. Calabrese et P. Le Doussal, “Exact Solution for the Kardar-Parisi-Zhang Equation with Flat Initial Conditions,” Physical Review Letters **106**, 250603 (2011). III.1.2, f, D.1, D.5, D.5, D.9.1, .1, E.1.1
- [178] P. Le Doussal et P. Calabrese, “The KPZ equation with flat initial condition and the directed polymer with one free end,” Journal of Statistical Mechanics: Theory and Experiment **6**, 06001 (2012). III.1.2, b, c, f
- [179] T. Gueudré, P. Le Doussal, A. Rosso, A. Henry, et P. Calabrese, “Short-time growth of a Kardar-Parisi-Zhang interface with flat initial conditions,” **86**, 041151 (2012). III.1.2, f
- [180] J. Ortmann, J. Quastel, et D. Remenik, “Exact formulas for random growth with half-flat initial data,” ArXiv e-prints (2014). III.1.2, D.1, E.1.1

- [181] P. L. Ferrari et H. Spohn, “Scaling Limit for the Space-Time Covariance of the Stationary Totally Asymmetric Simple Exclusion Process,” *Communications in Mathematical Physics* **265**, 1–44 (2006). III.1.2
- [182] J. Baik, P. L. Ferrari, et S. P ech e, “Limit process of stationary TASEP near the characteristic line,” *ArXiv e-prints* (2009). III.1.2
- [183] T. Imamura et T. Sasamoto, “Exact solution for the stationary kardar-parisi-zhang equation,” *Phys. Rev. Lett.* **108**, 190603 (2012). URL : <http://link.aps.org/doi/10.1103/PhysRevLett.108.190603>. III.1.2, f, D.1, E.1.1, E.8
- [184] T. Imamura et T. Sasamoto, “Stationary Correlations for the 1D KPZ Equation,” *Journal of Statistical Physics* **150**, 908–939 (2013). III.1.2, f
- [185] A. Borodin, I. Corwin, P. Ferrari, et B. Vet o, “Height fluctuations for the stationary kpz equation,” *Mathematical Physics, Analysis and Geometry* **18**, 1–95 (2015). URL : <http://dx.doi.org/10.1007/s11040-015-9189-2>. III.1.2, E.1.1, E.8
- [186] M. Hairer et J. Quastel, “A class of growth models rescaling to KPZ,” *ArXiv e-prints* (2015). III.1.3
- [187] L. Bertini et G. Giacomin, “Stochastic burgers and kpz equations from particle systems,” *Comm. Math. Phys.* **183**, 571–607 (1997). URL : <http://projecteuclid.org/euclid.cmp/1158328658>. III.1.3
- [188] T. Alberts, K. Khanin, et J. Quastel, “The intermediate disorder regime for directed polymers in dimension $1 + 1$,” *ArXiv e-prints* (2012). III.1.3, III.1.3
- [189] S. Bustingorry, P. Le Doussal, et A. Rosso, “Universal high-temperature regime of pinned elastic objects,” **82**, 140201 (2010). III.1.3
- [190] N. O’Connell et M. Yor, “Brownian analogues of Burke’s theorem,” *Stochastic Process. Appl.* **96**, 285–304 (2001). URL : [http://dx.doi.org/10.1016/S0304-4149\(01\)00119-3](http://dx.doi.org/10.1016/S0304-4149(01)00119-3). III.1.3, D.23, E.1.1
- [191] N. O’Connell, “Directed polymers and the quantum Toda lattice,” *ArXiv e-prints* (2009). III.1.3, D.1, .5, D.23, E.1.1
- [192] A. Borodin et I. Corwin, “Macdonald processes,” *Probability Theory and Related Fields* **158**, 225–400 (2014). URL : <http://dx.doi.org/10.1007/s00440-013-0482-3>. III.1.3, b, D.1, D.5, E.1.1, F.3.4, F.4.2
- [193] A. Auffinger, J. Baik, et I. Corwin, “Universality for directed polymers in thin rectangles,” *ArXiv e-prints* (2012). III.1.3, D.23
- [194] J. Bec et K. Khanin, “Burgers turbulence,” **447**, 1–66 (2007). III.2.1, E.1.1
- [195] D. Forster, D. R. Nelson, et M. J. Stephen, “Large-distance and long-time properties of a randomly stirred fluid,” *Phys. Rev. A* **16**, 732–749 (1977). URL : <http://link.aps.org/doi/10.1103/PhysRevA.16.732>. a, G.1, G.4.2

- [196] J. Krug, H. Spohn, et C. Godrèche, “Solids far from equilibrium,” *Solids far from equilibrium* (1991). a
- [197] T. Seppäläinen, “Scaling for a one-dimensional directed polymer with boundary conditions,” *ArXiv e-prints* (2009). b, b, a, III.3.1, III.3.5, D, D.1, D.2.1, .2, .1, E.1.1, F.1.1, G.1, G.2, G.4, a, G.6.4, G.9, G.8
- [198] I. Corwin, N. O’Connell, T. Seppäläinen, et N. Zygouras, “Tropical combinatorics and whittaker functions,” *Duke Math. J.* **163**, 513–563 (2014). URL : <http://dx.doi.org/10.1215/00127094-2410289>. b, a, III.3.1, D, D.1, .1, .1, D.13, .1, .2, D.23, E.1.1, c, E.5, F.1.1, G.1, G.8
- [199] P. J. Burke, “The output of a queuing system,” *Operations research* **4**, 699–704 (1956). c, G.5.1, c
- [200] G. M. Schütz, “Exact solution of the master equation for the asymmetric exclusion process,” *Journal of statistical physics* **88**, 427–445 (1997). c
- [201] M. Kardar, “Replica Bethe ansatz studies of two-dimensional interfaces with quenched random impurities,” *Nucl. Phys. B* **290**, 582–602 (1987). a, f, D.1, E.1.1, G.1
- [202] E. H. Lieb et W. Liniger, “Exact analysis of an interacting bose gas. i. the general solution and the ground state,” *Phys. Rev.* **130**, 1605–1616 (1963). URL : <http://link.aps.org/doi/10.1103/PhysRev.130.1605>. a, b, b, D.1, D.3.2, D.5, E.1.1
- [203] F. Franchini, “Notes on bethe ansatz techniques,” (2011). b
- [204] É. Brunet et B. Derrida, “Ground state energy of a non-integer number of particles with δ attractive interactions,” *Physica A Statistical Mechanics and its Applications* **279**, 398–407 (2000). c, f
- [205] É. Brunet et B. Derrida, “Probability distribution of the free energy of a directed polymer in a random medium,” *Phys. Rev. E* **61**, 6789–6801 (2000). c, f
- [206] S. Prolhac et H. Spohn, “The propagator of the attractive delta-Bose gas in one dimension,” *Journal of Mathematical Physics* **52**, 122106–122106 (2011). 6
- [207] J. B. McGuire, “Study of Exactly Soluble One-Dimensional N-Body Problems,” *Journal of Mathematical Physics* **5**, 622–636 (1964). c
- [208] A. Borodin, I. Corwin, L. Petrov, et T. Sasamoto, “Spectral Theory for Interacting Particle Systems Solvable by Coordinate Bethe Ansatz,” *Communications in Mathematical Physics* **339**, 1167–1245 (2015). c, f, D.1, D.7.5, E.1.1
- [209] P. Calabrese et J.-S. Caux, “Dynamics of the attractive 1D Bose gas: analytical treatment from integrability,” *Journal of Statistical Mechanics: Theory and Experiment* **8**, 08032 (2007). c, d, f, III.3.2, D.7.4, D.7.5, D.16, .2, E.1.1

- [210] M. Gaudin, *La fonction d'onde de Bethe*, Collection du Commissariat à l'Énergie Atomique / Ser. scientifique (Masson, 1983). URL : <https://books.google.fr/books?id=yLLvAAAAMAAJ>. d, D.3.2, D.6
- [211] F. Bornemann, “On the Numerical Evaluation of Fredholm Determinants,” ArXiv e-prints (2008). e
- [212] J. P. Bouchaud et H. Orland, “On the bethe ansatz for random directed polymers,” *Journal of Statistical Physics* **61**, 877–884 (1990). URL : <http://dx.doi.org/10.1007/BF01027306>. f
- [213] V. Dotsenko, “Two-point free energy distribution function in (1+1) directed polymers,” *Journal of Physics A: Mathematical and Theoretical* **46**, 355001 (2013). URL : <http://stacks.iop.org/1751-8121/46/i=35/a=355001>. f
- [214] P. Le Doussal, “Crossover from droplet to flat initial conditions in the KPZ equation from the replica Bethe ansatz,” *Journal of Statistical Mechanics: Theory and Experiment* **4**, 04018 (2014). f, D.1, E.1.1
- [215] V. Dotsenko, “Distribution function of the endpoint fluctuations of one-dimensional directed polymers in a random potential,” *Journal of Statistical Mechanics: Theory and Experiment* **2013**, P02012 (2013). URL : <http://stacks.iop.org/1742-5468/2013/i=02/a=P02012>. f, D.1, E.1.1
- [216] M. Draief, J. Mairesse, et N. O’Connell, “Queues, stores, and tableaux,” *J. Appl. Probab.* **42**, 1145–1167 (2005). URL : <http://dx.doi.org/10.1239/jap/1134587823>. a, III.3.5, G.1, G.5.1, b, c, G.8
- [217] N. O’Connell, “Directed polymers and the quantum Toda lattice,” ArXiv e-prints (2009). a
- [218] A. Borodin, I. Corwin, et D. Remenik, “Log-gamma polymer free energy fluctuations via a fredholm determinant identity,” *Communications in Mathematical Physics* **324**, 215–232 (2013). URL : <http://dx.doi.org/10.1007/s00220-013-1750-x>. a, III.3.1, III.3.2, D, D.1, D.9.2, .1, .1, D.12, D.23, E.1.1, c, c, F.1.1, G.1
- [219] I. Corwin, T. Seppäläinen, et H. Shen, “The strict-weak lattice polymer,” *Journal of Statistical Physics* **160**, 1027–1053 (2015). URL : <http://dx.doi.org/10.1007/s10955-015-1267-0>. a, III.3.3, E.1.1, b, E.4.3, F.1.1, 1, G.1, b, G.8
- [220] N. O’Connell et J. Ortmann, “Tracy-widom asymptotics for a random polymer model with gamma-distributed weights,” *Electron. J. Probab.* **20**, no. 25, 1–18 (2015). URL : <http://ejp.ejpecp.org/article/view/3787>. a, E.1.1, F.1.1, 1, G.1, G.8
- [221] K. Matveev et L. Petrov, “q-randomized Robinson-Schensted-Knuth correspondences and random polymers,” ArXiv e-prints (2015). a, 10, E.5, G.8

- [222] A. M. Povolotsky, “On the integrability of zero-range chipping models with factorized steady states,” *Journal of Physics A Mathematical General* **46**, 465205 (2013). III.3.1, III.3.3, .4, E, E.1.1, E.2.2, 3, E.2.3, E.2.3, E.2.3, E.2.3, E.2.3, a, E.5, F.3.1, G.8
- [223] I. Corwin et L. Petrov, “The q -pushasep: A new integrable model for traffic in $1+1$ dimension,” *Journal of Statistical Physics* **160**, 1005–1026 (2015). URL : <http://dx.doi.org/10.1007/s10955-015-1218-9>. 8
- [224] G. Barraquand et I. Corwin, “Random-walk in beta-distributed random environment,” *Probability Theory and Related Fields* p. 1–60 (2016). URL : <http://dx.doi.org/10.1007/s00440-016-0699-z>. III.3.1, III.3.3, III.3.4, III.3.4, III.3.4, E.1.1, E.1.2, b, a, F, F.1.1, F.1.2, F.2.2, F.2.3, F.2.3, F.3, F.3.1, F.3.4, F.5.1, F.5.1, F.5.1, F.6.1, F.6.1, F.6.1, 4, F.6.2, 5, F.7.2, F.8, 3, G.1
- [225] C. A. Tracy et H. Widom, “A Fredholm Determinant Representation in ASEP,” *Journal of Statistical Physics* **132**, 291–300 (2008). III.3.4, III.3.4, F.4.2, F.5.2
- [226] C. A. Tracy et H. Widom, “Asymptotics in ASEP with Step Initial Condition,” *Communications in Mathematical Physics* **290**, 129–154 (2009). III.3.4, E.1.1, F.4.2, F.5.2
- [227] F. Rassoul-Agha, T. Seppäläinen, et A. Yilmaz, “Quenched free energy and large deviations for random walks in random potentials,” *Communications on Pure and Applied Mathematics* **66**, 202–244 (2013). URL : <http://dx.doi.org/10.1002/cpa.21417>. III.3.4, F.1.1, F.5.1, F.5.4
- [228] N. Georgiou et T. Seppäläinen, “Large deviation rate functions for the partition function in a log-gamma distributed random potential,” *ArXiv e-prints* (2011). III.3.5
- [229] F. Comets et V.-L. Nguyen, “Localization in log-gamma polymers with boundaries,” *Probability Theory and Related Fields* p. 1–33 (2015). URL : <http://dx.doi.org/10.1007/s00440-015-0662-4>. III.3.5, G.1
- [230] L. Carraro et J. Duchon, “Équation de Burgers avec conditions initiales à accroissements indépendants et homogènes,” *Ann. Inst. Henri Poincaré* **15**, 431–458 (1998). A.4.1, .1, C.4.3, C.9
- [231] I. Dornic, H. Chaté, et M. A. Muñoz, “Integration of langevin equations with multiplicative noise and the viability of field theories for absorbing phase transitions,” *Phys. Rev. Lett.* **94**, 100601 (2005). URL : <http://link.aps.org/doi/10.1103/PhysRevLett.94.100601>. .1, B.2
- [232] W. Krauth, *Statistical mechanics: algorithms and computations*, vol. 13 (OUP Oxford, 2006). A.8.2
- [233] K. M. Salerno et M. O. Robbins, “Effect of inertia on sheared disordered solids: Critical scaling of avalanches in two and three dimensions,” *Phys. Rev. E* **88**, 062206 (2013). URL : <http://link.aps.org/doi/10.1103/PhysRevE.88.062206>. B.1

- [234] P. D. Ispánovity, L. Laurson, M. Zaiser, I. Groma, S. Zapperi, et M. J. Alava, “Avalanches in 2d dislocation systems: Plastic yielding is not depinning,” *Phys. Rev. Lett.* **112**, 235501 (2014). URL : <http://link.aps.org/doi/10.1103/PhysRevLett.112.235501>. B.1
- [235] G. Blatter, M. Feigel’man, V. Geshkenbein, A. Larkin, et V. Vinokur, “Vortices in high-temperature superconductors,” *Rev. Mod. Phys.* **66**, 1125 (1994). B.1, C.1, E.1.1
- [236] T. Nattermann et S. Scheidl, “Vortex-glass phases in type-II superconductors,” *Advances in Physics* **49**, 607–704 (2000). B.1, C.1
- [237] L. Laurson, X. Illa, S. Santucci, K. Tallakstad, K. M. løy, et M. Alava, “Evolution of the average avalanche shape with the universality class,” *Nat. Commun.* **4**, 2927 (2013). URL : <http://www.nature.com/ncomms/2013/131219/ncomms3927/abs/ncomms3927.html>. B.1
- [238] “See supplemental material below,” . B.1, B.3, B.1, B.1, B.1, B.1, B.1
- [239] “We thank matthieu wyart for this suggestion,” . B.1
- [240] A. Rosso, A. Hartmann, et W. Krauth, “Depinning of elastic manifolds,” *Phys. Rev. E* **67**, 021602 (2003). B.1
- [241] E. E. Ferrero, S. Bustingorry, et A. B. Kolton, “Non-steady relaxation and critical exponents at the depinning transition,” arXiv:**1211.7275** (2012). B.1, B.2, B.2
- [242] P. Calabrese, M. Kormos, et P. Le Doussal, “From the sine-Gordon field theory to the Kardar-Parisi-Zhang growth equation,” *EPL (Europhysics Letters)* **107**, 10011 (2014). D.1, E.1.1
- [243] A. Borodin, I. Corwin, et P. Ferrari, “Free energy fluctuations for directed polymers in random media in 1+ 1 dimension,” *Communications on Pure and Applied Mathematics* **67**, 1129–1214 (2014). D.1, .3, D.23, E.1.1
- [244] Éric Brunet, “private communication,” . D.1, D.3.2, D.3.2
- [245] Éric Brunet, “Phd thesis,” . D.5
- [246] M. Prähofer et H. Spohn, “Universal distributions for growth processes in 1 + 1 dimensions and random matrices,” *Phys. Rev. Lett.* **84**, 4882–4885 (2000). E.1.1
- [247] I. Corwin et L. Petrov, “Stochastic Higher Spin Vertex Models on the Line,” *Communications in Mathematical Physics* **343**, 651–700 (2016). E.1.1, E.2.2, 3, G.8
- [248] D. A. Huse, C. L. Henley, et D. S. Fisher, “Huse, henley, and fisher respond,” *Phys. Rev. Lett.* **55**, 2924–2924 (1985). URL : <http://link.aps.org/doi/10.1103/PhysRevLett.55.2924>. E.1.1, G.1, G.4.2

- [249] M. Kardar et Y.-C. Zhang, “Scaling of directed polymers in random media,” *Phys. Rev. Lett.* **58**, 2087–2090 (1987). URL : <http://link.aps.org/doi/10.1103/PhysRevLett.58.2087>. E.1.1, F.1.1
- [250] A. M. Somoza, M. Ortuño, et J. Prior, “Universal distribution functions in two-dimensional localized systems,” *Phys. Rev. Lett.* **99**, 116602 (2007). URL : <http://link.aps.org/doi/10.1103/PhysRevLett.99.116602>. E.1.1
- [251] T. Gueudré, A. Dobrinevski, et J.-P. Bouchaud, “Explore or Exploit? A Generic Model and an Exactly Solvable Case,” *Physical Review Letters* **112**, 050602 (2014). E.1.1
- [252] T. Hwa et M. Lässig, “Optimal detection of sequence similarity by local alignment,” (1998), RECOMB 98, p. 109–16. E.1.1
- [253] J. Otwinowski et J. Krug, “Clonal interference and muller’s ratchet in spatial habitats,” *Physical biology* **11**, 056003 (2014). E.1.1
- [254] A. Borodin et I. Corwin, “Discrete time q-taseps,” *International Mathematics Research Notices* (2013). URL : <http://imrn.oxfordjournals.org/content/early/2013/10/11/imrn.rnt206.abstract>. E.1.1, G.8
- [255] J.-P. Bouchaud et A. Georges, “Anomalous diffusion in disordered media: statistical mechanisms, models and physical applications,” *Phys. Rep.* **195**, 127–293 (1990). F.1.1
- [256] D. Fisher, P. L. Doussal, et C. Monthus, “Nonequilibrium dynamics of random field Ising spin chains: Exact results via real space renormalization group,” *Phys. Rev. E* **64**, 066107/1–41 (2001). F.1.1
- [257] F. Solomon, “Random walks in a random environment,” *Ann. Probab.* **3**, 1–31 (1975). URL : <http://dx.doi.org/10.1214/aop/1176996444>. F.1.1
- [258] E. Schertzer, R. Sun, et J. M. Swart, “The Brownian web, the Brownian net, and their universality,” *ArXiv e-prints* (2015). F.1.1
- [259] F. Rassoul-Agha et T. Seppäläinen, “An almost sure invariance principle for random walks in a space-time random environment,” *Probability Theory and Related Fields* **133**, 299–314 (2005). URL : <http://dx.doi.org/10.1007/s00440-004-0424-1>. F.1.1, F.4.5, F.4.5
- [260] J.-D. Deuschel, X. Guo, et A. F. Ramirez, “Quenched invariance principle for random walk in time-dependent balanced random environment,” *arXiv preprint arXiv:1503.01964* (2015). F.1.1
- [261] Y. Le Jan et S. Lemaire, “Products of Beta matrices and sticky flows,” *ArXiv Mathematics e-prints* (2003). 1
- [262] M. Balázs, F. Rassoul-Agha, et T. Seppäläinen, “The random average process and random walk in a space-time random environment in one dimension,” *Communications in mathematical physics* **266**, 499–545 (2006). F.1.1

- [263] A. Georges et P. Le Doussal, “From equilibrium spin models to probabilistic cellular automata,” *Journal of Statistical Physics* **54**, 1011–1064 (1989). URL : <http://dx.doi.org/10.1007/BF01019786>. F.1.1
- [264] A. Georges, D. Hansel, P. L. Doussal, et J. M. Maillard, “Dimensional reduction and correlation functions on 3d lattice models,” *Journal of Physics A: Mathematical and General* **20**, 5299 (1987). URL : <http://stacks.iop.org/0305-4470/20/i=15/a=041>. F.1.1
- [265] G. Barraquand et I. Corwin, “private communication,” . F.1.2, F.1.2, F.3.4, F.6, F.6.1, F.6.1, F.8
- [266] G. Barraquand et I. Corwin, “we thank guillaume barraquand and ivan corwin for this suggestion,” . F.4.5
- [267] T. S. Márton Balázs, Firas Rassoul-Agha, “Fluctuation bounds for the stationary beta polymer, work in preparation,” . G.1, G.8
- [268] N. Georgiou, F. Rassoul-Agha, T. Seppäläinen, et A. Yilmaz, “Ratios of partition functions for the log-gamma polymer,” *Ann. Probab.* **43**, 2282–2331 (2015). URL : <http://dx.doi.org/10.1214/14-AOP933>. G.2, G.6.3
- [269] J. B. Martin, “Batch queues, reversibility and first-passage percolation,” *Queueing Systems* **62**, 411–427 (2009). URL : <http://dx.doi.org/10.1007/s11134-009-9137-6>. G.5.1
- [270] N. Georgiou, F. Rassoul-Agha, et T. Seppäläinen, “Variational formulas and cocycle solutions for directed polymer and percolation models,” *Communications in Mathematical Physics* p. 1–39. G.6.3
- [271] M. Damron et J. Hanson, “Busemann functions and infinite geodesics in two-dimensional first-passage percolation,” *Communications in Mathematical Physics* **325**, 917–963 (2014). G.6.3
- [272] A. Borodin et L. Petrov, “Nearest neighbor Markov dynamics on Macdonald processes,” *ArXiv e-prints* (2013). G.8

Résumé

Cette thèse présente plusieurs aspects de la physique des systèmes élastiques désordonnés et des méthodes analytiques utilisées pour les étudier.

On s'intéressera d'une part aux propriétés universelles des processus d'avalanches statiques et dynamiques (à la transition de dépiégeage) d'interfaces élastiques de dimension arbitraire en milieu aléatoire à température nulle. Pour étudier ces questions nous utiliserons le groupe de renormalisation fonctionnel. Après une revue de ces aspects, nous présenterons plus particulièrement les résultats obtenus pendant la thèse sur (i) la structure spatiale des avalanches et (ii) les corrélations entre avalanches.

On s'intéressera d'autre part aux propriétés statiques à température finie de polymères dirigés en dimension 1+1, et en particulier aux observables liées à la classe d'universalité KPZ. Dans ce contexte l'étude de modèles exactement solubles a récemment permis de grands progrès. Après une revue de ces aspects, nous nous intéresserons plus particulièrement aux modèles exactement solubles de polymère dirigé sur le réseau carré, et présenterons les résultats obtenus pendant la thèse dans cette voie: (i) classification des modèles à température finie sur le réseau carré exactement solubles par ansatz de Bethe; (ii) universalité KPZ pour les modèles Log-Gamma et Inverse-Beta; (iii) universalité et non-universalité KPZ pour le modèle Beta; (iv) mesures stationnaires du modèle Inverse-Beta et des modèles à température nulle associés.

Mots Clés

Systèmes élastiques désordonnés, avalanches, polymère dirigé, KPZ, groupe de renormalisation fonctionnelle, modèles exactement solubles

Abstract

This thesis presents several aspects of the physics of disordered elastic systems and of the analytical methods used for their study.

On one hand we will be interested in universal properties of avalanche processes in the statics and dynamics (at the depinning transition) of elastic interfaces of arbitrary dimension in disordered media at zero temperature. To study these questions we will use the functional renormalization group. After a review of these aspects we will more particularly present the results obtained during the thesis on (i) the spatial structure of avalanches and (ii) the correlations between avalanches.

On the other hand we will be interested in static properties of directed polymers in 1+1 dimension, and in particular in observables related to the KPZ universality class. In this context the study of exactly solvable models has recently led to important progress. After a review of these aspects we will be more particularly interested in exactly solvable models of directed polymer on the square lattice and present the results obtained during the thesis in this direction: (i) classification of Bethe ansatz exactly solvable models of directed polymer at finite temperature on the square lattice; (ii) KPZ universality for the Log-Gamma and Inverse-Beta models; (iii) KPZ universality and non-universality for the Beta model; (iv) stationary measures of the Inverse-Beta model and of related zero temperature models.

Keywords

Disordered elastic systems, avalanches, directed polymer, KPZ, functional renormalization group, exactly solvable models